UNIVERZITET U BEOGRADU
INSTITUT ZA FIZIKU BEOGRAD
Pregrevica 118, 11080 Zemun – Beograd, Srbija
Tel: +381 11 3713000, Fax: +381 11 3162190, www.ipb.ac.rs
PIB/VAT: 100105980, Matični broj: 07018029, Tekući račun: 205-66984-23

Научном већу Института за физику

Предлог за Годишњу награду за научни рад Института за физику

Посебно нам је задовољство да предложимо др Ненада Врањеша, вишег научног сарадника, за Годишњу награду Института за физику за његов допринос прецизним мерењима параметара Стандардног модела физике честица, а посебно мерењу масе W бозона. Наведени резултати су остварени у периоду од 1. јануара 2016. до 31. децембра 2017. у оквиру експеримента АТЛАС на Великом сударачу хадрона (*Large Hadron Collider*, ЛХЦ) у ЦЕРН-у.

Тема истраживања. Основна тема истраживања колеге Врањеша односи се на прецизна мерења параметара Стандардног модела елементарних честица (СМ). Стандардни модел представља предиктиван теоријски оквир у коме су фундаментални параметри, масе и ширине честица као и њихове јачине спрезања, међусобно повезани скупом релација. Након потврде постојања Хигсовог бозона и првог мерења његове масе на експериментима АТЛАС и ЦМС на ЛХЦ-у тај скуп релација је надограничен, и упоређивање експериментално измерених вредности са теоријски предвиђеним вредностима омогућава даље тестирање конзистентности модела. У моделима која нису укључени у СМ вредност m_W зависи и од нових тешких честица које интерагују слабом интеракцијом, па тако упоређивање измерене вредности m_W са теоријском вредношћу представља ,,прозор" ка новој физици. Експериментална мерења маса познатих честица: масе W бозона (m_W), масе топ кварка (m_{top}), као и масе Хигсовог бозона (m_H) и јачине његових спрезања са фермионима и бозонима, омогућавају да се разјасни динамика нарушења симетрије у електрослабим интеракцијама. Ненад Врањеш је у претходне две године учествовао у свим овим истраживањима, а најзначајнији резултат односи се на мерење масе W бозона. Узимајући у обзир измерене вредности и неодређености m_{top} и m_H, m_W је предвиђена са прецизношћу ± 8 MeV. Вредност m_W добијена комбиновањем резултата мерења са више експеримената на сударачима ЛЕП и Теватрон износи 80385 ± 15 MeV. Крајњи циљ експеримената на ЛХЦ-у је постизање исте или боље прецизности у односу на теоријска предвиђања. У контексту глобалног фита параметара СМ, ограничења на параметарски простор физике изван СМ зависе највише од прецизног мерења m_W.

Опис резултата и личног доприноса кандидата. Мерење m_W у распадима $W \to \ell\nu$ (где ℓ означава електрон или мион а ν неутрино), представља велики изазов на хадронским сударачима. У питању је мерење екстремне прецизности: да би се резултати могли упоредити са теоријским предвиђањима потребно је достићи прецизност од 0.01%. Поређења ради, типична прецизна мерења на ЛХЦ-у имају за циљ прецизност реда величине 1%. У оквиру поменуте тематике колега Врањеш је имао кључни допринос у

калибрацији импулса миона, затим у мерењу ефикасности реконструкције и тригеровања миона, калибрацији хадронског узмака (недостајуће трансверзалне енергије), селекцији догађаја од интереса, као и у укупној анализи података у мионском каналу. Калибрација импулсне скале лептона (α_ℓ) је најкритичнија компонента мерења m_W на хадронским сударачима: осетљивост на импулсну скалу лептона износи $\delta m_W/\delta\alpha_\ell \approx 800$ MeV/%. Како би систематска неодређеност била доведена на потребан ниво $O(10^{-4})$ имплементирани су и експлоатисани иновативни алгоритми и технике за потребе калибрације импулса миона на експерименту АТЛАС. Коначна вредност m_W измерена је са неодређеношћу ± 19 MeV, што спада у најпрецизније мерење до данас остварено на експериментима у физици честица. Измерена вредност је компатибилна са тренутном светском средњом вредношћу као и последњим теоријским предвиђањима. Резултат је објављен у:

• Aaboud, M., ... ,Vranjes N., *et al.* [ATLAS Collaboration], *Measurement of the W-boson mass in pp collisions at* $\sqrt{s}$*= 7TeV with the ATLAS detector*, Eur.Phys.J. C78 (2018) no.2, 110, arXiv:1701.07240 [hep-ex], (**IF = 5.331**).

Као један од најкомпетентнијих сарадника са кључним доприносом у овој студији Ненад Врањеш је изабран да буде кореспондентни аутор наведене публикације. Рад је прихваћен за штампу у децембру 2017, а према бази `HEP-Inspire` до сада је цитиран већ 25 пута без аутоцитата. **Истиче се податак да је у питању прво (и за сада једино објављено) мерење $\mathbf{m_W}$ на ЛХЦ-у**. Резултат је до сада приказан на посебном ЦЕРН-овом семинару и најзначајнијим конференцијама из области. Због посебног значаја овај резултат је попримио ширу пажњу кроз ЦЕРН-ово саопштење за медије, и чланак у *CERN Courier*. Резултати су приказани и на семинару у Институту за физику.

Калибрација импулса миона, а нарочито ефеката који зависе од знака наелекетрисања мионских трагова у детектору примењена је у мерењу троструког диференцијалног пресека за продукцију Z бозона. Ненад Врањеш је учествовао и у овој студији чији су резултати објављени у:

• Aaboud, M., ... ,Vranjes N., *et al.* [ATLAS Collaboration], *Measurement of the Drell-Yan triple-differential cross section in pp collisions at* $\sqrt{s}$ *= 8 TeV*, JHEP 1712 (2017) 059, arXiv:1710.05167 [hep-ex], (**IF = 6.063**).

Ненад Врањеш је био члан рецензентских тимова за студије које се баве прецизним мерењем масе топ кварка и мерењем масе Хигсовог бозона. У оквиру колаборације АТЛАС, рецензентски тим заједно са непосредним ауторима има одговорност да произведе и објави научну публикацију врхунског квалитета. Резултат мерења масе топ кварка је објављен у престижном међународном часопису и за последње две године цитиран преко 30 пута, док су прелиминарни резултати мерења масе Хигсовог бозона приказани у једној јавној ноти:

• Aaboud, M., ... ,Vranjes N., *et al.* [ATLAS Collaboration], *Measurement of the top quark mass in the* $t\bar{t} \to$ *dilepton channel from* $\sqrt{s}$ *= 8 TeV ATLAS data*, Phys.Lett. B761 (2016) 350-371, arXiv:1606.02179 [hep-ex], (**IF = 4.087**).
• ATLAS Collaboration, *Measurement of the Higgs boson mass in the* $H \to ZZ \to 4\ell$ *and* $H \to \gamma\gamma$ *channels with* $\sqrt{s}$*=13 TeV pp collisions using the ATLAS detector*, `ATLAS-CONF-2017-046`.

Коначни резултат мерења масе Хигсовог бозона (са незнатним корекцијама у односу

на ноту) је у завршној фази унутрашње рецензије у оквиру АТЛАС колаборације и његово слање у часопис се очекује у наредним месецима.

Мерење пресека за продукцију честица СМ, пре свега W и Z бозона и топ кваркова, представља основ за разумевање квантне хромоднимаике и електрослабих процеса као и комплетности теоријског модела за опис феномена на хадронским сударачима. Предвиђања за пресеке зависе пре свега од партонских дистрибуција у протону те су стога осетљиве на динамику јако интерагујућих честица. Интегрална луминозност је кључна компонента ових мерења и често извор доминантне систематске неодређености. На ЛХЦ-у у основи поступка апсолутне калибрације луминозности је детаљна анализа специјалих судара протона, *van der Meer (vdM)* судара, где се луминозност измерена одговарајућим луминометрима калибрише вредношћу израчунатом из измерених параметара акцелератора. Од 2015. Ненад Врањеш је главни сарадник на анализи ових података, а резултати његових мерења су објављени у публикацији:

• Aaboud, M., ... ,Vranjes N., *et al.* [ATLAS Collaboration], *Luminosity determination in pp collisions at* $\sqrt{s}$ *= 8 TeV using the ATLAS detector at the LHC*, Eur.Phys.J. C76 (2016) no.12, 653, arXiv:1608.03953 [hep-ex], (**IF = 5.331**).

Наведена публикација је за последње две године цитирана 182 пута, и представља референтан резултат АТЛАС колаборације. Резултати мерења неодређености интегралне луминозности у којима је учествовао колега Врањеш представљају кључну компоненту за постигнуте прецизности мерења у:

• Aaboud, M., ... ,Vranjes N., *et al.* [ATLAS Collaboration], *Measurement of the* $t\bar{t}$ *production cross-section using* $e\mu$ *events with b−tagged jets in pp collisions at with the ATLAS detector* $\sqrt{s}$ *=13 TeV using the ATLAS detector*, Phys.Lett. B761 (2016) 136-157 (Erratum: Phys.Lett. B772 (2017) 879-879), arXiv:1606.02699 [hep-ex], (**IF = 4.087**).
• Aaboud, M., ... ,Vranjes N., *et al.* [ATLAS Collaboration], *Measurement of the* $t\bar{t}Z$ *and* $t\bar{t}W$ *production cross-section production cross sections in multilepton final states using 3.2* fb^{-1} *of pp at* $\sqrt{s}$ *=13 TeV with the ATLAS detector*, Eur.Phys.J. C77 (2017) no.1, 40, arXiv:1609.01599 [hep-ex], (**IF = 5.331**).
• Aaboud, M., ... ,Vranjes N., *et al.* [ATLAS Collaboration], *Measurements of the production cross section of a Z boson in association with jets in pp collisions at* $\sqrt{s}$ *=13 TeV with the ATLAS detector*, Eur.Phys.J. C77 (2017) no.6, 361, arXiv:1702.05725 [hep-ex], (**IF = 5.331**).
• Aaboud, M., ... ,Vranjes N., *et al.* [ATLAS Collaboration], *Measurement of the cross-section for electroweak production of dijets in association with a Z boson in pp collisions at* $\sqrt{s}$ *=13 TeV with the ATLAS detector*, Phys.Lett. B775 (2017) 206-228, arXiv:1709.10264 [hep-ex], (**IF = 4.087**).

Посебно желимо да истакнемо да је Ненад Врањеш од стране колаборације именован за руководиоца (convener-а) групе за анализу података са W и Z бозонима од 1. октобра 2017. на период од две године. У питању је једна од највећих група у АТЛАС колаборацији са преко 20 текућих пројеката на којима тренутно ради око 150 истраживача свих академских рангова. Активности групе се односе на мерење параметара СМ (m_W, Вајнбергов угао), тоталних и диференцијалних пресека за продукцију W и Z бозона (инклузивних, и у асоцијацији са џетовима, посебно са џетовима из тешких кваркова), као и спектара W и Z бозона у областима фазног простора од инетерса (ниски трансверзални импулси, ниске и високе вредности инваријантне масе дилептона) и други.

Статистика радова и импакт резултата на научну област. Ненад Врањеш је члан АТЛАС колаборације од 2004. и коаутор је свих радова објављених до данас. Унутар колаборације, допринос кандидата је демонстриран кроз престижну позицију руководиоца (*convener*-а), ауторство у интерним нотама које прате публикације у часописима, кроз едиторски рад, кроз презентације својих, као и резултата целокупних група у оквиру колаборације, и посебно кроз више предавања по позиву која је кандидат држао у име целе колаборације на међународним и националним конференцијама. У последње две године имао је суштински допринос у четири рада објављена у врхунским међународним часописима категорије М21. Према бази и `HEP-Inspire` ови радови су цитирани већ преко 200 пута. Резултати колеге Врањеша на мерењу луминозности од кључног су значаја за постигнуту прецизности мерења у четири рада објављена у часописима категорије М21 који су до сада цитирани преко 30 пута. Укупни импакт фактор наведених радова износи 41.8. Импакт добијених резултата огледа се кроз квалитет часописа у којима се резултати објављени као и кроз цитираност радова. Значај радова у којима је кандидат дао кључни допринос односи се на тестирање конзистентности Стандардног модела, кроз мерење масе W бозона, Хигсовог бозона и масе топ кварка. Ове теме представљају неке од кључних изазова програма ЛХЦ-а. Резултати на калибрацији луминозности имају значајну примену у великом броју резултата које је објавила колаборација у наведеном периоду.

Ненад Врањеш има развијену међународну сарадњу, пре свега са колегама из ЦЕРН-а, Француске и Немачке. Руководилац је једног билатералног DAAD пројекта. Био је ментор једне докторске дисертације одбрањене крајем 2017. Својим радом је изузетно допринео препознатљивости београдске групе у оквиру АТЛАС колаборације.

Због свега наведеног сматрамо да је др Ненад Врањеш постигао изузетне научне резултате у последње две године на самом фронту савремене физике елементарних честица, и задовољство нам је да га предложимо за Годишњу награду за научни рад Института за физику.

Београд, 14. март 2018.

др Лидија Живковић
научни саветник, руководилац пројекта ОИ 171004

академик проф. др Ђорђе Шијачки
Национални координатор АТЛАС експеримента за Србију

НЕНАД ВРАЊЕШ
CURRICULUM VITAE СА СПИСКОМ ПУБЛИКАЦИЈА

- **ЛИЧНЕ ИНФОРМАЦИЈЕ**

Афилијација: Институт за физику
Лабораторија за физику високих енергија
Датум и место рођења: 27. фебруар 1980, Земун.
email: nenadv@ipb.ac.rs
nenad.vranjes@cern.ch
Брачно стање : ожењен, једна кћерка

- **ОБРАЗОВАЊЕ**

Октобар 2007 – новембар 2011: **докторат,** докторска дисертација: ,,Трагање за новим тешким наелектрисаним градијентним бозонима на АТЛАС детектору" *(A Search for New Heavy Charged Gauge Bosons at ATLAS)* Заједнички докторат Универзитета у Београду и Националног и Каподистријског универзитета у Атини

Септембар 2004 – октобар 2007: **магистратура,** магистарски рад: ,,Могућности АТЛАС детектора за мерење продукције парова *W* бозона на Великом хадронском колајдеру", Физички факултет Универзитета у Београду

Октобар 1999 – јул 2004: **основне студије**, истраживачки смер, просек 9.44 Физички факултет Универзитета у Београду

- **РАДНО ИСКУСТВО**

Од новембра 2017: **виши научни сарадник,** Лабораторија за физику високих енергија, Институт за физику у Београду

мај 2012 – новембар 2017: **научни сарадник,** Лабораторија за физику високих енергија, Институт за физику у Београду

новембар 2011 – октобар 2014: **постдокторско усавршавање,** одсек за фундаментална истраживања, *CEA,Saclay* , Француска (базиран у ЦЕРН-у)

јун 2008 – мај 2012: **истраживач сарадник,** Лабораторија за физику високих енергија, Институт за физику у Београду

март 2005 – јун 2008: **истраживач приправник,** Лабораторија за физику високих енергија, Институт за физику у Београду

септембар 2004 – март 2005: **стипендиста министарства науке,** Институт за физику у Београду

- **НАУЧНА ИНТЕРЕСОВАЊА**
    - Физика на сударачима, посебно физика електрослабих инетракција
    - Мерење луминозности на хадронским сударачима
    - Реконструкција трагова, калибрација лептона
    - Физика изван Стандардног модела

- **ЗАДУЖЕЊА У ОКВИРУ АТЛАС КОЛАБОРАЦИЈЕ**
    - ***Convener*** *W,Z Standard Model* групе, октобар 2017. до сада
    - **Контакт** између ATLAS Standard Model групе и Muon performance групе, март-новембар 2017.
    - ***Contact editor*** рада Aaboud, M., ... ,Vranjes N., *et al,* [ATLAS Collaboration], {Measurement of the W-boson mass in pp collisions at \sqrt{s}= 7TeV with the ATLAS detector, Eur.Phys.J. C78 (2018) no.2, 110, arXiv:1701.07240 [hep-ex],
    - Члан ***Editorial board*** for the top quark mass measurement with 8 TeV data: Measurement of the top quark mass in the tt -> dilepton channel from s = 8 TeV ATLAS data, Phys.Lett. B761 (2016) 350-371, arXiv:1606.02179 [hep-ex].
    - Члан *Editorial board* for the Higsh boson quark mass measurement (4lepton + gammagamma) with 13 TeV data
    - ***Contact editor*** of the ATLAS Collaboration paper: G.Aad,…,N.Vranjes, *et al*. [ATLAS Collaboration], "*Measurement of the muon reconstruction performance of the ATLAS detector using 2011 and 2012 LHC proton-proton collision data*", arXiv:1407.3935 [hep-ex], Eur. Phys. J. C74 (2014) 3130.
    - ***Contact editor*** of the ATLAS Collaboration paper: G.Aad,…,N.Vranjes, *et al*. [ATLAS Collaboration], "*Search for new particles in events with one lepton and missing transverse momentum in pp collisions at sqrt{s} = 8 TeV with the ATLAS detector*," arXiv:1407.7494 [hep-ex], JHEP09 (2014) 037.

- **НАЈЗНАЧАЈНИЈЕ КОНФЕРЕНЦИЈЕ, РАДИОНИЦЕ И ШКОЛЕ**
    - LHCP 2016, Lund, Sweden, 13-18 June, 2016, **предавање по позиву**
    - 26th Rencontres de Blois, Particle Physics and Cosmology, Blois, France, May 18-23, 2014, **предавање по позиву**
    - LHC France 2013, Annecy 2013, Француска.
    - XII Конгрес физичара Србије, Врњачка бања , 2013.
    - Workshop on LHC on the march (IHEP-LHC-2011): Protvino, Russia, November 16-18, 2011, **предавање по позиву**
    - XXVIII Workshop on Recent Advances in Particle Physics and Cosmology, 25-28 March, 2010. Thessaloniki, Greece.
    - Signaling the Arrival of the LHC Era, 8 - 13 December 2008, ICTP, Trieste, Italy.
    - Physics at LHC - 2008, 29 September - 4 October 2008, Split, Croatia.
    - Fundamental interactions in Serbia, 26-28 September 2007, Iriski venac, Serbia.
    - Physics and Techniques of Event Generators, 1st MCnet School, IPPP, 18-20th Apr 2007, Durham, UK.
    - CERN-Fermilab summer school, Fermilab, USA, 2006.
    - 6th International Conference of the Balkan Physical Union, 22-26 Aug, 2006, Istanbul, Turkey.

- **МЕНТОРСТВА**

  - Једна докторска дисертација: А. Димитриевска, тема мерење масе W и калибрација миона (АТЛАС)
  - Мастер рада на тему будућег хадронског сударача високе енергије (FCC-hh) и други на тему унапређеног ЛХЦ (HL/HE - LHC), у току
  - Један *CERN summer student* (АТЛАС)

- **ВЕШТИНЕ**

  - Програмирање: C/C++, Python, Fortran, shell scripts, GRID Computing Linux, Mac OS
  - Језици: српски-матерњи, енглески - одлично, руски – основни ниво

- **НАГРАДЕ И ПРИЗНАЊА**

2004-2005 Стипендиста министарства науке
2002 Награда Краљевине Норвешке за 500 најбољих студената у Србији.
2000-2003 Стипендија министарства просвете

- **ОСТАЛЕ АКТИВНОСТИ**

  - Организација *International Masterclasses for High School Students 2009-2011*, у оквиру *International Particle Physics Outreach Group (IPPOG*).
  - Семинари на тему програма на ЛХЦ-у за студенте завршних година физике на ФФ (на курсевима физике честица и семинара савремене физике)
  - Ментор једног матурског рада у Математичкој гимназији (Потрага за Хигсовим бозоном коришћењем мионског спектрометра АТЛАС детектора) 2011.

- **ЛИСТА ИЗАБРАНИХ ПУБЛИКАЦИЈА**

1. M. Aaboud,.. N.Vranjes... [ATLAS Collaboration], *Measurement of the W-boson mass in pp collisions at $\sqrt{s}$= 7TeV with the ATLAS detector*, Eur.Phys.J. C78 (2018) no.2, 110, arXiv:1701.07240 [hep-ex]

2. M. Aaboud, M., ... ,Vranjes N., [ATLAS Collaboration], *Measurement of the Drell-Yan triple-differential cross section in pp collisions at $\sqrt{s} = 8$ TeV*, JHEP 1712 (2017) 059, arXiv:1710.05167 [hep-ex].

3. M. Aaboud, M., ... ,Vranjes N., [ATLAS Collaboration*], Luminosity determination in pp collisions at $\sqrt{s}$ = 8 TeV using the ATLAS detector at the LHC*, Eur.Phys.J. C76 (2016) no.12, 653.

4. Aaboud, M., ... ,Vranjes N., [ATLAS Collaboration], {\it Measurement of the $t\bar{t}$ production cross-section using $e\mu$ events with $b-$tagged jets in pp collisions at with the ATLAS detector $\sqrt{s} =$13 TeV using the ATLAS detector}, Phys.Lett. B761 (2016) 136-157 (Erratum: Phys.Lett. B772 (2017) 879-879), arXiv:1606.02699 [hep-ex]
5. Aaboud, M., ... ,Vranjes N., [ATLAS Collaboration], Measurement of the $t\bar{t}Z$ and $t\bar{t}W$ production cross-section production cross sections in multilepton final states using 3.2 fb^{-1} of pp at $\sqrt{s} =$13 TeV with the ATLAS detector, Eur.Phys.J. C77 (2017) no.1, 40, arXiv:1609.01599 [hep-ex]

6. Aaboud, M., ... ,Vranjes N., {\it et al.} [ATLAS Collaboration], {\it Measurements of the production cross section of a Z boson in association with jets in pp collisions at $\sqrt{s} =$13 TeV with the ATLAS detector}, Eur.Phys.J. C77 (2017) no.6, 361,

7. Aaboud, M., ... ,Vranjes N., {\it et al.} [ATLAS Collaboration], {\it Measurement of $W^{\pm}$ and Z-boson production cross sections in pp collisions at $\sqrt{s} =$13 TeV with the ATLAS detector}, Phys.Lett. B759 (2016) 601-621, arXiv:1603.09222 [hep-ex].

8. Aaboud, M., ... ,Vranjes N., {\it et al.} [ATLAS Collaboration], {\it Measurement of the cross-section for electroweak production of dijets in association with a Z boson in pp collisions at $\sqrt{s} =$13 TeV with the ATLAS detector}, Phys.Lett. B775 (2017) 206-228, arXiv:1709.10264 [hep-ex)

9. ATLAS Collaboration, "*Studies of theoretical uncertainties on the measurement of the mass of the W boson at the LHC*", ATL-PHYS-PUB-2014-015.

10. G.Aad,…,N.Vranjes, *et al.* [ATLAS Collaboration], "*Measurement of the muon reconstruction performance of the ATLAS detector using 2011 and 2012 LHC proton-proton collision data*", Eur. Phys. J. C74 (2014) 3130.

11. G.Aad,…,N.Vranjes, *et al.* [ATLAS Collaboration], "*Search for new particles in events with one lepton and missing transverse momentum in pp collisions at sqrt{s} = 8 TeV with the ATLAS detector*," JHEP09 (2014) 037.

12. G.Aad,…,N.Vranjes, *et al.* [ATLAS Collaboration], "*Measurement of the Higgs boson mass from the H -> gamma gamma and H -> ZZ* -> 4l channels with the ATLAS detector using 25 fb-1 of pp collision data*", Phys.Rev.D. 90, 052004 (2014).

13. G.Aad,…,N.Vranjes, *et al.* [ATLAS Collaboration], "*Fiducial and differential cross sections of Higgs boson production measured in the four-lepton decay channel in pp collisions at sqrt(s) = 8 TeV with the ATLAS detector*", Phys. Lett. B 738 (2014) 234-253.

14. G.Aad,…,N.Vranjes, *et al.* [ATLAS Collaboration], "*ATLAS search for a heavy gauge boson decaying to a charged lepton and a neutrino in pp collisions at sqrt(s)=7 TeV*", Eur.Phys.J.C 72 (2012) 2241.

15. G.Aad,…,N.Vranjes, *et al.* [ATLAS Collaboration], "*Search for a heavy gauge boson decaying to a charged lepton and a neutrino in 1 fb-1 of pp collisions at sqrt(s)=7 TeV using the ATLAS detector*", Phys. Lett. B 705, 28 (2011).

16. G.Aad,…,N.Vranjes, *et al.* [ATLAS Collaboration], "*Search for high-mass states with one lepton plus missing transverse momentum in proton-proton collisions at sqrt(s) = 7 TeV with the ATLAS detector"*, Phys.Lett.B 701:50-69, 2011.

17. ATLAS Collaboration, "*Physics potential of Z' and W' searches with the ATLAS Detector as a function of the LHC center-of-mass energy*", ATL-PHYS-PUB-2011-002.

18. ATLAS Collaboration, "*ATLAS sensitivity prospects to W' and Z' at 7 TeV*", ATL-PHYS-PUB-2010-007.

19. D.L. Adams, D. Fassouliotis, L.R. Flores Castillo, C. Kourkoumelis, B.R. Mellado Garcia, M.I. Pedraza Morales, N. Vranjes, S.L. Wu, "*Lepton plus Missing Transverse Energy Signals at High Mass*", ATL-PHYS-PUB-2009-071 (part of CERN-OPEN-2008-020).

20. K. Bachas,..., N.Vranjes, et al. "*Diboson Physics Studies*", ATL-PHYS-PUB-2009-038 (part of CERN-OPEN-2008-020).

- **ПРЕДАВАЊА НА КОНФЕРЕНЦИЈАМА**

1. N.Vranjes, on behalf of ATLAS and CMS Collaboration, "*Challages in W mass measurement*", LHCP2016, Lund, Sweden, 2016.

2. N.Vranjes, on behalf of ATLAS Collaboration, "*Electroweak tests at the LHC*", 26th Rencontres de Blois,
   Particle Physics and Cosmology, Blois, France, May 18-23, 2014.

3. N.Vranjes, on behalf of ATLAS Collaboration,"*Exotic Searches in ATLAS*", PoS IHEP-LHC-2011, 021 (2011) [arXiv:1202.3171 [hep-ex]].

4. N.Vranjes, on behalf of ATLAS and CMS collaborations, "*Muon reconstruction in ATLAS+CMS*",
   LHC France 2013, Annecy 2013, Francuska,

5. Н. Врањеш, *Последњи резултати експеримента АТЛАС*, Друштво физичара Србије, XII Конгрес физичара Србије.

6. N. Vranjes, C. Kourkoumelis, D. Fassouliotis, A. Antonaki, D. Popovic, "*Searches for new gauge bosons with the ATLAS detector*", XXVIII Workshop on Recent Advances in Particle Physics and Cosmology, 25-28 March 2010, Thessaloniki, Greece.

7. Nenad Vranjes for the ATLAS collaboration, "*Search for W' in lepton+missing ET final state with early data at ATLAS*", ATL-PHYS-PROC-2008-085, PoS(2008LHC)121.

5. K. Bachas,...,N.Vranjes et al. "*Studies of diboson production with the ATLAS detector*" Nucl.Phys.Proc.Suppl.177-178:255-257,2008.

- **ЛИСТА СВИХ ПУБЛИКАЦИЈА**

http://inspirehep.net/author/profile/N.Vranjes.1

Atlas Analysis Glance 18 December 2017 at 18:32 Hide

Analysis Paper STDM-2014-18 "W mass measurement 7 TeV" - Paper Acceptance

To: atlas-stdm-2014-18-contact-editors@cern.ch, atlas-stdm-2014-18-analysis-team@cern.ch, atlas-stdm-conveners@cern.ch, atlas-idet-conveners@cern.ch,

Cc: atlas-physics-coordinators@cern.ch, Nenad Vranjes, maarten.boonekamp@cea.fr, Matthias Schott, nansi.andari@cern.ch, Stefano Camarda, atlas-stdm-2014-18-editorial-board (Editorial Board of stdm-2014-18), Richard.Hawkings@cern.ch, atlas-spokesperson@cern.ch, atlas-publication-committee-chair@cern.ch, atlas-stdm-wz-conveners@cern.ch, atlas-phys-office-pub@cern.ch,

Reply-To: atlas-glance-support@cern.ch

Dear colleagues,

Congratulations, your paper W mass measurement 7 TeV is accepted!

Information about this paper can be found at the following Glance page:
https://glance.cern.ch/atlas/analysis/papers/details.php?id=6102

Best wishes,

(Automatic e-mail generated by Nuno Filipe Castro)

This message was automatically generated by Glance (hash 065d7957cc819b54721f7554a5f90857).

Eur. Phys. J. C (2018) 78:110
https://doi.org/10.1140/epjc/s10052-017-5475-4

THE EUROPEAN PHYSICAL JOURNAL C

Regular Article - Experimental Physics

Measurement of the W-boson mass in pp collisions at $\sqrt{s} = 7$ TeV with the ATLAS detector

ATLAS Collaboration[⋆]

CERN, 1211 Geneva 23, Switzerland

Received: 26 January 2017 / Accepted: 18 December 2017

Abstract A measurement of the mass of the W boson is presented based on proton–proton collision data recorded in 2011 at a centre-of-mass energy of 7 TeV with the ATLAS detector at the LHC, and corresponding to 4.6 fb^{-1} of integrated luminosity. The selected data sample consists of 7.8×10^6 candidates in the $W \to \mu\nu$ channel and 5.9×10^6 candidates in the $W \to e\nu$ channel. The W-boson mass is obtained from template fits to the reconstructed distributions of the charged lepton transverse momentum and of the W boson transverse mass in the electron and muon decay channels, yielding

$$\begin{aligned} m_W &= 80370 \pm 7\ (\text{stat.}) \pm 11 (\text{exp. syst.}) \\ &\quad \pm 14\ (\text{mod. syst.})\ \text{MeV} \\ &= 80370 \pm 19\ \text{MeV}, \end{aligned}$$

where the first uncertainty is statistical, the second corresponds to the experimental systematic uncertainty, and the third to the physics-modelling systematic uncertainty. A measurement of the mass difference between the W^+ and W^- bosons yields $m_{W^+} - m_{W^-} = -29 \pm 28$ MeV.

1 Introduction

The Standard Model (SM) of particle physics describes the electroweak interactions as being mediated by the W boson, the Z boson, and the photon, in a gauge theory based on the $\mathrm{SU(2)_L \times U(1)_Y}$ symmetry [1–3]. The theory incorporates the observed masses of the W and Z bosons through a symmetry-breaking mechanism. In the SM, this mechanism relies on the interaction of the gauge bosons with a scalar doublet field and implies the existence of an additional physical state known as the Higgs boson [4–7]. The existence of the W and Z bosons was first established at the CERN SPS in 1983 [8–11], and the LHC collaborations ATLAS and CMS reported the discovery of the Higgs boson in 2012 [12,13].

At lowest order in the electroweak theory, the W-boson mass, m_W, can be expressed solely as a function of the Z-boson mass, m_Z, the fine-structure constant, α, and the Fermi constant, G_μ. Higher-order corrections introduce an additional dependence of the W-boson mass on the gauge couplings and the masses of the heavy particles of the SM. The mass of the W boson can be expressed in terms of the other SM parameters as follows:

$$m_W^2 \left(1 - \frac{m_W^2}{m_Z^2}\right) = \frac{\pi\alpha}{\sqrt{2}G_\mu}(1 + \Delta r),$$

where Δr incorporates the effect of higher-order corrections [14,15]. In the SM, Δr is in particular sensitive to the top-quark and Higgs-boson masses; in extended theories, Δr receives contributions from additional particles and interactions. These effects can be probed by comparing the measured and predicted values of m_W. In the context of global fits to the SM parameters, constraints on physics beyond the SM are currently limited by the W-boson mass measurement precision [16]. Improving the precision of the measurement of m_W is therefore of high importance for testing the overall consistency of the SM.

Previous measurements of the mass of the W boson were performed at the CERN SPS proton–antiproton ($p\bar{p}$) collider with the UA1 and UA2 experiments [17,18] at centre-of-mass energies of $\sqrt{s} = 546$ GeV and $\sqrt{s} = 630$ GeV, at the Tevatron $p\bar{p}$ collider with the CDF and D0 detectors at $\sqrt{s} = 1.8$ TeV [19–21] and $\sqrt{s} = 1.96$ TeV [22–24], and at the LEP electron–positron collider by the ALEPH, DELPHI, L3, and OPAL collaborations at $\sqrt{s} = 161$–209 GeV [25–28]. The current Particle Data Group world average value of $m_W = 80385 \pm 15$ MeV [29] is dominated by the CDF and D0 measurements performed at $\sqrt{s} = 1.96$ TeV. Given the precisely measured values of α, G_μ and m_Z, and taking recent top-quark and Higgs-boson mass measurements, the SM prediction of m_W is $m_W = 80358 \pm 8$ MeV in Ref. [16] and $m_W = 80362 \pm 8$ MeV in Ref. [30]. The SM prediction uncertainty of 8 MeV represents a target for the precision of future measurements of m_W.

⋆ e-mail: atlas.publications@cern.ch

Published online: 06 February 2018

At hadron colliders, the W-boson mass can be determined in Drell–Yan production [31] from $W \to \ell\nu$ decays, where ℓ is an electron or muon. The mass of the W boson is extracted from the Jacobian edges of the final-state kinematic distributions, measured in the plane perpendicular to the beam direction. Sensitive observables include the transverse momenta of the charged lepton and neutrino and the W-boson transverse mass.

The ATLAS and CMS experiments benefit from large signal and calibration samples. The numbers of selected W- and Z-boson events, collected in a sample corresponding to approximately 4.6 fb^{-1} of integrated luminosity at a centre-of-mass energy of 7 TeV, are of the order of 10^7 for the $W \to \ell\nu$, and of the order of 10^6 for the $Z \to \ell\ell$ processes. The available data sample is therefore larger by an order of magnitude compared to the corresponding samples used for the CDF and D0 measurements. Given the precisely measured value of the Z-boson mass [32] and the clean leptonic final state, the $Z \to \ell\ell$ processes provide the primary constraints for detector calibration, physics modelling, and validation of the analysis strategy. The sizes of these samples correspond to a statistical uncertainty smaller than 10 MeV in the measurement of the W-boson mass.

Measurements of m_W at the LHC are affected by significant complications related to the strong interaction. In particular, in proton–proton (pp) collisions at $\sqrt{s} = 7$ TeV, approximately 25% of the inclusive W-boson production rate is induced by at least one second-generation quark, s or c, in the initial state. The amount of heavy-quark-initiated production has implications for the W-boson rapidity and transverse-momentum distributions [33]. As a consequence, the measurement of the W-boson mass is sensitive to the strange-quark and charm-quark parton distribution functions (PDFs) of the proton. In contrast, second-generation quarks contribute only to approximately 5% of the overall W-boson production rate at the Tevatron. Other important aspects of the measurement of the W-boson mass are the theoretical description of electroweak corrections, in particular the modelling of photon radiation from the W- and Z-boson decay leptons, and the modelling of the relative fractions of helicity cross sections in the Drell–Yan processes [34].

This paper is structured as follows. Section 2 presents an overview of the measurement strategy. Section 3 describes the ATLAS detector. Section 4 describes the data and simulation samples used for the measurement. Section 5 describes the object reconstruction and the event selection. Section 6 summarises the modelling of vector-boson production and decay, with emphasis on the QCD effects outlined above. Sections 7 and 8 are dedicated to the electron, muon, and recoil calibration procedures. Section 9 presents a set of validation tests of the measurement procedure, performed using the Z-boson event sample. Section 10 describes the analysis of the W-boson sample. Section 11 presents the extraction of m_W. The results are summarised in Sect. 12.

2 Measurement overview

This section provides the definition of the observables used in the analysis, an overview of the measurement strategy for the determination of the mass of the W boson, and a description of the methodology used to estimate the systematic uncertainties.

2.1 Observable definitions

ATLAS uses a right-handed coordinate system with its origin at the nominal interaction point (IP) in the centre of the detector and the z-axis along the beam pipe. The x-axis points from the IP to the centre of the LHC ring, and the y-axis points upward. Cylindrical coordinates (r, ϕ) are used in the transverse plane, ϕ being the azimuth around the z-axis. The pseudorapidity is defined in terms of the polar angle θ as $\eta = -\ln\tan(\theta/2)$.

The kinematic properties of charged leptons from W- and Z-boson decays are characterised by the measured transverse momentum, p_{T}^{ℓ}, pseudorapidity, η_ℓ, and azimuth, ϕ_ℓ. The mass of the lepton, m_ℓ, completes the four-vector. For Z-boson events, the invariant mass, $m_{\ell\ell}$, the rapidity, $y_{\ell\ell}$, and the transverse momentum, $p_{\mathrm{T}}^{\ell\ell}$, are obtained by combining the four-momenta of the decay-lepton pair.

The recoil in the transverse plane, $\vec{u}_{\mathrm{T}}$, is reconstructed from the vector sum of the transverse energy of all clusters reconstructed in the calorimeters (Sect. 3), excluding energy deposits associated with the decay leptons. It is defined as:

$$\vec{u}_{\mathrm{T}} = \sum_i \vec{E}_{\mathrm{T},i},$$

where $\vec{E}_{\mathrm{T},i}$ is the vector of the transverse energy of cluster i. The transverse-energy vector of a cluster has magnitude $E_{\mathrm{T}} = E/\cosh\eta$, with the energy deposit of the cluster E and its pseudorapidity η. The azimuth ϕ of the transverse-energy vector is defined from the coordinates of the cluster in the transverse plane. In W- and Z-boson events, $-\vec{u}_{\mathrm{T}}$ provides an estimate of the boson transverse momentum. The related quantities u_x and u_y are the projections of the recoil onto the axes of the transverse plane in the ATLAS coordinate system. In Z-boson events, $u_\parallel^Z$ and $u_\perp^Z$ represent the projections of the recoil onto the axes parallel and perpendicular to the Z-boson transverse momentum reconstructed from the decay-lepton pair. Whereas $u_\parallel^Z$ can be compared to $-p_{\mathrm{T}}^{\ell\ell}$ and probes the detector response to the recoil in terms of linearity and resolution, the $u_\perp^Z$ distribution satisfies $\langle u_\perp^Z \rangle = 0$ and its width provides an estimate of the recoil resolution. In W-boson events, $u_\parallel^\ell$ and $u_\perp^\ell$ are the projections of the recoil onto the

axes parallel and perpendicular to the reconstructed charged-lepton transverse momentum.

The resolution of the recoil is affected by additional event properties, namely the per-event number of pp interactions per bunch crossing (pile-up) μ, the average number of pp interactions per bunch crossing $\langle\mu\rangle$, the total reconstructed transverse energy, defined as the scalar sum of the transverse energy of all calorimeter clusters, $\Sigma E_{\mathrm{T}} \equiv \sum_i E_{\mathrm{T},i}$, and the quantity $\Sigma E_{\mathrm{T}}^{*} \equiv \Sigma E_{\mathrm{T}} - |\vec{u}_{\mathrm{T}}|$. The latter is less correlated with the recoil than ΣE_{T}, and better represents the event activity related to the pile-up and to the underlying event.

The magnitude and direction of the transverse-momentum vector of the decay neutrino, $\vec{p}_{\mathrm{T}}^{\,\nu}$, are inferred from the vector of the missing transverse momentum, $\vec{p}_{\mathrm{T}}^{\,\mathrm{miss}}$, which corresponds to the momentum imbalance in the transverse plane and is defined as:

$$\vec{p}_{\mathrm{T}}^{\,\mathrm{miss}} = -\left(\vec{p}_{\mathrm{T}}^{\,\ell} + \vec{u}_{\mathrm{T}}\right).$$

The W-boson transverse mass, m_{T}, is derived from $p_{\mathrm{T}}^{\mathrm{miss}}$ and from the transverse momentum of the charged lepton as follows:

$$m_{\mathrm{T}} = \sqrt{2 p_{\mathrm{T}}^{\ell} p_{\mathrm{T}}^{\mathrm{miss}} (1 - \cos\Delta\phi)},$$

where $\Delta\phi$ is the azimuthal opening angle between the charged lepton and the missing transverse momentum.

All vector-boson masses and widths are defined in the running-width scheme. Resonances are expressed by the relativistic Breit–Wigner mass distribution:

$$\frac{\mathrm{d}\sigma}{\mathrm{d}m} \propto \frac{m^2}{(m^2 - m_V^2)^2 + m^4\Gamma_V^2/m_V^2}, \tag{1}$$

where m is the invariant mass of the vector-boson decay products, and m_V and Γ_V, with $V = W, Z$, are the vector-boson masses and widths, respectively. This scheme was introduced in Ref. [35], and is consistent with earlier measurements of the W- and Z-boson resonance parameters [24,32].

2.2 Analysis strategy

The mass of the W boson is determined from fits to the transverse momentum of the charged lepton, p_{T}^{ℓ}, and to the transverse mass of the W boson, m_{T}. For W bosons at rest, the transverse-momentum distributions of the W decay leptons have a Jacobian edge at a value of $m/2$, whereas the distribution of the transverse mass has an endpoint at the value of m [36], where m is the invariant mass of the charged-lepton and neutrino system, which is related to m_W through the Breit–Wigner distribution of Eq. (1).

The expected final-state distributions, referred to as templates, are simulated for several values of m_W and include signal and background contributions. The templates are compared to the observed distribution by means of a χ^2 compatibility test. The χ^2 as a function of m_W is interpolated, and the measured value is determined by analytical minimisation of the χ^2 function. Predictions for different values of m_W are obtained from a single simulated reference sample, by reweighting the W-boson invariant mass distribution according to the Breit–Wigner parameterisation of Eq. (1). The W-boson width is scaled accordingly, following the SM relation $\Gamma_W \propto m_W^3$.

Experimentally, the p_{T}^{ℓ} and $p_{\mathrm{T}}^{\mathrm{miss}}$ distributions are affected by the lepton energy calibration. The latter is also affected by the calibration of the recoil. The p_{T}^{ℓ} and $p_{\mathrm{T}}^{\mathrm{miss}}$ distributions are broadened by the W-boson transverse-momentum distribution, and are sensitive to the W-boson helicity states, which are influenced by the proton PDFs [37]. Compared to p_{T}^{ℓ}, the m_{T} distribution has larger uncertainties due to the recoil, but smaller sensitivity to such physics-modelling effects. Imperfect modelling of these effects can distort the template distributions, and constitutes a significant source of uncertainties for the determination of m_W.

The calibration procedures described in this paper rely mainly on methods and results published earlier by ATLAS [38–40], and based on W and Z samples at $\sqrt{s} = 7$ TeV and $\sqrt{s} = 8$ TeV. The $Z \to \ell\ell$ event samples are used to calibrate the detector response. Lepton momentum corrections are derived exploiting the precisely measured value of the Z-boson mass, m_Z [32], and the recoil response is calibrated using the expected momentum balance with $p_{\mathrm{T}}^{\ell\ell}$. Identification and reconstruction efficiency corrections are determined from W- and Z-boson events using the tag-and-probe method [38,40]. The dependence of these corrections on p_{T}^{ℓ} is important for the measurement of m_W, as it affects the shape of the template distributions.

The detector response corrections and the physics modelling are verified in Z-boson events by performing measurements of the Z-boson mass with the same method used to determine the W-boson mass, and comparing the results to the LEP combined value of m_Z, which is used as input for the lepton calibration. The determination of m_Z from the lepton-pair invariant mass provides a first closure test of the lepton energy calibration. In addition, the extraction of m_Z from the p_{T}^{ℓ} distribution tests the p_{T}^{ℓ}-dependence of the efficiency corrections, and the modelling of the Z-boson transverse-momentum distribution and of the relative fractions of Z-boson helicity states. The $p_{\mathrm{T}}^{\mathrm{miss}}$ and m_{T} variables are defined in Z-boson events by treating one of the reconstructed decay leptons as a neutrino. The extraction of m_Z from the m_{T} distribution provides a test of the recoil calibration. The combination of the extraction of m_Z from the $m_{\ell\ell}$, p_{T}^{ℓ} and m_{T} distributions provides a closure test of the measurement procedure. The precision of this validation procedure is limited by the finite size of the Z-boson sample, which is approximately ten times smaller than the W-boson sample.

Table 1 Summary of categories and kinematic distributions used in the m_W measurement analysis for the electron and muon decay channels

Decay channel	$W \to e\nu$	$W \to \mu\nu$
Kinematic distributions	p_{T}^{ℓ}, m_{T}	p_{T}^{ℓ}, m_{T}
Charge categories	W^+, W^-	W^+, W^-
$\lvert\eta_\ell\rvert$ categories	[0, 0.6], [0.6, 1.2], [1.8, 2.4]	[0, 0.8], [0.8, 1.4], [1.4, 2.0], [2.0, 2.4]

The analysis of the Z-boson sample does not probe differences in the modelling of W- and Z-boson production processes. Whereas W-boson production at the Tevatron is charge symmetric and dominated by interactions with at least one valence quark, the sea-quark PDFs play a larger role at the LHC, and contributions from processes with heavy quarks in the initial state have to be modelled properly. The W^+-boson production rate exceeds that of W^- bosons by about 40%, with a broader rapidity distribution and a softer transverse-momentum distribution. Uncertainties in the modelling of these distributions and in the relative fractions of the W-boson helicity states are constrained using measurements of W- and Z-boson production performed with the ATLAS experiment at $\sqrt{s} = 7$ TeV and $\sqrt{s} = 8$ TeV [41–45].

The final measured value of the W-boson mass is obtained from the combination of various measurements performed in the electron and muon decay channels, and in charge- and $|\eta_\ell|$-dependent categories, as defined in Table 1. The boundaries of the $|\eta_\ell|$ categories are driven mainly by experimental and statistical constraints. The measurements of m_W used in the combination are based on the observed distributions of p_{T}^{ℓ} and m_{T}, which are only partially correlated. Measurements of m_W based on the $p_{\mathrm{T}}^{\mathrm{miss}}$ distributions are performed as consistency tests, but they are not used in the combination due to their significantly lower precision. The consistency of the results in the electron and muon channels provide a further test of the experimental calibrations, whereas the consistency of the results for the different charge and $|\eta_\ell|$ categories tests the W-boson production model.

Further consistency tests are performed by repeating the measurement in three intervals of $\langle\mu\rangle$, in two intervals of u_{T} and $u_{\parallel}^{\ell}$, and by removing the $p_{\mathrm{T}}^{\mathrm{miss}}$ selection requirement, which is applied in the nominal signal selection. The consistency of the values of m_W in these additional categories probes the modelling of the recoil response, and the modelling of the transverse-momentum spectrum of the W boson. Finally, the stability of the result with respect to the charged-lepton azimuth, and upon variations of the fitting ranges is verified.

Systematic uncertainties in the determination of m_W are evaluated using pseudodata samples produced from the nominal simulated event samples by varying the parameters corresponding to each source of uncertainty in turn. The differences between the values of m_W extracted from the pseudodata and nominal samples are used to estimate the uncertainty. When relevant, these variations are applied simultaneously in the W-boson signal samples and in the background contributions. The systematic uncertainties are estimated separately for each source and for fit ranges of $32 < p_{\mathrm{T}}^{\ell} < 45$ GeV and $66 < m_{\mathrm{T}} < 99$ GeV. These fit ranges minimise the total expected measurement uncertainty, and are used for the final result as discussed in Sect. 11.

In Sects. 6, 7, 8, and 10, which discuss the systematic uncertainties of the m_W measurement, the uncertainties are also given for combinations of measurement categories. This provides information showing the reduction of the systematic uncertainty obtained from the measurement categorisation. For these cases, the combined uncertainties are evaluated including only the expected statistical uncertainty in addition to the systematic uncertainty being considered. However, the total measurement uncertainty is estimated by adding all uncertainty contributions in quadrature for each measurement category, and combining the results accounting for correlations across categories.

During the analysis, an unknown offset was added to the value of m_W used to produce the templates. The offset was randomly selected from a uniform distribution in the range $[-100, 100]$ MeV, and the same value was used for the W^+ and W^- templates. The offset was removed after the m_W measurements performed in all categories were found to be compatible and the analysis procedure was finalised.

3 The ATLAS detector

The ATLAS experiment [46] is a multipurpose particle detector with a forward-backward symmetric cylindrical geometry. It consists of an inner tracking detector surrounded by a thin superconducting solenoid, electromagnetic and hadronic calorimeters, and a muon spectrometer incorporating three large superconducting toroid magnets.

The inner-detector system (ID) is immersed in a 2 T axial magnetic field and provides charged-particle tracking in the range $|\eta| < 2.5$. At small radii, a high-granularity silicon pixel detector covers the vertex region and typically provides three measurements per track. It is followed by the silicon microstrip tracker, which usually provides eight measurement points per track. These silicon detectors are complemented by a gas-filled straw-tube transition radiation tracker, which enables radially extended track reconstruction up to

$|\eta| = 2.0$. The transition radiation tracker also provides electron identification information based on the fraction of hits (typically 35 in total) above a higher energy-deposit threshold corresponding to transition radiation.

The calorimeter system covers the pseudorapidity range $|\eta| < 4.9$. Within the region $|\eta| < 3.2$, electromagnetic (EM) calorimetry is provided by high-granularity lead/liquid-argon (LAr) calorimeters, with an additional thin LAr presampler covering $|\eta| < 1.8$ to correct for upstream energy-loss fluctuations. The EM calorimeter is divided into a barrel section covering $|\eta| < 1.475$ and two endcap sections covering $1.375 < |\eta| < 3.2$. For $|\eta| < 2.5$ it is divided into three layers in depth, which are finely segmented in η and ϕ. Hadronic calorimetry is provided by a steel/scintillator-tile calorimeter, segmented into three barrel structures within $|\eta| < 1.7$ and two copper/LAr hadronic endcap calorimeters covering $1.5 < |\eta| < 3.2$. The solid-angle coverage is completed with forward copper/LAr and tungsten/LAr calorimeter modules in $3.1 < |\eta| < 4.9$, optimised for electromagnetic and hadronic measurements, respectively.

The muon spectrometer (MS) comprises separate trigger and high-precision tracking chambers measuring the deflection of muons in a magnetic field generated by superconducting air-core toroids. The precision chamber system covers the region $|\eta| < 2.7$ with three layers of monitored drift tubes, complemented by cathode strip chambers in the forward region. The muon trigger system covers the range $|\eta| < 2.4$ with resistive plate chambers in the barrel, and thin gap chambers in the endcap regions.

A three-level trigger system is used to select events for offline analysis [47]. The level-1 trigger is implemented in hardware and uses a subset of detector information to reduce the event rate to a design value of at most 75 kHz. This is followed by two software-based trigger levels which together reduce the event rate to about 300 Hz.

4 Data samples and event simulation

The data sample used in this analysis consists of W- and Z-boson candidate events, collected in 2011 with the ATLAS detector in proton–proton collisions at the LHC, at a centre-of-mass energy of $\sqrt{s} = 7$ TeV. The sample for the electron channel, with all relevant detector systems operational, corresponds to approximately 4.6 fb^{-1} of integrated luminosity. A smaller integrated luminosity of approximately 4.1 fb^{-1} is used in the muon channel, as part of the data was discarded due to a timing problem in the resistive plate chambers, which affected the muon trigger efficiency. The relative uncertainty of the integrated luminosity is 1.8% [48]. This data set provides approximately 1.4×10^7 reconstructed W-boson events and 1.8×10^6 Z-boson events, after all selection criteria have been applied.

The POWHEG MC generator [49–51] (v1/r1556) is used for the simulation of the hard-scattering processes of W- and Z-boson production and decay in the electron, muon, and tau channels, and is interfaced to PYTHIA 8 (v8.170) for the modelling of the parton shower, hadronisation, and underlying event [52,53], with parameters set according to the AZNLO tune [44]. The CT10 PDF set [54] is used for the hard-scattering processes, whereas the CTEQ6L1 PDF set [55] is used for the parton shower. In the Z-boson samples, the effect of virtual photon production (γ^*) and Z/γ^* interference is included. The effect of QED final-state radiation (FSR) is simulated with PHOTOS (v2.154) [56]. Tau lepton decays are handled by PYTHIA 8, taking into account polarisation effects. An alternative set of samples for W- and Z-boson production is generated with POWHEG interfaced to HERWIG (v6.520) for the modelling of the parton shower [57], and to JIMMY (v4.31) for the underlying event [58]. The W- and Z-boson masses are set to $m_W = 80.399$ GeV and $m_Z = 91.1875$ GeV, respectively. During the analysis, the value of the W-boson mass in the $W \to \ell\nu$ and $W \to \tau\nu$ samples was blinded using the reweighting procedure described in Sect. 2.

Top-quark pair production and the single-top-quark processes are modelled using the MC@NLO MC generator (v4.01) [59–61], interfaced to HERWIG and JIMMY. Gauge-boson pair production (WW, WZ, ZZ) is simulated with HERWIG (v6.520). In all the samples, the CT10 PDF set is used. Samples of heavy-flavour multijet events ($pp \to b\bar{b} + X$ and $pp \to c\bar{c} + X$) are simulated with PYTHIA 8 to validate the data-driven methods used to estimate backgrounds with non-prompt leptons in the final state.

Whereas the extraction of m_W is based on the shape of distributions, and is not sensitive to the overall normalisation of the predicted distributions, it is affected by theoretical uncertainties in the relative fractions of background and signal. The W- and Z-boson event yields are normalised according to their measured cross sections, and uncertainties of 1.8% and 2.3% are assigned to the W^+/Z and W^-/Z production cross-section ratios, respectively [41]. The $t\bar{t}$ sample is normalised according to its measured cross section [62] with an uncertainty of 3.9%, whereas the cross-section predictions for the single-top production processes of Refs. [63–65] are used for the normalisation of the corresponding sample, with an uncertainty of 7%. The samples of events with massive gauge-boson pair production are normalised to the NLO predictions calculated with MCFM [66], with an uncertainty of 10% to cover the differences to the NNLO predictions [67].

The response of the ATLAS detector is simulated using a program [68] based on GEANT 4 [69]. The ID and the MS were simulated assuming an ideal detector geometry; alignment corrections are applied to the data during event reconstruction. The description of the detector material incorporates the results of extensive studies of the electron and photon calibration [39]. The simulated hard-scattering process

is overlaid with additional proton–proton interactions, simulated with PYTHIA 8 (v8.165) using the A2 tune [70]. The distribution of the average number of interactions per bunch crossing $\langle\mu\rangle$ spans the range 2.5–16.0, with a mean value of approximately 9.0.

Simulation inaccuracies affecting the distributions of the signal, the response of the detector, and the underlying-event modelling, are corrected as described in the following sections. Physics-modelling corrections, such as those affecting the W-boson transverse-momentum distribution and the angular decay coefficients, are discussed in Sect. 6. Calibration and detector response corrections are presented in Sects. 7 and 8.

5 Particle reconstruction and event selection

This section describes the reconstruction and identification of electrons and muons, the reconstruction of the recoil, and the requirements used to select W- and Z-boson candidate events. The recoil provides an event-by-event estimate of the W-boson transverse momentum. The reconstructed kinematic properties of the leptons and of the recoil are used to infer the transverse momentum of the neutrino and the transverse-mass kinematic variables.

5.1 Reconstruction of electrons, muons and the recoil

Electron candidates are reconstructed from clusters of energy deposited in the electromagnetic calorimeter and associated with at least one track in the ID [38,39]. Quality requirements are applied to the associated tracks in order to reject poorly reconstructed charged-particle trajectories. The energy of the electron is reconstructed from the energy collected in calorimeter cells within an area of size $\Delta\eta \times \Delta\phi = 0.075 \times 0.175$ in the barrel, and 0.125×0.125 in the endcaps. A multivariate regression algorithm, developed and optimised on simulated events, is used to calibrate the energy reconstruction. The reconstructed electron energy is corrected to account for the energy deposited in front of the calorimeter and outside the cluster, as well as for variations of the energy response as a function of the impact point of the electron in the calorimeter. The energy calibration algorithm takes as inputs the energy collected by each calorimeter layer, including the presampler, the pseudorapidity of the cluster, and the local position of the shower within the cell of the second layer, which corresponds to the cluster centroid. The kinematic properties of the reconstructed electron are inferred from the energy measured in the EM calorimeter, and from the pseudorapidity and azimuth of the associated track. Electron candidates are required to have $p_{\mathrm{T}} > 15$ GeV and $|\eta| < 2.4$ and to fulfil a set of tight identification requirements [38]. The pseudorapidity range $1.2 < |\eta| < 1.82$ is excluded from the measurement, as the amount of passive material in front of the calorimeter and its uncertainty are largest in this region [39], preventing a sufficiently accurate description of non-Gaussian tails in the electron energy response. Additional isolation requirements on the nearby activity in the ID and calorimeter are applied to improve the background rejection. These isolation requirements are implemented by requiring the scalar sum of the p_{T} of tracks in a cone of size $\Delta R \equiv \sqrt{(\Delta\eta)^2 + (\Delta\phi)^2} < 0.4$ around the electron, $p_{\mathrm{T}}^{e,\mathrm{cone}}$, and the transverse energy deposited in the calorimeter within a cone of size $\Delta R < 0.2$ around the electron, $E_{\mathrm{T}}^{\mathrm{cone}}$, to be small. The contribution from the electron candidate itself is excluded. The specific criteria are optimised as a function of electron η and p_{T} to have a combined efficiency of about 95% in the simulation for isolated electrons from the decay of a W or Z boson.

The muon reconstruction is performed independently in the ID and in the MS, and a combined muon candidate is formed from the combination of a MS track with an ID track, based on the statistical combination of the track parameters [40]. The kinematic properties of the reconstructed muon are defined using the ID track parameters alone, which allows a simpler calibration procedure. The loss of resolution is small (10–15%) in the transverse-momentum range relevant for the measurement of the W-boson mass. The ID tracks associated with the muons must satisfy quality requirements on the number of hits recorded by each subdetector [40]. In order to reject muons from cosmic rays, the longitudinal coordinate of the point of closest approach of the track to the beamline is required to be within 10 mm of the collision vertex. Muon candidates are required to have $p_{\mathrm{T}} > 20$ GeV and $|\eta| < 2.4$. Similarly to the electrons, the rejection of multijet background is increased by applying an isolation requirement : the scalar sum of the p_{T} of tracks in a cone of size $\Delta R < 0.2$ around the muon candidate, $p_{\mathrm{T}}^{\mu,\mathrm{cone}}$, is required to be less than 10% of the muon p_{T}.

The recoil, $\vec{u}_{\mathrm{T}}$, is reconstructed from the vector sum of the transverse energy of all clusters measured in the calorimeters, as defined in Sect. 2.1. The ATLAS calorimeters measure energy depositions in the range $|\eta| < 4.9$ with a topological clustering algorithm [71], which starts from cells with an energy of at least four times the expected noise from electronics and pile-up. The momentum vector of each cluster is determined by the magnitude and coordinates of the energy deposition. Cluster energies are initially measured assuming that the energy deposition occurs only through electromagnetic interactions, and are then corrected for the different calorimeter responses to hadrons and electromagnetic particles, for losses due to dead material, and for energy which is not captured by the clustering process. The definition of $\vec{u}_{\mathrm{T}}$ and the inferred quantities $p_{\mathrm{T}}^{\mathrm{miss}}$ and m_{T} do not involve the explicit reconstruction of particle jets, to avoid possible threshold effects.

Clusters located a distance $\Delta R < 0.2$ from the reconstructed electron or muon candidates are not used for the reconstruction of $\vec{u}_{\mathrm{T}}$. This ensures that energy deposits originating from the lepton itself or from accompanying photons (from FSR or Bremsstrahlung) do not contribute to the recoil measurement. The energy of any soft particles removed along with the lepton is compensated for using the total transverse energy measured in a cone of the same size $\Delta R = 0.2$, placed at the same absolute pseudorapidity as the lepton with randomly chosen sign, and at different ϕ. The total transverse momentum measured in this cone is rotated to the position of the lepton and added to $\vec{u}_{\mathrm{T}}$.

5.2 Event selection

The W-boson sample is collected during data-taking with triggers requiring at least one muon candidate with transverse momentum larger than 18 GeV or at least one electron candidate with transverse momentum larger than 20 GeV. The transverse-momentum requirement for the electron candidate was raised to 22 GeV in later data-taking periods to cope with the increased instantaneous luminosity delivered by the LHC. Selected events are required to have a reconstructed primary vertex with at least three associated tracks.

W-boson candidate events are selected by requiring exactly one reconstructed electron or muon with $p_{\mathrm{T}}^{\ell} > 30$ GeV. The leptons are required to match the corresponding trigger object. In addition, the reconstructed recoil is required to be $u_{\mathrm{T}} < 30$ GeV, the missing transverse momentum $p_{\mathrm{T}}^{\mathrm{miss}} > 30$ GeV and the transverse mass $m_{\mathrm{T}} > 60$ GeV. These selection requirements are optimised to reduce the multijet background contribution, and to minimise model uncertainties from W bosons produced at high transverse momentum. A total of 5.89×10^6 W-boson candidate events are selected in the $W \to e\nu$ channel, and 7.84×10^6 events in the $W \to \mu\nu$ channel.

As mentioned in Sect. 2, Z-boson events are extensively used to calibrate the response of the detector to electrons and muons, and to derive recoil corrections. In addition, Z-boson events are used to test several aspects of the modelling of vector-boson production. Z-boson candidate events are collected with the same trigger selection used for the W-boson sample. The analysis selection requires exactly two reconstructed leptons with $p_{\mathrm{T}}^{\ell} > 25$ GeV, having the same flavour and opposite charges. The events are required to have an invariant mass of the dilepton system in the range $80 < m_{\ell\ell} < 100$ GeV. In both channels, selected leptons are required to be isolated in the same way as in the W-boson event selection. In total, 0.58×10^6 and 1.23×10^6 Z-boson candidate events are selected in the electron and muon decay channels, respectively.

6 Vector-boson production and decay

Samples of inclusive vector-boson production are produced using the POWHEG MC generator interfaced to PYTHIA 8, henceforth referred to as POWHEG+PYTHIA 8. The W- and Z-boson samples are reweighted to include the effects of higher-order QCD and electroweak (EW) corrections, as well as the results of fits to measured distributions which improve the agreement of the simulated lepton kinematic distributions with the data. The effect of virtual photon production and Z/γ^* interference is included in both the predictions and the POWHEG+PYTHIA 8 simulated Z-boson samples. The reweighting procedure used to include the corrections in the simulated event samples is detailed in Sect. 6.4.

The correction procedure is based on the factorisation of the fully differential leptonic Drell–Yan cross section [31] into four terms:

$$\frac{\mathrm{d}\sigma}{\mathrm{d}p_1\,\mathrm{d}p_2} = \left[\frac{\mathrm{d}\sigma(m)}{\mathrm{d}m}\right]\left[\frac{\mathrm{d}\sigma(y)}{\mathrm{d}y}\right]\left[\frac{\mathrm{d}\sigma(p_{\mathrm{T}},y)}{\mathrm{d}p_{\mathrm{T}}\,\mathrm{d}y}\left(\frac{\mathrm{d}\sigma(y)}{\mathrm{d}y}\right)^{-1}\right] \times \left[(1+\cos^2\theta)+\sum_{i=0}^{7} A_i(p_{\mathrm{T}},y)\,P_i(\cos\theta,\phi)\right], \tag{2}$$

where p_1 and p_2 are the lepton and anti-lepton four-momenta; m, p_{T}, and y are the invariant mass, transverse momentum, and rapidity of the dilepton system; θ and ϕ are the polar angle and azimuth of the lepton[1] in any given rest frame of the dilepton system; A_i are numerical coefficients, and P_i are spherical harmonics of order zero, one and two.

The differential cross section as a function of the invariant mass, $\mathrm{d}\sigma(m)/\mathrm{d}m$, is modelled with a Breit–Wigner parameterisation according to Eq. (1). In the case of the Z-boson samples, the photon propagator is included using the running electromagnetic coupling constant; further electroweak corrections are discussed in Sect. 6.1. The differential cross section as a function of boson rapidity, $\mathrm{d}\sigma(y)/\mathrm{d}y$, and the coefficients A_i are modelled with perturbative QCD fixed-order predictions, as described in Sect. 6.2. The transverse-momentum spectrum at a given rapidity, $\mathrm{d}\sigma(p_{\mathrm{T}},y)/(\mathrm{d}p_{\mathrm{T}}\,\mathrm{d}y)\cdot(\mathrm{d}\sigma(y)/\mathrm{d}y)^{-1}$, is modelled with predictions based on the PYTHIA 8 MC generator, as discussed in Sect. 6.3. An exhaustive review of available predictions for W- and Z-boson production at the LHC is given in Ref. [72].

Measurements of W- and Z-boson production are used to validate and constrain the modelling of the fully differential leptonic Drell–Yan cross section. The PDF central values and uncertainties, as well as the modelling of the differential cross section as a function of boson rapidity, are validated

[1] Here, lepton refers to the negatively charged lepton from a W^- or Z boson, and the neutrino from a W^+ boson.

by comparing to the 7 TeV W- and Z-boson rapidity measurements [41], based on the same data sample. The QCD parameters of the parton shower model were determined by fits to the transverse-momentum distribution of the Z boson measured at 7 TeV [44]. The modelling of the A_i coefficients is validated by comparing the theoretical predictions to the 8 TeV measurement of the angular coefficients in Z-boson decays [42].

6.1 Electroweak corrections and uncertainties

The dominant source of electroweak corrections to W- and Z-boson production originates from QED final-state radiation, and is simulated with PHOTOS. The effect of QED initial-state radiation (ISR) is also included through the PYTHIA 8 parton shower. The uncertainty in the modelling of QED FSR is evaluated by comparing distributions obtained using the default leading-order photon emission matrix elements with predictions obtained using NLO matrix elements, as well as by comparing PHOTOS with an alternative implementation based on the Yennie–Frautschi–Suura formalism [73], which is available in WINHAC [74]. The differences are small in both cases, and the associated uncertainty is considered negligible.

Other sources of electroweak corrections are not included in the simulated event samples, and their full effects are considered as systematic uncertainties. They include the interference between ISR and FSR QED corrections (IFI), pure weak corrections due to virtual-loop and box diagrams, and final-state emission of lepton pairs. Complete $O(\alpha)$ electroweak corrections to the $pp \to W + X$, $W \to \ell\nu$ process were initially calculated in Refs. [75,76]. Combined QCD and EW corrections are however necessary to evaluate the effect of the latter in presence of a realistic p_{T}^{W} distribution. Approximate $O(\alpha_{\mathrm{s}}\alpha)$ corrections including parton shower effects are available from WINHAC, SANC [77] and in the POWHEG framework [78–80]. A complete, fixed-order calculation of $O(\alpha_{\mathrm{s}}\alpha)$ corrections in the resonance region appeared in Ref. [81].

In the present work the effect of the NLO EW corrections are estimated using WINHAC, which employs the PYTHIA 6 MC generator for the simulation of QCD and QED ISR. The corresponding uncertainties are evaluated comparing the final state distributions obtained including QED FSR only with predictions using the complete NLO EW corrections in the $\alpha(0)$ and G_μ renormalisation schemes [82]. The latter predicts the larger correction and is used to assign the systematic uncertainty.

Final-state lepton pair production, through $\gamma^* \to \ell\ell$ radiation, is formally a higher-order correction but constitutes an significant additional source of energy loss for the W-boson decay products. This process is not included in the event simulation, and the impact on the determination of m_W is evaluated using PHOTOS and SANC.

Table 2 summarises the effect of the uncertainties associated with the electroweak corrections on the m_W measurements. All comparisons described above were performed at particle level. The impact is larger for the p_{T}^{ℓ} distribution than for the m_{T} distribution, and similar between the electron and muon decay channels. A detailed evaluation of these uncertainties was performed in Ref. [83] using POWHEG [78], and the results are in fair agreement with Table 2. The study of Ref. [83] also compares, at fixed order, the effect of the approximate $O(\alpha_{\mathrm{s}}\alpha)$ corrections with the full calculation of Ref. [81], and good agreement is found. The same sources of uncertainty affect the lepton momentum calibration through their impact on the $m_{\ell\ell}$ distribution in Z-boson events, as discussed in Sect. 7.

6.2 Rapidity distribution and angular coefficients

At leading order, W and Z bosons are produced with zero transverse momentum, and the angular distribution of the decay leptons depends solely on the polar angle of the lepton in the boson rest frame. Higher-order corrections give rise to sizeable boson transverse momentum, and to azimuthal asymmetries in the angular distribution of the decay leptons. The angular distribution of the W- and Z-boson decay leptons is determined by the relative fractions of helicity cross sections for the vector-boson production. The fully differential leptonic Drell–Yan cross section can be decomposed as a weighted sum of nine harmonic polynomials, with weights given by the helicity cross sections. The harmonic polyno-

Table 2 Impact on the m_W measurement of systematic uncertainties from higher-order electroweak corrections, for the p_{T}^{ℓ} and m_{T} distributions in the electron and muon decay channels

Decay channel	$W \to e\nu$		$W \to \mu\nu$	
Kinematic distribution	p_{T}^{ℓ}	m_{T}	p_{T}^{ℓ}	m_{T}
δm_W [MeV]				
FSR (real)	< 0.1	< 0.1	< 0.1	< 0.1
Pure weak and IFI corrections	3.3	2.5	3.5	2.5
FSR (pair production)	3.6	0.8	4.4	0.8
Total	4.9	2.6	5.6	2.6

mials depend on the polar angle, θ, and the azimuth, ϕ, of the lepton in a given rest frame of the boson. The helicity cross sections depend, in their most general expression, on the transverse momentum, p_{T}, rapidity, y, and invariant mass, m, of the boson. It is customary to factorise the unpolarised, or angular-integrated, cross section, $\mathrm{d}\sigma/(\mathrm{d}p_{\mathrm{T}}^2\,\mathrm{d}y\,\mathrm{d}m)$, and express the decomposition in terms of dimensionless angular coefficients, A_i, which represent the ratios of the helicity cross sections with respect to the unpolarised cross section [34], leading to the following expression for the fully differential Drell–Yan cross section:

$$\begin{aligned}\frac{\mathrm{d}\sigma}{\mathrm{d}p_{\mathrm{T}}^2\,\mathrm{d}y\,\mathrm{d}m\,\mathrm{d}\cos\theta\,\mathrm{d}\phi} = \frac{3}{16\pi}\frac{\mathrm{d}\sigma}{\mathrm{d}p_{\mathrm{T}}^2\,\mathrm{d}y\,\mathrm{d}m} \\ \times\Big[(1+\cos^2\theta)+A_0\,\frac{1}{2}(1-3\cos^2\theta) \\ +A_1\,\sin 2\theta\cos\phi + A_2\,\frac{1}{2}\sin^2\theta\cos 2\phi \\ +A_3\,\sin\theta\cos\phi + A_4\,\cos\theta \\ +A_5\,\sin^2\theta\sin 2\phi + A_6\,\sin 2\theta\sin\phi \\ +A_7\,\sin\theta\sin\phi\Big]. \end{aligned} \tag{3}$$

The angular coefficients depend in general on p_{T}, y and m. The A_5–A_7 coefficients are non-zero only at order $O(\alpha_{\mathrm{s}}^2)$ and above. They are small in the p_{T} region relevant for the present analysis, and are not considered further. The angles θ and ϕ are defined in the Collins–Soper (CS) frame [84].

The differential cross section as a function of boson rapidity, $\mathrm{d}\sigma(y)/\mathrm{d}y$, and the angular coefficients, A_i, are modelled with fixed-order perturbative QCD predictions, at $O(\alpha_{\mathrm{s}}^2)$ in the perturbative expansion of the strong coupling constant and using the CT10nnlo PDF set [85]. The dependence of the angular coefficients on m is neglected; the effect of this approximation on the measurement of m_W is discussed in Sect. 6.4. For the calculation of the predictions, an optimised version of DYNNLO [86] is used, which explicitly decomposes the calculation of the cross section into the different pieces of the q_{T}-subtraction formalism, and allows the computation of statistically correlated PDF variations. In this optimised version of DYNNLO, the Cuba library [87] is used for the numerical integration.

The values of the angular coefficients predicted by the POWHEG+PYTHIA 8 samples differ significantly from the corresponding NNLO predictions. In particular, large differences are observed in the predictions of A_0 at low values of $p_{\mathrm{T}}^{W,Z}$. Other coefficients, such as A_1 and A_2, are affected by significant NNLO corrections at high $p_{\mathrm{T}}^{W,Z}$. In Z-boson production, A_3 and A_4 are sensitive to the vector couplings between the Z boson and the fermions, and are predicted assuming the measured value of the effective weak mixing angle $\sin^2\theta_{\mathrm{eff}}^{\ell}$ [32].

6.3 Transverse-momentum distribution

Predictions of the vector-boson transverse-momentum spectrum cannot rely solely on fixed-order perturbative QCD. Most W-boson events used for the analysis have a low transverse-momentum value, in the kinematic region $p_{\mathrm{T}}^W < 30$ GeV, where large logarithmic terms of the type $\log(m_W/p_{\mathrm{T}}^W)$ need to be resummed, and non-perturbative effects must be included, either with parton showers or with predictions based on analytic resummation [88–92]. The modelling of the transverse-momentum spectrum of vector bosons at a given rapidity, expressed by the term $\mathrm{d}\sigma(p_{\mathrm{T}},y)/(\mathrm{d}p_{\mathrm{T}}\,\mathrm{d}y)\cdot(\mathrm{d}\sigma(y)/\mathrm{d}y)^{-1}$ in Eq. (2), is based on the PYTHIA 8 parton shower MC generator. The predictions of vector-boson production in the PYTHIA 8 MC generator employ leading-order matrix elements for the $q\bar{q}' \to W, Z$ processes and include a reweighting of the first parton shower emission to the leading-order V+jet cross section [93]. The resulting prediction of the boson p_{T} spectrum is comparable in accuracy to those of an NLO plus parton shower generator setup such as POWHEG+PYTHIA 8, and of resummed predictions at next-to-leading logarithmic order [94].

The values of the QCD parameters used in PYTHIA 8 were determined from fits to the Z-boson transverse momentum distribution measured with the ATLAS detector at a centre-of-mass energy of $\sqrt{s} = 7$ TeV [44]. Three QCD parameters were considered in the fit: the intrinsic transverse momentum of the incoming partons, the value of $\alpha_{\mathrm{s}}(m_Z)$ used for the QCD ISR, and the value of the ISR infrared cut-off. The resulting values of the PYTHIA 8 parameters constitute the AZ tune. The PYTHIA 8 AZ prediction was found to provide a satisfactory description of the p_{T}^Z distribution as a function of rapidity, contrarily to POWHEG+PYTHIA 8 AZNLO; hence the former is chosen to predict the p_{T}^W distribution. The good consistency of the m_W measurement results in $|\eta_\ell|$ categories, presented in Sect. 11, is also a consequence of this choice.

To illustrate the results of the parameters optimisation, the PYTHIA 8 AZ and 4C [95] predictions of the p_{T}^Z distribution are compared in Fig. 1a to the measurement used to determine the AZ tune. Kinematic requirements on the decay leptons are applied according to the experimental acceptance. For further validation, the predicted differential cross-section ratio,

$$R_{W/Z}(p_{\mathrm{T}}) = \left(\frac{1}{\sigma_W}\cdot\frac{\mathrm{d}\sigma_W(p_{\mathrm{T}})}{\mathrm{d}p_{\mathrm{T}}}\right)\left(\frac{1}{\sigma_Z}\cdot\frac{\mathrm{d}\sigma_Z(p_{\mathrm{T}})}{\mathrm{d}p_{\mathrm{T}}}\right)^{-1},$$

is compared to the corresponding ratio of ATLAS measurements of vector-boson transverse momentum [44,45]. The comparison is shown in Fig. 1b, where kinematic requirements on the decay leptons are applied according to the experimental acceptance. The measured Z-boson p_{T} distribution is

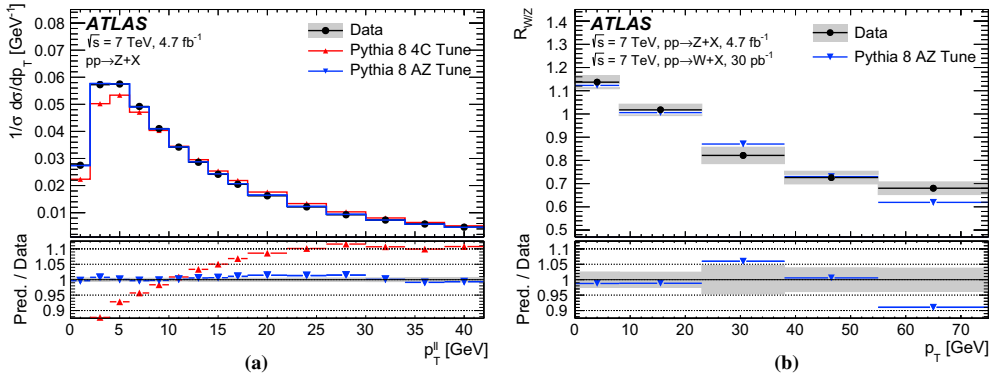

Fig. 1 **a** Normalised differential cross section as a function of $p_{\mathrm{T}}^{\ell\ell}$ in Z-boson events [44] and **b** differential cross-section ratio $R_{W/Z}(p_{\mathrm{T}})$ as a function of the boson p_{T} [44,45]. The measured cross sections are compared to the predictions of the PYTHIA 8 AZ tune and, in **a**, of the PYTHIA 8 4C tune. The shaded bands show the total experimental uncertainties

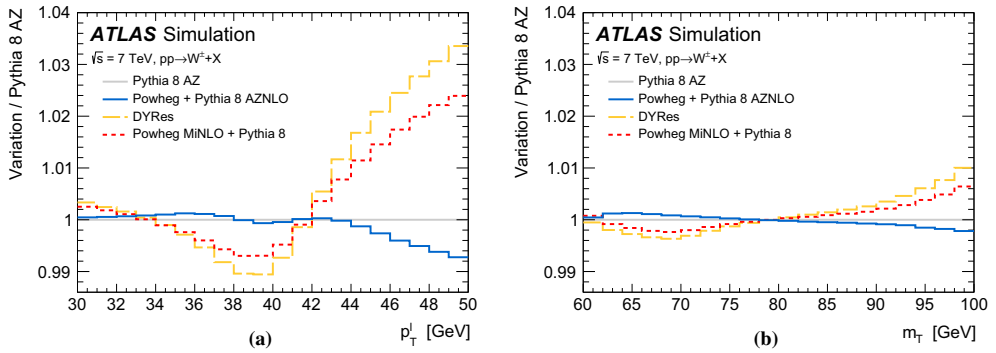

Fig. 2 Ratios of the reconstruction-level **a** p_{T}^{ℓ} and **b** m_{T} normalised distributions obtained using POWHEG+PYTHIA 8 AZNLO, DYRes and POWHEG MiNLO+PYTHIA 8 to the baseline normalised distributions obtained using PYTHIA 8 AZ

rebinned to match the coarser bins of the W-boson p_{T} distribution, which was measured using only 30 pb^{-1} of data. The theoretical prediction is in agreement with the experimental measurements for the region with $p_{\mathrm{T}} < 30$ GeV, which is relevant for the measurement of the W-boson mass.

The predictions of RESBOS [89,90], DYRes [91] and POWHEG MiNLO+PYTHIA 8 [96,97] are also considered. All predict a harder p_{T}^{W} distribution for a given p_{T}^{Z} distribution, compared to PYTHIA 8 AZ. Assuming the latter can be adjusted to match the measurement of Ref. [44], the corresponding p_{T}^{W} distribution induces a discrepancy with the detector-level u_{T} and $u_{\parallel}^{\ell}$ distributions observed in the W-boson data, as discussed in Sect. 11.2. This behaviour is observed using default values for the non-perturbative parameters of these programs, but is not expected to change significantly under variations of these parameters. These predictions are therefore not used in the determination of m_W or its uncertainty.

Figure 2 compares the reconstruction-level p_{T}^{ℓ} and m_{T} distributions obtained with POWHEG+PYTHIA 8 AZNLO, DYRes and POWHEG MiNLO+PYTHIA 8 to those of PYTHIA 8 AZ.[2] The effect of varying the p_{T}^{W} distribution is largest at high p_{T}^{ℓ}, which explains why the uncertainty due to the p_{T}^{W} modelling is reduced when limiting the p_{T}^{ℓ} fitting range as described in Sect. 11.3.

[2] Reconstruction-level distributions are obtained from the POWHEG+PYTHIA 8 signal sample by reweighting the particle-level p_{T}^{W} distribution according to the product of the p_{T}^{Z} distribution in PYTHIA 8 AZ, and of $R_{W/Z}(p_{\mathrm{T}})$ as predicted by POWHEG+PYTHIA 8 AZNLO, DYRes and POWHEG MiNLO+PYTHIA 8.

6.4 Reweighting procedure

The W and Z production and decay model described above is applied to the POWHEG+PYTHIA 8 samples through an event-by-event reweighting. Equation (3) expresses the factorisation of the cross section into the three-dimensional boson production phase space, defined by the variables m, p_{T}, and y, and the two-dimensional boson decay phase space, defined by the variables θ and ϕ. Accordingly, a prediction of the kinematic distributions of vector bosons and their decay products can be transformed into another prediction by applying separate reweighting of the three-dimensional boson production phase-space distributions, followed by a reweighting of the angular decay distributions.

The reweighting is performed in several steps. First, the inclusive rapidity distribution is reweighted according to the NNLO QCD predictions evaluated with DYNNLO. Then, at a given rapidity, the vector-boson transverse-momentum shape is reweighted to the PYTHIA 8 prediction with the AZ tune. This procedure provides the transverse-momentum distribution of vector bosons predicted by PYTHIA 8, preserving the rapidity distribution at NNLO. Finally, at given rapidity and transverse momentum, the angular variables are reweighted according to:

$$w(\cos\theta, \phi, p_{\mathrm{T}}, y) = \frac{1 + \cos^2\theta + \sum_i A_i'(p_{\mathrm{T}}, y)\, P_i(\cos\theta, \phi)}{1 + \cos^2\theta + \sum_i A_i(p_{\mathrm{T}}, y)\, P_i(\cos\theta, \phi)},$$

where A_i' are the angular coefficients evaluated at $O(\alpha_{\mathrm{s}}^2)$, and A_i are the angular coefficients of the POWHEG+PYTHIA 8 samples. This reweighting procedure neglects the small dependence of the two-dimensional (p_{T},y) distribution and of the angular coefficients on the final state invariant mass. The procedure is used to include the corrections described in Sects. 6.2 and 6.3, as well as to estimate the impact of the QCD modelling uncertainties described in Sect. 6.5.

The validity of the reweighting procedure is tested at particle level by generating independent W-boson samples using the CT10nnlo and NNPDF3.0 [98] NNLO PDF sets, and the same value of m_W. The relevant kinematic distributions are calculated for both samples and used to reweight the CT10nnlo sample to the NNPDF3.0 one. The procedure described in Sect. 2.2 is then used to determine the value of m_W by fitting the NNPDF3.0 sample using templates from the reweighted CT10nnlo sample. The fitted value agrees with the input value within 1.5 ± 2.0 MeV. The statistical precision of this test is used to assign the associated systematic uncertainty.

The resulting model is tested by comparing the predicted Z-boson differential cross section as a function of rapidity, the W-boson differential cross section as a function of lepton pseudorapidity, and the angular coefficients in Z-boson events, to the corresponding ATLAS measurements [41,42]. The comparison with the measured W and Z cross sections is shown in Fig. 3. Satisfactory agreement between the measurements and the theoretical predictions is observed. A χ^2 compatibility test is performed for the three distributions simultaneously, including the correlations between the uncertainties. The compatibility test yields a χ^2/dof value of 45/34. Other NNLO PDF sets such as NNPDF3.0, CT14 [99], MMHT2014 [100], and ABM12 [101] are in worse agreement with these distributions. Based on the quantitative comparisons performed in

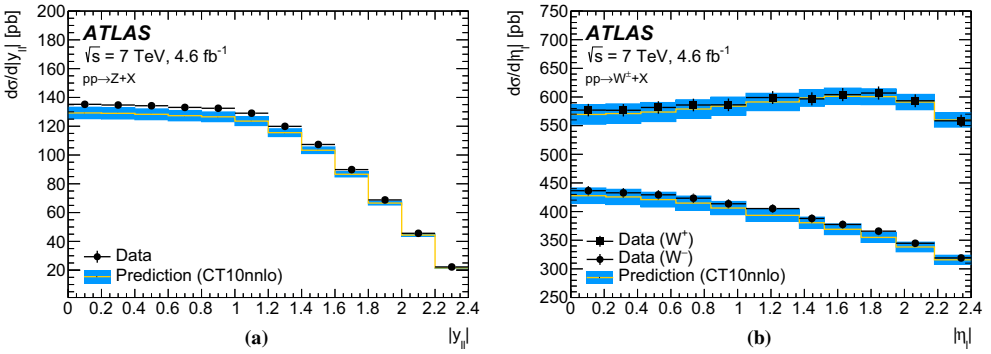

Fig. 3 **a** Differential Z-boson cross section as a function of boson rapidity, and **b** differential W^+ and W^- cross sections as a function of charged decay-lepton pseudorapidity at $\sqrt{s} = 7$ TeV [41]. The measured cross sections are compared to the POWHEG+PYTHIA 8 predictions, corrected to NNLO using DYNNLO with the CT10nnlo PDF set. The error bars show the total experimental uncertainties, including luminosity uncertainty, and the bands show the PDF uncertainties of the predictions

Ref. [41], only CT10nnlo, CT14 and MMHT2014 are considered further. The better agreement obtained with CT10nnlo can be ascribed to the weaker suppression of the strange quark density compared to the u- and d-quark sea densities in this PDF set.

The predictions of the angular coefficients in Z-boson events are compared to the ATLAS measurement at $\sqrt{s} = 8$ TeV [42]. Good agreement between the measurements and DYNNLO is observed for the relevant coefficients, except for A_2, where the measurement is significantly below the prediction. As an example, Fig. 4 shows the comparison for A_0 and A_2 as a function of p_{T}^{Z}. For A_2, an additional source of uncertainty in the theoretical prediction is considered to account for the observed disagreement with data, as discussed in Sect. 6.5.3.

6.5 Uncertainties in the QCD modelling

Several sources of uncertainty related to the perturbative and non-perturbative modelling of the strong interaction affect the dynamics of the vector-boson production and decay [33,102–104]. Their impact on the measurement of m_W is assessed through variations of the model parameters of the predictions for the differential cross sections as functions of the boson rapidity, transverse-momentum spectrum at a given rapidity, and angular coefficients, which correspond to the second, third, and fourth terms of the decomposition of Eq. (2), respectively. The parameter variations used to estimate the uncertainties are propagated to the simulated event samples by means of the reweighting procedure described in Sect. 6.4. Table 3 shows an overview of the uncertainties due to the QCD modelling which are discussed below.

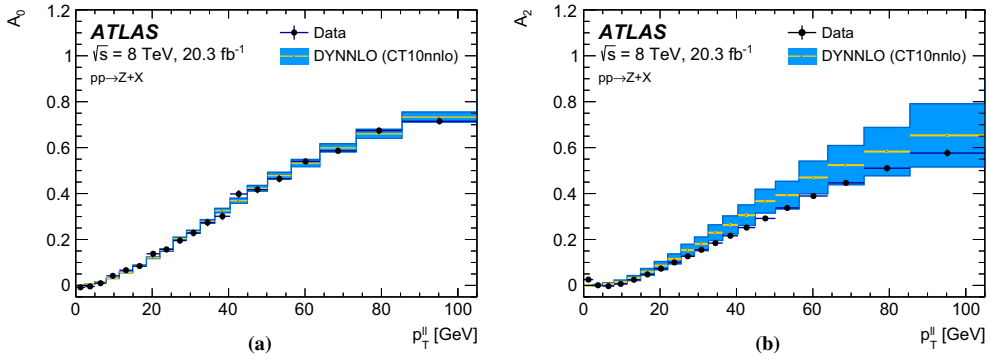

Fig. 4 The **a** A_0 and **b** A_2 angular coefficients in Z-boson events as a function of $p_{\mathrm{T}}^{\ell\ell}$ [42]. The measured coefficients are compared to the DYNNLO predictions using the CT10nnlo PDF set. The error bars show the total experimental uncertainties, and the bands show the uncertainties assigned to the DYNNLO predictions

Table 3 Systematic uncertainties in the m_W measurement due to QCD modelling, for the different kinematic distributions and W-boson charges. Except for the case of PDFs, the same uncertainties apply to W^+ and W^-. The fixed-order PDF uncertainty given for the separate W^+ and W^- final states corresponds to the quadrature sum of the CT10nnlo uncertainty variations; the charge-combined uncertainty also contains a 3.8 MeV contribution from comparing CT10nnlo to CT14 and MMHT2014

W-boson charge	W^+		W^-		Combined	
Kinematic distribution	p_{T}^{ℓ}	m_{T}	p_{T}^{ℓ}	m_{T}	p_{T}^{ℓ}	m_{T}
δm_W [MeV]						
Fixed-order PDF uncertainty	13.1	14.9	12.0	14.2	8.0	8.7
AZ tune	3.0	3.4	3.0	3.4	3.0	3.4
Charm-quark mass	1.2	1.5	1.2	1.5	1.2	1.5
Parton shower μ_{F} with heavy-flavour decorrelation	5.0	6.9	5.0	6.9	5.0	6.9
Parton shower PDF uncertainty	3.6	4.0	2.6	2.4	1.0	1.6
Angular coefficients	5.8	5.3	5.8	5.3	5.8	5.3
Total	15.9	18.1	14.8	17.2	11.6	12.9

6.5.1 Uncertainties in the fixed-order predictions

The imperfect knowledge of the PDFs affects the differential cross section as a function of boson rapidity, the angular coefficients, and the p_{T}^{W} distribution. The PDF contribution to the prediction uncertainty is estimated with the CT10nnlo PDF set by using the Hessian method [105]. There are 25 error eigenvectors, and a pair of PDF variations associated with each eigenvector. Each pair corresponds to positive and negative 90% CL excursions along the corresponding eigenvector. Symmetric PDF uncertainties are defined as the mean value of the absolute positive and negative excursions corresponding to each pair of PDF variations. The overall uncertainty of the CT10nnlo PDF set is scaled to 68% CL by applying a multiplicative factor of 1/1.645.

The effect of PDF variations on the rapidity distributions and angular coefficients are evaluated with DYNNLO, while their impact on the W-boson p_{T} distribution is evaluated using PYTHIA 8 and by reweighting event-by-event the PDFs of the hard-scattering process, which are convolved with the LO matrix elements. Similarly to other uncertainties which affect the p_{T}^{W} distribution (Sect. 6.5.2), only relative variations of the p_{T}^{W} and p_{T}^{Z} distributions induced by the PDFs are considered. The PDF variations are applied simultaneously to the boson rapidity, angular coefficients, and transverse-momentum distributions, and the overall PDF uncertainty is evaluated with the Hessian method as described above.

Uncertainties in the PDFs are the dominant source of physics-modelling uncertainty, contributing about 14 and 13 MeV when averaging p_{T}^{ℓ} and m_{T} fits for W^{+} and W^{-}, respectively. The PDF uncertainties are very similar when using p_{T}^{ℓ} or m_{T} for the measurement. They are strongly anti-correlated between positively and negatively charged W bosons, and the uncertainty is reduced to 7.4 MeV on average for p_{T}^{ℓ} and m_{T} fits, when combining opposite-charge categories. The anti-correlation of the PDF uncertainties is due to the fact that the total light-quark sea PDF is well constrained by deep inelastic scattering data, whereas the u-, d-, and s-quark decomposition of the sea is less precisely known [106]. An increase in the $\bar{u}$ PDF is at the expense of the $\bar{d}$ PDF, which produces opposite effects in the longitudinal polarisation of positively and negatively charged W bosons [37].

Other PDF sets are considered as alternative choices. The envelope of values of m_W extracted with the MMHT2014 and CT14 NNLO PDF sets is considered as an additional PDF uncertainty of 3.8 MeV, which is added in quadrature after combining the W^{+} and W^{-} categories, leading to overall PDF uncertainties of 8.0 MeV and 8.7 MeV for p_{T}^{ℓ} and m_{T} fits, respectively.

The effect of missing higher-order corrections on the NNLO predictions of the rapidity distributions of Z bosons, and the pseudorapidity distributions of the decay leptons of W bosons, is estimated by varying the renormalisation and factorisation scales by factors of 0.5 and 2.0 with respect to their nominal value $\mu_{\mathrm{R}} = \mu_{\mathrm{F}} = m_V$ in the DYNNLO predictions. The corresponding relative uncertainty in the normalised distributions is of the order of 0.1–0.3%, and significantly smaller than the PDF uncertainties. These uncertainties are expected to have a negligible impact on the measurement of m_W, and are not considered further.

The effect of the LHC beam-energy uncertainty of 0.65% [107] on the fixed-order predictions is studied. Relative variations of 0.65% around the nominal value of 3.5 TeV are considered, yielding variations of the inclusive W^{+} and W^{-} cross sections of 0.6 and 0.5%, respectively. No significant dependence as a function of lepton pseudorapidity is observed in the kinematic region used for the measurement, and the dependence as a function of p_{T}^{ℓ} and m_{T} is expected to be even smaller. This uncertainty is not considered further.

6.5.2 Uncertainties in the parton shower predictions

Several sources of uncertainty affect the PYTHIA 8 parton shower model used to predict the transverse momentum of the W boson. The values of the AZ tune parameters, determined by fits to the measurement of the Z-boson transverse momentum, are affected by the experimental uncertainty of the measurement. The corresponding uncertainties are propagated to the p_{T}^{W} predictions through variations of the orthogonal eigenvector components of the parameters error matrix [44]. The resulting uncertainty in m_W is 3.0 MeV for the p_{T}^{ℓ} distribution, and 3.4 MeV for the m_{T} distribution. In the present analysis, the impact of p_{T}^{W} distribution uncertainties is in general smaller when using p_{T}^{ℓ} than when using m_{T}, as a result of the comparatively narrow range used for the p_{T}^{ℓ} distribution fits.

Other uncertainties affecting predictions of the transverse-momentum spectrum of the W boson at a given rapidity, are propagated by considering relative variations of the p_{T}^{W} and p_{T}^{Z} distributions. The procedure is based on the assumption that model variations, when applied to p_{T}^{Z}, can be largely reabsorbed into new values of the AZ tune parameters fitted to the p_{T}^{Z} data. Variations that cannot be reabsorbed by the fit are excluded, since they would lead to a significant disagreement of the prediction with the measurement of p_{T}^{Z}. The uncertainties due to model variations which are largely correlated between p_{T}^{W} and p_{T}^{Z} cancel in this procedure. In contrast, the procedure allows a correct estimation of the uncertainties due to model variations which are uncorrelated between p_{T}^{W} and p_{T}^{Z}, and which represent the only relevant sources of theoretical uncertainties in the propagation of the QCD modelling from p_{T}^{Z} to p_{T}^{W}.

Uncertainties due to variations of parton shower parameters that are not fitted to the p_{T}^{Z} measurement include variations of the masses of the charm and bottom quarks, and variations of the factorisation scale used for the QCD ISR.

The mass of the charm quark is varied in PYTHIA 8, conservatively, by $\pm$ 0.5 GeV around its nominal value of 1.5 GeV. The resulting uncertainty contributes 1.2 MeV for the p_{T}^{ℓ} fits, and 1.5 MeV for the m_{T} fits. The mass of the bottom quark is varied in PYTHIA 8, conservatively, by $\pm$ 0.8 GeV around its nominal value of 4.8 GeV. The resulting variations have a negligible impact on the transverse-momentum distributions of Z and W bosons, and are not considered further.

The uncertainty due to higher-order QCD corrections to the parton shower is estimated through variations of the factorisation scale, μ_{F}, in the QCD ISR by factors of 0.5 and 2.0 with respect to the central choice $\mu_{\mathrm{F}}^2 = p_{\mathrm{T},0}^2 + p_{\mathrm{T}}^2$, where $p_{\mathrm{T},0}$ is an infrared cut-off, and p_{T} is the evolution variable of the parton shower [108]. Variations of the renormalisation scale in the QCD ISR are equivalent to a redefinition of $\alpha_{\mathrm{s}}(m_Z)$ used for the QCD ISR, which is fixed from the fits to the p_{T}^Z data. As a consequence, variations of the ISR renormalisation scale do not apply when estimating the uncertainty in the predicted p_{T}^W distribution.

Higher-order QCD corrections are expected to be largely correlated between W-boson and Z-boson production induced by the light quarks, u, d, and s, in the initial state. However, a certain degree of decorrelation between W- and Z-boson transverse-momentum distributions is expected, due to the different amounts of heavy-quark-initiated production, where heavy refers to charm and bottom flavours. The physical origin of this decorrelation can be ascribed to the presence of independent QCD scales corresponding to the three-to-four flavours and four-to-five flavours matching scales μ_c and μ_b in the variable-flavour-number scheme PDF evolution [109], which are of the order of the charm- and bottom-quark masses, respectively. To assess this effect, the variations of μ_{F} in the QCD ISR are performed simultaneously for all light-quark $q\bar{q} \to W, Z$ processes, with $q = u, d, s$, but independently for each of the $c\bar{c} \to Z$, $b\bar{b} \to Z$, and $c\bar{q} \to W$ processes, where $q = d, s$. The effect of the $c\bar{q} \to W$ variations on the determination of m_W is reduced by a factor of two, to account for the presence of only one heavy-flavour quark in the initial state. The resulting uncertainty in m_W is 5.0 MeV for the p_{T}^{ℓ} distribution, and 6.9 MeV for the m_{T} distribution. Since the μ_{F} variations affect all the branchings of the shower evolution and not only vertices involving heavy quarks, this procedure is expected to yield a sufficient estimate of the $\mu_{c,b}$-induced decorrelation between the W- and Z-boson p_{T} distributions. Treating the μ_{F} variations as correlated between all quark flavours, but uncorrelated between W- and Z-boson production, would yield a systematic uncertainty in m_W of approximately 30 MeV.

The predictions of the PYTHIA 8 MC generator include a reweighting of the first parton shower emission to the leading-order W+jet cross section, and do not include matching corrections to the higher-order W+jet cross section. As discussed in Sect. 11.2, predictions matched to the NLO W+jet cross section, such as POWHEG MiNLO+PYTHIA 8 and DYRes, are in disagreement with the observed $u_{\parallel}^{\ell}$ distribution and cannot be used to provide a reliable estimate of the associated uncertainty. The $u_{\parallel}^{\ell}$ distribution, on the other hand, validates the PYTHIA 8 AZ prediction and its uncertainty, which gives confidence that missing higher-order corrections to the W-boson p_{T} distribution are small in comparison to the uncertainties that are already included, and can be neglected at the present level of precision.

The sum in quadrature of the experimental uncertainties of the AZ tune parameters, the variations of the mass of the charm quark, and the factorisation scale variations, leads to uncertainties on m_W of 6.0 and 7.8 MeV when using the p_{T}^{ℓ} distribution and the m_{T} distribution, respectively. These sources of uncertainty are taken as fully correlated between the electron and muon channels, the positively and negatively charged W-boson production, and the $|\eta_{\ell}|$ bins.

The PYTHIA 8 parton shower simulation employs the CTEQ6L1 leading-order PDF set. An additional independent source of PDF-induced uncertainty in the p_{T}^W distribution is estimated by comparing several choices of the leading-order PDF used in the parton shower, corresponding to the CT14lo, MMHT2014lo and NNPDF2.3lo [110] PDF sets. The PDFs which give the largest deviation from the nominal ratio of the p_{T}^W and p_{T}^Z distributions are used to estimate the uncertainty. This procedure yields an uncertainty of about 4 MeV for W^+, and of about 2.5 MeV for W^-. Similarly to the case of fixed-order PDF uncertainties, there is a strong anti-correlation between positively and negatively charged W bosons, and the uncertainty is reduced to about 1.5 MeV when combining positive- and negative-charge categories.

The prediction of the p_{T}^W distribution relies on the p_{T}-ordered parton shower model of the PYTHIA 8 MC generator. In order to assess the impact of the choice of parton shower model on the determination of m_W, the PYTHIA 8 prediction of the ratio of the p_{T}^W and p_{T}^Z distributions is compared to the corresponding prediction of the HERWIG 7 MC generator [111,112], which implements an angular-ordered parton shower model. Differences between the PYTHIA 8 and HERWIG 7 predictions are smaller than the uncertainties in the PYTHIA 8 prediction, and no additional uncertainty is considered.

6.5.3 *Uncertainties in the angular coefficients*

The full set of angular coefficients can only be measured precisely for the production of Z bosons. The accuracy of the NNLO predictions of the angular coefficients is validated by comparison to the Z-boson measurement, and extrapolated to W-boson production assuming that NNLO predictions have similar accuracy for the W- and Z-boson processes. The ATLAS measurement of the angular coefficients in Z-boson

production at a centre-of-mass energy of $\sqrt{s} = 8$ TeV [42] is used for this validation. The $O(\alpha_s^2)$ predictions, evaluated with DYNNLO, are in agreement with the measurements of the angular coefficients within the experimental uncertainties, except for the measurement of A_2 as a function of Z-boson p_{T}.

Two sources of uncertainty affecting the modelling of the angular coefficients are considered, and propagated to the W-boson predictions. One source is defined from the experimental uncertainty of the Z-boson measurement of the angular coefficients which is used to validate the NNLO predictions. The uncertainty in the corresponding W-boson predictions is estimated by propagating the experimental uncertainty of the Z-boson measurement as follows. A set of pseudodata distributions are obtained by fluctuating the angular coefficients within the experimental uncertainties, preserving the correlations between the different measurement bins for the different coefficients. For each pseudoexperiment, the differences in the A_i coefficients between fluctuated and nominal Z-boson measurement results are propagated to the corresponding coefficient in W-boson production. The corresponding uncertainty is defined from the standard deviation of the m_W values as estimated from the pseudodata distributions.

The other source of uncertainty is considered to account for the disagreement between the measurement and the NNLO QCD predictions observed for the A_2 angular coefficient as a function of the Z-boson p_{T} (Fig. 4). The corresponding uncertainty in m_W is estimated by propagating the difference in A_2 between the Z-boson measurement and the theoretical prediction to the corresponding coefficient in W-boson production. The corresponding uncertainty in the measurement of m_W is 1.6 MeV for the extraction from the p_{T}^{ℓ} distribution. Including this contribution, total uncertainties of 5.8 and 5.3 MeV due to the modelling of the angular coefficients are estimated in the determination of the W-boson mass from the p_{T}^{ℓ} and m_{T} distributions, respectively. The uncertainty is dominated by the experimental uncertainty of the Z-boson measurement used to validate the theoretical predictions.

7 Calibration of electrons and muons

Any imperfect calibration of the detector response to electrons and muons impacts the measurement of the W-boson mass, as it affects the position and shape of the Jacobian edges reflecting the value of m_W. In addition, the p_{T}^{ℓ} and m_{T} distributions are broadened by the electron-energy and muon-momentum resolutions. Finally, the lepton-selection efficiencies depend on the lepton pseudorapidity and transverse momentum, further modifying these distributions. Corrections to the detector response are derived from the data, and presented below. In most cases, the corrections are applied to the simulation, with the exception of the muon sagitta bias corrections and electron energy response corrections, which are applied to the data. Backgrounds to the selected $Z \to \ell\ell$ samples are taken into account using the same procedures as discussed in Sect. 9. Since the Z samples are used separately for momentum calibration and efficiency measurements, as well as for the recoil response corrections discussed in Sect. 8, correlations among the corresponding uncertainties can appear. These correlations were investigated and found to be negligible.

7.1 Muon momentum calibration

As described in Sect. 5.1, the kinematic parameters of selected muons are determined from the associated inner-detector tracks. The accuracy of the momentum measurement is limited by imperfect knowledge of the detector alignment and resolution, of the magnetic field, and of the amount of passive material in the detector.

Biases in the reconstructed muon track momenta are classified as radial or sagitta biases. The former originate from detector movements along the particle trajectory and can be corrected by an η-dependent, charge-independent momentum-scale correction. The latter typically originate from curl distortions or linear twists of the detector around the z-axis [113], and can be corrected with η-dependent correction factors proportional to $q \times p_{\mathrm{T}}^{\ell}$, where q is the charge of the muon. The momentum scale and resolution corrections are applied to the simulation, while the sagitta bias correction is applied to the data:

$$p_{\mathrm{T}}^{\mathrm{MC,corr}} = p_{\mathrm{T}}^{\mathrm{MC}} \times [1 + \alpha(\eta, \phi)] \times \left[1 + \beta_{\mathrm{curv}}(\eta) \cdot G(0,1) \cdot p_{\mathrm{T}}^{\mathrm{MC}}\right],$$

$$p_{\mathrm{T}}^{\mathrm{data,corr}} = \frac{p_{\mathrm{T}}^{\mathrm{data}}}{1 + q \cdot \delta(\eta, \phi) \cdot p_{\mathrm{T}}^{\mathrm{data}}},$$

where $p_{\mathrm{T}}^{\mathrm{data,MC}}$ is the uncorrected muon transverse momentum in data and simulation, $G(0, 1)$ are normally distributed random variables with mean zero and unit width, and α, β_{curv}, and δ represent the momentum scale, intrinsic resolution and sagitta bias corrections, respectively. Multiple-scattering contributions to the resolution are relevant at low p_{T}, and the corresponding corrections are neglected.

Momentum scale and resolution corrections are derived using $Z \to \mu\mu$ decays, following the method described in Ref. [40]. Template histograms of the dimuon invariant mass are constructed from the simulated event samples, including momentum scale and resolution corrections in narrow steps within a range covering the expected uncertainty. The optimal values of α and β_{curv} are determined by means of a χ^2 minimisation, comparing data and simulation in the

range of twice the standard deviation on each side of the mean value of the invariant mass distribution. In the first step, the corrections are derived by averaging over ϕ, and for 24 pseudorapidity bins in the range $-2.4 < \eta_\ell < 2.4$. In the second iteration, ϕ-dependent correction factors are evaluated in coarser bins of η_ℓ. The typical size of α varies from -0.0005 to -0.0015 depending on η_ℓ, while β_{curv} values increase from $0.2\,\text{TeV}^{-1}$ in the barrel to $0.6\,\text{TeV}^{-1}$ in the high η_ℓ region. Before the correction, the ϕ-dependence has an amplitude at the level of 0.1%.

The α and β_{curv} corrections are sensitive to the following aspects of the calibration procedure, which are considered for the systematic uncertainty: the choice of the fitting range, methodological biases, background contributions, theoretical modelling of Z-boson production, non-linearity of the corrections, and material distribution in the ID. The uncertainty due to the choice of fitting range is estimated by varying the range by $\pm 10\%$, and repeating the procedure. The uncertainty due to the fit methodology is estimated by comparing the template fit results with an alternative approach, based on an iterative χ^2 minimisation. Background contributions from gauge-boson pair and top-quark pair production are estimated using the simulation. The uncertainty in these background contributions is evaluated by varying their normalisation within the theoretical uncertainties on the production cross sections. The uncertainty in the theoretical modelling of Z-boson production is evaluated by propagating the effect of electroweak corrections to QED FSR, QED radiation of fermion pairs, and other NLO electroweak corrections described in Sect. 6.1. The experimental uncertainty in the value of the Z-boson mass used as input is also accounted for. These sources of uncertainty are summed in quadrature, yielding an uncertainty $\delta\alpha$ in the muon momentum scale correction of approximately 0.5×10^{-4}; these sources are considered fully correlated across muon pseudorapidity.

The systematic uncertainty in the muon momentum scale due to the extrapolation from the $Z \to \mu\mu$ momentum range to the $W \to \mu\nu$ momentum range is estimated by evaluating momentum-scale corrections as a function of $1/p_{\text{T}}$ for muons in various $|\eta|$ ranges. The extrapolation uncertainty $\delta\alpha$ is parameterised as follows:

$$\delta\alpha = p_0 + \frac{p_1}{\left\langle\, p_{\text{T}}^{\ell}(W)\,\right\rangle},$$

where $\left\langle\, p_{\text{T}}^{\ell}(W)\,\right\rangle$ is the average p_{T} of muons in W-boson events, and p_0 and p_1 are free parameters. If the momentum-scale corrections are independent of $1/p_{\text{T}}$, the fitting parameters are expected to be $p_0 = 1$ and $p_1 = 0$. Deviations of p_1 from zero indicate a possible momentum dependence. The fitted values of $\delta\alpha$ are shown in Fig. 5a, and are consistent with one, within two standard deviations of the statistical error. The corresponding systematic uncertainty in m_W is defined assuming, in each bin of $|\eta|$, a momentum non-linearity given by the larger of the fitted value of p_1 and its uncertainty. This source of uncertainty is considered uncorrelated across muon pseudorapidity given that p_1 is dominated by statistical fluctuations. The effect of the imperfect knowledge of the material in the ID is studied using simulated event samples including an increase of the ID material by 10%, according to the uncertainty estimated in Ref. [114]. The impact of this variation is found to be negligible in comparison with the uncertainties discussed above.

Two methods are used for the determination of the sagitta bias δ. The first method exploits $Z \to \mu\mu$ events. Muons are categorised according to their charge and pseudorapidity, and for each of these categories, the position of the peak in the dimuon invariant mass distribution is determined for data and simulation. The procedure allows the determination of the charge dependence of the momentum scale for p_{T} values of approximately 42 GeV, which corresponds to the average transverse momentum of muons from Z-boson decays. The second method exploits identified electrons in a sample of $W \to e\nu$ decays. It is based on the ratio of the measured electron energy deposited in the calorimeter, E, to the electron momentum, p, measured in the ID. A clean sample of $W \to e\nu$ events with tightly identified electrons [38] is selected. Assuming that the response of the electromagnetic calorimeter is independent of the charge of the incoming particle, charge-dependent ID track momentum biases are extracted from the average differences in E/p for electrons and positrons [113]. This method benefits from a larger event sample compared to the first method, and allows the determination of charge-dependent corrections for p_{T} values of approximately 38 GeV, which corresponds to the average transverse momentum of muons in W-boson decays. The sagitta bias correction factors are derived using both methods separately in 40 η bins and 40 ϕ bins. The results are found to agree within uncertainties and are combined, as illustrated in Fig. 5b. The combined correction uncertainty is dominated by the finite size of the event samples.

Figure 6 shows the dimuon invariant mass distribution of $Z \to \mu\mu$ decays in data and simulation, after applying all corrections. Table 4 summarises the effect of the muon momentum scale and resolution uncertainties on the determination of m_W. The dominant systematic uncertainty in the momentum scale is due to the extrapolation of the correction from the Z-boson momentum range to the W-boson momentum range. The extrapolation uncertainty $\delta\alpha$ is (2–5) $\times 10^{-5}$ for $|\eta_\ell| < 2.0$, and (4–7) $\times 10^{-4}$ for $|\eta_\ell| > 2.0$. Systematic uncertainties from other sources are relatively small. The systematic uncertainty of the resolution corrections is dominated by the statistical uncertainty of the Z-boson event sample, and includes a contribution from the imperfect closure of the method. The latter is defined from the residual difference between the standard deviations of the dimuon invariant mass in data and simulation, after applying resolution corrections.

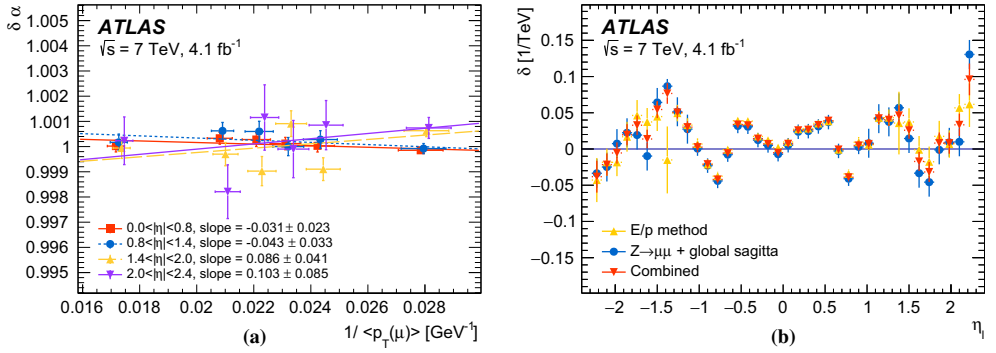

Fig. 5 **a** Residual muon momentum scale corrections as a function of muon $1/p_{\mathrm{T}}$ in four pseudorapidity regions, obtained with $Z \to \mu\mu$ events. The points are fitted using a linear function which parameterises the extrapolation of the muon momentum scale correction from Z to W events, as explained in the text. The error bars on the points show statistical uncertainties only. **b** Sagitta bias, δ, as a function of η_ℓ averaged over ϕ_ℓ. The results are obtained with the $Z \to \mu\mu$ and E/p methods and the combination of the two. The results obtained with the $Z \to \mu\mu$ method are corrected for the global sagitta bias. The E/p method uses electrons from $W \to e\nu$ decays. The two measurements are combined assuming they are uncorrelated. The error bars on the points show statistical uncertainties only

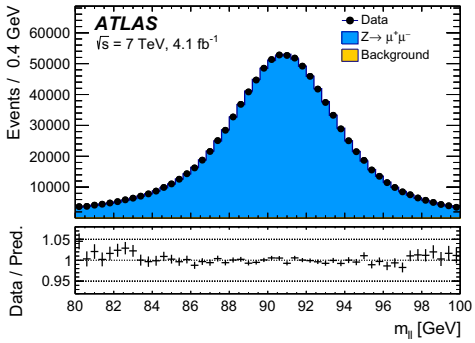

Fig. 6 Dimuon invariant mass distribution in $Z \to \mu\mu$ events. The data are compared to the simulation including signal and background contributions. Corrections for momentum scale and resolution, and for reconstruction, isolation, and trigger efficiencies are applied to the muons in the simulated events. Background events contribute less than 0.2% of the observed distribution. The lower panel shows the data-to-prediction ratio, with the error bars showing the statistical uncertainty

7.2 Muon selection efficiency

The selection of muon candidates in $W \to \mu\nu$ and $Z \to \mu\mu$ events requires an isolated track reconstructed in the inner detector and in the muon spectrometer. In addition, the events are required to pass the muon trigger selection. Differences in the efficiency of the reconstruction and selection requirements between data and simulation can introduce a systematic shift in the measurement of the W-boson mass, and have to be corrected. In particular, the extraction of m_W is sensitive to the dependence of the trigger, reconstruction and isolation efficiencies on the muon p_{T} and on the projection of the recoil on the lepton transverse momentum, $u_\parallel^\ell$.

For muons with p_{T} larger than approximately 15 GeV the detector simulation predicts constant efficiency as a function of p_{T}^ℓ, both for the muon trigger selection and the track reconstruction. In contrast, the efficiency of the isolation requirement is expected to vary as a function of p_{T}^ℓ and $u_\parallel^\ell$. The efficiency corrections also affect the muon selection inefficiency, and hence the estimation of the $Z \to \mu\mu$ background, which contributes to the $W \to \mu\nu$ selection when one of the decay muons fails the muon reconstruction or kinematic selection requirements.

Corrections to the muon reconstruction, trigger and isolation efficiencies are estimated by applying the tag-and-probe method [40] to $Z \to \mu\mu$ events in data and simulation. Efficiency corrections are defined as the ratio of efficiencies evaluated in data to efficiencies evaluated in simulated events. The corrections are evaluated as functions of two variables, p_{T}^ℓ and $u_\parallel^\ell$, and in various regions of the detector. The detector is segmented into regions corresponding to the η and ϕ coverage of the muon spectrometer. The subdivision accounts for the geometrical characteristics of the detector, such as the presence of uninstrumented or transition regions. The dependence of the efficiencies on $u_\parallel^\ell$ agree in data and simulation. Therefore, the muon efficiency corrections are evaluated only as a function of p_{T}^ℓ and η_ℓ, separately for positive and negative muon charges. The final efficiency correction factors are linearly interpolated as a function of muon p_{T}. No significant

Table 4 Systematic uncertainties in the m_W measurement from muon calibration and efficiency corrections, for the different kinematic distributions and $|\eta_\ell|$ categories, averaged over lepton charge. The momentum-scale uncertainties include the effects of both the momentum scale and linearity corrections. Combined uncertainties are evaluated as described in Sect. 2.2

$\lvert\eta_\ell\rvert$ range	[0.0, 0.8]		[0.8, 1.4]		[1.4, 2.0]		[2.0, 2.4]		Combined	
Kinematic distribution	p_{T}^{ℓ}	m_{T}	p_{T}^{ℓ}	m_{T}	p_{T}^{ℓ}	m_{T}	p_{T}^{ℓ}	m_{T}	p_{T}^{ℓ}	m_{T}
δm_W [MeV]										
Momentum scale	8.9	9.3	14.2	15.6	27.4	29.2	111.0	115.4	8.4	8.8
Momentum resolution	1.8	2.0	1.9	1.7	1.5	2.2	3.4	3.8	1.0	1.2
Sagitta bias	0.7	0.8	1.7	1.7	3.1	3.1	4.5	4.3	0.6	0.6
Reconstruction and isolation efficiencies	4.0	3.6	5.1	3.7	4.7	3.5	6.4	5.5	2.7	2.2
Trigger efficiency	5.6	5.0	7.1	5.0	11.8	9.1	12.1	9.9	4.1	3.2
Total	11.4	11.4	16.9	17.0	30.4	31.0	112.0	116.1	9.8	9.7

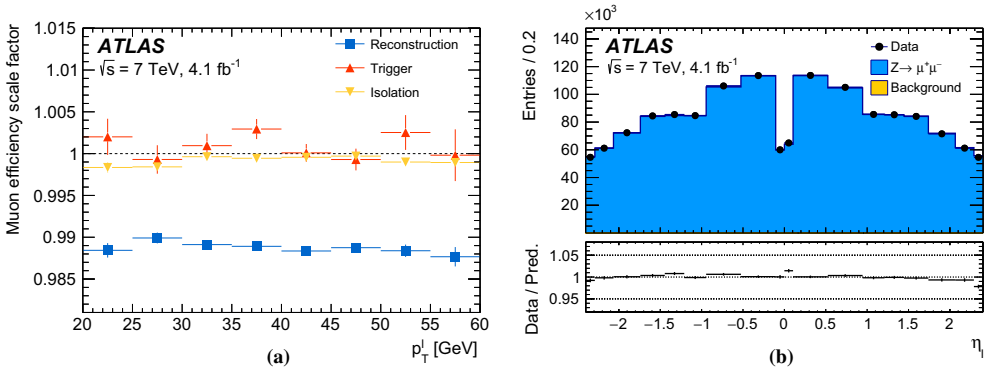

Fig. 7 **a** Scale factors for the muon reconstruction, trigger and isolation efficiency obtained with the tag and probe method as a function of the muon p_{T}. Scale factors for the trigger efficiency are averaged over two data-taking periods as explained in the text. The error bars on the points show statistical uncertainties only. **b** Distribution of the reconstructed muons η in $Z \to \mu\mu$ events. The data are compared to the simulation including signal and background contributions. Corrections for momentum scale and resolution, and for reconstruction, isolation, and trigger efficiencies are applied to the muons in the simulated events. Background events contribute less than 0.2% of the observed distribution. The lower panel shows the data-to-prediction ratio, with the error bars showing the statistical uncertainty

p_{T}-dependence of the corrections is observed in any of the detector regions.

The selection of tag-and-probe pairs from $Z \to \mu\mu$ events is based on the kinematic requirements described in Sect. 5.2. The tag muon is required to be a combined and energy-isolated muon candidate (see Sect. 5.1) which fulfils the muon trigger requirements. The selection requirements applied to the probe muon candidate differ for each efficiency determination: the selection requirement for which the efficiency is determined is removed from the set of requirements applied to the probe muon. All the efficiency corrections are derived inclusively for the full data set, with the exception of the trigger, for which they are derived separately for two different data-taking periods. The resulting scale factors are shown as a function of p_{T}^{ℓ} and averaged over η_ℓ in Fig. 7a.

The trigger and isolation efficiency corrections are typically below 0.3%, while the reconstruction efficiency correction is on average about 1.1%. The corresponding impact on muon selection inefficiency reaches up to about 20%.

The quality of the efficiency corrections is evaluated by applying the corrections to the $Z \to \mu\mu$ simulated sample, and comparing the simulated kinematic distributions to the corresponding distributions in data. Figure 7b illustrates this procedure for the η_ℓ distribution. Further distributions are shown in Sect. 9.

The dominant source of uncertainty in the determination of the muon efficiency corrections is the statistical uncertainty of the Z-boson data sample. The largest sources of systematic uncertainty are the multijet background contribution and the momentum-scale uncertainty. The correspond-

ing uncertainty in the measurement of m_W is approximately 5 MeV. The ID tracking efficiencies for muon candidates are above 99.5% without any significant p_{T} dependence, and the associated uncertainties are not considered further. An overview of the uncertainties associated with the muon efficiency corrections is shown in Table 4.

7.3 Electron energy response

The electron-energy corrections and uncertainties are largely based on the ATLAS Run 1 electron and photon calibration results [39]. The correction procedure starts with the intercalibration of the first and second layers of the EM calorimeter for minimum-ionising particles, using the energy deposits of muons in $Z \to \mu\mu$ decays. After the intercalibration of the calorimeter layers, the longitudinal shower-energy profiles of electrons and photons are used to determine the presampler energy scale and probe the passive material in front of the EM calorimeter, leading to an improved description of the detector material distribution and providing estimates of the residual passive material uncertainty. Finally, a dependence of the cell-level energy measurement on the read-out gain is observed in the second layer and corrected for. After these preliminary corrections, an overall energy-scale correction is determined as a function of η_ℓ from $Z \to ee$ decays, by comparing the reconstructed mass distributions in data and simulation. Simultaneously, an effective constant term for the calorimeter energy resolution is extracted by adjusting the width of the reconstructed dielectron invariant mass distribution in simulation to match the distribution in data.

Uncertainties in the energy-response corrections arise from the limited size of the $Z \to ee$ sample, from the physics modelling of the resonance and from the calibration algorithm itself. Physics-modelling uncertainties include uncertainties from missing higher-order electroweak corrections (dominated by the absence of lepton-pair emissions in the simulation) and from the experimental uncertainty in m_Z; these effects are taken fully correlated with the muon channel. Background contributions are small and the associated uncertainty is considered to be negligible. Uncertainties related to the calibration procedure are estimated by varying the invariant mass range used for the calibration, and with a closure test. For the closure test, a pseudodata sample of $Z \to ee$ events is obtained from the nominal sample by rescaling the electron energies by known η-dependent factors; the calibration algorithm is then applied, and the measured energy corrections are compared with the input rescaling factors.

These sources of uncertainty constitute a subset of those listed in Ref. [39], where additional variations were considered in order to generalise the applicability of the Z-boson calibration results to electrons and photons spanning a wide energy range. The effect of these uncertainties is averaged within the different η_ℓ categories. The overall relative energy-scale uncertainty, averaged over η_ℓ, is 9.4×10^{-5} for electrons from Z-boson decays.

In addition to the uncertainties in the energy-scale corrections arising from the Z-boson calibration procedure, possible differences in the energy response between electrons from Z-boson and W-boson decays constitute a significant source of uncertainty. The linearity of the response is affected by uncertainties in the intercalibration of the layers and in the passive material and calorimeter read-out corrections mentioned above. Additional uncertainties are assigned to cover imperfect electronics pedestal subtraction affecting the energy measurement in the cells of the calorimeter, and to the modelling of the interactions between the electrons and the detector material in GEANT4. The contribution from these sources to the relative energy-scale uncertainty is (3–12) $\times 10^{-5}$ in each η bin, and 5.4×10^{-5} when averaged over the full η range after taking into account the correlation between the η bins.

Azimuthal variations of the electron-energy response are expected from gravity-induced mechanical deformations of the EM calorimeter, and are observed especially in the endcaps, as illustrated in Fig. 8. As the Z-boson calibration averages over ϕ_ℓ and the azimuthal distributions of the selected electrons differ in the two processes, a small residual effect from this modulation is expected when applying the calibration results to the $W \to e\nu$ sample. Related effects are discussed in Sect. 8. A dedicated correction is derived using the azimuthal dependence of the mean of the electron energy/momentum ratio, $\langle E/p \rangle$, after correcting p for the momentum scale and curvature bias discussed in Sect. 7.1. The effect of this correction is a relative change of the average energy response of 3.8×10^{-5} in W-boson events, with negligible uncertainty.

The E/p distribution is also used to test the modelling of non-Gaussian tails in the energy response. An excess of events is observed in data at low values of E/p, and interpreted as the result of the mismodelling of the lateral development of EM showers in the calorimeter. Its impact is evaluated by removing the electrons with E/p values in the region where the discrepancy is observed. The effect of this removal is compatible for electrons from W- and Z-boson decays within 4.9×10^{-5}, which corresponds to the statistical uncertainty of the test and is considered as an additional systematic uncertainty.

The result of the complete calibration procedure is illustrated in Fig. 9, which shows the comparison of the dielectron invariant mass distribution for $Z \to ee$ events in data and simulation. The impact of the electron-energy calibration uncertainties on the m_W measurement is summarised in Table 5.

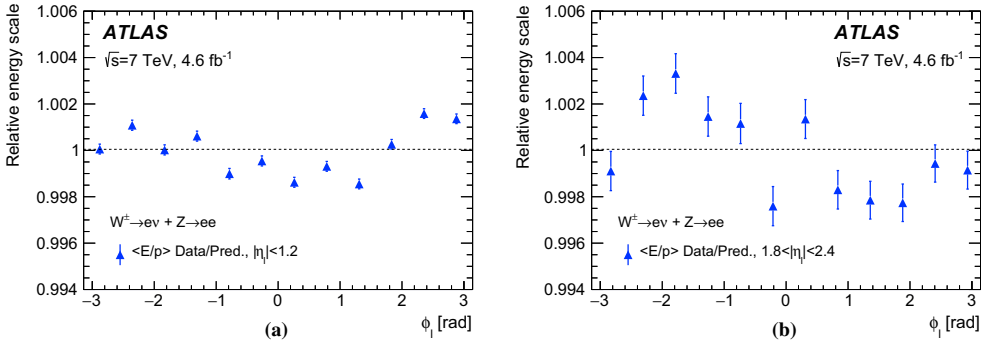

Fig. 8 Azimuthal variation of the data-to-prediction ratio of $\langle E/p \rangle$ in W and Z events, for electrons in **a** $|\eta_\ell| < 1.2$ and (b) $1.8 < |\eta_\ell| < 2.4$. The electron energy calibration based on $Z \to ee$ events is applied, and the track p is corrected for the momentum scale, resolution and sagitta bias. The mean for the E/p distribution integrated in ϕ is normalised to unity. The error bars are statistical only

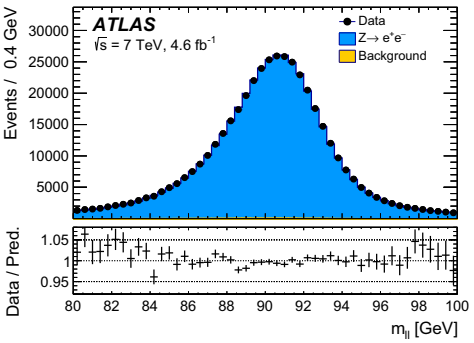

Fig. 9 Dielectron invariant mass distribution in $Z \to ee$ events. The data are compared to the simulation including signal and backgrounds. Corrections for energy resolution, and for reconstruction, identification, isolation and trigger efficiencies are applied to the simulation; energy-scale corrections are applied to the data. Background events contribute less than 0.2% of the observed distribution. The lower panel shows the data-to-prediction ratio, with the error bars showing the statistical uncertainty

7.4 Electron selection efficiency

Electron efficiency corrections are determined using samples of $W \to e\nu$, $Z \to ee$, and $J/\psi \to ee$ events, and measured separately for electron reconstruction, identification and trigger efficiencies [38], as a function of electron η and p_{T}. In the p_{T} range relevant for the measurement of the W-boson mass, the reconstruction and identification efficiency corrections have a typical uncertainty of 0.1–0.2% in the barrel, and 0.3% in the endcap. The trigger efficiency corrections have an uncertainty smaller than 0.1%, and are weakly dependent on p_{T}^{ℓ}.

For a data-taking period corresponding to approximately 20% of the integrated luminosity, the LAr calorimeter suffered from six front-end board failures. During this period, electrons could not be reconstructed in the region of $0 < \eta < 1.475$ and $-0.9 < \phi < -0.5$. The data-taking conditions are reflected in the simulation for the corresponding fraction of events. However, the trigger acceptance loss is not perfectly simulated, and dedicated efficiency corrections are derived as a function of η and ϕ to correct the mismodelling, and applied in addition to the initial corrections.

As described in Sect. 5, isolation requirements are applied to the identified electrons. Their efficiency is approximately 95% in the simulated event samples, and energy-isolation efficiency corrections are derived as for the reconstruction, identification, and trigger efficiencies. The energy-isolation efficiency corrections deviate from unity by less than 0.5%, with an uncertainty smaller than 0.2% on average.

Finally, as positively and negatively charged W-boson events have different final-state distributions, the W^+ contamination in the W^- sample, and vice versa, constitutes an additional source of uncertainty. The rate of electron charge mismeasurement in simulated events rises from about 0.2% in the barrel to 4% in the endcap. Estimates of charge mismeasurement in data confirm these predictions within better than 0.1%, apart from the high $|\eta|$ region where differences up to 1% are observed. The electron charge mismeasurement induces a systematic uncertainty in m_W of approximately 0.5 MeV in the regions of $|\eta_\ell| < 0.6$ and $0.6 < |\eta_\ell| < 1.2$, and of 5 MeV in the region of $1.8 < |\eta_\ell| < 2.4$, separately for W^+ and W^-. Since the W^+ and W^- samples contaminate each other, the effect

Table 5 Systematic uncertainties in the m_W measurement due to electron energy calibration, efficiency corrections and charge mismeasurement, for the different kinematic distributions and $|\eta_\ell|$ regions, averaged over lepton charge. Combined uncertainties are evaluated as described in Sect. 2.2

$\|\eta_\ell\|$ range	[0.0, 0.6]		[0.6, 1.2]		[1.8, 2.4]		Combined	
Kinematic distribution	p_{T}^{ℓ}	m_{T}	p_{T}^{ℓ}	m_{T}	p_{T}^{ℓ}	m_{T}	p_{T}^{ℓ}	m_{T}
δm_W [MeV]								
Energy scale	10.4	10.3	10.8	10.1	16.1	17.1	8.1	8.0
Energy resolution	5.0	6.0	7.3	6.7	10.4	15.5	3.5	5.5
Energy linearity	2.2	4.2	5.8	8.9	8.6	10.6	3.4	5.5
Energy tails	2.3	3.3	2.3	3.3	2.3	3.3	2.3	3.3
Reconstruction efficiency	10.5	8.8	9.9	7.8	14.5	11.0	7.2	6.0
Identification efficiency	10.4	7.7	11.7	8.8	16.7	12.1	7.3	5.6
Trigger and isolation efficiencies	0.2	0.5	0.3	0.5	2.0	2.2	0.8	0.9
Charge mismeasurement	0.2	0.2	0.2	0.2	1.5	1.5	0.1	0.1
Total	19.0	17.5	21.1	19.4	30.7	30.5	14.2	14.3

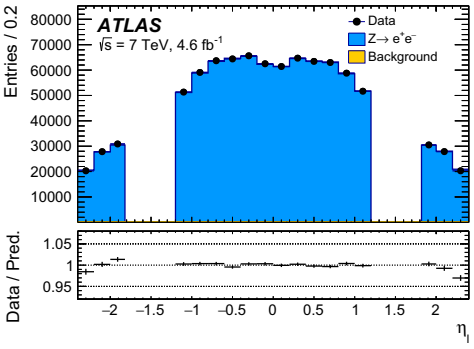

Fig. 10 Distribution of reconstructed electrons η in $Z \to ee$ events. The data are compared to the simulation including signal and background contributions. Corrections for energy resolution, and for reconstruction, identification, isolation and trigger efficiencies are applied to the simulation; energy-scale corrections are applied to the data. Background events contribute less than 0.2% of the observed distribution. The lower panel shows the data-to-prediction ratio, with the error bars showing the statistical uncertainty

is anti-correlated for the m_W measurements in the two different charge categories, and cancels in their combination, up to the asymmetry in the W^+/W^- production rate. After combination, the residual uncertainty in m_W is 0.2 MeV for $|\eta_\ell| < 1.2$, and 1.5 MeV for $1.8 < |\eta_\ell| < 2.4$, for both the p_{T}^{ℓ} and m_{T} distributions. The uncertainties are considered as uncorrelated across pseudorapidity bins.

Figure 10 compares the η_ℓ distribution in data and simulation for $Z \to ee$ events, after applying the efficiency corrections discussed above. The corresponding uncertainties in m_W due to the electron efficiency corrections are shown in Table 5.

8 Calibration of the recoil

The calibration of the recoil, u_{T}, affects the measurement of the W-boson mass through its impact on the m_{T} distribution, which is used to extract m_W. In addition, the recoil calibration affects the p_{T}^{ℓ} and m_{T} distributions through the $p_{\mathrm{T}}^{\mathrm{miss}}$, m_{T}, and u_{T} event-selection requirements. The calibration procedure proceeds in two steps. First, the dominant part of the u_{T} resolution mismodelling is addressed by correcting the modelling of the overall event activity in simulation. These corrections are derived separately in the W- and Z-boson samples. Second, corrections for residual differences in the recoil response and resolution are derived using Z-boson events in data, and transferred to the W-boson sample.

8.1 Event activity corrections

The pile-up of multiple proton–proton interactions has a significant impact on the resolution of the recoil. As described in Sect. 4, the pile-up is modelled by overlaying the simulated hard-scattering process with additional pp interactions simulated using PYTHIA 8 with the A2 tune. The average number of interactions per bunch crossing is defined, for each event, as $\langle\mu\rangle = \mathcal{L}\sigma_{\mathrm{in}}/f_{\mathrm{BC}}$, where $\mathcal{L}$ is the instantaneous luminosity, σ_{in} is the total pp inelastic cross section and f_{BC} is the average bunch-crossing rate. The distribution of $\langle\mu\rangle$ in the simulated event samples is reweighted to match the corresponding distribution in data. The distribution of $\langle\mu\rangle$ is affected in particular by the uncertainty in the cross section and properties of inelastic collisions. In the simulation, $\langle\mu\rangle$ is scaled by a factor α to optimise the modelling of observed data distributions which are relevant to the modelling of u_{T}. A value of $\alpha = 1.10 \pm 0.04$ is determined by minimising the χ^2 function of the compatibility test between data and simulation for the $\Sigma E_{\mathrm{T}}^{*}$ and $u_{\perp}^{Z}$ distributions, where the uncertainty accounts for differences in the values determined using the two distributions.

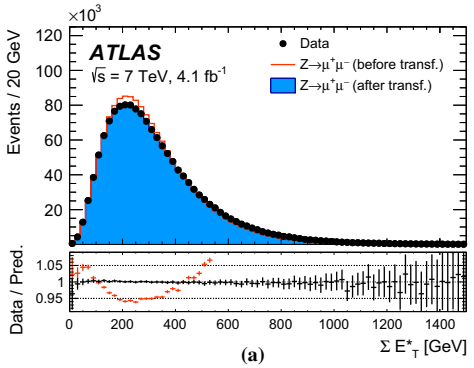

Fig. 11 Distributions of **a** $\Sigma E_{\mathrm{T}}^{*}$ and **b** azimuth ϕ of the recoil in data and simulation for $Z \to \mu\mu$ events. The $\Sigma E_{\mathrm{T}}^{*}$ distribution is shown before and after applying the Smirnov-transform correction, and the ϕ distribution is shown before and after the $u_{x,y}$ correction. The lower panels show the data-to-prediction ratios, with the vertical bars showing the statistical uncertainty

After the correction applied to the average number of pile-up interactions, residual data-to-prediction differences in the $\Sigma E_{\mathrm{T}}^{*}$ distribution are responsible for most of the remaining u_{T} resolution mismodelling. The $\Sigma E_{\mathrm{T}}^{*}$ distribution is corrected by means of a Smirnov transform, which is a mapping $x \to x'(x)$ such that a function $f(x)$ is transformed into another target function $g(x)$ through the relation $f(x) \to f(x') \equiv g(x)$ [115]. Accordingly, a mapping $\Sigma E_{\mathrm{T}}^{*} \to \Sigma E_{\mathrm{T}}^{*\prime}$ is defined such that the distribution of $\Sigma E_{\mathrm{T}}^{*}$ in simulation, $h_{\mathrm{MC}}(\Sigma E_{\mathrm{T}}^{*})$, is transformed into $h_{\mathrm{MC}}(\Sigma E_{\mathrm{T}}^{*\prime})$ to match the $\Sigma E_{\mathrm{T}}^{*}$ distribution in data, $h_{\mathrm{data}}(\Sigma E_{\mathrm{T}}^{*})$. The correction is derived for Z-boson events in bins of $p_{\mathrm{T}}^{\ell\ell}$, as the observed differences in the $\Sigma E_{\mathrm{T}}^{*}$ distribution depend on the Z-boson transverse momentum. The result of this procedure is illustrated in Fig. 11a. The modified distribution is used to parameterise the recoil response corrections discussed in the next section.

In W-boson events, the transverse momentum of the boson can only be inferred from u_{T}, which has worse resolution compared to $p_{\mathrm{T}}^{\ell\ell}$ in Z-boson events. To overcome this limitation, a p_{T}-dependent correction is defined assuming that the p_{T} dependence of differences between data and simulation in the $\Sigma E_{\mathrm{T}}^{*}$ distribution in W-boson events follows the corresponding differences observed in Z-boson events. The $\Sigma E_{\mathrm{T}}^{*}$ distribution to be matched by the simulation is defined as follows for W-boson events:

$$\tilde{h}^{W}_{\mathrm{data}}(\Sigma E_{\mathrm{T}}^{*}, p_{\mathrm{T}}^{W}) \equiv h^{Z}_{\mathrm{data}}(\Sigma E_{\mathrm{T}}^{*}, p_{\mathrm{T}}^{\ell\ell}) \left(\frac{h^{W}_{\mathrm{data}}(\Sigma E_{\mathrm{T}}^{*})}{h^{W}_{\mathrm{MC}}(\Sigma E_{\mathrm{T}}^{*})} \Big/ \frac{h^{Z}_{\mathrm{data}}(\Sigma E_{\mathrm{T}}^{*})}{h^{Z}_{\mathrm{MC}}(\Sigma E_{\mathrm{T}}^{*})} \right), \quad (4)$$

where p_{T}^{W} is the particle-level W-boson transverse momentum, and $p_{\mathrm{T}}^{\ell\ell}$ the transverse momentum measured from the decay-lepton pair, used as an approximation of the particle-level p_{T}^{Z}. The superscripts W and Z refer to W- or Z-boson event samples, and the double ratio in the second term accounts for the differences between the inclusive distributions in W- and Z-boson events. This correction is defined separately for positively and negatively charged W bosons, so as to incorporate the dependence of the p_{T}^{W} distribution on the charge of the W boson. Using $\tilde{h}^{W}_{\mathrm{data}}(\Sigma E_{\mathrm{T}}^{*}, p_{\mathrm{T}}^{W})$ defined in Eq. (4) as the target distribution, the p_{T}^{W}-dependent Smirnov transform of the $\Sigma E_{\mathrm{T}}^{*}$ distribution in W-boson events is defined as follows:

$$h^{W}_{\mathrm{MC}}(\Sigma E_{\mathrm{T}}^{*}; p_{\mathrm{T}}^{W}) \to h^{W}_{\mathrm{MC}}(\Sigma E_{\mathrm{T}}^{*\prime}; p_{\mathrm{T}}^{W}) \equiv \tilde{h}^{W}_{\mathrm{data}}(\Sigma E_{\mathrm{T}}^{*}; p_{\mathrm{T}}^{W}).$$

The validity of the approximation introduced in Eq. (4) is verified by comparing $h^{W}_{\mathrm{data}}(\Sigma E_{\mathrm{T}}^{*})/h^{W}_{\mathrm{MC}}(\Sigma E_{\mathrm{T}}^{*})$ and $h^{Z}_{\mathrm{data}}(\Sigma E_{\mathrm{T}}^{*})/h^{Z}_{\mathrm{MC}}(\Sigma E_{\mathrm{T}}^{*})$ in broad bins of u_{T}. The associated systematic uncertainties are discussed in Sect. 8.3.

8.2 Residual response corrections

In the ideal case of beams coinciding with the z-axis, the physical transverse momentum of W and Z bosons is uniformly distributed in ϕ. However, an offset of the interaction point with respect to the detector centre in the transverse plane, the non-zero crossing angle between the proton beams, and ϕ-dependent response of the calorimeters generate anisotropies in the reconstructed recoil distribution. Corresponding differences between data and simulation are addressed by effective corrections applied to u_x and u_y in simulation:

$$u_x' = u_x + \left(\langle u_x \rangle_{\mathrm{data}} - \langle u_x \rangle_{\mathrm{MC}} \right),$$
$$u_y' = u_y + \left(\langle u_y \rangle_{\mathrm{data}} - \langle u_y \rangle_{\mathrm{MC}} \right),$$

where $\langle u_{x,y} \rangle_{\text{data}}$ and $\langle u_{x,y} \rangle_{\text{MC}}$ are the mean values of these distributions in data and simulation, respectively. The corrections are evaluated in Z-boson events and parameterised as a function of ΣE_{T}^{*}. The effect of these corrections on the recoil ϕ distribution is illustrated in Fig. 11b.

The transverse momentum of Z bosons can be reconstructed from the decay-lepton pair with a resolution of 1–2 GeV, which is negligible compared to the recoil energy resolution. The recoil response can thus be calibrated from comparisons with the reconstructed $p_{\text{T}}^{\ell\ell}$ in data and simulation. Recoil energy scale and resolution corrections are derived in bins of ΣE_{T}^{*} and $p_{\text{T}}^{\ell\ell}$ at reconstruction level, and are applied in simulation as a function of the particle-level vector-boson momentum p_{T}^{V} in both the W- and Z-boson samples. The energy scale of the recoil is calibrated by comparing the $u_{\parallel}^{Z} + p_{\text{T}}^{\ell\ell}$ distribution in data and simulation, whereas resolution corrections are evaluated from the $u_{\perp}^{Z}$ distribution. Energy-scale corrections $b(p_{\text{T}}^{V}, \Sigma E_{\text{T}}^{*\prime})$ are defined as the difference between the average values of the $u_{\parallel}^{Z} + p_{\text{T}}^{\ell\ell}$ distributions in data and simulation, and the energy-resolution correction factors $r(p_{\text{T}}^{V}, \Sigma E_{\text{T}}^{*\prime})$ as the ratio of the standard deviations of the corresponding $u_{\perp}^{Z}$ distributions.

The parallel component of u_{T} in simulated events is corrected for energy scale and resolution, whereas the perpendicular component is corrected for energy resolution only. The corrections are defined as follows:

$$u_{\parallel}^{V,\text{corr}} = \left[u_{\parallel}^{V,\text{MC}} - \left\langle u_{\parallel}^{Z,\text{data}} \right\rangle (p_{\text{T}}^{V}, \Sigma E_{\text{T}}^{*\prime})\right] \cdot r(p_{\text{T}}^{V}, \Sigma E_{\text{T}}^{*\prime}) + \left\langle u_{\parallel}^{Z,\text{data}} \right\rangle (p_{\text{T}}^{V}, \Sigma E_{\text{T}}^{*\prime}) + b(p_{\text{T}}^{V}, \Sigma E_{\text{T}}^{*\prime}), \quad (5)$$

$$u_{\perp}^{V,\text{corr}} = u_{\perp}^{V,\text{MC}} \cdot r(p_{\text{T}}^{V}, \Sigma E_{\text{T}}^{*\prime}), \quad (6)$$

where $V = W, Z$, $u_{\parallel}^{V,\text{MC}}$ and $u_{\perp}^{V,\text{MC}}$ are the parallel and perpendicular components of u_{T} in the simulation, and $u_{\parallel}^{V,\text{corr}}$ and $u_{\perp}^{V,\text{corr}}$ are the corresponding corrected values. As for b and r, the average $\left\langle u_{\parallel}^{Z,\text{data}} \right\rangle$ is mapped as a function of the reconstructed $p_{\text{T}}^{\ell\ell}$ in Z-boson data, and used as a function of p_{T}^{V} in both W- and Z-boson simulation. Since the resolution of u_{T} has a sizeable dependence on the amount of pile-up, the correction procedure is defined in three bins of $\langle\mu\rangle$, corresponding to low, medium, and high pile-up conditions, and defined by the ranges of $\langle\mu\rangle \in [2.5, 6.5]$, $\langle\mu\rangle \in [6.5, 9.5]$, and $\langle\mu\rangle \in [9.5, 16.0]$, respectively. Values for $b(p_{\text{T}}^{V}, \Sigma E_{\text{T}}^{*\prime})$ are typically $O(100\,\text{MeV})$, and $r(p_{\text{T}}^{V}, \Sigma E_{\text{T}}^{*\prime})$ deviates from unity by 2% at most. The effect of the calibration is shown in Fig. 12 for $Z \to \mu\mu$ events. The level of agreement obtained after corrections is satisfactory, and similar performance is observed for $Z \to ee$ events.

A closure test of the applicability of Z-based corrections to W production is performed using W and Z samples simulated with POWHEG+HERWIG 6, which provide an alternative model for the description of hadronisation and the underlying event. The procedure described above is used to correct the recoil response from POWHEG+PYTHIA 8 to POWHEG+HERWIG 6, where the latter is treated as pseudo-data. As shown in Fig. 13, the corrected W recoil distributions in POWHEG+PYTHIA 8 match the corresponding distributions in POWHEG+HERWIG 6. For this study, the effect of the different particle-level p_{T}^{W} distributions in both samples is removed by reweighting the POWHEG+PYTHIA 8 prediction to POWHEG+HERWIG 6. This study is performed applying the standard lepton selection cuts, but avoiding further kinematic selections in order to maximize the statistics available for the test.

8.3 Systematic uncertainties

The recoil calibration procedure is sensitive to the following sources of systematic uncertainty: the uncertainty of the scale factor applied to the $\langle\mu\rangle$ distribution, uncertainties due to the Smirnov transform of the ΣE_{T}^{*} distribution, uncertainties in the correction of the average value of the $u_{x,y}$ distributions, statistical uncertainties in the residual correction factors and their p_{T} dependence, and expected differences in the recoil response between Z- and W-boson events.

The uncertainty from the $\langle\mu\rangle$ scale-factor α is evaluated by varying it by its uncertainty and repeating all steps of the recoil calibration procedure. These variations affect the determination of m_W by less than 1 MeV.

The systematic uncertainty related to the dependence of the ΣE_{T}^{*} correction on p_{T} is estimated by comparing with the results of a p_{T}-inclusive correction. This source contributes, averaging over W-boson charges, an uncertainty of approximately 1 MeV for the extraction of m_W from the p_{T}^{ℓ} distribution, and 11 MeV when using the m_{T} distribution.

The recoil energy scale and resolution corrections of Eqs. (5) and (6) are derived from the Z-boson sample and applied to W-boson events. Differences in the detector response to the recoil between W- and Z-boson processes are considered as a source of systematic uncertainty for these corrections. Differences between the $u_{\perp}^{W}$ and $u_{\perp}^{Z}$ distributions originating from different vector-boson kinematic properties, different ISR and FSR photon emission, and from different selection requirements are, however, discarded as they are either accurately modelled in the simulation or already incorporated in the correction procedure.

To remove the effect of such differences, the two-dimensional distribution $h_{\text{MC}}^{W}(p_{\text{T}}, \Sigma E_{\text{T}}^{*})$ in W-boson simulated events is corrected to match the corresponding distribution in Z-boson simulated events, treating the neutrinos in W-boson decays as charged leptons to calculate u_{T} as in Z-boson events. Finally, events containing a particle-level photon from final-state radiation are removed. After these corrections, the standard deviation of the $u_{\perp}$ distribution agrees within 0.03% between simulated W- and Z-boson

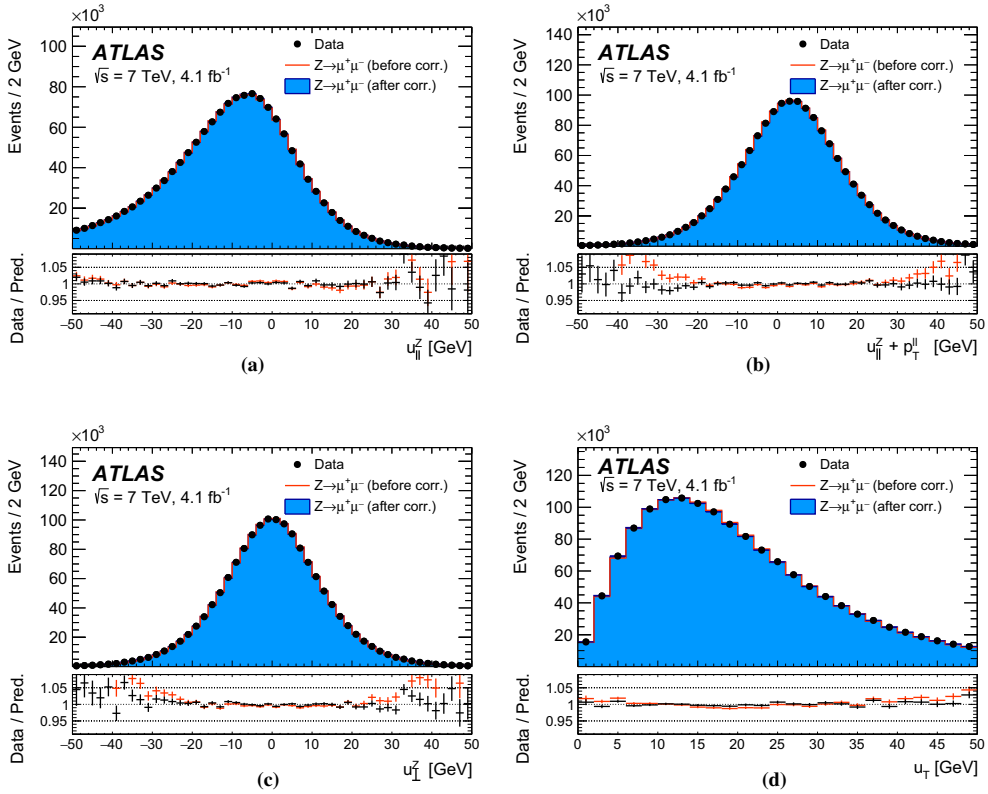

Fig. 12 Recoil distributions for **a** $u_{\parallel}^{Z}$, **b** $u_{\parallel}^{Z} + p_{\mathrm{T}}^{\ell\ell}$, (c) $u_{\perp}^{Z}$, and (d) u_{T} in $Z \to \mu\mu$ events. The data are compared to the simulation before and after applying the recoil corrections described in the text. The lower panels show the data-to-prediction ratios, with the vertical bars showing the statistical uncertainty

events. This difference is equivalent to 6% of the size of the residual resolution correction, which increases the standard deviation of the $u_{\perp}$ distribution by 0.5%. Accordingly, the corresponding systematic uncertainty due to the extrapolation of the recoil calibration from Z- to W-boson events is estimated by varying the energy resolution parameter r of Eqs. (5) and (6) by 6%. The impact of this uncertainty on the extraction of m_W is approximately 0.2 MeV for the p_{T}^{ℓ} distribution, and 5.1 MeV for the m_{T} distribution. The extrapolation uncertainty of the energy-scale correction b was found to be negligible in comparison.

In addition, the statistical uncertainty of the correction factors contributes 2.0 MeV for the p_{T}^{ℓ} distribution, and 2.7 MeV for the m_{T} distribution. Finally, instead of using a binned correction, a smooth interpolation of the correction values between the bins is performed. Comparing the binned and interpolated correction parameters $b(p_{\mathrm{T}}^{V}, \Sigma E_{\mathrm{T}}^{*\prime})$ and $r(p_{\mathrm{T}}^{V}, \Sigma E_{\mathrm{T}}^{*\prime})$ leads to a systematic uncertainty in m_W of 1.4 and 3.1 MeV for the p_{T}^{ℓ} and m_{T} distributions, respectively. Systematic uncertainties in the $u_{x,y}$ corrections are found to be small compared to the other systematic uncertainties, and are neglected.

The impact of the uncertainties of the recoil calibration on the extraction of the W-boson mass from the p_{T}^{ℓ} and m_{T} distributions are summarised in Table 6. The determination of m_W from the p_{T}^{ℓ} distribution is only slightly affected by the uncertainties of the recoil calibration, whereas larger uncertainties are estimated for the m_{T} distribution. The largest uncertainties are induced by the $\Sigma E_{\mathrm{T}}^{*}$ corrections and by the extrapolation of the recoil energy-scale and energy-resolution corrections from Z- to W-boson events. The systematic uncertainties are in general smaller for W^{-} events

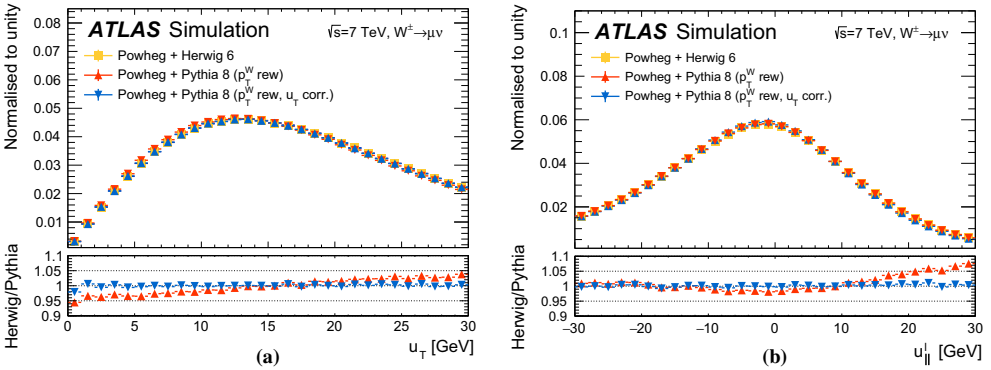

Fig. 13 Distributions of **a** u_{T} and **b** $u_{\parallel}^{\ell}$ in W events simulated using POWHEG+PYTHIA 8 and POWHEG+HERWIG 6. The recoil response in POWHEG+PYTHIA 8 is corrected to the POWHEG+HERWIG 6 response using simulated Z events following the method described in the text. The p_{T}^{W} distribution in POWHEG+PYTHIA 8 is reweighted to the POWHEG+HERWIG 6 prediction. The lower panels show the ratios of POWHEG+HERWIG 6 to POWHEG+PYTHIA 8, with and without the response correction in the POWHEG+PYTHIA 8 sample

Table 6 Systematic uncertainties in the m_W measurement due to recoil corrections, for the different kinematic distributions and W-boson charge categories. Combined uncertainties are evaluated as described in Sect. 2.2

W-boson charge	W^+		W^-		Combined	
Kinematic distribution	p_{T}^{ℓ}	m_{T}	p_{T}^{ℓ}	m_{T}	p_{T}^{ℓ}	m_{T}
δm_W [MeV]						
$\langle\mu\rangle$ scale factor	0.2	1.0	0.2	1.0	0.2	1.0
$\Sigma E_{\mathrm{T}}^{*}$ correction	0.9	12.2	1.1	10.2	1.0	11.2
Residual corrections (statistics)	2.0	2.7	2.0	2.7	2.0	2.7
Residual corrections (interpolation)	1.4	3.1	1.4	3.1	1.4	3.1
Residual corrections ($Z \to W$ extrapolation)	0.2	5.8	0.2	4.3	0.2	5.1
Total	2.6	14.2	2.7	11.8	2.6	13.0

than for W^+ events, as the $\Sigma E_{\mathrm{T}}^{*}$ distribution in W^- events is closer to the corresponding distribution in Z-boson events.

9 Consistency tests with Z-boson events

The $Z \to \ell\ell$ event sample allows several validation and consistency tests of the W-boson analysis to be performed. All the identification requirements of Sect. 5.1, the calibration and efficiency corrections of Sects. 7 and 8, as well as the physics-modelling corrections described in Sect. 6, are applied consistently in the W- and Z-boson samples. The Z-boson sample differs from the W-boson sample in the selection requirements, as described in Sect. 5.2. In addition to the event-selection requirements described there, the transverse momentum of the dilepton system, $p_{\mathrm{T}}^{\ell\ell}$, is required to be smaller than 30 GeV.

The missing transverse momentum in Z-boson events is defined by treating one of the two decay leptons as a neutrino and ignoring its transverse momentum when defining the event kinematics. This procedure allows the $p_{\mathrm{T}}^{\mathrm{miss}}$ and m_{T} variables to be defined in the Z-boson sample in close analogy to their definition in the W-boson sample. The procedure is repeated, removing the positive and negative lepton in turn.

In the Z-boson sample, the background contribution arising from top-quark and electroweak production is estimated using Monte Carlo samples. Each process is normalised using the corresponding theoretical cross sections, evaluated at NNLO in the perturbative expansion of the strong coupling constant. This background contributes a 0.12% fraction in each channel. In the muon channel, the background contribution from multijet events is estimated to be smaller than 0.05% using simulated event samples of $b\bar{b}$ and $c\bar{c}$ production, and neglected. In the electron channel, a data-driven estimate of the multijet background contributes about a 0.1% fraction, before applying the isolation selections, which reduce it to a negligible level.

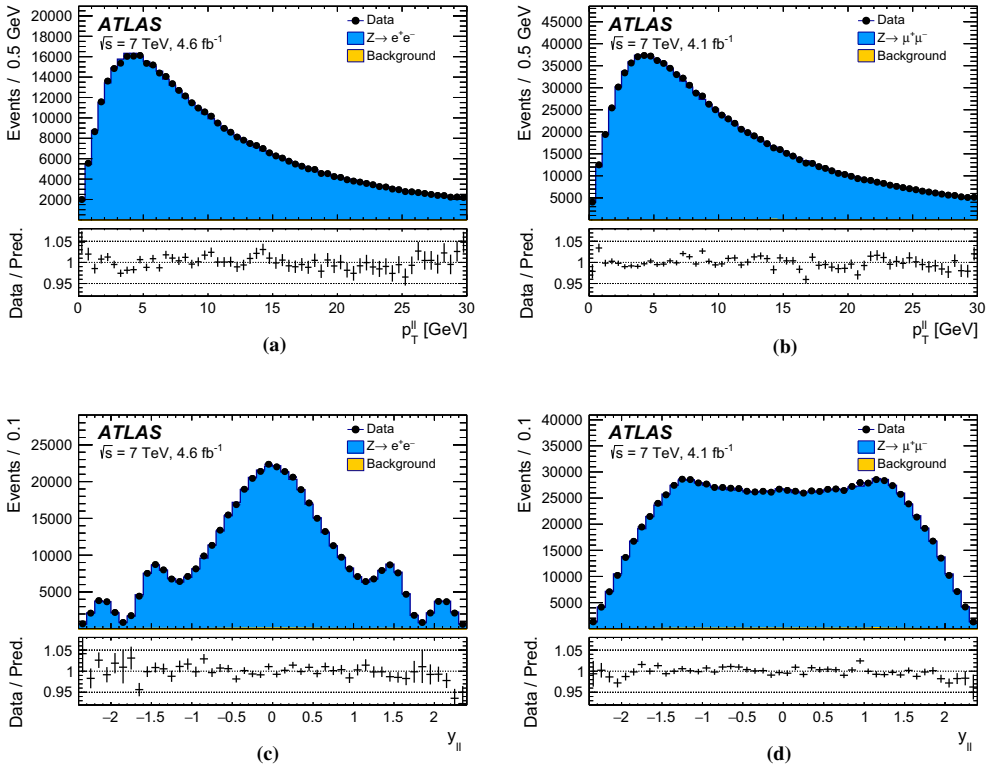

Fig. 14 The **a**, **b** $p_{\mathrm{T}}^{\ell\ell}$ and **c**, **d** $y_{\ell\ell}$ distributions in Z-boson events for the **a**, **c** electron and **b**, **d** muon decay channels. The data are compared to the simulation including signal and backgrounds. Detector calibration and physics-modelling corrections are applied to the simulated events. Background events contribute less than 0.2% of the observed distributions. The lower panels show the data-to-prediction ratios, with the error bars showing the statistical uncertainty

Figure 14 shows the reconstructed distributions of $p_{\mathrm{T}}^{\ell\ell}$ and $y_{\ell\ell}$ in selected Z-boson events; these distributions are not sensitive to the value of m_Z. Figure 15 shows the corresponding distributions for p_{T}^{ℓ} and m_{T}, variables which are sensitive to m_Z. Data and simulation agree at the level of 1–2% percent in all the distributions.

The mass of the Z boson is extracted with template fits to the $m_{\ell\ell}$, p_{T}^{ℓ}, and m_{T} kinematic distributions. The extraction of the Z-boson mass from the dilepton invariant mass distribution is expected to yield, by construction, the value of m_Z used as input for the muon-momentum and electron-energy calibrations, providing a closure test of the lepton calibration procedures. The p_{T}^{ℓ} distribution is very sensitive to the physics-modelling corrections described in Sect. 6. The comparison of the value of m_Z extracted from the p_{T}^{ℓ} distribution with the value used as input for the calibration tests the physics modelling and efficiency corrections. Finally, m_Z measurements from the m_{T} distribution provides a test of the recoil calibration.

Similarly to the W-boson mass, the value of m_Z is determined by minimising the χ^2 function of the compatibility test between the templates and the measured distributions. The templates are generated with values of m_Z in steps of 4 to 25 MeV within a range of ± 450 MeV, centred around a reference value corresponding to the LEP combined value, $m_Z = 91187.5$ MeV [32]. The χ^2 function is interpolated with a second order polynomial. The minimum of the χ^2 function yields the extracted value of m_Z, and the difference between the extracted value of m_Z and the reference value is defined as Δm_Z. The ranges used for the extraction are [80, 100] GeV for the $m_{\ell\ell}$ distributions, [30, 55] GeV for the p_{T}^{ℓ} distribution, and [40, 120] GeV for the m_{T} distribution.

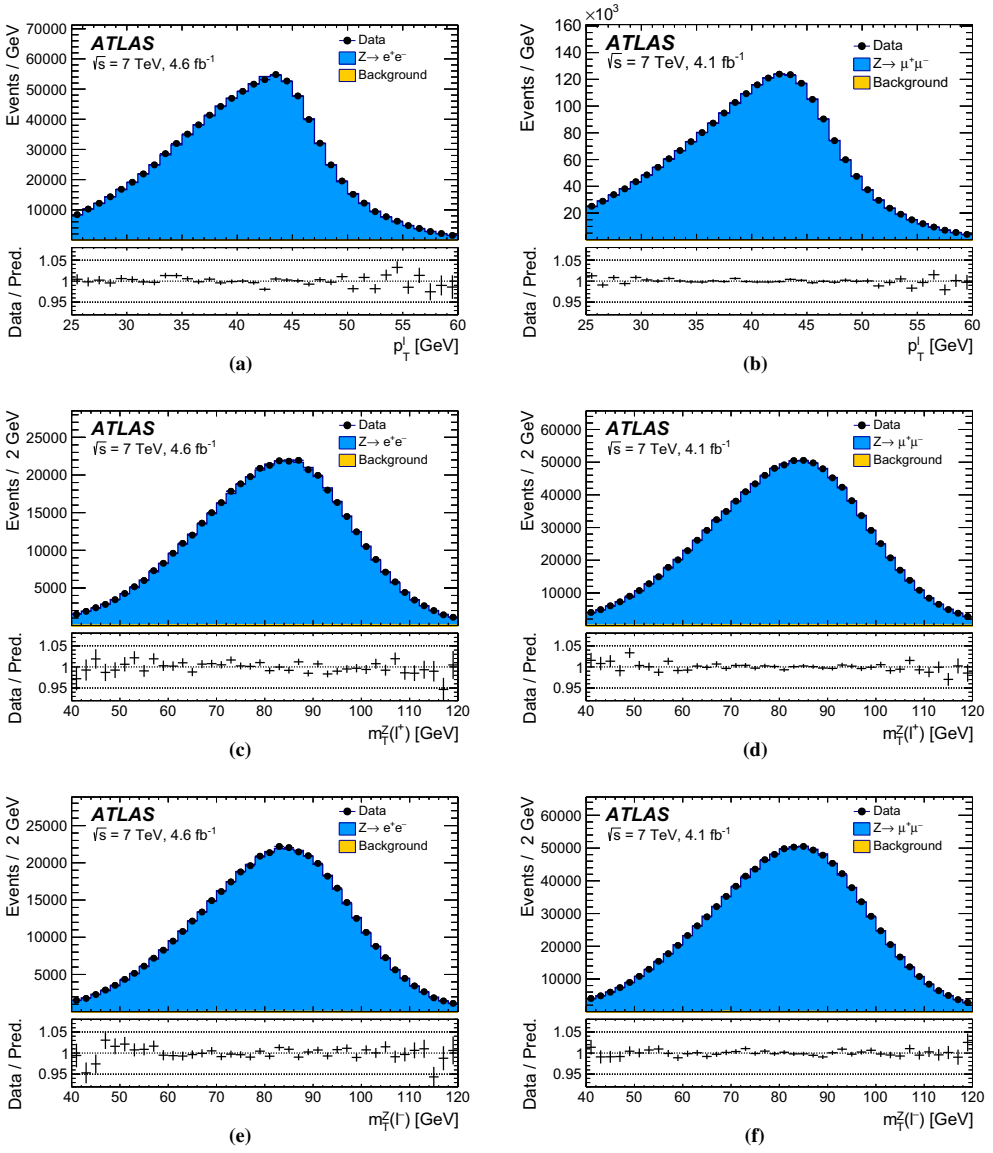

Fig. 15 The p_{T}^{ℓ} distribution in the **a** electron and **b** muon channels, and m_{T} distributions in the **c**, **e** electron and **d**, **f** muon decay channels for Z events when the **c**, **d** negatively charged, or **e**, **f** positively charged lepton is removed. The data are compared to the simulation including signal and backgrounds. Detector calibration and physics-modelling corrections are applied to the simulated events. Background events contribute less than 0.2% of the observed distributions. The lower panels show the data-to-prediction ratios, with the error bars showing the statistical uncertainty

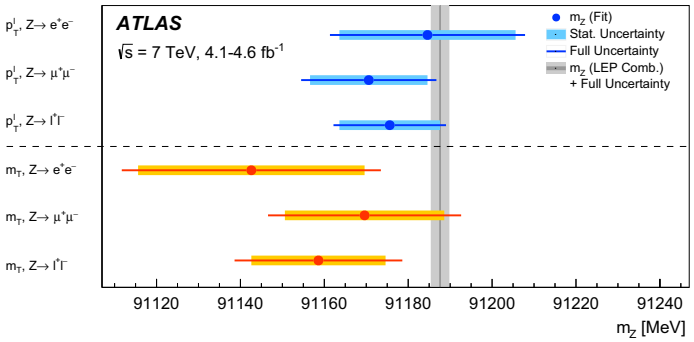

Fig. 16 Summary of the m_Z determinations from the p_{T}^{ℓ} and m_{T} distributions in the muon and electron decay channels. The LEP combined value of m_Z, which is used as input for the detector calibration, is also indicated. The horizontal and vertical bands show the uncertainties of the m_Z determinations and of the LEP combined value, respectively

Table 7 Difference between Z-boson mass, extracted from p_{T}^{ℓ} and m_{T} distributions, and the LEP combined value. The results are shown separately for the electron and muon decay channels, and their combination. The first quoted uncertainty is statistical, the second is the experimental systematic uncertainty, which includes lepton efficiency and recoil calibration uncertainties where applicable. Physics-modelling uncertainties are neglected

Lepton charge	ℓ^+		ℓ^-		Combined	
Kinematic distribution	p_{T}^{ℓ}	m_{T}	p_{T}^{ℓ}	m_{T}	p_{T}^{ℓ}	m_{T}
Δm_Z [MeV]						
$Z \to ee$	$13 \pm 31 \pm 10$	$-93 \pm 38 \pm 15$	$-20 \pm 31 \pm 10$	$4 \pm 38 \pm 15$	$-3 \pm 21 \pm 10$	$-45 \pm 27 \pm 15$
$Z \to \mu\mu$	$1 \pm 22 \pm 8$	$-35 \pm 28 \pm 13$	$-36 \pm 22 \pm 8$	$-1 \pm 27 \pm 13$	$-17 \pm 14 \pm 8$	$-18 \pm 19 \pm 13$
Combined	$5 \pm 18 \pm 6$	$-58 \pm 23 \pm 12$	$-31 \pm 18 \pm 6$	$1 \pm 22 \pm 12$	$-12 \pm 12 \pm 6$	$-29 \pm 16 \pm 12$

The extraction of m_Z from the m_{T} distribution is performed separately for positively and negatively charged leptons in the event, by reconstructing m_{T} from the kinematic properties of one of the two charged leptons and of the recoil reconstructed by treating the other as a neutrino.

Z-boson mass fits are performed using the m_{T} and p_{T}^{ℓ} distributions in the electron and muon decay channels, inclusively in η and separately for positively and negatively charged leptons. The results of the fits are summarised in Fig. 16 and Table 7. The p_{T}^{ℓ} fit results include all lepton reconstruction systematic uncertainties except the Z-based energy or momentum scale calibration uncertainties; the m_{T} fit results include recoil calibration systematic uncertainties in addition. Physics-modelling uncertainties are neglected.

The value of m_Z measured from positively charged leptons is correlated with the corresponding extraction from the negatively charged leptons. The p_{T}^{ℓ} distributions for positively and negatively charged leptons are statistically independent, but the m_{T} distributions share the same reconstructed recoil event by event, and are statistically correlated. In both cases, the decay of the Z-boson induces a kinematical correlation between the distributions of positively and negatively charged leptons. The correlation is estimated by constructing two-dimensional ℓ^+ and ℓ^- distributions, separately for p_{T}^{ℓ} and m_{T}, fluctuating the bin contents of these distributions within their uncertainties, and repeating the fits for each pseudodata sample. The correlation values are -7% for the p_{T}^{ℓ} distributions, and -12% for the m_{T} distributions.

Accounting for the experimental uncertainties as described above, the combined extraction of m_Z from the p_{T}^{ℓ} distribution yields a result compatible with the reference value within 0.9 standard deviations. The difference between the m_Z extractions from positively and negatively charged lepton distributions is compatible with zero within 1.4 standard deviations. For the extraction from the m_{T} distribution, the compatibility with the reference value of m_Z is at the level of 1.5 standard deviations. Fits using the lepton pair invariant mass distribution agree with the reference, yielding $\Delta m_Z = 1 \pm 3$ MeV in the muon channel and $\Delta m_Z = 3 \pm 5$ MeV in the electron channel, as expected from the calibration procedure. In summary, the consistency tests based on the Z-boson sample agree with the expectations within the experimental uncertainties.

10 Backgrounds in the W-boson sample

The W-boson event sample, selected as described in Sect. 5.2, includes events from various background processes. Background contributions from Z-boson, $W \to \tau\nu$, boson pair, and top-quark production are estimated using simulation.

Contributions from multijet production are estimated with data-driven techniques.

10.1 Electroweak and top-quark backgrounds

The dominant sources of background contribution in the $W \to \ell\nu$ sample are $Z \to \ell\ell$ events, in which one of the two leptons escapes detection, and $W \to \tau\nu$ events, where the τ decays to an electron or muon. These background contributions are estimated using the POWHEG+PYTHIA 8 samples after applying the modelling corrections discussed in Sect. 6, which include NNLO QCD corrections to the angular coefficients and rapidity distributions, and corrections to the vector-boson transverse momentum. The $Z \to ee$ background represents 2.9% of the $W^+ \to e\nu$ sample and 4.0% of the $W^- \to e\nu$ sample. In the muon channel, the $Z \to \mu\mu$ background represents 4.8 and 6.3% of the $W^+ \to \mu\nu$ and $W^- \to \mu\nu$ samples, respectively. The $W \to \tau\nu$ background represents 1.0% of the selected sample in both channels, and the $Z \to \tau\tau$ background contributes approximately 0.12%. The normalisation of these processes relative to the W-boson signal and the corresponding uncertainties are discussed in Sect. 4. A relative uncertainty of 0.2% is assigned to the normalisation of the $W \to \tau\nu$ samples with respect to the W-boson signal sample, to account for the uncertainty in the τ-lepton branching fractions to electrons and muons. In the determination of the W-boson mass, the variations of m_W are propagated to the $W \to \tau\nu$ background templates in the same way as for the signal.

Similarly, backgrounds involving top-quark (top-quark pairs and single top-quark) production, and boson-pair production are estimated using simulation, and normalisation uncertainties are assigned as discussed in Sect. 4. These processes represent 0.11 and 0.07% of the signal event selection, respectively.

Uncertainties in the distributions of the $W \to \tau\nu$ and $Z \to \ell\ell$ processes are described by the physics-modelling uncertainties discussed in Sect. 6, and are treated as fully correlated with the signal. Shape uncertainties for boson-pair production and top-quark production are considered negligible compared to the uncertainties in their cross sections, given the small contributions of these processes to the signal event selection.

10.2 Multijet background

Inclusive multijet production in strong-interaction processes constitutes a significant source of background. A fraction of multijet events contains semileptonic decays of bottom and charm hadrons to muons or electrons and neutrinos, and can pass the W-boson signal selection. In addition, inclusive jet production contributes to the background if one jet is misidentified as electron or muon, and sizeable missing transverse momentum is reconstructed in the event. In-flight decays of pions or kaons within the tracking region can mimic the W-boson signal in the muon channel. In the electron channel, events with photon conversions and hadrons misidentified as electrons can be selected as W-boson events. Due to the small selection probability for multijet events, their large production cross section, and the relatively complex modelling of the hadronisation processes, the multijet background contribution cannot be estimated precisely using simulation, and a data-driven method is used instead.

The estimation of the multijet background contribution follows similar procedures in the electron and muon decay channels, and relies on template fits to kinematic distributions in background-dominated regions. The analysis uses the distributions of $p_{\mathrm{T}}^{\mathrm{miss}}$, m_{T}, and the $p_{\mathrm{T}}^{\ell}/m_{\mathrm{T}}$ ratio, where jet-enriched regions are obtained by relaxing a subset of the signal event-selection requirements. The first kinematic region, denoted FR1, is defined by removing the $p_{\mathrm{T}}^{\mathrm{miss}}$ and m_{T} requirements from the event selection. A second kinematic region, FR2, is defined in the same way as FR1, but by also removing the requirement on u_{T}. Multijet background events, which tend to have smaller values of $p_{\mathrm{T}}^{\mathrm{miss}}$ and m_{T} than the signal, are enhanced by this selection. The $p_{\mathrm{T}}^{\ell}/m_{\mathrm{T}}$ distribution is sensitive to the angle between the p_{T}^{ℓ} and $p_{\mathrm{T}}^{\mathrm{miss}}$ vectors in the transverse plane. Whereas W-boson events are expected to peak at values of $p_{\mathrm{T}}^{\ell}/m_{\mathrm{T}} = 0.5$, relatively large tails are observed for multijet events.

Templates of the multijet background distributions for these observables are obtained from data by inverting the lepton energy-isolation requirements. Contamination of these control regions by electroweak and top production is estimated using simulation and subtracted. In the muon channel, the anti-isolation requirements are defined from the ratio of the scalar sum of the p_{T} of tracks in a cone of size $\Delta R < 0.2$ around the reconstructed muon to the muon p_{T}. The isolation variable $p_{\mathrm{T}}^{\mu,\mathrm{cone}}$, introduced in Sect. 5.1, is required to satisfy $c_1 < p_{\mathrm{T}}^{\mu,\mathrm{cone}}/p_{\mathrm{T}}^{\ell} < c_2$, where the anti-isolation boundaries c_1 and c_2 are varied as discussed below. In order to avoid overlap with the signal region, the lower boundary c_1 is always larger than 0.1. In the electron channel, the scalar sum of the p_{T} of tracks in a cone of size $\Delta R < 0.4$ around the reconstructed electron, defined as $p_{\mathrm{T}}^{e,\mathrm{cone}}$ in Sect. 5.1, is used to define the templates, while the requirements on the calorimeter isolation are omitted.

The multijet background normalisation is determined by fitting each of the $p_{\mathrm{T}}^{\mathrm{miss}}$, m_{T}, and $p_{\mathrm{T}}^{\ell}/m_{\mathrm{T}}$ distributions in the two kinematic regions FR1 and FR2, using templates of these distributions based on multijet events and obtained with several ranges of the anti-isolation variables. The multijet background in the signal region is determined by correcting the multijet fraction fitted in the FR1 and FR2 for the different

efficiencies of the selection requirements of the signal region. In the electron channel, c_1 is varied from 4 to 9 GeV in steps of 1 GeV, and c_2 is set to $c_2 = c_1 + 1$ GeV. In the muon channel, c_1 is varied from 0.1 to 0.37 in steps of 0.03, and c_2 is set to $c_2 = c_1 + 0.03$. Example results of template fits in the electron and muon channels are shown in Fig. 17. The results corresponding to the various observables and to the different kinematic regions are linearly extrapolated in the isolation variables to the signal regions, denoted by $c_1 = 0$. Figure 18 illustrates the extrapolation procedure.

The systematic uncertainty in the multijet background fraction is defined as half of the largest difference between the results extrapolated from the different kinematic regions and observables. The multijet background contribution is estimated separately in all measurement categories. In the electron channel, the multijet background fraction rises from $0.58 \pm 0.08\%$ at low $|\eta_\ell|$ to $1.73 \pm 0.19\%$ in the last measurement bin, averaging the W^+ and W^- channels. In the muon channel, the charge-averaged multijet background fraction decreases from $0.72 \pm 0.07\%$ to $0.49 \pm 0.03\%$, when going from low to high $|\eta_\ell|$. The uncertainties in the multijet background fractions are sufficient to account for the observed residual discrepancies between the fitted distributions and the data (see Fig. 17). The estimated multijet background yields are consistent between W^+ and W^-, but the multijet background fraction is smaller in the W^+ channels due to the higher signal yield.

Corrections to the shape of the multijet background contributions and corresponding uncertainties in the distributions used to measure the W-boson mass are estimated with a similar procedure. The kinematic distributions in the control regions are obtained for a set of anti-isolation ranges, and parameterised with linear functions of the lower bound of the anti-isolation requirement. The distributions are extrapolated to the signal regions accordingly. Uncertainties in the extrapolated distributions are dominated by the statistical uncertainty, which is determined with a toy MC method by fluctuating within their statistical uncertainty the bin contents of the histograms in the various anti-isolation ranges. The resulting multijet background distribution is propagated to the templates, and the standard deviation of the determined values of m_W yields the estimated uncertainty due to the shape of the multijet background. Uncertainties due to the choice of parameterisation are small in comparison and neglected.

Uncertainties in the normalisation of multijet, electroweak, and top-quark background processes are considered correlated across decay channels, boson charges and rapidity bins, whereas the uncertainty in the shape of multijet background is considered uncorrelated between decay channels and boson charges. The impact of the background systematic uncertainties on the determination of m_W is summarised in Table 8.

11 Measurement of the W-boson mass

This section presents the determination of the mass of the W boson from template fits to the kinematic distributions of the W-boson decay products. The final measured value is obtained from the combination of measurements performed using the lepton transverse momentum and transverse mass distributions in categories corresponding to the electron and muon decay channels, positively and negatively charged W bosons, and absolute pseudorapidity bins of the charged lepton, as illustrated in Table 1. The number of selected events in each category is shown in Table 9.

11.1 Control distributions

The detector calibration and the physics modelling are validated by comparing data with simulated W-boson signal and backgrounds for several kinematic distributions that are insensitive to the W-boson mass. The comparison is based on a χ^2 compatibility test, including statistical and systematic uncertainties, and the bin-to-bin correlations induced by the latter. The systematic uncertainty comprises all sources of experimental uncertainty related to the lepton and recoil calibration, and to the background subtraction, as well as sources of modelling uncertainty associated with electroweak corrections, or induced by the helicity fractions of vector-boson production, the vector-boson transverse-momentum distribution, and the PDFs. Comparisons of data and simulation for the η_ℓ, u_{T}, and $u_\parallel^\ell$ distributions, in positively and negatively charged W-boson events, are shown in Figs. 19 and 20 for the electron and muon decay channels, respectively.

Data and simulation agree within uncertainties for all distributions, as confirmed by the satisfactory χ^2/dof values. The effect of the residual discrepancies in the u_{T} distributions for $W^- \to \ell\nu$, visible at low values in Figs. 19d and 20d, is discussed in Sect. 11.5.

11.2 Data-driven check of the uncertainty in the p_{T}^W distribution

The uncertainty in the prediction of the $u_\parallel^\ell$ distribution is dominated by p_{T}^W distribution uncertainties, especially at negative values of $u_\parallel^\ell$ in the kinematic region corresponding to $u_\parallel^\ell < -15$ GeV. This is illustrated in Fig. 21, which compares the recoil distributions in the POWHEG+PYTHIA 8 and POWHEG+HERWIG 6 samples, before and after the corrections described in Sect. 8.2 (the p_{T}^W distribution predicted by POWHEG+PYTHIA 8 is not reweighted to that of POWHEG+HERWIG 6). As can be seen, the recoil corrections and the different p_{T}^W distributions have a comparable effect on the u_{T} distribution. In contrast, the effect of the recoil corrections is small at negative values of $u_\parallel^\ell$, whereas the

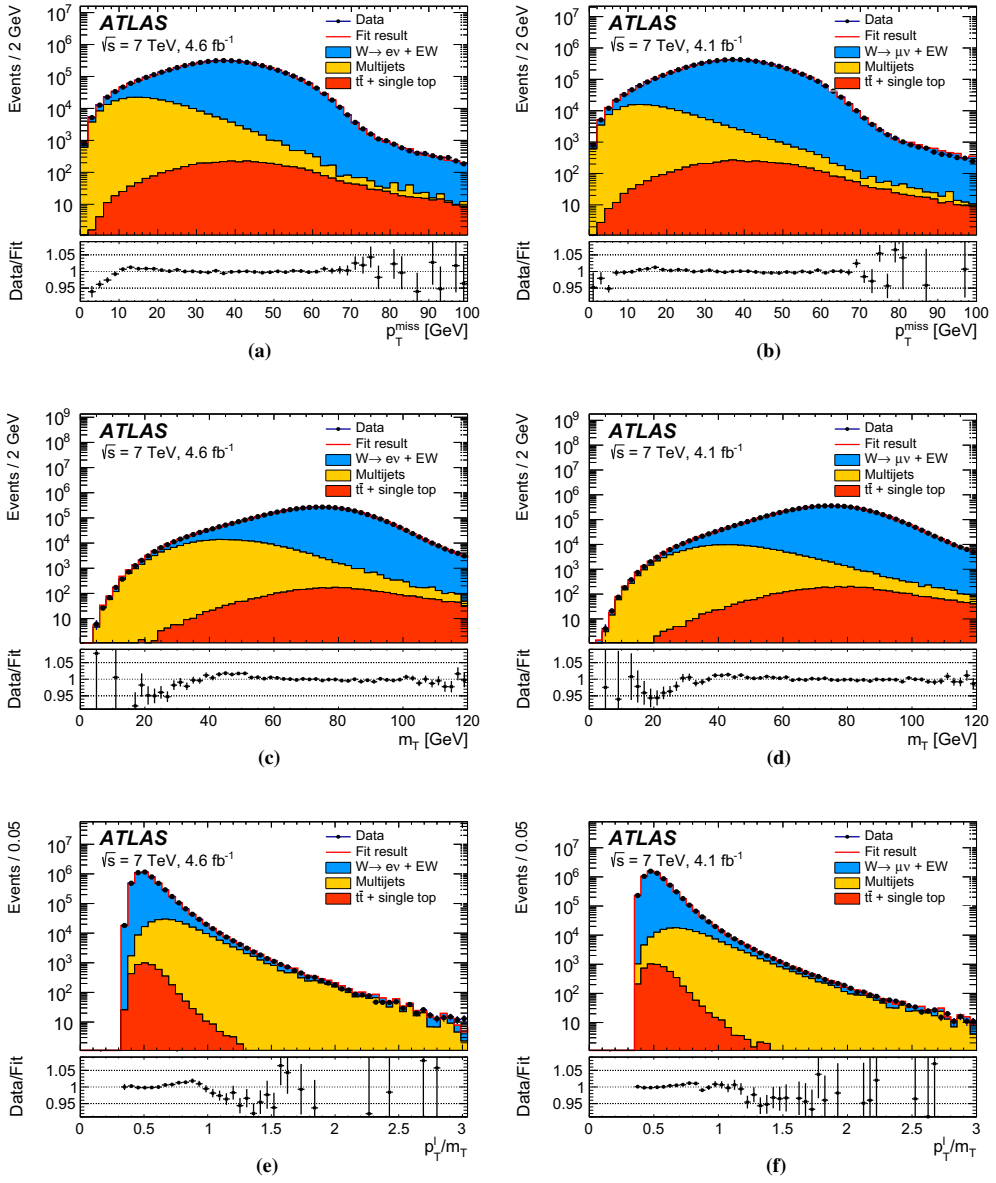

Fig. 17 Example template fits to the **a**, **b** $p_{\mathrm{T}}^{\mathrm{miss}}$, **c**, **d** m_{T}, and **e**, **f** $p_{\mathrm{T}}^{\ell}/m_{\mathrm{T}}$ distributions in the FR1 kinematic region, in the **a**, **c**, **e** electron and **b**, **d**, **f** muon decay channels. Multijet templates are derived from the data requiring $4\,\mathrm{GeV} < p_{\mathrm{T}}^{e,\mathrm{cone}} < 8\,\mathrm{GeV}$ in the electron channel, and $0.2 < p_{\mathrm{T}}^{\mu,\mathrm{cone}}/p_{\mathrm{T}}^{\ell} < 0.4$ in the muon channel. The data are compared to the simulation including signal and background contributions

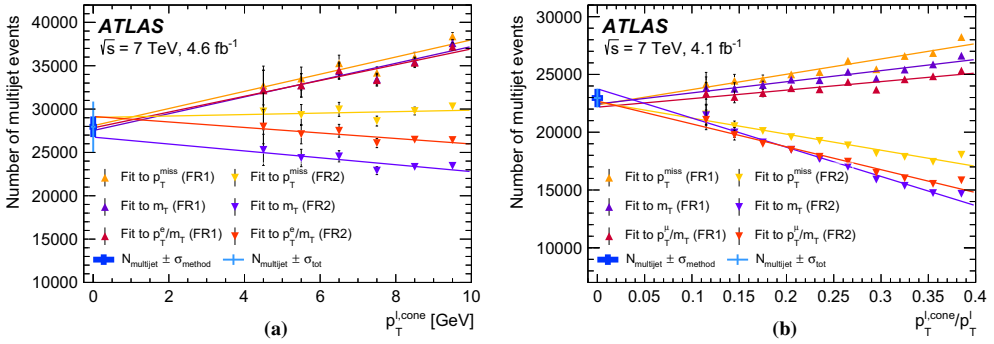

Fig. 18 Estimated number of multijet-background events as a function of the lower bound of the isolation-variable range used to define the control regions, for **a** electron and **b** muon decay channel. The estimation is performed for the two regions FR1 and FR2 and three distributions $p_{\mathrm{T}}^{\mathrm{miss}}$, m_{T}, and $p_{\mathrm{T}}^{\ell}/m_{\mathrm{T}}$, as described in the text. The linear extrapolations are indicated by the solid lines. The thick crosses show the results of the linear extrapolation of the background estimate to the signal region, including uncertainties from the extrapolation only. The thin crosses also include the uncertainty induced by the contamination of the control regions by EW and top-quark processes

Table 8 Systematic uncertainties in the m_W measurement due to electroweak, top-quark, and multijet background estimation, for fits to the p_{T}^{ℓ} and m_{T} distributions, in the electron and muon decay channels, with positively and negatively charged W bosons

Kinematic distribution	p_{T}^{ℓ}				m_{T}			
Decay channel	$W \to e\nu$		$W \to \mu\nu$		$W \to e\nu$		$W \to \mu\nu$	
W-boson charge	W^+	W^-	W^+	W^-	W^+	W^-	W^+	W^-
δm_W [MeV]								
$W \to \tau\nu$ (fraction, shape)	0.1	0.1	0.1	0.2	0.1	0.2	0.1	0.3
$Z \to ee$ (fraction, shape)	3.3	4.8	–	–	4.3	6.4	–	–
$Z \to \mu\mu$ (fraction, shape)	–	–	3.5	4.5	–	–	4.3	5.2
$Z \to \tau\tau$ (fraction, shape)	0.1	0.1	0.1	0.2	0.1	0.2	0.1	0.3
WW, WZ, ZZ (fraction)	0.1	0.1	0.1	0.1	0.4	0.4	0.3	0.4
Top (fraction)	0.1	0.1	0.1	0.1	0.3	0.3	0.3	0.3
Multijet (fraction)	3.2	3.6	1.8	2.4	8.1	8.6	3.7	4.6
Multijet (shape)	3.8	3.1	1.6	1.5	8.6	8.0	2.5	2.4
Total	6.0	6.8	4.3	5.3	12.6	13.4	6.2	7.4

Table 9 Numbers of selected W^+ and W^- events in the different decay channels in data, inclusively and for the various $|\eta_\ell|$ categories

$\lvert\eta_\ell\rvert$ range	0–0.8	0.8–1.4	1.4–2.0	2.0–2.4	Inclusive
$W^+ \to \mu^+\nu$	1 283 332	1 063 131	1 377 773	885 582	4 609 818
$W^- \to \mu^-\bar{\nu}$	1 001 592	769 876	916 163	547 329	3 234 960
$\lvert\eta_\ell\rvert$ range	0–0.6	0.6–1.2		1.8–2.4	Inclusive
$W^+ \to e^+\nu$	1 233 960	1 207 136		956 620	3 397 716
$W^- \to e^-\bar{\nu}$	969 170	908 327		610 028	2 487 525

difference in the p_{T}^{W} distributions has a large impact in this region.

The sensitivity of the $u_{\parallel}^{\ell}$ distribution is exploited to validate the modelling of the p_{T}^{W} distribution by PYTHIA 8 AZ, and its theory-driven uncertainty, described in Sect. 6.5.2, with a data-driven procedure. The parton-shower factorisation scale μ_{F} associated with the $c\bar{q} \to W$ processes constitutes the main source of uncertainty in the modelling of the p_{T}^{W} distribution. Variations of the $u_{\parallel}^{\ell}$ distribution induced by changes in the factorisation scale of the $c\bar{q} \to W$ processes are parameterised and fitted to the data. The $u_{\parallel}^{\ell}$ distribution is predicted for the two boundary values of μ_{F}, and assumed to vary linearly as a function of μ_{F}. Variations induced by changes in μ_{F} are parameterised using a variable

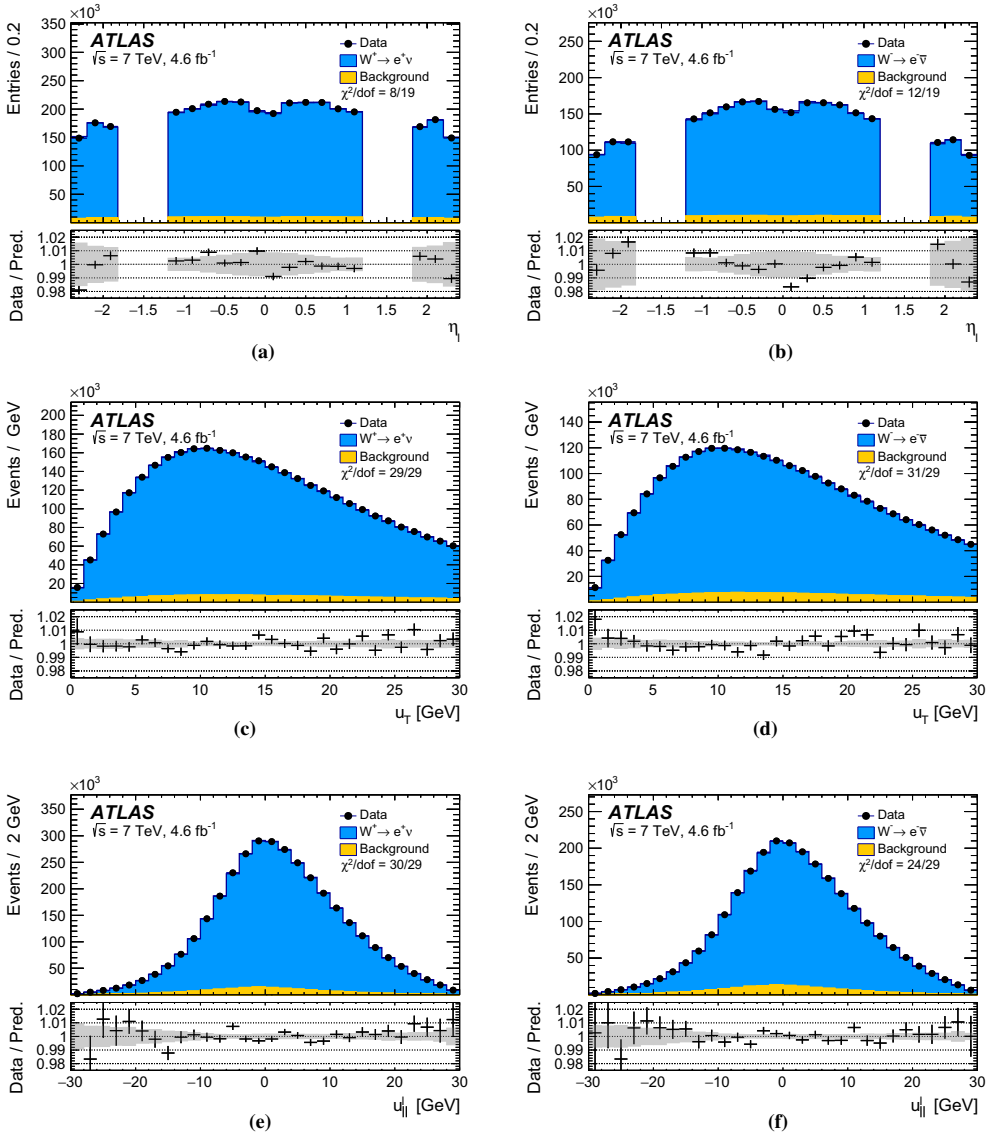

Fig. 19 The **a**, **b** η_ℓ, (c,d) u_{T}, and **e**, **f** $u^{\ell}_{\parallel}$ distributions for **a**, **c**, **e** W^+ events and **b**, **d**, **f** W^- events in the electron decay channel. The data are compared to the simulation including signal and background contributions. Detector calibration and physics-modelling corrections are applied to the simulated events. The lower panels show the data-to-prediction ratios, the error bars show the statistical uncertainty, and the band shows the systematic uncertainty of the prediction. The χ^2 values displayed in each figure account for all sources of uncertainty and include the effects of bin-to-bin correlations induced by the systematic uncertainties

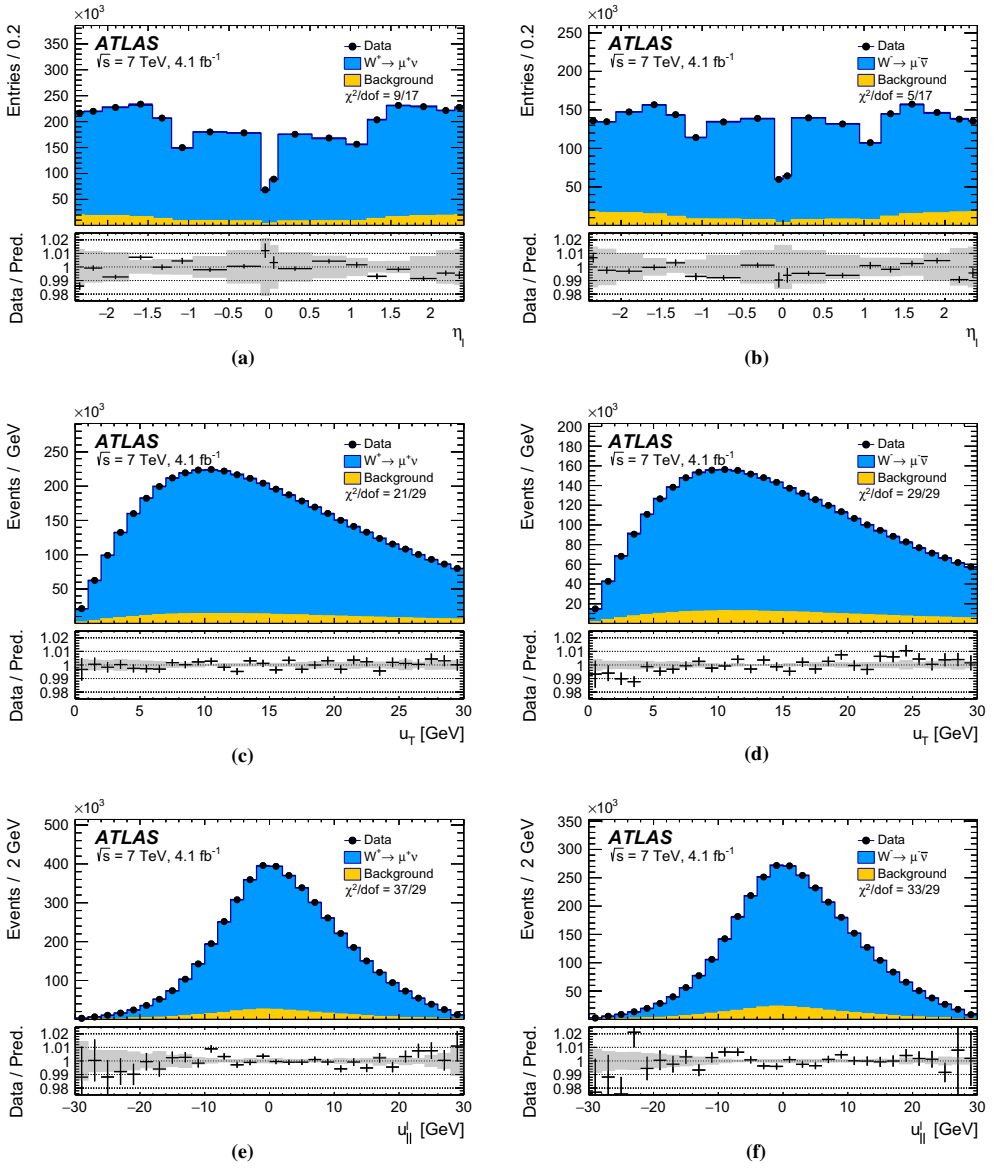

Fig. 20 The **a**, **b** η_ℓ, (c,d) u_{T}, and **e**, **f** $u_{\parallel}^{\ell}$ distributions for **a**, **c**, **e** W^+ events and **b**, **d**, **f** W^- events in the muon decay channel. The data are compared to the simulation including signal and background contributions. Detector calibration and physics-modelling corrections are applied to the simulated events. The lower panels show the data-to-prediction ratios, the error bars show the statistical uncertainty, and the band shows the systematic uncertainty of the prediction. The χ^2 values displayed in each figure account for all sources of uncertainty and include the effects of bin-to-bin correlations induced by the systematic uncertainties

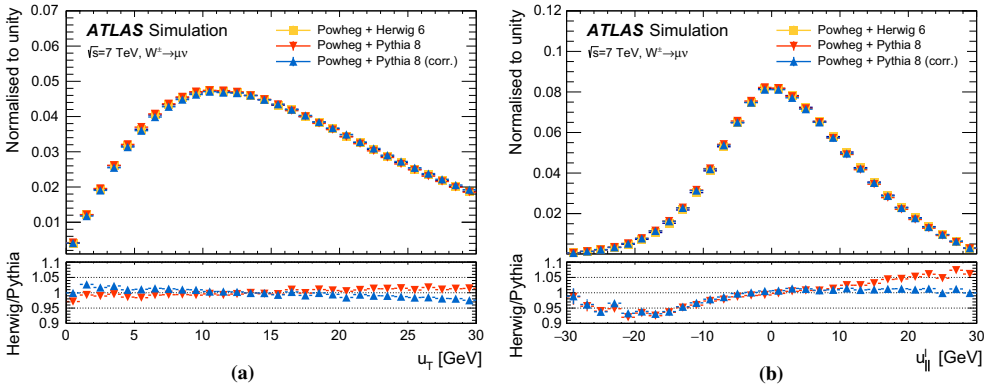

Fig. 21 Distributions of **a** u_{T} and **b** $u_{\parallel}^{\ell}$ in $W \to \mu\nu$ events simulated using POWHEG+PYTHIA 8 and POWHEG+HERWIG 6 after all analysis selection cuts are applied. The POWHEG+PYTHIA 8 distributions are shown before and after correction of the recoil response to that of POWHEG+HERWIG 6. The lower panels show the ratios of POWHEG+HERWIG 6 to POWHEG+PYTHIA 8, with and without the recoil response correction in the POWHEG+PYTHIA 8 sample. The discrepancy remaining after recoil corrections reflects the different p_{T}^{W} distributions

s defined in units of the initially allowed range, i.e. values of $s = -1, 0, +1$ correspond to half the effect[3] of changing from $\mu_{\mathrm{F}} = m_V$ to $\mu_{\mathrm{F}} = m_V/2, m_V, 2m_V$ respectively. The optimal value of s is determined by fitting the fraction of events in the kinematic region $-30 < u_{\parallel}^{\ell} < -15$ GeV. The fit accounts for all experimental and modelling uncertainties affecting the $u_{\parallel}^{\ell}$ distribution, and gives a value of $s = -0.22 \pm 1.06$. The best-fit value of s confirms the good agreement between the the PYTHIA 8 AZ prediction and the data; its uncertainty is dominated by PDF and recoil-calibration uncertainties, and matches the variation range of μ_{F} used for the initial estimation of the p_{T}^{W} distribution uncertainty.

This validation test supports the PYTHIA 8 AZ prediction of the p_{T}^{W} distribution and the theory-driven associated uncertainty estimate. On the other hand, as shown in Fig. 22, the data disagree with the DYRes and POWHEG MINLO+PYTHIA 8 predictions. The latter are obtained reweighting the initial p_{T}^{W} distribution in POWHEG+PYTHIA 8 according to the product of the p_{T}^{Z} distribution of PYTHIA 8 AZ, which matches the measurement of Ref. [44], and $R_{W/Z}(p_{\mathrm{T}})$ as predicted by DYRes and POWHEG MINLO+PYTHIA 8. The uncertainty bands in the DYRes prediction are calculated using variations of the factorisation, renormalisation and resummation scales μ_{F}, μ_{R} and μ_{Res} following the procedure described in Ref. [116,117]. The uncertainty obtained applying correlated scale variations in W and Z production does not cover the observed difference with the data. The potential effect of using $R_{W/Z}(p_{\mathrm{T}})$ as predicted by DYRes instead of PYTHIA 8 AZ for the determination of m_W is discussed in Sect. 11.5.

[3] Half the effect is used because only one of the two quarks in the initial state is heavy, as discussed in Sect. 6.5.2.

11.3 Results for m_W in the measurement categories

Measurements of m_W are performed using the p_{T}^{ℓ} and m_{T} distributions, separately for positively and negatively charged W bosons, in three bins of $|\eta_\ell|$ in the electron decay channel, and in four bins of $|\eta_\ell|$ in the muon decay channel, leading to a total of 28 m_W determinations. In each category, the value of m_W is determined by a χ^2 minimisation, comparing the p_{T}^{ℓ} and m_{T} distributions in data and simulation for different values of m_W. The templates are generated with values of m_W in steps of 1 to 10 MeV within a range of $\pm$ 400 MeV, centred around the reference value used in the Monte Carlo signal samples. The statistical uncertainty is estimated from the half width of the χ^2 function at the value corresponding to one unit above the minimum. Systematic uncertainties due to physics-modelling corrections, detector-calibration corrections, and background subtraction, are discussed in Sects. 6–8 and 10, respectively.

The lower and upper bounds of the range of the p_{T}^{ℓ} distribution used in the fit are varied from 30 to 35 GeV, and from 45 to 50 GeV respectively, in steps of 1 GeV. For the m_{T} distribution, the boundaries are varied from 65 to 70 GeV, and from 90 to 100 GeV. The total measurement uncertainty is evaluated for each range, after combining the measurement categories as described in Sect. 11.4 below. The

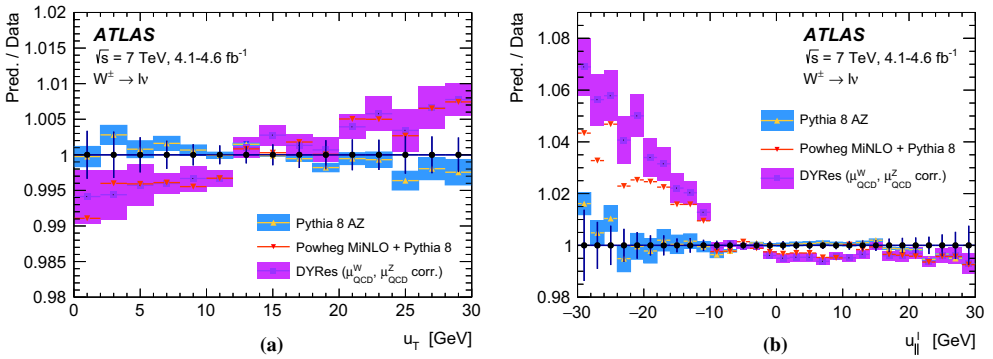

Fig. 22 Ratio between the predictions of PYTHIA 8 AZ, DYRes and POWHEG MiNLO+PYTHIA 8 and the data for the **a** u_{T} and **b** $u_{\parallel}^{\ell}$ distributions in $W \to \ell\nu$ events. The W-boson rapidity distribution is reweighted according to the NNLO prediction. The error bars on the data points display the total experimental uncertainty, and the band around the PYTHIA 8 AZ prediction reflects the uncertainty in the p_{T}^{W} distribution. The uncertainty band around the DYRes prediction assumes that uncertainties induced by variations of the QCD scales μ_{F}, μ_{R} and μ_{Res}, collectively referred to as μ_{QCD}, are fully correlated in W and Z production

smallest total uncertainty in m_W is found for the fit ranges $32 < p_{\mathrm{T}}^{\ell} < 45$ GeV and $66 < m_{\mathrm{T}} < 99$ GeV. The optimisation is performed before the unblinding of the m_W value and the optimised range is used for all the results described below.

The final measurement uncertainty is dominated by modelling uncertainties, with typical values in the range 25–35 MeV for the various charge and $|\eta_\ell|$ categories. Lepton-calibration uncertainties are the dominant sources of experimental systematic uncertainty for the extraction of m_W from the p_{T}^{ℓ} distribution. These uncertainties vary from about 15 MeV to about 35 MeV for most measurement categories, except the highest $|\eta|$ bin in the muon channel where the total uncertainty of about 120 MeV is dominated by the muon momentum linearity uncertainty. The uncertainty in the calibration of the recoil is the largest source of experimental systematic uncertainty for the m_{T} distribution, with a typical contribution of about 15 MeV for all categories. The determination of m_W from the p_{T}^{ℓ} and m_{T} distributions in the various categories is summarised in Table 10, including an overview of statistical and systematic uncertainties. The results are also shown in Fig. 23. No significant differences in the values of m_W corresponding to the different decay channels and to the various charge and $|\eta_\ell|$ categories are observed.

The comparison of data and simulation for kinematic distributions sensitive to the value of m_W provides further validation of the detector calibration and physics modelling. The comparison is performed in all measurement categories. The η-inclusive p_{T}^{ℓ}, m_{T} and $p_{\mathrm{T}}^{\mathrm{miss}}$ distributions for positively and negatively charged W bosons are shown in Figs. 24 and 25 for the electron and muon decay channels, respectively. The value of m_W used in the predictions is set to the overall measurement result presented in the next section. The χ^2 values quantifying the comparison between data and prediction are calculated over the full histogram range and account for all sources of uncertainty. The bin-to-bin correlations induced by the experimental and physics-modelling systematic uncertainties are also accounted for. Overall, satisfactory agreement is observed. The deficit of data visible for $p_{\mathrm{T}}^{\ell} \sim 40$–42 GeV in the $W^+ \to e\nu$ channel does not strongly affect the mass measurement, as the observed effect differs from that expected from m_W variations. Cross-checks of possible sources of this effect were performed, and its impact on the mass determination was shown to be within the corresponding systematic uncertainties.

11.4 Combination and final results

The measurements of m_W in the various categories are combined accounting for statistical and systematic uncertainties and their correlations. The statistical correlation of the m_W values determined from the p_{T}^{ℓ} and m_{T} distributions is evaluated with the bootstrap method [118], and is approximately 50% for all measurement categories.

The systematic uncertainties have specific correlation patterns across the m_W measurement categories. Muon-momentum and electron-energy calibration uncertainties are uncorrelated between the different decay channels, but largely correlated between the p_{T}^{ℓ} and m_{T} distributions. Recoil-calibration uncertainties are correlated between electron and muon decay channels, and they are small for p_{T}^{ℓ} distributions. The PDF-induced uncertainties are largely cor-

Table 10 Results of the m_W measurements in the electron and muon decay channels, for positively and negatively charged W bosons, in different lepton-$|\eta|$ ranges, using the m_{TT} and p_{T}^{ℓ} distributions in the optimised fitting range. The table shows the statistical uncertainties, together with all experimental uncertainties, divided into muon-, electron-, recoil- and background-related uncertainties, and all modelling uncertainties, separately for QCD modelling including scale variations, parton shower and angular coefficients, electroweak corrections, and PDFs. All uncertainties are given in MeV

Channel (m_{TT} fits)	m_W [MeV]	Stat. Unc.	Muon Unc.	Elec. Unc.	Recoil Unc.	Bckg. Unc.	QCD Unc.	EW Unc.	PDF Unc.	Total Unc.
$W^+ \to \mu\nu$, $\lvert\eta\rvert < 0.8$	80371.3	29.2	12.4	0.0	15.2	8.1	9.9	3.4	28.4	47.1
$W^+ \to \mu\nu$, $0.8 < \lvert\eta\rvert < 1.4$	80354.1	32.1	19.3	0.0	13.0	6.8	9.6	3.4	23.3	47.6
$W^+ \to \mu\nu$, $1.4 < \lvert\eta\rvert < 2.0$	80426.3	30.2	35.1	0.0	14.3	7.2	9.3	3.4	27.2	56.9
$W^+ \to \mu\nu$, $2.0 < \lvert\eta\rvert < 2.4$	80334.6	40.9	112.4	0.0	14.4	9.0	8.4	3.4	32.8	125.5
$W^- \to \mu\nu$, $\lvert\eta\rvert < 0.8$	80375.5	30.6	11.6	0.0	13.1	8.5	9.5	3.4	30.6	48.5
$W^- \to \mu\nu$, $0.8 < \lvert\eta\rvert < 1.4$	80417.5	36.4	18.5	0.0	12.2	7.7	9.7	3.4	22.2	49.7
$W^- \to \mu\nu$, $1.4 < \lvert\eta\rvert < 2.0$	80379.4	35.6	33.9	0.0	10.5	8.1	9.7	3.4	23.1	56.9
$W^- \to \mu\nu$, $2.0 < \lvert\eta\rvert < 2.4$	80334.2	52.4	123.7	0.0	11.6	10.2	9.9	3.4	34.1	139.9
$W^+ \to e\nu$, $\lvert\eta\rvert < 0.6$	80352.9	29.4	0.0	19.5	13.1	15.3	9.9	3.4	28.5	50.8
$W^+ \to e\nu$, $0.6 < \lvert\eta\rvert < 1.2$	80381.5	30.4	0.0	21.4	15.1	13.2	9.6	3.4	23.5	49.4
$W^+ \to e\nu$, $1.8 < \lvert\eta\rvert < 2.4$	80352.4	32.4	0.0	26.6	16.4	32.8	8.4	3.4	27.3	62.6
$W^- \to e\nu$, $\lvert\eta\rvert < 0.6$	80415.8	31.3	0.0	16.4	11.8	15.5	9.5	3.4	31.3	52.1
$W^- \to e\nu$, $0.6 < \lvert\eta\rvert < 1.2$	80297.5	33.0	0.0	18.7	11.2	12.8	9.7	3.4	23.9	49.0
$W^- \to e\nu$, $1.8 < \lvert\eta\rvert < 2.4$	80423.8	42.8	0.0	33.2	12.8	35.1	9.9	3.4	28.1	72.3
Channel (p_{T}^{ℓ} fits)										
$W^+ \to \mu\nu$, $\lvert\eta\rvert < 0.8$	80327.7	22.1	12.2	0.0	2.6	5.1	9.0	6.0	24.7	37.3
$W^+ \to \mu\nu$, $0.8 < \lvert\eta\rvert < 1.4$	80357.3	25.1	19.1	0.0	2.5	4.7	8.9	6.0	20.6	39.5
$W^+ \to \mu\nu$, $1.4 < \lvert\eta\rvert < 2.0$	80446.9	23.9	33.1	0.0	2.5	4.9	8.2	6.0	25.2	49.3
$W^+ \to \mu\nu$, $2.0 < \lvert\eta\rvert < 2.4$	80334.1	34.5	110.1	0.0	2.5	6.4	6.7	6.0	31.8	120.2
$W^- \to \mu\nu$, $\lvert\eta\rvert < 0.8$	80427.8	23.3	11.6	0.0	2.6	5.8	8.1	6.0	26.4	39.0
$W^- \to \mu\nu$, $0.8 < \lvert\eta\rvert < 1.4$	80395.6	27.9	18.3	0.0	2.5	5.6	8.0	6.0	19.8	40.5
$W^- \to \mu\nu$, $1.4 < \lvert\eta\rvert < 2.0$	80380.6	28.1	35.2	0.0	2.6	5.6	8.0	6.0	20.6	50.9
$W^- \to \mu\nu$, $2.0 < \lvert\eta\rvert < 2.4$	80315.2	45.5	116.1	0.0	2.6	7.6	8.3	6.0	32.7	129.6
$W^+ \to e\nu$, $\lvert\eta\rvert < 0.6$	80336.5	22.2	0.0	20.1	2.5	6.4	9.0	5.3	24.5	40.7
$W^+ \to e\nu$, $0.6 < \lvert\eta\rvert < 1.2$	80345.8	22.8	0.0	21.4	2.6	6.7	8.9	5.3	20.5	39.4
$W^+ \to e\nu$, $1.8 < \lvert\eta\rvert < 2.4$	80344.7	24.0	0.0	30.8	2.6	11.9	6.7	5.3	24.1	48.2
$W^- \to e\nu$, $\lvert\eta\rvert < 0.6$	80351.0	23.1	0.0	19.8	2.6	7.2	8.1	5.3	26.6	42.2
$W^- \to e\nu$, $0.6 < \lvert\eta\rvert < 1.2$	80309.8	24.9	0.0	19.7	2.7	7.3	8.0	5.3	20.9	39.9
$W^- \to e\nu$, $1.8 < \lvert\eta\rvert < 2.4$	80413.4	30.1	0.0	30.7	2.7	11.5	8.3	5.3	22.7	51.0

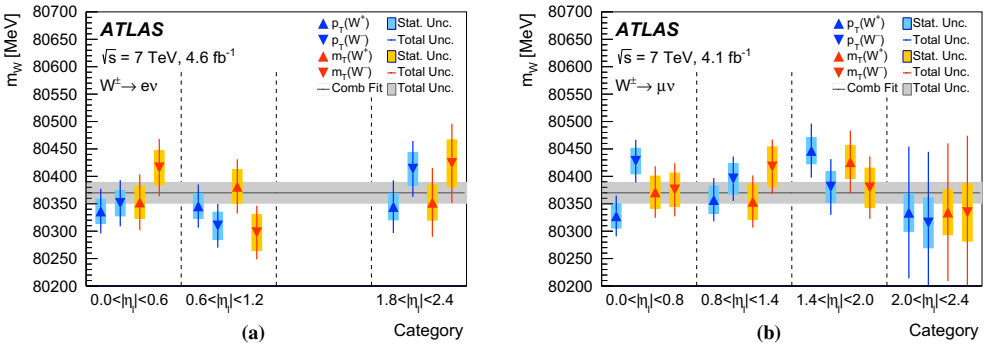

Fig. 23 Overview of the m_W measurements in the **a** electron and **b** muon decay channels. Results are shown for the p_{T}^{ℓ} and m_{T} distributions, for W^+ and W^- events in the different $|\eta_\ell|$ categories. The coloured bands and solid lines show the statistical and total uncertainties, respectively. The horizontal line and band show the fully combined result and its uncertainty

related between electron and muon decay channels, but significantly anti-correlated between positively and negatively charged W bosons, as discussed in Sect. 6. Due to the different balance of systematic uncertainties and to the variety of correlation patterns, a significant reduction of the uncertainties in the measurement of m_W is achieved by combining the different decay channels and the charge and $|\eta_\ell|$ categories.

As discussed in Sect. 2, the comparison of the results from the p_{T}^{ℓ} and m_{T} distributions, from the different decay channels, and in the various charge and $|\eta_\ell|$ categories, provides a test of the experimental and physics modelling corrections. Discrepancies between the positively and negatively charged lepton categories, or in the various $|\eta_\ell|$ bins would primarily indicate an insufficient understanding of physics-modelling effects, such as the PDFs and the p_{T}^{W} distribution. Inconsistencies between the electron and muon channels could indicate problems in the calibration of the muon-momentum and electron-energy responses. Significant differences between results from the p_{T}^{ℓ} and m_{T} distributions would point to either problems in the calibration of the recoil, or to an incorrect modelling of the transverse-momentum distribution of the W boson. Several measurement combinations are performed, using the best linear unbiased estimate (BLUE) method [119,120]. The results of the combinations are verified with the `HERAverager` program [121], which gives very close results.

Table 11 shows an overview of partial m_W measurement combinations. In the first step, determinations of m_W in the electron and muon decay channels from the m_{T} distribution are combined separately for the positive- and negative-charge categories, and together for both W-boson charges. The results are compatible, and the positively charged, negatively charged, and charge-inclusive combinations yield values of χ^2/dof corresponding to 2/6, 7/6, and 11/13, respectively. Compatibility of the results is also observed for the corresponding combinations from the p_{T}^{ℓ} distribution, with values of χ^2/dof of 5/6, 10/6, and 19/13, for positively charged, negatively charged, and charge-inclusive combinations, respectively. The χ^2 compatibility test validates the consistency of the results in the $W \to e\nu$ and $W \to \mu\nu$ decay channels. The precision of the determination of m_W from the m_{T} distribution is slightly worse than the result obtained from the p_{T}^{ℓ} distribution, due to the larger uncertainty induced by the recoil calibration. In addition, the impact of PDF- and p_{T}^{W}-related uncertainties on the p_{T}^{ℓ} fits is limited by the optimisation of the fitting range. In the second step, determinations of m_W from the p_{T}^{ℓ} and m_{T} distributions are combined separately for the electron and the muon decay channels. The results are compatible, with values of χ^2/dof of 4/5 and 8/5 in the electron channel for the p_{T}^{ℓ} and m_{T} distributions, respectively, and values of 7/7 and 3/7 in the muon channel for the p_{T}^{ℓ} and m_{T} distributions, respectively. The m_W determinations in the electron and in the muon channels agree, further validating the consistency of the electron and muon calibrations. Agreement between the m_W determinations from the p_{T}^{ℓ} and m_{T} distributions supports the calibration of the recoil, and the modelling of the transverse momentum of the W boson.

The results are summarised in Fig. 26. The combination of all the determinations of m_W reported in Table 10 has a value of χ^2/dof of 29/27, and yields a final result of

$$\begin{aligned} m_W &= 80369.5 \pm 6.8(\text{stat.}) \pm 10.6(\text{exp. syst.}) \\ &\quad \pm 13.6(\text{mod. syst.})\,\text{MeV} \\ &= 80369.5 \pm 18.5\,\text{MeV}, \end{aligned}$$

where the first uncertainty is statistical, the second corresponds to the experimental systematic uncertainty, and the

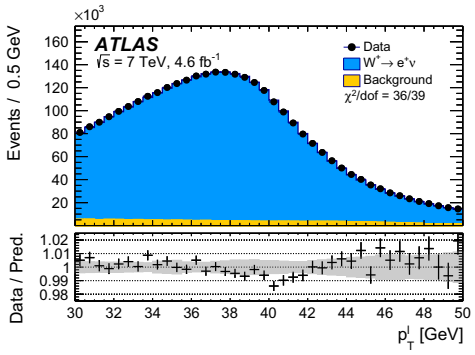

(a)

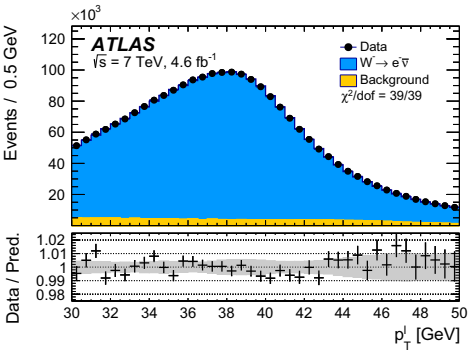

(b)

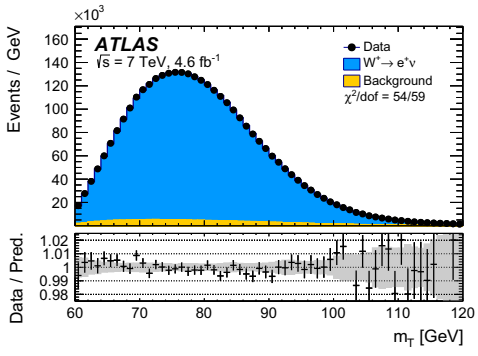

(c)

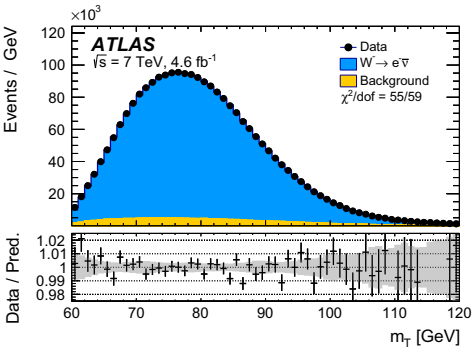

(d)

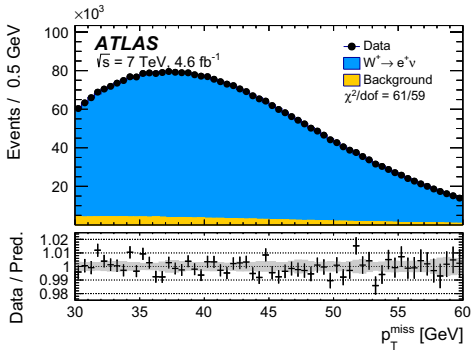

(e)

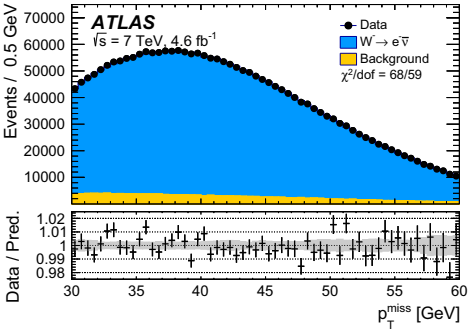

(f)

Fig. 24 The **a**, **b** p_{T}^{ℓ}, **c**, **d** m_{T}, and **e**, **f** $p_{\mathrm{T}}^{\mathrm{miss}}$ distributions for **a**, **c**, **e** W^+ events and **b**, **d**, **f** W^- events in the electron decay channel. The data are compared to the simulation including signal and background contributions. Detector calibration and physics-modelling corrections are applied to the simulated events. For all simulated distributions, m_W is set according to the overall measurement result. The lower panels show the data-to-prediction ratios, the error bars show the statistical uncertainty, and the band shows the systematic uncertainty of the prediction. The χ^2 values displayed in each figure account for all sources of uncertainty and include the effects of bin-to-bin correlations induced by the systematic uncertainties

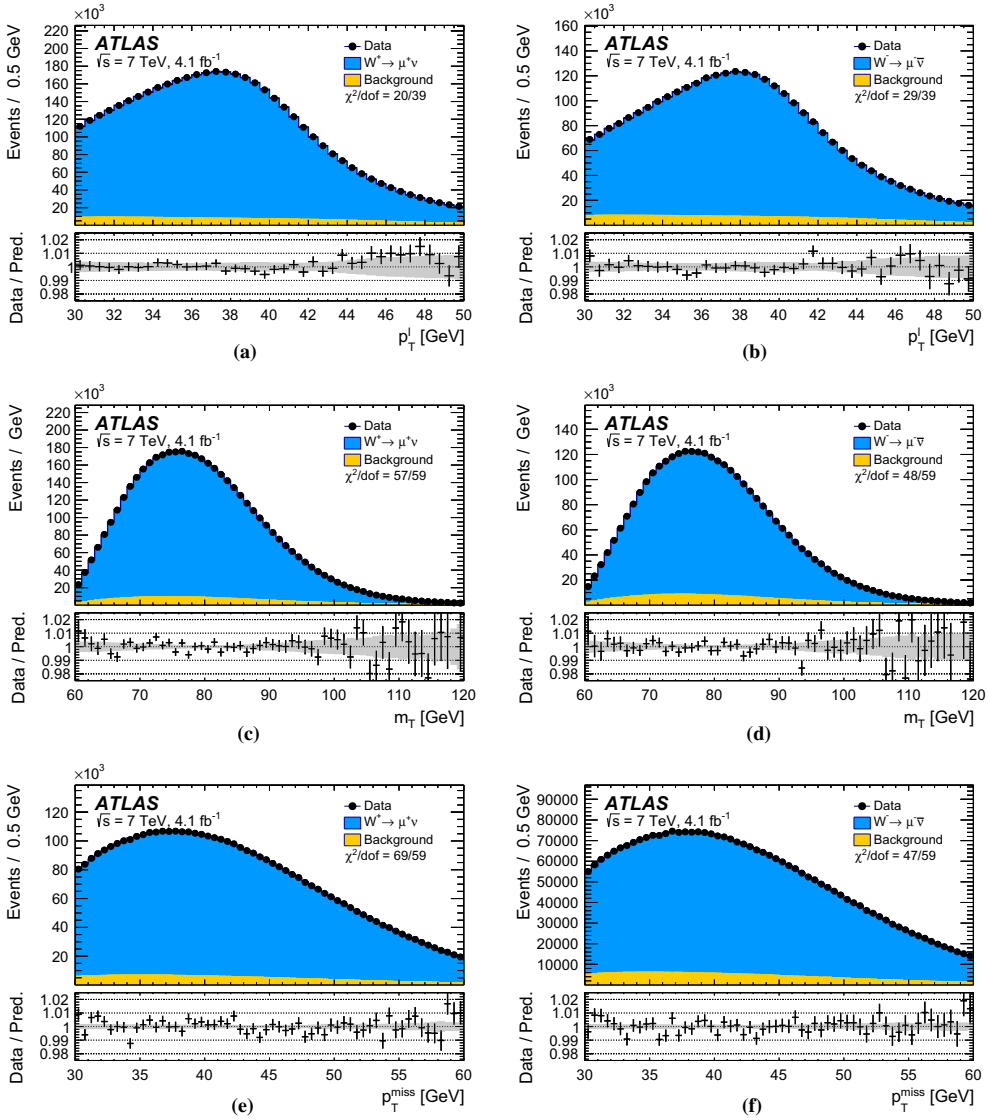

Fig. 25 The **a**, **b** p_{T}^{ℓ}, **c**, **d** m_{T}, and **e**, **f** $p_{\mathrm{T}}^{\mathrm{miss}}$ distributions for **a**, **c**, **e** W^+ events and **b**, **d**, **f** W^- events in the muon decay channel. The data are compared to the simulation including signal and background contributions. Detector calibration and physics-modelling corrections are applied to the simulated events. For all simulated distributions, m_W is set according to the overall measurement result. The lower panels show the data-to-prediction ratios, the error bars show the statistical uncertainty, and the band shows the systematic uncertainty of the prediction. The χ^2 values displayed in each figure account for all sources of uncertainty and include the effects of bin-to-bin correlations induced by the systematic uncertainties

Table 11 Results of the m_W measurements for various combinations of categories. The table shows the statistical uncertainties, together with all experimental uncertainties, divided into muon-, electron-, recoil- and background-related uncertainties, and all modelling uncertainties, separately for QCD modelling including scale variations, parton shower and angular coefficients, electroweak corrections, and PDFs. All uncertainties are given in MeV

Combined categories	m_W [MeV]	Stat. Unc.	Muon Unc.	Elec. Unc.	Recoil Unc.	Bckg. Unc.	QCD Unc.	EW Unc.	PDF Unc.	Total Unc.	χ^2/dof
m_T, W^+, e-μ	80370.0	12.3	8.3	6.7	14.5	9.7	9.4	3.4	16.9	30.9	2/6
m_T, W^-, e-μ	80381.1	13.9	8.8	6.6	11.8	10.2	9.7	3.4	16.2	30.5	7/6
m_T, $W^\pm$, e-μ	80375.7	9.6	7.8	5.5	13.0	8.3	9.6	3.4	10.2	25.1	11/13
p_T^ℓ, W^+, e-μ	80352.0	9.6	6.5	8.4	2.5	5.2	8.3	5.7	14.5	23.5	5/6
p_T^ℓ, W^-, e-μ	80383.4	10.8	7.0	8.1	2.5	6.1	8.1	5.7	13.5	23.6	10/6
p_T^ℓ, $W^\pm$, e-μ	80369.4	7.2	6.3	6.7	2.5	4.6	8.3	5.7	9.0	18.7	19/13
p_T^ℓ, $W^\pm$, e	80347.2	9.9	0.0	14.8	2.6	5.7	8.2	5.3	8.9	23.1	4/5
m_T, $W^\pm$, e	80364.6	13.5	0.0	14.4	13.2	12.8	9.5	3.4	10.2	30.8	8/5
m_T-p_T^ℓ, W^+, e	80345.4	11.7	0.0	16.0	3.8	7.4	8.3	5.0	13.7	27.4	1/5
m_T-p_T^ℓ, W^-, e	80359.4	12.9	0.0	15.1	3.9	8.5	8.4	4.9	13.4	27.6	8/5
m_T-p_T^ℓ, $W^\pm$, e	80349.8	9.0	0.0	14.7	3.3	6.1	8.3	5.1	9.0	22.9	12/11
p_T^ℓ, $W^\pm$, μ	80382.3	10.1	10.7	0.0	2.5	3.9	8.4	6.0	10.7	21.4	7/7
m_T, $W^\pm$, μ	80381.5	13.0	11.6	0.0	13.0	6.0	9.6	3.4	11.2	27.2	3/7
m_T-p_T^ℓ, W^+, μ	80364.1	11.4	12.4	0.0	4.0	4.7	8.8	5.4	17.6	27.2	5/7
m_T-p_T^ℓ, W^-, μ	80398.6	12.0	13.0	0.0	4.1	5.7	8.4	5.3	16.8	27.4	3/7
m_T-p_T^ℓ, $W^\pm$, μ	80382.0	8.6	10.7	0.0	3.7	4.3	8.6	5.4	10.9	21.0	10/15
m_T-p_T^ℓ, W^+, e-μ	80352.7	8.9	6.6	8.2	3.1	5.5	8.4	5.4	14.6	23.4	7/13
m_T-p_T^ℓ, W^-, e-μ	80383.6	9.7	7.2	7.8	3.3	6.6	8.3	5.3	13.6	23.4	15/13
m_T-p_T^ℓ, $W^\pm$, e-μ	80369.5	6.8	6.6	6.4	2.9	4.5	8.3	5.5	9.2	18.5	29/27

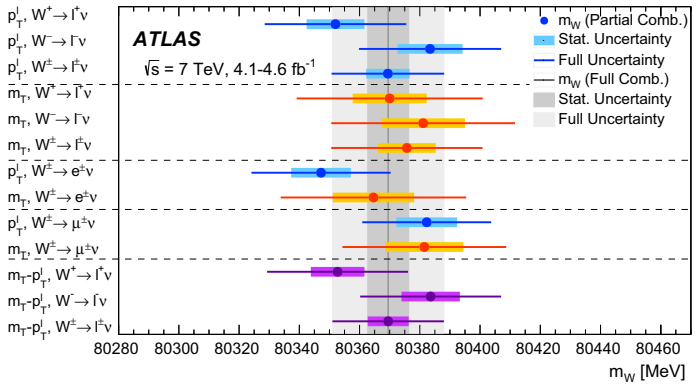

Fig. 26 Overview of the m_W determinations from the p_{T}^{ℓ} and m_{T} distributions, and for the combination of the p_{T}^{ℓ} and m_{T} distributions, in the muon and electron decay channels and for W^+ and W^- events. The horizontal lines and bands show the statistical and total uncertainties of the individual m_W determinations. The combined result for m_W and its statistical and total uncertainties are also indicated (vertical line and bands)

third to the physics-modelling systematic uncertainty. The latter dominates the total measurement uncertainty, and it itself dominated by strong interaction uncertainties. The experimental systematic uncertainties are dominated by the lepton calibration; backgrounds and the recoil calibration have a smaller impact. In the final combination, the muon decay channel has a weight of 57%, and the p_{T}^{ℓ} fit dominates the measurement with a weight of 86%. Finally, the charges contribute similarly with a weight of 52% for W^+ and of 48% for W^-.

The result is in agreement with the current world average of $m_W = 80385 \pm 15$ MeV [29], and has a precision comparable to the currently most precise single measurements of the CDF and D0 collaborations [22,23].

11.5 Additional validation tests

The final combination of m_W, presented above, depends only on template fits to the p_{T}^{ℓ} and m_{T} distributions. As a validation test, the value of m_W is determined from the $p_{\mathrm{T}}^{\mathrm{miss}}$ distribution, performing a fit in the range $30 < p_{\mathrm{T}}^{\mathrm{miss}} < 60$ GeV. Consistent results are observed in all measurement categories, leading to combined results of 80364 ± 26 (stat) MeV and 80367 ± 23 (stat) MeV for the electron and muon channels, respectively.

Several additional studies are performed to validate the stability of the m_W measurement. The stability of the result with respect to different pile-up conditions is tested by dividing the event sample into three bins of $\langle\mu\rangle$, namely [2.5, 6.5], [6.5, 9.5], and [9.5, 16]. In each bin, m_W measurements are performed independently using the p_{T}^{ℓ} and m_{T} distributions. This categorisation also tests the stability of m_W with respect to data-taking periods, as the later data-taking periods have on average more pile-up due to the increasing LHC luminosity.

The calibration of the recoil and the modelling of the p_{T}^{W} distribution are tested by performing m_W fits in two bins of the recoil corresponding to [0, 15] GeV and [15, 30] GeV, and in two regions corresponding to positive and negative values of $u_{\parallel}^{\ell}$. The analysis is also repeated with the $p_{\mathrm{T}}^{\mathrm{miss}}$ requirement removed from the signal selection, leading to a lower recoil modelling uncertainty but a higher multijet background contribution. The stability of the m_W measurements upon removal of this requirement is studied, and consistent results are obtained. All m_W determinations are consistent with the nominal result. An overview of the validation tests is shown in Table 12, where only statistical uncertainties are given. Fitting ranges of $30 < p_{\mathrm{T}}^{\ell} < 50$ GeV and $65 < m_{\mathrm{T}} < 100$ GeV are used for all these validation tests, to minimise the statistical uncertainty.

The lower and upper bounds of the range of the p_{T}^{ℓ} and m_{T} distributions are varied as in the optimisation procedure described in Sect. 11.3. The statistical and systematic uncertainties are evaluated for each range, and are only partially correlated between different ranges. Figure 27 shows measured values of m_W for selected ranges of the p_{T}^{ℓ} and m_{T} distributions, where only the uncorrelated statistical and systematic uncertainties with respect to the optimal range are shown. The observed variations are all within two standard deviations of the uncorrelated uncertainties, and small compared to the overall uncertainty of the measurement, which is illustrated by the band on Fig. 27. The largest dependence on the kinematic ranges used for the fits is observed for variations of the upper bound of the p_{T}^{ℓ} distribution in the $W^+ \to e\nu$ channel, and is related to the shape of the data-to-prediction ratio for this distribution in the region $40 < p_{\mathrm{T}}^{\ell} < 42$ GeV, as discussed in Sect. 11.3.

The effect of the residual discrepancies in the u_{T} distributions for $W^- \to \ell\nu$, visible at low values in Figs. 19-(d) and 20-(d), is estimated by adjusting, in turn, the particle-level p_{T}^{W} distribution and the recoil calibration

Table 12 Summary of consistency tests for the determination of m_W in several additional measurement categories. The Δm_W values correspond to the difference between the result for each category and the inclusive result for the corresponding observable (p_{T}^{ℓ} or m_{T}). The uncertainties correspond to the statistical uncertainty of the fit to the data of each category alone. Fitting ranges of $30 < p_{\mathrm{T}}^{\ell} < 50$ GeV and $65 < m_{\mathrm{T}} < 100$ GeV are used

Decay channel	$W \to e\nu$		$W \to \mu\nu$		Combined	
Kinematic distribution	p_{T}^{ℓ}	m_{T}	p_{T}^{ℓ}	m_{T}	p_{T}^{ℓ}	m_{T}
Δm_W [MeV]						
$\langle\mu\rangle$ in [2.5, 6.5]	8 ± 14	14 ± 18	-21 ± 12	0 ± 16	-9 ± 9	6 ± 12
$\langle\mu\rangle$ in [6.5, 9.5]	-6 ± 16	6 ± 23	12 ± 15	-8 ± 22	4 ± 11	-1 ± 16
$\langle\mu\rangle$ in [9.5, 16]	-1 ± 16	3 ± 27	25 ± 16	35 ± 26	12 ± 11	20 ± 19
u_{T} in [0, 15] GeV	0 ± 11	-8 ± 13	5 ± 10	8 ± 12	3 ± 7	-1 ± 9
u_{T} in [15, 30] GeV	10 ± 15	0 ± 24	-4 ± 14	-18 ± 22	2 ± 10	-10 ± 16
$u_{\parallel}^{\ell} < 0$ GeV	8 ± 15	20 ± 17	3 ± 13	-1 ± 16	5 ± 10	9 ± 12
$u_{\parallel}^{\ell} > 0$ GeV	-9 ± 10	1 ± 14	-12 ± 10	10 ± 13	-11 ± 7	6 ± 10
No $p_{\mathrm{T}}^{\mathrm{miss}}$-cut	14 ± 9	-1 ± 13	10 ± 8	-6 ± 12	12 ± 6	-4 ± 9

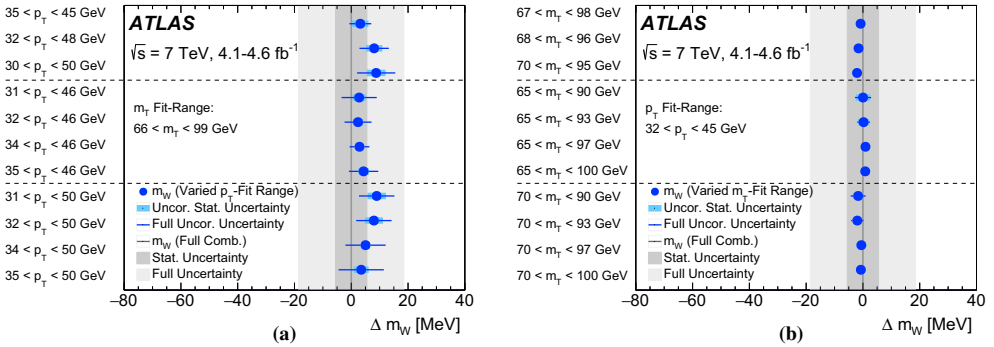

Fig. 27 Stability of the combined measurement of m_W with respect to variations of the kinematic ranges of **a** p_{T}^{ℓ} and **b** m_{T} used for the template fits. The optimal m_{T} range is used for the p_{T}^{ℓ} variations, and the optimal p_{T}^{ℓ} range is used for the m_{T} variations. The effect on the result of symmetric variations of the fitting range boundaries, and its dependence on variations of the lower (upper) boundary for two values of the upper (lower) boundary for p_{T}^{ℓ} (m_{T}) are shown. The bands and solid lines respectively show the statistical and total uncertainty on the difference with the optimal result

corrections to optimize the agreement between data and simulation. The impact of these variations on the determination of m_W is found to be small compared to the assigned p_{T}^{W} modelling and recoil calibration uncertainties, respectively.

When assuming $R_{W/Z}(p_{\mathrm{T}})$ as predicted by DYRes, instead of PYTHIA 8 AZ, to model the p_{T}^{W} distribution, deviations of about 3% appear in the distribution ratios of Figs. 24 and 25. This degrades the quality of the mass fits, and shifts the fitted values of m_W by about -20 to -90 MeV, depending on the channels, compared to the results of Table 11. Combining all channels, the shift is about -60 MeV. Since DYRes does not model the data distributions sensitive to p_{T}^{W}, as shown in Fig. 22, these shifts are given for information only and are not used to estimate the uncertainty in m_W.

11.6 Measurement of $m_{W^+} - m_{W^-}$

The results presented in the previous sections can be used to derive a measurement of the mass difference between the positively and negatively charged W bosons, $m_{W^+} - m_{W^-}$. Starting from the m_W measurement results in the 28 categories described above, 14 measurements of $m_{W^+} - m_{W^-}$ can be constructed by subtraction of the results obtained from the W^+ and W^- samples in the same decay channel and $|\eta|$ category. In practice, the m_W values measured in W^+ and W^- events are subtracted linearly, as are the effects of systematic uncertainties on these measurements, while the uncertainty contributions of a statistical nature are added in quadrature. Contrarily to the m_W measurement discussed above, no blinding procedure was applied for the measurement of $m_{W^+} - m_{W^-}$.

Table 13 Results of the $m_{W^+} - m_{W^-}$ measurements in the electron and muon decay channels, and of the combination. The table shows the statistical uncertainties; the experimental uncertainties, divided into muon-, electron-, recoil- and background-uncertainties; and the modelling uncertainties, separately for QCD modelling including scale variations, parton shower and angular coefficients, electroweak corrections, and PDFs. All uncertainties are given in MeV

Channel	$m_{W^+} - m_{W^-}$ [MeV]	Stat. Unc.	Muon Unc.	Elec. Unc.	Recoil Unc.	Bckg. Unc.	QCD Unc.	EW Unc.	PDF Unc.	Total Unc.
$W \to e\nu$	−29.7	17.5	0.0	4.9	0.9	5.4	0.5	0.0	24.1	30.7
$W \to \mu\nu$	−28.6	16.3	11.7	0.0	1.1	5.0	0.4	0.0	26.0	33.2
Combined	−29.2	12.8	3.3	4.1	1.0	4.5	0.4	0.0	23.9	28.0

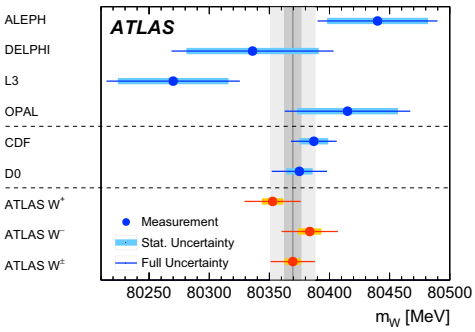

Fig. 28 The measured value of m_W is compared to other published results, including measurements from the LEP experiments ALEPH, DELPHI, L3 and OPAL [25–28], and from the Tevatron collider experiments CDF and D0 [22,23]. The vertical bands show the statistical and total uncertainties of the ATLAS measurement, and the horizontal bands and lines show the statistical and total uncertainties of the other published results. Measured values of m_W for positively and negatively charged W bosons are also shown

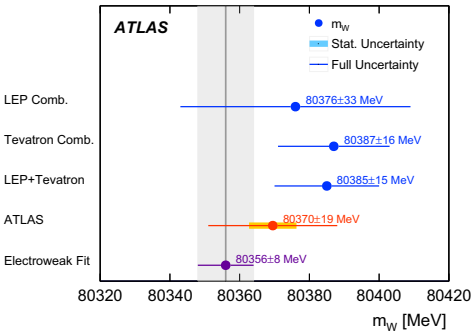

Fig. 29 The present measurement of m_W is compared to the SM prediction from the global electroweak fit [16] updated using recent measurements of the top-quark and Higgs-boson masses, $m_t = 172.84 \pm 0.70$ GeV [122] and $m_H = 125.09 \pm 0.24$ GeV [123], and to the combined values of m_W measured at LEP [124] and at the Tevatron collider [24]

In this process, uncertainties that are anti-correlated between W^+ and W^- and largely cancel for the m_W measurement become dominant when measuring $m_{W^+} - m_{W^-}$. On the physics-modelling side, the fixed-order PDF uncertainty and the parton shower PDF uncertainty give the largest contributions, while other sources of uncertainty only weakly depend on charge and tend to cancel. Among the sources of uncertainty related to lepton calibration, the track sagitta correction dominates in the muon channel, whereas several residual uncertainties contribute in the electron channel. Most lepton and recoil calibration uncertainties tend to cancel. Background systematic uncertainties contribute as the Z and multijet background fractions differ in the W^+ and W^- channels. The dominant statistical uncertainties arise from the size of the data and Monte Carlo signal samples, and of the control samples used to derive the multijet background.

The $m_{W^+} - m_{W^-}$ measurement results are shown in Table 13 for the electron and muon decay channels, and for the combination. The electron channel measurement combines six categories (p_{T}^{ℓ} and m_{T} fits in three $|\eta_\ell|$ bins), while the muon channel has four $|\eta_\ell|$ bins and eight categories in total. The fully combined result is

$$\begin{aligned} m_{W^+} - m_{W^-} &= -29.2 \pm 12.8(\text{stat.}) \\ &\quad \pm 7.0(\text{exp. syst.}) \\ &\quad \pm 23.9(\text{mod. syst.}) \text{ MeV} \\ &= -29.2 \pm 28.0 \text{ MeV}, \end{aligned}$$

where the first uncertainty is statistical, the second corresponds to the experimental systematic uncertainty, and the third to the physics-modelling systematic uncertainty.

12 Discussion and conclusions

This paper reports a measurement of the W-boson mass with the ATLAS detector, obtained through template fits to the kinematic properties of decay leptons in the electron and muon decay channels. The measurement is based on proton–proton collision data recorded in 2011 at a centre-of-mass energy of $\sqrt{s} = 7$ TeV at the LHC, and corresponding to an integrated luminosity of 4.6 fb^{-1}. The measurement relies

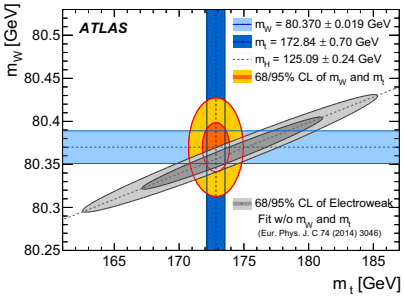

Fig. 30 The 68 and 95% confidence-level contours of the m_W and m_t indirect determination from the global electroweak fit [16] are compared to the 68 and 95% confidence-level contours of the ATLAS measurements of the top-quark and W-boson masses. The determination from the electroweak fit uses as input the LHC measurement of the Higgs-boson mass, $m_H = 125.09 \pm 0.24$ GeV [123]

on a thorough detector calibration based on the study of Z-boson events, leading to a precise modelling of the detector response to electrons, muons and the recoil. Templates for the W-boson kinematic distributions are obtained from the NLO MC generator POWHEG, interfaced to PYTHIA8 for the parton shower. The signal samples are supplemented with several additional physics-modelling corrections allowing for the inclusion of higher-order QCD and electroweak corrections, and by fits to measured distributions, so that agreement between the data and the model in the kinematic distributions is improved. The W-boson mass is obtained from the transverse-momentum distribution of charged leptons and from the transverse-mass distributions, for positively and negatively charged W bosons, in the electron and muon decay channels, and in several kinematic categories. The individual measurements of m_W are found to be consistent and their combination yields a value of

$$\begin{aligned} m_W &= 80370 \pm 7\ (\text{stat.}) \pm 11\ (\text{exp. syst.}) \\ &\quad \pm 14\ (\text{mod. syst.})\ \text{MeV} \\ &= 80370 \pm 19\ \text{MeV}, \end{aligned}$$

where the first uncertainty is statistical, the second corresponds to the experimental systematic uncertainty, and the third to the physics-modelling systematic uncertainty. A measurement of the W^+ and W^- mass difference yields $m_{W^+} - m_{W^-} = -29 \pm 28$ MeV.

The W-boson mass measurement is compatible with the current world average of $m_W = 80385 \pm 15$ MeV [29], and similar in precision to the currently leading measurements performed by the CDF and D0 collaborations [22,23]. An overview of the different m_W measurements is shown in Fig. 28. The compatibility of the measured value of m_W in the context of the global electroweak fit is illustrated in Figs. 29 and 30. Figure 29 compares the present measurement with earlier results, and with the SM prediction updated with regard to Ref. [16] using recent measurements of the top-quark and Higgs boson masses, $m_t = 172.84 \pm 0.70$ GeV [122] and $m_H = 125.09 \pm 0.24$ GeV [123]. This update gives a numerical value for the SM prediction of $m_W = 80356 \pm 8$ MeV. The corresponding two-dimensional 68 and 95% confidence limits for m_W and m_t are shown in Fig. 30, and compared to the present measurement of m_W and the average of the top-quark mass determinations performed by ATLAS [122].

The determination of the W-boson mass from the global fit of the electroweak parameters has an uncertainty of 8 MeV, which sets a natural target for the precision of the experimental measurement of the mass of the W boson. The modelling uncertainties, which currently dominate the overall uncertainty of the m_W measurement presented in this paper, need to be reduced in order to fully exploit the larger data samples available at centre-of-mass energies of 8 and 13 TeV. Better knowledge of the PDFs, as achievable with the inclusion in PDF fits of recent precise measurements of W- and Z-boson rapidity cross sections with the ATLAS detector [41], and improved QCD and electroweak predictions for Drell–Yan production, are therefore crucial for future measurements of the W-boson mass at the LHC.

Acknowledgements We thank CERN for the very successful operation of the LHC, as well as the support staff from our institutions without whom ATLAS could not be operated efficiently. We acknowledge the support of ANPCyT, Argentina; YerPhI, Armenia; ARC, Australia; BMWFW and FWF, Austria; ANAS, Azerbaijan; SSTC, Belarus; CNPq and FAPESP, Brazil; NSERC, NRC and CFI, Canada; CERN; CONICYT, Chile; CAS, MOST and NSFC, China; COLCIENCIAS, Colombia; MSMT CR, MPO CR and VSC CR, Czech Republic; DNRF and DNSRC, Denmark; IN2P3-CNRS, CEA-DSM/IRFU, France; SRNSF, Georgia; BMBF, HGF, and MPG, Germany; GSRT, Greece; RGC, Hong Kong SAR, China; ISF, I-CORE and Benoziyo Center, Israel; INFN, Italy; MEXT and JSPS, Japan; CNRST, Morocco; NWO, Netherlands; RCN, Norway; MNiSW and NCN, Poland; FCT, Portugal; MNE/IFA, Romania; MES of Russia and NRC KI, Russian Federation; JINR; MESTD, Serbia; MSSR, Slovakia; ARRS and MIZŠ, Slovenia; DST/NRF, South Africa; MINECO, Spain; SRC and Wallenberg Foundation, Sweden; SERI, SNSF and Cantons of Bern and Geneva, Switzerland; MOST, Taiwan; TAEK, Turkey; STFC, United Kingdom; DOE and NSF, United States of America. In addition, individual groups and members have received support from BCKDF, the Canada Council, CANARIE, CRC, Compute Canada, FQRNT, and the Ontario Innovation Trust, Canada; EPLANET, ERC, ERDF, FP7, Horizon 2020 and Marie Skłodowska-Curie Actions, European Union; Investissements d'Avenir Labex and Idex, ANR, Région Auvergne and Fondation Partager le Savoir, France; DFG and AvH Foundation, Germany; Herakleitos, Thales and Aristeia programmes co-financed by EU-ESF and the Greek NSRF; BSF, GIF and Minerva, Israel; BRF, Norway; CERCA Programme Generalitat de Catalunya, Generalitat Valenciana, Spain; the Royal Society and Leverhulme Trust, United Kingdom. The crucial computing support from all WLCG partners is acknowledged gratefully, in particular from CERN, the ATLAS Tier-1 facilities at TRIUMF (Canada), NDGF (Denmark, Norway, Sweden), CC-IN2P3 (France), KIT/GridKA (Germany), INFN-CNAF (Italy), NL-T1 (Netherlands), PIC (Spain), ASGC (Taiwan), RAL (UK) and BNL (USA), the Tier-2 facilities worldwide and large non-WLCG

resource providers. Major contributors of computing resources are listed in Ref. [125].

References

1. S.L. Glashow, Partial symmetries of weak interactions. Nucl. Phys. **22**, 579–588 (1961)
2. A. Salam, J.C. Ward, Electromagnetic and weak interactions. Phys. Lett. **13**, 168–171 (1964)
3. S. Weinberg, A model of leptons. Phys. Rev. Lett. **19**, 1264–1266 (1967)
4. F. Englert, R. Brout, Broken symmetry and the mass of gauge vector mesons. Phys. Rev. Lett. **13**, 321–323 (1964)
5. P.W. Higgs, Broken symmetries and the masses of gauge bosons. Phys. Rev. Lett. **13**, 508–509 (1964)
6. P.W. Higgs, Broken symmetries, massless particles and gauge fields. Phys. Lett. **12**, 132–133 (1964)
7. G.S. Guralnik, C.R. Hagen, T.W.B. Kibble, Global conservation laws and massless particles. Phys. Rev. Lett. **13**, 585–587 (1964)
8. UA1 Collaboration, G. Arnison, et al., Experimental observation of isolated large transverse energy electrons with associated missing energy at $\sqrt{s}$ = 540 GeV. Phys. Lett. B **122**, 103–116 (1983)
9. UA1 Collaboration, G. Arnison, et al., Experimental observation of lepton pairs of invariant mass around 95 GeV/c^2 at the CERN SPS Collider. Phys. Lett. B **126**, 398–410 (1983)
10. UA2 Collaboration, M. Banner, et al., Observation of single isolated electrons of high transverse momentum in events with missing transverse energy at the CERN $\bar{p}p$ Collider. Phys. Lett. B **122**, 476–485 (1983)
11. UA2 Collaboration, P. Bagnaia, et al., Evidence for $Z^0 \to e^+e^-$ at the CERN $\bar{p}p$ Collider. Phys. Lett. B **129**, 130–140 (1983)
12. ATLAS Collaboration, Observation of a new particle in the search for the Standard Model Higgs boson with the ATLAS detector at the LHC. Phys. Lett. B **716**, 1 (2012). arXiv: 1207.7214 [hep-ex]
13. CMS Collaboration, Observation of a new boson at a mass of 125 GeV with the CMS experiment at the LHC. Phys. Lett. B **716**, 30 (2012). arXiv: 1207.7235 [hep-ex]
14. M. Awramik, M. Czakon, A. Freitas, G. Weiglein, Precise prediction for the W boson mass in the standard model. Phys. Rev. D **69**, 053006 (2004). arXiv:hep-ph/0311148
15. A. Sirlin, Radiative corrections in the $SU(2)_L \times U(1)$ theory: a simple renormalization framework. Phys. Rev. D **22**, 971–981 (1980)
16. M. Baak et al., The global electroweak fit at NNLO and prospects for the LHC and ILC. Eur. Phys. J. C **74**, 3046 (2014). arXiv:1407.3792 [hep-ph]
17. UA1 Collaboration, G. Arnison, et al., Intermediate vector boson properties at the CERN super proton synchrotron collider. Europhys. Lett. **1**, 327–345 (1986)
18. UA2 Collaboration, J. Alitti, et al., An Improved determination of the ratio of W and Z masses at the CERN $\bar{p}p$ collider. Phys. Lett. B **276**, 354–364 (1992)
19. CDF Collaboration, T. Affolder et al., Measurement of the W boson mass with the collider detector at fermilab. Phys. Rev. D **64**, 052001 (2001). arXiv: hep-ex/0007044
20. D0 Collaboration, V. M. Abazov, et al., Improved W boson mass measurement with the DØ detector. Phys. Rev. D **66**, 012001 (2002). arXiv: hep-ex/0204014
21. CDF and D0 collaborations, V. M. Abazov et al. Combination of CDF and D0 results on W boson mass and width. Phys. Rev. D **70**, 092008 (2004). arXiv: hep-ex/0311039
22. CDF Collaboration, T. Aaltonen et al. Precise measurement of the W-boson mass with the CDF II detector. Phys. Rev. Lett. **108**, 151803 (2012). arXiv: 1203.0275 [hep-ex]
23. D0 Collaboration, V. M. Abazov et al. Measurement of the W boson mass with the D0 detector. Phys. Rev. Lett. **108**, 151804 (2012). arXiv: 1203.0293 [hep-ex]
24. CDF and D0 Collaborations, T. Aaltonen et al. Combination of CDF and D0 W-boson mass measurements. Phys. Rev. D **88**, 052018 (2013). arXiv: 1307.7627 [hep-ex]
25. ALEPH Collaboration, S. Schael et al. Measurement of the W boson mass and width in e^+e^- collisions at LEP. Eur. Phys. J. C **47**, 309-335 (2006). arXiv: hep-ex/0605011
26. DELPHI Collaboration, J. Abdallah et al. Measurement of the mass and width of the W Boson in e^+e^- collisions at $\sqrt{s}$ = 161 – 209 GeV. Eur. Phys. J. C **55**, 1-38 (2008). arXiv: 0803.2534 [hep-ex]
27. L3 Collaboration, P. Achard, et al., Measurement of the mass and the width of the W boson at LEP. Eur. Phys. J. C **45**, 569–587 (2006). arXiv: hep-ex/0511049
28. OPAL Collaboration, G. Abbiendi et al., Measurement of the mass and width of the W boson. Eur. Phys. J. C **45**, 307–335 (2006). arXiv: hep-ex/0508060
29. Particle Data Group, K. A. Olive et al, Review of particle physics. Chin. Phys. C **38**, 090001 (2014)
30. J. de Blas, et al., Electroweak precision observables and Higgs-boson signal strengths in the Standard Model and beyond: present and future. JHEP **12**, 135. arXiv: 1608.01509 [hep-ph] (2016)
31. S. D. Drell, T.-M. Yan, Massive lepton pair production in hadron-hadron collisions at high-energies. Phys. Rev. Lett. **25**, 316-320 (1970) [Erratum: Phys. Rev. Lett. 25, 902(1970)]
32. S. Schael et al., Precision electroweak measurements on the Z resonance. Phys. Rept. **427**, 257–454 (2006). arXiv:hep-ex/0509008
33. M. Krasny, F. Dydak, F. Fayette, W. Placzek, A. Siodmok, $\Delta M_W \leq 10 MeV/c^2$ at the LHC: a forlorn hope?. Eur. Phys. J. C **69**, 379–397 (2010). arXiv: 1004.2597 [hep-ex]
34. E. Mirkes, Angular decay distribution of leptons from W bosons at NLO in hadronic collisions. Nucl. Phys. B **387**, 3–85 (1992)
35. D.Yu. Bardin, A. Leike, T. Riemann, M. Sachwitz, Energy dependent width effects in e^+e^- annihilation near the Z boson pole. Phys. Lett. B **206**, 539–542 (1988)
36. J. Smith, W.L. van Neerven, J.A.M. Vermaseren, The transverse mass and width of the W boson. Phys. Rev. Lett. **50**, 1738 (1983)
37. ATLAS Collaboration, Studies of theoretical uncertainties on the measurement of the mass of the W boson at the LHC. ATL-PHYS-PUB-2014-015 (2014). https://cdsweb.cern.ch/record/1956455
38. ATLAS Collaboration, Electron reconstruction and identification efficiency measurements with the ATLAS detector using the 2011 LHC proton–proton collision data. Eur. Phys. J. C **74**, 2941 (2014). arXiv: 1404.2240 [hep-ex]
39. ATLAS Collaboration, Electron and photon energy calibration with the ATLAS detector using LHC Run 1 data. Eur. Phys. J. C **74**, 3071 (2014). arXiv: 1407.5063 [hep-ex]
40. ATLAS Collaboration, Measurement of the muon reconstruction performance of the ATLAS detector using 2011 and 2012 LHC proton–proton collision data. Eur. Phys. J. C **74**, 3130 (2014). arXiv: 1407.3935 [hep-ex]
41. ATLAS Collaboration, Precision measurement and interpretation of inclusive W^+, W^- and Z/γ^* production cross sections with the ATLAS detector. Eur. Phys. J. C **77**, 367 (2017). arXiv: 1612.03016 [hep-ex]

42. ATLAS Collaboration, Measurement of the angular coefficients in Z-boson events using electron and muon pairs from data taken at $\sqrt{s} = 8$ TeV with the ATLAS detector. JHEP **08**, 159 (2016). arXiv: 1606.00689 [hep-ex]
43. ATLAS Collaboration, Measurement of angular correlations in Drell-Yan lepton pairs to probe Z/γ^* boson transverse momentum at $\sqrt{s} = 7$ TeV with the ATLAS detector. Phys. Lett. B **720**, 32 (2013). arXiv: 1211.6899 [hep-ex]
44. ATLAS Collaboration, Measurement of the Z/γ^* boson transverse momentum distribution in pp collisions at $\sqrt{s} = 7$ TeV with the ATLAS detector. JHEP **09**, 145 (2014). arXiv: 1406.3660 [hep-ex]
45. ATLAS Collaboration, Measurement of the transverse momentum distribution of W bosons in pp collisions at $\sqrt{s} = 7$ TeV with the ATLAS detector. Phys. Rev. D **85**, 012005 (2012). arXiv: 1108.6308 [hep-ex]
46. ATLAS Collaboration, The ATLAS Experiment at the CERN large hadron collider. JINST **3**, S08003 (2008)
47. ATLAS Collaboration, Performance of the ATLAS Trigger System in 2010. Eur. Phys. J. C **72**, 1849 (2012). arXiv: 1110.1530 [hep-ex]
48. ATLAS Collaboration, Improved luminosity determination in pp collisions at $\sqrt{s} = 7$ TeV using the ATLAS detector at the LHC. Eur. Phys. J. C **73**, 2518 (2013). arXiv: 1302.4393 [hep-ex]
49. P. Nason, A New method for combining NLO QCD with shower Monte Carlo algorithms. JHEP **11**, 040 (2004). arXiv:hep-ph/0409146
50. S. Frixione, P. Nason, C. Oleari, Matching NLO QCD computations with Parton Shower simulations: the POWHEG method. JHEP **11**, 070 (2007). arXiv:0709.2092 [hep-ph]
51. S. Alioli, P. Nason, C. Oleari, E. Re, A general framework for implementing NLO calculations in shower Monte Carlo programs: the POWHEG BOX. JHEP **06**, 043 (2010). arXiv:1002.2581 [hep-ph]
52. T. Sjöstrand, S. Mrenna, P.Z. Skands, PYTHIA 6.4 physics and manual. JHEP **05**, 026 (2006). arXiv:hep-ph/0603175
53. T. Sjöstrand, S. Mrenna, P. Skands, A brief introduction to PYTHIA 8.1. Comput. Phys. Commun. **178**, 852–867 (2008). arXiv:0710.3820 [hep-ph]
54. H.-L. Lai et al., New parton distributions for collider physics Phys. Rev. D **82**, 074024 (2010). arXiv:1007.2241 [hep-ph]
55. J. Pumplin et al., New generation of parton distributions with uncertainties from global QCD analysis. JHEP **07**, 012 (2002). arXiv:hep-ph/0201195
56. P. Golonka, Z. Was, PHOTOS Monte Carlo: a precision tool for QED corrections in Z and W decays. Eur Phys. J. C **45**, 97 (2006). arXiv:hep-ph/0506026
57. G. Corcella et al., HERWIG 6: An Event generator for hadron emission reactions with interfering gluons (including supersymmetric processes). JHEP **01**, 010 (2001). arXiv:hep-ph/0011363
58. J. Butterworth, J.R. Forshaw, M. Seymour, Multiparton interactions in photoproduction at HERA. Z. Phys. C **72**, 637–646 (1996). arXiv:hep-ph/9601371
59. S. Frixione, B.R. Webber, Matching NLO QCD computations and parton shower simulations. JHEP **06**, 029 (2002). arXiv:hep-ph/0204244
60. S. Frixione, P. Nason, B.R. Webber, Matching NLO QCD and parton showers in heavy flavor production. JHEP **08**, 007 (2003). arXiv:hep-ph/0305252 [hep-ph]
61. S. Frixione, E. Laenen, P. Motylinski, B.R. Webber, Single-top production in MC@NLO. JHEP **03**, 092 (2006). arXiv:hep-ph/0512250 [hep-ph]
62. ATLAS Collaboration, Measurement of the $t\bar{t}$ production cross-section using $e\mu$ events with b-tagged jets in pp collisions at $\sqrt{s} = 7$ and 8 TeV with the ATLAS detector. Eur. Phys. J. C **74**, 3109 (2014). arXiv: 1406.5375 [hep-ex]
63. N. Kidonakis, Next-to-next-to-leading-order collinear and soft gluon corrections for t-channel single top quark production. Phys. Rev. D **83**, 091503 (2011). arXiv:1103.2792 [hep-ph]
64. N. Kidonakis, NNLL resummation for s-channel single top quark production. Phys. Rev. D **81**, 054028 (2010). arXiv:1001.5034 [hep-ph]
65. N. Kidonakis, Two-loop soft anomalous dimensions for single top quark associated production with a W^- or H^-. Phys. Rev. D **82**, 054018 (2010). arXiv:1005.4451 [hep-ph]
66. J.M. Campbell, R.K. Ellis, An Update on vector boson pair production at hadron colliders. Phys. Rev. D **60**, 113006 (1999). arXiv:hep-ph/9905386 [hep-ph]
67. T. Gehrmann et al., W^+W^- Production at hadron colliders in next to next to leading order QCD. Phys. Rev. Lett. **113**, 212001 (2014). arXiv:1408.5243 [hep-ph]
68. ATLAS Collaboration, The ATLAS simulation infrastructure. Eur. Phys. J. C **70**, 823 (2010). arXiv: 1005.4568 [hep-ex]
69. S. Agostinelli et al., GEANT4: a simulation toolkit. Nucl. Instrum. Meth. A **506**, 250–303 (2003)
70. ATLAS Collaboration. Summary of ATLAS Pythia 8 tunes, ATL-PHYS-PUB-2012-003. (2012). https://cds.cern.ch/record/1474107
71. ATLAS Collaboration. Topological cell clustering in the ATLAS calorimeters and its performance in LHC Run 1. Eur. Phys. J. C **77**, 490 (2017). arXiv: 1603.02934 [hep-ex]
72. S. Alioli, et al., Precision studies of observables in $pp \to W \to \ell\nu$ and $pp \to \gamma, Z \to \ell^+\ell^-$ processes at the LHC working group report. Eur. Phys. J. C **77**, 280 (2017). arXiv: 1606.02330 [hep-ph]
73. S. Jadach, W. Placzek, B.F.L. Ward, BHWIDE 1.00: $\mathcal{O}(\alpha)$ YFS exponentiated Monte Carlo for Bhabha scattering at wide angles for LEP-1 / SLC and LEP-2. Phys. Lett. B **390**, 298–308 (1997). arXiv:hep-ph/9608412
74. W. Płaczek, S. Jadach, M.W. Krasny, Drell-Yan processes with WINHAC. Acta Phys. Polon. B **44**, 2171–2178 (2013). arXiv:1310.5994 [hep-ph]
75. S. Dittmaier, M. Krämer, Electroweak radiative corrections to W boson production at hadron colliders. Phys. Rev. D **65**, 073007 (2002). arXiv:hep-ph/0109062
76. U. Baur, D. Wackeroth, Electroweak radiative corrections to $p\bar{p} \to W^\pm \to \ell^\pm\nu$ beyond the pole approximation. Phys. Rev. D **70**, 073015 (2004). arXiv:hep-ph/0405191
77. Arbuzov, A. et al., One-loop corrections to the Drell-Yan process in SANC: the charged current case. Eur. Phys. J. C **46**, 407–412 (2006). arXiv: hep-ph/0506110 [Erratum: Eur. Phys. J.C50,505(2007)]
78. L. Barzè, G. Montagna, P. Nason, O. Nicrosini, F. Piccinini, Implementation of electroweak corrections in the POWHEG BOX: single W production. JHEP **04**, 037 (2012). arXiv:1202.0465 [hep-ph]
79. C. Bernaciak, D. Wackeroth, N.L.O. Combining, QCD and electroweak radiative corrections to W boson production at hadron colliders in the POWHEG framework. Phys. Rev. D **85**, 093003 (2012). arXiv:1201.4804 [hep-ph]
80. Mück A. Oymanns L., Resonance-improved parton-shower matching for the Drell-Yan process including electroweak corrections. JHEP **05**, 090 (2017). arXiv: 1612.04292 [hep-ph]
81. S. Dittmaier, A. Huss, C. Schwinn, Dominant mixed QCD-electroweak $O(\alpha_s\alpha)$ corrections to Drell-Yan processes in the resonance region. Nucl. Phys. B **904**, 216–252 (2016). arXiv:1511.08016 [hep-ph]
82. G. Altarelli, R. H. P. Kleiss, C. Verzegnassi (eds.) Workshop on Z physics at LEP1: standard physics. (1989). https://cds.cern.ch/record/116932
83. C.M. Carloni Calame, et al., Precision measurement of the W-boson mass: theoretical contributions and uncertainties. Phys. Rev. D **96**, 093005 (2017). arXiv: 1612.02841 [hep-ph]

84. J.C. Collins, D.E. Soper, Angular distribution of dileptons in high-energy hadron collisions. Phys. Rev. D **16**, 2219 (1977)
85. J. Gao, M. Guzzi, J. Huston, H.-L. Lai, Z. Li et al., CT10 next-to-next-to-leading order global analysis of QCD. Phys. Rev. D **89**, 033009 (2014). arXiv:1302.6246 [hep-ph]
86. S. Catani, L. Cieri, G. Ferrera, D. de Florian, M. Grazzini, Vector boson production at hadron colliders: a fully exclusive QCD calculation at NNLO. Phys. Rev. Lett. **103**, 082001 (2009). arXiv:0903.2120 [hep-ph]
87. T. Hahn, CUBA: a library for multidimensional numerical integration. Comput. Phys. Commun. **168**, 78–95 (2005). arXiv:hep-ph/0404043
88. J.C. Collins, D.E. Soper, G.F. Sterman, Transverse momentum distribution in Drell–Yan pair and W and Z boson production. Nucl. Phys. B **250**, 199 (1985)
89. G.A. Ladinsky, C.P. Yuan, The nonperturbative regime in QCD resummation for gauge boson production at hadron colliders. Phys. Rev. D **50**, R4239 (1994). arXiv:hep-ph/9311341
90. C. Balazs, P. Yuan, Soft gluon effects on lepton pairs at hadron colliders. Phys. Rev. D **56**, 5558–5583 (1997). arXiv:hep-ph/9704258
91. S. Catani, D. Florian, G. de Ferrera, M. Grazzini, Vector boson production at hadron colliders: transverse-momentum resummation and leptonic decay. JHEP **12**, 047 (2015). arXiv:1507.06937 [hep-ph]
92. T. Becher, M. Neubert, D. Wilhelm, Electroweak gauge-boson production at small q_T: infrared safety from the collinear anomaly. JHEP **02**, 124 (2012). arXiv:1109.6027 [hep-ph]
93. G. Miu, T. Sjöstrand, W production in an improved parton shower approach. Phys. Lett. B **449**, 313–320 (1999). arXiv:hep-ph/9812455
94. S. Catani, B.R. Webber, G. Marchesini, QCD coherent branching and semiinclusive processes at large x. Nucl. Phys. B **349**, 635–654 (1991)
95. R. Corke, T. Sjöstrand, Interleaved parton showers and tuning prospects. JHEP **03**, 032 (2011). arXiv:1011.1759 [hep-ph]
96. K. Hamilton, P. Nason, G. Zanderighi, MINLO: Multi-scale improved NLO. JHEP **10**, 155 (2012). arXiv:1206.3572 [hep-ph]
97. K. Hamilton, P. Nason, C. Oleari, G. Zanderighi, Merging H/W/Z + 0 and 1 jet at NLO with no merging scale: a path to parton shower + NNLO matching. JHEP **05**, 082 (2013). arXiv:1212.4504 [hep-ph]
98. R.D. Ball et al., Parton distributions for the LHC Run II. JHEP **04**, 040 (2015). arXiv:1410.8849 [hep-ph]
99. S. Dulat et al., New parton distribution functions from a global analysis of quantum chromodynamics. Phys. Rev. D **93**, 033006 (2016). arXiv: 1506.07443 [hep-ph]
100. L.A. Harland-Lang, A.D. Martin, P. Motylinski, R.S. Thorne, Parton distributions in the LHC era: MMHT 2014 PDFs Eur. Phys. J. C **75**, 204 (2015). arXiv:1412.3989 [hep-ph]
101. S. Alekhin, J. Blümlein,, S. Moch, The ABM parton distributions tuned to LHC data. Phys. Rev. D **89**, 054028 (2014). arXiv:1310.3059 [hep-ph]
102. M. Krasny, F. Fayette, W. Placzek, A. Siodmok, Z-boson as "the standard candle" for high precision W-boson physics at LHC. Eur. Phys. J. C **51**, 607–617 (2007). arXiv:hep-ph/0702251
103. F. Fayette, M. Krasny, W. Placzek, A. Siodmok, Measurement of $M_{W^+} - M_{W^-}$ at LHC. Eur. Phys. J. C **63**, 33–56 (2009). arXiv:0812.2571 [hep-ph]
104. G. Bozzi, L. Citelli, A. Vicini, Parton density function uncertainties on the W boson mass measurement from the lepton transverse momentum distribution. Phys. Rev. D **91**, 113005 (2015). arXiv:1501.05587 [hep-ph]
105. J. Pumplin et al., Uncertainties of predictions from parton distribution functions. II. The Hessian method. Phys. Rev. D. **65**, 014013 (2001). arXiv:hep-ph/0101032
106. H1 and ZEUS Collaborations, H. Abramowicz et al., Combination of measurements of inclusive deep inelastic $e^{\pm}p$ scattering cross sections and QCD analysis of HERA data. Eur. Phys. J. C **75**, 580 (2015). arXiv: 1506.06042 [hep-ex]
107. Wenninger J., Energy calibration of the LHC Beams at 4 TeV. CERN-ATS-2013-040 (2013). https://cdsweb.cern.ch/record/1546734
108. T. Sjöstrand, P.Z. Skands, Transverse-momentum-ordered showers and interleaved multiple interactions. Eur. Phys. J. C **39**, 129–154 (2005). arXiv:hep-ph/0408302
109. M. Bonvini, A.S. Papanastasiou, F.J. Tackmann, Matched predictions for the $b\bar{b}H$ cross section at the 13 TeV LHC. JHEP **10**, 053 (2016). arXiv:1605.01733 [hep-ph]
110. R.D. Ball et al., Parton distributions with LHC data. Nucl. Phys. B **867**, 244–289 (2013). arXiv:1207.1303 [hep-ph]
111. J. Bellm et al., Herwig 7.0/Herwig++ 3.0 release note. Eur. Phys. J. C **76**, 196 (2016). arXiv:1512.01178 [hep-ph]
112. M. Bahr et al., Herwig++ physics and manual. Eur. Phys. J. C **58**, 639–707 (2008). arXiv:0803.0883 [hep-ph]
113. ATLAS Collaboration, Study of alignment-related systematic effects on the ATLAS inner detector track reconstruction. ATLAS-CONF-2012-141 (2012). https://cdsweb.cern.ch/record/1483518
114. ATLAS Collaboration, A study of the material in the ATLAS inner detector using secondary hadronic interactions. JINST **7**, P01013. (2012). arXiv: 1110.6191 [hep-ex]
115. Devroye L., Non-Uniform Random Variate Generation. Springer, 1986. http://www.eirene.de/Devroye.pdf
116. G. Bozzi, S. Catani, G. Ferrera, D. de Florian, M. Grazzini, Transverse-momentum resummation: a perturbative study of Z production at the tevatron. Nucl. Phys. B **815**, 174–197 (2009). arXiv:0812.2862 [hep-ph]
117. G. Bozzi, S. Catani, G. Ferrera, D. de Florian, M. Grazzini, Production of Drell-Yan lepton pairs in hadron collisions: transverse-momentum resummation at next-to-next-to-leading logarithmic accuracy. Phys. Lett. B **696**, 207–213 (2011). arXiv:1007.2351 [hep-ph]
118. B. Efron, Bootstrap methods: another look at the jackknife. Ann. Statist. **7**, 1–26 (1979)
119. L. Lyons, D. Gibaut, P. Clifford, How to combine correlated estimates of a single physical quantity. Nucl. Instrum. Meth. A **270**, 110 (1988)
120. A. Valassi, Combining correlated measurements of several different physical quantities. Nucl. Instrum. Meth. A **500**, 391–405 (2003)
121. H1 Collaboration, F.D. Aaron et al., Measurement of the Inclusive ep Scattering Cross Section at Low Q^2 and x at HERA. Eur. Phys. J. C **63**, 625-678 (2009). arXiv: 0904.0929 [hep-ex]
122. ATLAS Collaboration, Measurement of the top quark mass in the $t\bar{t} \to$ dilepton channel from $\sqrt{s} = 8$ TeV ATLAS data. Phys. Lett. B **761**, 350-371 (2016) arXiv: 1606.02179 [hep-ex]
123. ATLAS and CMS Collaborations, Combined measurement of the Higgs Boson Mass in pp collisions at $\sqrt{s} = 7$ and 8 TeV with the ATLAS and CMS experiments. Phys. Rev. Lett. **114**, 191803 (2015). arXiv: 1503.07589 [hep-ex]
124. ALEPH, DELPHI, L3, OPAL Collaborations, LEP Electroweak Working Group, S. Schael et al., Electroweak Measurements in Electron-Positron Collisions at W-Boson-Pair Energies at LEP. Phys. Rept. **532**, 119-244 (2013) arXiv: 1302.3415 [hep-ex]
125. ATLAS Collaboration, ATLAS Computing Acknowledgements 2016–2017, ATL-GEN-PUB-2016-002. https://cds.cern.ch/record/2202407

ATLAS Collaboration

M. Aaboud[137d], G. Aad[88], B. Abbott[115], J. Abdallah[8], O. Abdinov[12], B. Abeloos[119], S. H. Abidi[161], O. S. AbouZeid[139], N. L. Abraham[151], H. Abramowicz[155], H. Abreu[154], R. Abreu[118], Y. Abulaiti[148a,148b], B. S. Acharya[167a,167b,a], S. Adachi[157], L. Adamczyk[41a], D. L. Adams[27], J. Adelman[110], M. Adersberger[102], T. Adye[133], A. A. Affolder[139], T. Agatonovic-Jovin[14], C. Agheorghiesei[28b], J. A. Aguilar-Saavedra[128a,128f], S. P. Ahlen[24], F. Ahmadov[68,b], G. Aielli[135a,135b], S. Akatsuka[71], H. Akerstedt[148a,148b], T. P. A. Åkesson[84], A. V. Akimov[98], G. L. Alberghi[22a,22b], J. Albert[172], M. J. Alconada Verzini[74], M. Aleksa[32], I. N. Aleksandrov[68], C. Alexa[28b], G. Alexander[155], T. Alexopoulos[10], M. Alhroob[115], B. Ali[130], M. Aliev[76a,76b], G. Alimonti[94a], J. Alison[33], S. P. Alkire[38], B. M. M. Allbrooke[151], B. W. Allen[118], P. P. Allport[19], A. Aloisio[106a,106b], A. Alonso[39], F. Alonso[74], C. Alpigiani[140], A. A. Alshehri[56], M. Alstaty[88], B. Alvarez Gonzalez[32], D. Álvarez Piqueras[170], M. G. Alviggi[106a,106b], B. T. Amadio[16], Y. Amaral Coutinho[26a], C. Amelung[25], D. Amidei[92], S. P. Amor Dos Santos[128a,128c], A. Amorim[128a,128b], S. Amoroso[32], G. Amundsen[25], C. Anastopoulos[141], L. S. Ancu[52], N. Andari[19], T. Andeen[11], C. F. Anders[60b], J. K. Anders[77], K. J. Anderson[33], A. Andreazza[94a,94b], V. Andrei[60a], S. Angelidakis[9], I. Angelozzi[109], A. Angerami[38], F. Anghinolfi[32], A. V. Anisenkov[111,c], N. Anjos[13], A. Annovi[126a,126b], C. Antel[60a], M. Antonelli[50], A. Antonov[100,*], D. J. Antrim[166], F. Anulli[134a], M. Aoki[69], L. Aperio Bella[32], G. Arabidze[93], Y. Arai[69], J. P. Araque[128a], V. Araujo Ferraz[26a], A. T. H. Arce[48], R. E. Ardell[80], F. A. Arduh[74], J-F. Arguin[97], S. Argyropoulos[66], M. Arik[20a], A. J. Armbruster[145], L. J. Armitage[79], O. Arnaez[32], H. Arnold[51], M. Arratia[30], O. Arslan[23], A. Artamonov[99], G. Artoni[122], S. Artz[86], S. Asai[157], N. Asbah[45], A. Ashkenazi[155], L. Asquith[151], K. Assamagan[27], R. Astalos[146a], M. Atkinson[169], N. B. Atlay[143], K. Augsten[130], G. Avolio[32], B. Axen[16], M. K. Ayoub[119], G. Azuelos[97,d], A. E. Baas[60a], M. J. Baca[19], H. Bachacou[138], K. Bachas[76a,76b], M. Backes[122], M. Backhaus[32], P. Bagiacchi[134a,134b], P. Bagnaia[134a,134b], J. T. Baines[133], M. Bajic[39], O. K. Baker[179], E. M. Baldin[111,c], P. Balek[175], T. Balestri[150], F. Balli[138], W. K. Balunas[124], E. Banas[42], Sw. Banerjee[176,e], A. A. E. Bannoura[178], L. Barak[32], E. L. Barberio[91], D. Barberis[53a,53b], M. Barbero[88], T. Barillari[103], M-S. Barisits[32], T. Barklow[145], N. Barlow[30], S. L. Barnes[36c], B. M. Barnett[133], R. M. Barnett[16], Z. Barnovska-Blenessy[36a], A. Baroncelli[136a], G. Barone[25], A. J. Barr[122], L. Barranco Navarro[170], F. Barreiro[85], J. Barreiro Guimarães da Costa[35a], R. Bartoldus[145], A. E. Barton[75], P. Bartos[146a], A. Basalaev[125], A. Bassalat[119,f], R. L. Bates[56], S. J. Batista[161], J. R. Batley[30], M. Battaglia[139], M. Bauce[134a,134b], F. Bauer[138], H. S. Bawa[145,g], J. B. Beacham[113], M. D. Beattie[75], T. Beau[83], P. H. Beauchemin[165], P. Bechtle[23], H. P. Beck[18,h], K. Becker[122], M. Becker[86], M. Beckingham[173], C. Becot[112], A. J. Beddall[20d], A. Beddall[20b], V. A. Bednyakov[68], M. Bedognetti[109], C. P. Bee[150], T. A. Beermann[32], M. Begalli[26a], M. Begel[27], J. K. Behr[45], A. S. Bell[81], G. Bella[155], L. Bellagamba[22a], A. Bellerive[31], M. Bellomo[89], K. Belotskiy[100], O. Beltramello[32], N. L. Belyaev[100], O. Benary[155,*], D. Benchekroun[137a], M. Bender[102], K. Bendtz[148a,148b], N. Benekos[10], Y. Benhammou[155], E. Benhar Noccioli[179], J. Benitez[66], D. P. Benjamin[48], M. Benoit[52], J. R. Bensinger[25], S. Bentvelsen[109], L. Beresford[122], M. Beretta[50], D. Berge[109], E. Bergeaas Kuutmann[168], N. Berger[5], J. Beringer[16], S. Berlendis[58], N. R. Bernard[89], G. Bernardi[83], C. Bernius[112], F. U. Bernlochner[23], T. Berry[80], P. Berta[131], C. Bertella[86], G. Bertoli[148a,148b], F. Bertolucci[126a,126b], I. A. Bertram[75], C. Bertsche[45], D. Bertsche[115], G. J. Besjes[39], O. Bessidskaia Bylund[148a,148b], M. Bessner[45], N. Besson[138], C. Betancourt[51], A. Bethani[87], S. Bethke[103], A. J. Bevan[79], R. M. Bianchi[127], O. Biebel[102], D. Biedermann[17], M. Bianco[32], R. Bielski[87], N. V. Biesuz[126a,126b], M. Biglietti[136a], J. Bilbao De Mendizabal[52], T. R. V. Billoud[97], H. Bilokon[50], M. Bindi[57], A. Bingul[20b], C. Bini[134a,134b], S. Biondi[22a,22b], T. Bisanz[57], C. Bittrich[47], D. M. Bjergaard[48], C. W. Black[152], J. E. Black[145], K. M. Black[24], D. Blackburn[140], R. E. Blair[6], J.-B. Blanchard[138], T. Blazek[146a], I. Bloch[45], C. Blocker[25], A. Blue[56], W. Blum[86,*], U. Blumenschein[79], S. Blunier[34a], G. J. Bobbink[109], V. S. Bobrovnikov[111,c], S. S. Bocchetta[84], A. Bocci[48], C. Bock[102], M. Boehler[51], D. Boerner[178], D. Bogavac[102], A. G. Bogdanchikov[111], C. Bohm[148a], V. Boisvert[80], P. Bokan[168,i], T. Bold[41a], A. S. Boldyrev[101], M. Bomben[83], M. Bona[79], M. Boonekamp[138], A. Borisov[132], G. Borissov[75], J. Bortfeldt[32], D. Bortoletto[122], V. Bortolotto[62a,62b,62c], K. Bos[109], D. Boscherini[22a], M. Bosman[13], J. D. Bossio Sola[29], J. Boudreau[127], J. Bouffard[2], E. V. Bouhova-Thacker[75], D. Boumediene[37], C. Bourdarios[119], S. K. Boutle[56], A. Boveia[113], J. Boyd[32], I. R. Boyko[68], J. Bracinik[19], A. Brandt[8], G. Brandt[57], O. Brandt[60a], U. Bratzler[158], B. Brau[89], J. E. Brau[118], W. D. Breaden Madden[56], K. Brendlinger[45], A. J. Brennan[91], L. Brenner[109], R. Brenner[168], S. Bressler[175], D. L. Briglin[19], T. M. Bristow[49], D. Britton[56], D. Britzger[45], F. M. Brochu[30], I. Brock[23], R. Brock[93], G. Brooijmans[38], T. Brooks[80], W. K. Brooks[34b], J. Brosamer[16], E. Brost[110], J. H Broughton[19], P. A. Bruckman de Renstrom[42], D. Bruncko[146b], A. Bruni[22a], G. Bruni[22a], L. S. Bruni[109], B H Brunt[30], M. Bruschi[22a], N. Bruscino[23], P. Bryant[33], L. Bryngemark[84], T. Buanes[15], Q. Buat[144], P. Buchholz[143], A. G. Buckley[56], I. A. Budagov[68], F. Buehrer[51], M. K. Bugge[121], O. Bulekov[100], D. Bullock[8], H. Burckhart[32], S. Burdin[77], C. D. Burgard[51], A. M. Burger[5], B. Burghgrave[110], K. Burka[42], S. Burke[133], I. Burmeister[46], J. T. P. Burr[122], E. Busato[37], D. Büscher[51], V. Büscher[86], P. Bussey[56], J. M. Butler[24], C. M. Buttar[56], J. M. Butterworth[81], P. Butti[32], W. Buttinger[27],

A. Buzatu[35c], A. R. Buzykaev[111,c], S. Cabrera Urbán[170], D. Caforio[130], V. M. Cairo[40a,40b], O. Cakir[4a], N. Calace[52], P. Calafiura[16], A. Calandri[88], G. Calderini[83], P. Calfayan[64], G. Callea[40a,40b], L. P. Caloba[26a], S. Calvente Lopez[85], D. Calvet[37], S. Calvet[37], T. P. Calvet[88], R. Camacho Toro[33], S. Camarda[32], P. Camarri[135a,135b], D. Cameron[121], R. Caminal Armadans[169], C. Camincher[58], S. Campana[32], M. Campanelli[81], A. Camplani[94a,94b], A. Campoverde[143], V. Canale[106a,106b], M. Cano Bret[36c], J. Cantero[116], T. Cao[155], M. D. M. Capeans Garrido[32], I. Caprini[28b], M. Caprini[28b], M. Capua[40a,40b], R. M. Carbone[38], R. Cardarelli[135a], F. Cardillo[51], I. Carli[131], T. Carli[32], G. Carlino[106a], B. T. Carlson[127], L. Carminati[94a,94b], R. M. D. Carney[148a,148b], S. Caron[108], E. Carquin[34b], G. D. Carrillo-Montoya[32], J. Carvalho[128a,128c], D. Casadei[19], M. P. Casado[13,j], M. Casolino[13], D. W. Casper[166], R. Castelijn[109], A. Castelli[109], V. Castillo Gimenez[170], N. F. Castro[128a,k], A. Catinaccio[32], J. R. Catmore[121], A. Cattai[32], J. Caudron[23], V. Cavaliere[169], E. Cavallaro[13], D. Cavalli[94a], M. Cavalli-Sforza[13], V. Cavasinni[126a,126b], E. Celebi[20a], F. Ceradini[136a,136b], L. Cerda Alberich[170], A. S. Cerqueira[26b], A. Cerri[151], L. Cerrito[135a,135b], F. Cerutti[16], A. Cervelli[18], S. A. Cetin[20c], A. Chafaq[137a], D. Chakraborty[110], S. K. Chan[59], W. S. Chan[109], Y. L. Chan[62a], P. Chang[169], J. D. Chapman[30], D. G. Charlton[19], A. Chatterjee[52], C. C. Chau[161], C. A. Chavez Barajas[151], S. Che[113], S. Cheatham[167a,167c], A. Chegwidden[93], S. Chekanov[6], S. V. Chekulaev[163a], G. A. Chelkov[68,l], M. A. Chelstowska[32], C. Chen[67], H. Chen[27], S. Chen[35b], S. Chen[157], X. Chen[35c,m], Y. Chen[70], H. C. Cheng[92], H. J. Cheng[35a], Y. Cheng[33], A. Cheplakov[68], E. Cheremushkina[132], R. Cherkaoui El Moursli[137e], V. Chernyatin[27,*], E. Cheu[7], L. Chevalier[138], V. Chiarella[50], G. Chiarelli[126a,126b], G. Chiodini[76a], A. S. Chisholm[32], A. Chitan[28b], Y. H. Chiu[172], M. V. Chizhov[68], K. Choi[64], A. R. Chomont[37], S. Chouridou[159], B.K.B. Chow[102], V. Christodoulou[81], D. Chromek-Burckhart[32], M. C. Chu[62a], J. Chudoba[129], A. J. Chuinard[90], J. J. Chwastowski[42], L. Chytka[117], A. K. Ciftci[4a], D. Cinca[46], V. Cindro[78], I. A. Cioara[23], C. Ciocca[22a,22b], A. Ciocio[16], F. Cirotto[106a,106b], Z. H. Citron[175], M. Citterio[94a], M. Ciubancan[28b], A. Clark[52], B. L. Clark[59], M. R. Clark[38], P. J. Clark[49], R. N. Clarke[16], C. Clement[148a,148b], Y. Coadou[88], M. Cobal[167a,167c], A. Coccaro[52], J. Cochran[67], L. Colasurdo[108], B. Cole[38], A. P. Colijn[109], J. Collot[58], T. Colombo[166], P. Conde Muiño[128a,128b], E. Coniavitis[51], S. H. Connell[147b], I. A. Connelly[87], V. Consorti[51], S. Constantinescu[28b], G. Conti[32], F. Conventi[106a,n], M. Cooke[16], B. D. Cooper[81], A. M. Cooper-Sarkar[122], F. Cormier[171], K. J. R. Cormier[161], T. Cornelissen[178], M. Corradi[134a,134b], F. Corriveau[90,o], A. Cortes-Gonzalez[32], G. Cortiana[103], G. Costa[94a], M. J. Costa[170], D. Costanzo[141], G. Cottin[30], G. Cowan[80], B. E. Cox[87], K. Cranmer[112], S. J. Crawley[56], R. A. Creager[124], G. Cree[31], S. Crépé-Renaudin[58], F. Crescioli[83], W. A. Cribbs[148a,148b], M. Crispin Ortuzar[122], M. Cristinziani[23], V. Croft[108], G. Crosetti[40a,40b], A. Cueto[85], T. Cuhadar Donszelmann[141], J. Cummings[179], M. Curatolo[50], J. Cúth[86], H. Czirr[143], P. Czodrowski[32], G. D'amen[22a,22b], S. D'Auria[56], M. D'Onofrio[77], M. J. Da Cunha Sargedas De Sousa[128a,128b], C. Da Via[87], W. Dabrowski[41a], T. Dado[146a], T. Dai[92], O. Dale[15], F. Dallaire[97], C. Dallapiccola[89], M. Dam[39], J. R. Dandoy[124], N. P. Dang[51], A. C. Daniells[19], N. S. Dann[87], M. Danninger[171], M. Dano Hoffmann[138], V. Dao[150], G. Darbo[53a], S. Darmora[8], J. Dassoulas[3], A. Dattagupta[118], T. Daubney[45], W. Davey[23], C. David[45], T. Davidek[131], M. Davies[155], P. Davison[81], E. Dawe[91], I. Dawson[141], K. De[8], R. de Asmundis[106a], A. De Benedetti[115], S. De Castro[22a,22b], S. De Cecco[83], N. De Groot[108], P. de Jong[109], H. De la Torre[93], F. De Lorenzi[67], A. De Maria[57], D. De Pedis[134a], A. De Salvo[134a], U. De Sanctis[151], A. De Santo[151], K. De Vasconcelos Corga[88], J. B. De Vivie De Regie[119], W. J. Dearnaley[75], R. Debbe[27], C. Debenedetti[139], D. V. Dedovich[68], N. Dehghanian[3], I. Deigaard[109], M. Del Gaudio[40a,40b], J. Del Peso[85], T. Del Prete[126a,126b], D. Delgove[119], F. Deliot[138], C. M. Delitzsch[52], A. Dell'Acqua[32], L. Dell'Asta[24], M. Dell'Orso[126a,126b], M. Della Pietra[106a,106b], D. della Volpe[52], M. Delmastro[5], P. A. Delsart[58], D. A. DeMarco[161], S. Demers[179], M. Demichev[68], A. Demilly[83], S. P. Denisov[132], D. Denysiuk[138], D. Derendarz[42], J. E. Derkaoui[137d], F. Derue[83], P. Dervan[77], K. Desch[23], C. Deterre[45], K. Dette[46], P. O. Deviveiros[32], A. Dewhurst[133], S. Dhaliwal[25], A. Di Ciaccio[135a,135b], L. Di Ciaccio[5], W. K. Di Clemente[124], C. Di Donato[106a,106b], A. Di Girolamo[32], B. Di Girolamo[32], B. Di Micco[136a,136b], R. Di Nardo[32], K. F. Di Petrillo[59], A. Di Simone[51], R. Di Sipio[161], D. Di Valentino[31], C. Diaconu[88], M. Diamond[161], F. A. Dias[49], M. A. Diaz[34a], E. B. Diehl[92], J. Dietrich[17], S. Díez Cornell[45], A. Dimitrievska[14], J. Dingfelder[23], P. Dita[28b], S. Dita[28b], F. Dittus[32], F. Djama[88], T. Djobava[54b], J. I. Djuvsland[60a], M. A. B. do Vale[26c], D. Dobos[32], M. Dobre[28b], C. Doglioni[84], J. Dolejsi[131], Z. Dolezal[131], M. Donadelli[26d], S. Donati[126a,126b], P. Dondero[123a,123b], J. Donini[37], J. Dopke[133], A. Doria[106a], M. T. Dova[74], A. T. Doyle[56], E. Drechsler[57], M. Dris[10], Y. Du[36b], J. Duarte-Campderros[155], E. Duchovni[175], G. Duckeck[102], O. A. Ducu[97,p], D. Duda[109], A. Dudarev[32], A. Chr. Dudder[86], E. M. Duffield[16], L. Duflot[119], M. Dührssen[32], M. Dumancic[175], A. E. Dumitriu[28b], A. K. Duncan[56], M. Dunford[60a], H. Duran Yildiz[4a], M. Düren[55], A. Durglishvili[54b], D. Duschinger[47], B. Dutta[45], M. Dyndal[45], C. Eckardt[45], K. M. Ecker[103], R. C. Edgar[92], T. Eifert[32], G. Eigen[15], K. Einsweiler[16], T. Ekelof[168], M. El Kacimi[137c], V. Ellajosyula[88], M. Ellert[168], S. Elles[5], F. Ellinghaus[178], A. A. Elliot[172], N. Ellis[32], J. Elmsheuser[27], M. Elsing[32], D. Emeliyanov[133], Y. Enari[157], O. C. Endner[86], J. S. Ennis[173], J. Erdmann[46], A. Ereditato[18], G. Ernis[178], M. Ernst[27], S. Errede[169], E. Ertel[86], M. Escalier[119], H. Esch[46], C. Escobar[127], B. Esposito[50], A. I. Etienvre[138], E. Etzion[155], H. Evans[64], A. Ezhilov[125], F. Fabbri[22a,22b], L. Fabbri[22a,22b], G. Facini[33], R. M. Fakhrutdinov[132],

S. Falciano[134a], R. J. Falla[81], J. Faltova[32], Y. Fang[35a], M. Fanti[94a,94b], A. Farbin[8], A. Farilla[136a], C. Farina[127], E. M. Farina[123a,123b], T. Farooque[93], S. Farrell[16], S. M. Farrington[173], P. Farthouat[32], F. Fassi[137e], P. Fassnacht[32], D. Fassouliotis[9], M. Faucci Giannelli[80], A. Favareto[53a,53b], W. J. Fawcett[122], L. Fayard[119], O. L. Fedin[125,q], W. Fedorko[171], S. Feigl[121], L. Feligioni[88], C. Feng[36b], E. J. Feng[32], H. Feng[92], A. B. Fenyuk[132], L. Feremenga[8], P. Fernandez Martinez[170], S. Fernandez Perez[13], J. Ferrando[45], A. Ferrari[168], P. Ferrari[109], R. Ferrari[123a], D. E. Ferreira de Lima[60b], A. Ferrer[170], D. Ferrere[52], C. Ferretti[92], F. Fiedler[86], A. Filipčič[78], M. Filipuzzi[45], F. Filthaut[108], M. Fincke-Keeler[172], K. D. Finelli[152], M. C. N. Fiolhais[128a,128c,r], L. Fiorini[170], A. Fischer[2], C. Fischer[13], J. Fischer[178], W. C. Fisher[93], N. Flaschel[45], I. Fleck[143], P. Fleischmann[92], R. R. M. Fletcher[124], T. Flick[178], B. M. Flierl[102], L. R. Flores Castillo[62a], M. J. Flowerdew[103], G. T. Forcolin[87], A. Formica[138], A. Forti[87], A. G. Foster[19], D. Fournier[119], H. Fox[75], S. Fracchia[113], P. Francavilla[83], M. Franchini[22a,22b], D. Francis[32], L. Franconi[121], M. Franklin[59], M. Frate[166], M. Fraternali[123a,123b], D. Freeborn[81], S. M. Fressard-Batraneanu[32], B. Freund[97], D. Froidevaux[32], J. A. Frost[122], C. Fukunaga[158], E. Fullana Torregrosa[86], T. Fusayasu[104], J. Fuster[170], C. Gabaldon[58], O. Gabizon[154], A. Gabrielli[22a,22b], A. Gabrielli[16], G. P. Gach[41a], S. Gadatsch[32], S. Gadomski[80], G. Gagliardi[53a,53b], L. G. Gagnon[97], P. Gagnon[64], C. Galea[108], B. Galhardo[128a,128c], E. J. Gallas[122], B. J. Gallop[133], P. Gallus[130], G. Galster[39], K. K. Gan[113], S. Ganguly[37], J. Gao[36a], Y. Gao[77], Y. S. Gao[145,g], F. M. Garay Walls[49], C. García[170], J. E. García Navarro[170], M. Garcia-Sciveres[16], R. W. Gardner[33], N. Garelli[145], V. Garonne[121], A. Gascon Bravo[45], K. Gasnikova[45], C. Gatti[50], A. Gaudiello[53a,53b], G. Gaudio[123a], I. L. Gavrilenko[98], C. Gay[171], G. Gaycken[23], E. N. Gazis[10], C. N. P. Gee[133], M. Geisen[86], M. P. Geisler[60a], K. Gellerstedt[148a,148b], C. Gemme[53a], M. H. Genest[58], C. Geng[36a,s], S. Gentile[134a,134b], C. Gentsos[156], S. George[80], D. Gerbaudo[13], A. Gershon[155], S. Ghasemi[143], M. Ghneimat[23], B. Giacobbe[22a], S. Giagu[134a,134b], P. Giannetti[126a,126b], S. M. Gibson[80], M. Gignac[171], M. Gilchriese[16], D. Gillberg[31], G. Gilles[178], D. M. Gingrich[3,d], N. Giokaris[9,*], M. P. Giordani[167a,167c], F. M. Giorgi[22a], P. F. Giraud[138], P. Giromini[59], D. Giugni[94a], F. Giuli[122], C. Giuliani[103], M. Giulini[60b], B. K. Gjelsten[121], S. Gkaitatzis[156], I. Gkialas[9], E. L. Gkougkousis[139], L. K. Gladilin[101], C. Glasman[85], J. Glatzer[13], P. C. F. Glaysher[45], A. Glazov[45], M. Goblirsch-Kolb[25], J. Godlewski[42], S. Goldfarb[91], T. Golling[52], D. Golubkov[132], A. Gomes[128a,128b,128d], R. Gonçalo[128a], R. Goncalves Gama[26a], J. Goncalves Pinto Firmino Da Costa[138], G. Gonella[51], L. Gonella[19], A. Gongadze[68], S. González de la Hoz[170], S. Gonzalez-Sevilla[52], L. Goossens[32], P. A. Gorbounov[99], H. A. Gordon[27], I. Gorelov[107], B. Gorini[32], E. Gorini[76a,76b], A. Gorišek[78], A. T. Goshaw[48], C. Gössling[46], M. I. Gostkin[68], C. R. Goudet[119], D. Goujdami[137c], A. G. Goussiou[140], N. Govender[147b,t], E. Gozani[154], L. Graber[57], I. Grabowska-Bold[41a], P. O. J. Gradin[58], J. Gramling[52], E. Gramstad[121], S. Grancagnolo[17], V. Gratchev[125], P. M. Gravila[28f], H. M. Gray[32], Z. D. Greenwood[82,u], C. Grefe[23], K. Gregersen[81], I. M. Gregor[45], P. Grenier[145], K. Grevtsov[5], J. Griffiths[8], A. A. Grillo[139], K. Grimm[75], S. Grinstein[13,v], Ph. Gris[37], J.-F. Grivaz[119], S. Groh[86], E. Gross[175], J. Grosse-Knetter[57], G. C. Grossi[82], Z. J. Grout[81], L. Guan[92], W. Guan[176], J. Guenther[65], F. Guescini[163a], D. Guest[166], O. Gueta[155], B. Gui[113], E. Guido[53a,53b], T. Guillemin[5], S. Guindon[2], U. Gul[56], C. Gumpert[32], J. Guo[36c], W. Guo[92], Y. Guo[36a], R. Gupta[43], S. Gupta[122], G. Gustavino[134a,134b], P. Gutierrez[115], N. G. Gutierrez Ortiz[81], C. Gutschow[81], C. Guyot[138], M. P. Guzik[41a], C. Gwenlan[122], C. B. Gwilliam[77], A. Haas[112], C. Haber[16], H. K. Hadavand[8], A. Hadef[88], S. Hageböck[23], M. Hagihara[164], H. Hakobyan[180,*], M. Haleem[45], J. Haley[116], G. Halladjian[93], G. D. Hallewell[88], K. Hamacher[178], P. Hamal[117], K. Hamano[172], A. Hamilton[147a], G. N. Hamity[141], P. G. Hamnett[45], L. Han[36a], S. Han[35a], K. Hanagaki[69,w], K. Hanawa[157], M. Hance[139], B. Haney[124], P. Hanke[60a], R. Hanna[138], J. B. Hansen[39], J. D. Hansen[39], M. C. Hansen[23], P. H. Hansen[39], K. Hara[164], A. S. Hard[176], T. Harenberg[178], F. Hariri[119], S. Harkusha[95], R. D. Harrington[49], P. F. Harrison[173], F. Hartjes[109], N. M. Hartmann[102], M. Hasegawa[70], Y. Hasegawa[142], A. Hasib[49], S. Hassani[138], S. Haug[18], R. Hauser[93], L. Hauswald[47], L. B. Havener[38], M. Havranek[130], C. M. Hawkes[19], R. J. Hawkings[32], D. Hayakawa[159], D. Hayden[93], C. P. Hays[122], J. M. Hays[79], H. S. Hayward[77], S. J. Haywood[133], S. J. Head[19], T. Heck[86], V. Hedberg[84], L. Heelan[8], K. K. Heidegger[51], S. Heim[45], T. Heim[16], B. Heinemann[45,x], J. J. Heinrich[102], L. Heinrich[112], C. Heinz[55], J. Hejbal[129], L. Helary[32], A. Held[171], S. Hellman[148a,148b], C. Helsens[32], J. Henderson[122], R. C. W. Henderson[75], Y. Heng[176], S. Henkelmann[171], A. M. Henriques Correia[32], S. Henrot-Versille[119], G. H. Herbert[17], H. Herde[25], V. Herget[177], Y. Hernández Jiménez[147c], G. Herten[51], R. Hertenberger[102], L. Hervas[32], T. C. Herwig[124], G. G. Hesketh[81], N. P. Hessey[163a], J. W. Hetherly[43], S. Higashino[69], E. Higón-Rodriguez[170], E. Hill[172], J. C. Hill[30], K. H. Hiller[45], S. J. Hillier[19], I. Hinchliffe[16], M. Hirose[51], D. Hirschbuehl[178], B. Hiti[78], O. Hladik[129], X. Hoad[49], J. Hobbs[150], N. Hod[163a], M. C. Hodgkinson[141], P. Hodgson[141], A. Hoecker[32], M. R. Hoeferkamp[107], F. Hoenig[102], D. Hohn[23], T. R. Holmes[16], M. Homann[46], S. Honda[164], T. Honda[69], T. M. Hong[127], B. H. Hooberman[169], W. H. Hopkins[118], Y. Horii[105], A. J. Horton[144], J-Y. Hostachy[58], S. Hou[153], A. Hoummada[137a], J. Howarth[45], J. Hoya[74], M. Hrabovsky[117], I. Hristova[17], J. Hrivnac[119], T. Hryn'ova[5], A. Hrynevich[96], P. J. Hsu[63], S.-C. Hsu[140], Q. Hu[36a], S. Hu[36c], Y. Huang[35a], Z. Hubacek[130], F. Hubaut[88], F. Huegging[23], T. B. Huffman[122], E. W. Hughes[38], G. Hughes[75], M. Huhtinen[32], P. Huo[150], N. Huseynov[68,b], J. Huston[93], J. Huth[59], G. Iacobucci[52], G. Iakovidis[27], I. Ibragimov[143], L. Iconomidou-Fayard[119], P. Iengo[32], O. Igonkina[109,x], T. Iizawa[174],

Y. Ikegami[69], M. Ikeno[69], Y. Ilchenko[11,y], D. Iliadis[156], N. Ilic[145], G. Introzzi[123a,123b], P. Ioannou[9,*], M. Iodice[136a], K. Iordanidou[38], V. Ippolito[59], N. Ishijima[120], M. Ishino[157], M. Ishitsuka[159], C. Issever[122], S. Istin[20a], F. Ito[164], J. M. Iturbe Ponce[87], R. Iuppa[162a,162b], H. Iwasaki[69], J. M. Izen[44], V. Izzo[106a], S. Jabbar[3], P. Jackson[1], V. Jain[2], K. B. Jakobi[86], K. Jakobs[51], S. Jakobsen[32], T. Jakoubek[129], D. O. Jamin[116], D. K. Jana[82], R. Jansky[65], J. Janssen[23], M. Janus[57], P. A. Janus[41a], G. Jarlskog[84], N. Javadov[68,b], T. Javůrek[51], M. Javurkova[51], F. Jeanneau[138], L. Jeanty[16], J. Jejelava[54a,aa], A. Jelinskas[173], P. Jenni[51,ab], C. Jeske[173], S. Jézéquel[5], H. Ji[176], J. Jia[150], H. Jiang[67], Y. Jiang[36a], Z. Jiang[145], S. Jiggins[81], J. Jimenez Pena[170], S. Jin[35a], A. Jinaru[28b], O. Jinnouchi[159], H. Jivan[147c], P. Johansson[141], K. A. Johns[7], C. A. Johnson[64], W. J. Johnson[140], K. Jon-And[148a,148b], R. W. L. Jones[75], S. Jones[7], T. J. Jones[77], J. Jongmanns[60a], P. M. Jorge[128a,128b], J. Jovicevic[163a], X. Ju[176], A. Juste Rozas[13,v], M. K. Köhler[175], A. Kaczmarska[42], M. Kado[119], H. Kagan[113], M. Kagan[145], S. J. Kahn[88], T. Kaji[174], E. Kajomovitz[48], C. W. Kalderon[84], A. Kaluza[86], S. Kama[43], A. Kamenshchikov[132], N. Kanaya[157], S. Kaneti[30], L. Kanjir[78], V. A. Kantserov[100], J. Kanzaki[69], B. Kaplan[112], L. S. Kaplan[176], D. Kar[147c], K. Karakostas[10], N. Karastathis[10], M. J. Kareem[57], E. Karentzos[10], M. Karnevskiy[86], S. N. Karpov[68], Z. M. Karpova[68], K. Karthik[112], V. Kartvelishvili[75], A. N. Karyukhin[132], K. Kasahara[164], L. Kashif[176], R. D. Kass[113], A. Kastanas[149], Y. Kataoka[157], C. Kato[157], A. Katre[52], J. Katzy[45], K. Kawade[105], K. Kawagoe[73], T. Kawamoto[157], G. Kawamura[57], E. F. Kay[77], V. F. Kazanin[111,c], R. Keeler[172], R. Kehoe[43], J. S. Keller[45], J. J. Kempster[80], H. Keoshkerian[161], O. Kepka[129], B. P. Kerševan[78], S. Kersten[178], R. A. Keyes[90], M. Khader[169], F. Khalil-zada[12], A. Khanov[116], A. G. Kharlamov[111,c], T. Kharlamova[111,c], A. Khodinov[160], T. J. Khoo[52], V. Khovanskiy[99,*], E. Khramov[68], J. Khubua[54b,ac], S. Kido[70], C. R. Kilby[80], H. Y. Kim[8], S. H. Kim[164], Y. K. Kim[33], N. Kimura[156], O. M. Kind[17], B. T. King[77], D. Kirchmeier[47], J. Kirk[133], A. E. Kiryunin[103], T. Kishimoto[157], D. Kisielewska[41a], K. Kiuchi[164], O. Kivernyk[138], E. Kladiva[146b], T. Klapdor-Kleingrothaus[51], M. H. Klein[38], M. Klein[77], U. Klein[77], K. Kleinknecht[86], P. Klimek[110], A. Klimentov[27], R. Klingenberg[46], T. Klioutchnikova[32], E.-E. Kluge[60a], P. Kluit[109], S. Kluth[103], J. Knapik[42], E. Kneringer[65], E. B. F. G. Knoops[88], A. Knue[103], A. Kobayashi[157], D. Kobayashi[159], T. Kobayashi[157], M. Kobel[47], M. Kocian[145], P. Kodys[131], T. Koffas[31], E. Koffeman[109], N. M. Köhler[103], T. Koi[145], M. Kolb[60b], I. Koletsou[5], A. A. Komar[98,*], Y. Komori[157], T. Kondo[69], N. Kondrashova[36c], K. Köneke[51], A. C. König[108], T. Kono[69,ad], R. Konoplich[112,ae], N. Konstantinidis[81], R. Kopeliansky[64], S. Koperny[41a], A. K. Kopp[51], K. Korcyl[42], K. Kordas[156], A. Korn[81], A. A. Korol[111,c], I. Korolkov[13], E. V. Korolkova[141], O. Kortner[103], S. Kortner[103], T. Kosek[131], V. V. Kostyukhin[23], A. Kotwal[48], A. Koulouris[10], A. Kourkoumeli-Charalampidi[123a,123b], C. Kourkoumelis[9], V. Kouskoura[27], A. B. Kowalewska[42], R. Kowalewski[172], T. Z. Kowalski[41a], C. Kozakai[157], W. Kozanecki[138], A. S. Kozhin[132], V. A. Kramarenko[101], G. Kramberger[78], D. Krasnopevtsev[100], M. W. Krasny[83], A. Krasznahorkay[32], D. Krauss[103], A. Kravchenko[27], J. A. Kremer[41a], M. Kretz[60c], J. Kretzschmar[77], K. Kreutzfeldt[55], P. Krieger[161], K. Krizka[33], K. Kroeninger[46], H. Kroha[103], J. Kroll[124], J. Kroseberg[23], J. Krstic[14], U. Kruchonak[68], H. Krüger[23], N. Krumnack[67], M. C. Kruse[48], M. Kruskal[24], T. Kubota[91], H. Kucuk[81], S. Kuday[4b], J. T. Kuechler[178], S. Kuehn[51], A. Kugel[60c], F. Kuger[177], T. Kuhl[45], V. Kukhtin[68], R. Kukla[88], Y. Kulchitsky[95], S. Kuleshov[34b], Y. P. Kulinich[169], M. Kuna[134a,134b], T. Kunigo[71], A. Kupco[129], O. Kuprash[155], H. Kurashige[70], L. L. Kurchaninov[163a], Y. A. Kurochkin[95], M. G. Kurth[35a], V. Kus[129], E. S. Kuwertz[172], M. Kuze[159], J. Kvita[117], T. Kwan[172], D. Kyriazopoulos[141], A. La Rosa[103], J. L. La Rosa Navarro[26d], L. La Rotonda[40a,40b], C. Lacasta[170], F. Lacava[134a,134b], J. Lacey[45], H. Lacker[17], D. Lacour[83], E. Ladygin[68], R. Lafaye[5], B. Laforge[83], T. Lagouri[179], S. Lai[57], S. Lammers[64], W. Lampl[7], E. Lançon[27], U. Landgraf[51], M. P. J. Landon[79], M. C. Lanfermann[52], V. S. Lang[60a], J. C. Lange[13], A. J. Lankford[166], F. Lanni[27], K. Lantzsch[23], A. Lanza[123a], A. Lapertosa[53a,53b], S. Laplace[83], J. F. Laporte[138], T. Lari[94a], F. Lasagni Manghi[22a,22b], M. Lassnig[32], P. Laurelli[50], W. Lavrijsen[16], A. T. Law[139], P. Laycock[77], T. Lazovich[59], M. Lazzaroni[94a,94b], B. Le[91], O. Le Dortz[83], E. Le Guirriec[88], E. P. Le Quilleuc[138], M. LeBlanc[172], T. LeCompte[6], F. Ledroit-Guillon[58], C. A. Lee[27], S. C. Lee[153], L. Lee[1], B. Lefebvre[90], G. Lefebvre[83], M. Lefebvre[172], F. Legger[102], C. Leggett[16], A. Lehan[77], G. Lehmann Miotto[32], X. Lei[7], W. A. Leight[45], A. G. Leister[179], M. A. L. Leite[26d], R. Leitner[131], D. Lellouch[175], B. Lemmer[57], K. J. C. Leney[81], T. Lenz[23], B. Lenzi[32], R. Leone[7], S. Leone[126a,126b], C. Leonidopoulos[49], G. Lerner[151], C. Leroy[97], A. A. J. Lesage[138], C. G. Lester[30], M. Levchenko[125], J. Levêque[5], D. Levin[92], L. J. Levinson[175], M. Levy[19], D. Lewis[79], M. Leyton[44], B. Li[36a,s], C. Li[36a], H. Li[150], L. Li[48], L. Li[36c], Q. Li[35a], S. Li[48], X. Li[36c], Y. Li[143], Z. Liang[35a], B. Liberti[135a], A. Liblong[161], K. Lie[169], J. Liebal[23], W. Liebig[15], A. Limosani[152], S. C. Lin[153,af], T. H. Lin[86], B. E. Lindquist[150], A. E. Lionti[52], E. Lipeles[124], A. Lipniacka[15], M. Lisovyi[60b], T. M. Liss[169], A. Lister[171], A. M. Litke[139], B. Liu[153,ag], H. Liu[92], H. Liu[27], J. Liu[36b], J. B. Liu[36a], K. Liu[88], L. Liu[169], M. Liu[36a], Y. L. Liu[36a], Y. Liu[36a], M. Livan[123a,123b], A. Lleres[58], J. Llorente Merino[35a], S. L. Lloyd[79], C. Y. Lo[62b], F. Lo Sterzo[153], E. M. Lobodzinska[45], P. Loch[7], F. K. Loebinger[87], K. M. Loew[25], A. Loginov[179,*], T. Lohse[17], K. Lohwasser[45], M. Lokajicek[129], B. A. Long[24], J. D. Long[169], R. E. Long[75], L. Longo[76a,76b], K. A. Looper[113], J. A. Lopez[34b], D. Lopez Mateos[59], I. Lopez Paz[13], A. Lopez Solis[83], J. Lorenz[102], N. Lorenzo Martinez[64], M. Losada[21], P. J. Lösel[102], X. Lou[35a], A. Lounis[119], J. Love[6], P. A. Love[75], H. Lu[62a], N. Lu[92],

Y. J. Lu[63], H. J. Lubatti[140], C. Luci[134a,134b], A. Lucotte[58], C. Luedtke[51], F. Luehring[64], W. Lukas[65], L. Luminari[134a], O. Lundberg[148a,148b], B. Lund-Jensen[149], P. M. Luzi[83], D. Lynn[27], R. Lysak[129], E. Lytken[84], V. Lyubushkin[68], H. Ma[27], L. L. Ma[36b], Y. Ma[36b], G. Maccarrone[50], A. Macchiolo[103], C. M. Macdonald[141], B. Maček[78], J. Machado Miguens[124,128b], D. Madaffari[88], R. Madar[37], H. J. Maddocks[168], W. F. Mader[47], A. Madsen[45], J. Maeda[70], S. Maeland[15], T. Maeno[27], A. Maevskiy[101], E. Magradze[57], J. Mahlstedt[109], C. Maiani[119], C. Maidantchik[26a], A. A. Maier[103], T. Maier[102], A. Maio[128a,128b,128d], S. Majewski[118], Y. Makida[69], N. Makovec[119], B. Malaescu[83], Pa. Malecki[42], V. P. Maleev[125], F. Malek[58], U. Mallik[66], D. Malon[6], C. Malone[30], S. Maltezos[10], S. Malyukov[32], J. Mamuzic[170], G. Mancini[50], L. Mandelli[94a], I. Mandić[78], J. Maneira[128a,128b], L. Manhaes de Andrade Filho[26b], J. Manjarres Ramos[163b], A. Mann[102], A. Manousos[32], B. Mansoulie[138], J. D. Mansour[35a], R. Mantifel[90], M. Mantoani[57], S. Manzoni[94a,94b], L. Mapelli[32], G. Marceca[29], L. March[52], G. Marchiori[83], M. Marcisovsky[129], M. Marjanovic[37], D. E. Marley[92], F. Marroquim[26a], S. P. Marsden[87], Z. Marshall[16], M. U. F Martensson[168], S. Marti-Garcia[170], C. B. Martin[113], T. A. Martin[173], V. J. Martin[49], B. Martin dit Latour[15], M. Martinez[13,v], V. I. Martinez Outschoorn[169], S. Martin-Haugh[133], V. S. Martoiu[28b], A. C. Martyniuk[81], A. Marzin[115], L. Masetti[86], T. Mashimo[157], R. Mashinistov[98], J. Masik[87], A. L. Maslennikov[111,c], L. Massa[135a,135b], P. Mastrandrea[5], A. Mastroberardino[40a,40b], T. Masubuchi[157], P. Mättig[178], J. Maurer[28b], S. J. Maxfield[77], D. A. Maximov[111,c], R. Mazini[153], I. Maznas[156], S. M. Mazza[94a,94b], N. C. Mc Fadden[107], G. Mc Goldrick[161], S. P. Mc Kee[92], A. McCarn[92], R. L. McCarthy[150], T. G. McCarthy[103], L. I. McClymont[81], E. F. McDonald[91], J. A. Mcfayden[81], G. Mchedlidze[57], S. J. McMahon[133], P. C. McNamara[91], R. A. McPherson[172,o], S. Meehan[140], T. J. Megy[51], S. Mehlhase[102], A. Mehta[77], T. Meideck[58], K. Meier[60a], C. Meineck[102], B. Meirose[44], D. Melini[170,ah], B. R. Mellado Garcia[147c], M. Melo[146a], F. Meloni[18], S. B. Menary[87], L. Meng[77], X. T. Meng[92], A. Mengarelli[22a,22b], S. Menke[103], E. Meoni[165], S. Mergelmeyer[17], P. Mermod[52], L. Merola[106a,106b], C. Meroni[94a], F. S. Merritt[33], A. Messina[134a,134b], J. Metcalfe[6], A. S. M ete[166], C. Meyer[124], J-P. Meyer[138], J. Meyer[109], H. Meyer Zu Theenhausen[60a], F. Miano[151], R. P. Middleton[133], S. Miglioranzi[53a,53b], L. Mijović[49], G. Mikenberg[175], M. Mikestikova[129], M. Mikuž[78], M. Milesi[91], A. Milic[27], D. W. Miller[33], C. Mills[49], A. Milov[175], D. A. Milstead[148a,148b], A. A. Minaenko[132], Y. Minami[157], I. A. Minashvili[68], A. I. Mincer[112], B. Mindur[41a], M. Mineev[68], Y. Minegishi[157], Y. Ming[176], L. M. Mir[13], K. P. Mistry[124], T. Mitani[174], J. Mitrevski[102], V. A. Mitsou[170], A. Miucci[18], P. S. Miyagawa[141], A. Mizukami[69], J. U. Mjörnmark[84], M. Mlynarikova[131], T. Moa[148a,148b], K. Mochizuki[97], P. Mogg[51], S. Mohapatra[38], S. Molander[148a,148b], R. Moles-Valls[23], R. Monden[71], M. C. Mondragon[93], K. Mönig[45], J. Monk[39], E. Monnier[88], A. Montalbano[150], J. Montejo Berlingen[32], F. Monticelli[74], S. Monzani[94a,94b], R. W. Moore[3], N. Morange[119], D. Moreno[21], M. Moreno Llácer[57], P. Morettini[53a], S. Morgenstern[32], D. Mori[144], T. Mori[157], M. Morii[59], M. Morinaga[157], V. Morisbak[121], A. K. Morley[152], G. Mornacchi[32], J. D. Morris[79], L. Morvaj[150], P. Moschovakos[10], M. Mosidze[54b], H. J. Moss[141], J. Moss[145,ai], K. Motohashi[159], R. Mount[145], E. Mountricha[27], E. J. W. Moyse[89], S. Muanza[88], R. D. Mudd[19], F. Mueller[103], J. Mueller[127], R. S. P. Mueller[102], D. Muenstermann[75], P. Mullen[56], G. A. Mullier[18], F. J. Munoz Sanchez[87], W. J. Murray[173,133], H. Musheghyan[157], M. Muškinja[78], A. G. Myagkov[132,aj], M. Myska[130], B. P. Nachman[16], O. Nackenhorst[52], K. Nagai[122], R. Nagai[69,ad], K. Nagano[69], Y. Nagasaka[61], K. Nagata[164], M. Nagel[51], E. Nagy[88], A. M. Nairz[32], Y. Nakahama[105], K. Nakamura[69], T. Nakamura[157], I. Nakano[114], R. F. Naranjo Garcia[45], R. Narayan[11], D. I. Narrias Villar[60a], I. Naryshkin[125], T. Naumann[45], G. Navarro[21], R. Nayyar[7], H. A. Neal[92], P. Yu. Nechaeva[98], T. J. Neep[138], A. Negri[123a,123b], M. Negrini[22a], S. Nektarijevic[108], C. Nellist[119], A. Nelson[166], M. E. Nelson[122], S. Nemecek[129], P. Nemethy[112], A. A. Nepomuceno[26a], M. Nessi[32,ak], M. S. Neubauer[169], M. Neumann[178], R. M. Neves[112], P. Nevski[27], P. R. Newman[19], T. Y. Ng[62c], T. Nguyen Manh[97], R. B. Nickerson[122], R. Nicolaidou[138], J. Nielsen[139], V. Nikolaenko[132,aj], I. Nikolic-Audit[83], K. Nikolopoulos[19], J. K. Nilsen[121], P. Nilsson[27], Y. Ninomiya[157], A. Nisati[134a], N. Nishu[35c], R. Nisius[103], T. Nobe[157], Y. Noguchi[71], M. Nomachi[120], I. Nomidis[31], M. A. Nomura[27], T. Nooney[79], M. Nordberg[32], N. Norjoharuddeen[122], O. Novgorodova[47], S. Nowak[103], M. Nozaki[69], L. Nozka[117], K. Ntekas[166], E. Nurse[81], F. Nuti[91], D. C. O'Neil[144], A. A. O'Rourke[45], V. O'Shea[56], F. G. Oakham[31,d], H. Oberlack[103], T. Obermann[23], J. Ocariz[83], A. Ochi[70], I. Ochoa[38], J. P. Ochoa-Ricoux[34a], S. Oda[73], S. Odaka[69], H. Ogren[64], A. Oh[87], S. H. Oh[48], C. C. Ohm[16], H. Ohman[168], H. Oide[53a,53b], H. Okawa[164], Y. Okumura[157], T. Okuyama[69], A. Olariu[28b], L. F. Oleiro Seabra[128a], S. A. Olivares Pino[49], D. Oliveira Damazio[27], A. Olszewski[42], J. Olszowska[42], A. Onofre[128a,128e], K. Onogi[105], P. U. E. Onyisi[11,z], M. J. Oreglia[33], Y. Oren[155], D. Orestano[136a,136b], N. Orlando[62b], R. S. Orr[161], B. Osculati[53a,53b,*], R. Ospanov[87], G. Otero y Garzon[29], H. Otono[73], M. Ouchrif[137d], F. Ould-Saada[121], A. Ouraou[138], K. P. Oussoren[109], Q. Ouyang[35a], M. Owen[56], R. E. Owen[19], V. E. Ozcan[20a], N. Ozturk[8], K. Pachal[144], A. Pacheco Pages[13], L. Pacheco Rodriguez[138], C. Padilla Aranda[13], S. Pagan Griso[16], M. Paganini[179], F. Paige[27], P. Pais[89], G. Palacino[64], S. Palazzo[40a,40b], S. Palestini[32], M. Palka[41b], D. Pallin[37], E. St. Panagiotopoulou[10], I. Panagoulias[10], C. E. Pandini[83], J. G. Panduro Vazquez[80], P. Pani[32], S. Panitkin[27], D. Pantea[28b], L. Paolozzi[52], Th. D. Papadopoulou[10], K. Papageorgiou[9], A. Paramonov[6], D. Paredes Hernandez[179], A. J. Parker[75], M. A. Parker[30], K. A. Parker[45], F. Parodi[53a,53b], J. A. Parsons[38], U. Parzefall[51],

V. R. Pascuzzi[161], J. M. Pasner[139], E. Pasqualucci[134a], S. Passaggio[53a], Fr. Pastore[80], S. Pataraia[178], J. R. Pater[87], T. Pauly[32], J. Pearce[172], B. Pearson[103], L. E. Pedersen[39], S. Pedraza Lopez[170], R. Pedro[128a,128b], S. V. Peleganchuk[111,c], O. Penc[129], C. Peng[35a], H. Peng[36a], J. Penwell[64], B. S. Peralva[26b], M. M. Perego[138], D. V. Perepelitsa[27], L. Perini[94a,94b], H. Pernegger[32], S. Perrella[106a,106b], R. Peschke[45], V. D. Peshekhonov[68], K. Peters[45], R. F. Y. Peters[87], B. A. Petersen[32], T. C. Petersen[39], E. Petit[58], A. Petridis[1], C. Petridou[156], P. Petroff[119], E. Petrolo[134a], M. Petrov[122], F. Petrucci[136a,136b], N. E. Pettersson[89], A. Peyaud[138], R. Pezoa[34b], P. W. Phillips[133], G. Piacquadio[150], E. Pianori[173], A. Picazio[89], E. Piccaro[79], M. A. Pickering[122], R. Piegaia[29], J. E. Pilcher[33], A. D. Pilkington[87], A. W. J. Pin[87], M. Pinamonti[167a,167c,al], J. L. Pinfold[3], H. Pirumov[45], M. Pitt[175], L. Plazak[146a], M.-A. Pleier[27], V. Pleskot[86], E. Plotnikova[68], D. Pluth[67], P. Podberezko[111], R. Poettgen[148a,148b], L. Poggioli[119], D. Pohl[23], G. Polesello[123a], A. Poley[45], A. Policicchio[40a,40b], R. Polifka[32], A. Polini[22a], C. S. Pollard[56], V. Polychronakos[27], K. Pommès[32], L. Pontecorvo[134a], B. G. Pope[93], G. A. Popeneciu[28d], A. Poppleton[32], S. Pospisil[130], K. Potamianos[16], I. N. Potrap[68], C. J. Potter[30], C. T. Potter[118], G. Poulard[32], J. Poveda[32], M. E. Pozo Astigarraga[32], P. Pralavorio[88], A. Pranko[16], S. Prell[67], D. Price[87], L. E. Price[6], M. Primavera[76a], S. Prince[90], K. Prokofiev[62c], F. Prokoshin[34b], S. Protopopescu[27], J. Proudfoot[6], M. Przybycien[41a], D. Puddu[136a,136b], A. Puri[169], P. Puzo[119], J. Qian[92], G. Qin[56], Y. Qin[87], A. Quadt[57], W. B. Quayle[167a,167b], M. Queitsch-Maitland[45], D. Quilty[56], S. Raddum[121], V. Radeka[27], V. Radescu[122], S. K. Radhakrishnan[150], P. Radloff[118], P. Rados[91], F. Ragusa[94a,94b], G. Rahal[181], J. A. Raine[87], S. Rajagopalan[27], C. Rangel-Smith[168], M. G. Ratti[94a,94b], D. M. Rauch[45], F. Rauscher[102], S. Rave[86], T. Ravenscroft[56], I. Ravinovich[175], M. Raymond[32], A. L. Read[121], N. P. Readioff[77], M. Reale[76a,76b], D. M. Rebuzzi[123a,123b], A. Redelbach[177], G. Redlinger[27], R. Reece[139], R. G. Reed[147c], K. Reeves[44], L. Rehnisch[17], J. Reichert[124], A. Reiss[86], C. Rembser[32], H. Ren[35a], M. Rescigno[134a], S. Resconi[94a], E. D. Resseguie[124], S. Rettie[171], E. Reynolds[19], O. L. Rezanova[111,c], P. Reznicek[131], R. Rezvani[97], R. Richter[103], S. Richter[81], E. Richter-Was[41b], O. Ricken[23], M. Ridel[83], P. Rieck[103], C. J. Riegel[178], J. Rieger[57], O. Rifki[115], M. Rijssenbeek[150], A. Rimoldi[123a,123b], M. Rimoldi[18], L. Rinaldi[22a], B. Ristić[52], E. Ritsch[32], I. Riu[13], F. Rizatdinova[116], E. Rizvi[79], C. Rizzi[13], R. T. Roberts[87], S. H. Robertson[90,o], A. Robichaud-Veronneau[90], D. Robinson[30], J. E. M. Robinson[45], A. Robson[56], C. Roda[126a,126b], Y. Rodina[88], A. Rodriguez Perez[13], D. Rodriguez Rodriguez[170], S. Roe[32], C. S. Rogan[59], O. Røhne[121], J. Roloff[59], A. Romaniouk[100], M. Romano[22a,22b], S. M. Romano Saez[37], E. Romero Adam[170], N. Rompotis[77], M. Ronzani[51], L. Roos[83], S. Rosati[134a], K. Rosbach[51], P. Rose[139], N.-A. Rosien[57], V. Rossetti[148a,148b], E. Rossi[106a,106b], L. P. Rossi[53a], J. H. N. Rosten[30], R. Rosten[140], M. Rotaru[28b], I. Roth[175], J. Rothberg[140], D. Rousseau[119], A. Rozanov[88], Y. Rozen[154], X. Ruan[147c], F. Rubbo[145], F. Rühr[51], A. Ruiz-Martinez[31], Z. Rurikova[51], N. A. Rusakovich[68], A. Ruschke[102], H. L. Russell[140], J. P. Rutherfoord[7], N. Ruthmann[32], Y. F. Ryabov[125], M. Rybar[169], G. Rybkin[119], S. Ryu[6], A. Ryzhov[132], G. F. Rzehorz[57], A. F. Saavedra[152], G. Sabato[109], S. Sacerdoti[29], H. F-W. Sadrozinski[139], R. Sadykov[68], F. Safai Tehrani[134a], P. Saha[110], M. Sahinsoy[60a], M. Saimpert[45], M. Saito[157], T. Saito[157], H. Sakamoto[157], Y. Sakurai[174], G. Salamanna[136a,136b], J. E. Salazar Loyola[34b], D. Salek[109], P. H. Sales De Bruin[140], D. Salihagic[103], A. Salnikov[145], J. Salt[170], D. Salvatore[40a,40b], F. Salvatore[151], A. Salvucci[62a,62b,62c], A. Salzburger[32], D. Sammel[51], D. Sampsonidis[156], J. Sánchez[170], V. Sanchez Martinez[170], A. Sanchez Pineda[106a,106b], H. Sandaker[121], R. L. Sandbach[79], C. O. Sander[45], M. Sandhoff[178], C. Sandoval[21], D. P. C. Sankey[133], M. Sannino[53a,53b], A. Sansoni[50], C. Santoni[37], R. Santonico[135a,135b], H. Santos[128a], I. Santoyo Castillo[151], K. Sapp[127], A. Sapronov[68], J. G. Saraiva[128a,128d], B. Sarrazin[23], O. Sasaki[69], K. Sato[164], E. Sauvan[5], G. Savage[80], P. Savard[161,d], N. Savic[103], C. Sawyer[133], L. Sawyer[82,u], J. Saxon[33], C. Sbarra[22a], A. Sbrizzi[22a,22b], T. Scanlon[81], D. A. Scannicchio[166], M. Scarcella[152], V. Scarfone[40a,40b], J. Schaarschmidt[140], P. Schacht[103], B. M. Schachtner[102], D. Schaefer[32], L. Schaefer[124], R. Schaefer[45], J. Schaeffer[86], S. Schaepe[23], S. Schaetzel[60b], U. Schäfer[86], A. C. Schaffer[119], D. Schaile[102], R. D. Schamberger[150], V. Scharf[60a], V. A. Schegelsky[125], D. Scheirich[131], M. Schernau[166], C. Schiavi[53a,53b], S. Schier[139], C. Schillo[51], M. Schioppa[40a,40b], S. Schlenker[32], K. R. Schmidt-Sommerfeld[103], K. Schmieden[32], C. Schmitt[86], S. Schmitt[45], S. Schmitz[86], B. Schneider[163a], U. Schnoor[51], L. Schoeffel[138], A. Schoening[60b], B. D. Schoenrock[93], E. Schopf[23], M. Schott[86], J. F. P. Schouwenberg[108], J. Schovancova[8], S. Schramm[52], N. Schuh[86], A. Schulte[86], M. J. Schultens[23], H.-C. Schultz-Coulon[60a], H. Schulz[17], M. Schumacher[51], B. A. Schumm[139], Ph. Schune[138], A. Schwartzman[145], T. A. Schwarz[92], H. Schweiger[87], Ph. Schwemling[138], R. Schwienhorst[93], J. Schwindling[138], T. Schwindt[23], G. Sciolla[25], F. Scuri[126a,126b], F. Scutti[91], J. Searcy[92], P. Seema[23], S. C. Seidel[107], A. Seiden[139], J. M. Seixas[26a], G. Sekhniaidze[106a], K. Sekhon[92], S. J. Sekula[43], N. Semprini-Cesari[22a,22b], C. Serfon[121], L. Serin[119], L. Serkin[167a,167b], M. Sessa[136a,136b], R. Seuster[172], H. Severini[115], T. Sfiligoj[78], F. Sforza[32], A. Sfyrla[52], E. Shabalina[57], N. W. Shaikh[148a,148b], L. Y. Shan[35a], R. Shang[169], J. T. Shank[24], M. Shapiro[16], P. B. Shatalov[99], K. Shaw[167a,167b], S. M. Shaw[87], A. Shcherbakova[148a,148b], C. Y. Shehu[151], Y. Shen[115], P. Sherwood[81], L. Shi[153,an], S. Shimizu[70], C. O. Shimmin[179], M. Shimojima[104], S. Shirabe[73], M. Shiyakova[68,ao], J. Shlomi[175], A. Shmeleva[98], D. Shoaleh Saadi[97], M. J. Shochet[33], S. Shojaii[94a], D. R. Shope[115], S. Shrestha[113], E. Shulga[100], M. A. Shupe[7], P. Sicho[129], A. M. Sickles[169], P. E. Sidebo[149], E. Sideras Haddad[147c], O. Sidiropoulou[177], D. Sidorov[116],

A. Sidoti[22a,22b], F. Siegert[47], Dj. Sijacki[14], J. Silva[128a,128d], S. B. Silverstein[148a], V. Simak[130], Lj. Simic[14], S. Simion[119], E. Simioni[86], B. Simmons[81], M. Simon[86], P. Sinervo[161], N. B. Sinev[118], M. Sioli[22a,22b], G. Siragusa[177], I. Siral[92], S. Yu. Sivoklokov[101], J. Sjölin[148a,148b], M. B. Skinner[75], P. Skubic[115], M. Slater[19], T. Slavicek[130], M. Slawinska[109], K. Sliwa[165], R. Slovak[131], V. Smakhtin[175], B. H. Smart[5], L. Smestad[15], J. Smiesko[146a], S. Yu. Smirnov[100], Y. Smirnov[100], L. N. Smirnova[101,ap], O. Smirnova[84], J. W. Smith[57], M. N. K. Smith[38], R. W. Smith[38], M. Smizanska[75], K. Smolek[130], A. A. Snesarev[98], I. M. Snyder[118], S. Snyder[27], R. Sobie[172,o], F. Socher[47], A. Soffer[155], D. A. Soh[153], G. Sokhrannyi[78], C. A. Solans Sanchez[32], M. Solar[130], E. Yu. Soldatov[100], U. Soldevila[170], A. A. Solodkov[132], A. Soloshenko[68], O. V. Solovyanov[132], V. Solovyev[125], P. Sommer[51], H. Son[165], H. Y. Song[36a,aq], A. Sopczak[130], V. Sorin[13], D. Sosa[60b], C. L. Sotiropoulou[126a,126b], R. Soualah[167a,167c], A. M. Soukharev[111,c], D. South[45], B. C. Sowden[80], S. Spagnolo[76a,76b], M. Spalla[126a,126b], M. Spangenberg[173], F. Spanò[80], D. Sperlich[17], F. Spettel[103], T. M. Spieker[60a], R. Spighi[22a], G. Spigo[32], L. A. Spiller[91], M. Spousta[131], R. D. St. Denis[56,*], A. Stabile[94a], R. Stamen[60a], S. Stamm[17], E. Stanecka[42], R. W. Stanek[6], C. Stanescu[136a], M. M. Stanitzki[45], S. Stapnes[121], E. A. Starchenko[132], G. H. Stark[33], J. Stark[58], S. H Stark[39], P. Staroba[129], P. Starovoitov[60a], S. Stärz[32], R. Staszewski[42], P. Steinberg[27], B. Stelzer[144], H. J. Stelzer[32], O. Stelzer-Chilton[163a], H. Stenzel[55], G. A. Stewart[56], J. A. Stillings[23], M. C. Stockton[90], M. Stoebe[90], G. Stoicea[28b], P. Stolte[57], S. Stonjek[103], A. R. Stradling[8], A. Straessner[47], M. E. Stramaglia[18], J. Strandberg[149], S. Strandberg[148a,148b], A. Strandlie[121], M. Strauss[115], P. Strizenec[146b], R. Ströhmer[177], D. M. Strom[118], R. Stroynowski[43], A. Strubig[108], S. A. Stucci[27], B. Stugu[15], N. A. Styles[45], D. Su[145], J. Su[127], S. Suchek[60a], Y. Sugaya[120], M. Suk[130], V. V. Sulin[98], S. Sultansoy[4c], T. Sumida[71], S. Sun[59], X. Sun[3], K. Suruliz[151], C. J. E. Suster[152], M. R. Sutton[151], S. Suzuki[69], M. Svatos[129], M. Swiatlowski[33], S. P. Swift[2], I. Sykora[146a], T. Sykora[131], D. Ta[51], K. Tackmann[45], J. Taenzer[155], A. Taffard[166], R. Tafirout[163a], N. Taiblum[155], H. Takai[27], R. Takashima[72], T. Takeshita[142], Y. Takubo[69], M. Talby[88], A. A. Talyshev[111,c], J. Tanaka[157], M. Tanaka[159], R. Tanaka[119], S. Tanaka[69], R. Tanioka[70], B. B. Tannenwald[113], S. Tapia Araya[34b], S. Tapprogge[86], S. Tarem[154], G. F. Tartarelli[94a], P. Tas[131], M. Tasevsky[129], T. Tashiro[71], E. Tassi[40a,40b], A. Tavares Delgado[128a,128b], Y. Tayalati[137e], A. C. Taylor[107], G. N. Taylor[91], P. T. E. Taylor[91], W. Taylor[163b], P. Teixeira-Dias[80], D. Temple[144], H. Ten Kate[32], P. K. Teng[153], J. J. Teoh[120], F. Tepel[178], S. Terada[69], K. Terashi[157], J. Terron[85], S. Terzo[13], M. Testa[50], R. J. Teuscher[161,o], T. Theveneaux-Pelzer[88], J. P. Thomas[19], J. Thomas-Wilsker[80], P. D. Thompson[19], A. S. Thompson[56], L. A. Thomsen[179], E. Thomson[124], M. J. Tibbetts[16], R. E. Ticse Torres[88], V. O. Tikhomirov[98,ar], Yu. A. Tikhonov[111,c], S. Timoshenko[100], P. Tipton[179], S. Tisserant[88], K. Todome[159], S. Todorova-Nova[5], J. Tojo[73], S. Tokár[146a], K. Tokushuku[69], E. Tolley[59], L. Tomlinson[87], M. Tomoto[105], L. Tompkins[145,as], K. Toms[107], B. Tong[59], P. Tornambe[51], E. Torrence[118], H. Torres[144], E. Torró Pastor[140], J. Toth[88,at], F. Touchard[88], D. R. Tovey[141], C. J. Treado[112], T. Trefzger[177], A. Tricoli[27], I. M. Trigger[163a], S. Trincaz-Duvoid[83], M. F. Tripiana[13], W. Trischuk[161], B. Trocmé[58], A. Trofymov[45], C. Troncon[94a], M. Trottier-McDonald[16], M. Trovatelli[172], L. Truong[167a,167c], M. Trzebinski[42], A. Trzupek[42], K. W. Tsang[62a], J. C-L. Tseng[122], P. V. Tsiareshka[95], G. Tsipolitis[10], N. Tsirintanis[9], S. Tsiskaridze[13], V. Tsiskaridze[51], E. G. Tskhadadze[54a], K. M. Tsui[62a], I. I. Tsukerman[99], V. Tsulaia[16], S. Tsuno[69], D. Tsybychev[150], Y. Tu[62b], A. Tudorache[28b], V. Tudorache[28b], T. T. Tulbure[28a], A. N. Tuna[59], S. A. Tupputi[22a,22b], S. Turchikhin[68], D. Turgeman[175], I. Turk Cakir[4b,au], R. Turra[94a,94b], P. M. Tuts[38], G. Ucchielli[22a,22b], I. Ueda[69], M. Ughetto[148a,148b], F. Ukegawa[164], G. Unal[32], A. Undrus[27], G. Unel[166], F. C. Ungaro[91], Y. Unno[69], C. Unverdorben[102], J. Urban[146b], P. Urquijo[91], P. Urrejola[86], G. Usai[8], J. Usui[69], L. Vacavant[88], V. Vacek[130], B. Vachon[90], C. Valderanis[102], E. Valdes Santurio[148a,148b], N. Valencic[109], S. Valentinetti[22a,22b], A. Valero[170], L. Valéry[13], S. Valkar[131], A. Vallier[5], J. A. Valls Ferrer[170], W. Van Den Wollenberg[109], H. van der Graaf[109], N. van Eldik[154], P. van Gemmeren[6], J. Van Nieuwkoop[144], I. van Vulpen[109], M. C. van Woerden[109], M. Vanadia[134a,134b], W. Vandelli[32], R. Vanguri[124], A. Vaniachine[160], P. Vankov[109], G. Vardanyan[180], R. Vari[134a], E. W. Varnes[7], C. Varni[53a,53b], T. Varol[43], D. Varouchas[83], A. Vartapetian[8], K. E. Varvell[152], J. G. Vasquez[179], G. A. Vasquez[34b], F. Vazeille[37], T. Vazquez Schroeder[90], J. Veatch[57], V. Veeraraghavan[7], L. M. Veloce[161], F. Veloso[128a,128c], S. Veneziano[134a], A. Ventura[76a,76b], M. Venturi[172], N. Venturi[161], A. Venturini[25], V. Vercesi[123a], M. Verducci[136a,136b], W. Verkerke[109], J. C. Vermeulen[109], M. C. Vetterli[144,d], N. Viaux Maira[34a], O. Viazlo[84], I. Vichou[169,*], T. Vickey[141], O. E. Vickey Boeriu[141], G. H. A. Viehhauser[122], S. Viel[16], L. Vigani[122], M. Villa[22a,22b], M. Villaplana Perez[94a,94b], E. Vilucchi[50], M. G. Vincter[31], V. B. Vinogradov[68], A. Vishwakarma[45], C. Vittori[22a,22b], I. Vivarelli[151], S. Vlachos[10], M. Vlasak[130], M. Vogel[178], P. Vokac[130], G. Volpi[126a,126b], M. Volpi[91], H. von der Schmitt[103], E. von Toerne[23], V. Vorobel[131], K. Vorobev[100], M. Vos[170], R. Voss[32], J. H. Vossebeld[77], N. Vranjes[14], M. Vranjes Milosavljevic[14], V. Vrba[130], M. Vreeswijk[109], R. Vuillermet[32], I. Vukotic[33], P. Wagner[23], W. Wagner[178], H. Wahlberg[74], S. Wahrmund[47], J. Wakabayashi[105], J. Walder[75], R. Walker[102], W. Walkowiak[143], V. Wallangen[148a,148b], C. Wang[35b], C. Wang[36b,av], F. Wang[176], H. Wang[16], H. Wang[3], J. Wang[45], J. Wang[152], Q. Wang[115], R. Wang[6], S. M. Wang[153], T. Wang[38], W. Wang[153,aw], W. Wang[36a], C. Wanotayaroj[118], A. Warburton[90], C. P. Ward[30], D. R. Wardrope[81], A. Washbrook[49], P. M. Watkins[19], A. T. Watson[19], M. F. Watson[19], G. Watts[140], S. Watts[87], B. M. Waugh[81], A. F. Webb[11], S. Webb[86], M. S. Weber[18], S. W. Weber[177], S. A. Weber[31],

J. S. Webster[6], A. R. Weidberg[122], B. Weinert[64], J. Weingarten[57], C. Weiser[51], H. Weits[109], P. S. Wells[32], T. Wenaus[27], T. Wengler[32], S. Wenig[32], N. Wermes[23], M. D. Werner[67], P. Werner[32], M. Wessels[60a], K. Whalen[118], N. L. Whallon[140], A. M. Wharton[75], A. White[8], M. J. White[1], R. White[34b], D. Whiteson[166], F. J. Wickens[133], W. Wiedenmann[176], M. Wielers[133], C. Wiglesworth[39], L. A. M. Wiik-Fuchs[23], A. Wildauer[103], F. Wilk[87], H. G. Wilkens[32], H. H. Williams[124], S. Williams[109], C. Willis[93], S. Willocq[89], J. A. Wilson[19], I. Wingerter-Seez[5], F. Winklmeier[118], O. J. Winston[151], B. T. Winter[23], M. Wittgen[145], M. Wobisch[82,u], T. M. H. Wolf[109], R. Wolff[88], M. W. Wolter[42], H. Wolters[128a,128c], S. D. Worm[19], B. K. Wosiek[42], J. Wotschack[32], M. J. Woudstra[87], K. W. Wozniak[42], M. Wu[33], S. L. Wu[176], X. Wu[52], Y. Wu[92], T. R. Wyatt[87], B. M. Wynne[49], S. Xella[39], Z. Xi[92], L. Xia[35c], D. Xu[35a], L. Xu[27], B. Yabsley[152], S. Yacoob[147a], D. Yamaguchi[159], Y. Yamaguchi[120], A. Yamamoto[69], S. Yamamoto[157], T. Yamanaka[157], K. Yamauchi[105], Y. Yamazaki[70], Z. Yan[24], H. Yang[36c], H. Yang[16], Y. Yang[153], Z. Yang[15], W-M. Yao[16], Y. C. Yap[83], Y. Yasu[69], E. Yatsenko[5], K. H. Yau Wong[23], J. Ye[43], S. Ye[27], I. Yeletskikh[68], E. Yildirim[86], K. Yorita[174], K. Yoshihara[124], C. Young[145], C. J. S. Young[32], S. Youssef[24], D. R. Yu[16], J. Yu[8], J. Yu[67], L. Yuan[70], S. P. Y. Yuen[23], I. Yusuff[30,ax], B. Zabinski[42], G. Zacharis[10], R. Zaidan[13], A. M. Zaitsev[132,aj], N. Zakharchuk[45], J. Zalieckas[15], A. Zaman[150], S. Zambito[59], D. Zanzi[91], C. Zeitnitz[178], M. Zeman[130], A. Zemla[41a], J. C. Zeng[169], Q. Zeng[145], O. Zenin[132], T. Ženiš[146a], D. Zerwas[119], D. Zhang[92], F. Zhang[176], G. Zhang[36a,aq], H. Zhang[35b], J. Zhang[6], L. Zhang[51], L. Zhang[36a], M. Zhang[169], R. Zhang[23], R. Zhang[36a,av], X. Zhang[36b], Y. Zhang[35a], Z. Zhang[119], X. Zhao[43], Y. Zhao[36b,ay], Z. Zhao[36a], A. Zhemchugov[68], J. Zhong[122], B. Zhou[92], C. Zhou[176], L. Zhou[43], M. Zhou[35a], M. Zhou[150], N. Zhou[35c], C. G. Zhu[36b], H. Zhu[35a], J. Zhu[92], Y. Zhu[36a], X. Zhuang[35a], K. Zhukov[98], A. Zibell[177], D. Zieminska[64], N. I. Zimine[68], C. Zimmermann[86], S. Zimmermann[51], Z. Zinonos[103], M. Zinser[86], M. Ziolkowski[143], L. Živković[14], G. Zobernig[176], A. Zoccoli[22a,22b], R. Zou[33], M. zur Nedden[17], L. Zwalinski[32]

[1] Department of Physics, University of Adelaide, Adelaide, Australia
[2] Physics Department, SUNY Albany, Albany, NY, USA
[3] Department of Physics, University of Alberta, Edmonton, AB, Canada
[4] [(a)]Department of Physics, Ankara University, Ankara, Turkey; [(b)]Istanbul Aydin University, Istanbul, Turkey; [(c)]Division of Physics, TOBB University of Economics and Technology, Ankara, Turkey
[5] LAPP, CNRS/IN2P3 and Université Savoie Mont Blanc, Annecy-le-Vieux, France
[6] High Energy Physics Division, Argonne National Laboratory, Argonne, IL, USA
[7] Department of Physics, University of Arizona, Tucson, AZ, USA
[8] Department of Physics, The University of Texas at Arlington, Arlington, TX, USA
[9] Physics Department, National and Kapodistrian University of Athens, Athens, Greece
[10] Physics Department, National Technical University of Athens, Zografou, Greece
[11] Department of Physics, The University of Texas at Austin, Austin, TX, USA
[12] Institute of Physics, Azerbaijan Academy of Sciences, Baku, Azerbaijan
[13] Institut de Física d'Altes Energies (IFAE), The Barcelona Institute of Science and Technology, Barcelona, Spain
[14] Institute of Physics, University of Belgrade, Belgrade, Serbia
[15] Department for Physics and Technology, University of Bergen, Bergen, Norway
[16] Physics Division, Lawrence Berkeley National Laboratory, University of California, Berkeley, CA, USA
[17] Department of Physics, Humboldt University, Berlin, Germany
[18] Albert Einstein Center for Fundamental Physics, Laboratory for High Energy Physics, University of Bern, Bern, Switzerland
[19] School of Physics and Astronomy, University of Birmingham, Birmingham, UK
[20] [(a)]Department of Physics, Bogazici University, Istanbul, Turkey; [(b)]Department of Physics Engineering, Gaziantep University, Gaziantep, Turkey; [(c)]Faculty of Engineering and Natural Sciences, Istanbul Bilgi University, Istanbul, Turkey; [(d)]Faculty of Engineering and Natural Sciences, Bahcesehir University, Istanbul, Turkey
[21] Centro de Investigaciones, Universidad Antonio Narino, Bogotá, Colombia
[22] [(a)]INFN Sezione di Bologna, Bologna, Italy; [(b)]Dipartimento di Fisica e Astronomia, Università di Bologna, Bologna, Italy
[23] Physikalisches Institut, University of Bonn, Bonn, Germany
[24] Department of Physics, Boston University, Boston, MA, USA
[25] Department of Physics, Brandeis University, Waltham, MA, USA

[26] [(a)]Universidade Federal do Rio De Janeiro COPPE/EE/IF, Rio de Janeiro, Brazil; [(b)]Electrical Circuits Department, Federal University of Juiz de Fora (UFJF), Juiz de Fora, Brazil; [(c)]Federal University of Sao Joao del Rei (UFSJ), Sao Joao del Rei, Brazil; [(d)]Instituto de Fisica, Universidade de Sao Paulo, São Paulo, Brazil
[27] Physics Department, Brookhaven National Laboratory, Upton, NY, USA
[28] [(a)]Transilvania University of Brasov, Brasov, Romania; [(b)]Horia Hulubei National Institute of Physics and Nuclear Engineering, Bucharest, Romania; [(c)]Department of Physics, Alexandru Ioan Cuza University of Iasi, Iasi, Romania; [(d)]Physics Department, National Institute for Research and Development of Isotopic and Molecular Technologies, Cluj-Napoca, Romania; [(e)]University Politehnica Bucharest, Bucharest, Romania; [(f)]West University in Timisoara, Timisoara, Romania
[29] Departamento de Física, Universidad de Buenos Aires, Buenos Aires, Argentina
[30] Cavendish Laboratory, University of Cambridge, Cambridge, UK
[31] Department of Physics, Carleton University, Ottawa, ON, Canada
[32] CERN, Geneva, Switzerland
[33] Enrico Fermi Institute, University of Chicago, Chicago, IL, USA
[34] [(a)]Departamento de Física, Pontificia Universidad Católica de Chile, Santiago, Chile; [(b)]Departamento de Física, Universidad Técnica Federico Santa María, Valparaiso, Chile
[35] [(a)]Institute of High Energy Physics, Chinese Academy of Sciences, Beijing, China; [(b)]Department of Physics, Nanjing University, Nanjing, Jiangsu, China; [(c)]Physics Department, Tsinghua University, Beijing 100084, China
[36] [(a)]Department of Modern Physics, University of Science and Technology of China, Hefei, Anhui, China; [(b)]School of Physics, Shandong University, Jinan, Shandong, China; [(c)]Department of Physics and Astronomy, Key Laboratory for Particle Physics, Astrophysics and Cosmology, Ministry of Education, Shanghai Key Laboratory for Particle Physics and Cosmology, Shanghai Jiao Tong University, Shanghai (also at PKU-CHEP), Shanghai, China
[37] Université Clermont Auvergne, CNRS/IN2P3, LPC, Clermont-Ferrand, France
[38] Nevis Laboratory, Columbia University, Irvington, NY, USA
[39] Niels Bohr Institute, University of Copenhagen, Copenhagen, Denmark
[40] [(a)]INFN Gruppo Collegato di Cosenza, Laboratori Nazionali di Frascati, Frascati, Italy; [(b)]Dipartimento di Fisica, Università della Calabria, Rende, Italy
[41] [(a)]Faculty of Physics and Applied Computer Science, AGH University of Science and Technology, Kraków, Poland; [(b)]Marian Smoluchowski Institute of Physics, Jagiellonian University, Kraków, Poland
[42] Institute of Nuclear Physics, Polish Academy of Sciences, Kraków, Poland
[43] Physics Department, Southern Methodist University, Dallas, TX, USA
[44] Physics Department, University of Texas at Dallas, c, TX, USA
[45] DESY, Hamburg and Zeuthen, Germany
[46] Lehrstuhl für Experimentelle Physik IV, Technische Universität Dortmund, Dortmund, Germany
[47] Institut für Kern- und Teilchenphysik, Technische Universität Dresden, Dresden, Germany
[48] Department of Physics, Duke University, Durham, NC, USA
[49] SUPA-School of Physics and Astronomy, University of Edinburgh, Edinburgh, UK
[50] INFN Laboratori Nazionali di Frascati, Frascati, Italy
[51] Fakultät für Mathematik und Physik, Albert-Ludwigs-Universität, Freiburg, Germany
[52] Departement de Physique Nucleaire et Corpusculaire, Université de Genève, Geneva, Switzerland
[53] [(a)]INFN Sezione di Genova, Genoa, Italy; [(b)]Dipartimento di Fisica, Università di Genova, Genoa, Italy
[54] [(a)]E. Andronikashvili Institute of Physics, Iv. Javakhishvili Tbilisi State University, Tbilisi, Georgia; [(b)]High Energy Physics Institute, Tbilisi State University, Tbilisi, Georgia
[55] II Physikalisches Institut, Justus-Liebig-Universität Giessen, Giessen, Germany
[56] SUPA-School of Physics and Astronomy, University of Glasgow, Glasgow, UK
[57] II Physikalisches Institut, Georg-August-Universität, Göttingen, Germany
[58] Laboratoire de Physique Subatomique et de Cosmologie, Université Grenoble-Alpes, CNRS/IN2P3, Grenoble, France
[59] Laboratory for Particle Physics and Cosmology, Harvard University, Cambridge, MA, USA
[60] [(a)]Kirchhoff-Institut für Physik, Ruprecht-Karls-Universität Heidelberg, Heidelberg, Germany; [(b)]Physikalisches Institut, Ruprecht-Karls-Universität Heidelberg, Heidelberg, Germany; [(c)]ZITI Institut für technische Informatik, Ruprecht-Karls-Universität Heidelberg, Mannheim, Germany
[61] Faculty of Applied Information Science, Hiroshima Institute of Technology, Hiroshima, Japan

[62] [(a)]Department of Physics, The Chinese University of Hong Kong, Shatin, NT, Hong Kong; [(b)]Department of Physics, The University of Hong Kong, Hong Kong, China; [(c)]Department of Physics, Institute for Advanced Study, The Hong Kong University of Science and Technology, Clear Water Bay, Kowloon, Hong Kong, China
[63] Department of Physics, National Tsing Hua University, Taiwan, Taiwan
[64] Department of Physics, Indiana University, Bloomington, IN, USA
[65] Institut für Astro- und Teilchenphysik, Leopold-Franzens-Universität, Innsbruck, Austria
[66] University of Iowa, Iowa City, IA, USA
[67] Department of Physics and Astronomy, Iowa State University, Ames, IA, USA
[68] Joint Institute for Nuclear Research, JINR Dubna, Dubna, Russia
[69] KEK, High Energy Accelerator Research Organization, Tsukuba, Japan
[70] Graduate School of Science, Kobe University, Kobe, Japan
[71] Faculty of Science, Kyoto University, Kyoto, Japan
[72] Kyoto University of Education, Kyoto, Japan
[73] Department of Physics, Kyushu University, Fukuoka, Japan
[74] Instituto de Física La Plata, Universidad Nacional de La Plata and CONICET, La Plata, Argentina
[75] Physics Department, Lancaster University, Lancaster, UK
[76] [(a)]INFN Sezione di Lecce, Lecce, Italy; [(b)]Dipartimento di Matematica e Fisica, Università del Salento, Lecce, Italy
[77] Oliver Lodge Laboratory, University of Liverpool, Liverpool, UK
[78] Department of Experimental Particle Physics, Jožef Stefan Institute and Department of Physics, University of Ljubljana, Ljubljana, Slovenia
[79] School of Physics and Astronomy, Queen Mary University of London, London, UK
[80] Department of Physics, Royal Holloway University of London, Surrey, UK
[81] Department of Physics and Astronomy, University College London, London, UK
[82] Louisiana Tech University, Ruston, LA, USA
[83] Laboratoire de Physique Nucléaire et de Hautes Energies, UPMC and Université Paris-Diderot and CNRS/IN2P3, Paris, France
[84] Fysiska institutionen, Lunds universitet, Lund, Sweden
[85] Departamento de Fisica Teorica C-15, Universidad Autonoma de Madrid, Madrid, Spain
[86] Institut für Physik, Universität Mainz, Mainz, Germany
[87] School of Physics and Astronomy, University of Manchester, Manchester, UK
[88] CPPM, Aix-Marseille Université and CNRS/IN2P3, Marseille, France
[89] Department of Physics, University of Massachusetts, Amherst, MA, USA
[90] Department of Physics, McGill University, Montreal, QC, Canada
[91] School of Physics, University of Melbourne, Victoria, Australia
[92] Department of Physics, The University of Michigan, Ann Arbor, MI, USA
[93] Department of Physics and Astronomy, Michigan State University, East Lansing, MI, USA
[94] [(a)]INFN Sezione di Milano, Milan, Italy; [(b)]Dipartimento di Fisica, Università di Milano, Milan, Italy
[95] B.I. Stepanov Institute of Physics, National Academy of Sciences of Belarus, Minsk, Republic of Belarus
[96] Research Institute for Nuclear Problems of Byelorussian State University, Minsk, Republic of Belarus
[97] Group of Particle Physics, University of Montreal, Montreal, QC, Canada
[98] P.N. Lebedev Physical Institute of the Russian Academy of Sciences, Moscow, Russia
[99] Institute for Theoretical and Experimental Physics (ITEP), Moscow, Russia
[100] National Research Nuclear University MEPhI, Moscow, Russia
[101] D.V. Skobeltsyn Institute of Nuclear Physics, M.V. Lomonosov Moscow State University, Moscow, Russia
[102] Fakultät für Physik, Ludwig-Maximilians-Universität München, Munich, Germany
[103] Max-Planck-Institut für Physik (Werner-Heisenberg-Institut), Munich, Germany
[104] Nagasaki Institute of Applied Science, Nagasaki, Japan
[105] Graduate School of Science and Kobayashi-Maskawa Institute, Nagoya University, Nagoya, Japan
[106] [(a)]INFN Sezione di Napoli, Naples, Italy; [(b)]Dipartimento di Fisica, Università di Napoli, Naples, Italy
[107] Department of Physics and Astronomy, University of New Mexico, Albuquerque, NM, USA
[108] Institute for Mathematics, Astrophysics and Particle Physics, Radboud University Nijmegen/Nikhef, Nijmegen, The Netherlands
[109] Nikhef National Institute for Subatomic Physics, University of Amsterdam, Amsterdam, The Netherlands

[110] Department of Physics, Northern Illinois University, DeKalb, IL, USA
[111] Budker Institute of Nuclear Physics, SB RAS, Novosibirsk, Russia
[112] Department of Physics, New York University, New York, NY, USA
[113] Ohio State University, Columbus, OH, USA
[114] Faculty of Science, Okayama University, Okayama, Japan
[115] Homer L. Dodge Department of Physics and Astronomy, University of Oklahoma, Norman, OK, USA
[116] Department of Physics, Oklahoma State University, Stillwater, OK, USA
[117] Palacký University, RCPTM, Olomouc, Czech Republic
[118] Center for High Energy Physics, University of Oregon, Eugene, OR, USA
[119] LAL, Univ. Paris-Sud, CNRS/IN2P3, Université Paris-Saclay, Orsay, France
[120] Graduate School of Science, Osaka University, Osaka, Japan
[121] Department of Physics, University of Oslo, Oslo, Norway
[122] Department of Physics, Oxford University, Oxford, UK
[123] [(a)]INFN Sezione di Pavia, Pavia, Italy; [(b)]Dipartimento di Fisica, Università di Pavia, Pavia, Italy
[124] Department of Physics, University of Pennsylvania, Philadelphia, PA, USA
[125] National Research Centre "Kurchatov Institute" B.P. Konstantinov Petersburg Nuclear Physics Institute, St. Petersburg, Russia
[126] [(a)]INFN Sezione di Pisa, Pisa, Italy; [(b)]Dipartimento di Fisica E. Fermi, Università di Pisa, Pisa, Italy
[127] Department of Physics and Astronomy, University of Pittsburgh, Pittsburgh, PA, USA
[128] [(a)]Laboratório de Instrumentação e Física Experimental de Partículas-LIP, Lisbon, Portugal; [(b)]Faculdade de Ciências, Universidade de Lisboa, Lisbon, Portugal; [(c)]Department of Physics, University of Coimbra, Coimbra, Portugal; [(d)]Centro de Física Nuclear da Universidade de Lisboa, Lisbon, Portugal; [(e)]Departamento de Fisica, Universidade do Minho, Braga, Portugal; [(f)]Departamento de Fisica Teorica y del Cosmos and CAFPE, Universidad de Granada, Granada, Spain; [(g)]Dep Fisica and CEFITEC of Faculdade de Ciencias e Tecnologia, Universidade Nova de Lisboa, Caparica, Portugal
[129] Institute of Physics, Academy of Sciences of the Czech Republic, Prague, Czech Republic
[130] Czech Technical University in Prague, Prague, Czech Republic
[131] Faculty of Mathematics and Physics, Charles University, Prague, Czech Republic
[132] State Research Center Institute for High Energy Physics (Protvino), NRC KI, Protvino, Russia
[133] Particle Physics Department, Rutherford Appleton Laboratory, Didcot, UK
[134] [(a)]INFN Sezione di Roma, Rome, Italy; [(b)]Dipartimento di Fisica, Sapienza Università di Roma, Rome, Italy
[135] [(a)]INFN Sezione di Roma Tor Vergata, Rome, Italy; [(b)]Dipartimento di Fisica, Università di Roma Tor Vergata, Rome, Italy
[136] [(a)]INFN Sezione di Roma Tre, Rome, Italy; [(b)]Dipartimento di Matematica e Fisica, Università Roma Tre, Rome, Italy
[137] [(a)]Faculté des Sciences Ain Chock, Réseau Universitaire de Physique des Hautes Energies-Université Hassan II, Casablanca, Morocco; [(b)]Centre National de l'Energie des Sciences Techniques Nucleaires, Rabat, Morocco; [(c)]Faculté des Sciences Semlalia, Université Cadi Ayyad, LPHEA-Marrakech, Marrakech, Morocco; [(d)]Faculté des Sciences, Université Mohamed Premier and LPTPM, Oujda, Morocco; [(e)]Faculté des Sciences, Université Mohammed V, Rabat, Morocco
[138] DSM/IRFU (Institut de Recherches sur les Lois Fondamentales de l'Univers), CEA Saclay (Commissariat à l'Energie Atomique et aux Energies Alternatives), Gif-sur-Yvette, France
[139] Santa Cruz Institute for Particle Physics, University of California Santa Cruz, Santa Cruz, CA, USA
[140] Department of Physics, University of Washington, Seattle, WA, USA
[141] Department of Physics and Astronomy, University of Sheffield, Sheffield, UK
[142] Department of Physics, Shinshu University, Nagano, Japan
[143] Department Physik, Universität Siegen, Siegen, Germany
[144] Department of Physics, Simon Fraser University, Burnaby, BC, Canada
[145] SLAC National Accelerator Laboratory, Stanford, CA, USA
[146] [(a)]Faculty of Mathematics, Physics and Informatics, Comenius University, Bratislava, Slovak Republic; [(b)]Department of Subnuclear Physics, Institute of Experimental Physics of the Slovak Academy of Sciences, Kosice, Slovak Republic

[147] [(a)]Department of Physics, University of Cape Town, Cape Town, South Africa; [(b)]Department of Physics, University of Johannesburg, Johannesburg, South Africa; [(c)]School of Physics, University of the Witwatersrand, Johannesburg, South Africa
[148] [(a)]Department of Physics, Stockholm University, Stockholm, Sweden; [(b)]The Oskar Klein Centre, Stockholm, Sweden
[149] Physics Department, Royal Institute of Technology, Stockholm, Sweden
[150] Departments of Physics and Astronomy and Chemistry, Stony Brook University, Stony Brook, NY, USA
[151] Department of Physics and Astronomy, University of Sussex, Brighton, UK
[152] School of Physics, University of Sydney, Sydney, Australia
[153] Institute of Physics, Academia Sinica, Taipei, Taiwan
[154] Department of Physics, Technion: Israel Institute of Technology, Haifa, Israel
[155] Raymond and Beverly Sackler School of Physics and Astronomy, Tel Aviv University, Tel Aviv, Israel
[156] Department of Physics, Aristotle University of Thessaloniki, Thessaloníki, Greece
[157] International Center for Elementary Particle Physics and Department of Physics, The University of Tokyo, Tokyo, Japan
[158] Graduate School of Science and Technology, Tokyo Metropolitan University, Tokyo, Japan
[159] Department of Physics, Tokyo Institute of Technology, Tokyo, Japan
[160] Tomsk State University, Tomsk, Russia
[161] Department of Physics, University of Toronto, Toronto, ON, Canada
[162] [(a)]INFN-TIFPA, Trento, Italy; [(b)]University of Trento, Trento, Italy
[163] [(a)]TRIUMF, Vancouver, BC, Canada; [(b)]Department of Physics and Astronomy, York University, Toronto, ON, Canada
[164] Faculty of Pure and Applied Sciences, and Center for Integrated Research in Fundamental Science and Engineering, University of Tsukuba, Tsukuba, Japan
[165] Department of Physics and Astronomy, Tufts University, Medford, MA, USA
[166] Department of Physics and Astronomy, University of California Irvine, Irvine, CA, USA
[167] [(a)]INFN Gruppo Collegato di Udine, Sezione di Trieste, Udine, Italy; [(b)]ICTP, Trieste, Italy; [(c)]Dipartimento di Chimica, Fisica e Ambiente, Università di Udine, Udine, Italy
[168] Department of Physics and Astronomy, University of Uppsala, Uppsala, Sweden
[169] Department of Physics, University of Illinois, Urbana, IL, USA
[170] Instituto de Fisica Corpuscular (IFIC) and Departamento de Fisica Atomica, Molecular y Nuclear and Departamento de Ingeniería Electrónica and Instituto de Microelectrónica de Barcelona (IMB-CNM), University of Valencia and CSIC, Valencia, Spain
[171] Department of Physics, University of British Columbia, Vancouver, BC, Canada
[172] Department of Physics and Astronomy, University of Victoria, Victoria, BC, Canada
[173] Department of Physics, University of Warwick, Coventry, UK
[174] Waseda University, Tokyo, Japan
[175] Department of Particle Physics, The Weizmann Institute of Science, Rehovot, Israel
[176] Department of Physics, University of Wisconsin, Madison, WI, USA
[177] Fakultät für Physik und Astronomie, Julius-Maximilians-Universität, Würzburg, Germany
[178] Fakultät für Mathematik und Naturwissenschaften, Fachgruppe Physik, Bergische Universität Wuppertal, Wuppertal, Germany
[179] Department of Physics, Yale University, New Haven, CT, USA
[180] Yerevan Physics Institute, Yerevan, Armenia
[181] Centre de Calcul de l'Institut National de Physique Nucléaire et de Physique des Particules (IN2P3), Villeurbanne, France

[a] Also at Department of Physics, King's College London, London, UK
[b] Also at Institute of Physics, Azerbaijan Academy of Sciences, Baku, Azerbaijan
[c] Also at Novosibirsk State University, Novosibirsk, Russia
[d] Also at TRIUMF, Vancouver, BC, Canada
[e] Also at Department of Physics and Astronomy, University of Louisville, Louisville, KY, USA
[f] Also at Physics Department, An-Najah National University, Nablus, Palestine
[g] Also at Department of Physics, California State University, Fresno, CA, USA
[h] Also at Department of Physics, University of Fribourg, Fribourg, Switzerland
[i] Also at II Physikalisches Institut, Georg-August-Universität, Göttingen, Germany

[j] Also at Department de Fisica de la Universitat Autonoma de Barcelona, Barcelona, Spain
[k] Also at Departamento de Fisica e Astronomia, Faculdade de Ciencias, Universidade do Porto, Porto, Portugal
[l] Also at Tomsk State University, Tomsk, Russia
[m] Also at The Collaborative Innovation Center of Quantum Matter (CICQM), Beijing, China
[n] Also at Universita di Napoli Parthenope, Napoli, Italy
[o] Also at Institute of Particle Physics (IPP), Canada
[p] Also at Horia Hulubei National Institute of Physics and Nuclear Engineering, Bucharest, Romania
[q] Also at Department of Physics, St. Petersburg State Polytechnical University, St. Petersburg, Russia
[r] Also at Borough of Manhattan Community College, City University of New York, New York, USA
[s] Also at Department of Physics, The University of Michigan, Ann Arbor MI, United States of America
[t] Also at Centre for High Performance Computing, CSIR Campus, Rosebank, Cape Town, South Africa
[u] Also at Louisiana Tech University, Ruston, LA, USA
[v] Also at Institucio Catalana de Recerca i Estudis Avancats, ICREA, Barcelona, Spain
[w] Also at Graduate School of Science, Osaka University, Osaka, Japan
[x] Also at Fakultät für Mathematik und Physik, Albert-Ludwigs-Universität, Freiburg, Germany
[y] Also at Institute for Mathematics, Astrophysics and Particle Physics, Radboud University Nijmegen/Nikhef, Nijmegen, The Netherlands
[z] Also at Department of Physics, The University of Texas at Austin, Austin, TX, USA
[aa] Also at Institute of Theoretical Physics, Ilia State University, Tbilisi, Georgia
[ab] Also at CERN, Geneva, Switzerland
[ac] Also at Georgian Technical University (GTU), Tbilisi, Georgia
[ad] Also at Ochadai Academic Production, Ochanomizu University, Tokyo, Japan
[ae] Also at Manhattan College, New York, NY, USA
[af] Also at Academia Sinica Grid Computing, Institute of Physics, Academia Sinica, Taipei, Taiwan
[ag] Also at School of Physics, Shandong University, Shandong, China
[ah] Also at Departamento de Fisica Teorica y del Cosmos and CAFPE, Universidad de Granada, Granada, Spain
[ai] Also at Department of Physics, California State University, Sacramento, CA, USA
[aj] Also at Moscow Institute of Physics and Technology State University, Dolgoprudny, Russia
[ak] Also at Departement de Physique Nucleaire et Corpusculaire, Université de Genève, Geneva, Switzerland
[al] Also at International School for Advanced Studies (SISSA), Trieste, Italy
[am] Also at Institut de Física d'Altes Energies (IFAE), The Barcelona Institute of Science and Technology, Barcelona, Spain
[an] Also at School of Physics, Sun Yat-sen University, Guangzhou, China
[ao] Also at Institute for Nuclear Research and Nuclear Energy (INRNE) of the Bulgarian Academy of Sciences, Sofia, Bulgaria
[ap] Also at Faculty of Physics, M.V. Lomonosov Moscow State University, Moscow, Russia
[aq] Also at Institute of Physics, Academia Sinica, Taipei, Taiwan
[ar] Also at National Research Nuclear University MEPhI, Moscow, Russia
[as] Also at Department of Physics, Stanford University, Stanford, CA, USA
[at] Also at Institute for Particle and Nuclear Physics, Wigner Research Centre for Physics, Budapest, Hungary
[au] Also at Faculty of Engineering, Giresun University, Giresun, Turkey
[av] Also at CPPM, Aix-Marseille Université and CNRS/IN2P3, Marseille, France
[aw] Also at Department of Physics, Nanjing University, Jiangsu, China
[ax] Also at Department of Physics, University of Malaya, Kuala Lumpur, Malaysia
[ay] Also at LAL, Univ. Paris-Sud, CNRS/IN2P3, Université Paris-Saclay, Orsay, France
*Deceased

Published for SISSA by Springer

Received: October 17, 2017
Accepted: November 3, 2017
Published: December 12, 2017

Measurement of the Drell-Yan triple-differential cross section in pp collisions at $\sqrt{s} = 8$ TeV

The ATLAS collaboration

E-mail: atlas.publications@cern.ch

Abstract: This paper presents a measurement of the triple-differential cross section for the Drell-Yan process $Z/\gamma^* \to \ell^+\ell^-$ where ℓ is an electron or a muon. The measurement is performed for invariant masses of the lepton pairs, $m_{\ell\ell}$, between 46 and 200 GeV using a sample of 20.2 fb^{-1} of pp collisions data at a centre-of-mass energy of $\sqrt{s} = 8$ TeV collected by the ATLAS detector at the LHC in 2012. The data are presented in bins of invariant mass, absolute dilepton rapidity, $|y_{\ell\ell}|$, and the angular variable $\cos\theta^*$ between the outgoing lepton and the incoming quark in the Collins-Soper frame. The measurements are performed in the range $|y_{\ell\ell}| < 2.4$ in the muon channel, and extended to $|y_{\ell\ell}| < 3.6$ in the electron channel. The cross sections are used to determine the Z boson forward-backward asymmetry as a function of $|y_{\ell\ell}|$ and $m_{\ell\ell}$. The measurements achieve high-precision, below the percent level in the pole region, excluding the uncertainty in the integrated luminosity, and are in agreement with predictions. These precision data are sensitive to the parton distribution functions and the effective weak mixing angle.

Keywords: Hadron-Hadron scattering (experiments)

ArXiv ePrint: 1710.05167

https://doi.org/10.1007/JHEP12(2017)059

JHEP12(2017)059

Contents

JHEP12(2017)059

JHEP12(2017)059

1 Introduction

In the Drell-Yan process [1, 2] $q\bar{q} \to Z/\gamma^* \to \ell^+\ell^-$, parity violation in the neutral weak coupling of the mediator to fermions induces a forward-backward asymmetry, A_{FB}, in the decay angle distribution of the outgoing lepton (ℓ^-) relative to the incoming quark direction as measured in the dilepton rest frame. This decay angle depends on the sine of the weak mixing angle, $\sin^2\theta_{\mathrm{W}}$, which enters in the fermionic vector couplings to the Z boson. At leading order in electroweak (EW) theory it is given by $\sin^2\theta_{\mathrm{W}} = 1 - m_W^2/m_Z^2$, where m_W and m_Z are the W and Z boson masses, respectively. Higher-order loop corrections modify this relation depending on the renormalisation scheme used, and so experimental measurements are often given in terms of the sine of the effective weak mixing angle, $\sin^2\theta^{\mathrm{eff}}$ [3]. High-precision cross-section measurements sensitive to the asymmetry, and therefore to the effective weak mixing angle, provide a testing ground for EW theory and could offer some insight into physics beyond the Standard Model (SM).

Previous measurements by ATLAS and CMS of the Drell-Yan (DY) process include measurements of fiducial cross sections [4–7], and one-dimensional differential cross sections as a function of rapidity [8, 9], transverse momentum [9–12], and invariant mass [13–15]. Double-differential cross-section measurements as a function of invariant mass and either rapidity or transverse momentum [16–21] have also been published, as well as Z boson polarisation coefficients [22, 23] and the forward-backward asymmetry [24, 25]. Extraction of the effective weak mixing angle in leptonic Z boson decays, $\sin^2\theta^{\mathrm{eff}}_{\mathrm{lept}}$, from A_{FB} measurements has been performed by ATLAS using $5\,\mathrm{fb}^{-1}$ of proton-proton collision data at $\sqrt{s} = 7$ TeV [24] — a result in which the largest contribution to the uncertainty was due to limited knowledge of the parton distribution functions (PDFs) of the proton.

A complete description of the Drell-Yan cross section to all orders in quantum chromodynamics (QCD) depends on five kinematic variables of the Born-level leptons, namely $m_{\ell\ell}$, the invariant mass of the lepton pair; $y_{\ell\ell}$, the rapidity of the dilepton system; θ and ϕ, the lepton decay angles in the rest frame of the two incident quarks; and $p_{\mathrm{T},Z}$, the transverse momentum of the vector boson. In this paper, measurements of the triple-differential Drell-Yan cross section, $\mathrm{d}^3\sigma/\mathrm{d}m_{\ell\ell}\mathrm{d}|y_{\ell\ell}|\mathrm{d}\cos\theta^*$, are reported as a function of $m_{\ell\ell}$, $|y_{\ell\ell}|$, and $\cos\theta^*$, where the lepton decay angle is defined in the Collins-Soper (CS) reference frame [26]. These cross-section measurements are designed to be simultaneously sensitive to $\sin^2\theta^{\mathrm{eff}}_{\mathrm{lept}}$ and to the PDFs, therefore allowing a coherent determination of both. A simultaneous extraction has the potential to reduce the PDF-induced uncertainty in the extracted value of the effective weak mixing angle.

At leading order (LO) in perturbative electroweak and QCD theory, the Drell-Yan triple-differential cross section can be written as

$$\frac{\mathrm{d}^3\sigma}{\mathrm{d}m_{\ell\ell}\mathrm{d}y_{\ell\ell}\mathrm{d}\cos\theta^*} = \frac{\pi\alpha^2}{3m_{\ell\ell}s}\sum_q P_q\left[f_q(x_1,Q^2)f_{\bar{q}}(x_2,Q^2) + (q\leftrightarrow\bar{q})\right], \tag{1.1}$$

where s is the squared proton-proton (pp) centre-of-mass energy; the incoming parton momentum fractions are $x_{1,2} = (m_{\ell\ell}/\sqrt{s})\mathrm{e}^{\pm y_{\ell\ell}}$; and $f_q(x_1,Q^2)$ are the PDFs for parton flavour q. Here, Q^2 is the four-momentum transfer squared and is set to the dilepton centre-of-mass energy, $m_{\ell\ell}$, which is equal to the partonic centre-of-mass energy. The $q\leftrightarrow\bar{q}$ term accounts for the case in which the parent protons of the q and $\bar{q}$ are interchanged. The function P_q in equation (1.1) is given by

$$\begin{aligned} P_q = {} & e_\ell^2 e_q^2(1+\cos^2\theta^*) \\ & + e_\ell e_q \frac{2m_{\ell\ell}^2(m_{\ell\ell}^2-m_Z^2)}{\sin^2\theta_{\mathrm{W}}\cos^2\theta_{\mathrm{W}}\left[(m_{\ell\ell}^2-m_Z^2)^2+\Gamma_Z^2m_Z^2\right]}\left[v_\ell v_q(1+\cos^2\theta^*)+2a_\ell a_q\cos\theta^*\right] \\ & + \frac{m_{\ell\ell}^4}{\sin^4\theta_{\mathrm{W}}\cos^4\theta_{\mathrm{W}}\left[(m_{\ell\ell}^2-m_Z^2)^2+\Gamma_Z^2m_Z^2\right]}\left[(a_\ell^2+v_\ell^2)(a_q^2+v_q^2)(1+\cos^2\theta^*)+8a_\ell v_\ell a_q v_q\cos\theta^*\right]. \end{aligned} \tag{1.2}$$

In this relation m_Z and Γ_Z are the Z boson mass and width, respectively; e_ℓ and e_q are the lepton and quark electric charges; and $v_\ell = -\frac{1}{4}+\sin^2\theta_{\mathrm{W}}$, $a_\ell = -\frac{1}{4}$, $v_q = \frac{1}{2}I_q^3 - e_q\sin^2\theta_{\mathrm{W}}$, and $a_q = \frac{1}{2}I_q^3$ are the vector and axial-vector lepton and quark couplings, respectively where I_q^3 is the third component of the weak isospin.

The first term in equation (1.2) corresponds to pure virtual photon, γ^*, exchange in the scattering process, the second corresponds to the interference of γ^* and Z exchange, and the last term corresponds to pure Z exchange. Thus the DY invariant mass spectrum is characterized by a $1/m_{\ell\ell}^2$ fall-off from γ^* exchange contribution, an $m_{\ell\ell}$-dependent Breit-Wigner peaking at the mass of the Z boson, and a Z/γ^* interference contribution which changes sign from negative to positive as $m_{\ell\ell}$ increases across the m_Z threshold.

The terms which are linear in $\cos\theta^*$ induce the forward-backward asymmetry. The largest contribution comes from the interference term, except at $m_{\ell\ell} = m_Z$ where the interference term is zero, and only the Z exchange term contributes to the asymmetry. The resulting asymmetry is, however, numerically small due to the small value of v_ℓ. The

JHEP12(2017)059

net effect is an asymmetry which is negative for $m_{\ell\ell} < m_Z$ and increases, becoming positive for $m_{\ell\ell} > m_Z$. The point of zero asymmetry occurs slightly below $m_{\ell\ell} = m_Z$.

The forward-backward asymmetry varies with $|y_{\ell\ell}|$. The incoming quark direction can only be determined probabilistically: for increasing $|y_{\ell\ell}|$ the momentum fraction of one parton reaches larger x where the valence quark PDFs dominate because the valence quarks typically carry more momentum than the antiquarks. Therefore, the Z/γ^* is more likely to be boosted in the quark direction. Conversely, at small boson rapidity, $|y_{\ell\ell}| \sim 0$, it becomes almost impossible to identify the direction of the quark since the quark and antiquark have nearly equal momenta.

The sensitivity of the cross section to the PDFs arises primarily from its dependence on $y_{\ell\ell}$ (and therefore x_1 and x_2) in equation (1.1). Further sensitivity is gained by analysing the cross section in the $m_{\ell\ell}$ dimension, since in the Z resonance peak the partons couple through the weak interaction and off-peak the electric couplings to the γ^* dominate. Therefore, the relative contributions of up-type and down-type quarks vary with $m_{\ell\ell}$. Finally, the $\cos\theta^*$ dependence of the cross section provides sensitivity to terms containing $a_\ell a_q$ and $v_\ell v_q a_\ell a_q$ in equation (1.2). Three different combinations of couplings to the incident quarks contribute to the LO cross section. The magnitude of the asymmetry is proportional to the valence quark PDFs and offers direct sensitivity to the corresponding PDF component.

The full five-dimensional cross section can also be decomposed into harmonic polynomials for the lepton decay angle scattering amplitudes and their corresponding coefficients A_{0-7} [22]. Higher-order QCD corrections to the LO $q\bar{q}$ process involve $qg + \bar{q}g$ terms at next-to-leading order (NLO), and gg terms at next-to-next-to-leading order (NNLO). These higher-order terms modify the decay angle dependence of the cross section. Measuring the $|\cos\theta^*|$ distribution provides additional sensitivity to the gluon versus sea-quark PDFs and is related to the measurements of the angular coefficients as a function of the Z boson transverse momentum [22, 23].

Initial-state QCD radiation can introduce a non-zero transverse momentum for the final-state lepton pair, leading to quark directions which may no longer be aligned with the incident proton directions. Hence, in this paper, the decay angle is measured in the CS reference frame [26] in which the decay angle is measured from an axis symmetric with respect to the two incoming partons. The decay angle in the CS frame (θ^*) is given by

$$\cos\theta^* = \frac{p_{\mathrm{z},\ell\ell}}{m_{\ell\ell}|p_{\mathrm{z},\ell\ell}|} \frac{p_1^+ p_2^- - p_1^- p_2^+}{\sqrt{m_{\ell\ell}^2 + p_{\mathrm{T},\ell\ell}^2}},$$

where $p_i^\pm = E_i \pm p_{\mathrm{z},i}$ and $i = 1$ corresponds to the negatively-charged lepton and $i = 2$ to the positively-charged antilepton. Here, E and p_z are the energy and longitudinal z-components of the leptonic four-momentum, respectively; $p_{\mathrm{z},\ell\ell}$ is the dilepton z-component of the momentum; and $p_{\mathrm{T},\ell\ell}$ the dilepton transverse momentum.

The triple-differential cross sections are measured using 20.2 fb^{-1} of pp collision data at $\sqrt{s} = 8$ TeV. The measurements are performed in the electron and muon decay channels for $|y_{\ell\ell}| < 2.4$. The electron channel analysis is extended to high rapidity in the region $1.2 < |y_{\ell\ell}| < 3.6$. The measured cross sections cover the kinematic range $46 < m_{\ell\ell} <$

JHEP12(2017)059

200 GeV, $0 < |y_{\ell\ell}| < 3.6$, and $-1 < \cos\theta^* < +1$. For convenience the notation

$$\mathrm{d}^3\sigma \equiv \frac{\mathrm{d}^3\sigma}{\mathrm{d}m_{\ell\ell}\mathrm{d}|y_{\ell\ell}|\mathrm{d}\cos\theta^*}$$

is used. The cross sections are classified as either *forward* ($\cos\theta^* > 0$) or *backward* ($\cos\theta^* < 0$) and used to obtain an experimental measurement of A_{FB} differentially in $m_{\ell\ell}$ and $|y_{\ell\ell}|$:

$$A_{\mathrm{FB}} = \frac{\mathrm{d}^3\sigma(\cos\theta^* > 0) - \mathrm{d}^3\sigma(\cos\theta^* < 0)}{\mathrm{d}^3\sigma(\cos\theta^* > 0) + \mathrm{d}^3\sigma(\cos\theta^* < 0)} \,. \tag{1.3}$$

2 ATLAS detector

The ATLAS detector [27] consists of an inner tracking detector (ID) surrounded by a thin superconducting solenoid, electromagnetic and hadronic calorimeters, and a muon spectrometer (MS). Charged particles in the pseudorapidity[1] range $|\eta| < 2.5$ are reconstructed with the ID, which consists of layers of silicon pixel and microstrip detectors and a straw-tube transition-radiation tracker having a coverage of $|\eta| < 2.0$. The ID is immersed in a 2 T magnetic field provided by the solenoid. The latter is surrounded by a hermetic calorimeter that covers $|\eta| < 4.9$ and provides three-dimensional reconstruction of particle showers. The electromagnetic calorimeter is a liquid-argon sampling calorimeter, which uses lead absorbers for $|\eta| < 3.2$. The hadronic sampling calorimeter uses plastic scintillator tiles as the active material and steel absorbers in the region $|\eta| < 1.7$. In the region $1.5 < |\eta| < 3.2$, liquid argon is used as the active material, with copper absorbers. A forward calorimeter covers the range $3.2 < |\eta| < 4.9$ which also uses liquid argon as the active material, and copper and tungsten absorbers for the EM and hadronic sections of the subdetector, respectively.

Outside the calorimeters, air-core toroids supply the magnetic field for the MS. There, three layers of precision chambers allow the accurate measurement of muon track curvature in the region $|\eta| < 2.7$. The majority of these precision chambers is composed of drift tubes, while cathode-strip chambers provide coverage in the inner layers of the forward region $2.0 < |\eta| < 2.7$. The muon trigger in the range $|\eta| < 2.4$ uses resistive-plate chambers in the central region and thin-gap chambers in the forward region. A three-level trigger system [28] selects events to be recorded for offline analysis.

3 Simulated event samples

Monte Carlo (MC) simulation samples are used to model the expected signal and background yields, with the exception of certain data-driven background estimates. The MC samples are normalised using the highest-order cross-section predictions available in perturbation theory.

[1] ATLAS uses a right-handed coordinate system with its origin at the nominal interaction point in the centre of the detector and the z-axis along the beam pipe. The x-axis points from the interaction point to the centre of the LHC ring, and the y-axis points upward. Cylindrical coordinates (r, ϕ) are used in the transverse plane, ϕ being the azimuthal angle around the beam pipe. The pseudorapidity is defined in terms of the polar angle θ as $\eta = -\ln\tan(\theta/2)$.

JHEP12(2017)059

The DY process was generated at NLO using Powheg-Box (referred to as Powheg in the following) [29–32] and the CT10 PDF set [33], with Pythia 8 [34] to model parton showering, hadronisation, and the underlying event (UEPS). The $Z/\gamma^* \to \ell^+\ell^-$ differential cross section as a function of mass has been calculated at NNLO in perturbative QCD (pQCD) using FEWZ 3.1 [35–37] with the MSTW2008NNLO PDF set [38]. The renormalisation, μ_r, and factorisation, μ_f, scales were both set equal to $m_{\ell\ell}$. The calculation includes NLO EW corrections beyond final-state photon radiation (FSR) using the G_μ EW scheme [39]. A mass-dependent K-factor used to scale the $Z/\gamma^* \to \ell^+\ell^-$ MC sample is obtained from the ratio of the calculated total NNLO pQCD cross section with the additional EW corrections, to the total cross section from the Powheg sample. This one-dimensional (and therefore partial) NNLO K-factor is found to vary from 1.035 at the lowest invariant mass values considered in this analysis to 1.025 at the highest. This factor also improves the modelling of the Z boson lineshape. The DY production of τ pairs was modelled using Powheg in the same way as the signal simulation.

The scattering amplitude coefficients describing the distributions of lepton decay angles are known to be not accurately modelled in Powheg particularly A_0 at low $p_{\mathrm{T},Z}$ [22]. For this reason, the signal MC events are reweighted as a function of $p_{\mathrm{T},Z}$ and $y_{\ell\ell}$ to improve their modelling. These weights were calculated using the cross-section calculator DYNNLO [40].

The photon-induced process, $\gamma\gamma \to \ell\ell$, is simulated at LO using Pythia 8 and the MRST2004qed PDF set [41]. The expected yield for this process also accounts for NLO QED/EW corrections from references [42, 43], which decrease the yield by approximately 30%.

The production of top quark pairs with prompt isolated leptons from electroweak boson decays constitutes a dominant background. It is estimated at NLO in QCD using Powheg and the CT10 PDF set, with Pythia 6 [44] for UEPS. The $t\bar{t}$ sample is normalized using a cross section calculated at NNLO in QCD including resummation effects [45–50]. Small compared to the $t\bar{t}$ contribution, single-top production in association with a W boson (Wt) is also modelled by Powheg and the CT10 PDF set, with Pythia 6 for UEPS. Both the $t\bar{t}$ and Wt contributions are summed and collectively referred to as the top quark background.

Further small background contributions are due to diboson (WW, WZ and ZZ) production with decays to final states with at least two leptons. The diboson processes were generated at LO with Herwig, using the CTEQ6L1 PDF set [51]. The samples are scaled to NLO calculations [52, 53] or to ATLAS measurements as described in reference [17]. Additionally, the background arising from W boson production in association with jets (W+jets) is studied with MC samples generated with Powheg under identical conditions as the DY signal samples.

All MC samples used in the analysis include the effects of QED FSR, multiple interactions per bunch crossing ("pile-up"), and detector simulation. QED FSR was simulated using Photos [54], while the effects of pile-up were accounted for by overlaying simulated minimum-bias events [55] generated with Pythia8 [34]. The interactions of particles with the detector were modelled using a full ATLAS detector simulation [55] based on Geant4 [56]. Finally, several corrections are applied to the simulated samples, ac-

JHEP12(2017)059

Process	Generator	Parton shower & underlying event	Generator PDF	Model parameters ("Tune")
$Z/\gamma^* \to \ell\ell$	Powheg v1(r1556)	Pythia 8.162	CT10	AU2 [62]
$Z/\gamma^* \to \tau\tau$	Powheg v1(r1556)	Pythia 8.162	CT10	AU2
$\gamma\gamma \to \ell\ell$	Pythia 8.170	Pythia 8.170	MRST2004qed	4C [63]
$t\bar{t}$	Powheg v1(r1556)	Pythia 6.427.2	CT10	AUET2 [64]
Wt	Powheg v1(r1556)	Pythia 6.427.2	CT10	AUET2
Diboson	Herwig 6.520	Herwig 6.520	CTEQ6L1	AUET2
$W \to \ell\nu$	Powheg v1(r1556)	Pythia 8.162	CT10	AU2

Table 1. Overview of the Monte Carlo samples used in this analysis.

counting for differences between data and simulation in the lepton trigger, reconstruction, identification, and isolation efficiencies as well as lepton resolution and muon momentum scale [57–61, 61]. The electron energy scale corrections are applied to the data.

An overview of the simulated event samples is given in table 1.

4 Event selection

Events are required to have been recorded during stable beam condition periods and must pass detector and data-quality requirements. This corresponds to an integrated luminosity of $20.2\,\text{fb}^{-1}$ for the muon channel. Small losses in the data processing chain lead to an integrated luminosity of $20.1\,\text{fb}^{-1}$ for the electron channel. Due to differences in the detector response to electrons and muons the selection is optimised separately for each channel and is described in the following.

4.1 Central rapidity electron channel

The electron data were collected using a dilepton trigger which uses calorimetric and tracking information to identify compact electromagnetic energy depositions. Identification algorithms use calorimeter shower shape information and the energy deposited in the vicinity of the electron candidates to find candidate electron pairs with a minimum transverse energy of 12 GeV for both the leading and subleading electron.

Electrons are reconstructed by clustering energy deposits in the electromagnetic calorimeter using a sliding-window algorithm. These clusters are then matched to tracks reconstructed in the inner detector. The calorimeter provides the energy measurement and the track is used to determine the angular information of the electron trajectory. An energy scale correction determined from $Z \to e^+e^-$, $W \to e\nu$, and $J/\psi \to e^+e^-$ decays [57] is applied to data. Central electron candidates are required to have $|\eta^e| < 2.4$. Furthermore, candidates reconstructed within the transition region between the barrel and endcap calorimeters, $1.37 < |\eta^e| < 1.52$, are excluded from the measurement. Each candidate is required to satisfy the "medium" electron identification [58, 59] criteria, based on calorimetric shower shapes and track parameters. To ensure the selected electrons are on the efficiency plateau of the trigger, electrons are required to have $E_{\text{T}}^e > 20\,\text{GeV}$. Candidate events are

JHEP12(2017)059

required to have exactly one pair of oppositely-charged electrons and their invariant mass is required to be in the range $46 < m_{ee} < 200\,\text{GeV}$.

4.2 High rapidity electron channel

In this channel, the rapidity range of the measurement is extended by selecting one central electron and one forward electron. Forward electrons are defined as having pseudorapidities in the range $2.5 < |\eta^e| < 4.9$, reconstructed by the endcap or forward calorimeters. The data were collected using two single-electron triggers in the central calorimeter region with $E_{\text{T}}^e > 24\,\text{GeV}$ or $E_{\text{T}}^e > 60\,\text{GeV}$. The lower-threshold trigger has additional criteria for the shower shape and energy deposited in the vicinity of the electron candidate. The reconstructed central electrons are required to have $E_{\text{T}}^e > 25\,\text{GeV}$, $|\eta^e| < 2.4$, and must satisfy the "tight" identification criteria. Electrons in the calorimeter transition regions $1.37 < |\eta^e| < 1.52$ are rejected. Leptons produced in the Drell-Yan process are expected to be well isolated from other particles not associated with the lepton. This provides a good discriminant against the multijet background arising from the semileptonic decays of heavy quarks or hadrons faking electrons. The track isolation is defined as the scalar sum of the transverse momenta, $\sum p_{\text{T}}$, of the additional tracks contained in a cone of size $\Delta R = \sqrt{(\Delta\phi)^2 + (\Delta\eta)^2} = 0.2$ around the electron (omitting the contribution from the electron track). Central electrons are required to have a track isolation less than 14% of E_{T}^e.

The forward electron is required to satisfy "tight" identification criteria, $E_{\text{T}}^e > 20\,\text{GeV}$, and $2.5 < |\eta^e| < 4.9$, excluding the transition region between the endcap and forward calorimeters, $3.00 < |\eta^e| < 3.35$. Due to insufficient accuracy in the modelling of the material in front of the endcap calorimeter, forward electrons in the region $2.70 < |\eta^e| < 2.80$ are also rejected.

A dedicated calibration procedure is performed for the forward electrons. Energy scale and Gaussian resolution corrections are derived in bins of η^e by comparing the peak position and the width of the m_{ee} distributions in data and simulation. The scale and resolution corrections are the values that bring the peak regions, $80 < m_{ee} < 100\,\text{GeV}$, of the data and simulation into the best agreement.

No isolation criteria are applied to the forward electron and due to the absence of tracking information in the forward region, no charge requirements are placed on the selected electron pair. Lastly, events in the high rapidity electron channel are required to have exactly one central-forward pair of electrons with an invariant mass in the range $66 < m_{ee} < 150\,\text{GeV}$. Events with more than one possible central-forward pair are not used in this measurement channel.

4.3 Central rapidity muon channel

Candidate events in the muon channel were collected using two sets of triggers with the set of triggers used depending on the p_{T}^{μ} of the muon with the larger transverse momentum. For $p_{\text{T}}^{\mu} > 25\,\text{GeV}$, two single-muon triggers are used, with transverse momentum thresholds of 24 GeV and 36 GeV. The low-threshold trigger requires the muon to be isolated. This combination of triggers collected the majority of the events in the data sample. For $p_{\text{T}}^{\mu} <$

25 GeV, a dimuon trigger is used which requires two muons with transverse momentum thresholds of 18 GeV for one muon and 8 GeV for the other.

Muons are identified by tracks reconstructed in the muon spectrometer matched to tracks reconstructed in the inner detector, and are required to have $p_{\mathrm{T}}^{\mu} > 20\,\mathrm{GeV}$ and $|\eta^{\mu}| < 2.4$. Additionally, they must satisfy identification criteria based on the number of hits in the inner detector and muon spectrometer, and on the consistency between the charge and momentum measurements in both systems [60]. Backgrounds from multijet events are efficiently suppressed by imposing an isolation condition requiring that the sum of the transverse momentum, $\sum p_{\mathrm{T}}$, of the tracks contained in a cone of size $\Delta R = 0.2$ around the muon (omitting the contribution from the muon track) to be less than 10% of p_{T}^{μ}. A small contribution of cosmic muons is removed by requiring the magnitude of the longitudinal impact parameter with respect to the primary interaction vertex z_0 to be less than 10 mm. Events are selected if they contain exactly two oppositely-charged muons satisfying the isolation and impact parameter requirements. Finally, the dilepton invariant mass must be in the range $46 < m_{\mu\mu} < 200\,\mathrm{GeV}$.

In order to minimise the influence of residual misalignments between the ID and MS, muon kinematic variables are measured using the ID only. A small residual η^{μ}- and charge-dependent bias in the muon momentum was observed, most likely arising from residual rotational misalignments of the inner detector. Such ID misalignments bias the measurement of the muon track sagitta and have an opposite effect on the momentum of positively- and negatively-charged muons. Hence, the reconstructed invariant mass or rapidity of muon pairs are not affected, in contrast to measurements of $\cos\theta^*$ which are charge-dependent. These residual inner detector misalignments are corrected for based on two methods, one which uses $Z \to \mu^+\mu^-$ events, and another using $Z \to e^+e^-$ events as described in reference [65]. Together with a χ^2 minimisation technique, the dimuon data sample is used to determine the corrections binned finely, which are however insensitive to the η-independent component of the track curvature bias. This bias is corrected for using dielectron data by comparing the ratio of the calorimeter energy to the track momentum for electrons and positrons.

4.4 Measurement bins

The measurement bins are chosen by taking into consideration several competing demands on the analysis such as its sensitivity to the underlying physics, the statistical precision in each bin, and detector resolution effects particularly in the $m_{\ell\ell}$ dimension. The binning must also match those used in recent ATLAS cross section measurements [13, 18].

The measurement is performed in seven bins of $m_{\ell\ell}$ from 46 GeV to 200 GeV with edges set at 66, 80, 91, 102, 116, and 150 GeV; 12 equidistant bins of $|y_{\ell\ell}|$ from 0 to 2.4; and bins of $\cos\theta^*$ from -1 to $+1$, separated at -0.7, -0.4, 0.0, $+0.4$, $+0.7$ giving 6 bins. In total, 504 measurement bins are used for the central rapidity electron and muon channel measurements.

For the high rapidity electron channel the measurement is restricted to the 5 invariant mass bins in the region $66 < m_{\ell\ell} < 150\,\mathrm{GeV}$. The $|y_{\ell\ell}|$ region measured in this channel ranges from 1.2 to 3.6 in 5 bins with boundaries at 1.6, 2.0, 2.4, 2.8. The $\cos\theta^*$ binning is

JHEP12(2017)059

identical to the binning of the central analyses. A total of 150 measurement bins is used in this channel.

5 Background estimation

The background from processes with two isolated final-state leptons of the same flavour is estimated using MC simulation. The processes with non-negligible contributions are $Z/\gamma^* \to \tau\tau$, diboson (WW, WZ and ZZ), and photon-induced dilepton production — together termed the *electroweak* background sources. The top quark background arising from $t\bar{t}$ and Wt production is also estimated using MC simulation. The samples used for these estimates are listed in table 1.

Background contributions from events where at least one final state jet satisfies the electron or muon selection criteria, hereafter referred to as the *fake lepton* background, are determined using a combination of data-driven methods and MC simulation. By far the largest contribution to the fake lepton background comes from light- and heavy-flavour multijet production, referred to as the *multijet* background, which is determined from data. Descriptions on the fake background estimations used in each of the three channels are given in the following subsections.

5.1 Fake lepton background estimation in the central rapidity electron channel

To separate the signal from the multijet background, the analysis relies on the electron relative transverse energy isolation distribution (I^e). This is a good discriminant for the multijet contribution, which has larger values of I^e than the signal process. It is defined as the ratio of the summed calorimetric transverse energy contained in a cone of size $\Delta R = 0.2$ around the electron to the electron transverse energy: $I^e = \sum E_{\mathrm{T}}(\Delta R = 0.2)/E^e_{\mathrm{T}}$. The smaller of the I^e values of the two electron candidates is chosen to represent each event, as it was found to provide optimal discrimination.

The multijet fraction is then estimated from data by fitting this distribution using a template method. The background template is selected with inverted electron identification requirements and the signal, electroweak, and W+jet templates are taken from simulation. The non-isolated sample where the smaller I^e of the two electrons exceeds a certain value is found to be dominated by multijet background and is used to adjust the normalization of the background template, taking into account the small signal contamination. Since the multijet background is not expected to exhibit any parity violating effects and the $\cos\theta^*$ background templates in data were found not to show any asymmetry about $\cos\theta^* = 0$, the method is symmetrised in bins of $|\cos\theta^*|$, resulting in a doubling of the sample sizes and therefore more stable results.

The multijet contribution is found to be largest at low m_{ee} and also at large $|\cos\theta^*|$ for $|y_{ee}| \sim 0$, where it reaches 15% of the expected number of signal events. In the pole region, $80 < m_{ee} < 102\,\mathrm{GeV}$, the contribution is less than 0.1%.

The contribution of W+jet production to the fake lepton background is estimated from MC simulation. It is small compared to the multijet background for all kinematic regions, and therefore does not introduce any significant charge asymmetry.

JHEP12(2017)059

5.2 Fake lepton background estimation in the high rapidity electron channel

The multijet background in the high rapidity electron channel is estimated using a template method similar to the one used in the central electron channel with, however, some small adjustments. The isolation variable is used for the normalisation of the multijet background only for the mass bins in the range $80 < m_{ee} < 102\,\text{GeV}$. The size of the isolation cone in this case is increased to $\Delta R = 0.3$, which was found to improve the stability of the fits. For the off-peak mass bins, the transverse energy of the forward electron is used as an alternative discriminating variable, where the multijet background contributes mostly at low E_{T}. This decreases the statistical uncertainty of the estimation and reduces its dependence on the W+jet background modelling, as discussed below.

The multijet background is the dominant contribution to the background in this measurement channel and is typically about 5–10% of the expected signal, but increases rapidly at large $|\cos\theta^*|$. It can be as large as 30–60% in some bins at large $|y_{ee}|$ where the $|A_{\text{FB}}|$ is large and the signal cross section is suppressed, i.e. $\cos\theta^* < 0$ for $m_{ee} > m_Z$.

The W+jet background is estimated using MC simulation. As was the case in the central electron analysis, it is found to be small under the peak of the Z resonance. It is found to be more significant off peak, reaching 30% of the fake lepton background.

5.3 Fake lepton background estimation in the central rapidity muon channel

The multijet background remaining after event selection in the muon channel is largely due to heavy-flavour b- and c-quark decays, and is estimated in two steps. First, the shape as a function of $|y_{\mu\mu}|$ and $|\cos\theta^*|$ is estimated in each $m_{\mu\mu}$ bin. Next its overall normalisation is then determined in each invariant mass region.

Three orthogonal control regions with inverted muon isolation requirements defined by $I^\mu = \sum p_{\text{T}}(\Delta R = 0.2)/p_{\text{T}}^\mu > 0.1$, and/or inverted muon pair charge requirements are used to determine the multijet background. In each control region the contamination from signal and electroweak background is subtracted using simulation.

A comparison of the shape of the I^μ distributions for muons in events with same-charge and opposite-charge muon pairs shows a small linear deviation from unity of up to +10% when extrapolated into the isolated signal region $I^\mu < 0.1$. This is found to be independent of $m_{\mu\mu}$, and is accounted for in the extrapolation. The $|y_{\mu\mu}|$ and $|\cos\theta^*|$ dependence of the background in each $m_{\mu\mu}$ bin is obtained in the multijet enriched data control region in which pairs of same-charge and opposite-charge muons satisfy $I^\mu > 0.1$. Finally, the resulting $|y_{\mu\mu}|$ and $|\cos\theta^*|$ spectra are normalised in the signal region using the constraint that the yield ratio of opposite-charge to same-charge muon pairs is similar in the isolated and non-isolated control regions.

This method does not account for a potential W+jets background contribution. This component is estimated from simulation and found to be negligible.

The estimated fake lepton background contribution in the muon channel is everywhere smaller than its contribution in the central electron channel, and never more than 5% of the expected signal yield.

JHEP12(2017)059

5.4 Top quark and electroweak backgrounds

These sources of background arise from QCD and EW processes in which two prompt isolated leptons are produced. Their contributions are estimated using MC simulation.

Background events from top quark processes increase with $m_{\ell\ell}$ and are typically below 2% of the expected signal yields. The contribution is largest at the extremes of $\cos\theta^*$ where it can reach 10–20% of the expected signal in the central channels. At high rapidity, this background source is typically below 5% everywhere.

The diboson background increases with invariant mass and reaches about 6% of the expected signal yield at large $|\cos\theta^*|$ in both the central electron and muon channels. In the high rapidity electron channel it reaches about 3% at moderate $|y_{\ell\ell}|$.

The background from $Z \to \tau\tau$ is significant only at low $m_{\ell\ell}$, where it can reach 7% in the central rapidity channels and 3% in the high rapidity channel.

Photon-induced production of dilepton pairs gives a small background contribution of 2% or less in all channels. However, for large values of $m_{\ell\ell}$, this contribution can reach about 5%.

6 Cross-section measurement

As defined in section 4.4, the binning scheme used for the triple-differential measurements consists of 504 bins for the central rapidity electron and muon channels, and 150 bins in the high rapidity electron channel. The Drell-Yan cross section is measured in the central rapidity channels within the fiducial region defined by $p_{\mathrm{T}}^{\ell} > 20\,\mathrm{GeV}$, $|\eta^{\ell}| < 2.4$, and $46 < m_{\ell\ell} < 200\,\mathrm{GeV}$. In the high rapidity electron channel the fiducial region of the measurement is defined by $p_{\mathrm{T}}^{\ell} > 25\,\mathrm{GeV}$ and $|\eta^{\ell}| < 2.4$ for the central electron, $p_{\mathrm{T}}^{\ell} > 20\,\mathrm{GeV}$ and $2.5 < |\eta^{\ell}| < 4.9$ for the forward electron, and $66 < m_{\ell\ell} < 150\,\mathrm{GeV}$.

The cross-section results are first unfolded to the "dressed"-level, defined at the particle-level using leptons after FSR recombined with radiated photons within a cone of $\Delta R = 0.1$. The unfolded data are then corrected to the Born-level, before final-state QED radiation at the particle-level, using a correction factor obtained from the Powheg MC sample. This procedure neglects the bin migrations between the dressed- and Born-level kinematics, an approximation which was verified to have a negligible impact on the central values and uncertainties of the results presented in this paper.

The triple-differential cross section is calculated as

$$\left.\frac{\mathrm{d}^3\sigma}{\mathrm{d}m_{\ell\ell}\,\mathrm{d}|y_{\ell\ell}|\,\mathrm{d}\cos\theta^*}\right|_{l,m,n} = \mathcal{M}_{ijk}^{lmn} \cdot \frac{N_{ijk}^{\mathrm{data}} - N_{ijk}^{\mathrm{bkg}}}{\mathcal{L}_{\mathrm{int}}} \frac{1}{\Delta_{m_{\ell\ell}} \cdot 2\Delta_{|y_{\ell\ell}|} \cdot \Delta_{\cos\theta^*}} \ , \qquad (6.1)$$

where i, j, k are the bin indices for reconstructed final-state kinematics; l, m, n are the bin indices for the generator-level kinematics; and $\mathcal{L}_{\mathrm{int}}$ is the integrated luminosity of the data set. Quantity N^{data} is the number of candidate signal events observed in a given bin of width $\Delta_{m_{\ell\ell}}$, $\Delta_{|y_{\ell\ell}|}$, and $\Delta_{\cos\theta^*}$, while N^{bkg} is the number of background events in the same bin. The factor of two in the denominator accounts for the modulus in the rapidity bin

JHEP12(2017)059

width. Integrated single- and double-differential cross sections are measured by summing over the corresponding indices of equation (6.1).

The factor $\mathcal{M}$ is the inverted response matrix and takes into account the efficiency of the signal selection and bin migration effects. It gives the probability that a selected event reconstructed in some measurement bin was originally generated in a given fiducial (generator-level) bin. The factor $\mathcal{M}$ is obtained from the Drell-Yan signal samples after correcting for differences in the reconstruction, identification, trigger, and isolation efficiencies between data and simulation, as well as for momentum scale and resolution mismodelling effects. It also accounts for events originally outside of the fiducial selection that migrate into the reconstructed event sample. Finally, $\mathcal{M}$ also includes extrapolations over the regions that are excluded from the electron selection ($1.37 < |\eta^e| < 1.52$, $2.70 < |\eta^e| < 2.80$, and $3.00 < |\eta^e| < 3.35$).

The quality of the simulation and its ability to describe the data are checked in figures 1–4, comparing data and prediction for the $y_{\ell\ell}$, $\cos\theta^*$, and $m_{\ell\ell}$ distributions in selected regions of the measured kinematic range, as indicated in the figure captions. The expected number of events is calculated as the sum of expected signal and background yields. Acceptable agreement is found in all channels, given that the simulation is only accurate to NLO for the observables shown in figures 1–3, and to NNLO accuracy for the $m_{\ell\ell}$ distribution shown in figure 4.

The background-subtracted data are unfolded to fiducial cross sections using the inverse of the response matrix obtained using an iterative Bayesian unfolding method [66] in which the prior is improved at each iteration. When using such methods the statistical and systematic uncertainties (discussed in section 7) increase with each unfolding iteration, while the residual bias from the initial prior decreases. A balance between these two competing effects must be struck when deciding on the number of iterations to be used to unfold the measurement. Only small changes to the prior are expected, however, since the lineshape of the Z boson resonance and the PDFs are known to high-precision. Moreover, the prior (Powheg) is enhanced using QCD and EW corrections and describes the data within experimental uncertainties. An optimum was found using two iterations in this analysis.

Finally, measurement bins which are predicted by signal MC simulation to have fewer than 25 signal events are expected to have large statistical uncertainties and therefore these bins are removed from the analysis. Approximately 50 bins are discarded in each of the central electron and muon channels. They typically lie at large $|y_{\ell\ell}|$ and large $|\cos\theta^*|$. In the high rapidity electron channel, 27 bins are removed, all corresponding to small $|\cos\theta^*|$. In all cases the discarded bins correspond to ones for which the signal prediction at LO in QCD is consistent with zero.

JHEP12(2017)059

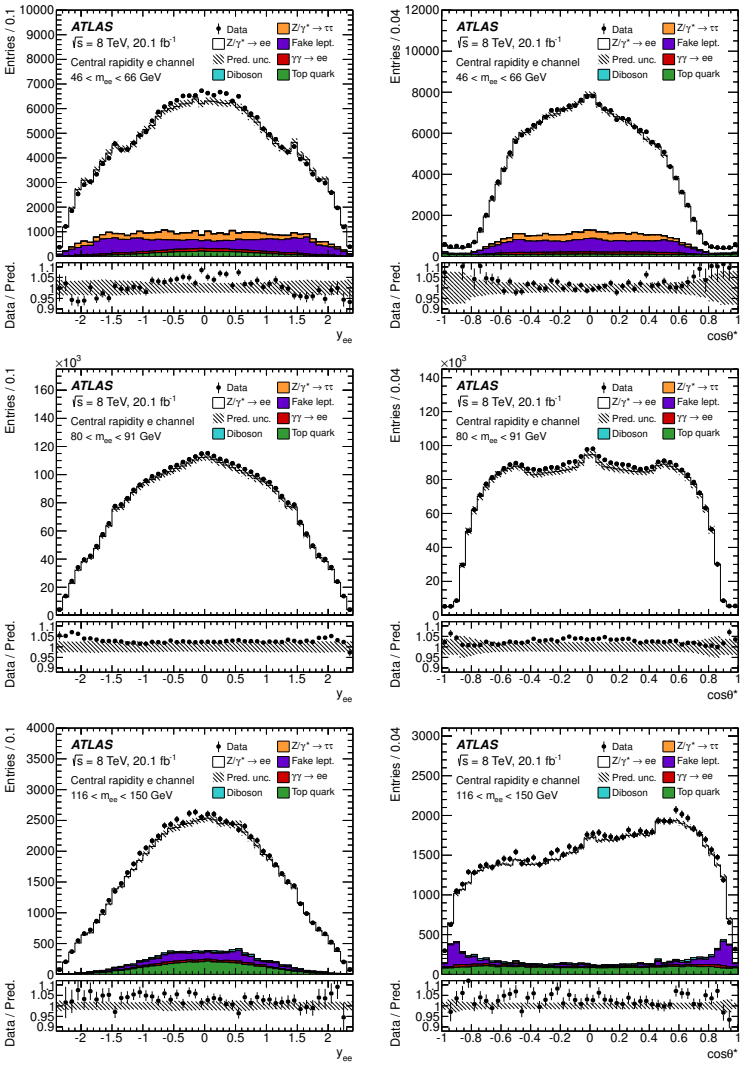

Figure 1. Distributions of dilepton rapidity (left) and $\cos\theta^*$ (right) in the central rapidity electron channel for m_{ee} bins 46–66 GeV (top row), 80–91 GeV (middle), and 116–150 GeV (bottom). The data (solid markers) and the prediction (stacked histogram) are shown after event selection. The lower panels in each plot show the ratio of data to prediction. The error bars represent the data statistical uncertainty while the hatched band represents the systematic uncertainty in the prediction.

JHEP12(2017)059

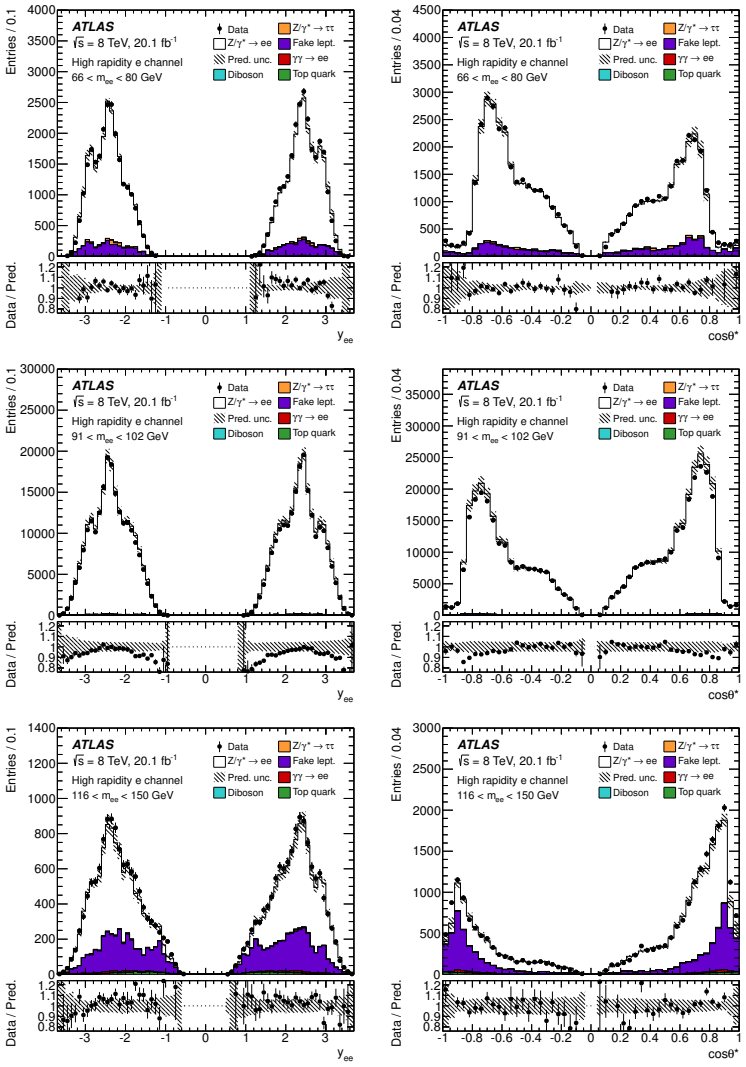

Figure 2. Distributions of dilepton rapidity (left) and $\cos\theta^*$ (right) in the high rapidity electron channel for m_{ee} bins 66–80 GeV (top row), 91–102 GeV (middle), and 116–150 GeV (bottom). The data (solid markers) and the prediction (stacked histogram) are shown after event selection. The lower panels in each plot show the ratio of data to prediction. The error bars represent the data statistical uncertainty while the hatched band represents the systematic uncertainty in the prediction.

JHEP12(2017)059

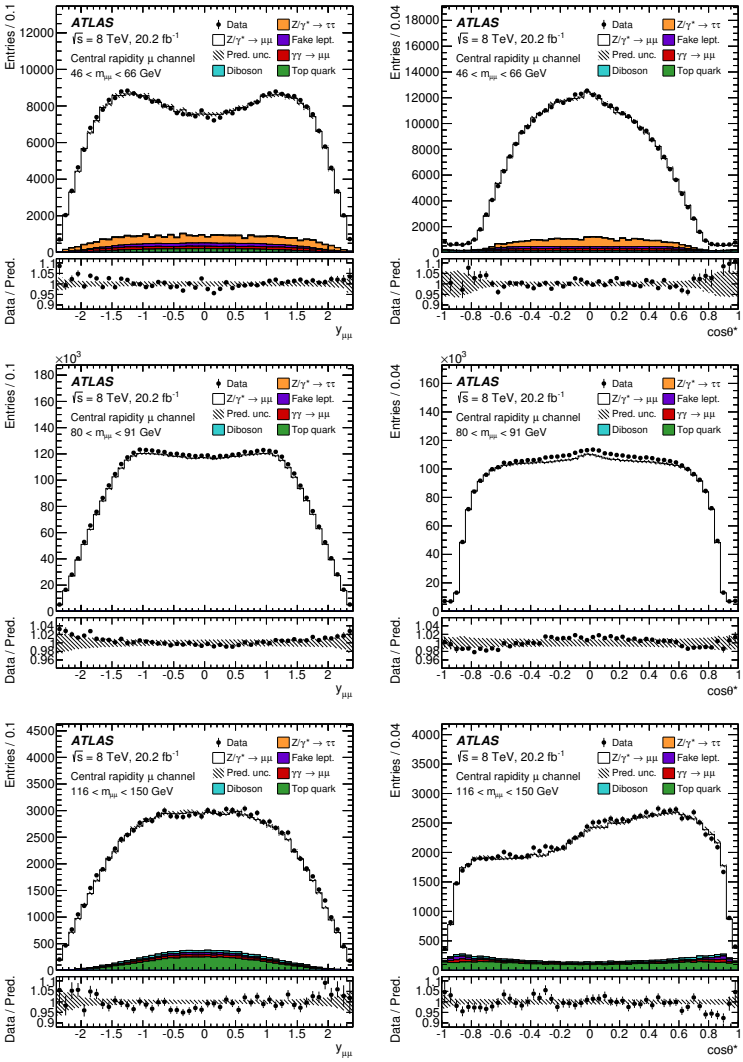

Figure 3. Distributions of dilepton rapidity (left) and $\cos\theta^*$ (right) in the central rapidity muon channel for $m_{\mu\mu}$ bins 46–66 GeV (top row), 80–91 GeV (middle), and 116–150 GeV (bottom). The data (solid markers) and the prediction (stacked histogram) are shown after event selection. The lower panels in each plot show the ratio of data to prediction. The error bars represent the data statistical uncertainty while the hatched band represents the systematic uncertainty in the prediction.

JHEP12(2017)059

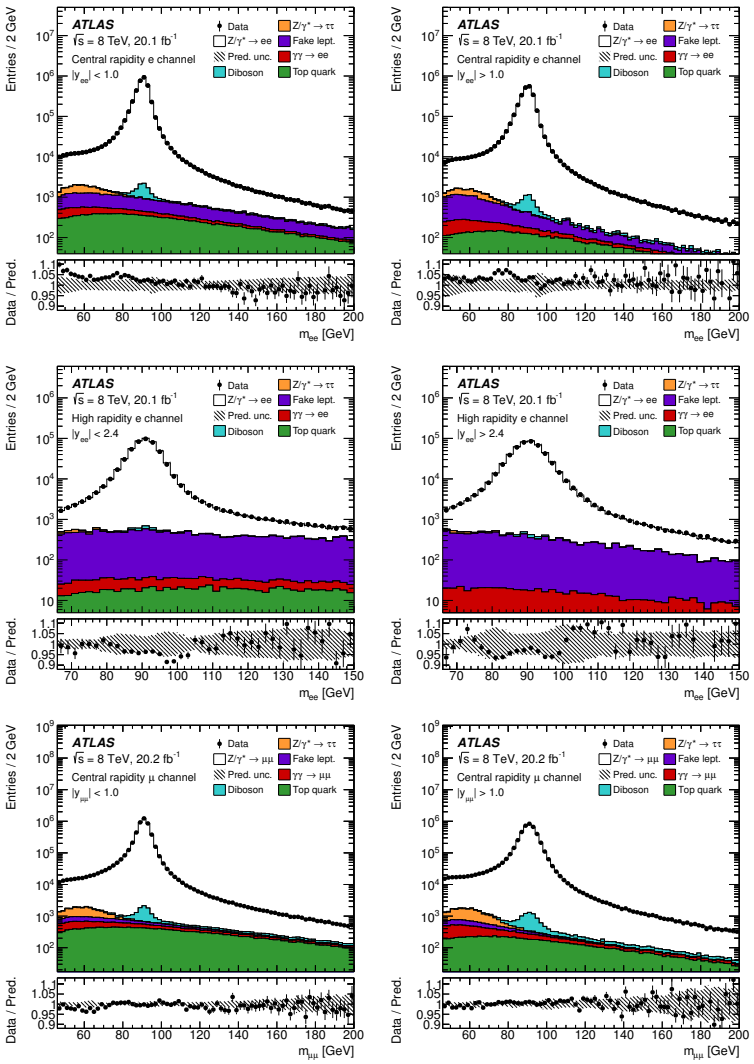

Figure 4. Distributions of invariant mass for all three measurements: the central rapidity electron (top row), the high rapidity electron channel (middle), and the central rapidity muon (bottom) channels. For the central measurements, the distributions are plotted for $|y_{\ell\ell}| < 1.0$ (left) and $|y_{\ell\ell}| > 1.0$ (right) while for the high rapidity measurement, regions $|y_{ee}| < 2.4$ (left) and $|y_{ee}| > 2.4$ (right) are shown. The data (solid markers) and the prediction (stacked histogram) are shown after event selection. The lower panels in each plot show the ratio of data to prediction. The error bars represent the data statistical uncertainty while the hatched band represents the systematic uncertainty in the prediction.

JHEP12(2017)059

7 Measurement uncertainties

The uncertainties in the measurements are discussed separately starting with the sources relevant to both electron channels, then the sources only appearing in the high rapidity electron channel. Next, sources of uncertainty specific to the muon channel are given followed by the sources common to all three measurements. Uncertainties due to statistical sources from both the data and MC samples, the modelling of the energy and momentum response to leptons, lepton selection efficiencies, background subtraction, and theoretical uncertainties are covered in this section. Each source is classified as being correlated or uncorrelated between measurement bins in a single channel. The sources are propagated using one of three techniques: the bootstrap method [67], the pseudo-experiment method, or the offset method.

7.1 Statistical uncertainties

The impact of the statistical uncertainty in the number of events in the data and MC simulations on the cross-section measurement is quantified using the bootstrap method, a statistical resampling technique in which each event is reweighted with a random number drawn from a Poisson distribution with a mean of unity. This reweighting procedure is done 1000 times producing 1000 replicas of the measurement. All replicas are then unfolded and the uncertainty is taken as the standard deviation of the measured cross sections. In the case of the signal MC sample the bootstrap replicas are used to produce an ensemble of 1000 response matrices which are used to unfold the measurement. The standard deviation of the unfolded cross sections is used as the signal MC statistical uncertainty.

7.2 Systematic uncertainties

The pseudo-experiment method is used for correction factors determined in bins of lepton kinematics, typically η and transverse energy/momentum. These correction factors have statistical and systematic uncertainties which are fluctuated randomly using 1000 pseudo-experiments according to a Gaussian distribution whose mean and standard deviation are set to the value and uncertainty of the correction factor, respectively. For correlated sources, a single set of varied correction factors is used for all measurement bins, whereas for uncorrelated sources the random shifts are applied separately for each bin. The uncertainties are propagated via the unfolding procedure yielding 1000 cross-section results which are used to determine a covariance matrix.

In the offset method the correction factor values from each source are coherently shifted upwards and downwards by one standard deviation and the measurement is remade using the varied values. The uncertainty is taken as half the difference between the two unfolded measurements.

7.3 Central and high rapidity electron channels

The systematic uncertainties in the cross section that are unique to the electron channels are dominated by the uncertainties in the electron energy scale, and the electron reconstruction and identification efficiency uncertainties. In addition, a large contribution to the

JHEP12(2017)059

uncertainty arises from the electron energy resolution uncertainty in the two neighbouring m_{ee} bins at the Z-peak, $80 < m_{ee} < 91\,\text{GeV}$ and $91 < m_{ee} < 102\,\text{GeV}$.

7.3.1 Energy scale and resolution

The electron energy scale and resolution and their corresponding uncertainties are determined using $Z \to e^+e^-$, $W \to e\nu$, and $J/\psi \to e^+e^-$ decays. The uncertainty in the energy scale is separated into a statistical component and 14 uncorrelated systematic sources. Some of these sources are split into fine η^e bins, while others are coarsely binned into barrel and endcap regions as described in reference [57]. These sources are found to be strongly anti-correlated between the regions $m_{ee} < m_Z$ and $m_{ee} > m_Z$. The statistical uncertainty in the energy scale is found to be negligible. Adding the effects of the 14 sources of uncertainty in the energy scale in quadrature after propagating to the measured cross sections, the combined uncertainty is 1–2% for the mass bins $80 < m_{ee} < 91\,\text{GeV}$ and $91 < m_{ee} < 102\,\text{GeV}$, but is less than 1% at low and high m_{ee}. However, in the integrated m_{ee} cross-section measurement the effect of these sources is strongly reduced as a result of the anti-correlation between these two m_{ee} bins.

The uncertainty in the energy resolution is separated into seven uncorrelated systematic sources which are propagated to the cross-section measurements individually. This combined uncertainty is typically 0.1–0.5% except in the invariant mass regions neighbouring the Z-peak where it reaches 1%.

7.3.2 Reconstruction and identification efficiencies

The reconstruction and identification efficiencies of electrons are determined from data using various tag-and-probe methods in Z and J/ψ decays, following the prescription in reference [58] with certain improvements and adjustments for the 2012 conditions [68]. The uncertainties arise from variations in the tag-and-probe selection and the background subtraction methods. The correlated systematic uncertainty is taken from the RMS of all variations, separately for the reconstruction and identification efficiency sources, and propagated using the pseudo-experiment method.

The influence of the identification efficiency uncertainty is found to be 0.2–0.4% increasing for larger $|\cos\theta^*|$, and up to 2% at low m_{ee}. The reconstruction efficiency uncertainty translates into a variation of the measured cross section which is generally below 0.2% but as large as 0.4% at low m_{ee}.

7.3.3 Trigger efficiency

The trigger efficiency is measured in both the data and MC simulation using a tag-and-probe method in $Z \to e^+e^-$ decays and is composed of a statistical uncorrelated component which is small, and a correlated piece which is propagated using the pseudo-experiment method. The resulting uncertainty in the cross section amounts to approximately 0.5% at low m_{ee} but decreases to approximately 0.1% for $m_{ee} > 116\,\text{GeV}$.

JHEP12(2017)059

7.3.4 Charge misidentification

The electron charge is determined from the sign of the curvature of the associated ID track. Bremsstrahlung radiation and subsequent conversion of the radiated photons can lead to misidentification of the charge. This is measured in Z boson decays in which one lepton has an incorrectly reconstructed charge. Such events are selected by requiring the electron pair to possess the same electric charge and an invariant mass to be near m_Z, consistent with a Z boson decay. The resulting correlated uncertainty is propagated with the offset method and found to be less than 0.2% everywhere.

7.3.5 Multijet background

Uncertainties in the multijet estimation arise from the sample size used in the method, the subtracted signal and EW contamination, the shape of the multijet distribution, and the range of the isolation distribution used. The subtracted top quark and diboson contamination is varied coherently within the theoretical cross-section uncertainties. The subtracted signal contamination is varied by ±5%. The shape of the multijet distribution is varied by relaxing the same-sign charge requirement in the case of the central electron channel, and using the transverse energy E_{T}^{e} of the forward electron as an alternative discriminant in the high rapidity electron channel. The range of the isolation distribution used is varied by ±15%.

The variations made to account for systematic uncertainties in the method lead to changes in the estimated multijet yield in the central electron channel. The variations in the multijet yields range from about 10% at low m_{ee} and $\cos\theta^* \sim 0$, to more than 100% in regions where the nominal multijet yield is small, e.g. at large $|\cos\theta^*|$ and high m_{ee}.

The uncorrelated statistical component is propagated to the measured cross sections with the bootstrap replica method. The remaining two correlated components are propagated with the offset method, which when summed in quadrature amount to a measurement uncertainty of less than 0.1% of the cross section, except at low m_{ee} and large $|\cos\theta^*|$ where it grows to almost 1% in the central electron channel.

In the high rapidity channel the multijet yields range from 15% to more than 100% due to systematic uncertainties in the method. At small $\cos\theta^*$ and high invariant masses where the signal contribution is suppressed, the expected multijet background can be very large, as noted in section 5.2. Here, the systematic uncertainty in the multijet background is 20–70% depending on $|y_{ee}|$, resulting in a measurement uncertainty of 30% or greater when propagated to the triple-differential cross section.

7.4 High rapidity electron channel

The high rapidity electron analysis differs from the central electron channel measurement by requiring one electron to be in the forward region $2.5 < |\eta^e| < 4.9$ where there is no tracking system, which leads to larger background contamination. This is compensated for by the addition of an isolation requirement on the central electron, and more restrictive identification requirements (see section 4.2) on the central and forward electrons. The technique used to calibrate the forward calorimeters is also different, and the impact of

JHEP12(2017)059

potential charge misidentification is different. Since the charge can be measured only for the central electron, the impact of misidentification is to swap the sign of $\cos\theta^*$. Each of these leads to additional sources of systematic uncertainty which are discussed in the following.

The energy scale and resolution corrections for forward electrons lead to correlated sources of uncertainty propagated using the offset method. They arise from changes in the event selection used to perform the calibration as well as variations of the methodology. The influence of the scale uncertainty on the measurement is about 1% but can reach 5% at high $|\cos\theta^*|$. The resolution uncertainty amounts to 0.1–0.3% increasing to 3–5% at large $|\cos\theta^*|$ and off-peak mass bins.

The uncertainty in the cross-section measurement due to the identification efficiency of forward electrons is considered to be correlated across the measurement bins and is estimated using the pseudo-experiment method. It amounts to about 1% uncertainty in the cross section.

The efficiency of the isolation selection for central electrons is derived using a tag-and-probe method in central $Z \to e^+e^-$ decays and is well described by the simulation. The resulting uncertainty in the cross section is negligible.

To verify that the modelling of the W+jet background does not affect the estimation of the total fake lepton background in the high rapidity channel, its normalisation is varied by 60% (as motivated by reference [18]) and the fit of the multijet background is repeated. Since the shape of the E_{T} distribution is similar for the W+jet and multijet backgrounds, the total fake lepton background remains almost invariant for the off-peak regions while for the peak mass bins the variation is small compared to the multijet background uncertainty.

7.5 Central rapidity muon channel

Uncertainties related to the muon momentum scale and resolution, and the efficiencies of the muon trigger, reconstruction, and isolation and impact parameter selections are all studied using $Z \to \mu^+\mu^-$ events, and in some cases $J/\psi \to \mu^+\mu^-$ events are also used. The efficiencies are determined using a tag-and-probe method. The largest contributions to the systematic uncertainty in the measurements typically arise from the reconstruction efficiency and isolation efficiency modelling, and from the muon momentum scale calibration.

7.5.1 Momentum scale and resolution

Corrections to the muon momentum scale and resolution are obtained from fits to the $Z \to \mu^+\mu^-$ and $J/\psi \to \mu^+\mu^-$ lineshapes with scale and resolution parameters derived in local detector regions [60]. These sources are separated into 12 correlated components for the resolution in fine η^μ bins and one correlated component for the momentum scale. Uncertainties in the momentum scale arising from the methodology, and uncertainties in the ID material simulation, muon angle reconstruction, and alignment are propagated using the offset method. They result in a systematic uncertainty correlated in η^μ bins of the measured cross sections of typically 0.3%, increasing for larger $|y_{\mu\mu}|$, $|\cos\theta^*|$, and $m_{\mu\mu}$

JHEP12(2017)059

to 2%. The correlated resolution uncertainty has a small influence on the measurement and is also propagated with the offset method.

The influence of residual misalignments is estimated from two sources. The first arises from the statistical uncertainty of the alignment corrections derived using $Z \to \mu^+\mu^-$ data and is considered uncorrelated. This component is propagated to the cross section using the pseudo-experiment method, and is separated into 84 uncorrelated components. The second source accounts for biases in the correction method, and is defined as the difference between the corrections derived for data and simulation in bins of η^μ. This uncertainty is separated into 40 correlated components. After propagating this correlated source to the cross section using the pseudo-experiment method, the resulting uncertainty is found to be about 0.2%, increasing significantly with $|\cos\theta^*|$ at large $|y_{\mu\mu}|$.

7.5.2 Reconstruction efficiency

The uncertainty due to the muon reconstruction efficiency is parameterised as a function of η^μ and p_{T}^μ [60] and is decomposed into correlated and uncorrelated parts. The uncertainty is propagated to the cross section using the offset and pseudo-experiment methods for the correlated and uncorrelated components, respectively. The correlated component has an uncertainty of 0.1%, which corresponds to an uncertainty in the measured cross section of 0.2–0.4%.

7.5.3 Trigger efficiency

The efficiency corrections for single-muon and dimuon triggers are obtained using the tag-and-probe method as described in reference [61]. They are parameterised in terms of muon pseudorapidity η^μ, azimuthal angle ϕ^μ, and electric charge. The correlated uncertainty components arise from the background contamination, a possible residual dependence on muon p_{T}^μ, and an uncertainty based on the event topology, which are propagated using the offset method. The uncorrelated statistical uncertainty is propagated to the cross section using the pseudo-experiment method. Events selected with the single-muon triggers ($p_{\mathrm{T}}^\mu > 25\,\mathrm{GeV}$) cover most of the kinematic range of the measurement, whereas the dimuon triggers supplement the selection at low $m_{\mu\mu}$ and have somewhat larger uncertainties. This translates into a correlated uncertainty in the measured cross section which is typically 0.1% where the single-muon triggers are used, and can reach 0.6% at large $|\cos\theta^*|$ in the lowest $m_{\mu\mu}$ bin.

7.5.4 Isolation and impact parameter efficiency

Muon isolation and impact parameter selection efficiencies give rise to additional systematic uncertainties and are estimated together. The sources considered include the remaining background contamination, the residual variation in η^μ, and a possible bias from the event topology estimated by varying the azimuthal opening angle between the two muons used in the tag-and-probe method. The resulting correlated cross-section uncertainty determined with the pseudo-experiment method is found to be typically 0.2%, rising to 0.5% at high $m_{\mu\mu}$.

JHEP12(2017)059

7.5.5 Multijet background

The uncertainty in the multijet background estimate comes from several sources. The uncorrelated statistical uncertainty of the control regions is propagated using the bootstrap replica method and can be significant, in particular from the isolated same-charge control sample. The subtracted top quark and diboson contamination in the control regions is varied coherently within the theoretical cross-section uncertainties given in section 3. The subtracted signal contamination is varied by ±5%. The correlated uncertainty in the shape of the $|y_{\mu\mu}|$ and $|\cos\theta^*|$ spectra is determined from the RMS of these distributions in five regions of increasing non-isolation of the muon pairs obtained from the control regions. The final contribution comes from the fit extrapolation of the background estimate into the signal region and is assessed by varying the range of the fit. Systematic components lead to changes in the multijet yields of 15% to 30% of the expected signal contribution. This is largest in the regions of large $|\cos\theta^*|$. The variations can be up to 60% for large $|\cos\theta^*|$ and large $|y_{\ell\ell}|$.

Both the shape and extrapolation uncertainties are propagated to the cross section using the offset method and dominate the total uncertainty. The combined uncertainty in the background estimate when propagated to the cross-section measurement is below 0.1% in all measurement bins except in the lowest $m_{\mu\mu}$ bin where it reaches 1% at large $|\cos\theta^*|$ and small $|y_{\mu\mu}|$.

7.6 Systematic uncertainties common to all channels

The systematic uncertainties common to all three channels are derived using identical methods. With the exception of the statistical uncertainties arising from the MC samples used, which are uncorrelated between the measurement channels, common systematic uncertainties are assumed to be fully correlated between the channels. The dominant common uncertainty is the uncertainty in the luminosity measurement.

7.6.1 Top, diboson, W+jet, $Z/\gamma^* \to \tau\tau$, and photon-induced background normalisation

The normalisation uncertainties considered for these background sources arise from variations in the PDFs, α_S, and the QCD scales used in the theoretical predictions. The normalisation uncertainty in the top quark background, which is dominated by $t\bar{t}$ production, is taken to be 6% following the PDF4LHC prescription [69]. The uncertainty includes scale and α_S variations and also takes into account the uncertainty in the top-quark mass. Diboson (WW, WZ and ZZ) production is another important background source for which the normalisation uncertainties are about 10%. See reference [17] for additional information on the normalisation uncertainties of the various Monte Carlo samples used.

The background contributions from W+jet processes are assigned a normalisation uncertainty of 5% for the central rapidity measurements. For the high rapidity electron channel, where W+jet is a dominant background, a variation of 60% is considered (see section 7.4).

The background contribution from $Z/\gamma^* \to \tau\tau$ decays is assigned a normalisation uncertainty of 5%. The photon-induced background is assigned an uncertainty of 40%,

JHEP12(2017)059

derived by calculating the photon-induced contribution in a constituent and a current mass scheme for the quark [41], and taking the magnitude of the difference between either scheme and their average [13]. In all cases the normalisation uncertainties are propagated to the final cross sections using the offset method.

7.6.2 Unfolding bias

The simulation used as an initial prior in the unfolding process could lead to a potential bias in the measured cross sections. This potential bias is quantified by varying the predictions within theoretical uncertainties. The PDF bias is probed using signal MC events reweighted to each of the 26 different eigenvector variations of the CT10 PDF set in the determination of $\mathcal{M}$. For each variation the change in the unfolded cross section is found to be much smaller than the change in the predicted cross section using each eigenvector PDF set. Changing the PDF set can alter the predicted cross section by up to a few percent but the influence on the unfolded result is less than 0.1%. Furthermore, the change in the unfolded result, using one to five iterations of unfolding, is much smaller than the total uncertainty in the data. This study is repeated by reweighting the signal MC events to different values of the scattering amplitude coefficient $A_4 = \frac{8}{3}A_{\mathrm{FB}}$, which is proportional to $\sin^2\theta_W$. A variation of ± 0.01 is used, corresponding to a maximum change of 0.5% in the cross-section prior, which results in a change in the unfolded cross section of less than 0.1%. These studies show that potential biases are small for five iterations or less.

A potential overestimate or underestimate of the statistical and systematic uncertainties of the measurement due to the chosen number of unfolding iterations is also studied. Tests of the statistical uncertainty are performed using pseudo-data generated using an alternative PDF. Ultimately, two unfolding iterations are used for the final cross-section determination. This number has a negligible bias due to the initial prior and produces a negligible bias in the data statistical and systematic uncertainties.

7.6.3 MC modelling

The Z boson p_{T} distribution is not well modelled in MC simulation and could influence the measurement. The potential bias is estimated by reweighting the signal MC events to the observed data spectrum at reconstruction-level. This reweighted MC sample is used to unfold the cross section and the difference to the nominal measurement is taken as the uncertainty, which is typically below 0.1%, rising to about 1% at large $|\cos\theta^*|$ and large $|y_{\ell\ell}|$.

Adjustments to the reweighting of the scattering amplitude coefficients in the Powheg MC sample are found to have negligible impact on the measured cross sections.

The MC simulations used for modelling the underlying event and parton shower processes are not explicitly studied here, but are only expected to influence this measurement via the lepton isolation selection efficiencies. Studies presented in reference [18] indicate that such effects are small.

7.6.4 PDF uncertainty

As discussed in section 6, the response matrix $\mathcal{M}$ also includes a small acceptance interpolation from the measured region to the fiducial region. These acceptance corrections differ in each of the three measurement channels due to $\eta^{e,\mu}$ gaps in the detector. The corrections are 5–10% but can be larger in certain bins of the triple-differential cross-section measurement. The PDF uncertainties due to these acceptance corrections are estimated using the CT10 PDF eigenvector set at 68% confidence level. They are found to be small, with uncertainties on the order of 0.1% or below for most cross-section measurement bins in the electron channel. In the high rapidity electron channel the uncertainty is also found to be small, except at large $|\cos\theta^*|$ where it can reach 0.6%. The uncertainty evaluated in the muon channel is found to be about 0.5% at low $m_{\mu\mu}$, negligible for $m_{\mu\mu}$ at m_Z, and reaches 0.6% for large $|\cos\theta^*|$ and large $|y_{\mu\mu}|$.

7.6.5 Luminosity

The uncertainty in the integrated luminosity is 1.9%, which is derived following the methodology detailed in reference [70]. This is fully correlated across all measurement bins and analysis channels.

7.7 Summary of measurement uncertainties

Tables 2–4 present the contributions of the individual uncertainties discussed above for each channel in selected analysis bins. The influence of the experimental systematic uncertainties on the measurements of $\mathrm{d}^3\sigma$ can be divided into three regions of $m_{\ell\ell}$ — below the resonance peak, on the peak region, and above the resonance. In the electron channels, the largest measurement uncertainties arise from background and efficiency correction uncertainties at low and high $m_{\ell\ell}$. In the peak region the uncertainty is dominated by the energy scale sources. The muon channel precision is limited by the background uncertainty at low $m_{\ell\ell}$, and by both the momentum scale and misalignment uncertainties in the peak region. At larger invariant mass the uncertainties related to the muon reconstruction and isolation efficiency also become important.

JHEP12(2017)059

Bin	m_{ee} [GeV]	$\lvert y_{ee}\rvert$	$\cos\theta^*$	$\delta^{\rm stat}_{\rm unc}$ [%]	$\delta^{\rm sig}_{\rm unc}$ [%]	$\delta^{\rm bkg}_{\rm unc}$ [%]	$\delta^{\rm mj}_{\rm unc}$ [%]	$\delta^{\rm bkg}_{\rm cor}$ [%]	$\delta^{\rm mj}_{\rm cor}$ [%]	$\delta^{\rm scl}_{\rm cor}$ [%]	$\delta^{\rm res}_{\rm cor}$ [%]	$\delta^{\rm rec}_{\rm cor}$ [%]	$\delta^{\rm id}_{\rm cor}$ [%]	$\delta^{\rm trig}_{\rm cor}$ [%]	$\delta^{\rm qmid}_{\rm cor}$ [%]	$\delta^{\rm kfac}_{\rm cor}$ [%]	$\delta^{\rm zpt}_{\rm cor}$ [%]	$\delta^{\rm pdf}_{\rm cor}$ [%]	$\delta^{\rm tot}$ [%]
1	46, 66	0.0, 0.2	−1.0, −0.7	6.7	2.4	3.4	3.1	1.9	5.2	0.5	0.7	0.5	2.5	0.7	0.2	0.0	0.9	0.2	10.6
2	46, 66	0.0, 0.2	−0.7, −0.4	2.3	0.8	1.2	0.9	1.1	2.0	0.2	0.2	0.5	2.7	0.9	0.0	0.0	0.0	0.1	4.7
3	46, 66	0.0, 0.2	−0.4, 0.0	1.4	0.5	0.9	0.4	0.9	0.9	0.3	0.1	0.3	1.9	0.3	0.0	0.0	0.0	0.0	2.9
4	46, 66	0.0, 0.2	0.0, +0.4	1.4	0.5	0.8	0.5	0.9	0.9	0.3	0.1	0.3	1.9	0.3	0.0	0.0	0.0	0.1	3.0
5	46, 66	0.0, 0.2	+0.4, +0.7	2.2	0.8	0.9	0.9	1.1	2.0	0.2	0.1	0.5	2.6	0.8	0.0	0.0	0.0	0.1	4.5
6	46, 66	0.0, 0.2	+0.7, +1.0	6.7	2.3	4.8	3.1	1.8	4.9	0.9	0.5	0.5	2.6	0.7	0.1	0.0	0.9	0.2	10.9
79	66, 80	0.2, 0.4	−1.0, −0.7	2.7	1.3	0.5	0.7	0.5	1.6	1.5	1.1	0.6	3.7	1.2	0.1	0.0	0.3	0.2	5.6
80	66, 80	0.2, 0.4	−0.7, −0.4	1.3	0.6	0.4	0.3	0.3	0.3	0.4	0.4	0.3	1.7	0.4	0.1	0.0	0.0	0.0	2.5
81	66, 80	0.2, 0.4	−0.4, 0.0	1.3	0.4	0.4	0.3	0.3	0.1	0.3	0.1	0.1	0.7	0.2	0.0	0.0	0.0	0.0	1.6
82	66, 80	0.2, 0.4	0.0, +0.4	1.2	0.5	0.3	0.4	0.3	0.1	0.3	0.1	0.1	0.7	0.2	0.1	0.0	0.0	0.0	1.7
83	66, 80	0.2, 0.4	+0.4, +0.7	1.4	0.6	0.3	0.3	0.3	0.3	0.6	0.2	0.3	1.7	0.4	0.1	0.0	0.1	0.0	2.6
84	66, 80	0.2, 0.4	+0.7, +1.0	2.7	1.4	0.4	0.7	0.4	1.6	2.8	1.0	0.6	3.8	1.2	0.2	0.0	0.3	0.1	6.1
157	80, 91	0.4, 0.6	−1.0, −0.7	0.6	0.3	0.0	0.1	0.0	0.1	1.4	0.3	0.3	3.2	0.4	0.1	0.0	0.0	0.1	3.6
158	80, 91	0.4, 0.6	−0.7, −0.4	0.4	0.2	0.0	0.0	0.0	0.0	1.0	0.1	0.1	0.5	0.2	0.1	0.0	0.1	0.0	1.2
159	80, 91	0.4, 0.6	−0.4, 0.0	0.4	0.1	0.0	0.0	0.0	0.0	1.0	0.1	0.0	0.3	0.1	0.1	0.0	0.0	0.0	1.1
160	80, 91	0.4, 0.6	0.0, +0.4	0.4	0.1	0.0	0.0	0.0	0.0	1.0	0.0	0.0	0.3	0.1	0.1	0.0	0.0	0.0	1.2
161	80, 91	0.4, 0.6	+0.4, +0.7	0.4	0.2	0.0	0.0	0.0	0.0	1.0	0.1	0.1	0.5	0.2	0.1	0.0	0.1	0.0	1.2
162	80, 91	0.4, 0.6	+0.7, +1.0	0.6	0.3	0.0	0.0	0.0	0.1	1.6	0.2	0.3	3.2	0.4	0.1	0.0	0.0	0.1	3.7
235	91, 102	0.6, 0.8	−1.0, −0.7	0.5	0.2	0.0	0.1	0.0	0.0	2.1	0.2	0.3	2.6	0.5	0.0	0.0	0.2	0.0	3.5
236	91, 102	0.6, 0.8	−0.7, −0.4	0.4	0.2	0.0	0.0	0.0	0.0	1.3	0.0	0.1	0.5	0.2	0.0	0.0	0.1	0.0	1.5
237	91, 102	0.6, 0.8	−0.4, 0.0	0.4	0.1	0.0	0.0	0.0	0.0	1.0	0.1	0.0	0.2	0.1	0.0	0.0	0.0	0.0	1.1
238	91, 102	0.6, 0.8	0.0, +0.4	0.3	0.1	0.0	0.0	0.0	0.0	1.0	0.0	0.0	0.2	0.1	0.0	0.0	0.0	0.0	1.1
239	91, 102	0.6, 0.8	+0.4, +0.7	0.4	0.2	0.0	0.0	0.0	0.0	1.2	0.0	0.1	0.5	0.2	0.0	0.0	0.1	0.0	1.4
240	91, 102	0.6, 0.8	+0.7, +1.0	0.5	0.2	0.0	0.1	0.0	0.1	2.1	0.1	0.3	2.6	0.5	0.0	0.0	0.2	0.0	3.4
313	102, 116	0.8, 1.0	−1.0, −0.7	2.8	1.2	0.6	0.8	0.5	0.7	2.1	0.9	0.2	1.4	0.3	0.1	0.0	0.1	0.0	4.3
314	102, 116	0.8, 1.0	−0.7, −0.4	2.6	1.2	0.2	0.5	0.2	0.9	2.3	1.0	0.0	0.4	0.2	0.0	0.0	0.1	0.1	4.0
315	102, 116	0.8, 1.0	−0.4, 0.0	2.0	0.8	1.6	0.3	0.2	0.2	1.0	0.3	0.1	0.3	0.1	0.1	0.0	0.0	0.0	2.9
316	102, 116	0.8, 1.0	0.0, +0.4	1.8	0.7	0.1	0.2	0.2	0.1	0.9	0.5	0.1	0.3	0.1	0.0	0.0	0.1	0.1	2.2
317	102, 116	0.8, 1.0	+0.4, +0.7	2.3	1.0	0.5	0.4	0.2	0.7	1.7	1.3	0.0	0.4	0.2	0.1	0.0	0.0	0.1	3.5
318	102, 116	0.8, 1.0	+0.7, +1.0	2.3	1.0	0.2	0.6	0.3	0.6	2.1	0.6	0.2	1.4	0.3	0.0	0.0	0.0	0.1	3.8
391	116, 150	1.0, 1.2	−1.0, −0.7	4.8	1.0	2.8	1.8	1.3	5.1	0.2	0.4	0.1	0.4	0.2	0.1	0.0	0.0	0.1	8.0
392	116, 150	1.0, 1.2	−0.7, −0.4	3.5	0.9	0.4	0.7	0.7	0.6	0.6	0.1	0.1	0.3	0.2	0.1	0.0	0.2	0.1	3.9
393	116, 150	1.0, 1.2	−0.4, 0.0	3.1	0.8	1.3	0.4	0.5	0.8	0.6	0.1	0.1	0.4	0.2	0.1	0.0	0.0	0.2	3.7
394	116, 150	1.0, 1.2	0.0, +0.4	3.0	0.8	0.6	0.5	0.4	0.9	0.6	0.2	0.1	0.4	0.2	0.1	0.0	0.1	0.0	3.5
395	116, 150	1.0, 1.2	+0.4, +0.7	2.8	0.7	0.5	0.5	0.5	0.4	0.6	0.4	0.1	0.3	0.2	0.1	0.0	0.1	0.1	3.2
396	116, 150	1.0, 1.2	+0.7, +1.0	3.7	0.8	2.2	1.1	0.8	3.4	0.4	0.2	0.1	0.4	0.2	0.1	0.0	0.0	0.1	5.7
469	150, 200	1.2, 1.4	−1.0, −0.7	11.9	1.4	2.0	3.6	2.2	1.5	0.4	0.3	0.1	0.5	0.3	0.1	0.0	0.0	0.2	12.9
470	150, 200	1.2, 1.4	−0.7, −0.4	6.6	0.8	1.0	5.9	1.6	0.9	0.9	0.2	0.1	0.5	0.3	0.1	0.0	0.0	0.1	9.2
471	150, 200	1.2, 1.4	−0.4, 0.0	6.6	1.0	3.1	1.9	1.0	0.4	1.0	0.1	0.2	0.6	0.3	0.2	0.0	0.0	0.1	7.8
472	150, 200	1.2, 1.4	0.0, +0.4	5.3	0.9	0.8	0.9	0.6	0.2	0.6	0.2	0.2	0.6	0.3	0.2	0.0	0.1	0.0	5.6
473	150, 200	1.2, 1.4	+0.4, +0.7	4.4	0.6	0.5	1.9	0.7	0.4	0.9	0.2	0.1	0.5	0.3	0.1	0.0	0.0	0.0	5.0
474	150, 200	1.2, 1.4	+0.7, +1.0	7.6	0.9	1.1	2.3	1.1	0.7	0.3	0.2	0.1	0.5	0.3	0.2	0.0	0.0	0.1	8.3

Table 2. Central rapidity electron channel uncertainties in selected bins. All uncertainties quoted are in units of percent, relative to the measured differential cross section. The uncertainties are separated into those which are bin-to-bin correlated within a single channel (marked "cor") and those which are uncorrelated (marked "unc"). The sources are the uncertainties arising from the data sample size ($\delta^{\rm stat}_{\rm unc}$); the signal MC sample size ($\delta^{\rm sig}_{\rm unc}$); the sizes of the background MC samples ($\delta^{\rm bkg}_{\rm unc}$); the statistical component of the multijet estimation ($\delta^{\rm mj}_{\rm unc}$); the combined correlated (normalisation) component of all background MC samples ($\delta^{\rm bkg}_{\rm cor}$); the multijet estimation ($\delta^{\rm mj}_{\rm cor}$); the electron energy scale ($\delta^{\rm scl}_{\rm cor}$) and resolution ($\delta^{\rm res}_{\rm cor}$); the reconstruction ($\delta^{\rm rec}_{\rm cor}$), identification ($\delta^{\rm id}_{\rm cor}$), and trigger efficiencies ($\delta^{\rm trig}_{\rm cor}$); the electron charge misidentification ($\delta^{\rm qmid}_{\rm cor}$); the K-factors ($\delta^{\rm kfac}_{\rm cor}$); the Z boson $p_{\rm T}$ modelling ($\delta^{\rm zpt}_{\rm cor}$); the PDF variation ($\delta^{\rm pdf}_{\rm cor}$); and the total measurement uncertainty ($\delta^{\rm tot}$). The luminosity uncertainty is not included in these tables.

JHEP12(2017)059

Bin	m_{ee} [GeV]	$\lvert y_{ee}\rvert$	$\cos\theta^*$	$\delta^{\text{stat}}_{\text{unc}}$ [%]	$\delta^{\text{sig}}_{\text{unc}}$ [%]	$\delta^{\text{bkg}}_{\text{unc}}$ [%]	$\delta^{\text{mj}}_{\text{unc}}$ [%]	$\delta^{\text{bkg}}_{\text{cor}}$ [%]	$\delta^{\text{mj}}_{\text{cor}}$ [%]	$\delta^{\text{scl}}_{\text{cor}}$ [%]	$\delta^{\text{res}}_{\text{cor}}$ [%]	$\delta^{\text{fscl}}_{\text{cor}}$ [%]	$\delta^{\text{fres}}_{\text{cor}}$ [%]	$\delta^{\text{rec}}_{\text{cor}}$ [%]	$\delta^{\text{id}}_{\text{cor}}$ [%]	$\delta^{\text{trig}}_{\text{cor}}$ [%]	$\delta^{\text{iso}}_{\text{cor}}$ [%]	$\delta^{\text{fid}}_{\text{cor}}$ [%]	$\delta^{\text{qmid}}_{\text{cor}}$ [%]	$\delta^{\text{kfac}}_{\text{cor}}$ [%]	$\delta^{\text{zpt}}_{\text{cor}}$ [%]	$\delta^{\text{pdf}}_{\text{cor}}$ [%]	δ^{tot} [%]
1	66, 80	1.2, 1.6	−1.0, −0.7	6.4	3.0	6.0	4.5	0.9	11.5	0.4	0.6	3.1	2.1	0.2	0.8	0.3	0.0	0.7	0.0	0.0	0.8	0.6	16.0
2	66, 80	1.2, 1.6	−0.7, −0.4	16.4	8.7	8.0	9.9	0.5	11.4	0.5	1.2	5.8	2.5	0.1	0.2	0.1	0.0	0.8	0.0	0.0	0.8	0.3	26.0
3	66, 80	1.2, 1.6	−0.4, 0.0	—	—	—	—	—	—	—	—	—	—	—	—	—	—	—	—	—	—	—	—
4	66, 80	1.2, 1.6	0.0, +0.4	—	—	—	—	—	—	—	—	—	—	—	—	—	—	—	—	—	—	—	—
5	66, 80	1.2, 1.6	+0.4, +0.7	15.7	8.0	6.7	7.9	0.5	10.7	0.9	0.8	3.8	5.5	0.1	0.1	0.1	0.0	0.8	0.0	0.0	1.6	1.4	24.1
6	66, 80	1.2, 1.6	+0.7, +1.0	7.9	3.3	8.8	5.8	1.6	15.3	0.7	0.7	2.3	2.9	0.2	0.8	0.3	0.0	0.7	0.0	0.0	0.9	0.3	20.9
19	66, 80	2.4, 2.8	−1.0, −0.7	3.4	2.2	1.4	2.8	0.3	3.4	2.5	0.7	4.3	5.2	0.2	1.6	0.4	0.1	1.4	0.0	0.0	2.4	0.2	10.1
20	66, 80	2.4, 2.8	−0.7, −0.4	2.2	1.3	0.8	1.6	0.3	1.1	1.2	0.6	3.1	3.9	0.1	0.8	0.2	0.0	1.3	0.0	0.0	0.5	0.1	6.4
21	66, 80	2.4, 2.8	−0.4, 0.0	2.3	1.0	0.8	1.4	0.2	1.5	0.4	0.2	0.9	0.3	0.1	0.5	0.2	0.0	0.8	0.0	0.0	0.1	0.0	3.6
22	66, 80	2.4, 2.8	0.0, +0.4	2.8	1.2	1.5	1.9	0.4	2.0	0.4	0.5	1.3	0.3	0.1	0.5	0.2	0.0	0.7	0.0	0.0	0.3	0.1	4.7
23	66, 80	2.4, 2.8	+0.4, +0.7	2.7	1.6	1.3	2.3	0.4	1.7	1.6	0.2	4.0	6.0	0.1	0.8	0.2	0.0	1.4	0.1	0.0	1.1	0.2	8.8
24	66, 80	2.4, 2.8	+0.7, +1.0	4.2	2.7	3.4	3.7	0.7	5.5	2.8	0.9	4.9	6.5	0.2	1.6	0.4	0.1	1.4	0.0	0.0	3.6	0.3	13.2
73	91, 102	2.0, 2.4	−1.0, −0.7	0.9	0.6	0.2	0.3	0.0	0.8	0.8	0.1	1.9	0.1	0.2	0.8	0.2	0.0	1.2	0.0	0.0	0.8	0.1	2.9
74	91, 102	2.0, 2.4	−0.7, −0.4	0.5	0.3	0.0	0.2	0.0	0.7	0.9	0.1	1.5	0.2	0.0	0.4	0.1	0.0	0.8	0.0	0.0	0.1	0.1	2.1
75	91, 102	2.0, 2.4	−0.4, 0.0	0.7	0.3	0.1	0.4	0.0	0.6	0.6	0.1	1.7	0.1	0.0	0.2	0.1	0.0	0.7	0.0	0.0	0.1	0.0	2.2
76	91, 102	2.0, 2.4	0.0, +0.4	0.6	0.3	0.1	0.4	0.0	0.5	0.5	0.1	1.5	0.1	0.0	0.2	0.1	0.0	0.7	0.0	0.0	0.1	0.1	2.0
77	91, 102	2.0, 2.4	+0.4, +0.7	0.5	0.3	0.1	0.1	0.0	0.5	0.9	0.2	1.3	0.3	0.0	0.4	0.1	0.0	0.8	0.0	0.0	0.2	0.1	2.0
78	91, 102	2.0, 2.4	+0.7, +1.0	0.9	0.5	0.2	0.3	0.0	0.3	0.7	0.2	1.6	0.2	0.2	0.7	0.2	0.0	1.2	0.0	0.0	0.8	0.0	2.6
97	102, 116	1.6, 2.0	−1.0, −0.7	3.8	1.8	2.0	2.9	0.7	4.2	0.6	0.3	2.4	2.2	0.1	0.3	0.1	0.0	0.8	0.0	0.0	1.5	0.1	7.9
98	102, 116	1.6, 2.0	−0.7, −0.4	4.4	2.1	2.0	3.4	0.3	3.6	1.2	0.6	2.1	1.2	0.0	0.2	0.0	0.0	0.7	0.0	0.0	1.5	0.2	8.0
99	102, 116	1.6, 2.0	−0.4, 0.0	—	—	—	—	—	—	—	—	—	—	—	—	—	—	—	—	—	—	—	—
100	102, 116	1.6, 2.0	0.0, +0.4	—	—	—	—	—	—	—	—	—	—	—	—	—	—	—	—	—	—	—	—
101	102, 116	1.6, 2.0	+0.4, +0.7	3.3	1.5	1.6	2.1	0.2	2.2	1.0	0.7	1.7	1.0	0.0	0.2	0.0	0.0	0.7	0.0	0.0	1.1	0.1	5.6
102	102, 116	1.6, 2.0	+0.7, +1.0	2.6	1.4	1.3	1.5	0.3	1.9	0.3	0.1	2.1	1.0	0.1	0.3	0.1	0.0	0.8	0.0	0.0	0.9	0.2	4.9
109	102, 116	2.4, 2.8	−1.0, −0.7	3.7	2.2	2.3	3.4	0.8	6.2	3.3	1.2	6.7	6.6	0.1	0.6	0.1	0.0	1.4	0.0	0.0	3.3	0.3	13.7
110	102, 116	2.4, 2.8	−0.7, −0.4	4.2	2.3	1.0	3.7	0.3	3.3	1.4	1.2	5.5	4.2	0.0	0.2	0.1	0.0	1.2	0.0	0.0	2.0	0.2	10.2
111	102, 116	2.4, 2.8	−0.4, 0.0	3.9	1.9	1.5	4.5	0.2	4.6	0.7	0.9	2.3	1.2	0.1	0.3	0.2	0.0	0.7	0.0	0.0	0.9	0.2	8.5
112	102, 116	2.4, 2.8	0.0, +0.4	3.1	1.5	0.7	2.9	0.1	3.2	0.6	0.4	2.3	1.3	0.1	0.3	0.1	0.0	0.8	0.0	0.0	0.9	0.1	6.3
113	102, 116	2.4, 2.8	+0.4, +0.7	2.7	1.6	1.1	1.7	0.2	1.6	1.2	0.8	4.0	2.1	0.0	0.2	0.1	0.0	1.2	0.0	0.0	1.4	0.2	6.5
114	102, 116	2.4, 2.8	+0.7, +1.0	2.2	1.4	1.3	1.5	0.3	2.4	2.0	0.8	3.3	3.2	0.1	0.6	0.1	0.0	1.3	0.0	0.0	2.2	0.1	7.0
127	116, 150	1.6, 2.0	−1.0, −0.7	8.4	1.7	8.7	7.1	2.9	29.0	0.2	0.4	1.8	1.2	0.0	0.1	0.0	0.0	0.6	0.0	0.0	0.7	0.2	32.5
128	116, 150	1.6, 2.0	−0.7, −0.4	7.6	2.0	4.2	9.0	1.3	8.6	0.6	0.2	0.3	0.5	0.0	0.1	0.0	0.0	0.6	0.0	0.0	0.5	0.2	15.4
129	116, 150	1.6, 2.0	−0.4, 0.0	—	—	—	—	—	—	—	—	—	—	—	—	—	—	—	—	—	—	—	—
130	116, 150	1.6, 2.0	0.0, +0.4	—	—	—	—	—	—	—	—	—	—	—	—	—	—	—	—	—	—	—	—
131	116, 150	1.6, 2.0	+0.4, +0.7	4.4	1.2	3.1	3.8	0.5	3.1	0.2	0.1	0.3	0.2	0.0	0.1	0.0	0.0	0.6	0.0	0.0	0.3	0.1	7.4
132	116, 150	1.6, 2.0	+0.7, +1.0	3.9	0.9	5.5	2.5	1.2	9.8	0.2	0.1	0.9	0.2	0.0	0.1	0.0	0.0	0.7	0.0	0.0	0.5	0.1	12.3
139	116, 150	2.4, 2.8	−1.0, −0.7	16.3	2.9	11.4	14.0	5.4	29.3	1.3	0.5	5.4	1.7	0.1	0.3	0.1	0.0	1.1	0.1	0.0	1.3	0.3	39.1
140	116, 150	2.4, 2.8	−0.7, −0.4	7.5	3.0	7.5	7.3	1.2	10.7	0.2	0.2	1.2	1.4	0.0	0.2	0.1	0.0	0.9	0.0	0.0	1.6	0.3	17.2
141	116, 150	2.4, 2.8	−0.4, 0.0	6.0	1.7	3.8	5.6	0.5	6.8	0.2	0.1	1.8	0.5	0.1	0.4	0.1	0.0	0.6	0.1	0.0	0.9	0.1	11.6
142	116, 150	2.4, 2.8	0.0, +0.4	4.5	1.4	3.1	3.2	0.5	3.4	0.1	0.5	0.8	0.2	0.1	0.4	0.1	0.0	0.6	0.0	0.0	0.5	0.1	7.4
143	116, 150	2.4, 2.8	+0.4, +0.7	3.8	1.4	2.4	2.4	0.4	3.3	0.3	0.3	0.9	0.7	0.0	0.2	0.1	0.0	1.0	0.0	0.0	0.9	0.1	6.5
144	116, 150	2.4, 2.8	+0.7, +1.0	3.3	1.0	1.7	2.0	0.7	3.8	0.7	0.2	1.8	0.6	0.1	0.3	0.1	0.0	1.1	0.0	0.0	0.2	0.1	6.3

Table 3. High rapidity electron channel uncertainties in selected bins. All uncertainties quoted are in units of percent, relative to the measured differential cross section. Bins with blank entries ("−") are those that have been omitted from the measurement due to a lack of expected events. The uncertainties are separated into those which are bin-to-bin correlated within a single channel (marked "cor") and those which are uncorrelated (marked "unc"). The sources are the uncertainties arising from the data sample size ($\delta^{\text{stat}}_{\text{unc}}$); the signal MC sample size ($\delta^{\text{sig}}_{\text{unc}}$); the sizes of the background MC samples ($\delta^{\text{bkg}}_{\text{unc}}$); the statistical component of the multijet estimation ($\delta^{\text{mj}}_{\text{unc}}$); the combined correlated (normalisation) component of all background MC samples ($\delta^{\text{bkg}}_{\text{cor}}$); the multijet estimation ($\delta^{\text{mj}}_{\text{cor}}$); the electron energy scale ($\delta^{\text{scl}}_{\text{cor}}$) and resolution ($\delta^{\text{res}}_{\text{cor}}$); the forward electron energy scale ($\delta^{\text{fscl}}_{\text{cor}}$) and resolution ($\delta^{\text{fres}}_{\text{cor}}$); the reconstruction ($\delta^{\text{rec}}_{\text{cor}}$), identification ($\delta^{\text{id}}_{\text{cor}}$), trigger ($\delta^{\text{trig}}_{\text{cor}}$), isolation ($\delta^{\text{iso}}_{\text{cor}}$), and forward identification efficiencies ($\delta^{\text{fid}}_{\text{cor}}$); the electron charge misidentification ($\delta^{\text{qmid}}_{\text{cor}}$); the K-factors ($\delta^{\text{kfac}}_{\text{cor}}$); the Z boson p_{T} modelling ($\delta^{\text{zpt}}_{\text{cor}}$); the PDF variation ($\delta^{\text{pdf}}_{\text{cor}}$); and the total measurement uncertainty (δ^{tot}). The luminosity uncertainty is not included in these tables.

JHEP12(2017)059

Bin	$m_{\mu\mu}$ [GeV]	$\lvert y_{\mu\mu}\rvert$	$\cos\theta^*$	$\delta^{\text{stat}}_{\text{unc}}$ [%]	$\delta^{\text{sig}}_{\text{unc}}$ [%]	$\delta^{\text{bkg}}_{\text{unc}}$ [%]	$\delta^{\text{bkg}}_{\text{cor}}$ [%]	$\delta^{\text{mj}}_{\text{cor}}$ [%]	$\delta^{\text{scl}}_{\text{cor}}$ [%]	$\delta^{\text{sag}}_{\text{cor}}$ [%]	$\delta^{\text{res}}_{\text{cor}}$ [%]	$\delta^{\text{rec}}_{\text{cor}}$ [%]	$\delta^{\text{id}}_{\text{cor}}$ [%]	$\delta^{\text{trig}}_{\text{cor}}$ [%]	$\delta^{\text{kfac}}_{\text{cor}}$ [%]	$\delta^{\text{zpt}}_{\text{cor}}$ [%]	$\delta^{\text{pdf}}_{\text{cor}}$ [%]	δ^{tot} [%]
1	46, 66	0.0, 0.2	−1.0, −0.7	5.4	2.0	2.1	1.5	0.5	0.2	0.5	0.6	0.3	0.3	0.7	0.0	0.5	0.3	6.6
2	46, 66	0.0, 0.2	−0.7, −0.4	1.8	0.7	1.1	1.2	0.0	0.0	0.1	0.1	0.2	0.2	0.5	0.2	0.3	0.2	2.7
3	46, 66	0.0, 0.2	−0.4, 0.0	1.5	0.6	0.8	0.9	0.5	0.0	0.1	0.0	0.5	0.4	0.0	0.2	0.4	0.2	2.3
4	46, 66	0.0, 0.2	0.0, +0.4	1.5	0.6	0.9	0.9	0.5	0.0	0.1	0.1	0.5	0.4	0.0	0.2	0.5	0.2	2.3
5	46, 66	0.0, 0.2	+0.4, +0.7	1.9	0.6	1.2	1.2	0.0	0.1	0.1	0.4	0.2	0.2	0.5	0.2	0.3	0.2	2.8
6	46, 66	0.0, 0.2	+0.7, +1.0	5.7	2.0	3.6	1.8	0.5	0.1	1.0	0.1	0.3	0.3	0.8	0.2	0.6	0.8	7.7
79	66, 80	0.2, 0.4	−1.0, −0.7	2.3	1.1	0.5	0.6	0.7	0.1	0.7	0.4	0.2	0.2	0.3	0.0	0.0	0.1	3.0
80	66, 80	0.2, 0.4	−0.7, −0.4	1.3	0.7	0.3	0.4	0.1	0.1	0.2	0.1	0.3	0.3	0.0	0.0	0.0	0.1	1.7
81	66, 80	0.2, 0.4	−0.4, 0.0	1.4	0.7	0.4	0.3	0.2	0.1	0.2	0.2	0.4	0.4	0.0	0.1	0.1	0.3	1.8
82	66, 80	0.2, 0.4	0.0, +0.4	1.4	0.7	0.3	0.3	0.2	0.1	0.1	0.2	0.4	0.4	0.1	0.1	0.1	0.2	1.8
83	66, 80	0.2, 0.4	+0.4, +0.7	1.4	0.7	0.4	0.4	0.1	0.1	0.2	0.2	0.3	0.3	0.0	0.1	0.1	0.1	1.8
84	66, 80	0.2, 0.4	+0.7, +1.0	2.2	1.1	0.4	0.6	0.8	0.2	0.7	0.1	0.2	0.2	0.3	0.0	0.0	0.3	3.0
157	80, 91	0.4, 0.6	−1.0, −0.7	0.4	0.2	0.0	0.0	0.0	0.1	1.0	0.1	0.3	0.3	0.0	0.0	0.0	0.1	1.4
158	80, 91	0.4, 0.6	−0.7, −0.4	0.4	0.2	0.0	0.0	0.0	0.2	0.6	0.1	0.4	0.4	0.1	0.0	0.0	0.0	1.1
159	80, 91	0.4, 0.6	−0.4, 0.0	0.3	0.1	0.0	0.0	0.0	0.2	0.3	0.1	0.3	0.3	0.0	0.0	0.0	0.0	0.9
160	80, 91	0.4, 0.6	0.0, +0.4	0.3	0.1	0.0	0.0	0.0	0.2	0.3	0.1	0.3	0.3	0.0	0.0	0.0	0.0	0.9
161	80, 91	0.4, 0.6	+0.4, +0.7	0.4	0.2	0.0	0.0	0.0	0.2	0.6	0.0	0.4	0.4	0.1	0.0	0.0	0.0	1.1
162	80, 91	0.4, 0.6	+0.7, +1.0	0.4	0.2	0.0	0.0	0.0	0.2	1.1	0.1	0.3	0.3	0.1	0.0	0.1	0.0	1.4
235	91, 102	0.6, 0.8	−1.0, −0.7	0.4	0.2	0.0	0.0	0.0	0.1	0.5	0.0	0.3	0.3	0.1	0.0	0.1	0.0	1.0
236	91, 102	0.6, 0.8	−0.7, −0.4	0.3	0.2	0.0	0.0	0.0	0.1	1.0	0.0	0.4	0.4	0.2	0.0	0.0	0.0	1.3
237	91, 102	0.6, 0.8	−0.4, 0.0	0.3	0.1	0.0	0.0	0.0	0.1	0.3	0.0	0.2	0.2	0.0	0.0	0.0	0.0	0.8
238	91, 102	0.6, 0.8	0.0, +0.4	0.3	0.1	0.0	0.0	0.0	0.2	0.3	0.0	0.3	0.2	0.0	0.0	0.0	0.0	0.8
239	91, 102	0.6, 0.8	+0.4, +0.7	0.3	0.2	0.0	0.0	0.0	0.2	1.0	0.0	0.4	0.4	0.1	0.0	0.0	0.0	1.3
240	91, 102	0.6, 0.8	+0.7, +1.0	0.4	0.2	0.0	0.0	0.0	0.1	0.5	0.0	0.3	0.3	0.1	0.0	0.1	0.1	1.0
313	102, 116	0.8, 1.0	−1.0, −0.7	2.1	1.0	0.1	0.4	0.0	0.2	0.9	1.4	0.4	0.4	0.2	0.0	0.0	0.1	3.0
314	102, 116	0.8, 1.0	−0.7, −0.4	1.8	0.8	0.0	0.2	0.1	0.2	1.8	0.3	0.3	0.3	0.2	0.0	0.0	0.0	2.8
315	102, 116	0.8, 1.0	−0.4, 0.0	1.7	0.7	0.0	0.1	0.0	0.1	0.4	0.6	0.3	0.3	0.1	0.0	0.0	0.0	2.0
316	102, 116	0.8, 1.0	0.0, +0.4	1.6	0.6	0.0	0.1	0.0	0.2	0.4	0.5	0.3	0.3	0.0	0.0	0.0	0.0	2.0
317	102, 116	0.8, 1.0	+0.4, +0.7	1.6	0.7	0.0	0.2	0.1	0.2	2.0	0.8	0.4	0.3	0.1	0.0	0.0	0.1	2.8
318	102, 116	0.8, 1.0	+0.7, +1.0	2.0	0.9	0.1	0.3	0.0	0.2	0.8	1.5	0.4	0.4	0.0	0.0	0.0	0.0	2.7
391	116, 150	1.0, 1.2	−1.0, −0.7	4.1	1.2	0.3	1.3	0.0	0.1	0.5	0.3	0.5	0.5	0.2	0.1	0.0	0.1	4.8
392	116, 150	1.0, 1.2	−0.7, −0.4	2.9	0.7	0.2	0.7	0.1	0.1	0.7	0.4	0.4	0.3	0.2	0.0	0.1	0.1	3.4
393	116, 150	1.0, 1.2	−0.4, 0.0	2.5	0.6	0.1	0.5	0.1	0.1	0.5	0.1	0.3	0.3	0.2	0.0	0.1	0.1	2.8
394	116, 150	1.0, 1.2	0.0, +0.4	2.2	0.6	0.1	0.4	0.0	0.0	0.5	0.0	0.3	0.3	0.1	0.0	0.1	0.1	2.5
395	116, 150	1.0, 1.2	+0.4, +0.7	2.3	0.6	0.2	0.5	0.0	0.0	0.4	0.3	0.3	0.3	0.0	0.0	0.1	0.0	2.6
396	116, 150	1.0, 1.2	+0.7, +1.0	3.2	0.9	0.3	0.7	0.1	0.1	0.8	0.1	0.5	0.5	0.0	0.0	0.0	0.1	3.8
469	150, 200	1.2, 1.4	−1.0, −0.7	11.1	1.5	1.2	2.9	0.1	0.3	2.7	0.5	0.7	0.5	0.2	0.1	0.0	0.1	13.6
470	150, 200	1.2, 1.4	−0.7, −0.4	5.6	0.8	0.5	1.4	0.0	0.1	1.3	0.1	0.5	0.4	0.2	0.0	0.0	0.1	6.2
471	150, 200	1.2, 1.4	−0.4, 0.0	4.6	0.6	0.3	0.9	0.1	0.0	1.0	0.2	0.4	0.4	0.2	0.0	0.0	0.1	5.1
472	150, 200	1.2, 1.4	0.0, +0.4	4.1	0.5	0.2	0.7	0.1	0.0	1.1	0.0	0.4	0.4	0.1	0.0	0.0	0.0	4.5
473	150, 200	1.2, 1.4	+0.4, +0.7	4.0	0.5	0.2	0.8	0.0	0.1	0.8	0.2	0.4	0.4	0.0	0.0	0.0	0.1	4.3
474	150, 200	1.2, 1.4	+0.7, +1.0	6.6	0.9	0.5	1.2	0.1	0.0	1.7	0.0	0.6	0.5	0.0	0.0	0.1	0.1	8.0

Table 4. Central rapidity muon channel uncertainties in selected bins. All uncertainties quoted are in units of percent, relative to the measured differential cross section. The uncertainties are separated into those which are bin-to-bin correlated within a single channel (marked "cor") and those which are uncorrelated (marked "unc"). The sources are the uncertainties arising from the data sample size ($\delta^{\text{stat}}_{\text{unc}}$); the signal MC sample size ($\delta^{\text{sig}}_{\text{unc}}$); the sizes of the background MC samples ($\delta^{\text{bkg}}_{\text{unc}}$); the combined correlated (normalisation) component of all background MC samples ($\delta^{\text{bkg}}_{\text{cor}}$); the multijet estimation ($\delta^{\text{mj}}_{\text{cor}}$); the muon momentum scale ($\delta^{\text{scl}}_{\text{cor}}$); the sagitta bias corrections ($\delta^{\text{sag}}_{\text{cor}}$); the muon momentum resolution ($\delta^{\text{res}}_{\text{cor}}$); the reconstruction ($\delta^{\text{rec}}_{\text{cor}}$), identification ($\delta^{\text{id}}_{\text{cor}}$), and trigger efficiencies ($\delta^{\text{trig}}_{\text{cor}}$); the K-factors ($\delta^{\text{kfac}}_{\text{cor}}$); the Z boson p_{T} modelling ($\delta^{\text{zpt}}_{\text{cor}}$); the PDF variation ($\delta^{\text{pdf}}_{\text{cor}}$); and the total measurement uncertainty (δ^{tot}). The luminosity uncertainty is not included in these tables.

JHEP12(2017)059

8 Results

In the two invariant mass bins in the region $80 < m_{\ell\ell} < 102\,\text{GeV}$, the measurement of $\mathrm{d}^3\sigma$ in the central electron channel achieves a total uncertainty (excluding the luminosity contribution) of 1–2% per bin. In the muon channel the precision is better than 1%. In both cases the measurement precision is dominated by the experimental systematic uncertainties, compared to a data statistical uncertainty of about 0.5% per bin in this high-precision region. In the high rapidity electron channel, the precision of the measurement reaches 2–3% per bin, of which the statistical uncertainty is about 0.5%.

The data tables provided in this paper contain compact summaries of the measurement uncertainties; however, complete tables with the full breakdown of all systematic uncertainties and their correlated components are provided in HEPData [71, 72]. These complete tables also include the correction factors used to translate the unfolded measurements from the dressed-level to the Born-level as discussed in section 6.

8.1 Combination of the central rapidity electron and muon channels

The central rapidity electron and muon measurement channels are defined with a common fiducial region given in section 6 and therefore are combined to further reduce the experimental uncertainties. A χ^2-minimisation technique is used to combine the cross sections [73–75]. This method introduces a nuisance parameter for each systematic error source which contributes to the total χ^2. The sources of uncertainty considered are discussed in section 7. Correlated sources of uncertainty which are propagated with the pseudo-experiment or bootstrap resampling methods can be represented in covariance matrix form for each source. The covariance matrices are decomposed into eigenvector representations as input to the χ^2-minimisation function. For each covariance matrix the eigenvectors are sorted by the magnitude of their corresponding eigenvalues. The largest of the eigenvalues are added in order of decreasing value until their sum exceeds a certain fraction of the sum of all eigenvalues, f_{eig}. At which point the correlation information for the eigenvectors whose eigenvalues were not included in the sum is ignored and the eigenvectors are added in quadrature to form a diagonal uncorrelated uncertainty matrix. The resulting numbers of nuisance parameters depends on the complexity of the correlation pattern and on f_{eig}, for which values between 99% and 20% are chosen depending on the source.

This method of decomposition can accurately describe the full covariance matrix, and simultaneously reduce the number of nuisance parameters. The method preserves the total uncertainty and marginally enhances the uncorrelated component of the uncertainty by construction. The original and decomposed covariance matrices are compared and found to agree well such that the combined results are found to be stable in terms of χ^2 and the central values and their uncertainties when f_{eig} is varied around the chosen value in a wide range.

Bin-to-bin correlated sources of uncertainty which are also correlated between the two measurement channels share common nuisance parameters, and are listed in section 7.6. In total, 275 nuisance parameters are used in the procedure. The behaviour of the uncertainties with respect to the combined cross-section values can lead to non-Gaussian

JHEP12(2017)059

distributions of the nuisance parameters. For example, sources related to the selection efficiencies are expected to be proportional to the combined cross-section value, i.e. have multiplicative behaviour; sources related to background subtraction are expected to be independent of the combined cross section and therefore have an additive behaviour. Finally, data statistical sources are expected to be proportional to the square-root of the combined cross section, and have Poisson-like behaviour even after unfolding.

The combination of the central electron and muon channels introduces shifts and constraints to the nuisance parameters. These shifts are propagated to high rapidity electron channel measurement but only have a small impact on this channel since it is dominated by the forward calorimeter uncertainties. The combination of the electron and muon channel cross-section measurements results in a χ^2 per degree of freedom (dof) of 489/451 (p-value of 10%). The pulls of the individual channel measurements to the combined data are found to be Gaussian-distributed about zero with unit RMS. They do not indicate any trends as a function of the kinematic variables. The pulls of the nuisance parameters are similarly found to be Gaussian-distributed about zero with a somewhat larger width of 1.18. Only six nuisance parameters have shifts exceeding three standard deviations, which are sources related to the calibration of the electromagnetic calorimeter, and the source describing the normalisation of the $Z \to \tau\tau$ background MC sample. These particular sources have negligible impact on the measurement.

8.2 Compatibility tests and integrated measurements

In the following subsections, the triple-differential cross sections measured in each of the three channels are compared to one another. The compatibility of the combined data with published ATLAS DY measurements made using the same 2012 dataset is briefly discussed. Moreover, the combined triple-differential cross section is integrated to produce single- and double-differential cross sections which are then compared to theoretical predictions.

8.2.1 Compatibility of the central and high rapidity measurements

The measurements performed in the central electron and muon channels are compared with the high rapidity analysis to test for compatibility. The measurements are made in two different fiducial regions and therefore a common fiducial volume is defined within which the comparison is made. This volume is chosen to be $66 < m_{\ell\ell} < 150\,\text{GeV}$, $p_{\text{T}}^{\ell} > 20\,\text{GeV}$, and no requirement is made on the pseudorapidity of the lepton. The comparison is performed in the overlapping $|y_{\ell\ell}|$ bins of the central and high rapidity analyses.

The corresponding acceptance corrections are obtained from the Powheg simulation for each individual measurement bin. Bins with extrapolation factors smaller than 0.1 are excluded from this test, since they correspond to very restricted regions of phase space. Such regions are subject to large modelling uncertainties, in particular the uncertainty associated with modelling the Z boson transverse momentum. In each bin, the sum of the extrapolation factors for the central and high rapidity channels are found to be close to 80%, indicating that the two sets of measurements cover most of the phase space for $66 < m_{\ell\ell} < 150\,\text{GeV}$ and $p_{\text{T}}^{\ell} > 20\,\text{GeV}$. A second calculation of the extrapolation factors to the full phase space (i.e. $p_{\text{T}}^{\ell} > 0\,\text{GeV}$) has an uncertainty of 1.5%. This is assumed to be

JHEP12(2017)059

strongly anti-correlated between the factors for the central and high rapidity channels since the sum of factors is close to unity. Therefore, an additional 1% anti-correlated uncertainty in the extrapolation factors is used.

The uncertainties arising from electron efficiency corrections are taken to be uncorrelated between the central and high rapidity electron channels since they use different identification criteria and triggers. The multijet uncertainty is also taken to be uncorrelated. The χ^2/dof of the compatibility test is found to be 32/30 (p-value of 37%) for the electron channel and 39/30 (p-value of 13%) for the muon channel.

8.2.2 Compatibility with published data

The cross-section measurements in the central electron and muon channels partially overlap with published DY measurements from ATLAS using the same data set. They are differential measurements of the Z boson transverse momentum spectrum [16] and of the high-mass DY cross section for $m_{\ell\ell} > 116\,\text{GeV}$ [17]. The compatibility of the data presented here with these two published measurements has been tested in identical fiducial regions, separately for the electron and muon channels. The measurements are in good agreement with each other.

The reader is referred to [16] where the most precise measurements of integrated and p_{T}-differential Z cross sections were made in the fiducial region $p_{\text{T}}^{\ell} > 20\,\text{GeV}$ and $|\eta^{\ell}| < 2.4$.

For cross sections differential in $m_{\ell\ell}$ and $|y_{\ell\ell}|$ in the region $m_{\ell\ell} > 116\,\text{GeV}$, see the results presented in reference [17]. These measurements are given in the fiducial region of $p_{\text{T}}^{\ell} > 40, 30\,\text{GeV}$ for leading and subleading leptons, and $|\eta^{\ell}| < 2.5$. Note that the published cross sections include the $\gamma\gamma \to \ell^+\ell^-$ process.

For cross sections measured in the region $m_{\ell\ell} < 116\,\text{GeV}$ and differential in $m_{\ell\ell}$ and $|y_{\ell\ell}|$, the data presented in this paper should be used.

8.2.3 Integrated cross sections

The combined measurements are integrated over the kinematic variables $\cos\theta^*$ and $y_{\ell\ell}$ in order to determine the cross section $\text{d}\sigma/\text{d}m_{\ell\ell}$. Similarly, the integration is performed in $\cos\theta^*$ to determine the cross section $\text{d}^2\sigma/\text{d}m_{\ell\ell}\text{d}|y_{\ell\ell}|$. The integration is firstly performed for the electron and muon channels separately to allow a χ^2-test for compatibility of the two channels. The measurements are simply summed in the e and μ channels for the bins in which both electron and muon measurements are present. Statistical and uncorrelated uncertainties are added in quadrature, whereas correlated systematic uncertainties are propagated linearly. The compatibility tests return $\chi^2/\text{dof} = 12.8/7$ (p-value of 7.7%) for the one-dimensional cross section, and 103/84 (p-value of 7.4%) for the two-dimensional cross section.

The integrated cross sections $\text{d}\sigma/\text{d}m_{\ell\ell}$ and $\text{d}^2\sigma/\text{d}m_{\ell\ell}\text{d}|y_{\ell\ell}|$ are determined from the combined Born-level fiducial triple-differential cross sections. The one-dimensional result is shown in figure 5. The corresponding table of measurements is given in table 5 located in the appendix. The data shows that the combined Born-level fiducial cross section falls by three orders of magnitude in the invariant mass region from the resonant peak to 200 GeV. The data have an uncertainty of about 2%, dominated by the luminosity uncertainty of

JHEP12(2017)059

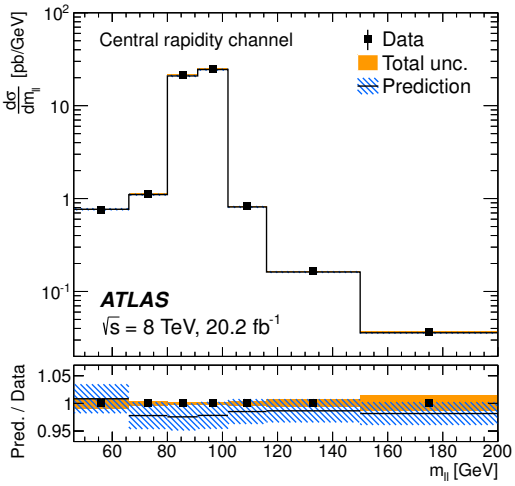

Figure 5. The combined Born-level fiducial cross section $\mathrm{d}\sigma/\mathrm{d}m_{\ell\ell}$. The data are shown as solid markers and the prediction from Powheg including NNLO QCD and NLO EW K-factors is shown as the solid line. The lower panel shows the ratio of prediction to measurement. The inner error bars represent the data statistical uncertainty and the solid band shows the total experimental uncertainty. The contribution to the uncertainty from the luminosity measurement is excluded. The hatched band represents the statistical and PDF uncertainties in the prediction.

1.9%, while uncertainties from the experimental systematic sources can be as low as 0.5% for the peak region. The statistical precision is 0.5% or better, even for the highest invariant mass bin. The fiducial measurements are well predicted by the NLO QCD and parton shower simulation from Powheg partially corrected for NNLO QCD and NLO EW effects, and scattering amplitude coefficients as described in section 3. The uncertainties in the predictions include those arising from the sample size and the PDF variations. No renormalization, factorisation and matching scale variation uncertainties are included although they can be sizeable — as large as 5% for NLO predictions. Except in the lowest mass bin, the predictions underestimate the cross section by about 1–2% (smaller than the luminosity uncertainty), as seen in the lower panel of the figure which shows the ratio of prediction to the measurement.

The two-dimensional Born-level fiducial cross section, $\mathrm{d}^2\sigma/\mathrm{d}m_{\ell\ell}\mathrm{d}|y_{\ell\ell}|$, is illustrated in figure 6 and listed in table 6 of the appendix. In each measured invariant mass bin, the shape of the rapidity distribution shows a plateau at small $|y_{\ell\ell}|$ leading to a broad shoulder followed by a cross section falling to zero at the highest accessible $|y_{\ell\ell}|$. The width of the plateau narrows with increasing $m_{\ell\ell}$. In the two high-precision Z-peak mass bins, the measured cross-section values have a total uncertainty (excluding the common luminosity uncertainty) of 0.4% for $|y_{\ell\ell}| < 1$ rising to 0.7% at $|y_{\ell\ell}| = 2.4$. At high invariant mass, the statistical and experimental uncertainty components contribute equally

JHEP12(2017)059

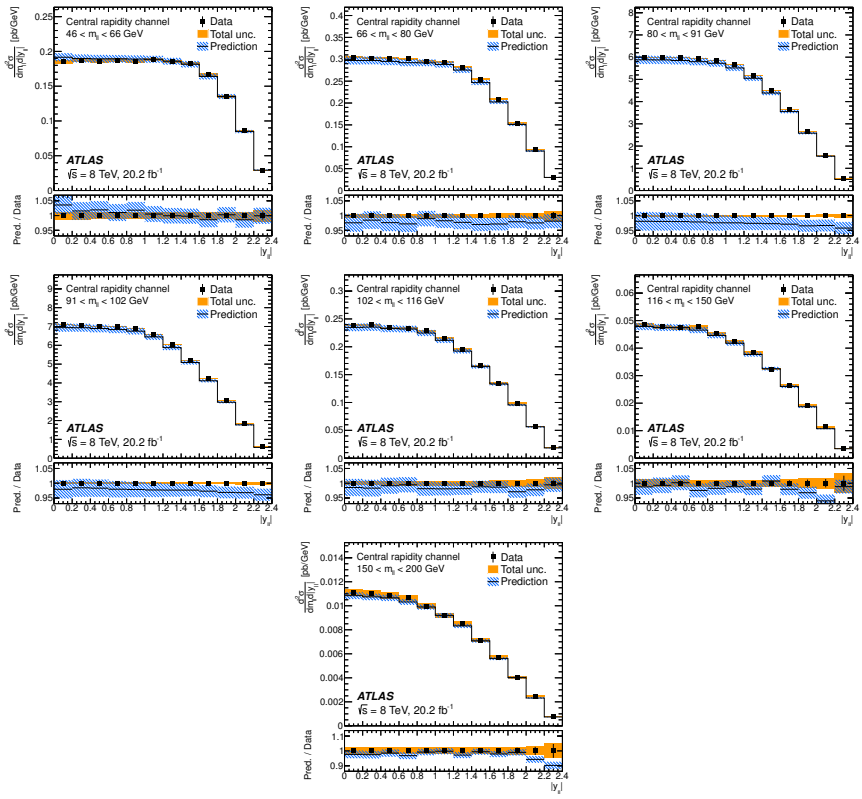

Figure 6. The combined Born-level fiducial cross section $\mathrm{d}^2\sigma/\mathrm{d}m_{\ell\ell}\mathrm{d}|y_{\ell\ell}|$ in the seven invariant mass bins of the central measurements. The data are shown as solid markers and the prediction from Powheg including NNLO QCD and NLO EW K-factors is shown as the solid line. The lower panel shows the ratio of prediction to measurement. The inner error bars represent the data statistical uncertainty and the solid band shows the total experimental uncertainty. The contribution to the uncertainty from the luminosity measurement is excluded. The hatched band represents the statistical and PDF uncertainties in the prediction.

to the total measurement precision in the plateau region, increasing from 0.5% to 1.8%. The theoretical predictions replicate the features in the data well. The lower panel of each figure shows the ratio of the prediction to the measurement. Here, in addition to overall rate difference already observed in the one-dimensional distribution, a small tendency of the data to exceed the predictions at the highest $|y_{\ell\ell}|$ can be seen in some of the mass bins.

JHEP12(2017)059

8.3 Triple-differential cross sections

The combined triple-differential Born-level cross section is shown in figures 7–10. For each invariant mass bin, the data are presented as a function of $|y_{\ell\ell}|$, with each of the six $\cos\theta^*$ regions overlaid in the main panel of the figures. The lower panels show in more detail the ratio of the prediction to the data for each $\cos\theta^*$ bin in turn. The statistical and total, excluding the contribution from the luminosity, uncertainties in the data are shown in the ratio panels.

The accessible range of the $|y_{\ell\ell}|$ distribution is largest for the region close to $\cos\theta^* \simeq 0$, and smallest at the extremes of $\cos\theta^*$. In the lowest invariant mass bin, the cross-section measurements in $\cos\theta^*$ bins with the same absolute value, e.g. bins $-1.0 < \cos\theta^* < -0.7$ and $+0.7 < \cos\theta^* < +1.0$, are consistent with each other at low $|y_{\ell\ell}| \simeq 0$, but exhibit an asymmetry which increases with $|y_{\ell\ell}|$. At large $|y_{\ell\ell}|$, the cross sections for $\cos\theta^* < 0$ are up to 35% larger than the corresponding measurements at $\cos\theta^* > 0$. In the $66 < m_{\ell\ell} < 80\,\text{GeV}$ bin, all cross sections are larger, for large $|\cos\theta^*|$ in particular, due to reduced influence of the fiducial selection on p_{T}^{ℓ}.

The next two invariant mass bins show the peak of the cross section where the asymmetry is smallest. In fact, for $80 < m_{\ell\ell} < 91\,\text{GeV}$ the difference between $\cos\theta^* > 0$ and $\cos\theta^* < 0$ is close to zero. The dramatic improvement in the overall precision of the measurements in this region is also apparent. For the $91 < m_{\ell\ell} < 102\,\text{GeV}$ region, the small asymmetry is observed to change sign, yielding larger cross sections for the $\cos\theta^* < 0$ part of the phase space. This behaviour is expected from the interference effects between the Z and γ^* contributions to the scattering amplitudes. For bins of higher invariant mass the asymmetry increases albeit with larger uncertainties due to the limited statistical precision of the data. The combined measurement is listed in table 7 with its uncertainties.

The predictions describe the data very well, as can be seen from the ratio panels, apart from some bins at large $|y_{\ell\ell}|$ and $|\cos\theta^*|$. These bins correspond to edges of the fiducial acceptance and may be affected by the $p_{\text{T},\ell\ell}$ modelling uncertainties which are not shown for the predictions.

In figures 11–15 the measured triple differential Born-level cross section for the high rapidity electron channel analysis is presented as a function of $\cos\theta^*$. In this channel the region of small $|\cos\theta^*|$ is experimentally accessible only for moderate values of rapidity, i.e. $|y_{\ell\ell}| \simeq 2.0$–$2.8$. Nevertheless the same features of the cross section are observed: the cross sections are largest for the region $m_{\ell\ell} \sim m_Z$; an asymmetry in the $\cos\theta^*$ spectrum is observed with larger cross sections at negative $\cos\theta^*$ for $m_{\ell\ell} < m_Z$, and larger cross sections at positive $\cos\theta^*$ for $m_{\ell\ell} > m_Z$; the magnitude of the asymmetry is smallest for $80 < m_{\ell\ell} < 91\,\text{GeV}$ and increases with $m_{\ell\ell}$. The triple-differential measurement is listed in table 8 with its uncertainties.

JHEP12(2017)059

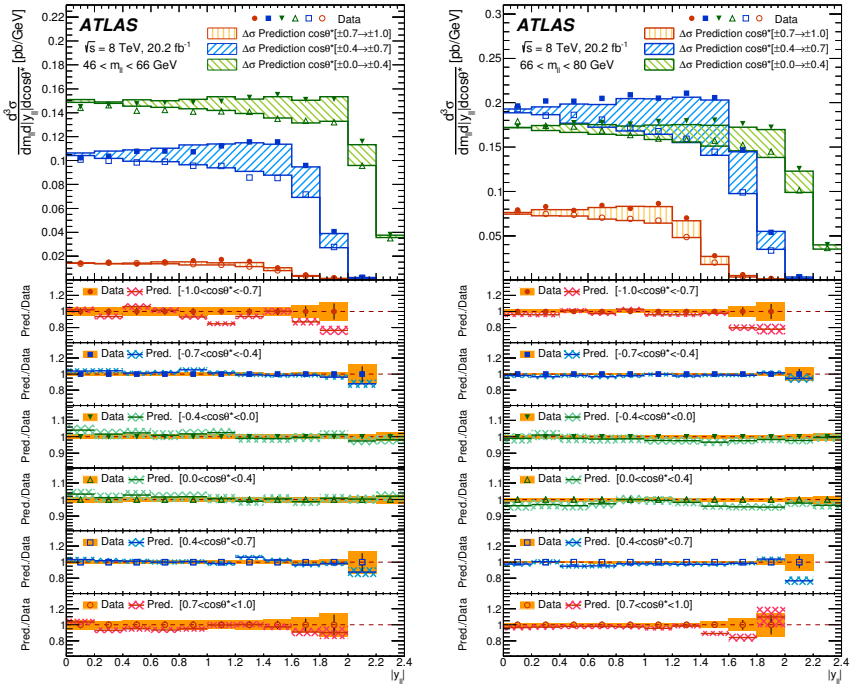

Figure 7. The combined Born-level fiducial cross sections $\mathrm{d}^3\sigma$. The kinematic region shown is labelled in each plot. The data are shown as solid ($\cos\theta^* < 0$) and open ($\cos\theta^* > 0$) markers and the prediction from Powheg including NNLO QCD and NLO EW K-factors is shown as the solid line. The difference, $\Delta\sigma$, between the predicted cross sections in the two measurement bins at equal $|\cos\theta^*|$ symmetric around $\cos\theta^* = 0$ is represented by the hatched shading. In each plot, the lower panel shows the ratio of prediction to measurement. The inner error bars represent the statistical uncertainty of the data and the solid band shows the total experimental uncertainty. The contribution to the uncertainty from the luminosity measurement is excluded. The crosshatched band represents the statistical and PDF uncertainties in the prediction.

JHEP12(2017)059

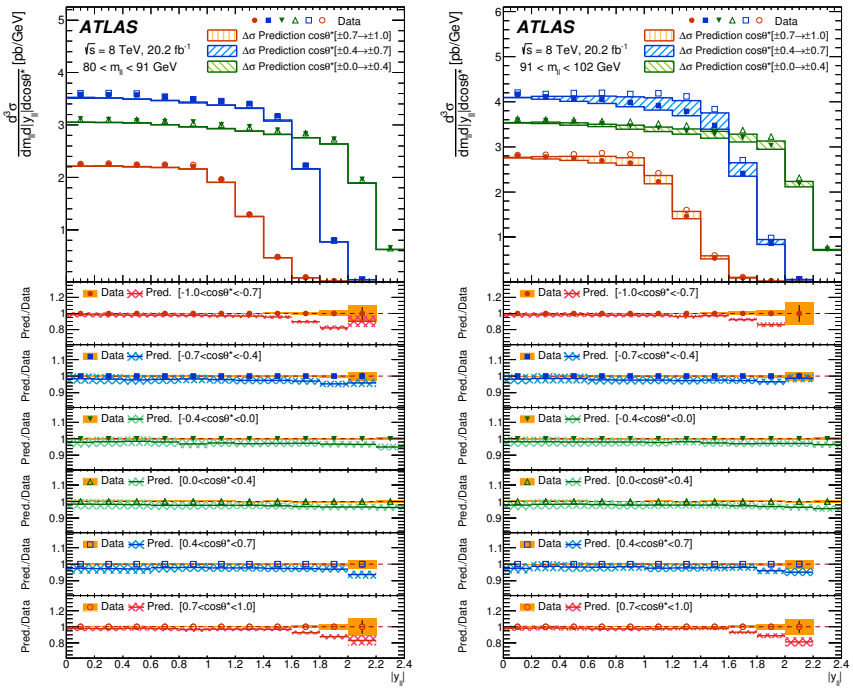

Figure 8. The combined Born-level fiducial cross sections $\mathrm{d}^3\sigma$. The kinematic region shown is labelled in each plot. The data are shown as solid ($\cos\theta^* < 0$) and open ($\cos\theta^* > 0$) markers and the prediction from Powheg including NNLO QCD and NLO EW K-factors is shown as the solid line. The difference, $\Delta\sigma$, between the predicted cross sections in the two measurement bins at equal $|\cos\theta^*|$ symmetric around $\cos\theta^* = 0$ is represented by the hatched shading. In each plot, the lower panel shows the ratio of prediction to measurement. The inner error bars represent the statistical uncertainty of the data and the solid band shows the total experimental uncertainty. The contribution to the uncertainty from the luminosity measurement is excluded. The crosshatched band represents the statistical and PDF uncertainties in the prediction.

JHEP12(2017)059

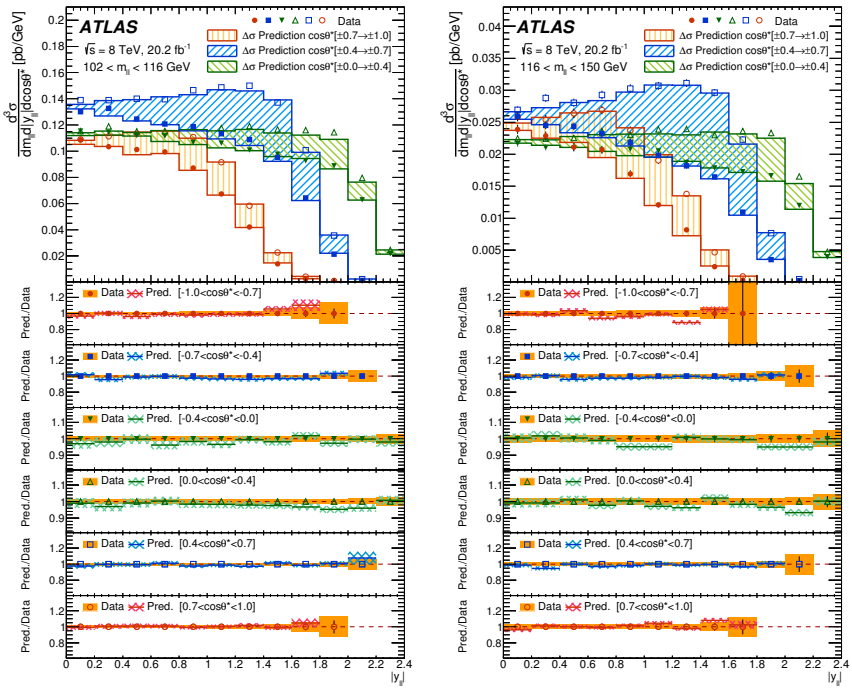

Figure 9. The combined Born-level fiducial cross sections $\mathrm{d}^3\sigma$. The kinematic region shown is labelled in each plot. The data are shown as solid ($\cos\theta^* < 0$) and open ($\cos\theta^* > 0$) markers and the prediction from Powheg including NNLO QCD and NLO EW K-factors is shown as the solid line. The difference, $\Delta\sigma$, between the predicted cross sections in the two measurement bins at equal $|\cos\theta^*|$ symmetric around $\cos\theta^* = 0$ is represented by the hatched shading. In each plot, the lower panel shows the ratio of prediction to measurement. The inner error bars represent the statistical uncertainty of the data and the solid band shows the total experimental uncertainty. The contribution to the uncertainty from the luminosity measurement is excluded. The crosshatched band represents the statistical and PDF uncertainties in the prediction.

JHEP12(2017)059

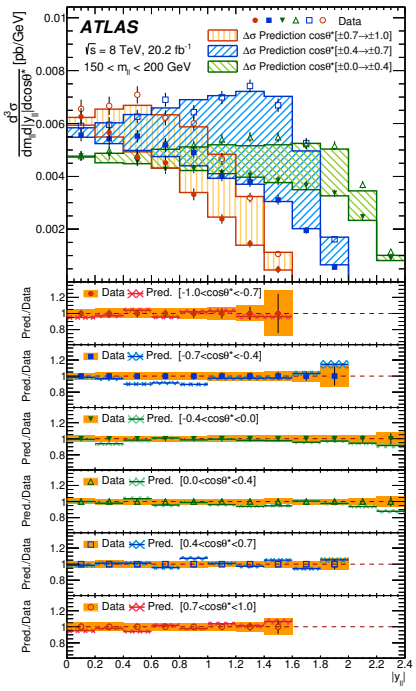

Figure 10. The combined Born-level fiducial cross sections $\mathrm{d}^3\sigma$. The kinematic region shown is labelled in each plot. The data are shown as solid ($\cos\theta^* < 0$) and open ($\cos\theta^* > 0$) markers and the prediction from Powheg including NNLO QCD and NLO EW K-factors is shown as the solid line. The difference, $\Delta\sigma$, between the predicted cross sections in the two measurement bins at equal $|\cos\theta^*|$ symmetric around $\cos\theta^* = 0$ is represented by the hatched shading. In each plot, the lower panel shows the ratio of prediction to measurement. The inner error bars represent the statistical uncertainty of the data and the solid band shows the total experimental uncertainty. The contribution to the uncertainty from the luminosity measurement is excluded. The crosshatched band represents the statistical and PDF uncertainties in the prediction.

JHEP12(2017)059

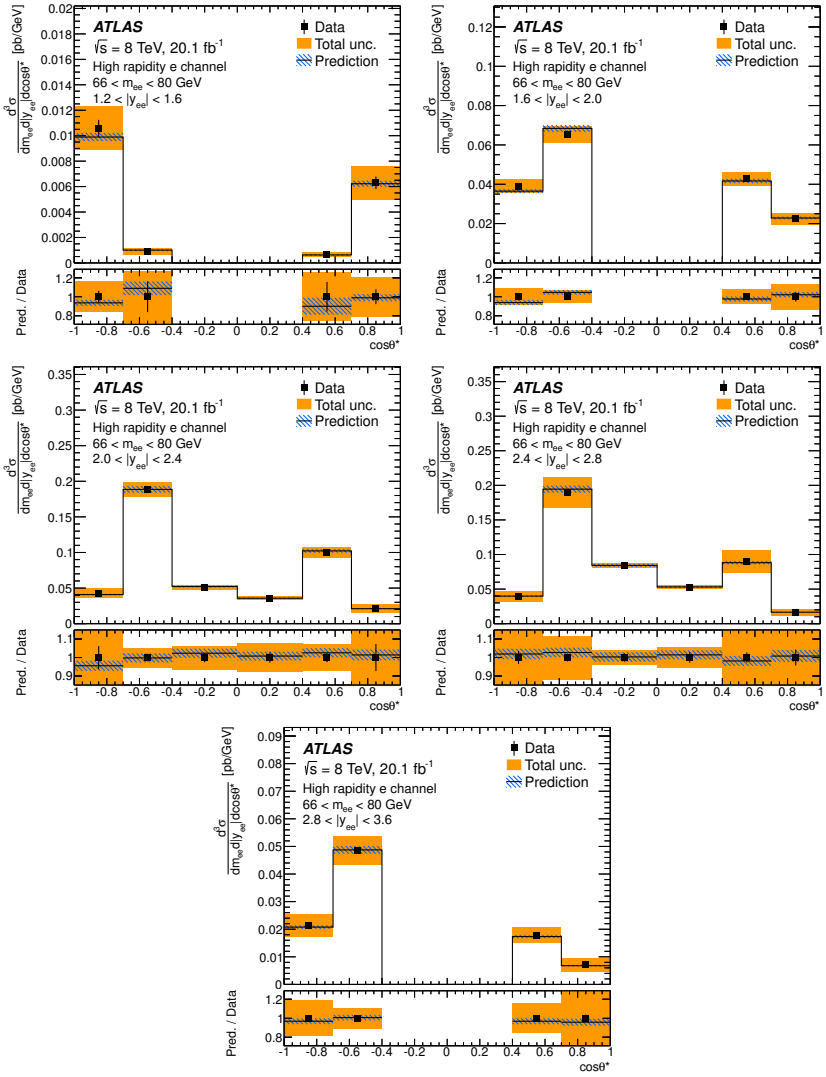

Figure 11. The high rapidity electron channel Born-level fiducial cross section $d^3\sigma$. The kinematic region shown is labelled in each plot. The data are shown as solid markers and the prediction from Powheg including NNLO QCD and NLO EW K-factors is shown as the solid line. In each plot, the lower panel shows the ratio of prediction to measurement. The inner error bars represent the statistical uncertainty of the data and the solid band shows the total experimental uncertainty. The contribution from the uncertainty of the luminosity measurement is excluded. The hatched band represents the statistical and PDF uncertainties in the prediction.

JHEP12(2017)059

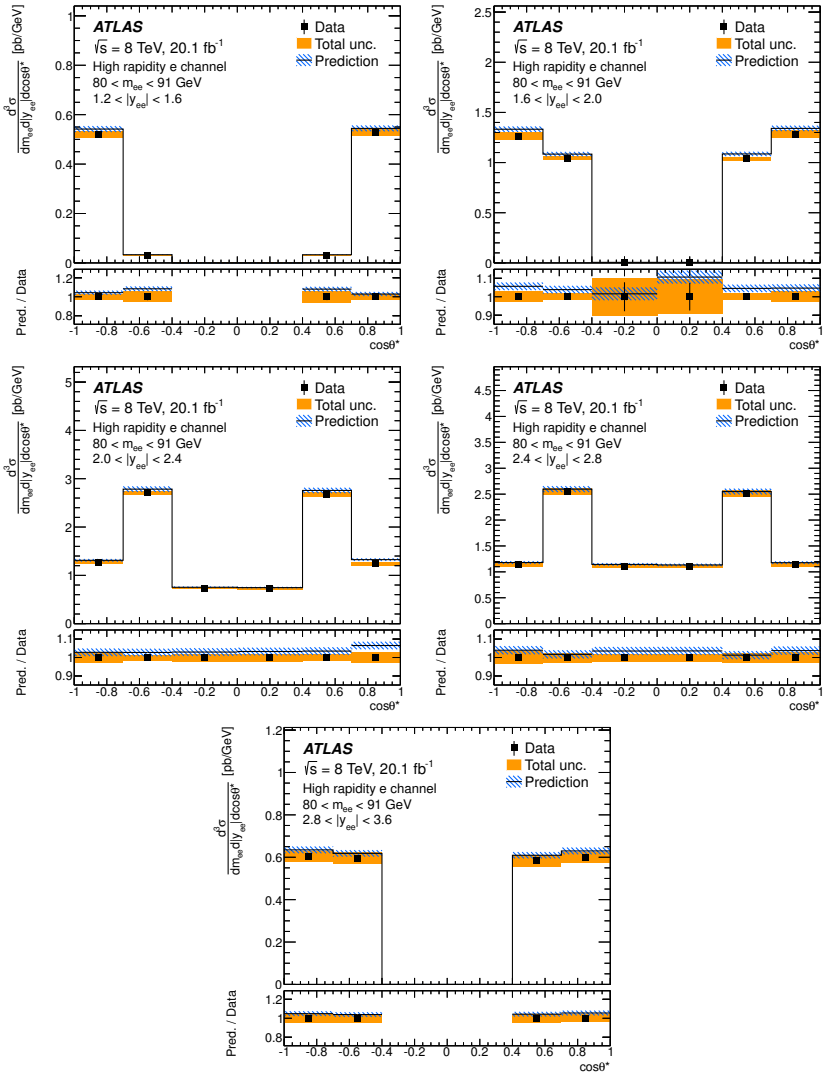

Figure 12. The high rapidity electron channel Born-level fiducial cross section $d^3\sigma$. The kinematic region shown is labelled in each plot. The data are shown as solid markers and the prediction from Powheg including NNLO QCD and NLO EW K-factors is shown as the solid line. In each plot, the lower panel shows the ratio of prediction to measurement. The inner error bars represent the statistical uncertainty of the data and the solid band shows the total experimental uncertainty. The contribution from the uncertainty of the luminosity measurement is excluded. The hatched band represents the statistical and PDF uncertainties in the prediction.

JHEP12(2017)059

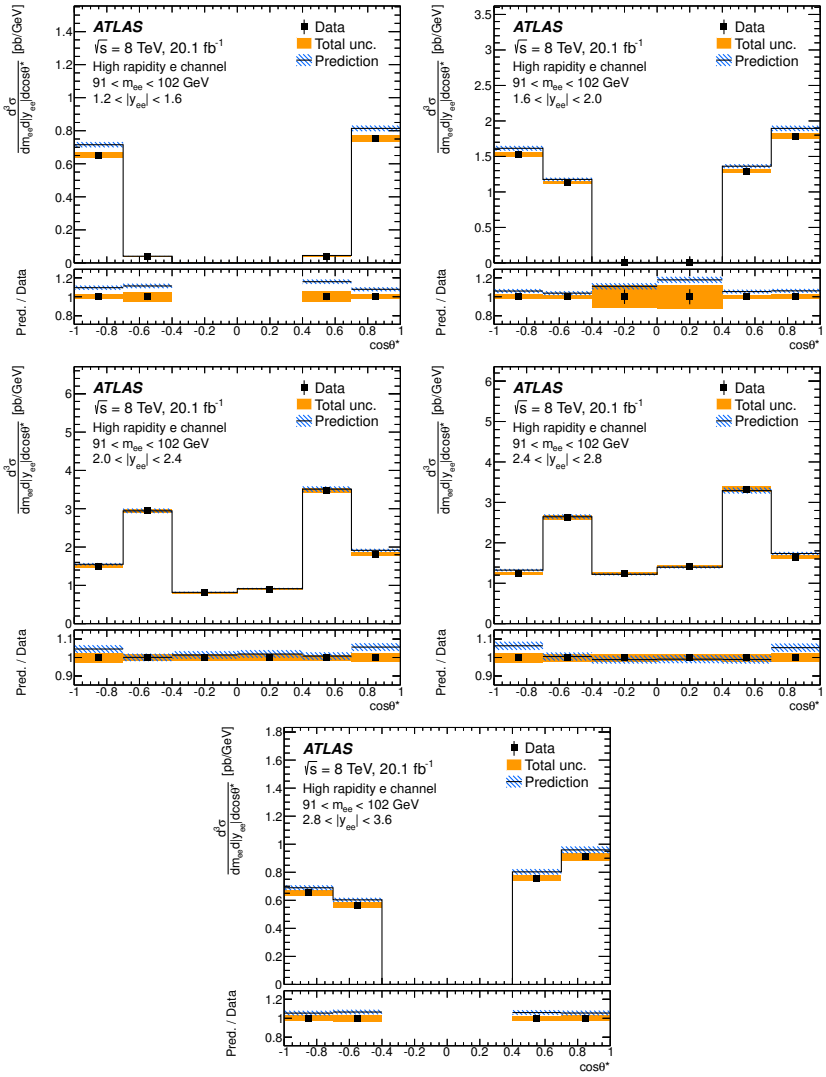

Figure 13. The high rapidity electron channel Born-level fiducial cross section $d^3\sigma$. The kinematic region shown is labelled in each plot. The data are shown as solid markers and the prediction from Powheg including NNLO QCD and NLO EW K-factors is shown as the solid line. In each plot, the lower panel shows the ratio of prediction to measurement. The inner error bars represent the statistical uncertainty of the data and the solid band shows the total experimental uncertainty. The contribution from the uncertainty of the luminosity measurement is excluded. The hatched band represents the statistical and PDF uncertainties in the prediction.

JHEP12(2017)059

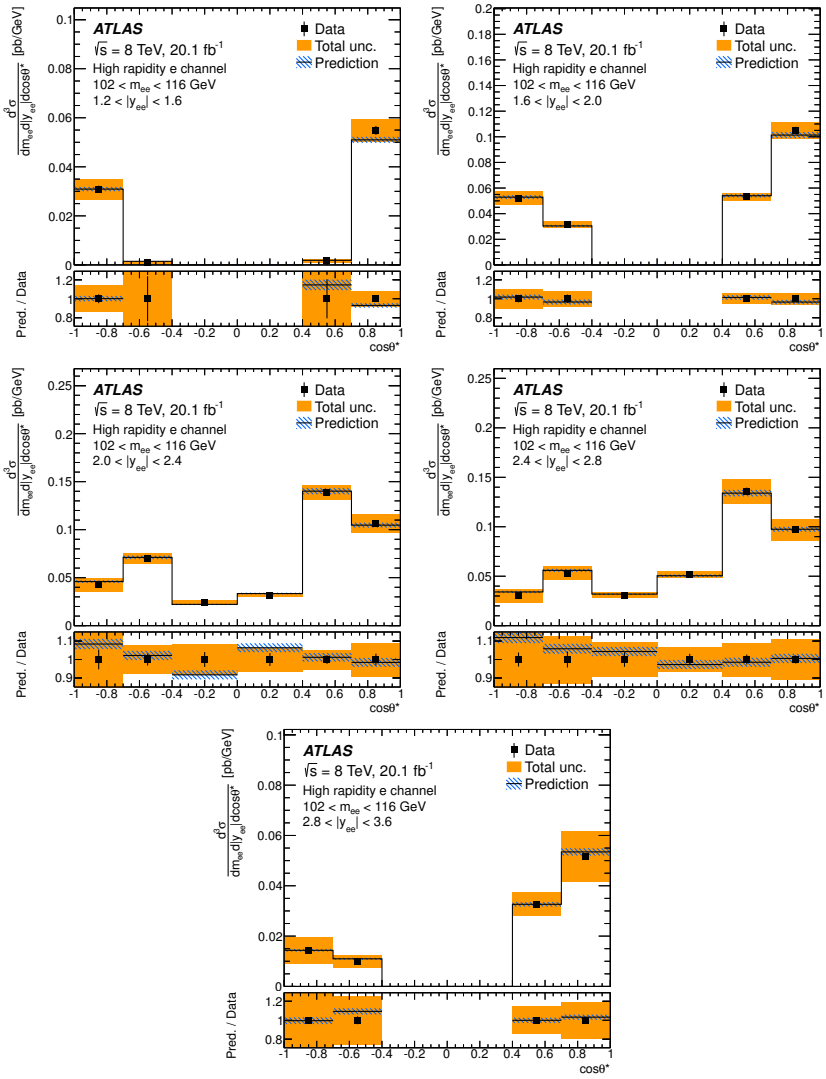

Figure 14. The high rapidity electron channel Born-level fiducial cross section $d^3\sigma$. The kinematic region shown is labelled in each plot. The data are shown as solid markers and the prediction from Powheg including NNLO QCD and NLO EW K-factors is shown as the solid line. In each plot, the lower panel shows the ratio of prediction to measurement. The inner error bars represent the statistical uncertainty of the data and the solid band shows the total experimental uncertainty. The contribution from the uncertainty of the luminosity measurement is excluded. The hatched band represents the statistical and PDF uncertainties in the prediction.

JHEP12(2017)059

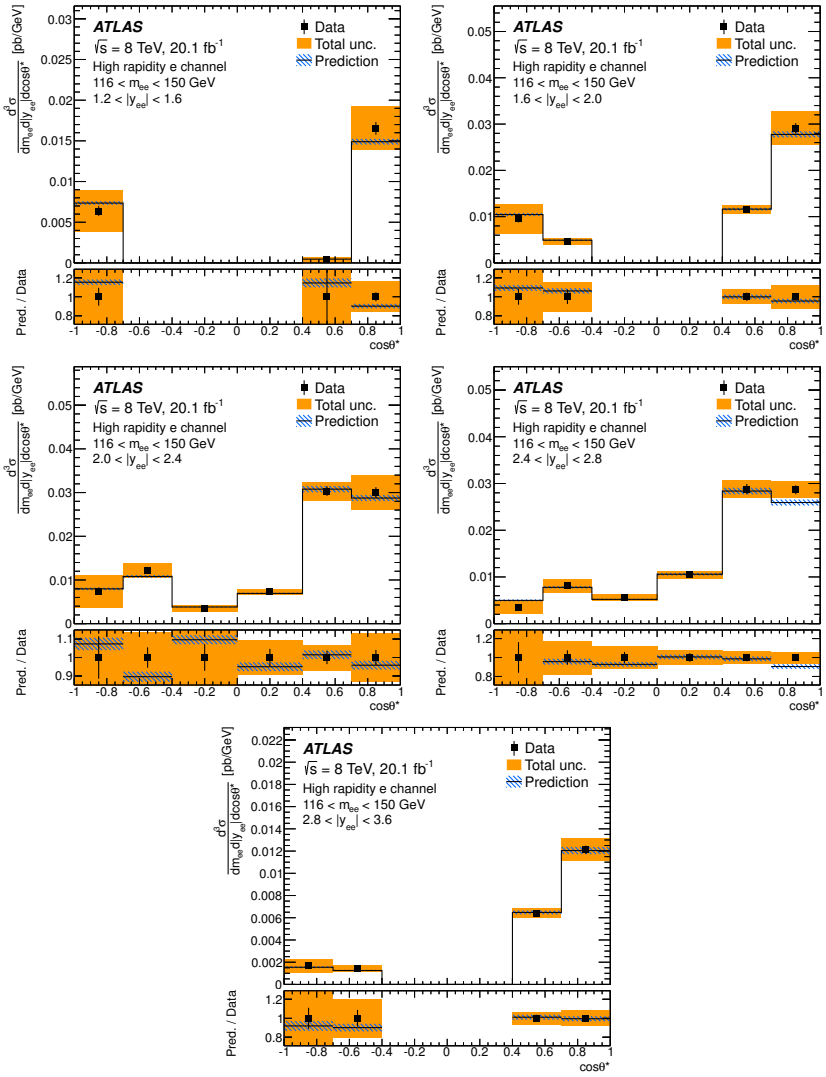

Figure 15. The high rapidity electron channel Born-level fiducial cross section $d^3\sigma$. The kinematic region shown is labelled in each plot. The data are shown as solid markers and the prediction from Powheg including NNLO QCD and NLO EW K-factors is shown as the solid line. In each plot, the lower panel shows the ratio of prediction to measurement. The inner error bars represent the statistical uncertainty of the data and the solid band shows the total experimental uncertainty. The contribution from the uncertainty of the luminosity measurement is excluded. The hatched band represents the statistical and PDF uncertainties in the prediction.

JHEP12(2017)059

8.4 Forward-backward asymmetry

The effect of parity violation in Z boson decays is more clearly visible in the forward-backward asymmetry, A_{FB}, derived from the cross-section measurements of $\mathrm{d}^3\sigma$. The combined Born-level cross sections are used to determine A_{FB} in the region $0 < |y_{\ell\ell}| < 2.4$ by summing the measurement bins for $\cos\theta^* > 0$ and for $\cos\theta^* < 0$ and calculating the asymmetry according to equation (1.3).

The uncorrelated uncertainty in A_{FB} is determined using standard error propagation. The correlated uncertainty is determined for each source in turn by coherently shifting $\mathrm{d}^3\sigma$ by the associated correlated uncertainty and calculating the difference to the nominal value of A_{FB}. Finally, the total uncertainty in A_{FB} is taken as the sum in quadrature of the correlated and uncorrelated components. The uncertainties in A_{FB} are significantly reduced, especially the correlated uncertainties such as the electron energy scale and resolution. The total uncertainty is dominated by the data statistical uncertainty everywhere. An experimental uncertainty of 1×10^{-3} is reached for the combined measurement, and 4×10^{-3} for the high rapidity electron channel measurement. In the high-precision region of $80 < m_{\ell\ell} < 102\,\mathrm{GeV}$ the largest systematic uncertainty contributions are from the MC sample size (which are a factor two smaller than the data statistical uncertainty) and the lepton scale contributions, which are an order of magnitude smaller. At low $m_{\ell\ell}$ the uncorrelated and statistical contributions from the background sources are also of comparable size. Summary tables of these measurements are given in tables 9 and 10 in the appendix.

The measurements of A_{FB} are shown in figure 16 for the combined data. The data are compared to a Born-level prediction from Powheg including K-factors for NNLO QCD and NLO EW corrections. The value of $\sin^2\theta^{\mathrm{eff}}_{\mathrm{lept}}$ used in the simulation is 0.23113 [76]. The measured asymmetry is found to generally increase with $m_{\ell\ell}$ from a negative to a positive asymmetry which is close to zero near $m_{\ell\ell} = m_Z$. The magnitude of A_{FB} is smallest for $|y_{\ell\ell}| = 0$ and increases to a maximum in the region $1.0 < |y_{\ell\ell}| < 2.0$, before decreasing at larger rapidity. This is expected from the effect of dilution and the unknown direction of the incident q on an event-by-event basis. At larger $|y_{\ell\ell}|$, and hence larger x, the influence of the higher-momentum valence u- and d-quarks becomes increasingly apparent through the longitudinal boost in the valence direction. This allows a correct determination of the q direction to be made on average and is well modelled by the Powheg prediction. At even larger $|y_{\ell\ell}|$ in the combined measurements the maximum of $|A_{\mathrm{FB}}|$ decreases again due to the limited acceptance of the detector in $\eta^{e,\mu}$.

The measurements of A_{FB} in the high rapidity electron channel analysis, which is expected to be more sensitive to the asymmetry, are presented in figure 17. Qualitatively, the asymmetry shows behaviour similar to that seen in the combined measurement: the asymmetry increases with m_{ee} and values of $|A_{\mathrm{FB}}|$ reaching 0.7 are observed at the highest $|y_{ee}|$ where the influence of dilution is smallest. As was the case in the combined measurement, the high rapidity A_{FB} measurement is well-described by the Powheg prediction.

JHEP12(2017)059

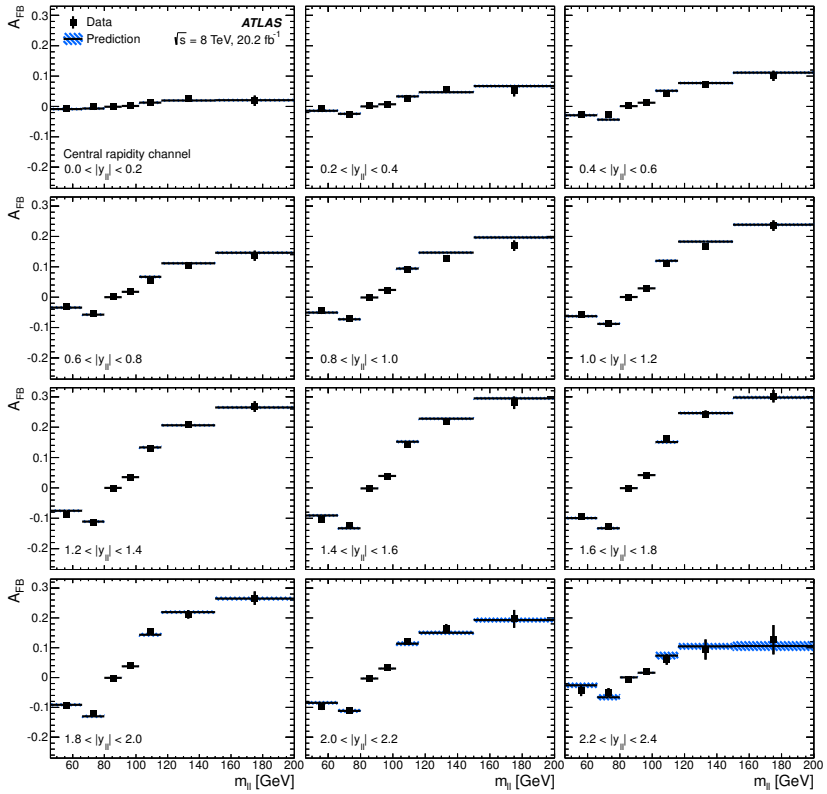

Figure 16. Forward-backward asymmetry, A_{FB}, determined from the combined Born-level fiducial cross section. The kinematic region shown is labelled in each plot. The data are shown as solid markers and the error bars represent the total experimental uncertainty. The prediction from Powheg including NNLO QCD and NLO EW K-factors is shown as the solid line and the hatched band represents the statistical and PDF uncertainties in the prediction.

JHEP12(2017)059

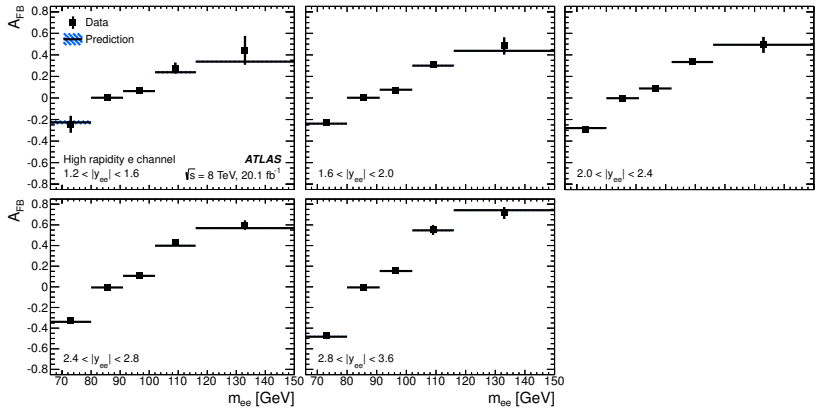

Figure 17. Forward-backward asymmetry, A_{FB}, determined from the high rapidity electron Born-level fiducial cross section. The kinematic region shown is labelled in each plot. The data are shown as solid markers and the error bars represent the total experimental uncertainty. The prediction from Powheg including NNLO QCD and NLO EW K-factors is shown as the solid line and the hatched band represents the statistical and PDF uncertainties in the prediction.

9 Conclusion

The triple-differential Drell-Yan production cross section $\mathrm{d}^3\sigma/\mathrm{d}m_{\ell\ell}\mathrm{d}|y_{\ell\ell}|\mathrm{d}\cos\theta^*$ is measured in the range $46 < m_{\ell\ell} < 200\,\mathrm{GeV}$ and $|y_{\ell\ell}| < 2.4$ for electron and muon pairs. The measurements are extended to high rapidity in the electron channel up to $|y_{ee}| = 3.6$ in the mass range $66 < m_{\ell\ell} < 150\,\mathrm{GeV}$. The analysis uses $20.2\,\mathrm{fb}^{-1}$ of pp collision data at $\sqrt{s} = 8$ TeV collected in 2012 by the ATLAS detector at the LHC. The central rapidity measurement channels are combined taking into account the systematic uncertainty correlations. Their combination achieves an experimental precision of better than 0.5%, excluding the overall uncertainty in the luminosity measurement of 1.9%.

The combined cross sections are integrated to produce the single- and double-differential cross sections $\mathrm{d}\sigma/\mathrm{d}m_{\ell\ell}$ and $\mathrm{d}^2\sigma/\mathrm{d}m_{\ell\ell}\mathrm{d}|y_{\ell\ell}|$. The fiducial cross sections are compared to a theoretical prediction calculated using Powheg at NLO with matched leading-logarithm parton showers. The calculation is approximately corrected for NNLO QCD effects and for additional higher-order electroweak effects applied as a function of $m_{\ell\ell}$. The single- and double-differential measurements are well described by the prediction. Having applied corrections to the scattering amplitude coefficients in Powheg the prediction also provides a good description of the triple-differential measurements.

The measured cross sections are used to determine the forward-backward asymmetry A_{FB} as a function of dilepton invariant mass and rapidity. The Powheg predictions enhanced with NNLO QCD and NLO EW K-factors describe the observed behaviour of A_{FB} well.

Acknowledgments

We thank CERN for the very successful operation of the LHC, as well as the support staff from our institutions without whom ATLAS could not be operated efficiently.

We acknowledge the support of ANPCyT, Argentina; YerPhI, Armenia; ARC, Australia; BMWFW and FWF, Austria; ANAS, Azerbaijan; SSTC, Belarus; CNPq and FAPESP, Brazil; NSERC, NRC and CFI, Canada; CERN; CONICYT, Chile; CAS, MOST and NSFC, China; COLCIENCIAS, Colombia; MSMT CR, MPO CR and VSC CR, Czech Republic; DNRF and DNSRC, Denmark; IN2P3-CNRS, CEA-DSM/IRFU, France; SRNSF, Georgia; BMBF, HGF, and MPG, Germany; GSRT, Greece; RGC, Hong Kong SAR, China; ISF, I-CORE and Benoziyo Center, Israel; INFN, Italy; MEXT and JSPS, Japan; CNRST, Morocco; NWO, Netherlands; RCN, Norway; MNiSW and NCN, Poland; FCT, Portugal; MNE/IFA, Romania; MES of Russia and NRC KI, Russian Federation; JINR; MESTD, Serbia; MSSR, Slovakia; ARRS and MIZŠ, Slovenia; DST/NRF, South Africa; MINECO, Spain; SRC and Wallenberg Foundation, Sweden; SERI, SNSF and Cantons of Bern and Geneva, Switzerland; MOST, Taiwan; TAEK, Turkey; STFC, United Kingdom; DOE and NSF, United States of America. In addition, individual groups and members have received support from BCKDF, the Canada Council, CANARIE, CRC, Compute Canada, FQRNT, and the Ontario Innovation Trust, Canada; EPLANET, ERC, ERDF, FP7, Horizon 2020 and Marie Skłodowska-Curie Actions, European Union; In-

JHEP12(2017)059

vestissements d'Avenir Labex and Idex, ANR, Région Auvergne and Fondation Partager le Savoir, France; DFG and AvH Foundation, Germany; Herakleitos, Thales and Aristeia programmes co-financed by EU-ESF and the Greek NSRF; BSF, GIF and Minerva, Israel; BRF, Norway; CERCA Programme Generalitat de Catalunya, Generalitat Valenciana, Spain; the Royal Society and Leverhulme Trust, United Kingdom.

The crucial computing support from all WLCG partners is acknowledged gratefully, in particular from CERN, the ATLAS Tier-1 facilities at TRIUMF (Canada), NDGF (Denmark, Norway, Sweden), CC-IN2P3 (France), KIT/GridKA (Germany), INFN-CNAF (Italy), NL-T1 (Netherlands), PIC (Spain), ASGC (Taiwan), RAL (U.K.) and BNL (U.S.A.), the Tier-2 facilities worldwide and large non-WLCG resource providers. Major contributors of computing resources are listed in ref. [77].

A Data tables

Summary tables of $\mathrm{d}^3\sigma/\mathrm{d}m_{\ell\ell}\mathrm{d}|y_{\ell\ell}|\mathrm{d}\cos\theta^*$ cross sections and A_{FB} are given in this appendix. Tables containing the complete breakdown of systematic uncertainties are available in HEPData [71, 72].

A.1 Integrated cross-section tables

$m_{\ell\ell}$ [GeV]	$\mathrm{d}\sigma/\mathrm{d}m_{\ell\ell}$ [pb/GeV]	δ^{stat} [%]	$\delta^{\mathrm{syst}}_{\mathrm{unc}}$ [%]	$\delta^{\mathrm{syst}}_{\mathrm{cor}}$ [%]	δ^{total} [%]
46, 66	7.61×10^{-1}	0.2	0.1	0.9	0.9
66, 80	1.13	0.1	0.1	0.4	0.4
80, 91	21.4	0.0	0.0	0.2	0.2
91, 102	25.0	0.0	0.0	0.2	0.2
102, 116	8.25×10^{-1}	0.2	0.1	0.4	0.4
116, 150	1.64×10^{-1}	0.3	0.1	0.7	0.7
150, 200	3.66×10^{-2}	0.5	0.2	1.3	1.4

Table 5. The combined Born-level single-differential cross section $\mathrm{d}\sigma/\mathrm{d}m_{\ell\ell}$. The measurements are listed together with the statistical (δ^{stat}), uncorrelated systematic ($\delta^{\mathrm{syst}}_{\mathrm{unc}}$), correlated systematic ($\delta^{\mathrm{syst}}_{\mathrm{cor}}$), and total ($\delta^{\mathrm{total}}$) uncertainties. The luminosity uncertainty of 1.9% is not shown and not included in the overall systematic and total uncertainties.

JHEP12(2017)059

$m_{\ell\ell}$ [GeV]	$\lvert y_{\ell\ell}\rvert$	$\mathrm{d}^2\sigma/\mathrm{d}m_{\ell\ell}\mathrm{d}\lvert y_{\ell\ell}\rvert$ [pb/GeV]	δ^{stat} [%]	$\delta^{\mathrm{syst}}_{\mathrm{unc}}$ [%]	$\delta^{\mathrm{syst}}_{\mathrm{cor}}$ [%]	δ^{total} [%]	m_{ee} [GeV]	$\lvert y_{\ell\ell}\rvert$	$\mathrm{d}^2\sigma/\mathrm{d}m_{\ell\ell}\mathrm{d}\lvert y_{\ell\ell}\rvert$ [pb/GeV]	δ^{stat} [%]	$\delta^{\mathrm{syst}}_{\mathrm{unc}}$ [%]	$\delta^{\mathrm{syst}}_{\mathrm{cor}}$ [%]	δ^{total} [%]
46, 66	0.0, 0.2	1.85×10^{-1}	0.6	0.4	1.0	1.2	46, 66	1.2, 1.4	1.86×10^{-1}	0.6	0.4	0.9	1.1
46, 66	0.2, 0.4	1.87×10^{-1}	0.6	0.5	1.0	1.2	46, 66	1.4, 1.6	1.82×10^{-1}	0.6	0.4	0.9	1.1
46, 66	0.4, 0.6	1.86×10^{-1}	0.6	0.4	0.9	1.2	46, 66	1.6, 1.8	1.66×10^{-1}	0.6	0.5	0.9	1.2
46, 66	0.6, 0.8	1.87×10^{-1}	0.6	0.4	0.9	1.2	46, 66	1.8, 2.0	1.35×10^{-1}	0.7	0.5	0.8	1.2
46, 66	0.8, 1.0	1.86×10^{-1}	0.6	0.4	0.9	1.2	46, 66	2.0, 2.2	8.60×10^{-2}	0.8	0.6	0.8	1.3
46, 66	1.0, 1.2	1.88×10^{-1}	0.6	0.4	0.9	1.1	46, 66	2.2, 2.4	2.93×10^{-2}	1.4	1.1	0.9	2.0
66, 80	0.0, 0.2	3.05×10^{-1}	0.4	0.2	0.4	0.6	66, 80	1.2, 1.4	2.82×10^{-1}	0.4	0.2	0.4	0.6
66, 80	0.2, 0.4	3.02×10^{-1}	0.4	0.2	0.4	0.6	66, 80	1.4, 1.6	2.54×10^{-1}	0.5	0.3	0.4	0.6
66, 80	0.4, 0.6	3.02×10^{-1}	0.4	0.2	0.4	0.6	66, 80	1.6, 1.8	2.08×10^{-1}	0.5	0.3	0.4	0.7
66, 80	0.6, 0.8	3.01×10^{-1}	0.4	0.2	0.4	0.6	66, 80	1.8, 2.0	1.54×10^{-1}	0.6	0.3	0.5	0.8
66, 80	0.8, 1.0	2.95×10^{-1}	0.4	0.2	0.4	0.6	66, 80	2.0, 2.2	9.27×10^{-2}	0.7	0.4	0.6	1.0
66, 80	1.0, 1.2	2.93×10^{-1}	0.4	0.2	0.4	0.6	66, 80	2.2, 2.4	3.05×10^{-2}	1.2	0.7	0.9	1.7
80, 91	0.0, 0.2	6.00	0.1	0.0	0.2	0.2	80, 91	1.2, 1.4	5.19	0.1	0.1	0.2	0.3
80, 91	0.2, 0.4	6.00	0.1	0.0	0.2	0.2	80, 91	1.4, 1.6	4.51	0.1	0.1	0.2	0.3
80, 91	0.4, 0.6	5.97	0.1	0.1	0.2	0.2	80, 91	1.6, 1.8	3.66	0.1	0.1	0.3	0.3
80, 91	0.6, 0.8	5.93	0.1	0.0	0.2	0.3	80, 91	1.8, 2.0	2.67	0.1	0.1	0.3	0.3
80, 91	0.8, 1.0	5.87	0.1	0.1	0.2	0.3	80, 91	2.0, 2.2	1.60	0.2	0.1	0.3	0.4
80, 91	1.0, 1.2	5.66	0.1	0.1	0.2	0.3	80, 91	2.2, 2.4	5.20×10^{-1}	0.3	0.2	0.4	0.5
91, 102	0.0, 0.2	7.08	0.1	0.1	0.2	0.2	91, 102	1.2, 1.4	6.02	0.1	0.0	0.2	0.3
91, 102	0.2, 0.4	7.04	0.1	0.1	0.2	0.2	91, 102	1.4, 1.6	5.21	0.1	0.1	0.2	0.3
91, 102	0.4, 0.6	7.01	0.1	0.1	0.2	0.2	91, 102	1.6, 1.8	4.23	0.1	0.1	0.3	0.3
91, 102	0.6, 0.8	6.98	0.1	0.0	0.2	0.2	91, 102	1.8, 2.0	3.07	0.2	0.1	0.3	0.3
91, 102	0.8, 1.0	6.90	0.1	0.0	0.2	0.2	91, 102	2.0, 2.2	1.83	0.2	0.1	0.3	0.4
91, 102	1.0, 1.2	6.60	0.1	0.1	0.2	0.3	91, 102	2.2, 2.4	5.96×10^{-1}	0.3	0.2	0.4	0.5
102, 116	0.0, 0.2	2.38×10^{-1}	0.5	0.2	0.3	0.7	102, 116	1.2, 1.4	1.96×10^{-1}	0.5	0.3	0.5	0.7
102, 116	0.2, 0.4	2.39×10^{-1}	0.5	0.2	0.4	0.7	102, 116	1.4, 1.6	1.66×10^{-1}	0.5	0.3	0.5	0.8
102, 116	0.4, 0.6	2.35×10^{-1}	0.5	0.2	0.4	0.7	102, 116	1.6, 1.8	1.35×10^{-1}	0.6	0.4	0.7	1.0
102, 116	0.6, 0.8	2.33×10^{-1}	0.5	0.3	0.4	0.7	102, 116	1.8, 2.0	9.84×10^{-2}	0.6	0.4	0.8	1.1
102, 116	0.8, 1.0	2.29×10^{-1}	0.5	0.3	0.4	0.7	102, 116	2.0, 2.2	5.76×10^{-2}	0.7	0.5	1.0	1.3
102, 116	1.0, 1.2	2.16×10^{-1}	0.5	0.3	0.4	0.7	102, 116	2.2, 2.4	1.85×10^{-2}	1.0	0.9	1.3	1.9
116, 150	0.0, 0.2	4.84×10^{-2}	0.8	0.3	0.8	1.2	116, 150	1.2, 1.4	3.84×10^{-2}	0.9	0.4	0.6	1.1
116, 150	0.2, 0.4	4.79×10^{-2}	0.8	0.3	0.8	1.2	116, 150	1.4, 1.6	3.23×10^{-2}	0.9	0.4	0.5	1.1
116, 150	0.4, 0.6	4.74×10^{-2}	0.8	0.3	0.8	1.2	116, 150	1.6, 1.8	2.66×10^{-2}	1.0	0.5	0.5	1.2
116, 150	0.6, 0.8	4.77×10^{-2}	0.8	0.3	0.8	1.2	116, 150	1.8, 2.0	1.93×10^{-2}	1.2	0.7	0.6	1.5
116, 150	0.8, 1.0	4.54×10^{-2}	0.8	0.3	0.7	1.1	116, 150	2.0, 2.2	1.14×10^{-2}	1.4	0.7	0.7	1.7
116, 150	1.0, 1.2	4.23×10^{-2}	0.8	0.4	0.6	1.1	116, 150	2.2, 2.4	3.48×10^{-3}	2.6	1.7	1.2	3.3
150, 200	0.0, 0.2	1.11×10^{-2}	1.6	0.6	1.8	2.4	150, 200	1.2, 1.4	8.56×10^{-3}	1.6	0.6	1.0	2.0
150, 200	0.2, 0.4	1.10×10^{-2}	1.5	0.7	1.8	2.4	150, 200	1.4, 1.6	7.12×10^{-3}	1.8	0.9	0.9	2.2
150, 200	0.4, 0.6	1.08×10^{-2}	1.5	0.6	1.7	2.3	150, 200	1.6, 1.8	5.72×10^{-3}	1.9	0.7	0.8	2.2
150, 200	0.6, 0.8	1.07×10^{-2}	1.5	0.5	1.5	2.2	150, 200	1.8, 2.0	4.06×10^{-3}	2.2	0.7	0.7	2.4
150, 200	0.8, 1.0	9.98×10^{-3}	1.6	0.5	1.3	2.1	150, 200	2.0, 2.2	2.46×10^{-3}	2.8	1.0	0.7	3.0
150, 200	1.0, 1.2	9.22×10^{-3}	1.6	0.6	1.2	2.1	150, 200	2.2, 2.4	8.20×10^{-4}	4.7	1.3	1.0	5.0

Table 6. The combined Born-level double-differential cross section $\mathrm{d}^2\sigma/\mathrm{d}m_{\ell\ell}\mathrm{d}\lvert y_{\ell\ell}\rvert$. The measurements are listed together with the statistical (δ^{stat}), uncorrelated systematic ($\delta^{\mathrm{syst}}_{\mathrm{unc}}$), correlated systematic ($\delta^{\mathrm{syst}}_{\mathrm{cor}}$), and total ($\delta^{\mathrm{total}}$) uncertainties. The luminosity uncertainty of 1.9% is not shown and not included in the overall systematic and total uncertainties.

JHEP12(2017)059

A.2 Triple-differential cross-section tables

Bin	$m_{\ell\ell}$ [GeV]	$\lvert y_{\ell\ell}\rvert$	$\cos\theta^*$	$\mathrm{d}^3\sigma$ [pb/GeV]	δ^{stat} [%]	$\delta^{\text{syst}}_{\text{unc}}$ [%]	$\delta^{\text{syst}}_{\text{cor}}$ [%]	δ^{total} [%]	Bin	$m_{\ell\ell}$ [GeV]	$\lvert y_{\ell\ell}\rvert$	$\cos\theta^*$	$\mathrm{d}^3\sigma$ [pb/GeV]	δ^{stat} [%]	$\delta^{\text{syst}}_{\text{unc}}$ [%]	$\delta^{\text{syst}}_{\text{cor}}$ [%]	δ^{total} [%]
1	46, 66	0.0, 0.2	−1.0, −0.7	1.42×10^{-2}	4.0	2.5	1.8	5.1	6	46, 66	0.0, 0.2	+0.7, +1.0	1.37×10^{-2}	4.2	3.4	2.0	5.7
2	46, 66	0.0, 0.2	−0.7, −0.4	1.02×10^{-1}	1.4	1.1	1.2	2.1	5	46, 66	0.0, 0.2	+0.4, +0.7	1.01×10^{-1}	1.4	1.1	1.2	2.1
3	46, 66	0.0, 0.2	−0.4, 0.0	1.45×10^{-1}	1.0	0.8	0.9	1.5	4	46, 66	0.0, 0.2	0.0, +0.4	1.44×10^{-1}	1.0	0.8	0.9	1.6
7	46, 66	0.2, 0.4	−1.0, −0.7	1.48×10^{-2}	3.9	2.1	1.8	4.8	12	46, 66	0.2, 0.4	+0.7, +1.0	1.46×10^{-2}	3.9	1.9	1.8	4.7
8	46, 66	0.2, 0.4	−0.7, −0.4	1.03×10^{-1}	1.4	1.3	1.2	2.2	11	46, 66	0.2, 0.4	+0.4, +0.7	9.99×10^{-2}	1.4	1.1	1.2	2.2
9	46, 66	0.2, 0.4	−0.4, 0.0	1.47×10^{-1}	1.0	0.8	0.9	1.5	10	46, 66	0.2, 0.4	0.0, +0.4	1.46×10^{-1}	1.0	0.9	0.9	1.6
13	46, 66	0.4, 0.6	−1.0, −0.7	1.35×10^{-2}	4.5	3.3	1.9	5.9	18	46, 66	0.4, 0.6	+0.7, +1.0	1.43×10^{-2}	4.2	2.5	1.8	5.2
14	46, 66	0.4, 0.6	−0.7, −0.4	1.08×10^{-1}	1.4	1.1	1.0	2.1	17	46, 66	0.4, 0.6	+0.4, +0.7	9.84×10^{-2}	1.6	1.3	1.2	2.3
15	46, 66	0.4, 0.6	−0.4, 0.0	1.47×10^{-1}	0.9	0.7	0.9	1.5	16	46, 66	0.4, 0.6	0.0, +0.4	1.42×10^{-1}	1.0	0.8	0.9	1.5
19	46, 66	0.6, 0.8	−1.0, −0.7	1.50×10^{-2}	4.0	2.8	1.8	5.2	24	46, 66	0.6, 0.8	+0.7, +1.0	1.46×10^{-2}	4.1	3.0	1.9	5.5
20	46, 66	0.6, 0.8	−0.7, −0.4	1.08×10^{-1}	1.4	1.0	1.1	2.1	23	46, 66	0.6, 0.8	+0.4, +0.7	9.90×10^{-2}	1.5	1.1	1.2	2.2
21	46, 66	0.6, 0.8	−0.4, 0.0	1.48×10^{-1}	0.9	0.7	0.8	1.4	22	46, 66	0.6, 0.8	0.0, +0.4	1.42×10^{-1}	0.9	0.8	0.9	1.5
25	46, 66	0.8, 1.0	−1.0, −0.7	1.63×10^{-2}	4.1	2.7	1.5	5.1	30	46, 66	0.8, 1.0	+0.7, +1.0	1.33×10^{-2}	4.4	3.2	2.0	5.8
26	46, 66	0.8, 1.0	−0.7, −0.4	1.07×10^{-1}	1.5	1.1	1.1	2.1	29	46, 66	0.8, 1.0	+0.4, +0.7	9.57×10^{-2}	1.6	1.1	1.3	2.3
27	46, 66	0.8, 1.0	−0.4, 0.0	1.49×10^{-1}	0.9	0.7	0.8	1.4	28	46, 66	0.8, 1.0	0.0, +0.4	1.41×10^{-1}	1.0	0.8	0.8	1.5
31	46, 66	1.0, 1.2	−1.0, −0.7	1.71×10^{-2}	3.5	2.2	1.4	4.4	36	46, 66	1.0, 1.2	+0.7, +1.0	1.27×10^{-2}	4.2	2.5	1.8	5.2
32	46, 66	1.0, 1.2	−0.7, −0.4	1.12×10^{-1}	1.4	1.0	1.1	2.0	35	46, 66	1.0, 1.2	+0.4, +0.7	9.56×10^{-2}	1.5	1.1	1.2	2.2
33	46, 66	1.0, 1.2	−0.4, 0.0	1.50×10^{-1}	1.0	0.8	0.8	1.5	34	46, 66	1.0, 1.2	0.0, +0.4	1.41×10^{-1}	1.0	0.8	0.8	1.5
37	46, 66	1.2, 1.4	−1.0, −0.7	1.57×10^{-2}	3.8	2.3	1.6	4.7	42	46, 66	1.2, 1.4	+0.7, +1.0	1.13×10^{-2}	4.4	3.3	1.9	5.8
38	46, 66	1.2, 1.4	−0.7, −0.4	1.16×10^{-1}	1.3	0.9	1.0	1.9	41	46, 66	1.2, 1.4	+0.4, +0.7	8.57×10^{-2}	1.6	1.2	1.4	2.4
39	46, 66	1.2, 1.4	−0.4, 0.0	1.53×10^{-1}	1.0	0.7	0.8	1.4	40	46, 66	1.2, 1.4	0.0, +0.4	1.41×10^{-1}	1.0	0.8	0.8	1.5
43	46, 66	1.4, 1.6	−1.0, −0.7	1.04×10^{-2}	4.4	2.4	1.5	5.3	48	46, 66	1.4, 1.6	+0.7, +1.0	8.25×10^{-3}	5.0	3.9	1.7	6.6
44	46, 66	1.4, 1.6	−0.7, −0.4	1.16×10^{-1}	1.3	0.9	0.9	1.8	47	46, 66	1.4, 1.6	+0.4, +0.7	8.55×10^{-2}	1.6	1.3	1.3	2.5
45	46, 66	1.4, 1.6	−0.4, 0.0	1.55×10^{-1}	1.0	0.7	0.7	1.4	46	46, 66	1.4, 1.6	0.0, +0.4	1.35×10^{-1}	1.1	0.8	0.9	1.6
49	46, 66	1.6, 1.8	−1.0, −0.7	4.44×10^{-3}	6.6	3.2	1.8	7.5	54	46, 66	1.6, 1.8	+0.7, +1.0	3.58×10^{-3}	7.8	4.2	2.3	9.1
50	46, 66	1.6, 1.8	−0.7, −0.4	9.59×10^{-2}	1.4	1.0	1.0	2.0	53	46, 66	1.6, 1.8	+0.4, +0.7	7.16×10^{-2}	1.7	1.4	1.3	2.6
51	46, 66	1.6, 1.8	−0.4, 0.0	1.51×10^{-1}	1.0	0.8	0.8	1.5	52	46, 66	1.6, 1.8	0.0, +0.4	1.33×10^{-1}	1.1	0.8	0.9	1.6
55	46, 66	1.8, 2.0	−1.0, −0.7	1.97×10^{-3}	10.0	4.7	2.4	11.4	60	46, 66	1.8, 2.0	+0.7, +1.0	1.38×10^{-3}	12.8	6.6	2.7	14.7
56	46, 66	1.8, 2.0	−0.7, −0.4	4.05×10^{-2}	2.3	1.4	1.0	2.9	59	46, 66	1.8, 2.0	+0.4, +0.7	2.76×10^{-2}	2.8	2.0	1.3	3.6
57	46, 66	1.8, 2.0	−0.4, 0.0	1.51×10^{-1}	1.0	0.8	0.8	1.5	58	46, 66	1.8, 2.0	0.0, +0.4	1.32×10^{-1}	1.1	0.8	0.9	1.6
61	46, 66	2.0, 2.2	−1.0, −0.7	—	—	—	—	—	66	46, 66	2.0, 2.2	+0.7, +1.0	—	—	—	—	—
62	46, 66	2.0, 2.2	−0.7, −0.4	2.48×10^{-3}	9.7	7.1	3.0	12.3	65	46, 66	2.0, 2.2	+0.4, +0.7	1.64×10^{-3}	11.1	6.4	5.2	13.8
63	46, 66	2.0, 2.2	−0.4, 0.0	1.16×10^{-1}	1.1	0.8	0.7	1.6	64	46, 66	2.0, 2.2	0.0, +0.4	9.58×10^{-2}	1.2	1.0	0.9	1.8
67	46, 66	2.2, 2.4	−1.0, −0.7	—	—	—	—	—	72	46, 66	2.2, 2.4	+0.7, +1.0	—	—	—	—	—
68	46, 66	2.2, 2.4	−0.7, −0.4	—	—	—	—	—	71	46, 66	2.2, 2.4	+0.4, +0.7	—	—	—	—	—
69	46, 66	2.2, 2.4	−0.4, 0.0	3.82×10^{-2}	1.9	1.5	0.9	2.6	70	46, 66	2.2, 2.4	0.0, +0.4	3.50×10^{-2}	2.0	1.4	1.0	2.6
73	66, 80	0.0, 0.2	−1.0, −0.7	7.92×10^{-2}	1.6	0.9	0.8	2.0	78	66, 80	0.0, 0.2	+0.7, +1.0	7.70×10^{-2}	1.6	0.9	0.8	2.0
74	66, 80	0.0, 0.2	−0.7, −0.4	1.96×10^{-1}	0.9	0.5	0.4	1.1	77	66, 80	0.0, 0.2	+0.4, +0.7	1.93×10^{-1}	1.0	0.5	0.4	1.1
75	66, 80	0.0, 0.2	−0.4, 0.0	1.74×10^{-1}	0.9	0.6	0.3	1.1	76	66, 80	0.0, 0.2	0.0, +0.4	1.79×10^{-1}	0.9	0.4	0.3	1.0
79	66, 80	0.2, 0.4	−1.0, −0.7	8.29×10^{-2}	1.7	0.9	0.8	2.0	84	66, 80	0.2, 0.4	+0.7, +1.0	7.47×10^{-2}	1.6	0.9	0.8	2.0
80	66, 80	0.2, 0.4	−0.7, −0.4	2.02×10^{-1}	0.9	0.5	0.4	1.1	83	66, 80	0.2, 0.4	+0.4, +0.7	1.85×10^{-1}	1.0	0.5	0.4	1.2
81	66, 80	0.2, 0.4	−0.4, 0.0	1.72×10^{-1}	0.9	0.5	0.3	1.0	82	66, 80	0.2, 0.4	0.0, +0.4	1.74×10^{-1}	0.9	0.5	0.3	1.0
85	66, 80	0.4, 0.6	−1.0, −0.7	7.86×10^{-2}	1.6	0.9	0.9	2.0	90	66, 80	0.4, 0.6	+0.7, +1.0	7.37×10^{-2}	1.7	0.9	0.9	2.1
86	66, 80	0.4, 0.6	−0.7, −0.4	2.02×10^{-1}	1.0	0.5	0.4	1.2	89	66, 80	0.4, 0.6	+0.4, +0.7	1.86×10^{-1}	1.0	0.5	0.4	1.2
87	66, 80	0.4, 0.6	−0.4, 0.0	1.77×10^{-1}	0.8	0.4	0.3	1.0	88	66, 80	0.4, 0.6	0.0, +0.4	1.73×10^{-1}	0.8	0.4	0.3	1.0
91	66, 80	0.6, 0.8	−1.0, −0.7	8.41×10^{-2}	1.6	0.8	0.8	2.0	96	66, 80	0.6, 0.8	+0.7, +1.0	7.03×10^{-2}	1.6	1.0	0.8	2.1
92	66, 80	0.6, 0.8	−0.7, −0.4	2.05×10^{-1}	1.0	0.5	0.4	1.2	95	66, 80	0.6, 0.8	+0.4, +0.7	1.81×10^{-1}	1.0	0.7	0.5	1.3
93	66, 80	0.6, 0.8	−0.4, 0.0	1.78×10^{-1}	0.8	0.4	0.3	1.0	94	66, 80	0.6, 0.8	0.0, +0.4	1.69×10^{-1}	0.9	0.4	0.3	1.0
97	66, 80	0.8, 1.0	−1.0, −0.7	8.08×10^{-2}	1.7	1.0	0.8	2.1	102	66, 80	0.8, 1.0	+0.7, +1.0	6.90×10^{-2}	1.8	1.0	0.9	2.2
98	66, 80	0.8, 1.0	−0.7, −0.4	2.09×10^{-1}	1.0	0.5	0.4	1.2	101	66, 80	0.8, 1.0	+0.4, +0.7	1.72×10^{-1}	1.0	0.6	0.5	1.3
99	66, 80	0.8, 1.0	−0.4, 0.0	1.76×10^{-1}	0.8	0.4	0.3	1.0	100	66, 80	0.8, 1.0	0.0, +0.4	1.63×10^{-1}	0.9	0.5	0.3	1.0
103	66, 80	1.0, 1.2	−1.0, −0.7	8.63×10^{-2}	1.6	0.9	0.7	2.0	108	66, 80	1.0, 1.2	+0.7, +1.0	6.71×10^{-2}	1.7	1.0	0.8	2.1
104	66, 80	1.0, 1.2	−0.7, −0.4	2.05×10^{-1}	0.9	0.5	0.4	1.1	107	66, 80	1.0, 1.2	+0.4, +0.7	1.68×10^{-1}	1.0	0.6	0.5	1.2
105	66, 80	1.0, 1.2	−0.4, 0.0	1.79×10^{-1}	0.9	0.5	0.3	1.0	106	66, 80	1.0, 1.2	0.0, +0.4	1.60×10^{-1}	0.9	0.5	0.4	1.1
109	66, 80	1.2, 1.4	−1.0, −0.7	7.00×10^{-2}	1.6	1.0	0.8	2.1	114	66, 80	1.2, 1.4	+0.7, +1.0	4.86×10^{-2}	1.9	1.0	1.0	2.3
110	66, 80	1.2, 1.4	−0.7, −0.4	2.11×10^{-1}	0.9	0.5	0.4	1.1	113	66, 80	1.2, 1.4	+0.4, +0.7	1.59×10^{-1}	1.0	0.6	0.5	1.2
111	66, 80	1.2, 1.4	−0.4, 0.0	1.79×10^{-1}	0.9	0.5	0.4	1.1	112	66, 80	1.2, 1.4	0.0, +0.4	1.58×10^{-1}	0.9	0.5	0.4	1.2
115	66, 80	1.4, 1.6	−1.0, −0.7	2.74×10^{-2}	2.6	1.5	0.8	3.1	120	66, 80	1.4, 1.6	+0.7, +1.0	1.97×10^{-2}	2.9	2.3	1.1	3.9
116	66, 80	1.4, 1.6	−0.7, −0.4	2.06×10^{-1}	0.9	0.5	0.4	1.1	119	66, 80	1.4, 1.6	+0.4, +0.7	1.45×10^{-1}	1.0	0.6	0.5	1.3
117	66, 80	1.4, 1.6	−0.4, 0.0	1.80×10^{-1}	0.9	0.5	0.4	1.1	118	66, 80	1.4, 1.6	0.0, +0.4	1.57×10^{-1}	0.9	0.5	0.4	1.1
121	66, 80	1.6, 1.8	−1.0, −0.7	6.28×10^{-3}	5.1	3.5	1.8	6.5	126	66, 80	1.6, 1.8	+0.7, +1.0	4.06×10^{-3}	6.1	4.2	1.8	7.7
122	66, 80	1.6, 1.8	−0.7, −0.4	1.47×10^{-1}	1.0	0.6	0.5	1.3	125	66, 80	1.6, 1.8	+0.4, +0.7	9.89×10^{-2}	1.2	0.8	0.6	1.6
123	66, 80	1.6, 1.8	−0.4, 0.0	1.76×10^{-1}	0.9	0.5	0.4	1.1	124	66, 80	1.6, 1.8	0.0, +0.4	1.52×10^{-1}	0.9	0.5	0.5	1.1
127	66, 80	1.8, 2.0	−1.0, −0.7	1.90×10^{-3}	9.4	5.8	3.5	11.6	132	66, 80	1.8, 2.0	+0.7, +1.0	8.82×10^{-4}	11.9	7.4	4.3	14.7
128	66, 80	1.8, 2.0	−0.7, −0.4	5.38×10^{-2}	1.8	1.2	0.9	2.3	131	66, 80	1.8, 2.0	+0.4, +0.7	3.34×10^{-2}	2.1	1.3	1.0	2.7
129	66, 80	1.8, 2.0	−0.4, 0.0	1.72×10^{-1}	0.8	0.5	0.5	1.1	130	66, 80	1.8, 2.0	0.0, +0.4	1.45×10^{-1}	0.9	0.5	0.5	1.2
133	66, 80	2.0, 2.2	−1.0, −0.7	—	—	—	—	—	138	66, 80	2.0, 2.2	+0.7, +1.0	—	—	—	—	—
134	66, 80	2.0, 2.2	−0.7, −0.4	3.68×10^{-3}	6.5	4.8	3.0	8.6	137	66, 80	2.0, 2.2	+0.4, +0.7	2.62×10^{-3}	7.8	5.4	3.9	10.2
135	66, 80	2.0, 2.2	−0.4, 0.0	1.26×10^{-1}	1.0	0.5	0.6	1.3	136	66, 80	2.0, 2.2	0.0, +0.4	1.01×10^{-1}	1.0	0.6	0.7	1.4
139	66, 80	2.2, 2.4	−1.0, −0.7	—	—	—	—	—	144	66, 80	2.2, 2.4	+0.7, +1.0	—	—	—	—	—
140	66, 80	2.2, 2.4	−0.7, −0.4	—	—	—	—	—	143	66, 80	2.2, 2.4	+0.4, +0.7	—	—	—	—	—
141	66, 80	2.2, 2.4	−0.4, 0.0	4.01×10^{-2}	1.6	1.0	1.1	2.2	142	66, 80	2.2, 2.4	0.0, +0.4	3.62×10^{-2}	1.7	1.1	1.1	2.3

JHEP12(2017)059

Bin	$m_{\ell\ell}$ [GeV]	$\lvert y_{\ell\ell}\rvert$	$\cos\theta^*$	$\mathrm{d}^3\sigma$ [pb/GeV]	δ^{stat} [%]	$\delta^{\text{syst}}_{\text{unc}}$ [%]	$\delta^{\text{syst}}_{\text{cor}}$ [%]	δ^{total} [%]	Bin	$m_{\ell\ell}$ [GeV]	$\lvert y_{\ell\ell}\rvert$	$\cos\theta^*$	$\mathrm{d}^3\sigma$ [pb/GeV]	δ^{stat} [%]	$\delta^{\text{syst}}_{\text{unc}}$ [%]	$\delta^{\text{syst}}_{\text{cor}}$ [%]	δ^{total} [%]
145	91, 102	0.0, 0.2	−1.0, −0.7	2.25	0.3	0.2	0.3	0.5	150	91, 102	0.0, 0.2	+0.7, +1.0	2.26	0.3	0.2	0.3	0.5
146	91, 102	0.0, 0.2	−0.7, −0.4	3.58	0.3	0.1	0.2	0.3	149	91, 102	0.0, 0.2	+0.4, +0.7	3.60	0.3	0.1	0.2	0.3
147	91, 102	0.0, 0.2	−0.4, 0.0	3.12	0.3	0.1	0.2	0.4	148	91, 102	0.0, 0.2	0.0, +0.4	3.10	0.3	0.1	0.2	0.4
151	91, 102	0.2, 0.4	−1.0, −0.7	2.26	0.3	0.2	0.3	0.5	156	91, 102	0.2, 0.4	+0.7, +1.0	2.27	0.3	0.2	0.3	0.5
152	91, 102	0.2, 0.4	−0.7, −0.4	3.58	0.3	0.1	0.2	0.3	155	91, 102	0.2, 0.4	+0.4, +0.7	3.61	0.3	0.1	0.2	0.4
153	91, 102	0.2, 0.4	−0.4, 0.0	3.10	0.3	0.1	0.2	0.4	154	91, 102	0.2, 0.4	0.0, +0.4	3.10	0.2	0.1	0.2	0.4
157	91, 102	0.4, 0.6	−1.0, −0.7	2.24	0.3	0.2	0.3	0.5	162	91, 102	0.4, 0.6	+0.7, +1.0	2.24	0.3	0.2	0.3	0.5
158	91, 102	0.4, 0.6	−0.7, −0.4	3.57	0.3	0.1	0.2	0.4	161	91, 102	0.4, 0.6	+0.4, +0.7	3.60	0.3	0.1	0.2	0.4
159	91, 102	0.4, 0.6	−0.4, 0.0	3.08	0.2	0.1	0.2	0.3	160	91, 102	0.4, 0.6	0.0, +0.4	3.10	0.2	0.1	0.2	0.3
163	91, 102	0.6, 0.8	−1.0, −0.7	2.24	0.3	0.2	0.3	0.5	168	91, 102	0.6, 0.8	+0.7, +1.0	2.24	0.3	0.2	0.3	0.5
164	91, 102	0.6, 0.8	−0.7, −0.4	3.54	0.3	0.1	0.3	0.4	167	91, 102	0.6, 0.8	+0.4, +0.7	3.54	0.3	0.1	0.3	0.4
165	91, 102	0.6, 0.8	−0.4, 0.0	3.06	0.2	0.1	0.2	0.3	166	91, 102	0.6, 0.8	0.0, +0.4	3.08	0.2	0.1	0.2	0.3
169	91, 102	0.8, 1.0	−1.0, −0.7	2.21	0.3	0.2	0.3	0.5	174	91, 102	0.8, 1.0	+0.7, +1.0	2.24	0.3	0.2	0.3	0.5
170	91, 102	0.8, 1.0	−0.7, −0.4	3.50	0.3	0.1	0.3	0.4	173	91, 102	0.8, 1.0	+0.4, +0.7	3.49	0.3	0.1	0.3	0.4
171	91, 102	0.8, 1.0	−0.4, 0.0	3.06	0.2	0.1	0.2	0.3	172	91, 102	0.8, 1.0	0.0, +0.4	3.03	0.2	0.1	0.2	0.3
175	91, 102	1.0, 1.2	−1.0, −0.7	1.96	0.4	0.2	0.3	0.5	180	91, 102	1.0, 1.2	+0.7, +1.0	1.96	0.3	0.2	0.3	0.5
176	91, 102	1.0, 1.2	−0.7, −0.4	3.45	0.3	0.1	0.3	0.4	179	91, 102	1.0, 1.2	+0.4, +0.7	3.46	0.2	0.1	0.3	0.4
177	91, 102	1.0, 1.2	−0.4, 0.0	3.01	0.2	0.1	0.3	0.4	178	91, 102	1.0, 1.2	0.0, +0.4	3.00	0.2	0.1	0.3	0.4
181	91, 102	1.2, 1.4	−1.0, −0.7	1.29	0.4	0.2	0.4	0.6	186	91, 102	1.2, 1.4	+0.7, +1.0	1.29	0.4	0.2	0.4	0.6
182	91, 102	1.2, 1.4	−0.7, −0.4	3.41	0.3	0.1	0.3	0.4	185	91, 102	1.2, 1.4	+0.4, +0.7	3.39	0.2	0.1	0.2	0.4
183	91, 102	1.2, 1.4	−0.4, 0.0	2.97	0.3	0.1	0.3	0.4	184	91, 102	1.2, 1.4	0.0, +0.4	2.95	0.2	0.1	0.3	0.4
187	91, 102	1.4, 1.6	−1.0, −0.7	4.87×10^{-1}	0.7	0.4	0.4	0.8	192	91, 102	1.4, 1.6	+0.7, +1.0	4.80×10^{-1}	0.6	0.4	0.4	0.8
188	91, 102	1.4, 1.6	−0.7, −0.4	3.18	0.2	0.1	0.3	0.4	191	91, 102	1.4, 1.6	+0.4, +0.7	3.16	0.2	0.1	0.3	0.4
189	91, 102	1.4, 1.6	−0.4, 0.0	2.90	0.2	0.1	0.3	0.4	190	91, 102	1.4, 1.6	0.0, +0.4	2.90	0.2	0.1	0.3	0.4
193	91, 102	1.6, 1.8	−1.0, −0.7	9.17×10^{-2}	1.5	0.9	0.5	1.8	198	91, 102	1.6, 1.8	+0.7, +1.0	9.08×10^{-2}	1.5	0.9	0.6	1.8
194	91, 102	1.6, 1.8	−0.7, −0.4	2.24	0.3	0.2	0.3	0.5	197	91, 102	1.6, 1.8	+0.4, +0.7	2.22	0.3	0.2	0.3	0.5
195	91, 102	1.6, 1.8	−0.4, 0.0	2.83	0.2	0.1	0.3	0.4	196	91, 102	1.6, 1.8	0.0, +0.4	2.84	0.2	0.1	0.3	0.4
199	91, 102	1.8, 2.0	−1.0, −0.7	2.11×10^{-2}	2.9	1.9	0.7	3.5	204	91, 102	1.8, 2.0	+0.7, +1.0	2.02×10^{-2}	2.9	1.9	1.1	3.6
200	91, 102	1.8, 2.0	−0.7, −0.4	8.08×10^{-1}	0.5	0.3	0.4	0.7	203	91, 102	1.8, 2.0	+0.4, +0.7	7.92×10^{-1}	0.5	0.3	0.4	0.7
201	91, 102	1.8, 2.0	−0.4, 0.0	2.73	0.2	0.1	0.3	0.4	202	91, 102	1.8, 2.0	0.0, +0.4	2.73	0.2	0.1	0.3	0.4
205	91, 102	2.0, 2.2	−1.0, −0.7	2.53×10^{-3}	7.9	6.1	2.2	10.3	210	91, 102	2.0, 2.2	+0.7, +1.0	2.74×10^{-3}	8.3	5.6	3.4	10.6
206	91, 102	2.0, 2.2	−0.7, −0.4	4.99×10^{-2}	2.1	1.5	0.7	2.7	209	91, 102	2.0, 2.2	+0.4, +0.7	5.03×10^{-2}	2.1	1.5	0.7	2.7
207	91, 102	2.0, 2.2	−0.4, 0.0	1.96	0.3	0.2	0.3	0.5	208	91, 102	2.0, 2.2	0.0, +0.4	1.95	0.3	0.2	0.3	0.5
211	91, 102	2.2, 2.4	−1.0, −0.7	—	—	—	—	—	216	91, 102	2.2, 2.4	+0.7, +1.0	—	—	—	—	—
212	91, 102	2.2, 2.4	−0.7, −0.4	—	—	—	—	—	215	91, 102	2.2, 2.4	+0.4, +0.7	—	—	—	—	—
213	91, 102	2.2, 2.4	−0.4, 0.0	6.54×10^{-1}	0.4	0.3	0.4	0.7	214	91, 102	2.2, 2.4	0.0, +0.4	6.46×10^{-1}	0.4	0.3	0.4	0.7
217	91, 102	0.0, 0.2	−1.0, −0.7	2.80	0.3	0.2	0.3	0.4	222	91, 102	0.0, 0.2	+0.7, +1.0	2.82	0.3	0.2	0.3	0.4
218	91, 102	0.0, 0.2	−0.7, −0.4	4.17	0.2	0.1	0.2	0.3	221	91, 102	0.0, 0.2	+0.4, +0.7	4.21	0.2	0.1	0.2	0.3
219	91, 102	0.0, 0.2	−0.4, 0.0	3.59	0.2	0.1	0.2	0.4	220	91, 102	0.0, 0.2	0.0, +0.4	3.62	0.2	0.1	0.2	0.4
223	91, 102	0.2, 0.4	−1.0, −0.7	2.78	0.3	0.2	0.3	0.4	228	91, 102	0.2, 0.4	+0.7, +1.0	2.83	0.3	0.2	0.3	0.4
224	91, 102	0.2, 0.4	−0.7, −0.4	4.11	0.3	0.1	0.2	0.3	227	91, 102	0.2, 0.4	+0.4, +0.7	4.17	0.2	0.1	0.2	0.3
225	91, 102	0.2, 0.4	−0.4, 0.0	3.58	0.2	0.1	0.2	0.4	226	91, 102	0.2, 0.4	0.0, +0.4	3.61	0.2	0.1	0.2	0.3
229	91, 102	0.4, 0.6	−1.0, −0.7	2.75	0.3	0.2	0.3	0.5	234	91, 102	0.4, 0.6	+0.7, +1.0	2.84	0.3	0.2	0.3	0.5
230	91, 102	0.4, 0.6	−0.7, −0.4	4.07	0.3	0.1	0.2	0.4	233	91, 102	0.4, 0.6	+0.4, +0.7	4.19	0.3	0.1	0.2	0.4
231	91, 102	0.4, 0.6	−0.4, 0.0	3.55	0.2	0.1	0.2	0.3	232	91, 102	0.4, 0.6	0.0, +0.4	3.59	0.2	0.1	0.2	0.3
235	91, 102	0.6, 0.8	−1.0, −0.7	2.70	0.3	0.2	0.3	0.4	240	91, 102	0.6, 0.8	+0.7, +1.0	2.86	0.3	0.1	0.3	0.4
236	91, 102	0.6, 0.8	−0.7, −0.4	4.05	0.3	0.1	0.3	0.4	239	91, 102	0.6, 0.8	+0.4, +0.7	4.20	0.3	0.1	0.3	0.4
237	91, 102	0.6, 0.8	−0.4, 0.0	3.52	0.2	0.1	0.2	0.3	238	91, 102	0.6, 0.8	0.0, +0.4	3.57	0.2	0.1	0.2	0.3
241	91, 102	0.8, 1.0	−1.0, −0.7	2.64	0.3	0.2	0.3	0.5	246	91, 102	0.8, 1.0	+0.7, +1.0	2.83	0.3	0.2	0.3	0.5
242	91, 102	0.8, 1.0	−0.7, −0.4	3.98	0.3	0.1	0.3	0.4	245	91, 102	0.8, 1.0	+0.4, +0.7	4.17	0.3	0.1	0.3	0.4
243	91, 102	0.8, 1.0	−0.4, 0.0	3.46	0.2	0.1	0.2	0.3	244	91, 102	0.8, 1.0	0.0, +0.4	3.56	0.2	0.1	0.2	0.3
247	91, 102	1.0, 1.2	−1.0, −0.7	2.23	0.3	0.2	0.3	0.5	252	91, 102	1.0, 1.2	+0.7, +1.0	2.42	0.3	0.2	0.3	0.5
248	91, 102	1.0, 1.2	−0.7, −0.4	3.91	0.2	0.1	0.3	0.4	251	91, 102	1.0, 1.2	+0.4, +0.7	4.19	0.2	0.1	0.2	0.4
249	91, 102	1.0, 1.2	−0.4, 0.0	3.41	0.2	0.1	0.3	0.4	250	91, 102	1.0, 1.2	0.0, +0.4	3.52	0.2	0.1	0.2	0.4
253	91, 102	1.2, 1.4	−1.0, −0.7	1.46	0.4	0.2	0.3	0.5	258	91, 102	1.2, 1.4	+0.7, +1.0	1.60	0.4	0.2	0.3	0.5
254	91, 102	1.2, 1.4	−0.7, −0.4	3.79	0.3	0.1	0.2	0.4	257	91, 102	1.2, 1.4	+0.4, +0.7	4.12	0.2	0.1	0.2	0.3
255	91, 102	1.2, 1.4	−0.4, 0.0	3.34	0.2	0.1	0.3	0.4	256	91, 102	1.2, 1.4	0.0, +0.4	3.48	0.2	0.1	0.3	0.4
259	91, 102	1.4, 1.6	−1.0, −0.7	5.29×10^{-1}	0.6	0.3	0.4	0.8	264	91, 102	1.4, 1.6	+0.7, +1.0	5.95×10^{-1}	0.6	0.3	0.4	0.8
260	91, 102	1.4, 1.6	−0.7, −0.4	3.48	0.2	0.1	0.3	0.4	263	91, 102	1.4, 1.6	+0.4, +0.7	3.84	0.2	0.1	0.2	0.4
261	91, 102	1.4, 1.6	−0.4, 0.0	3.27	0.2	0.1	0.3	0.4	262	91, 102	1.4, 1.6	0.0, +0.4	3.42	0.2	0.1	0.3	0.4
265	91, 102	1.6, 1.8	−1.0, −0.7	9.80×10^{-2}	1.5	1.0	0.7	1.9	270	91, 102	1.6, 1.8	+0.7, +1.0	1.13×10^{-1}	1.3	0.9	0.6	1.7
266	91, 102	1.6, 1.8	−0.7, −0.4	2.41	0.3	0.1	0.3	0.5	269	91, 102	1.6, 1.8	+0.4, +0.7	2.70	0.3	0.1	0.3	0.4
267	91, 102	1.6, 1.8	−0.4, 0.0	3.20	0.2	0.1	0.3	0.4	268	91, 102	1.6, 1.8	0.0, +0.4	3.37	0.2	0.1	0.3	0.4
271	91, 102	1.8, 2.0	−1.0, −0.7	2.17×10^{-2}	3.0	1.8	0.9	3.7	276	91, 102	1.8, 2.0	+0.7, +1.0	2.36×10^{-2}	2.8	1.7	0.8	3.4
272	91, 102	1.8, 2.0	−0.7, −0.4	8.61×10^{-1}	0.5	0.3	0.5	0.7	275	91, 102	1.8, 2.0	+0.4, +0.7	9.82×10^{-1}	0.5	0.3	0.4	0.7
273	91, 102	1.8, 2.0	−0.4, 0.0	3.03	0.2	0.1	0.3	0.4	274	91, 102	1.8, 2.0	0.0, +0.4	3.23	0.2	0.1	0.3	0.4
277	91, 102	2.0, 2.2	−1.0, −0.7	2.30×10^{-3}	10.6	8.0	5.2	14.3	282	91, 102	2.0, 2.2	+0.7, +1.0	3.47×10^{-3}	7.6	5.2	2.6	9.6
278	91, 102	2.0, 2.2	−0.7, −0.4	5.15×10^{-2}	2.0	1.3	1.0	2.6	281	91, 102	2.0, 2.2	+0.4, +0.7	6.30×10^{-2}	1.9	1.2	1.0	2.5
279	91, 102	2.0, 2.2	−0.4, 0.0	2.17	0.3	0.1	0.3	0.4	280	91, 102	2.0, 2.2	0.0, +0.4	2.32	0.3	0.1	0.3	0.4
283	91, 102	2.2, 2.4	−1.0, −0.7	—	—	—	—	—	288	91, 102	2.2, 2.4	+0.7, +1.0	—	—	—	—	—
284	91, 102	2.2, 2.4	−0.7, −0.4	—	—	—	—	—	287	91, 102	2.2, 2.4	+0.4, +0.7	—	—	—	—	—
285	91, 102	2.2, 2.4	−0.4, 0.0	7.30×10^{-1}	0.4	0.2	0.4	0.7	286	91, 102	2.2, 2.4	0.0, +0.4	7.59×10^{-1}	0.4	0.2	0.4	0.6

JHEP12(2017)059

Bin	$m_{\ell\ell}$ [GeV]	$\lvert y_{\ell\ell}\rvert$	$\cos\theta^*$	$\mathrm{d}^3\sigma$ [pb/GeV]	δ^{stat} [%]	$\delta^{\text{syst}}_{\text{unc}}$ [%]	$\delta^{\text{syst}}_{\text{cor}}$ [%]	δ^{total} [%]	Bin	$m_{\ell\ell}$ [GeV]	$\lvert y_{\ell\ell}\rvert$	$\cos\theta^*$	$\mathrm{d}^3\sigma$ [pb/GeV]	δ^{stat} [%]	$\delta^{\text{syst}}_{\text{unc}}$ [%]	$\delta^{\text{syst}}_{\text{cor}}$ [%]	δ^{total} [%]
289	102, 116	0.0, 0.2	−1.0, −0.7	1.09×10^{-1}	1.4	0.8	0.6	1.7	294	102, 116	0.0, 0.2	+0.7, +1.0	1.09×10^{-1}	1.4	0.8	0.6	1.7
290	102, 116	0.0, 0.2	−0.7, −0.4	1.30×10^{-1}	1.2	0.6	0.4	1.4	293	102, 116	0.0, 0.2	+0.4, +0.7	1.39×10^{-1}	1.2	0.5	0.3	1.4
291	102, 116	0.0, 0.2	−0.4, 0.0	1.15×10^{-1}	1.2	0.5	0.3	1.4	292	102, 116	0.0, 0.2	0.0, +0.4	1.15×10^{-1}	1.2	0.5	0.4	1.4
295	102, 116	0.2, 0.4	−1.0, −0.7	1.03×10^{-1}	1.5	0.8	0.6	1.8	300	102, 116	0.2, 0.4	+0.7, +1.0	1.11×10^{-1}	1.5	0.8	0.6	1.7
296	102, 116	0.2, 0.4	−0.7, −0.4	1.33×10^{-1}	1.2	0.6	0.4	1.4	299	102, 116	0.2, 0.4	+0.4, +0.7	1.39×10^{-1}	1.2	0.5	0.4	1.4
297	102, 116	0.2, 0.4	−0.4, 0.0	1.14×10^{-1}	1.2	0.5	0.4	1.3	298	102, 116	0.2, 0.4	0.0, +0.4	1.19×10^{-1}	1.2	0.5	0.4	1.3
301	102, 116	0.4, 0.6	−1.0, −0.7	1.01×10^{-1}	1.5	0.8	0.6	1.8	306	102, 116	0.4, 0.6	+0.7, +1.0	1.13×10^{-1}	1.4	0.7	0.6	1.7
302	102, 116	0.4, 0.6	−0.7, −0.4	1.25×10^{-1}	1.3	0.7	0.4	1.5	305	102, 116	0.4, 0.6	+0.4, +0.7	1.40×10^{-1}	1.2	0.6	0.4	1.4
303	102, 116	0.4, 0.6	−0.4, 0.0	1.12×10^{-1}	1.1	0.5	0.4	1.3	304	102, 116	0.4, 0.6	0.0, +0.4	1.15×10^{-1}	1.1	0.5	0.3	1.3
307	102, 116	0.6, 0.8	−1.0, −0.7	9.95×10^{-2}	1.4	0.8	0.7	1.8	312	102, 116	0.6, 0.8	+0.7, +1.0	1.14×10^{-1}	1.4	0.7	0.7	1.7
308	102, 116	0.6, 0.8	−0.7, −0.4	1.21×10^{-1}	1.4	0.7	0.5	1.6	311	102, 116	0.6, 0.8	+0.4, +0.7	1.40×10^{-1}	1.3	0.7	0.5	1.6
309	102, 116	0.6, 0.8	−0.4, 0.0	1.12×10^{-1}	1.1	0.5	0.4	1.3	310	102, 116	0.6, 0.8	0.0, +0.4	1.15×10^{-1}	1.1	0.5	0.3	1.3
313	102, 116	0.8, 1.0	−1.0, −0.7	8.72×10^{-2}	1.6	0.9	0.6	1.9	318	102, 116	0.8, 1.0	+0.7, +1.0	1.11×10^{-1}	1.4	0.8	0.6	1.7
314	102, 116	0.8, 1.0	−0.7, −0.4	1.19×10^{-1}	1.3	0.7	0.5	1.6	317	102, 116	0.8, 1.0	+0.4, +0.7	1.47×10^{-1}	1.2	0.6	0.5	1.4
315	102, 116	0.8, 1.0	−0.4, 0.0	1.07×10^{-1}	1.1	0.7	0.4	1.4	316	102, 116	0.8, 1.0	0.0, +0.4	1.18×10^{-1}	1.0	0.5	0.4	1.2
319	102, 116	1.0, 1.2	−1.0, −0.7	6.74×10^{-2}	1.7	1.0	0.7	2.1	324	102, 116	1.0, 1.2	+0.7, +1.0	9.14×10^{-2}	1.5	0.8	0.6	1.8
320	102, 116	1.0, 1.2	−0.7, −0.4	1.13×10^{-1}	1.2	0.7	0.5	1.5	323	102, 116	1.0, 1.2	+0.4, +0.7	1.49×10^{-1}	1.1	0.6	0.5	1.3
321	102, 116	1.0, 1.2	−0.4, 0.0	1.06×10^{-1}	1.1	0.6	0.5	1.4	322	102, 116	1.0, 1.2	0.0, +0.4	1.18×10^{-1}	1.1	0.5	0.5	1.3
325	102, 116	1.2, 1.4	−1.0, −0.7	4.21×10^{-2}	1.9	1.2	1.1	2.5	330	102, 116	1.2, 1.4	+0.7, +1.0	5.84×10^{-2}	1.7	1.0	0.8	2.1
326	102, 116	1.2, 1.4	−0.7, −0.4	1.09×10^{-1}	1.2	0.6	0.6	1.5	329	102, 116	1.2, 1.4	+0.4, +0.7	1.50×10^{-1}	1.0	0.6	0.5	1.3
327	102, 116	1.2, 1.4	−0.4, 0.0	1.01×10^{-1}	1.1	0.6	0.6	1.4	328	102, 116	1.2, 1.4	0.0, +0.4	1.19×10^{-1}	1.1	0.7	0.7	1.5
331	102, 116	1.4, 1.6	−1.0, −0.7	1.39×10^{-2}	2.5	1.9	1.5	3.5	336	102, 116	1.4, 1.6	+0.7, +1.0	2.25×10^{-2}	2.2	1.6	1.5	3.1
332	102, 116	1.4, 1.6	−0.7, −0.4	9.53×10^{-2}	1.2	0.7	0.6	1.5	335	102, 116	1.4, 1.6	+0.4, +0.7	1.37×10^{-1}	1.1	0.6	0.6	1.3
333	102, 116	1.4, 1.6	−0.4, 0.0	9.77×10^{-2}	1.1	0.6	0.7	1.5	334	102, 116	1.4, 1.6	0.0, +0.4	1.17×10^{-1}	1.0	0.6	0.6	1.3
337	102, 116	1.6, 1.8	−1.0, −0.7	2.35×10^{-3}	4.6	4.9	2.8	7.3	342	102, 116	1.6, 1.8	+0.7, +1.0	4.19×10^{-3}	4.2	3.8	2.2	6.1
338	102, 116	1.6, 1.8	−0.7, −0.4	6.43×10^{-2}	1.2	0.9	1.0	1.8	341	102, 116	1.6, 1.8	+0.4, +0.7	1.01×10^{-1}	1.1	0.7	0.9	1.6
339	102, 116	1.6, 1.8	−0.4, 0.0	9.25×10^{-2}	1.1	0.7	1.0	1.6	340	102, 116	1.6, 1.8	0.0, +0.4	1.16×10^{-1}	1.0	0.7	0.8	1.5
343	102, 116	1.8, 2.0	−1.0, −0.7	4.34×10^{-4}	6.1	11.4	3.4	13.4	348	102, 116	1.8, 2.0	+0.7, +1.0	8.65×10^{-4}	8.2	9.1	2.9	12.6
344	102, 116	1.8, 2.0	−0.7, −0.4	2.13×10^{-2}	1.7	1.5	1.6	2.8	347	102, 116	1.8, 2.0	+0.4, +0.7	3.56×10^{-2}	1.5	1.3	1.5	2.5
345	102, 116	1.8, 2.0	−0.4, 0.0	8.89×10^{-2}	1.0	0.6	0.9	1.5	346	102, 116	1.8, 2.0	0.0, +0.4	1.14×10^{-1}	0.9	0.6	0.9	1.4
349	102, 116	2.0, 2.2	−1.0, −0.7	—	—	—	—	—	354	102, 116	2.0, 2.2	+0.7, +1.0	—	—	—	—	—
350	102, 116	2.0, 2.2	−0.7, −0.4	1.39×10^{-3}	3.3	5.6	3.5	7.4	353	102, 116	2.0, 2.2	+0.4, +0.7	2.22×10^{-3}	3.6	4.9	2.2	6.5
351	102, 116	2.0, 2.2	−0.4, 0.0	6.28×10^{-2}	1.0	0.8	1.3	1.8	352	102, 116	2.0, 2.2	0.0, +0.4	7.95×10^{-2}	0.9	0.7	1.1	1.6
355	102, 116	2.2, 2.4	−1.0, −0.7	—	—	—	—	—	360	102, 116	2.2, 2.4	+0.7, +1.0	—	—	—	—	—
356	102, 116	2.2, 2.4	−0.7, −0.4	—	—	—	—	—	359	102, 116	2.2, 2.4	+0.4, +0.7	—	—	—	—	—
357	102, 116	2.2, 2.4	−0.4, 0.0	2.17×10^{-2}	1.4	1.4	1.9	2.7	358	102, 116	2.2, 2.4	0.0, +0.4	2.45×10^{-2}	1.3	1.3	1.6	2.5
361	116, 150	0.0, 0.2	−1.0, −0.7	2.39×10^{-2}	2.4	1.1	1.4	3.0	366	116, 150	0.0, 0.2	+0.7, +1.0	2.59×10^{-2}	2.2	1.0	1.3	2.7
362	116, 150	0.0, 0.2	−0.7, −0.4	2.59×10^{-2}	1.9	0.6	0.8	2.1	365	116, 150	0.0, 0.2	+0.4, +0.7	2.69×10^{-2}	1.9	0.6	0.7	2.1
363	116, 150	0.0, 0.2	−0.4, 0.0	2.16×10^{-2}	1.9	0.9	0.6	2.2	364	116, 150	0.0, 0.2	0.0, +0.4	2.25×10^{-2}	1.8	0.7	0.6	2.0
367	116, 150	0.2, 0.4	−1.0, −0.7	2.29×10^{-2}	2.3	1.2	1.5	3.0	372	116, 150	0.2, 0.4	+0.7, +1.0	2.54×10^{-2}	2.3	1.2	1.3	2.8
368	116, 150	0.2, 0.4	−0.7, −0.4	2.45×10^{-2}	2.1	0.8	0.8	2.4	371	116, 150	0.2, 0.4	+0.4, +0.7	2.88×10^{-2}	1.9	0.6	0.7	2.1
369	116, 150	0.2, 0.4	−0.4, 0.0	2.10×10^{-2}	1.9	0.6	0.7	2.1	370	116, 150	0.2, 0.4	0.0, +0.4	2.25×10^{-2}	1.8	0.5	0.6	2.0
373	116, 150	0.4, 0.6	−1.0, −0.7	2.11×10^{-2}	2.4	1.0	1.6	3.1	378	116, 150	0.4, 0.6	+0.7, +1.0	2.64×10^{-2}	2.3	1.1	1.3	2.8
374	116, 150	0.4, 0.6	−0.7, −0.4	2.44×10^{-2}	2.1	0.7	0.8	2.4	377	116, 150	0.4, 0.6	+0.4, +0.7	2.81×10^{-2}	2.0	0.7	0.7	2.2
375	116, 150	0.4, 0.6	−0.4, 0.0	2.10×10^{-2}	1.8	0.7	0.6	2.0	376	116, 150	0.4, 0.6	0.0, +0.4	2.26×10^{-2}	1.7	0.5	0.6	1.9
379	116, 150	0.6, 0.8	−1.0, −0.7	2.07×10^{-2}	2.4	1.0	1.5	3.0	384	116, 150	0.6, 0.8	+0.7, +1.0	2.69×10^{-2}	2.0	0.8	1.1	2.4
380	116, 150	0.6, 0.8	−0.7, −0.4	2.32×10^{-2}	2.3	0.8	0.9	2.5	383	116, 150	0.6, 0.8	+0.4, +0.7	2.93×10^{-2}	2.0	0.8	0.7	2.3
381	116, 150	0.6, 0.8	−0.4, 0.0	2.06×10^{-2}	1.8	0.6	0.6	2.0	382	116, 150	0.6, 0.8	0.0, +0.4	2.36×10^{-2}	1.7	0.5	0.5	1.9
385	116, 150	0.8, 1.0	−1.0, −0.7	1.69×10^{-2}	2.6	1.2	1.5	3.3	390	116, 150	0.8, 1.0	+0.7, +1.0	2.37×10^{-2}	2.1	0.9	1.1	2.6
386	116, 150	0.8, 1.0	−0.7, −0.4	2.18×10^{-2}	2.3	0.9	0.8	2.6	389	116, 150	0.8, 1.0	+0.4, +0.7	3.03×10^{-2}	1.9	0.7	0.6	2.1
387	116, 150	0.8, 1.0	−0.4, 0.0	2.08×10^{-2}	1.8	0.6	0.6	2.0	388	116, 150	0.8, 1.0	0.0, +0.4	2.30×10^{-2}	1.7	0.6	0.5	1.9
391	116, 150	1.0, 1.2	−1.0, −0.7	1.21×10^{-2}	3.1	1.6	1.3	3.7	396	116, 150	1.0, 1.2	+0.7, +1.0	1.90×10^{-2}	2.4	1.2	1.1	2.9
392	116, 150	1.0, 1.2	−0.7, −0.4	1.99×10^{-2}	2.2	0.9	0.8	2.5	395	116, 150	1.0, 1.2	+0.4, +0.7	3.07×10^{-2}	1.8	0.6	0.6	2.0
393	116, 150	1.0, 1.2	−0.4, 0.0	2.05×10^{-2}	1.9	0.8	0.6	2.1	394	116, 150	1.0, 1.2	0.0, +0.4	2.39×10^{-2}	1.7	0.6	0.6	1.9
397	116, 150	1.2, 1.4	−1.0, −0.7	8.16×10^{-3}	3.6	1.5	1.3	4.1	402	116, 150	1.2, 1.4	+0.7, +1.0	1.38×10^{-2}	2.7	1.0	0.8	3.0
398	116, 150	1.2, 1.4	−0.7, −0.4	1.82×10^{-2}	2.2	1.1	0.8	2.6	401	116, 150	1.2, 1.4	+0.4, +0.7	3.11×10^{-2}	1.7	0.7	0.6	1.9
399	116, 150	1.2, 1.4	−0.4, 0.0	1.87×10^{-2}	2.0	0.8	0.6	2.2	400	116, 150	1.2, 1.4	0.0, +0.4	2.39×10^{-2}	1.8	0.7	0.6	2.0
403	116, 150	1.4, 1.6	−1.0, −0.7	2.40×10^{-3}	6.3	2.9	2.0	7.2	408	116, 150	1.4, 1.6	+0.7, +1.0	4.68×10^{-3}	4.4	2.5	1.2	5.2
404	116, 150	1.4, 1.6	−0.7, −0.4	1.64×10^{-2}	2.2	0.9	0.8	2.6	407	116, 150	1.4, 1.6	+0.4, +0.7	2.96×10^{-2}	1.7	0.7	0.6	1.9
405	116, 150	1.4, 1.6	−0.4, 0.0	1.79×10^{-2}	2.0	0.9	0.7	2.3	406	116, 150	1.4, 1.6	0.0, +0.4	2.30×10^{-2}	1.7	0.8	0.5	2.0
409	116, 150	1.6, 1.8	−1.0, −0.7	3.00×10^{-4}	70.7	18.8	4.6	73.3	414	116, 150	1.6, 1.8	+0.7, +1.0	9.12×10^{-4}	9.2	7.6	2.1	12.2
410	116, 150	1.6, 1.8	−0.7, −0.4	1.09×10^{-2}	2.8	1.2	0.9	3.1	413	116, 150	1.6, 1.8	+0.4, +0.7	2.23×10^{-2}	2.0	0.9	0.7	2.3
411	116, 150	1.6, 1.8	−0.4, 0.0	1.72×10^{-2}	2.0	0.9	0.7	2.3	412	116, 150	1.6, 1.8	0.0, +0.4	2.36×10^{-2}	1.8	0.9	0.6	2.0
415	116, 150	1.8, 2.0	−1.0, −0.7	—	—	—	—	—	420	116, 150	1.8, 2.0	+0.7, +1.0	—	—	—	—	—
416	116, 150	1.8, 2.0	−0.7, −0.4	3.51×10^{-3}	4.7	2.7	1.8	5.7	419	116, 150	1.8, 2.0	+0.4, +0.7	7.66×10^{-3}	3.5	2.0	1.3	4.2
417	116, 150	1.8, 2.0	−0.4, 0.0	1.66×10^{-2}	2.1	1.2	0.8	2.6	418	116, 150	1.8, 2.0	0.0, +0.4	2.33×10^{-2}	1.8	1.0	0.7	2.2
421	116, 150	2.0, 2.2	−1.0, −0.7	—	—	—	—	—	426	116, 150	2.0, 2.2	+0.7, +1.0	—	—	—	—	—
422	116, 150	2.0, 2.2	−0.7, −0.4	2.20×10^{-4}	8.3	8.9	6.0	13.5	425	116, 150	2.0, 2.2	+0.4, +0.7	4.66×10^{-4}	9.7	7.6	3.8	12.9
423	116, 150	2.0, 2.2	−0.4, 0.0	1.20×10^{-2}	2.1	1.0	0.9	2.5	424	116, 150	2.0, 2.2	0.0, +0.4	1.65×10^{-2}	1.9	0.9	0.8	2.2
427	116, 150	2.2, 2.4	−1.0, −0.7	—	—	—	—	—	432	116, 150	2.2, 2.4	+0.7, +1.0	—	—	—	—	—
428	116, 150	2.2, 2.4	−0.7, −0.4	—	—	—	—	—	431	116, 150	2.2, 2.4	+0.4, +0.7	—	—	—	—	—
429	116, 150	2.2, 2.4	−0.4, 0.0	3.94×10^{-3}	3.8	2.5	1.9	4.9	430	116, 150	2.2, 2.4	0.0, +0.4	4.75×10^{-3}	3.5	2.2	1.9	4.5

JHEP12(2017)059

Bin	$m_{\ell\ell}$ [GeV]	$\lvert y_{\ell\ell}\rvert$	$\cos\theta^*$	$\mathrm{d}^3\sigma$ [pb/GeV]	δ^{stat} [%]	$\delta^{\mathrm{syst}}_{\mathrm{unc}}$ [%]	$\delta^{\mathrm{syst}}_{\mathrm{cor}}$ [%]	δ^{total} [%]	Bin	$m_{\ell\ell}$ [GeV]	$\lvert y_{\ell\ell}\rvert$	$\cos\theta^*$	$\mathrm{d}^3\sigma$ [pb/GeV]	δ^{stat} [%]	$\delta^{\mathrm{syst}}_{\mathrm{unc}}$ [%]	$\delta^{\mathrm{syst}}_{\mathrm{cor}}$ [%]	δ^{total} [%]
433	150, 200	0.0, 0.2	−1.0, −0.7	6.26×10^{-3}	4.2	1.6	2.8	5.3	438	150, 200	0.0, 0.2	+0.7, +1.0	6.55×10^{-3}	4.3	1.7	2.8	5.4
434	150, 200	0.0, 0.2	−0.7, −0.4	5.56×10^{-3}	3.7	1.2	1.6	4.2	437	150, 200	0.0, 0.2	+0.4, +0.7	5.91×10^{-3}	3.6	1.3	1.6	4.1
435	150, 200	0.0, 0.2	−0.4, 0.0	4.77×10^{-3}	3.4	1.3	1.2	3.8	436	150, 200	0.0, 0.2	0.0, +0.4	4.76×10^{-3}	3.5	0.7	1.1	3.7
439	150, 200	0.2, 0.4	−1.0, −0.7	5.66×10^{-3}	4.6	1.7	3.2	5.8	444	150, 200	0.2, 0.4	+0.7, +1.0	6.67×10^{-3}	4.0	2.0	2.7	5.2
440	150, 200	0.2, 0.4	−0.7, −0.4	5.41×10^{-3}	3.9	1.9	1.6	4.7	443	150, 200	0.2, 0.4	+0.4, +0.7	5.96×10^{-3}	3.6	1.9	2.5	4.8
441	150, 200	0.2, 0.4	−0.4, 0.0	4.81×10^{-3}	3.4	0.9	1.2	3.7	442	150, 200	0.2, 0.4	0.0, +0.4	4.97×10^{-3}	3.2	1.0	1.2	3.6
445	150, 200	0.4, 0.6	−1.0, −0.7	4.73×10^{-3}	4.8	2.2	3.3	6.2	450	150, 200	0.4, 0.6	+0.7, +1.0	7.08×10^{-3}	3.7	1.3	2.3	4.6
446	150, 200	0.4, 0.6	−0.7, −0.4	5.52×10^{-3}	3.9	1.0	1.6	4.3	449	150, 200	0.4, 0.6	+0.4, +0.7	6.26×10^{-3}	3.6	1.2	1.4	4.0
447	150, 200	0.4, 0.6	−0.4, 0.0	4.56×10^{-3}	3.4	0.8	1.1	3.7	448	150, 200	0.4, 0.6	0.0, +0.4	4.79×10^{-3}	3.4	1.9	1.1	4.1
451	150, 200	0.6, 0.8	−1.0, −0.7	4.51×10^{-3}	4.7	1.9	3.0	5.9	456	150, 200	0.6, 0.8	+0.7, +1.0	6.21×10^{-3}	3.8	1.3	2.2	4.6
452	150, 200	0.6, 0.8	−0.7, −0.4	5.18×10^{-3}	4.2	1.5	1.7	4.8	455	150, 200	0.6, 0.8	+0.4, +0.7	6.90×10^{-3}	3.5	0.8	1.2	3.8
453	150, 200	0.6, 0.8	−0.4, 0.0	4.26×10^{-3}	3.4	1.2	1.2	3.8	454	150, 200	0.6, 0.8	0.0, +0.4	5.26×10^{-3}	3.1	0.6	1.0	3.3
457	150, 200	0.8, 1.0	−1.0, −0.7	3.32×10^{-3}	5.4	2.3	3.2	6.7	462	150, 200	0.8, 1.0	+0.7, +1.0	6.01×10^{-3}	3.8	1.5	1.8	4.5
458	150, 200	0.8, 1.0	−0.7, −0.4	4.91×10^{-3}	4.3	1.1	1.7	4.8	461	150, 200	0.8, 1.0	+0.4, +0.7	6.43×10^{-3}	3.7	1.3	1.3	4.1
459	150, 200	0.8, 1.0	−0.4, 0.0	4.28×10^{-3}	3.5	0.8	1.1	3.7	460	150, 200	0.8, 1.0	0.0, +0.4	5.18×10^{-3}	3.1	0.7	0.9	3.3
463	150, 200	1.0, 1.2	−1.0, −0.7	2.39×10^{-3}	6.4	2.4	3.0	7.5	468	150, 200	1.0, 1.2	+0.7, +1.0	4.66×10^{-3}	4.2	1.8	1.8	4.9
464	150, 200	1.0, 1.2	−0.7, −0.4	4.03×10^{-3}	4.4	1.7	1.8	5.1	467	150, 200	1.0, 1.2	+0.4, +0.7	6.99×10^{-3}	3.2	1.1	1.0	3.5
465	150, 200	1.0, 1.2	−0.4, 0.0	4.13×10^{-3}	3.7	1.2	1.3	4.1	466	150, 200	1.0, 1.2	0.0, +0.4	5.40×10^{-3}	3.1	1.2	0.9	3.5
469	150, 200	1.2, 1.4	−1.0, −0.7	1.46×10^{-3}	8.1	4.1	2.8	9.5	474	150, 200	1.2, 1.4	+0.7, +1.0	3.19×10^{-3}	5.0	2.4	1.5	5.7
470	150, 200	1.2, 1.4	−0.7, −0.4	3.80×10^{-3}	4.4	2.1	1.8	5.2	473	150, 200	1.2, 1.4	+0.4, +0.7	7.42×10^{-3}	3.0	1.0	0.9	3.3
471	150, 200	1.2, 1.4	−0.4, 0.0	4.04×10^{-3}	3.8	1.3	1.2	4.2	472	150, 200	1.2, 1.4	0.0, +0.4	5.48×10^{-3}	3.3	0.8	0.9	3.5
475	150, 200	1.4, 1.6	−1.0, −0.7	4.78×10^{-4}	24.4	14.5	3.2	28.6	480	150, 200	1.4, 1.6	+0.7, +1.0	1.06×10^{-3}	8.4	5.8	2.2	10.4
476	150, 200	1.4, 1.6	−0.7, −0.4	3.12×10^{-3}	4.9	2.4	2.0	5.9	479	150, 200	1.4, 1.6	+0.4, +0.7	6.69×10^{-3}	3.1	2.0	0.9	3.8
477	150, 200	1.4, 1.6	−0.4, 0.0	3.84×10^{-3}	3.8	1.4	1.2	4.2	478	150, 200	1.4, 1.6	0.0, +0.4	5.48×10^{-3}	3.1	1.1	0.8	3.4
481	150, 200	1.6, 1.8	−1.0, −0.7	—	—	—	—	—	486	150, 200	1.6, 1.8	+0.7, +1.0	—	—	—	—	—
482	150, 200	1.6, 1.8	−0.7, −0.4	1.96×10^{-3}	5.9	2.0	2.0	6.5	485	150, 200	1.6, 1.8	+0.4, +0.7	5.25×10^{-3}	3.5	1.2	0.9	3.8
483	150, 200	1.6, 1.8	−0.4, 0.0	3.65×10^{-3}	3.9	1.6	1.5	4.5	484	150, 200	1.6, 1.8	0.0, +0.4	5.22×10^{-3}	3.2	1.1	0.8	3.5
487	150, 200	1.8, 2.0	−1.0, −0.7	—	—	—	—	—	492	150, 200	1.8, 2.0	+0.7, +1.0	—	—	—	—	—
488	150, 200	1.8, 2.0	−0.7, −0.4	5.67×10^{-4}	11.8	4.8	4.4	13.4	491	150, 200	1.8, 2.0	+0.4, +0.7	1.62×10^{-3}	6.4	1.9	1.6	6.9
489	150, 200	1.8, 2.0	−0.4, 0.0	3.36×10^{-3}	3.8	0.9	1.0	4.0	490	150, 200	1.8, 2.0	0.0, +0.4	5.16×10^{-3}	3.0	0.9	0.7	3.2
493	150, 200	2.0, 2.2	−1.0, −0.7	—	—	—	—	—	498	150, 200	2.0, 2.2	+0.7, +1.0	—	—	—	—	—
494	150, 200	2.0, 2.2	−0.7, −0.4	—	—	—	—	—	497	150, 200	2.0, 2.2	+0.4, +0.7	—	—	—	—	—
495	150, 200	2.0, 2.2	−0.4, 0.0	2.47×10^{-3}	4.4	1.7	1.3	4.9	496	150, 200	2.0, 2.2	0.0, +0.4	3.68×10^{-3}	3.5	1.2	0.8	3.8
499	150, 200	2.2, 2.4	−1.0, −0.7	—	—	—	—	—	504	150, 200	2.2, 2.4	+0.7, +1.0	—	—	—	—	—
500	150, 200	2.2, 2.4	−0.7, −0.4	—	—	—	—	—	503	150, 200	2.2, 2.4	+0.4, +0.7	—	—	—	—	—
501	150, 200	2.2, 2.4	−0.4, 0.0	8.93×10^{-4}	7.0	2.0	1.7	7.5	502	150, 200	2.2, 2.4	0.0, +0.4	1.15×10^{-3}	6.3	1.8	1.3	6.6

Table 7. The combined Born-level triple-differential cross section $\mathrm{d}^3\sigma/\mathrm{d}m_{\ell\ell}\mathrm{d}|y_{\ell\ell}|\mathrm{d}\cos\theta^*$. The measurements are listed together with the statistical (δ^{stat}), uncorrelated systematic ($\delta^{\mathrm{syst}}_{\mathrm{unc}}$), correlated systematic ($\delta^{\mathrm{syst}}_{\mathrm{cor}}$), and total ($\delta^{\mathrm{total}}$) uncertainties. The luminosity uncertainty of 1.9% is not shown and not included in the overall systematic and total uncertainties.

JHEP12(2017)059

Bin	m_{ee} [GeV]	$\lvert y_{ee}\rvert$	$\cos\theta^*$	$\mathrm{d}^3\sigma$ [pb/GeV]	δ^{stat} [%]	$\delta^{\mathrm{syst}}_{\mathrm{unc}}$ [%]	$\delta^{\mathrm{syst}}_{\mathrm{cor}}$ [%]	δ^{total} [%]	Bin	m_{ee} [GeV]	$\lvert y_{ee}\rvert$	$\cos\theta^*$	$\mathrm{d}^3\sigma$ [pb/GeV]	δ^{stat} [%]	$\delta^{\mathrm{syst}}_{\mathrm{unc}}$ [%]	$\delta^{\mathrm{syst}}_{\mathrm{cor}}$ [%]	δ^{total} [%]
1	66, 80	1.2, 1.6	−1.0, −0.7	1.06×10^{-2}	6.4	8.1	12.4	16.1	6	66, 80	1.2, 1.6	+0.7, +1.0	6.29×10^{-3}	7.8	11.0	16.1	21.0
2	66, 80	1.2, 1.6	−0.7, −0.4	9.24×10^{-4}	16.2	15.4	15.3	27.1	5	66, 80	1.2, 1.6	+0.4, +0.7	6.97×10^{-4}	15.7	13.1	15.5	25.7
3	66, 80	1.2, 1.6	−0.4, 0.0	—	—	—	—	—	4	66, 80	1.2, 1.6	0.0, +0.4	—	—	—	—	—
7	66, 80	1.6, 2.0	−1.0, −0.7	3.89×10^{-2}	3.9	3.8	7.0	8.9	12	66, 80	1.6, 2.0	+0.7, +1.0	2.24×10^{-2}	5.1	6.7	10.4	13.3
8	66, 80	1.6, 2.0	−0.7, −0.4	6.54×10^{-2}	2.8	2.6	5.1	6.4	11	66, 80	1.6, 2.0	+0.4, +0.7	4.27×10^{-2}	3.2	3.5	6.1	7.8
9	66, 80	1.6, 2.0	−0.4, 0.0	—	—	—	—	—	10	66, 80	1.6, 2.0	0.0, +0.4	—	—	—	—	—
13	66, 80	2.0, 2.4	−1.0, −0.7	4.28×10^{-2}	6.2	6.6	13.1	16.0	18	66, 80	2.0, 2.4	+0.7, +1.0	2.08×10^{-2}	7.3	8.6	25.4	27.8
14	66, 80	2.0, 2.4	−0.7, −0.4	1.89×10^{-1}	2.0	2.1	4.4	5.2	17	66, 80	2.0, 2.4	+0.4, +0.7	9.97×10^{-2}	2.6	3.4	6.0	7.3
15	66, 80	2.0, 2.4	−0.4, 0.0	5.10×10^{-2}	2.5	2.5	5.4	6.5	16	66, 80	2.0, 2.4	0.0, +0.4	3.55×10^{-2}	2.8	3.2	6.3	7.6
19	66, 80	2.4, 2.8	−1.0, −0.7	3.91×10^{-2}	3.5	3.8	19.5	20.2	24	66, 80	2.4, 2.8	+0.7, +1.0	1.65×10^{-2}	4.3	5.7	26.9	27.9
20	66, 80	2.4, 2.8	−0.7, −0.4	1.89×10^{-1}	2.2	2.2	11.3	11.8	23	66, 80	2.4, 2.8	+0.4, +0.7	8.98×10^{-2}	2.7	3.1	17.5	18.0
21	66, 80	2.4, 2.8	−0.4, 0.0	8.40×10^{-2}	2.3	1.9	2.4	3.8	22	66, 80	2.4, 2.8	0.0, +0.4	5.24×10^{-2}	2.8	2.7	3.9	5.5
25	66, 80	2.8, 3.6	−1.0, −0.7	2.14×10^{-2}	3.0	3.1	18.4	18.9	30	66, 80	2.8, 3.6	+0.7, +1.0	7.09×10^{-3}	3.8	7.4	32.7	33.8
26	66, 80	2.8, 3.6	−0.7, −0.4	4.84×10^{-2}	2.1	1.9	10.3	10.7	29	66, 80	2.8, 3.6	+0.4, +0.7	1.79×10^{-2}	2.8	3.2	15.2	15.7
27	66, 80	2.8, 3.6	−0.4, 0.0	—	—	—	—	—	28	66, 80	2.8, 3.6	0.0, +0.4	—	—	—	—	—
31	80, 91	1.2, 1.6	−1.0, −0.7	5.20×10^{-1}	0.9	0.7	2.4	2.7	36	80, 91	1.2, 1.6	+0.7, +1.0	5.29×10^{-1}	0.9	0.7	2.6	2.8
32	80, 91	1.2, 1.6	−0.7, −0.4	3.07×10^{-2}	3.6	2.6	3.4	5.6	35	80, 91	1.2, 1.6	+0.4, +0.7	3.07×10^{-2}	3.5	2.8	3.6	5.8
33	80, 91	1.2, 1.6	−0.4, 0.0	—	—	—	—	—	34	80, 91	1.2, 1.6	0.0, +0.4	—	—	—	—	—
37	80, 91	1.6, 2.0	−1.0, −0.7	1.26	0.7	0.4	2.7	2.8	42	80, 91	1.6, 2.0	+0.7, +1.0	1.28	0.6	0.4	2.6	2.7
38	80, 91	1.6, 2.0	−0.7, −0.4	1.04	0.7	0.5	1.7	1.9	41	80, 91	1.6, 2.0	+0.4, +0.7	1.04	0.7	0.5	1.7	1.9
39	80, 91	1.6, 2.0	−0.4, 0.0	5.59×10^{-3}	7.9	4.4	4.4	10.0	40	80, 91	1.6, 2.0	0.0, +0.4	5.05×10^{-3}	7.4	4.6	3.5	9.4
43	80, 91	2.0, 2.4	−1.0, −0.7	1.28	0.9	0.8	2.7	2.9	48	80, 91	2.0, 2.4	+0.7, +1.0	1.24	0.9	0.7	2.6	2.9
44	80, 91	2.0, 2.4	−0.7, −0.4	2.71	0.5	0.4	1.4	1.5	47	80, 91	2.0, 2.4	+0.4, +0.7	2.66	0.5	0.4	1.5	1.6
45	80, 91	2.0, 2.4	−0.4, 0.0	7.32×10^{-1}	0.6	0.6	1.8	2.0	46	80, 91	2.0, 2.4	0.0, +0.4	7.23×10^{-1}	0.6	0.6	1.9	2.1
49	80, 91	2.4, 2.8	−1.0, −0.7	1.14	0.7	0.6	3.2	3.4	54	80, 91	2.4, 2.8	+0.7, +1.0	1.14	0.6	0.6	2.7	2.9
50	80, 91	2.4, 2.8	−0.7, −0.4	2.55	0.6	0.5	2.4	2.5	53	80, 91	2.4, 2.8	+0.4, +0.7	2.52	0.6	0.5	2.5	2.6
51	80, 91	2.4, 2.8	−0.4, 0.0	1.10	0.6	0.5	1.7	1.9	52	80, 91	2.4, 2.8	0.0, +0.4	1.10	0.6	0.5	1.7	1.9
55	80, 91	2.8, 3.6	−1.0, −0.7	6.05×10^{-1}	0.6	0.6	4.1	4.2	60	80, 91	2.8, 3.6	+0.7, +1.0	5.97×10^{-1}	0.6	0.6	4.0	4.1
56	80, 91	2.8, 3.6	−0.7, −0.4	5.95×10^{-1}	0.5	0.5	4.6	4.6	59	80, 91	2.8, 3.6	+0.4, +0.7	5.84×10^{-1}	0.5	0.5	4.5	4.5
57	80, 91	2.8, 3.6	−0.4, 0.0	—	—	—	—	—	58	80, 91	2.8, 3.6	0.0, +0.4	—	—	—	—	—
61	91, 102	1.2, 1.6	−1.0, −0.7	6.53×10^{-1}	0.8	0.6	2.2	2.4	66	91, 102	1.2, 1.6	+0.7, +1.0	7.55×10^{-1}	0.8	0.6	2.3	2.5
62	91, 102	1.2, 1.6	−0.7, −0.4	3.64×10^{-2}	3.5	2.8	2.7	5.2	65	91, 102	1.2, 1.6	+0.4, +0.7	3.88×10^{-2}	3.5	3.0	3.2	5.6
63	91, 102	1.2, 1.6	−0.4, 0.0	—	—	—	—	—	64	91, 102	1.2, 1.6	0.0, +0.4	—	—	—	—	—
67	91, 102	1.6, 2.0	−1.0, −0.7	1.52	0.6	0.4	2.2	2.3	72	91, 102	1.6, 2.0	+0.7, +1.0	1.78	0.6	0.4	2.1	2.3
68	91, 102	1.6, 2.0	−0.7, −0.4	1.13	0.7	0.5	1.5	1.7	71	91, 102	1.6, 2.0	+0.4, +0.7	1.29	0.7	0.4	1.4	1.6
69	91, 102	1.6, 2.0	−0.4, 0.0	6.15×10^{-3}	7.6	6.1	6.4	11.6	70	91, 102	1.6, 2.0	0.0, +0.4	5.73×10^{-3}	8.0	6.7	6.3	12.2
73	91, 102	2.0, 2.4	−1.0, −0.7	1.48	0.9	0.7	2.3	2.6	78	91, 102	2.0, 2.4	+0.7, +1.0	1.81	0.8	0.6	2.2	2.4
74	91, 102	2.0, 2.4	−0.7, −0.4	2.94	0.5	0.3	1.6	1.7	77	91, 102	2.0, 2.4	+0.4, +0.7	3.48	0.4	0.3	1.5	1.6
75	91, 102	2.0, 2.4	−0.4, 0.0	8.06×10^{-1}	0.7	0.6	1.6	1.9	76	91, 102	2.0, 2.4	0.0, +0.4	8.97×10^{-1}	0.6	0.6	1.5	1.7
79	91, 102	2.4, 2.8	−1.0, −0.7	1.25	0.7	0.6	2.3	2.5	84	91, 102	2.4, 2.8	+0.7, +1.0	1.65	0.6	0.5	2.3	2.4
80	91, 102	2.4, 2.8	−0.7, −0.4	2.63	0.6	0.5	2.0	2.1	83	91, 102	2.4, 2.8	+0.4, +0.7	3.33	0.5	0.5	1.8	2.0
81	91, 102	2.4, 2.8	−0.4, 0.0	1.24	0.6	1.0	1.7	2.1	82	91, 102	2.4, 2.8	0.0, +0.4	1.41	0.6	0.8	1.5	1.8
85	91, 102	2.8, 3.6	−1.0, −0.7	6.54×10^{-1}	0.6	0.6	3.0	3.1	90	91, 102	2.8, 3.6	+0.7, +1.0	9.09×10^{-1}	0.5	0.6	2.9	3.0
86	91, 102	2.8, 3.6	−0.7, −0.4	5.66×10^{-1}	0.6	0.5	3.3	3.4	89	91, 102	2.8, 3.6	+0.4, +0.7	7.57×10^{-1}	0.5	0.4	2.5	2.6
87	91, 102	2.8, 3.6	−0.4, 0.0	—	—	—	—	—	88	91, 102	2.8, 3.6	0.0, +0.4	—	—	—	—	—
91	102, 116	1.2, 1.6	−1.0, −0.7	3.09×10^{-2}	4.6	6.3	11.4	13.8	96	102, 116	1.2, 1.6	+0.7, +1.0	5.49×10^{-2}	3.3	4.0	6.5	8.3
92	102, 116	1.2, 1.6	−0.7, −0.4	1.06×10^{-3}	23.7	22.9	33.4	46.9	95	102, 116	1.2, 1.6	+0.4, +0.7	1.64×10^{-3}	20.6	29.7	24.2	43.5
93	102, 116	1.2, 1.6	−0.4, 0.0	—	—	—	—	—	94	102, 116	1.2, 1.6	0.0, +0.4	—	—	—	—	—
97	102, 116	1.6, 2.0	−1.0, −0.7	5.20×10^{-2}	3.8	4.0	8.5	10.1	102	102, 116	1.6, 2.0	+0.7, +1.0	1.05×10^{-1}	2.6	2.4	5.0	6.2
98	102, 116	1.6, 2.0	−0.7, −0.4	3.15×10^{-2}	4.4	4.4	4.9	8.0	101	102, 116	1.6, 2.0	+0.4, +0.7	5.32×10^{-2}	3.3	3.0	3.5	5.7
99	102, 116	1.6, 2.0	−0.4, 0.0	—	—	—	—	—	100	102, 116	1.6, 2.0	0.0, +0.4	—	—	—	—	—
103	102, 116	2.0, 2.4	−1.0, −0.7	4.24×10^{-2}	5.3	5.0	15.5	17.1	108	102, 116	2.0, 2.4	+0.7, +1.0	1.06×10^{-1}	3.2	3.1	7.8	9.0
104	102, 116	2.0, 2.4	−0.7, −0.4	6.96×10^{-2}	3.2	3.5	5.9	7.6	107	102, 116	2.0, 2.4	+0.4, +0.7	1.38×10^{-1}	2.4	2.2	4.4	5.4
105	102, 116	2.0, 2.4	−0.4, 0.0	2.42×10^{-2}	4.0	4.4	5.9	8.4	106	102, 116	2.0, 2.4	0.0, +0.4	3.15×10^{-2}	3.5	3.5	4.0	6.3
109	102, 116	2.4, 2.8	−1.0, −0.7	3.05×10^{-2}	3.8	4.6	22.0	22.8	114	102, 116	2.4, 2.8	+0.7, +1.0	9.69×10^{-2}	2.2	2.4	10.5	11.0
110	102, 116	2.4, 2.8	−0.7, −0.4	5.28×10^{-2}	4.3	4.5	11.4	12.9	113	102, 116	2.4, 2.8	+0.4, +0.7	1.36×10^{-1}	2.7	2.6	8.4	9.2
111	102, 116	2.4, 2.8	−0.4, 0.0	3.06×10^{-2}	4.0	5.1	6.9	9.5	112	102, 116	2.4, 2.8	0.0, +0.4	5.19×10^{-2}	3.1	3.3	4.8	6.6
115	102, 116	2.8, 3.6	−1.0, −0.7	1.44×10^{-2}	3.4	3.9	35.9	36.3	120	102, 116	2.8, 3.6	+0.7, +1.0	5.18×10^{-2}	2.0	1.8	19.3	19.4
116	102, 116	2.8, 3.6	−0.7, −0.4	1.00×10^{-2}	4.2	4.6	24.8	25.5	119	102, 116	2.8, 3.6	+0.4, +0.7	3.27×10^{-2}	2.4	2.1	14.2	14.6
117	102, 116	2.8, 3.6	−0.4, 0.0	—	—	—	—	—	118	102, 116	2.8, 3.6	0.0, +0.4	—	—	—	—	—

JHEP12(2017)059

Bin	m_{ee} [GeV]	$\lvert y_{ee}\rvert$	$\cos\theta^*$	$\mathrm{d}^3\sigma$ [pb/GeV]	δ^{stat} [%]	$\delta^{\mathrm{syst}}_{\mathrm{unc}}$ [%]	$\delta^{\mathrm{syst}}_{\mathrm{cor}}$ [%]	δ^{total} [%]	Bin	m_{ee} [GeV]	$\lvert y_{ee}\rvert$	$\cos\theta^*$	$\mathrm{d}^3\sigma$ [pb/GeV]	δ^{stat} [%]	$\delta^{\mathrm{syst}}_{\mathrm{unc}}$ [%]	$\delta^{\mathrm{syst}}_{\mathrm{cor}}$ [%]	δ^{total} [%]
121	116, 150	1.2, 1.6	−1.0, −0.7	6.38×10^{-3}	9.4	13.8	36.2	39.9	126	116, 150	1.2, 1.6	+0.7, +1.0	1.65×10^{-2}	4.7	5.6	14.4	16.1
122	116, 150	1.2, 1.6	−0.7, −0.4	—	—	—	—	—	125	116, 150	1.2, 1.6	+0.4, +0.7	4.05×10^{-4}	33.3	55.4	43.5	78.0
123	116, 150	1.2, 1.6	−0.4, 0.0	—	—	—	—	—	124	116, 150	1.2, 1.6	0.0, +0.4	—	—	—	—	—
127	116, 150	1.6, 2.0	−1.0, −0.7	9.56×10^{-3}	8.4	11.4	29.7	32.9	132	116, 150	1.6, 2.0	+0.7, +1.0	2.91×10^{-2}	3.9	6.2	9.9	12.3
128	116, 150	1.6, 2.0	−0.7, −0.4	4.62×10^{-3}	7.6	10.1	9.1	15.6	131	116, 150	1.6, 2.0	+0.4, +0.7	1.16×10^{-2}	4.4	5.1	3.3	7.5
129	116, 150	1.6, 2.0	−0.4, 0.0	—	—	—	—	—	130	116, 150	1.6, 2.0	0.0, +0.4	—	—	—	—	—
133	116, 150	2.0, 2.4	−1.0, −0.7	7.42×10^{-3}	11.5	16.3	46.1	50.3	138	116, 150	2.0, 2.4	+0.7, +1.0	3.00×10^{-2}	4.1	5.2	11.3	13.1
134	116, 150	2.0, 2.4	−0.7, −0.4	1.21×10^{-2}	5.5	6.4	11.2	14.0	137	116, 150	2.0, 2.4	+0.4, +0.7	3.03×10^{-2}	3.6	3.8	4.7	7.0
135	116, 150	2.0, 2.4	−0.4, 0.0	3.48×10^{-3}	7.2	12.2	14.1	20.1	136	116, 150	2.0, 2.4	0.0, +0.4	7.29×10^{-3}	4.7	5.9	5.6	9.4
139	116, 150	2.4, 2.8	−1.0, −0.7	3.36×10^{-3}	16.2	18.3	30.4	39.0	144	116, 150	2.4, 2.8	+0.7, +1.0	2.87×10^{-2}	3.3	3.0	4.3	6.2
140	116, 150	2.4, 2.8	−0.7, −0.4	8.13×10^{-3}	7.6	10.9	11.6	17.6	143	116, 150	2.4, 2.8	+0.4, +0.7	2.88×10^{-2}	3.8	3.8	3.9	6.7
141	116, 150	2.4, 2.8	−0.4, 0.0	5.61×10^{-3}	5.9	7.0	7.1	11.6	142	116, 150	2.4, 2.8	0.0, +0.4	1.05×10^{-2}	4.5	4.7	3.8	7.5
145	116, 150	2.8, 3.6	−1.0, −0.7	1.68×10^{-3}	11.1	13.6	32.3	36.8	150	116, 150	2.8, 3.6	+0.7, +1.0	1.21×10^{-2}	3.1	3.6	6.8	8.3
146	116, 150	2.8, 3.6	−0.7, −0.4	1.39×10^{-3}	8.8	11.4	14.1	20.1	149	116, 150	2.8, 3.6	+0.4, +0.7	6.41×10^{-3}	3.7	4.0	3.8	6.6
147	116, 150	2.8, 3.6	−0.4, 0.0	—	—	—	—	—	148	116, 150	2.8, 3.6	0.0, +0.4	—	—	—	—	—

Table 8. The high rapidity electron channel Born-level triple-differential cross section $\mathrm{d}^3\sigma/\mathrm{d}m_{\ell\ell}\mathrm{d}|y_{\ell\ell}|\mathrm{d}\cos\theta^*$. The measurements are listed together with the statistical (δ^{stat}), uncorrelated systematic ($\delta^{\mathrm{syst}}_{\mathrm{unc}}$), correlated systematic ($\delta^{\mathrm{syst}}_{\mathrm{cor}}$), and total ($\delta^{\mathrm{total}}$) uncertainties. The luminosity uncertainty of 1.9% is not shown and not included in the overall systematic and total uncertainties.

A.3 Forward-backward asymmetry tables

$\lvert y_{\ell\ell}\rvert$	$m_{\ell\ell}$ [GeV]	A_{FB}	Δ^{stat}	$\Delta^{\mathrm{syst}}_{\mathrm{unc}}$	$\Delta^{\mathrm{syst}}_{\mathrm{cor}}$	Δ^{total}	$\lvert y_{\ell\ell}\rvert$	$m_{\ell\ell}$ [GeV]	A_{FB}	Δ^{stat}	$\Delta^{\mathrm{syst}}_{\mathrm{unc}}$	$\Delta^{\mathrm{syst}}_{\mathrm{cor}}$	Δ^{total}
0.0, 0.2	46, 66	-5.97×10^{-3}	5.6×10^{-3}	4.5×10^{-3}	7.2×10^{-4}	7.3×10^{-3}	0.2, 0.4	46, 66	-8.12×10^{-3}	5.7×10^{-3}	4.7×10^{-3}	8.7×10^{-4}	7.4×10^{-3}
0.0, 0.2	66, 80	-2.48×10^{-4}	4.2×10^{-3}	2.3×10^{-3}	7.5×10^{-4}	4.8×10^{-3}	0.2, 0.4	66, 80	-2.61×10^{-2}	4.2×10^{-3}	2.3×10^{-3}	6.7×10^{-4}	4.9×10^{-3}
0.0, 0.2	80, 91	8.26×10^{-4}	1.1×10^{-3}	5.6×10^{-4}	3.5×10^{-4}	1.3×10^{-3}	0.2, 0.4	80, 91	1.85×10^{-3}	1.1×10^{-3}	5.5×10^{-4}	5.5×10^{-4}	1.4×10^{-3}
0.0, 0.2	91, 102	3.78×10^{-3}	1.1×10^{-3}	5.1×10^{-4}	3.2×10^{-4}	1.2×10^{-3}	0.2, 0.4	91, 102	6.49×10^{-3}	1.1×10^{-3}	5.0×10^{-4}	5.1×10^{-4}	1.3×10^{-3}
0.0, 0.2	102, 116	1.29×10^{-2}	5.3×10^{-3}	2.5×10^{-3}	9.1×10^{-4}	5.9×10^{-3}	0.2, 0.4	102, 116	2.59×10^{-2}	5.3×10^{-3}	2.5×10^{-3}	1.1×10^{-3}	5.9×10^{-3}
0.0, 0.2	116, 150	2.60×10^{-2}	8.3×10^{-3}	3.3×10^{-3}	1.3×10^{-3}	9.0×10^{-3}	0.2, 0.4	116, 150	5.69×10^{-2}	8.4×10^{-3}	3.6×10^{-3}	1.5×10^{-3}	9.2×10^{-3}
0.0, 0.2	150, 200	1.88×10^{-2}	1.6×10^{-2}	5.8×10^{-3}	2.9×10^{-3}	1.7×10^{-2}	0.2, 0.4	150, 200	5.11×10^{-2}	1.6×10^{-2}	6.9×10^{-3}	4.2×10^{-3}	1.8×10^{-2}
0.4, 0.6	46, 66	-2.71×10^{-2}	5.9×10^{-3}	4.5×10^{-3}	9.1×10^{-4}	7.5×10^{-3}	0.6, 0.8	46, 66	-2.96×10^{-2}	5.7×10^{-3}	4.3×10^{-3}	9.5×10^{-4}	7.2×10^{-3}
0.4, 0.6	66, 80	-2.76×10^{-2}	4.3×10^{-3}	2.3×10^{-3}	7.6×10^{-4}	4.9×10^{-3}	0.6, 0.8	66, 80	-5.27×10^{-2}	4.4×10^{-3}	2.5×10^{-3}	9.2×10^{-4}	5.1×10^{-3}
0.4, 0.6	80, 91	2.61×10^{-3}	1.1×10^{-3}	5.5×10^{-4}	6.0×10^{-4}	1.4×10^{-3}	0.6, 0.8	80, 91	1.48×10^{-3}	1.1×10^{-3}	5.6×10^{-4}	6.6×10^{-4}	1.4×10^{-3}
0.4, 0.6	91, 102	1.23×10^{-2}	1.1×10^{-3}	5.2×10^{-4}	5.7×10^{-4}	1.3×10^{-3}	0.6, 0.8	91, 102	1.74×10^{-2}	1.1×10^{-3}	5.1×10^{-4}	6.4×10^{-4}	1.4×10^{-3}
0.4, 0.6	102, 116	4.39×10^{-2}	5.2×10^{-3}	2.6×10^{-3}	1.2×10^{-3}	6.0×10^{-3}	0.6, 0.8	102, 116	5.37×10^{-2}	5.2×10^{-3}	2.7×10^{-3}	1.7×10^{-3}	6.1×10^{-3}
0.4, 0.6	116, 150	7.39×10^{-2}	8.5×10^{-3}	3.3×10^{-3}	1.7×10^{-3}	9.3×10^{-3}	0.6, 0.8	116, 150	1.06×10^{-1}	8.3×10^{-3}	3.1×10^{-3}	1.8×10^{-3}	9.1×10^{-3}
0.4, 0.6	150, 200	1.01×10^{-1}	1.6×10^{-2}	5.8×10^{-3}	2.7×10^{-3}	1.7×10^{-2}	0.6, 0.8	150, 200	1.37×10^{-1}	1.6×10^{-2}	5.3×10^{-3}	3.2×10^{-3}	1.7×10^{-2}
0.8, 1.0	46, 66	-4.28×10^{-2}	5.8×10^{-3}	4.4×10^{-3}	8.9×10^{-4}	7.3×10^{-3}	1.0, 1.2	46, 66	-5.60×10^{-2}	5.7×10^{-3}	4.2×10^{-3}	1.2×10^{-3}	7.2×10^{-3}
0.8, 1.0	66, 80	-7.03×10^{-2}	4.4×10^{-3}	2.4×10^{-3}	9.0×10^{-4}	5.1×10^{-3}	1.0, 1.2	66, 80	-8.76×10^{-2}	4.3×10^{-3}	2.4×10^{-3}	9.5×10^{-4}	5.0×10^{-3}
0.8, 1.0	80, 91	-7.42×10^{-5}	1.1×10^{-3}	5.7×10^{-4}	7.5×10^{-4}	1.5×10^{-3}	1.0, 1.2	80, 91	8.90×10^{-5}	1.1×10^{-3}	5.7×10^{-4}	7.8×10^{-4}	1.5×10^{-3}
0.8, 1.0	91, 102	2.33×10^{-2}	1.1×10^{-3}	5.2×10^{-4}	6.9×10^{-4}	1.4×10^{-3}	1.0, 1.2	91, 102	2.88×10^{-2}	1.1×10^{-3}	5.1×10^{-4}	7.4×10^{-4}	1.4×10^{-3}
0.8, 1.0	102, 116	9.15×10^{-2}	5.2×10^{-3}	2.8×10^{-3}	1.6×10^{-3}	6.1×10^{-3}	1.0, 1.2	102, 116	1.10×10^{-1}	5.1×10^{-3}	2.7×10^{-3}	1.7×10^{-3}	6.0×10^{-3}
0.8, 1.0	116, 150	1.28×10^{-1}	8.4×10^{-3}	3.4×10^{-3}	1.8×10^{-3}	9.2×10^{-3}	1.0, 1.2	116, 150	1.68×10^{-1}	8.4×10^{-3}	3.6×10^{-3}	2.0×10^{-3}	9.3×10^{-3}
0.8, 1.0	150, 200	1.69×10^{-1}	1.6×10^{-2}	5.3×10^{-3}	4.0×10^{-3}	1.7×10^{-2}	1.0, 1.2	150, 200	2.36×10^{-1}	1.6×10^{-2}	5.9×10^{-3}	4.2×10^{-3}	1.7×10^{-2}
1.2, 1.4	46, 66	-8.88×10^{-2}	5.7×10^{-3}	4.2×10^{-3}	1.4×10^{-3}	7.2×10^{-3}	1.4, 1.6	46, 66	-1.03×10^{-1}	5.8×10^{-3}	4.3×10^{-3}	1.7×10^{-3}	7.5×10^{-3}
1.2, 1.4	66, 80	-1.14×10^{-1}	4.2×10^{-3}	2.4×10^{-3}	1.1×10^{-3}	5.0×10^{-3}	1.4, 1.6	66, 80	-1.25×10^{-1}	4.4×10^{-3}	2.6×10^{-3}	1.3×10^{-3}	5.3×10^{-3}
1.2, 1.4	80, 91	-2.23×10^{-3}	1.1×10^{-3}	5.7×10^{-4}	8.7×10^{-4}	1.5×10^{-3}	1.4, 1.6	80, 91	-2.59×10^{-3}	1.2×10^{-3}	6.2×10^{-4}	9.2×10^{-4}	1.6×10^{-3}
1.2, 1.4	91, 102	3.38×10^{-2}	1.1×10^{-3}	5.2×10^{-4}	8.5×10^{-4}	1.5×10^{-3}	1.4, 1.6	91, 102	3.77×10^{-2}	1.1×10^{-3}	5.7×10^{-4}	8.9×10^{-4}	1.6×10^{-3}
1.2, 1.4	102, 116	1.30×10^{-1}	5.0×10^{-3}	2.8×10^{-3}	2.0×10^{-3}	6.1×10^{-3}	1.4, 1.6	102, 116	1.44×10^{-1}	5.1×10^{-3}	3.0×10^{-3}	2.2×10^{-3}	6.3×10^{-3}
1.2, 1.4	116, 150	2.09×10^{-1}	8.5×10^{-3}	3.7×10^{-3}	2.6×10^{-3}	9.6×10^{-3}	1.4, 1.6	116, 150	2.19×10^{-1}	8.9×10^{-3}	3.9×10^{-3}	2.8×10^{-3}	1.0×10^{-2}
1.2, 1.4	150, 200	2.68×10^{-1}	1.6×10^{-2}	6.6×10^{-3}	4.3×10^{-3}	1.8×10^{-2}	1.4, 1.6	150, 200	2.80×10^{-1}	1.8×10^{-2}	9.0×10^{-3}	4.5×10^{-3}	2.1×10^{-2}
1.6, 1.8	46, 66	-9.35×10^{-2}	6.1×10^{-3}	4.6×10^{-3}	1.4×10^{-3}	7.8×10^{-3}	1.8, 2.0	46, 66	-9.23×10^{-2}	6.7×10^{-3}	4.9×10^{-3}	1.5×10^{-3}	8.5×10^{-3}
1.6, 1.8	66, 80	-1.26×10^{-1}	4.9×10^{-3}	2.8×10^{-3}	1.5×10^{-3}	5.8×10^{-3}	1.8, 2.0	66, 80	-1.20×10^{-1}	5.6×10^{-3}	3.3×10^{-3}	2.0×10^{-3}	6.8×10^{-3}
1.6, 1.8	80, 91	-7.79×10^{-4}	1.3×10^{-3}	7.0×10^{-4}	1.0×10^{-3}	1.8×10^{-3}	1.8, 2.0	80, 91	-2.65×10^{-3}	1.5×10^{-3}	8.1×10^{-4}	1.1×10^{-3}	2.0×10^{-3}
1.6, 1.8	91, 102	3.96×10^{-2}	1.3×10^{-3}	6.3×10^{-4}	9.6×10^{-4}	1.7×10^{-3}	1.8, 2.0	91, 102	3.97×10^{-2}	1.5×10^{-3}	7.4×10^{-4}	1.1×10^{-3}	2.0×10^{-3}
1.6, 1.8	102, 116	1.63×10^{-1}	5.3×10^{-3}	3.6×10^{-3}	2.8×10^{-3}	7.0×10^{-3}	1.8, 2.0	102, 116	1.54×10^{-1}	5.6×10^{-3}	3.9×10^{-3}	3.5×10^{-3}	7.7×10^{-3}
1.6, 1.8	116, 150	2.43×10^{-1}	1.0×10^{-2}	4.6×10^{-3}	2.6×10^{-3}	1.2×10^{-2}	1.8, 2.0	116, 150	2.12×10^{-1}	1.2×10^{-2}	6.8×10^{-3}	3.9×10^{-3}	1.4×10^{-2}
1.6, 1.8	150, 200	3.02×10^{-1}	1.8×10^{-2}	6.8×10^{-3}	5.6×10^{-3}	2.0×10^{-2}	1.8, 2.0	150, 200	2.66×10^{-1}	2.1×10^{-2}	6.3×10^{-3}	4.2×10^{-3}	2.3×10^{-2}
2.0, 2.2	46, 66	-9.82×10^{-2}	8.3×10^{-3}	6.2×10^{-3}	2.6×10^{-3}	1.1×10^{-2}	2.2, 2.4	46, 66	-4.44×10^{-2}	1.4×10^{-2}	1.1×10^{-2}	3.1×10^{-3}	1.8×10^{-2}
2.0, 2.2	66, 80	-1.10×10^{-1}	6.9×10^{-3}	4.2×10^{-3}	3.0×10^{-3}	8.6×10^{-3}	2.2, 2.4	66, 80	-5.03×10^{-2}	1.2×10^{-2}	7.5×10^{-3}	6.1×10^{-3}	1.5×10^{-2}
2.0, 2.2	80, 91	-3.33×10^{-3}	1.9×10^{-3}	1.1×10^{-3}	1.5×10^{-3}	2.7×10^{-3}	2.2, 2.4	80, 91	-6.44×10^{-3}	3.1×10^{-3}	1.9×10^{-3}	2.1×10^{-3}	4.2×10^{-3}
2.0, 2.2	91, 102	3.33×10^{-2}	1.9×10^{-3}	9.8×10^{-4}	1.5×10^{-3}	2.6×10^{-3}	2.2, 2.4	91, 102	1.99×10^{-2}	3.1×10^{-3}	1.6×10^{-3}	2.3×10^{-3}	4.2×10^{-3}
2.0, 2.2	102, 116	1.20×10^{-1}	6.5×10^{-3}	5.1×10^{-3}	6.3×10^{-3}	1.0×10^{-2}	2.2, 2.4	102, 116	6.06×10^{-2}	9.7×10^{-3}	9.3×10^{-3}	1.2×10^{-2}	1.8×10^{-2}
2.0, 2.2	116, 150	1.64×10^{-1}	1.4×10^{-2}	6.6×10^{-3}	3.9×10^{-3}	1.6×10^{-2}	2.2, 2.4	116, 150	9.40×10^{-2}	2.6×10^{-2}	1.6×10^{-2}	1.5×10^{-2}	3.4×10^{-2}
2.0, 2.2	150, 200	1.97×10^{-1}	2.7×10^{-2}	1.0×10^{-2}	7.7×10^{-3}	3.0×10^{-2}	2.2, 2.4	150, 200	1.27×10^{-1}	4.6×10^{-2}	1.3×10^{-2}	1.0×10^{-2}	4.9×10^{-2}

Table 9. The asymmetry A_{FB} determined from the combined triple-differential cross-section measurements. The measurements are listed together with the statistical (Δ^{stat}), uncorrelated systematic ($\Delta^{\mathrm{syst}}_{\mathrm{unc}}$), correlated systematic ($\Delta^{\mathrm{syst}}_{\mathrm{cor}}$), and total ($\Delta^{\mathrm{total}}$) uncertainties.

$\lvert y_{ee}\rvert$	m_{ee} [GeV]	A_{FB}	Δ^{stat}	$\Delta^{\mathrm{syst}}_{\mathrm{unc}}$	$\Delta^{\mathrm{syst}}_{\mathrm{cor}}$	Δ^{total}
1.2, 1.6	66, 80	-2.44×10^{-1}	4.4×10^{-2}	5.9×10^{-2}	2.5×10^{-2}	7.8×10^{-2}
1.2, 1.6	80, 91	8.57×10^{-3}	6.2×10^{-3}	4.6×10^{-3}	3.6×10^{-3}	8.5×10^{-3}
1.2, 1.6	91, 102	7.03×10^{-2}	5.7×10^{-3}	4.1×10^{-3}	4.9×10^{-3}	8.6×10^{-3}
1.2, 1.6	102, 116	2.78×10^{-1}	2.6×10^{-2}	3.4×10^{-2}	2.6×10^{-2}	5.0×10^{-2}
1.2, 1.6	116, 150	4.43×10^{-1}	4.2×10^{-2}	6.0×10^{-2}	1.1×10^{-1}	1.3×10^{-1}
1.6, 2.0	66, 80	-2.32×10^{-1}	1.7×10^{-2}	1.9×10^{-2}	1.1×10^{-2}	2.7×10^{-2}
1.6, 2.0	80, 91	3.08×10^{-3}	3.3×10^{-3}	2.3×10^{-3}	2.5×10^{-3}	4.7×10^{-3}
1.6, 2.0	91, 102	7.30×10^{-2}	3.2×10^{-3}	2.1×10^{-3}	1.8×10^{-3}	4.2×10^{-3}
1.6, 2.0	102, 116	3.09×10^{-1}	1.6×10^{-2}	1.6×10^{-2}	1.3×10^{-2}	2.6×10^{-2}
1.6, 2.0	116, 150	4.83×10^{-1}	2.6×10^{-2}	3.7×10^{-2}	6.5×10^{-2}	7.9×10^{-2}
2.0, 2.4	66, 80	-2.89×10^{-1}	1.2×10^{-2}	1.4×10^{-2}	1.3×10^{-2}	2.3×10^{-2}
2.0, 2.4	80, 91	-9.15×10^{-3}	2.8×10^{-3}	2.1×10^{-3}	1.7×10^{-3}	3.9×10^{-3}
2.0, 2.4	91, 102	8.43×10^{-2}	2.7×10^{-3}	1.9×10^{-3}	2.7×10^{-3}	4.3×10^{-3}
2.0, 2.4	102, 116	3.40×10^{-1}	1.3×10^{-2}	1.3×10^{-2}	1.6×10^{-2}	2.5×10^{-2}
2.0, 2.4	116, 150	4.93×10^{-1}	2.1×10^{-2}	2.7×10^{-2}	6.5×10^{-2}	7.3×10^{-2}
2.4, 2.8	66, 80	-3.26×10^{-1}	1.1×10^{-2}	1.1×10^{-2}	1.7×10^{-2}	2.3×10^{-2}
2.4, 2.8	80, 91	-4.68×10^{-3}	2.6×10^{-3}	2.2×10^{-3}	2.4×10^{-3}	4.2×10^{-3}
2.4, 2.8	91, 102	1.11×10^{-1}	2.6×10^{-3}	2.5×10^{-3}	2.1×10^{-3}	4.1×10^{-3}
2.4, 2.8	102, 116	4.29×10^{-1}	1.2×10^{-2}	1.3×10^{-2}	1.8×10^{-2}	2.6×10^{-2}
2.4, 2.8	116, 150	5.98×10^{-1}	1.8×10^{-2}	2.3×10^{-2}	3.3×10^{-2}	4.4×10^{-2}
2.8, 3.6	66, 80	-4.73×10^{-1}	1.1×10^{-2}	1.4×10^{-2}	2.7×10^{-2}	3.2×10^{-2}
2.8, 3.6	80, 91	-8.07×10^{-3}	2.8×10^{-3}	2.7×10^{-3}	2.3×10^{-3}	4.5×10^{-3}
2.8, 3.6	91, 102	1.55×10^{-1}	2.7×10^{-3}	2.7×10^{-3}	5.0×10^{-3}	6.2×10^{-3}
2.8, 3.6	102, 116	5.51×10^{-1}	1.1×10^{-2}	1.1×10^{-2}	4.5×10^{-2}	4.8×10^{-2}
2.8, 3.6	116, 150	7.15×10^{-1}	1.9×10^{-2}	2.3×10^{-2}	4.8×10^{-2}	5.7×10^{-2}

Table 10. The asymmetry A_{FB} determined from the high rapidity electron channel triple-differential cross-section measurement. The measurement is listed together with the statistical (Δ^{stat}), uncorrelated systematic ($\Delta^{\mathrm{syst}}_{\mathrm{unc}}$), correlated systematic ($\Delta^{\mathrm{syst}}_{\mathrm{cor}}$), and total ($\Delta^{\mathrm{total}}$) uncertainties.

JHEP12(2017)059

References

[1] S.D. Drell and T.-M. Yan, *Massive Lepton Pair Production in Hadron-Hadron Collisions at High-Energies*, *Phys. Rev. Lett.* **25** (1970) 316 [*Erratum ibid.* **25** (1970) 902] [INSPIRE].

[2] S.D. Drell and T.-M. Yan, *Partons and their Applications at High-Energies*, *Annals Phys.* **66** (1971) 578 [INSPIRE].

[3] SLD Electroweak Group, DELPHI, ALEPH, SLD, SLD Heavy Flavour Group, OPAL, LEP Electroweak Working Group and L3 collaborations, S. Schael et al., *Precision electroweak measurements on the Z resonance*, *Phys. Rept.* **427** (2006) 257 [hep-ex/0509008] [INSPIRE].

[4] ATLAS collaboration, *Measurement of $W^{\pm}$ and Z-boson production cross sections in pp collisions at $\sqrt{s} = 13$ TeV with the ATLAS detector*, *Phys. Lett.* **B 759** (2016) 601 [arXiv:1603.09222] [INSPIRE].

[5] ATLAS collaboration, *Measurements of top-quark pair to Z-boson cross-section ratios at $\sqrt{s} = 13$, 8, 7 TeV with the ATLAS detector*, *JHEP* **02** (2017) 117 [arXiv:1612.03636] [INSPIRE].

[6] CMS collaboration, *Measurement of the Inclusive W and Z Production Cross sections in pp Collisions at $\sqrt{s} = 7$ TeV*, *JHEP* **10** (2011) 132 [arXiv:1107.4789] [INSPIRE].

[7] CMS collaboration, *Measurement of inclusive W and Z boson production cross sections in pp collisions at $\sqrt{s} = 8$ TeV*, *Phys. Rev. Lett.* **112** (2014) 191802 [arXiv:1402.0923] [INSPIRE].

[8] ATLAS collaboration, *Measurement of the inclusive $W^{\pm}$ and Z/gamma cross sections in the electron and muon decay channels in pp collisions at $\sqrt{s} = 7$ TeV with the ATLAS detector*, *Phys. Rev.* **D 85** (2012) 072004 [arXiv:1109.5141] [INSPIRE].

[9] CMS collaboration, *Measurement of the Rapidity and Transverse Momentum Distributions of Z Bosons in pp Collisions at $\sqrt{s} = 7$ TeV*, *Phys. Rev.* **D 85** (2012) 032002 [arXiv:1110.4973] [INSPIRE].

[10] ATLAS collaboration, *Measurement of angular correlations in Drell-Yan lepton pairs to probe Z/gamma* boson transverse momentum at $\sqrt{s} = 7$ TeV with the ATLAS detector*, *Phys. Lett.* **B 720** (2013) 32 [arXiv:1211.6899] [INSPIRE].

[11] ATLAS collaboration, *Measurement of the Z/γ^* boson transverse momentum distribution in pp collisions at $\sqrt{s} = 7$ TeV with the ATLAS detector*, *JHEP* **09** (2014) 145 [arXiv:1406.3660] [INSPIRE].

[12] CMS collaboration, *Measurement of the transverse momentum spectra of weak vector bosons produced in proton-proton collisions at $\sqrt{s} = 8$ TeV*, *JHEP* **02** (2017) 096 [arXiv:1606.05864] [INSPIRE].

[13] ATLAS collaboration, *Measurement of the high-mass Drell-Yan differential cross-section in pp collisions at $\sqrt{s} = 7$ TeV with the ATLAS detector*, *Phys. Lett.* **B 725** (2013) 223 [arXiv:1305.4192] [INSPIRE].

JHEP12(2017)059

[14] ATLAS collaboration, *Measurement of the low-mass Drell-Yan differential cross section at $\sqrt{s} = 7$ TeV using the ATLAS detector*, *JHEP* **06** (2014) 112 [arXiv:1404.1212] [INSPIRE].

[15] CMS collaboration, *Measurement of the Drell-Yan Cross section in pp Collisions at $\sqrt{s} = 7$ TeV*, *JHEP* **10** (2011) 007 [arXiv:1108.0566] [INSPIRE].

[16] ATLAS collaboration, *Measurement of the transverse momentum and ϕ^*_η distributions of Drell-Yan lepton pairs in proton-proton collisions at $\sqrt{s} = 8$ TeV with the ATLAS detector*, *Eur. Phys. J.* **C 76** (2016) 291 [arXiv:1512.02192] [INSPIRE].

[17] ATLAS collaboration, *Measurement of the double-differential high-mass Drell-Yan cross section in pp collisions at $\sqrt{s} = 8$ TeV with the ATLAS detector*, *JHEP* **08** (2016) 009 [arXiv:1606.01736] [INSPIRE].

[18] ATLAS collaboration, *Precision measurement and interpretation of inclusive W^+, W^- and Z/γ^* production cross sections with the ATLAS detector*, *Eur. Phys. J.* **C 77** (2017) 367 [arXiv:1612.03016] [INSPIRE].

[19] CMS collaboration, *Measurement of the Z boson differential cross section in transverse momentum and rapidity in proton-proton collisions at 8 TeV*, *Phys. Lett.* **B 749** (2015) 187 [arXiv:1504.03511] [INSPIRE].

[20] CMS collaboration, *Measurements of differential and double-differential Drell-Yan cross sections in proton-proton collisions at 8 TeV*, *Eur. Phys. J.* **C 75** (2015) 147 [arXiv:1412.1115] [INSPIRE].

[21] CMS collaboration, *Measurement of the differential and double-differential Drell-Yan cross sections in proton-proton collisions at $\sqrt{s} = 7$ TeV*, *JHEP* **12** (2013) 030 [arXiv:1310.7291] [INSPIRE].

[22] ATLAS collaboration, *Measurement of the angular coefficients in Z-boson events using electron and muon pairs from data taken at $\sqrt{s} = 8$ TeV with the ATLAS detector*, *JHEP* **08** (2016) 159 [arXiv:1606.00689] [INSPIRE].

[23] CMS collaboration, *Angular coefficients of Z bosons produced in pp collisions at $\sqrt{s} = 8$ TeV and decaying to $\mu^+\mu^-$ as a function of transverse momentum and rapidity*, *Phys. Lett.* **B 750** (2015) 154 [arXiv:1504.03512] [INSPIRE].

[24] ATLAS collaboration, *Measurement of the forward-backward asymmetry of electron and muon pair-production in pp collisions at $\sqrt{s} = 7$ TeV with the ATLAS detector*, *JHEP* **09** (2015) 049 [arXiv:1503.03709] [INSPIRE].

[25] CMS collaboration, *Forward-backward asymmetry of Drell-Yan lepton pairs in pp collisions at $\sqrt{s} = 7$ TeV*, *Phys. Lett.* **B 718** (2013) 752 [arXiv:1207.3973] [INSPIRE].

[26] J.C. Collins and D.E. Soper, *Angular Distribution of Dileptons in High-Energy Hadron Collisions*, *Phys. Rev.* **D 16** (1977) 2219 [INSPIRE].

[27] ATLAS collaboration, *The ATLAS Experiment at the CERN Large Hadron Collider*, 2008 *JINST* **3** S08003 [INSPIRE].

[28] ATLAS collaboration, *Performance of the ATLAS Trigger System in 2010*, *Eur. Phys. J.* **C 72** (2012) 1849 [arXiv:1110.1530] [INSPIRE].

[29] P. Nason, *A new method for combining NLO QCD with shower Monte Carlo algorithms*, *JHEP* **11** (2004) 040 [hep-ph/0409146] [INSPIRE].

JHEP12(2017)059

[30] S. Frixione, P. Nason and C. Oleari, *Matching NLO QCD computations with Parton Shower simulations: the POWHEG method*, *JHEP* **11** (2007) 070 [arXiv:0709.2092] [INSPIRE].

[31] S. Alioli, P. Nason, C. Oleari and E. Re, *NLO vector-boson production matched with shower in POWHEG*, *JHEP* **07** (2008) 060 [arXiv:0805.4802] [INSPIRE].

[32] S. Alioli, P. Nason, C. Oleari and E. Re, *A general framework for implementing NLO calculations in shower Monte Carlo programs: the POWHEG BOX*, *JHEP* **06** (2010) 043 [arXiv:1002.2581] [INSPIRE].

[33] H.-L. Lai et al., *New parton distributions for collider physics*, *Phys. Rev.* **D 82** (2010) 074024 [arXiv:1007.2241] [INSPIRE].

[34] T. Sjöstrand, S. Mrenna and P.Z. Skands, *A Brief Introduction to PYTHIA 8.1*, *Comput. Phys. Commun.* **178** (2008) 852 [arXiv:0710.3820] [INSPIRE].

[35] K. Melnikov and F. Petriello, *Electroweak gauge boson production at hadron colliders through* $\mathcal{O}(\alpha_s^2)$, *Phys. Rev.* **D 74** (2006) 114017 [hep-ph/0609070] [INSPIRE].

[36] R. Gavin, Y. Li, F. Petriello and S. Quackenbush, *FEWZ 2.0: A code for hadronic Z production at next-to-next-to-leading order*, *Comput. Phys. Commun.* **182** (2011) 2388 [arXiv:1011.3540] [INSPIRE].

[37] Y. Li and F. Petriello, *Combining QCD and electroweak corrections to dilepton production in FEWZ*, *Phys. Rev.* **D 86** (2012) 094034 [arXiv:1208.5967] [INSPIRE].

[38] A.D. Martin, W.J. Stirling, R.S. Thorne and G. Watt, *Parton distributions for the LHC*, *Eur. Phys. J.* **C 63** (2009) 189 [arXiv:0901.0002] [INSPIRE].

[39] W.F.L. Hollik, *Radiative Corrections in the Standard Model and their Role for Precision Tests of the Electroweak Theory*, *Fortsch. Phys.* **38** (1990) 165 [INSPIRE].

[40] S. Catani, L. Cieri, G. Ferrera, D. de Florian and M. Grazzini, *Vector boson production at hadron colliders: a fully exclusive QCD calculation at NNLO*, *Phys. Rev. Lett.* **103** (2009) 082001 [arXiv:0903.2120] [INSPIRE].

[41] A.D. Martin, R.G. Roberts, W.J. Stirling and R.S. Thorne, *Parton distributions incorporating QED contributions*, *Eur. Phys. J.* **C 39** (2005) 155 [hep-ph/0411040] [INSPIRE].

[42] D. Bardin et al., *SANC integrator in the progress: QCD and EW contributions*, *JETP Lett.* **96** (2012) 285 [arXiv:1207.4400] [INSPIRE].

[43] S.G. Bondarenko and A.A. Sapronov, *NLO EW and QCD proton-proton cross section calculations with mcsanc-v1.01*, *Comput. Phys. Commun.* **184** (2013) 2343 [arXiv:1301.3687] [INSPIRE].

[44] T. Sjöstrand, S. Mrenna and P.Z. Skands, *PYTHIA 6.4 Physics and Manual*, *JHEP* **05** (2006) 026 [hep-ph/0603175] [INSPIRE].

[45] M. Cacciari, M. Czakon, M. Mangano, A. Mitov and P. Nason, *Top-pair production at hadron colliders with next-to-next-to-leading logarithmic soft-gluon resummation*, *Phys. Lett.* **B 710** (2012) 612 [arXiv:1111.5869] [INSPIRE].

[46] P. Bärnreuther, M. Czakon and A. Mitov, *Percent Level Precision Physics at the Tevatron: First Genuine NNLO QCD Corrections to* $q\bar{q} \to t\bar{t} + X$, *Phys. Rev. Lett.* **109** (2012) 132001 [arXiv:1204.5201] [INSPIRE].

JHEP12(2017)059

[47] M. Czakon and A. Mitov, *NNLO corrections to top-pair production at hadron colliders: the all-fermionic scattering channels*, *JHEP* **12** (2012) 054 [arXiv:1207.0236] [INSPIRE].

[48] M. Czakon and A. Mitov, *NNLO corrections to top pair production at hadron colliders: the quark-gluon reaction*, *JHEP* **01** (2013) 080 [arXiv:1210.6832] [INSPIRE].

[49] M. Czakon, P. Fiedler and A. Mitov, *Total Top-Quark Pair-Production Cross section at Hadron Colliders Through $O(\alpha_S^4)$*, *Phys. Rev. Lett.* **110** (2013) 252004 [arXiv:1303.6254] [INSPIRE].

[50] M. Czakon and A. Mitov, *Top++: A Program for the Calculation of the Top-Pair Cross-Section at Hadron Colliders*, *Comput. Phys. Commun.* **185** (2014) 2930 [arXiv:1112.5675] [INSPIRE].

[51] J. Pumplin, D.R. Stump, J. Huston, H.L. Lai, P.M. Nadolsky and W.K. Tung, *New generation of parton distributions with uncertainties from global QCD analysis*, *JHEP* **07** (2002) 012 [hep-ph/0201195] [INSPIRE].

[52] J.M. Campbell and R.K. Ellis, *An update on vector boson pair production at hadron colliders*, *Phys. Rev.* **D 60** (1999) 113006 [hep-ph/9905386] [INSPIRE].

[53] J.M. Campbell, R.K. Ellis and C. Williams, *Vector boson pair production at the LHC*, *JHEP* **07** (2011) 018 [arXiv:1105.0020] [INSPIRE].

[54] P. Golonka and Z. Was, *PHOTOS Monte Carlo: A precision tool for QED corrections in Z and W decays*, *Eur. Phys. J.* **C 45** (2006) 97 [hep-ph/0506026] [INSPIRE].

[55] ATLAS collaboration, *The ATLAS Simulation Infrastructure*, *Eur. Phys. J.* **C 70** (2010) 823 [arXiv:1005.4568] [INSPIRE].

[56] GEANT4 collaboration, S. Agostinelli et al., *GEANT4: A simulation toolkit*, *Nucl. Instrum. Meth.* **A 506** (2003) 250 [INSPIRE].

[57] ATLAS collaboration, *Electron and photon energy calibration with the ATLAS detector using LHC Run 1 data*, *Eur. Phys. J.* **C 74** (2014) 3071 [arXiv:1407.5063] [INSPIRE].

[58] ATLAS collaboration, *Electron reconstruction and identification efficiency measurements with the ATLAS detector using the 2011 LHC proton-proton collision data*, *Eur. Phys. J.* **C 74** (2014) 2941 [arXiv:1404.2240] [INSPIRE].

[59] ATLAS collaboration, *Electron efficiency measurements with the ATLAS detector using 2012 LHC proton-proton collision data*, *Eur. Phys. J.* **C 77** (2017) 195 [arXiv:1612.01456] [INSPIRE].

[60] ATLAS collaboration, *Measurement of the muon reconstruction performance of the ATLAS detector using 2011 and 2012 LHC proton-proton collision data*, *Eur. Phys. J.* **C 74** (2014) 3130 [arXiv:1407.3935] [INSPIRE].

[61] ATLAS collaboration, *Performance of the ATLAS muon trigger in pp collisions at $\sqrt{s} = 8$ TeV*, *Eur. Phys. J.* **C 75** (2015) 120 [arXiv:1408.3179] [INSPIRE].

[62] ATLAS collaboration, *Summary of ATLAS Pythia 8 tunes*, ATL-PHYS-PUB-2012-003 (2012).

[63] R. Corke and T. Sjöstrand, *Interleaved Parton Showers and Tuning Prospects*, *JHEP* **03** (2011) 032 [arXiv:1011.1759] [INSPIRE].

[64] ATLAS collaboration, *New ATLAS event generator tunes to 2010 data*, ATL-PHYS-PUB-2011-008 (2011).

JHEP12(2017)059

[65] ATLAS collaboration, *Measurement of the W-boson mass in pp collisions at $\sqrt{s} = 7$ TeV with the ATLAS detector*, arXiv:1701.07240 [INSPIRE].

[66] G. D'Agostini, *A multidimensional unfolding method based on Bayes' theorem*, *Nucl. Instrum. Meth.* **A 362** (1995) 487 [INSPIRE].

[67] B. Efron, *Bootstrap methods: Another look at the jackknife*, *Ann. Statist.* **7** (1979) 1.

[68] ATLAS collaboration, *Electron efficiency measurements with the ATLAS detector using the 2012 LHC proton-proton collision data*, ATLAS-CONF-2014-032 (2014).

[69] M. Botje et al., *The PDF4LHC Working Group Interim Recommendations*, arXiv:1101.0538 [INSPIRE].

[70] ATLAS collaboration, *Luminosity determination in pp collisions at $\sqrt{s} = 8$ TeV using the ATLAS detector at the LHC*, *Eur. Phys. J.* **C 76** (2016) 653 [arXiv:1608.03953] [INSPIRE].

[71] *The durham high energy physics database*, https://www.hepdata.net.

[72] E. Maguire, L. Heinrich and G. Watt, *HEPData: a repository for high energy physics data*, arXiv:1704.05473 [INSPIRE].

[73] A. Glazov, *Averaging of DIS cross section data*, *AIP Conf. Proc.* **792** (2005) 237 [INSPIRE].

[74] H1 collaboration, F.D. Aaron et al., *Measurement of the Inclusive ep Scattering Cross section at Low Q^2 and x at HERA*, *Eur. Phys. J.* **C 63** (2009) 625 [arXiv:0904.0929] [INSPIRE].

[75] ZEUS and H1 collaborations, F.D. Aaron et al., *Combined Measurement and QCD Analysis of the Inclusive e+- p Scattering Cross sections at HERA*, *JHEP* **01** (2010) 109 [arXiv:0911.0884] [INSPIRE].

[76] Particle Data Group collaboration, C. Patrignani et al., *Review of Particle Physics*, *Chin. Phys.* **C 40** (2016) 100001 [INSPIRE].

[77] ATLAS collaboration, *ATLAS Computing Acknowledgements 2016-2017*, ATL-GEN-PUB-2016-002 (2016).

JHEP12(2017)059

The ATLAS collaboration

M. Aaboud[137d], G. Aad[88], B. Abbott[115], O. Abdinov[12,*], B. Abeloos[119], S.H. Abidi[161], O.S. AbouZeid[139], N.L. Abraham[151], H. Abramowicz[155], H. Abreu[154], R. Abreu[118], Y. Abulaiti[148a,148b], B.S. Acharya[167a,167b,a], S. Adachi[157], L. Adamczyk[41a], J. Adelman[110], M. Adersberger[102], T. Adye[133], A.A. Affolder[139], Y. Afik[154], T. Agatonovic-Jovin[14], C. Agheorghiesei[28c], J.A. Aguilar-Saavedra[128a,128f], S.P. Ahlen[24], F. Ahmadov[68,b], G. Aielli[135a,135b], S. Akatsuka[71], H. Akerstedt[148a,148b], T.P.A. Åkesson[84], E. Akilli[52], A.V. Akimov[98], G.L. Alberghi[22a,22b], J. Albert[172], P. Albicocco[50], M.J. Alconada Verzini[74], S.C. Alderweireldt[108], M. Aleksa[32], I.N. Aleksandrov[68], C. Alexa[28b], G. Alexander[155], T. Alexopoulos[10], M. Alhroob[115], B. Ali[130], M. Aliev[76a,76b], G. Alimonti[94a], J. Alison[33], S.P. Alkire[38], B.M.M. Allbrooke[151], B.W. Allen[118], P.P. Allport[19], A. Aloisio[106a,106b], A. Alonso[39], F. Alonso[74], C. Alpigiani[140], A.A. Alshehri[56], M.I. Alstaty[88], B. Alvarez Gonzalez[32], D. Álvarez Piqueras[170], M.G. Alviggi[106a,106b], B.T. Amadio[16], Y. Amaral Coutinho[26a], C. Amelung[25], D. Amidei[92], S.P. Amor Dos Santos[128a,128c], S. Amoroso[32], G. Amundsen[25], C. Anastopoulos[141], L.S. Ancu[52], N. Andari[19], T. Andeen[11], C.F. Anders[60b], J.K. Anders[77], K.J. Anderson[33], A. Andreazza[94a,94b], V. Andrei[60a], S. Angelidakis[37], I. Angelozzi[109], A. Angerami[38], A.V. Anisenkov[111,c], N. Anjos[13], A. Annovi[126a,126b], C. Antel[60a], M. Antonelli[50], A. Antonov[100,*], D.J. Antrim[166], F. Anulli[134a], M. Aoki[69], L. Aperio Bella[32], G. Arabidze[93], Y. Arai[69], J.P. Araque[128a], V. Araujo Ferraz[26a], A.T.H. Arce[48], R.E. Ardell[80], F.A. Arduh[74], J-F. Arguin[97], S. Argyropoulos[66], M. Arik[20a], A.J. Armbruster[32], L.J. Armitage[79], O. Arnaez[161], H. Arnold[51], M. Arratia[30], O. Arslan[23], A. Artamonov[99,*], G. Artoni[122], S. Artz[86], S. Asai[157], N. Asbah[45], A. Ashkenazi[155], L. Asquith[151], K. Assamagan[27], R. Astalos[146a], M. Atkinson[169], N.B. Atlay[143], K. Augsten[130], G. Avolio[32], B. Axen[16], M.K. Ayoub[35a], G. Azuelos[97,d], A.E. Baas[60a], M.J. Baca[19], H. Bachacou[138], K. Bachas[76a,76b], M. Backes[122], P. Bagnaia[134a,134b], M. Bahmani[42], H. Bahrasemani[144], J.T. Baines[133], M. Bajic[39], O.K. Baker[179], P.J. Bakker[109], E.M. Baldin[111,c], P. Balek[175], F. Balli[138], W.K. Balunas[124], E. Banas[42], A. Bandyopadhyay[23], Sw. Banerjee[176,e], A.A.E. Bannoura[178], L. Barak[155], E.L. Barberio[91], D. Barberis[53a,53b], M. Barbero[88], T. Barillari[103], M-S Barisits[32], J.T. Barkeloo[118], T. Barklow[145], N. Barlow[30], S.L. Barnes[36c], B.M. Barnett[133], R.M. Barnett[16], Z. Barnovska-Blenessy[36a], A. Baroncelli[136a], G. Barone[25], A.J. Barr[122], L. Barranco Navarro[170], F. Barreiro[85], J. Barreiro Guimarães da Costa[35a], R. Bartoldus[145], A.E. Barton[75], P. Bartos[146a], A. Basalaev[125], A. Bassalat[119,f], R.L. Bates[56], S.J. Batista[161], J.R. Batley[30], M. Battaglia[139], M. Bauce[134a,134b], F. Bauer[138], H.S. Bawa[145,g], J.B. Beacham[113], M.D. Beattie[75], T. Beau[83], P.H. Beauchemin[165], P. Bechtle[23], H.P. Beck[18,h], H.C. Beck[57], K. Becker[122], M. Becker[86], C. Becot[112], A.J. Beddall[20e], A. Beddall[20b], V.A. Bednyakov[68], M. Bedognetti[109], C.P. Bee[150], T.A. Beermann[32], M. Begalli[26a], M. Begel[27], J.K. Behr[45], A.S. Bell[81], G. Bella[155], L. Bellagamba[22a], A. Bellerive[31], M. Bellomo[154], K. Belotskiy[100], O. Beltramello[32], N.L. Belyaev[100], O. Benary[155,*], D. Benchekroun[137a], M. Bender[102], N. Benekos[10], Y. Benhammou[155], E. Benhar Noccioli[179], J. Benitez[66], D.P. Benjamin[48], M. Benoit[52], J.R. Bensinger[25], S. Bentvelsen[109], L. Beresford[122], M. Beretta[50], D. Berge[109], E. Bergeaas Kuutmann[168], N. Berger[5], J. Beringer[16], S. Berlendis[58], N.R. Bernard[89], G. Bernardi[83], C. Bernius[145], F.U. Bernlochner[23], T. Berry[80], P. Berta[86], C. Bertella[35a], G. Bertoli[148a,148b], I.A. Bertram[75], C. Bertsche[45], D. Bertsche[115], G.J. Besjes[39], O. Bessidskaia Bylund[148a,148b], M. Bessner[45], N. Besson[138], A. Bethani[87], S. Bethke[103], A.J. Bevan[79], J. Beyer[103], R.M. Bianchi[127], O. Biebel[102], D. Biedermann[17], R. Bielski[87], K. Bierwagen[86], N.V. Biesuz[126a,126b], M. Biglietti[136a], T.R.V. Billoud[97], H. Bilokon[50], M. Bindi[57], A. Bingul[20b], C. Bini[134a,134b], S. Biondi[22a,22b], T. Bisanz[57], C. Bittrich[47], D.M. Bjergaard[48], J.E. Black[145], K.M. Black[24], R.E. Blair[6], T. Blazek[146a], I. Bloch[45], C. Blocker[25], A. Blue[56],

JHEP12(2017)059

W. Blum[86,*], U. Blumenschein[79], S. Blunier[34a], G.J. Bobbink[109], V.S. Bobrovnikov[111,c], S.S. Bocchetta[84], A. Bocci[48], C. Bock[102], M. Boehler[51], D. Boerner[178], D. Bogavac[102], A.G. Bogdanchikov[111], C. Bohm[148a], V. Boisvert[80], P. Bokan[168,i], T. Bold[41a], A.S. Boldyrev[101], A.E. Bolz[60b], M. Bomben[83], M. Bona[79], M. Boonekamp[138], A. Borisov[132], G. Borissov[75], J. Bortfeldt[32], D. Bortoletto[122], V. Bortolotto[62a,62b,62c], D. Boscherini[22a], M. Bosman[13], J.D. Bossio Sola[29], J. Boudreau[127], J. Bouffard[2], E.V. Bouhova-Thacker[75], D. Boumediene[37], C. Bourdarios[119], S.K. Boutle[56], A. Boveia[113], J. Boyd[32], I.R. Boyko[68], A.J. Bozson[80], J. Bracinik[19], A. Brandt[8], G. Brandt[57], O. Brandt[60a], F. Braren[45], U. Bratzler[158], B. Brau[89], J.E. Brau[118], W.D. Breaden Madden[56], K. Brendlinger[45], A.J. Brennan[91], L. Brenner[109], R. Brenner[168], S. Bressler[175], D.L. Briglin[19], T.M. Bristow[49], D. Britton[56], D. Britzger[45], F.M. Brochu[30], I. Brock[23], R. Brock[93], G. Brooijmans[38], T. Brooks[80], W.K. Brooks[34b], J. Brosamer[16], E. Brost[110], J.H Broughton[19], P.A. Bruckman de Renstrom[42], D. Bruncko[146b], A. Bruni[22a], G. Bruni[22a], L.S. Bruni[109], S. Bruno[135a,135b], BH Brunt[30], M. Bruschi[22a], N. Bruscino[127], P. Bryant[33], L. Bryngemark[45], T. Buanes[15], Q. Buat[144], P. Buchholz[143], A.G. Buckley[56], I.A. Budagov[68], F. Buehrer[51], M.K. Bugge[121], O. Bulekov[100], D. Bullock[8], T.J. Burch[110], S. Burdin[77], C.D. Burgard[51], A.M. Burger[5], B. Burghgrave[110], K. Burka[42], S. Burke[133], I. Burmeister[46], J.T.P. Burr[122], E. Busato[37], D. Büscher[51], V. Büscher[86], P. Bussey[56], J.M. Butler[24], C.M. Buttar[56], J.M. Butterworth[81], P. Butti[32], W. Buttinger[27], A. Buzatu[153], A.R. Buzykaev[111,c], S. Cabrera Urbán[170], D. Caforio[130], H. Cai[169], V.M. Cairo[40a,40b], O. Cakir[4a], N. Calace[52], P. Calafiura[16], A. Calandri[88], G. Calderini[83], P. Calfayan[64], G. Callea[40a,40b], L.P. Caloba[26a], S. Calvente Lopez[85], D. Calvet[37], S. Calvet[37], T.P. Calvet[88], R. Camacho Toro[33], S. Camarda[32], P. Camarri[135a,135b], D. Cameron[121], R. Caminal Armadans[169], C. Camincher[58], S. Campana[32], M. Campanelli[81], A. Camplani[94a,94b], A. Campoverde[143], V. Canale[106a,106b], M. Cano Bret[36c], J. Cantero[116], T. Cao[155], M.D.M. Capeans Garrido[32], I. Caprini[28b], M. Caprini[28b], M. Capua[40a,40b], R.M. Carbone[38], R. Cardarelli[135a], F. Cardillo[51], I. Carli[131], T. Carli[32], G. Carlino[106a], B.T. Carlson[127], L. Carminati[94a,94b], R.M.D. Carney[148a,148b], S. Caron[108], E. Carquin[34b], S. Carrá[94a,94b], G.D. Carrillo-Montoya[32], D. Casadei[19], M.P. Casado[13,j], M. Casolino[13], D.W. Casper[166], R. Castelijn[109], V. Castillo Gimenez[170], N.F. Castro[128a,k], A. Catinaccio[32], J.R. Catmore[121], A. Cattai[32], J. Caudron[23], V. Cavaliere[169], E. Cavallaro[13], D. Cavalli[94a], M. Cavalli-Sforza[13], V. Cavasinni[126a,126b], E. Celebi[20d], F. Ceradini[136a,136b], L. Cerda Alberich[170], A.S. Cerqueira[26b], A. Cerri[151], L. Cerrito[135a,135b], F. Cerutti[16], A. Cervelli[22a,22b], S.A. Cetin[20d], A. Chafaq[137a], D. Chakraborty[110], S.K. Chan[59], W.S. Chan[109], Y.L. Chan[62a], P. Chang[169], J.D. Chapman[30], D.G. Charlton[19], C.C. Chau[31], C.A. Chavez Barajas[151], S. Che[113], S. Cheatham[167a,167c], A. Chegwidden[93], S. Chekanov[6], S.V. Chekulaev[163a], G.A. Chelkov[68,l], M.A. Chelstowska[32], C. Chen[36a], C. Chen[67], H. Chen[27], J. Chen[36a], S. Chen[35b], S. Chen[157], X. Chen[35c,m], Y. Chen[70], H.C. Cheng[92], H.J. Cheng[35a], A. Cheplakov[68], E. Cheremushkina[132], R. Cherkaoui El Moursli[137e], E. Cheu[7], K. Cheung[63], L. Chevalier[138], V. Chiarella[50], G. Chiarelli[126a,126b], G. Chiodini[76a], A.S. Chisholm[32], A. Chitan[28b], Y.H. Chiu[172], M.V. Chizhov[68], K. Choi[64], A.R. Chomont[37], S. Chouridou[156], Y.S. Chow[62a], V. Christodoulou[81], M.C. Chu[62a], J. Chudoba[129], A.J. Chuinard[90], J.J. Chwastowski[42], L. Chytka[117], A.K. Ciftci[4a], D. Cinca[46], V. Cindro[78], I.A. Cioara[23], A. Ciocio[16], F. Cirotto[106a,106b], Z.H. Citron[175], M. Citterio[94a], M. Ciubancan[28b], A. Clark[52], B.L. Clark[59], M.R. Clark[38], P.J. Clark[49], R.N. Clarke[16], C. Clement[148a,148b], Y. Coadou[88], M. Cobal[167a,167c], A. Coccaro[52], J. Cochran[67], L. Colasurdo[108], B. Cole[38], A.P. Colijn[109], J. Collot[58], T. Colombo[166], P. Conde Muiño[128a,128b], E. Coniavitis[51], S.H. Connell[147b], I.A. Connelly[87], S. Constantinescu[28b], G. Conti[32], F. Conventi[106a,n], M. Cooke[16], A.M. Cooper-Sarkar[122], F. Cormier[171], K.J.R. Cormier[161], M. Corradi[134a,134b], F. Corriveau[90,o], A. Cortes-Gonzalez[32], G. Costa[94a], M.J. Costa[170], D. Costanzo[141], G. Cottin[30],

JHEP12(2017)059

G. Cowan[80], B.E. Cox[87], K. Cranmer[112], S.J. Crawley[56], R.A. Creager[124], G. Cree[31], S. Crépé-Renaudin[58], F. Crescioli[83], W.A. Cribbs[148a,148b], M. Cristinziani[23], V. Croft[112], G. Crosetti[40a,40b], A. Cueto[85], T. Cuhadar Donszelmann[141], A.R. Cukierman[145], J. Cummings[179], M. Curatolo[50], J. Cúth[86], S. Czekierda[42], P. Czodrowski[32], G. D'amen[22a,22b], S. D'Auria[56], L. D'eramo[83], M. D'Onofrio[77], M.J. Da Cunha Sargedas De Sousa[128a,128b], C. Da Via[87], W. Dabrowski[41a], T. Dado[146a], T. Dai[92], O. Dale[15], F. Dallaire[97], C. Dallapiccola[89], M. Dam[39], J.R. Dandoy[124], M.F. Daneri[29], N.P. Dang[176], A.C. Daniells[19], N.S. Dann[87], M. Danninger[171], M. Dano Hoffmann[138], V. Dao[150], G. Darbo[53a], S. Darmora[8], J. Dassoulas[3], A. Dattagupta[118], T. Daubney[45], W. Davey[23], C. David[45], T. Davidek[131], D.R. Davis[48], P. Davison[81], E. Dawe[91], I. Dawson[141], K. De[8], R. de Asmundis[106a], A. De Benedetti[115], S. De Castro[22a,22b], S. De Cecco[83], N. De Groot[108], P. de Jong[109], H. De la Torre[93], F. De Lorenzi[67], A. De Maria[57], D. De Pedis[134a], A. De Salvo[134a], U. De Sanctis[135a,135b], A. De Santo[151], K. De Vasconcelos Corga[88], J.B. De Vivie De Regie[119], R. Debbe[27], C. Debenedetti[139], D.V. Dedovich[68], N. Dehghanian[3], I. Deigaard[109], M. Del Gaudio[40a,40b], J. Del Peso[85], D. Delgove[119], F. Deliot[138], C.M. Delitzsch[7], A. Dell'Acqua[32], L. Dell'Asta[24], M. Dell'Orso[126a,126b], M. Della Pietra[106a,106b], D. della Volpe[52], M. Delmastro[5], C. Delporte[119], P.A. Delsart[58], D.A. DeMarco[161], S. Demers[179], M. Demichev[68], A. Demilly[83], S.P. Denisov[132], D. Denysiuk[138], D. Derendarz[42], J.E. Derkaoui[137d], F. Derue[83], P. Dervan[77], K. Desch[23], C. Deterre[45], K. Dette[161], M.R. Devesa[29], P.O. Deviveiros[32], A. Dewhurst[133], S. Dhaliwal[25], F.A. Di Bello[52], A. Di Ciaccio[135a,135b], L. Di Ciaccio[5], W.K. Di Clemente[124], C. Di Donato[106a,106b], A. Di Girolamo[32], B. Di Girolamo[32], B. Di Micco[136a,136b], R. Di Nardo[32], K.F. Di Petrillo[59], A. Di Simone[51], R. Di Sipio[161], D. Di Valentino[31], C. Diaconu[88], M. Diamond[161], F.A. Dias[39], M.A. Diaz[34a], E.B. Diehl[92], J. Dietrich[17], S. Díez Cornell[45], A. Dimitrievska[14], J. Dingfelder[23], P. Dita[28b], S. Dita[28b], F. Dittus[32], F. Djama[88], T. Djobava[54b], J.I. Djuvsland[60a], M.A.B. do Vale[26c], D. Dobos[32], M. Dobre[28b], D. Dodsworth[25], C. Doglioni[84], J. Dolejsi[131], Z. Dolezal[131], M. Donadelli[26d], S. Donati[126a,126b], P. Dondero[123a,123b], J. Donini[37], J. Dopke[133], A. Doria[106a], M.T. Dova[74], A.T. Doyle[56], E. Drechsler[57], M. Dris[10], Y. Du[36b], J. Duarte-Campderros[155], A. Dubreuil[52], E. Duchovni[175], G. Duckeck[102], A. Ducourthial[83], O.A. Ducu[97,p], D. Duda[109], A. Dudarev[32], A.Chr. Dudder[86], E.M. Duffield[16], L. Duflot[119], M. Dührssen[32], C. Dulsen[178], M. Dumancic[175], A.E. Dumitriu[28b], A.K. Duncan[56], M. Dunford[60a], A. Duperrin[88], H. Duran Yildiz[4a], M. Düren[55], A. Durglishvili[54b], D. Duschinger[47], B. Dutta[45], D. Duvnjak[1], M. Dyndal[45], B.S. Dziedzic[42], C. Eckardt[45], K.M. Ecker[103], R.C. Edgar[92], T. Eifert[32], G. Eigen[15], K. Einsweiler[16], T. Ekelof[168], M. El Kacimi[137c], R. El Kosseifi[88], V. Ellajosyula[88], M. Ellert[168], S. Elles[5], F. Ellinghaus[178], A.A. Elliot[172], N. Ellis[32], J. Elmsheuser[27], M. Elsing[32], D. Emeliyanov[133], Y. Enari[157], O.C. Endner[86], J.S. Ennis[173], M.B. Epland[48], J. Erdmann[46], A. Ereditato[18], M. Ernst[27], S. Errede[169], M. Escalier[119], C. Escobar[170], B. Esposito[50], O. Estrada Pastor[170], A.I. Etienvre[138], E. Etzion[155], H. Evans[64], A. Ezhilov[125], M. Ezzi[137e], F. Fabbri[22a,22b], L. Fabbri[22a,22b], V. Fabiani[108], G. Facini[81], R.M. Fakhrutdinov[132], S. Falciano[134a], R.J. Falla[81], J. Faltova[32], Y. Fang[35a], M. Fanti[94a,94b], A. Farbin[8], A. Farilla[136a], C. Farina[127], E.M. Farina[123a,123b], T. Farooque[93], S. Farrell[16], S.M. Farrington[173], P. Farthouat[32], F. Fassi[137e], P. Fassnacht[32], D. Fassouliotis[9], M. Faucci Giannelli[49], A. Favareto[53a,53b], W.J. Fawcett[122], L. Fayard[119], O.L. Fedin[125,q], W. Fedorko[171], S. Feigl[121], L. Feligioni[88], C. Feng[36b], E.J. Feng[32], M.J. Fenton[56], A.B. Fenyuk[132], L. Feremenga[8], P. Fernandez Martinez[170], S. Fernandez Perez[13], J. Ferrando[45], A. Ferrari[168], P. Ferrari[109], R. Ferrari[123a], D.E. Ferreira de Lima[60b], A. Ferrer[170], D. Ferrere[52], C. Ferretti[92], F. Fiedler[86], A. Filipčič[78], M. Filipuzzi[45], F. Filthaut[108], M. Fincke-Keeler[172], K.D. Finelli[152], M.C.N. Fiolhais[128a,128c,r], L. Fiorini[170], A. Fischer[2], C. Fischer[13], J. Fischer[178], W.C. Fisher[93], N. Flaschel[45], I. Fleck[143], P. Fleischmann[92], R.R.M. Fletcher[124], T. Flick[178], B.M. Flierl[102],

JHEP12(2017)059

L.R. Flores Castillo[62a], M.J. Flowerdew[103], G.T. Forcolin[87], A. Formica[138], F.A. Förster[13], A. Forti[87], A.G. Foster[19], D. Fournier[119], H. Fox[75], S. Fracchia[141], P. Francavilla[83], M. Franchini[22a,22b], S. Franchino[60a], D. Francis[32], L. Franconi[121], M. Franklin[59], M. Frate[166], M. Fraternali[123a,123b], D. Freeborn[81], S.M. Fressard-Batraneanu[32], B. Freund[97], D. Froidevaux[32], J.A. Frost[122], C. Fukunaga[158], T. Fusayasu[104], J. Fuster[170], O. Gabizon[154], A. Gabrielli[22a,22b], A. Gabrielli[16], G.P. Gach[41a], S. Gadatsch[32], S. Gadomski[80], G. Gagliardi[53a,53b], L.G. Gagnon[97], C. Galea[108], B. Galhardo[128a,128c], E.J. Gallas[122], B.J. Gallop[133], P. Gallus[130], G. Galster[39], K.K. Gan[113], S. Ganguly[37], Y. Gao[77], Y.S. Gao[145,g], F.M. Garay Walls[34a], C. García[170], J.E. García Navarro[170], J.A. García Pascual[35a], M. Garcia-Sciveres[16], R.W. Gardner[33], N. Garelli[145], V. Garonne[121], A. Gascon Bravo[45], K. Gasnikova[45], C. Gatti[50], A. Gaudiello[53a,53b], G. Gaudio[123a], I.L. Gavrilenko[98], C. Gay[171], G. Gaycken[23], E.N. Gazis[10], C.N.P. Gee[133], J. Geisen[57], M. Geisen[86], M.P. Geisler[60a], K. Gellerstedt[148a,148b], C. Gemme[53a], M.H. Genest[58], C. Geng[92], S. Gentile[134a,134b], C. Gentsos[156], S. George[80], D. Gerbaudo[13], G. Geßner[46], S. Ghasemi[143], M. Ghneimat[23], B. Giacobbe[22a], S. Giagu[134a,134b], N. Giangiacomi[22a,22b], P. Giannetti[126a,126b], S.M. Gibson[80], M. Gignac[171], M. Gilchriese[16], D. Gillberg[31], G. Gilles[178], D.M. Gingrich[3,d], M.P. Giordani[167a,167c], F.M. Giorgi[22a], P.F. Giraud[138], P. Giromini[59], G. Giugliarelli[167a,167c], D. Giugni[94a], F. Giuli[122], C. Giuliani[103], M. Giulini[60b], B.K. Gjelsten[121], S. Gkaitatzis[156], I. Gkialas[9,s], E.L. Gkougkousis[13], P. Gkountoumis[10], L.K. Gladilin[101], C. Glasman[85], J. Glatzer[13], P.C.F. Glaysher[45], A. Glazov[45], M. Goblirsch-Kolb[25], J. Godlewski[42], S. Goldfarb[91], T. Golling[52], D. Golubkov[132], A. Gomes[128a,128b,128d], R. Gonçalo[128a], R. Goncalves Gama[26a], J. Goncalves Pinto Firmino Da Costa[138], G. Gonella[51], L. Gonella[19], A. Gongadze[68], S. González de la Hoz[170], S. Gonzalez-Sevilla[52], L. Goossens[32], P.A. Gorbounov[99], H.A. Gordon[27], I. Gorelov[107], B. Gorini[32], E. Gorini[76a,76b], A. Gorišek[78], A.T. Goshaw[48], C. Gössling[46], M.I. Gostkin[68], C.A. Gottardo[23], C.R. Goudet[119], D. Goujdami[137c], A.G. Goussiou[140], N. Govender[147b,t], E. Gozani[154], I. Grabowska-Bold[41a], P.O.J. Gradin[168], J. Gramling[166], E. Gramstad[121], S. Grancagnolo[17], V. Gratchev[125], P.M. Gravila[28f], C. Gray[56], H.M. Gray[16], Z.D. Greenwood[82,u], C. Grefe[23], K. Gregersen[81], I.M. Gregor[45], P. Grenier[145], K. Grevtsov[5], J. Griffiths[8], A.A. Grillo[139], K. Grimm[75], S. Grinstein[13,v], Ph. Gris[37], J.-F. Grivaz[119], S. Groh[86], E. Gross[175], J. Grosse-Knetter[57], G.C. Grossi[82], Z.J. Grout[81], A. Grummer[107], L. Guan[92], W. Guan[176], J. Guenther[32], F. Guescini[163a], D. Guest[166], O. Gueta[155], B. Gui[113], E. Guido[53a,53b], T. Guillemin[5], S. Guindon[32], U. Gul[56], C. Gumpert[32], J. Guo[36c], W. Guo[92], Y. Guo[36a], R. Gupta[43], S. Gupta[122], S. Gurbuz[20a], G. Gustavino[115], B.J. Gutelman[154], P. Gutierrez[115], N.G. Gutierrez Ortiz[81], C. Gutschow[81], C. Guyot[138], M.P. Guzik[41a], C. Gwenlan[122], C.B. Gwilliam[77], A. Haas[112], C. Haber[16], H.K. Hadavand[8], N. Haddad[137e], A. Hadef[88], S. Hageböck[23], M. Hagihara[164], H. Hakobyan[180,*], M. Haleem[45], J. Haley[116], G. Halladjian[93], G.D. Hallewell[88], K. Hamacher[178], P. Hamal[117], K. Hamano[172], A. Hamilton[147a], G.N. Hamity[141], P.G. Hamnett[45], L. Han[36a], S. Han[35a], K. Hanagaki[69,w], K. Hanawa[157], M. Hance[139], B. Haney[124], P. Hanke[60a], J.B. Hansen[39], J.D. Hansen[39], M.C. Hansen[23], P.H. Hansen[39], K. Hara[164], A.S. Hard[176], T. Harenberg[178], F. Hariri[119], S. Harkusha[95], P.F. Harrison[173], N.M. Hartmann[102], Y. Hasegawa[142], A. Hasib[49], S. Hassani[138], S. Haug[18], R. Hauser[93], L. Hauswald[47], L.B. Havener[38], M. Havranek[130], C.M. Hawkes[19], R.J. Hawkings[32], D. Hayakawa[159], D. Hayden[93], C.P. Hays[122], J.M. Hays[79], H.S. Hayward[77], S.J. Haywood[133], S.J. Head[19], T. Heck[86], V. Hedberg[84], L. Heelan[8], S. Heer[23], K.K. Heidegger[51], S. Heim[45], T. Heim[16], B. Heinemann[45,x], J.J. Heinrich[102], L. Heinrich[112], C. Heinz[55], J. Hejbal[129], L. Helary[32], A. Held[171], S. Hellman[148a,148b], C. Helsens[32], R.C.W. Henderson[75], Y. Heng[176], S. Henkelmann[171], A.M. Henriques Correia[32], S. Henrot-Versille[119], G.H. Herbert[17], H. Herde[25], V. Herget[177], Y. Hernández Jiménez[147c], H. Herr[86], G. Herten[51], R. Hertenberger[102], L. Hervas[32], T.C. Herwig[124], G.G. Hesketh[81], N.P. Hessey[163a], J.W. Hetherly[43], S. Higashino[69],

JHEP12(2017)059

E. Higón-Rodriguez[170], K. Hildebrand[33], E. Hill[172], J.C. Hill[30], K.H. Hiller[45], S.J. Hillier[19], M. Hils[47], I. Hinchliffe[16], M. Hirose[51], D. Hirschbuehl[178], B. Hiti[78], O. Hladik[129], X. Hoad[49], J. Hobbs[150], N. Hod[163a], M.C. Hodgkinson[141], P. Hodgson[141], A. Hoecker[32], M.R. Hoeferkamp[107], F. Hoenig[102], D. Hohn[23], T.R. Holmes[33], M. Homann[46], S. Honda[164], T. Honda[69], T.M. Hong[127], B.H. Hooberman[169], W.H. Hopkins[118], Y. Horii[105], A.J. Horton[144], J-Y. Hostachy[58], A. Hostiuc[140], S. Hou[153], A. Hoummada[137a], J. Howarth[87], J. Hoya[74], M. Hrabovsky[117], J. Hrdinka[32], I. Hristova[17], J. Hrivnac[119], T. Hryn'ova[5], A. Hrynevich[96], P.J. Hsu[63], S.-C. Hsu[140], Q. Hu[36a], S. Hu[36c], Y. Huang[35a], Z. Hubacek[130], F. Hubaut[88], F. Huegging[23], T.B. Huffman[122], E.W. Hughes[38], G. Hughes[75], M. Huhtinen[32], R.F.H. Hunter[31], P. Huo[150], N. Huseynov[68,b], J. Huston[93], J. Huth[59], R. Hyneman[92], G. Iacobucci[52], G. Iakovidis[27], I. Ibragimov[143], L. Iconomidou-Fayard[119], Z. Idrissi[137e], P. Iengo[32], O. Igonkina[109,y], T. Iizawa[174], Y. Ikegami[69], M. Ikeno[69], Y. Ilchenko[11,z], D. Iliadis[156], N. Ilic[145], F. Iltzsche[47], G. Introzzi[123a,123b], P. Ioannou[9,*], M. Iodice[136a], K. Iordanidou[38], V. Ippolito[59], M.F. Isacson[168], N. Ishijima[120], M. Ishino[157], M. Ishitsuka[159], C. Issever[122], S. Istin[20a], F. Ito[164], J.M. Iturbe Ponce[62a], R. Iuppa[162a,162b], H. Iwasaki[69], J.M. Izen[44], V. Izzo[106a], S. Jabbar[3], P. Jackson[1], R.M. Jacobs[23], V. Jain[2], K.B. Jakobi[86], K. Jakobs[51], S. Jakobsen[65], T. Jakoubek[129], D.O. Jamin[116], D.K. Jana[82], R. Jansky[52], J. Janssen[23], M. Janus[57], P.A. Janus[41a], G. Jarlskog[84], N. Javadov[68,b], T. Javůrek[51], M. Javurkova[51], F. Jeanneau[138], L. Jeanty[16], J. Jejelava[54a,aa], A. Jelinskas[173], P. Jenni[51,ab], C. Jeske[173], S. Jézéquel[5], H. Ji[176], J. Jia[150], H. Jiang[67], Y. Jiang[36a], Z. Jiang[145], S. Jiggins[81], J. Jimenez Pena[170], S. Jin[35a], A. Jinaru[28b], O. Jinnouchi[159], H. Jivan[147c], P. Johansson[141], K.A. Johns[7], C.A. Johnson[64], W.J. Johnson[140], K. Jon-And[148a,148b], R.W.L. Jones[75], S.D. Jones[151], S. Jones[7], T.J. Jones[77], J. Jongmanns[60a], P.M. Jorge[128a,128b], J. Jovicevic[163a], X. Ju[176], A. Juste Rozas[13,v], M.K. Köhler[175], A. Kaczmarska[42], M. Kado[119], H. Kagan[113], M. Kagan[145], S.J. Kahn[88], T. Kaji[174], E. Kajomovitz[154], C.W. Kalderon[84], A. Kaluza[86], S. Kama[43], A. Kamenshchikov[132], N. Kanaya[157], L. Kanjir[78], V.A. Kantserov[100], J. Kanzaki[69], B. Kaplan[112], L.S. Kaplan[176], D. Kar[147c], K. Karakostas[10], N. Karastathis[10], M.J. Kareem[163b], E. Karentzos[10], S.N. Karpov[68], Z.M. Karpova[68], K. Karthik[112], V. Kartvelishvili[75], A.N. Karyukhin[132], K. Kasahara[164], L. Kashif[176], R.D. Kass[113], A. Kastanas[149], Y. Kataoka[157], C. Kato[157], A. Katre[52], J. Katzy[45], K. Kawade[70], K. Kawagoe[73], T. Kawamoto[157], G. Kawamura[57], E.F. Kay[77], V.F. Kazanin[111,c], R. Keeler[172], R. Kehoe[43], J.S. Keller[31], E. Kellermann[84], J.J. Kempster[80], J Kendrick[19], H. Keoshkerian[161], O. Kepka[129], B.P. Kerševan[78], S. Kersten[178], R.A. Keyes[90], M. Khader[169], F. Khalil-zada[12], A. Khanov[116], A.G. Kharlamov[111,c], T. Kharlamova[111,c], A. Khodinov[160], T.J. Khoo[52], V. Khovanskiy[99,*], E. Khramov[68], J. Khubua[54b,ac], S. Kido[70], C.R. Kilby[80], H.Y. Kim[8], S.H. Kim[164], Y.K. Kim[33], N. Kimura[156], O.M. Kind[17], B.T. King[77], D. Kirchmeier[47], J. Kirk[133], A.E. Kiryunin[103], T. Kishimoto[157], D. Kisielewska[41a], V. Kitali[45], O. Kivernyk[5], E. Kladiva[146b], T. Klapdor-Kleingrothaus[51], M.H. Klein[92], M. Klein[77], U. Klein[77], K. Kleinknecht[86], P. Klimek[110], A. Klimentov[27], R. Klingenberg[46], T. Klingl[23], T. Klioutchnikova[32], E.-E. Kluge[60a], P. Kluit[109], S. Kluth[103], E. Kneringer[65], E.B.F.G. Knoops[88], A. Knue[103], A. Kobayashi[157], D. Kobayashi[73], T. Kobayashi[157], M. Kobel[47], M. Kocian[145], P. Kodys[131], T. Koffas[31], E. Koffeman[109], N.M. Köhler[103], T. Koi[145], M. Kolb[60b], I. Koletsou[5], A.A. Komar[98,*], T. Kondo[69], N. Kondrashova[36c], K. Köneke[51], A.C. König[108], T. Kono[69,ad], R. Konoplich[112,ae], N. Konstantinidis[81], R. Kopeliansky[64], S. Koperny[41a], A.K. Kopp[51], K. Korcyl[42], K. Kordas[156], A. Korn[81], A.A. Korol[111,c], I. Korolkov[13], E.V. Korolkova[141], O. Kortner[103], S. Kortner[103], T. Kosek[131], V.V. Kostyukhin[23], A. Kotwal[48], A. Koulouris[10], A. Kourkoumeli-Charalampidi[123a,123b], C. Kourkoumelis[9], E. Kourlitis[141], V. Kouskoura[27], A.B. Kowalewska[42], R. Kowalewski[172], T.Z. Kowalski[41a], C. Kozakai[157], W. Kozanecki[138], A.S. Kozhin[132], V.A. Kramarenko[101], G. Kramberger[78], D. Krasnopevtsev[100], M.W. Krasny[83],

JHEP12(2017)059

A. Krasznahorkay[32], D. Krauss[103], J.A. Kremer[41a], J. Kretzschmar[77], K. Kreutzfeldt[55], P. Krieger[161], K. Krizka[16], K. Kroeninger[46], H. Kroha[103], J. Kroll[129], J. Kroll[124], J. Kroseberg[23], J. Krstic[14], U. Kruchonak[68], H. Krüger[23], N. Krumnack[67], M.C. Kruse[48], T. Kubota[91], H. Kucuk[81], S. Kuday[4b], J.T. Kuechler[178], S. Kuehn[32], A. Kugel[60a], F. Kuger[177], T. Kuhl[45], V. Kukhtin[68], R. Kukla[88], Y. Kulchitsky[95], S. Kuleshov[34b], Y.P. Kulinich[169], M. Kuna[134a,134b], T. Kunigo[71], A. Kupco[129], T. Kupfer[46], O. Kuprash[155], H. Kurashige[70], L.L. Kurchaninov[163a], Y.A. Kurochkin[95], M.G. Kurth[35a], E.S. Kuwertz[172], M. Kuze[159], J. Kvita[117], T. Kwan[172], D. Kyriazopoulos[141], A. La Rosa[103], J.L. La Rosa Navarro[26d], L. La Rotonda[40a,40b], F. La Ruffa[40a,40b], C. Lacasta[170], F. Lacava[134a,134b], J. Lacey[45], D.P.J. Lack[87], H. Lacker[17], D. Lacour[83], E. Ladygin[68], R. Lafaye[5], B. Laforge[83], T. Lagouri[179], S. Lai[57], S. Lammers[64], W. Lampl[7], E. Lançon[27], U. Landgraf[51], M.P.J. Landon[79], M.C. Lanfermann[52], V.S. Lang[45], J.C. Lange[13], R.J. Langenberg[32], A.J. Lankford[166], F. Lanni[27], K. Lantzsch[23], A. Lanza[123a], A. Lapertosa[53a,53b], S. Laplace[83], J.F. Laporte[138], T. Lari[94a], F. Lasagni Manghi[22a,22b], M. Lassnig[32], T.S. Lau[62a], P. Laurelli[50], W. Lavrijsen[16], A.T. Law[139], P. Laycock[77], T. Lazovich[59], M. Lazzaroni[94a,94b], B. Le[91], O. Le Dortz[83], E. Le Guirriec[88], E.P. Le Quilleuc[138], M. LeBlanc[172], T. LeCompte[6], F. Ledroit-Guillon[58], C.A. Lee[27], G.R. Lee[34a], S.C. Lee[153], L. Lee[59], B. Lefebvre[90], G. Lefebvre[83], M. Lefebvre[172], F. Legger[102], C. Leggett[16], G. Lehmann Miotto[32], X. Lei[7], W.A. Leight[45], M.A.L. Leite[26d], R. Leitner[131], D. Lellouch[175], B. Lemmer[57], K.J.C. Leney[81], T. Lenz[23], B. Lenzi[32], R. Leone[7], S. Leone[126a,126b], C. Leonidopoulos[49], G. Lerner[151], C. Leroy[97], R. Les[161], A.A.J. Lesage[138], C.G. Lester[30], M. Levchenko[125], J. Levêque[5], D. Levin[92], L.J. Levinson[175], M. Levy[19], D. Lewis[79], B. Li[36a,af], Changqiao Li[36a], H. Li[150], L. Li[36c], Q. Li[35a], Q. Li[36a], S. Li[48], X. Li[36c], Y. Li[143], Z. Liang[35a], B. Liberti[135a], A. Liblong[161], K. Lie[62c], J. Liebal[23], W. Liebig[15], A. Limosani[152], K. Lin[93], S.C. Lin[182], T.H. Lin[86], R.A. Linck[64], B.E. Lindquist[150], A.E. Lionti[52], E. Lipeles[124], A. Lipniacka[15], M. Lisovyi[60b], T.M. Liss[169,ag], A. Lister[171], A.M. Litke[139], B. Liu[67], H. Liu[92], H. Liu[27], J.K.K. Liu[122], J. Liu[36b], J.B. Liu[36a], K. Liu[88], L. Liu[169], M. Liu[36a], Y.L. Liu[36a], Y. Liu[36a], M. Livan[123a,123b], A. Lleres[58], J. Llorente Merino[35a], S.L. Lloyd[79], C.Y. Lo[62b], F. Lo Sterzo[43], E.M. Lobodzinska[45], P. Loch[7], F.K. Loebinger[87], A. Loesle[51], K.M. Loew[25], T. Lohse[17], K. Lohwasser[141], M. Lokajicek[129], B.A. Long[24], J.D. Long[169], R.E. Long[75], L. Longo[76a,76b], K.A. Looper[113], J.A. Lopez[34b], I. Lopez Paz[13], A. Lopez Solis[83], J. Lorenz[102], N. Lorenzo Martinez[5], M. Losada[21], P.J. Lösel[102], X. Lou[35a], A. Lounis[119], J. Love[6], P.A. Love[75], H. Lu[62a], N. Lu[92], Y.J. Lu[63], H.J. Lubatti[140], C. Luci[134a,134b], A. Lucotte[58], C. Luedtke[51], F. Luehring[64], W. Lukas[65], L. Luminari[134a], O. Lundberg[148a,148b], B. Lund-Jensen[149], M.S. Lutz[89], P.M. Luzi[83], D. Lynn[27], R. Lysak[129], E. Lytken[84], F. Lyu[35a], V. Lyubushkin[68], H. Ma[27], L.L. Ma[36b], Y. Ma[36b], G. Maccarrone[50], A. Macchiolo[103], C.M. Macdonald[141], B. Maček[78], J. Machado Miguens[124,128b], D. Madaffari[170], R. Madar[37], W.F. Mader[47], A. Madsen[45], N. Madysa[47], J. Maeda[70], S. Maeland[15], T. Maeno[27], A.S. Maevskiy[101], V. Magerl[51], C. Maiani[119], C. Maidantchik[26a], T. Maier[102], A. Maio[128a,128b,128d], O. Majersky[146a], S. Majewski[118], Y. Makida[69], N. Makovec[119], B. Malaescu[83], Pa. Malecki[42], V.P. Maleev[125], F. Malek[58], U. Mallik[66], D. Malon[6], C. Malone[30], S. Maltezos[10], S. Malyukov[32], J. Mamuzic[170], G. Mancini[50], I. Mandić[78], J. Maneira[128a,128b], L. Manhaes de Andrade Filho[26b], J. Manjarres Ramos[47], K.H. Mankinen[84], A. Mann[102], A. Manousos[32], B. Mansoulie[138], J.D. Mansour[35a], R. Mantifel[90], M. Mantoani[57], S. Manzoni[94a,94b], L. Mapelli[32], G. Marceca[29], L. March[52], L. Marchese[122], G. Marchiori[83], M. Marcisovsky[129], C.A. Marin Tobon[32], M. Marjanovic[37], D.E. Marley[92], F. Marroquim[26a], S.P. Marsden[87], Z. Marshall[16], M.U.F Martensson[168], S. Marti-Garcia[170], C.B. Martin[113], T.A. Martin[173], V.J. Martin[49], B. Martin dit Latour[15], M. Martinez[13,v], V.I. Martinez Outschoorn[169], S. Martin-Haugh[133], V.S. Martoiu[28b], A.C. Martyniuk[81], A. Marzin[32], L. Masetti[86], T. Mashimo[157], R. Mashinistov[98],

JHEP12(2017)059

J. Masik[87], A.L. Maslennikov[111,c], L.H. Mason[91], L. Massa[135a,135b], P. Mastrandrea[5], A. Mastroberardino[40a,40b], T. Masubuchi[157], P. Mättig[178], J. Maurer[28b], S.J. Maxfield[77], D.A. Maximov[111,c], R. Mazini[153], I. Maznas[156], S.M. Mazza[94a,94b], N.C. Mc Fadden[107], G. Mc Goldrick[161], S.P. Mc Kee[92], A. McCarn[92], R.L. McCarthy[150], T.G. McCarthy[103], L.I. McClymont[81], E.F. McDonald[91], J.A. Mcfayden[32], G. Mchedlidze[57], S.J. McMahon[133], P.C. McNamara[91], C.J. McNicol[173], R.A. McPherson[172,o], S. Meehan[140], T.J. Megy[51], S. Mehlhase[102], A. Mehta[77], T. Meideck[58], K. Meier[60a], B. Meirose[44], D. Melini[170,ah], B.R. Mellado Garcia[147c], J.D. Mellenthin[57], M. Melo[146a], F. Meloni[18], A. Melzer[23], S.B. Menary[87], L. Meng[77], X.T. Meng[92], A. Mengarelli[22a,22b], S. Menke[103], E. Meoni[40a,40b], S. Mergelmeyer[17], C. Merlassino[18], P. Mermod[52], L. Merola[106a,106b], C. Meroni[94a], F.S. Merritt[33], A. Messina[134a,134b], J. Metcalfe[6], A.S. Mete[166], C. Meyer[124], J-P. Meyer[138], J. Meyer[109], H. Meyer Zu Theenhausen[60a], F. Miano[151], R.P. Middleton[133], S. Miglioranzi[53a,53b], L. Mijović[49], G. Mikenberg[175], M. Mikestikova[129], M. Mikuž[78], M. Milesi[91], A. Milic[161], D.A. Millar[79], D.W. Miller[33], C. Mills[49], A. Milov[175], D.A. Milstead[148a,148b], A.A. Minaenko[132], Y. Minami[157], I.A. Minashvili[54b], A.I. Mincer[112], B. Mindur[41a], M. Mineev[68], Y. Minegishi[157], Y. Ming[176], L.M. Mir[13], A. Mirto[76a,76b], K.P. Mistry[124], T. Mitani[174], J. Mitrevski[102], V.A. Mitsou[170], A. Miucci[18], P.S. Miyagawa[141], A. Mizukami[69], J.U. Mjörnmark[84], T. Mkrtchyan[180], M. Mlynarikova[131], T. Moa[148a,148b], K. Mochizuki[97], P. Mogg[51], S. Mohapatra[38], S. Molander[148a,148b], R. Moles-Valls[23], M.C. Mondragon[93], K. Mönig[45], J. Monk[39], E. Monnier[88], A. Montalbano[150], J. Montejo Berlingen[32], F. Monticelli[74], S. Monzani[94a,94b], R.W. Moore[3], N. Morange[119], D. Moreno[21], M. Moreno Llácer[32], P. Morettini[53a], S. Morgenstern[32], D. Mori[144], T. Mori[157], M. Morii[59], M. Morinaga[174], V. Morisbak[121], A.K. Morley[32], G. Mornacchi[32], J.D. Morris[79], L. Morvaj[150], P. Moschovakos[10], M. Mosidze[54b], H.J. Moss[141], J. Moss[145,ai], K. Motohashi[159], R. Mount[145], E. Mountricha[27], E.J.W. Moyse[89], S. Muanza[88], F. Mueller[103], J. Mueller[127], R.S.P. Mueller[102], D. Muenstermann[75], P. Mullen[56], G.A. Mullier[18], F.J. Munoz Sanchez[87], W.J. Murray[173,133], H. Musheghyan[32], M. Muškinja[78], A.G. Myagkov[132,aj], M. Myska[130], B.P. Nachman[16], O. Nackenhorst[52], K. Nagai[122], R. Nagai[69,ad], K. Nagano[69], Y. Nagasaka[61], K. Nagata[164], M. Nagel[51], E. Nagy[88], A.M. Nairz[32], Y. Nakahama[105], K. Nakamura[69], T. Nakamura[157], I. Nakano[114], R.F. Naranjo Garcia[45], R. Narayan[11], D.I. Narrias Villar[60a], I. Naryshkin[125], T. Naumann[45], G. Navarro[21], R. Nayyar[7], H.A. Neal[92], P.Yu. Nechaeva[98], T.J. Neep[138], A. Negri[123a,123b], M. Negrini[22a], S. Nektarijevic[108], C. Nellist[57], A. Nelson[166], M.E. Nelson[122], S. Nemecek[129], P. Nemethy[112], M. Nessi[32,ak], M.S. Neubauer[169], M. Neumann[178], P.R. Newman[19], T.Y. Ng[62c], T. Nguyen Manh[97], R.B. Nickerson[122], R. Nicolaidou[138], J. Nielsen[139], N. Nikiforou[11], V. Nikolaenko[132,aj], I. Nikolic-Audit[83], K. Nikolopoulos[19], J.K. Nilsen[121], P. Nilsson[27], Y. Ninomiya[157], A. Nisati[134a], N. Nishu[36c], R. Nisius[103], I. Nitsche[46], T. Nitta[174], T. Nobe[157], Y. Noguchi[71], M. Nomachi[120], I. Nomidis[31], M.A. Nomura[27], T. Nooney[79], M. Nordberg[32], N. Norjoharuddeen[122], O. Novgorodova[47], M. Nozaki[69], L. Nozka[117], K. Ntekas[166], E. Nurse[81], F. Nuti[91], K. O'connor[25], D.C. O'Neil[144], A.A. O'Rourke[45], V. O'Shea[56], F.G. Oakham[31,d], H. Oberlack[103], T. Obermann[23], J. Ocariz[83], A. Ochi[70], I. Ochoa[38], J.P. Ochoa-Ricoux[34a], S. Oda[73], S. Odaka[69], A. Oh[87], S.H. Oh[48], C.C. Ohm[149], H. Ohman[168], H. Oide[53a,53b], H. Okawa[164], Y. Okumura[157], T. Okuyama[69], A. Olariu[28b], L.F. Oleiro Seabra[128a], S.A. Olivares Pino[34a], D. Oliveira Damazio[27], A. Olszewski[42], J. Olszowska[42], A. Onofre[128a,128e], K. Onogi[105], P.U.E. Onyisi[11,z], H. Oppen[121], M.J. Oreglia[33], Y. Oren[155], D. Orestano[136a,136b], N. Orlando[62b], R.S. Orr[161], B. Osculati[53a,53b,*], R. Ospanov[36a], G. Otero y Garzon[29], H. Otono[73], M. Ouchrif[137d], F. Ould-Saada[121], A. Ouraou[138], K.P. Oussoren[109], Q. Ouyang[35a], M. Owen[56], R.E. Owen[19], V.E. Ozcan[20a], N. Ozturk[8], K. Pachal[144], A. Pacheco Pages[13], L. Pacheco Rodriguez[138], C. Padilla Aranda[13], S. Pagan Griso[16], M. Paganini[179], F. Paige[27], G. Palacino[64], S. Palazzo[40a,40b], S. Palestini[32],

JHEP12(2017)059

M. Palka[41b], D. Pallin[37], E.St. Panagiotopoulou[10], I. Panagoulias[10], C.E. Pandini[52], J.G. Panduro Vazquez[80], P. Pani[32], S. Panitkin[27], D. Pantea[28b], L. Paolozzi[52], Th.D. Papadopoulou[10], K. Papageorgiou[9,s], A. Paramonov[6], D. Paredes Hernandez[179], A.J. Parker[75], M.A. Parker[30], K.A. Parker[45], F. Parodi[53a,53b], J.A. Parsons[38], U. Parzefall[51], V.R. Pascuzzi[161], J.M. Pasner[139], E. Pasqualucci[134a], S. Passaggio[53a], Fr. Pastore[80], S. Pataraia[86], J.R. Pater[87], T. Pauly[32], B. Pearson[103], S. Pedraza Lopez[170], R. Pedro[128a,128b], S.V. Peleganchuk[111,c], O. Penc[129], C. Peng[35a], H. Peng[36a], J. Penwell[64], B.S. Peralva[26b], M.M. Perego[138], D.V. Perepelitsa[27], F. Peri[17], L. Perini[94a,94b], H. Pernegger[32], S. Perrella[106a,106b], R. Peschke[45], V.D. Peshekhonov[68,*], K. Peters[45], R.F.Y. Peters[87], B.A. Petersen[32], T.C. Petersen[39], E. Petit[58], A. Petridis[1], C. Petridou[156], P. Petroff[119], E. Petrolo[134a], M. Petrov[122], F. Petrucci[136a,136b], N.E. Pettersson[89], A. Peyaud[138], R. Pezoa[34b], F.H. Phillips[93], P.W. Phillips[133], G. Piacquadio[150], E. Pianori[173], A. Picazio[89], E. Piccaro[79], M.A. Pickering[122], R. Piegaia[29], J.E. Pilcher[33], A.D. Pilkington[87], M. Pinamonti[135a,135b], J.L. Pinfold[3], H. Pirumov[45], M. Pitt[175], L. Plazak[146a], M.-A. Pleier[27], V. Pleskot[86], E. Plotnikova[68], D. Pluth[67], P. Podberezko[111], R. Poettgen[84], R. Poggi[123a,123b], L. Poggioli[119], I. Pogrebnyak[93], D. Pohl[23], I. Pokharel[57], G. Polesello[123a], A. Poley[45], A. Policicchio[40a,40b], R. Polifka[32], A. Polini[22a], C.S. Pollard[56], V. Polychronakos[27], K. Pommès[32], D. Ponomarenko[100], L. Pontecorvo[134a], G.A. Popeneciu[28d], D.M. Portillo Quintero[83], S. Pospisil[130], K. Potamianos[45], I.N. Potrap[68], C.J. Potter[30], H. Potti[11], T. Poulsen[84], J. Poveda[32], M.E. Pozo Astigarraga[32], P. Pralavorio[88], A. Pranko[16], S. Prell[67], D. Price[87], M. Primavera[76a], S. Prince[90], N. Proklova[100], K. Prokofiev[62c], F. Prokoshin[34b], S. Protopopescu[27], J. Proudfoot[6], M. Przybycien[41a], A. Puri[169], P. Puzo[119], J. Qian[92], G. Qin[56], Y. Qin[87], A. Quadt[57], M. Queitsch-Maitland[45], D. Quilty[56], S. Raddum[121], V. Radeka[27], V. Radescu[122], S.K. Radhakrishnan[150], P. Radloff[118], P. Rados[91], F. Ragusa[94a,94b], G. Rahal[181], J.A. Raine[87], S. Rajagopalan[27], C. Rangel-Smith[168], T. Rashid[119], S. Raspopov[5], M.G. Ratti[94a,94b], D.M. Rauch[45], F. Rauscher[102], S. Rave[86], I. Ravinovich[175], J.H. Rawling[87], M. Raymond[32], A.L. Read[121], N.P. Readioff[58], M. Reale[76a,76b], D.M. Rebuzzi[123a,123b], A. Redelbach[177], G. Redlinger[27], R. Reece[139], R.G. Reed[147c], K. Reeves[44], L. Rehnisch[17], J. Reichert[124], A. Reiss[86], C. Rembser[32], H. Ren[35a], M. Rescigno[134a], S. Resconi[94a], E.D. Resseguie[124], S. Rettie[171], E. Reynolds[19], O.L. Rezanova[111,c], P. Reznicek[131], R. Rezvani[97], R. Richter[103], S. Richter[81], E. Richter-Was[41b], O. Ricken[23], M. Ridel[83], P. Rieck[103], C.J. Riegel[178], J. Rieger[57], O. Rifki[115], M. Rijssenbeek[150], A. Rimoldi[123a,123b], M. Rimoldi[18], L. Rinaldi[22a], G. Ripellino[149], B. Ristić[32], E. Ritsch[32], I. Riu[13], F. Rizatdinova[116], E. Rizvi[79], C. Rizzi[13], R.T. Roberts[87], S.H. Robertson[90,o], A. Robichaud-Veronneau[90], D. Robinson[30], J.E.M. Robinson[45], A. Robson[56], E. Rocco[86], C. Roda[126a,126b], Y. Rodina[88,al], S. Rodriguez Bosca[170], A. Rodriguez Perez[13], D. Rodriguez Rodriguez[170], S. Roe[32], C.S. Rogan[59], O. Røhne[121], J. Roloff[59], A. Romaniouk[100], M. Romano[22a,22b], S.M. Romano Saez[37], E. Romero Adam[170], N. Rompotis[77], M. Ronzani[51], L. Roos[83], S. Rosati[134a], K. Rosbach[51], P. Rose[139], N.-A. Rosien[57], E. Rossi[106a,106b], L.P. Rossi[53a], J.H.N. Rosten[30], R. Rosten[140], M. Rotaru[28b], J. Rothberg[140], D. Rousseau[119], A. Rozanov[88], Y. Rozen[154], X. Ruan[147c], F. Rubbo[145], F. Rühr[51], A. Ruiz-Martinez[31], Z. Rurikova[51], N.A. Rusakovich[68], H.L. Russell[90], J.P. Rutherfoord[7], N. Ruthmann[32], Y.F. Ryabov[125], M. Rybar[169], G. Rybkin[119], S. Ryu[6], A. Ryzhov[132], G.F. Rzehorz[57], A.F. Saavedra[152], G. Sabato[109], S. Sacerdoti[29], H.F-W. Sadrozinski[139], R. Sadykov[68], F. Safai Tehrani[134a], P. Saha[110], M. Sahinsoy[60a], M. Saimpert[45], M. Saito[157], T. Saito[157], H. Sakamoto[157], Y. Sakurai[174], G. Salamanna[136a,136b], J.E. Salazar Loyola[34b], D. Salek[109], P.H. Sales De Bruin[168], D. Salihagic[103], A. Salnikov[145], J. Salt[170], D. Salvatore[40a,40b], F. Salvatore[151], A. Salvucci[62a,62b,62c], A. Salzburger[32], D. Sammel[51], D. Sampsonidis[156], D. Sampsonidou[156], J. Sánchez[170], V. Sanchez Martinez[170], A. Sanchez Pineda[167a,167c], H. Sandaker[121], R.L. Sandbach[79], C.O. Sander[45], M. Sandhoff[178],

JHEP12(2017)059

C. Sandoval[21], D.P.C. Sankey[133], M. Sannino[53a,53b], Y. Sano[105], A. Sansoni[50], C. Santoni[37], H. Santos[128a], I. Santoyo Castillo[151], A. Sapronov[68], J.G. Saraiva[128a,128d], B. Sarrazin[23], O. Sasaki[69], K. Sato[164], E. Sauvan[5], G. Savage[80], P. Savard[161,d], N. Savic[103], C. Sawyer[133], L. Sawyer[82,u], J. Saxon[33], C. Sbarra[22a], A. Sbrizzi[22a,22b], T. Scanlon[81], D.A. Scannicchio[166], J. Schaarschmidt[140], P. Schacht[103], B.M. Schachtner[102], D. Schaefer[33], L. Schaefer[124], R. Schaefer[45], J. Schaeffer[86], S. Schaepe[23], S. Schaetzel[60b], U. Schäfer[86], A.C. Schaffer[119], D. Schaile[102], R.D. Schamberger[150], V.A. Schegelsky[125], D. Scheirich[131], M. Schernau[166], C. Schiavi[53a,53b], S. Schier[139], L.K. Schildgen[23], C. Schillo[51], M. Schioppa[40a,40b], S. Schlenker[32], K.R. Schmidt-Sommerfeld[103], K. Schmieden[32], C. Schmitt[86], S. Schmitt[45], S. Schmitz[86], U. Schnoor[51], L. Schoeffel[138], A. Schoening[60b], B.D. Schoenrock[93], E. Schopf[23], M. Schott[86], J.F.P. Schouwenberg[108], J. Schovancova[32], S. Schramm[52], N. Schuh[86], A. Schulte[86], M.J. Schultens[23], H.-C. Schultz-Coulon[60a], H. Schulz[17], M. Schumacher[51], B.A. Schumm[139], Ph. Schune[138], A. Schwartzman[145], T.A. Schwarz[92], H. Schweiger[87], Ph. Schwemling[138], R. Schwienhorst[93], J. Schwindling[138], A. Sciandra[23], G. Sciolla[25], M. Scornajenghi[40a,40b], F. Scuri[126a,126b], F. Scutti[91], J. Searcy[92], P. Seema[23], S.C. Seidel[107], A. Seiden[139], J.M. Seixas[26a], G. Sekhniaidze[106a], K. Sekhon[92], S.J. Sekula[43], N. Semprini-Cesari[22a,22b], S. Senkin[37], C. Serfon[121], L. Serin[119], L. Serkin[167a,167b], M. Sessa[136a,136b], R. Seuster[172], H. Severini[115], T. Sfiligoj[78], F. Sforza[165], A. Sfyrla[52], E. Shabalina[57], N.W. Shaikh[148a,148b], L.Y. Shan[35a], R. Shang[169], J.T. Shank[24], M. Shapiro[16], P.B. Shatalov[99], K. Shaw[167a,167b], S.M. Shaw[87], A. Shcherbakova[148a,148b], C.Y. Shehu[151], Y. Shen[115], N. Sherafati[31], P. Sherwood[81], L. Shi[153,am], S. Shimizu[70], C.O. Shimmin[179], M. Shimojima[104], I.P.J. Shipsey[122], S. Shirabe[73], M. Shiyakova[68,an], J. Shlomi[175], A. Shmeleva[98], D. Shoaleh Saadi[97], M.J. Shochet[33], S. Shojaii[94a,94b], D.R. Shope[115], S. Shrestha[113], E. Shulga[100], M.A. Shupe[7], P. Sicho[129], A.M. Sickles[169], P.E. Sidebo[149], E. Sideras Haddad[147c], O. Sidiropoulou[177], A. Sidoti[22a,22b], F. Siegert[47], Dj. Sijacki[14], J. Silva[128a,128d], S.B. Silverstein[148a], V. Simak[130], Lj. Simic[68], S. Simion[119], E. Simioni[86], B. Simmons[81], M. Simon[86], P. Sinervo[161], N.B. Sinev[118], M. Sioli[22a,22b], G. Siragusa[177], I. Siral[92], S.Yu. Sivoklokov[101], J. Sjölin[148a,148b], M.B. Skinner[75], P. Skubic[115], M. Slater[19], T. Slavicek[130], M. Slawinska[42], K. Sliwa[165], R. Slovak[131], V. Smakhtin[175], B.H. Smart[5], J. Smiesko[146a], N. Smirnov[100], S.Yu. Smirnov[100], Y. Smirnov[100], L.N. Smirnova[101,ao], O. Smirnova[84], J.W. Smith[57], M.N.K. Smith[38], R.W. Smith[38], M. Smizanska[75], K. Smolek[130], A.A. Snesarev[98], I.M. Snyder[118], S. Snyder[27], R. Sobie[172,o], F. Socher[47], A. Soffer[155], A. Søgaard[49], D.A. Soh[153], G. Sokhrannyi[78], C.A. Solans Sanchez[32], M. Solar[130], E.Yu. Soldatov[100], U. Soldevila[170], A.A. Solodkov[132], A. Soloshenko[68], O.V. Solovyanov[132], V. Solovyev[125], P. Sommer[51], H. Son[165], A. Sopczak[130], D. Sosa[60b], C.L. Sotiropoulou[126a,126b], S. Sottocornola[123a,123b], R. Soualah[167a,167c], A.M. Soukharev[111,c], D. South[45], B.C. Sowden[80], S. Spagnolo[76a,76b], M. Spalla[126a,126b], M. Spangenberg[173], F. Spanò[80], D. Sperlich[17], F. Spettel[103], T.M. Spieker[60a], R. Spighi[22a], G. Spigo[32], L.A. Spiller[91], M. Spousta[131], R.D. St. Denis[56,*], A. Stabile[94a], R. Stamen[60a], S. Stamm[17], E. Stanecka[42], R.W. Stanek[6], C. Stanescu[136a], M.M. Stanitzki[45], B.S. Stapf[109], S. Stapnes[121], E.A. Starchenko[132], G.H. Stark[33], J. Stark[58], S.H Stark[39], P. Staroba[129], P. Starovoitov[60a], S. Stärz[32], R. Staszewski[42], M. Stegler[45], P. Steinberg[27], B. Stelzer[144], H.J. Stelzer[32], O. Stelzer-Chilton[163a], H. Stenzel[55], G.A. Stewart[56], M.C. Stockton[118], M. Stoebe[90], G. Stoicea[28b], P. Stolte[57], S. Stonjek[103], A.R. Stradling[8], A. Straessner[47], M.E. Stramaglia[18], J. Strandberg[149], S. Strandberg[148a,148b], M. Strauss[115], P. Strizenec[146b], R. Ströhmer[177], D.M. Strom[118], R. Stroynowski[43], A. Strubig[49], S.A. Stucci[27], B. Stugu[15], N.A. Styles[45], D. Su[145], J. Su[127], S. Suchek[60a], Y. Sugaya[120], M. Suk[130], V.V. Sulin[98], DMS Sultan[162a,162b], S. Sultansoy[4c], T. Sumida[71], S. Sun[59], X. Sun[3], K. Suruliz[151], C.J.E. Suster[152], M.R. Sutton[151], S. Suzuki[69], M. Svatos[129], M. Swiatlowski[33], S.P. Swift[2], I. Sykora[146a], T. Sykora[131], D. Ta[51],

JHEP12(2017)059

K. Tackmann[45], J. Taenzer[155], A. Taffard[166], R. Tafirout[163a], E. Tahirovic[79], N. Taiblum[155], H. Takai[27], R. Takashima[72], E.H. Takasugi[103], K. Takeda[70], T. Takeshita[142], Y. Takubo[69], M. Talby[88], A.A. Talyshev[111,c], J. Tanaka[157], M. Tanaka[159], R. Tanaka[119], S. Tanaka[69], R. Tanioka[70], B.B. Tannenwald[113], S. Tapia Araya[34b], S. Tapprogge[86], S. Tarem[154], G.F. Tartarelli[94a], P. Tas[131], M. Tasevsky[129], T. Tashiro[71], E. Tassi[40a,40b], A. Tavares Delgado[128a,128b], Y. Tayalati[137e], A.C. Taylor[107], A.J. Taylor[49], G.N. Taylor[91], P.T.E. Taylor[91], W. Taylor[163b], P. Teixeira-Dias[80], D. Temple[144], H. Ten Kate[32], P.K. Teng[153], J.J. Teoh[120], F. Tepel[178], S. Terada[69], K. Terashi[157], J. Terron[85], S. Terzo[13], M. Testa[50], R.J. Teuscher[161,o], T. Theveneaux-Pelzer[88], F. Thiele[39], J.P. Thomas[19], J. Thomas-Wilsker[80], P.D. Thompson[19], A.S. Thompson[56], L.A. Thomsen[179], E. Thomson[124], Y. Tian[38], M.J. Tibbetts[16], R.E. Ticse Torres[88], V.O. Tikhomirov[98,ap], Yu.A. Tikhonov[111,c], S. Timoshenko[100], P. Tipton[179], S. Tisserant[88], K. Todome[159], S. Todorova-Nova[5], S. Todt[47], J. Tojo[73], S. Tokár[146a], K. Tokushuku[69], E. Tolley[59], L. Tomlinson[87], M. Tomoto[105], L. Tompkins[145,aq], K. Toms[107], B. Tong[59], P. Tornambe[51], E. Torrence[118], H. Torres[47], E. Torró Pastor[140], J. Toth[88,ar], F. Touchard[88], D.R. Tovey[141], C.J. Treado[112], T. Trefzger[177], F. Tresoldi[151], A. Tricoli[27], I.M. Trigger[163a], S. Trincaz-Duvoid[83], M.F. Tripiana[13], W. Trischuk[161], B. Trocmé[58], A. Trofymov[45], C. Troncon[94a], M. Trottier-McDonald[16], M. Trovatelli[172], L. Truong[147b], M. Trzebinski[42], A. Trzupek[42], K.W. Tsang[62a], J.C-L. Tseng[122], P.V. Tsiareshka[95], G. Tsipolitis[10], N. Tsirintanis[9], S. Tsiskaridze[13], V. Tsiskaridze[51], E.G. Tskhadadze[54a], I.I. Tsukerman[99], V. Tsulaia[16], S. Tsuno[69], D. Tsybychev[150], Y. Tu[62b], A. Tudorache[28b], V. Tudorache[28b], T.T. Tulbure[28a], A.N. Tuna[59], S. Turchikhin[68], D. Turgeman[175], I. Turk Cakir[4b,as], R. Turra[94a], P.M. Tuts[38], G. Ucchielli[22a,22b], I. Ueda[69], M. Ughetto[148a,148b], F. Ukegawa[164], G. Unal[32], A. Undrus[27], G. Unel[166], F.C. Ungaro[91], Y. Unno[69], K. Uno[157], C. Unverdorben[102], J. Urban[146b], P. Urquijo[91], P. Urrejola[86], G. Usai[8], J. Usui[69], L. Vacavant[88], V. Vacek[130], B. Vachon[90], K.O.H. Vadla[121], A. Vaidya[81], C. Valderanis[102], E. Valdes Santurio[148a,148b], M. Valente[52], S. Valentinetti[22a,22b], A. Valero[170], L. Valéry[13], S. Valkar[131], A. Vallier[5], J.A. Valls Ferrer[170], W. Van Den Wollenberg[109], H. van der Graaf[109], P. van Gemmeren[6], J. Van Nieuwkoop[144], I. van Vulpen[109], M.C. van Woerden[109], M. Vanadia[135a,135b], W. Vandelli[32], A. Vaniachine[160], P. Vankov[109], G. Vardanyan[180], R. Vari[134a], E.W. Varnes[7], C. Varni[53a,53b], T. Varol[43], D. Varouchas[119], A. Vartapetian[8], K.E. Varvell[152], J.G. Vasquez[179], G.A. Vasquez[34b], F. Vazeille[37], D. Vazquez Furelos[13], T. Vazquez Schroeder[90], J. Veatch[57], V. Veeraraghavan[7], L.M. Veloce[161], F. Veloso[128a,128c], S. Veneziano[134a], A. Ventura[76a,76b], M. Venturi[172], N. Venturi[32], A. Venturini[25], V. Vercesi[123a], M. Verducci[136a,136b], W. Verkerke[109], A.T. Vermeulen[109], J.C. Vermeulen[109], M.C. Vetterli[144,d], N. Viaux Maira[34b], O. Viazlo[84], I. Vichou[169,*], T. Vickey[141], O.E. Vickey Boeriu[141], G.H.A. Viehhauser[122], S. Viel[16], L. Vigani[122], M. Villa[22a,22b], M. Villaplana Perez[94a,94b], E. Vilucchi[50], M.G. Vincter[31], V.B. Vinogradov[68], A. Vishwakarma[45], C. Vittori[22a,22b], I. Vivarelli[151], S. Vlachos[10], M. Vogel[178], P. Vokac[130], G. Volpi[13], H. von der Schmitt[103], E. von Toerne[23], V. Vorobel[131], K. Vorobev[100], M. Vos[170], R. Voss[32], J.H. Vossebeld[77], N. Vranjes[14], M. Vranjes Milosavljevic[14], V. Vrba[130], M. Vreeswijk[109], R. Vuillermet[32], I. Vukotic[33], P. Wagner[23], W. Wagner[178], J. Wagner-Kuhr[102], H. Wahlberg[74], S. Wahrmund[47], J. Walder[75], R. Walker[102], W. Walkowiak[143], V. Wallangen[148a,148b], C. Wang[35b], C. Wang[36b,at], F. Wang[176], H. Wang[16], H. Wang[3], J. Wang[45], J. Wang[152], Q. Wang[115], R.-J. Wang[83], R. Wang[6], S.M. Wang[153], T. Wang[38], W. Wang[153,au], W. Wang[36a,av], Z. Wang[36c], C. Wanotayaroj[45], A. Warburton[90], C.P. Ward[30], D.R. Wardrope[81], A. Washbrook[49], P.M. Watkins[19], A.T. Watson[19], M.F. Watson[19], G. Watts[140], S. Watts[87], B.M. Waugh[81], A.F. Webb[11], S. Webb[86], M.S. Weber[18], S.M. Weber[60a], S.W. Weber[177], S.A. Weber[31], J.S. Webster[6], A.R. Weidberg[122], B. Weinert[64], J. Weingarten[57], M. Weirich[86],

JHEP12(2017)059

C. Weiser[51], H. Weits[109], P.S. Wells[32], T. Wenaus[27], T. Wengler[32], S. Wenig[32], N. Wermes[23], M.D. Werner[67], P. Werner[32], M. Wessels[60a], T.D. Weston[18], K. Whalen[118], N.L. Whallon[140], A.M. Wharton[75], A.S. White[92], A. White[8], M.J. White[1], R. White[34b], D. Whiteson[166], B.W. Whitmore[75], F.J. Wickens[133], W. Wiedenmann[176], M. Wielers[133], C. Wiglesworth[39], L.A.M. Wiik-Fuchs[51], A. Wildauer[103], F. Wilk[87], H.G. Wilkens[32], H.H. Williams[124], S. Williams[109], C. Willis[93], S. Willocq[89], J.A. Wilson[19], I. Wingerter-Seez[5], E. Winkels[151], F. Winklmeier[118], O.J. Winston[151], B.T. Winter[23], M. Wittgen[145], M. Wobisch[82,u], T.M.H. Wolf[109], R. Wolff[88], M.W. Wolter[42], H. Wolters[128a,128c], V.W.S. Wong[171], N.L. Woods[139], S.D. Worm[19], B.K. Wosiek[42], J. Wotschack[32], K.W. Wozniak[42], M. Wu[33], S.L. Wu[176], X. Wu[52], Y. Wu[92], T.R. Wyatt[87], B.M. Wynne[49], S. Xella[39], Z. Xi[92], L. Xia[35c], D. Xu[35a], L. Xu[27], T. Xu[138], B. Yabsley[152], S. Yacoob[147a], D. Yamaguchi[159], Y. Yamaguchi[159], A. Yamamoto[69], S. Yamamoto[157], T. Yamanaka[157], F. Yamane[70], M. Yamatani[157], Y. Yamazaki[70], Z. Yan[24], H. Yang[36c], H. Yang[16], Y. Yang[153], Z. Yang[15], W-M. Yao[16], Y.C. Yap[45], Y. Yasu[69], E. Yatsenko[5], K.H. Yau Wong[23], J. Ye[43], S. Ye[27], I. Yeletskikh[68], E. Yigitbasi[24], E. Yildirim[86], K. Yorita[174], K. Yoshihara[124], C. Young[145], C.J.S. Young[32], J. Yu[8], J. Yu[67], S.P.Y. Yuen[23], I. Yusuff[30,aw], B. Zabinski[42], G. Zacharis[10], R. Zaidan[13], A.M. Zaitsev[132,aj], N. Zakharchuk[45], J. Zalieckas[15], A. Zaman[150], S. Zambito[59], D. Zanzi[91], C. Zeitnitz[178], G. Zemaityte[122], A. Zemla[41a], J.C. Zeng[169], Q. Zeng[145], O. Zenin[132], T. Ženiš[146a], D. Zerwas[119], D. Zhang[36b], D. Zhang[92], F. Zhang[176], G. Zhang[36a,av], H. Zhang[119], J. Zhang[6], L. Zhang[51], L. Zhang[36a], M. Zhang[169], P. Zhang[35b], R. Zhang[23], R. Zhang[36a,at], X. Zhang[36b], Y. Zhang[35a], Z. Zhang[119], X. Zhao[43], Y. Zhao[36b,ax], Z. Zhao[36a], A. Zhemchugov[68], B. Zhou[92], C. Zhou[176], L. Zhou[43], M. Zhou[35a], M. Zhou[150], N. Zhou[35c], C.G. Zhu[36b], H. Zhu[35a], J. Zhu[92], Y. Zhu[36a], X. Zhuang[35a], K. Zhukov[98], A. Zibell[177], D. Zieminska[64], N.I. Zimine[68], C. Zimmermann[86], S. Zimmermann[51], Z. Zinonos[103], M. Zinser[86], M. Ziolkowski[143], L. Živković[14], G. Zobernig[176], A. Zoccoli[22a,22b], R. Zou[33], M. zur Nedden[17], L. Zwalinski[32].

[1] *Department of Physics, University of Adelaide, Adelaide, Australia*
[2] *Physics Department, SUNY Albany, Albany NY, United States of America*
[3] *Department of Physics, University of Alberta, Edmonton AB, Canada*
[4] [(a)] *Department of Physics, Ankara University, Ankara;* [(b)] *Istanbul Aydin University, Istanbul;* [(c)] *Division of Physics, TOBB University of Economics and Technology, Ankara, Turkey*
[5] *LAPP, CNRS/IN2P3 and Université Savoie Mont Blanc, Annecy-le-Vieux, France*
[6] *High Energy Physics Division, Argonne National Laboratory, Argonne IL, United States of America*
[7] *Department of Physics, University of Arizona, Tucson AZ, United States of America*
[8] *Department of Physics, The University of Texas at Arlington, Arlington TX, United States of America*
[9] *Physics Department, National and Kapodistrian University of Athens, Athens, Greece*
[10] *Physics Department, National Technical University of Athens, Zografou, Greece*
[11] *Department of Physics, The University of Texas at Austin, Austin TX, United States of America*
[12] *Institute of Physics, Azerbaijan Academy of Sciences, Baku, Azerbaijan*
[13] *Institut de Física d'Altes Energies (IFAE), The Barcelona Institute of Science and Technology, Barcelona, Spain*
[14] *Institute of Physics, University of Belgrade, Belgrade, Serbia*
[15] *Department for Physics and Technology, University of Bergen, Bergen, Norway*
[16] *Physics Division, Lawrence Berkeley National Laboratory and University of California, Berkeley CA, United States of America*
[17] *Department of Physics, Humboldt University, Berlin, Germany*
[18] *Albert Einstein Center for Fundamental Physics and Laboratory for High Energy Physics, University of Bern, Bern, Switzerland*
[19] *School of Physics and Astronomy, University of Birmingham, Birmingham, United Kingdom*

JHEP12(2017)059

[20] [(a)] Department of Physics, Bogazici University, Istanbul; [(b)] Department of Physics Engineering, Gaziantep University, Gaziantep; [(d)] Istanbul Bilgi University, Faculty of Engineering and Natural Sciences, Istanbul; [(e)] Bahcesehir University, Faculty of Engineering and Natural Sciences, Istanbul, Turkey
[21] Centro de Investigaciones, Universidad Antonio Narino, Bogota, Colombia
[22] [(a)] INFN Sezione di Bologna; [(b)] Dipartimento di Fisica e Astronomia, Università di Bologna, Bologna, Italy
[23] Physikalisches Institut, University of Bonn, Bonn, Germany
[24] Department of Physics, Boston University, Boston MA, United States of America
[25] Department of Physics, Brandeis University, Waltham MA, United States of America
[26] [(a)] Universidade Federal do Rio De Janeiro COPPE/EE/IF, Rio de Janeiro; [(b)] Electrical Circuits Department, Federal University of Juiz de Fora (UFJF), Juiz de Fora; [(c)] Federal University of Sao Joao del Rei (UFSJ), Sao Joao del Rei; [(d)] Instituto de Fisica, Universidade de Sao Paulo, Sao Paulo, Brazil
[27] Physics Department, Brookhaven National Laboratory, Upton NY, United States of America
[28] [(a)] Transilvania University of Brasov, Brasov; [(b)] Horia Hulubei National Institute of Physics and Nuclear Engineering, Bucharest; [(c)] Department of Physics, Alexandru Ioan Cuza University of Iasi, Iasi; [(d)] National Institute for Research and Development of Isotopic and Molecular Technologies, Physics Department, Cluj Napoca; [(e)] University Politehnica Bucharest, Bucharest; [(f)] West University in Timisoara, Timisoara, Romania
[29] Departamento de Física, Universidad de Buenos Aires, Buenos Aires, Argentina
[30] Cavendish Laboratory, University of Cambridge, Cambridge, United Kingdom
[31] Department of Physics, Carleton University, Ottawa ON, Canada
[32] CERN, Geneva, Switzerland
[33] Enrico Fermi Institute, University of Chicago, Chicago IL, United States of America
[34] [(a)] Departamento de Física, Pontificia Universidad Católica de Chile, Santiago; [(b)] Departamento de Física, Universidad Técnica Federico Santa María, Valparaíso, Chile
[35] [(a)] Institute of High Energy Physics, Chinese Academy of Sciences, Beijing; [(b)] Department of Physics, Nanjing University, Jiangsu; [(c)] Physics Department, Tsinghua University, Beijing 100084, China
[36] [(a)] Department of Modern Physics and State Key Laboratory of Particle Detection and Electronics, University of Science and Technology of China, Anhui; [(b)] School of Physics, Shandong University, Shandong; [(c)] Department of Physics and Astronomy, Key Laboratory for Particle Physics, Astrophysics and Cosmology, Ministry of Education; Shanghai Key Laboratory for Particle Physics and Cosmology, Shanghai Jiao Tong University, Shanghai(also at PKU-CHEP), China
[37] Université Clermont Auvergne, CNRS/IN2P3, LPC, Clermont-Ferrand, France
[38] Nevis Laboratory, Columbia University, Irvington NY, United States of America
[39] Niels Bohr Institute, University of Copenhagen, Kobenhavn, Denmark
[40] [(a)] INFN Gruppo Collegato di Cosenza, Laboratori Nazionali di Frascati; [(b)] Dipartimento di Fisica, Università della Calabria, Rende, Italy
[41] [(a)] AGH University of Science and Technology, Faculty of Physics and Applied Computer Science, Krakow; [(b)] Marian Smoluchowski Institute of Physics, Jagiellonian University, Krakow, Poland
[42] Institute of Nuclear Physics Polish Academy of Sciences, Krakow, Poland
[43] Physics Department, Southern Methodist University, Dallas TX, United States of America
[44] Physics Department, University of Texas at Dallas, Richardson TX, United States of America
[45] DESY, Hamburg and Zeuthen, Germany
[46] Lehrstuhl für Experimentelle Physik IV, Technische Universität Dortmund, Dortmund, Germany
[47] Institut für Kern- und Teilchenphysik, Technische Universität Dresden, Dresden, Germany
[48] Department of Physics, Duke University, Durham NC, United States of America
[49] SUPA - School of Physics and Astronomy, University of Edinburgh, Edinburgh, United Kingdom
[50] INFN e Laboratori Nazionali di Frascati, Frascati, Italy
[51] Fakultät für Mathematik und Physik, Albert-Ludwigs-Universität, Freiburg, Germany

JHEP12(2017)059

[52] Departement de Physique Nucleaire et Corpusculaire, Université de Genève, Geneva, Switzerland
[53] [(a)] INFN Sezione di Genova; [(b)] Dipartimento di Fisica, Università di Genova, Genova, Italy
[54] [(a)] E. Andronikashvili Institute of Physics, Iv. Javakhishvili Tbilisi State University, Tbilisi; [(b)] High Energy Physics Institute, Tbilisi State University, Tbilisi, Georgia
[55] II Physikalisches Institut, Justus-Liebig-Universität Giessen, Giessen, Germany
[56] SUPA - School of Physics and Astronomy, University of Glasgow, Glasgow, United Kingdom
[57] II Physikalisches Institut, Georg-August-Universität, Göttingen, Germany
[58] Laboratoire de Physique Subatomique et de Cosmologie, Université Grenoble-Alpes, CNRS/IN2P3, Grenoble, France
[59] Laboratory for Particle Physics and Cosmology, Harvard University, Cambridge MA, United States of America
[60] [(a)] Kirchhoff-Institut für Physik, Ruprecht-Karls-Universität Heidelberg, Heidelberg; [(b)] Physikalisches Institut, Ruprecht-Karls-Universität Heidelberg, Heidelberg, Germany
[61] Faculty of Applied Information Science, Hiroshima Institute of Technology, Hiroshima, Japan
[62] [(a)] Department of Physics, The Chinese University of Hong Kong, Shatin, N.T., Hong Kong; [(b)] Department of Physics, The University of Hong Kong, Hong Kong; [(c)] Department of Physics and Institute for Advanced Study, The Hong Kong University of Science and Technology, Clear Water Bay, Kowloon, Hong Kong, China
[63] Department of Physics, National Tsing Hua University, Taiwan, Taiwan
[64] Department of Physics, Indiana University, Bloomington IN, United States of America
[65] Institut für Astro- und Teilchenphysik, Leopold-Franzens-Universität, Innsbruck, Austria
[66] University of Iowa, Iowa City IA, United States of America
[67] Department of Physics and Astronomy, Iowa State University, Ames IA, United States of America
[68] Joint Institute for Nuclear Research, JINR Dubna, Dubna, Russia
[69] KEK, High Energy Accelerator Research Organization, Tsukuba, Japan
[70] Graduate School of Science, Kobe University, Kobe, Japan
[71] Faculty of Science, Kyoto University, Kyoto, Japan
[72] Kyoto University of Education, Kyoto, Japan
[73] Research Center for Advanced Particle Physics and Department of Physics, Kyushu University, Fukuoka, Japan
[74] Instituto de Física La Plata, Universidad Nacional de La Plata and CONICET, La Plata, Argentina
[75] Physics Department, Lancaster University, Lancaster, United Kingdom
[76] [(a)] INFN Sezione di Lecce; [(b)] Dipartimento di Matematica e Fisica, Università del Salento, Lecce, Italy
[77] Oliver Lodge Laboratory, University of Liverpool, Liverpool, United Kingdom
[78] Department of Experimental Particle Physics, Jožef Stefan Institute and Department of Physics, University of Ljubljana, Ljubljana, Slovenia
[79] School of Physics and Astronomy, Queen Mary University of London, London, United Kingdom
[80] Department of Physics, Royal Holloway University of London, Surrey, United Kingdom
[81] Department of Physics and Astronomy, University College London, London, United Kingdom
[82] Louisiana Tech University, Ruston LA, United States of America
[83] Laboratoire de Physique Nucléaire et de Hautes Energies, UPMC and Université Paris-Diderot and CNRS/IN2P3, Paris, France
[84] Fysiska institutionen, Lunds universitet, Lund, Sweden
[85] Departamento de Fisica Teorica C-15, Universidad Autonoma de Madrid, Madrid, Spain
[86] Institut für Physik, Universität Mainz, Mainz, Germany
[87] School of Physics and Astronomy, University of Manchester, Manchester, United Kingdom
[88] CPPM, Aix-Marseille Université and CNRS/IN2P3, Marseille, France
[89] Department of Physics, University of Massachusetts, Amherst MA, United States of America
[90] Department of Physics, McGill University, Montreal QC, Canada
[91] School of Physics, University of Melbourne, Victoria, Australia
[92] Department of Physics, The University of Michigan, Ann Arbor MI, United States of America

JHEP12(2017)059

[93] Department of Physics and Astronomy, Michigan State University, East Lansing MI, United States of America
[94] [(a)] INFN Sezione di Milano; [(b)] Dipartimento di Fisica, Università di Milano, Milano, Italy
[95] B.I. Stepanov Institute of Physics, National Academy of Sciences of Belarus, Minsk, Republic of Belarus
[96] Research Institute for Nuclear Problems of Byelorussian State University, Minsk, Republic of Belarus
[97] Group of Particle Physics, University of Montreal, Montreal QC, Canada
[98] P.N. Lebedev Physical Institute of the Russian Academy of Sciences, Moscow, Russia
[99] Institute for Theoretical and Experimental Physics (ITEP), Moscow, Russia
[100] National Research Nuclear University MEPhI, Moscow, Russia
[101] D.V. Skobeltsyn Institute of Nuclear Physics, M.V. Lomonosov Moscow State University, Moscow, Russia
[102] Fakultät für Physik, Ludwig-Maximilians-Universität München, München, Germany
[103] Max-Planck-Institut für Physik (Werner-Heisenberg-Institut), München, Germany
[104] Nagasaki Institute of Applied Science, Nagasaki, Japan
[105] Graduate School of Science and Kobayashi-Maskawa Institute, Nagoya University, Nagoya, Japan
[106] [(a)] INFN Sezione di Napoli; [(b)] Dipartimento di Fisica, Università di Napoli, Napoli, Italy
[107] Department of Physics and Astronomy, University of New Mexico, Albuquerque NM, United States of America
[108] Institute for Mathematics, Astrophysics and Particle Physics, Radboud University Nijmegen/Nikhef, Nijmegen, Netherlands
[109] Nikhef National Institute for Subatomic Physics and University of Amsterdam, Amsterdam, Netherlands
[110] Department of Physics, Northern Illinois University, DeKalb IL, United States of America
[111] Budker Institute of Nuclear Physics, SB RAS, Novosibirsk, Russia
[112] Department of Physics, New York University, New York NY, United States of America
[113] Ohio State University, Columbus OH, United States of America
[114] Faculty of Science, Okayama University, Okayama, Japan
[115] Homer L. Dodge Department of Physics and Astronomy, University of Oklahoma, Norman OK, United States of America
[116] Department of Physics, Oklahoma State University, Stillwater OK, United States of America
[117] Palacký University, RCPTM, Olomouc, Czech Republic
[118] Center for High Energy Physics, University of Oregon, Eugene OR, United States of America
[119] LAL, Univ. Paris-Sud, CNRS/IN2P3, Université Paris-Saclay, Orsay, France
[120] Graduate School of Science, Osaka University, Osaka, Japan
[121] Department of Physics, University of Oslo, Oslo, Norway
[122] Department of Physics, Oxford University, Oxford, United Kingdom
[123] [(a)] INFN Sezione di Pavia; [(b)] Dipartimento di Fisica, Università di Pavia, Pavia, Italy
[124] Department of Physics, University of Pennsylvania, Philadelphia PA, United States of America
[125] National Research Centre "Kurchatov Institute" B.P.Konstantinov Petersburg Nuclear Physics Institute, St. Petersburg, Russia
[126] [(a)] INFN Sezione di Pisa; [(b)] Dipartimento di Fisica E. Fermi, Università di Pisa, Pisa, Italy
[127] Department of Physics and Astronomy, University of Pittsburgh, Pittsburgh PA, United States of America
[128] [(a)] Laboratório de Instrumentação e Física Experimental de Partículas - LIP, Lisboa; [(b)] Faculdade de Ciências, Universidade de Lisboa, Lisboa; [(c)] Department of Physics, University of Coimbra, Coimbra; [(d)] Centro de Física Nuclear da Universidade de Lisboa, Lisboa; [(e)] Departamento de Fisica, Universidade do Minho, Braga; [(f)] Departamento de Fisica Teorica y del Cosmos, Universidad de Granada, Granada; [(g)] Dep Fisica and CEFITEC of Faculdade de Ciencias e Tecnologia, Universidade Nova de Lisboa, Caparica, Portugal
[129] Institute of Physics, Academy of Sciences of the Czech Republic, Praha, Czech Republic

JHEP12(2017)059

[130] Czech Technical University in Prague, Praha, Czech Republic
[131] Charles University, Faculty of Mathematics and Physics, Prague, Czech Republic
[132] State Research Center Institute for High Energy Physics (Protvino), NRC KI, Russia
[133] Particle Physics Department, Rutherford Appleton Laboratory, Didcot, United Kingdom
[134] [(a)] INFN Sezione di Roma; [(b)] Dipartimento di Fisica, Sapienza Università di Roma, Roma, Italy
[135] [(a)] INFN Sezione di Roma Tor Vergata; [(b)] Dipartimento di Fisica, Università di Roma Tor Vergata, Roma, Italy
[136] [(a)] INFN Sezione di Roma Tre; [(b)] Dipartimento di Matematica e Fisica, Università Roma Tre, Roma, Italy
[137] [(a)] Faculté des Sciences Ain Chock, Réseau Universitaire de Physique des Hautes Energies - Université Hassan II, Casablanca; [(b)] Centre National de l'Energie des Sciences Techniques Nucleaires, Rabat; [(c)] Faculté des Sciences Semlalia, Université Cadi Ayyad, LPHEA-Marrakech; [(d)] Faculté des Sciences, Université Mohamed Premier and LPTPM, Oujda; [(e)] Faculté des sciences, Université Mohammed V, Rabat, Morocco
[138] DSM/IRFU (Institut de Recherches sur les Lois Fondamentales de l'Univers), CEA Saclay (Commissariat à l'Energie Atomique et aux Energies Alternatives), Gif-sur-Yvette, France
[139] Santa Cruz Institute for Particle Physics, University of California Santa Cruz, Santa Cruz CA, United States of America
[140] Department of Physics, University of Washington, Seattle WA, United States of America
[141] Department of Physics and Astronomy, University of Sheffield, Sheffield, United Kingdom
[142] Department of Physics, Shinshu University, Nagano, Japan
[143] Department Physik, Universität Siegen, Siegen, Germany
[144] Department of Physics, Simon Fraser University, Burnaby BC, Canada
[145] SLAC National Accelerator Laboratory, Stanford CA, United States of America
[146] [(a)] Faculty of Mathematics, Physics & Informatics, Comenius University, Bratislava; [(b)] Department of Subnuclear Physics, Institute of Experimental Physics of the Slovak Academy of Sciences, Kosice, Slovak Republic
[147] [(a)] Department of Physics, University of Cape Town, Cape Town; [(b)] Department of Physics, University of Johannesburg, Johannesburg; [(c)] School of Physics, University of the Witwatersrand, Johannesburg, South Africa
[148] [(a)] Department of Physics, Stockholm University; [(b)] The Oskar Klein Centre, Stockholm, Sweden
[149] Physics Department, Royal Institute of Technology, Stockholm, Sweden
[150] Departments of Physics & Astronomy and Chemistry, Stony Brook University, Stony Brook NY, United States of America
[151] Department of Physics and Astronomy, University of Sussex, Brighton, United Kingdom
[152] School of Physics, University of Sydney, Sydney, Australia
[153] Institute of Physics, Academia Sinica, Taipei, Taiwan
[154] Department of Physics, Technion: Israel Institute of Technology, Haifa, Israel
[155] Raymond and Beverly Sackler School of Physics and Astronomy, Tel Aviv University, Tel Aviv, Israel
[156] Department of Physics, Aristotle University of Thessaloniki, Thessaloniki, Greece
[157] International Center for Elementary Particle Physics and Department of Physics, The University of Tokyo, Tokyo, Japan
[158] Graduate School of Science and Technology, Tokyo Metropolitan University, Tokyo, Japan
[159] Department of Physics, Tokyo Institute of Technology, Tokyo, Japan
[160] Tomsk State University, Tomsk, Russia
[161] Department of Physics, University of Toronto, Toronto ON, Canada
[162] [(a)] INFN-TIFPA; [(b)] University of Trento, Trento, Italy
[163] [(a)] TRIUMF, Vancouver BC; [(b)] Department of Physics and Astronomy, York University, Toronto ON, Canada
[164] Faculty of Pure and Applied Sciences, and Center for Integrated Research in Fundamental Science and Engineering, University of Tsukuba, Tsukuba, Japan

JHEP12(2017)059

[165] Department of Physics and Astronomy, Tufts University, Medford MA, United States of America
[166] Department of Physics and Astronomy, University of California Irvine, Irvine CA, United States of America
[167] [(a)] INFN Gruppo Collegato di Udine, Sezione di Trieste, Udine; [(b)] ICTP, Trieste; [(c)] Dipartimento di Chimica, Fisica e Ambiente, Università di Udine, Udine, Italy
[168] Department of Physics and Astronomy, University of Uppsala, Uppsala, Sweden
[169] Department of Physics, University of Illinois, Urbana IL, United States of America
[170] Instituto de Fisica Corpuscular (IFIC), Centro Mixto Universidad de Valencia - CSIC, Spain
[171] Department of Physics, University of British Columbia, Vancouver BC, Canada
[172] Department of Physics and Astronomy, University of Victoria, Victoria BC, Canada
[173] Department of Physics, University of Warwick, Coventry, United Kingdom
[174] Waseda University, Tokyo, Japan
[175] Department of Particle Physics, The Weizmann Institute of Science, Rehovot, Israel
[176] Department of Physics, University of Wisconsin, Madison WI, United States of America
[177] Fakultät für Physik und Astronomie, Julius-Maximilians-Universität, Würzburg, Germany
[178] Fakultät für Mathematik und Naturwissenschaften, Fachgruppe Physik, Bergische Universität Wuppertal, Wuppertal, Germany
[179] Department of Physics, Yale University, New Haven CT, United States of America
[180] Yerevan Physics Institute, Yerevan, Armenia
[181] Centre de Calcul de l'Institut National de Physique Nucléaire et de Physique des Particules (IN2P3), Villeurbanne, France
[182] Academia Sinica Grid Computing, Institute of Physics, Academia Sinica, Taipei, Taiwan

[a] Also at Department of Physics, King's College London, London, United Kingdom
[b] Also at Institute of Physics, Azerbaijan Academy of Sciences, Baku, Azerbaijan
[c] Also at Novosibirsk State University, Novosibirsk, Russia
[d] Also at TRIUMF, Vancouver BC, Canada
[e] Also at Department of Physics & Astronomy, University of Louisville, Louisville, KY, United States of America
[f] Also at Physics Department, An-Najah National University, Nablus, Palestine
[g] Also at Department of Physics, California State University, Fresno CA, United States of America
[h] Also at Department of Physics, University of Fribourg, Fribourg, Switzerland
[i] Also at II Physikalisches Institut, Georg-August-Universität, Göttingen, Germany
[j] Also at Departament de Fisica de la Universitat Autonoma de Barcelona, Barcelona, Spain
[k] Also at Departamento de Fisica e Astronomia, Faculdade de Ciencias, Universidade do Porto, Portugal
[l] Also at Tomsk State University, Tomsk, and Moscow Institute of Physics and Technology State University, Dolgoprudny, Russia
[m] Also at The Collaborative Innovation Center of Quantum Matter (CICQM), Beijing, China
[n] Also at Universita di Napoli Parthenope, Napoli, Italy
[o] Also at Institute of Particle Physics (IPP), Canada
[p] Also at Horia Hulubei National Institute of Physics and Nuclear Engineering, Bucharest, Romania
[q] Also at Department of Physics, St. Petersburg State Polytechnical University, St. Petersburg, Russia
[r] Also at Borough of Manhattan Community College, City University of New York, New York City, United States of America
[s] Also at Department of Financial and Management Engineering, University of the Aegean, Chios, Greece
[t] Also at Centre for High Performance Computing, CSIR Campus, Rosebank, Cape Town, South Africa
[u] Also at Louisiana Tech University, Ruston LA, United States of America
[v] Also at Institucio Catalana de Recerca i Estudis Avancats, ICREA, Barcelona, Spain

JHEP12(2017)059

[w] Also at Graduate School of Science, Osaka University, Osaka, Japan
[x] Also at Fakultät für Mathematik und Physik, Albert-Ludwigs-Universität, Freiburg, Germany
[y] Also at Institute for Mathematics, Astrophysics and Particle Physics, Radboud University Nijmegen/Nikhef, Nijmegen, Netherlands
[z] Also at Department of Physics, The University of Texas at Austin, Austin TX, United States of America
[aa] Also at Institute of Theoretical Physics, Ilia State University, Tbilisi, Georgia
[ab] Also at CERN, Geneva, Switzerland
[ac] Also at Georgian Technical University (GTU),Tbilisi, Georgia
[ad] Also at Ochadai Academic Production, Ochanomizu University, Tokyo, Japan
[ae] Also at Manhattan College, New York NY, United States of America
[af] Also at Department of Physics, The University of Michigan, Ann Arbor MI, United States of America
[ag] Also at The City College of New York, New York NY, United States of America
[ah] Also at Departamento de Fisica Teorica y del Cosmos, Universidad de Granada, Granada, Portugal
[ai] Also at Department of Physics, California State University, Sacramento CA, United States of America
[aj] Also at Moscow Institute of Physics and Technology State University, Dolgoprudny, Russia
[ak] Also at Departement de Physique Nucleaire et Corpusculaire, Université de Genève, Geneva, Switzerland
[al] Also at Institut de Física d'Altes Energies (IFAE), The Barcelona Institute of Science and Technology, Barcelona, Spain
[am] Also at School of Physics, Sun Yat-sen University, Guangzhou, China
[an] Also at Institute for Nuclear Research and Nuclear Energy (INRNE) of the Bulgarian Academy of Sciences, Sofia, Bulgaria
[ao] Also at Faculty of Physics, M.V.Lomonosov Moscow State University, Moscow, Russia
[ap] Also at National Research Nuclear University MEPhI, Moscow, Russia
[aq] Also at Department of Physics, Stanford University, Stanford CA, United States of America
[ar] Also at Institute for Particle and Nuclear Physics, Wigner Research Centre for Physics, Budapest, Hungary
[as] Also at Giresun University, Faculty of Engineering, Turkey
[at] Also at CPPM, Aix-Marseille Université and CNRS/IN2P3, Marseille, France
[au] Also at Department of Physics, Nanjing University, Jiangsu, China
[av] Also at Institute of Physics, Academia Sinica, Taipei, Taiwan
[aw] Also at University of Malaya, Department of Physics, Kuala Lumpur, Malaysia
[ax] Also at LAL, Univ. Paris-Sud, CNRS/IN2P3, Université Paris-Saclay, Orsay, France
[*] Deceased

JHEP12(2017)059

Eur. Phys. J. C (2016) 76:653
DOI 10.1140/epjc/s10052-016-4466-1

THE EUROPEAN PHYSICAL JOURNAL C

Regular Article - Experimental Physics

Luminosity determination in pp collisions at $\sqrt{s} = 8$ TeV using the ATLAS detector at the LHC

ATLAS Collaboration[⋆]

CERN, 1211 Geneva 23, Switzerland

Received: 16 August 2016 / Accepted: 26 October 2016 / Published online: 28 November 2016

Abstract The luminosity determination for the ATLAS detector at the LHC during pp collisions at $\sqrt{s} = 8$ TeV in 2012 is presented. The evaluation of the luminosity scale is performed using several luminometers, and comparisons between these luminosity detectors are made to assess the accuracy, consistency and long-term stability of the results. A luminosity uncertainty of $\delta\mathcal{L}/\mathcal{L} = \pm 1.9\%$ is obtained for the 22.7 fb^{-1} of pp collision data delivered to ATLAS at $\sqrt{s} = 8$ TeV in 2012.

1 Introduction

An accurate measurement of the delivered luminosity is a key component of the ATLAS [1] physics programme. For cross-section measurements, the uncertainty in the delivered luminosity is often one of the major systematic uncertainties. Searches for, and eventual discoveries of, physical phenomena beyond the Standard Model also rely on accurate information about the delivered luminosity to evaluate background levels and determine sensitivity to the signatures of new phenomena.

This paper describes the measurement of the luminosity delivered to the ATLAS detector at the LHC in pp collisions at a centre-of-mass energy of $\sqrt{s} = 8$ TeV during 2012. It is structured as follows. The strategy for measuring and calibrating the luminosity is outlined in Sect. 2, followed in Sect. 3 by a brief description of the detectors and algorithms used for luminosity determination. The absolute calibration of these algorithms by the van der Meer (*vdM*) method [2], which must be carried out under specially tailored beam conditions, is described in Sect. 4; the associated systematic uncertainties are detailed in Sect. 5. The comparison of the relative response of several independent luminometers during physics running reveals that significant time- and rate-dependent effects impacted the performance of the ATLAS bunch-by-bunch luminometers during the 2012 run (Sect. 6). Therefore this absolute *vdM* calibration cannot be invoked as is. Instead, it must be transferred, at one point in time and using an independent relative-luminosity monitor, from the low-luminosity regime of *vdM* scans to the high-luminosity conditions typical of routine physics running. Additional corrections must be applied over the course of the 2012 data-taking period to compensate for detector aging (Sect. 7). The various contributions to the systematic uncertainty affecting the integrated luminosity delivered to ATLAS in 2012 are recapitulated in Sect. 8, and the final results are summarized in Sect. 9.

⋆ e-mail: atlas.publications@cern.ch

2 Luminosity-determination methodology

The analysis presented in this paper closely parallels, and where necessary expands, the one used to determine the luminosity in pp collisions at $\sqrt{s} = 7$ TeV [3].

The bunch luminosity $\mathcal{L}_\mathrm{b}$ produced by a single pair of colliding bunches can be expressed as

$$\mathcal{L}_\mathrm{b} = \frac{\mu f_\mathrm{r}}{\sigma_\mathrm{inel}}, \tag{1}$$

where the pile-up parameter μ is the average number of inelastic interactions per bunch crossing, f_r is the bunch revolution frequency, and σ_inel is the pp inelastic cross-section. The total instantaneous luminosity is given by

$$\mathcal{L} = \sum_{\mathrm{b}=1}^{n_\mathrm{b}} \mathcal{L}_\mathrm{b} = n_\mathrm{b} \langle \mathcal{L}_\mathrm{b} \rangle = n_\mathrm{b} \frac{\langle \mu \rangle f_\mathrm{r}}{\sigma_\mathrm{inel}}.$$

Here the sum runs over the n_b bunch pairs colliding at the interaction point (IP), $\langle \mathcal{L}_\mathrm{b} \rangle$ is the mean bunch luminosity and $\langle \mu \rangle$ is the bunch-averaged pile-up parameter. Table 1 highlights the operational conditions of the LHC during Run 1 from 2010 to 2012. Compared to previous years, operating conditions did not vary significantly during 2012, with typically 1368 bunches colliding and a peak instantaneous luminosity delivered by the LHC at the start of a fill of

Table 1 Selected LHC parameters for pp collisions at $\sqrt{s} = 7$ TeV in 2010 and 2011, and at $\sqrt{s} = 8$ TeV in 2012. Values shown are representative of the best accelerator performance during normal physics operation

Parameter	2010	2011	2012
Number of bunch pairs colliding (n_b)	348	1331	1380
Bunch spacing (ns)	150	50	50
Typical bunch population (10^{11} protons)	0.9	1.2	1.7
Peak luminosity $\mathcal{L}_{\text{peak}}$ (10^{33} cm^{-2} s^{-1})	0.2	3.6	7.7
Peak number of inelastic interactions per crossing	∼5	∼20	∼40
Average number of interactions per crossing (luminosity weighted)	∼2	∼9	∼21
Total integrated luminosity delivered	47 pb^{-1}	5.5 fb^{-1}	23 fb^{-1}

$\mathcal{L}_{\text{peak}} \approx 6$–$8 \times 10^{33}\,\text{cm}^{-2}\,\text{s}^{-1}$, on the average three times higher than in 2011.

ATLAS monitors the delivered luminosity by measuring μ_{vis}, the visible interaction rate per bunch crossing, with a variety of independent detectors and using several different algorithms (Sect. 3). The bunch luminosity can then be written as

$$\mathcal{L}_{\text{b}} = \frac{\mu_{\text{vis}}\, f_{\text{r}}}{\sigma_{\text{vis}}}, \tag{2}$$

where $\mu_{\text{vis}} = \varepsilon\, \mu$, ε is the efficiency of the detector and algorithm under consideration, and the visible cross-section for that same detector and algorithm is defined by $\sigma_{\text{vis}} \equiv \varepsilon\, \sigma_{\text{inel}}$. Since μ_{vis} is a directly measurable quantity, the calibration of the luminosity scale for a particular detector and algorithm amounts to determining the visible cross-section σ_{vis}. This calibration, described in detail in Sect. 4, is performed using dedicated beam-separation scans, where the absolute luminosity can be inferred from direct measurements of the beam parameters [2,4]. This known luminosity is then combined with the simultaneously measured interaction rate μ_{vis} to extract σ_{vis}.

A fundamental ingredient of the ATLAS strategy to assess and control the systematic uncertainties affecting the absolute luminosity determination is to compare the measurements of several luminometers, most of which use more than one algorithm to determine the luminosity. These multiple detectors and algorithms are characterized by significantly different acceptance, response to pile-up, and sensitivity to instrumental effects and to beam-induced backgrounds. Since the calibration of the absolute luminosity scale is carried out only two or three times per year, this calibration must either remain constant over extended periods of time and under different machine conditions, or be corrected for long-term drifts. The level of consistency across the various methods, over the full range of luminosities and beam conditions, and across many months of LHC operation, provides a direct test of the accuracy and stability of the results. A full discussion of the systematic uncertainties is presented in Sects. 5–8.

The information needed for physics analyses is the integrated luminosity for some well-defined data samples. The basic time unit for storing ATLAS luminosity information for physics use is the luminosity block (LB). The boundaries of each LB are defined by the ATLAS central trigger processor (CTP), and in general the duration of each LB is approximately one minute. Configuration changes, such as a trigger prescale adjustment, prompt a luminosity-block transition, and data are analysed assuming that each luminosity block contains data taken under uniform conditions, including luminosity. For each LB, the instantaneous luminosity from each detector and algorithm, averaged over the luminosity block, is stored in a relational database along with a variety of general ATLAS data-quality information. To define a data sample for physics, quality criteria are applied to select LBs where conditions are acceptable; then the instantaneous luminosity in that LB is multiplied by the LB duration to provide the integrated luminosity delivered in that LB. Additional corrections can be made for trigger deadtime and trigger prescale factors, which are also recorded on a per-LB basis. Adding up the integrated luminosity delivered in a specific set of luminosity blocks provides the integrated luminosity of the entire data sample.

3 Luminosity detectors and algorithms

The ATLAS detector is discussed in detail in Ref. [1]. The two primary luminometers, the BCM (Beam Conditions Monitor) and LUCID (LUminosity measurement using a Cherenkov Integrating Detector), both make deadtime-free, bunch-by-bunch luminosity measurements (Sect. 3.1). These are compared with the results of the track-counting method (Sect. 3.2), a new approach developed by ATLAS which monitors the multiplicity of charged particles produced in randomly selected colliding-bunch crossings, and is essential to assess the calibration-transfer correction from the *vdM* to the high-luminosity regime. Additional methods have been developed to disentangle the relative long-term drifts and run-to-run variations between the BCM, LUCID and track-counting measurements during high-luminosity running, thereby reducing the associated systematic uncertain-

ties to the sub-percent level. These techniques measure the total instantaneous luminosity, summed over all bunches, by monitoring detector currents sensitive to average particle fluxes through the ATLAS calorimeters, or by reporting fluences observed in radiation-monitoring equipment; they are described in Sect. 3.3.

3.1 Dedicated bunch-by-bunch luminometers

The BCM consists of four $8 \times 8\,\mathrm{mm}^2$ diamond sensors arranged around the beampipe in a cross pattern at $z = \pm 1.84\,\mathrm{m}$ on each side of the ATLAS IP.[1] If one of the sensors produces a signal over a preset threshold, a *hit* is recorded for that bunch crossing, thereby providing a low-acceptance bunch-by-bunch luminosity signal at $|\eta| = 4.2$ with subnanosecond time resolution. The horizontal and vertical pairs of BCM sensors are read out separately, leading to two luminosity measurements labelled BCMH and BCMV respectively. Because the thresholds, efficiencies and noise levels may exhibit small differences between BCMH and BCMV, these two measurements are treated for calibration and monitoring purposes as being produced by independent devices, although the overall response of the two devices is expected to be very similar.

LUCID is a Cherenkov detector specifically designed to measure the luminosity in ATLAS. Sixteen aluminium tubes originally filled with C_4F_{10} gas surround the beampipe on each side of the IP at a distance of 17 m, covering the pseudorapidity range $5.6 < |\eta| < 6.0$. For most of 2012, the LUCID tubes were operated under vacuum to reduce the sensitivity of the device, thereby mitigating pile-up effects and providing a wider operational dynamic range. In this configuration, Cherenkov photons are produced only in the quartz windows that separate the gas volumes from the photomultiplier tubes (PMTs) situated at the back of the detector. If one of the LUCID PMTs produces a signal over a preset threshold, that tube records a hit for that bunch crossing.

Each colliding-bunch pair is identified numerically by a bunch-crossing identifier (BCID) which labels each of the 3564 possible 25 ns slots in one full revolution of the nominal LHC fill pattern. Both BCM and LUCID are fast detectors with electronics capable of reading out the diamond-sensor and PMT hit patterns separately for each bunch crossing, thereby making full use of the available statistics. These FPGA-based front-end electronics run autonomously from the main data acquisition system, and are not affected by any deadtime imposed by the CTP.[2] They execute in real time several different online algorithms, characterized by diverse efficiencies, background sensitivities, and linearity characteristics [5].

The BCM and LUCID detectors consist of two symmetric arms placed in the forward ("A") and backward ("C") direction from the IP, which can also be treated as independent devices. The baseline luminosity algorithm is an inclusive hit requirement, known as the EventOR algorithm, which requires that at least one hit be recorded anywhere in the detector considered. Assuming that the number of interactions in a bunch crossing obeys a Poisson distribution, the probability of observing an event which satisfies the EventOR criteria can be computed as

$$P_{\mathrm{EventOR}}(\mu_{\mathrm{vis}}^{\mathrm{OR}}) = N_{\mathrm{OR}}/N_{\mathrm{BC}} = 1 - \mathrm{e}^{-\mu_{\mathrm{vis}}^{\mathrm{OR}}}. \quad (3)$$

Here the raw event count N_{OR} is the number of bunch crossings, during a given time interval, in which at least one pp interaction satisfies the event-selection criteria of the OR algorithm under consideration, and N_{BC} is the total number of bunch crossings during the same interval. Solving for μ_{vis} in terms of the event-counting rate yields

$$\mu_{\mathrm{vis}}^{\mathrm{OR}} = -\ln\left(1 - \tfrac{N_{\mathrm{OR}}}{N_{\mathrm{BC}}}\right). \quad (4)$$

When $\mu_{\mathrm{vis}} \gg 1$, event counting algorithms lose sensitivity as fewer and fewer bunch crossings in a given time interval report zero observed interactions. In the limit where $N_{\mathrm{OR}}/N_{\mathrm{BC}} = 1$, event counting algorithms can no longer be used to determine the interaction rate μ_{vis}: this is referred to as *saturation*. The sensitivity of the LUCID detector is high enough (even without gas in the tubes) that the LUCID_EventOR algorithm saturates in a one-minute interval at around 20 interactions per crossing, while the single-arm inclusive LUCID_EventA and LUCID_EventC algorithms can be used up to around 30 interactions per crossing. The lower acceptance of the BCM detector allowed event counting to remain viable for all of 2012.

3.2 Tracker-based luminosity algorithms

The ATLAS inner detector (ID) measures the trajectories of charged particles over the pseudorapidity range $|\eta| < 2.5$ and the full azimuth. It consists [1] of a silicon pixel detector (Pixel), a silicon micro-strip detector (SCT) and a straw-tube transition-radiation detector (TRT). Charged particles are reconstructed as tracks using an inside-out algorithm,

[1] ATLAS uses a right-handed coordinate system with its origin at the nominal interaction point in the centre of the detector, and the z-axis along the beam line. The x-axis points from the IP to the centre of the LHC ring, and the y-axis points upwards. Cylindrical coordinates (r, ϕ) are used in the transverse plane, ϕ being the azimuthal angle around the beam line. The pseudorapidity is defined in terms of the polar angle θ as $\eta = -\ln\tan(\theta/2)$.

[2] The CTP inhibits triggers (causing deadtime) for a variety of reasons, but especially for several bunch crossings after a triggered event to allow time for the detector readout to conclude. Any new triggers which occur during this time are ignored.

which starts with three-point seeds from the silicon detectors and then adds hits using a combinatoric Kalman filter [6].

The luminosity is assumed to be proportional to the number of reconstructed charged-particle tracks, with the visible interaction rate μ_{vis} taken as the number of tracks per bunch crossing averaged over a given time window (typically a luminosity block). In standard physics operation, silicon-detector data are recorded in a dedicated partial-event stream using a random trigger at a typical rate of 100 Hz, sampling each colliding-bunch pair with equal probability. Although a bunch-by-bunch luminosity measurement is possible in principle, over 1300 bunches were colliding in ATLAS for most of 2012, so that in practice only the bunch-integrated luminosity can be determined with percent-level statistical precision in a given luminosity block. During *vdM* scans, Pixel and SCT data are similarly routed to a dedicated data stream for a subset of the colliding-bunch pairs at a typical rate of 5 kHz per BCID, thereby allowing the bunch-by-bunch determination of σ_{vis}.

For the luminosity measurements presented in this paper, charged-particle track reconstruction uses hits from the silicon detectors only. Reconstructed tracks are required to have at least nine silicon hits, zero holes[3] in the Pixel detector and transverse momentum in excess of 0.9 GeV. Furthermore, the absolute transverse impact parameter with respect to the luminous centroid [7] is required to be no larger than seven times its uncertainty, as determined from the covariance matrix of the fit.

This default track selection makes no attempt to distinguish tracks originating from primary vertices from those produced in secondary interactions, as the yields of both are expected to be proportional to the luminosity. Previous studies of track reconstruction in ATLAS show that in low pile-up conditions ($\mu \leq 1$) and with a track selection looser than the above-described default, single-beam backgrounds remain well below the per-mille level [8]. However, for pile-up parameters typical of 2012 physics running, tracks formed from random hit combinations, known as *fake tracks*, can become significant [9]. The track selection above is expected to be robust against such non-linearities, as demonstrated by analysing simulated events of overlaid inelastic pp interactions produced using the PYTHIA 8 Monte Carlo event generator [10]. In the simulation, the fraction of fake tracks per event can be parameterized as a function of the true pile-up parameter, yielding a fake-track fraction of less than 0.2% at $\mu = 20$ for the default track selection. In data, this fake-track contamination is subtracted from the measured track multiplicity using the simulation-based parameterization with, as input, the $\langle\mu\rangle$ value reported by the BCMH_EventOR luminosity algorithm. An uncertainty equal to half the correction is assigned to the measured track multiplicity to account for possible systematic differences between data and simulation.

Biases in the track-counting luminosity measurement can arise from μ-dependent effects in the track reconstruction or selection requirements, which would change the reported track-counting yield per collision between the low pile-up *vdM*-calibration regime and the high-μ regime typical of physics data-taking. Short- and long-term variations in the track reconstruction and selection efficiency can also arise from changing ID conditions, for example because of temporarily disabled silicon readout modules. In general, looser track selections are less sensitive to such fluctuations in instrumental coverage; however, they typically suffer from larger fake-track contamination.

To assess the impact of such potential biases, several looser track selections, or *working points* (WP), are investigated. Most are found to be consistent with the default working point once the uncertainty affecting the simulation-based fake-track subtraction is accounted for. In the case where the Pixel-hole requirement is relaxed from zero to no more than one, a moderate difference in excess of the fake-subtraction uncertainty is observed in the data. This working point, labelled "Pixel holes $\leq$1", is used as an alternative algorithm when evaluating the systematic uncertainties associated with track-counting luminosity measurements.

In order to all but eliminate fake-track backgrounds and minimize the associated μ-dependence, another alternative is to remove the impact-parameter requirement and use the resulting superset of tracks as input to the primary-vertex reconstruction algorithm. Those tracks which, after the vertex-reconstruction fit, have a non-negligible probability of being associated to any primary vertex are counted to provide an alternative luminosity measurement. In the simulation, the performance of this "vertex-associated" working point is comparable, in terms of fake-track fraction and other residual non-linearities, to that of the default and "Pixel holes $\leq$1" track selections discussed above.

3.3 Bunch-integrating detectors

Additional algorithms, sensitive to the instantaneous luminosity summed over all bunches, provide relative-luminosity monitoring on time scales of a few seconds rather than of a bunch crossing, allowing independent checks of the linearity and long-term stability of the BCM, LUCID and track-counting algorithms. The first technique measures the particle flux from pp collisions as reflected in the current drawn by the PMTs of the hadronic calorimeter (TileCal). This flux, which is proportional to the instantaneous luminosity, is also monitored by the total ionization current flowing through a

[3] In this context, a hole is counted when a hit is expected in an active sensor located on the track trajectory between the first and the last hit associated with this track, but no such hit is found. If the corresponding sensor is known to be inactive and therefore not expected to provide a hit, no hole is counted.

well-chosen set of liquid-argon (LAr) calorimeter cells. A third technique, using Medipix radiation monitors, measures the average particle flux observed in these devices.

3.3.1 Photomultiplier currents in the central hadronic calorimeter

The TileCal [11] is constructed from plastic-tile scintillators as the active medium and from steel absorber plates. It covers the pseudorapidity range $|\eta| < 1.7$ and consists of a long central cylindrical barrel and two smaller extended barrels, one on each side of the long barrel. Each of these three cylinders is divided azimuthally into 64 modules and segmented into three radial sampling layers. Cells are defined in each layer according to a projective geometry, and each cell is connected by optical fibres to two photomultiplier tubes. The current drawn by each PMT is proportional to the total number of particles interacting in a given TileCal cell, and provides a signal proportional to the luminosity summed over all the colliding bunches. This current is monitored by an integrator system with a time constant of 10 ms and is sensitive to currents from 0.1 nA to 1.2 μA. The calibration and the monitoring of the linearity of the integrator electronics are ensured by a dedicated high-precision current-injection system.

The collision-induced PMT current depends on the pseudorapidity of the cell considered and on the radial sampling in which it is located. The cells most sensitive to luminosity variations are located near $|\eta| \approx 1.25$; at a given pseudorapidity, the current is largest in the innermost sampling layer, because the hadronic showers are progressively absorbed as they expand in the middle and outer radial layers. Long-term variations of the TileCal response are monitored, and corrected if appropriate [3], by injecting a laser pulse directly into the PMT, as well as by integrating the counting rate from a ^{137}Cs radioactive source that circulates between the calorimeter cells during calibration runs.

The TileCal luminosity measurement is not directly calibrated by the *vdM* procedure, both because its slow and asynchronous readout is not optimized to keep in step with the scan protocol, and because the luminosity is too low during the scan for many of its cells to provide accurate measurements. Instead, the TileCal luminosity calibration is performed in two steps. The PMT currents, corrected for electronics pedestals and for non-collision backgrounds[4] and averaged over the most sensitive cells, are first cross-calibrated to the absolute luminosity reported by the BCM during the April 2012 *vdM* scan session (Sect. 4). Since these high-sensitivity cells would incur radiation damage at the highest luminosities encountered during 2012, thereby requiring large calibration corrections, their luminosity scale is transferred, during an early intermediate-luminosity run and on a cell-by-cell basis, to the currents measured in the remaining cells (the sensitivities of which are insufficient under the low-luminosity conditions of *vdM* scans). The luminosity reported in any other physics run is then computed as the average, over the usable cells, of the individual cell luminosities, determined by multiplying the baseline-subtracted PMT current from that cell by the corresponding calibration constant.

3.3.2 LAr-gap currents

The electromagnetic endcap (EMEC) and forward (FCal) calorimeters are sampling devices that cover the pseudorapidity ranges of, respectively, $1.5 < |\eta| < 3.2$ and $3.2 < |\eta| < 4.9$. They are housed in the two endcap cryostats along with the hadronic endcap calorimeters.

The EMECs consist of accordion-shaped lead/stainless-steel absorbers interspersed with honeycomb-insulated electrodes that distribute the high voltage (HV) to the LAr-filled gaps where the ionization electrons drift, and that collect the associated electrical signal by capacitive coupling. In order to keep the electric field across each LAr gap constant over time, the HV supplies are regulated such that any voltage drop induced by the particle flux through a given HV sector is counterbalanced by a continuous injection of electrical current. The value of this current is proportional to the particle flux and thereby provides a relative-luminosity measurement using the EMEC HV line considered.

Both forward calorimeters are divided longitudinally into three modules. Each of these consists of a metallic absorber matrix (copper in the first module, tungsten elsewhere) containing cylindrical electrodes arranged parallel to the beam axis. The electrodes are formed by a copper (or tungsten) tube, into which a rod of slightly smaller diameter is inserted. This rod, in turn, is positioned concentrically using a helically wound radiation-hard plastic fibre, which also serves to electrically isolate the anode rod from the cathode tube. The remaining small annular gap is filled with LAr as the active medium. Only the first sampling is used for luminosity measurements. It is divided into 16 azimuthal sectors, each fed by 4 independent HV lines. As in the EMEC, the HV system provides a stable electric field across the LAr gaps and the current drawn from each line is directly proportional to the average particle flux through the corresponding FCal cells.

After correction for electronic pedestals and single-beam backgrounds, the observed currents are assumed to be proportional to the luminosity summed over all bunches; the validity of this assumption is assessed in Sect. 6. The EMEC and FCal gap currents cannot be calibrated during a *vdM* scan, because the instantaneous luminosity during these scans remains below the sensitivity of the current-measurement

[4] For each LHC fill, the currents are baseline-corrected using data recorded shortly before the LHC beams are brought into collision.

circuitry. Instead, the calibration constant associated with an individual HV line is evaluated as the ratio of the absolute luminosity reported by the baseline bunch-by-bunch luminosity algorithm (BCMH_EventOR) and integrated over one high-luminosity reference physics run, to the HV current drawn through that line, pedestal-subtracted and integrated over exactly the same time interval. This is done for each usable HV line independently. The luminosity reported in any other physics run by either the EMEC or the FCal, separately for the A and C detector arms, is then computed as the average, over the usable cells, of the individual HV-line luminosities.

3.3.3 Hit counting in the Medipix system

The Medipix (MPX) detectors are hybrid silicon pixel devices, which are distributed around the ATLAS detector [12] and are primarily used to monitor radiation conditions in the experimental hall. Each of these 12 devices consists of a 2 cm^2 silicon sensor matrix, segmented in 256×256 cells and bump-bonded to a readout chip. Each pixel in the matrix counts hits from individual particle interactions observed during a software-triggered "frame", which integrates over 5–120 s, depending upon the typical particle flux at the location of the detector considered. In order to provide calibrated luminosity measurements, the total number of pixel clusters observed in each sensor is counted and scaled to the TileCal luminosity in the same reference run as the EMEC and FCal. The six MPX detectors with the highest counting rate are analysed in this fashion for the 2012 running period; their mutual consistency is discussed in Sect. 6.

The hit-counting algorithm described above is primarily sensitive to charged particles. The MPX detectors offer the additional capability to detect thermal neutrons via $^6\mathrm{Li}(n,\alpha)^3\mathrm{H}$ reactions in a ^{6}LiF converter layer. This neutron-counting rate provides a further measure of the luminosity, which is consistent with, but statistically inferior to, the MPX hit counting measurement [12].

4 Absolute luminosity calibration by the van der Meer method

In order to use the measured interaction rate μ_{vis} as a luminosity monitor, each detector and algorithm must be calibrated by determining its visible cross-section σ_{vis}. The primary calibration technique to determine the absolute luminosity scale of each bunch-by-bunch luminosity detector and algorithm employs dedicated *vdM* scans to infer the delivered luminosity at one point in time from the measurable parameters of the colliding bunches. By comparing the known luminosity delivered in the *vdM* scan to the visible interaction rate μ_{vis}, the visible cross-section can be determined from Eq. (2).

This section is organized as follows. The formalism of the van der Meer method is recalled in Sect. 4.1, followed in Sect. 4.2 by a description of the *vdM*-calibration datasets collected during the 2012 running period. The step-by-step determination of the visible cross-section is outlined in Sect. 4.3, and each ingredient is discussed in detail in Sects. 4.4–4.10. The resulting absolute calibrations of the bunch-by-bunch luminometers, as applicable to the low-luminosity conditions of *vdM* scans, are summarized in Sect. 4.11.

4.1 Absolute luminosity from measured beam parameters

In terms of colliding-beam parameters, the bunch luminosity $\mathcal{L}_{\mathrm{b}}$ is given by

$$\mathcal{L}_{\mathrm{b}} = f_{\mathrm{r}}\, n_1 n_2 \int \hat{\rho}_1(x,y)\, \hat{\rho}_2(x,y)\, \mathrm{d}x\, \mathrm{d}y, \tag{5}$$

where the beams are assumed to collide with zero crossing angle, $n_1 n_2$ is the bunch-population product and $\hat{\rho}_{1(2)}(x,y)$ is the normalized particle density in the transverse $(x$–$y)$ plane of beam 1 (2) at the IP. With the standard assumption that the particle densities can be factorized into independent horizontal and vertical component distributions, $\hat{\rho}(x,y) = \rho_x(x)\,\rho_y(y)$, Eq. (5) can be rewritten as

$$\mathcal{L}_{\mathrm{b}} = f_{\mathrm{r}}\, n_1 n_2\, \Omega_x(\rho_{x1},\rho_{x2})\, \Omega_y(\rho_{y1},\rho_{y2}), \tag{6}$$

where

$$\Omega_x(\rho_{x1},\rho_{x2}) = \int \rho_{x1}(x)\,\rho_{x2}(x)\,\mathrm{d}x$$

is the beam-overlap integral in the x direction (with an analogous definition in the y direction). In the method proposed by van der Meer [2], the overlap integral (for example in the x direction) can be calculated as

$$\Omega_x(\rho_{x1},\rho_{x2}) = \frac{R_x(0)}{\int R_x(\delta)\,\mathrm{d}\delta}, \tag{7}$$

where $R_x(\delta)$ is the luminosity (at this stage in arbitrary units) measured during a horizontal scan at the time the two beams are separated horizontally by the distance δ, and $\delta = 0$ represents the case of zero beam separation. Because the luminosity $R_x(\delta)$ is normalized to that at zero separation $R_x(0)$, any quantity proportional to the luminosity (such as μ_{vis}) can be substituted in Eq. (7) in place of R.

Defining the horizontal convolved beam size Σ_x [7,13] as

$$\Sigma_x = \frac{1}{\sqrt{2\pi}} \frac{\int R_x(\delta)\,\mathrm{d}\delta}{R_x(0)}, \tag{8}$$

and similarly for Σ_y, the bunch luminosity in Eq. (6) can be rewritten as

$$\mathcal{L}_{\mathrm{b}} = \frac{f_{\mathrm{r}} n_1 n_2}{2\pi\,\Sigma_x\,\Sigma_y}, \tag{9}$$

which allows the absolute bunch luminosity to be determined from the revolution frequency f_{r}, the bunch-population product $n_1 n_2$, and the product $\Sigma_x \Sigma_y$ which is measured directly during a pair of orthogonal *vdM* (beam-separation) scans. In the case where the luminosity curve $R_x(\delta)$ is Gaussian, Σ_x coincides with the standard deviation of that distribution. It is important to note that the *vdM* method does not rely on any particular functional form of $R_x(\delta)$: the quantities Σ_x and Σ_y can be determined for any observed luminosity curve from Eq. (8) and used with Eq. (9) to determine the absolute luminosity at $\delta = 0$.

In the more general case where the factorization assumption breaks down, i.e. when the particle densities [or more precisely the dependence of the luminosity on the beam separation (δ_x, δ_y)] cannot be factorized into a product of uncorrelated x and y components, the formalism can be extended to yield [4]

$$\Sigma_x \Sigma_y = \frac{1}{2\pi} \frac{\int R_{x,y}(\delta_x, \delta_y)\,\mathrm{d}\delta_x\,\mathrm{d}\delta_y}{R_{x,y}(0,0)}, \tag{10}$$

with Eq. (9) remaining formally unaffected. Luminosity calibration in the presence of non-factorizable bunch-density distributions is discussed extensively in Sect. 4.8.

The measured product of the transverse convolved beam sizes $\Sigma_x \Sigma_y$ is directly related to the reference specific luminosity:[5]

$$\mathcal{L}_{\mathrm{spec}} \equiv \frac{\mathcal{L}_{\mathrm{b}}}{n_1 n_2} = \frac{f_{\mathrm{r}}}{2\pi\,\Sigma_x\,\Sigma_y}$$

which, together with the bunch currents, determines the absolute luminosity scale. To calibrate a given luminosity algorithm, one can equate the absolute luminosity computed from beam parameters using Eq. (9) to that measured according to Eq. (2) to get

$$\sigma_{\mathrm{vis}} = \mu_{\mathrm{vis}}^{\mathrm{MAX}} \frac{2\pi\ \Sigma_x \Sigma_y}{n_1 n_2}, \tag{11}$$

where $\mu_{\mathrm{vis}}^{\mathrm{MAX}}$ is the visible interaction rate per bunch crossing reported at the peak of the scan curve by that particular algorithm. Equation (11) provides a direct calibration of the visible cross-section σ_{vis} for each algorithm in terms of the peak visible interaction rate $\mu_{\mathrm{vis}}^{\mathrm{MAX}}$, the product of the convolved beam widths $\Sigma_x \Sigma_y$, and the bunch-population product $n_1 n_2$.

In the presence of a significant crossing angle in one of the scan planes, the formalism becomes considerably more involved [14], but the conclusions remain unaltered and Eqs. (8)–(11) remain valid. The non-zero vertical crossing angle in some scan sessions widens the luminosity curve by a factor that depends on the bunch length, the transverse beam size and the crossing angle, but reduces the peak luminosity by the same factor. The corresponding increase in the measured value of Σ_y is exactly compensated by the decrease in $\mu_{\mathrm{vis}}^{\mathrm{MAX}}$, so that no correction for the crossing angle is needed in the determination of σ_{vis}.

4.2 Luminosity-scan datasets

The beam conditions during *vdM* scans are different from those in normal physics operation, with lower bunch intensities and only a few tens of widely spaced bunches circulating. These conditions are optimized to reduce various systematic uncertainties in the calibration procedure [7]. Three scan sessions were performed during 2012: in April, July, and November (Table 2). The April scans were performed with nominal collision optics ($\beta^\star = 0.6\,\mathrm{m}$), which minimizes the accelerator set-up time but yields conditions which are inadequate for achieving the best possible calibration accuracy.[6] The July and November scans were performed using dedicated *vdM*-scan optics with $\beta^\star = 11\,\mathrm{m}$, in order to increase the transverse beam sizes while retaining a sufficiently high collision rate even in the tails of the scans. This strategy limits the impact of the vertex-position resolution on the non-factorization analysis, which is detailed in Sect. 4.8, and also reduces potential μ-dependent calibration biases. In addition, the observation of large non-factorization effects in the April and July scan data motivated, for the November scan, a dedicated set-up of the LHC injector chain [16] to produce more Gaussian and less correlated transverse beam profiles.

Since the luminosity can be different for each colliding-bunch pair, both because the beam sizes differ from bunch to bunch and because the bunch populations n_1 and n_2 can each vary by up to $\pm 10\%$, the determination of Σ_x and Σ_y and the measurement of $\mu_{\mathrm{vis}}^{\mathrm{MAX}}$ are performed independently for each colliding-bunch pair. As a result, and taking the November session as an example, each scan set provides 29 independent measurements of σ_{vis}, allowing detailed consistency checks.

[5] The specific luminosity is defined as the luminosity per bunch and per unit bunch-population product [7].

[6] The β function describes the single-particle motion and determines the variation of the beam envelope along the beam trajectory. It is calculated from the focusing properties of the magnetic lattice (see for example Ref. [15]). The symbol $\beta^\star$ denotes the value of the β function at the IP.

Table 2 Summary of the main characteristics of the 2012 *vdM* scans performed at the ATLAS interaction point. The nominal tranverse beam size is computed using the nominal LHC emittance ($\epsilon_N = 3.75$ μm-radians). The actual transverse emittance and single-beam size are estimated by combining the convolved transverse widths measured in the first scan of each session with the nominal IP β-function. The values of the luminosity/bunch and of μ are given for zero beam separation during the first scan. The specific luminosity decreases by 6–17% over the duration of a given scan session

Scan labels	I–III	IV–IX	X–XV
Date	16 April 2012	19 July 2012	22, 24 November 2012
LHC fill number	2520	2855, 2856	3311, 3316
Total number of bunches per beam	48	48	39
Number of bunches colliding in ATLAS	35	35	29
Typical number of protons per bunch $n_{1,2}$	0.6×10^{11}	0.9×10^{11}	0.9×10^{11}
Nominal β-function at the IP ($\beta^\star$) (m)	0.6	11	11
Nominal transverse single-beam size σ_b^{nom} (μm)	23	98	98
Actual transverse emittance ϵ_N (μm-radians)	2.3	3.2	3.1
Actual transverse single-beam size σ_b (μm)	18	91	89
Actual transverse luminous size $\sigma_{\mathcal{L}}$ ($\approx \sigma_b/\sqrt{2}$) ($\mu$m)	13	65	63
Nominal vertical half crossing-angle (μrad)	$\pm$145	0	0
Typical luminosity/bunch ($\mu b^{-1}\,s^{-1}$)	0.8	0.09	0.09
Pile-up parameter μ (interactions/crossing)	5.2	0.6	0.6
Scan sequence	3 sets of centred $x + y$ scans (I–III)	4 sets of centred $x + y$ scans (IV–VI, VIII) plus 2 sets of $x + y$ off-axis scans (VII, IX)	4 sets of centred $x + y$ scans (X, XI, XIV, XV) plus 2 sets of $x + y$ off-axis scans (XII, XIII)
Total scan steps per plane	25	25 (sets IV–VII) 17 (sets VIII–IX)	25
Maximum beam separation	$\pm 6\sigma_b^{nom}$	$\pm 6\sigma_b^{nom}$	$\pm 6\sigma_b^{nom}$
Scan duration per step (s)	20	30	30

To further test the reproducibility of the calibration procedure, multiple centred-scan[7] sets, each consisting of one horizontal scan and one vertical scan, are executed in the same scan session. In November for instance, two sets of centred scans (X and XI) were performed in quick succession, followed by two sets of off-axis scans (XII and XIII), where the beams were separated by 340 and 200 μm respectively in the non-scanning direction. A third set of centred scans (XIV) was then performed as a reproducibility check. A fourth centred scan set (XV) was carried out approximately one day later in a different LHC fill.

The variation of the calibration results between individual scan sets in a given scan session is used to quantify the reproducibility of the optimal relative beam position, the convolved beam sizes, and the visible cross-sections. The reproducibility and consistency of the visible cross-section results across the April, July and November scan sessions provide a measure of the long-term stability of the response of each detector, and are used to assess potential systematic biases in the *vdM*-calibration technique under different accelerator conditions.

4.3 *vdM*-scan analysis methodology

The 2012 *vdM* scans were used to derive calibrations for the LUCID_EventOR, BCM_EventOR and track-counting algorithms. Since there are two distinct BCM readouts, calibrations are determined separately for the horizontal (BCMH) and vertical (BCMV) detector pairs. Similarly, the fully inclusive (EventOR) and single-arm inclusive (EventA, EventC) algorithms are calibrated independently. For the April scan session, the dedicated track-counting event stream (Sect. 3.2) used the same random trigger as during physics operation. For the July and November sessions, where the typical event rate was lower by an order of magnitude, track counting was performed on events triggered by the ATLAS Minimum Bias Trigger Scintillator (MBTS) [1]. Corrections for MBTS trigger inefficiency and for CTP-induced deadtime are applied, at each scan step separately, when calculating the average number of tracks per event.

For each individual algorithm, the *vdM* data are analysed in the same manner. The specific visible interaction rate

[7] A *centred* (or *on-axis*) beam-separation scan is one where the beams are kept centred on each other in the transverse direction orthogonal to the scan axis. An *offset* (or *off-axis*) scan is one where the beams are partially separated in the non-scanning direction.

$\mu_{\rm vis}/(n_1 n_2)$ is measured, for each colliding-bunch pair, as a function of the nominal beam separation (i.e. the separation specified by the LHC control system) in two orthogonal scan directions (x and y). The value of $\mu_{\rm vis}$ is determined from the raw counting rate using the formalism described in Sect. 3.1 or 3.2. The specific interaction rate is used so that the calculation of Σ_x and Σ_y properly takes into account the bunch-current variation during the scan; the measurement of the bunch-population product $n_1 n_2$ is detailed in Sect. 4.10.

Figure 1 shows examples of horizontal-scan curves measured for a single BCID using two different algorithms. At each scan step, the visible interaction rate $\mu_{\rm vis}$ is first corrected for afterglow, instrumental noise and beam-halo backgrounds as described in Sect. 4.4, and the nominal beam separation is rescaled using the calibrated beam-separation scale (Sect. 4.5). The impact of orbit drifts is addressed in Sect. 4.6, and that of beam–beam deflections and of the dynamic-β effect is discussed in Sect. 4.7. For each BCID and each scan independently, a characteristic function is fitted to the corrected data; the peak of the fitted function provides a measurement of $\mu_{\rm vis}^{\rm MAX}$, while the convolved width Σ is computed from the integral of the function using Eq. (8). Depending on the beam conditions, this function can be a single-Gaussian function plus a constant term, a double-Gaussian function plus a constant term, a Gaussian function times a polynomial (plus a constant term), or other variations. As described in Sect. 5, the differences between the results extracted using different characteristic functions are taken into account as a systematic uncertainty in the calibration result.

The combination of one horizontal (x) scan and one vertical (y) scan is the minimum needed to perform a measurement of $\sigma_{\rm vis}$. In principle, while the $\mu_{\rm vis}^{\rm MAX}$parameter is detector- and algorithm-specific, the convolved widths Σ_x and Σ_y, which together specify the head-on reference luminosity, do not need to be determined using that same detector and algorithm. In practice, it is convenient to extract all the parameters associated with a given algorithm consistently from a single set of scan curves, and the average value of $\mu_{\rm vis}^{\rm MAX}$ between the two scan planes is used. The correlations between the fitted values of $\mu_{\rm vis}^{\rm MAX}$, Σ_x and Σ_y are taken into account when evaluating the statistical uncertainty affecting $\sigma_{\rm vis}$.

Each BCID should yield the same measured $\sigma_{\rm vis}$ value, and so the average over all BCIDs is taken as the $\sigma_{\rm vis}$ measurement for the scan set under consideration. The bunch-to-bunch consistency of the visible cross-section for a given luminosity algorithm, as well as the level of agreement between Σ values measured by different detectors and algorithms in a given scan set, are discussed in Sect. 5 as part of the systematic uncertainty.

Once visible cross-sections have been determined from each scan set as described above, two beam-dynamical effects must be considered (and if appropriate corrected for), both associated with the shape of the colliding bunches in transverse phase space: non-factorization and emittance growth. These are discussed in Sects. 4.8 and 4.9 respectively.

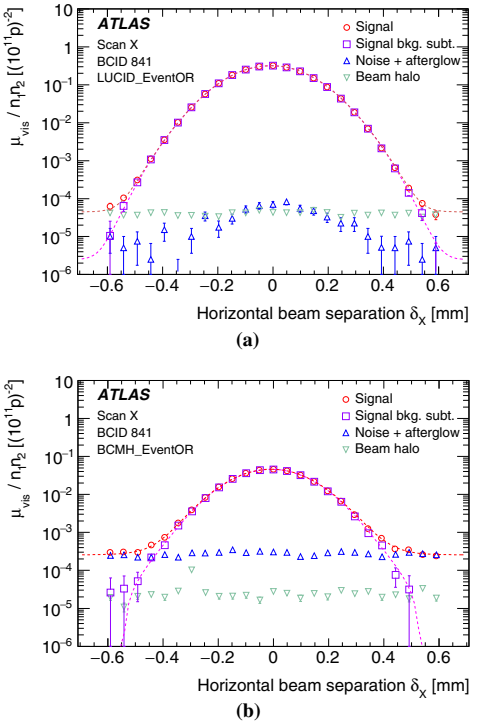

Fig. 1 Beam-separation dependence of the specific visible interaction rate measured using the **a** LUCID_EventOR and **b** BCMH_EventOR algorithms during horizontal scan X, before (*red circles*) and after (*purple squares*) afterglow, noise and single-beam background subtraction. The subtracted contributions are shown as triangles. The scan curves are fitted to a Gaussian function multiplied by a sixth-order polynomial, plus a constant

4.4 Background subtraction

The *vdM* calibration procedure is affected by three distinct background contributions to the luminosity signal: afterglow, instrumental noise, and single-beam backgrounds.

As detailed in Refs. [3,5], both the LUCID and BCM detectors observe some small activity in the BCIDs immediately following a collision, which in later BCIDs decays to a baseline value with several different time constants. This afterglow is most likely caused by photons from nuclear de-excitation, which in turn is induced by the hadronic cascades initiated by pp collision products. For a given bunch pat-

tern, the afterglow level is observed to be proportional to the luminosity in the colliding-bunch slots. During *vdM* scans, it lies three to four orders of magnitude below the luminosity signal, but reaches a few tenths of a percent during physics running because of the much denser bunch pattern.

Instrumental noise is, under normal circumstances, a few times smaller than the single-beam backgrounds, and remains negligible except at the largest beam separations. However, during a one-month period in late 2012 that includes the November *vdM* scans, the A arm of both BCM detectors was affected by high-rate electronic noise corresponding to about 0.5% (1%) of the visible interaction rate, at the peak of the scan, in the BCMH (BCMV) diamond sensors (Fig. 1b). This temporary perturbation, the cause of which could not be identified, disappeared a few days after the scan session. Nonetheless, it was large enough that a careful subtraction procedure had to be implemented in order for this noise not to bias the fit of the BCM luminosity-scan curves.

Since afterglow and instrumental noise both induce random hits at a rate that varies slowly from one BCID to the next, they are subtracted together from the raw visible interaction rate μ_{vis} in each colliding-bunch slot. Their combined magnitude is estimated using the rate measured in the immediately preceding bunch slot, assuming that the variation of the afterglow level from one bunch slot to the next can be neglected.

A third background contribution arises from activity correlated with the passage of a single beam through the detector. This activity is attributed to a combination of shower debris from beam–gas interactions and from beam-tail particles that populate the beam halo and impinge on the luminosity detectors in time with the circulating bunch. It is observed to be proportional to the bunch population, can differ slightly between beams 1 and 2, but is otherwise uniform for all bunches in a given beam. The total single-beam background in a colliding-bunch slot is estimated by measuring the single-beam rates in unpaired bunches (after subtracting the afterglow and noise as done for colliding-bunch slots), separately for beam 1 and beam 2, rescaling them by the ratio of the bunch populations in the unpaired and colliding bunches, and summing the contributions from the two beams. This background typically amounts to 2×10^{-4} (8×10^{-4}) of the luminosity at the peak of the scan for the LUCID (BCM) EventOR algorithms. Because it depends neither on the luminosity nor on the beam separation, it can become comparable to the actual luminosity in the tails of the scans.

4.5 Determination of the absolute beam-separation scale

Another key input to the *vdM* scan technique is the knowledge of the beam separation at each scan step. The ability to measure Σ depends upon knowing the absolute distance by which the beams are separated during the *vdM* scan, which is controlled by a set of closed orbit bumps[8] applied locally near the ATLAS IP. To determine this beam-separation scale, dedicated calibration measurements were performed close in time to the April and July scan sessions using the same optical configuration at the interaction point. Such length-scale scans are performed by displacing both beams transversely by five steps over a range of up to $\pm 3\sigma_{\mathrm{b}}^{\mathrm{nom}}$, at each step keeping the beams well centred on each other in the scanning plane. The actual displacement of the luminous region can then be measured with high accuracy using the primary-vertex position reconstructed by the ATLAS tracking detectors. Since each of the four bump amplitudes (two beams in two transverse directions) depends on different magnet and lattice functions, the length-scale calibration scans are performed so that each of these four calibration constants can be extracted independently. The July 2012 calibration data for the horizontal bump of beam 2 are presented in Fig. 2. The scale factor which relates the nominal beam displacement to the measured displacement of the luminous centroid is given by the slope of the fitted straight line; the intercept is irrelevant.

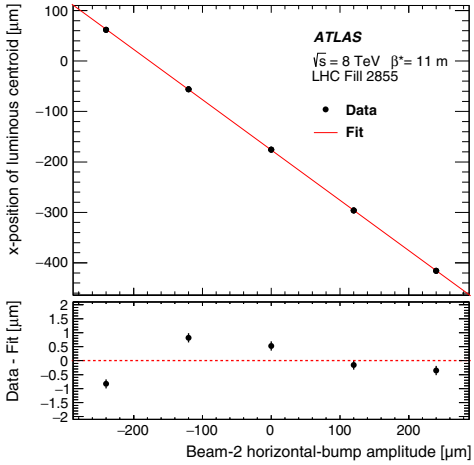

Fig. 2 Length-scale calibration scan for the x direction of beam 2. Shown is the measured displacement of the luminous centroid as a function of the expected displacement based on the corrector bump amplitude. The *line* is a linear fit to the data, and the residual is shown in the *bottom panel*. *Error bars* are statistical only

Since the coefficients relating magnet currents to beam displacements depend on the interaction-region optics, the absolute length scale depends on the $\beta^{\star}$ setting and must

[8] A closed orbit bump is a local distortion of the beam orbit that is implemented using pairs of steering dipoles located on either side of the affected region. In this particular case, these bumps are tuned to offset the trajectory of either beam parallel to itself at the IP, in either the horizontal or the vertical direction.

Table 3 Length-scale calibrations at the ATLAS interaction point at $\sqrt{s} = 8$ TeV. Values shown are the ratio of the beam displacement measured by ATLAS using the average primary-vertex position, to the nominal displacement entered into the accelerator control system. Ratios are shown for each individual beam in both planes, as well as for the beam-separation scale that determines that of the convolved beam sizes in the *vdM* scan. The uncertainties are statistical only

Calibration session(s)	April 2012		July 2012 (applicable to November)	
$\beta^\star$	0.6 m		11 m	
	Horizontal	Vertical	Horizontal	Vertical
Displacement scale				
Beam 1	0.9882 ± 0.0008	0.9881 ± 0.0008	0.9970 ± 0.0004	0.9961 ± 0.0006
Beam 2	0.9822 ± 0.0008	0.9897 ± 0.0009	0.9964 ± 0.0004	0.9951 ± 0.0004
Separation scale	0.9852 ± 0.0006	0.9889 ± 0.0006	0.9967 ± 0.0003	0.9956 ± 0.0004

be recalibrated when the latter changes. The results of the 2012 length-scale calibrations are summarized in Table 3. Because the beam-separation scans discussed in Sect. 4.2 are performed by displacing the two beams symmetrically in opposite directions, the relevant scale factor in the determination of Σ is the average of the scale factors for beam 1 and beam 2 in each plane. A total correction of -2.57% (-0.77%) is applied to the convolved-width product $\Sigma_x \Sigma_y$ and to the visible cross-sections measured during the April (July and November) 2012 *vdM* scans.

4.6 Orbit-drift corrections

Transverse drifts of the individual beam orbits at the IP during a scan session can distort the luminosity-scan curves and, if large enough, bias the determination of the overlap integrals and/or of the peak interaction rate. Such effects are monitored by extrapolating to the IP beam-orbit segments measured using beam-position monitors (BPMs) located in the LHC arcs [17], where the beam trajectories should remain unaffected by the *vdM* closed-orbit bumps across the IP. This procedure is applied to each beam separately and provides measurements of the relative drift of the two beams during the scan session, which are used to correct the beam separation at each scan step as well as between the x and y scans. The resulting impact on the visible cross-section varies from one scan set to the next; it does not exceed $\pm 0.6\%$ in any 2012 scan set, except for scan set X where the orbits drifted rapidly enough for the correction to reach $+1.1\%$.

4.7 Beam–beam corrections

When charged-particle bunches collide, the electromagnetic field generated by a bunch in beam 1 distorts the individual particle trajectories in the corresponding bunch of beam 2 (and vice-versa). This so-called *beam–beam interaction* affects the scan data in two ways.

First, when the bunches are not exactly centred on each other in the x–y plane, their electromagnetic repulsion induces a mutual angular kick [18] of a fraction of a microradian and modulates the actual transverse separation at the IP in a manner that depends on the separation itself. The phenomenon is well known from e^+e^- colliders and has been observed at the LHC at a level consistent with predictions [17]. If left unaccounted for, these *beam–beam deflections* would bias the measurement of the overlap integrals in a manner that depends on the bunch parameters.

The second phenomenon, called *dynamic* β [19], arises from the mutual defocusing of the two colliding bunches: this effect is conceptually analogous to inserting a small quadrupole at the collision point. The resulting fractional change in $\beta^\star$, or equivalently the optical demagnification between the LHC arcs and the collision point, varies with the transverse beam separation, slightly modifying, at each scan step, the effective beam separation in both planes (and thereby also the collision rate), and resulting in a distortion of the shape of the *vdM* scan curves.

The amplitude and the beam-separation dependence of both effects depend similarly on the beam energy, the tunes[9] and the unperturbed β-functions, as well as on the bunch intensities and transverse beam sizes. The beam–beam deflections and associated orbit distortions are calculated analytically [13] assuming elliptical Gaussian beams that collide in ATLAS only. For a typical bunch, the peak angular kick during the November 2012 scans is about $\pm 0.25\,\mu$rad, and the corresponding peak increase in relative beam separation amounts to $\pm 1.7\,\mu$m. The MAD-X optics code [20] is used to validate this analytical calculation, and to verify that higher-order dynamical effects (such as the orbit shifts induced at other collision points by beam–beam deflections at the ATLAS IP) result in negligible corrections to the analytical prediction.

The dynamic evolution of $\beta^\star$ during the scan is modelled using the MAD-X simulation assuming bunch parameters representative of the May 2011 *vdM* scan [3], and then scaled

[9] The tune of a storage ring is defined as the betatron phase advance per turn, or equivalently as the number of betatron oscillations over one full ring circumference.

using the beam energies, the $\beta^\star$ settings, as well as the measured intensities and convolved beam sizes of each colliding-bunch pair. The correction function is intrinsically independent of whether the bunches collide in ATLAS only, or also at other LHC interaction points [19]. For the November session, the peak-to-peak $\beta^\star$ variation during a scan is about 1.1%.

At each scan step, the predicted deflection-induced change in beam separation is added to the nominal beam separation, and the dynamic-β effect is accounted for by rescaling both the effective beam separation and the measured visible interaction rate to reflect the beam-separation dependence of the IP β-functions. Comparing the results of the 2012 scan analysis without and with beam–beam corrections, it is found that the visible cross-sections are increased by 1.2–1.8% by the deflection correction, and reduced by 0.2–0.3% by the dynamic-β correction. The net combined effect of these beam–beam corrections is a 0.9–1.5% increase of the visible cross-sections, depending on the scan set considered.

4.8 Non-factorization effects

The original *vdM* formalism [2] explicitly assumes that the particle densities in each bunch can be factorized into independent horizontal and vertical components, such that the term $1/2\pi\,\Sigma_x\,\Sigma_y$ in Eq. (9) fully describes the overlap integral of the two beams. If this factorization assumption is violated, the horizontal (vertical) convolved beam width Σ_x (Σ_y) is no longer independent of the vertical (horizontal) beam separation δ_y (δ_x); similarly, the transverse luminous size [7] in one plane ($\sigma_{x\mathcal{L}}$ or $\sigma_{y\mathcal{L}}$), as extracted from the spatial distribution of reconstructed collision vertices, depends on the separation in the other plane. The generalized *vdM* formalism summarized by Eq. (10) correctly handles such two-dimensional luminosity distributions, provided the dependence of these distributions on the beam separation in the transverse plane is known with sufficient accuracy.

Non-factorization effects are unambiguously observed in some of the 2012 scan sessions, both from significant differences in Σ_x (Σ_y) between a standard scan and an off-axis scan, during which the beams are partially separated in the non-scanning plane (Sect. 4.8.1), and from the δ_x (δ_y) dependence of $\sigma_{y\mathcal{L}}$ ($\sigma_{x\mathcal{L}}$) during a standard horizontal (vertical) scan (Sect. 4.8.2). Non-factorization effects can also be quantified, albeit with more restrictive assumptions, by performing a simultaneous fit to horizontal and vertical *vdM* scan curves using a non-factorizable function to describe the simultaneous dependence of the luminosity on the x and y beam separation (Sect. 4.8.3).

A large part of the scan-to-scan irreproducibility observed during the April and July scan sessions can be attributed to non-factorization effects, as discussed for ATLAS in Sect. 4.8.4 below and as independently reported by the LHCb Collaboration [21]. The strength of the effect varies widely across *vdM* scan sessions, differs somewhat from one bunch to the next and evolves with time within one LHC fill. Overall, the body of available observations can be explained neither by residual linear x–y coupling in the LHC optics [3,22], nor by crossing-angle or beam–beam effects; instead, it points to non-linear transverse correlations in the phase space of the individual bunches. This phenomenon was never envisaged at previous colliders, and was considered for the first time at the LHC [3] as a possible source of systematic uncertainty in the absolute luminosity scale. More recently, the non-factorizability of individual bunch density distributions was demonstrated directly by an LHCb beam–gas imaging analysis [21].

4.8.1 *Off-axis* vdM *scans*

An unambiguous signature of non-factorization can be provided by comparing the transverse convolved width measured during centred (or on-axis) *vdM* scans with the same quantity extracted from an offset (or off-axis) scan, i.e. one where the two beams are significantly separated in the direction orthogonal to that of the scan. This is illustrated in Fig. 3a. The beams remained vertically centred on each other during the first three horizontal scans (the first horizontal scan) of LHC fill 2855 (fill 2856), and were separated vertically by approximately 340 μm (roughly $4\sigma_b$) during the last horizontal scan in each fill. In both fills, the horizontal convolved beam size is significantly larger when the beams are vertically separated, demonstrating that the horizontal luminosity distribution depends on the vertical beam separation, i.e. that the horizontal and vertical luminosity distributions do not factorize.

The same measurement was carried out during the November scan session: the beams remained vertically centred on each other during the first, second and last scans (Fig. 3b), and were separated vertically by about 340 (200) μm during the third (fourth) scan. The horizontal convolved beam size increases with time at an approximately constant rate, reflecting transverse-emittance growth. No significant deviation from this trend is observed when the beams are separated vertically, suggesting that the horizontal luminosity distribution is independent of the vertical beam separation, i.e. that during the November scan session the horizontal and vertical luminosity distributions approximately factorize.

4.8.2 *Determination of single-beam parameters from luminous-region and luminosity-scan data*

While a single off-axis scan can provide convincing evidence for non-factorization, it samples only one thin slice in the (δ_x, δ_y) beam-separation space and is therefore insufficient to fully determine the two-dimensional luminosity distribution. Characterizing the latter by performing an x–

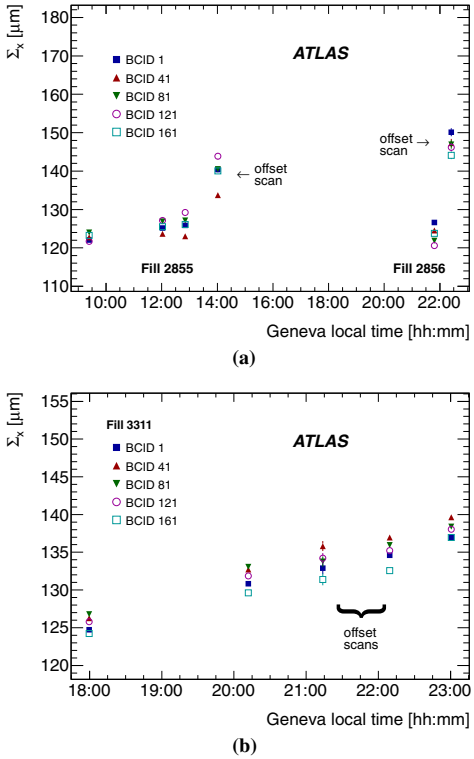

Fig. 3 Time evolution of the horizontal convolved beam size Σ_x for five different colliding-bunch pairs (BCIDs), measured using the LUCID_EventOR luminosity algorithm during the **a** July and **b** November 2012 *vdM*-scan sessions

y grid scan (rather than two one-dimensional x and y scans) would be prohibitively expensive in terms of beam time, as well as limited by potential emittance-growth biases. The strategy, therefore, is to retain the standard *vdM* technique (which assumes factorization) as the baseline calibration method, and to use the data to constrain possible non-factorization biases. In the absence of input from beam–gas imaging (which requires a vertex-position resolution within the reach of LHCb only), the most powerful approach so far has been the modelling of the simultaneous beam-separation-dependence of the luminosity and of the luminous-region geometry. In this procedure, the parameters describing the transverse proton-density distribution of individual bunches are determined by fitting the evolution, during *vdM* scans, not only of the luminosity itself but also of the position, orientation and shape of its spatial distribution, as reflected by that of reconstructed pp-collision vertices [23]. Luminosity profiles are then generated for simulated *vdM* scans using these fitted single-beam parameters, and analysed in the same fashion as real *vdM* scan data. The impact of non-factorization on the absolute luminosity scale is quantified by the ratio R_{NF} of the "measured" luminosity extracted from the one-dimensional simulated luminosity profiles using the standard *vdM* method, to the "true" luminosity from the computed four-dimensional (x, y, z, t) overlap integral [7] of the single-bunch distributions at zero beam separation. This technique is closely related to beam–beam imaging [7,24,25], with the notable difference that it is much less sensitive to the vertex-position resolution because it is used only to estimate a small fractional correction to the overlap integral, rather than its full value.

The luminous region is modelled by a three-dimensional (3D) ellipsoid [7]. Its parameters are extracted, at each scan step, from an unbinned maximum-likelihood fit of a 3D Gaussian function to the spatial distribution of the reconstructed primary vertices that were collected, at the corresponding beam separation, from the limited subset of colliding-bunch pairs monitored by the high-rate, dedicated ID-only data stream (Sect. 3.2). The vertex-position resolution, which is somewhat larger (smaller) than the transverse luminous size during scan sets I–III (scan sets IV–XV), is determined from the data as part of the fitting procedure [23]. It potentially impacts the reported horizontal and vertical luminous sizes, but not the measured position, orientation nor length of the luminous ellipsoid.

The single-bunch proton-density distributions $\rho_B(x, y, z)$ are parameterized, independently for each beam B ($B = 1$, 2), as the non-factorizable sum of up to three 3D Gaussian or super-Gaussian [26] distributions (G_{a}, G_{b}, G_{c}) with arbitrary widths and orientations [27,28]:

$$\rho_B = w_{\mathrm{a}B} \times G_{\mathrm{a}B} + (1 - w_{\mathrm{a}B})[w_{\mathrm{b}B} \times G_{\mathrm{b}B} + (1 - w_{\mathrm{b}B}) \times G_{\mathrm{c}B}],$$

where the weights $w_{\mathrm{a(b)}B}$, $(1 - w_{\mathrm{a(b)}B})$ add up to one by construction. The overlap integral of these density distributions, which allows for a crossing angle in both planes, is evaluated at each scan step to predict the produced luminosity and the geometry of the luminous region for a given set of bunch parameters. This calculation takes into account the impact, on the relevant observables, of the luminosity backgrounds, orbit drifts and beam–beam corrections. The bunch parameters are then adjusted, by means of a χ^2-minimization procedure, to provide the best possible description of the centroid position, the orientation and the resolution-corrected widths of the luminous region measured at each step of a given set of on-axis x and y scans. Such a fit is illustrated in Fig. 4 for one of the horizontal scans in the July 2012 session. The goodness of fit is satisfactory ($\chi^2 = 1.3$ per degree of freedom), even if some systematic deviations are apparent in the tails of the scan. The strong horizontal-separation dependence of the

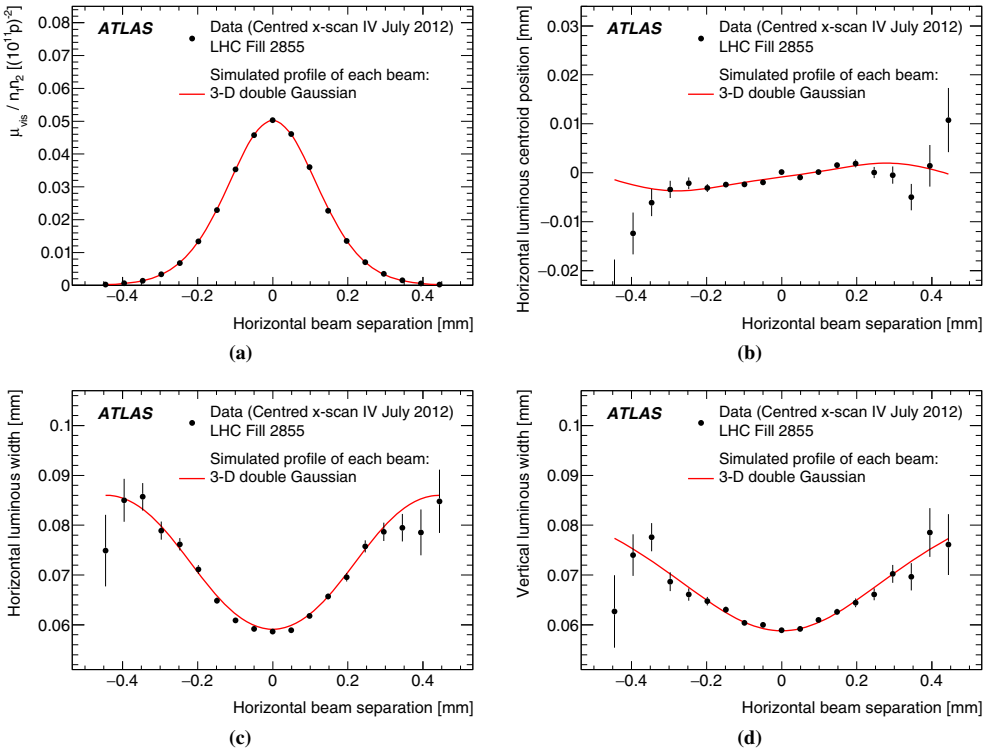

Fig. 4 Beam-separation dependence of the luminosity and of a subset of luminous-region parameters during horizontal *vdM* scan IV. The *points* represent **a** the specific visible interaction rate (or equivalently the specific luminosity), **b** the *horizontal* position of the luminous centroid, **c**, **d** the *horizontal* and *vertical* luminous widths $\sigma_{x\mathcal{L}}$ and $\sigma_{y\mathcal{L}}$. The *red line* is the result of the fit described in the text

vertical luminous size (Fig. 4d) confirms the presence of significant non-factorization effects, as already established from the off-axis luminosity data for that scan session (Fig. 3a).

This procedure is applied to all 2012 *vdM* scan sets, and the results are summarized in Fig. 5. The luminosity extracted from the standard *vdM* analysis with the assumption that factorization is valid, is larger than that computed from the reconstructed single-bunch parameters. This implies that neglecting non-factorization effects in the *vdM* calibration leads to overestimating the absolute luminosity scale (or equivalently underestimating the visible cross-section) by up to 3% (4.5%) in the April (July) scan session. Non-factorization biases remain below 0.8% in the November scans, thanks to bunch-tailoring in the LHC injector chain [16]. These observations are consistent, in terms both of absolute magnitude and of time evolution within a scan session, with those reported by LHCb [21] and CMS [29,30] in the same fills.

4.8.3 Non-factorizable vdM *fits to luminosity-scan data*

A second approach, which does not use luminous-region data, performs a combined fit of the measured beam-separation dependence of the specific visible interaction rate to horizontal- and vertical-scan data simultaneously, in order to determine the overlap integral(s) defined by either Eq. (8) or Eq. (10). Considered fit functions include factorizable or non-factorizable combinations of two-dimensional Gaussian or other functions (super-Gaussian, Gaussian times polynomial) where the (non-)factorizability between the two scan directions is imposed by construction.

The fractional difference between σ_{vis} values extracted from such factorizable and non-factorizable fits, i.e. the multiplicative correction factor to be applied to visible cross-sections extracted from a standard *vdM* analysis, is consistent with the equivalent ratio R_{NF} extracted from the analysis of Sect. 4.8.2 within 0.5% or less for all scan sets. Com-

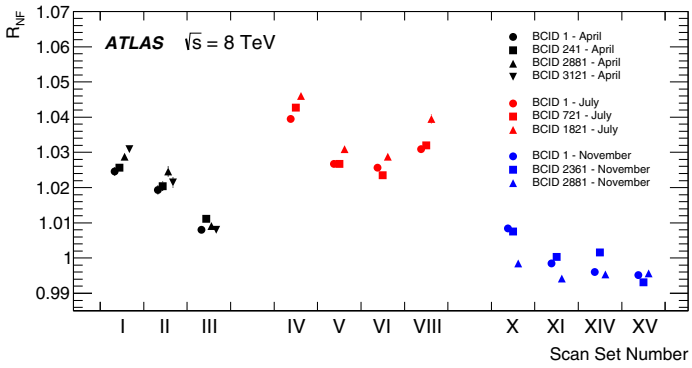

Fig. 5 Ratio R_{NF} of the luminosity determined by the *vdM* method assuming factorization, to that evaluated from the overlap integral of the reconstructed single-bunch profiles at the peak of each scan set. The results are *colour-coded* by scan session. *Each point* corresponds to one colliding-bunch pair in the dedicated ID-only stream. The statistical errors are smaller than the symbols

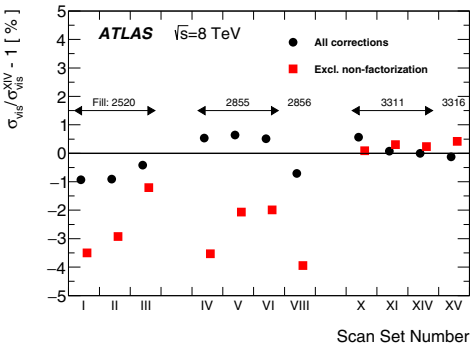

Fig. 6 Comparison of *vdM*-calibrated visible cross-sections for the default track-counting algorithm, with all corrections applied (*black circles*) and with all corrections except for non-factorization (*red squares*). Shown is the fractional difference between the visible cross-section from a given scan set, and the fully corrected visible cross-section from scan set XIV. The LHC fill numbers corresponding to each scan set are indicated

bined with the results of the off-axis scans, this confirms that while the April and July *vdM* analyses require substantial non-factorization corrections, non-factorization biases during the November scan session remain small.

4.8.4 *Non-factorization corrections and scan-to-scan consistency*

Non-factorization corrections significantly improve the reproducibility of the calibration results (Fig. 6). Within a given LHC fill and in the absence of non-factorization corrections, the visible cross-section increases with time, as also observed at other IPs in the same fills [21,29], suggesting that the underlying non-linear correlations evolve over time. Applying the non-factorization corrections extracted from the luminous-region analysis dramatically improves the scan-to-scan consistency within the April and July scan sessions, as well as from one session to the next. The 1.0–1.4% inconsistency between the fully corrected cross-sections (black circles) in scan sets I–III and in later scans, as well as the difference between fills 2855 and 2856 in the July session, are discussed in Sect. 4.11.

4.9 Emittance-growth correction

The *vdM* scan formalism assumes that both convolved beam sizes Σ_x, Σ_y (and therefore the transverse emittances of each beam) remain constant, both during a single x or y scan and in the interval between the horizontal scan and the associated vertical scan.

Emittance growth within a scan would manifest itself by a slight distortion of the scan curve. The associated systematic uncertainty, determined from pseudo-scans simulated with the observed level of emittance growth, was found to be negligible.

Emittance growth between scans manifests itself by a slight increase of the measured value of Σ from one scan to the next, and by a simultaneous decrease in specific luminosity. Each scan set requires 40–60 min, during which time the convolved beam sizes each grow by 1–2%, and the peak specific interaction rate decreases accordingly as $1/(\Sigma_x \Sigma_y)$. This is illustrated in Fig. 7, which displays the Σ_x and $\mu_{\mathrm{vis}}^{\mathrm{MAX}}/(n_1 n_2)$ values measured by the BCMH_EventOR algorithm during scan sets XI, XIV and XV. For each BCID, the convolved beam sizes increase, and the peak specific interaction rate decreases, from scan XI to scan XIV; since scan XV took place very early in the following fill, the corresponding transverse beam sizes (specific rates) are smaller (larger) than for the previous scan sets.

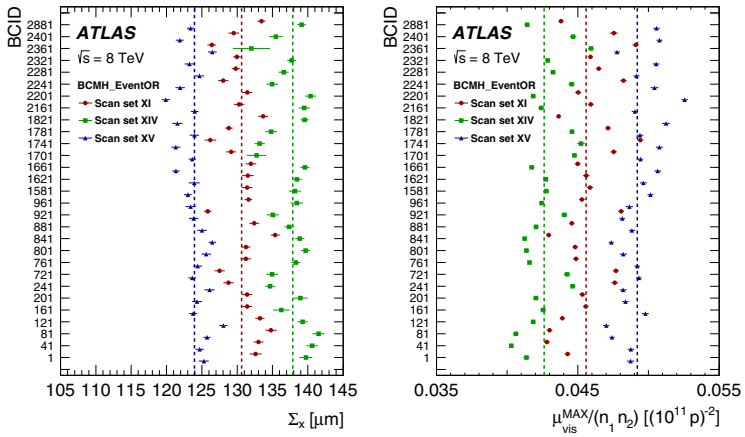

Fig. 7 Bunch-by-bunch **a** horizontal convolved beam size and **b** peak specific interaction rate measured in scan sets XI, XIV, and XV for the BCMH_EventOR algorithm. The *vertical lines* represent the weighted average over colliding-bunch pairs for each scan set separately. The *error bars* are statistical only, and are approximately the size of the marker

If the horizontal and vertical emittances grow at identical rates, the procedure described in Sect. 4.3 remains valid without any need for correction, provided that the decrease in peak rate is fully accounted for by the increase in $(\Sigma_x \Sigma_y)$, and that the peak specific interaction rate in Eq. (11) is computed as the average of the specific rates at the peak of the horizontal and the vertical scan:

$$\mu_{\mathrm{vis}}^{\mathrm{MAX}}/n_1 n_2 = \frac{(\mu_{\mathrm{vis}}^{\mathrm{MAX}}/n_1 n_2)_x + (\mu_{\mathrm{vis}}^{\mathrm{MAX}}/n_1 n_2)_y}{2} .$$

The horizontal-emittance growth rate is measured from the bunch-by-bunch difference in fitted convolved width between two consecutive horizontal scans in the same LHC fill, and similarly for the vertical emittance. For LHC fill 3311 (scan sets X–XIV), these measurements reveal that the horizontal convolved width grew 1.5–2 times faster than the vertical width. The potential bias associated with unequal horizontal and vertical growth rates can be corrected for by interpolating the measured values of Σ_x, Σ_y and $\mu_{\mathrm{vis}}^{\mathrm{MAX}}$ to a common reference time, assuming that all three observables evolve linearly with time. This reference time is in principle arbitrary: it can be, for instance, the peak of the x scan (in which case only Σ_y needs to be interpolated), or the peak of the y scan, or any other value. The visible cross-section, computed from Eq. (11) using measured values projected to a common reference time, should be independent of the reference time chosen.

Applying this procedure to the November scan session results in fractional corrections to σ_{vis} of 1.38, 0.22 and 0.04% for scan sets X, XI and XIV, respectively. The correction for scan set X is exceptionally large because operational difficulties forced an abnormally long delay (almost two hours) between the horizontal scan and the vertical scan, exacerbating the impact of the unequal horizontal and vertical growth rates; its magnitude is validated by the noticeable improvement it brings to the scan-to-scan reproducibility of σ_{vis}.

No correction is available for scan set XV, as no other scans were performed in LHC fill 3316. However, in that case the delay between the x and y scans was short enough, and the consistency of the resulting σ_{vis} values with those in scan sets XI and XIV sufficiently good (Fig. 6), that this missing correction is small enough to be covered by the systematic uncertainties discussed in Sects. 5.2.6 and 5.2.8.

Applying the same procedure to the July scan session yields emittance-growth corrections below 0.3% in all cases. However, the above-described correction procedure is, strictly speaking, applicable only when non-factorization effects are small enough to be neglected. When the factorization hypothesis no longer holds, the very concept of separating horizontal and vertical emittance growth is ill-defined. In addition, the time evolution of the fitted one-dimensional convolved widths and of the associated peak specific rates is presumably more influenced by the progressive dilution, over time, of the non-factorization effects discussed in Sect. 4.8 above. Therefore, and given that the non-factorization cor-

Table 4 Systematic uncertainties affecting the bunch-population product $n_1 n_2$ during the 2012 *vdM* scans

Scan set number	I–III	IV–VII	VIII–IX	X–XIV	XV
LHC fill number	2520	2855	2856	3311	3316
Fractional systematic uncertainty (%)					
Total intensity scale (DCCT)	0.26	0.21	0.21	0.22	0.23
Bunch-by-bunch fraction (FBCT)	0.03	0.04	0.04	0.04	0.04
Ghost charge (LHCb beam–gas)	0.04	0.03	0.04	0.04	0.02
Satellites (longitudinal density monitor)	0.07	0.02	0.03	0.01	<0.01
Total	0.27	0.22	0.22	0.24	0.23

rections applied to scan sets I–VIII (Fig. 5) are up to ten times larger than a typical emittance-growth correction, no such correction is applied to the April and July scan results; an appropriately conservative systematic uncertainty must be assigned instead.

4.10 Bunch-population determination

The bunch-population measurements are performed by the LHC Bunch-Current Normalization Working Group and have been described in detail in Refs. [21,27,31–33]. A brief summary of the analysis is presented here. The fractional uncertainties affecting the bunch-population product ($n_1 n_2$) are summarized in Table 4.

The LHC bunch currents are determined in a multi-step process due to the different capabilities of the available instrumentation. First, the total intensity of each beam is monitored by two identical and redundant DC current transformers (DCCT), which are high-accuracy devices but have no ability to distinguish individual bunch populations. Each beam is also monitored by two fast beam-current transformers (FBCT), which measure relative bunch currents individually for each of the 3564 nominal 25 ns slots in each beam; these fractional bunch populations are converted into absolute bunch currents using the overall current scale provided by the DCCT. Finally, corrections are applied to account for out-of-time charge present in a given BCID but not colliding at the interaction point.

A precision current source with a relative accuracy of 0.05% is used to calibrate the DCCT at regular intervals. An exhaustive analysis of the various sources of systematic uncertainty in the absolute scale of the DCCT, including in particular residual non-linearities, long-term stability and dependence on beam conditions, is documented in Ref. [31]. In practice, the uncertainty depends on the beam intensity and the acquisition conditions, and must be evaluated on a fill-by-fill basis; it typically translates into a 0.2–0.3% uncertainty in the absolute luminosity scale.

Because of the highly demanding bandwidth specifications dictated by single-bunch current measurements, the FBCT response is potentially sensitive to the frequency spectrum radiated by the circulating bunches, timing adjustments with respect to the RF phase, and bunch-to-bunch intensity or length variations. Dedicated laboratory measurements and beam experiments, comparisons with the response of other bunch-aware beam instrumentation (such as the ATLAS beam pick-up timing system), as well as the imposition of constraints on the bunch-to-bunch consistency of the measured visible cross-sections, resulted in a <0.04% systematic luminosity-calibration uncertainty in the luminosity scale arising from the relative-intensity measurements [27,32].

Additional corrections to the bunch-by-bunch population are made to correct for *ghost charge* and *satellite bunches*. Ghost charge refers to protons that are present in nominally empty bunch slots at a level below the FBCT threshold (and hence invisible), but which still contribute to the current measured by the more accurate DCCT. Highly precise measurements of these tiny currents (normally at most a few per mille of the total intensity) have been achieved [27] by comparing the number of beam–gas vertices reconstructed by LHCb in nominally empty bunch slots, to that in non-colliding bunches whose current is easily measurable. For the 2012 luminosity-calibration fills, the ghost-charge correction to the bunch-population product ranges from −0.21 to −0.65%; its systematic uncertainty is dominated by that affecting the LHCb trigger efficiency for beam–gas events.

Satellite bunches describe out-of-time protons present in collision bunch slots that are measured by the FBCT, but that remain captured in an RF bucket at least one period (2.5 ns) away from the nominally filled LHC bucket. As such, they experience at most long-range encounters with the nominally filled bunches in the other beam. The best measurements are obtained using the longitudinal density monitor. This instrument uses avalanche photodiodes with 90 ps timing resolution to compare the number of infrared synchrotron-radiation photons originating from satellite RF buckets, to that from the nominally filled buckets. The corrections to the bunch-population product range from −0.03 to −0.65%, with the lowest satellite fraction achieved in scans X–XV. The measurement techniques, as well as the associ-

ated corrections and systematic uncertainties, are detailed in Ref. [33].

4.11 Calibration results

4.11.1 Summary of calibration corrections

With the exception of the noise and single-beam background subtractions (which depend on the location, geometry and instrumental response of individual subdetectors), all the above corrections to the *vdM*-calibrated visible cross-sections are intrinsically independent of the luminometer and luminosity algorithm considered. The beam-separation scale, as well as the orbit-drift and beam–beam corrections, impact the effective beam separation at each scan step; the non-factorization and emittance-growth corrections depend on the properties of each colliding bunch-pair and on their time evolution over the course of a fill; and corrections to the bunch-population product translate into an overall scale factor that is common to all scan sets within a given LHC fill. The mutual consistency of these corrections was explicitly verified for the LUCID_EventOR and BCM_EventOR visible cross-sections, for which independently determined corrections are in excellent agreement. As the other algorithms (in particular track counting) are statistically less precise during *vdM* scans, their visible cross-sections are corrected using scale factors extracted from the LUCID_EventOR scan analysis.

The dominant correction in scan sets I–VIII (Fig. 8) is associated with non-factorization; it is also the most uncertain, because it is sensitive to the vertex-position resolution, especially in scan sets I–III where the transverse luminous size is significantly smaller than the resolution. In contrast, non-factorization corrections are moderate in scan sets X–XV, suggesting a correspondingly minor contribution to the systematic uncertainty for the November scan session.

The next largest correction in scan sets I–III is that of the beam-separation scale, which, because of different $\beta^\star$ settings, is uncorrelated between the April session and the other two sessions, and fully correlated across scan sets IV–XV (Sect. 5.1.3). The correction to the bunch-population product is equally shared among FBCT, ghost-charge and satellite corrections in scan sets I–III, and dominated by the ghost-charge subtraction in scans IV–XV. This correction is uncorrelated between scan sessions, but fully correlated between scan sets in the same fill.

Of comparable magnitude across all scan sets, and partially correlated between them, is the beam–beam correction; its systematic uncertainty is moderate and can be calculated reliably (Sect. 5.2.3). The uncertainties associated with orbit drifts (Sect. 5.2.1) and emittance growth (Sect. 5.2.6) are small, except for scan set X where these corrections are largest.

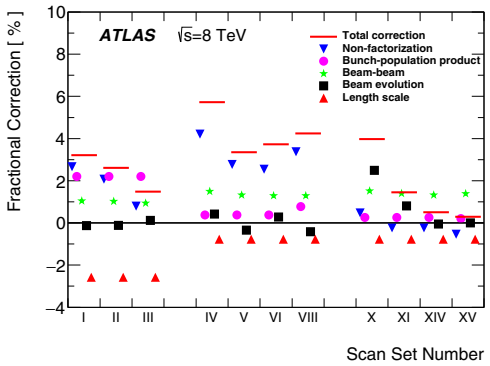

Fig. 8 Luminometer-independent corrections to the visible cross-sections calibrated by the van der Meer method, averaged over all colliding bunches and displayed separately for each scan set. The length–scale, beam–beam, non-factorization and bunch–population corrections are discussed in Sects. 4.5, 4.7, 4.8 and 4.10, respectively. The orbit–drift (Sect. 4.6) and emittance–growth (Sect. 4.9) corrections are combined for clarity, and their cumulative effect is displayed as "beam evolution". The sum of all corrections is shown, for each scan set, by the red line

4.11.2 Consistency of vdM *calibrations across 2012 scan sessions*

The relative stability of *vdM* calibrations, across scan sets within a scan session and from one scan session to the next, can be quantified by the ratio $S^k_{\text{calib},j}$ of the visible cross-section for luminosity algorithm k (k = BCMH_EventOR, BCMV_EventOR, LUCID_EventA,…) in a given scan set j to that in a reference scan set, arbitrarily chosen as scan set XIV:

$$S^k_{\text{calib},j} = \sigma^k_{\text{vis},j}/\sigma^k_{\text{vis, XIV}} \,.$$

The ratio $S^k_{\text{calib},j}$ is presented in Fig. 9a for a subset of BCM, LUCID and track-counting algorithms. Several features are apparent.

- The visible cross-section associated with the LUCID_EventA algorithm drops significantly between the April and July scan sessions, and then again between July and November.
- For each algorithm separately, the σ_{vis} variation across scan sets within a given LHC fill (scan sets I–III, IV–VI and X–XIV) remains below 0.5%, except for scan set X which stands out by 1%.
- The absolute calibrations of the BCMH_EventOR and track-counting algorithms are stable to better than ±0.8% across scan sets IV–VI and X–XV, with the inconsistency being again dominated by scan set X.

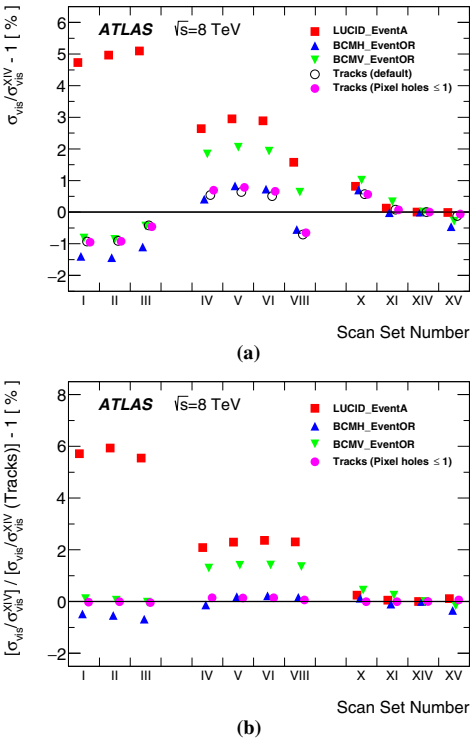

Fig. 9 **a** Stability of absolutely calibrated visible cross-sections across scan sets, as quantified by the ratio of the visible cross-section in a given scan set to that of the same luminosity algorithm in scan set XIV. **b** Relative instrumental stability of different luminosity algorithms across scan sets, as quantified by the ratio shown in **a** for a given algorithm, divided by the same ratio for the default track-counting algorithm

- Between scan sets IV–VI and X–XV, the calibrations of the track counting, BCMH_EventOR and BCMV_EventOR algorithms drop on the average by 0.5, 0.6 and 1.7% respectively.
- The calibrations of the BCM_EventOR (track-counting) algorithm in scan sets I–III and VIII are lower by up to 1.4% (2%) compared to the other scan sets. This structure, which is best visible in Fig. 6, is highly correlated across all algorithms. Since the corresponding luminosity detectors use very different technologies, this particular feature cannot be caused by luminometer instrumental effects.

In order to separate purely instrumental drifts in the ATLAS luminometers from *vdM*-calibration inconsistencies linked to other sources (such as accelerator parameters or beam conditions), Fig. 9b shows the variation, across scan sets j, of the double ratio

$$S^k_{\text{instr},\,j} = S^k_{\text{calib},\,j} / S^{\text{track counting}}_{\text{calib},\,j} = \frac{\sigma^k_{\text{vis},\,j}/\sigma^k_{\text{vis, XIV}}}{\sigma^{\text{track counting}}_{\text{vis},\,j}/\sigma^{\text{track counting}}_{\text{vis, XIV}}},$$

which quantifies the stability of algorithm k relative to that of the default track-counting algorithm. Track counting is chosen as the reference here because it is the bunch-by-bunch algorithm whose absolute calibration is the most stable over time (Figs. 6 and 9a), and that displays the best stability relative to all bunch-integrating luminosity algorithms during physics running across the entire 2012 running period (this is demonstrated in Sect. 6.1). By construction, the instrumental-stability parameter $S^k_{\text{instr},\,j}$ is sensitive only to instrumental effects, because the corrections described in Sects. 4.5–4.10 are intrinsically independent of the luminosity algorithm considered. The following features emerge.

- For each algorithm individually, the instrumental stability is typically better than 0.5% within each scan session.
- The instrumental stability of both the "Pixel holes $\leq$1" selection and the vertex-associated track selection (not shown) is better than 0.2% across all scan sets.
- Relative to track counting, the LUCID efficiency drops by 3.5% between the April and July scan sessions, and by an additional 2.2% between July and November. This degradation is understood to be caused by PMT aging.
- The BCMH_EventOR efficiency increases by about 0.7% with respect to that of track counting between the April and July sessions, and then remains stable to within 0.2–0.4% across the July and November sessions. In contrast, the efficiency of the BCMV_EventOR algorithm compared to that of track counting increases by about 1.3% from April to July, and drops back to its original level by the November session. These long-term variations in the response of various subsets of diamond sensors in the low-luminosity regime of *vdM* scans are possibly related to subtle solid-state physics effects arising from the combination of radiation damage during physics running [3,34] and of partial annealing during beam-off and low-luminosity periods. Aging effects of comparable magnitude are observed at high luminosity (Sect. 6).
- Given the 0.7% relative stability, between scan sets I–III and IV–VI, of the track-counting and BCMH_EventOR calibrations (Fig. 9b), the 1.4–2.0% discrepancy, between the April and July *vdM*-scan sessions, that affects the absolute calibrations of both the BCMH_EventOR and the track-counting algorithms (Fig. 9a) cannot be primarily instrumental in nature. The actual cause could not be identified with certainty. Since the transverse luminous size $\sigma_{\mathcal{L}}$ in the April session (Table 2) is approximately three times smaller than the vertex-position resolution, a plausible scenario is that a small error in the estimated resolution biases the reconstructed luminous size in such

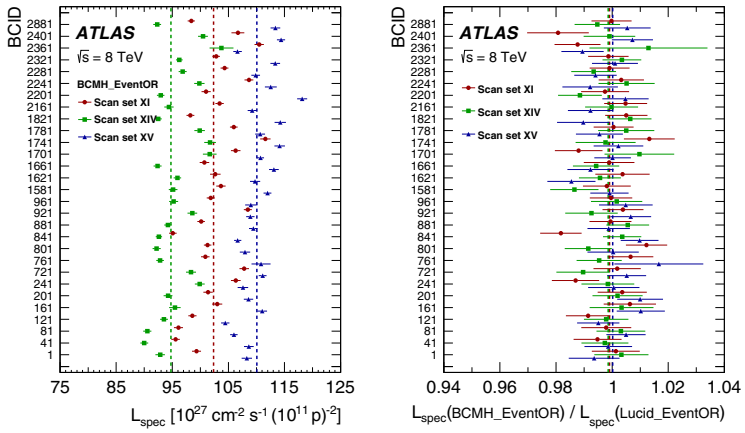

Fig. 10 **a** Bunch-by-bunch specific luminosity for scan sets XI, XIV and XV determined using the BCMH_EventOR algorithm. **b** Bunch-by-bunch ratio of the $\mathcal{L}_{\text{spec}}$ values reported by the BCMH_EventOR and LUCID_EventOR algorithms. The *vertical lines* indicate the weighted average over BCIDs for the three scan sets separately. The *error bars* represent statistical uncertainties only

ences in transverse emittance also seen during normal physics fills. A systematic reduction in $\mathcal{L}_{\text{spec}}$ can be observed from scan XI to scan XIV, caused by emittance growth over the duration of the fill. Although the two algorithms appear statistically consistent for each bunch pair separately (Fig. 10b), their bunch-averaged ratio systematically differs from unity by a small amount. The largest such discrepancy in scan sets XI–XV among the BCM, LUCID and track-counting algorithms amounts to 0.5% and is adopted as the systematic uncertainty associated with the choice of reference specific-luminosity value.

5.1.2 Noise and background subtraction

To assess possible uncertainties in the default subtraction scheme, an alternative fit is performed to data without applying the background-correction procedure of Sect. 4.4, but interpreting the constant (i.e. separation-independent) term in the fitting function as the sum of instrumental noise and single-beam backgrounds. The maximum difference observed between these two background treatments, averaged over scan sets XI–XV, amounts to less than 0.3% (0.02%) for the BCMH_EventOR (LUCID_EventOR) algorithm. A systematic uncertainty of $\pm 0.3\%$ is thus assigned to the background-subtraction procedure during *vdM* scans.

5.1.3 Length-scale calibration

The length scale of each scan step enters the extraction of $\Sigma_{x,y}$ and hence directly affects the absolute luminosity scale. The corresponding calibration procedure is described in Sect. 4.5. Combining in quadrature the statistical errors in the horizontal and vertical beam-separation scales (Table 3) yields a statistical uncertainty of $\pm 0.08\%$ in the length-scale product.

The residual non-linearity visible in Fig. 2, and also observed in length-scale calibration scans performed in 2011, could be caused either by the power converters that drive the steering correctors forming the closed-orbit bumps, by the response of the steering correctors themselves, or by magnetic imperfections (higher multipole components) at large betatron amplitudes in the quadrupoles located within those orbit bumps. The potential impact of such a non-linearity on the luminosity calibration is estimated to be less than 0.05%.

Another potential source of bias is associated with orbit drifts. These were monitored during each of the four length-scale scans using the method outlined in Sect. 4.6, revealing no significant drift. Small inconsistencies in the transverse beam positions extrapolated to the IP from the BPMs in the left and right arcs are used to set an upper limit on the potential orbit drift, during each scan, of the beam being calibrated, resulting in an overall $\pm 0.4\%$ uncertainty in the length-scale product and therefore in the visible cross-section.

5.1.4 Absolute length scale of the inner detector

The determination of the beam-separation scale is based on comparing the scan step requested by the LHC control system with the actual transverse displacement of the luminous centroid measured by ATLAS. This measurement relies on

the length scale of the ATLAS inner detector tracking system (primarily the Pixel detector) being correct in measuring displacements of vertex positions away from the centre of the detector. The determination of the uncertainty in this absolute length scale is described in Ref. [3]; its impact amounts to a systematic uncertainty of ±0.3% in the visible cross-section.

5.2 Beam conditions

5.2.1 Orbit drifts during vdM *scans*

The systematic uncertainty associated with orbit drifts is taken as half of the correction described in Sect. 4.6, averaged over scan sets XI–XV. It translates into a ±0.1% systematic uncertainty in $\overline{\sigma}_{\mathrm{vis}}$. Because the sign and amplitude of the orbit drifts vary over time, this uncertainty is uncorrelated with that affecting the length-scale calibration.

5.2.2 Beam-position jitter

At each step of a scan, the actual beam separation may be affected by random deviations of the beam positions from their nominal settings, which in turn induce fluctuations in the luminosity measured at each scan point. The magnitude of this potential jitter was evaluated from the variation between consecutive measurements, a few seconds apart, of the relative beam separation at the IP extracted from single-beam orbits measured by BPMs in the nearby LHC arcs and extrapolated to the IP (Sect. 4.6). The typical jitter in transverse beam separation observed during the November scan session amounts to 0.75 μm RMS. The resulting systematic uncertainty in σ_{vis} is obtained by random Gaussian smearing of the nominal separation by this amount, independently at each scan step, in a series of simulated scans. The RMS of the resulting fluctuations in fitted visible cross-section yields a ±0.2% systematic uncertainty associated with beam-position jitter.

5.2.3 Beam–beam corrections

For given values of the bunch intensity and transverse convolved beam sizes, which are precisely measured, the deflection-induced orbit distortion and the relative variation of $\beta^\star$ are both proportional to $\beta^\star$ itself; they also depend on the fractional tune. Assigning a ±20% uncertainty to each β-function value at the IP and a ±0.01 upper limit to each tune variation results in a ±0.28% uncertainty in σ_{vis}. This uncertainty is computed with the conservative assumption that β-function and tune uncertainties are correlated between the horizontal and vertical planes, but uncorrelated between the two LHC rings.

5.2.4 Fit model

The choice of the fit function is arbitrary, but guided by the requirement that the fit provides faithful measurements of the integral under the luminosity-scan curve and of the rate at zero beam separation. The choice of functional form therefore depends on the underlying shapes of the colliding bunches, as manifested in the beam-separation dependence of the luminosity. Scan sets I–VIII are best modelled using a double Gaussian function plus a constant. The beam shapes are different in scan sets X–XV [16]: here the best fit is obtained using a Gaussian function multiplied by a sixth-order polynomial. Additional fits are performed with different model assumptions: a super-Gaussian function, and a Gaussian function multiplied by a fourth-order polynomial (plus a constant term in all cases). The maximum fractional difference between the results of these different fits, across scan sets XI–XV and across the BCM, LUCID and track-counting algorithms, amounts to 0.5%. This value is assigned as the uncertainty associated with the fit model.

5.2.5 Non-factorization correction

The non-factorization corrections extracted from the luminous-region analysis (Sect. 4.8.2) and the non-factorizable *vdM* fits (Sect. 4.8.3), are consistent to within 0.5% or less in all scan sets. This value is chosen as the systematic uncertainty associated with non-factorization biases in the November scans.

5.2.6 Emittance-growth correction

The uncertainty in the correction described in Sect. 4.9 is estimated as the largest difference in the scan-averaged correction for extreme choices of reference times, and amounts to ±0.1% in $\overline{\sigma}_{\mathrm{vis}}$.

5.2.7 Consistency of bunch-by-bunch visible cross-sections

The calibrated σ_{vis} value associated with a given luminometer and algorithm should be a universal scale factor independent of beam conditions or BCID. The variation in σ_{vis} across colliding-bunch pairs in a given scan set, as well as between scan sets, is used to quantify the reproducibility and stability of the calibration procedure during a scan session.

The comparison of Fig. 11a, b for scan sets XI, XIV and XV suggests that some of the σ_{vis} variation from one bunch pair to the next is not statistical in nature, but rather correlated across bunch slots. The non-statistical component of this variation, i.e. the difference in quadrature between the RMS bunch-by-bunch variation of σ_{vis} within a given scan set and the average statistical uncertainty affecting a single-BCID σ_{vis} measurement, is taken as a systematic uncertainty in the calibration technique. The largest such difference across scan

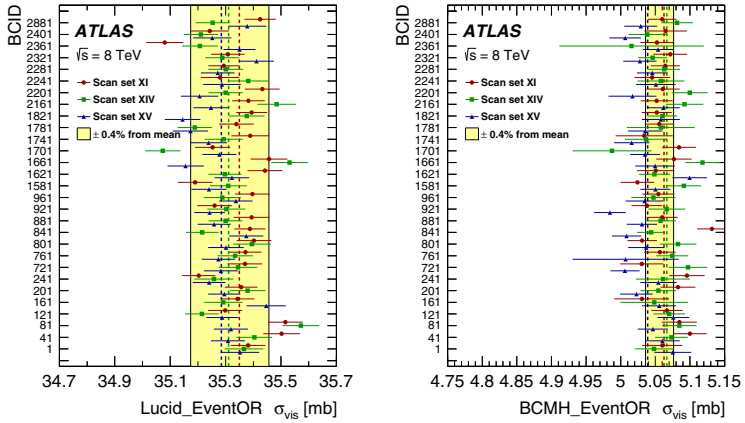

Fig. 11 Bunch-by-bunch σ_{vis} values measured in scan sets XI, XIV, and XV for the **a** LUCID_EventOR and **b** BCMH_EventOR algorithm. The *error bars* are statistical only. The *vertical lines* represent the weighted average over colliding-bunch pairs, separately for each scan set. The *shaded band* indicates a ±0.4% variation from the average, which is the sum in quadrature of the systematic uncertainties associated with bunch-by-bunch and scan-to-scan σ_{vis} consistency

sets XI–XV, evaluated using the measured LUCID_EventOR visible cross-section, amounts to 0.23%. The RMS bunch-by-bunch fluctuation of the BCM cross-sections is, in all cases but one, slightly smaller than the corresponding bunch-averaged statistical uncertainty, indicating that the statistical sensitivity of the BCM algorithms is insufficient to provide a reliable estimate of this uncertainty; the LUCID result is therefore adopted as a measure of the σ_{vis} bunch-by-bunch consistency.

5.2.8 Scan-to-scan reproducibility

The reproducibility of the visible cross-sections across the selected November scan sets, as illustrated in Fig. 9a, is used as a measure of the residual inconsistencies potentially associated with imperfect correction procedures and unidentified sources of non-reproducibility. The largest such difference in visible cross-section between scan sets XI–XV, as reported by any of the BCM_EventOR, LUCID_EventOR or track-counting algorithms, amounts to ±0.31%.

5.3 Bunch-population product

The determination of this uncertainty (±0.24%) is discussed in Sect. 4.10 and summarized in Table 4.

5.4 Summary of van der Meer calibration uncertainties

The systematic uncertainties affecting the November 2012 *vdM* calibration are summarized in Table 6; they apply equally to all *vdM*-calibrated luminosity algorithms. The statistical uncertainties, in contrast, are algorithm dependent (Table 5), but small by comparison.

The uncertainties affecting the April and July 2012 calibrations have not been evaluated in detail. Most of them would be of comparable magnitude to their November counterparts, except for additional sizeable contributions from the non-factorization effects and scan-to-scan inconsistencies discussed in Sect. 4.11.

6 Consistency of relative-luminosity measurements during physics running

The calibration of $\overline{\sigma}_{\text{vis}}$ was performed at only a few points in time (Table 2), and at values of μ low compared to the pile-up levels routinely encountered during physics operation (Fig. 12). In this section, the stability of the luminosity measurement over the 2012 high-luminosity data sample is characterized from two distinct viewpoints: time stability of the relative response of various luminosity algorithms across the entire running period (Sect. 6.1), and linearity of the calibrated luminosity values with respect to the actual pile-up parameter μ (Sect. 6.2). The relative con-

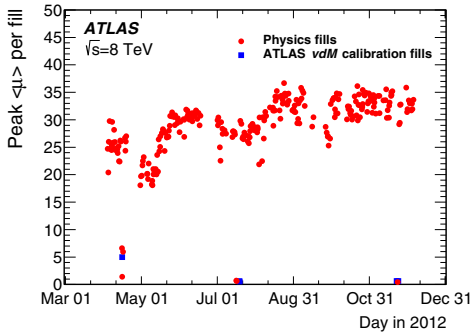

Fig. 12 History of the peak bunch-averaged pile-up parameter $\langle\mu\rangle$ during 2012, restricted to stable-beam periods

sistency across all available luminosity detectors and algorithms is used to assess the robustness of the results and to quantify systematic variations in the response of the various luminometers.

6.1 Relative stability of luminosity measurements over time

6.1.1 Consistency within individual luminometer subsystems

Figure 13a illustrates the internal consistency of the luminosity values reported by independent bunch-by-bunch algorithms during the 2012 running period, noise- and afterglow-subtracted as described in Sect. 4.4, then summed over all colliding bunches and integrated over the stable-beam period in each ATLAS run. In order to better illustrate their relative time evolution, these run-integrated luminosity ratios are shown *anchored*, i.e. normalized to the corresponding ratio in a high-luminosity run close in time to the November *vdM*-scan session.

During most of 2012, the ratio of the luminosity values reported by the horizontal and vertical pairs of BCM sensors is stable within a $\pm 0.4\%$ envelope, with the notable exception of a sharp -0.6% step, lasting approximately one month, during which the BCM was affected by electronic noise (Sect. 4.4). While during physics operation the noise itself has a negligible impact on the measured luminosity, its onset was accompanied by step changes in the response of individual diamond sensors; similar efficiency shifts in the opposite direction were observed when the noise disappeared, a few days after the November *vdM* session.

The history of the luminosity ratio between the A and C arms of LUCID exhibits two distinct bands, each with a peak-to-peak scatter of up to $\pm 0.8\%$ and separated by 1.5% on the average. The step change in late June 2012 is associated with turning off two PMTs in the C arm, which were drawing excessive current. To mitigate the impact of this operational change on the LUCID performance, the LUCID luminosity before (after) this step change is determined using the April (November) 2012 *vdM* calibrations.

While relative efficiency variations among individual BCM sensors, or between the two LUCID arms, can be monitored using such internal luminosity ratios, quantifying the associated shifts in their absolute calibration requires an external reference. This can be provided, for instance, by the calorimeter- or MPX-based hit-counting luminosity algorithms presented in Sect. 3.3. Among these, the best internal performance is offered by the EMEC and the TileCal: in the high-luminosity regime, both achieve an arm-to-arm consistency better than $\pm 0.4\%$ across the 2012 running period (Fig. 13b). The two FCal arms display a relative drift of about 1% which is highly correlated among all channels in each arm. The run-to-run spread of the MPX luminosity ratios (Fig. 13c) lies in the 2% range.

While calorimeter algorithms lack sensitivity in the *vdM*-calibration regime, the track-counting method can be absolutely calibrated with a precision comparable to that of the BCM and LUCID algorithms (Table 5). As demonstrated below, it also offers competitive precision for the run-integrated luminosity[10] during physics operation, thereby providing additional constraints on the performance of the other bunch-by-bunch algorithms.

Figure 14 displays the history of the luminosity reported by the two alternative track-counting working points introduced in Sect. 3.2, normalized to that from the default WP. In contrast to what is presented in Fig. 13, these ratios are not anchored, but directly reflect the relative response of the three algorithms as calibrated in the November 2012 *vdM*-scan session. While the three working points are consistent within 0.2% at the very beginning of the 2012 running period (which corresponds to the April *vdM*-scan session), counting vertex-associated tracks results, during most of the year, in a luminosity value lower by about 1.3% compared to the other two WPs. Comparison with the history of the mean pile-up parameter (Fig. 12) suggests that this inconsistency is not time-related but μ-dependent, as further discussed in Sect. 6.2.

6.1.2 Consistency between luminometer subsystems

Figure 15 shows the ratio of the integrated luminosity per ATLAS run as measured by a variety of luminosity algo-

[10] Except for *vdM*-scan sessions, track–counting-based luminosity measurements on shorter time scales (a few luminosity blocks), or on a bunch-by-bunch basis, are statistically limited by the available data-acquisition bandwidth.

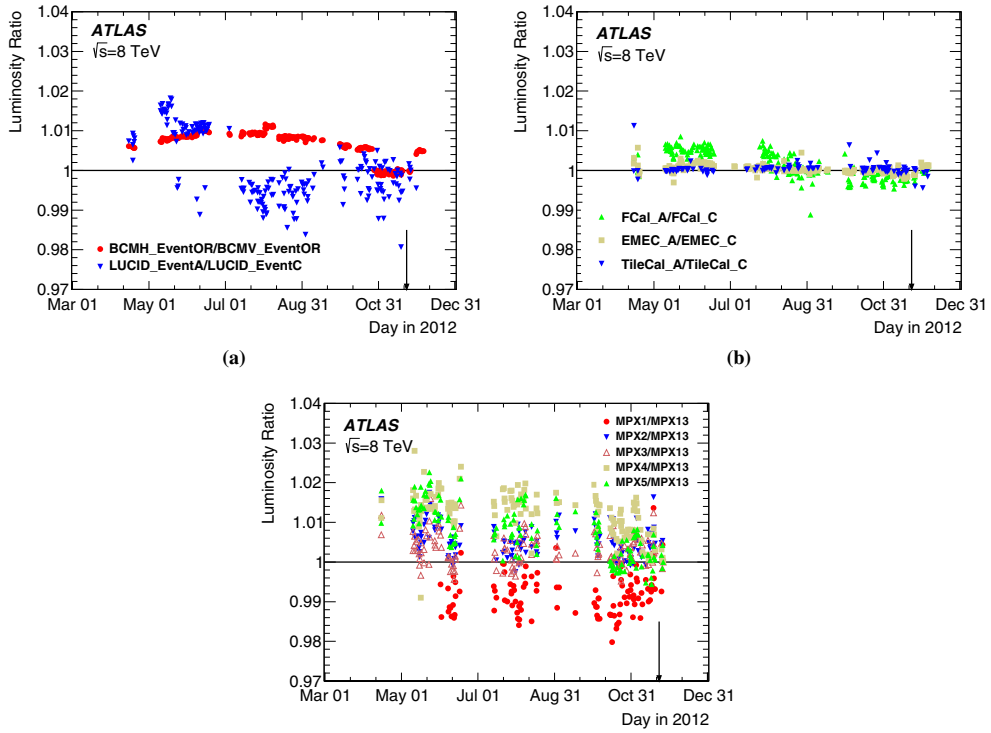

Fig. 13 **a** History of the ratio of the integrated luminosities per run reported by the BCM inclusive–OR algorithms (BCMV_EventOR/BCMH_EventOR) and by the LUCID single-arm algorithms (LUCID_EventA/LUCID_EventC), during routine physics operation at high luminosity. **b** History of the ratio of the integrated luminosities per run reported by the A and C arms of the electromagnetic endcap (EMEC), hadronic (TileCal) and forward (FCal) calorimeters. **c** History of the ratio of the integrated luminosities per run reported by five of the six individual MPX sensors, to that reported by the sixth sensor in the same run. In all figures, *each point* shows the ratio for a single run relative to that in a reference run taken on November 25, 2012 (LHC fill 3323). Statistical uncertainties are negligible. The *vertical arrows* indicate the time of the November 2012 *vdM* scan session

rithms, to that reported by the TileCal. Even though a systematic trend between the LAr and TileCal measurements is apparent, the calorimeter algorithms are consistent to better than ±0.7%. The TileCal luminosity is consistent with that from the default track-counting algorithm to within ±0.4% or less.

In contrast, both BCM and LUCID exhibit significant variations in response over the course of 2012, which vary from channel to channel and are attributed to, respectively, radiation-induced lattice defects and PMT aging. Among these, the BCMH_EventOR algorithm exhibits the least severe deviation from its response at the time of the November *vdM*-scan session. Its long-term drift is, however, large enough to warrant a time-dependent response correction that is based on one of the more stable relative-luminosity monitors shown in Fig. 15, and that is described in Sect. 7.3.2.

6.2 μ dependence

As the pile-up response of a given luminosity algorithm is determined by the instrumental characteristics of the luminometer considered, the BCMH_EventOR and BCMV_EventOR algorithms are expected to exhibit little μ-dependence with respect to each other, even if both may be affected by a common non-linearity with respect to the actual instantaneous luminosity. The same applies to ratios of luminosity values reported independently by the A and C arms of FCal, EMEC, LUCID and TileCal.

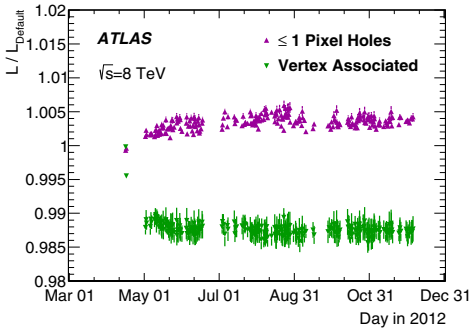

Fig. 14 History of the integrated-luminosity values reported by the two alternative track-counting methods, normalized to that from the default track selection, each as absolutely calibrated by the *vdM* method. *Each point* represents the mean over a single ATLAS run. The *error bars* reflect the systematic uncertainty associated with the simulation-based fake-track subtraction. No track-counting data are available prior to the first *vdM*-scan session (16 April 2012)

In contrast, the track-counting luminosities obtained using the three track selections defined in Sect. 3.2 exhibit a noticeable relative non-linearity (Fig. 16a). The pattern is consistent with that observed in Fig. 14. At very low μ, the three working points are fully consistent, as expected from having been *vdM*-calibrated at $\mu \sim 0.5$. As μ increases, loosening the pixel-hole requirement on the selected tracks results, after fake-track subtraction, in a residual positive non-linearity of at most 0.7% in the reported $\langle\mu\rangle$ value. In contrast, the vertex-associated track count exhibits, also after fake-track correction, a negative non-linearity with respect to the default WP, which peaks at -1.3% and then decreases in magnitude. Even though the simulation should account for the pile-up dependence of the fake-track fraction and of the track- and vertex-reconstruction efficiencies, it fails to explain the relative μ-dependence observed in the data between the three track-counting selections. The onset of the discrepancies appears to lie in the range $2 < \mu < 10$. However, only very limited data, all from a single run with a small number of isolated bunches, are available in that μ range, so that no firm conclusions can be drawn. A conservative approach is therefore adopted: the observed discrepancy between track-counting WPs is used as a data-driven upper limit on a potential bias affecting the absolute track-based luminosity scale in the high-μ regime. The impact of this systematic uncertainty is discussed in Sect. 7.3.1.

In the absence of any absolute linearity reference, potential pile–up-dependent biases in the high-μ regime can be constrained by the relative μ-dependence of the luminosity values reported by luminometers based on very different technologies (Fig. 16b). The relative non-linearity between the BCMH_EventOR and the TileCal (the default track-counting) algorithm does not exceed $\pm 0.3\%$ ($\pm 0.5\%$) over the $\langle\mu\rangle$ range accessible in this run; the root causes of the relative μ-dependence between these three luminometers remain under investigation. An extensive analysis of the more severe LUCID non-linearity indicates that under typical physics operating conditions, the large currents drawn by the LUCID PMTs significantly distort their response.

The run-averaged pile-up parameter changes from one run to the next, because of variations both in the initial luminosity and in the duration of LHC fills. Therefore, the larger the relative μ-dependence between two algorithms, the larger the fill-to-fill fluctuations in the ratio of the run-integrated luminosities reported by these two algorithms. This effect contributes significantly to the point-to-point scatter that is apparent in Fig. 15.

7 Luminosity determination during physics running

To determine the integrated luminosity used in ATLAS physics analyses, a single bunch-by-bunch algorithm is selected as the baseline to provide the central value for a certain time range (Sect. 7.1). The corresponding *vdM*-calibrated luminosity values are first background-subtracted (Sect. 7.2), and then corrected for rate- and time-dependent biases that impact high-luminosity operation (Sect. 7.3). The consistency of the various ATLAS luminosity measurements after all corrections is quantified in Sect. 7.4, together with the associated systematic uncertainty.

7.1 Baseline luminosity algorithm

The choice of algorithm is determined in part by the reproducibility and long-term stability of its absolute calibration. Figure 9 shows that in this respect, the BCMH_EventOR and track-counting algorithms perform noticeably better than BCMV_EventOR and LUCID. Studies of relative stability during physics running (Fig. 15) and of μ dependence (Fig. 16b) lead to the same conclusion. As track counting is active only during stable-beam operation and is statistically marginal at the luminosity-block level, it is not suitable for use as a baseline algorithm, but it is retained as a reference method to assess systematic biases. The BCMH_EventOR algorithm supplies the absolute luminosity during most of the 2012 running period; it is supplemented by the LUCID_EventA algorithm during the few runs where the BCM is not available, and which represent less than 1% of the 2012 integrated luminosity.

7.2 Background subtraction

During high-luminosity physics running, instrumental noise and single-beam backgrounds become negligible by com-

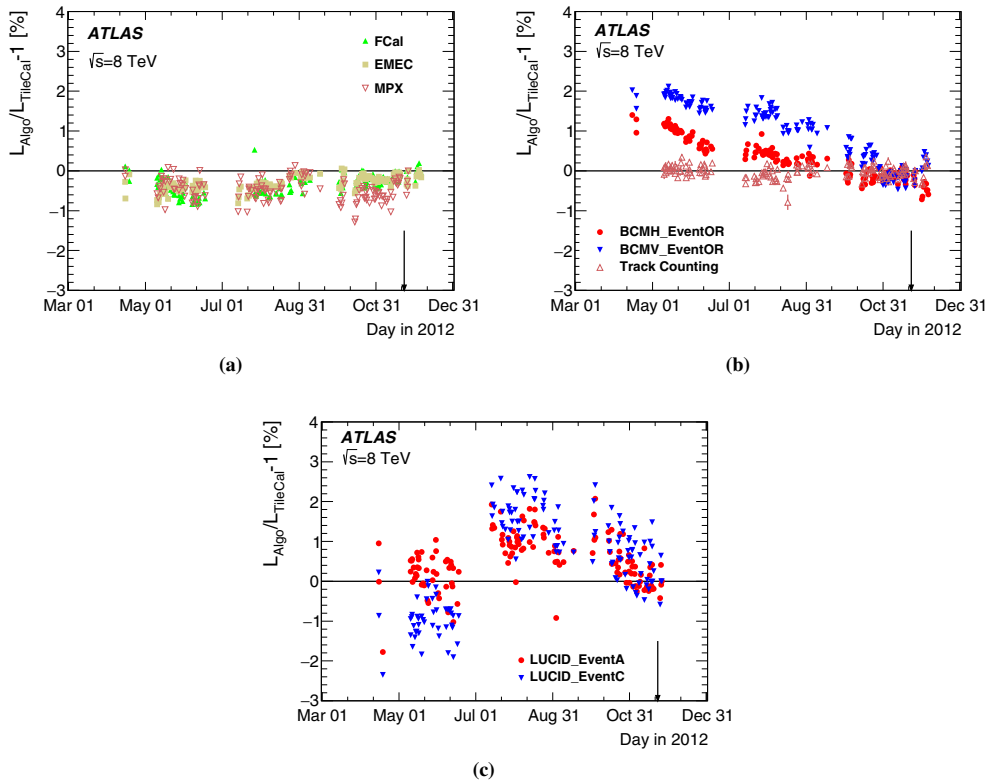

Fig. 15 History of the luminosity per run, compared to the value measured by TileCal, for **a** bunch-integrating, **b** BCM and track-counting, and **c** LUCID algorithms, during routine physics operation at high luminosity. *Each point* shows for a single run the mean deviation from a reference run taken on November 25, 2012 (LHC fill 3323). The EMEC, FCal and TileCal values are computed using the average of the luminosities reported by the A and C arms of the corresponding calorimeter; the MPX values reflect the average over the six sensors. The step in LUCID response is moderate thanks to the use of the April calibration for the LUCID data recorded before July. The *vertical arrows* indicate the time of the November *vdM* scan session

parison to the luminosity; only afterglow remains as a significant background. With a 2012 bunch spacing of 50 ns and typically over 1000 colliding bunches, it reaches a fairly stable equilibrium after the first few bunches in a train. It is observed to scale with the instantaneous luminosity and typically amounts to 0.2–0.5% of the luminosity signal.

The bunch-by-bunch noise- and afterglow-subtraction procedure described in Sect. 4.4 is applied to all BCM and LUCID luminosity determinations. Since the afterglow level in the BCID immediately following a colliding-bunch slot may differ from that in the second BCID after this slot (i.e. in the next colliding-bunch slot), BCIDs at the end of a bunch train were used to evaluate a possible bias in the method. This study suggests that the subtraction over-corrects the BCMH_EventOR luminosity by approximately 0.2%. A systematic uncertainty of ±0.2% is therefore assigned to the afterglow correction.

7.3 Corrections to the absolute calibration in the high-luminosity regime

Extrapolating the curves of Fig. 16b to very low $\langle\mu\rangle$ suggests that for some algorithms, the *vdM*-based luminosity scale may not be directly applicable in the pile-up regime typical of physics operation. Percent-level corrections are indeed required (Sect. 7.3.1) to transfer, at one point in time, the absolute calibration of BCM and LUCID from the low-luminosity regime of *vdM* scans ($\mu \sim 0.5$, $\mathcal{L} \sim$

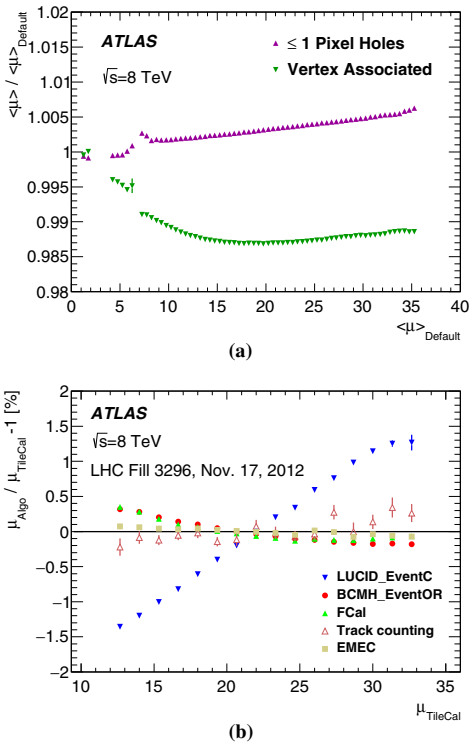

Fig. 16 **a** Ratio of the bunch-averaged pile-up parameter $\langle\mu\rangle$ reported using different track-counting working points, to that from the default WP, as a function of the $\langle\mu\rangle$ value obtained using the default WP. The data are averaged over all stable-beam runs. **b** Fractional deviation of the bunch-averaged pile-up parameter $\langle\mu\rangle$, obtained using different algorithms, from the TileCal value, as a function of $\langle\mu\rangle_{\text{TileCal}}$, during a physics run selected to cover the widest possible $\langle\mu\rangle$ range. The data are normalized such that all algorithms yield the same integrated luminosity in the run considered

2×10^{30} cm^{-2}s^{-1}) to that of routine physics operation ($\mu\sim$ 20–25, $\mathcal{L}>10^{33}$ cm^{-2}s^{-1}). In addition, a time-dependent correction (Sect. 7.3.2) must be applied to the luminosity of the baseline algorithm to compensate for the long-term drifts apparent in Fig. 15.

7.3.1 *Calibration transfer from the* vdM *regime to physics conditions*

The history of the instantaneous-luminosity values reported during part of the November *vdM*-scan session by the track-counting and LUCID_EventA algorithms, relative to the BCMH_EventOR algorithm and using the calibrations listed in Table 5, is presented in Fig. 17a. The ratio of the default track-counting (LUCID) luminosity integrated over several hours immediately before and after scan set XV, to that from the BCMH_EventOR algorithm, is consistent with unity within 0.5% (0.4%). The run-integrated luminosity values associated, in that same fill, with the other two track selections (not shown) are consistent with the default track selection within less than one per mille.

However, at high luminosity these ratios differ from unity by several percent (Fig. 17b), with all BCM (LUCID) algorithms reporting a lower (higher) luminosity compared to the track-counting method. In addition, the vertex-associated track selection is no longer consistent with the other two, as discussed in Sect. 6.

To provide consistent luminosity measurements, all algorithms must be corrected to some common absolute scale in the high-luminosity regime. As calorimeter-based luminometers lack sensitivity in the *vdM*-scan regime, only track counting remains to quantify the relative shifts in response of the BCM and LUCID algorithms between the *vdM*-scan and high-luminosity regimes. First, the run-to-run fluctuations in Fig. 17b are smoothed by parameterizing the luminosity ratios as a linear function of the cumulative integrated-luminosity fraction, used here as a proxy for calendar time. Then, for each BCM algorithm and for a given track selection, the difference between the fitted ratio in the high-luminosity reference fill where the calibration transfer is performed (LHC fill 3323), and the corresponding run-integrated luminosity ratio under *vdM* conditions (LHC fill 3316), quantifies the shift in the BCM luminosity scale with respect to track counting. The same procedure is applied to LUCID.

The results are summarized in Table 7 for the default track selection. The BCMH_EventOR efficiency drops by 2.5% with respect to track counting. Naively extrapolating the relative μ-dependence of these two algorithms from the high-μ regime (Fig. 16b) to $\mu\sim0.5$ predicts a shift of 1.3%, about half of the effect observed.[11] Similarly, the μ-dependence of LUCID_EventC predicts a 3% increase in response when going from the *vdM*-scan regime to the high-luminosity regime, while the measured step amounts to +3.9%. These observations suggest that while the measured relative μ-dependence of the three algorithms is consistent with the signs of the calibration shifts and appears to account for a large fraction of their magnitude, other effects also play a role. For instance, studies of the CMS diamond sensors [34] suggest that the response of the BCM may depend on the

[11] Since the mechanisms driving the μ-dependence are neither well characterized nor understood, and in the absence of sufficient data linking the μ range in routine physics operation (Fig. 16b) to that in the *vdM*-scan regime ($\mu\sim0.5$), such an extrapolation is indicative only: it cannot be relied upon for a quantitative evaluation of the calibration-transfer correction.

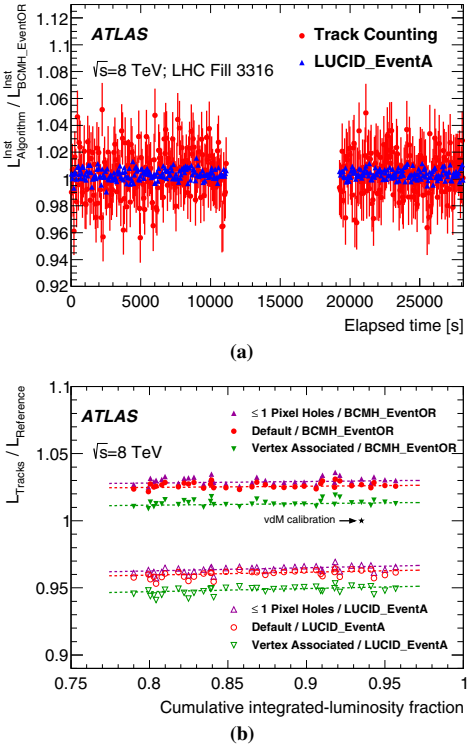

Fig. 17 **a** History of the ratio of the instantaneous luminosity reported by the default track-counting and LUCID_EventA algorithms to that from the BCMH_EventOR algorithm under *vdM*-scan conditions, during LHC fill 3316. The gap corresponds to scan set XV. The *error bars* are statistical. **b** Evolution of the ratio of the integrated luminosity per run reported by the three track-counting algorithms to that from the BCMH_EventOR and LUCID_EventA algorithms, in the few weeks in late 2012 during which the BCM response is approximately constant, as a function of the cumulative delivered luminosity (normalized to the 2012 total). Each point shows the ratio for a single high-luminosity run. The *dashed lines* are *straight-line* fits to the data. The reference run (LHC fill 3323) took place the day following the November *vdM*-scan session, which is indicated by the *star*

total instantaneous collision rate (i.e. on the product of $\langle\mu\rangle$ and the total number of colliding bunches) through a polarization mechanism associated with radiation-induced lattice defects.

The track-counting results lie between BCM and LUCID, and using the track scale as a proxy for the true scale is consistent to within 0.5% with taking the average scale from all the algorithms listed in Table 7. The choice of which track selection to use as reference is somewhat arbitrary. The default working point appears as the natural choice given that

Table 7 Measured fractional shift in luminosity scale between the *vdM*-scan regime (LHC fill 3316) and a nearby high-luminosity ATLAS run (LHC fill 3323), using the default track-counting algorithm as the reference. The errors shown are statistical only; they are dominated by track-counting statistics in the *vdM*-scan fill, and are therefore fully correlated across the four ratios

Luminosity algorithm	Calibration shift w.r.t. track counting (%)
BCMH_eventOR	-2.5 ± 0.1
BCMV_eventOR	-2.9 ± 0.1
LUCID_eventA	$+3.5 \pm 0.1$
LUCID_eventC	$+3.9 \pm 0.1$

it exhibits the smallest relative μ-dependence with respect to TileCal, suffers from the smallest uncertainty arising from the simulation-based fake-track subtraction, and lies between the extremes of the three track selections.

The systematic uncertainty in the calibration-transfer corrections of Table 7 is estimated to be $\pm 1.4\%$. It is dominated by the 1.3% inconsistency (Figs. 16a, 17b) between the default and the vertex-associated track selections. Additional contributions arise from the small inconsistency between the BCM-based and track-based luminosity measurements during the *vdM*-scan fill (0.5%), from a small deadtime correction that affects the *vdM*-scan track-counting data only (0.2%), and from the track-counting statistics during the *vdM*-scan fill (0.1%). The slight integrated-luminosity (or time) dependence of the BCM to track-counting luminosity ratio visible in Fig. 17b is accounted for as part of the long-term drift correction, discussed next.

7.3.2 *Long-term drift correction*

The second step in transferring the *vdM*-based calibrations to an arbitrary high-luminosity physics run consists in correcting for the long-term drifts apparent in Fig. 15, using one of the more stable monitors (EMEC, FCal, TileCal or track counting) as a reference. The absolute luminosity scale of the selected reference monitor is first anchored to that of BCM (or LUCID) in the high-luminosity reference run where the calibration transfer is performed (LHC fill 3323). The run-by-run luminosity ratio of the considered bunch-by-bunch algorithm to the chosen reference is then parameterized as a function of the cumulative integrated-luminosity fraction. This choice of variable, instead of calendar time, is inspired by (but not dependent upon) the assumption that detector aging increases smoothly with integrated radiation dose; it also simplifies the analysis by eliminating the gaps between running periods (Fig. 15). A two-segment, piece-wise linear fit is used to smooth the run-to-run fluctuations, with one segment covering the entire year except for the BCM

Table 8 Impact of the long-term drift correction on the 2012 integrated luminosity

Reference algorithm	Fractional change in integrated luminosity [%]			
	BCMH_EventOR	BCMV_EventOR	LUCID_EventA	LUCID_EventC
EMEC	−0.59	−1.26	−0.70	−0.49
FCal	−0.70	−1.36	−0.68	−0.52
TileCal	−0.44	−1.09	−0.54	−0.26
Track counting	−0.45	−1.12	−0.57	−0.34

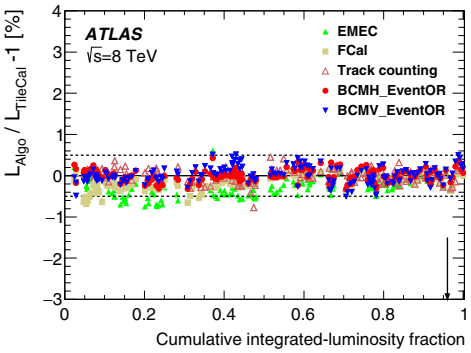

(a)

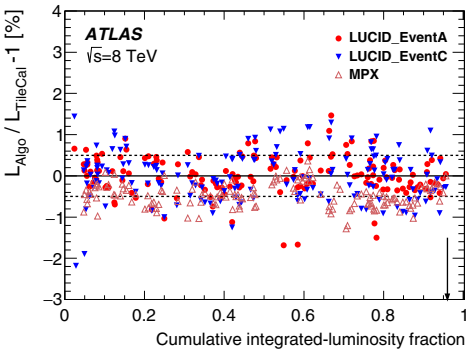

(b)

Fig. 19 History of the fractional difference in run-integrated luminosity between the TileCal algorithm and the drift-corrected **a** BCM and **b** LUCID and MPX algorithms. The results of the other possible reference monitors (EMEC, FCal and track counting) are taken from Fig. 15 and included here for comparison. *Each point* shows the mean difference for a single run compared to that in the reference fill indicated by the arrow. The *dashed horizontal lines* delimit a ±0.5% window around zero

9 Summary

The ATLAS luminosity scale for the 2012 LHC run has been calibrated using data from dedicated beam-separation scans, also known as van der Meer scans. The *vdM*-calibration uncertainty is smaller than for the 2011 data set [3], thanks to improved control of beam-dynamical effects (beam–beam deflections, dynamic β, non-factorization) and to a refined analysis of the non-reproducibility of beam conditions (orbit drift, emittance growth). The total systematic uncertainty in the delivered luminosity is no longer dominated by *vdM*-calibration uncertainties. The largest contribution arises from instrumental effects that require the transfer of the absolute luminosity scale from the low-rate *vdM*-scan regime to the high-luminosity conditions of routine physics operation; residual run-to-run and long-term inconsistencies between independent luminosity measurements also contribute significantly.

Table 9 Relative uncertainty in the calibrated luminosity scale, broken down by source

Uncertainty source	$\delta\mathcal{L}/\mathcal{L}$ [%]
van der Meer calibration	1.2
Afterglow subtraction	0.2
Calibration transfer from *vdM*-scan to high-luminosity regime	1.4
Long-term drift correction	0.3
Run-to-run consistency	0.5
Total	1.9

The combination of these systematic uncertainties results in a final uncertainty of $\delta\mathcal{L}/\mathcal{L} = \pm 1.9\%$ in the luminosity measured by ATLAS during pp collisions at $\sqrt{s} = 8$ TeV for the 22.7 fb^{-1} of data delivered to ATLAS in 2012. This uncertainty applies to the high-luminosity data sample and any subset thereof, but not necessarily to a few special runs taken under very low pile-up conditions, such as those dedicated to elastic-scattering measurements: the latter require a separate analysis tailored to their specific experimental conditions.

Acknowledgements We thank CERN for the very successful operation of the LHC, as well as the support staff from our institutions without whom ATLAS could not be operated efficiently. We acknowledge the support of ANPCyT, Argentina; YerPhI, Armenia; ARC, Australia; BMWFW and FWF, Austria; ANAS, Azerbaijan; SSTC, Belarus; CNPq and FAPESP, Brazil; NSERC, NRC and CFI, Canada; CERN; CONICYT, Chile; CAS, MOST and NSFC, China; COLCIENCIAS, Colombia; MSMT CR, MPO CR and VSC CR, Czech Republic; DNRF and

DNSRC, Denmark; IN2P3-CNRS, CEA-DSM/IRFU, France; GNSF, Georgia; BMBF, HGF, and MPG, Germany; GSRT, Greece; RGC, Hong Kong SAR, China; ISF, I-CORE and Benoziyo Center, Israel; INFN, Italy; MEXT and JSPS, Japan; CNRST, Morocco; FOM and NWO, Netherlands; RCN, Norway; MNiSW and NCN, Poland; FCT, Portugal; MNE/IFA, Romania; MES of Russia and NRC KI, Russian Federation; JINR; MESTD, Serbia; MSSR, Slovakia; ARRS and MIZŠ, Slovenia; DST/NRF, South Africa; MINECO, Spain; SRC and Wallenberg Foundation, Sweden; SERI, SNSF and Cantons of Bern and Geneva, Switzerland; MOST, Taiwan; TAEK, Turkey; STFC, United Kingdom; DOE and NSF, United States of America. In addition, individual groups and members have received support from BCKDF, the Canada Council, CANARIE, CRC, Compute Canada, FQRNT, and the Ontario Innovation Trust, Canada; EPLANET, ERC, FP7, Horizon 2020 and Marie Skłodowska-Curie Actions, European Union; Investissements d'Avenir Labex and Idex, ANR, Région Auvergne and Fondation Partager le Savoir, France; DFG and AvH Foundation, Germany; Herakleitos, Thales and Aristeia programmes co-financed by EU-ESF and the Greek NSRF; BSF, GIF and Minerva, Israel; BRF, Norway; Generalitat de Catalunya, Generalitat Valenciana, Spain; the Royal Society and Leverhulme Trust, United Kingdom. The crucial computing support from all WLCG partners is acknowledged gratefully, in particular from CERN, the ATLAS Tier-1 facilities at TRIUMF (Canada), NDGF (Denmark, Norway, Sweden), CC-IN2P3 (France), KIT/GridKA (Germany), INFN-CNAF (Italy), NL-T1 (Netherlands), PIC (Spain), ASGC (Taiwan), RAL (UK) and BNL (USA), the Tier-2 facilities worldwide and large non-WLCG resource providers. Major contributors of computing resources are listed in Ref. [35].

Funded by SCOAP[3].

References

1. ATLAS Collaboration, The ATLAS Experiment at the CERN Large Hadron Collider. JINST **3**, S08003 (2008). doi:10.1088/1748-0221/3/08/S08003
2. S. van der Meer, Calibration of the effective beam height in the ISR. CERN-ISR-PO-68-31 (1968). http://cds.cern.ch/record/296752
3. ATLAS Collaboration, Improved luminosity determination in pp collisions at $\sqrt{s} = 7$ TeV using the ATLAS detector at the LHC. Eur. Phys. J. C **73**, 2518 (2013). doi:10.1140/epjc/s10052-013-2518-3, arXiv:1302.4393 [hep-ex]
4. C. Rubbia, Measurement of the luminosity of $p\bar{p}$ collider with a (generalized) van der Meer Method. CERN-$p\bar{p}$-Note-38 (1977). http://cds.cern.ch/record/1025746
5. ATLAS Collaboration, Luminosity determination in pp collisions at $\sqrt{s} = 7$ TeV using the ATLAS detector at the LHC. Eur. Phys. J. C **71** 1630 (2011). doi:10.1140/epjc/s10052-011-1630-5, arXiv:1101.2185 [hep-ex]
6. ATLAS Collaboration, Concepts, design and implementation of the ATLAS new tracking (NEWT). ATL-SOFT-PUB-2007-007 (2007). http://cds.cern.ch/record/1020106
7. P. Grafström, W. Kozanecki, Luminosity determination at proton colliders. Progr. Part. Nucl. Phys. **81**, 97–148 (2015). doi:10.1016/j.ppnp.2014.11.002
8. ATLAS Collaboration, Charged-particle multiplicities in pp interactions measured with the ATLAS detector at the LHC. New J. Phys. **13** 053033 (2011). doi:10.1088/1367-2630/13/5/053033, arXiv:1012.5104 [hep-ex]
9. ATLAS Collaboration, Performance of the atlas inner detector track and vertex reconstruction in the high pile-up LHC environment. ATLAS-CONF-2012-042 (2012). http://cdsweb.cern.ch/record/1435196
10. T. Sjöstrand, S. Mrenna, P. Skands, A brief introduction to PYTHIA 8.1. Comput. Phys. Commun. **178**, 852 (2008). doi:10.1016/j.cpc.2008.01.036. arXiv:0710.3820 [hep-ph]
11. Tile Calorimeter Collaboration, Tile calorimeter technical design report. CERN-LHCC-96-042 (1996). http://cds.cern.ch/record/331062
12. A. Sopczak et al., MPX detectors as LHC luminosity monitor. IEEE Trans. Nucl. Sci. **62**, 3225 (2015). http://ieeexplore.ieee.org/stamp/stamp.jsp?arnumber=7349015
13. M. Venturini, W. Kozanecki, Out-of-plane deflections as a diagnostic tool and application to PEP-II. SLAC-PUB-8700 (2001). http://slac.stanford.edu/pubs/slacpubs/8500/slac-pub-8700.pdf
14. W. Herr, B. Muratori, Concept of luminosity. Yellow Report CERN 2006-002 (2006). http://cds.cern.ch/record/941318
15. H. Wiedemann, Particle accelerator physics, graduate texts in physics. Springer, ISBN 9783319183169, 9783319183176 (2015). http://www.springer.com/us/book/9783319183169?wt_mc=ThirdParty.SpringerLink.3.EPR653.About_eBook
16. H. Bartosik, G. Rumolo, Production of the single bunch for Van der Meer scans in the LHC injector chain. CERN-ACC-NOTE-2013-0008 (2013). http://cds.cern.ch/record/1590405
17. W. Kozanecki, T. Pieloni, J. Wenninger, Observation of beam-beam deflections with LHC orbit data. CERN-ACC-NOTE-2013-0006 (2013). http://cds.cern.ch/record/1581723
18. P. Bambade et al., Observation of beam-beam deflections at the interaction point of the SLAC linear collider. Phys. Rev. Lett. **62**, 2949 (1989). doi:10.1103/PhysRevLett.62.2949
19. W. Herr, Beam-beam effects and dynamic β^*. Proc. LHC Lumi Days (2012). http://indico.cern.ch/event/162948/contributions/1417430/attachments/191879/269237/S3_WH.pdf
20. CERN Accelerator Beam Physics Group, MAD–Methodical Accelerator Design. http://mad.web.cern.ch/mad/
21. LHCb Collaboration, R. Aaij et al., Precision luminosity measurements at LHCb. JINST **9**, P12005 (2014). doi:10.1088/1748-0221/9/12/P12005, arXiv:1410.0149 [hep-ex]
22. S.M. White, Determination of the absolute luminosity at the LHC. CERN-THESIS-2010-139 (2010). http://cds.cern.ch/record/1308187
23. ATLAS Collaboration, Characterization of interaction-point beam parameters using the pp event-vertex distribution reconstructed in the ATLAS detector at the LHC. ATLAS-CONF-2010-027 (2010). http://cdsweb.cern.ch/record/1277659
24. V. Balagura, Notes on van der Meer scan for absolute luminosity measurement. Nucl. Instrum. Methods A **654**, 634–638 (2011). doi:10.1016/j.nima.2011.06.007, arXiv:1103.1129 [physics.ins-det]
25. LHCb Collaboration, R. Aaij et al., Absolute luminosity measurements with the LHCb detector at the LHC. JINST **7**, P01010 (2012). doi:10.1088/1748-0221/7/01/P01010, arXiv:1110.2866 [hep-ex]
26. F.J. Decker, Beam distributions beyond RMS. SLAC-PUB-95-6684 (1994). http://www.slac.stanford.edu/cgi-wrap/getdoc/slac-pub-6841.pdf
27. C. Barschel, Precision luminosity measurement at LHCb with beam-gas imaging. CERN-THESIS-2013-301 (2014). http://cds.cern.ch/record/1693671

28. S.N. Webb, Factorisation of beams in van der Meer scans and measurements of the ϕ_η^* distribution of $Z \to e^+e^-$ events in pp collisions at $\sqrt{s} = 8$ TeV with the ATLAS detector. CERN-THESIS-2015-054 (2015). http://cds.cern.ch/record/2020875
29. CMS Collaboration, CMS luminosity based on pixel cluster counting—summer 2012 update. CMS-PAS-LUM-12-001 (2012). http://cds.cern.ch/record/1482193
30. CMS Collaboration, CMS luminosity based on pixel cluster counting—summer 2013 update. CMS-PAS-LUM-13-001 (2013). http://cds.cern.ch/record/1598864
31. C. Barschel et al., Results of the LHC DCCT calibration studies. CERN-ATS-Note-2012-026 PERF (2012). http://cdsweb.cern.ch/record/1425904
32. G. Anders et al., Study of the Relative Bunch Populations for Luminosity Calibration, CERN-ATS-Note-2012-028 PERF (2012). http://cdsweb.cern.ch/record/1427726
33. A Boccardi et al., LHC luminosity calibration using the longitudinal density monitor. CERN-ATS-Note-2013-034 TECH (2013). http://cds.cern.ch/record/1556087
34. M. Guthoff et al., Radiation damage in the diamond based beam condition monitors of the CMS experiment at the Large Hadron Collider (LHC) at CERN. Nucl. Instrum. Methods. A **730** 168–173 (2013). doi:10.1016/j.nima.2013.05.041
35. ATLAS Collaboration, ATLAS computing acknowledgements 2016–2017. ATL-GEN-PUB-2016-002 (2016). http://cds.cern.ch/record/2202407

ATLAS Collaboration

M. Aaboud[136d], G. Aad[87], B. Abbott[114], J. Abdallah[65], O. Abdinov[12], B. Abeloos[118], R. Aben[108], O. S. AbouZeid[138], N. L. Abraham[150], H. Abramowicz[154], H. Abreu[153], R. Abreu[117], Y. Abulaiti[147a,147b], B. S. Acharya[164a,164b,a], L. Adamczyk[40a], D. L. Adams[27], J. Adelman[109], S. Adomeit[101], T. Adye[132], A. A. Affolder[76], T. Agatonovic-Jovin[14], J. Agricola[56], J. A. Aguilar-Saavedra[127a,127f], S. P. Ahlen[24], F. Ahmadov[67,b], G. Aielli[134a,134b], H. Akerstedt[147a,147b], T. P. A. Åkesson[83], A. V. Akimov[97], G. L. Alberghi[22a,22b], J. Albert[169], S. Albrand[57], M. J. Alconada Verzini[73], M. Aleksa[32], I. N. Aleksandrov[67], C. Alexa[28b], G. Alexander[154], T. Alexopoulos[10], M. Alhroob[114], M. Aliev[75a,75b], G. Alimonti[93a], J. Alison[33], S. P. Alkire[37], B. M. M. Allbrooke[150], B. W. Allen[117], P. P. Allport[19], A. Aloisio[105a,105b], A. Alonso[38], F. Alonso[73], C. Alpigiani[139], M. Alstaty[87], B. Alvarez Gonzalez[32], D. Álvarez Piqueras[167], M. G. Alviggi[105a,105b], B. T. Amadio[16], K. Amako[68], Y. Amaral Coutinho[26a], C. Amelung[25], D. Amidei[91], S. P. Amor Dos Santos[127a,127c], A. Amorim[127a,127b], S. Amoroso[32], G. Amundsen[25], C. Anastopoulos[140], L. S. Ancu[51], N. Andari[109], T. Andeen[11], C. F. Anders[60b], G. Anders[32], J. K. Anders[76], K. J. Anderson[33], A. Andreazza[93a,93b], V. Andrei[60a], S. Angelidakis[9], I. Angelozzi[108], P. Anger[46], A. Angerami[37], F. Anghinolfi[32], A. V. Anisenkov[110,c], N. Anjos[13], A. Annovi[125a,125b], M. Antonelli[49], A. Antonov[99,*], F. Anulli[133a], M. Aoki[68], L. Aperio Bella[19], G. Arabidze[92], Y. Arai[68], J. P. Araque[127a], A. T. H. Arce[47], F. A. Arduh[73], J.-F. Arguin[96], S. Argyropoulos[65], M. Arik[20a], A. J. Armbruster[144], L. J. Armitage[78], O. Arnaez[32], H. Arnold[50], M. Arratia[30], O. Arslan[23], A. Artamonov[98], G. Artoni[121], S. Artz[85], S. Asai[156], N. Asbah[44], A. Ashkenazi[154], B. Åsman[147a,147b], L. Asquith[150], K. Assamagan[27], R. Astalos[145a], M. Atkinson[166], N. B. Atlay[142], K. Augsten[129], G. Avolio[32], B. Axen[16], M. K. Ayoub[118], G. Azuelos[96,d], M. A. Baak[32], A. E. Baas[60a], M. J. Baca[19], H. Bachacou[137], K. Bachas[75a,75b], M. Backes[32], M. Backhaus[32], P. Bagiacchi[133a,133b], P. Bagnaia[133a,133b], Y. Bai[35a], J. T. Baines[132], O. K. Baker[176], E. M. Baldin[110,c], P. Balek[130], T. Balestri[149], F. Balli[137], W. K. Balunas[123], E. Banas[41], Sw. Banerjee[173,e], A. A. E. Bannoura[175], L. Barak[32], E. L. Barberio[90], D. Barberis[52a,52b], M. Barbero[87], T. Barillari[102], T. Barklow[144], N. Barlow[30], S. L. Barnes[86], B. M. Barnett[132], R. M. Barnett[16], Z. Barnovska[5], A. Baroncelli[135a], G. Barone[25], A. J. Barr[121], L. Barranco Navarro[167], F. Barreiro[84], J. Barreiro Guimarães da Costa[35a], R. Bartoldus[144], A. E. Barton[74], P. Bartos[145a], A. Basalaev[124], A. Bassalat[118], R. L. Bates[55], S. J. Batista[159], J. R. Batley[30], M. Battaglia[138], M. Bauce[133a,133b], F. Bauer[137], H. S. Bawa[144,f], J. B. Beacham[112], M. D. Beattie[74], T. Beau[82], P. H. Beauchemin[162], P. Bechtle[23], H. P. Beck[18,g], K. Becker[121], M. Becker[85], M. Beckingham[170], C. Becot[111], A. J. Beddall[20d], A. Beddall[20b], V. A. Bednyakov[67], M. Bedognetti[108], C. P. Bee[149], L. J. Beemster[108], T. A. Beermann[32], M. Begel[27], J. K. Behr[44], C. Belanger-Champagne[89], A. S. Bell[80], G. Bella[154], L. Bellagamba[22a], A. Bellerive[31], M. Bellomo[88], K. Belotskiy[99], O. Beltramello[32], N. L. Belyaev[99], O. Benary[154], D. Benchekroun[136a], M. Bender[101], K. Bendtz[147a,147b], N. Benekos[10], Y. Benhammou[154], E. Benhar Noccioli[176], J. Benitez[65], D. P. Benjamin[47], J. R. Bensinger[25], S. Bentvelsen[108], L. Beresford[121], M. Beretta[49], D. Berge[108], E. Bergeaas Kuutmann[165], N. Berger[5], J. Beringer[16], S. Berlendis[57], N. R. Bernard[88], C. Bernius[111], F. U. Bernlochner[23], T. Berry[79], P. Berta[130], C. Bertella[85], G. Bertoli[147a,147b], F. Bertolucci[125a,125b], I. A. Bertram[74], C. Bertsche[44], D. Bertsche[114], G. J. Besjes[38], O. Bessidskaia Bylund[147a,147b], M. Bessner[44], N. Besson[137], C. Betancourt[50], S. Bethke[102], A. J. Bevan[78], W. Bhimji[16], R. M. Bianchi[126], L. Bianchini[25], M. Bianco[32], O. Biebel[101], D. Biedermann[17], R. Bielski[86], N. V. Biesuz[125a,125b], M. Biglietti[135a], J. Bilbao De Mendizabal[51], H. Bilokon[49], M. Bindi[56], S. Binet[118], A. Bingul[20b], C. Bini[133a,133b], S. Biondi[22a,22b], D. M. Bjergaard[47], C. W. Black[151], J. E. Black[144], K. M. Black[24], D. Blackburn[139], R. E. Blair[6], J.-B. Blanchard[137], J. E. Blanco[79], T. Blazek[145a], I. Bloch[44], C. Blocker[25], W. Blum[85,*], U. Blumenschein[56], S. Blunier[34a], G. J. Bobbink[108], V. S. Bobrovnikov[110,c], S. S. Bocchetta[83], A. Bocci[47], C. Bock[101], M. Boehler[50],

D. Boerner[175], J. A. Bogaerts[32], D. Bogavac[14], A. G. Bogdanchikov[110], C. Bohm[147a], V. Boisvert[79], P. Bokan[14], T. Bold[40a], A. S. Boldyrev[164a,164c], M. Bomben[82], M. Bona[78], M. Boonekamp[137], A. Borisov[131], G. Borissov[74], J. Bortfeldt[101], D. Bortoletto[121], V. Bortolotto[62a,62b,62c], K. Bos[108], D. Boscherini[22a], M. Bosman[13], J. D. Bossio Sola[29], J. Boudreau[126], J. Bouffard[2], E. V. Bouhova-Thacker[74], D. Boumediene[36], C. Bourdarios[118], S. K. Boutle[55], A. Boveia[32], J. Boyd[32], I. R. Boyko[67], J. Bracinik[19], A. Brandt[8], G. Brandt[56], O. Brandt[60a], U. Bratzler[157], B. Brau[88], J. E. Brau[117], H. M. Braun[175,*], W. D. Breaden Madden[55], K. Brendlinger[123], A. J. Brennan[90], L. Brenner[108], R. Brenner[165], S. Bressler[172], T. M. Bristow[48], D. Britton[55], D. Britzger[44], F. M. Brochu[30], I. Brock[23], R. Brock[92], G. Brooijmans[37], T. Brooks[79], W. K. Brooks[34b], J. Brosamer[16], E. Brost[117], J. H Broughton[19], P. A. Bruckman de Renstrom[41], D. Bruncko[145b], R. Bruneliere[50], A. Bruni[22a], G. Bruni[22a], L. S. Bruni[108], BH Brunt[30], M. Bruschi[22a], N. Bruscino[23], P. Bryant[33], L. Bryngemark[83], T. Buanes[15], Q. Buat[143], P. Buchholz[142], A. G. Buckley[55], I. A. Budagov[67], F. Buehrer[50], M. K. Bugge[120], O. Bulekov[99], D. Bullock[8], H. Burckhart[32], S. Burdin[76], C. D. Burgard[50], B. Burghgrave[109], K. Burka[41], S. Burke[132], I. Burmeister[45], E. Busato[36], D. Büscher[50], V. Büscher[85], P. Bussey[55], J. M. Butler[24], C. M. Buttar[55], J. M. Butterworth[80], P. Butti[108], W. Buttinger[27], A. Buzatu[55], A. R. Buzykaev[110,c], S. Cabrera Urbán[167], D. Caforio[129], V. M. Cairo[39a,39b], O. Cakir[4a], N. Calace[51], P. Calafiura[16], A. Calandri[87], G. Calderini[82], P. Calfayan[101], L. P. Caloba[26a], D. Calvet[36], S. Calvet[36], T. P. Calvet[87], R. Camacho Toro[33], S. Camarda[32], P. Camarri[134a,134b], D. Cameron[120], R. Caminal Armadans[166], C. Camincher[57], S. Campana[32], M. Campanelli[80], A. Camplani[93a,93b], A. Campoverde[142], V. Canale[105a,105b], A. Canepa[160a], M. Cano Bret[35e], J. Cantero[115], R. Cantrill[127a], T. Cao[42], M. D. M. Capeans Garrido[32], I. Caprini[28b], M. Caprini[28b], M. Capua[39a,39b], R. Caputo[85], R. M. Carbone[37], R. Cardarelli[134a], F. Cardillo[50], I. Carli[130], T. Carli[32], G. Carlino[105a], L. Carminati[93a,93b], S. Caron[107], E. Carquin[34b], G. D. Carrillo-Montoya[32], J. R. Carter[30], J. Carvalho[127a,127c], D. Casadei[19], M. P. Casado[13,h], M. Casolino[13], D. W. Casper[163], E. Castaneda-Miranda[146a], R. Castelijn[108], A. Castelli[108], V. Castillo Gimenez[167], N. F. Castro[127a,i], A. Catinaccio[32], J. R. Catmore[120], A. Cattai[32], J. Caudron[85], V. Cavaliere[166], E. Cavallaro[13], D. Cavalli[93a], M. Cavalli-Sforza[13], V. Cavasinni[125a,125b], F. Ceradini[135a,135b], L. Cerda Alberich[167], B. C. Cerio[47], A. S. Cerqueira[26b], A. Cerri[150], L. Cerrito[78], F. Cerutti[16], M. Cerv[32], A. Cervelli[18], S. A. Cetin[20c], A. Chafaq[136a], D. Chakraborty[109], S. K. Chan[59], Y. L. Chan[62a], P. Chang[166], J. D. Chapman[30], D. G. Charlton[19], A. Chatterjee[51], C. C. Chau[159], C. A. Chavez Barajas[150], S. Che[112], S. Cheatham[74], A. Chegwidden[92], S. Chekanov[6], S. V. Chekulaev[160a], G. A. Chelkov[67,j], M. A. Chelstowska[91], C. Chen[66], H. Chen[27], K. Chen[149], S. Chen[35c], S. Chen[156], X. Chen[35f], Y. Chen[69], H. C. Cheng[91], H. J Cheng[35a], Y. Cheng[33], A. Cheplakov[67], E. Cheremushkina[131], R. Cherkaoui El Moursli[136e], V. Chernyatin[27,*], E. Cheu[7], L. Chevalier[137], V. Chiarella[49], G. Chiarelli[125a,125b], G. Chiodini[75a], A. S. Chisholm[19], A. Chitan[28b], M. V. Chizhov[67], K. Choi[63], A. R. Chomont[36], S. Chouridou[9], B. K. B. Chow[101], V. Christodoulou[80], D. Chromek-Burckhart[32], J. Chudoba[128], A. J. Chuinard[89], J. J. Chwastowski[41], L. Chytka[116], G. Ciapetti[133a,133b], A. K. Ciftci[4a], D. Cinca[55], V. Cindro[77], I. A. Cioara[23], A. Ciocio[16], F. Cirotto[105a,105b], Z. H. Citron[172], M. Citterio[93a], M. Ciubancan[28b], A. Clark[51], B. L. Clark[59], M. R. Clark[37], P. J. Clark[48], R. N. Clarke[16], C. Clement[147a,147b], Y. Coadou[87], M. Cobal[164a,164c], A. Coccaro[51], J. Cochran[66], L. Coffey[25], L. Colasurdo[107], B. Cole[37], A. P. Colijn[108], J. Collot[57], T. Colombo[32], G. Compostella[102], P. Conde Muiño[127a,127b], E. Coniavitis[50], S. H. Connell[146b], I. A. Connelly[79], V. Consorti[50], S. Constantinescu[28b], G. Conti[32], F. Conventi[105a,k], M. Cooke[16], B. D. Cooper[80], A. M. Cooper-Sarkar[121], K. J. R. Cormier[159], T. Cornelissen[175], M. Corradi[133a,133b], F. Corriveau[89,l], A. Corso-Radu[163], A. Cortes-Gonzalez[13], G. Cortiana[102], G. Costa[93a], M. J. Costa[167], D. Costanzo[140], G. Cottin[30], G. Cowan[79], B. E. Cox[86], K. Cranmer[111], S. J. Crawley[55], G. Cree[31], S. Crépé-Renaudin[57], F. Crescioli[82], W. A. Cribbs[147a,147b], M. Crispin Ortuzar[121], M. Cristinziani[23], V. Croft[107], G. Crosetti[39a,39b], T. Cuhadar Donszelmann[140], J. Cummings[176], M. Curatolo[49], J. Cúth[85], C. Cuthbert[151], H. Czirr[142], P. Czodrowski[3], G. D'amen[22a,22b], S. D'Auria[55], M. D'Onofrio[76], M. J. Da Cunha Sargedas De Sousa[127a,127b], C. Da Via[86], W. Dabrowski[40a], T. Dado[145a], T. Dai[91], O. Dale[15], F. Dallaire[96], C. Dallapiccola[88], M. Dam[38], J. R. Dandoy[33], N. P. Dang[50], A. C. Daniells[19], N. S. Dann[86], M. Danninger[168], M. Dano Hoffmann[137], V. Dao[50], G. Darbo[52a], S. Darmora[8], J. Dassoulas[3], A. Dattagupta[63], W. Davey[23], C. David[169], T. Davidek[130], M. Davies[154], P. Davison[80], E. Dawe[90], I. Dawson[140], R. K. Daya-Ishmukhametova[88], K. De[8], R. de Asmundis[105a], A. De Benedetti[114], S. De Castro[22a,22b], S. De Cecco[82], N. De Groot[107], P. de Jong[108], H. De la Torre[84], F. De Lorenzi[66], A. De Maria[56], D. De Pedis[133a], A. De Salvo[133a], U. De Sanctis[150], A. De Santo[150], J. B. De Vivie De Regie[118], W. J. Dearnaley[74], R. Debbe[27], C. Debenedetti[138], D. V. Dedovich[67], N. Dehghanian[3], I. Deigaard[108], M. Del Gaudio[39a,39b], J. Del Peso[84], T. Del Prete[125a,125b], D. Delgove[118], F. Deliot[137], C. M. Delitzsch[51], M. Deliyergiyev[77], A. Dell'Acqua[32], L. Dell'Asta[24], M. Dell'Orso[125a,125b], M. Della Pietra[105a,k], D. della Volpe[51], M. Delmastro[5], P. A. Delsart[57], C. Deluca[108], D. A. DeMarco[159], S. Demers[176], M. Demichev[67], A. Demilly[82], S. P. Denisov[131], D. Denysiuk[137], D. Derendarz[41], J. E. Derkaoui[136d], F. Derue[82], P. Dervan[76], K. Desch[23], C. Deterre[44], K. Dette[45], P. O. Deviveiros[32], A. Dewhurst[132], S. Dhaliwal[25], A. Di Ciaccio[134a,134b], L. Di Ciaccio[5], W. K. Di Clemente[123], C. Di Donato[133a,133b], A. Di Girolamo[32], B. Di Girolamo[32], B. Di Micco[135a,135b], R. Di Nardo[32], A. Di Simone[50],

R. Di Sipio[159], D. Di Valentino[31], C. Diaconu[87], M. Diamond[159], F. A. Dias[48], M. A. Diaz[34a], E. B. Diehl[91], J. Dietrich[17], S. Diglio[87], A. Dimitrievska[14], J. Dingfelder[23], P. Dita[28b], S. Dita[28b], F. Dittus[32], F. Djama[87], T. Djobava[53b], J. I. Djuvsland[60a], M. A. B. do Vale[26c], D. Dobos[32], M. Dobre[28b], C. Doglioni[83], T. Dohmae[156], J. Dolejsi[130], Z. Dolezal[130], B. A. Dolgoshein[99,*], M. Donadelli[26d], S. Donati[125a,125b], P. Dondero[122a,122b], J. Donini[36], J. Dopke[132], A. Doria[105a], M. T. Dova[73], A. T. Doyle[55], E. Drechsler[56], M. Dris[10], Y. Du[35d], J. Duarte-Campderros[154], E. Duchovni[172], G. Duckeck[101], O. A. Ducu[96,m], D. Duda[108], A. Dudarev[32], E. M. Duffield[16], L. Duflot[118], L. Duguid[79], M. Dührssen[32], M. Dumancic[172], M. Dunford[60a], H. Duran Yildiz[4a], M. Düren[54], A. Durglishvili[53b], D. Duschinger[46], B. Dutta[44], M. Dyndal[44], C. Eckardt[44], K. M. Ecker[102], R. C. Edgar[91], N. C. Edwards[48], T. Eifert[32], G. Eigen[15], K. Einsweiler[16], T. Ekelof[165], M. El Kacimi[136c], V. Ellajosyula[87], M. Ellert[165], S. Elles[5], F. Ellinghaus[175], A. A. Elliot[169], N. Ellis[32], J. Elmsheuser[27], M. Elsing[32], D. Emeliyanov[132], Y. Enari[156], O. C. Endner[85], M. Endo[119], J. S. Ennis[170], J. Erdmann[45], A. Ereditato[18], G. Ernis[175], J. Ernst[2], M. Ernst[27], S. Errede[166], E. Ertel[85], M. Escalier[118], H. Esch[45], C. Escobar[126], B. Esposito[49], A. I. Etienvre[137], E. Etzion[154], H. Evans[63], A. Ezhilov[124], F. Fabbri[22a,22b], L. Fabbri[22a,22b], G. Facini[33], R. M. Fakhrutdinov[131], S. Falciano[133a], R. J. Falla[80], J. Faltova[32], Y. Fang[35a], M. Fanti[93a,93b], A. Farbin[8], A. Farilla[135a], C. Farina[126], T. Farooque[13], S. Farrell[16], S. M. Farrington[170], P. Farthouat[32], F. Fassi[136e], P. Fassnacht[32], D. Fassouliotis[9], M. Faucci Giannelli[79], A. Favareto[52a,52b], W. J. Fawcett[121], L. Fayard[118], O. L. Fedin[124,n], W. Fedorko[168], S. Feigl[120], L. Feligioni[87], C. Feng[35d], E. J. Feng[32], H. Feng[91], A. B. Fenyuk[131], L. Feremenga[8], P. Fernandez Martinez[167], S. Fernandez Perez[13], J. Ferrando[55], A. Ferrari[165], P. Ferrari[108], R. Ferrari[122a], D. E. Ferreira de Lima[60b], A. Ferrer[167], D. Ferrere[51], C. Ferretti[91], A. Ferretto Parodi[52a,52b], F. Fiedler[85], A. Filipčič[77], M. Filipuzzi[44], F. Filthaut[107], M. Fincke-Keeler[169], K. D. Finelli[151], M. C. N. Fiolhais[127a,127c], L. Fiorini[167], A. Firan[42], A. Fischer[2], C. Fischer[13], J. Fischer[175], W. C. Fisher[92], N. Flaschel[44], I. Fleck[142], P. Fleischmann[91], G. T. Fletcher[140], R. R. M. Fletcher[123], T. Flick[175], A. Floderus[83], L. R. Flores Castillo[62a], M. J. Flowerdew[102], G. T. Forcolin[86], A. Formica[137], A. Forti[86], A. G. Foster[19], D. Fournier[118], H. Fox[74], S. Fracchia[13], P. Francavilla[82], M. Franchini[22a,22b], D. Francis[32], L. Franconi[120], M. Franklin[59], M. Frate[163], M. Fraternali[122a,122b], D. Freeborn[80], S. M. Fressard-Batraneanu[32], F. Friedrich[46], D. Froidevaux[32], J. A. Frost[121], C. Fukunaga[157], E. Fullana Torregrosa[85], T. Fusayasu[103], J. Fuster[167], C. Gabaldon[57], O. Gabizon[175], A. Gabrielli[22a,22b], A. Gabrielli[16], G. P. Gach[40a], S. Gadatsch[32], S. Gadomski[51], G. Gagliardi[52a,52b], L. G. Gagnon[96], P. Gagnon[63], C. Galea[107], B. Galhardo[127a,127c], E. J. Gallas[121], B. J. Gallop[132], P. Gallus[129], G. Galster[38], K. K. Gan[112], J. Gao[35b,87], Y. Gao[48], Y. S. Gao[144,f], F. M. Garay Walls[48], C. García[167], J. E. García Navarro[167], M. Garcia-Sciveres[16], R. W. Gardner[33], N. Garelli[144], V. Garonne[120], A. Gascon Bravo[44], C. Gatti[49], A. Gaudiello[52a,52b], G. Gaudio[122a], B. Gaur[142], L. Gauthier[96], I. L. Gavrilenko[97], C. Gay[168], G. Gaycken[23], E. N. Gazis[10], Z. Gecse[168], C. N. P. Gee[132], Ch. Geich-Gimbel[23], M. Geisen[85], M. P. Geisler[60a], C. Gemme[52a], M. H. Genest[57], C. Geng[35b,o], S. Gentile[133a,133b], S. George[79], D. Gerbaudo[13], A. Gershon[154], S. Ghasemi[142], H. Ghazlane[136b], M. Ghneimat[23], B. Giacobbe[22a], S. Giagu[133a,133b], P. Giannetti[125a,125b], B. Gibbard[27], S. M. Gibson[79], M. Gignac[168], M. Gilchriese[16], T. P. S. Gillam[30], D. Gillberg[31], G. Gilles[175], D. M. Gingrich[3,d], N. Giokaris[9], M. P. Giordani[164a,164c], F. M. Giorgi[22a], F. M. Giorgi[17], P. F. Giraud[137], P. Giromini[59], D. Giugni[93a], F. Giuli[121], C. Giuliani[102], M. Giulini[60b], B. K. Gjelsten[120], S. Gkaitatzis[155], I. Gkialas[155], E. L. Gkougkousis[118], L. K. Gladilin[100], C. Glasman[84], J. Glatzer[50], P. C. F. Glaysher[48], A. Glazov[44], M. Goblirsch-Kolb[102], J. Godlewski[41], S. Goldfarb[91], T. Golling[51], D. Golubkov[131], A. Gomes[127a,127b,127d], R. Gonçalo[127a], J. Goncalves Pinto Firmino Da Costa[137], G. Gonella[50], L. Gonella[19], A. Gongadze[67], S. González de la Hoz[167], G. Gonzalez Parra[13], S. Gonzalez-Sevilla[51], L. Goossens[32], P. A. Gorbounov[98], H. A. Gordon[27], I. Gorelov[106], B. Gorini[32], E. Gorini[75a,75b], A. Gorišek[77], E. Gornicki[41], A. T. Goshaw[47], C. Gössling[45], M. I. Gostkin[67], C. R. Goudet[118], D. Goujdami[136c], A. G. Goussiou[139], N. Govender[146b,p], E. Gozani[153], L. Graber[56], I. Grabowska-Bold[40a], P. O. J. Gradin[57], P. Grafström[22a,22b], J. Gramling[51], E. Gramstad[120], S. Grancagnolo[17], V. Gratchev[124], P. M. Gravila[28e], H. M. Gray[32], E. Graziani[135a], Z. D. Greenwood[81,q], C. Grefe[23], K. Gregersen[80], I. M. Gregor[44], P. Grenier[144], K. Grevtsov[5], J. Griffiths[8], A. A. Grillo[138], K. Grimm[74], S. Grinstein[13,r], Ph. Gris[36], J. -F. Grivaz[118], S. Groh[85], J. P. Grohs[46], E. Gross[172], J. Grosse-Knetter[56], G. C. Grossi[81], Z. J. Grout[150], L. Guan[91], W. Guan[173], J. Guenther[129], F. Guescini[51], D. Guest[163], O. Gueta[154], E. Guido[52a,52b], T. Guillemin[5], S. Guindon[2], U. Gul[55], C. Gumpert[32], J. Guo[35e], Y. Guo[35b,o], S. Gupta[121], G. Gustavino[133a,133b], P. Gutierrez[114], N. G. Gutierrez Ortiz[80], C. Gutschow[46], C. Guyot[137], C. Gwenlan[121], C. B. Gwilliam[76], A. Haas[111], C. Haber[16], H. K. Hadavand[8], N. Haddad[136e], A. Hadef[87], P. Haefner[23], S. Hageböck[23], Z. Hajduk[41], H. Hakobyan[177,*], M. Haleem[44], J. Haley[115], G. Halladjian[92], G. D. Hallewell[87], K. Hamacher[175], P. Hamal[116], K. Hamano[169], A. Hamilton[146a], G. N. Hamity[140], P. G. Hamnett[44], L. Han[35b], K. Hanagaki[68,s], K. Hanawa[156], M. Hance[138], B. Haney[123], P. Hanke[60a], R. Hanna[137], J. B. Hansen[38], J. D. Hansen[38], M. C. Hansen[23], P. H. Hansen[38], K. Hara[161], A. S. Hard[173], T. Harenberg[175], F. Hariri[118], S. Harkusha[94], R. D. Harrington[48], P. F. Harrison[170], F. Hartjes[108], N. M. Hartmann[101], M. Hasegawa[69], Y. Hasegawa[141], A. Hasib[114], S. Hassani[137], S. Haug[18], R. Hauser[92], L. Hauswald[46], M. Havranek[128], C. M. Hawkes[19],

R. J. Hawkings[32], D. Hayden[92], C. P. Hays[121], J. M. Hays[78], H. S. Hayward[76], S. J. Haywood[132], S. J. Head[19], T. Heck[85], V. Hedberg[83], L. Heelan[8], S. Heim[123], T. Heim[16], B. Heinemann[16], J. J. Heinrich[101], L. Heinrich[111], C. Heinz[54], J. Hejbal[128], L. Helary[24], S. Hellman[147a,147b], C. Helsens[32], J. Henderson[121], R. C. W. Henderson[74], Y. Heng[173], S. Henkelmann[168], A. M. Henriques Correia[32], S. Henrot-Versille[118], G. H. Herbert[17], Y. Hernández Jiménez[167], G. Herten[50], R. Hertenberger[101], L. Hervas[32], G. G. Hesketh[80], N. P. Hessey[108], J. W. Hetherly[42], R. Hickling[78], E. Higón-Rodriguez[167], E. Hill[169], J. C. Hill[30], K. H. Hiller[44], S. J. Hillier[19], I. Hinchliffe[16], E. Hines[123], R. R. Hinman[16], M. Hirose[158], D. Hirschbuehl[175], J. Hobbs[149], N. Hod[160a], M. C. Hodgkinson[140], P. Hodgson[140], A. Hoecker[32], M. R. Hoeferkamp[106], F. Hoenig[101], D. Hohn[23], T. R. Holmes[16], M. Homann[45], T. M. Hong[126], B. H. Hooberman[166], W. H. Hopkins[117], Y. Horii[104], A. J. Horton[143], J-Y. Hostachy[57], S. Hou[152], A. Hoummada[136a], J. Howarth[44], M. Hrabovsky[116], I. Hristova[17], J. Hrivnac[118], T. Hryn'ova[5], A. Hrynevich[95], C. Hsu[146c], P. J. Hsu[152,t], S. -C. Hsu[139], D. Hu[37], Q. Hu[35b], Y. Huang[44], Z. Hubacek[129], F. Hubaut[87], F. Huegging[23], T. B. Huffman[121], E. W. Hughes[37], G. Hughes[74], M. Huhtinen[32], T. A. Hülsing[85], P. Huo[149], N. Huseynov[67,b], J. Huston[92], J. Huth[59], G. Iacobucci[51], G. Iakovidis[27], I. Ibragimov[142], L. Iconomidou-Fayard[118], E. Ideal[176], Z. Idrissi[136e], P. Iengo[32], O. Igonkina[108,u], T. Iizawa[171], Y. Ikegami[68], M. Ikeno[68], Y. Ilchenko[11,v], D. Iliadis[155], N. Ilic[144], T. Ince[102], G. Introzzi[122a,122b], P. Ioannou[9,*], M. Iodice[135a], K. Iordanidou[37], V. Ippolito[59], M. Ishino[70], M. Ishitsuka[158], R. Ishmukhametov[112], C. Issever[121], S. Istin[20a], F. Ito[161], J. M. Iturbe Ponce[86], R. Iuppa[134a,134b], W. Iwanski[41], H. Iwasaki[68], J. M. Izen[43], V. Izzo[105a], S. Jabbar[3], B. Jackson[123], M. Jackson[76], P. Jackson[1], V. Jain[2], K. B. Jakobi[85], K. Jakobs[50], S. Jakobsen[32], T. Jakoubek[128], D. O. Jamin[115], D. K. Jana[81], E. Jansen[80], R. Jansky[64], J. Janssen[23], M. Janus[56], G. Jarlskog[83], N. Javadov[67,b], T. Javůrek[50], F. Jeanneau[137], L. Jeanty[16], J. Jejelava[53a,w], G. -Y. Jeng[151], D. Jennens[90], P. Jenni[50,x], J. Jentzsch[45], C. Jeske[170], S. Jézéquel[5], H. Ji[173], J. Jia[149], H. Jiang[66], Y. Jiang[35b], S. Jiggins[80], J. Jimenez Pena[167], S. Jin[35a], A. Jinaru[28b], O. Jinnouchi[158], P. Johansson[140], K. A. Johns[7], W. J. Johnson[139], K. Jon-And[147a,147b], G. Jones[170], R. W. L. Jones[74], S. Jones[7], T. J. Jones[76], J. Jongmanns[60a], P. M. Jorge[127a,127b], J. Jovicevic[160a], X. Ju[173], A. Juste Rozas[13,r], M. K. Köhler[172], A. Kaczmarska[41], M. Kado[118], H. Kagan[112], M. Kagan[144], S. J. Kahn[87], E. Kajomovitz[47], C. W. Kalderon[121], A. Kaluza[85], S. Kama[42], A. Kamenshchikov[131], N. Kanaya[156], S. Kaneti[30], L. Kanjir[77], V. A. Kantserov[99], J. Kanzaki[68], B. Kaplan[111], L. S. Kaplan[173], A. Kapliy[33], D. Kar[146c], K. Karakostas[10], A. Karamaoun[3], N. Karastathis[10], M. J. Kareem[56], E. Karentzos[10], M. Karnevskiy[85], S. N. Karpov[67], Z. M. Karpova[67], K. Karthik[111], V. Kartvelishvili[74], A. N. Karyukhin[131], K. Kasahara[161], L. Kashif[173], R. D. Kass[112], A. Kastanas[15], Y. Kataoka[156], C. Kato[156], A. Katre[51], J. Katzy[44], K. Kawagoe[72], T. Kawamoto[156], G. Kawamura[56], S. Kazama[156], V. F. Kazanin[110,c], R. Keeler[169], R. Kehoe[42], J. S. Keller[44], J. J. Kempster[79], K. Kawade[104], H. Keoshkerian[159], O. Kepka[128], B. P. Kerševan[77], S. Kersten[175], R. A. Keyes[89], F. Khalil-zada[12], A. Khanov[115], A. G. Kharlamov[110,c], T. J. Khoo[51], V. Khovanskiy[98], E. Khramov[67], J. Khubua[53b,y], S. Kido[69], H. Y. Kim[8], S. H. Kim[161], Y. K. Kim[33], N. Kimura[155], O. M. Kind[17], B. T. King[76], M. King[167], S. B. King[168], J. Kirk[132], A. E. Kiryunin[102], T. Kishimoto[69], D. Kisielewska[40a], F. Kiss[50], K. Kiuchi[161], O. Kivernyk[137], E. Kladiva[145b], M. H. Klein[37], M. Klein[76], U. Klein[76], K. Kleinknecht[85], P. Klimek[147a,147b], A. Klimentov[27], R. Klingenberg[45], J. A. Klinger[140], T. Klioutchnikova[32], E. -E. Kluge[60a], P. Kluit[108], S. Kluth[102], J. Knapik[41], E. Kneringer[64], E. B. F. G. Knoops[87], A. Knue[55], A. Kobayashi[156], D. Kobayashi[158], T. Kobayashi[156], M. Kobel[46], M. Kocian[144], P. Kodys[130], T. Koffas[31], E. Koffeman[108], T. Koi[144], H. Kolanoski[17], M. Kolb[60b], I. Koletsou[5], A. A. Komar[97,*], Y. Komori[156], T. Kondo[68], N. Kondrashova[44], K. Köneke[50], A. C. König[107], T. Kono[68,z], R. Konoplich[111,aa], N. Konstantinidis[80], R. Kopeliansky[63], S. Koperny[40a], L. Köpke[85], A. K. Kopp[50], K. Korcyl[41], K. Kordas[155], A. Korn[80], A. A. Korol[110,c], I. Korolkov[13], E. V. Korolkova[140], O. Kortner[102], S. Kortner[102], T. Kosek[130], V. V. Kostyukhin[23], A. Kotwal[47], A. Kourkoumeli-Charalampidi[155], C. Kourkoumelis[9], V. Kouskoura[27], A. B. Kowalewska[41], R. Kowalewski[169], T. Z. Kowalski[40a], C. Kozakai[156], W. Kozanecki[137], A. S. Kozhin[131], V. A. Kramarenko[100], G. Kramberger[77], D. Krasnopevtsev[99], M. W. Krasny[82], A. Krasznahorkay[32], J. K. Kraus[23], A. Kravchenko[27], M. Kretz[60c], J. Kretzschmar[76], K. Kreutzfeldt[54], P. Krieger[159], K. Krizka[33], K. Kroeninger[45], H. Kroha[102], J. Kroll[123], J. Kroseberg[23], J. Krstic[14], U. Kruchonak[67], H. Krüger[23], N. Krumnack[66], A. Kruse[173], M. C. Kruse[47], M. Kruskal[24], T. Kubota[90], H. Kucuk[80], S. Kuday[4b], J. T. Kuechler[175], S. Kuehn[50], A. Kugel[60c], F. Kuger[174], A. Kuhl[138], T. Kuhl[44], V. Kukhtin[67], R. Kukla[137], Y. Kulchitsky[94], S. Kuleshov[34b], M. Kuna[133a,133b], T. Kunigo[70], A. Kupco[128], H. Kurashige[69], Y. A. Kurochkin[94], V. Kus[128], E. S. Kuwertz[169], M. Kuze[158], J. Kvita[116], T. Kwan[169], D. Kyriazopoulos[140], A. La Rosa[102], J. L. La Rosa Navarro[26d], L. La Rotonda[39a,39b], C. Lacasta[167], F. Lacava[133a,133b], J. Lacey[31], H. Lacker[17], D. Lacour[82], V. R. Lacuesta[167], E. Ladygin[67], R. Lafaye[5], B. Laforge[82], T. Lagouri[176], S. Lai[56], S. Lammers[63], W. Lampl[7], E. Lançon[137], U. Landgraf[50], M. P. J. Landon[78], V. S. Lang[60a], J. C. Lange[13], A. J. Lankford[163], F. Lanni[27], K. Lantzsch[23], A. Lanza[122a], S. Laplace[82], C. Lapoire[32], J. F. Laporte[137], T. Lari[93a], F. Lasagni Manghi[22a,22b], M. Lassnig[32], P. Laurelli[49], W. Lavrijsen[16], A. T. Law[138], P. Laycock[76], T. Lazovich[59], M. Lazzaroni[93a,93b], B. Le[90], O. Le Dortz[82], E. Le Guirriec[87], E. P. Le Quilleuc[137], M. LeBlanc[169], T. LeCompte[6], F. Ledroit-Guillon[57], C. A. Lee[27],

S. C. Lee[152], L. Lee[1], G. Lefebvre[82], M. Lefebvre[169], F. Legger[101], C. Leggett[16], A. Lehan[76], G. Lehmann Miotto[32], X. Lei[7], W. A. Leight[31], A. Leisos[155,ab], A. G. Leister[176], M. A. L. Leite[26d], R. Leitner[130], D. Lellouch[172], B. Lemmer[56], K. J. C. Leney[80], T. Lenz[23], B. Lenzi[32], R. Leone[7], S. Leone[125a,125b], C. Leonidopoulos[48], S. Leontsinis[10], G. Lerner[150], C. Leroy[96], A. A. J. Lesage[137], C. G. Lester[30], M. Levchenko[124], J. Levêque[5], D. Levin[91], L. J. Levinson[172], M. Levy[19], D. Lewis[78], A. M. Leyko[23], M. Leyton[43], B. Li[35b,o], H. Li[149], H. L. Li[33], L. Li[47], L. Li[35e], Q. Li[35a], S. Li[47], X. Li[86], Y. Li[142], Z. Liang[35a], B. Liberti[134a], A. Liblong[159], P. Lichard[32], K. Lie[166], J. Liebal[23], W. Liebig[15], A. Limosani[151], S. C. Lin[152,ac], T. H. Lin[85], B. E. Lindquist[149], A. E. Lionti[51], E. Lipeles[123], A. Lipniacka[15], M. Lisovyi[60b], T. M. Liss[166], A. Lister[168], A. M. Litke[138], B. Liu[152,ad], D. Liu[152], H. Liu[91], H. Liu[27], J. Liu[87], J. B. Liu[35b], K. Liu[87], L. Liu[166], M. Liu[47], M. Liu[35b], Y. L. Liu[35b], Y. Liu[35b], M. Livan[122a,122b], A. Lleres[57], J. Llorente Merino[35a], S. L. Lloyd[78], F. Lo Sterzo[152], E. Lobodzinska[44], P. Loch[7], W. S. Lockman[138], F. K. Loebinger[86], A. E. Loevschall-Jensen[38], K. M. Loew[25], A. Loginov[176,*], T. Lohse[17], K. Lohwasser[44], M. Lokajicek[128], B. A. Long[24], J. D. Long[166], R. E. Long[74], L. Longo[75a,75b], K. A. Looper[112], L. Lopes[127a], D. Lopez Mateos[59], B. Lopez Paredes[140], I. Lopez Paz[13], A. Lopez Solis[82], J. Lorenz[101], N. Lorenzo Martinez[63], M. Losada[21], P. J. Lösel[101], X. Lou[35a], A. Lounis[118], J. Love[6], P. A. Love[74], H. Lu[62a], N. Lu[91], H. J. Lubatti[139], C. Luci[133a,133b], A. Lucotte[57], C. Luedtke[50], F. Luehring[63], W. Lukas[64], L. Luminari[133a], O. Lundberg[147a,147b], B. Lund-Jensen[148], P. M. Luzi[82], D. Lynn[27], R. Lysak[128], E. Lytken[83], V. Lyubushkin[67], H. Ma[27], L. L. Ma[35d], Y. Ma[35d], G. Maccarrone[49], A. Macchiolo[102], C. M. Macdonald[140], B. Maček[77], J. Machado Miguens[123,127b], D. Madaffari[87], R. Madar[36], H. J. Maddocks[165], W. F. Mader[46], A. Madsen[44], J. Maeda[69], S. Maeland[15], T. Maeno[27], A. Maevskiy[100], E. Magradze[56], J. Mahlstedt[108], C. Maiani[118], C. Maidantchik[26a], A. A. Maier[102], T. Maier[101], A. Maio[127a,127b,127d], S. Majewski[117], Y. Makida[68], N. Makovec[118], B. Malaescu[82], Pa. Malecki[41], V. P. Maleev[124], F. Malek[57], U. Mallik[65], D. Malon[6], C. Malone[144], S. Maltezos[10], S. Malyukov[32], J. Mamuzic[167], G. Mancini[49], B. Mandelli[32], L. Mandelli[93a], I. Mandić[77], J. Maneira[127a,127b], L. Manhaes de Andrade Filho[26b], J. Manjarres Ramos[160b], A. Mann[101], A. Manousos[32], B. Mansoulie[137], J. D. Mansour[35a], R. Mantifel[89], M. Mantoani[56], S. Manzoni[93a,93b], L. Mapelli[32], G. Marceca[29], L. March[51], G. Marchiori[82], M. Marcisovsky[128], M. Marjanovic[14], D. E. Marley[91], F. Marroquim[26a], S. P. Marsden[86], Z. Marshall[16], S. Marti-Garcia[167], B. Martin[92], T. A. Martin[170], V. J. Martin[48], B. Martin dit Latour[15], M. Martinez[13,r], S. Martin-Haugh[132], V. S. Martoiu[28b], A. C. Martyniuk[80], M. Marx[139], A. Marzin[32], L. Masetti[85], T. Mashimo[156], R. Mashinistov[97], J. Masik[86], A. L. Maslennikov[110,c], I. Massa[22a,22b], L. Massa[22a,22b], P. Mastrandrea[5], A. Mastroberardino[39a,39b], T. Masubuchi[156], P. Mättig[175], J. Mattmann[85], J. Maurer[28b], S. J. Maxfield[76], D. A. Maximov[110,c], R. Mazini[152], S. M. Mazza[93a,93b], N. C. Mc Fadden[106], G. Mc Goldrick[159], S. P. Mc Kee[91], A. McCarn[91], R. L. McCarthy[149], T. G. McCarthy[102], L. I. McClymont[80], E. F. McDonald[90], K. W. McFarlane[58,*], J. A. Mcfayden[80], G. Mchedlidze[56], S. J. McMahon[132], R. A. McPherson[169,l], M. Medinnis[44], S. Meehan[139], S. Mehlhase[101], A. Mehta[76], K. Meier[60a], C. Meineck[101], B. Meirose[43], D. Melini[167], B. R. Mellado Garcia[146c], M. Melo[145a], F. Meloni[18], S. B. Menary[86], A. Mengarelli[22a,22b], S. Menke[102], E. Meoni[162], S. Mergelmeyer[17], P. Mermod[51], L. Merola[105a,105b], C. Meroni[93a], F. S. Merritt[33], A. Messina[133a,133b], J. Metcalfe[6], A. S. Mete[163], C. Meyer[85], C. Meyer[123], J-P. Meyer[137], J. Meyer[108], H. Meyer Zu Theenhausen[60a], F. Miano[150], R. P. Middleton[132], S. Miglioranzi[52a,52b], L. Mijović[23], G. Mikenberg[172], M. Mikestikova[128], M. Mikuž[77], M. Milesi[90], A. Milic[64], D. W. Miller[33], C. Mills[48], A. Milov[172], D. A. Milstead[147a,147b], A. A. Minaenko[131], Y. Minami[156], I. A. Minashvili[67], A. I. Mincer[111], B. Mindur[40a], M. Mineev[67], Y. Ming[173], L. M. Mir[13], K. P. Mistry[123], T. Mitani[171], J. Mitrevski[101], V. A. Mitsou[167], A. Miucci[51], P. S. Miyagawa[140], J. U. Mjörnmark[83], T. Moa[147a,147b], K. Mochizuki[96], S. Mohapatra[37], S. Molander[147a,147b], R. Moles-Valls[23], R. Monden[70], M. C. Mondragon[92], K. Mönig[44], J. Monk[38], E. Monnier[87], A. Montalbano[149], J. Montejo Berlingen[32], F. Monticelli[73], S. Monzani[93a,93b], R. W. Moore[3], N. Morange[118], D. Moreno[21], M. Moreno Llácer[56], P. Morettini[52a], D. Mori[143], T. Mori[156], M. Morii[59], M. Morinaga[156], V. Morisbak[120], S. Moritz[85], A. K. Morley[151], G. Mornacchi[32], J. D. Morris[78], S. S. Mortensen[38], L. Morvaj[149], M. Mosidze[53b], J. Moss[144], K. Motohashi[158], R. Mount[144], E. Mountricha[27], S. V. Mouraviev[97,*], E. J. W. Moyse[88], S. Muanza[87], R. D. Mudd[19], F. Mueller[102], J. Mueller[126], R. S. P. Mueller[101], T. Mueller[30], D. Muenstermann[74], P. Mullen[55], G. A. Mullier[18], F. J. Munoz Sanchez[86], J. A. Murillo Quijada[19], W. J. Murray[170,132], H. Musheghyan[56], M. Muškinja[77], A. G. Myagkov[131,ae], M. Myska[129], B. P. Nachman[144], O. Nackenhorst[51], K. Nagai[121], R. Nagai[68,z], K. Nagano[68], Y. Nagasaka[61], K. Nagata[161], M. Nagel[50], E. Nagy[87], A. M. Nairz[32], Y. Nakahama[32], K. Nakamura[68], T. Nakamura[156], I. Nakano[113], H. Namasivayam[43], R. F. Naranjo Garcia[44], R. Narayan[11], D. I. Narrias Villar[60a], I. Naryshkin[124], T. Naumann[44], G. Navarro[21], R. Nayyar[7], H. A. Neal[91], P. Yu. Nechaeva[97], T. J. Neep[86], P. D. Nef[144], A. Negri[122a,122b], M. Negrini[22a], S. Nektarijevic[107], C. Nellist[118], A. Nelson[163], S. Nemecek[128], P. Nemethy[111], A. A. Nepomuceno[26a], M. Nessi[32,af], M. S. Neubauer[166], M. Neumann[175], R. M. Neves[111], P. Nevski[27], P. R. Newman[19], D. H. Nguyen[6], T. Nguyen Manh[96], R. B. Nickerson[121], R. Nicolaidou[137], J. Nielsen[138], A. Nikiforov[17], V. Nikolaenko[131,ae], I. Nikolic-Audit[82], K. Nikolopoulos[19], J. K. Nilsen[120],

P. Nilsson[27], Y. Ninomiya[156], A. Nisati[133a], R. Nisius[102], T. Nobe[156], L. Nodulman[6], M. Nomachi[119], I. Nomidis[31], T. Nooney[78], S. Norberg[114], M. Nordberg[32], N. Norjoharuddeen[121], O. Novgorodova[46], S. Nowak[102], M. Nozaki[68], L. Nozka[116], K. Ntekas[10], E. Nurse[80], F. Nuti[90], F. O'grady[7], D. C. O'Neil[143], A. A. O'Rourke[44], V. O'Shea[55], F. G. Oakham[31,d], H. Oberlack[102], T. Obermann[23], J. Ocariz[82], A. Ochi[69], I. Ochoa[37], J. P. Ochoa-Ricoux[34a], S. Oda[72], S. Odaka[68], H. Ogren[63], A. Oh[86], S. H. Oh[47], C. C. Ohm[16], H. Ohman[165], H. Oide[32], H. Okawa[161], Y. Okumura[33], T. Okuyama[68], A. Olariu[28b], L. F. Oleiro Seabra[127a], S. A. Olivares Pino[48], D. Oliveira Damazio[27], A. Olszewski[41], J. Olszowska[41], A. Onofre[127a,127e], K. Onogi[104], P. U. E. Onyisi[11,v], M. J. Oreglia[33], Y. Oren[154], D. Orestano[135a,135b], N. Orlando[62b], R. S. Orr[159], B. Osculati[52a,52b], R. Ospanov[86], G. Otero y Garzon[29], H. Otono[72], M. Ouchrif[136d], F. Ould-Saada[120], A. Ouraou[137], K. P. Oussoren[108], Q. Ouyang[35a], M. Owen[55], R. E. Owen[19], V. E. Ozcan[20a], N. Ozturk[8], K. Pachal[143], A. Pacheco Pages[13], C. Padilla Aranda[13], M. Pagáčová[50], S. Pagan Griso[16], F. Paige[27], P. Pais[88], K. Pajchel[120], G. Palacino[160b], S. Palestini[32], M. Palka[40b], D. Pallin[36], A. Palma[127a,127b], E. St. Panagiotopoulou[10], C. E. Pandini[82], J. G. Panduro Vazquez[79], P. Pani[147a,147b], S. Panitkin[27], D. Pantea[28b], L. Paolozzi[51], Th. D. Papadopoulou[10], K. Papageorgiou[155], A. Paramonov[6], D. Paredes Hernandez[176], A. J. Parker[74], M. A. Parker[30], K. A. Parker[140], F. Parodi[52a,52b], J. A. Parsons[37], U. Parzefall[50], V. R. Pascuzzi[159], E. Pasqualucci[133a], S. Passaggio[52a], Fr. Pastore[79], G. Pásztor[31,ag], S. Pataraia[175], J. R. Pater[86], T. Pauly[32], J. Pearce[169], B. Pearson[114], L. E. Pedersen[38], M. Pedersen[120], S. Pedraza Lopez[167], R. Pedro[127a,127b], S. V. Peleganchuk[110,c], D. Pelikan[165], O. Penc[128], C. Peng[35a], H. Peng[35b], J. Penwell[63], B. S. Peralva[26b], M. M. Perego[137], D. V. Perepelitsa[27], E. Perez Codina[160a], L. Perini[93a,93b], H. Pernegger[32], S. Perrella[105a,105b], R. Peschke[44], V. D. Peshekhonov[67], K. Peters[44], R. F. Y. Peters[86], B. A. Petersen[32], T. C. Petersen[38], E. Petit[57], A. Petridis[1], C. Petridou[155], P. Petroff[118], E. Petrolo[133a], M. Petrov[121], F. Petrucci[135a,135b], N. E. Pettersson[88], A. Peyaud[137], R. Pezoa[34b], P. W. Phillips[132], G. Piacquadio[144,ah], E. Pianori[170], A. Picazio[88], E. Piccaro[78], M. Piccinini[22a,22b], M. A. Pickering[121], R. Piegaia[29], J. E. Pilcher[33], A. D. Pilkington[86], A. W. J. Pin[86], M. Pinamonti[164a164c,ai], J. L. Pinfold[3], A. Pingel[38], S. Pires[82], H. Pirumov[44], M. Pitt[172], L. Plazak[145a], M.-A. Pleier[27], V. Pleskot[85], E. Plotnikova[67], P. Plucinski[92], D. Pluth[66], R. Poettgen[147a,147b], L. Poggioli[118], D. Pohl[23], G. Polesello[122a], A. Poley[44], A. Policicchio[39a,39b], R. Polifka[159], A. Polini[22a], C. S. Pollard[55], V. Polychronakos[27], K. Pommès[32], L. Pontecorvo[133a], B. G. Pope[92], G. A. Popeneciu[28c], D. S. Popovic[14], A. Poppleton[32], S. Pospisil[129], K. Potamianos[16], I. N. Potrap[67], C. J. Potter[30], C. T. Potter[117], G. Poulard[32], J. Poveda[32], V. Pozdnyakov[67], M. E. Pozo Astigarraga[32], P. Pralavorio[87], A. Pranko[16], S. Prell[66], D. Price[86], L. E. Price[6], M. Primavera[75a], S. Prince[89], M. Proissl[48], K. Prokofiev[62c], F. Prokoshin[34b], S. Protopopescu[27], J. Proudfoot[6], M. Przybycien[40a], D. Puddu[135a,135b], M. Purohit[27,aj], P. Puzo[118], J. Qian[91], G. Qin[55], Y. Qin[86], A. Quadt[56], W. B. Quayle[164a,164b], M. Queitsch-Maitland[86], D. Quilty[55], S. Raddum[120], V. Radeka[27], V. Radescu[60b], S. K. Radhakrishnan[149], P. Radloff[117], P. Rados[90], F. Ragusa[93a,93b], G. Rahal[178], J. A. Raine[86], S. Rajagopalan[27], M. Rammensee[32], C. Rangel-Smith[165], M. G. Ratti[93a,93b], F. Rauscher[101], S. Rave[85], T. Ravenscroft[55], I. Ravinovich[172], M. Raymond[32], A. L. Read[120], N. P. Readioff[76], M. Reale[75a,75b], D. M. Rebuzzi[122a,122b], A. Redelbach[174], G. Redlinger[27], R. Reece[138], K. Reeves[43], L. Rehnisch[17], J. Reichert[123], H. Reisin[29], C. Rembser[32], H. Ren[35a], M. Rescigno[133a], S. Resconi[93a], O. L. Rezanova[110,c], P. Reznicek[130], R. Rezvani[96], R. Richter[102], S. Richter[80], E. Richter-Was[40b], O. Ricken[23], M. Ridel[82], P. Rieck[17], C. J. Riegel[175], J. Rieger[56], O. Rifki[114], M. Rijssenbeek[149], A. Rimoldi[122a,122b], M. Rimoldi[18], L. Rinaldi[22a], B. Ristić[51], E. Ritsch[32], I. Riu[13], F. Rizatdinova[115], E. Rizvi[78], C. Rizzi[13], S. H. Robertson[89,l], A. Robichaud-Veronneau[89], D. Robinson[30], J. E. M. Robinson[44], A. Robson[55], C. Roda[125a,125b], Y. Rodina[87], A. Rodriguez Perez[13], D. Rodriguez Rodriguez[167], S. Roe[32], C. S. Rogan[59], O. Røhne[120], A. Romaniouk[99], M. Romano[22a,22b], S. M. Romano Saez[36], E. Romero Adam[167], N. Rompotis[139], M. Ronzani[50], L. Roos[82], E. Ros[167], S. Rosati[133a], K. Rosbach[50], P. Rose[138], O. Rosenthal[142], N. -A. Rosien[56], V. Rossetti[147a,147b], E. Rossi[105a,105b], L. P. Rossi[52a], J. H. N. Rosten[30], R. Rosten[139], M. Rotaru[28b], I. Roth[172], J. Rothberg[139], D. Rousseau[118], C. R. Royon[137], A. Rozanov[87], Y. Rozen[153], X. Ruan[146c], F. Rubbo[144], M. S. Rudolph[159], F. Rühr[50], A. Ruiz-Martinez[31], Z. Rurikova[50], N. A. Rusakovich[67], A. Ruschke[101], H. L. Russell[139], J. P. Rutherfoord[7], N. Ruthmann[32], Y. F. Ryabov[124], M. Rybar[166], G. Rybkin[118], S. Ryu[6], A. Ryzhov[131], G. F. Rzehorz[56], A. F. Saavedra[151], G. Sabato[108], S. Sacerdoti[29], H. F.-W. Sadrozinski[138], R. Sadykov[67], F. Safai Tehrani[133a], P. Saha[109], M. Sahinsoy[60a], M. Saimpert[137], T. Saito[156], H. Sakamoto[156], Y. Sakurai[171], G. Salamanna[135a,135b], A. Salamon[134a,134b], J. E. Salazar Loyola[34b], D. Salek[108], P. H. Sales De Bruin[139], D. Salihagic[102], A. Salnikov[144], J. Salt[167], D. Salvatore[39a,39b], F. Salvatore[150], A. Salvucci[62a], A. Salzburger[32], D. Sammel[50], D. Sampsonidis[155], A. Sanchez[105a,105b], J. Sánchez[167], V. Sanchez Martinez[167], H. Sandaker[120], R. L. Sandbach[78], H. G. Sander[85], M. Sandhoff[175], C. Sandoval[21], R. Sandstroem[102], D. P. C. Sankey[132], M. Sannino[52a,52b], A. Sansoni[49], C. Santoni[36], R. Santonico[134a,134b], H. Santos[127a], I. Santoyo Castillo[150], K. Sapp[126], A. Sapronov[67], J. G. Saraiva[127a,127d], B. Sarrazin[23], O. Sasaki[68], Y. Sasaki[156], K. Sato[161], G. Sauvage[5,*], E. Sauvan[5], G. Savage[79], P. Savard[159,d], C. Sawyer[132], L. Sawyer[81,q], J. Saxon[33], C. Sbarra[22a], A. Sbrizzi[22a,22b], T. Scanlon[80], D. A. Scannicchio[163], M. Scarcella[151], V. Scarfone[39a,39b], J. Schaarschmidt[172], P. Schacht[102], B. M. Schachtner[101],

D. Schaefer[32], R. Schaefer[44], J. Schaeffer[85], S. Schaepe[23], S. Schaetzel[60b], U. Schäfer[85], A. C. Schaffer[118], D. Schaile[101], R. D. Schamberger[149], V. Scharf[60a], V. A. Schegelsky[124], D. Scheirich[130], M. Schernau[163], C. Schiavi[52a,52b], S. Schier[138], C. Schillo[50], M. Schioppa[39a,39b], S. Schlenker[32], K. R. Schmidt-Sommerfeld[102], K. Schmieden[32], C. Schmitt[85], S. Schmitt[44], S. Schmitz[85], B. Schneider[160a], U. Schnoor[50], L. Schoeffel[137], A. Schoening[60b], B. D. Schoenrock[92], E. Schopf[23], M. Schott[85], J. Schovancova[8], S. Schramm[51], M. Schreyer[174], N. Schuh[85], M. J. Schultens[23], H. -C. Schultz-Coulon[60a], H. Schulz[17], M. Schumacher[50], B. A. Schumm[138], Ph. Schune[137], A. Schwartzman[144], T. A. Schwarz[91], Ph. Schwegler[102], H. Schweiger[86], Ph. Schwemling[137], R. Schwienhorst[92], J. Schwindling[137], T. Schwindt[23], G. Sciolla[25], F. Scuri[125a,125b], F. Scutti[90], J. Searcy[91], P. Seema[23], S. C. Seidel[106], A. Seiden[138], F. Seifert[129], J. M. Seixas[26a], G. Sekhniaidze[105a], K. Sekhon[91], S. J. Sekula[42], D. M. Seliverstov[124,*], N. Semprini-Cesari[22a,22b], C. Serfon[120], L. Serin[118], L. Serkin[164a,164b], M. Sessa[135a,135b], R. Seuster[169], H. Severini[114], T. Sfiligoj[77], F. Sforza[32], A. Sfyrla[51], E. Shabalina[56], N. W. Shaikh[147a,147b], L. Y. Shan[35a], R. Shang[166], J. T. Shank[24], M. Shapiro[16], P. B. Shatalov[98], K. Shaw[164a,164b], S. M. Shaw[86], A. Shcherbakova[147a,147b], C. Y. Shehu[150], P. Sherwood[80], L. Shi[152,ak], S. Shimizu[69], C. O. Shimmin[163], M. Shimojima[103], M. Shiyakova[67,al], A. Shmeleva[97], D. Shoaleh Saadi[96], M. J. Shochet[33], S. Shojaii[93a,93b], S. Shrestha[112], E. Shulga[99], M. A. Shupe[7], P. Sicho[128], A. M. Sickles[166], P. E. Sidebo[148], O. Sidiropoulou[174], D. Sidorov[115], A. Sidoti[22a,22b], F. Siegert[46], Dj. Sijacki[14], J. Silva[127a,127d], S. B. Silverstein[147a], V. Simak[129], O. Simard[5], Lj. Simic[14], S. Simion[118], E. Simioni[85], B. Simmons[80], D. Simon[36], M. Simon[85], P. Sinervo[159], N. B. Sinev[117], M. Sioli[22a,22b], G. Siragusa[174], S. Yu. Sivoklokov[100], J. Sjölin[147a,147b], T. B. Sjursen[15], M. B. Skinner[74], H. P. Skottowe[59], P. Skubic[114], M. Slater[19], T. Slavicek[129], M. Slawinska[108], K. Sliwa[162], R. Slovak[130], V. Smakhtin[172], B. H. Smart[5], L. Smestad[15], J. Smiesko[145a], S. Yu. Smirnov[99], Y. Smirnov[99], L. N. Smirnova[100,am], O. Smirnova[83], M. N. K. Smith[37], R. W. Smith[37], M. Smizanska[74], K. Smolek[129], A. A. Snesarev[97], S. Snyder[27], R. Sobie[169,l], F. Socher[46], A. Soffer[154], D. A. Soh[152], G. Sokhrannyi[77], C. A. Solans Sanchez[32], M. Solar[129], E. Yu. Soldatov[99], U. Soldevila[167], A. A. Solodkov[131], A. Soloshenko[67], O. V. Solovyanov[131], V. Solovyev[124], P. Sommer[50], H. Son[162], H. Y. Song[35b,an], A. Sood[16], A. Sopczak[129], V. Sopko[129], V. Sorin[13], D. Sosa[60b], C. L. Sotiropoulou[125a,125b], R. Soualah[164a,164c], A. M. Soukharev[110,c], D. South[44], B. C. Sowden[79], S. Spagnolo[75a,75b], M. Spalla[125a,125b], M. Spangenberg[170], F. Spanò[79], D. Sperlich[17], F. Spettel[102], R. Spighi[22a], G. Spigo[32], L. A. Spiller[90], M. Spousta[130], R. D. St. Denis[55,*], A. Stabile[93a], R. Stamen[60a], S. Stamm[17], E. Stanecka[41], R. W. Stanek[6], C. Stanescu[135a], M. Stanescu-Bellu[44], M. M. Stanitzki[44], S. Stapnes[120], E. A. Starchenko[131], G. H. Stark[33], J. Stark[57], P. Staroba[128], P. Starovoitov[60a], S. Stärz[32], R. Staszewski[41], P. Steinberg[27], B. Stelzer[143], H. J. Stelzer[32], O. Stelzer-Chilton[160a], H. Stenzel[54], G. A. Stewart[55], J. A. Stillings[23], M. C. Stockton[89], M. Stoebe[89], G. Stoicea[28b], P. Stolte[56], S. Stonjek[102], A. R. Stradling[8], A. Straessner[46], M. E. Stramaglia[18], J. Strandberg[148], S. Strandberg[147a,147b], A. Strandlie[120], M. Strauss[114], P. Strizenec[145b], R. Ströhmer[174], D. M. Strom[117], R. Stroynowski[42], A. Strubig[107], S. A. Stucci[18], B. Stugu[15], N. A. Styles[44], D. Su[144], J. Su[126], R. Subramaniam[81], S. Suchek[60a], Y. Sugaya[119], M. Suk[129], V. V. Sulin[97], S. Sultansoy[4c], T. Sumida[70], S. Sun[59], X. Sun[35a], J. E. Sundermann[50], K. Suruliz[150], G. Susinno[39a,39b], M. R. Sutton[150], S. Suzuki[68], M. Svatos[128], M. Swiatlowski[33], I. Sykora[145a], T. Sykora[130], D. Ta[50], C. Taccini[135a,135b], K. Tackmann[44], J. Taenzer[159], A. Taffard[163], R. Tafirout[160a], N. Taiblum[154], H. Takai[27], R. Takashima[71], T. Takeshita[141], Y. Takubo[68], M. Talby[87], A. A. Talyshev[110,c], K. G. Tan[90], J. Tanaka[156], R. Tanaka[118], S. Tanaka[68], B. B. Tannenwald[112], S. Tapia Araya[34b], S. Tapprogge[85], S. Tarem[153], G. F. Tartarelli[93a], P. Tas[130], M. Tasevsky[128], T. Tashiro[70], E. Tassi[39a,39b], A. Tavares Delgado[127a,127b], Y. Tayalati[136d], A. C. Taylor[106], G. N. Taylor[90], P. T. E. Taylor[90], W. Taylor[160b], F. A. Teischinger[32], P. Teixeira-Dias[79], K. K. Temming[50], D. Temple[143], H. Ten Kate[32], P. K. Teng[152], J. J. Teoh[119], F. Tepel[175], S. Terada[68], K. Terashi[156], J. Terron[84], S. Terzo[102], M. Testa[49], R. J. Teuscher[159,l], T. Theveneaux-Pelzer[87], J. P. Thomas[19], J. Thomas-Wilsker[79], E. N. Thompson[37], P. D. Thompson[19], A. S. Thompson[55], L. A. Thomsen[176], E. Thomson[123], M. Thomson[30], M. J. Tibbetts[16], R. E. Ticse Torres[87], V. O. Tikhomirov[97,ao], Yu. A. Tikhonov[110,c], S. Timoshenko[99], P. Tipton[176], S. Tisserant[87], K. Todome[158], T. Todorov[5,*], S. Todorova-Nova[130], J. Tojo[72], S. Tokár[145a], K. Tokushuku[68], E. Tolley[59], L. Tomlinson[86], M. Tomoto[104], L. Tompkins[144,ap], K. Toms[106], B. Tong[59], E. Torrence[117], H. Torres[143], E. Torró Pastor[139], J. Toth[87,aq], F. Touchard[87], D. R. Tovey[140], T. Trefzger[174], A. Tricoli[27], I. M. Trigger[160a], S. Trincaz-Duvoid[82], M. F. Tripiana[13], W. Trischuk[159], B. Trocmé[57], A. Trofymov[44], C. Troncon[93a], M. Trottier-McDonald[16], M. Trovatelli[169], L. Truong[164a,164c], M. Trzebinski[41], A. Trzupek[41], J. C.-L. Tseng[121], P. V. Tsiareshka[94], G. Tsipolitis[10], N. Tsirintanis[9], S. Tsiskaridze[13], V. Tsiskaridze[50], E. G. Tskhadadze[53a], K. M. Tsui[62a], I. I. Tsukerman[98], V. Tsulaia[16], S. Tsuno[68], D. Tsybychev[149], A. Tudorache[28b], V. Tudorache[28b], A. N. Tuna[59], S. A. Tupputi[22a,22b], S. Turchikhin[100,am], D. Turecek[129], D. Turgeman[172], R. Turra[93a,93b], A. J. Turvey[42], P. M. Tuts[37], M. Tyndel[132], G. Ucchielli[22a,22b], I. Ueda[156], R. Ueno[31], M. Ughetto[147a,147b], F. Ukegawa[161], G. Unal[32], A. Undrus[27], G. Unel[163], F. C. Ungaro[90], Y. Unno[68], C. Unverdorben[101], J. Urban[145b], P. Urquijo[90], P. Urrejola[85], G. Usai[8], A. Usanova[64], L. Vacavant[87], V. Vacek[129], B. Vachon[89], C. Valderanis[101], E. Valdes Santurio[147a,147b], N. Valencic[108], S. Valentinetti[22a,22b], A. Valero[167],

L. Valery[13], S. Valkar[130], S. Vallecorsa[51], J. A. Valls Ferrer[167], W. Van Den Wollenberg[108], P. C. Van Der Deijl[108], R. van der Geer[108], H. van der Graaf[108], N. van Eldik[153], P. van Gemmeren[6], J. Van Nieuwkoop[143], I. van Vulpen[108], M. C. van Woerden[32], M. Vanadia[133a,133b], W. Vandelli[32], R. Vanguri[123], A. Vaniachine[131], P. Vankov[108], G. Vardanyan[177], R. Vari[133a], E. W. Varnes[7], T. Varol[42], D. Varouchas[82], A. Vartapetian[8], K. E. Varvell[151], J. G. Vasquez[176], F. Vazeille[36], T. Vazquez Schroeder[89], J. Veatch[56], L. M. Veloce[159], F. Veloso[127a,127c], S. Veneziano[133a], A. Ventura[75a,75b], M. Venturi[169], N. Venturi[159], A. Venturini[25], V. Vercesi[122a], M. Verducci[133a,133b], W. Verkerke[108], J. C. Vermeulen[108], A. Vest[46,ar], M. C. Vetterli[143,d], O. Viazlo[83], I. Vichou[166,*], T. Vickey[140], O. E. Vickey Boeriu[140], G. H. A. Viehhauser[121], S. Viel[16], L. Vigani[121], R. Vigne[64], M. Villa[22a,22b], M. Villaplana Perez[93a,93b], E. Vilucchi[49], M. G. Vincter[31], V. B. Vinogradov[67], C. Vittori[22a,22b], I. Vivarelli[150], S. Vlachos[10], M. Vlasak[129], M. Vogel[175], P. Vokac[129], G. Volpi[125a,125b], M. Volpi[90], H. von der Schmitt[102], E. von Toerne[23], V. Vorobel[130], K. Vorobev[99], M. Vos[167], R. Voss[32], J. H. Vossebeld[76], N. Vranjes[14], M. Vranjes Milosavljevic[14], V. Vrba[128], M. Vreeswijk[108], R. Vuillermet[32], I. Vukotic[33], Z. Vykydal[129], P. Wagner[23], W. Wagner[175], H. Wahlberg[73], S. Wahrmund[46], J. Wakabayashi[104], J. Walder[74], R. Walker[101], W. Walkowiak[142], V. Wallangen[147a,147b], C. Wang[35c], C. Wang[35d,87], F. Wang[173], H. Wang[16], H. Wang[42], J. Wang[44], J. Wang[151], K. Wang[89], R. Wang[6], S. M. Wang[152], T. Wang[23], T. Wang[37], W. Wang[35b], X. Wang[176], C. Wanotayaroj[117], A. Warburton[89], C. P. Ward[30], D. R. Wardrope[80], A. Washbrook[48], P. M. Watkins[19], A. T. Watson[19], M. F. Watson[19], G. Watts[139], S. Watts[86], B. M. Waugh[80], S. Webb[85], M. S. Weber[18], S. W. Weber[174], J. S. Webster[6], A. R. Weidberg[121], B. Weinert[63], J. Weingarten[56], C. Weiser[50], H. Weits[108], P. S. Wells[32], T. Wenaus[27], T. Wengler[32], S. Wenig[32], N. Wermes[23], M. Werner[50], M. D. Werner[66], P. Werner[32], M. Wessels[60a], J. Wetter[162], K. Whalen[117], N. L. Whallon[139], A. M. Wharton[74], A. White[8], M. J. White[1], R. White[34b], D. Whiteson[163], F. J. Wickens[132], W. Wiedenmann[173], M. Wielers[132], P. Wienemann[23], C. Wiglesworth[38], L. A. M. Wiik-Fuchs[23], A. Wildauer[102], F. Wilk[86], H. G. Wilkens[32], H. H. Williams[123], S. Williams[108], C. Willis[92], S. Willocq[88], J. A. Wilson[19], I. Wingerter-Seez[5], F. Winklmeier[117], O. J. Winston[150], B. T. Winter[23], M. Wittgen[144], J. Wittkowski[101], S. J. Wollstadt[85], M. W. Wolter[41], H. Wolters[127a,127c], B. K. Wosiek[41], J. Wotschack[32], M. J. Woudstra[86], K. W. Wozniak[41], M. Wu[57], M. Wu[33], S. L. Wu[173], X. Wu[51], Y. Wu[91], T. R. Wyatt[86], B. M. Wynne[48], S. Xella[38], D. Xu[35a], L. Xu[27], B. Yabsley[151], S. Yacoob[146a], R. Yakabe[69], D. Yamaguchi[158], Y. Yamaguchi[119], A. Yamamoto[68], S. Yamamoto[156], T. Yamanaka[156], K. Yamauchi[104], Y. Yamazaki[69], Z. Yan[24], H. Yang[35e], H. Yang[173], Y. Yang[152], Z. Yang[15], W.-M. Yao[16], Y. C. Yap[82], Y. Yasu[68], E. Yatsenko[5], K. H. Yau Wong[23], J. Ye[42], S. Ye[27], I. Yeletskikh[67], A. L. Yen[59], E. Yildirim[85], K. Yorita[171], R. Yoshida[6], K. Yoshihara[123], C. Young[144], C. J. S. Young[32], S. Youssef[24], D. R. Yu[16], J. Yu[8], J. M. Yu[91], J. Yu[66], L. Yuan[69], S. P. Y. Yuen[23], I. Yusuff[30,as], B. Zabinski[41], R. Zaidan[35d], A. M. Zaitsev[131,ae], N. Zakharchuk[44], J. Zalieckas[15], A. Zaman[149], S. Zambito[59], L. Zanello[133a,133b], D. Zanzi[90], C. Zeitnitz[175], M. Zeman[129], A. Zemla[40a], J. C. Zeng[166], Q. Zeng[144], K. Zengel[25], O. Zenin[131], T. Ženiš[145a], D. Zerwas[118], D. Zhang[91], F. Zhang[173], G. Zhang[35b,an], H. Zhang[35c], J. Zhang[6], L. Zhang[50], R. Zhang[23], R. Zhang[35b,at], X. Zhang[35d], Z. Zhang[118], X. Zhao[42], Y. Zhao[35d], Z. Zhao[35b], A. Zhemchugov[67], J. Zhong[121], B. Zhou[91], C. Zhou[47], L. Zhou[37], L. Zhou[42], M. Zhou[149], N. Zhou[35f], C. G. Zhu[35d], H. Zhu[35a], J. Zhu[91], Y. Zhu[35b], X. Zhuang[35a], K. Zhukov[97], A. Zibell[174], D. Zieminska[63], N. I. Zimine[67], C. Zimmermann[85], S. Zimmermann[50], Z. Zinonos[56], M. Zinser[85], M. Ziolkowski[142], L. Živković[14], G. Zobernig[173], A. Zoccoli[22a,22b], M. zur Nedden[17], G. Zurzolo[105a,105b], L. Zwalinski[32]

[1] Department of Physics, University of Adelaide, Adelaide, Australia
[2] Physics Department, SUNY Albany, Albany, NY, USA
[3] Department of Physics, University of Alberta, Edmonton, AB, Canada
[4] [(a)]Department of Physics, Ankara University, Ankara, Turkey; [(b)]Istanbul Aydin University, Istanbul, Turkey; [(c)]Division of Physics, TOBB University of Economics and Technology, Ankara, Turkey
[5] LAPP, CNRS/IN2P3 and Université Savoie Mont Blanc, Annecy-le-Vieux, France
[6] High Energy Physics Division, Argonne National Laboratory, Argonne, IL, USA
[7] Department of Physics, University of Arizona, Tucson, AZ, USA
[8] Department of Physics, The University of Texas at Arlington, Arlington, TX, USA
[9] Physics Department, University of Athens, Athens, Greece
[10] Physics Department, National Technical University of Athens, Zografou, Greece
[11] Department of Physics, The University of Texas at Austin, Austin, TX, USA
[12] Institute of Physics, Azerbaijan Academy of Sciences, Baku, Azerbaijan
[13] Institut de Física d'Altes Energies (IFAE), The Barcelona Institute of Science and Technology, Barcelona, Spain
[14] Institute of Physics, University of Belgrade, Belgrade, Serbia
[15] Department for Physics and Technology, University of Bergen, Bergen, Norway
[16] Physics Division, Lawrence Berkeley National Laboratory, University of California, Berkeley, CA, USA

[17] Department of Physics, Humboldt University, Berlin, Germany
[18] Albert Einstein Center for Fundamental Physics and Laboratory for High Energy Physics, University of Bern, Bern, Switzerland
[19] School of Physics and Astronomy, University of Birmingham, Birmingham, UK
[20] [(a)]Department of Physics, Bogazici University, Istanbul, Turkey; [(b)]Department of Physics Engineering, Gaziantep University, Gaziantep, Turkey; [(c)]Faculty of Engineering and Natural Sciences, Istanbul Bilgi University, Istanbul, Turkey; [(d)]Faculty of Engineering and Natural Sciences, Bahcesehir University, Istanbul, Turkey
[21] Centro de Investigaciones, Universidad Antonio Narino, Bogotá, Colombia
[22] [(a)]INFN Sezione di Bologna, Bologna, Italy; [(b)]Dipartimento di Fisica e Astronomia, Università di Bologna, Bologna, Italy
[23] Physikalisches Institut, University of Bonn, Bonn, Germany
[24] Department of Physics, Boston University, Boston, MA, USA
[25] Department of Physics, Brandeis University, Waltham, MA, USA
[26] [(a)]Universidade Federal do Rio De Janeiro COPPE/EE/IF, Rio de Janeiro, Brazil; [(b)]Electrical Circuits Department, Federal University of Juiz de Fora (UFJF), Juiz de Fora, Brazil; [(c)]Federal University of Sao Joao del Rei (UFSJ), São João del Rei, Brazil; [(d)]Instituto de Fisica, Universidade de Sao Paulo, São Paulo, Brazil
[27] Physics Department, Brookhaven National Laboratory, Upton, NY, USA
[28] [(a)]Transilvania University of Brasov, Brasov, Romania; [(b)]National Institute of Physics and Nuclear Engineering, Bucharest, Romania; [(c)]Physics Department, National Institute for Research and Development of Isotopic and Molecular Technologies, Cluj-Napoca, Romania; [(d)]University Politehnica Bucharest, Bucharest, Romania; [(e)]West University in Timisoara, Timisoara, Romania
[29] Departamento de Física, Universidad de Buenos Aires, Buenos Aires, Argentina
[30] Cavendish Laboratory, University of Cambridge, Cambridge, UK
[31] Department of Physics, Carleton University, Ottawa, ON, Canada
[32] CERN, Geneva, Switzerland
[33] Enrico Fermi Institute, University of Chicago, Chicago, IL, USA
[34] [(a)]Departamento de Física, Pontificia Universidad Católica de Chile, Santiago, Chile; [(b)]Departamento de Física, Universidad Técnica Federico Santa María, Valparaíso, Chile
[35] [(a)]Institute of High Energy Physics, Chinese Academy of Sciences, Beijing, China; [(b)]Department of Modern Physics, University of Science and Technology of China, Anhui, China; [(c)]Department of Physics, Nanjing University, Jiangsu, China; [(d)]School of Physics, Shandong University, Shandong, China; [(e)]Department of Physics and Astronomy, Shanghai Key Laboratory for Particle Physics and Cosmology, Shanghai Jiao Tong University (also affiliated with PKU-CHEP), Shanghai, China; [(f)]Physics Department, Tsinghua University, Beijing 100084, China
[36] Laboratoire de Physique Corpusculaire, Clermont Université and Université Blaise Pascal and CNRS/IN2P3, Clermont-Ferrand, France
[37] Nevis Laboratory, Columbia University, Irvington, NY, USA
[38] Niels Bohr Institute, University of Copenhagen, Copenhagen, Denmark
[39] [(a)]INFN Gruppo Collegato di Cosenza, Laboratori Nazionali di Frascati, Cosenza, Italy; [(b)]Dipartimento di Fisica, Università della Calabria, Rende, Italy
[40] [(a)]AGH University of Science and Technology, Faculty of Physics and Applied Computer Science, Kraków, Poland; [(b)]Marian Smoluchowski Institute of Physics, Jagiellonian University, Kraków, Poland
[41] Institute of Nuclear Physics, Polish Academy of Sciences, Kraków, Poland
[42] Physics Department, Southern Methodist University, Dallas, TX, USA
[43] Physics Department, University of Texas at Dallas, Richardson, TX, USA
[44] DESY, Hamburg and Zeuthen, Germany
[45] Lehrstuhl für Experimentelle Physik IV, Technische Universität Dortmund, Dortmund, Germany
[46] Institut für Kern–und Teilchenphysik, Technische Universität Dresden, Dresden, Germany
[47] Department of Physics, Duke University, Durham, NC, USA
[48] SUPA-School of Physics and Astronomy, University of Edinburgh, Edinburgh, UK
[49] INFN Laboratori Nazionali di Frascati, Frascati, Italy
[50] Fakultät für Mathematik und Physik, Albert-Ludwigs-Universität, Freiburg, Germany
[51] Section de Physique, Université de Genève, Geneva, Switzerland
[52] [(a)]INFN Sezione di Genova, Genoa, Italy; [(b)]Dipartimento di Fisica, Università di Genova, Genoa, Italy

[53] [(a)]E. Andronikashvili Institute of Physics, Iv. Javakhishvili Tbilisi State University, Tbilisi, Georgia; [(b)]High Energy Physics Institute, Tbilisi State University, Tbilisi, Georgia
[54] II Physikalisches Institut, Justus-Liebig-Universität Giessen, Giessen, Germany
[55] SUPA-School of Physics and Astronomy, University of Glasgow, Glasgow, UK
[56] II Physikalisches Institut, Georg-August-Universität, Göttingen, Germany
[57] Laboratoire de Physique Subatomique et de Cosmologie, Université Grenoble-Alpes, CNRS/IN2P3, Grenoble, France
[58] Department of Physics, Hampton University, Hampton, VA, USA
[59] Laboratory for Particle Physics and Cosmology, Harvard University, Cambridge, MA, USA
[60] [(a)]Kirchhoff-Institut für Physik, Ruprecht-Karls-Universität Heidelberg, Heidelberg, Germany; [(b)]Physikalisches Institut, Ruprecht-Karls-Universität Heidelberg, Heidelberg, Germany; [(c)]ZITI Institut für technische Informatik, Ruprecht-Karls-Universität Heidelberg, Mannheim, Germany
[61] Faculty of Applied Information Science, Hiroshima Institute of Technology, Hiroshima, Japan
[62] [(a)]Department of Physics, The Chinese University of Hong Kong, Shatin, NT, Hong Kong; [(b)]Department of Physics, The University of Hong Kong, Pokfulam, Hong Kong; [(c)]Department of Physics, The Hong Kong University of Science and Technology, Clear Water Bay, Kowloon, Hong Kong, China
[63] Department of Physics, Indiana University, Bloomington, IN, USA
[64] Institut für Astro–und Teilchenphysik, Leopold-Franzens-Universität, Innsbruck, Austria
[65] University of Iowa, Iowa City, IA, USA
[66] Department of Physics and Astronomy, Iowa State University, Ames, IA, USA
[67] Joint Institute for Nuclear Research, JINR Dubna, Dubna, Russia
[68] KEK, High Energy Accelerator Research Organization, Tsukuba, Japan
[69] Graduate School of Science, Kobe University, Kobe, Japan
[70] Faculty of Science, Kyoto University, Kyoto, Japan
[71] Kyoto University of Education, Kyoto, Japan
[72] Department of Physics, Kyushu University, Fukuoka, Japan
[73] Instituto de Física La Plata, Universidad Nacional de La Plata and CONICET, La Plata, Argentina
[74] Physics Department, Lancaster University, Lancaster, UK
[75] [(a)]INFN Sezione di Lecce, Lecce, Italy; [(b)]Dipartimento di Matematica e Fisica, Università del Salento, Lecce, Italy
[76] Oliver Lodge Laboratory, University of Liverpool, Liverpool, UK
[77] Department of Physics, Jožef Stefan Institute, University of Ljubljana, Ljubljana, Slovenia
[78] School of Physics and Astronomy, Queen Mary University of London, London, UK
[79] Department of Physics, Royal Holloway University of London, Surrey, UK
[80] Department of Physics and Astronomy, University College London, London, UK
[81] Louisiana Tech University, Ruston, LA, USA
[82] Laboratoire de Physique Nucléaire et de Hautes Energies, UPMC and Université Paris-Diderot and CNRS/IN2P3, Paris, France
[83] Fysiska institutionen, Lunds universitet, Lund, Sweden
[84] Departamento de Fisica Teorica C-15, Universidad Autonoma de Madrid, Madrid, Spain
[85] Institut für Physik, Universität Mainz, Mainz, Germany
[86] School of Physics and Astronomy, University of Manchester, Manchester, UK
[87] CPPM, Aix-Marseille Université and CNRS/IN2P3, Marseille, France
[88] Department of Physics, University of Massachusetts, Amherst, MA, USA
[89] Department of Physics, McGill University, Montreal, QC, Canada
[90] School of Physics, University of Melbourne, Victoria, Australia
[91] Department of Physics, The University of Michigan, Ann Arbor, MI, USA
[92] Department of Physics and Astronomy, Michigan State University, East Lansing, MI, USA
[93] [(a)]INFN Sezione di Milano, Milan, Italy; [(b)]Dipartimento di Fisica, Università di Milano, Milan, Italy
[94] B.I. Stepanov Institute of Physics, National Academy of Sciences of Belarus, Minsk, Republic of Belarus
[95] National Scientific and Educational Centre for Particle and High Energy Physics, Minsk, Republic of Belarus
[96] Group of Particle Physics, University of Montreal, Montreal, QC, Canada
[97] P.N. Lebedev Physical Institute of the Russian, Academy of Sciences, Moscow, Russia
[98] Institute for Theoretical and Experimental Physics (ITEP), Moscow, Russia
[99] National Research Nuclear University MEPhI, Moscow, Russia

[100] D.V. Skobeltsyn Institute of Nuclear Physics, M.V. Lomonosov Moscow State University, Moscow, Russia
[101] Fakultät für Physik, Ludwig-Maximilians-Universität München, Munich, Germany
[102] Max-Planck-Institut für Physik (Werner-Heisenberg-Institut), Munich, Germany
[103] Nagasaki Institute of Applied Science, Nagasaki, Japan
[104] Graduate School of Science and Kobayashi-Maskawa Institute, Nagoya University, Nagoya, Japan
[105] [(a)]INFN Sezione di Napoli, Naples, Italy; [(b)]Dipartimento di Fisica, Università di Napoli, Naples, Italy
[106] Department of Physics and Astronomy, University of New Mexico, Albuquerque, NM, USA
[107] Institute for Mathematics Astrophysics and Particle Physics, Radboud University Nijmegen/Nikhef, Nijmegen, The Netherlands
[108] Nikhef National Institute for Subatomic Physics and University of Amsterdam, Amsterdam, The Netherlands
[109] Department of Physics, Northern Illinois University, DeKalb, IL, USA
[110] Budker Institute of Nuclear Physics, SB RAS, Novosibirsk, Russia
[111] Department of Physics, New York University, New York, NY, USA
[112] Ohio State University, Columbus, OH, USA
[113] Faculty of Science, Okayama University, Okayama, Japan
[114] Homer L. Dodge Department of Physics and Astronomy, University of Oklahoma, Norman, OK, USA
[115] Department of Physics, Oklahoma State University, Stillwater, OK, USA
[116] Palacký University, RCPTM, Olomouc, Czech Republic
[117] Center for High Energy Physics, University of Oregon, Eugene, OR, USA
[118] LAL, Univ. Paris-Sud, CNRS/IN2P3, Université Paris-Saclay, Orsay, France
[119] Graduate School of Science, Osaka University, Osaka, Japan
[120] Department of Physics, University of Oslo, Oslo, Norway
[121] Department of Physics, Oxford University, Oxford, UK
[122] [(a)]INFN Sezione di Pavia, Pavia, Italy; [(b)]Dipartimento di Fisica, Università di Pavia, Pavia, Italy
[123] Department of Physics, University of Pennsylvania, Philadelphia, PA, USA
[124] National Research Centre "Kurchatov Institute" B.P. Konstantinov Petersburg Nuclear Physics Institute, St. Petersburg, Russia
[125] [(a)]INFN Sezione di Pisa, Pisa, Italy; [(b)]Dipartimento di Fisica E. Fermi, Università di Pisa, Pisa, Italy
[126] Department of Physics and Astronomy, University of Pittsburgh, Pittsburgh, PA, USA
[127] [(a)]Laboratório de Instrumentação e Física Experimental de Partículas-LIP, Lisbon, Portugal; [(b)]Faculdade de Ciências, Universidade de Lisboa, Lisbon, Portugal; [(c)]Department of Physics, University of Coimbra, Coimbra, Portugal; [(d)]Centro de Física Nuclear da Universidade de Lisboa, Lisbon, Portugal; [(e)]Departamento de Fisica, Universidade do Minho, Braga, Portugal; [(f)]Departamento de Fisica Teorica y del Cosmos and CAFPE, Universidad de Granada, Granada, Spain; [(g)]Dep Fisica and CEFITEC of Faculdade de Ciencias e Tecnologia, Universidade Nova de Lisboa, Caparica, Portugal
[128] Institute of Physics, Academy of Sciences of the Czech Republic, Prague, Czech Republic
[129] Czech Technical University in Prague, Prague, Czech Republic
[130] Faculty of Mathematics and Physics, Charles University in Prague, Prague, Czech Republic
[131] State Research Center Institute for High Energy Physics (Protvino), NRC KI, Moscow, Russia
[132] Particle Physics Department, Rutherford Appleton Laboratory, Didcot, UK
[133] [(a)]INFN Sezione di Roma, Rome, Italy; [(b)]Dipartimento di Fisica, Sapienza Università di Roma, Rome, Italy
[134] [(a)]INFN Sezione di Roma Tor Vergata, Rome, Italy; [(b)]Dipartimento di Fisica, Università di Roma Tor Vergata, Rome, Italy
[135] [(a)]INFN Sezione di Roma Tre, Rome, Italy; [(b)]Dipartimento di Matematica e Fisica, Università Roma Tre, Rome, Italy
[136] [(a)]Faculté des Sciences Ain Chock, Réseau Universitaire de Physique des Hautes Energies-Université Hassan II, Casablanca, Morocco; [(b)]Centre National de l'Energie des Sciences Techniques Nucleaires, Rabat, Morocco; [(c)]Faculté des Sciences Semlalia, Université Cadi Ayyad, LPHEA-Marrakech, Marrakesh, Morocco; [(d)]Faculté des Sciences, Université Mohamed Premier and LPTPM, Oujda, Morocco; [(e)]Faculté des , Sciences, Université Mohammed V, Rabat, Morocco
[137] DSM/IRFU (Institut de Recherches sur les Lois Fondamentales de l'Univers), CEA Saclay (Commissariat à l'Energie Atomique et aux Energies Alternatives), Gif-sur-Yvette, France
[138] Santa Cruz Institute for Particle Physics, University of California Santa Cruz, Santa Cruz, CA, USA
[139] Department of Physics, University of Washington, Seattle, WA, USA

[140] Department of Physics and Astronomy, University of Sheffield, Sheffield, UK
[141] Department of Physics, Shinshu University, Nagano, Japan
[142] Fachbereich Physik, Universität Siegen, Siegen, Germany
[143] Department of Physics, Simon Fraser University, Burnaby, BC, Canada
[144] SLAC National Accelerator Laboratory, Stanford, CA, USA
[145] [(a)]Faculty of Mathematics, Physics and Informatics, Comenius University, Bratislava, Slovakia; [(b)]Department of Subnuclear Physics, Institute of Experimental Physics of the Slovak Academy of Sciences, Kosice, Slovak Republic
[146] [(a)]Department of Physics, University of Cape Town, Cape Town, South Africa; [(b)]Department of Physics, University of Johannesburg, Johannesburg, South Africa; [(c)]School of Physics, University of the Witwatersrand, Johannesburg, South Africa
[147] [(a)]Department of Physics, Stockholm University, Stockholm, Sweden; [(b)]The Oskar Klein Centre, Stockholm, Sweden
[148] Physics Department, Royal Institute of Technology, Stockholm, Sweden
[149] Departments of Physics and Astronomy and Chemistry, Stony Brook University, Stony Brook, NY, USA
[150] Department of Physics and Astronomy, University of Sussex, Brighton, UK
[151] School of Physics, University of Sydney, Sydney, Australia
[152] Institute of Physics, Academia Sinica, Taipei, Taiwan
[153] Department of Physics, Technion: Israel Institute of Technology, Haifa, Israel
[154] Raymond and Beverly Sackler School of Physics and Astronomy, Tel Aviv University, Tel Aviv, Israel
[155] Department of Physics, Aristotle University of Thessaloniki, Thessaloniki, Greece
[156] International Center for Elementary Particle Physics and Department of Physics, The University of Tokyo, Tokyo, Japan
[157] Graduate School of Science and Technology, Tokyo Metropolitan University, Tokyo, Japan
[158] Department of Physics, Tokyo Institute of Technology, Tokyo, Japan
[159] Department of Physics, University of Toronto, Toronto, ON, Canada
[160] [(a)]TRIUMF, Vancouver, BC, Canada; [(b)]Department of Physics and Astronomy, York University, Toronto, ON, Canada
[161] Faculty of Pure and Applied Sciences, and Center for Integrated Research in Fundamental Science and Engineering, University of Tsukuba, Tsukuba, Japan
[162] Department of Physics and Astronomy, Tufts University, Medford, MA, United States of America
[163] Department of Physics and Astronomy, University of California Irvine, Irvine, CA, USA
[164] [(a)]INFN Gruppo Collegato di Udine, Sezione di Trieste, Udine, Italy; [(b)]ICTP, Trieste, Italy; [(c)]Dipartimento di Chimica, Fisica e Ambiente, Università di Udine, Udine, Italy
[165] Department of Physics and Astronomy, University of Uppsala, Uppsala, Sweden
[166] Department of Physics, University of Illinois, Urbana, IL, USA
[167] Instituto de Fisica Corpuscular (IFIC) and Departamento de Fisica Atomica, Molecular y Nuclear and Departamento de Ingeniería Electrónica and Instituto de Microelectrónica de Barcelona (IMB-CNM), University of Valencia and CSIC, Valencia, Spain
[168] Department of Physics, University of British Columbia, Vancouver, BC, Canada
[169] Department of Physics and Astronomy, University of Victoria, Victoria, BC, Canada
[170] Department of Physics, University of Warwick, Coventry, UK
[171] Waseda University, Tokyo, Japan
[172] Department of Particle Physics, The Weizmann Institute of Science, Rehovot, Israel
[173] Department of Physics, University of Wisconsin, Madison, WI, USA
[174] Fakultät für Physik und Astronomie, Julius-Maximilians-Universität, Würzburg, Germany
[175] Fakultät für Mathematik und Naturwissenschaften, Fachgruppe Physik, Bergische Universität Wuppertal, Wuppertal, Germany
[176] Department of Physics, Yale University, New Haven, CT, USA
[177] Yerevan Physics Institute, Yerevan, Armenia
[178] Centre de Calcul de l'Institut National de Physique Nucléaire et de Physique des Particules (IN2P3), Villeurbanne, France

[a] Also at Department of Physics, King's College London, London, UK
[b] Also at Institute of Physics, Azerbaijan Academy of Sciences, Baku, Azerbaijan
[c] Also at Novosibirsk State University, Novosibirsk, Russia
[d] Also at TRIUMF, Vancouver, BC, Canada
[e] Also at Department of Physics & Astronomy, University of Louisville, Louisville, KY, USA

[f] Also at Department of Physics, California State University, Fresno, CA, USA
[g] Also at Department of Physics, University of Fribourg, Fribourg, Switzerland
[h] Also at Departament de Fisica de la Universitat Autonoma de Barcelona, Barcelona, Spain
[i] Also at Departamento de Fisica e Astronomia, Faculdade de Ciencias, Universidade do Porto, Portugal
[j] Also at Tomsk State University, Tomsk, Russia
[k] Also at Universita di Napoli Parthenope, Napoli, Italy
[l] Also at Institute of Particle Physics (IPP), Canada
[m] Also at National Institute of Physics and Nuclear Engineering, Bucharest, Romania
[n] Also at Department of Physics, St. Petersburg State Polytechnical University, St. Petersburg, Russia
[o] Also at Department of Physics, The University of Michigan, Ann Arbor, MI, USA
[p] Also at Centre for High Performance Computing, CSIR Campus, Rosebank, Cape Town, South Africa
[q] Also at Louisiana Tech University, Ruston, LA, USA
[r] Also at Institucio Catalana de Recerca i Estudis Avancats, ICREA, Barcelona, Spain
[s] Also at Graduate School of Science, Osaka University, Osaka, Japan
[t] Also at Department of Physics, National Tsing Hua University, Taiwan
[u] Also at Institute for Mathematics, Astrophysics and Particle Physics, Radboud University Nijmegen/Nikhef, Nijmegen, Netherlands
[v] Also at Department of Physics, The University of Texas at Austin, Austin, TX, USA
[w] Also at Institute of Theoretical Physics, Ilia State University, Tbilisi, Georgia
[x] Also at CERN, Geneva, Switzerland
[y] Also at Georgian Technical University (GTU),Tbilisi, Georgia
[z] Also at Ochadai Academic Production, Ochanomizu University, Tokyo, Japan
[aa] Also at Manhattan College, New York, NY, USA
[ab] Also at Hellenic Open University, Patras, Greece
[ac] Also at Academia Sinica Grid Computing, Institute of Physics, Academia Sinica, Taipei, Taiwan
[ad] Also at School of Physics, Shandong University, Shandong, China
[ae] Also at Moscow Institute of Physics and Technology State University, Dolgoprudny, Russia
[af] Also at Section de Physique, Université de Genève, Geneva, Switzerland
[ag] Also at Eotvos Lorand University, Budapest, Hungary
[ah] Also at Departments of Physics & Astronomy and Chemistry, Stony Brook University, Stony Brook, NY, USA
[ai] Also at International School for Advanced Studies (SISSA), Trieste, Italy
[aj] Also at Department of Physics and Astronomy, University of South Carolina, Columbia, SC, USA
[ak] Also at School of Physics and Engineering, Sun Yat-sen University, Guangzhou, China
[al] Also at Institute for Nuclear Research and Nuclear Energy (INRNE) of the Bulgarian Academy of Sciences, Sofia, Bulgaria
[am] Also at Faculty of Physics, M.V. Lomonosov Moscow State University, Moscow, Russia
[an] Also at Institute of Physics, Academia Sinica, Taipei, Taiwan
[ao] Also at National Research Nuclear University MEPhI, Moscow, Russia
[ap] Also at Department of Physics, Stanford University, Stanford, CA, USA
[aq] Also at Institute for Particle and Nuclear Physics, Wigner Research Centre for Physics, Budapest, Hungary
[ar] Also at Flensburg University of Applied Sciences, Flensburg, Germany
[as] Also at University of Malaya, Department of Physics, Kuala Lumpur, Malaysia
[at] Also at CPPM, Aix-Marseille Université and CNRS/IN2P3, Marseille, France
* Deceased

Physics Letters B 761 (2016) 350–371

Contents lists available at ScienceDirect

Physics Letters B

www.elsevier.com/locate/physletb

Measurement of the top quark mass in the $t\bar{t} \to$ dilepton channel from $\sqrt{s} = 8$ TeV ATLAS data

The ATLAS Collaboration *

ARTICLE INFO

Article history:
Received 8 June 2016
Received in revised form 21 July 2016
Accepted 8 August 2016
Available online 24 August 2016
Editor: W.-D. Schlatter

ABSTRACT

The top quark mass is measured in the $t\bar{t} \to$ dilepton channel (lepton $= e, \mu$) using ATLAS data recorded in the year 2012 at the LHC. The data were taken at a proton–proton centre-of-mass energy of $\sqrt{s} = 8$ TeV and correspond to an integrated luminosity of about 20.2 fb^{-1}. Exploiting the template method, and using the distribution of invariant masses of lepton–b-jet pairs, the top quark mass is measured to be $m_{\text{top}} = 172.99 \pm 0.41$ (stat) ± 0.74 (syst) GeV, with a total uncertainty of 0.84 GeV. Finally, a combination with previous ATLAS m_{top} measurements from $\sqrt{s} = 7$ TeV data in the $t\bar{t} \to$ dilepton and $t\bar{t} \to$ lepton + jets channels results in $m_{\text{top}} = 172.84 \pm 0.34$ (stat) ± 0.61 (syst) GeV, with a total uncertainty of 0.70 GeV.

1. Introduction

The mass of the top quark (m_{top}) is an important parameter of the Standard Model (SM) of particle physics. Precise measurements of m_{top} provide crucial information for global fits of electroweak parameters [1–3] which help assess the internal consistency of the SM and to probe its extensions. In addition, the value of m_{top} affects the stability of the SM Higgs potential, which has cosmological implications [4–6]. Many measurements of m_{top} have been performed by the Tevatron and LHC Collaborations. Combining a selection of those, the first Tevatron+LHC m_{top} result is $m_{\text{top}} = 173.34 \pm 0.27$ (stat) ± 0.71 (syst) GeV, with a total uncertainty of 0.76 GeV [7]. Meanwhile, a number of new results have become available [8–13], some of which are more precise than the above combination. The latest ATLAS results in the $t\bar{t} \to$ lepton + jets and $t\bar{t} \to$ dilepton decay channels, both with electrons (e) and muons (μ) in the final state [14], are $m_{\text{top}} = 172.33 \pm 0.75$ (stat) $\pm$ 1.02 (syst) GeV and $m_{\text{top}} = 173.79 \pm 0.54$ (stat) ± 1.30 (syst) GeV, respectively.

This Letter presents a new measurement of m_{top} obtained in the $t\bar{t} \to$ dilepton decay channel using 2012 data taken at a proton–proton (pp) centre-of-mass energy of $\sqrt{s} = 8$ TeV, with an integrated luminosity of about 20.2 fb^{-1}. The analysis exploits the decay $t\bar{t} \to W^+W^-b\bar{b} \to \ell^+\ell^-\nu\bar{\nu}b\bar{b}$, which is realised when both W bosons decay into a charged lepton and its corresponding neutrino. In the analysis, the $t\bar{t}$ decay channels ee, $e\mu$ and $\mu\mu$ (including $\tau \to e, \mu$) are combined and referred to as the dilepton channel. Single-top-quark events with the same lepton final states are included in the signal. Given the larger data sample compared to Ref. [14], the event selection was optimised to achieve the smallest total uncertainty. The measurement is based on the implementation of the template method described in Ref. [14], which is calibrated using signal Monte Carlo (MC) samples. Consequently, the top quark mass measured in this way corresponds to the mass definition used in the MC program.

2. ATLAS detector

The ATLAS experiment [15] at the LHC is a multi-purpose particle detector with a forward–backward symmetric cylindrical geometry and a near 4π coverage in solid angle.[1] It consists of an inner tracking detector surrounded by a thin superconducting solenoid providing a 2 T axial magnetic field, electromagnetic and hadron calorimeters, and a muon spectrometer. The inner tracking detector covers the pseudorapidity range $|\eta| < 2.5$. It consists of silicon pixel, silicon microstrip, and transition radiation tracking detectors. Lead/liquid-argon (LAr) sampling calorimeters provide electromagnetic (EM) energy measurements with high granularity. A hadronic (steel/scintillator-tile) calorimeter covers the central pseudorapidity range ($|\eta| < 1.7$). The end-cap and forward regions are instrumented with LAr calorimeters for EM and hadronic energy mea-

[1] ATLAS uses a right-handed coordinate system with its origin at the nominal interaction point (IP) in the centre of the detector and the z-axis along the beam pipe. The x-axis points from the IP to the centre of the LHC ring, and the y-axis points upwards. Cylindrical coordinates (r, ϕ) are used in the transverse plane, ϕ being the azimuthal angle around the z-axis. The pseudorapidity is defined in terms of the polar angle θ as $\eta = -\ln\tan(\theta/2)$. Angular distance is measured in units of $\Delta R \equiv \sqrt{(\Delta\eta)^2 + (\Delta\phi)^2}$.

* *E-mail address:* atlas.publications@cern.ch.

http://dx.doi.org/10.1016/j.physletb.2016.08.042

surements up to $|\eta| = 4.9$. The muon spectrometer surrounds the calorimeters and is based on three large air–core toroid superconducting magnets with eight coils each. Its bending power is in the range from 2.0 to 7.5 T m. It includes a system of precision tracking chambers and fast detectors for triggering. A three-level trigger system is used to select events. The first-level trigger is implemented in hardware and uses a subset of the detector information to reduce the accepted event rate to at most 75 kHz. This is followed by two software-based trigger levels that together reduce the accepted rate to 400 Hz on average depending on the data-taking conditions during 2012.

3. Data and MC samples

This analysis is based on pp collision data recorded in 2012 at $\sqrt{s} = 8$ TeV. The integrated data luminosity amounts to 20.2 fb^{-1} with an uncertainty of 1.9% determined with the procedures described in Ref. [16].

The modelling of $t\bar{t}$ and single-top-quark signal events and of most background processes relies on MC simulations. For the simulation of signal events the POWHEG-BOX program [17–19] is used. The simulation of the top quark pair [20] and single-top-quark production in the Wt-channel [21] uses matrix elements at next-to-leading order (NLO) in the strong coupling constant α_S, with the NLO CT10 [22] parton distribution function (PDF) and the parameter $h_{\text{damp}} = \infty$. The h_{damp} parameter sets the resummation scale, which controls the transition from the matrix element to the parton shower (PS) simulation. Given that the event selection described below requires leptonic decay products of two W bosons, single-top-quark events in the s-channel and t-channel are found not to contribute to the sample.

The PYTHIA (v6.425) program [23] with the P2011C [24] set of tuned parameters (tune) and the corresponding CTEQ6L1 PDF [25] are employed to provide the parton shower, hadronisation and underlying-event modelling. The uncertainties due to QCD initial- and final-state radiation (ISR/FSR) modelling are estimated with samples generated with the POWHEG-BOX program interfaced to the PYTHIA program for which the parameters of the generation are varied to span the ranges compatible with the results of measurements of $t\bar{t}$ production in association with jets [26–28].

For m_{top} hypothesis testing, the $t\bar{t}$ and single-top-quark event samples are generated for five values of m_{top} in the range 167.5 to 177.5 GeV in steps of 2.5 GeV. For each m_{top} value, the MC samples are normalised according to the best available cross-section calculations, which for $m_{\text{top}} = 172.5$ GeV are $\sigma_{t\bar{t}} = 253^{+13}_{-15}$ pb [29–34] for $t\bar{t}$ production and $\sigma_{Wt} = 22.4 \pm 1.5$ pb [35] for single-top-quark production in the Wt-channel. The PDF + α_S-induced uncertainties in these cross-sections are calculated using the PDF4LHC prescription [36] with the MSTW2008 68% CL NNLO PDF [37,38], CT10 NNLO PDF [22,39] and NNPDF2.3 5f FFN PDF [40], and are added in quadrature with the uncertainties due to the choices of the factorisation and renormalisation scales.

The simulation of $W^{\pm}$ or Z boson production in association with jets is performed with the ALPGEN (v2.13) program [41] interfaced to the PYTHIA6 program using the CTEQ6L1 PDF and the corresponding AUET2 tune [42]. Diboson production processes (WW, WZ and ZZ) are simulated using the ALPGEN program interfaced to the HERWIG (v6.520) program [43] with the AUET2 tune and to the JIMMY (v4.31) program [44]. All samples are simulated taking into account the effects of multiple soft pp interactions (pile-up) registered in the 2012 data. These interactions are modelled by overlaying simulated hits from events with exactly one inelastic (signal) collision per bunch crossing with hits from minimum-bias events that are produced with the PYTHIA (v8.160) program [45] using the A2M tune [46] and the MSTW2008 LO PDF. For this analysis, the observed values of the pile-up-related quantities $\langle\mu\rangle$, the mean number of interactions per bunch crossing, and n_{vtx}, the average number of vertices per event, are $\langle\mu\rangle = 20.7$ and $n_{\text{vtx}} = 9.2$.

Finally, the samples undergo a simulation of the ATLAS detector [47] based on GEANT4 [48], and are then processed through the same reconstruction software as the data. A number of samples used to assess systematic uncertainties are produced with a faster version of the simulation which, in addition to the full simulation of the tracking, uses smearing functions and interpolates particle behaviour and calorimeter response, based on resolution functions measured in full-simulation studies, to approximate the results of the full simulation.

4. Data selection and event reconstruction

Triggers based on isolated single electrons or muons with energy or momentum thresholds of 24 GeV are used. The detector objects resulting from the top quark pair decay are electron and muon candidates, jets and missing transverse momentum ($E_{\text{T}}^{\text{miss}}$). In the following, the term lepton is used for charged leptons (excluding τ leptons) exclusively.

Electron candidates [49] are required to have a transverse energy of $E_{\text{T}} > 25$ GeV, a pseudorapidity of the corresponding EM cluster of $|\eta_{\text{cluster}}| < 2.47$, with the transition region $1.37 < |\eta_{\text{cluster}}| < 1.52$ between the barrel and the end-cap calorimeter excluded. The muon candidates [50] are required to have transverse momentum $p_{\text{T}} > 25$ GeV and $|\eta| < 2.5$. To reduce the contamination by leptons from heavy-flavour decays inside jets or from photon conversions, referred to as non-prompt (NP) leptons, strict isolation criteria are applied to the amount of activity in the vicinity of the lepton candidate [49,50].

Jets are built from topological clusters of calorimeter cells [51] with the anti-k_t jet clustering algorithm [52] using a radius parameter of $R = 0.4$. Jets are reconstructed using the local cluster weighting (LCW) and global sequential calibration (GSC) algorithms [53–55] and required to satisfy $p_{\text{T}} > 25$ GeV and $|\eta| < 2.5$. Muons reconstructed within a $\Delta R = 0.4$ cone around the axis of a jet with $p_{\text{T}} > 25$ GeV are not considered as charged-lepton candidates. In addition, jets within a $\Delta R = 0.2$ cone around an electron candidate are removed and finally electrons within a $\Delta R = 0.4$ cone around any of the remaining jets are discarded. The identification of jets containing b-hadrons, b-tagging, is used for event reconstruction and background suppression. In the following, irrespective of their origin, jets tagged by the b-tagging algorithm are referred to as b-tagged jets, whereas those not tagged are referred to as untagged jets. Similarly, whether they are tagged or not, jets originating from bottom quarks are referred to as b-jets and those from (u, d, c, s)-quarks or gluons as light jets. The working point of the neural-network-based MV1 b-tagging algorithm [56] corresponds to an average b-tagging efficiency of 70% for b-jets in simulated $t\bar{t}$ events and rejection factors of 5 for jets containing a c-hadron and 137 for jets containing only lighter-flavour hadrons. To match the b-tagging performance in the data, p_{T}- and η-dependent scale factors [56], obtained from dijet and $t\bar{t} \rightarrow$ dilepton events, are applied to MC jets depending on their true flavour. The reconstruction of the $E_{\text{T}}^{\text{miss}}$ is based on the vector sum of energy deposits in the calorimeters, projected onto the transverse plane. Muons are included in the $E_{\text{T}}^{\text{miss}}$ using their reconstructed momentum in the tracking detectors [57].

The contribution of events wrongly reconstructed as $t\bar{t} \rightarrow$ dilepton events due to the presence of objects misidentified as leptons (fake leptons), is estimated from data [58]. The technique employed uses fake-lepton and real-lepton efficiencies that depend on η and p_{T}, measured in a background-enhanced control region

Table 1
The observed numbers of events in data after the pre-selection and the final selection. In addition, the expected numbers of signal events for $m_{\text{top}} = 172.5$ GeV and background events corresponding to the integrated data luminosity are given. Two significant digits are used for the uncertainties of the predicted numbers of events explained in the text. The lower rows report the matching performance evaluated for $m_{\text{top}} = 172.5$ GeV, using one significant digit for the statistical uncertainties.

Selection	Pre-selection	Final selection
Data	36 359	9426
$t\bar{t}$ signal	$34\,300 \pm 2700$	9670 ± 770
Single-top-quark signal	1690 ± 110	363 ± 23
Fake leptons	240 ± 240	31 ± 31
Z + jets	212 ± 83	20.6 ± 8.5
$WW/WZ/ZZ$	57 ± 21	10.2 ± 3.8
Signal + background	$36\,600 \pm 2800$	$10\,100 \pm 770$
Expected background fraction	0.01 ± 0.01	0.01 ± 0.00
Data/(Signal + background)	0.99 ± 0.07	0.93 ± 0.07
Matching efficiency [%]	78.4 ± 0.2	95.3 ± 0.4
Selection purity [%]	51.6 ± 0.1	69.8 ± 0.3
Unmatched events [%]	34.2 ± 0.1	26.7 ± 0.1
Wrongly matched events [%]	14.2 ± 0.1	3.4 ± 0.0

with low $E_{\text{T}}^{\text{miss}}$ and from events with dilepton masses around the Z peak [59].

The selection from Ref. [14] is applied as a pre-selection as follows:

1. Events are required to have a signal from the single-electron or single-muon trigger and at least one primary vertex with at least five associated tracks.
2. Exactly two oppositely charged leptons are required, with at least one of them matching the reconstructed object that fired the corresponding trigger.
3. In the same-lepton-flavour channels, ee and $\mu\mu$, $E_{\text{T}}^{\text{miss}} > 60$ GeV is required. In addition, the invariant mass of the lepton pair must satisfy $m_{\ell\ell} > 15$ GeV, and must not be compatible with the Z mass within 10 GeV.
4. In the $e\mu$ channel the scalar sum of p_{T} of the two selected leptons and all jets is required to be larger than 130 GeV.
5. The presence of at least two jets with $p_{\text{T}} > 25$ GeV and $|\eta| < 2.5$ is required, and at least one of these jets has to be b-tagged.

The observed numbers of events in the data after this pre-selection, together with the expected numbers of signal and background events corresponding to the integrated data luminosity, are given in Table 1. Assuming a top quark mass of $m_{\text{top}} = 172.5$ GeV, the predicted number of events is consistent with the one observed in the data within uncertainties. For all predictions, the uncertainties are estimated as the sum in quadrature of the statistical uncertainty, a 1.9% uncertainty in the integrated luminosity, and a number of additional components. For the signal, these are a 5.4% uncertainty in the $t\bar{t}$ cross-section, or a 6.0% uncertainty in the single-top-quark cross-section, as given in Sect. 3. Finally, global 4.1%, 2.2% and 2.8% uncertainties are added, corresponding to the envelopes of the results from the eigenvector variations of the jet energy scale (JES), the relative b-to-light-jet energy scale (bJES) and the b-tagging scale factors, respectively. The background uncertainties contain jet-multiplicity-dependent uncertainties of about 40% in the normalisation of the Z + jets background and a 100% uncertainty in the normalisation of fake-lepton background.

The two jets carrying the highest MV1 weight are taken as the two b-jets originating from the decays of the two top quarks, and the two leptons are taken as the leptons from the leptonic W decays. From the two possible assignments of the two pairs, the combination leading to the lowest average invariant mass of the two lepton–b-jet pairs ($m_{\ell b}$) is retained. To estimate the performance of this algorithm in MC simulated samples, the reconstruction-level objects are matched to the closest generator-level object based on a maximum allowed ΔR, being 0.1 for leptons and 0.3 for jets. A matched object is defined as a reconstruction-level object that falls within ΔR of any generator-level object of that type, and a correct match means that this generator-level object is the one it originated from. Due to acceptance losses and reconstruction inefficiency, not all reconstruction-level objects can successfully be matched to their generator-level counterparts, resulting in unmatched events. The matching efficiency is the fraction of correctly matched events among all the matched events, and the selection purity is the fraction of correctly matched events among all events, regardless of whether they could be matched or not. The corresponding numbers for $m_{\text{top}} = 172.5$ GeV are reported in Table 1.

Starting from this pre-selection, an optimisation of the total uncertainty in m_{top} is performed. A phase-space restriction based on the average p_{T} of the two lepton–b-jet pairs ($p_{\text{T},\ell b}$) is used to obtain the smallest total uncertainty in m_{top}. The corresponding $p_{\text{T},\ell b}$ distribution is shown in Fig. 1(a). The smallest uncertainty in m_{top} corresponds to $p_{\text{T},\ell b} > 120$ GeV. The difference in shape between data and prediction is covered by the systematic uncertainty as detailed in Sect. 6. This restriction is found to also increase the fraction of correctly matched events in the $t\bar{t}$ sample, and reduces the number of unmatched or wrongly matched events.

To perform the template parameterisation described in Sect. 5, an additional selection criterion is applied, restricting the reconstructed $m_{\ell b}$ value ($m_{\ell b}^{\text{reco}}$) to the range $30\ \text{GeV} < m_{\ell b}^{\text{reco}} < 170$ GeV. Applying both restrictions, the numbers of predicted and observed events resulting from the final selection are reported in Table 1. Using this optimisation, the matching efficiency and the sample purity are much improved as reported in the bottom rows of Table 1, while retaining about 26% of the events. Using this selection, and the objects assigned to the two lepton–b-jet pairs, the kinematic distributions in the data are well described by the predictions, as shown in Fig. 1 for the transverse momenta of b-jets and leptons, and for the $\Delta R_{\ell b}$ of the two lepton–b-jet pairs.

5. Template fit and results in the data

The implementation of the template method used in this analysis is described in Ref. [14]. For this analysis, the templates are simulated distributions of $m_{\ell b}^{\text{reco}}$, constructed for a number of discrete values of m_{top}. Appropriate functions are fitted to these templates, interpolating between different input m_{top}. The remaining parameters of the functions are fixed by a simultaneous fit to all templates, imposing linear dependences of the parameters on m_{top}. The resulting template fit function has m_{top} as the only free parameter and an unbinned likelihood maximisation gives the value of m_{top} that best describes the data. Statistically independent signal templates, comprising $t\bar{t}$ and single-top-quark events, are constructed as a function of the top quark mass used in the MC generator. Within the statistical uncertainties, the sum of a Gaussian distribution and a Landau function gives a good description of the shape of the $m_{\ell b}^{\text{reco}}$ distribution as shown in Fig. 2(a) for three values of m_{top}. With this signal choice, the background distribution is independent of m_{top}, and a Landau function is fitted to it. The sum of the signal template at $m_{\text{top}} = 172.5$ GeV and the background is compared to data in Fig. 2(b). It gives a good description of the data except for differences that can be accounted for by a different

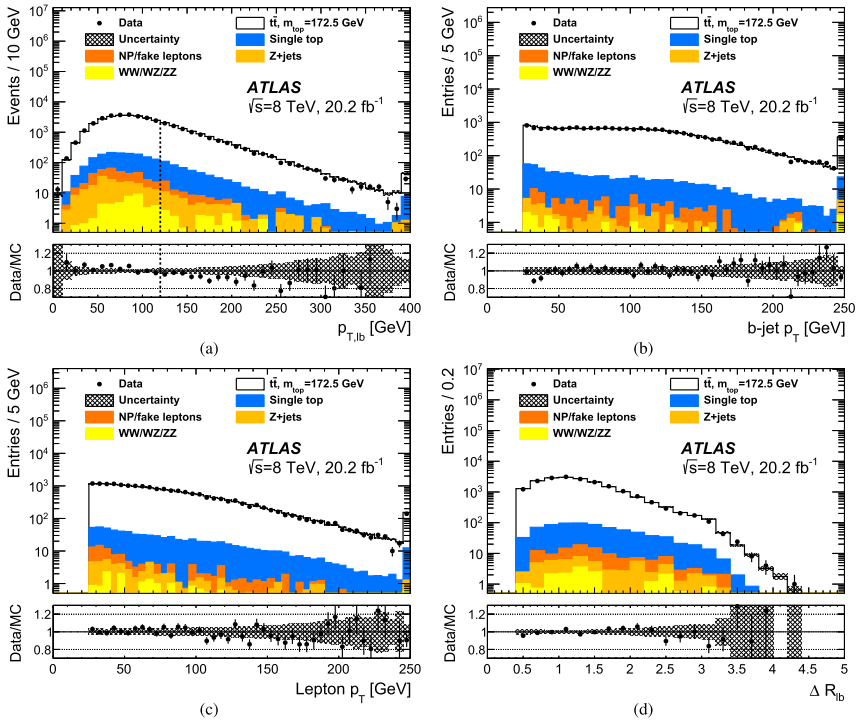

Fig. 1. Kinematic distributions obtained from the objects assigned to the two lepton–b-jet pairs for (a) the pre-selection, or (b)–(d) the final selection. The average p_{T} of the two lepton–b-jet pairs, denoted by $p_{\mathrm{T},\ell b}$, is shown in (a). The $p_{\mathrm{T},\ell b}$ requirement for the final selection is indicated by the vertical dashed line. The remaining distributions show the p_{T} of the b-jets in (b), the p_{T} of the leptons in (c), and the $\Delta R_{\ell b}$ of the lepton and the b-jet for the two lepton–b-jet pairs in (d). The rightmost bin contains the overflow, if present. For all distributions, the number of predicted events is normalised to the one observed in the data. The hatched area corresponds to the statistical uncertainties in the prediction, the uncertainty bars to the statistical uncertainties in the data. For each figure, the ratio of data and prediction is also presented.

top quark mass. In this distribution, the correctly matched events are concentrated in the central part, whereas the remainder is less peaked and accounts for most of the tails.

In this analysis the expected statistical precision as well as all systematic uncertainties are obtained from pseudo-experiments generated from MC simulated samples mimicking ATLAS data. To verify the internal consistency of the method, 1000 pseudo-experiments per mass point are performed, correcting for oversampling [60]. Within uncertainties, and for all m_{top} values, the residuals and pull means are consistent with zero and the pull widths are consistent with unity, i.e. the estimator is unbiased and uncertainties are calculated properly. The expected statistical uncertainty is obtained from the distribution of the statistical uncertainty in the fitted m_{top} of the pseudo-experiments. For $m_{\mathrm{top}} = 172.5$ GeV and the data luminosity it amounts to 0.41 ± 0.03 GeV, where the quoted precision is statistical. The $m_{\ell b}^{\mathrm{reco}}$ distribution in the data is shown in Fig. 2(c) together with the corresponding fitted probability density functions for the background alone and for the sum of signal and background. The value obtained fixing the background contribution to its prediction is $m_{\mathrm{top}} = 172.99 \pm 0.41$ (stat) GeV. The statistical uncertainty in m_{top} is taken from the parabolic approximation of the logarithm of the likelihood as shown in Fig. 2(d). The observed and predicted values of the statistical uncertainty agree.

6. Uncertainties affecting the m_{top} determination

The same systematic uncertainty sources as in Ref. [14] are investigated. Their impact on the analysis is mostly evaluated from pairs of samples expressing a particular systematic uncertainty, by constructing the corresponding templates and measuring the average difference in m_{top} of the pair from 1000 pseudo-experiments. To facilitate a combination with other results, every systematic uncertainty is assigned a statistical uncertainty, taking into account the statistical correlation of the considered samples. Following Ref. [61], the resulting uncertainty components are given in Table 2 irrespective of their statistical significance. The uncertainty sources are constructed so as to be uncorrelated with each another and thus the total uncertainty squared is calculated as the sum in quadrature of all components. The various sources of systematic uncertainties and the evaluation of their effect on m_{top} are briefly described in the following. The values are given in Table 2.

Method: The mean value of the differences between the fitted and generated m_{top} for the MC samples at various input top quark masses is assigned as the method calibration uncertainty. This also covers effects from limited numbers of MC simulated events in the templates.

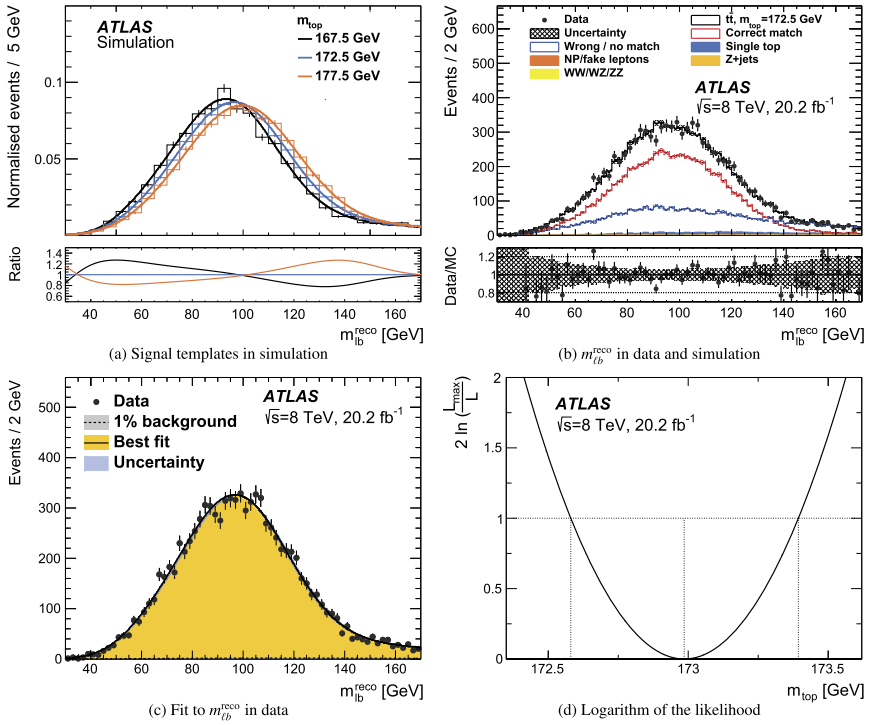

(a) Signal templates in simulation

(b) $m_{\ell b}^{\text{reco}}$ in data and simulation

(c) Fit to $m_{\ell b}^{\text{reco}}$ in data

(d) Logarithm of the likelihood

Fig. 2. Simulated signal templates (histograms) for different values of m_{top} together with the template fits (curves) are given in (a). The $m_{\ell b}^{\text{reco}}$ distribution observed in data in comparison to the prediction is shown in (b). Both figures show statistical uncertainties only. In (b) the background contributions are too small to be distinguished. The $m_{\ell b}^{\text{reco}}$ distribution is shown in (c) for data with statistical uncertainties together with the fitted probability density functions for the background alone (barely visible at the bottom of the figure) and for the sum of signal and background. The uncertainty band corresponds to the total uncertainty in m_{top}. Finally, the corresponding logarithm of the likelihood as a function of m_{top} is displayed in (d).

Signal Monte Carlo generator: The difference in m_{top} between the event sample produced with the MC@NLO program [62,63] and the default POWHEG sample, both generated at $m_{\text{top}} = 172.5$ GeV and using the HERWIG program for parton shower, hadronisation and underlying event, is quoted as a systematic uncertainty.

Hadronisation: The difference in m_{top} between samples produced with the POWHEG-BOX program and showered with either the PYTHIA6 program using the P2011C tune or the HERWIG and JIMMY programs using the ATLAS AUET2 tune [42] is quoted as a systematic uncertainty. This includes different approaches in parton-shower modelling and hadronisation, namely the Lund string model [64,65] and the cluster model [66]. The difference in shape between data and prediction observed for the $p_{\text{T},\ell b}$ distribution shown in Fig. 1(a) is much reduced when using the POWHEG+HERWIG sample and therefore covered by this uncertainty. As a check to assess the maximum possible difference in m_{top} caused by the mismodelling of the $p_{\text{T},\ell b}$ distribution, the predicted distribution is reweighted to the data distribution and the fit is repeated. The observed difference in m_{top} from the nominal sample is about 0.2 GeV, well below the statistical uncertainty in the data. Consequently, no additional uncertainty is applied. Finally, the calibration of the JES and bJES, discussed below, is also partially based on a comparison of jet energy responses in event samples produced with the Herwig++ [67] and PYTHIA6 programs. However, it was verified [68] that the amount of double-counting of JES and hadronisation effects for the $t\bar{t} \to$ lepton + jets channel is small.

Initial- and final-state QCD radiation (ISR/FSR): The uncertainty due to this effect is evaluated by comparing two dedicated samples generated with the POWHEG-BOX and PYTHIA6 programs that differ in several parameters, namely: the QCD scale Λ_{QCD}, the transverse momentum scale for space-like parton-shower evolution Q^2_{max} and the h_{damp} parameter [69]. Half the observed difference between the up variation and the down variation is quoted as a systematic uncertainty. For comparison, using the signal samples generated at $m_{\text{top}} = 172.5$ GeV, and only changing the h_{damp} parameter but using a much larger range, i.e. from ∞ to m_{top}, the measured m_{top} is lowered by 0.23 ± 0.13 GeV, where the uncertainty is statistical.

Underlying event (UE): The difference in UE modelling is assessed by comparing POWHEG samples based on the same partonic events generated with the CT10 PDFs. The difference in m_{top} for a sample with the Perugia 2012 tune (P2012) and a sample with the P2012 mpiHi tune [24] is assigned as a systematic uncertainty.

Colour reconnection (CR): This systematic uncertainty is estimated using samples with the same partonic events as for the UE uncertainty evaluation, but with the P2012 tune and the P2012 loCR tune [24] for PS and hadronisation. The difference in m_{top} is quoted as a systematic uncertainty.

Parton distribution function (PDF): The PDF systematic uncertainty is the sum in quadrature of three contributions. These are:

Table 2
The three measured values of m_{top} together with their statistical and systematic uncertainty components are shown on the left. The middle part reports the estimated correlations ρ_{ij} per pair of measurements, with 0, 1 and 2 denoting the ℓ + jets and dilepton measurements at $\sqrt{s} = 7$ TeV (from Ref. [14]) and the dilepton measurement at $\sqrt{s} = 8$ TeV, respectively. Finally, the right part lists the m_{top} results for the combinations of the two measurements at $\sqrt{s} = 7$ TeV, the two measurements in the dilepton channel and all measurements. For the individual measurements, the systematic uncertainty in m_{top} and its associated statistical uncertainty is given for each source of uncertainty. Assigned correlations are given as integer values, determined correlations as real values. The last line refers to the sum in quadrature of the statistical and systematic uncertainty components or the total correlations, respectively.

	$\sqrt{s} = 7$ TeV		$\sqrt{s} = 8$ TeV	Correlations			Combinations		
	$m_{\text{top}}^{\ell+\text{jets}}$ [GeV]	$m_{\text{top}}^{\text{dil}}$ [GeV]	$m_{\text{top}}^{\text{dil}}$ [GeV]	ρ_{01}	ρ_{02}	ρ_{12}	$m_{\text{top}}^{7\text{ TeV}}$ [GeV]	$m_{\text{top}}^{\text{dil}}$ [GeV]	$m_{\text{top}}^{\text{all}}$ [GeV]
Results	172.33	173.79	172.99				172.99	173.04	172.84
Statistics	0.75	0.54	0.41	0	0	0	0.48	0.38	0.34
Method	0.11 ± 0.10	0.09 ± 0.07	0.05 ± 0.07	0	0	0	0.07	0.05	0.05
Signal Monte Carlo generator	0.22 ± 0.21	0.26 ± 0.16	0.09 ± 0.15	+1.00	+1.00	+1.00	0.24	0.10	0.14
Hadronisation	0.18 ± 0.12	0.53 ± 0.09	0.22 ± 0.09	+1.00	+1.00	+1.00	0.34	0.24	0.23
Initial- and final-state QCD radiation	0.32 ± 0.06	0.47 ± 0.05	0.23 ± 0.07	−1.00	−1.00	+1.00	0.04	0.24	0.08
Underlying event	0.15 ± 0.07	0.05 ± 0.05	0.10 ± 0.14	−1.00	−1.00	+1.00	0.06	0.10	0.02
Colour reconnection	0.11 ± 0.07	0.14 ± 0.05	0.03 ± 0.14	−1.00	−1.00	+1.00	0.01	0.03	0.01
Parton distribution function	0.25 ± 0.00	0.11 ± 0.00	0.05 ± 0.00	+0.57	−0.29	+0.03	0.17	0.04	0.08
Background normalisation	0.10 ± 0.00	0.04 ± 0.00	0.03 ± 0.00	+1.00	+0.23	+0.23	0.07	0.03	0.04
W/Z + jets shape	0.29 ± 0.00	0.00 ± 0.00	0	0			0.16	0.00	0.09
Fake leptons shape	0.05 ± 0.00	0.01 ± 0.00	0.08 ± 0.00	+0.23	+0.20	−0.08	0.03	0.07	0.05
Jet energy scale	0.58 ± 0.11	0.75 ± 0.08	0.54 ± 0.04	−0.23	+0.06	+0.35	0.41	0.52	0.41
Relative b-to-light-jet energy scale	0.06 ± 0.03	0.68 ± 0.02	0.30 ± 0.01	+1.00	+1.00	+1.00	0.34	0.32	0.25
Jet energy resolution	0.22 ± 0.11	0.19 ± 0.04	0.09 ± 0.05	−1.00	0	0	0.03	0.08	0.08
Jet reconstruction efficiency	0.12 ± 0.00	0.07 ± 0.00	0.01 ± 0.00	+1.00	+1.00	+1.00	0.10	0.01	0.04
Jet vertex fraction	0.01 ± 0.00	0.00 ± 0.00	0.02 ± 0.00	−1.00	+1.00	−1.00	0.00	0.02	0.02
b-tagging	0.50 ± 0.00	0.07 ± 0.00	0.03 ± 0.02	−0.77	0	0	0.25	0.03	0.15
Leptons	0.04 ± 0.00	0.13 ± 0.00	0.14 ± 0.01	−0.34	−0.52	+0.96	0.05	0.14	0.09
$E_{\text{T}}^{\text{miss}}$	0.15 ± 0.04	0.04 ± 0.03	0.01 ± 0.01	−0.15	+0.25	−0.24	0.08	0.01	0.05
Pile-up	0.02 ± 0.01	0.01 ± 0.00	0.05 ± 0.01	0	0	0	0.01	0.05	0.03
Total systematic uncertainty	1.03 ± 0.31	1.31 ± 0.23	0.74 ± 0.29				0.77	0.74	0.61
Total	1.27 ± 0.33	1.41 ± 0.24	0.84 ± 0.29	−0.07	0.00	0.51	0.91	0.84	0.70

the sum in quadrature of the differences in m_{top} for the 26 eigenvector variations of the CTEQ PDF [25] and two differences in m_{top} obtained from reweighting the central CT10 PDF set to the MSTW2008 PDF [37] and the NNPDF23 PDF [40].

Background normalisation: The normalisations are varied simultaneously for the MC-based and the data-driven background estimates according to the above mentioned uncertainties.

Background shapes: Given the negligible uncertainty in the dilepton channel observed in Ref. [14], no shape uncertainty is evaluated for the MC-based background. For the data-driven background the shape uncertainty is obtained from the estimate of fake-lepton events using the matrix method [58].

Jet energy scale (JES): Mean jet energies are measured with a relative precision of about 1% to 4%, typically falling with jet p_{T} and rising with jet $|\eta|$ [70,71]. The large number of subcomponents of the total JES uncertainty are reduced by a matrix diagonalisation of the full JES covariance matrix. For each of the resulting 25 significant nuisance parameters [54] the corresponding uncertainty in m_{top} is calculated. The total JES-induced uncertainty in m_{top} is obtained by the sum in quadrature of the results for the subcomponents.

Relative *b*-to-light-jet energy scale (bJES): The bJES is an additional uncertainty for the remaining differences between b-jets and light jets after the global JES is applied and therefore the corresponding uncertainty is uncorrelated with the JES uncertainty. Jets containing b-hadrons are assigned an additional uncertainty of 0.2% to 1.2%, with lowest uncertainties for high-p_{T} b-jets [54].

Jet energy resolution (JER): The JER uncertainty is determined by the sum in quadrature of the m_{top} differences between the varied samples and the nominal sample or, where applicable, half the fitted difference between the up variation and the down variation of the components of the eigenvector decomposition.

Jet reconstruction efficiency (JRE): The JRE uncertainty is evaluated by randomly removing 2% of the jets with $p_{\text{T}} < 30$ GeV from the MC simulated events prior to the event selection to reflect the precision with which the data-to-MC JRE ratio is known [53]. The m_{top} difference with respect to the nominal sample is taken as a systematic uncertainty.

Jet vertex fraction (JVF): When summing the scalar p_{T} of all tracks in a jet, the JVF is the fraction contributed by tracks originating at the primary vertex. The uncertainty is evaluated by varying the requirement on the JVF within its uncertainty [72].

***b*-tagging**: Mismodelling of the b-tagging efficiency and mistag rate is accounted for by the application of scale factors which depend on jet p_{T} and jet η to MC simulated events [56]. The eigenvector decomposition [56,73] accounts for the uncertainties in the b-tagging, c/τ-tagging and mistagging scale factors. The final b-tagging uncertainty is the sum in quadrature of these uncorrelated components.

Lepton uncertainties: The lepton uncertainties measured in $J/\psi \to \ell\ell$ and $Z \to \ell\ell$ events are related to the electron energy or muon momentum scales and resolutions, and the trigger and identification efficiencies [49,50,74]. For each component, the corresponding uncertainty is propagated to the analysis including the recalculation of the $E_{\text{T}}^{\text{miss}}$.

Missing transverse momentum ($E_{\text{T}}^{\text{miss}}$): The remaining contribution to the $E_{\text{T}}^{\text{miss}}$ uncertainty stems from the uncertainties in calorimeter cell energies associated with low-p_{T} jets (7 GeV $< p_{\text{T}} <$ 20 GeV), without any corresponding reconstructed physics object or from pile-up interactions. Their impact is accounted for as described in Ref. [57].

Pile-up: Besides the component treated in the JES, the residual dependence of the fitted m_{top} on the amount of pile-up activity and a possible MC mismodelling is determined. The m_{top} dependence as functions of n_{vtx} and $\langle\mu\rangle$ is found to be consistent in data and simulation. The corresponding uncertainty evaluated from the remaining difference is small.

The systematic uncertainties quoted in Table 2 carry statistical uncertainties. The statistical precision of a single sample fit is about 100 MeV. The statistical correlation of the samples is calculated from the fraction of shared events. Pairs of samples with only a change in a single parameter have high correlation and correspondingly low statistical uncertainty in the difference in m_{top}, while a pair of statistically independent samples results in a larger uncertainty.

In summary, the result in the dilepton channel at $\sqrt{s} = 8$ TeV of $m_{\text{top}} = 172.99 \pm 0.41\,(\text{stat}) \pm 0.74\,(\text{syst})$ GeV is about 40% more precise than the one obtained from the $\sqrt{s} = 7$ TeV data and the most precise single result in this decay channel to date. The increased precision is partly driven by a better knowledge of the JES and bJES. In addition, the applied optimisation procedure significantly reduces the total systematic uncertainty, mostly due to a lower impact of the JES and theory modelling uncertainties.

7. Combination with previous ATLAS measurements

The combination of the m_{top} results follows the approach developed for the combination of the $\sqrt{s} = 7$ TeV measurements in Ref. [14] including the evaluation of the correlations. For combining the measurements from data at different centre-of-mass energies a mapping of uncertainty categories is performed. Complex cases are the uncertainty components involving eigenvector decompositions such as the JES, the JER and the b-tagging scale factor uncertainties. The $\sqrt{s} = 7$ and 8 TeV measurements are treated as uncorrelated for the nuisance parameters of the JER and the b-tagging, c/τ-tagging and mistagging uncertainties. A correlated treatment of the estimators for the flavour-tagging nuisance parameters results in an insignificant change in the combination. The total JES uncertainty consists of about 20 eigenvector components, which partly differ for the analyses of $\sqrt{s} = 7$ and 8 TeV data, which make use of the EM+JES and the LCW+GSC [70] jet calibrations, respectively. For the combination, a mapping between uncertainty components at the different centre-of-mass energies is employed to identify the corresponding ones. The combination was found to be stable against variations of the assumptions for ambiguous cases.

The combination is performed using the best linear unbiased estimate (BLUE) method [75,76], implying Gaussian probability density functions for all uncertainties, using the implementation described in Ref. [77]. The central values, the list of uncertainty components and the correlations ρ of the estimators for each uncertainty component have to be provided. For the statistical, method calibration, MC-based background shape at $\sqrt{s} = 7$ TeV, and pile-up uncertainties in m_{top} the measurements are assumed to be uncorrelated. For the remaining uncertainties in m_{top}, when using $\pm 1\sigma$ variations of a systematic effect, e.g. when changing the bJES by $\pm 1\sigma$, there are two possibilities. When simultaneously applying a variation for a systematic uncertainty, e.g. $+1\sigma$ for the bJES to a pair of analyses, e.g. the dilepton measurements at $\sqrt{s} = 7$ and 8 TeV, both analyses can result in a larger or smaller m_{top} value than what is obtained for the nominal case (full correlation, $\rho = +1$), or one analysis can obtain a larger and the other a smaller value (full anti-correlation, $\rho = -1$). Consequently, an uncertainty from a source only consisting of a single variation, such as the uncertainty related to the choice of MC generator for signal events, results in a correlation of $\rho = \pm 1$. The estimator correlations for composite uncertainties are evaluated by adding the covariance terms of the subcomponents i with $\rho_i = \pm 1$ and dividing by the total uncertainties for that source. The resulting estimator

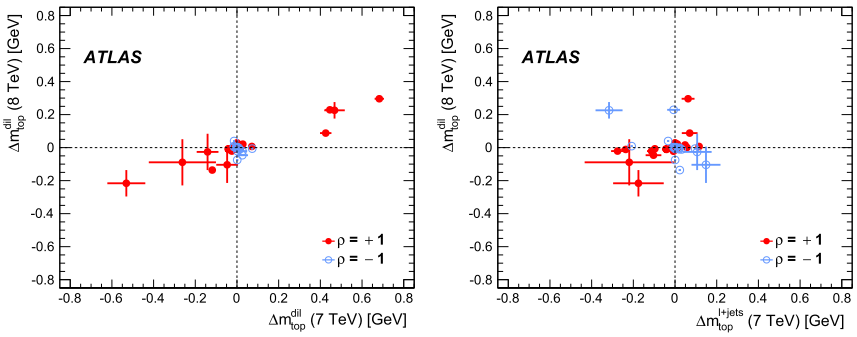

(a) $\sqrt{s}$ = 7 TeV versus $\sqrt{s}$ = 8 TeV dilepton (b) $\sqrt{s}$ = 7 TeV ℓ+jets versus $\sqrt{s}$ = 8 TeV dilepton

Fig. 3. The pairwise differences in m_{top} when simultaneously varying both analyses for a systematic uncertainty. Each cross indicates the statistical precisions of the systematic uncertainty. The red full points indicate $\rho = 1$, the blue open points $\rho = -1$.

correlation per uncertainty is quoted in Table 2 and used in the combination.

The evaluated uncertainties in m_{top} for the uncertainty components for the two dilepton analyses, denoted by Δm_{top}^{dil}, are shown in Fig. 3(a). Each point represents a systematic uncertainty together with a cross, indicating the respective statistical precision of the systematic uncertainty in the two analyses. The red full points indicate $\rho = 1$, the blue open points $\rho = -1$. Given the similarity of the analyses, a positive estimator correlation is observed for most uncertainty components of the two measurements in the dilepton channel. The corresponding distribution for the ℓ + jets measurement at $\sqrt{s} = 7$ TeV and the dilepton measurement at $\sqrt{s} = 8$ TeV is given in Fig. 3(b). In this figure, the estimates are anti-correlated for several significant uncertainties. This is caused by the in-situ measurement of the jet energy scale factor (JSF) and relative b-to-light-jet energy scale factor (bJSF) in the three-dimensional ℓ + jets analysis, detailed in Ref. [14]. The resulting total correlation for this pair is very low as shown in Table 2. The combination strongly profits from this.

The central values of the three measurements, their uncertainty components, the determined correlations per pair of measurements and the results of the combinations are given in Table 2. The pairwise differences in the three measurements are 0.75σ for the $\sqrt{s} = 7$ TeV measurements, 0.43σ for the ℓ + jets measurement at $\sqrt{s} = 7$ TeV and the dilepton measurement at $\sqrt{s} = 8$ TeV and 0.66σ for the two dilepton measurements. For all three cases σ denotes the one standard deviation of the respective m_{top} difference. The combined result in the dilepton channel alone is $m_{top}^{dil} = 173.04 \pm 0.38\,(stat) \pm 0.74\,(syst)$ GeV $= 173.04 \pm 0.84$ GeV, providing no significant improvement with respect to the more precise result at $\sqrt{s} = 8$ TeV which carries a BLUE combination weight of 0.94. This is a mere consequence of the measurement correlation of 0.51, which is close to the ratio of uncertainties (see Ref. [76]). The χ^2 probability of the combination is 51%. The stability of the combination is assessed from the results of 1000 combinations for which all input uncertainties are varied within their statistical uncertainties, which for some cases also result in different correlations (see Fig. 3). The corresponding distributions of the central values and uncertainties of the combinations are approximately Gaussian, with a width of 0.03 GeV and of 0.04 GeV, respectively.

The combination of all three measurements provides a 17% improvement with respect to the most precise single input measurement. The combined result is $m_{top}^{all} = 172.84 \pm 0.34\,(stat) \pm 0.61\,(syst)$ GeV $= 172.84 \pm 0.70$ GeV. The χ^2 probability of the combination is 73% and the BLUE combination weights of the ℓ+jets and dilepton measurements at $\sqrt{s} = 7$ TeV and the dilepton measurement at $\sqrt{s} = 8$ TeV are 0.30, 0.07 and 0.63, respectively. Again, the central value and the combined total uncertainty are both stable at the level of 0.03 GeV.

8. Conclusion

The top quark mass is measured in the $t\bar{t} \to$ dilepton channel from about 20.2 fb^{-1} of $\sqrt{s} = 8$ TeV proton–proton collision data recorded by the ATLAS detector at the LHC. Compared to the latest ATLAS measurement in this decay channel, the event selection is refined exploiting the average p_T of the lepton–b-jet pairs to enhance the fraction of correctly reconstructed events, thereby reducing the systematic uncertainties. Using the optimal point in terms of total uncertainty observed in a phase-space scan of this variable as an additional event selection criterion, the measured value of m_{top} is

$$m_{top} = 172.99 \pm 0.41\,(stat) \pm 0.74\,(syst)\ \text{GeV},$$

with a total uncertainty of 0.84 GeV. The precision is mainly limited by systematic uncertainties, mostly by the calibration of the jet energy scale, and to a lesser extent by the calibration of the relative b-to-light-jet energy scale and by the Monte Carlo modelling of signal events.

This measurement is combined with the ATLAS measurements in the $t\bar{t} \to$ lepton + jets and $t\bar{t} \to$ dilepton decay channels from $\sqrt{s} = 7$ TeV data. The correlations of the measurements are evaluated for all sources of the systematic uncertainty. Using a dedicated mapping of uncertainty categories, the combination of the three measurements results in

$$m_{top} = 172.84 \pm 0.34\,(stat) \pm 0.61\,(syst)\ \text{GeV},$$

with a total uncertainty of 0.70 GeV, i.e. a relative precision of 0.4%. The result is mostly limited by the calibration of the jet energy scales and by the Monte Carlo modelling of signal events.

Acknowledgements

We thank CERN for the very successful operation of the LHC, as well as the support staff from our institutions without whom ATLAS could not be operated efficiently.

We acknowledge the support of ANPCyT, Argentina; YerPhI, Armenia; ARC, Australia; BMWFW and FWF, Austria; ANAS, Azerbaijan; SSTC, Belarus; CNPq and FAPESP, Brazil; NSERC, NRC and CFI, Canada; CERN; CONICYT, Chile; CAS, MOST and NSFC, China; COLCIENCIAS, Colombia; MSMT CR, MPO CR and VSC CR, Czech Republic; DNRF and DNSRC, Denmark; IN2P3-CNRS, CEA-DSM/IRFU, France; GNSF, Georgia; BMBF, HGF, and MPG, Germany; GSRT, Greece; RGC, Hong Kong SAR, China; ISF, I-CORE and Benoziyo Center, Israel; INFN, Italy; MEXT and JSPS, Japan; CNRST, Morocco; FOM and NWO, Netherlands; RCN, Norway; MNiSW and NCN, Poland; FCT, Portugal; MNE/IFA, Romania; MES of Russia and NRC KI, Russian Federation; JINR; MESTD, Serbia; MSSR, Slovakia; ARRS and MIZŠ, Slovenia; DST/NRF, South Africa; MINECO, Spain; SRC and Wallenberg Foundation, Sweden; SERI, SNSF and Cantons of Bern and Geneva, Switzerland; MOST, Taiwan; TAEK, Turkey; STFC, United Kingdom; DOE and NSF, United States of America. In addition, individual groups and members have received support from BCKDF, the Canada Council, CANARIE, CRC, Compute Canada, FQRNT, and the Ontario Innovation Trust, Canada; EPLANET, ERC, FP7, Horizon 2020 and Marie Skłodowska-Curie Actions, European Union; Investissements d'Avenir Labex and Idex, ANR, Région Auvergne and Fondation Partager le Savoir, France; DFG and AvH Foundation, Germany; Herakleitos, Thales and Aristeia programmes co-financed by EU-ESF and the Greek NSRF; BSF, GIF and Minerva, Israel; BRF, Norway; Generalitat de Catalunya, Generalitat Valenciana, Spain; the Royal Society and Leverhulme Trust, United Kingdom.

The crucial computing support from all WLCG partners is acknowledged gratefully, in particular from CERN and the ATLAS Tier-1 facilities at TRIUMF (Canada), NDGF (Denmark, Norway, Sweden), CC-IN2P3 (France), KIT/GridKA (Germany), INFN-CNAF (Italy), NL-T1 (Netherlands), PIC (Spain), ASGC (Taiwan), RAL (UK) and BNL (USA) and in the Tier-2 facilities worldwide.

References

[1] ALEPH Collaboration, CDF Collaboration, D0 Collaboration, DELPHI Collaboration, L3 Collaboration, OPAL Collaboration, SLD Collaboration, The LEP Electroweak Working Group, The Tevatron Electroweak Working Group, The SLD Electroweak and Heavy Flavour Groups, arXiv:1012.2367 [hep-ex].
[2] M. Baak, et al., The global electroweak fit at NNLO and prospects for the LHC and ILC, Eur. Phys. J. C 74 (2014) 3046.
[3] K.A. Olive, et al., Particle Data Group, Review of particle physics, Chin. Phys. C 38 (2014) 090001.
[4] G. Degrassi, et al., Higgs mass and vacuum stability in the standard model at NNLO, J. High Energy Phys. 8 (2012) 98.
[5] F. Bezrukov, et al., The standard model Higgs boson as the inflaton, Phys. Lett. B 659 (2008) 703.
[6] A. De Simone, et al., Running inflation in the standard model, Phys. Lett. B 678 (2009) 1.
[7] ATLAS Collaboration, CDF Collaboration, CMS Collaboration, D0 Collaboration, First combination of Tevatron and LHC measurements of the top-quark mass, arXiv:1403.4427 [hep-ex].
[8] ATLAS Collaboration, Measurement of the top-quark mass in the fully hadronic decay channel from ATLAS data at $\sqrt{s} = 7$ TeV, Eur. Phys. J. C 75 (2015) 158.
[9] CDF Collaboration, T. Aaltonen, et al., Measurement of the top-quark mass in the $t\bar{t}$ dilepton channel using the full CDF Run II data set, Phys. Rev. D 92 (2015) 032003.
[10] CDF Collaboration, T. Aaltonen, et al., Measurement of the top-quark mass in the all-hadronic channel using the full CDF data set, Phys. Rev. D 90 (2014) 091101(R).
[11] CMS Collaboration, Measurement of the top quark mass using proton–proton data at $\sqrt{(s)} = 7$ and 8 TeV, Phys. Rev. D 93 (2016) 072004.
[12] DØ Collaboration, V.M. Abazov, et al., Precise measurement of the top quark mass in dilepton decays using optimized neutrino weighting, Phys. Lett. B 752 (2016) 18.
[13] DØ Collaboration, V.M. Abazov, et al., Precision measurement of the top quark mass in lepton + jets final states, Phys. Rev. Lett. 113 (2014) 032002.
[14] ATLAS Collaboration, Measurement of the top quark mass in the $t\bar{t} \to$ lepton + jets and $t\bar{t} \to$ dilepton channels using $\sqrt{s} = 7$ TeV ATLAS data, Eur. Phys. J. C 75 (2015) 330.
[15] ATLAS Collaboration, The ATLAS experiment at the CERN Large Hadron Collider, J. Instrum. 3 (2008) S08003.
[16] ATLAS Collaboration, Improved luminosity determination in pp collisions at $\sqrt{s} = 7$ TeV using the ATLAS detector at the LHC, Eur. Phys. J. C 73 (2013) 2518.
[17] P. Nason, A new method for combining NLO QCD with shower Monte Carlo algorithms, J. High Energy Phys. 11 (2004) 040.
[18] S. Frixione, et al., Matching NLO QCD computations with parton shower simulations: the POWHEG method, J. High Energy Phys. 11 (2007) 70.
[19] S. Alioli, P. Nason, C. Oleari, E. Re, A general framework for implementing NLO calculations in shower Monte Carlo programs: the POWHEG BOX, J. High Energy Phys. 06 (2010) 043.
[20] S. Frixione, P. Nason, G. Ridolfi, A positive-weight next-to-leading-order Monte Carlo for heavy flavour hadroproduction, J. High Energy Phys. 09 (2007) 126.
[21] E. Re, Single-top Wt-channel production matched with parton showers using the POWHEG method, Eur. Phys. J. C 71 (2011) 1547.
[22] H.L. Lai, et al., New parton distributions for collider physics, Phys. Rev. D 82 (2010) 74024.
[23] S. Mrenna, et al., PYTHIA 6.4 physics and manual, J. High Energy Phys. 05 (2006) 26.
[24] P.Z. Skands, Tuning Monte Carlo generators: the Perugia tunes, Phys. Rev. D 82 (2010) 74018.
[25] J. Pumplin, et al., New generation of parton distributions with uncertainties from global QCD analysis, J. High Energy Phys. 07 (2002) 12.
[26] ATLAS Collaboration, Measurement of $t\bar{t}$ production with a veto on additional central jet activity in pp collisions at $\sqrt{s} = 7$ TeV using the ATLAS detector, Eur. Phys. J. C 72 (2012) 2043.
[27] ATLAS Collaboration, Measurement of the $t\bar{t}$ production cross-section as a function of jet multiplicity and jet transverse momentum in 7 TeV proton–proton collisions with the ATLAS detector, J. High Energy Phys. 01 (2015) 20.
[28] ATLAS Collaboration, Comparison of Monte Carlo generator predictions to ATLAS measurements of top pair production at 7 TeV, ATL-PHYS-PUB-2015-002, 2015, http://cds.cern.ch/record/1981319.
[29] M. Cacciari, et al., Top-pair production at hadron colliders with next-to-next-to-leading logarithmic soft-gluon resummation, Phys. Lett. B 710 (2012) 612.
[30] P. Bärnreuther, et al., Percent level precision physics at the Tevatron: first genuine NNLO QCD corrections to $q\bar{q} \to t\bar{t} + X$, Phys. Rev. Lett. 109 (2012) 132001.
[31] M. Czakon, A. Mitov, NNLO corrections to top-pair production at hadron colliders: the all-fermionic scattering channels, J. High Energy Phys. 12 (2012) 54.
[32] M. Czakon, A. Mitov, NNLO corrections to top pair production at hadron colliders: the quark–gluon reaction, J. High Energy Phys. 01 (2013) 80.
[33] M. Czakon, et al., The total top quark pair production cross-section at hadron colliders through $\mathcal{O}(\alpha_S^4)$, Phys. Rev. Lett. 110 (2013) 252004.
[34] M. Czakon, A. Mitov, Top++: a program for the calculation of the top-pair cross-section at hadron colliders, Comput. Phys. Commun. 185 (2014) 2930.
[35] N. Kidonakis, Two-loop soft anomalous dimensions for single top quark associated production with a W^- or H^-, Phys. Rev. D 82 (2010) 54018.
[36] M. Botje, et al., The PDF4LHC working group interim recommendations, arXiv:1101.0538 [hep-ph].
[37] A.D. Martin, et al., Parton distributions for the LHC, Eur. Phys. J. C 63 (2009) 189.
[38] A.D. Martin, et al., Uncertainties on α_S in global PDF analyses and implications for predicted hadronic cross sections, Eur. Phys. J. C 64 (2009) 653.
[39] J. Gao, et al., The CT10 NNLO global analysis of QCD, Phys. Rev. D 89 (2014) 33009.
[40] R.D. Ball, et al., Parton distributions with LHC data, Nucl. Phys. B 867 (2013) 244.
[41] M.L. Mangano, et al., ALPGEN, a generator for hard multiparton processes in hadronic collisions, J. High Energy Phys. 07 (2003) 1.
[42] ATLAS Collaboration, New ATLAS event generator tunes to 2010 data, ATL-PHYS-PUB-2011-008, 2011, http://cds.cern.ch/record/1345343.
[43] G. Corcella, et al., HERWIG 6.5: an event generator for hadron emission reactions with interfering gluons (including supersymmetric processes), J. High Energy Phys. 01 (2001) 10.
[44] J.M. Butterworth, et al., Multiparton interactions in photoproduction at HERA, Z. Phys. C 72 (1996) 637.
[45] T. Sjöstrand, S. Mrenna, P. Skands, A brief introduction to PYTHIA 8.1, Comput. Phys. Commun. 178 (2008) 852.
[46] ATLAS Collaboration, Summary of ATLAS PYTHIA 8 tunes, ATL-PHYS-PUB-2012-003, 2012, http://cdsweb.cern.ch/record/1474107.
[47] ATLAS Collaboration, The ATLAS simulation infrastructure, Eur. Phys. J. C 70 (2010) 823.
[48] S. Agostinelli, et al., GEANT4: a simulation toolkit, Nucl. Instrum. Methods A 506 (2003) 250.
[49] ATLAS Collaboration, Electron reconstruction and identification efficiency measurements with the ATLAS detector using the 2011 LHC proton–proton collision data, Eur. Phys. J. C 74 (2014) 2941.
[50] ATLAS Collaboration, Measurement of the muon reconstruction performance of the ATLAS detector using 2011 and 2012 LHC proton–proton collision data, Eur. Phys. J. C 74 (2014) 3130.

[51] ATLAS Collaboration, Topological cell clustering in the ATLAS calorimeters and its performance in LHC Run 1, Eur. Phys. J. C (2016), in press, arXiv:1603.02934 [hep-ex].
[52] M. Cacciari, et al., The anti-k_t jet clustering algorithm, J. High Energy Phys. 04 (2008) 63.
[53] ATLAS Collaboration, Jet energy measurement with the ATLAS detector in proton–proton collisions at $\sqrt{s} = 7$ TeV, Eur. Phys. J. C 73 (2013) 2304.
[54] ATLAS Collaboration, Jet energy measurement and its systematic uncertainty in proton–proton collisions at $\sqrt{s} = 7$ TeV with the ATLAS detector, Eur. Phys. J. C 75 (2015) 17.
[55] ATLAS Collaboration, Monte Carlo calibration and combination of *in-situ* measurements of jet energy scale, jet energy resolution and jet mass in ATLAS, ATLAS-CONF-2015-037, 2015, http://cds.cern.ch/record/2044941.
[56] ATLAS Collaboration, Performance of b-jet identification in the ATLAS experiment, J. Instrum. 11 (2016) P04008.
[57] ATLAS Collaboration, Performance of missing transverse momentum reconstruction in proton–proton collisions at $\sqrt{s} = 7$ TeV with ATLAS, Eur. Phys. J. C 72 (2012) 1844.
[58] ATLAS Collaboration, Estimation of non-prompt and fake lepton backgrounds in final states with top quarks produced in proton–proton collisions at $\sqrt{s} = 8$ TeV with the ATLAS detector, ATLAS-CONF-2014-058, 2014, http://cds.cern.ch/record/1951336.
[59] ATLAS Collaboration, Measurement of the top quark-pair production cross section with ATLAS in pp collisions at $\sqrt{s} = 7$ TeV, Eur. Phys. J. C 71 (2011) 1577.
[60] R.J. Barlow, Application of the bootstrap resampling technique to particle physics experiments, http://www.hep.man.ac.uk/preprints/1999.html.
[61] R. Barlow, Systematic errors: facts and fictions, arXiv:hep-ex/0207026.
[62] S. Frixione, B.R. Webber, Matching NLO QCD computations and parton shower simulations, J. High Energy Phys. 06 (2002) 029.
[63] S. Frixione, et al., Matching NLO QCD and parton showers in heavy flavour production, J. High Energy Phys. 08 (2003) 007.
[64] B. Andersson, et al., Parton fragmentation and string dynamics, Phys. Rep. 97 (1983) 31.
[65] B. Andersson, The Lund Model, Cambridge University Press, ISBN 9780521017343, 1997.
[66] B. Webber, A QCD model for jet fragmentation including soft gluon interference, Nucl. Phys. B 238 (1984) 492.
[67] M. Bahr, et al., Herwig++ physics and manual, Eur. Phys. J. C 58 (2008) 639.
[68] ATLAS Collaboration, Impact of fragmentation modelling on the top quark mass measurement using the ATLAS detector, ATL-PHYS-PUB-2015-042, 2015, http://cds.cern.ch/record/2054420.
[69] ATLAS Collaboration, Comparison of Monte Carlo generator predictions for gap fraction and jet multiplicity observables in $t\bar{t}$ events, ATL-PHYS-PUB-2014-005, 2014, http://cds.cern.ch/record/1703034.
[70] ATLAS Collaboration, Determination of the jet energy scale and resolution at ATLAS using Z/γ-jet events in data at $\sqrt{s} = 8$ TeV, ATLAS-CONF-2015-057, 2015, http://cds.cern.ch/record/2059846.
[71] ATLAS Collaboration, Data-driven determination of the energy scale and resolution of jets reconstructed in the ATLAS calorimeters using dijet and multijet events at $\sqrt{s} = 8$ TeV, ATLAS-CONF-2015-017, 2015, http://cds.cern.ch/record/2008678.
[72] ATLAS Collaboration, Pile-up subtraction and suppression for jets in ATLAS, ATLAS-CONF-2013-083, 2013, http://cds.cern.ch/record/1570994.
[73] ATLAS Collaboration, Calibration of b-tagging using dileptonic top pair events in a combinatorial likelihood approach with the ATLAS experiment, ATLAS-CONF-2014-004, 2014, http://cdsweb.cern.ch/record/1664335.
[74] ATLAS Collaboration, Electron and photon energy calibration with the ATLAS detector using LHC Run 1 data, Eur. Phys. J. C 74 (2014) 3071.
[75] L. Lyons, et al., How to combine correlated estimates of a single physical quantity, Nucl. Instrum. Methods A 270 (1988) 110.
[76] R. Nisius, On the combination of correlated estimates of a physics observable, Eur. Phys. J. C 74 (2014) 3004.
[77] R. Nisius, A ROOT class to combine a number of correlated estimates of one or more observables using the best linear unbiased estimate method, http://blue.hepforge.org/Bluemanual.pdf.

ATLAS Collaboration

M. Aaboud [135d], G. Aad [86], B. Abbott [113], J. Abdallah [64], O. Abdinov [12], B. Abeloos [117], R. Aben [107], O.S. AbouZeid [137], N.L. Abraham [149], H. Abramowicz [153], H. Abreu [152], R. Abreu [116], Y. Abulaiti [146a,146b], B.S. Acharya [163a,163b,a], L. Adamczyk [40a], D.L. Adams [27], J. Adelman [108], S. Adomeit [100], T. Adye [131], A.A. Affolder [75], T. Agatonovic-Jovin [14], J. Agricola [56], J.A. Aguilar-Saavedra [126a,126f], S.P. Ahlen [24], F. Ahmadov [66,b], G. Aielli [133a,133b], H. Akerstedt [146a,146b], T.P.A. Åkesson [82], A.V. Akimov [96], G.L. Alberghi [22a,22b], J. Albert [168], S. Albrand [57], M.J. Alconada Verzini [72], M. Aleksa [32], I.N. Aleksandrov [66], C. Alexa [28b], G. Alexander [153], T. Alexopoulos [10], M. Alhroob [113], B. Ali [128], M. Aliev [74a,74b], G. Alimonti [92a], J. Alison [33], S.P. Alkire [37], B.M.M. Allbrooke [149], B.W. Allen [116], P.P. Allport [19], A. Aloisio [104a,104b], A. Alonso [38], F. Alonso [72], C. Alpigiani [138], M. Alstaty [86], B. Alvarez Gonzalez [32], D. Álvarez Piqueras [166], M.G. Alviggi [104a,104b], B.T. Amadio [16], K. Amako [67], Y. Amaral Coutinho [26a], C. Amelung [25], D. Amidei [90], S.P. Amor Dos Santos [126a,126c], A. Amorim [126a,126b], S. Amoroso [32], G. Amundsen [25], C. Anastopoulos [139], L.S. Ancu [51], N. Andari [19], T. Andeen [11], C.F. Anders [59b], G. Anders [32], J.K. Anders [75], K.J. Anderson [33], A. Andreazza [92a,92b], V. Andrei [59a], S. Angelidakis [9], I. Angelozzi [107], P. Anger [46], A. Angerami [37], F. Anghinolfi [32], A.V. Anisenkov [109,c], N. Anjos [13], A. Annovi [124a,124b], C. Antel [59a], M. Antonelli [49], A. Antonov [98,*], F. Anulli [132a], M. Aoki [67], L. Aperio Bella [19], G. Arabidze [91], Y. Arai [67], J.P. Araque [126a], A.T.H. Arce [47], F.A. Arduh [72], J-F. Arguin [95], S. Argyropoulos [64], M. Arik [20a], A.J. Armbruster [143], L.J. Armitage [77], O. Arnaez [32], H. Arnold [50], M. Arratia [30], O. Arslan [23], A. Artamonov [97], G. Artoni [120], S. Artz [84], S. Asai [155], N. Asbah [44], A. Ashkenazi [153], B. Åsman [146a,146b], L. Asquith [149], K. Assamagan [27], R. Astalos [144a], M. Atkinson [165], N.B. Atlay [141], K. Augsten [128], G. Avolio [32], B. Axen [16], M.K. Ayoub [117], G. Azuelos [95,d], M.A. Baak [32], A.E. Baas [59a], M.J. Baca [19], H. Bachacou [136], K. Bachas [74a,74b], M. Backes [148], M. Backhaus [32], P. Bagiacchi [132a,132b], P. Bagnaia [132a,132b], Y. Bai [35a], J.T. Baines [131], O.K. Baker [175], E.M. Baldin [109,c], P. Balek [171], T. Balestri [148], F. Balli [136], W.K. Balunas [122], E. Banas [41], Sw. Banerjee [172,e], A.A.E. Bannoura [174], L. Barak [32], E.L. Barberio [89], D. Barberis [52a,52b], M. Barbero [86], T. Barillari [101], M-S Barisits [32], T. Barklow [143], N. Barlow [30], S.L. Barnes [85], B.M. Barnett [131], R.M. Barnett [16], Z. Barnovska [5], A. Baroncelli [134a], G. Barone [25], A.J. Barr [120], L. Barranco Navarro [166], F. Barreiro [83], J. Barreiro Guimarães da Costa [35a], R. Bartoldus [143], A.E. Barton [73], P. Bartos [144a], A. Basalaev [123], A. Bassalat [117], R.L. Bates [55], S.J. Batista [158], J.R. Batley [30], M. Battaglia [137], M. Bauce [132a,132b], F. Bauer [136], H.S. Bawa [143,f], J.B. Beacham [111], M.D. Beattie [73], T. Beau [81], P.H. Beauchemin [161], P. Bechtle [23],

H.P. Beck [18,g], K. Becker [120], M. Becker [84], M. Beckingham [169], C. Becot [110], A.J. Beddall [20e], A. Beddall [20b], V.A. Bednyakov [66], M. Bedognetti [107], C.P. Bee [148], L.J. Beemster [107], T.A. Beermann [32], M. Begel [27], J.K. Behr [44], C. Belanger-Champagne [88], A.S. Bell [79], G. Bella [153], L. Bellagamba [22a], A. Bellerive [31], M. Bellomo [87], K. Belotskiy [98], O. Beltramello [32], N.L. Belyaev [98], O. Benary [153], D. Benchekroun [135a], M. Bender [100], K. Bendtz [146a,146b], N. Benekos [10], Y. Benhammou [153], E. Benhar Noccioli [175], J. Benitez [64], D.P. Benjamin [47], J.R. Bensinger [25], S. Bentvelsen [107], L. Beresford [120], M. Beretta [49], D. Berge [107], E. Bergeaas Kuutmann [164], N. Berger [5], J. Beringer [16], S. Berlendis [57], N.R. Bernard [87], C. Bernius [110], F.U. Bernlochner [23], T. Berry [78], P. Berta [129], C. Bertella [84], G. Bertoli [146a,146b], F. Bertolucci [124a,124b], I.A. Bertram [73], C. Bertsche [44], D. Bertsche [113], G.J. Besjes [38], O. Bessidskaia Bylund [146a,146b], M. Bessner [44], N. Besson [136], C. Betancourt [50], A. Bethani [57], S. Bethke [101], A.J. Bevan [77], R.M. Bianchi [125], L. Bianchini [25], M. Bianco [32], O. Biebel [100], D. Biedermann [17], R. Bielski [85], N.V. Biesuz [124a,124b], M. Biglietti [134a], J. Bilbao De Mendizabal [51], T.R.V. Billoud [95], H. Bilokon [49], M. Bindi [56], S. Binet [117], A. Bingul [20b], C. Bini [132a,132b], S. Biondi [22a,22b], D.M. Bjergaard [47], C.W. Black [150], J.E. Black [143], K.M. Black [24], D. Blackburn [138], R.E. Blair [6], J.-B. Blanchard [136], T. Blazek [144a], I. Bloch [44], C. Blocker [25], W. Blum [84,*], U. Blumenschein [56], S. Blunier [34a], G.J. Bobbink [107], V.S. Bobrovnikov [109,c], S.S. Bocchetta [82], A. Bocci [47], C. Bock [100], M. Boehler [50], D. Boerner [174], J.A. Bogaerts [32], D. Bogavac [14], A.G. Bogdanchikov [109], C. Bohm [146a], V. Boisvert [78], P. Bokan [14], T. Bold [40a], A.S. Boldyrev [163a,163c], M. Bomben [81], M. Bona [77], M. Boonekamp [136], A. Borisov [130], G. Borissov [73], J. Bortfeldt [32], D. Bortoletto [120], V. Bortolotto [61a,61b,61c], K. Bos [107], D. Boscherini [22a], M. Bosman [13], J.D. Bossio Sola [29], J. Boudreau [125], J. Bouffard [2], E.V. Bouhova-Thacker [73], D. Boumediene [36], C. Bourdarios [117], S.K. Boutle [55], A. Boveia [32], J. Boyd [32], I.R. Boyko [66], J. Bracinik [19], A. Brandt [8], G. Brandt [56], O. Brandt [59a], U. Bratzler [156], B. Brau [87], J.E. Brau [116], H.M. Braun [174,*], W.D. Breaden Madden [55], K. Brendlinger [122], A.J. Brennan [89], L. Brenner [107], R. Brenner [164], S. Bressler [171], T.M. Bristow [48], D. Britton [55], D. Britzger [44], F.M. Brochu [30], I. Brock [23], R. Brock [91], G. Brooijmans [37], T. Brooks [78], W.K. Brooks [34b], J. Brosamer [16], E. Brost [108], J.H Broughton [19], P.A. Bruckman de Renstrom [41], D. Bruncko [144b], R. Bruneliere [50], A. Bruni [22a], G. Bruni [22a], L.S. Bruni [107], BH Brunt [30], M. Bruschi [22a], N. Bruscino [23], P. Bryant [33], L. Bryngemark [82], T. Buanes [15], Q. Buat [142], P. Buchholz [141], A.G. Buckley [55], I.A. Budagov [66], F. Buehrer [50], M.K. Bugge [119], O. Bulekov [98], D. Bullock [8], H. Burckhart [32], S. Burdin [75], C.D. Burgard [50], B. Burghgrave [108], K. Burka [41], S. Burke [131], I. Burmeister [45], J.T.P. Burr [120], E. Busato [36], D. Büscher [50], V. Büscher [84], P. Bussey [55], J.M. Butler [24], C.M. Buttar [55], J.M. Butterworth [79], P. Butti [107], W. Buttinger [27], A. Buzatu [55], A.R. Buzykaev [109,c], S. Cabrera Urbán [166], D. Caforio [128], V.M. Cairo [39a,39b], O. Cakir [4a], N. Calace [51], P. Calafiura [16], A. Calandri [86], G. Calderini [81], P. Calfayan [100], G. Callea [39a,39b], L.P. Caloba [26a], S. Calvente Lopez [83], D. Calvet [36], S. Calvet [36], T.P. Calvet [86], R. Camacho Toro [33], S. Camarda [32], P. Camarri [133a,133b], D. Cameron [119], R. Caminal Armadans [165], C. Camincher [57], S. Campana [32], M. Campanelli [79], A. Camplani [92a,92b], A. Campoverde [141], V. Canale [104a,104b], A. Canepa [159a], M. Cano Bret [35e], J. Cantero [114], R. Cantrill [126a], T. Cao [42], M.D.M. Capeans Garrido [32], I. Caprini [28b], M. Caprini [28b], M. Capua [39a,39b], R. Caputo [84], R.M. Carbone [37], R. Cardarelli [133a], F. Cardillo [50], I. Carli [129], T. Carli [32], G. Carlino [104a], L. Carminati [92a,92b], S. Caron [106], E. Carquin [34b], G.D. Carrillo-Montoya [32], J.R. Carter [30], J. Carvalho [126a,126c], D. Casadei [19], M.P. Casado [13,h], M. Casolino [13], D.W. Casper [162], E. Castaneda-Miranda [145a], R. Castelijn [107], A. Castelli [107], V. Castillo Gimenez [166], N.F. Castro [126a,i], A. Catinaccio [32], J.R. Catmore [119], A. Cattai [32], J. Caudron [23], V. Cavaliere [165], E. Cavallaro [13], D. Cavalli [92a], M. Cavalli-Sforza [13], V. Cavasinni [124a,124b], F. Ceradini [134a,134b], L. Cerda Alberich [166], B.C. Cerio [47], A.S. Cerqueira [26b], A. Cerri [149], L. Cerrito [133a,133b], F. Cerutti [16], M. Cerv [32], A. Cervelli [18], S.A. Cetin [20d], A. Chafaq [135a], D. Chakraborty [108], S.K. Chan [58], Y.L. Chan [61a], P. Chang [165], J.D. Chapman [30], D.G. Charlton [19], A. Chatterjee [51], C.C. Chau [158], C.A. Chavez Barajas [149], S. Che [111], S. Cheatham [73], A. Chegwidden [91], S. Chekanov [6], S.V. Chekulaev [159a], G.A. Chelkov [66,j], M.A. Chelstowska [90], C. Chen [65], H. Chen [27], K. Chen [148], S. Chen [35c], S. Chen [155], X. Chen [35f], Y. Chen [68], H.C. Cheng [90], H.J Cheng [35a], Y. Cheng [33], A. Cheplakov [66], E. Cheremushkina [130], R. Cherkaoui El Moursli [135e], V. Chernyatin [27,*], E. Cheu [7], L. Chevalier [136], V. Chiarella [49], G. Chiarelli [124a,124b], G. Chiodini [74a], A.S. Chisholm [19], A. Chitan [28b], M.V. Chizhov [66], K. Choi [62], A.R. Chomont [36], S. Chouridou [9], B.K.B. Chow [100], V. Christodoulou [79], D. Chromek-Burckhart [32], J. Chudoba [127], A.J. Chuinard [88], J.J. Chwastowski [41], L. Chytka [115], G. Ciapetti [132a,132b], A.K. Ciftci [4a], D. Cinca [45], V. Cindro [76], I.A. Cioara [23], C. Ciocca [22a,22b], A. Ciocio [16], F. Cirotto [104a,104b], Z.H. Citron [171],

M. Citterio [92a], M. Ciubancan [28b], A. Clark [51], B.L. Clark [58], M.R. Clark [37], P.J. Clark [48], R.N. Clarke [16], C. Clement [146a,146b], Y. Coadou [86], M. Cobal [163a,163c], A. Coccaro [51], J. Cochran [65], L. Colasurdo [106], B. Cole [37], A.P. Colijn [107], J. Collot [57], T. Colombo [32], G. Compostella [101], P. Conde Muiño [126a,126b], E. Coniavitis [50], S.H. Connell [145b], I.A. Connelly [78], V. Consorti [50], S. Constantinescu [28b], G. Conti [32], F. Conventi [104a,k], M. Cooke [16], B.D. Cooper [79], A.M. Cooper-Sarkar [120], K.J.R. Cormier [158], T. Cornelissen [174], M. Corradi [132a,132b], F. Corriveau [88,l], A. Corso-Radu [162], A. Cortes-Gonzalez [32], G. Cortiana [101], G. Costa [92a], M.J. Costa [166], D. Costanzo [139], G. Cottin [30], G. Cowan [78], B.E. Cox [85], K. Cranmer [110], S.J. Crawley [55], G. Cree [31], S. Crépé-Renaudin [57], F. Crescioli [81], W.A. Cribbs [146a,146b], M. Crispin Ortuzar [120], M. Cristinziani [23], V. Croft [106], G. Crosetti [39a,39b], A. Cueto [83], T. Cuhadar Donszelmann [139], J. Cummings [175], M. Curatolo [49], J. Cúth [84], H. Czirr [141], P. Czodrowski [3], G. D'amen [22a,22b], S. D'Auria [55], M. D'Onofrio [75], M.J. Da Cunha Sargedas De Sousa [126a,126b], C. Da Via [85], W. Dabrowski [40a], T. Dado [144a], T. Dai [90], O. Dale [15], F. Dallaire [95], C. Dallapiccola [87], M. Dam [38], J.R. Dandoy [33], N.P. Dang [50], A.C. Daniells [19], N.S. Dann [85], M. Danninger [167], M. Dano Hoffmann [136], V. Dao [50], G. Darbo [52a], S. Darmora [8], J. Dassoulas [3], A. Dattagupta [62], W. Davey [23], C. David [168], T. Davidek [129], M. Davies [153], P. Davison [79], E. Dawe [89], I. Dawson [139], R.K. Daya-Ishmukhametova [87], K. De [8], R. de Asmundis [104a], A. De Benedetti [113], S. De Castro [22a,22b], S. De Cecco [81], N. De Groot [106], P. de Jong [107], H. De la Torre [83], F. De Lorenzi [65], A. De Maria [56], D. De Pedis [132a], A. De Salvo [132a], U. De Sanctis [149], A. De Santo [149], J.B. De Vivie De Regie [117], W.J. Dearnaley [73], R. Debbe [27], C. Debenedetti [137], D.V. Dedovich [66], N. Dehghanian [3], I. Deigaard [107], M. Del Gaudio [39a,39b], J. Del Peso [83], T. Del Prete [124a,124b], D. Delgove [117], F. Deliot [136], C.M. Delitzsch [51], M. Deliyergiyev [76], A. Dell'Acqua [32], L. Dell'Asta [24], M. Dell'Orso [124a,124b], M. Della Pietra [104a,k], D. della Volpe [51], M. Delmastro [5], P.A. Delsart [57], D.A. DeMarco [158], S. Demers [175], M. Demichev [66], A. Demilly [81], S.P. Denisov [130], D. Denysiuk [136], D. Derendarz [41], J.E. Derkaoui [135d], F. Derue [81], P. Dervan [75], K. Desch [23], C. Deterre [44], K. Dette [45], P.O. Deviveiros [32], A. Dewhurst [131], S. Dhaliwal [25], A. Di Ciaccio [133a,133b], L. Di Ciaccio [5], W.K. Di Clemente [122], C. Di Donato [132a,132b], A. Di Girolamo [32], B. Di Girolamo [32], B. Di Micco [134a,134b], R. Di Nardo [32], A. Di Simone [50], R. Di Sipio [158], D. Di Valentino [31], C. Diaconu [86], M. Diamond [158], F.A. Dias [48], M.A. Diaz [34a], E.B. Diehl [90], J. Dietrich [17], S. Diglio [86], A. Dimitrievska [14], J. Dingfelder [23], P. Dita [28b], S. Dita [28b], F. Dittus [32], F. Djama [86], T. Djobava [53b], J.I. Djuvsland [59a], M.A.B. do Vale [26c], D. Dobos [32], M. Dobre [28b], C. Doglioni [82], J. Dolejsi [129], Z. Dolezal [129], M. Donadelli [26d], S. Donati [124a,124b], P. Dondero [121a,121b], J. Donini [36], J. Dopke [131], A. Doria [104a], M.T. Dova [72], A.T. Doyle [55], E. Drechsler [56], M. Dris [10], Y. Du [35d], J. Duarte-Campderros [153], E. Duchovni [171], G. Duckeck [100], O.A. Ducu [95,m], D. Duda [107], A. Dudarev [32], A.Chr. Dudder [84], E.M. Duffield [16], L. Duflot [117], M. Dührssen [32], M. Dumancic [171], M. Dunford [59a], H. Duran Yildiz [4a], M. Düren [54], A. Durglishvili [53b], D. Duschinger [46], B. Dutta [44], M. Dyndal [44], C. Eckardt [44], K.M. Ecker [101], R.C. Edgar [90], N.C. Edwards [48], T. Eifert [32], G. Eigen [15], K. Einsweiler [16], T. Ekelof [164], M. El Kacimi [135c], V. Ellajosyula [86], M. Ellert [164], S. Elles [5], F. Ellinghaus [174], A.A. Elliot [168], N. Ellis [32], J. Elmsheuser [27], M. Elsing [32], D. Emeliyanov [131], Y. Enari [155], O.C. Endner [84], J.S. Ennis [169], J. Erdmann [45], A. Ereditato [18], G. Ernis [174], J. Ernst [2], M. Ernst [27], S. Errede [165], E. Ertel [84], M. Escalier [117], H. Esch [45], C. Escobar [125], B. Esposito [49], A.I. Etienvre [136], E. Etzion [153], H. Evans [62], A. Ezhilov [123], F. Fabbri [22a,22b], L. Fabbri [22a,22b], G. Facini [33], R.M. Fakhrutdinov [130], S. Falciano [132a], R.J. Falla [79], J. Faltova [129], Y. Fang [35a], M. Fanti [92a,92b], A. Farbin [8], A. Farilla [134a], C. Farina [125], E.M. Farina [121a,121b], T. Farooque [13], S. Farrell [16], S.M. Farrington [169], P. Farthouat [32], F. Fassi [135e], P. Fassnacht [32], D. Fassouliotis [9], M. Faucci Giannelli [78], A. Favareto [52a,52b], W.J. Fawcett [120], L. Fayard [117], O.L. Fedin [123,n], W. Fedorko [167], S. Feigl [119], L. Feligioni [86], C. Feng [35d], E.J. Feng [32], H. Feng [90], A.B. Fenyuk [130], L. Feremenga [8], P. Fernandez Martinez [166], S. Fernandez Perez [13], J. Ferrando [55], A. Ferrari [164], P. Ferrari [107], R. Ferrari [121a], D.E. Ferreira de Lima [59b], A. Ferrer [166], D. Ferrere [51], C. Ferretti [90], A. Ferretto Parodi [52a,52b], F. Fiedler [84], A. Filipčič [76], M. Filipuzzi [44], F. Filthaut [106], M. Fincke-Keeler [168], K.D. Finelli [150], M.C.N. Fiolhais [126a,126c], L. Fiorini [166], A. Firan [42], A. Fischer [2], C. Fischer [13], J. Fischer [174], W.C. Fisher [91], N. Flaschel [44], I. Fleck [141], P. Fleischmann [90], G.T. Fletcher [139], R.R.M. Fletcher [122], T. Flick [174], A. Floderus [82], L.R. Flores Castillo [61a], M.J. Flowerdew [101], G.T. Forcolin [85], A. Formica [136], A. Forti [85], A.G. Foster [19], D. Fournier [117], H. Fox [73], S. Fracchia [13], P. Francavilla [81], M. Franchini [22a,22b], D. Francis [32], L. Franconi [119], M. Franklin [58], M. Frate [162], M. Fraternali [121a,121b], D. Freeborn [79], S.M. Fressard-Batraneanu [32], F. Friedrich [46], D. Froidevaux [32], J.A. Frost [120], C. Fukunaga [156],

E. Fullana Torregrosa[84], T. Fusayasu[102], J. Fuster[166], C. Gabaldon[57], O. Gabizon[174], A. Gabrielli[22a,22b], A. Gabrielli[16], G.P. Gach[40a], S. Gadatsch[32], S. Gadomski[51], G. Gagliardi[52a,52b], L.G. Gagnon[95], P. Gagnon[62], C. Galea[106], B. Galhardo[126a,126c], E.J. Gallas[120], B.J. Gallop[131], P. Gallus[128], G. Galster[38], K.K. Gan[111], J. Gao[35b,86], Y. Gao[48], Y.S. Gao[143,f], F.M. Garay Walls[48], C. García[166], J.E. García Navarro[166], M. Garcia-Sciveres[16], R.W. Gardner[33], N. Garelli[143], V. Garonne[119], A. Gascon Bravo[44], K. Gasnikova[44], C. Gatti[49], A. Gaudiello[52a,52b], G. Gaudio[121a], L. Gauthier[95], I.L. Gavrilenko[96], C. Gay[167], G. Gaycken[23], E.N. Gazis[10], Z. Gecse[167], C.N.P. Gee[131], Ch. Geich-Gimbel[23], M. Geisen[84], M.P. Geisler[59a], C. Gemme[52a], M.H. Genest[57], C. Geng[35b,o], S. Gentile[132a,132b], C. Gentsos[154], S. George[78], D. Gerbaudo[13], A. Gershon[153], S. Ghasemi[141], H. Ghazlane[135b], M. Ghneimat[23], B. Giacobbe[22a], S. Giagu[132a,132b], P. Giannetti[124a,124b], B. Gibbard[27], S.M. Gibson[78], M. Gignac[167], M. Gilchriese[16], T.P.S. Gillam[30], D. Gillberg[31], G. Gilles[174], D.M. Gingrich[3,d], N. Giokaris[9], M.P. Giordani[163a,163c], F.M. Giorgi[22a], F.M. Giorgi[17], P.F. Giraud[136], P. Giromini[58], D. Giugni[92a], F. Giuli[120], C. Giuliani[101], M. Giulini[59b], B.K. Gjelsten[119], S. Gkaitatzis[154], I. Gkialas[154], E.L. Gkougkousis[117], L.K. Gladilin[99], C. Glasman[83], J. Glatzer[32], P.C.F. Glaysher[48], A. Glazov[44], M. Goblirsch-Kolb[25], J. Godlewski[41], S. Goldfarb[89], T. Golling[51], D. Golubkov[130], A. Gomes[126a,126b,126d], R. Gonçalo[126a], J. Goncalves Pinto Firmino Da Costa[136], G. Gonella[50], L. Gonella[19], A. Gongadze[66], S. González de la Hoz[166], G. Gonzalez Parra[13], S. Gonzalez-Sevilla[51], L. Goossens[32], P.A. Gorbounov[97], H.A. Gordon[27], I. Gorelov[105], B. Gorini[32], E. Gorini[74a,74b], A. Gorišek[76], E. Gornicki[41], A.T. Goshaw[47], C. Gössling[45], M.I. Gostkin[66], C.R. Goudet[117], D. Goujdami[135c], A.G. Goussiou[138], N. Govender[145b,p], E. Gozani[152], L. Graber[56], I. Grabowska-Bold[40a], P.O.J. Gradin[57], P. Grafström[22a,22b], J. Gramling[51], E. Gramstad[119], S. Grancagnolo[17], V. Gratchev[123], P.M. Gravila[28e], H.M. Gray[32], E. Graziani[134a], Z.D. Greenwood[80,q], C. Grefe[23], K. Gregersen[79], I.M. Gregor[44], P. Grenier[143], K. Grevtsov[5], J. Griffiths[8], A.A. Grillo[137], K. Grimm[73], S. Grinstein[13,r], Ph. Gris[36], J.-F. Grivaz[117], S. Groh[84], J.P. Grohs[46], E. Gross[171], J. Grosse-Knetter[56], G.C. Grossi[80], Z.J. Grout[149], L. Guan[90], W. Guan[172], J. Guenther[63], F. Guescini[51], D. Guest[162], O. Gueta[153], E. Guido[52a,52b], T. Guillemin[5], S. Guindon[2], U. Gul[55], C. Gumpert[32], J. Guo[35e], Y. Guo[35b,o], R. Gupta[42], S. Gupta[120], G. Gustavino[132a,132b], P. Gutierrez[113], N.G. Gutierrez Ortiz[79], C. Gutschow[46], C. Guyot[136], C. Gwenlan[120], C.B. Gwilliam[75], A. Haas[110], C. Haber[16], H.K. Hadavand[8], N. Haddad[135e], A. Hadef[86], S. Hageböck[23], Z. Hajduk[41], H. Hakobyan[176,*], M. Haleem[44], J. Haley[114], G. Halladjian[91], G.D. Hallewell[86], K. Hamacher[174], P. Hamal[115], K. Hamano[168], A. Hamilton[145a], G.N. Hamity[139], P.G. Hamnett[44], L. Han[35b], K. Hanagaki[67,s], K. Hanawa[155], M. Hance[137], B. Haney[122], S. Hanisch[32], P. Hanke[59a], R. Hanna[136], J.B. Hansen[38], J.D. Hansen[38], M.C. Hansen[23], P.H. Hansen[38], K. Hara[160], A.S. Hard[172], T. Harenberg[174], F. Hariri[117], S. Harkusha[93], R.D. Harrington[48], P.F. Harrison[169], F. Hartjes[107], N.M. Hartmann[100], M. Hasegawa[68], Y. Hasegawa[140], A. Hasib[113], S. Hassani[136], S. Haug[18], R. Hauser[91], L. Hauswald[46], M. Havranek[127], C.M. Hawkes[19], R.J. Hawkings[32], D. Hayakawa[157], D. Hayden[91], C.P. Hays[120], J.M. Hays[77], H.S. Hayward[75], S.J. Haywood[131], S.J. Head[19], T. Heck[84], V. Hedberg[82], L. Heelan[8], S. Heim[122], T. Heim[16], B. Heinemann[16], J.J. Heinrich[100], L. Heinrich[110], C. Heinz[54], J. Hejbal[127], L. Helary[32], S. Hellman[146a,146b], C. Helsens[32], J. Henderson[120], R.C.W. Henderson[73], Y. Heng[172], S. Henkelmann[167], A.M. Henriques Correia[32], S. Henrot-Versille[117], G.H. Herbert[17], V. Herget[173], Y. Hernández Jiménez[166], G. Herten[50], R. Hertenberger[100], L. Hervas[32], G.G. Hesketh[79], N.P. Hessey[107], J.W. Hetherly[42], R. Hickling[77], E. Higón-Rodriguez[166], E. Hill[168], J.C. Hill[30], K.H. Hiller[44], S.J. Hillier[19], I. Hinchliffe[16], E. Hines[122], R.R. Hinman[16], M. Hirose[50], D. Hirschbuehl[174], J. Hobbs[148], N. Hod[159a], M.C. Hodgkinson[139], P. Hodgson[139], A. Hoecker[32], M.R. Hoeferkamp[105], F. Hoenig[100], D. Hohn[23], T.R. Holmes[16], M. Homann[45], T.M. Hong[125], B.H. Hooberman[165], W.H. Hopkins[116], Y. Horii[103], A.J. Horton[142], J-Y. Hostachy[57], S. Hou[151], A. Hoummada[135a], J. Howarth[44], M. Hrabovsky[115], I. Hristova[17], J. Hrivnac[117], T. Hryn'ova[5], A. Hrynevich[94], C. Hsu[145c], P.J. Hsu[151,t], S.-C. Hsu[138], D. Hu[37], Q. Hu[35b], S. Hu[35e], Y. Huang[44], Z. Hubacek[128], F. Hubaut[86], F. Huegging[23], T.B. Huffman[120], E.W. Hughes[37], G. Hughes[73], M. Huhtinen[32], P. Huo[148], N. Huseynov[66,b], J. Huston[91], J. Huth[58], G. Iacobucci[51], G. Iakovidis[27], I. Ibragimov[141], L. Iconomidou-Fayard[117], E. Ideal[175], Z. Idrissi[135e], P. Iengo[32], O. Igonkina[107,u], T. Iizawa[170], Y. Ikegami[67], M. Ikeno[67], Y. Ilchenko[11,v], D. Iliadis[154], N. Ilic[143], T. Ince[101], G. Introzzi[121a,121b], P. Ioannou[9,*], M. Iodice[134a], K. Iordanidou[37], V. Ippolito[58], N. Ishijima[118], M. Ishino[155], M. Ishitsuka[157], R. Ishmukhametov[111], C. Issever[120], S. Istin[20a], F. Ito[160],

J.M. Iturbe Ponce [85], R. Iuppa [133a,133b], W. Iwanski [41], H. Iwasaki [67], J.M. Izen [43], V. Izzo [104a], S. Jabbar [3], B. Jackson [122], P. Jackson [1], V. Jain [2], K.B. Jakobi [84], K. Jakobs [50], S. Jakobsen [32], T. Jakoubek [127], D.O. Jamin [114], D.K. Jana [80], E. Jansen [79], R. Jansky [63], J. Janssen [23], M. Janus [56], G. Jarlskog [82], N. Javadov [66,b], T. Javůrek [50], F. Jeanneau [136], L. Jeanty [16], J. Jejelava [53a,w], G.-Y. Jeng [150], D. Jennens [89], P. Jenni [50,x], C. Jeske [169], S. Jézéquel [5], H. Ji [172], J. Jia [148], H. Jiang [65], Y. Jiang [35b], S. Jiggins [79], J. Jimenez Pena [166], S. Jin [35a], A. Jinaru [28b], O. Jinnouchi [157], P. Johansson [139], K.A. Johns [7], W.J. Johnson [138], K. Jon-And [146a,146b], G. Jones [169], R.W.L. Jones [73], S. Jones [7], T.J. Jones [75], J. Jongmanns [59a], P.M. Jorge [126a,126b], J. Jovicevic [159a], X. Ju [172], A. Juste Rozas [13,r], M.K. Köhler [171], A. Kaczmarska [41], M. Kado [117], H. Kagan [111], M. Kagan [143], S.J. Kahn [86], T. Kaji [170], E. Kajomovitz [47], C.W. Kalderon [120], A. Kaluza [84], S. Kama [42], A. Kamenshchikov [130], N. Kanaya [155], S. Kaneti [30], L. Kanjir [76], V.A. Kantserov [98], J. Kanzaki [67], B. Kaplan [110], L.S. Kaplan [172], A. Kapliy [33], D. Kar [145c], K. Karakostas [10], A. Karamaoun [3], N. Karastathis [10], M.J. Kareem [56], E. Karentzos [10], M. Karnevskiy [84], S.N. Karpov [66], Z.M. Karpova [66], K. Karthik [110], V. Kartvelishvili [73], A.N. Karyukhin [130], K. Kasahara [160], L. Kashif [172], R.D. Kass [111], A. Kastanas [15], Y. Kataoka [155], C. Kato [155], A. Katre [51], J. Katzy [44], K. Kawagoe [71], T. Kawamoto [155], G. Kawamura [56], V.F. Kazanin [109,c], R. Keeler [168], R. Kehoe [42], J.S. Keller [44], J.J. Kempster [78], K Kentaro [103], H. Keoshkerian [158], O. Kepka [127], B.P. Kerševan [76], S. Kersten [174], R.A. Keyes [88], M. Khader [165], F. Khalil-zada [12], A. Khanov [114], A.G. Kharlamov [109,c], T.J. Khoo [51], V. Khovanskiy [97], E. Khramov [66], J. Khubua [53b,y], S. Kido [68], C.R. Kilby [78], H.Y. Kim [8], S.H. Kim [160], Y.K. Kim [33], N. Kimura [154], O.M. Kind [17], B.T. King [75], M. King [166], S.B. King [167], J. Kirk [131], A.E. Kiryunin [101], T. Kishimoto [155], D. Kisielewska [40a], F. Kiss [50], K. Kiuchi [160], O. Kivernyk [136], E. Kladiva [144b], M.H. Klein [37], M. Klein [75], U. Klein [75], K. Kleinknecht [84], P. Klimek [108], A. Klimentov [27], R. Klingenberg [45], J.A. Klinger [139], T. Klioutchnikova [32], E.-E. Kluge [59a], P. Kluit [107], S. Kluth [101], J. Knapik [41], E. Kneringer [63], E.B.F.G. Knoops [86], A. Knue [55], A. Kobayashi [155], D. Kobayashi [157], T. Kobayashi [155], M. Kobel [46], M. Kocian [143], P. Kodys [129], N.M. Koehler [101], T. Koffas [31], E. Koffeman [107], T. Koi [143], H. Kolanoski [17], M. Kolb [59b], I. Koletsou [5], A.A. Komar [96,*], Y. Komori [155], T. Kondo [67], N. Kondrashova [44], K. Köneke [50], A.C. König [106], T. Kono [67,z], R. Konoplich [110,aa], N. Konstantinidis [79], R. Kopeliansky [62], S. Koperny [40a], L. Köpke [84], A.K. Kopp [50], K. Korcyl [41], K. Kordas [154], A. Korn [79], A.A. Korol [109,c], I. Korolkov [13], E.V. Korolkova [139], O. Kortner [101], S. Kortner [101], T. Kosek [129], V.V. Kostyukhin [23], A. Kotwal [47], A. Kourkoumeli-Charalampidi [154], C. Kourkoumelis [9], V. Kouskoura [27], A.B. Kowalewska [41], R. Kowalewski [168], T.Z. Kowalski [40a], C. Kozakai [155], W. Kozanecki [136], A.S. Kozhin [130], V.A. Kramarenko [99], G. Kramberger [76], D. Krasnopevtsev [98], M.W. Krasny [81], A. Krasznahorkay [32], A. Kravchenko [27], M. Kretz [59c], J. Kretzschmar [75], K. Kreutzfeldt [54], P. Krieger [158], K. Krizka [33], K. Kroeninger [45], H. Kroha [101], J. Kroll [122], J. Kroseberg [23], J. Krstic [14], U. Kruchonak [66], H. Krüger [23], N. Krumnack [65], A. Kruse [172], M.C. Kruse [47], M. Kruskal [24], T. Kubota [89], H. Kucuk [79], S. Kuday [4b], J.T. Kuechler [174], S. Kuehn [50], A. Kugel [59c], F. Kuger [173], A. Kuhl [137], T. Kuhl [44], V. Kukhtin [66], R. Kukla [136], Y. Kulchitsky [93], S. Kuleshov [34b], M. Kuna [132a,132b], T. Kunigo [69], A. Kupco [127], H. Kurashige [68], Y.A. Kurochkin [93], V. Kus [127], E.S. Kuwertz [168], M. Kuze [157], J. Kvita [115], T. Kwan [168], D. Kyriazopoulos [139], A. La Rosa [101], J.L. La Rosa Navarro [26d], L. La Rotonda [39a,39b], C. Lacasta [166], F. Lacava [132a,132b], J. Lacey [31], H. Lacker [17], D. Lacour [81], V.R. Lacuesta [166], E. Ladygin [66], R. Lafaye [5], B. Laforge [81], T. Lagouri [175], S. Lai [56], S. Lammers [62], W. Lampl [7], E. Lançon [136], U. Landgraf [50], M.P.J. Landon [77], M.C. Lanfermann [51], V.S. Lang [59a], J.C. Lange [13], A.J. Lankford [162], F. Lanni [27], K. Lantzsch [23], A. Lanza [121a], S. Laplace [81], C. Lapoire [32], J.F. Laporte [136], T. Lari [92a], F. Lasagni Manghi [22a,22b], M. Lassnig [32], P. Laurelli [49], W. Lavrijsen [16], A.T. Law [137], P. Laycock [75], T. Lazovich [58], M. Lazzaroni [92a,92b], B. Le [89], O. Le Dortz [81], E. Le Guirriec [86], E.P. Le Quilleuc [136], M. LeBlanc [168], T. LeCompte [6], F. Ledroit-Guillon [57], C.A. Lee [27], S.C. Lee [151], L. Lee [1], B. Lefebvre [88], G. Lefebvre [81], M. Lefebvre [168], F. Legger [100], C. Leggett [16], A. Lehan [75], G. Lehmann Miotto [32], X. Lei [7], W.A. Leight [31], A. Leisos [154,ab], A.G. Leister [175], M.A.L. Leite [26d], R. Leitner [129], D. Lellouch [171], B. Lemmer [56], K.J.C. Leney [79], T. Lenz [23], B. Lenzi [32], R. Leone [7], S. Leone [124a,124b], C. Leonidopoulos [48], S. Leontsinis [10], G. Lerner [149], C. Leroy [95], A.A.J. Lesage [136], C.G. Lester [30], M. Levchenko [123], J. Levêque [5], D. Levin [90], L.J. Levinson [171], M. Levy [19], D. Lewis [77], A.M. Leyko [23], M. Leyton [43], B. Li [35b,o], C. Li [35b], H. Li [148], H.L. Li [33], L. Li [47], L. Li [35e], Q. Li [35a], S. Li [47], X. Li [85], Y. Li [141], Z. Liang [35a], B. Liberti [133a], A. Liblong [158], P. Lichard [32], K. Lie [165], J. Liebal [23], W. Liebig [15], A. Limosani [150], S.C. Lin [151,ac], T.H. Lin [84], B.E. Lindquist [148], A.E. Lionti [51], E. Lipeles [122], A. Lipniacka [15], M. Lisovyi [59b], T.M. Liss [165], A. Lister [167],

A.M. Litke [137], B. Liu [151,ad], D. Liu [151], H. Liu [90], H. Liu [27], J. Liu [86], J.B. Liu [35b], K. Liu [86], L. Liu [165], M. Liu [47], M. Liu [35b], Y.L. Liu [35b], Y. Liu [35b], M. Livan [121a,121b], A. Lleres [57], J. Llorente Merino [35a], S.L. Lloyd [77], F. Lo Sterzo [151], E. Lobodzinska [44], P. Loch [7], W.S. Lockman [137], F.K. Loebinger [85], A.E. Loevschall-Jensen [38], K.M. Loew [25], A. Loginov [175], T. Lohse [17], K. Lohwasser [44], M. Lokajicek [127], B.A. Long [24], J.D. Long [165], R.E. Long [73], L. Longo [74a,74b], K.A. Looper [111], L. Lopes [126a], D. Lopez Mateos [58], B. Lopez Paredes [139], I. Lopez Paz [13], A. Lopez Solis [81], J. Lorenz [100], N. Lorenzo Martinez [62], M. Losada [21], P.J. Lösel [100], X. Lou [35a], A. Lounis [117], J. Love [6], P.A. Love [73], H. Lu [61a], N. Lu [90], H.J. Lubatti [138], C. Luci [132a,132b], A. Lucotte [57], C. Luedtke [50], F. Luehring [62], W. Lukas [63], L. Luminari [132a], O. Lundberg [146a,146b], B. Lund-Jensen [147], P.M. Luzi [81], D. Lynn [27], R. Lysak [127], E. Lytken [82], V. Lyubushkin [66], H. Ma [27], L.L. Ma [35d], Y. Ma [35d], G. Maccarrone [49], A. Macchiolo [101], C.M. Macdonald [139], B. Maček [76], J. Machado Miguens [122,126b], D. Madaffari [86], R. Madar [36], H.J. Maddocks [164], W.F. Mader [46], A. Madsen [44], J. Maeda [68], S. Maeland [15], T. Maeno [27], A. Maevskiy [99], E. Magradze [56], J. Mahlstedt [107], C. Maiani [117], C. Maidantchik [26a], A.A. Maier [101], T. Maier [100], A. Maio [126a,126b,126d], S. Majewski [116], Y. Makida [67], N. Makovec [117], B. Malaescu [81], Pa. Malecki [41], V.P. Maleev [123], F. Malek [57], U. Mallik [64], D. Malon [6], C. Malone [143], S. Maltezos [10], S. Malyukov [32], J. Mamuzic [166], G. Mancini [49], B. Mandelli [32], L. Mandelli [92a], I. Mandić [76], J. Maneira [126a,126b], L. Manhaes de Andrade Filho [26b], J. Manjarres Ramos [159b], A. Mann [100], A. Manousos [32], B. Mansoulie [136], J.D. Mansour [35a], R. Mantifel [88], M. Mantoani [56], S. Manzoni [92a,92b], L. Mapelli [32], G. Marceca [29], L. March [51], G. Marchiori [81], M. Marcisovsky [127], M. Marjanovic [14], D.E. Marley [90], F. Marroquim [26a], S.P. Marsden [85], Z. Marshall [16], S. Marti-Garcia [166], B. Martin [91], T.A. Martin [169], V.J. Martin [48], B. Martin dit Latour [15], M. Martinez [13,r], V.I. Martinez Outschoorn [165], S. Martin-Haugh [131], V.S. Martoiu [28b], A.C. Martyniuk [79], M. Marx [138], A. Marzin [32], L. Masetti [84], T. Mashimo [155], R. Mashinistov [96], J. Masik [85], A.L. Maslennikov [109,c], I. Massa [22a,22b], L. Massa [22a,22b], P. Mastrandrea [5], A. Mastroberardino [39a,39b], T. Masubuchi [155], P. Mättig [174], J. Mattmann [84], J. Maurer [28b], S.J. Maxfield [75], D.A. Maximov [109,c], R. Mazini [151], S.M. Mazza [92a,92b], N.C. Mc Fadden [105], G. Mc Goldrick [158], S.P. Mc Kee [90], A. McCarn [90], R.L. McCarthy [148], T.G. McCarthy [101], L.I. McClymont [79], E.F. McDonald [89], J.A. Mcfayden [79], G. Mchedlidze [56], S.J. McMahon [131], R.A. McPherson [168,l], M. Medinnis [44], S. Meehan [138], S. Mehlhase [100], A. Mehta [75], K. Meier [59a], C. Meineck [100], B. Meirose [43], D. Melini [166], B.R. Mellado Garcia [145c], M. Melo [144a], F. Meloni [18], A. Mengarelli [22a,22b], S. Menke [101], E. Meoni [161], S. Mergelmeyer [17], P. Mermod [51], L. Merola [104a,104b], C. Meroni [92a], F.S. Merritt [33], A. Messina [132a,132b], J. Metcalfe [6], A.S. Mete [162], C. Meyer [84], C. Meyer [122], J-P. Meyer [136], J. Meyer [107], H. Meyer Zu Theenhausen [59a], F. Miano [149], R.P. Middleton [131], S. Miglioranzi [52a,52b], L. Mijović [48], G. Mikenberg [171], M. Mikestikova [127], M. Mikuž [76], M. Milesi [89], A. Milic [63], D.W. Miller [33], C. Mills [48], A. Milov [171], D.A. Milstead [146a,146b], A.A. Minaenko [130], Y. Minami [155], I.A. Minashvili [66], A.I. Mincer [110], B. Mindur [40a], M. Mineev [66], Y. Ming [172], L.M. Mir [13], K.P. Mistry [122], T. Mitani [170], J. Mitrevski [100], V.A. Mitsou [166], A. Miucci [51], P.S. Miyagawa [139], J.U. Mjörnmark [82], T. Moa [146a,146b], K. Mochizuki [95], S. Mohapatra [37], S. Molander [146a,146b], R. Moles-Valls [23], R. Monden [69], M.C. Mondragon [91], K. Mönig [44], J. Monk [38], E. Monnier [86], A. Montalbano [148], J. Montejo Berlingen [32], F. Monticelli [72], S. Monzani [92a,92b], R.W. Moore [3], N. Morange [117], D. Moreno [21], M. Moreno Llácer [56], P. Morettini [52a], D. Mori [142], T. Mori [155], M. Morii [58], M. Morinaga [155], V. Morisbak [119], S. Moritz [84], A.K. Morley [150], G. Mornacchi [32], J.D. Morris [77], S.S. Mortensen [38], L. Morvaj [148], M. Mosidze [53b], J. Moss [143], K. Motohashi [157], R. Mount [143], E. Mountricha [27], S.V. Mouraviev [96,*], E.J.W. Moyse [87], S. Muanza [86], R.D. Mudd [19], F. Mueller [101], J. Mueller [125], R.S.P. Mueller [100], T. Mueller [30], D. Muenstermann [73], P. Mullen [55], G.A. Mullier [18], F.J. Munoz Sanchez [85], J.A. Murillo Quijada [19], W.J. Murray [169,131], H. Musheghyan [56], M. Muškinja [76], A.G. Myagkov [130,ae], M. Myska [128], B.P. Nachman [143], O. Nackenhorst [51], K. Nagai [120], R. Nagai [67,z], K. Nagano [67], Y. Nagasaka [60], K. Nagata [160], M. Nagel [50], E. Nagy [86], A.M. Nairz [32], Y. Nakahama [103], K. Nakamura [67], T. Nakamura [155], I. Nakano [112], H. Namasivayam [43], R.F. Naranjo Garcia [44], R. Narayan [11], D.I. Narrias Villar [59a], I. Naryshkin [123], T. Naumann [44], G. Navarro [21], R. Nayyar [7], H.A. Neal [90], P.Yu. Nechaeva [96], T.J. Neep [85], A. Negri [121a,121b], M. Negrini [22a], S. Nektarijevic [106], C. Nellist [117], A. Nelson [162], S. Nemecek [127], P. Nemethy [110], A.A. Nepomuceno [26a], M. Nessi [32,af], M.S. Neubauer [165], M. Neumann [174], R.M. Neves [110], P. Nevski [27], P.R. Newman [19], D.H. Nguyen [6], T. Nguyen Manh [95], R.B. Nickerson [120], R. Nicolaidou [136], J. Nielsen [137], A. Nikiforov [17], V. Nikolaenko [130,ae], I. Nikolic-Audit [81], K. Nikolopoulos [19], J.K. Nilsen [119], P. Nilsson [27], Y. Ninomiya [155], A. Nisati [132a], R. Nisius [101], T. Nobe [155],

M. Nomachi [118], I. Nomidis [31], T. Nooney [77], S. Norberg [113], M. Nordberg [32], N. Norjoharuddeen [120], O. Novgorodova [46], S. Nowak [101], M. Nozaki [67], L. Nozka [115], K. Ntekas [10], E. Nurse [79], F. Nuti [89], F. O'grady [7], D.C. O'Neil [142], A.A. O'Rourke [44], V. O'Shea [55], F.G. Oakham [31,d], H. Oberlack [101], T. Obermann [23], J. Ocariz [81], A. Ochi [68], I. Ochoa [37], J.P. Ochoa-Ricoux [34a], S. Oda [71], S. Odaka [67], H. Ogren [62], A. Oh [85], S.H. Oh [47], C.C. Ohm [16], H. Ohman [164], H. Oide [32], H. Okawa [160], Y. Okumura [155], T. Okuyama [67], A. Olariu [28b], L.F. Oleiro Seabra [126a], S.A. Olivares Pino [48], D. Oliveira Damazio [27], A. Olszewski [41], J. Olszowska [41], A. Onofre [126a,126e], K. Onogi [103], P.U.E. Onyisi [11,v], M.J. Oreglia [33], Y. Oren [153], D. Orestano [134a,134b], N. Orlando [61b], R.S. Orr [158], B. Osculati [52a,52b], R. Ospanov [85], G. Otero y Garzon [29], H. Otono [71], M. Ouchrif [135d], F. Ould-Saada [119], A. Ouraou [136], K.P. Oussoren [107], Q. Ouyang [35a], M. Owen [55], R.E. Owen [19], V.E. Ozcan [20a], N. Ozturk [8], K. Pachal [142], A. Pacheco Pages [13], L. Pacheco Rodriguez [136], C. Padilla Aranda [13], M. Pagáčová [50], S. Pagan Griso [16], F. Paige [27], P. Pais [87], K. Pajchel [119], G. Palacino [159b], S. Palestini [32], M. Palka [40b], D. Pallin [36], E.St. Panagiotopoulou [10], C.E. Pandini [81], J.G. Panduro Vazquez [78], P. Pani [146a,146b], S. Panitkin [27], D. Pantea [28b], L. Paolozzi [51], Th.D. Papadopoulou [10], K. Papageorgiou [154], A. Paramonov [6], D. Paredes Hernandez [175], A.J. Parker [73], M.A. Parker [30], K.A. Parker [139], F. Parodi [52a,52b], J.A. Parsons [37], U. Parzefall [50], V.R. Pascuzzi [158], E. Pasqualucci [132a], S. Passaggio [52a], Fr. Pastore [78], G. Pásztor [31,ag], S. Pataraia [174], J.R. Pater [85], T. Pauly [32], J. Pearce [168], B. Pearson [113], L.E. Pedersen [38], M. Pedersen [119], S. Pedraza Lopez [166], R. Pedro [126a,126b], S.V. Peleganchuk [109,c], O. Penc [127], C. Peng [35a], H. Peng [35b], J. Penwell [62], B.S. Peralva [26b], M.M. Perego [136], D.V. Perepelitsa [27], E. Perez Codina [159a], L. Perini [92a,92b], H. Pernegger [32], S. Perrella [104a,104b], R. Peschke [44], V.D. Peshekhonov [66], K. Peters [44], R.F.Y. Peters [85], B.A. Petersen [32], T.C. Petersen [38], E. Petit [57], A. Petridis [1], C. Petridou [154], P. Petroff [117], E. Petrolo [132a], M. Petrov [120], F. Petrucci [134a,134b], N.E. Pettersson [87], A. Peyaud [136], R. Pezoa [34b], P.W. Phillips [131], G. Piacquadio [143], E. Pianori [169], A. Picazio [87], E. Piccaro [77], M. Piccinini [22a,22b], M.A. Pickering [120], R. Piegaia [29], J.E. Pilcher [33], A.D. Pilkington [85], A.W.J. Pin [85], M. Pinamonti [163a,163c,ah], J.L. Pinfold [3], A. Pingel [38], S. Pires [81], H. Pirumov [44], M. Pitt [171], L. Plazak [144a], M.-A. Pleier [27], V. Pleskot [84], E. Plotnikova [66], P. Plucinski [91], D. Pluth [65], R. Poettgen [146a,146b], L. Poggioli [117], D. Pohl [23], G. Polesello [121a], A. Poley [44], A. Policicchio [39a,39b], R. Polifka [158], A. Polini [22a], C.S. Pollard [55], V. Polychronakos [27], K. Pommès [32], L. Pontecorvo [132a], B.G. Pope [91], G.A. Popeneciu [28c], D.S. Popovic [14], A. Poppleton [32], S. Pospisil [128], K. Potamianos [16], I.N. Potrap [66], C.J. Potter [30], C.T. Potter [116], G. Poulard [32], J. Poveda [32], V. Pozdnyakov [66], M.E. Pozo Astigarraga [32], P. Pralavorio [86], A. Pranko [16], S. Prell [65], D. Price [85], L.E. Price [6], M. Primavera [74a], S. Prince [88], K. Prokofiev [61c], F. Prokoshin [34b], S. Protopopescu [27], J. Proudfoot [6], M. Przybycien [40a], D. Puddu [134a,134b], M. Purohit [27,ai], P. Puzo [117], J. Qian [90], G. Qin [55], Y. Qin [85], A. Quadt [56], W.B. Quayle [163a,163b], M. Queitsch-Maitland [85], D. Quilty [55], S. Raddum [119], V. Radeka [27], V. Radescu [59b], S.K. Radhakrishnan [148], P. Radloff [116], P. Rados [89], F. Ragusa [92a,92b], G. Rahal [177], J.A. Raine [85], S. Rajagopalan [27], M. Rammensee [32], C. Rangel-Smith [164], M.G. Ratti [92a,92b], F. Rauscher [100], S. Rave [84], T. Ravenscroft [55], I. Ravinovich [171], M. Raymond [32], A.L. Read [119], N.P. Readioff [75], M. Reale [74a,74b], D.M. Rebuzzi [121a,121b], A. Redelbach [173], G. Redlinger [27], R. Reece [137], K. Reeves [43], L. Rehnisch [17], J. Reichert [122], H. Reisin [29], C. Rembser [32], H. Ren [35a], M. Rescigno [132a], S. Resconi [92a], O.L. Rezanova [109,c], P. Reznicek [129], R. Rezvani [95], R. Richter [101], S. Richter [79], E. Richter-Was [40b], O. Ricken [23], M. Ridel [81], P. Rieck [17], C.J. Riegel [174], J. Rieger [56], O. Rifki [113], M. Rijssenbeek [148], A. Rimoldi [121a,121b], M. Rimoldi [18], L. Rinaldi [22a], B. Ristić [51], E. Ritsch [32], I. Riu [13], F. Rizatdinova [114], E. Rizvi [77], C. Rizzi [13], S.H. Robertson [88,l], A. Robichaud-Veronneau [88], D. Robinson [30], J.E.M. Robinson [44], A. Robson [55], C. Roda [124a,124b], Y. Rodina [86], A. Rodriguez Perez [13], D. Rodriguez Rodriguez [166], S. Roe [32], C.S. Rogan [58], O. Røhne [119], A. Romaniouk [98], M. Romano [22a,22b], S.M. Romano Saez [36], E. Romero Adam [166], N. Rompotis [138], M. Ronzani [50], L. Roos [81], E. Ros [166], S. Rosati [132a], K. Rosbach [50], P. Rose [137], O. Rosenthal [141], N.-A. Rosien [56], V. Rossetti [146a,146b], E. Rossi [104a,104b], L.P. Rossi [52a], J.H.N. Rosten [30], R. Rosten [138], M. Rotaru [28b], I. Roth [171], J. Rothberg [138], D. Rousseau [117], C.R. Royon [136], A. Rozanov [86], Y. Rozen [152], X. Ruan [145c], F. Rubbo [143], M.S. Rudolph [158], F. Rühr [50], A. Ruiz-Martinez [31], Z. Rurikova [50], N.A. Rusakovich [66], A. Ruschke [100], H.L. Russell [138], J.P. Rutherfoord [7], N. Ruthmann [32], Y.F. Ryabov [123], M. Rybar [165], G. Rybkin [117], S. Ryu [6], A. Ryzhov [130], G.F. Rzehorz [56], A.F. Saavedra [150], G. Sabato [107], S. Sacerdoti [29], H.F-W. Sadrozinski [137], R. Sadykov [66], F. Safai Tehrani [132a], P. Saha [108], M. Sahinsoy [59a], M. Saimpert [136], T. Saito [155], H. Sakamoto [155], Y. Sakurai [170], G. Salamanna [134a,134b], A. Salamon [133a,133b], J.E. Salazar Loyola [34b], D. Salek [107],

P.H. Sales De Bruin [138], D. Salihagic [101], A. Salnikov [143], J. Salt [166], D. Salvatore [39a,39b], F. Salvatore [149], A. Salvucci [61a], A. Salzburger [32], D. Sammel [50], D. Sampsonidis [154], A. Sanchez [104a,104b], J. Sánchez [166], V. Sanchez Martinez [166], H. Sandaker [119], R.L. Sandbach [77], H.G. Sander [84], M. Sandhoff [174], C. Sandoval [21], R. Sandstroem [101], D.P.C. Sankey [131], M. Sannino [52a,52b], A. Sansoni [49], C. Santoni [36], R. Santonico [133a,133b], H. Santos [126a], I. Santoyo Castillo [149], K. Sapp [125], A. Sapronov [66], J.G. Saraiva [126a,126d], B. Sarrazin [23], O. Sasaki [67], Y. Sasaki [155], K. Sato [160], G. Sauvage [5,*], E. Sauvan [5], G. Savage [78], P. Savard [158,d], N. Savic [101], C. Sawyer [131], L. Sawyer [80,q], J. Saxon [33], C. Sbarra [22a], A. Sbrizzi [22a,22b], T. Scanlon [79], D.A. Scannicchio [162], M. Scarcella [150], V. Scarfone [39a,39b], J. Schaarschmidt [171], P. Schacht [101], B.M. Schachtner [100], D. Schaefer [32], R. Schaefer [44], J. Schaeffer [84], S. Schaepe [23], S. Schaetzel [59b], U. Schäfer [84], A.C. Schaffer [117], D. Schaile [100], R.D. Schamberger [148], V. Scharf [59a], V.A. Schegelsky [123], D. Scheirich [129], M. Schernau [162], C. Schiavi [52a,52b], S. Schier [137], C. Schillo [50], M. Schioppa [39a,39b], S. Schlenker [32], K.R. Schmidt-Sommerfeld [101], K. Schmieden [32], C. Schmitt [84], S. Schmitt [44], S. Schmitz [84], B. Schneider [159a], U. Schnoor [50], L. Schoeffel [136], A. Schoening [59b], B.D. Schoenrock [91], E. Schopf [23], M. Schott [84], J. Schovancova [8], S. Schramm [51], M. Schreyer [173], N. Schuh [84], A. Schulte [84], M.J. Schultens [23], H.-C. Schultz-Coulon [59a], H. Schulz [17], M. Schumacher [50], B.A. Schumm [137], Ph. Schune [136], A. Schwartzman [143], T.A. Schwarz [90], H. Schweiger [85], Ph. Schwemling [136], R. Schwienhorst [91], J. Schwindling [136], T. Schwindt [23], G. Sciolla [25], F. Scuri [124a,124b], F. Scutti [89], J. Searcy [90], P. Seema [23], S.C. Seidel [105], A. Seiden [137], F. Seifert [128], J.M. Seixas [26a], G. Sekhniaidze [104a], K. Sekhon [90], S.J. Sekula [42], D.M. Seliverstov [123,*], N. Semprini-Cesari [22a,22b], C. Serfon [119], L. Serin [117], L. Serkin [163a,163b], M. Sessa [134a,134b], R. Seuster [168], H. Severini [113], T. Sfiligoj [76], F. Sforza [32], A. Sfyrla [51], E. Shabalina [56], N.W. Shaikh [146a,146b], L.Y. Shan [35a], R. Shang [165], J.T. Shank [24], M. Shapiro [16], P.B. Shatalov [97], K. Shaw [163a,163b], S.M. Shaw [85], A. Shcherbakova [146a,146b], C.Y. Shehu [149], P. Sherwood [79], L. Shi [151,aj], S. Shimizu [68], C.O. Shimmin [162], M. Shimojima [102], M. Shiyakova [66,ak], A. Shmeleva [96], D. Shoaleh Saadi [95], M.J. Shochet [33], S. Shojaii [92a,92b], S. Shrestha [111], E. Shulga [98], M.A. Shupe [7], P. Sicho [127], A.M. Sickles [165], P.E. Sidebo [147], O. Sidiropoulou [173], D. Sidorov [114], A. Sidoti [22a,22b], F. Siegert [46], Dj. Sijacki [14], J. Silva [126a,126d], S.B. Silverstein [146a], V. Simak [128], Lj. Simic [14], S. Simion [117], E. Simioni [84], B. Simmons [79], D. Simon [36], M. Simon [84], P. Sinervo [158], N.B. Sinev [116], M. Sioli [22a,22b], G. Siragusa [173], S.Yu. Sivoklokov [99], J. Sjölin [146a,146b], M.B. Skinner [73], H.P. Skottowe [58], P. Skubic [113], M. Slater [19], T. Slavicek [128], M. Slawinska [107], K. Sliwa [161], R. Slovak [129], V. Smakhtin [171], B.H. Smart [5], L. Smestad [15], J. Smiesko [144a], S.Yu. Smirnov [98], Y. Smirnov [98], L.N. Smirnova [99,al], O. Smirnova [82], M.N.K. Smith [37], R.W. Smith [37], M. Smizanska [73], K. Smolek [128], A.A. Snesarev [96], S. Snyder [27], R. Sobie [168,l], F. Socher [46], A. Soffer [153], D.A. Soh [151], G. Sokhrannyi [76], C.A. Solans Sanchez [32], M. Solar [128], E.Yu. Soldatov [98], U. Soldevila [166], A.A. Solodkov [130], A. Soloshenko [66], O.V. Solovyanov [130], V. Solovyev [123], P. Sommer [50], H. Son [161], H.Y. Song [35b,am], A. Sood [16], A. Sopczak [128], V. Sopko [128], V. Sorin [13], D. Sosa [59b], C.L. Sotiropoulou [124a,124b], R. Soualah [163a,163c], A.M. Soukharev [109,c], D. South [44], B.C. Sowden [78], S. Spagnolo [74a,74b], M. Spalla [124a,124b], M. Spangenberg [169], F. Spanò [78], D. Sperlich [17], F. Spettel [101], R. Spighi [22a], G. Spigo [32], L.A. Spiller [89], M. Spousta [129], R.D. St. Denis [55,*], A. Stabile [92a], R. Stamen [59a], S. Stamm [17], E. Stanecka [41], R.W. Stanek [6], C. Stanescu [134a], M. Stanescu-Bellu [44], M.M. Stanitzki [44], S. Stapnes [119], E.A. Starchenko [130], G.H. Stark [33], J. Stark [57], P. Staroba [127], P. Starovoitov [59a], S. Stärz [32], R. Staszewski [41], P. Steinberg [27], B. Stelzer [142], H.J. Stelzer [32], O. Stelzer-Chilton [159a], H. Stenzel [54], G.A. Stewart [55], J.A. Stillings [23], M.C. Stockton [88], M. Stoebe [88], G. Stoicea [28b], P. Stolte [56], S. Stonjek [101], A.R. Stradling [8], A. Straessner [46], M.E. Stramaglia [18], J. Strandberg [147], S. Strandberg [146a,146b], A. Strandlie [119], M. Strauss [113], P. Strizenec [144b], R. Ströhmer [173], D.M. Strom [116], R. Stroynowski [42], A. Strubig [106], S.A. Stucci [18], B. Stugu [15], N.A. Styles [44], D. Su [143], J. Su [125], S. Suchek [59a], Y. Sugaya [118], M. Suk [128], V.V. Sulin [96], S. Sultansoy [4c], T. Sumida [69], S. Sun [58], X. Sun [35a], J.E. Sundermann [50], K. Suruliz [149], G. Susinno [39a,39b], M.R. Sutton [149], S. Suzuki [67], M. Svatos [127], M. Swiatlowski [33], I. Sykora [144a], T. Sykora [129], D. Ta [50], C. Taccini [134a,134b], K. Tackmann [44], J. Taenzer [158], A. Taffard [162], R. Tafirout [159a], N. Taiblum [153], H. Takai [27], R. Takashima [70], T. Takeshita [140], Y. Takubo [67], M. Talby [86], A.A. Talyshev [109,c], K.G. Tan [89], J. Tanaka [155], M. Tanaka [157], R. Tanaka [117], S. Tanaka [67], B.B. Tannenwald [111], S. Tapia Araya [34b], S. Tapprogge [84], S. Tarem [152], G.F. Tartarelli [92a], P. Tas [129], M. Tasevsky [127], T. Tashiro [69], E. Tassi [39a,39b], A. Tavares Delgado [126a,126b], Y. Tayalati [135e], A.C. Taylor [105], G.N. Taylor [89], P.T.E. Taylor [89], W. Taylor [159b], F.A. Teischinger [32], P. Teixeira-Dias [78], K.K. Temming [50],

D. Temple [142], H. Ten Kate [32], P.K. Teng [151], J.J. Teoh [118], F. Tepel [174], S. Terada [67], K. Terashi [155], J. Terron [83], S. Terzo [101], M. Testa [49], R.J. Teuscher [158,l], T. Theveneaux-Pelzer [86], J.P. Thomas [19], J. Thomas-Wilsker [78], E.N. Thompson [37], P.D. Thompson [19], A.S. Thompson [55], L.A. Thomsen [175], E. Thomson [122], M. Thomson [30], M.J. Tibbetts [16], R.E. Ticse Torres [86], V.O. Tikhomirov [96,an], Yu.A. Tikhonov [109,c], S. Timoshenko [98], P. Tipton [175], S. Tisserant [86], K. Todome [157], T. Todorov [5,*], S. Todorova-Nova [129], J. Tojo [71], S. Tokár [144a], K. Tokushuku [67], E. Tolley [58], L. Tomlinson [85], M. Tomoto [103], L. Tompkins [143,ao], K. Toms [105], B. Tong [58], E. Torrence [116], H. Torres [142], E. Torró Pastor [138], J. Toth [86,ap], F. Touchard [86], D.R. Tovey [139], T. Trefzger [173], A. Tricoli [27], I.M. Trigger [159a], S. Trincaz-Duvoid [81], M.F. Tripiana [13], W. Trischuk [158], B. Trocmé [57], A. Trofymov [44], C. Troncon [92a], M. Trottier-McDonald [16], M. Trovatelli [168], L. Truong [163a,163c], M. Trzebinski [41], A. Trzupek [41], J.C-L. Tseng [120], P.V. Tsiareshka [93], G. Tsipolitis [10], N. Tsirintanis [9], S. Tsiskaridze [13], V. Tsiskaridze [50], E.G. Tskhadadze [53a], K.M. Tsui [61a], I.I. Tsukerman [97], V. Tsulaia [16], S. Tsuno [67], D. Tsybychev [148], Y. Tu [61b], A. Tudorache [28b], V. Tudorache [28b], A.N. Tuna [58], S.A. Tupputi [22a,22b], S. Turchikhin [66], D. Turecek [128], D. Turgeman [171], R. Turra [92a,92b], A.J. Turvey [42], P.M. Tuts [37], M. Tyndel [131], G. Ucchielli [22a,22b], I. Ueda [155], M. Ughetto [146a,146b], F. Ukegawa [160], G. Unal [32], A. Undrus [27], G. Unel [162], F.C. Ungaro [89], Y. Unno [67], C. Unverdorben [100], J. Urban [144b], P. Urquijo [89], P. Urrejola [84], G. Usai [8], A. Usanova [63], L. Vacavant [86], V. Vacek [128], B. Vachon [88], C. Valderanis [100], E. Valdes Santurio [146a,146b], N. Valencic [107], S. Valentinetti [22a,22b], A. Valero [166], L. Valery [13], S. Valkar [129], J.A. Valls Ferrer [166], W. Van Den Wollenberg [107], P.C. Van Der Deijl [107], H. van der Graaf [107], N. van Eldik [152], P. van Gemmeren [6], J. Van Nieuwkoop [142], I. van Vulpen [107], M.C. van Woerden [32], M. Vanadia [132a,132b], W. Vandelli [32], R. Vanguri [122], A. Vaniachine [130], P. Vankov [107], G. Vardanyan [176], R. Vari [132a], E.W. Varnes [7], T. Varol [42], D. Varouchas [81], A. Vartapetian [8], K.E. Varvell [150], J.G. Vasquez [175], F. Vazeille [36], T. Vazquez Schroeder [88], J. Veatch [56], V. Veeraraghavan [7], L.M. Veloce [158], F. Veloso [126a,126c], S. Veneziano [132a], A. Ventura [74a,74b], M. Venturi [168], N. Venturi [158], A. Venturini [25], V. Vercesi [121a], M. Verducci [132a,132b], W. Verkerke [107], J.C. Vermeulen [107], A. Vest [46,aq], M.C. Vetterli [142,d], O. Viazlo [82], I. Vichou [165], T. Vickey [139], O.E. Vickey Boeriu [139], G.H.A. Viehhauser [120], S. Viel [16], L. Vigani [120], M. Villa [22a,22b], M. Villaplana Perez [92a,92b], E. Vilucchi [49], M.G. Vincter [31], V.B. Vinogradov [66], C. Vittori [22a,22b], I. Vivarelli [149], S. Vlachos [10], M. Vlasak [128], M. Vogel [174], P. Vokac [128], G. Volpi [124a,124b], M. Volpi [89], H. von der Schmitt [101], E. von Toerne [23], V. Vorobel [129], K. Vorobev [98], M. Vos [166], R. Voss [32], J.H. Vossebeld [75], N. Vranjes [14], M. Vranjes Milosavljevic [14], V. Vrba [127], M. Vreeswijk [107], R. Vuillermet [32], I. Vukotic [33], Z. Vykydal [128], P. Wagner [23], W. Wagner [174], H. Wahlberg [72], S. Wahrmund [46], J. Wakabayashi [103], J. Walder [73], R. Walker [100], W. Walkowiak [141], V. Wallangen [146a,146b], C. Wang [35c], C. Wang [35d,86], F. Wang [172], H. Wang [16], H. Wang [42], J. Wang [44], J. Wang [150], K. Wang [88], R. Wang [6], S.M. Wang [151], T. Wang [23], T. Wang [37], W. Wang [35b], X. Wang [175], C. Wanotayaroj [116], A. Warburton [88], C.P. Ward [30], D.R. Wardrope [79], A. Washbrook [48], P.M. Watkins [19], A.T. Watson [19], M.F. Watson [19], G. Watts [138], S. Watts [85], B.M. Waugh [79], S. Webb [84], M.S. Weber [18], S.W. Weber [173], J.S. Webster [6], A.R. Weidberg [120], B. Weinert [62], J. Weingarten [56], C. Weiser [50], H. Weits [107], P.S. Wells [32], T. Wenaus [27], T. Wengler [32], S. Wenig [32], N. Wermes [23], M. Werner [50], M.D. Werner [65], P. Werner [32], M. Wessels [59a], J. Wetter [161], K. Whalen [116], N.L. Whallon [138], A.M. Wharton [73], A. White [8], M.J. White [1], R. White [34b], D. Whiteson [162], F.J. Wickens [131], W. Wiedenmann [172], M. Wielers [131], P. Wienemann [23], C. Wiglesworth [38], L.A.M. Wiik-Fuchs [23], A. Wildauer [101], F. Wilk [85], H.G. Wilkens [32], H.H. Williams [122], S. Williams [107], C. Willis [91], S. Willocq [87], J.A. Wilson [19], I. Wingerter-Seez [5], F. Winklmeier [116], O.J. Winston [149], B.T. Winter [23], M. Wittgen [143], J. Wittkowski [100], T.M.H. Wolf [107], M.W. Wolter [41], H. Wolters [126a,126c], S.D. Worm [131], B.K. Wosiek [41], J. Wotschack [32], M.J. Woudstra [85], K.W. Wozniak [41], M. Wu [57], M. Wu [33], S.L. Wu [172], X. Wu [51], Y. Wu [90], T.R. Wyatt [85], B.M. Wynne [48], S. Xella [38], D. Xu [35a], L. Xu [27], B. Yabsley [150], S. Yacoob [145a], D. Yamaguchi [157], Y. Yamaguchi [118], A. Yamamoto [67], S. Yamamoto [155], T. Yamanaka [155], K. Yamauchi [103], Y. Yamazaki [68], Z. Yan [24], H. Yang [35e], H. Yang [172], Y. Yang [151], Z. Yang [15], W-M. Yao [16], Y.C. Yap [81], Y. Yasu [67], E. Yatsenko [5], K.H. Yau Wong [23], J. Ye [42], S. Ye [27], I. Yeletskikh [66], A.L. Yen [58], E. Yildirim [84], K. Yorita [170], R. Yoshida [6], K. Yoshihara [122], C. Young [143], C.J.S. Young [32], S. Youssef [24], D.R. Yu [16], J. Yu [8], J.M. Yu [90], J. Yu [65], L. Yuan [68], S.P.Y. Yuen [23], I. Yusuff [30,ar], B. Zabinski [41], R. Zaidan [35d], A.M. Zaitsev [130,ae], N. Zakharchuk [44], J. Zalieckas [15], A. Zaman [148], S. Zambito [58], L. Zanello [132a,132b], D. Zanzi [89], C. Zeitnitz [174], M. Zeman [128], A. Zemla [40a], J.C. Zeng [165], Q. Zeng [143], K. Zengel [25], O. Zenin [130], T. Ženiš [144a], D. Zerwas [117], D. Zhang [90], F. Zhang [172],

G. Zhang [35b,am], H. Zhang [35c], J. Zhang [6], L. Zhang [50], R. Zhang [23], R. Zhang [35b,as], X. Zhang [35d], Z. Zhang [117], X. Zhao [42], Y. Zhao [35d], Z. Zhao [35b], A. Zhemchugov [66], J. Zhong [120], B. Zhou [90], C. Zhou [47], L. Zhou [37], L. Zhou [42], M. Zhou [148], N. Zhou [35f], C.G. Zhu [35d], H. Zhu [35a], J. Zhu [90], Y. Zhu [35b], X. Zhuang [35a], K. Zhukov [96], A. Zibell [173], D. Zieminska [62], N.I. Zimine [66], C. Zimmermann [84], S. Zimmermann [50], Z. Zinonos [56], M. Zinser [84], M. Ziolkowski [141], L. Živković [14], G. Zobernig [172], A. Zoccoli [22a,22b], M. zur Nedden [17], L. Zwalinski [32]

[1] *Department of Physics, University of Adelaide, Adelaide, Australia*
[2] *Physics Department, SUNY Albany, Albany NY, United States*
[3] *Department of Physics, University of Alberta, Edmonton AB, Canada*
[4] [(a)] *Department of Physics, Ankara University, Ankara;* [(b)] *Istanbul Aydin University, Istanbul;* [(c)] *Division of Physics, TOBB University of Economics and Technology, Ankara, Turkey*
[5] *LAPP, CNRS/IN2P3 and Université Savoie Mont Blanc, Annecy-le-Vieux, France*
[6] *High Energy Physics Division, Argonne National Laboratory, Argonne IL, United States*
[7] *Department of Physics, University of Arizona, Tucson AZ, United States*
[8] *Department of Physics, The University of Texas at Arlington, Arlington TX, United States*
[9] *Physics Department, University of Athens, Athens, Greece*
[10] *Physics Department, National Technical University of Athens, Zografou, Greece*
[11] *Department of Physics, The University of Texas at Austin, Austin TX, United States*
[12] *Institute of Physics, Azerbaijan Academy of Sciences, Baku, Azerbaijan*
[13] *Institut de Física d'Altes Energies (IFAE), The Barcelona Institute of Science and Technology, Barcelona, Spain*
[14] *Institute of Physics, University of Belgrade, Belgrade, Serbia*
[15] *Department for Physics and Technology, University of Bergen, Bergen, Norway*
[16] *Physics Division, Lawrence Berkeley National Laboratory and University of California, Berkeley CA, United States*
[17] *Department of Physics, Humboldt University, Berlin, Germany*
[18] *Albert Einstein Center for Fundamental Physics and Laboratory for High Energy Physics, University of Bern, Bern, Switzerland*
[19] *School of Physics and Astronomy, University of Birmingham, Birmingham, United Kingdom*
[20] [(a)] *Department of Physics, Bogazici University, Istanbul;* [(b)] *Department of Physics Engineering, Gaziantep University, Gaziantep;* [(d)] *Istanbul Bilgi University, Faculty of Engineering and Natural Sciences, Istanbul;* [(e)] *Bahcesehir University, Faculty of Engineering and Natural Sciences, Istanbul, Turkey*
[21] *Centro de Investigaciones, Universidad Antonio Narino, Bogota, Colombia*
[22] [(a)] *INFN Sezione di Bologna;* [(b)] *Dipartimento di Fisica e Astronomia, Università di Bologna, Bologna, Italy*
[23] *Physikalisches Institut, University of Bonn, Bonn, Germany*
[24] *Department of Physics, Boston University, Boston MA, United States*
[25] *Department of Physics, Brandeis University, Waltham MA, United States*
[26] [(a)] *Universidade Federal do Rio De Janeiro COPPE/EE/IF, Rio de Janeiro;* [(b)] *Electrical Circuits Department, Federal University of Juiz de Fora (UFJF), Juiz de Fora;* [(c)] *Federal University of Sao Joao del Rei (UFSJ), Sao Joao del Rei;* [(d)] *Instituto de Fisica, Universidade de Sao Paulo, Sao Paulo, Brazil*
[27] *Physics Department, Brookhaven National Laboratory, Upton NY, United States*
[28] [(a)] *Transilvania University of Brasov, Brasov;* [(b)] *National Institute of Physics and Nuclear Engineering, Bucharest;* [(c)] *National Institute for Research and Development of Isotopic and Molecular Technologies, Physics Department, Cluj Napoca;* [(d)] *University Politehnica Bucharest, Bucharest;* [(e)] *West University in Timisoara, Timisoara, Romania*
[29] *Departamento de Física, Universidad de Buenos Aires, Buenos Aires, Argentina*
[30] *Cavendish Laboratory, University of Cambridge, Cambridge, United Kingdom*
[31] *Department of Physics, Carleton University, Ottawa ON, Canada*
[32] *CERN, Geneva, Switzerland*
[33] *Enrico Fermi Institute, University of Chicago, Chicago IL, United States*
[34] [(a)] *Departamento de Física, Pontificia Universidad Católica de Chile, Santiago;* [(b)] *Departamento de Física, Universidad Técnica Federico Santa María, Valparaíso, Chile*
[35] [(a)] *Institute of High Energy Physics, Chinese Academy of Sciences, Beijing;* [(b)] *Department of Modern Physics, University of Science and Technology of China, Anhui;* [(c)] *Department of Physics, Nanjing University, Jiangsu;* [(d)] *School of Physics, Shandong University, Shandong;* [(e)] *Department of Physics and Astronomy, Shanghai Key Laboratory for Particle Physics and Cosmology, Shanghai Jiao Tong University, Shanghai* [at]; [(f)] *Physics Department, Tsinghua University, Beijing 100084, China*
[36] *Laboratoire de Physique Corpusculaire, Clermont Université and Université Blaise Pascal and CNRS/IN2P3, Clermont-Ferrand, France*
[37] *Nevis Laboratory, Columbia University, Irvington NY, United States*
[38] *Niels Bohr Institute, University of Copenhagen, Kobenhavn, Denmark*
[39] [(a)] *INFN Gruppo Collegato di Cosenza, Laboratori Nazionali di Frascati;* [(b)] *Dipartimento di Fisica, Università della Calabria, Rende, Italy*
[40] [(a)] *AGH University of Science and Technology, Faculty of Physics and Applied Computer Science, Krakow;* [(b)] *Marian Smoluchowski Institute of Physics, Jagiellonian University, Krakow, Poland*
[41] *Institute of Nuclear Physics Polish Academy of Sciences, Krakow, Poland*
[42] *Physics Department, Southern Methodist University, Dallas TX, United States*
[43] *Physics Department, University of Texas at Dallas, Richardson TX, United States*
[44] *DESY, Hamburg and Zeuthen, Germany*
[45] *Institut für Experimentelle Physik IV, Technische Universität Dortmund, Dortmund, Germany*
[46] *Institut für Kern- und Teilchenphysik, Technische Universität Dresden, Dresden, Germany*
[47] *Department of Physics, Duke University, Durham NC, United States*
[48] *SUPA - School of Physics and Astronomy, University of Edinburgh, Edinburgh, United Kingdom*
[49] *INFN Laboratori Nazionali di Frascati, Frascati, Italy*
[50] *Fakultät für Mathematik und Physik, Albert-Ludwigs-Universität, Freiburg, Germany*
[51] *Section de Physique, Université de Genève, Geneva, Switzerland*
[52] [(a)] *INFN Sezione di Genova;* [(b)] *Dipartimento di Fisica, Università di Genova, Genova, Italy*
[53] [(a)] *E. Andronikashvili Institute of Physics, Iv. Javakhishvili Tbilisi State University, Tbilisi;* [(b)] *High Energy Physics Institute, Tbilisi State University, Tbilisi, Georgia*
[54] *II Physikalisches Institut, Justus-Liebig-Universität Giessen, Giessen, Germany*
[55] *SUPA - School of Physics and Astronomy, University of Glasgow, Glasgow, United Kingdom*
[56] *II Physikalisches Institut, Georg-August-Universität, Göttingen, Germany*
[57] *Laboratoire de Physique Subatomique et de Cosmologie, Université Grenoble-Alpes, CNRS/IN2P3, Grenoble, France*
[58] *Laboratory for Particle Physics and Cosmology, Harvard University, Cambridge MA, United States*
[59] [(a)] *Kirchhoff-Institut für Physik, Ruprecht-Karls-Universität Heidelberg, Heidelberg;* [(b)] *Physikalisches Institut, Ruprecht-Karls-Universität Heidelberg, Heidelberg;* [(c)] *ZITI Institut für technische Informatik, Ruprecht-Karls-Universität Heidelberg, Mannheim, Germany*
[60] *Faculty of Applied Information Science, Hiroshima Institute of Technology, Hiroshima, Japan*

[61] [(a)] Department of Physics, The Chinese University of Hong Kong, Shatin, N.T., Hong Kong; [(b)] Department of Physics, The University of Hong Kong, Hong Kong; [(c)] Department of Physics, The Hong Kong University of Science and Technology, Clear Water Bay, Kowloon, Hong Kong, China
[62] Department of Physics, Indiana University, Bloomington IN, United States
[63] Institut für Astro- und Teilchenphysik, Leopold-Franzens-Universität, Innsbruck, Austria
[64] University of Iowa, Iowa City IA, United States
[65] Department of Physics and Astronomy, Iowa State University, Ames IA, United States
[66] Joint Institute for Nuclear Research, JINR Dubna, Dubna, Russia
[67] KEK, High Energy Accelerator Research Organization, Tsukuba, Japan
[68] Graduate School of Science, Kobe University, Kobe, Japan
[69] Faculty of Science, Kyoto University, Kyoto, Japan
[70] Kyoto University of Education, Kyoto, Japan
[71] Department of Physics, Kyushu University, Fukuoka, Japan
[72] Instituto de Física La Plata, Universidad Nacional de La Plata and CONICET, La Plata, Argentina
[73] Physics Department, Lancaster University, Lancaster, United Kingdom
[74] [(a)] INFN Sezione di Lecce; [(b)] Dipartimento di Matematica e Fisica, Università del Salento, Lecce, Italy
[75] Oliver Lodge Laboratory, University of Liverpool, Liverpool, United Kingdom
[76] Department of Physics, Jožef Stefan Institute and University of Ljubljana, Ljubljana, Slovenia
[77] School of Physics and Astronomy, Queen Mary University of London, London, United Kingdom
[78] Department of Physics, Royal Holloway University of London, Surrey, United Kingdom
[79] Department of Physics and Astronomy, University College London, London, United Kingdom
[80] Louisiana Tech University, Ruston LA, United States
[81] Laboratoire de Physique Nucléaire et de Hautes Energies, UPMC and Université Paris-Diderot and CNRS/IN2P3, Paris, France
[82] Fysiska institutionen, Lunds universitet, Lund, Sweden
[83] Departamento de Fisica Teorica C-15, Universidad Autonoma de Madrid, Madrid, Spain
[84] Institut für Physik, Universität Mainz, Mainz, Germany
[85] School of Physics and Astronomy, University of Manchester, Manchester, United Kingdom
[86] CPPM, Aix-Marseille Université and CNRS/IN2P3, Marseille, France
[87] Department of Physics, University of Massachusetts, Amherst MA, United States
[88] Department of Physics, McGill University, Montreal QC, Canada
[89] School of Physics, University of Melbourne, Victoria, Australia
[90] Department of Physics, The University of Michigan, Ann Arbor MI, United States
[91] Department of Physics and Astronomy, Michigan State University, East Lansing MI, United States
[92] [(a)] INFN Sezione di Milano; [(b)] Dipartimento di Fisica, Università di Milano, Milano, Italy
[93] B.I. Stepanov Institute of Physics, National Academy of Sciences of Belarus, Minsk, Belarus
[94] National Scientific and Educational Centre for Particle and High Energy Physics, Minsk, Belarus
[95] Group of Particle Physics, University of Montreal, Montreal QC, Canada
[96] P.N. Lebedev Physical Institute of the Russian Academy of Sciences, Moscow, Russia
[97] Institute for Theoretical and Experimental Physics (ITEP), Moscow, Russia
[98] National Research Nuclear University MEPhI, Moscow, Russia
[99] D.V. Skobeltsyn Institute of Nuclear Physics, M.V. Lomonosov Moscow State University, Moscow, Russia
[100] Fakultät für Physik, Ludwig-Maximilians-Universität München, München, Germany
[101] Max-Planck-Institut für Physik (Werner-Heisenberg-Institut), München, Germany
[102] Nagasaki Institute of Applied Science, Nagasaki, Japan
[103] Graduate School of Science and Kobayashi-Maskawa Institute, Nagoya University, Nagoya, Japan
[104] [(a)] INFN Sezione di Napoli; [(b)] Dipartimento di Fisica, Università di Napoli, Napoli, Italy
[105] Department of Physics and Astronomy, University of New Mexico, Albuquerque NM, United States
[106] Institute for Mathematics, Astrophysics and Particle Physics, Radboud University Nijmegen/Nikhef, Nijmegen, Netherlands
[107] Nikhef National Institute for Subatomic Physics and University of Amsterdam, Amsterdam, Netherlands
[108] Department of Physics, Northern Illinois University, DeKalb IL, United States
[109] Budker Institute of Nuclear Physics, SB RAS, Novosibirsk, Russia
[110] Department of Physics, New York University, New York NY, United States
[111] Ohio State University, Columbus OH, United States
[112] Faculty of Science, Okayama University, Okayama, Japan
[113] Homer L. Dodge Department of Physics and Astronomy, University of Oklahoma, Norman OK, United States
[114] Department of Physics, Oklahoma State University, Stillwater OK, United States
[115] Palacký University, RCPTM, Olomouc, Czech Republic
[116] Center for High Energy Physics, University of Oregon, Eugene OR, United States
[117] LAL, Univ. Paris-Sud, CNRS/IN2P3, Université Paris-Saclay, Orsay, France
[118] Graduate School of Science, Osaka University, Osaka, Japan
[119] Department of Physics, University of Oslo, Oslo, Norway
[120] Department of Physics, Oxford University, Oxford, United Kingdom
[121] [(a)] INFN Sezione di Pavia; [(b)] Dipartimento di Fisica, Università di Pavia, Pavia, Italy
[122] Department of Physics, University of Pennsylvania, Philadelphia PA, United States
[123] National Research Centre "Kurchatov Institute" B.P. Konstantinov Petersburg Nuclear Physics Institute, St. Petersburg, Russia
[124] [(a)] INFN Sezione di Pisa; [(b)] Dipartimento di Fisica E. Fermi, Università di Pisa, Pisa, Italy
[125] Department of Physics and Astronomy, University of Pittsburgh, Pittsburgh PA, United States
[126] [(a)] Laboratório de Instrumentação e Física Experimental de Partículas – LIP, Lisboa; [(b)] Faculdade de Ciências, Universidade de Lisboa, Lisboa; [(c)] Department of Physics, University of Coimbra, Coimbra; [(d)] Centro de Física Nuclear da Universidade de Lisboa, Lisboa; [(e)] Departamento de Fisica, Universidade do Minho, Braga; [(f)] Departamento de Fisica Teorica y del Cosmos and CAFPE, Universidad de Granada, Granada (Spain); [(g)] Dep Fisica and CEFITEC of Faculdade de Ciencias e Tecnologia, Universidade Nova de Lisboa, Caparica, Portugal
[127] Institute of Physics, Academy of Sciences of the Czech Republic, Praha, Czech Republic
[128] Czech Technical University in Prague, Praha, Czech Republic
[129] Faculty of Mathematics and Physics, Charles University in Prague, Praha, Czech Republic
[130] State Research Center Institute for High Energy Physics (Protvino), NRC KI, Russia
[131] Particle Physics Department, Rutherford Appleton Laboratory, Didcot, United Kingdom
[132] [(a)] INFN Sezione di Roma; [(b)] Dipartimento di Fisica, Sapienza Università di Roma, Roma, Italy
[133] [(a)] INFN Sezione di Roma Tor Vergata; [(b)] Dipartimento di Fisica, Università di Roma Tor Vergata, Roma, Italy
[134] [(a)] INFN Sezione di Roma Tre; [(b)] Dipartimento di Matematica e Fisica, Università Roma Tre, Roma, Italy

[135] [(a)] Faculté des Sciences Ain Chock, Réseau Universitaire de Physique des Hautes Energies - Université Hassan II, Casablanca; [(b)] Centre National de l'Energie des Sciences Techniques Nucleaires, Rabat; [(c)] Faculté des Sciences Semlalia, Université Cadi Ayyad, LPHEA-Marrakech; [(d)] Faculté des Sciences, Université Mohamed Premier and LPTPM, Oujda; [(e)] Faculté des sciences, Université Mohammed V, Rabat, Morocco
[136] DSM/IRFU (Institut de Recherches sur les Lois Fondamentales de l'Univers), CEA Saclay (Commissariat à l'Energie Atomique et aux Energies Alternatives), Gif-sur-Yvette, France
[137] Santa Cruz Institute for Particle Physics, University of California Santa Cruz, Santa Cruz CA, United States
[138] Department of Physics, University of Washington, Seattle WA, United States
[139] Department of Physics and Astronomy, University of Sheffield, Sheffield, United Kingdom
[140] Department of Physics, Shinshu University, Nagano, Japan
[141] Fachbereich Physik, Universität Siegen, Siegen, Germany
[142] Department of Physics, Simon Fraser University, Burnaby BC, Canada
[143] SLAC National Accelerator Laboratory, Stanford CA, United States
[144] [(a)] Faculty of Mathematics, Physics & Informatics, Comenius University, Bratislava; [(b)] Department of Subnuclear Physics, Institute of Experimental Physics of the Slovak Academy of Sciences, Kosice, Slovak Republic
[145] [(a)] Department of Physics, University of Cape Town, Cape Town; [(b)] Department of Physics, University of Johannesburg, Johannesburg; [(c)] School of Physics, University of the Witwatersrand, Johannesburg, South Africa
[146] [(a)] Department of Physics, Stockholm University; [(b)] The Oskar Klein Centre, Stockholm, Sweden
[147] Physics Department, Royal Institute of Technology, Stockholm, Sweden
[148] Departments of Physics & Astronomy and Chemistry, Stony Brook University, Stony Brook NY, United States
[149] Department of Physics and Astronomy, University of Sussex, Brighton, United Kingdom
[150] School of Physics, University of Sydney, Sydney, Australia
[151] Institute of Physics, Academia Sinica, Taipei, Taiwan
[152] Department of Physics, Technion: Israel Institute of Technology, Haifa, Israel
[153] Raymond and Beverly Sackler School of Physics and Astronomy, Tel Aviv University, Tel Aviv, Israel
[154] Department of Physics, Aristotle University of Thessaloniki, Thessaloniki, Greece
[155] International Center for Elementary Particle Physics and Department of Physics, The University of Tokyo, Tokyo, Japan
[156] Graduate School of Science and Technology, Tokyo Metropolitan University, Tokyo, Japan
[157] Department of Physics, Tokyo Institute of Technology, Tokyo, Japan
[158] Department of Physics, University of Toronto, Toronto ON, Canada
[159] [(a)] TRIUMF, Vancouver BC; [(b)] Department of Physics and Astronomy, York University, Toronto ON, Canada
[160] Faculty of Pure and Applied Sciences, and Center for Integrated Research in Fundamental Science and Engineering, University of Tsukuba, Tsukuba, Japan
[161] Department of Physics and Astronomy, Tufts University, Medford MA, United States
[162] Department of Physics and Astronomy, University of California Irvine, Irvine CA, United States
[163] [(a)] INFN Gruppo Collegato di Udine, Sezione di Trieste, Udine; [(b)] ICTP, Trieste; [(c)] Dipartimento di Chimica, Fisica e Ambiente, Università di Udine, Udine, Italy
[164] Department of Physics and Astronomy, University of Uppsala, Uppsala, Sweden
[165] Department of Physics, University of Illinois, Urbana IL, United States
[166] Instituto de Fisica Corpuscular (IFIC) and Departamento de Fisica Atomica, Molecular y Nuclear and Departamento de Ingeniería Electrónica and Instituto de Microelectrónica de Barcelona (IMB-CNM), University of Valencia and CSIC, Valencia, Spain
[167] Department of Physics, University of British Columbia, Vancouver BC, Canada
[168] Department of Physics and Astronomy, University of Victoria, Victoria BC, Canada
[169] Department of Physics, University of Warwick, Coventry, United Kingdom
[170] Waseda University, Tokyo, Japan
[171] Department of Particle Physics, The Weizmann Institute of Science, Rehovot, Israel
[172] Department of Physics, University of Wisconsin, Madison WI, United States
[173] Fakultät für Physik und Astronomie, Julius-Maximilians-Universität, Würzburg, Germany
[174] Fakultät für Mathematik und Naturwissenschaften, Fachgruppe Physik, Bergische Universität Wuppertal, Wuppertal, Germany
[175] Department of Physics, Yale University, New Haven CT, United States
[176] Yerevan Physics Institute, Yerevan, Armenia
[177] Centre de Calcul de l'Institut National de Physique Nucléaire et de Physique des Particules (IN2P3), Villeurbanne, France

[a] Also at Department of Physics, King's College London, London, United Kingdom.
[b] Also at Institute of Physics, Azerbaijan Academy of Sciences, Baku, Azerbaijan.
[c] Also at Novosibirsk State University, Novosibirsk, Russia.
[d] Also at TRIUMF, Vancouver BC, Canada.
[e] Also at Department of Physics & Astronomy, University of Louisville, Louisville, KY, United States of America.
[f] Also at Department of Physics, California State University, Fresno CA, United States of America.
[g] Also at Department of Physics, University of Fribourg, Fribourg, Switzerland.
[h] Also at Departament de Fisica de la Universitat Autonoma de Barcelona, Barcelona, Spain.
[i] Also at Departamento de Fisica e Astronomia, Faculdade de Ciencias, Universidade do Porto, Portugal.
[j] Also at Tomsk State University, Tomsk, Russia.
[k] Also at Universita di Napoli Parthenope, Napoli, Italy.
[l] Also at Institute of Particle Physics (IPP), Canada.
[m] Also at National Institute of Physics and Nuclear Engineering, Bucharest, Romania.
[n] Also at Department of Physics, St. Petersburg State Polytechnical University, St. Petersburg, Russia.
[o] Also at Department of Physics, The University of Michigan, Ann Arbor MI, United States of America.
[p] Also at Centre for High Performance Computing, CSIR Campus, Rosebank, Cape Town, South Africa.
[q] Also at Louisiana Tech University, Ruston LA, United States of America.
[r] Also at Institucio Catalana de Recerca i Estudis Avancats, ICREA, Barcelona, Spain.
[s] Also at Graduate School of Science, Osaka University, Osaka, Japan.
[t] Also at Department of Physics, National Tsing Hua University, Taiwan.
[u] Also at Institute for Mathematics, Astrophysics and Particle Physics, Radboud University Nijmegen/Nikhef, Nijmegen, Netherlands.
[v] Also at Department of Physics, The University of Texas at Austin, Austin TX, United States of America.
[w] Also at Institute of Theoretical Physics, Ilia State University, Tbilisi, Georgia.
[x] Also at CERN, Geneva, Switzerland.
[y] Also at Georgian Technical University (GTU), Tbilisi, Georgia.
[z] Also at Ochadai Academic Production, Ochanomizu University, Tokyo, Japan.
[aa] Also at Manhattan College, New York NY, United States of America.
[ab] Also at Hellenic Open University, Patras, Greece.

[ac] Also at Academia Sinica Grid Computing, Institute of Physics, Academia Sinica, Taipei, Taiwan.
[ad] Also at School of Physics, Shandong University, Shandong, China.
[ae] Also at Moscow Institute of Physics and Technology State University, Dolgoprudny, Russia.
[af] Also at Section de Physique, Université de Genève, Geneva, Switzerland.
[ag] Also at Eotvos Lorand University, Budapest, Hungary.
[ah] Also at International School for Advanced Studies (SISSA), Trieste, Italy.
[ai] Also at Department of Physics and Astronomy, University of South Carolina, Columbia SC, United States of America.
[aj] Also at School of Physics and Engineering, Sun Yat-sen University, Guangzhou, China.
[ak] Also at Institute for Nuclear Research and Nuclear Energy (INRNE) of the Bulgarian Academy of Sciences, Sofia, Bulgaria.
[al] Also at Faculty of Physics, M.V. Lomonosov Moscow State University, Moscow, Russia.
[am] Also at Institute of Physics, Academia Sinica, Taipei, Taiwan.
[an] Also at National Research Nuclear University MEPhI, Moscow, Russia.
[ao] Also at Department of Physics, Stanford University, Stanford CA, United States of America.
[ap] Also at Institute for Particle and Nuclear Physics, Wigner Research Centre for Physics, Budapest, Hungary.
[aq] Also at Flensburg University of Applied Sciences, Flensburg, Germany.
[ar] Also at University of Malaya, Department of Physics, Kuala Lumpur, Malaysia.
[as] Also at CPPM, Aix-Marseille Université and CNRS/IN2P3, Marseille, France.
[at] Also affiliated with PKU-CHEP.
[*] Deceased.

Physics Letters B 775 (2017) 206–228

Contents lists available at ScienceDirect

Physics Letters B

www.elsevier.com/locate/physletb

Measurement of the cross-section for electroweak production of dijets in association with a Z boson in pp collisions at $\sqrt{s} = 13$ TeV with the ATLAS detector

The ATLAS Collaboration *

ARTICLE INFO

Article history:
Received 2 October 2017
Received in revised form 19 October 2017
Accepted 19 October 2017
Available online 27 October 2017
Editor: W.-D. Schlatter

ABSTRACT

The cross-section for the production of two jets in association with a leptonically decaying Z boson (Zjj) is measured in proton–proton collisions at a centre-of-mass energy of 13 TeV, using data recorded with the ATLAS detector at the Large Hadron Collider, corresponding to an integrated luminosity of 3.2 fb^{-1}. The electroweak Zjj cross-section is extracted in a fiducial region chosen to enhance the electroweak contribution relative to the dominant Drell–Yan Zjj process, which is constrained using a data-driven approach. The measured fiducial electroweak cross-section is $\sigma_{\mathrm{EW}}^{Zjj} = 119 \pm 16$ (stat.) $\pm$ 20 (syst.) ± 2 (lumi.) fb for dijet invariant mass greater than 250 GeV, and 34.2 ± 5.8 (stat.) ± 5.5 (syst.) $\pm$ 0.7 (lumi.) fb for dijet invariant mass greater than 1 TeV. Standard Model predictions are in agreement with the measurements. The inclusive Zjj cross-section is also measured in six different fiducial regions with varying contributions from electroweak and Drell–Yan Zjj production.

1. Introduction

At the Large Hadron Collider (LHC) events containing a Z boson and at least two jets (Zjj) are produced predominantly via initial-state QCD radiation from the incoming partons in the Drell–Yan process (QCD-Zjj), as shown in Fig. 1(a). In contrast, the production of Zjj events via t-channel electroweak gauge boson exchange (EW-Zjj events), including the vector-boson fusion (VBF) process shown in Fig. 1(b), is a much rarer process. Such VBF processes for vector-boson production are of great interest as a 'standard candle' for other VBF processes at the LHC: e.g., the production of Higgs bosons or the search for weakly interacting particles beyond the Standard Model.

The kinematic properties of Zjj events allow some discrimination between the QCD and EW production mechanisms. The emission of a virtual W boson from the quark in EW-Zjj events results in the presence of two high-energy jets, with moderate transverse momentum (p_{T}), separated by a large interval in rapidity (y)[1] and therefore with large dijet mass (m_{jj}) that characterises the EW-Zjj signal. A consequence of the exchange of a vector boson in Fig. 1(b) is that there is no colour connection between the hadronic systems produced by the break-up of the two incoming protons. As a result, EW-Zjj events are less likely to contain additional hadronic activity in the rapidity interval between the two high-p_{T} jets than corresponding QCD-Zjj events.

The first studies of EW-Zjj production were performed [1] in pp collisions at a centre-of-mass energy ($\sqrt{s}$) of 7 TeV by the CMS Collaboration, where the background-only hypothesis was rejected at the 2.6σ level. The first observation of the EW-Zjj process was performed by the ATLAS Collaboration at a centre-of-mass energy ($\sqrt{s}$) of 8 TeV [2]. The cross-section measurement is in agreement with predictions from the Powheg-box event generator [3–5] and allowed limits to be placed on anomalous triple gauge couplings. The CMS Collaboration has also observed and measured [6] the cross-section for EW-Zjj production at 8 TeV. This Letter presents measurements of the cross-section for EW-Zjj production and inclusive Zjj production at high dijet invariant mass in pp collisions at $\sqrt{s} = 13$ TeV using data corresponding to an integrated luminosity of 3.2 fb^{-1} collected by the ATLAS detector at the LHC. These measurements allow the dependence of the cross-section on $\sqrt{s}$

* *E-mail address:* atlas.publications@cern.ch.

[1] ATLAS uses a right-handed coordinate system with its origin at the nominal interaction point in the centre of the detector and the z-axis along the beam pipe. In the transverse plane, the x-axis points from the interaction point to the centre of the LHC ring, the y-axis points upward, and ϕ is the azimuthal angle around the z-axis. The pseudorapidity is defined in terms of the polar angle θ as $\eta = -\ln\tan(\theta/2)$. The rapidity is defined as $y = 0.5\ln[(E + p_z)/(E - p_z)]$, where E and p_z are the energy and longitudinal momentum respectively. An angular separation between two objects is defined as $\Delta R = \sqrt{(\Delta\phi)^2 + (\Delta\eta)^2}$, where $\Delta\phi$ and $\Delta\eta$ are the separations in ϕ and η respectively. Momentum in the transverse plane is denoted by p_{T}.

https://doi.org/10.1016/j.physletb.2017.10.040

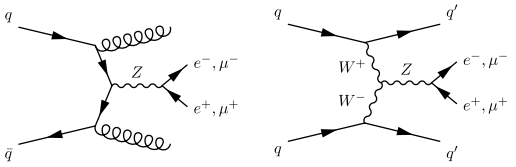

(a) QCD-Zjj. (b) EW-Zjj.

Fig. 1. Examples of leading-order Feynman diagrams for the two production mechanisms for a leptonically decaying Z boson and at least two jets (Zjj) in proton–proton collisions: (a) QCD radiation from the incoming partons (QCD-Zjj) and (b) t-channel exchange of an EW gauge boson (EW-Zjj).

to be studied. The increased $\sqrt{s}$ allows exploration of higher dijet masses, where the EW-Zjj contribution to the total Zjj rate becomes more pronounced.

2. ATLAS detector

The ATLAS detector is described in detail in Refs. [7,8]. It consists of an inner detector for tracking, surrounded by a thin superconducting solenoid, electromagnetic and hadronic calorimeters, and a muon spectrometer incorporating three large superconducting toroidal magnet systems. The inner detector is immersed in a 2 T axial magnetic field and provides charged-particle tracking in the range $|\eta| < 2.5$.

The calorimeters cover the pseudorapidity range $|\eta| < 4.9$. Electromagnetic calorimetry is provided by barrel and end-cap lead/liquid-argon (LAr) calorimeters in the region $|\eta| < 3.2$. Within $|\eta| < 2.47$ the calorimeter is finely segmented in the lateral direction of the showers, allowing measurement of the energy and position of electrons, and providing electron identification in conjunction with the inner detector. Hadronic calorimetry is provided by the steel/scintillator-tile calorimeter, segmented into three barrel structures within $|\eta| < 1.7$, and two hadronic end-cap calorimeters. A copper/LAr hadronic calorimeter covers the $1.5 < |\eta| < 3.2$ region, and a forward copper/tungsten/LAr calorimeter with electromagnetic-shower identification capabilities covers the $3.1 < |\eta| < 4.9$ region.

The muon spectrometer comprises separate trigger and high-precision tracking chambers. The tracking chambers cover the region $|\eta| < 2.7$ with three layers of monitored drift tubes, complemented by cathode strip chambers in part of the forward region, where the hit rate is highest. The muon trigger system covers the range $|\eta| < 2.4$ with resistive plate chambers in the barrel region, and thin gap chambers in the end-cap regions.

A two-level trigger system is used to select events of interest [9]. The Level-1 trigger is implemented in hardware and uses a subset of the detector information to reduce the event rate to around 100 kHz. This is followed by the software-based high-level trigger system which reduces the event rate to about 1 kHz.

3. Monte Carlo samples

The production of EW-Zjj events was simulated at next-to-leading-order (NLO) accuracy in perturbative QCD using the Powheg-box v1 Monte Carlo (MC) event generator [4,5,10] and, alternatively, at leading-order (LO) accuracy in perturbative QCD using the Sherpa 2.2.0 event generator [11]. For modelling of the parton shower, fragmentation, hadronisation and underlying event (UEPS), Powheg-box was interfaced to Pythia 8 [12] with a dedicated set of parton-shower-generator parameters (tune) denoted AZNLO [13] and the CT10 NLO parton distribution function (PDF) set [14]. The renormalisation and factorisation scales were set to the Z boson mass. Sherpa predictions used the Comix [15] and OpenLoops [16] matrix element event generators, and the CKKW method was used to combine the various final-state topologies from the matrix element and match them to the parton shower [17]. The matrix elements were merged with the Sherpa parton shower [18] using the ME+PS@LO prescription [19,20], and using Sherpa's native dynamical scale-setting algorithm to set the renormalisation and factorisation scales. Sherpa predictions used the NNPDF30NNLO PDF set [21].

The production of QCD-Zjj events was simulated using three event generators, Sherpa 2.2.1, Alpgen 2.14 [22] and MadGraph5_aMC@NLO 2.2.2 [23]. Sherpa provides $Z + n$-parton predictions calculated for up to two partons at NLO accuracy and up to four partons at LO accuracy in perturbative QCD. Sherpa predictions used the NNPDF30NLO PDF set together with the tuning of the UEPS parameters developed by the Sherpa authors using the ME+PS@NLO prescription [19,20]. Alpgen is an LO event generator which uses explicit matrix elements for up to five partons and was interfaced to Pythia 6.426 [24] using the Perugia2011C tune [25] and the CTEQ6L1 PDF set [26]. Only matrix elements for light-flavour production in Alpgen are included, with heavy-flavour contributions modelled by the parton shower. MadGraph5_aMC@NLO 2.2.2 (MG5_aMC) uses explicit matrix elements for up to four partons at LO, and was interfaced to Pythia 8 with the A14 tune [27] and using the NNPDF23LO PDF set [28]. For reconstruction-level studies, total Z boson production rates predicted by all three event generators used to produce QCD-Zjj predictions are normalised using the next-to-next-to-leading-order (NNLO) predictions calculated with the FEWZ 3.1 program [29–31] using the CT10 NNLO PDF set [14]. However, when comparing particle-level theoretical predictions to detector-corrected measurements, the normalisation of quoted predictions is provided by the event generator in question rather than an external NNLO prediction.

The production of a pair of EW vector bosons (diboson), where one decays leptonically and the other hadronically, or where both decay leptonically and are produced in association with two or more jets, through WZ or ZZ production with at least one Z boson decaying to leptons, was simulated separately using Sherpa 2.1.1 and the CT10 NLO PDF set.

The largest background to the selected Zjj samples arises from $t\bar{t}$ and single-top (Wt) production. These were generated using Powheg-box v2 and Pythia 6.428 with the Perugia2012 tune [25], and normalised using the cross-section calculated at NNLO+NNLL (next-to-next-to-leading log) accuracy using the Top++2.0 program [32].

All the above MC samples were fully simulated through the Geant 4 [33] simulation of the ATLAS detector [34]. The effect of additional pp interactions (pile-up) in the same or nearby bunch crossings was also simulated, using Pythia v8.186 with the A2 tune [35] and the MSTW2008LO PDF set [36]. The MC samples were reweighted so that the distribution of the average number of pile-up interactions per bunch crossing matches that observed in data. For the data considered in this Letter, the average number of interactions is 13.7.

4. Event preselection

The Z bosons are measured in their dielectron and dimuon decay modes. Candidate events are selected using triggers requiring at least one identified electron or muon with transverse momentum thresholds of $p_{\mathrm{T}} = 24$ GeV and 20 GeV respectively, with additional isolation requirements imposed in these triggers. At higher transverse momenta, the efficiency of selecting candidate events is improved through the use of additional electron and

muon triggers without isolation requirements and with thresholds of $p_{\mathrm{T}} = 60$ GeV and 50 GeV respectively.

Candidate electrons are reconstructed from clusters of energy in the electromagnetic calorimeter matched to inner-detector tracks [37]. They must satisfy the *Medium* identification requirements described in Ref. [37] and have $p_{\mathrm{T}} > 25$ GeV and $|\eta| < 2.47$, excluding the transition region between the barrel and end-cap calorimeters at $1.37 < |\eta| < 1.52$. Candidate muons are identified as tracks in the inner detector matched and combined with track segments in the muon spectrometer. They must satisfy the *Medium* identification requirements described in Ref. [38], and have $p_{\mathrm{T}} > 25$ GeV and $|\eta| < 2.4$. Candidate leptons must also satisfy a set of isolation criteria based on reconstructed tracks and calorimeter activity. Events are required to contain exactly two leptons of the same flavour but of opposite charge. The dilepton invariant mass must satisfy $81 < \mathrm{m}_{\ell\ell} < 101$ GeV.

Candidate hadronic jets are required to satisfy $p_{\mathrm{T}} > 25$ GeV and $|y| < 4.4$. They are reconstructed from clusters of energy in the calorimeter [39] using the anti-k_t algorithm [40,41] with radius parameter $R = 0.4$. Jet energies are calibrated by applying p_{T}- and y-dependent corrections derived from Monte Carlo simulation with additional in situ correction factors determined from data [42]. To reduce the impact of pile-up contributions, all jets with $|y| < 2.4$ and $p_{\mathrm{T}} < 60$ GeV are required to be compatible with having originated from the primary vertex (the vertex with the highest sum of track p_{T}^2), as defined by the jet vertex tagger algorithm [43]. Selected electrons and muons are discarded if they lie within $\Delta R = 0.4$ of a reconstructed jet. This requirement is imposed to remove non-prompt non-isolated leptons produced in heavy-flavour decays or from the decay in flight of a kaon or pion.

5. Measurement of inclusive Zjj fiducial cross-sections

5.1. Definition of particle-level cross-sections

Cross-sections are measured for inclusive Zjj production that includes the EW-Zjj and QCD-Zjj processes, as well as diboson events. The particle-level production cross-section for inclusive Zjj production in a given fiducial region f is given by

$$\sigma^f = \frac{N^f_{\mathrm{obs}} - N^f_{\mathrm{bkg}}}{L \cdot \mathcal{C}^f}, \tag{1}$$

where N^f_{obs} is the number of events observed in the data passing the selection requirements of the fiducial region under study at detector level, N^f_{bkg} is the corresponding number of expected background (non-Zjj) events, L is the integrated luminosity corresponding to the analysed data sample, and $\mathcal{C}^f$ is a correction factor applied to the observed data yields, which accounts for experimental efficiency and detector resolution effects, and is derived from MC simulation with data-driven efficiency and energy/momentum scale corrections. This correction factor is calculated as:

$$\mathcal{C}^f = \frac{N^f_{\mathrm{det}}}{N^f_{\mathrm{particle}}},$$

where N^f_{det} is the number of signal events that satisfy the fiducial selection criteria at detector level in the MC simulation, and N^f_{particle} is the number of signal events that pass the equivalent selection but at particle level. These correction factors have values between 0.63 and 0.77, depending on the fiducial region.

With the exception of background from multijet and W + jets processes (henceforth referred to together simply as multijet processes), contributions to N^f_{bkg} are estimated using the Monte Carlo samples described in Section 3. Background from multijet events is estimated from the data by reversing requirements on lepton identification or isolation to derive a template for the contribution of jets mis-reconstructed as lepton candidates as a function of dilepton mass. Non-multijet background is subtracted from the template using simulation. The normalisation is derived by fitting the nominal dilepton mass distribution in each fiducial region with the sum of the multijet template and a template comprising signal and background contributions determined from simulation. The multijet contribution is found to be less than 0.3% in each fiducial region. The contribution from W + jets processes was checked using MC simulation and found to be much smaller than the total multijet background as determined from data.

At particle level, only final-state particles with proper lifetime $c\tau > 10$ mm are considered. Prompt leptons are dressed using the four-momentum combination of an electron or muon and all photons (not originating from hadron decays) within a cone of size $\Delta R = 0.1$ centred on the lepton. These dressed leptons are required to satisfy $p_{\mathrm{T}} > 25$ GeV and $|\eta| < 2.47$. Events are required to contain exactly two dressed leptons of the same flavour but of opposite charge, and the dilepton invariant mass must satisfy $81 < \mathrm{m}_{\ell\ell} < 101$ GeV. Jets are reconstructed using the anti-k_t algorithm with radius parameter $R = 0.4$. Prompt leptons and the photons used to dress these leptons are not included in the particle-level jet reconstruction. All remaining final-state particles are included in the particle-level jet clustering. Prompt leptons with a separation $\Delta R_{j,\ell} < 0.4$ from any jet are rejected.

The cross-section measurements are performed in the six phase-space regions defined in Table 1. These regions are chosen to have varying contributions from EW-Zjj and QCD-Zjj processes.

5.2. Event selection

Following Ref. [2], events are selected in six detector fiducial regions. As far as possible, these are defined with the same kinematic requirements as the six phase-space regions in which the cross-section is measured (Table 1). This minimises systematic uncertainties in the modelling of the acceptance.

The baseline fiducial region represents an inclusive selection of events containing a leptonically decaying Z boson and at least two jets with $p_{\mathrm{T}} > 45$ GeV, at least one of which satisfies $p_{\mathrm{T}} > 55$ GeV. The two highest-p_{T} (leading and sub-leading) jets in a given event define the dijet system. The baseline region is dominated by QCD-Zjj events. The requirement of $81 < m_{\ell\ell} < 101$ GeV suppresses other sources of dilepton events, such as $t\bar{t}$ and $Z \to \tau\tau$, as well as the multijet background.

Because the energy scale of the dijet system is typically higher in events produced by the EW-Zjj process than in those produced by the QCD-Zjj process, two subsets of the baseline region are defined which probe the EW-Zjj contribution in different ways: in the high-mass fiducial region a high value of the invariant mass of the dijet system ($m_{jj} > 1$ TeV) is required, and in the high-p_{T} fiducial region the minimum p_{T} of the leading and sub-leading jets is increased to 85 GeV and 75 GeV respectively. The EW-Zjj process typically produces harder jet transverse momenta and results in a harder dijet invariant mass spectrum than the QCD-Zjj process.

Three additional fiducial regions allow the separate contributions from the EW-Zjj and QCD-Zjj processes to be measured. The EW-enriched fiducial region is designed to enhance the EW-Zjj contribution relative to that from QCD-Zjj, particularly at high m_{jj}. The EW-enriched region is derived from the baseline region requiring $m_{jj} > 250$ GeV, a dilepton transverse momentum of $p_{\mathrm{T}}^{\ell\ell} > 20$ GeV, and that the normalised transverse momentum balance between the two leptons and the two highest transverse

Table 1
Summary of the particle-level selection criteria defining the six fiducial regions (see text for details).

	Fiducial region					
Object	Baseline	High-mass	High-p_{T}	EW-enriched	EW-enriched, $m_{jj} > 1$ TeV	QCD-enriched
Leptons	$\lvert\eta\rvert < 2.47$, $p_{\mathrm{T}} > 25$ GeV, $\Delta R_{j,\ell} > 0.4$					
Dilepton pair	$81 < m_{\ell\ell} < 101$ GeV					
	–			$p_{\mathrm{T}}^{\ell\ell} > 20$ GeV		
Jets	$\lvert y\rvert < 4.4$					
	$p_{\mathrm{T}}^{j_1} > 55$ GeV		$p_{\mathrm{T}}^{j_1} > 85$ GeV	$p_{\mathrm{T}}^{j_1} > 55$ GeV		
	$p_{\mathrm{T}}^{j_2} > 45$ GeV		$p_{\mathrm{T}}^{j_2} > 75$ GeV	$p_{\mathrm{T}}^{j_2} > 45$ GeV		
Dijet system	–	$m_{jj} > 1$ TeV	–	$m_{jj} > 250$ GeV	$m_{jj} > 1$ TeV	$m_{jj} > 250$ GeV
Interval jets	–			$N_{\text{jet }(p_{\mathrm{T}}>25\text{ GeV})}^{\text{interval}} = 0$		$N_{\text{jet }(p_{\mathrm{T}}>25\text{ GeV})}^{\text{interval}} \geq 1$
Zjj system	–			$p_{\mathrm{T}}^{\text{balance}} < 0.15$		$p_{\mathrm{T}}^{\text{balance},3} < 0.15$

momentum jets satisfy $p_{\mathrm{T}}^{\text{balance}} < 0.15$. The latter quantity is given by

$$p_{\mathrm{T}}^{\text{balance}} = \frac{\left|\vec{p}_{\mathrm{T}}^{\,\ell_1} + \vec{p}_{\mathrm{T}}^{\,\ell_2} + \vec{p}_{\mathrm{T}}^{\,j_1} + \vec{p}_{\mathrm{T}}^{\,j_2}\right|}{\left|\vec{p}_{\mathrm{T}}^{\,\ell_1}\right| + \left|\vec{p}_{\mathrm{T}}^{\,\ell_2}\right| + \left|\vec{p}_{\mathrm{T}}^{\,j_1}\right| + \left|\vec{p}_{\mathrm{T}}^{\,j_2}\right|}, \tag{2}$$

where $\vec{p}_{\mathrm{T}}^{\,i}$ is the transverse momentum vector of object i, ℓ_1 and ℓ_2 label the two leptons that define the Z boson candidate, and j_1 and j_2 refer to the leading and sub-leading jets. These requirements help remove events in which the jets arise from pile-up or multiple parton interactions. The requirement on $p_{\mathrm{T}}^{\text{balance}}$ also helps suppress events in which the p_{T} of one or more jets is badly measured and it enhances the EW-Zjj contribution, where the lower probability of additional radiation causes the Z boson and the dijet system to be well balanced. The EW-enriched region requires a veto [44] on any jets with $p_{\mathrm{T}} > 25$ GeV reconstructed within the rapidity interval bounded by the dijet system ($N_{\text{jet }(p_{\mathrm{T}}>25\text{ GeV})}^{\text{interval}} = 0$). A second fiducial region, denoted EW-enriched ($m_{jj} > 1$ TeV), has identical selection criteria, except for a raised m_{jj} threshold of 1 TeV which further enhances the EW-Zjj contribution to the total Zjj signal rate.

In contrast, the QCD-enriched fiducial region is designed to suppress the EW-Zjj contribution relative to QCD-Zjj by requiring at least one jet with $p_{\mathrm{T}} > 25$ GeV to be reconstructed within the rapidity interval bounded by the dijet system ($N_{\text{jet }(p_{\mathrm{T}}>25\text{ GeV})}^{\text{interval}} \geq 1$). In the QCD-enriched region, the definition of the normalised transverse momentum balance is modified from that given in Eq. (2) to include in the calculation of the numerator and denominator the p_{T} of the highest p_{T} jet within the rapidity interval bounded by the dijet system ($p_{\mathrm{T}}^{\text{balance},3}$). In all other respects, the kinematic requirements in the EW-enriched region and QCD-enriched region are identical.

5.3. Detector-level results

In the baseline region, 30 686 events are selected in the dielectron channel and 36 786 events are selected in the dimuon channel. The total observed yields are in agreement with the expected yields within statistical uncertainties in each dilepton channel. The largest deviation across all fiducial regions is a 2σ (statistical) difference between the expected to observed ratio in the electron versus muon channel in the high-p_{T} region.

The expected composition of the selected data samples in the six Zjj fiducial regions is summarised in Table 2, averaging across the dielectron and dimuon channels as these compositions in the two dilepton channels are in agreement within statistical uncertainties. The numbers of selected events in data and expectations from total signal plus background estimates are also given for each region. The largest discrepancy between observed and expected yields is seen in the high-mass region, and results from a mismodelling of the m_{jj} spectrum in the QCD-Zjj MC simulations used, which is discussed below and accounted for in the assessment of systematic uncertainties in the measurement.

5.4. Systematic uncertainties in the inclusive Zjj fiducial cross-sections

Experimental systematic uncertainties affect the determination of the $\mathcal{C}^f$ correction factor and the background estimates. The dominant systematic uncertainty in the inclusive Zjj fiducial cross-sections arises from the calibration of the jet energy scale and resolution. This uncertainty varies from around 4% in the EW-enriched region to around 12% in the QCD-enriched region. The larger uncertainty in the QCD-enriched region is due to the higher average jet multiplicity (an average of 1.7 additional jets in addition to the leading and sub-leading jets) compared with the EW-enriched region (an average of 0.4 additional jets). Other experimental systematic uncertainties arising from lepton efficiencies related to reconstruction, identification, isolation and trigger, and lepton energy/momentum scale and resolution as well as from the effect of pile-up, amount to a total of around 1–2%, depending on the fiducial region.

The systematic uncertainty arising from the MC modelling of the m_{jj} distribution in the QCD-Zjj and EW-Zjj signal processes is around 3% in the EW-enriched region, around 1% in the QCD-enriched region, 2% in the high-mass region, and below 1% elsewhere. This is assessed by comparing the correction factors obtained by using the different MC event generators listed in Section 3 and by performing a data-driven reweighting of the QCD-Zjj MC sample to describe the m_{jj} distribution of the observed data in a given fiducial region. Additional contributions arise from varying the QCD renormalisation and factorisation scales up and down by a factor of two independently, and from the propagation of uncertainties in the PDF sets. The normalisation of the diboson contribution is varied according to PDF and scale variations in these predictions [45], and results in up to a 0.1% effect on the measured Zjj cross-sections depending on the fiducial region. The uncertainty from varying the normalisation and shape in m_{jj} of the estimated background from top-quark production is at most 1% (in the high-mass region), arising from changes in the extracted Zjj cross-sections when using modified top-quark background MC samples with PDF and scale variations, suppressed or enhanced additional

Table 2
Estimated composition (in percent) of the data samples selected in the six Zjj fiducial regions for the dielectron and dimuon channels combined, using the EW-Zjj sample from Powheg, and the QCD-Zjj sample from Sherpa (normalised using NNLO predictions for the inclusive Z cross-section calculated with FEWZ). Uncertainties in the sample contributions are statistical only. Also shown are the total expected yields and the total observed yields in each fiducial region. Uncertainties in the total expected yields are statistical (first) and systematic (second), see Section 5.4 for details.

Process	Composition [%]					
	Baseline	High-mass	High-p_{T}	EW-enriched	EW-enriched, $m_{jj} > 1$ TeV	QCD-enriched
QCD-Zjj	94.2 ± 0.4	86.8 ± 1.6	92.3 ± 0.4	93.4 ± 0.9	72.9 ± 2.1	95.4 ± 0.8
EW-Zjj	$1.5 \pm < 0.1$	10.6 ± 0.2	$2.6 \pm < 0.1$	$4.8 \pm < 0.1$	26.1 ± 0.5	$1.6 \pm < 0.1$
Diboson	$1.6 \pm < 0.1$	1.5 ± 0.7	2.0 ± 0.5	1.0 ± 0.5	0.8 ± 0.4	1.8 ± 0.4
$t\bar{t}$	$2.6 \pm < 0.1$	1.1 ± 0.1	3.1 ± 0.1	$0.7 \pm < 0.1$	0.1 ± 0.1	1.2 ± 0.1
Single-t	<0.2	<0.2	<0.2	<0.1	<0.1	<0.1
Multijet	<0.3	<0.3	<0.3	<0.3	<0.3	<0.3
Total expected	64800 $\pm$ 130 $\pm$ 5220	2220 $\pm$ 20 $\pm$ 200	21900 $\pm$ 40 $\pm$ 1210	11100 $\pm$ 50 $\pm$ 520	640 $\pm$ 10 $\pm$ 40	7120 $\pm$ 30 $\pm$ 880
Total observed	67472	1471	22461	11630	490	6453

radiation (generated with the Perugia2012radHi/Lo tunes [25]), or using an alternative top-quark production sample from MadGraph5_aMC@NLO interfaced to Herwig++ v2.7.1 [23,46].

The systematic uncertainty in the integrated luminosity is 2.1%. This is derived following a methodology similar to that detailed in Ref. [47], from a calibration of the luminosity scale using x–y beam-separation scans performed in June 2015.

5.5. Inclusive Zjj results

The measured cross-sections in the dielectron and dimuon channels are combined and presented here as a weighted average (taking into account total uncertainties) across both channels. These cross-sections are determined using each of the correction factors derived from the six combinations of the three QCD-Zjj (Alpgen, MG5_aMC, and Sherpa) and two EW-Zjj (Powheg and Sherpa) MC samples. For a given fiducial region (Table 1) the cross-section averaged over all six variations is presented in Table 3. The envelope of variation between QCD-Zjj and EW-Zjj models is assigned as a source of systematic uncertainty (1% in all regions except the EW-enriched region where the variation is 3% and the high-mass region where the variation is 2%).

The theoretical predictions from Sherpa (QCD-Zjj) + Powheg (EW-Zjj), MG5_aMC (QCD-Zjj) + Powheg (EW-Zjj), and Alpgen (QCD-Zjj) + Powheg (EW-Zjj) are found to be in agreement with the measurements in most cases. The uncertainties in the theoretical predictions are significantly larger than the uncertainties in the corresponding measurements.

The largest differences between predictions and measurement are in the high-mass and EW-enriched ($m_{jj} > 250$ GeV and > 1 TeV) regions. Predictions from Sherpa (QCD-Zjj) + Powheg (EW-Zjj) and MG5_aMC (QCD-Zjj) + Powheg (EW-Zjj) exceed measurements in the high-mass region by 54% and 34% respectively, where the predictions have relative uncertainties with respect to the measurement of 36% and 32%. For the EW-enriched region, Sherpa (QCD-Zjj) + Powheg (EW-Zjj) describes the observed rates well, but MG5_aMC (QCD-Zjj) + Powheg (EW-Zjj) overestimates measurements by 28% with a relative uncertainty of 11%. In the EW-enriched ($m_{jj} > 1$ TeV) region the same predictions overestimate measured rates by 33% and 57%, with relative uncertainties of 16% and 15%. Some of these differences arise from a significant mismodelling of the QCD-Zjj contribution, as investigated and discussed in detail in Section 6.1. Predictions from Alpgen (QCD-Zjj) + Powheg (EW-Zjj) are in agreement with the data for the high-mass and EW-enriched ($m_{jj} > 250$ GeV and > 1 TeV) regions.

6. Measurement of EW-Zjj fiducial cross-sections

The EW-enriched fiducial region (defined in Table 1) is used to measure the production cross-section of the EW-Zjj process. The EW-enriched region has an overall expected EW-Zjj signal fraction of 4.8% (Table 2) and this signal fraction grows with increasing m_{jj} to 26.1% for $m_{jj} > 1$ TeV. The QCD-enriched region has an overall expected EW-Zjj signal fraction of 1.6% increasing to 4.4% for $m_{jj} > 1$ TeV. The dominant background to the EW-Zjj cross-section measurement is QCD-Zjj production. It is subtracted in the same way as non-Zjj backgrounds in the inclusive measurement described in Section 5. Although diboson production includes contributions from purely EW processes, in this measurement it is considered as part of the background and is estimated from simulation.

A particle-level production cross-section measurement of EW-Zjj production in a given fiducial region f is thus given by

$$\sigma_{\mathrm{EW}}^{f} = \frac{N_{\mathrm{obs}}^{f} - N_{\mathrm{QCD\text{-}}Zjj}^{f} - N_{\mathrm{bkg}}^{f}}{L \cdot \mathcal{C}_{\mathrm{EW}}^{f}}, \tag{3}$$

with the same notations as in Eq. (1) and where $N_{\mathrm{QCD\text{-}}Zjj}^{f}$ is the expected number of QCD-Zjj events passing the selection requirements of the fiducial region at detector level, N_{bkg}^{f} is the expected number of background (non-Zjj and diboson) events, and $\mathcal{C}_{\mathrm{EW}}^{f}$ is a correction factor applied to the observed background-subtracted data yields that accounts for experimental efficiency and detector resolution effects, and is derived from EW-Zjj MC simulation with data-driven efficiency and energy/momentum scale corrections. For the $m_{jj} > 250$ GeV ($m_{jj} > 1$ TeV) region this correction factor is determined to be 0.66 (0.67) when using the Sherpa EW-Zjj prediction, and 0.67 (0.68) when using the Powheg EW-Zjj prediction.

Detector-level comparisons of the m_{jj} distribution between data and simulation in (a) the EW-enriched region and (b) the QCD-enriched region are shown in Fig. 2. It can be seen in Fig. 2(a)

Table 3
Measured and predicted inclusive Zjj production cross-sections in the six fiducial regions defined in Table 1. For the measured cross-sections, the first uncertainty given is statistical, the second is systematic and the third is due to the luminosity determination. For the predictions, the statistical uncertainty is added in quadrature to the systematic uncertainties arising from the PDFs and factorisation and renormalisation scale variations.

Fiducial region	Inclusive Zjj cross-sections [pb]						
	Measured				Prediction		
	value	± stat.	± syst.	± lumi.	SHERPA (QCD-Zjj) +POWHEG (EW-Zjj)	MG5_aMC (QCD-Zjj) +POWHEG (EW-Zjj)	ALPGEN (QCD-Zjj) +POWHEG (EW-Zjj)
Baseline	13.9	± 0.1	± 1.1	± 0.3	13.5 ± 1.9	15.2 ± 2.2	11.7 ± 1.7
High-p_{T}	4.77	± 0.05	± 0.27	± 0.10	4.7 ± 0.8	5.5 ± 0.9	4.2 ± 0.7
EW-enriched	2.77	± 0.04	± 0.13	± 0.06	2.7 ± 0.2	3.6 ± 0.3	2.4 ± 0.2
QCD-enriched	1.34	± 0.02	± 0.17	± 0.03	1.5 ± 0.4	1.4 ± 0.3	1.1 ± 0.3
High-mass	0.30	± 0.01	± 0.03	± 0.01	0.46 ± 0.11	0.40 ± 0.09	0.27 ± 0.06
EW-enriched ($m_{jj} > 1$ TeV)	0.118	± 0.008	± 0.006	± 0.002	0.156 ± 0.019	0.185 ± 0.023	0.120 ± 0.015

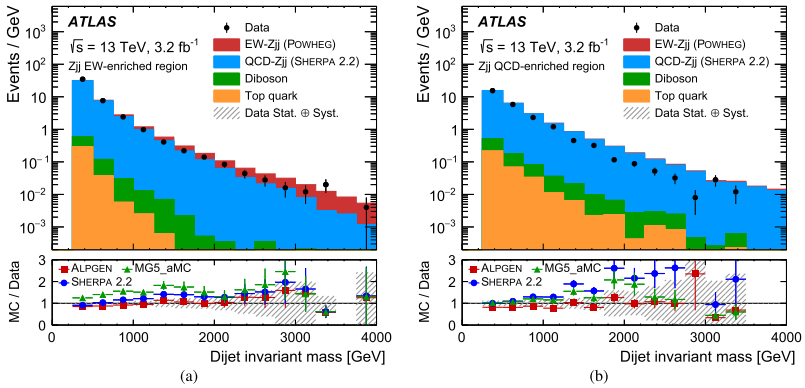

Fig. 2. Detector-level comparisons of the dijet invariant mass distribution between data and simulation in (a) the EW-enriched region and (b) the QCD-enriched region, for the dielectron and dimuon channel combined. Uncertainties shown on the data are statistical only. The EW-Zjj simulation sample comes from the POWHEG event generator and the QCD-Zjj MC sample comes from the SHERPA event generator. The lower panels show the ratio of simulation to data for three QCD-Zjj models, from ALPGEN, MG5_aMC, and SHERPA. The hatched band centred at unity represents the size of statistical and experimental systematic uncertainties added in quadrature.

that in the EW-enriched region the EW-Zjj component becomes prominent at large values of m_{jj}. However, Fig. 2(b) demonstrates that the shape of the m_{jj} distribution for QCD-Zjj production is poorly modelled in simulation. The same trend is seen for all three QCD-Zjj event generators listed in Section 3. ALPGEN provides the best description of the data over the whole m_{jj} range. In comparison, MG5_aMC and SHERPA overestimate the data by 80% and 120% respectively, for $m_{jj} = 2$ TeV, well outside the uncertainties on these predictions described in Table 3. These discrepancies have been observed previously in Zjj [2,48] and Wjj [49–51] production at high dijet invariant mass and at high jet rapidities. For the purpose of extracting the cross-section for EW-Zjj production, this mismodelling of QCD-Zjj is corrected for using a data-driven approach, as discussed in the following.

6.1. Corrections for mismodelling of QCD-Zjj production and fitting procedure

The normalisation of the QCD-Zjj background is extracted from a fit of the QCD-Zjj and EW-Zjj m_{jj} simulated distributions to the data in the EW-enriched region, after subtraction of non-Zjj and diboson background, using a log-likelihood maximisation [52]. Following the procedure adopted in Ref. [2], the data in the QCD-enriched region are used to evaluate detector-level shape correction factors for the QCD-Zjj MC predictions bin-by-bin in m_{jj}. These data-to-simulation ratio correction factors are applied to the simulation-predicted shape in m_{jj} of the QCD-Zjj contribution in the EW-enriched region. This procedure is motivated by two observations:

(a) the QCD-enriched region and EW-enriched region are designed to be kinematically very similar, differing only with regard to the presence/absence of jets reconstructed within the rapidity interval bounded by the dijet system,
(b) the contribution of EW-Zjj to the region of high m_{jj} is suppressed in the QCD-enriched region (4.4% for $m_{jj} > 1$ TeV) relative to that in the EW-enriched region (26.1% for $m_{jj} > 1$ TeV) (also illustrated in Fig. 2); the impact of the residual EW-Zjj contamination in the QCD-enriched region is assigned as a component of the systematic uncertainty in the QCD-Zjj background.

The shape correction factors in m_{jj} obtained using the three different QCD-Zjj MC samples are shown in Fig. 3(a). These are derived as the ratio of the data to simulation in bins of m_{jj} after normalisation of the total yield in simulation to that observed

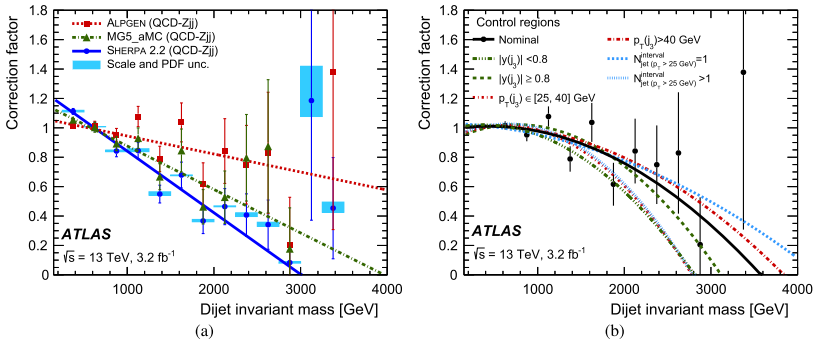

Fig. 3. Binned data-to-simulation normalised ratio shape correction factors as a function of dijet invariant mass in the QCD-enriched region. (a) Ratio for three different QCD-Zjj MC samples with uncertainties corresponding to the combined statistical uncertainties in the data and QCD-Zjj MC samples added in quadrature. Scale and PDF uncertainties in SHERPA predictions are indicated by the shaded bands. Lines represent fits to the ratios using a linear fit. (b) Ratio for subregions of the QCD-enriched region for the ALPGEN MC sample. Curves represent the result of fits with a quadratic function for the various subregions.

in data in the QCD-enriched region. A binned fit to the correction factors derived in dijet invariant mass is performed with a linear fit function (and also with a quadratic fit function) to produce a continuous correction factor. The linear fit is illustrated overlaid on the binned correction factors in Fig. 3(a). The nominal value of the EW-Zjj cross-section corresponding to a particular QCD-Zjj event generator template is determined using the correction factors from the linear fit. The change in resultant EW-Zjj cross-section from using binned correction factors directly is assessed as a systematic uncertainty. The change in the extracted EW-Zjj cross-section when using a quadratic fit was found to be negligible. The variations observed between event generators may be partly due to differences in the modelling of QCD radiation within the rapidity interval bounded by the dijet system, which affects the extrapolation from the central-jet-enriched QCD-enriched region to the central-jet-suppressed EW-enriched region. The variation between event generators is much larger than the effect of PDF and scale uncertainties in a particular prediction (indicated in Fig. 3(a) by a shaded band on the predictions from SHERPA). Estimating the uncertainties associated with QCD-Zjj mismodelling from PDF and scale variations around a single generator prediction would thus result in an underestimate of the true theoretical uncertainty associated with this mismodelling. In this measurement, the span of resultant EW-Zjj cross-sections extracted from the use of each of the three QCD-Zjj templates is assessed as a systematic uncertainty. The variation in the EW-Zjj cross-section measurement due to a change in the EW-Zjj signal template used in the derivation of the m_{jj} correction factors (from POWHEG to SHERPA) is found to be negligible.

To test the dependence of the QCD-Zjj correction factors on the modelling of any additional jet emitted in the dijet rapidity interval, the QCD-enriched control region is divided into pairs of mutually exclusive subsets according to the $|y|$ of the highest p_{T} jet within the rapidity interval bounded by the dijet system, the p_{T} of that jet, or the value of $N^{\text{interval}}_{\text{jet }(p_{\mathrm{T}}>25\text{ GeV})}$. The continuous correction factors are determined from each subregion using both a linear and a quadratic fit to the data. Correction factors derived in the subregions using quadratic fits result in the largest variation in the extracted cross-sections. These fits are shown in Fig. 3(b) for the ALPGEN QCD-Zjj sample, which displays the largest variation between subregions of the three event generators used to produce QCD-Zjj predictions. Within statistical uncertainties the measured EW-Zjj cross-sections are not sensitive to the definition of the control region used.

The normalisations of the corrected QCD-Zjj templates and the EW-Zjj templates are allowed to vary independently in a fit to the background-subtracted m_{jj} distribution in the EW-enriched region. The measured electroweak production cross-section is determined from the data minus the QCD-Zjj contribution determined from these fits (Eq. (3)). As the choice of EW-Zjj template can influence the normalisation of the QCD-Zjj template in the EW-enriched region fit, the measured EW-Zjj cross-section determination is repeated for each QCD-Zjj template using either the POWHEG or SHERPA EW-Zjj template in the fit. The central value of the result quoted is the average of the measured EW-Zjj cross-sections determined with each of the six combinations of the three QCD-Zjj and two EW-Zjj templates, with the envelope of measured results from these variations taken as an uncertainty associated with the dependence on the modelling of the templates in the EW-enriched region. Separate uncertainties are assigned for the determination of the QCD-Zjj correction factors in the QCD-enriched region and their propagation into the EW-enriched region. The measurement of the EW-Zjj cross-section in the EW-enriched region for $m_{jj} > 1$ TeV is extracted from the same fit procedure, with data and QCD-Zjj yields integrated for $m_{jj} > 1$ TeV.

Fig. 4(a) shows a comparison in the EW-enriched region of the fitted EW-Zjj and m_{jj}-reweighted QCD-Zjj templates to the background-subtracted data, from which the measured EW-Zjj cross-section is extracted. Fig. 4(b) demonstrates how the data in the EW-enriched region is modelled with the fitted EW-Zjj and m_{jj}-reweighted QCD-Zjj templates, for the three different QCD-Zjj event generators (and their corresponding correction factors derived in the QCD-enriched region shown in Fig. 3(a)). Despite significantly different modelling of the m_{jj} distribution between event generators, and different models for additional QCD radiation, the results of the combined correction and fit procedure give a consistent description of the data.

6.2. *Systematic uncertainties in the EW-Zjj fiducial cross-section*

The total systematic uncertainty in the cross-section for EW-Zjj production in the EW-enriched fiducial region is 17% (16% in the EW-enriched $m_{jj} > 1$ TeV region). The sources and size of each systematic uncertainty are summarised in Table 4.

Systematic uncertainties associated with the EW-Zjj signal template used in the fit and EW-Zjj signal extraction are obtained from the variation in the measured cross-section when using either of the individual EW-Zjj MC samples (POWHEG and SHERPA)

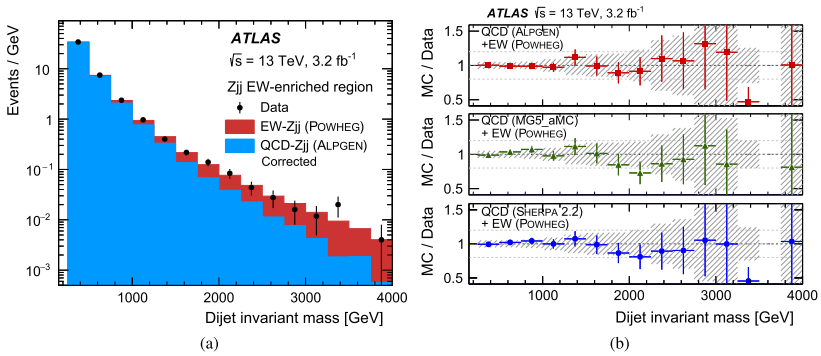

Fig. 4. (a) Comparison in the EW-enriched region of the sum of EW-Zjj and m_{jj}-reweighted QCD-Zjj templates to the data (minus the non-Zjj backgrounds). The normalisation of the templates is adjusted to the results of the fit (see text for details). The EW-Zjj MC sample comes from the POWHEG event generator and the QCD-Zjj MC sample comes from the ALPGEN event generator. (b) The ratio of the sum of the EW-Zjj and m_{jj}-reweighted QCD-Zjj templates to the background-subtracted data in the EW-enriched region, for three different QCD-Zjj MC predictions. The normalisation of the templates is adjusted to the results of the fit. Error bars represent the statistical uncertainties in the data and combined QCD-Zjj plus EW-Zjj MC samples added in quadrature. The hatched band represents experimental systematic uncertainties in the m_{jj} distribution.

Table 4
Systematic uncertainties contributing to the measurement of the EW-Zjj cross-sections for $m_{jj} > 250$ GeV and $m_{jj} > 1$ TeV. Uncertainties are grouped into EW-Zjj signal modelling, QCD-Zjj background modelling, QCD-EW interference, non-Zjj backgrounds, and experimental sources.

Source	Relative systematic uncertainty [%]	
	$\sigma_{\text{EW}}^{m_{jj}>250\text{ GeV}}$	$\sigma_{\text{EW}}^{m_{jj}>1\text{ TeV}}$
EW-Zjj signal modelling (QCD scales, PDF and UEPS)	± 7.4	± 1.7
EW-Zjj template statistical uncertainty	± 0.5	± 0.04
EW-Zjj contamination in QCD-enriched region	−0.1	−0.2
QCD-Zjj modelling (m_{jj} shape constraint / third-jet veto)	± 11	± 11
Stat. uncertainty in QCD control region constraint	± 6.2	± 6.4
QCD-Zjj signal modelling (QCD scales, PDF and UEPS)	± 4.5	± 6.5
QCD-Zjj template statistical uncertainty	± 2.5	± 3.5
QCD-EW interference	± 1.3	± 1.5
$\bar{t}t$ and single-top background modelling	± 1.0	± 1.2
Diboson background modelling	± 0.1	± 0.1
Jet energy resolution	± 2.3	± 1.1
Jet energy scale	+5.3/−4.1	+3.5/−4.2
Lepton identification, momentum scale, trigger, pile-up	+1.3/−2.5	+3.2/−1.5
Luminosity	± 2.1	± 2.1
Total	± 17	± 16

compared to the average of the two, taken as the central value. Uncertainties in the EW-Zjj templates due to variations of the QCD scales, of the PDFs, and of the UEPS model are also included as are statistical uncertainties in the templates themselves.

Following the extraction of the EW-Zjj cross-section in the EW-enriched regions, the normalisations of the EW-Zjj MC samples are modified to agree with the measurements and the potential EW contamination of the QCD-enriched region is recalculated, which leads to a modification of the QCD-Zjj correction factors. The EW-Zjj cross-section measurement is repeated with these modified QCD-Zjj templates and the change in the resultant cross-sections is assigned as a systematic uncertainty associated with the EW-Zjj contamination of the QCD-enriched region.

As discussed in Section 6.1, the use of a QCD-enriched region provides a way to correct for QCD-Zjj modelling issues and also constrains theoretical and experimental uncertainties associated with observables constructed from the two leading jets. Nevertheless, the largest contribution to the total uncertainty arises from modelling uncertainties associated with propagation of the m_{jj} correction factors for QCD-Zjj in the QCD-enriched region into the EW-enriched region, and these correction factors depend on the modelling of the additional jet activity in the QCD-Zjj MC samples used in the measurement. The uncertainty is assessed by repeating the EW-Zjj cross-section measurement with m_{jj}-reweighted QCD-Zjj MC templates from ALPGEN, MG5_aMC, and SHERPA, and assigning the variation of the measured cross-sections from the central EW-Zjj result as a systematic uncertainty. Statistical uncertainties from data and simulation in the m_{jj} correction factors derived in the QCD-enriched region are also propagated through to the measured EW-Zjj cross-section as a systematic uncertainty. Uncertainties associated with QCD renormalisation and factorisation scales, PDF error sets, and UEPS modelling are assessed by studying the change in the extracted EW-Zjj cross-sections when repeating the measurement procedure, including rederiving

m_{jj} correction factors in the QCD-enriched region and repeating fits in the EW-enriched region, using modified QCD-Zjj MC templates. Statistical uncertainties in the QCD-Zjj template in the EW-enriched region are also propagated as a systematic uncertainty in the EW-Zjj cross-section measurement.

Potential quantum-mechanical interference between the QCD-Zjj and EW-Zjj processes is assessed using MG5_aMC to derive a correction to the QCD-Zjj template as a function of m_{jj}. The impact of interference on the measurement is determined by repeating the EW-Zjj measurement procedure twice, either applying this correction to the QCD-Zjj template only in the QCD-enriched region or only in the EW-enriched region and taking the maximum change in the measured EW-Zjj cross-section as a symmetrised uncertainty. This approach assumes the interference affects only one of the two fiducial regions and therefore has a maximal impact on the signal extraction. Potential interference between the Zjj and diboson processes was found to be negligible.

Normalisation and shape uncertainties in the estimated background from top-quark and diboson production are assessed with varied background templates as described in Section 5.4, albeit with significantly larger uncertainties in the EW-enriched fiducial region compared to the baseline region.

Experimental systematic uncertainties arising from the jet energy scale and resolution, from lepton efficiencies related to reconstruction, identification, isolation and trigger, and lepton energy/momentum scale and resolution, and from pile-up modelling, are independently assessed by repeating the EW-Zjj measurement procedure using modified QCD-Zjj and EW-Zjj templates. Here, the QCD-enriched QCD-Zjj template constraint procedure described in Section 6.1 has the added benefit of significantly reducing the jet-based experimental uncertainties, as can be seen in Table 4 from their small impact on the total systematic uncertainty.

6.3. Electroweak Zjj results

As in the inclusive Zjj cross-section measurements, the quoted EW-Zjj cross-section measurements are the average of the cross-sections determined with each of the six combinations of the three QCD-Zjj MC templates and two EW-Zjj MC templates. The measured cross-sections for the EW production of a leptonically decaying Z boson and at least two jets satisfying the fiducial requirements for the EW-enriched regions as given in Table 1 with the requirements $m_{jj} > 250$ GeV and $m_{jj} > 1$ TeV are shown in Table 5, where they are compared to predictions from Powheg+Pythia. The use of a differential template fit in m_{jj} to extract the EW-Zjj signal allows systematic uncertainties on the EW-Zjj cross-section measurements to be constrained by the bins with the most favourable balance of EW-Zjj signal purity and minimal shape and normalisation uncertainty. For the $m_{jj} > 250$ GeV region, although all m_{jj} bins contribute to the fit, the individually most-constraining m_{jj} interval is the 900–1000 GeV bin. The use of this method results in very similar relative systematic uncertainties in the EW-Zjj cross-section measurements at the two different m_{jj} thresholds, despite the measured relative EW-Zjj contribution to the total Zjj rate for $m_{jj} > 1$ TeV being more than six times the relative contribution of EW-Zjj for $m_{jj} > 250$ GeV.

The EW-Zjj cross-sections at $\sqrt{s} = 13$ TeV are in agreement with the predictions from Powheg+Pythia for both $m_{jj} > 250$ GeV and $m_{jj} > 1$ TeV. The effect on the measurement of inclusive Zjj production rates (Section 5.5) from correcting the EW-Zjj production rates predicted by Powheg+Pythia to the measured rates presented here was found to be negligible. Modifications to the m_{jj} distribution shape are already accounted for as a systematic uncertainty in the inclusive Zjj measurements.

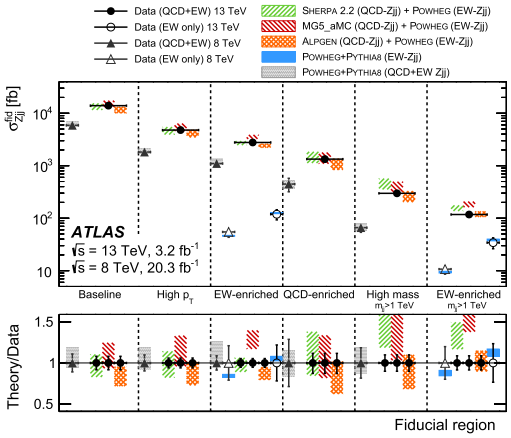

Fig. 5. Fiducial cross-sections for a leptonically decaying Z boson and at least two jets (solid data points) and EW-Zjj production (open data points) at 13 TeV (circles) compared to equivalent results at 8 TeV [2] (triangles) and to theoretical predictions (shaded/hatched bands). Measurements of Zjj at 13 TeV are compared to predictions from Sherpa (QCD-Zjj) + Powheg (EW-Zjj), MG5_aMC (QCD-Zjj) + Powheg (EW-Zjj), and Alpgen (QCD-Zjj) + Powheg (EW-Zjj), while measurements of EW-Zjj production are compared to Powheg (EW-Zjj). Results at 8 TeV are compared to predictions from Powheg+Pythia (QCD-Zjj + EW-Zjj). The bottom panel shows the ratio of the various theory predictions to data as shaded bands. Relative uncertainties in the measured data are represented by an error bar centred at unity.

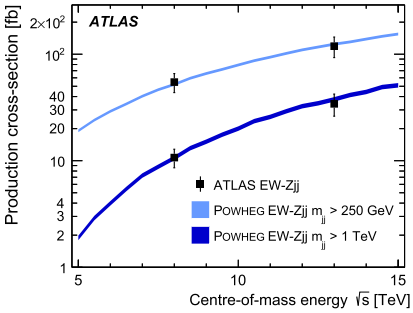

Fig. 6. Measurements of the EW-Zjj process presented in this Letter at a centre-of-mass energy of 13 TeV, compared with previous measurements at 8 TeV [2], for two different dijet invariant mass thresholds, $m_{jj} > 0.25$ TeV and $m_{jj} > 1$ TeV. The error bars on the measurements represent statistical and systematic uncertainties added in quadrature. Predictions from the Powheg event generator with their total uncertainty are also shown.

Fig. 5 shows a summary of the fiducial cross-sections for a leptonically decaying Z boson and at least two jets at 13 TeV compared to equivalent results at 8 TeV [2] and to theoretical predictions with their uncertainties. A significant rise in cross-section is observed between $\sqrt{s} = 8$ TeV and $\sqrt{s} = 13$ TeV within each fiducial region. In the EW-enriched region, for m_{jj} thresholds of 250 GeV and 1 TeV, the measured EW-Zjj cross-sections at 13 TeV are found to be respectively 2.2 and 3.2 times as large as those measured at 8 TeV, as illustrated in Fig. 6.

Table 5
Measured and predicted EW-Zjj production cross-sections in the EW-enriched fiducial regions with and without an additional kinematic requirement of $m_{jj} > 1$ TeV. For the measured cross-sections, the first uncertainty given is statistical, the second is systematic and the third is due to the luminosity determination. For the predictions, the quoted uncertainty represents the statistical uncertainty, plus systematic uncertainties from the PDFs and factorisation and renormalisation scale variations, all added in quadrature.

Fiducial region	EW-Zjj cross-sections [fb]				
	Measured				Powheg+Pythia
EW-enriched, $m_{jj} > 250$ GeV	119	$\pm$ 16	$\pm$ 20	$\pm$ 2	125.2 ± 3.4
EW-enriched, $m_{jj} > 1$ TeV	34.2	$\pm$ 5.8	$\pm$ 5.5	$\pm$ 0.7	38.5 ± 1.5

7. Summary

Fiducial cross-sections for the electroweak production of two jets in association with a leptonically decaying Z boson in proton–proton collisions are measured at a centre-of-mass energy of 13 TeV, using data corresponding to an integrated luminosity of 3.2 fb^{-1} recorded with the ATLAS detector at the Large Hadron Collider. The EW-Zjj cross-section is extracted in a fiducial region chosen to enhance the EW contribution relative to the dominant QCD-Zjj process, which is constrained using a data-driven approach. The measured fiducial EW cross-section is $\sigma_{\mathrm{EW}}^{Zjj} = 119 \pm 16$ (stat.) ± 20 (syst.) ± 2 (lumi.) fb for dijet invariant mass greater than 250 GeV, and 34.2 ± 5.8 (stat.) ± 5.5 (syst.) ± 0.7 (lumi.) fb for dijet invariant mass greater than 1 TeV. A comparison with previously published measurements at $\sqrt{s} = 8$ TeV is presented, with measured EW-Zjj cross-sections at $\sqrt{s} = 13$ TeV found to be 2.2 (3.2) times as large as those measured at $\sqrt{s} = 8$ TeV in the low (high) dijet mass EW-enriched regions. Relative to measurements at $\sqrt{s} = 8$ TeV, the increased $\sqrt{s}$ allows a region of higher dijet mass to be explored, in which the EW-Zjj signal is more prominent. The Standard Model predictions are in agreement with the EW-Zjj measurements.

The inclusive Zjj cross-section is also measured in six different fiducial regions with varying contributions from EW-Zjj and QCD-Zjj production. At higher dijet invariant masses (> 1 TeV), particularly crucial for precision measurements of EW-Zjj production and for searches for new phenomena in vector-boson fusion topologies, predictions from Sherpa (QCD-Zjj) + Powheg (EW-Zjj) and MG5_aMC (QCD-Zjj) + Powheg (EW-Zjj) are found to significantly overestimate the observed Zjj production rates in data. Alpgen (QCD-Zjj) + Powheg (EW-Zjj) provides a better description of the m_{jj} shape.

Acknowledgements

We thank CERN for the very successful operation of the LHC, as well as the support staff from our institutions without whom ATLAS could not be operated efficiently.

We acknowledge the support of ANPCyT, Argentina; YerPhI, Armenia; ARC, Australia; BMWFW and FWF, Austria; ANAS, Azerbaijan; SSTC, Belarus; CNPq and FAPESP, Brazil; NSERC, NRC and CFI, Canada; CERN; CONICYT, Chile; CAS, MOST and NSFC, China; COLCIENCIAS, Colombia; MSMT CR, MPO CR and VSC CR, Czech Republic; DNRF and DNSRC, Denmark; IN2P3-CNRS, CEA-DSM/IRFU, France; SRNSF, Georgia; BMBF, HGF, and MPG, Germany; GSRT, Greece; RGC, Hong Kong SAR, China; ISF, I-CORE and Benoziyo Center, Israel; INFN, Italy; MEXT and JSPS, Japan; CNRST, Morocco; NWO, Netherlands; RCN, Norway; MNiSW and NCN, Poland; FCT, Portugal; MNE/IFA, Romania; MES of Russia and NRC KI, Russian Federation; JINR; MESTD, Serbia; MSSR, Slovakia; ARRS and MIZŠ, Slovenia; DST/NRF, South Africa; MINECO, Spain; SRC and Knut and Alice Wallenberg Foundation, Sweden; SERI, SNSF and Cantons of Bern and Geneva, Switzerland; MOST, Taiwan; TAEK, Turkey; STFC, United Kingdom; DOE and NSF, United States of America. In addition, individual groups and members have received support from BCKDF, the Canada Council, Canarie, CRC, Compute Canada, FQRNT, and the Ontario Innovation Trust, Canada; EPLANET, ERC, ERDF, FP7, Horizon 2020 and Marie Skłodowska-Curie Actions, European Union; Investissements d'Avenir Labex and Idex, ANR, Région Auvergne and Fondation Partager le Savoir, France; DFG and AvH Foundation, Germany; Herakleitos, Thales and Aristeia programmes co-financed by EU-ESF and the Greek NSRF; BSF, GIF and Minerva, Israel; BRF, Norway; CERCA Programme Generalitat de Catalunya, Generalitat Valenciana, Spain; the Royal Society and Leverhulme Trust, United Kingdom.

The crucial computing support from all WLCG partners is acknowledged gratefully, in particular from CERN, the ATLAS Tier-1 facilities at TRIUMF (Canada), NDGF (Denmark, Norway, Sweden), CC-IN2P3 (France), KIT/GridKA (Germany), INFN-CNAF (Italy), NL-T1 (Netherlands), PIC (Spain), ASGC (Taiwan), RAL (UK) and BNL (USA), the Tier-2 facilities worldwide and large non-WLCG resource providers. Major contributors of computing resources are listed in Ref. [53].

References

[1] CMS Collaboration, Measurement of the hadronic activity in events with a Z and two jets and extraction of the cross section for the electroweak production of a Z with two jets in pp collisions at $\sqrt{s} = 7$ TeV, J. High Energy Phys. 10 (2013) 062, arXiv:1305.7389 [hep-ex].

[2] ATLAS Collaboration, Measurement of the electroweak production of dijets in association with a Z-boson and distributions sensitive to vector boson fusion in proton–proton collisions at $\sqrt{s} = 8$ TeV using the ATLAS detector, J. High Energy Phys. 04 (2014) 031, arXiv:1401.7610 [hep-ex].

[3] P. Nason, A new method for combining NLO QCD with shower Monte Carlo algorithms, J. High Energy Phys. 11 (2004) 040, arXiv:hep-ph/0409146.

[4] S. Frixione, P. Nason, C. Oleari, Matching NLO QCD computations with Parton Shower simulations: the POWHEG method, J. High Energy Phys. 11 (2007) 070, arXiv:0709.2092 [hep-ph].

[5] S. Alioli, et al., A general framework for implementing NLO calculations in shower Monte Carlo programs: the POWHEG BOX, J. High Energy Phys. 06 (2010) 043, arXiv:1002.2581 [hep-ph].

[6] CMS Collaboration, Measurement of electroweak production of two jets in association with a Z boson in proton–proton collisions at $\sqrt{s} = 8$ TeV, Eur. Phys. J. C 75 (2015) 66, arXiv:1410.3153 [hep-ex].

[7] ATLAS Collaboration, The ATLAS experiment at the CERN Large Hadron Collider, J. Instrum. 3 (2008) S08003.

[8] ATLAS Collaboration, ATLAS Insertable B-Layer, Technical Design Report, ATLAS-TDR-19, 2010, https://cds.cern.ch/record/1291633;
ATLAS Insertable B-Layer, Technical Design Report Addendum, ATLAS-TDR-19-ADD-1, https://cds.cern.ch/record/1451888, 2012.

[9] ATLAS Collaboration, Performance of the ATLAS trigger system in 2015, Eur. Phys. J. C 77 (2017) 317, arXiv:1611.09661 [hep-ex].

[10] F. Schissler, D. Zeppenfeld, Parton shower effects on W and Z production via vector boson fusion at NLO QCD, J. High Energy Phys. 04 (2013) 057, arXiv:1302.2884 [hep-ph].

[11] T. Gleisberg, et al., Event generation with SHERPA 1.1, J. High Energy Phys. 02 (2009) 007, arXiv:0811.4622 [hep-ph].

[12] T. Sjöstrand, et al., An introduction to PYTHIA 8.2, Comput. Phys. Commun. 191 (2015) 159, arXiv:1410.3012 [hep-ph].

[13] ATLAS Collaboration, Measurement of the Z/γ^* boson transverse momentum distribution in pp collisions at $\sqrt{s} = 7$ TeV with the ATLAS detector, J. High Energy Phys. 09 (2014) 145, arXiv:1406.3660 [hep-ex].

[14] H.-L. Lai, et al., New parton distributions for collider physics, Phys. Rev. D 82 (2010) 074024, arXiv:1007.2241 [hep-ph].
[15] T. Gleisberg, S. Höche, Comix, a new matrix element generator, J. High Energy Phys. 12 (2008) 039, arXiv:0808.3674 [hep-ph].
[16] F. Cascioli, P. Maierhöfer, S. Pozzorini, Scattering amplitudes with open loops, Phys. Rev. Lett. 108 (2012) 111601, arXiv:1111.5206 [hep-ph].
[17] S. Catani, et al., QCD matrix elements + parton showers, J. High Energy Phys. 11 (2001) 063, arXiv:hep-ph/0109231.
[18] S. Schumann, F. Krauss, A parton shower algorithm based on Catani–Seymour dipole factorisation, J. High Energy Phys. 03 (2008) 038, arXiv:0709.1027 [hep-ph].
[19] T. Gehrmann, S. Hoche, F. Krauss, M. Schonherr, F. Siegert, NLO QCD matrix elements + parton showers in $e^+e^- \to$ hadrons, J. High Energy Phys. 01 (2013) 144, arXiv:1207.5031 [hep-ph].
[20] S. Höche, et al., QCD matrix elements + parton showers: the NLO case, J. High Energy Phys. 04 (2013) 027, arXiv:1207.5030 [hep-ph].
[21] NNPDF Collaboration, R. Ball, et al., Parton distributions for the LHC Run II, J. High Energy Phys. 04 (2015) 040, arXiv:1410.8849 [hep-ph].
[22] M.L. Mangano, F. Piccinini, A. Polosa, M. Moretti, R. Pittau, ALPGEN, a generator for hard multiparton processes in hadronic collisions, J. High Energy Phys. 07 (2003) 001, arXiv:hep-ph/0206293.
[23] J. Alwall, et al., The automated computation of tree-level and next-to-leading order differential cross sections, and their matching to parton shower simulations, J. High Energy Phys. 07 (2014) 079, arXiv:1405.0301 [hep-ph].
[24] T. Sjöstrand, S. Mrenna, P.Z. Skands, PYTHIA 6.4 physics and manual, J. High Energy Phys. 05 (2006) 026, arXiv:hep-ph/0603175.
[25] P.Z. Skands, Tuning Monte Carlo generators: the Perugia tunes, Phys. Rev. D 82 (2010) 074018, arXiv:1005.3457 [hep-ph].
[26] J. Pumplin, et al., New generation of parton distributions with uncertainties from global QCD analysis, J. High Energy Phys. 07 (2002) 012, arXiv:hep-ph/0201195.
[27] ATLAS Collaboration, ATLAS Pythia 8 Tunes to 7 TeV Data, ATL-PHYS-PUB-2014-021, 2014–2014, https://cds.cern.ch/record/1966419.
[28] NNPDF Collaboration, R. Ball, et al., Parton distributions with LHC data, Nucl. Phys. B 867 (2013) 244, arXiv:1207.1303 [hep-ph].
[29] C. Anastasiou, L.J. Dixon, K. Melnikov, F. Petriello, High precision QCD at hadron colliders: electroweak gauge boson rapidity distributions at next-to-next-to leading order, Phys. Rev. D 69 (2004) 094008, arXiv:hep-ph/0312266.
[30] R. Gavin, Y. Li, F. Petriello, S. Quackenbush, FEWZ 2.0: a code for hadronic Z production at next-to-next-to-leading order, Comput. Phys. Commun. 182 (2011) 2388, arXiv:1011.3540 [hep-ph].
[31] Y. Li, F. Petriello, Combining QCD and electroweak corrections to dilepton production in the framework of the FEWZ simulation code, Phys. Rev. D 86 (2012) 094034, arXiv:1208.5967 [hep-ph].
[32] M. Czakon, A. Mitov, Top++: a program for the calculation of the top-pair cross-section at hadron colliders, Comput. Phys. Commun. 185 (2014) 2930, arXiv:1112.5675 [hep-ph].
[33] S. Agostinelli, et al., GEANT4 – a simulation toolkit, Nucl. Instrum. Methods A 506 (2003) 250.
[34] ATLAS Collaboration, The ATLAS simulation infrastructure, Eur. Phys. J. C 70 (2010) 823, arXiv:1005.4568 [physics.ins-det].
[35] ATLAS Collaboration, Summary of ATLAS Pythia 8 Tunes, ATL-PHYS-PUB-2012-003, 2012, https://cds.cern.ch/record/1474107.
[36] A.D. Martin, W.J. Stirling, R.S. Thorne, G. Watt, Parton distributions for the LHC, Eur. Phys. J. C 63 (2009) 189, arXiv:0901.0002 [hep-ph].
[37] ATLAS Collaboration, Electron Efficiency Measurements with the ATLAS Detector Using the 2015 LHC Proton–Proton Collision Data, ATLAS-CONF-2016-024, 2016, https://cds.cern.ch/record/2157687.
[38] ATLAS Collaboration, Muon reconstruction performance of the ATLAS detector in proton–proton collision data at $\sqrt{s} = 13$ TeV, Eur. Phys. J. C 76 (2016) 292, arXiv:1603.05598 [hep-ex].
[39] W. Lampl, et al., Calorimeter Clustering Algorithms: Description and Performance, ATL-LARG-PUB-2008-002, 2008, https://cds.cern.ch/record/1099735.
[40] M. Cacciari, G.P. Salam, G. Soyez, The anti-k_t jet clustering algorithm, J. High Energy Phys. 04 (2008) 063, arXiv:0802.1189 [hep-ph].
[41] M. Cacciari, G.P. Salam, G. Soyez, FastJet user manual, Eur. Phys. J. C 72 (2012) 1896, arXiv:1111.6097 [hep-ph].
[42] ATLAS Collaboration, Jet energy scale measurements and their systematic uncertainties in proton–proton collisions at $\sqrt{s} = 13$ TeV with the ATLAS detector, arXiv:1703.09665 [hep-ex], 2017.
[43] ATLAS Collaboration, Tagging and Suppression of Pileup Jets with the ATLAS Detector, ATLAS-CONF-2014-018, 2014, https://cds.cern.ch/record/1700870.
[44] D.L. Rainwater, R. Szalapski, D. Zeppenfeld, Probing color singlet exchange in Z + two jet events at the CERN LHC, Phys. Rev. D 54 (1996) 6680, arXiv:hep-ph/9605444.
[45] ATLAS Collaboration, Multi-Boson Simulation for 13 TeV ATLAS Analyses, ATL-PHYS-PUB-2016-002, 2016, https://cds.cern.ch/record/2119986.
[46] M. Bahr, et al., Herwig++ physics and manual, Eur. Phys. J. C 58 (2008) 639, arXiv:0803.0883 [hep-ph].
[47] ATLAS Collaboration, Luminosity determination in pp collisions at $\sqrt{s} =$ 8 TeV using the ATLAS detector at the LHC, Eur. Phys. J. C 76 (2016) 653, arXiv:1608.03953 [hep-ex].
[48] ATLAS Collaboration, Measurements of the production cross section of a Z boson in association with jets in pp collisions at $\sqrt{s} = 13$ TeV with the ATLAS detector, Eur. Phys. J. C 77 (2017) 361, arXiv:1702.05725 [hep-ex].
[49] DØ Collaboration, V.M. Abazov, et al., Studies of W boson plus jets production in $p\bar{p}$ collisions at $\sqrt{s} = 1.96$ TeV, Phys. Rev. D 88 (2013) 092001, arXiv:1302.6508 [hep-ex].
[50] CMS Collaboration, Measurements of differential cross sections for associated production of a W boson and jets in proton–proton collisions at $\sqrt{s} = 8$ TeV, Phys. Rev. D 95 (2017) 052002, arXiv:1610.04222 [hep-ex].
[51] ATLAS Collaboration, Measurements of electroweak W_{jj} production and constraints on anomalous gauge couplings with the ATLAS detector, Eur. Phys. J. C 77 (2017) 474, arXiv:1703.04362 [hep-ex].
[52] W. Verkerke, D. Kirkby, The RooFit toolkit for data modeling, arXiv:physics/0306116, 2003.
[53] ATLAS Collaboration, ATLAS Computing Acknowledgements 2016–2017, 2016, ATL-GEN-PUB-2016-002, http://cdsweb.cern.ch/record/2202407.

The ATLAS Collaboration

M. Aaboud [137d], G. Aad [88], B. Abbott [115], O. Abdinov [12,*], B. Abeloos [119], S.H. Abidi [161], O.S. AbouZeid [139], N.L. Abraham [151], H. Abramowicz [155], H. Abreu [154], R. Abreu [118], Y. Abulaiti [148a,148b], B.S. Acharya [167a,167b,a], S. Adachi [157], L. Adamczyk [41a], J. Adelman [110], M. Adersberger [102], T. Adye [133], A.A. Affolder [139], Y. Afik [154], T. Agatonovic-Jovin [14], C. Agheorghiesei [28c], J.A. Aguilar-Saavedra [128a,128f], S.P. Ahlen [24], F. Ahmadov [68,b], G. Aielli [135a,135b], S. Akatsuka [71], H. Akerstedt [148a,148b], T.P.A. Åkesson [84], E. Akilli [52], A.V. Akimov [98], G.L. Alberghi [22a,22b], J. Albert [172], P. Albicocco [50], M.J. Alconada Verzini [74], S.C. Alderweireldt [108], M. Aleksa [32], I.N. Aleksandrov [68], C. Alexa [28b], G. Alexander [155], T. Alexopoulos [10], M. Alhroob [115], B. Ali [130], M. Aliev [76a,76b], G. Alimonti [94a], J. Alison [33], S.P. Alkire [38], B.M.M. Allbrooke [151], B.W. Allen [118], P.P. Allport [19], A. Aloisio [106a,106b], A. Alonso [39], F. Alonso [74], C. Alpigiani [140], A.A. Alshehri [56], M.I. Alstaty [88], B. Alvarez Gonzalez [32], D. Álvarez Piqueras [170], M.G. Alviggi [106a,106b], B.T. Amadio [16], Y. Amaral Coutinho [26a], C. Amelung [25], D. Amidei [92], S.P. Amor Dos Santos [128a,128c], S. Amoroso [32], G. Amundsen [25], C. Anastopoulos [141], L.S. Ancu [52], N. Andari [19], T. Andeen [11], C.F. Anders [60b], J.K. Anders [77], K.J. Anderson [33], A. Andreazza [94a,94b], V. Andrei [60a], S. Angelidakis [37], I. Angelozzi [109], A. Angerami [38], A.V. Anisenkov [111,c], N. Anjos [13], A. Annovi [126a,126b], C. Antel [60a], M. Antonelli [50], A. Antonov [100,*], D.J. Antrim [166], F. Anulli [134a], M. Aoki [69], L. Aperio Bella [32], G. Arabidze [93], Y. Arai [69], J.P. Araque [128a], V. Araujo Ferraz [26a], A.T.H. Arce [48], R.E. Ardell [80], F.A. Arduh [74], J-F. Arguin [97], S. Argyropoulos [66], M. Arik [20a], A.J. Armbruster [32], L.J. Armitage [79], O. Arnaez [161],

H. Arnold [51], M. Arratia [30], O. Arslan [23], A. Artamonov [99], G. Artoni [122], S. Artz [86], S. Asai [157], N. Asbah [45], A. Ashkenazi [155], L. Asquith [151], K. Assamagan [27], R. Astalos [146a], M. Atkinson [169], N.B. Atlay [143], K. Augsten [130], G. Avolio [32], B. Axen [16], M.K. Ayoub [119], G. Azuelos [97,d], A.E. Baas [60a], M.J. Baca [19], H. Bachacou [138], K. Bachas [76a,76b], M. Backes [122], P. Bagnaia [134a,134b], M. Bahmani [42], H. Bahrasemani [144], J.T. Baines [133], M. Bajic [39], O.K. Baker [179], E.M. Baldin [111,c], P. Balek [175], F. Balli [138], W.K. Balunas [124], E. Banas [42], A. Bandyopadhyay [23], Sw. Banerjee [176,e], A.A.E. Bannoura [178], L. Barak [155], E.L. Barberio [91], D. Barberis [53a,53b], M. Barbero [88], T. Barillari [103], M-S Barisits [32], J.T. Barkeloo [118], T. Barklow [145], N. Barlow [30], S.L. Barnes [36c], B.M. Barnett [133], R.M. Barnett [16], Z. Barnovska-Blenessy [36a], A. Baroncelli [136a], G. Barone [25], A.J. Barr [122], L. Barranco Navarro [170], F. Barreiro [85], J. Barreiro Guimarães da Costa [35a], R. Bartoldus [145], A.E. Barton [75], P. Bartos [146a], A. Basalaev [125], A. Bassalat [119,f], R.L. Bates [56], S.J. Batista [161], J.R. Batley [30], M. Battaglia [139], M. Bauce [134a,134b], F. Bauer [138], H.S. Bawa [145,g], J.B. Beacham [113], M.D. Beattie [75], T. Beau [83], P.H. Beauchemin [165], P. Bechtle [23], H.P. Beck [18,h], H.C. Beck [57], K. Becker [122], M. Becker [86], C. Becot [112], A.J. Beddall [20d], A. Beddall [20b], V.A. Bednyakov [68], M. Bedognetti [109], C.P. Bee [150], T.A. Beermann [32], M. Begalli [26a], M. Begel [27], J.K. Behr [45], A.S. Bell [81], G. Bella [155], L. Bellagamba [22a], A. Bellerive [31], M. Bellomo [154], K. Belotskiy [100], O. Beltramello [32], N.L. Belyaev [100], O. Benary [155,*], D. Benchekroun [137a], M. Bender [102], K. Bendtz [148a,148b], N. Benekos [10], Y. Benhammou [155], E. Benhar Noccioli [179], J. Benitez [66], D.P. Benjamin [48], M. Benoit [52], J.R. Bensinger [25], S. Bentvelsen [109], L. Beresford [122], M. Beretta [50], D. Berge [109], E. Bergeaas Kuutmann [168], N. Berger [5], J. Beringer [16], S. Berlendis [58], N.R. Bernard [89], G. Bernardi [83], C. Bernius [145], F.U. Bernlochner [23], T. Berry [80], P. Berta [86], C. Bertella [35a], G. Bertoli [148a,148b], F. Bertolucci [126a,126b], I.A. Bertram [75], C. Bertsche [45], D. Bertsche [115], G.J. Besjes [39], O. Bessidskaia Bylund [148a,148b], M. Bessner [45], N. Besson [138], A. Bethani [87], S. Bethke [103], A.J. Bevan [79], J. Beyer [103], R.M. Bianchi [127], O. Biebel [102], D. Biedermann [17], R. Bielski [87], K. Bierwagen [86], N.V. Biesuz [126a,126b], M. Biglietti [136a], T.R.V. Billoud [97], H. Bilokon [50], M. Bindi [57], A. Bingul [20b], C. Bini [134a,134b], S. Biondi [22a,22b], T. Bisanz [57], C. Bittrich [47], D.M. Bjergaard [48], J.E. Black [145], K.M. Black [24], R.E. Blair [6], T. Blazek [146a], I. Bloch [45], C. Blocker [25], A. Blue [56], W. Blum [86,*], U. Blumenschein [79], S. Blunier [34a], G.J. Bobbink [109], V.S. Bobrovnikov [111,c], S.S. Bocchetta [84], A. Bocci [48], C. Bock [102], M. Boehler [51], D. Boerner [178], D. Bogavac [102], A.G. Bogdanchikov [111], C. Bohm [148a], V. Boisvert [80], P. Bokan [168,i], T. Bold [41a], A.S. Boldyrev [101], A.E. Bolz [60b], M. Bomben [83], M. Bona [79], M. Boonekamp [138], A. Borisov [132], G. Borissov [75], J. Bortfeldt [32], D. Bortoletto [122], V. Bortolotto [62a,62b,62c], D. Boscherini [22a], M. Bosman [13], J.D. Bossio Sola [29], J. Boudreau [127], J. Bouffard [2], E.V. Bouhova-Thacker [75], D. Boumediene [37], C. Bourdarios [119], S.K. Boutle [56], A. Boveia [113], J. Boyd [32], I.R. Boyko [68], J. Bracinik [19], A. Brandt [8], G. Brandt [57], O. Brandt [60a], U. Bratzler [158], B. Brau [89], J.E. Brau [118], W.D. Breaden Madden [56], K. Brendlinger [45], A.J. Brennan [91], L. Brenner [109], R. Brenner [168], S. Bressler [175], D.L. Briglin [19], T.M. Bristow [49], D. Britton [56], D. Britzger [45], F.M. Brochu [30], I. Brock [23], R. Brock [93], G. Brooijmans [38], T. Brooks [80], W.K. Brooks [34b], J. Brosamer [16], E. Brost [110], J.H Broughton [19], P.A. Bruckman de Renstrom [42], D. Bruncko [146b], A. Bruni [22a], G. Bruni [22a], L.S. Bruni [109], BH Brunt [30], M. Bruschi [22a], N. Bruscino [23], P. Bryant [33], L. Bryngemark [45], T. Buanes [15], Q. Buat [144], P. Buchholz [143], A.G. Buckley [56], I.A. Budagov [68], F. Buehrer [51], M.K. Bugge [121], O. Bulekov [100], D. Bullock [8], T.J. Burch [110], S. Burdin [77], C.D. Burgard [51], A.M. Burger [5], B. Burghgrave [110], K. Burka [42], S. Burke [133], I. Burmeister [46], J.T.P. Burr [122], E. Busato [37], D. Büscher [51], V. Büscher [86], P. Bussey [56], J.M. Butler [24], C.M. Buttar [56], J.M. Butterworth [81], P. Butti [32], W. Buttinger [27], A. Buzatu [153], A.R. Buzykaev [111,c], S. Cabrera Urbán [170], D. Caforio [130], V.M. Cairo [40a,40b], O. Cakir [4a], N. Calace [52], P. Calafiura [16], A. Calandri [88], G. Calderini [83], P. Calfayan [64], G. Callea [40a,40b], L.P. Caloba [26a], S. Calvente Lopez [85], D. Calvet [37], S. Calvet [37], T.P. Calvet [88], R. Camacho Toro [33], S. Camarda [32], P. Camarri [135a,135b], D. Cameron [121], R. Caminal Armadans [169], C. Camincher [58], S. Campana [32], M. Campanelli [81], A. Camplani [94a,94b], A. Campoverde [143], V. Canale [106a,106b], M. Cano Bret [36c], J. Cantero [116], T. Cao [155], M.D.M. Capeans Garrido [32], I. Caprini [28b], M. Caprini [28b], M. Capua [40a,40b], R.M. Carbone [38], R. Cardarelli [135a], F. Cardillo [51], I. Carli [131], T. Carli [32], G. Carlino [106a], B.T. Carlson [127], L. Carminati [94a,94b], R.M.D. Carney [148a,148b], S. Caron [108], E. Carquin [34b], S. Carrá [94a,94b], G.D. Carrillo-Montoya [32], D. Casadei [19], M.P. Casado [13,j], M. Casolino [13], D.W. Casper [166], R. Castelijn [109], V. Castillo Gimenez [170], N.F. Castro [128a,k], A. Catinaccio [32], J.R. Catmore [121], A. Cattai [32], J. Caudron [23], V. Cavaliere [169], E. Cavallaro [13], D. Cavalli [94a], M. Cavalli-Sforza [13], V. Cavasinni [126a,126b], E. Celebi [20c], F. Ceradini [136a,136b], L. Cerda Alberich [170], A.S. Cerqueira [26b], A. Cerri [151], L. Cerrito [135a,135b], F. Cerutti [16],

A. Cervelli [18], S.A. Cetin [20c], A. Chafaq [137a], D. Chakraborty [110], S.K. Chan [59], W.S. Chan [109], Y.L. Chan [62a], P. Chang [169], J.D. Chapman [30], D.G. Charlton [19], C.C. Chau [31], C.A. Chavez Barajas [151], S. Che [113], S. Cheatham [167a,167c], A. Chegwidden [93], S. Chekanov [6], S.V. Chekulaev [163a], G.A. Chelkov [68,l], M.A. Chelstowska [32], C. Chen [67], H. Chen [27], J. Chen [36a], S. Chen [35b], S. Chen [157], X. Chen [35c,m], Y. Chen [70], H.C. Cheng [92], H.J. Cheng [35a], A. Cheplakov [68], E. Cheremushkina [132], R. Cherkaoui El Moursli [137e], E. Cheu [7], K. Cheung [63], L. Chevalier [138], V. Chiarella [50], G. Chiarelli [126a,126b], G. Chiodini [76a], A.S. Chisholm [32], A. Chitan [28b], Y.H. Chiu [172], M.V. Chizhov [68], K. Choi [64], A.R. Chomont [37], S. Chouridou [156], Y.S. Chow [62a], V. Christodoulou [81], M.C. Chu [62a], J. Chudoba [129], A.J. Chuinard [90], J.J. Chwastowski [42], L. Chytka [117], A.K. Ciftci [4a], D. Cinca [46], V. Cindro [78], I.A. Cioara [23], C. Ciocca [22a,22b], A. Ciocio [16], F. Cirotto [106a,106b], Z.H. Citron [175], M. Citterio [94a], M. Ciubancan [28b], A. Clark [52], B.L. Clark [59], M.R. Clark [38], P.J. Clark [49], R.N. Clarke [16], C. Clement [148a,148b], Y. Coadou [88], M. Cobal [167a,167c], A. Coccaro [52], J. Cochran [67], L. Colasurdo [108], B. Cole [38], A.P. Colijn [109], J. Collot [58], T. Colombo [166], P. Conde Muiño [128a,128b], E. Coniavitis [51], S.H. Connell [147b], I.A. Connelly [87], S. Constantinescu [28b], G. Conti [32], F. Conventi [106a,n], M. Cooke [16], A.M. Cooper-Sarkar [122], F. Cormier [171], K.J.R. Cormier [161], M. Corradi [134a,134b], F. Corriveau [90,o], A. Cortes-Gonzalez [32], G. Cortiana [103], G. Costa [94a], M.J. Costa [170], D. Costanzo [141], G. Cottin [30], G. Cowan [80], B.E. Cox [87], K. Cranmer [112], S.J. Crawley [56], R.A. Creager [124], G. Cree [31], S. Crépé-Renaudin [58], F. Crescioli [83], W.A. Cribbs [148a,148b], M. Cristinziani [23], V. Croft [108], G. Crosetti [40a,40b], A. Cueto [85], T. Cuhadar Donszelmann [141], A.R. Cukierman [145], J. Cummings [179], M. Curatolo [50], J. Cúth [86], S. Czekierda [42], P. Czodrowski [32], G. D'amen [22a,22b], S. D'Auria [56], L. D'eramo [83], M. D'Onofrio [77], M.J. Da Cunha Sargedas De Sousa [128a,128b], C. Da Via [87], W. Dabrowski [41a], T. Dado [146a], T. Dai [92], O. Dale [15], F. Dallaire [97], C. Dallapiccola [89], M. Dam [39], J.R. Dandoy [124], M.F. Daneri [29], N.P. Dang [176], A.C. Daniells [19], N.S. Dann [87], M. Danninger [171], M. Dano Hoffmann [138], V. Dao [150], G. Darbo [53a], S. Darmora [8], J. Dassoulas [3], A. Dattagupta [118], T. Daubney [45], W. Davey [23], C. David [45], T. Davidek [131], D.R. Davis [48], P. Davison [81], E. Dawe [91], I. Dawson [141], K. De [8], R. de Asmundis [106a], A. De Benedetti [115], S. De Castro [22a,22b], S. De Cecco [83], N. De Groot [108], P. de Jong [109], H. De la Torre [93], F. De Lorenzi [67], A. De Maria [57], D. De Pedis [134a], A. De Salvo [134a], U. De Sanctis [135a,135b], A. De Santo [151], K. De Vasconcelos Corga [88], J.B. De Vivie De Regie [119], R. Debbe [27], C. Debenedetti [139], D.V. Dedovich [68], N. Dehghanian [3], I. Deigaard [109], M. Del Gaudio [40a,40b], J. Del Peso [85], D. Delgove [119], F. Deliot [138], C.M. Delitzsch [7], A. Dell'Acqua [32], L. Dell'Asta [24], M. Dell'Orso [126a,126b], M. Della Pietra [106a,106b], D. della Volpe [52], M. Delmastro [5], C. Delporte [119], P.A. Delsart [58], D.A. DeMarco [161], S. Demers [179], M. Demichev [68], A. Demilly [83], S.P. Denisov [132], D. Denysiuk [138], D. Derendarz [42], J.E. Derkaoui [137d], F. Derue [83], P. Dervan [77], K. Desch [23], C. Deterre [45], K. Dette [161], M.R. Devesa [29], P.O. Deviveiros [32], A. Dewhurst [133], S. Dhaliwal [25], F.A. Di Bello [52], A. Di Ciaccio [135a,135b], L. Di Ciaccio [5], W.K. Di Clemente [124], C. Di Donato [106a,106b], A. Di Girolamo [32], B. Di Girolamo [32], B. Di Micco [136a,136b], R. Di Nardo [32], K.F. Di Petrillo [59], A. Di Simone [51], R. Di Sipio [161], D. Di Valentino [31], C. Diaconu [88], M. Diamond [161], F.A. Dias [39], M.A. Diaz [34a], E.B. Diehl [92], J. Dietrich [17], S. Díez Cornell [45], A. Dimitrievska [14], J. Dingfelder [23], P. Dita [28b], S. Dita [28b], F. Dittus [32], F. Djama [88], T. Djobava [54b], J.I. Djuvsland [60a], M.A.B. do Vale [26c], D. Dobos [32], M. Dobre [28b], C. Doglioni [84], J. Dolejsi [131], Z. Dolezal [131], M. Donadelli [26d], S. Donati [126a,126b], P. Dondero [123a,123b], J. Donini [37], J. Dopke [133], A. Doria [106a], M.T. Dova [74], A.T. Doyle [56], E. Drechsler [57], M. Dris [10], Y. Du [36b], J. Duarte-Campderros [155], A. Dubreuil [52], E. Duchovni [175], G. Duckeck [102], A. Ducourthial [83], O.A. Ducu [97,p], D. Duda [109], A. Dudarev [32], A.Chr. Dudder [86], E.M. Duffield [16], L. Duflot [119], M. Dührssen [32], M. Dumancic [175], A.E. Dumitriu [28b], A.K. Duncan [56], M. Dunford [60a], H. Duran Yildiz [4a], M. Düren [55], A. Durglishvili [54b], D. Duschinger [47], B. Dutta [45], D. Duvnjak [1], M. Dyndal [45], B.S. Dziedzic [42], C. Eckardt [45], K.M. Ecker [103], R.C. Edgar [92], T. Eifert [32], G. Eigen [15], K. Einsweiler [16], T. Ekelof [168], M. El Kacimi [137c], R. El Kosseifi [88], V. Ellajosyula [88], M. Ellert [168], S. Elles [5], F. Ellinghaus [178], A.A. Elliot [172], N. Ellis [32], J. Elmsheuser [27], M. Elsing [32], D. Emeliyanov [133], Y. Enari [157], O.C. Endner [86], J.S. Ennis [173], J. Erdmann [46], A. Ereditato [18], M. Ernst [27], S. Errede [169], M. Escalier [119], C. Escobar [170], B. Esposito [50], O. Estrada Pastor [170], A.I. Etienvre [138], E. Etzion [155], H. Evans [64], A. Ezhilov [125], M. Ezzi [137e], F. Fabbri [22a,22b], L. Fabbri [22a,22b], V. Fabiani [108], G. Facini [81], R.M. Fakhrutdinov [132], S. Falciano [134a], R.J. Falla [81], J. Faltova [32], Y. Fang [35a], M. Fanti [94a,94b], A. Farbin [8], A. Farilla [136a], C. Farina [127], E.M. Farina [123a,123b], T. Farooque [93], S. Farrell [16], S.M. Farrington [173], P. Farthouat [32], F. Fassi [137e], P. Fassnacht [32], D. Fassouliotis [9], M. Faucci Giannelli [49],

A. Favareto [53a,53b], W.J. Fawcett [122], L. Fayard [119], O.L. Fedin [125,q], W. Fedorko [171], S. Feigl [121], L. Feligioni [88], C. Feng [36b], E.J. Feng [32], H. Feng [92], M.J. Fenton [56], A.B. Fenyuk [132], L. Feremenga [8], P. Fernandez Martinez [170], S. Fernandez Perez [13], J. Ferrando [45], A. Ferrari [168], P. Ferrari [109], R. Ferrari [123a], D.E. Ferreira de Lima [60b], A. Ferrer [170], D. Ferrere [52], C. Ferretti [92], F. Fiedler [86], A. Filipčič [78], M. Filipuzzi [45], F. Filthaut [108], M. Fincke-Keeler [172], K.D. Finelli [152], M.C.N. Fiolhais [128a,128c,r], L. Fiorini [170], A. Fischer [2], C. Fischer [13], J. Fischer [178], W.C. Fisher [93], N. Flaschel [45], I. Fleck [143], P. Fleischmann [92], R.R.M. Fletcher [124], T. Flick [178], B.M. Flierl [102], L.R. Flores Castillo [62a], M.J. Flowerdew [103], G.T. Forcolin [87], A. Formica [138], F.A. Förster [13], A. Forti [87], A.G. Foster [19], D. Fournier [119], H. Fox [75], S. Fracchia [141], P. Francavilla [83], M. Franchini [22a,22b], S. Franchino [60a], D. Francis [32], L. Franconi [121], M. Franklin [59], M. Frate [166], M. Fraternali [123a,123b], D. Freeborn [81], S.M. Fressard-Batraneanu [32], B. Freund [97], D. Froidevaux [32], J.A. Frost [122], C. Fukunaga [158], T. Fusayasu [104], J. Fuster [170], C. Gabaldon [58], O. Gabizon [154], A. Gabrielli [22a,22b], A. Gabrielli [16], G.P. Gach [41a], S. Gadatsch [32], S. Gadomski [80], G. Gagliardi [53a,53b], L.G. Gagnon [97], C. Galea [108], B. Galhardo [128a,128c], E.J. Gallas [122], B.J. Gallop [133], P. Gallus [130], G. Galster [39], K.K. Gan [113], S. Ganguly [37], Y. Gao [77], Y.S. Gao [145,g], F.M. Garay Walls [34a], C. García [170], J.E. García Navarro [170], J.A. García Pascual [35a], M. Garcia-Sciveres [16], R.W. Gardner [33], N. Garelli [145], V. Garonne [121], A. Gascon Bravo [45], K. Gasnikova [45], C. Gatti [50], A. Gaudiello [53a,53b], G. Gaudio [123a], I.L. Gavrilenko [98], C. Gay [171], G. Gaycken [23], E.N. Gazis [10], C.N.P. Gee [133], J. Geisen [57], M. Geisen [86], M.P. Geisler [60a], K. Gellerstedt [148a,148b], C. Gemme [53a], M.H. Genest [58], C. Geng [92], S. Gentile [134a,134b], C. Gentsos [156], S. George [80], D. Gerbaudo [13], A. Gershon [155], G. Geßner [46], S. Ghasemi [143], M. Ghneimat [23], B. Giacobbe [22a], S. Giagu [134a,134b], N. Giangiacomi [22a,22b], P. Giannetti [126a,126b], S.M. Gibson [80], M. Gignac [171], M. Gilchriese [16], D. Gillberg [31], G. Gilles [178], D.M. Gingrich [3,d], M.P. Giordani [167a,167c], F.M. Giorgi [22a], P.F. Giraud [138], P. Giromini [59], G. Giugliarelli [167a,167c], D. Giugni [94a], F. Giuli [122], C. Giuliani [103], M. Giulini [60b], B.K. Gjelsten [121], S. Gkaitatzis [156], I. Gkialas [9,s], E.L. Gkougkousis [13], P. Gkountoumis [10], L.K. Gladilin [101], C. Glasman [85], J. Glatzer [13], P.C.F. Glaysher [45], A. Glazov [45], M. Goblirsch-Kolb [25], J. Godlewski [42], S. Goldfarb [91], T. Golling [52], D. Golubkov [132], A. Gomes [128a,128b,128d], R. Gonçalo [128a], R. Goncalves Gama [26a], J. Goncalves Pinto Firmino Da Costa [138], G. Gonella [51], L. Gonella [19], A. Gongadze [68], S. González de la Hoz [170], S. Gonzalez-Sevilla [52], L. Goossens [32], P.A. Gorbounov [99], H.A. Gordon [27], I. Gorelov [107], B. Gorini [32], E. Gorini [76a,76b], A. Gorišek [78], A.T. Goshaw [48], C. Gössling [46], M.I. Gostkin [68], C.A. Gottardo [23], C.R. Goudet [119], D. Goujdami [137c], A.G. Goussiou [140], N. Govender [147b,t], E. Gozani [154], L. Graber [57], I. Grabowska-Bold [41a], P.O.J. Gradin [168], J. Gramling [166], E. Gramstad [121], S. Grancagnolo [17], V. Gratchev [125], P.M. Gravila [28f], C. Gray [56], H.M. Gray [16], Z.D. Greenwood [82,u], C. Grefe [23], K. Gregersen [81], I.M. Gregor [45], P. Grenier [145], K. Grevtsov [5], J. Griffiths [8], A.A. Grillo [139], K. Grimm [75], S. Grinstein [13,v], Ph. Gris [37], J.-F. Grivaz [119], S. Groh [86], E. Gross [175], J. Grosse-Knetter [57], G.C. Grossi [82], Z.J. Grout [81], A. Grummer [107], L. Guan [92], W. Guan [176], J. Guenther [65], F. Guescini [163a], D. Guest [166], O. Gueta [155], B. Gui [113], E. Guido [53a,53b], T. Guillemin [5], S. Guindon [32], U. Gul [56], C. Gumpert [32], J. Guo [36c], W. Guo [92], Y. Guo [36a], R. Gupta [43], S. Gupta [122], G. Gustavino [115], B.J. Gutelman [154], P. Gutierrez [115], N.G. Gutierrez Ortiz [81], C. Gutschow [81], C. Guyot [138], M.P. Guzik [41a], C. Gwenlan [122], C.B. Gwilliam [77], A. Haas [112], C. Haber [16], H.K. Hadavand [8], N. Haddad [137e], A. Hadef [88], S. Hageböck [23], M. Hagihara [164], H. Hakobyan [180,*], M. Haleem [45], J. Haley [116], G. Halladjian [93], G.D. Hallewell [88], K. Hamacher [178], P. Hamal [117], K. Hamano [172], A. Hamilton [147a], G.N. Hamity [141], P.G. Hamnett [45], L. Han [36a], S. Han [35a], K. Hanagaki [69,w], K. Hanawa [157], M. Hance [139], B. Haney [124], P. Hanke [60a], J.B. Hansen [39], J.D. Hansen [39], M.C. Hansen [23], P.H. Hansen [39], K. Hara [164], A.S. Hard [176], T. Harenberg [178], F. Hariri [119], S. Harkusha [95], R.D. Harrington [49], P.F. Harrison [173], N.M. Hartmann [102], Y. Hasegawa [142], A. Hasib [49], S. Hassani [138], S. Haug [18], R. Hauser [93], L. Hauswald [47], L.B. Havener [38], M. Havranek [130], C.M. Hawkes [19], R.J. Hawkings [32], D. Hayakawa [159], D. Hayden [93], C.P. Hays [122], J.M. Hays [79], H.S. Hayward [77], S.J. Haywood [133], S.J. Head [19], T. Heck [86], V. Hedberg [84], L. Heelan [8], S. Heer [23], K.K. Heidegger [51], S. Heim [45], T. Heim [16], B. Heinemann [45,x], J.J. Heinrich [102], L. Heinrich [112], C. Heinz [55], J. Hejbal [129], L. Helary [32], A. Held [171], S. Hellman [148a,148b], C. Helsens [32], R.C.W. Henderson [75], Y. Heng [176], S. Henkelmann [171], A.M. Henriques Correia [32], S. Henrot-Versille [119], G.H. Herbert [17], H. Herde [25], V. Herget [177], Y. Hernández Jiménez [147c], H. Herr [86], G. Herten [51], R. Hertenberger [102], L. Hervas [32], T.C. Herwig [124], G.G. Hesketh [81], N.P. Hessey [163a], J.W. Hetherly [43], S. Higashino [69], E. Higón-Rodriguez [170], K. Hildebrand [33], E. Hill [172], J.C. Hill [30], K.H. Hiller [45], S.J. Hillier [19],

M. Hils [47], I. Hinchliffe [16], M. Hirose [51], D. Hirschbuehl [178], B. Hiti [78], O. Hladik [129], X. Hoad [49], J. Hobbs [150], N. Hod [163a], M.C. Hodgkinson [141], P. Hodgson [141], A. Hoecker [32], M.R. Hoeferkamp [107], F. Hoenig [102], D. Hohn [23], T.R. Holmes [33], M. Homann [46], S. Honda [164], T. Honda [69], T.M. Hong [127], B.H. Hooberman [169], W.H. Hopkins [118], Y. Horii [105], A.J. Horton [144], J-Y. Hostachy [58], S. Hou [153], A. Hoummada [137a], J. Howarth [87], J. Hoya [74], M. Hrabovsky [117], J. Hrdinka [32], I. Hristova [17], J. Hrivnac [119], T. Hryn'ova [5], A. Hrynevich [96], P.J. Hsu [63], S.-C. Hsu [140], Q. Hu [36a], S. Hu [36c], Y. Huang [35a], Z. Hubacek [130], F. Hubaut [88], F. Huegging [23], T.B. Huffman [122], E.W. Hughes [38], G. Hughes [75], M. Huhtinen [32], P. Huo [150], N. Huseynov [68,b], J. Huston [93], J. Huth [59], G. Iacobucci [52], G. Iakovidis [27], I. Ibragimov [143], L. Iconomidou-Fayard [119], Z. Idrissi [137e], P. Iengo [32], O. Igonkina [109,y], T. Iizawa [174], Y. Ikegami [69], M. Ikeno [69], Y. Ilchenko [11,z], D. Iliadis [156], N. Ilic [145], G. Introzzi [123a,123b], P. Ioannou [9,*], M. Iodice [136a], K. Iordanidou [38], V. Ippolito [59], M.F. Isacson [168], N. Ishijima [120], M. Ishino [157], M. Ishitsuka [159], C. Issever [122], S. Istin [20a], F. Ito [164], J.M. Iturbe Ponce [62a], R. Iuppa [162a,162b], H. Iwasaki [69], J.M. Izen [44], V. Izzo [106a], S. Jabbar [3], P. Jackson [1], R.M. Jacobs [23], V. Jain [2], K.B. Jakobi [86], K. Jakobs [51], S. Jakobsen [65], T. Jakoubek [129], D.O. Jamin [116], D.K. Jana [82], R. Jansky [52], J. Janssen [23], M. Janus [57], P.A. Janus [41a], G. Jarlskog [84], N. Javadov [68,b], T. Javůrek [51], M. Javurkova [51], F. Jeanneau [138], L. Jeanty [16], J. Jejelava [54a,aa], A. Jelinskas [173], P. Jenni [51,ab], C. Jeske [173], S. Jézéquel [5], H. Ji [176], J. Jia [150], H. Jiang [67], Y. Jiang [36a], Z. Jiang [145], S. Jiggins [81], J. Jimenez Pena [170], S. Jin [35a], A. Jinaru [28b], O. Jinnouchi [159], H. Jivan [147c], P. Johansson [141], K.A. Johns [7], C.A. Johnson [64], W.J. Johnson [140], K. Jon-And [148a,148b], R.W.L. Jones [75], S.D. Jones [151], S. Jones [7], T.J. Jones [77], J. Jongmanns [60a], P.M. Jorge [128a,128b], J. Jovicevic [163a], X. Ju [176], A. Juste Rozas [13,v], M.K. Köhler [175], A. Kaczmarska [42], M. Kado [119], H. Kagan [113], M. Kagan [145], S.J. Kahn [88], T. Kaji [174], E. Kajomovitz [48], C.W. Kalderon [84], A. Kaluza [86], S. Kama [43], A. Kamenshchikov [132], N. Kanaya [157], L. Kanjir [78], V.A. Kantserov [100], J. Kanzaki [69], B. Kaplan [112], L.S. Kaplan [176], D. Kar [147c], K. Karakostas [10], N. Karastathis [10], M.J. Kareem [57], E. Karentzos [10], S.N. Karpov [68], Z.M. Karpova [68], K. Karthik [112], V. Kartvelishvili [75], A.N. Karyukhin [132], K. Kasahara [164], L. Kashif [176], R.D. Kass [113], A. Kastanas [149], Y. Kataoka [157], C. Kato [157], A. Katre [52], J. Katzy [45], K. Kawade [70], K. Kawagoe [73], T. Kawamoto [157], G. Kawamura [57], E.F. Kay [77], V.F. Kazanin [111,c], R. Keeler [172], R. Kehoe [43], J.S. Keller [31], E. Kellermann [84], J.J. Kempster [80], J Kendrick [19], H. Keoshkerian [161], O. Kepka [129], B.P. Kerševan [78], S. Kersten [178], R.A. Keyes [90], M. Khader [169], F. Khalil-zada [12], A. Khanov [116], A.G. Kharlamov [111,c], T. Kharlamova [111,c], A. Khodinov [160], T.J. Khoo [52], V. Khovanskiy [99,*], E. Khramov [68], J. Khubua [54b,ac], S. Kido [70], C.R. Kilby [80], H.Y. Kim [8], S.H. Kim [164], Y.K. Kim [33], N. Kimura [156], O.M. Kind [17], B.T. King [77], D. Kirchmeier [47], J. Kirk [133], A.E. Kiryunin [103], T. Kishimoto [157], D. Kisielewska [41a], V. Kitali [45], O. Kivernyk [5], E. Kladiva [146b], T. Klapdor-Kleingrothaus [51], M.H. Klein [38], M. Klein [77], U. Klein [77], K. Kleinknecht [86], P. Klimek [110], A. Klimentov [27], R. Klingenberg [46], T. Klingl [23], T. Klioutchnikova [32], E.-E. Kluge [60a], P. Kluit [109], S. Kluth [103], E. Kneringer [65], E.B.F.G. Knoops [88], A. Knue [103], A. Kobayashi [157], D. Kobayashi [159], T. Kobayashi [157], M. Kobel [47], M. Kocian [145], P. Kodys [131], T. Koffas [31], E. Koffeman [109], N.M. Köhler [103], T. Koi [145], M. Kolb [60b], I. Koletsou [5], A.A. Komar [98,*], T. Kondo [69], N. Kondrashova [36c], K. Köneke [51], A.C. König [108], T. Kono [69,ad], R. Konoplich [112,ae], N. Konstantinidis [81], R. Kopeliansky [64], S. Koperny [41a], A.K. Kopp [51], K. Korcyl [42], K. Kordas [156], A. Korn [81], A.A. Korol [111,c], I. Korolkov [13], E.V. Korolkova [141], O. Kortner [103], S. Kortner [103], T. Kosek [131], V.V. Kostyukhin [23], A. Kotwal [48], A. Koulouris [10], A. Kourkoumeli-Charalampidi [123a,123b], C. Kourkoumelis [9], E. Kourlitis [141], V. Kouskoura [27], A.B. Kowalewska [42], R. Kowalewski [172], T.Z. Kowalski [41a], C. Kozakai [157], W. Kozanecki [138], A.S. Kozhin [132], V.A. Kramarenko [101], G. Kramberger [78], D. Krasnopevtsev [100], M.W. Krasny [83], A. Krasznahorkay [32], D. Krauss [103], J.A. Kremer [41a], J. Kretzschmar [77], K. Kreutzfeldt [55], P. Krieger [161], K. Krizka [16], K. Kroeninger [46], H. Kroha [103], J. Kroll [129], J. Kroll [124], J. Kroseberg [23], J. Krstic [14], U. Kruchonak [68], H. Krüger [23], N. Krumnack [67], M.C. Kruse [48], T. Kubota [91], H. Kucuk [81], S. Kuday [4b], J.T. Kuechler [178], S. Kuehn [32], A. Kugel [60a], F. Kuger [177], T. Kuhl [45], V. Kukhtin [68], R. Kukla [88], Y. Kulchitsky [95], S. Kuleshov [34b], Y.P. Kulinich [169], M. Kuna [134a,134b], T. Kunigo [71], A. Kupco [129], T. Kupfer [46], O. Kuprash [155], H. Kurashige [70], L.L. Kurchaninov [163a], Y.A. Kurochkin [95], M.G. Kurth [35a], V. Kus [129], E.S. Kuwertz [172], M. Kuze [159], J. Kvita [117], T. Kwan [172], D. Kyriazopoulos [141], A. La Rosa [103], J.L. La Rosa Navarro [26d], L. La Rotonda [40a,40b], F. La Ruffa [40a,40b], C. Lacasta [170], F. Lacava [134a,134b], J. Lacey [45], D.P.J. Lack [87], H. Lacker [17], D. Lacour [83], E. Ladygin [68], R. Lafaye [5], B. Laforge [83], T. Lagouri [179], S. Lai [57], S. Lammers [64], W. Lampl [7], E. Lançon [27], U. Landgraf [51], M.P.J. Landon [79], M.C. Lanfermann [52], V.S. Lang [45], J.C. Lange [13],

R.J. Langenberg [32], A.J. Lankford [166], F. Lanni [27], K. Lantzsch [23], A. Lanza [123a], A. Lapertosa [53a,53b], S. Laplace [83], J.F. Laporte [138], T. Lari [94a], F. Lasagni Manghi [22a,22b], M. Lassnig [32], T.S. Lau [62a], P. Laurelli [50], W. Lavrijsen [16], A.T. Law [139], P. Laycock [77], T. Lazovich [59], M. Lazzaroni [94a,94b], B. Le [91], O. Le Dortz [83], E. Le Guirriec [88], E.P. Le Quilleuc [138], M. LeBlanc [172], T. LeCompte [6], F. Ledroit-Guillon [58], C.A. Lee [27], G.R. Lee [133,af], S.C. Lee [153], L. Lee [59], B. Lefebvre [90], G. Lefebvre [83], M. Lefebvre [172], F. Legger [102], C. Leggett [16], G. Lehmann Miotto [32], X. Lei [7], W.A. Leight [45], M.A.L. Leite [26d], R. Leitner [131], D. Lellouch [175], B. Lemmer [57], K.J.C. Leney [81], T. Lenz [23], B. Lenzi [32], R. Leone [7], S. Leone [126a,126b], C. Leonidopoulos [49], G. Lerner [151], C. Leroy [97], A.A.J. Lesage [138], C.G. Lester [30], M. Levchenko [125], J. Levêque [5], D. Levin [92], L.J. Levinson [175], M. Levy [19], D. Lewis [79], B. Li [36a,ag], Changqiao Li [36a], H. Li [150], L. Li [36c], Q. Li [35a], Q. Li [36a], S. Li [48], X. Li [36c], Y. Li [143], Z. Liang [35a], B. Liberti [135a], A. Liblong [161], K. Lie [62c], J. Liebal [23], W. Liebig [15], A. Limosani [152], S.C. Lin [182], T.H. Lin [86], R.A. Linck [64], B.E. Lindquist [150], A.E. Lionti [52], E. Lipeles [124], A. Lipniacka [15], M. Lisovyi [60b], T.M. Liss [169,ah], A. Lister [171], A.M. Litke [139], B. Liu [67], H. Liu [92], H. Liu [27], J.K.K. Liu [122], J. Liu [36b], J.B. Liu [36a], K. Liu [88], L. Liu [169], M. Liu [36a], Y.L. Liu [36a], Y. Liu [36a], M. Livan [123a,123b], A. Lleres [58], J. Llorente Merino [35a], S.L. Lloyd [79], C.Y. Lo [62b], F. Lo Sterzo [153], E.M. Lobodzinska [45], P. Loch [7], F.K. Loebinger [87], A. Loesle [51], K.M. Loew [25], A. Loginov [179,*], T. Lohse [17], K. Lohwasser [141], M. Lokajicek [129], B.A. Long [24], J.D. Long [169], R.E. Long [75], L. Longo [76a,76b], K.A. Looper [113], J.A. Lopez [34b], D. Lopez Mateos [59], I. Lopez Paz [13], A. Lopez Solis [83], J. Lorenz [102], N. Lorenzo Martinez [5], M. Losada [21], P.J. Lösel [102], X. Lou [35a], A. Lounis [119], J. Love [6], P.A. Love [75], H. Lu [62a], N. Lu [92], Y.J. Lu [63], H.J. Lubatti [140], C. Luci [134a,134b], A. Lucotte [58], C. Luedtke [51], F. Luehring [64], W. Lukas [65], L. Luminari [134a], O. Lundberg [148a,148b], B. Lund-Jensen [149], M.S. Lutz [89], P.M. Luzi [83], D. Lynn [27], R. Lysak [129], E. Lytken [84], F. Lyu [35a], V. Lyubushkin [68], H. Ma [27], L.L. Ma [36b], Y. Ma [36b], G. Maccarrone [50], A. Macchiolo [103], C.M. Macdonald [141], B. Maček [78], J. Machado Miguens [124,128b], D. Madaffari [170], R. Madar [37], W.F. Mader [47], A. Madsen [45], J. Maeda [70], S. Maeland [15], T. Maeno [27], A.S. Maevskiy [101], V. Magerl [51], J. Mahlstedt [109], C. Maiani [119], C. Maidantchik [26a], A.A. Maier [103], T. Maier [102], A. Maio [128a,128b,128d], O. Majersky [146a], S. Majewski [118], Y. Makida [69], N. Makovec [119], B. Malaescu [83], Pa. Malecki [42], V.P. Maleev [125], F. Malek [58], U. Mallik [66], D. Malon [6], C. Malone [30], S. Maltezos [10], S. Malyukov [32], J. Mamuzic [170], G. Mancini [50], I. Mandić [78], J. Maneira [128a,128b], L. Manhaes de Andrade Filho [26b], J. Manjarres Ramos [47], K.H. Mankinen [84], A. Mann [102], A. Manousos [32], B. Mansoulie [138], J.D. Mansour [35a], R. Mantifel [90], M. Mantoani [57], S. Manzoni [94a,94b], L. Mapelli [32], G. Marceca [29], L. March [52], L. Marchese [122], G. Marchiori [83], M. Marcisovsky [129], M. Marjanovic [37], D.E. Marley [92], F. Marroquim [26a], S.P. Marsden [87], Z. Marshall [16], M.U.F Martensson [168], S. Marti-Garcia [170], C.B. Martin [113], T.A. Martin [173], V.J. Martin [49], B. Martin dit Latour [15], M. Martinez [13,v], V.I. Martinez Outschoorn [169], S. Martin-Haugh [133], V.S. Martoiu [28b], A.C. Martyniuk [81], A. Marzin [32], L. Masetti [86], T. Mashimo [157], R. Mashinistov [98], J. Masik [87], A.L. Maslennikov [111,c], L. Massa [135a,135b], P. Mastrandrea [5], A. Mastroberardino [40a,40b], T. Masubuchi [157], P. Mättig [178], J. Maurer [28b], S.J. Maxfield [77], D.A. Maximov [111,c], R. Mazini [153], I. Maznas [156], S.M. Mazza [94a,94b], N.C. Mc Fadden [107], G. Mc Goldrick [161], S.P. Mc Kee [92], A. McCarn [92], R.L. McCarthy [150], T.G. McCarthy [103], L.I. McClymont [81], E.F. McDonald [91], J.A. Mcfayden [32], G. Mchedlidze [57], S.J. McMahon [133], P.C. McNamara [91], C.J. McNicol [173], R.A. McPherson [172,o], S. Meehan [140], T.J. Megy [51], S. Mehlhase [102], A. Mehta [77], T. Meideck [58], K. Meier [60a], B. Meirose [44], D. Melini [170,ai], B.R. Mellado Garcia [147c], J.D. Mellenthin [57], M. Melo [146a], F. Meloni [18], A. Melzer [23], S.B. Menary [87], L. Meng [77], X.T. Meng [92], A. Mengarelli [22a,22b], S. Menke [103], E. Meoni [40a,40b], S. Mergelmeyer [17], C. Merlassino [18], P. Mermod [52], L. Merola [106a,106b], C. Meroni [94a], F.S. Merritt [33], A. Messina [134a,134b], J. Metcalfe [6], A.S. Mete [166], C. Meyer [124], J-P. Meyer [138], J. Meyer [109], H. Meyer Zu Theenhausen [60a], F. Miano [151], R.P. Middleton [133], S. Miglioranzi [53a,53b], L. Mijović [49], G. Mikenberg [175], M. Mikestikova [129], M. Mikuž [78], M. Milesi [91], A. Milic [161], D.A. Millar [79], D.W. Miller [33], C. Mills [49], A. Milov [175], D.A. Milstead [148a,148b], A.A. Minaenko [132], Y. Minami [157], I.A. Minashvili [68], A.I. Mincer [112], B. Mindur [41a], M. Mineev [68], Y. Minegishi [157], Y. Ming [176], L.M. Mir [13], K.P. Mistry [124], T. Mitani [174], J. Mitrevski [102], V.A. Mitsou [170], A. Miucci [18], P.S. Miyagawa [141], A. Mizukami [69], J.U. Mjörnmark [84], T. Mkrtchyan [180], M. Mlynarikova [131], T. Moa [148a,148b], K. Mochizuki [97], P. Mogg [51], S. Mohapatra [38], S. Molander [148a,148b], R. Moles-Valls [23], M.C. Mondragon [93], K. Mönig [45], J. Monk [39], E. Monnier [88], A. Montalbano [150], J. Montejo Berlingen [32], F. Monticelli [74], S. Monzani [94a,94b], R.W. Moore [3], N. Morange [119], D. Moreno [21], M. Moreno Llácer [32], P. Morettini [53a], S. Morgenstern [32],

D. Mori [144], T. Mori [157], M. Morii [59], M. Morinaga [174], V. Morisbak [121], A.K. Morley [32], G. Mornacchi [32], J.D. Morris [79], L. Morvaj [150], P. Moschovakos [10], M. Mosidze [54b], H.J. Moss [141], J. Moss [145,aj], K. Motohashi [159], R. Mount [145], E. Mountricha [27], E.J.W. Moyse [89], S. Muanza [88], F. Mueller [103], J. Mueller [127], R.S.P. Mueller [102], D. Muenstermann [75], P. Mullen [56], G.A. Mullier [18], F.J. Munoz Sanchez [87], W.J. Murray [173,133], H. Musheghyan [32], M. Muškinja [78], A.G. Myagkov [132,ak], M. Myska [130], B.P. Nachman [16], O. Nackenhorst [52], K. Nagai [122], R. Nagai [69,ad], K. Nagano [69], Y. Nagasaka [61], K. Nagata [164], M. Nagel [51], E. Nagy [88], A.M. Nairz [32], Y. Nakahama [105], K. Nakamura [69], T. Nakamura [157], I. Nakano [114], R.F. Naranjo Garcia [45], R. Narayan [11], D.I. Narrias Villar [60a], I. Naryshkin [125], T. Naumann [45], G. Navarro [21], R. Nayyar [7], H.A. Neal [92], P.Yu. Nechaeva [98], T.J. Neep [138], A. Negri [123a,123b], M. Negrini [22a], S. Nektarijevic [108], C. Nellist [119], A. Nelson [166], M.E. Nelson [122], S. Nemecek [129], P. Nemethy [112], M. Nessi [32,al], M.S. Neubauer [169], M. Neumann [178], P.R. Newman [19], T.Y. Ng [62c], T. Nguyen Manh [97], R.B. Nickerson [122], R. Nicolaidou [138], J. Nielsen [139], V. Nikolaenko [132,ak], I. Nikolic-Audit [83], K. Nikolopoulos [19], J.K. Nilsen [121], P. Nilsson [27], Y. Ninomiya [157], A. Nisati [134a], N. Nishu [36c], R. Nisius [103], I. Nitsche [46], T. Nitta [174], T. Nobe [157], Y. Noguchi [71], M. Nomachi [120], I. Nomidis [31], M.A. Nomura [27], T. Nooney [79], M. Nordberg [32], N. Norjoharuddeen [122], O. Novgorodova [47], S. Nowak [103], M. Nozaki [69], L. Nozka [117], K. Ntekas [166], E. Nurse [81], F. Nuti [91], K. O'connor [25], D.C. O'Neil [144], A.A. O'Rourke [45], V. O'Shea [56], F.G. Oakham [31,d], H. Oberlack [103], T. Obermann [23], J. Ocariz [83], A. Ochi [70], I. Ochoa [38], J.P. Ochoa-Ricoux [34a], S. Oda [73], S. Odaka [69], A. Oh [87], S.H. Oh [48], C.C. Ohm [16], H. Ohman [168], H. Oide [53a,53b], H. Okawa [164], Y. Okumura [157], T. Okuyama [69], A. Olariu [28b], L.F. Oleiro Seabra [128a], S.A. Olivares Pino [34a], D. Oliveira Damazio [27], A. Olszewski [42], J. Olszowska [42], A. Onofre [128a,128e], K. Onogi [105], P.U.E. Onyisi [11,z], H. Oppen [121], M.J. Oreglia [33], Y. Oren [155], D. Orestano [136a,136b], N. Orlando [62b], R.S. Orr [161], B. Osculati [53a,53b,*], R. Ospanov [36a], G. Otero y Garzon [29], H. Otono [73], M. Ouchrif [137d], F. Ould-Saada [121], A. Ouraou [138], K.P. Oussoren [109], Q. Ouyang [35a], M. Owen [56], R.E. Owen [19], V.E. Ozcan [20a], N. Ozturk [8], K. Pachal [144], A. Pacheco Pages [13], L. Pacheco Rodriguez [138], C. Padilla Aranda [13], S. Pagan Griso [16], M. Paganini [179], F. Paige [27], G. Palacino [64], S. Palazzo [40a,40b], S. Palestini [32], M. Palka [41b], D. Pallin [37], E.St. Panagiotopoulou [10], I. Panagoulias [10], C.E. Pandini [126a,126b], J.G. Panduro Vazquez [80], P. Pani [32], S. Panitkin [27], D. Pantea [28b], L. Paolozzi [52], Th.D. Papadopoulou [10], K. Papageorgiou [9,s], A. Paramonov [6], D. Paredes Hernandez [179], A.J. Parker [75], M.A. Parker [30], K.A. Parker [45], F. Parodi [53a,53b], J.A. Parsons [38], U. Parzefall [51], V.R. Pascuzzi [161], J.M. Pasner [139], E. Pasqualucci [134a], S. Passaggio [53a], Fr. Pastore [80], S. Pataraia [86], J.R. Pater [87], T. Pauly [32], B. Pearson [103], S. Pedraza Lopez [170], R. Pedro [128a,128b], S.V. Peleganchuk [111,c], O. Penc [129], C. Peng [35a], H. Peng [36a], J. Penwell [64], B.S. Peralva [26b], M.M. Perego [138], D.V. Perepelitsa [27], F. Peri [17], L. Perini [94a,94b], H. Pernegger [32], S. Perrella [106a,106b], R. Peschke [45], V.D. Peshekhonov [68,*], K. Peters [45], R.F.Y. Peters [87], B.A. Petersen [32], T.C. Petersen [39], E. Petit [58], A. Petridis [1], C. Petridou [156], P. Petroff [119], E. Petrolo [134a], M. Petrov [122], F. Petrucci [136a,136b], N.E. Pettersson [89], A. Peyaud [138], R. Pezoa [34b], F.H. Phillips [93], P.W. Phillips [133], G. Piacquadio [150], E. Pianori [173], A. Picazio [89], E. Piccaro [79], M.A. Pickering [122], R. Piegaia [29], J.E. Pilcher [33], A.D. Pilkington [87], A.W.J. Pin [87], M. Pinamonti [135a,135b], J.L. Pinfold [3], H. Pirumov [45], M. Pitt [175], L. Plazak [146a], M.-A. Pleier [27], V. Pleskot [86], E. Plotnikova [68], D. Pluth [67], P. Podberezko [111], R. Poettgen [84], R. Poggi [123a,123b], L. Poggioli [119], I. Pogrebnyak [93], D. Pohl [23], G. Polesello [123a], A. Poley [45], A. Policicchio [40a,40b], R. Polifka [32], A. Polini [22a], C.S. Pollard [56], V. Polychronakos [27], K. Pommès [32], D. Ponomarenko [100], L. Pontecorvo [134a], G.A. Popeneciu [28d], S. Pospisil [130], K. Potamianos [16], I.N. Potrap [68], C.J. Potter [30], T. Poulsen [84], J. Poveda [32], M.E. Pozo Astigarraga [32], P. Pralavorio [88], A. Pranko [16], S. Prell [67], D. Price [87], M. Primavera [76a], S. Prince [90], N. Proklova [100], K. Prokofiev [62c], F. Prokoshin [34b], S. Protopopescu [27], J. Proudfoot [6], M. Przybycien [41a], A. Puri [169], P. Puzo [119], J. Qian [92], G. Qin [56], Y. Qin [87], A. Quadt [57], M. Queitsch-Maitland [45], D. Quilty [56], S. Raddum [121], V. Radeka [27], V. Radescu [122], S.K. Radhakrishnan [150], P. Radloff [118], P. Rados [91], F. Ragusa [94a,94b], G. Rahal [181], J.A. Raine [87], S. Rajagopalan [27], C. Rangel-Smith [168], T. Rashid [119], S. Raspopov [5], M.G. Ratti [94a,94b], D.M. Rauch [45], F. Rauscher [102], S. Rave [86], I. Ravinovich [175], J.H. Rawling [87], M. Raymond [32], A.L. Read [121], N.P. Readioff [58], M. Reale [76a,76b], D.M. Rebuzzi [123a,123b], A. Redelbach [177], G. Redlinger [27], R. Reece [139], R.G. Reed [147c], K. Reeves [44], L. Rehnisch [17], J. Reichert [124], A. Reiss [86], C. Rembser [32], H. Ren [35a], M. Rescigno [134a], S. Resconi [94a], E.D. Resseguie [124], S. Rettie [171], E. Reynolds [19], O.L. Rezanova [111,c], P. Reznicek [131], R. Rezvani [97], R. Richter [103], S. Richter [81],

E. Richter-Was [41b], O. Ricken [23], M. Ridel [83], P. Rieck [103], C.J. Riegel [178], J. Rieger [57], O. Rifki [115], M. Rijssenbeek [150], A. Rimoldi [123a,123b], M. Rimoldi [18], L. Rinaldi [22a], G. Ripellino [149], B. Ristić [32], E. Ritsch [32], I. Riu [13], F. Rizatdinova [116], E. Rizvi [79], C. Rizzi [13], R.T. Roberts [87], S.H. Robertson [90,o], A. Robichaud-Veronneau [90], D. Robinson [30], J.E.M. Robinson [45], A. Robson [56], E. Rocco [86], C. Roda [126a,126b], Y. Rodina [88,am], S. Rodriguez Bosca [170], A. Rodriguez Perez [13], D. Rodriguez Rodriguez [170], S. Roe [32], C.S. Rogan [59], O. Røhne [121], J. Roloff [59], A. Romaniouk [100], M. Romano [22a,22b], S.M. Romano Saez [37], E. Romero Adam [170], N. Rompotis [77], M. Ronzani [51], L. Roos [83], S. Rosati [134a], K. Rosbach [51], P. Rose [139], N.-A. Rosien [57], E. Rossi [106a,106b], L.P. Rossi [53a], J.H.N. Rosten [30], R. Rosten [140], M. Rotaru [28b], J. Rothberg [140], D. Rousseau [119], A. Rozanov [88], Y. Rozen [154], X. Ruan [147c], F. Rubbo [145], F. Rühr [51], A. Ruiz-Martinez [31], Z. Rurikova [51], N.A. Rusakovich [68], H.L. Russell [90], J.P. Rutherfoord [7], N. Ruthmann [32], Y.F. Ryabov [125], M. Rybar [169], G. Rybkin [119], S. Ryu [6], A. Ryzhov [132], G.F. Rzehorz [57], A.F. Saavedra [152], G. Sabato [109], S. Sacerdoti [29], H.F-W. Sadrozinski [139], R. Sadykov [68], F. Safai Tehrani [134a], P. Saha [110], M. Sahinsoy [60a], M. Saimpert [45], M. Saito [157], T. Saito [157], H. Sakamoto [157], Y. Sakurai [174], G. Salamanna [136a,136b], J.E. Salazar Loyola [34b], D. Salek [109], P.H. Sales De Bruin [168], D. Salihagic [103], A. Salnikov [145], J. Salt [170], D. Salvatore [40a,40b], F. Salvatore [151], A. Salvucci [62a,62b,62c], A. Salzburger [32], D. Sammel [51], D. Sampsonidis [156], D. Sampsonidou [156], J. Sánchez [170], V. Sanchez Martinez [170], A. Sanchez Pineda [167a,167c], H. Sandaker [121], R.L. Sandbach [79], C.O. Sander [45], M. Sandhoff [178], C. Sandoval [21], D.P.C. Sankey [133], M. Sannino [53a,53b], Y. Sano [105], A. Sansoni [50], C. Santoni [37], H. Santos [128a], I. Santoyo Castillo [151], A. Sapronov [68], J.G. Saraiva [128a,128d], B. Sarrazin [23], O. Sasaki [69], K. Sato [164], E. Sauvan [5], G. Savage [80], P. Savard [161,d], N. Savic [103], C. Sawyer [133], L. Sawyer [82,u], J. Saxon [33], C. Sbarra [22a], A. Sbrizzi [22a,22b], T. Scanlon [81], D.A. Scannicchio [166], J. Schaarschmidt [140], P. Schacht [103], B.M. Schachtner [102], D. Schaefer [32], L. Schaefer [124], R. Schaefer [45], J. Schaeffer [86], S. Schaepe [23], S. Schaetzel [60b], U. Schäfer [86], A.C. Schaffer [119], D. Schaile [102], R.D. Schamberger [150], V.A. Schegelsky [125], D. Scheirich [131], M. Schernau [166], C. Schiavi [53a,53b], S. Schier [139], L.K. Schildgen [23], C. Schillo [51], M. Schioppa [40a,40b], S. Schlenker [32], K.R. Schmidt-Sommerfeld [103], K. Schmieden [32], C. Schmitt [86], S. Schmitt [45], S. Schmitz [86], U. Schnoor [51], L. Schoeffel [138], A. Schoening [60b], B.D. Schoenrock [93], E. Schopf [23], M. Schott [86], J.F.P. Schouwenberg [108], J. Schovancova [32], S. Schramm [52], N. Schuh [86], A. Schulte [86], M.J. Schultens [23], H.-C. Schultz-Coulon [60a], H. Schulz [17], M. Schumacher [51], B.A. Schumm [139], Ph. Schune [138], A. Schwartzman [145], T.A. Schwarz [92], H. Schweiger [87], Ph. Schwemling [138], R. Schwienhorst [93], J. Schwindling [138], A. Sciandra [23], G. Sciolla [25], M. Scornajenghi [40a,40b], F. Scuri [126a,126b], F. Scutti [91], J. Searcy [92], P. Seema [23], S.C. Seidel [107], A. Seiden [139], J.M. Seixas [26a], G. Sekhniaidze [106a], K. Sekhon [92], S.J. Sekula [43], N. Semprini-Cesari [22a,22b], S. Senkin [37], C. Serfon [121], L. Serin [119], L. Serkin [167a,167b], M. Sessa [136a,136b], R. Seuster [172], H. Severini [115], T. Sfiligoj [78], F. Sforza [165], A. Sfyrla [52], E. Shabalina [57], N.W. Shaikh [148a,148b], L.Y. Shan [35a], R. Shang [169], J.T. Shank [24], M. Shapiro [16], P.B. Shatalov [99], K. Shaw [167a,167b], S.M. Shaw [87], A. Shcherbakova [148a,148b], C.Y. Shehu [151], Y. Shen [115], N. Sherafati [31], P. Sherwood [81], L. Shi [153,an], S. Shimizu [70], C.O. Shimmin [179], M. Shimojima [104], I.P.J. Shipsey [122], S. Shirabe [73], M. Shiyakova [68,ao], J. Shlomi [175], A. Shmeleva [98], D. Shoaleh Saadi [97], M.J. Shochet [33], S. Shojaii [94a], D.R. Shope [115], S. Shrestha [113], E. Shulga [100], M.A. Shupe [7], P. Sicho [129], A.M. Sickles [169], P.E. Sidebo [149], E. Sideras Haddad [147c], O. Sidiropoulou [177], A. Sidoti [22a,22b], F. Siegert [47], Dj. Sijacki [14], J. Silva [128a,128d], S.B. Silverstein [148a], V. Simak [130], Lj. Simic [14], S. Simion [119], E. Simioni [86], B. Simmons [81], M. Simon [86], P. Sinervo [161], N.B. Sinev [118], M. Sioli [22a,22b], G. Siragusa [177], I. Siral [92], S.Yu. Sivoklokov [101], J. Sjölin [148a,148b], M.B. Skinner [75], P. Skubic [115], M. Slater [19], T. Slavicek [130], M. Slawinska [42], K. Sliwa [165], R. Slovak [131], V. Smakhtin [175], B.H. Smart [5], J. Smiesko [146a], N. Smirnov [100], S.Yu. Smirnov [100], Y. Smirnov [100], L.N. Smirnova [101,ap], O. Smirnova [84], J.W. Smith [57], M.N.K. Smith [38], R.W. Smith [38], M. Smizanska [75], K. Smolek [130], A.A. Snesarev [98], I.M. Snyder [118], S. Snyder [27], R. Sobie [172,o], F. Socher [47], A. Soffer [155], A. Søgaard [49], D.A. Soh [153], G. Sokhrannyi [78], C.A. Solans Sanchez [32], M. Solar [130], E.Yu. Soldatov [100], U. Soldevila [170], A.A. Solodkov [132], A. Soloshenko [68], O.V. Solovyanov [132], V. Solovyev [125], P. Sommer [51], H. Son [165], A. Sopczak [130], D. Sosa [60b], C.L. Sotiropoulou [126a,126b], R. Soualah [167a,167c], A.M. Soukharev [111,c], D. South [45], B.C. Sowden [80], S. Spagnolo [76a,76b], M. Spalla [126a,126b], M. Spangenberg [173], F. Spanò [80], D. Sperlich [17], F. Spettel [103], T.M. Spieker [60a], R. Spighi [22a], G. Spigo [32], L.A. Spiller [91], M. Spousta [131], R.D. St. Denis [56,*], A. Stabile [94a], R. Stamen [60a], S. Stamm [17], E. Stanecka [42], R.W. Stanek [6], C. Stanescu [136a], M.M. Stanitzki [45],

B.S. Stapf [109], S. Stapnes [121], E.A. Starchenko [132], G.H. Stark [33], J. Stark [58], S.H Stark [39], P. Staroba [129], P. Starovoitov [60a], S. Stärz [32], R. Staszewski [42], P. Steinberg [27], B. Stelzer [144], H.J. Stelzer [32], O. Stelzer-Chilton [163a], H. Stenzel [55], G.A. Stewart [56], M.C. Stockton [118], M. Stoebe [90], G. Stoicea [28b], P. Stolte [57], S. Stonjek [103], A.R. Stradling [8], A. Straessner [47], M.E. Stramaglia [18], J. Strandberg [149], S. Strandberg [148a,148b], M. Strauss [115], P. Strizenec [146b], R. Ströhmer [177], D.M. Strom [118], R. Stroynowski [43], A. Strubig [49], S.A. Stucci [27], B. Stugu [15], N.A. Styles [45], D. Su [145], J. Su [127], S. Suchek [60a], Y. Sugaya [120], M. Suk [130], V.V. Sulin [98], DMS Sultan [162a,162b], S. Sultansoy [4c], T. Sumida [71], S. Sun [59], X. Sun [3], K. Suruliz [151], C.J.E. Suster [152], M.R. Sutton [151], S. Suzuki [69], M. Svatos [129], M. Swiatlowski [33], S.P. Swift [2], I. Sykora [146a], T. Sykora [131], D. Ta [51], K. Tackmann [45], J. Taenzer [155], A. Taffard [166], R. Tafirout [163a], E. Tahirovic [79], N. Taiblum [155], H. Takai [27], R. Takashima [72], E.H. Takasugi [103], T. Takeshita [142], Y. Takubo [69], M. Talby [88], A.A. Talyshev [111,c], J. Tanaka [157], M. Tanaka [159], R. Tanaka [119], S. Tanaka [69], R. Tanioka [70], B.B. Tannenwald [113], S. Tapia Araya [34b], S. Tapprogge [86], S. Tarem [154], G.F. Tartarelli [94a], P. Tas [131], M. Tasevsky [129], T. Tashiro [71], E. Tassi [40a,40b], A. Tavares Delgado [128a,128b], Y. Tayalati [137e], A.C. Taylor [107], A.J. Taylor [49], G.N. Taylor [91], P.T.E. Taylor [91], W. Taylor [163b], P. Teixeira-Dias [80], D. Temple [144], H. Ten Kate [32], P.K. Teng [153], J.J. Teoh [120], F. Tepel [178], S. Terada [69], K. Terashi [157], J. Terron [85], S. Terzo [13], M. Testa [50], R.J. Teuscher [161,o], T. Theveneaux-Pelzer [88], F. Thiele [39], J.P. Thomas [19], J. Thomas-Wilsker [80], P.D. Thompson [19], A.S. Thompson [56], L.A. Thomsen [179], E. Thomson [124], M.J. Tibbetts [16], R.E. Ticse Torres [88], V.O. Tikhomirov [98,aq], Yu.A. Tikhonov [111,c], S. Timoshenko [100], P. Tipton [179], S. Tisserant [88], K. Todome [159], S. Todorova-Nova [5], S. Todt [47], J. Tojo [73], S. Tokár [146a], K. Tokushuku [69], E. Tolley [59], L. Tomlinson [87], M. Tomoto [105], L. Tompkins [145,ar], K. Toms [107], B. Tong [59], P. Tornambe [51], E. Torrence [118], H. Torres [47], E. Torró Pastor [140], J. Toth [88,as], F. Touchard [88], D.R. Tovey [141], C.J. Treado [112], T. Trefzger [177], F. Tresoldi [151], A. Tricoli [27], I.M. Trigger [163a], S. Trincaz-Duvoid [83], M.F. Tripiana [13], W. Trischuk [161], B. Trocmé [58], A. Trofymov [45], C. Troncon [94a], M. Trottier-McDonald [16], M. Trovatelli [172], L. Truong [147b], M. Trzebinski [42], A. Trzupek [42], K.W. Tsang [62a], J.C-L. Tseng [122], P.V. Tsiareshka [95], G. Tsipolitis [10], N. Tsirintanis [9], S. Tsiskaridze [13], V. Tsiskaridze [51], E.G. Tskhadadze [54a], K.M. Tsui [62a], I.I. Tsukerman [99], V. Tsulaia [16], S. Tsuno [69], D. Tsybychev [150], Y. Tu [62b], A. Tudorache [28b], V. Tudorache [28b], T.T. Tulbure [28a], A.N. Tuna [59], S.A. Tupputi [22a,22b], S. Turchikhin [68], D. Turgeman [175], I. Turk Cakir [4b,at], R. Turra [94a], P.M. Tuts [38], G. Ucchielli [22a,22b], I. Ueda [69], M. Ughetto [148a,148b], F. Ukegawa [164], G. Unal [32], A. Undrus [27], G. Unel [166], F.C. Ungaro [91], Y. Unno [69], C. Unverdorben [102], J. Urban [146b], P. Urquijo [91], P. Urrejola [86], G. Usai [8], J. Usui [69], L. Vacavant [88], V. Vacek [130], B. Vachon [90], K.O.H. Vadla [121], A. Vaidya [81], C. Valderanis [102], E. Valdes Santurio [148a,148b], M. Valente [52], S. Valentinetti [22a,22b], A. Valero [170], L. Valéry [13], S. Valkar [131], A. Vallier [5], J.A. Valls Ferrer [170], W. Van Den Wollenberg [109], H. van der Graaf [109], P. van Gemmeren [6], J. Van Nieuwkoop [144], I. van Vulpen [109], M.C. van Woerden [109], M. Vanadia [135a,135b], W. Vandelli [32], A. Vaniachine [160], P. Vankov [109], G. Vardanyan [180], R. Vari [134a], E.W. Varnes [7], C. Varni [53a,53b], T. Varol [43], D. Varouchas [119], A. Vartapetian [8], K.E. Varvell [152], J.G. Vasquez [179], G.A. Vasquez [34b], F. Vazeille [37], T. Vazquez Schroeder [90], J. Veatch [57], V. Veeraraghavan [7], L.M. Veloce [161], F. Veloso [128a,128c], S. Veneziano [134a], A. Ventura [76a,76b], M. Venturi [172], N. Venturi [32], A. Venturini [25], V. Vercesi [123a], M. Verducci [136a,136b], W. Verkerke [109], A.T. Vermeulen [109], J.C. Vermeulen [109], M.C. Vetterli [144,d], N. Viaux Maira [34b], O. Viazlo [84], I. Vichou [169,*], T. Vickey [141], O.E. Vickey Boeriu [141], G.H.A. Viehhauser [122], S. Viel [16], L. Vigani [122], M. Villa [22a,22b], M. Villaplana Perez [94a,94b], E. Vilucchi [50], M.G. Vincter [31], V.B. Vinogradov [68], A. Vishwakarma [45], C. Vittori [22a,22b], I. Vivarelli [151], S. Vlachos [10], M. Vogel [178], P. Vokac [130], G. Volpi [13], H. von der Schmitt [103], E. von Toerne [23], V. Vorobel [131], K. Vorobev [100], M. Vos [170], R. Voss [32], J.H. Vossebeld [77], N. Vranjes [14], M. Vranjes Milosavljevic [14], V. Vrba [130], M. Vreeswijk [109], R. Vuillermet [32], I. Vukotic [33], P. Wagner [23], W. Wagner [178], J. Wagner-Kuhr [102], H. Wahlberg [74], S. Wahrmund [47], J. Walder [75], R. Walker [102], W. Walkowiak [143], V. Wallangen [148a,148b], C. Wang [35b], C. Wang [36b,au], F. Wang [176], H. Wang [16], H. Wang [3], J. Wang [45], J. Wang [152], Q. Wang [115], R. Wang [6], S.M. Wang [153], T. Wang [38], W. Wang [153,av], W. Wang [36a], Z. Wang [36c], C. Wanotayaroj [118], A. Warburton [90], C.P. Ward [30], D.R. Wardrope [81], A. Washbrook [49], P.M. Watkins [19], A.T. Watson [19], M.F. Watson [19], G. Watts [140], S. Watts [87], B.M. Waugh [81], A.F. Webb [11], S. Webb [86], M.S. Weber [18], S.W. Weber [177], S.A. Weber [31], J.S. Webster [6], A.R. Weidberg [122], B. Weinert [64], J. Weingarten [57], M. Weirich [86], C. Weiser [51], H. Weits [109], P.S. Wells [32], T. Wenaus [27], T. Wengler [32], S. Wenig [32], N. Wermes [23], M.D. Werner [67], P. Werner [32],

M. Wessels [60a], T.D. Weston [18], K. Whalen [118], N.L. Whallon [140], A.M. Wharton [75], A.S. White [92], A. White [8], M.J. White [1], R. White [34b], D. Whiteson [166], B.W. Whitmore [75], F.J. Wickens [133], W. Wiedenmann [176], M. Wielers [133], C. Wiglesworth [39], L.A.M. Wiik-Fuchs [51], A. Wildauer [103], F. Wilk [87], H.G. Wilkens [32], H.H. Williams [124], S. Williams [109], C. Willis [93], S. Willocq [89], J.A. Wilson [19], I. Wingerter-Seez [5], E. Winkels [151], F. Winklmeier [118], O.J. Winston [151], B.T. Winter [23], M. Wittgen [145], M. Wobisch [82,u], T.M.H. Wolf [109], R. Wolff [88], M.W. Wolter [42], H. Wolters [128a,128c], V.W.S. Wong [171], S.D. Worm [19], B.K. Wosiek [42], J. Wotschack [32], K.W. Wozniak [42], M. Wu [33], S.L. Wu [176], X. Wu [52], Y. Wu [92], T.R. Wyatt [87], B.M. Wynne [49], S. Xella [39], Z. Xi [92], L. Xia [35c], D. Xu [35a], L. Xu [27], T. Xu [138], B. Yabsley [152], S. Yacoob [147a], D. Yamaguchi [159], Y. Yamaguchi [159], A. Yamamoto [69], S. Yamamoto [157], T. Yamanaka [157], F. Yamane [70], M. Yamatani [157], Y. Yamazaki [70], Z. Yan [24], H. Yang [36c], H. Yang [16], Y. Yang [153], Z. Yang [15], W-M. Yao [16], Y.C. Yap [83], Y. Yasu [69], E. Yatsenko [5], K.H. Yau Wong [23], J. Ye [43], S. Ye [27], I. Yeletskikh [68], E. Yigitbasi [24], E. Yildirim [86], K. Yorita [174], K. Yoshihara [124], C. Young [145], C.J.S. Young [32], J. Yu [8], J. Yu [67], S.P.Y. Yuen [23], I. Yusuff [30,aw], B. Zabinski [42], G. Zacharis [10], R. Zaidan [13], A.M. Zaitsev [132,ak], N. Zakharchuk [45], J. Zalieckas [15], A. Zaman [150], S. Zambito [59], D. Zanzi [91], C. Zeitnitz [178], G. Zemaityte [122], A. Zemla [41a], J.C. Zeng [169], Q. Zeng [145], O. Zenin [132], T. Ženiš [146a], D. Zerwas [119], D. Zhang [92], F. Zhang [176], G. Zhang [36a,ax], H. Zhang [35b], J. Zhang [6], L. Zhang [51], L. Zhang [36a], M. Zhang [169], P. Zhang [35b], R. Zhang [23], R. Zhang [36a,au], X. Zhang [36b], Y. Zhang [35a], Z. Zhang [119], X. Zhao [43], Y. Zhao [36b,ay], Z. Zhao [36a], A. Zhemchugov [68], B. Zhou [92], C. Zhou [176], L. Zhou [43], M. Zhou [35a], M. Zhou [150], N. Zhou [35c], C.G. Zhu [36b], H. Zhu [35a], J. Zhu [92], Y. Zhu [36a], X. Zhuang [35a], K. Zhukov [98], A. Zibell [177], D. Zieminska [64], N.I. Zimine [68], C. Zimmermann [86], S. Zimmermann [51], Z. Zinonos [103], M. Zinser [86], M. Ziolkowski [143], L. Živković [14], G. Zobernig [176], A. Zoccoli [22a,22b], R. Zou [33], M. zur Nedden [17], L. Zwalinski [32]

[1] *Department of Physics, University of Adelaide, Adelaide, Australia*
[2] *Physics Department, SUNY Albany, Albany NY, United States*
[3] *Department of Physics, University of Alberta, Edmonton AB, Canada*
[4] [(a)] *Department of Physics, Ankara University, Ankara;* [(b)] *Istanbul Aydin University, Istanbul;* [(c)] *Division of Physics, TOBB University of Economics and Technology, Ankara, Turkey*
[5] *LAPP, CNRS/IN2P3 and Université Savoie Mont Blanc, Annecy-le-Vieux, France*
[6] *High Energy Physics Division, Argonne National Laboratory, Argonne IL, United States*
[7] *Department of Physics, University of Arizona, Tucson AZ, United States*
[8] *Department of Physics, The University of Texas at Arlington, Arlington TX, United States*
[9] *Physics Department, National and Kapodistrian University of Athens, Athens, Greece*
[10] *Physics Department, National Technical University of Athens, Zografou, Greece*
[11] *Department of Physics, The University of Texas at Austin, Austin TX, United States*
[12] *Institute of Physics, Azerbaijan Academy of Sciences, Baku, Azerbaijan*
[13] *Institut de Física d'Altes Energies (IFAE), The Barcelona Institute of Science and Technology, Barcelona, Spain*
[14] *Institute of Physics, University of Belgrade, Belgrade, Serbia*
[15] *Department for Physics and Technology, University of Bergen, Bergen, Norway*
[16] *Physics Division, Lawrence Berkeley National Laboratory and University of California, Berkeley CA, United States*
[17] *Department of Physics, Humboldt University, Berlin, Germany*
[18] *Albert Einstein Center for Fundamental Physics and Laboratory for High Energy Physics, University of Bern, Bern, Switzerland*
[19] *School of Physics and Astronomy, University of Birmingham, Birmingham, United Kingdom*
[20] [(a)] *Department of Physics, Bogazici University, Istanbul;* [(b)] *Department of Physics Engineering, Gaziantep University, Gaziantep;* [(c)] *Istanbul Bilgi University, Faculty of Engineering and Natural Sciences, Istanbul;* [(d)] *Bahcesehir University, Faculty of Engineering and Natural Sciences, Istanbul, Turkey*
[21] *Centro de Investigaciones, Universidad Antonio Narino, Bogota, Colombia*
[22] [(a)] *INFN Sezione di Bologna;* [(b)] *Dipartimento di Fisica e Astronomia, Università di Bologna, Bologna, Italy*
[23] *Physikalisches Institut, University of Bonn, Bonn, Germany*
[24] *Department of Physics, Boston University, Boston MA, United States*
[25] *Department of Physics, Brandeis University, Waltham MA, United States*
[26] [(a)] *Universidade Federal do Rio De Janeiro COPPE/EE/IF, Rio de Janeiro;* [(b)] *Electrical Circuits Department, Federal University of Juiz de Fora (UFJF), Juiz de Fora;* [(c)] *Federal University of Sao Joao del Rei (UFSJ), Sao Joao del Rei;* [(d)] *Instituto de Fisica, Universidade de Sao Paulo, Sao Paulo, Brazil*
[27] *Physics Department, Brookhaven National Laboratory, Upton NY, United States*
[28] [(a)] *Transilvania University of Brasov, Brasov;* [(b)] *Horia Hulubei National Institute of Physics and Nuclear Engineering, Bucharest;* [(c)] *Department of Physics, Alexandru Ioan Cuza University of Iasi, Iasi;* [(d)] *National Institute for Research and Development of Isotopic and Molecular Technologies, Physics Department, Cluj Napoca;* [(e)] *University Politehnica Bucharest, Bucharest;* [(f)] *West University in Timisoara, Timisoara, Romania*
[29] *Departamento de Física, Universidad de Buenos Aires, Buenos Aires, Argentina*
[30] *Cavendish Laboratory, University of Cambridge, Cambridge, United Kingdom*
[31] *Department of Physics, Carleton University, Ottawa ON, Canada*
[32] *CERN, Geneva, Switzerland*
[33] *Enrico Fermi Institute, University of Chicago, Chicago IL, United States*
[34] [(a)] *Departamento de Física, Pontificia Universidad Católica de Chile, Santiago;* [(b)] *Departamento de Física, Universidad Técnica Federico Santa María, Valparaíso, Chile*
[35] [(a)] *Institute of High Energy Physics, Chinese Academy of Sciences, Beijing;* [(b)] *Department of Physics, Nanjing University, Jiangsu;* [(c)] *Physics Department, Tsinghua University, Beijing 100084, China*
[36] [(a)] *Department of Modern Physics and State Key Laboratory of Particle Detection and Electronics, University of Science and Technology of China, Anhui;* [(b)] *School of Physics, Shandong University, Shandong;* [(c)] *Department of Physics and Astronomy, Key Laboratory for Particle Physics, Astrophysics and Cosmology, Ministry of Education, Shanghai Key Laboratory for Particle Physics and Cosmology, Shanghai Jiao Tong University, Shanghai* [az]*, China*
[37] *Université Clermont Auvergne, CNRS/IN2P3, LPC, Clermont-Ferrand, France*
[38] *Nevis Laboratory, Columbia University, Irvington NY, United States*
[39] *Niels Bohr Institute, University of Copenhagen, Kobenhavn, Denmark*

[40] [(a)] INFN Gruppo Collegato di Cosenza, Laboratori Nazionali di Frascati; [(b)] Dipartimento di Fisica, Università della Calabria, Rende, Italy
[41] [(a)] AGH University of Science and Technology, Faculty of Physics and Applied Computer Science, Krakow; [(b)] Marian Smoluchowski Institute of Physics, Jagiellonian University, Krakow, Poland
[42] Institute of Nuclear Physics Polish Academy of Sciences, Krakow, Poland
[43] Physics Department, Southern Methodist University, Dallas TX, United States
[44] Physics Department, University of Texas at Dallas, Richardson TX, United States
[45] DESY, Hamburg and Zeuthen, Germany
[46] Lehrstuhl für Experimentelle Physik IV, Technische Universität Dortmund, Dortmund, Germany
[47] Institut für Kern- und Teilchenphysik, Technische Universität Dresden, Dresden, Germany
[48] Department of Physics, Duke University, Durham NC, United States
[49] SUPA - School of Physics and Astronomy, University of Edinburgh, Edinburgh, United Kingdom
[50] INFN e Laboratori Nazionali di Frascati, Frascati, Italy
[51] Fakultät für Mathematik und Physik, Albert-Ludwigs-Universität, Freiburg, Germany
[52] Departement de Physique Nucleaire et Corpusculaire, Université de Genève, Geneva, Switzerland
[53] [(a)] INFN Sezione di Genova; [(b)] Dipartimento di Fisica, Università di Genova, Genova, Italy
[54] [(a)] E. Andronikashvili Institute of Physics, Iv. Javakhishvili Tbilisi State University, Tbilisi; [(b)] High Energy Physics Institute, Tbilisi State University, Tbilisi, Georgia
[55] II Physikalisches Institut, Justus-Liebig-Universität Giessen, Giessen, Germany
[56] SUPA - School of Physics and Astronomy, University of Glasgow, Glasgow, United Kingdom
[57] II Physikalisches Institut, Georg-August-Universität, Göttingen, Germany
[58] Laboratoire de Physique Subatomique et de Cosmologie, Université Grenoble-Alpes, CNRS/IN2P3, Grenoble, France
[59] Laboratory for Particle Physics and Cosmology, Harvard University, Cambridge MA, United States
[60] [(a)] Kirchhoff-Institut für Physik, Ruprecht-Karls-Universität Heidelberg, Heidelberg; [(b)] Physikalisches Institut, Ruprecht-Karls-Universität Heidelberg, Heidelberg, Germany
[61] Faculty of Applied Information Science, Hiroshima Institute of Technology, Hiroshima, Japan
[62] [(a)] Department of Physics, The Chinese University of Hong Kong, Shatin, N.T.; [(b)] Department of Physics, The University of Hong Kong; [(c)] Department of Physics and Institute for Advanced Study, The Hong Kong University of Science and Technology, Clear Water Bay, Kowloon, Hong Kong, China
[63] Department of Physics, National Tsing Hua University, Taiwan
[64] Department of Physics, Indiana University, Bloomington IN, United States
[65] Institut für Astro- und Teilchenphysik, Leopold-Franzens-Universität, Innsbruck, Austria
[66] University of Iowa, Iowa City IA, United States
[67] Department of Physics and Astronomy, Iowa State University, Ames IA, United States
[68] Joint Institute for Nuclear Research, JINR Dubna, Dubna, Russia
[69] KEK, High Energy Accelerator Research Organization, Tsukuba, Japan
[70] Graduate School of Science, Kobe University, Kobe, Japan
[71] Faculty of Science, Kyoto University, Kyoto, Japan
[72] Kyoto University of Education, Kyoto, Japan
[73] Research Center for Advanced Particle Physics and Department of Physics, Kyushu University, Fukuoka, Japan
[74] Instituto de Física La Plata, Universidad Nacional de La Plata and CONICET, La Plata, Argentina
[75] Physics Department, Lancaster University, Lancaster, United Kingdom
[76] [(a)] INFN Sezione di Lecce; [(b)] Dipartimento di Matematica e Fisica, Università del Salento, Lecce, Italy
[77] Oliver Lodge Laboratory, University of Liverpool, Liverpool, United Kingdom
[78] Department of Experimental Particle Physics, Jožef Stefan Institute and Department of Physics, University of Ljubljana, Ljubljana, Slovenia
[79] School of Physics and Astronomy, Queen Mary University of London, London, United Kingdom
[80] Department of Physics, Royal Holloway University of London, Surrey, United Kingdom
[81] Department of Physics and Astronomy, University College London, London, United Kingdom
[82] Louisiana Tech University, Ruston LA, United States
[83] Laboratoire de Physique Nucléaire et de Hautes Energies, UPMC and Université Paris-Diderot and CNRS/IN2P3, Paris, France
[84] Fysiska institutionen, Lunds universitet, Lund, Sweden
[85] Departamento de Fisica Teorica C-15, Universidad Autonoma de Madrid, Madrid, Spain
[86] Institut für Physik, Universität Mainz, Mainz, Germany
[87] School of Physics and Astronomy, University of Manchester, Manchester, United Kingdom
[88] CPPM, Aix-Marseille Université and CNRS/IN2P3, Marseille, France
[89] Department of Physics, University of Massachusetts, Amherst MA, United States
[90] Department of Physics, McGill University, Montreal QC, Canada
[91] School of Physics, University of Melbourne, Victoria, Australia
[92] Department of Physics, The University of Michigan, Ann Arbor MI, United States
[93] Department of Physics and Astronomy, Michigan State University, East Lansing MI, United States
[94] [(a)] INFN Sezione di Milano; [(b)] Dipartimento di Fisica, Università di Milano, Milano, Italy
[95] B.I. Stepanov Institute of Physics, National Academy of Sciences of Belarus, Minsk, Belarus
[96] Research Institute for Nuclear Problems of Byelorussian State University, Minsk, Belarus
[97] Group of Particle Physics, University of Montreal, Montreal QC, Canada
[98] P.N. Lebedev Physical Institute of the Russian Academy of Sciences, Moscow, Russia
[99] Institute for Theoretical and Experimental Physics (ITEP), Moscow, Russia
[100] National Research Nuclear University MEPhI, Moscow, Russia
[101] D.V. Skobeltsyn Institute of Nuclear Physics, M.V. Lomonosov Moscow State University, Moscow, Russia
[102] Fakultät für Physik, Ludwig-Maximilians-Universität München, München, Germany
[103] Max-Planck-Institut für Physik (Werner-Heisenberg-Institut), München, Germany
[104] Nagasaki Institute of Applied Science, Nagasaki, Japan
[105] Graduate School of Science and Kobayashi-Maskawa Institute, Nagoya University, Nagoya, Japan
[106] [(a)] INFN Sezione di Napoli; [(b)] Dipartimento di Fisica, Università di Napoli, Napoli, Italy
[107] Department of Physics and Astronomy, University of New Mexico, Albuquerque NM, United States
[108] Institute for Mathematics, Astrophysics and Particle Physics, Radboud University Nijmegen/Nikhef, Nijmegen, Netherlands
[109] Nikhef National Institute for Subatomic Physics and University of Amsterdam, Amsterdam, Netherlands
[110] Department of Physics, Northern Illinois University, DeKalb IL, United States
[111] Budker Institute of Nuclear Physics, SB RAS, Novosibirsk, Russia
[112] Department of Physics, New York University, New York NY, United States
[113] Ohio State University, Columbus OH, United States
[114] Faculty of Science, Okayama University, Okayama, Japan
[115] Homer L. Dodge Department of Physics and Astronomy, University of Oklahoma, Norman OK, United States
[116] Department of Physics, Oklahoma State University, Stillwater OK, United States

[117] Palacký University, RCPTM, Olomouc, Czech Republic
[118] Center for High Energy Physics, University of Oregon, Eugene OR, United States
[119] LAL, Univ. Paris-Sud, CNRS/IN2P3, Université Paris-Saclay, Orsay, France
[120] Graduate School of Science, Osaka University, Osaka, Japan
[121] Department of Physics, University of Oslo, Oslo, Norway
[122] Department of Physics, Oxford University, Oxford, United Kingdom
[123] [(a)] INFN Sezione di Pavia; [(b)] Dipartimento di Fisica, Università di Pavia, Pavia, Italy
[124] Department of Physics, University of Pennsylvania, Philadelphia PA, United States
[125] National Research Centre "Kurchatov Institute" B.P. Konstantinov Petersburg Nuclear Physics Institute, St. Petersburg, Russia
[126] [(a)] INFN Sezione di Pisa; [(b)] Dipartimento di Fisica E. Fermi, Università di Pisa, Pisa, Italy
[127] Department of Physics and Astronomy, University of Pittsburgh, Pittsburgh PA, United States
[128] [(a)] Laboratório de Instrumentação e Física Experimental de Partículas - LIP, Lisboa; [(b)] Faculdade de Ciências, Universidade de Lisboa, Lisboa; [(c)] Department of Physics, University of Coimbra, Coimbra; [(d)] Centro de Física Nuclear da Universidade de Lisboa, Lisboa; [(e)] Departamento de Fisica, Universidade do Minho, Braga; [(f)] Departamento de Fisica Teorica y del Cosmos and CAFPE, Universidad de Granada, Granada; [(g)] Dep Fisica and CEFITEC of Faculdade de Ciencias e Tecnologia, Universidade Nova de Lisboa, Caparica, Portugal
[129] Institute of Physics, Academy of Sciences of the Czech Republic, Praha, Czech Republic
[130] Czech Technical University in Prague, Praha, Czech Republic
[131] Charles University, Faculty of Mathematics and Physics, Prague, Czech Republic
[132] State Research Center Institute for High Energy Physics (Protvino), NRC KI, Russia
[133] Particle Physics Department, Rutherford Appleton Laboratory, Didcot, United Kingdom
[134] [(a)] INFN Sezione di Roma; [(b)] Dipartimento di Fisica, Sapienza Università di Roma, Roma, Italy
[135] [(a)] INFN Sezione di Roma Tor Vergata; [(b)] Dipartimento di Fisica, Università di Roma Tor Vergata, Roma, Italy
[136] [(a)] INFN Sezione di Roma Tre; [(b)] Dipartimento di Matematica e Fisica, Università Roma Tre, Roma, Italy
[137] [(a)] Faculté des Sciences Ain Chock, Réseau Universitaire de Physique des Hautes Energies - Université Hassan II, Casablanca; [(b)] Centre National de l'Energie des Sciences Techniques Nucleaires, Rabat; [(c)] Faculté des Sciences Semlalia, Université Cadi Ayyad, LPHEA-Marrakech; [(d)] Faculté des Sciences, Université Mohamed Premier and LPTPM, Oujda; [(e)] Faculté des sciences, Université Mohammed V, Rabat, Morocco
[138] DSM/IRFU (Institut de Recherches sur les Lois Fondamentales de l'Univers), CEA Saclay (Commissariat à l'Energie Atomique et aux Energies Alternatives), Gif-sur-Yvette, France
[139] Santa Cruz Institute for Particle Physics, University of California Santa Cruz, Santa Cruz CA, United States
[140] Department of Physics, University of Washington, Seattle WA, United States
[141] Department of Physics and Astronomy, University of Sheffield, Sheffield, United Kingdom
[142] Department of Physics, Shinshu University, Nagano, Japan
[143] Department Physik, Universität Siegen, Siegen, Germany
[144] Department of Physics, Simon Fraser University, Burnaby BC, Canada
[145] SLAC National Accelerator Laboratory, Stanford CA, United States
[146] [(a)] Faculty of Mathematics, Physics & Informatics, Comenius University, Bratislava; [(b)] Department of Subnuclear Physics, Institute of Experimental Physics of the Slovak Academy of Sciences, Kosice, Slovak Republic
[147] [(a)] Department of Physics, University of Cape Town, Cape Town; [(b)] Department of Physics, University of Johannesburg, Johannesburg; [(c)] School of Physics, University of the Witwatersrand, Johannesburg, South Africa
[148] [(a)] Department of Physics, Stockholm University; [(b)] The Oskar Klein Centre, Stockholm, Sweden
[149] Physics Department, Royal Institute of Technology, Stockholm, Sweden
[150] Departments of Physics & Astronomy and Chemistry, Stony Brook University, Stony Brook NY, United States
[151] Department of Physics and Astronomy, University of Sussex, Brighton, United Kingdom
[152] School of Physics, University of Sydney, Sydney, Australia
[153] Institute of Physics, Academia Sinica, Taipei, Taiwan
[154] Department of Physics, Technion: Israel Institute of Technology, Haifa, Israel
[155] Raymond and Beverly Sackler School of Physics and Astronomy, Tel Aviv University, Tel Aviv, Israel
[156] Department of Physics, Aristotle University of Thessaloniki, Thessaloniki, Greece
[157] International Center for Elementary Particle Physics and Department of Physics, The University of Tokyo, Tokyo, Japan
[158] Graduate School of Science and Technology, Tokyo Metropolitan University, Tokyo, Japan
[159] Department of Physics, Tokyo Institute of Technology, Tokyo, Japan
[160] Tomsk State University, Tomsk, Russia
[161] Department of Physics, University of Toronto, Toronto ON, Canada
[162] [(a)] INFN-TIFPA; [(b)] University of Trento, Trento, Italy
[163] [(a)] TRIUMF, Vancouver BC; [(b)] Department of Physics and Astronomy, York University, Toronto ON, Canada
[164] Faculty of Pure and Applied Sciences, and Center for Integrated Research in Fundamental Science and Engineering, University of Tsukuba, Tsukuba, Japan
[165] Department of Physics and Astronomy, Tufts University, Medford MA, United States
[166] Department of Physics and Astronomy, University of California Irvine, Irvine CA, United States
[167] [(a)] INFN Gruppo Collegato di Udine, Sezione di Trieste, Udine; [(b)] ICTP, Trieste; [(c)] Dipartimento di Chimica, Fisica e Ambiente, Università di Udine, Udine, Italy
[168] Department of Physics and Astronomy, University of Uppsala, Uppsala, Sweden
[169] Department of Physics, University of Illinois, Urbana IL, United States
[170] Instituto de Fisica Corpuscular (IFIC), Centro Mixto Universidad de Valencia - CSIC, Spain
[171] Department of Physics, University of British Columbia, Vancouver BC, Canada
[172] Department of Physics and Astronomy, University of Victoria, Victoria BC, Canada
[173] Department of Physics, University of Warwick, Coventry, United Kingdom
[174] Waseda University, Tokyo, Japan
[175] Department of Particle Physics, The Weizmann Institute of Science, Rehovot, Israel
[176] Department of Physics, University of Wisconsin, Madison WI, United States
[177] Fakultät für Physik und Astronomie, Julius-Maximilians-Universität, Würzburg, Germany
[178] Fakultät für Mathematik und Naturwissenschaften, Fachgruppe Physik, Bergische Universität Wuppertal, Wuppertal, Germany
[179] Department of Physics, Yale University, New Haven CT, United States
[180] Yerevan Physics Institute, Yerevan, Armenia
[181] Centre de Calcul de l'Institut National de Physique Nucléaire et de Physique des Particules (IN2P3), Villeurbanne, France
[182] Academia Sinica Grid Computing, Institute of Physics, Academia Sinica, Taipei, Taiwan

[a] Also at Department of Physics, King's College London, London, United Kingdom.
[b] Also at Institute of Physics, Azerbaijan Academy of Sciences, Baku, Azerbaijan.
[c] Also at Novosibirsk State University, Novosibirsk, Russia.
[d] Also at TRIUMF, Vancouver BC, Canada.
[e] Also at Department of Physics & Astronomy, University of Louisville, Louisville, KY, United States of America.

[f] Also at Physics Department, An-Najah National University, Nablus, Palestine.
[g] Also at Department of Physics, California State University, Fresno, CA, United States of America.
[h] Also at Department of Physics, University of Fribourg, Fribourg, Switzerland.
[i] Also at II Physikalisches Institut, Georg-August-Universität, Göttingen, Germany.
[j] Also at Departament de Fisica de la Universitat Autonoma de Barcelona, Barcelona, Spain.
[k] Also at Departamento de Fisica e Astronomia, Faculdade de Ciencias, Universidade do Porto, Portugal.
[l] Also at Tomsk State University, Tomsk, Russia.
[m] Also at The Collaborative Innovation Center of Quantum Matter (CICQM), Beijing, China.
[n] Also at Universita di Napoli Parthenope, Napoli, Italy.
[o] Also at Institute of Particle Physics (IPP), Canada.
[p] Also at Horia Hulubei National Institute of Physics and Nuclear Engineering, Bucharest, Romania.
[q] Also at Department of Physics, St. Petersburg State Polytechnical University, St. Petersburg, Russia.
[r] Also at Borough of Manhattan Community College, City University of New York, New York City, United States of America.
[s] Also at Department of Financial and Management Engineering, University of the Aegean, Chios, Greece.
[t] Also at Centre for High Performance Computing, CSIR Campus, Rosebank, Cape Town, South Africa.
[u] Also at Louisiana Tech University, Ruston LA, United States of America.
[v] Also at Institucio Catalana de Recerca i Estudis Avancats, ICREA, Barcelona, Spain.
[w] Also at Graduate School of Science, Osaka University, Osaka, Japan.
[x] Also at Fakultät für Mathematik und Physik, Albert-Ludwigs-Universität, Freiburg, Germany.
[y] Also at Institute for Mathematics, Astrophysics and Particle Physics, Radboud University Nijmegen/Nikhef, Nijmegen, Netherlands.
[z] Also at Department of Physics, The University of Texas at Austin, Austin TX, United States of America.
[aa] Also at Institute of Theoretical Physics, Ilia State University, Tbilisi, Georgia.
[ab] Also at CERN, Geneva, Switzerland.
[ac] Also at Georgian Technical University (GTU), Tbilisi, Georgia.
[ad] Also at Ochadai Academic Production, Ochanomizu University, Tokyo, Japan.
[ae] Also at Manhattan College, New York NY, United States of America.
[af] Also at Departamento de Física, Pontificia Universidad Católica de Chile, Santiago, Chile.
[ag] Also at Department of Physics, The University of Michigan, Ann Arbor MI, United States of America.
[ah] Also at The City College of New York, New York NY, United States of America.
[ai] Also at Departamento de Fisica Teorica y del Cosmos and CAFPE, Universidad de Granada, Granada, Portugal.
[aj] Also at Department of Physics, California State University, Sacramento CA, United States of America.
[ak] Also at Moscow Institute of Physics and Technology State University, Dolgoprudny, Russia.
[al] Also at Departement de Physique Nucleaire et Corpusculaire, Université de Genève, Geneva, Switzerland.
[am] Also at Institut de Física d'Altes Energies (IFAE), The Barcelona Institute of Science and Technology, Barcelona, Spain.
[an] Also at School of Physics, Sun Yat-sen University, Guangzhou, China.
[ao] Also at Institute for Nuclear Research and Nuclear Energy (INRNE) of the Bulgarian Academy of Sciences, Sofia, Bulgaria.
[ap] Also at Faculty of Physics, M.V. Lomonosov Moscow State University, Moscow, Russia.
[aq] Also at National Research Nuclear University MEPhI, Moscow, Russia.
[ar] Also at Department of Physics, Stanford University, Stanford CA, United States of America.
[as] Also at Institute for Particle and Nuclear Physics, Wigner Research Centre for Physics, Budapest, Hungary.
[at] Also at Giresun University, Faculty of Engineering, Turkey.
[au] Also at CPPM, Aix-Marseille Université and CNRS/IN2P3, Marseille, France.
[av] Also at Department of Physics, Nanjing University, Jiangsu, China.
[aw] Also at University of Malaya, Department of Physics, Kuala Lumpur, Malaysia.
[ax] Also at Institute of Physics, Academia Sinica, Taipei, Taiwan.
[ay] Also at LAL, Univ. Paris-Sud, CNRS/IN2P3, Université Paris-Saclay, Orsay, France.
[az] Also at PKU-CHEP.
[*] Deceased.

Eur. Phys. J. C (2017) 77:361
DOI 10.1140/epjc/s10052-017-4900-z

THE EUROPEAN PHYSICAL JOURNAL C

Regular Article - Experimental Physics

Measurements of the production cross section of a Z boson in association with jets in pp collisions at $\sqrt{s} = 13$ TeV with the ATLAS detector

ATLAS Collaboration[*]

CERN, 1211 Geneva 23, Switzerland

Received: 21 February 2017 / Accepted: 8 May 2017 / Published online: 31 May 2017

Abstract Measurements of the production cross section of a Z boson in association with jets in proton–proton collisions at $\sqrt{s} = 13$ TeV are presented, using data corresponding to an integrated luminosity of 3.16 fb^{-1} collected by the ATLAS experiment at the CERN Large Hadron Collider in 2015. Inclusive and differential cross sections are measured for events containing a Z boson decaying to electrons or muons and produced in association with up to seven jets with $p_{\mathrm{T}} > 30$ GeV and $|y| < 2.5$. Predictions from different Monte Carlo generators based on leading-order and next-to-leading-order matrix elements for up to two additional partons interfaced with parton shower and fixed-order predictions at next-to-leading order and next-to-next-to-leading order are compared with the measured cross sections. Good agreement within the uncertainties is observed for most of the modelled quantities, in particular with the generators which use next-to-leading-order matrix elements and the more recent next-to-next-to-leading-order fixed-order predictions.

Contents

[*] e-mail: atlas.publications@cern.ch

1 Introduction

The measurement of the production of a Z boson[1] in association with jets, Z + jets, constitutes a powerful test of perturbative quantum chromodynamics (QCD) [1,2]. The large production cross section and easily identifiable decays of the Z boson to charged leptonic final states offer clean experimental signatures which can be precisely measured. Such processes also constitute a non-negligible background for studies of the Higgs boson and in searches for new phenomena; typically in these studies, the multiplicity and kinematics of the jets are exploited to achieve a separation of the signal of interest from the Standard Model (SM) Z + jets process. These quantities are often measured in control regions and subsequently extrapolated to the signal region with the use of Monte Carlo (MC) generators, which are themselves subject to systematic uncertainty and must be tuned and validated using data. Predictions from the most recent generators combine next-to-leading-order (NLO) multi-leg matrix elements with a parton shower (PS) and a hadronisation model. Fixed-order parton-level predictions for Z+jets production at next-to-next-to-leading order (NNLO) are also available [3–6].

The Z + jets production differential cross section was previously measured by the ATLAS [7], CMS [8], and

[1] Throughout this paper, Z/γ^*-boson production is denoted simply by Z-boson production.

LHCb [9] collaborations at the CERN Large Hadron Collider (LHC) [10] at centre-of-mass energies of $\sqrt{s} = 7$ TeV [11–15] and 8 TeV [16–18], and by the CDF and D0 collaborations at the Tevatron collider at $\sqrt{s} = 1.96$ TeV [19,20]. In this paper, proton–proton (pp) collision data corresponding to an integrated luminosity of 3.16 fb^{-1}, collected at $\sqrt{s} = 13$ TeV with the ATLAS detector during 2015, are used for measurements of the Z-boson production cross section in association with up to seven jets within a fiducial region defined by the detector acceptance. The Z boson is identified using its decays to electron or muon pairs ($Z \to e^+e^-$, $Z \to \mu^+\mu^-$). Cross sections are measured separately for these two channels, and for their combination, as a function of the inclusive and exclusive jet multiplicity N_{jets} and the ratio of successive inclusive jet multiplicities $(N_{\text{jets}} + 1)/N_{\text{jets}}$, the transverse momentum of the leading jet $p_{\text{T}}^{\text{jet}}$ for several jet multiplicities, the jet rapidity y^{jet}, the azimuthal separation between the two leading jets $\Delta\phi_{\text{jj}}$, the two leading jet invariant mass m_{jj}, and the scalar sum H_{T} of the transverse momenta of all selected leptons and jets.

The paper is organised as follows. Section 2 contains a brief description of the ATLAS detector. The data and simulated samples as well as the Z + jets predictions used in the analysis are described in Sect. 3. The event selection and its associated uncertainties are presented in Sect. 4, while the methods employed to estimate the backgrounds are shown in Sect. 5. Comparisons between data and Monte Carlo predictions for reconstructed distributions are found in Sect. 6, while the unfolding procedure is described in Sect. 7. Section 8 presents the analysis results, the comparisons to predictions, and a discussion of their interpretation. Conclusions are provided in Sect. 9.

2 The ATLAS detector

The ATLAS experiment at the LHC is a multi-purpose particle detector with a forward-backward symmetric cylindrical geometry and nearly 4π coverage in solid angle.[2] It consists of an inner tracking detector, electromagnetic and hadronic calorimeters, and a muon spectrometer. The inner tracker is surrounded by a thin superconducting solenoid magnet and provides precision tracking of charged particles and momentum measurements in the pseudorapidity range $|\eta| < 2.5$. This region is matched to a high-granularity electromagnetic (EM) sampling calorimeter covering the pseudorapidity range $|\eta| < 3.2$, and a coarser granularity calorimeter up to $|\eta| = 4.9$. The hadronic calorimeter system covers the entire pseudorapidity range up to $|\eta| = 4.9$. The muon spectrometer consists of three large superconducting toroids each containing eight coils, a system of trigger chambers, and precision tracking chambers, which provide trigger and tracking capabilities in the range $|\eta| < 2.4$ and $|\eta| < 2.7$, respectively. A two-level trigger system [21] is used to select events. The first-level trigger is implemented in hardware and uses a subset of the detector information. This is followed by the software-based high-level trigger system, which runs offline reconstruction, reducing the event rate to approximately 1 kHz.

3 Data set, simulated event samples, and predictions

3.1 Data set

The data used in this analysis were collected by the ATLAS detector during August to November 2015. During this period, the LHC circulated 6.5 TeV proton beams with a 25 ns bunch spacing. The peak delivered instantaneous luminosity was $L = 5 \times 10^{33}\,\text{cm}^{-2}\,\text{s}^1$ and the mean number of pp interactions per bunch crossing (hard scattering and pile-up events) was $\langle\mu\rangle = 13$. The data set used in this measurement corresponds to a total integrated luminosity of 3.16 fb^{-1}.

3.2 Simulated event samples

Monte Carlo simulations, normalised to higher-order calculations, are used to estimate most of the contributions from background events, to unfold the data to the particle level, and to compare with the unfolded data distributions. All samples are processed with a GEANT4-based simulation [22] of the ATLAS detector [23]. An overview of all signal and background processes considered and of the generators used for the simulation is given in Table 1. Total production cross sections for the samples, their respective uncertainties (mainly coming from parton distribution function (PDF) and factorisation and renormalisation scale variations), and references to higher-order QCD corrections, where available, are also listed in Table 1.

Signal events (i.e. containing a Z boson with associated jets) are simulated using the SHERPA v2.2.1 [31] generator, denoted by SHERPA 2.2. Matrix elements (ME) are calculated for up to two additional partons at NLO and up to four partons at leading order (LO) using the Comix [34]

[2] ATLAS uses a right-handed coordinate system with its origin at the nominal interaction point (IP) in the centre of the detector and the z-axis along the beam pipe. The x-axis points from the IP to the centre of the LHC ring, and the y-axis points upwards. Cylindrical coordinates (r, ϕ) are used in the transverse plane, ϕ being the azimuthal angle around the z-axis. The pseudorapidity is defined in terms of the polar angle θ as $\eta = -\ln\tan(\theta/2)$. Angular distance is measured in units of $\Delta R \equiv \sqrt{(\Delta\eta)^2 + (\Delta\phi)^2}$. When dealing with massive jets and particles, the rapidity $y = \frac{1}{2}\ln\left(\frac{E+p_z}{E-p_z}\right)$ is used, where E is the jet/particle energy and p_z is the z-component of the jet/particle momentum.

Table 1 Signal and background Monte Carlo samples and the generators used in the simulation. Each sample is normalised to the appropriate production cross section σ and multiplied by the relevant branching ratios (BR) per lepton flavour for this sample, as shown in the third column. For W-boson and top-quark production, contributions from higher-order QCD corrections were calculated following the references given in the fifth column for the stated order. Similarly, for Z-boson production, higher-order QCD corrections were evaluated in the dilepton invariant mass range $66 < m_{\ell\ell} < 116$ GeV following the references given in the fifth column for the stated order, and extrapolation scaling factors were applied to match mass ranges used by each simulation as given in the first column. The theory uncertainties as given in the final column correspond to PDF and scale variations. The diboson samples include on-shell and off-shell WW, WZ and ZZ production. Recently, NNLO QCD predictions have been made available for the diboson processes [32,33]. However, these higher-order corrections have a negligible impact on this analysis

Process	Generator	$(\sigma \cdot \text{BR})$ [pb]	Normalisation order	References	Theory uncert. (%)
$Z(\to \ell^+\ell^-)$ + jets ($\ell = e, \mu$; $m_{\ell\ell} > 40$ GeV)	SHERPA 2.2	2106	NNLO	[24–27]	5
$Z(\to \ell^+\ell^-)$ + jets ($\ell = e, \mu, \tau$; $m_{\ell\ell} > 40$ GeV)	MG5_aMC@NLO+PY8	2103	NNLO	[24–27]	5
$W \to \ell\nu$ ($\ell = e, \mu$)	MG5_aMC@NLO+PY8	20,080	NNLO	[24–27]	5
$t\bar{t}$ ($m_t = 172.5$ GeV)					
PERUGIA2012(RADHI/RADLO)	POWHEG+PY6	831	NNLO+NNLL	[28]	6
UE- EE- 5	MG5_aMC@NLO+Herwig++	831	NNLO+NNLL	[28]	6
Single top quark (Wt)	POWHEG+PY6	72	NLO+NNLL	[29]	6
Single top quark (t-channel)	POWHEG+PY6	136	NLO+NNLL	[30]	6
Single top anti-quark (t-channel)	POWHEG+PY6	81	NLO+NNLL	[30]	6
Dibosons	SHERPA 2.1	97	NLO	[31]	6

and OpenLoops [35] matrix element generators. They are merged with the SHERPA parton shower [36] (with a matching scale of 20 GeV) using the ME+PS@NLO prescription [37]. A five-flavour scheme is used for these predictions. The NNPDF30NLO PDF set [38] is used in conjunction with a dedicated set of parton-shower-generator parameters (tune) developed by the SHERPA authors. This sample is used for the nominal unfolding of the data distributions, to compare to the cross-section measurements, and to estimate the systematic uncertainties.

A simulated sample of Z + jets production is also produced with the MADGRAPH_aMC@NLO (denoted by MG5_aMC@NLO) v2.2.2 generator [39], using matrix elements including up to four partons at leading order and employing the NNPDF30NLO PDF set, interfaced to PYTHIA v8.186 [40] to model the parton shower, using the CKKWL merging scheme [41] (with a matching scale of 30 GeV). A five-flavour scheme is used. The A14 [42] parton-shower tune is used together with the NNPDF23LO PDF set [43]. The sample is denoted by MG5_aMC+PY8 CKKWL and is used to provide cross-checks of the systematic uncertainty in the unfolding and to model the small $Z \to \tau\tau$ background. In addition, a MG5_aMC@NLO sample with matrix elements for up to two jets and with parton showers beyond this, employing the NNPDF30NLO PDF set and interfaced to PYTHIA v8.186 to model the parton shower, is generated using the FxFx merging scheme [44] (with a matching scale of 25 GeV [45]) and is denoted by MG5_aMC+PY8 FxFx. This sample also uses a five-flavour scheme and the A14 parton-shower tune with the NNPDF23LO PDF set. Both MG5_aMC@NLO samples are used for comparison with the unfolded cross-section measurements.

The measured cross sections are also compared to predictions from the leading-order matrix element generator ALPGEN v2.14 [46] interfaced to PYTHIA v6.426 [47] to model the parton shower, denoted by ALPGEN+PY6, using the PERUGIA2011C [48] parton-shower tune and the CTEQ6L1 PDF set [49]. A four-flavour scheme is used. Up to five additional partons are modelled by the matrix elements merged with the MLM prescription [46] (with a matching scale of 20 GeV). The matrix elements for the production of $Z + b\bar{b}$ and $Z + c\bar{c}$ events are explicitly included and a heavy-flavour overlap procedure is used to remove the double counting of heavy quarks from gluon splitting in the parton shower.

The Z-boson samples are normalised to the NNLO prediction calculated with the Fewz 3.1 program [24–27] with CT10NNLO PDFs [50].

Contributions from the top-quark, single-boson, and diboson components of the background (described in Sect. 5) are estimated from the following Monte Carlo samples. Samples of top-quark pair and single top-quark production are generated at NLO with the POWHEG-Box generator [51–53] [versions v2 (r3026) for top-quark pairs and v1 for single top quarks (r2556 and r2819 for t-and Wt-channels, respectively)] and PYTHIA v6.428 (PERUGIA2012 tune [48]). Samples with enhanced or suppressed additional

radiation are generated with the PERUGIA2012RADHI/LO tunes [48]. An alternative top-quark pair sample is produced using the MG5_aMC@NLO generator interfaced with Herwig++ v2.7.1 [39,54], using the UE- EE- 5 tune [55]. The samples are normalised to the cross section calculated at NNLO+NNLL (next-to-next-to-leading log) with the Top++2.0 program [28].

The W-boson backgrounds are modelled using the MG5_aMC+PY8 CKKWL v2.2.2 generator, interfaced to PYTHIA v8.186 and are normalised to the NNLO values given in Table 1. Diboson processes with fully leptonic and semileptonic decays are simulated [56] using the SHERPA v2.1.1 generator with the CT10NLO PDF set. The matrix elements contain the doubly resonant WW, WZ and ZZ processes, and all other diagrams with four electroweak vertices. They are calculated for one or zero additional partons at NLO and up to three additional partons at LO and merged with the SHERPA parton shower using the ME+PS@NLO prescription.

Events involving semileptonic decays of heavy quarks, hadrons misidentified as leptons, and, in the case of the electron channel, electrons from photon conversions are referred to collectively as "multijet events". The multijet background was estimated using data-driven techniques, as described in Sect. 5.

Multiple overlaid pp collisions are simulated with the soft QCD processes of PYTHIA v.8.186 using the A2 tune [57] and the MSTW2008LO PDF set [58]. All Monte Carlo samples are reweighted so that the pile-up distribution matches that observed in the data.

3.3 Fixed-order predictions

In addition to these Monte Carlo samples, parton-level fixed-order predictions at NLO are calculated by the BLACKHAT+SHERPA collaboration for the production of Z bosons with up to four partons [59,60]. The BLACKHAT+SHERPA predictions use the CT14 PDF set [61] including variations of its eigenvectors at the 68% confidence level, rescaled from 90% confidence level using a factor of 1/1.645. The nominal predictions use a factorisation and renormalisation scale of $H_{\mathrm{T}}/2$ with uncertainties derived from the envelope of a common variation of the scales by factors of 0.5, $1/\sqrt{2}$, $\sqrt{2}$, and 2. The effects of PDF and scale uncertainties range from 1 to 4% and from 0.1 to 10%, respectively, for the cross sections of Z-boson production in association with at least one to four partons, and are included in the predictions which are provided by the BLACKHAT+SHERPA authors for the fiducial phase space of this analysis. Since these predictions are defined before the decay leptons emit photons via final-state radiation (Born-level FSR), corrections to the dressed level (where all photons found within a cone of size $\Delta R = 0.1$ of the lepton from the decay of the Z boson are included) are derived from MG5_aMC+PY8 CKKWL, separately for each kinematic observable used to measure cross sections, with associated systematic uncertainties obtained by comparing to the ALPGEN+PY6 generator. This correction is needed in order to match the prediction to the lepton definition used in the measurements. The average size of these corrections is approximately -2%. To bring the prediction from parton to particle level, corrections for the non-perturbative effects of hadronisation and the underlying event are also calculated separately for each observable using the SHERPA v2.2 generator by turning on and off in the simulation both the fragmentation and the interactions between the proton remnants. The net size of the corrections is up to approximately 10% at small values of $p_{\mathrm{T}}^{\mathrm{jet}}$ and vanishes for large values of $p_{\mathrm{T}}^{\mathrm{jet}}$. An uncertainty of approximately 2% for this correction is included in the total systematic uncertainty of the prediction.

Calculations of cross sections at NNLO QCD have recently become available [3–6]. In this paper, the results are compared to the calculation, denoted by $Z+ \geq 1$ jet $\mathrm{N_{jetti}}$ NNLO [3,4], which uses a new subtraction technique based on *N-jettiness* [62] and relies on the theoretical formalism provided in soft-collinear effective theory. The predictions, which are provided by the authors of this calculation for the fiducial phase space of this analysis, use a factorisation and renormalisation scale of $\sqrt{m_{\ell\ell}^2 + \sum \left(p_{\mathrm{T}}^{\mathrm{jet}}\right)^2}$ (where $m_{\ell\ell}$ is the invariant mass of the dilepton system) and the CT14 PDF set. The QCD renormalisation and factorisation scales were jointly varied by a common factor of two, and are included in the uncertainties. Non-perturbative and FSR corrections and their associated uncertainties as discussed above are also included in the predictions.

4 Event selection

Electron- and muon-candidate events are selected using triggers which require at least one electron or muon with transverse momentum thresholds of $p_{\mathrm{T}} = 24\,\mathrm{GeV}$ or 20 GeV, respectively, with some isolation requirements for the muon trigger. To recover possible efficiency losses at high momenta, additional electron and muon triggers which do not make any isolation requirements are included with thresholds of $p_{\mathrm{T}} \geq 60\,\mathrm{GeV}$ and $p_{\mathrm{T}} = 50\,\mathrm{GeV}$, respectively. Candidate events are required to have a primary vertex, defined as the vertex with the highest sum of track p_{T}^2, with at least two associated tracks with $p_{\mathrm{T}} > 400\,\mathrm{MeV}$.

Electron candidates are required to have $p_{\mathrm{T}} > 25\,\mathrm{GeV}$ and to pass "medium" likelihood-based identification requirements [63,64] optimised for the 2015 operating conditions, within the fiducial region of $|\eta| < 2.47$, excluding candidates in the transition region between the barrel and endcap electromagnetic calorimeters, $1.37 < |\eta| < 1.52$. Muons

are reconstructed for $|\eta| < 2.4$ with $p_{\mathrm{T}} > 25\,\mathrm{GeV}$ and must pass "medium" identification requirements [65] also optimised for the 2015 operating conditions. At least one of the lepton candidates is required to match the lepton that triggered the event. The electrons and muons must also satisfy p_{T}-dependent cone-based isolation requirements, using both tracking detector and calorimeter information (described in Refs. [66,67], respectively). The isolation requirements are tuned so that the lepton isolation efficiency is at least 90% for $p_{\mathrm{T}} > 25\,\mathrm{GeV}$, increasing to 99% at 60 GeV. Both the electron and muon tracks are required to be associated with the primary vertex, using constraints on the transverse impact parameter significance $|d_0|/\Delta d_0$, where d_0 is the transverse impact parameter and Δd_0 is its uncertainty, and on the longitudinal impact parameter z_0 corrected for the reconstructed position of the primary vertex. The transverse impact parameter significance is required to be less than five for electrons and three for muons, while the absolute value of the corrected z_0 multiplied by the sine of the track polar angle is required to be less than 0.5 mm.

Jets of hadrons are reconstructed with the anti-k_t algorithm [68] with radius parameter $R = 0.4$ using topological clusters of energy deposited in the calorimeters [69]. Jets are calibrated using a simulation-based calibration scheme, followed by in situ corrections to account for differences between simulation and data [70]. In order to reduce the effects of pile-up contributions, jets with pseudorapidity $|\eta| < 2.4$ and $p_{\mathrm{T}} < 60$ GeV are required to have a significant fraction of their tracks with an origin compatible with the primary vertex, as defined by the jet vertex tagger algorithm [71]. In addition, the expected average energy contribution from pile-up clusters is subtracted according to the η–ϕ catchment area of the jet [72]. Jets used in the analysis are required to have p_{T} greater than 30 GeV and rapidity $|y| < 2.5$.

The overlap between leptons and jets is removed in a two-step process. The first step removes jets closer than $\Delta R = 0.2$ to a selected electron, and jets closer than $\Delta R = 0.2$ to a selected muon, if they are likely to be reconstructed from photons radiated by the muon. In a second step, electrons and muons are discarded if they are located closer than $\Delta R = 0.4$ to a remaining selected jet. This requirement effectively removes events with leptons and jets which are not reliably simulated in the Monte Carlo simulation.

Events containing a Z-boson candidate are selected by requiring exactly two leptons of the same flavour but of opposite charge with dilepton invariant mass in the range $71 < m_{\ell\ell} < 111\,\mathrm{GeV}$. The expected and observed numbers of Z-boson candidates selected for each inclusive jet multiplicity, for $N_{\mathrm{jets}} \geq 0 - 7$, are summarised in Table 2, separately for the $Z \to e^+e^-$ and the $Z \to \mu^+\mu^-$ channels. The background evaluation that appears in this table is discussed in Sect. 5. After all requirements, 248,816 and 311,183 $Z+ \geq 1$ jet events are selected in the electron and muon channels, respectively.

4.1 Correction factors and related systematic uncertainties

Some of the object and event selection efficiencies as well as the energy and momentum calibrations modelled by the simulation must be corrected with simulation-to-data correction factors to better match those observed in the data. These corrections and their corresponding uncertainties fall into the following two categories: dependent and not dependent on lepton flavour.

The corrections and uncertainties specific to each leptonic final state ($Z \to e^+e^-$ and $Z \to \mu^+\mu^-$) are as follows:

- **Trigger:** The lepton trigger efficiency is estimated in simulation, with a separate data-driven analysis performed to obtain the simulation-to-data trigger correction factors and their corresponding uncertainties [21].
- **Lepton reconstruction, identification, and isolation:** The lepton selection efficiencies as determined from simulation are also corrected with simulation-to-data correction factors, with corresponding uncertainties [64,65].
- **Energy, momentum scale/resolution:** Uncertainties in the lepton calibrations are estimated [65] because they can cause a change of acceptance because of migration of events across the p_{T} threshold and $m_{\ell\ell}$ boundaries.

The corrections and uncertainties common to the electron and muon final states are as follows:

- **Jet energy scale and resolution**: Uncertainties in the jet energy-scale calibration and resolution have a significant impact on the measurements, especially for the higher jet multiplicities. The jet energy-scale calibration is based on 13 TeV simulation and on in situ corrections obtained from data [70]. The uncertainties are estimated using a decorrelation scheme, resulting in a set of 19 independent parameters which cover all of the relevant calibration uncertainties. The jet energy scale is the dominant systematic uncertainty for all bins with at least one jet. The jet energy-resolution uncertainty is derived by oversmearing the jet energy in the simulation and using the symmetrised variations as the uncertainty.
- **Jet vertex tagger**: The modelling of the output variable from the jet vertex tagger is validated using data events where the Z boson recoils against a jet. A percent-level correction is derived and its statistical and systematic uncertainties are used as additional uncertainties in the efficiency to select jets from the primary vertex [71].
- **Pile-up**: The imperfect modelling of the effects of pile-up leads to acceptance changes at the percent level for different jet multiplicities. To assess this uncertainty, the

Table 2 Fraction of signal and background processes in % in the final selection and expected and observed numbers of events for the various inclusive jet multiplicities considered in the electron (top) and muon (bottom) channels

	+ ≥ 0 jets	+ ≥ 1 jets	+ ≥ 2 jets	+ ≥ 3 jets	+ ≥ 4 jets	+ ≥ 5 jets	+ ≥ 6 jets	+ ≥ 7 jets
Electron channel								
$Z \to e^+e^-$ (%)	99.3	97.6	93.9	90.3	87.3	85.2	83.3	81.2
Top quark (%)	0.2	1.2	3.8	6.5	8.6	9.7	10.5	11.6
Diboson (%)	0.2	0.8	1.6	2.4	3.4	4.4	5.5	6.6
$Z \to \tau^+\tau^-$ (%)	<0.1	<0.1	<0.1	<0.1	<0.1	<0.1	<0.1	<0.1
$W \to e\nu$ (%)	<0.1	<0.1	<0.1	<0.1	<0.1	<0.1	<0.1	<0.1
Multijet (%)	0.2	0.4	0.6	0.7	0.7	0.7	0.7	0.7
Expected	1,327,900	239,500	57,310	14,080	3637	978	252	63
Observed	1,347,900	248,816	59,998	14,377	3587	898	217	48
Muon channel								
$Z \to \mu^+\mu^-$ (%)	99.3	97.5	94.0	90.7	88.3	86.7	84.8	84.6
Top quark (%)	0.2	1.1	3.6	6.0	7.7	8.1	8.7	7.7
Diboson (%)	0.2	0.7	1.6	2.4	3.4	4.5	5.9	7.0
$Z \to \tau^+\tau^-$ (%)	<0.1	<0.1	<0.1	<0.1	<0.1	<0.1	<0.1	<0.1
$W \to \mu\nu$ (%)	<0.1	<0.1	<0.1	<0.1	<0.1	<0.1	<0.1	<0.1
Multijet (%)	0.3	0.6	0.9	0.9	0.7	0.7	0.7	0.7
Expected	1,693,000	300,600	71,230	17,740	4523	1187	307	76
Observed	1,708,602	311,183	74,510	17,865	4387	1081	240	57

average number of interactions per bunch crossing $\langle\mu\rangle$ is varied in simulation so that the behaviour of variables sensitive to pile-up matches that observed in data.

- **Luminosity**: The cross sections have a 2.1% uncertainty from the measurement of the integrated luminosity, which is derived, following a methodology similar to that detailed in Refs. [73,74], from a calibration of the luminosity using x–y beam-separation scans performed in August 2015.

5 Background estimation

Contributions from the electroweak (single boson and diboson) and top-quark (single top-quark and top-quark pair) components of the background are estimated using the Monte Carlo samples described in Sect. 3 with corresponding uncertainties as listed in Table 1. Contributions from multijet events are evaluated with data-driven techniques as described below. A summary of the composition and relative importance of the backgrounds in the candidate Z + jets events is given in Table 2. The overall purity of the Z + jets selections (fraction of signal events in the final selection) ranges from 99% in the inclusive sample to 80–85% in the ≥ 7 jets bin.

5.1 Top-quark and electroweak backgrounds

The dominant contribution to the background at high jet multiplicities comes from $t\bar{t}$ production, with the subsequent leptonic decays of the W bosons originating from the top quarks and is evaluated from simulation. An overall uncertainty of 6%, corresponding to the PDF and scale variations on the theoretical predictions of the inclusive cross sections, is assigned (see Table 1). The $t\bar{t}$ background estimate is validated through a cross-section measurement of $t\bar{t}$ production in the dilepton channel at $\sqrt{s} = 13\,\text{TeV}$ [75] as a function of the jet multiplicity, and the modelling of the additional parton radiation in $t\bar{t}$ events by POWHEG+PY6 was found to be in good agreement with this measurement. In addition, a systematic uncertainty in the modelling of the shape of the distributions is derived by modifying the parton-shower intensity in the nominal simulation sample and by comparing to the predictions from the alternative generator MG5_aMC@NLO+Herwig++ (both listed in Table 1). The small contribution from single-top-quark events is also estimated using POWHEG+PY6 samples and assigned a 6% uncertainty.

Diboson production in leptonic and semileptonic final states with at least two leptons of the same flavour constitutes a co-dominant background for high jet multiplicities (see Table 2). The production of WZ bosons in association with jets at $\sqrt{s} = 13\,\text{TeV}$ was found to be well modelled by

the SHERPA 2.1 generator [76]. A 6% uncertainty, again corresponding to PDF and scale variations on the predictions, is assessed. Since in Ref. [76] the measurement is limited by the statistical precision for dibosons $+ \geq 4$ jets (resulting in ≥ 6 hadronic jets for semileptonic diboson decays), an additional systematic uncertainty of 50% in the normalisation of the diboson background is added for $Z+ \geq 6$ jets.

Minor background contributions also arise from single-W-boson production decaying to leptonic final states and from single-Z-boson production in the $Z \to \tau^+\tau^-$ process, both estimated with simulation and assigned a 5% uncertainty (as given in Table 1).

5.2 Multijet background

Background-enriched data control regions are used to estimate the multijet contribution in both the electron and muon channels. They are constructed by loosening the lepton identification and isolation requirements. Templates are built from the dilepton invariant mass distribution, a variable that shows discrimination between multijet background and other processes in regions of its kinematic range, but is largely uncorrelated with the variables used to build the multijet control regions. The templates are subsequently normalised to events passing the Z-boson signal selection.

In the electron channel, the multijet templates are built for each jet multiplicity from events with two same-charge leptons with no isolation requirement, whose identification criteria are looser than those of the signal selection, which the leptons must not satisfy. In the muon channel, the control region is similarly built from events with two leptons which are selected with looser identification requirements than the signal selection and also fail the nominal isolation requirement. In both cases, dedicated triggers better suited to this purpose are used to populate the templates. The small electroweak and top-quark contamination is subtracted using simulated events.

The normalisation of the multijet template is estimated with a log-likelihood fit to the measured dilepton invariant mass distribution for the inclusive Z selection, using templates for $Z \to \ell^+\ell^-$ and for the electroweak and top-quark background derived from simulation. The fit is performed in the invariant mass windows of $52 < m_{ee} < 148\,\text{GeV}$ and $40 < m_{\mu\mu} < 80\,\text{GeV}$ for the electron and muon channels, respectively, in order to benefit from the larger multijet contribution in the mass sidebands. The normalisation of the multijet template is allowed to float freely while the remaining non-multijet templates are constrained to be within 6% of the predicted cross sections for these processes as given in Table 1. The multijet fractions are evaluated separately for each jet multiplicity, except for very high jet multiplicities where the templates are statistically limited, and so these fractions are taken from the estimates of the ≥ 5 jets and ≥ 4 jets bins in the electron and muon channels, respectively.

The systematic uncertainties on the multijet background are derived by varying the mass range and bin width of the nominal fit, using the lepton transverse impact parameter d_0 as the fitting variable instead of the invariant mass, using alternative simulation samples for the templates, allowing the normalisations of the non-multijet components to vary independently or within a wider range, and varying the lepton resolution and energy/momentum scales. In addition, given the multiple sources of multijet background in the electron channel, an alternative template is constructed by requiring that the electrons fail to meet an isolation criterion instead of failing to meet the nominal signal selection electron identification criterion.

The resulting estimated multijet fractions in each jet multiplicity bin are given in Table 2. Their corresponding total uncertainties are dominated by their systematic components. These systematic components are approximately 70% of the multijet fraction as estimated in the electron and muon channels.

6 Kinematic distributions

The level of agreement between data and predictions is evaluated from the comparison of kinematic distributions. Figure 1, which presents the dilepton mass for the $Z+ \geq 1$ jet topology and the inclusive jet multiplicity, shows how well the SHERPA 2.2 and MG5_aMC+PY8 CKKWL predictions agree with data. The uncertainty bands shown in these distributions include the statistical uncertainties due to the simulation sample sizes, the event-selection uncertainties described in Sect. 4.1 (omitting the common 2.1% luminosity uncertainty), and the background normalisation uncertainties described in Sect. 5.

7 Unfolding of detector effects

The cross-section measurements presented in this paper are performed within the fiducial acceptance region defined by the following requirements:

- $p_{\text{T}}^{\ell} > 25\,\text{GeV}$, $|\eta^{\ell}| < 2.5$
- $p_{\text{T}}^{\text{jet}} > 30\,\text{GeV}$, $|y^{\text{jet}}| < 2.5$
- $\Delta R(\ell, \text{jet}) > 0.4$
- $71 < m_{\ell\ell} < 111\,\text{GeV}$.

The cross sections are defined at particle ("truth") level, corresponding to dressed electrons and muons from the Z bosons. The particle level also includes jets clustered using

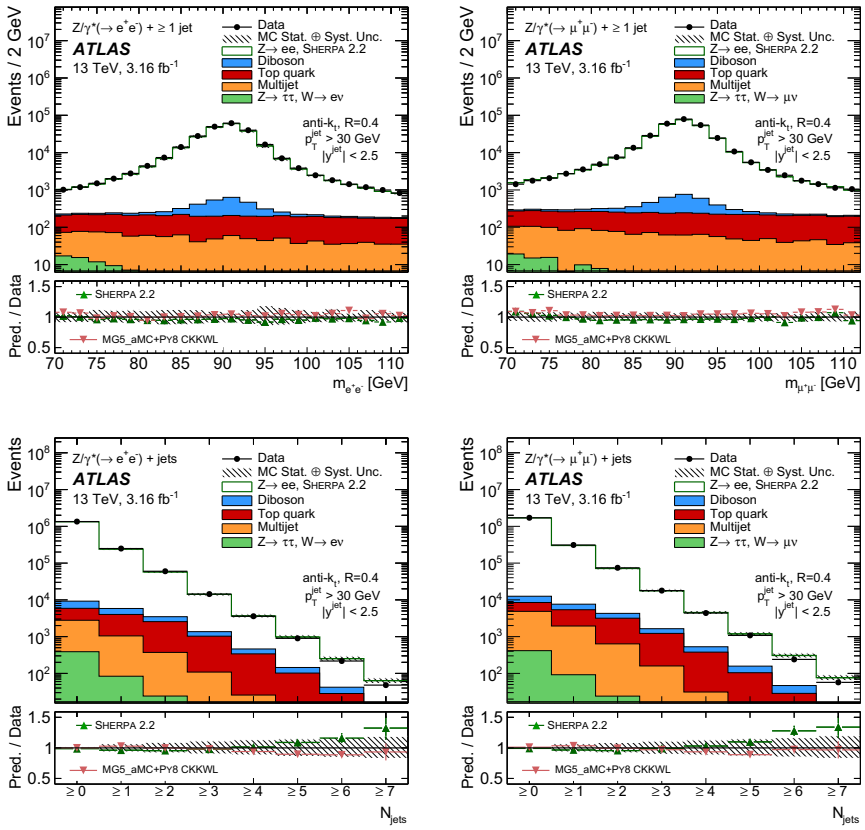

Fig. 1 Dilepton invariant mass for $Z+\geq 1$ jet (*top*) and inclusive jet multiplicity (*bottom*) in the $Z(\rightarrow e^+e^-)+$ jets (*left*) and the $Z(\rightarrow \mu^+\mu^-)+$ jets (*right*) channels. All backgrounds and the signal samples are stacked to produce the figures. Systematic uncertainties for the signal and background distributions are combined in the *hatched band*, and the statistical uncertainty is shown on the *data points*. The uncertainty in the luminosity and the theory uncertainty in the signal prediction are not included in the *uncertainty band*

the anti-k_t algorithm [68] with radius parameter $R = 0.4$ for final-state particles with decay length $c\tau > 10$ mm, excluding the dressed Z-boson decay products.

The fiducial cross sections are estimated from the reconstructed kinematic observables: jet multiplicity, $p_{\mathrm{T}}^{\mathrm{jet}}$ for different jet multiplicities, y^{jet}, $\Delta\phi_{\mathrm{jj}}$, m_{jj}, and H_{T}, for events that pass the selection described in Sect. 4. The expected background components as described in Sect. 5 are subtracted from the distributions in data. A variable-width binning of these observables is used, such that the purity is at least 50% in each bin and the size of the statistical uncertainty in most of the bins remains below 10%.

An iterative Bayesian unfolding technique [77], as implemented in the RooUnfold package [78], is used to unfold the measurements to the particle level, thereby accounting for detector effects related to inefficiencies, resolution, and systematic biases in the central values of the kinematic variables describing both the leptons and the jets. The iterative unfolding technique updates the initial estimators for the generated ("truth") distribution in consecutive steps, using Bayes' theorem in each iteration to derive an unfolding matrix from the initial response matrix (which relates truth and reconstructed distributions of given observables) and the current truth estimator.

The response matrices are constructed using the SHERPA 2.2 $Z(\rightarrow \ell^+\ell^-) +$ jets samples. SHERPA 2.2 is also used to derive the initial truth estimator. In order to enter the response matrix, events must pass the Z-boson selection at generator level and at detector level and contain the number of jets required by the preselection for a given observable at both generator and detector level. Reconstructed jets are required to match the corresponding generator-level jets within a cone of size $\Delta R = 0.4$ for all distributions except global quantities such as the jet multiplicity and H_{T}. A given bin (i, j) in the response matrix therefore corresponds to the probability that a true jet object in bin j is reconstructed in bin i of the distribution. Figure 2 illustrates two examples of response matrices. The resulting ratios of detector-level to truth-level event yields are typically 0.65 and 0.8 for the electron and muon channels, respectively.

The background-subtracted data are corrected for the expected fraction of events with reconstructed objects unmatched to any generator object before entering the iterative unfolding. The number of iterations used for the iterative unfolding of each distribution (two) is chosen by unfolding the SHERPA 2.2 samples reweighted to data and comparing to the generated reweighted distribution. The unfolded event yields are divided by the integrated luminosity of the data sample and the bin width of the distribution in question to provide the final fiducial cross sections. The final result is given by

$$\sigma_i = \frac{1}{\epsilon_i L} \sum_j U_{ij} N_j^{\mathrm{data}} \left(1 - f_j^{\mathrm{unmatched}}\right), \tag{1}$$

where L is the integrated luminosity, ϵ_i is the reconstruction efficiency for truth bin i, N_j^{data} corresponds to the number of events observed in data in reconstructed bin j and $f_j^{\mathrm{unmatched}}$ is its fraction of unmatched events calculated from simulation, and U_{ij} is the unfolding matrix calculated after two iterations, using the updated prior from the first iteration and the response matrix.

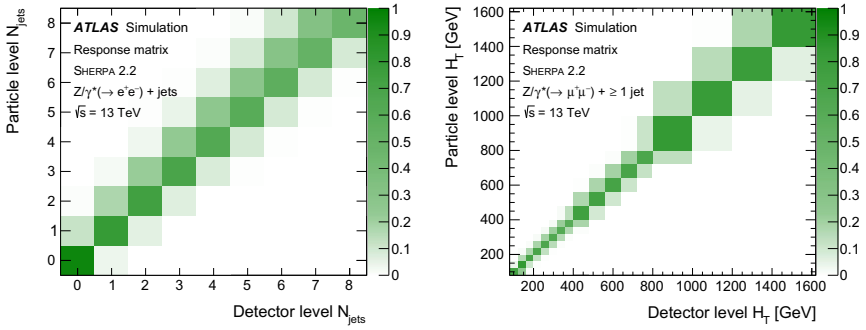

Fig. 2 Response matrices corresponding to the exclusive jet multiplicity for $Z +$ jets events in the electron channel (*left*) and to the H_{T} for $Z+ \geq 1$ jet events in the muon channel (*right*). The sum of the entries in each row is normalised to unity. Both matrices are obtained from SHERPA 2.2

Table 3 Measured fiducial cross sections in the electron and muon channels for successive inclusive jet multiplicities. The total statistical and systematic uncertainties are given, along with the uncertainty in the luminosity

Jet multiplicity	Measured cross section ± (stat.) ± (syst.) ± (lumi.) [pb]							
	$Z \rightarrow ee$				$Z \rightarrow \mu\mu$			
≥0 jets	743±	1±	24±	16	738±	1±	23±	16
≥1 jets	116.6±	0.3±	9.9±	2.5	115.7±	0.2±	9.7±	2.5
≥2 jets	27.1±	0.1±	2.9±	0.6	27.0±	0.1±	2.8±	0.6
≥3 jets	6.20±	0.06±	0.82±	0.14	6.22±	0.05±	0.83±	0.14
≥4 jets	1.49±	0.03±	0.23±	0.04	1.48±	0.03±	0.23±	0.04
≥5 jets	0.357±	0.013±	0.069±	0.009	0.354±	0.012±	0.068±	0.009
≥6 jets	0.082±	0.006±	0.019±	0.002	0.076±	0.005±	0.019±	0.002
≥7 jets	0.0180±	0.0029±	0.0051±	0.0005	0.0166±	0.0027±	0.0060±	0.0004

7.1 Systematic uncertainties associated with the unfolding procedure

The limited size of a simulation sample can create biases in the distributions. Systematic uncertainties account for possible residual biases in the unfolding procedure due to, e.g. modelling of the hadronisation in the simulation, migrations into other kinematic distributions not explicitly part of the unfolding, or the finite bin width used in each distribution. The following uncertainties arise from the unfolding procedure.

- The statistical uncertainties of the response matrices derived from SHERPA 2.2 are propagated to the unfolded cross sections with a toy simulation method. A total of 5000 ensembles (pseudo-experiments) of unfolded samples are generated. For each sample, the number of reconstructed events in each bin is generated randomly according to a Gaussian distribution, where the mean is the nominal number of events before unfolding and the width is its corresponding statistical uncertainty. Unfolding is performed for each ensemble. The widths of resulting distributions are taken as a systematic uncertainty of the unfolding.
- The SHERPA 2.2 samples are reweighted at generator level, such that the distribution of the leading jet p_{T} at detector level matches that observed in the data. The modified SHERPA 2.2 samples are then used to unfold the data again and the variations in the resulting cross sections are used to derive a systematic uncertainty.
- An additional check is performed by unfolding reconstructed MG5_aMC+PY8 CKKWL events using SHERPA 2.2 response matrices. The residual non-closure is accounted for by an additional flat uncertainty of 3% for all distributions.

8 Results

The measured cross sections, presented in Sect. 8.1, are calculated in the electron and muon channels separately and the compatibility of the results of the two channels is evaluated.

Table 4 Relative statistical and systematic uncertainties (in %) in the measured cross sections of Z + jets production for successive inclusive jet multiplicities in the electron (top) and muon (bottom) channels

Systematic source	Relative uncertainty in $\sigma(Z(\to \ell^+\ell^-)+\geq N_{\mathrm{jets}})$ (%)							
	+ ≥ 0 jets	+ ≥ 1 jets	+ ≥ 2 jets	+ ≥ 3 jets	+ ≥ 4 jets	+ ≥ 5 jets	+ ≥ 6 jets	+ ≥ 7 jets
$Z \to e^+e^-$								
Electron trigger	0.1	0.1	0.1	0.2	0.2	0.2	0.3	0.3
Electron selection	1.2	1.6	1.8	1.9	2.3	2.7	2.9	3.8
Jet energy scale	<0.1	6.6	9.2	11.5	13.8	17.3	20.6	23.7
Jet energy resolution	<0.1	3.7	3.7	4.4	5.3	5.2	6.2	7.3
Jet vertex tagger	<0.1	1.3	2.1	2.8	3.6	4.5	5.5	6.3
Pile-up	0.4	0.2	0.1	0.2	0.2	0.1	0.4	0.8
Luminosity	2.1	2.1	2.2	2.3	2.4	2.5	2.6	2.8
Unfolding	3.0	3.0	3.0	3.0	3.0	3.1	3.1	3.2
Background	0.1	0.3	0.6	1.0	1.6	3.3	6.0	11.6
Total syst. Uncertainty	3.9	8.7	11.0	13.4	15.9	19.5	23.6	28.7
Stat. uncertainty	0.1	0.2	0.5	0.9	1.9	3.7	7.7	15.9
$Z \to \mu^+\mu^-$								
Muon trigger	0.4	0.5	0.4	0.5	0.4	0.5	0.9	0.6
Muon selection	0.8	0.9	1.0	1.0	1.0	1.5	4.2	16.6
Jet energy scale	<0.1	6.8	9.1	11.9	14.0	17.0	20.9	23.7
Jet energy resolution	<0.1	3.6	3.6	4.1	5.0	5.9	6.2	9.3
Jet vertex tagger	<0.1	1.3	2.1	3.1	3.6	4.4	5.6	6.6
Pile-up	0.4	0.1	<0.1	0.3	0.5	0.1	0.4	0.9
Luminosity	2.1	2.1	2.2	2.3	2.4	2.5	2.6	2.7
Unfolding	3.0	3.0	3.0	3.0	3.0	3.1	3.1	3.2
Background	0.2	0.4	0.6	0.9	1.7	4.0	7.4	12.9
Total syst. Uncertainty	3.8	8.7	10.8	13.6	16.0	19.4	24.6	36.3
Stat. uncertainty	0.1	0.2	0.4	0.8	1.7	3.4	7.2	16.3

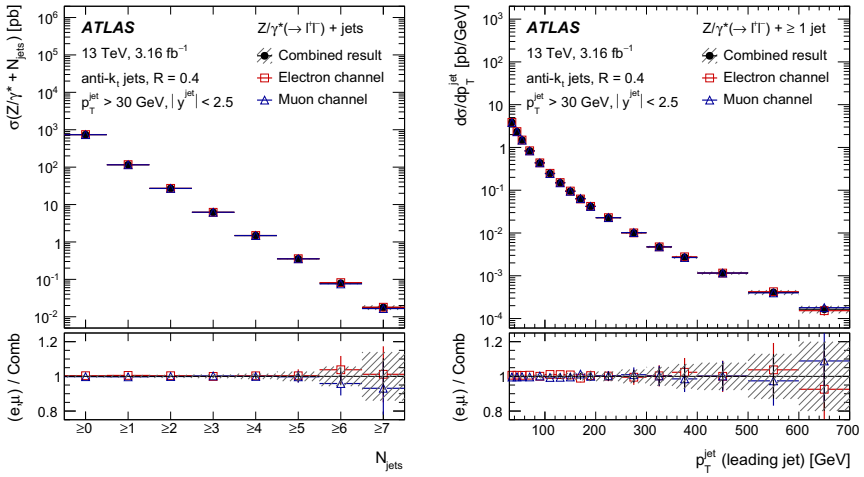

Fig. 3 Measured fiducial cross section as a function of the inclusive jet multiplicity (*left*) and the leading jet p_{T} for inclusive $Z+\geq 1$ jet events (*right*) in the electron and the muon channels and compared to their combined value. The ratios of the two measurements to the combined results are also shown in the *bottom panels*. The *error bars* indicate the statistical uncertainty, and the *hatched bands* the statistical and the flavour-uncorrelated systematic uncertainties of the combined result, added in quadrature

Table 5 Measured combined fiducial cross sections for successive inclusive jet multiplicities. The statistical, systematic, and luminosity uncertainties are given

Jet multiplicity	Measured cross section $\pm$(stat.) $\pm$(syst.) $\pm$(lumi.) [pb] $Z \to \ell\ell$
$\geq$0 jets	$740 \pm 1 \pm 23 \pm 16$
$\geq$1 jets	$116.0 \pm 0.3 \pm 9.7 \pm 2.5$
$\geq$2 jets	$27.0 \pm 0.1 \pm 2.8 \pm 0.6$
$\geq$3 jets	$6.20 \pm 0.04 \pm 0.82 \pm 0.14$
$\geq$4 jets	$1.48 \pm 0.02 \pm 0.23 \pm 0.04$
$\geq$5 jets	$0.36 \pm 0.01 \pm 0.07 \pm 0.01$
$\geq$6 jets	$0.079 \pm 0.004 \pm 0.018 \pm 0.002$
$\geq$7 jets	$0.0178 \pm 0.0019 \pm 0.0049 \pm 0.0005$

Table 6 Measured combined ratios of the fiducial cross sections for successive inclusive jet multiplicities. The statistical, systematic, and luminosity uncertainties are given

Jet multiplicity	Measured cross-section ratio $\pm$(stat.) $\pm$(syst.) $\pm$(lumi.) $Z \to \ell\ell$
$\geq$1 jets/$\geq$0 jets	$0.1568 \pm 0.0004 \pm 0.0131 \pm 0.0001$
$\geq$2 jets/$\geq$1 jets	$0.2327 \pm 0.0011 \pm 0.0093 \pm 0.0002$
$\geq$3 jets/$\geq$2 jets	$0.2299 \pm 0.0018 \pm 0.0095 \pm 0.0002$
$\geq$4 jets/$\geq$3 jets	$0.2390 \pm 0.0035 \pm 0.0094 \pm 0.0002$
$\geq$5 jets/$\geq$4 jets	$0.2397 \pm 0.0068 \pm 0.0111 \pm 0.0002$
$\geq$6 jets/$\geq$5 jets	$0.2213 \pm 0.0127 \pm 0.0123 \pm 0.0003$
$\geq$7 jets/$\geq$6 jets	$0.2240 \pm 0.0264 \pm 0.0222 \pm 0.0003$

In order to improve the precision of the measurement, these results are then combined, taking into account the correlations of the systematic uncertainties. The comparisons of the combined results to the predictions are presented in Sect. 8.2.

8.1 Results in the individual channels and the combination

The fiducial cross-section measurements in the $Z(\to e^+e^-)+$ jets and $Z(\to \mu^+\mu^-)+$ jets channels as a function of the inclusive jet multiplicities are presented in Table 3. The data statistical uncertainties are propagated through the unfolding by using pseudo-experiments. As mentioned in Sect. 7, the systematic uncertainties are propagated through the unfolding via the migration matrices and via the variation of the subtracted background. Table 4 shows the resulting total relative statistical and systematic uncertainties as well as the systematic components [lepton trigger, lepton selection, jet energy scale and resolution, jet vertex tagging, pile-up, luminosity (all described in Sect. 4.1)], unfolding (described in Sect. 7), and background (described in Sect. 5) as a function of the inclusive jet multiplicity, presented separately for the electron and muon channels. The jet energy scale is the

dominant systematic uncertainty for all bins with at least one jet.

Figure 3 shows a comparison of the electron and muon channels for the measured fiducial cross section as a function of the inclusive jet multiplicity and of the leading jet p_{T} for inclusive $Z+ \geq 1$ jet events. This figure demonstrates that the results in the electron and muon channels are compatible and hence can be combined to improve the precision of the measurement. This figure also shows the result of this combination described below.

The results from the electron and muon channels are combined at dressed level for each distribution separately: inclusive and exclusive jet multiplicities, ratio for successive inclusive jet multiplicities, leading jet p_{T} for $Z+ \geq 1, 2, 3, 4$ jet events and jet p_{T} for exclusive $Z + 1$ jet events, leading jet rapidity for inclusive $Z+ \geq 1$ jet events, H_{T}, $\Delta\phi_{\mathrm{jj}}$, and m_{jj}. A χ^2 function whose sum runs over all measurement sets (electrons and muons), measurement points, and some of the uncertainty sources, is used for the combination [79,80] and distinguishes between bin-to-bin correlated and uncorrelated sources of uncertainties, the latter comprising the statistical uncertainty of the data and the statistical unfolding uncertainty. Uncertainties specific to the lepton flavour and to the background are included in the χ^2 function, while the remaining, flavour-uncorrelated, systematic uncertainties related to jets, pile-up, luminosity, and unfolding are averaged after the combination.

8.2 Comparisons of results to predictions

The cross-section measurement for different inclusive $Z +$ jets multiplicities and their ratios obtained from the combination are found in Tables 5 and 6. Figure 4 shows the comparison of these results with the NLO QCD fixed-order calculations from BLACKHAT+SHERPA and with the predictions from SHERPA 2.2, ALPGEN+PY6, MG5_aMC+PY8 CKKWL, and MG5_aMC+PY8 FxFx. The plots show the particle-level cross section with the generator predictions normalised to the inclusive NNLO cross sections in the top panel, accompanied by the ratios of the various predictions with respect to the data in the bottom panels. Uncertainties from the parton distribution functions and QCD scale variations are included in the BLACKHAT+SHERPA predictions, as described in Sect. 3.3. A constant 5% theoretical uncertainty is used for SHERPA 2.2, ALPGEN+PY6, MG5_aMC+PY8 CKKWL, and MG5_aMC+PY8 FxFx, as described in Table 1. The

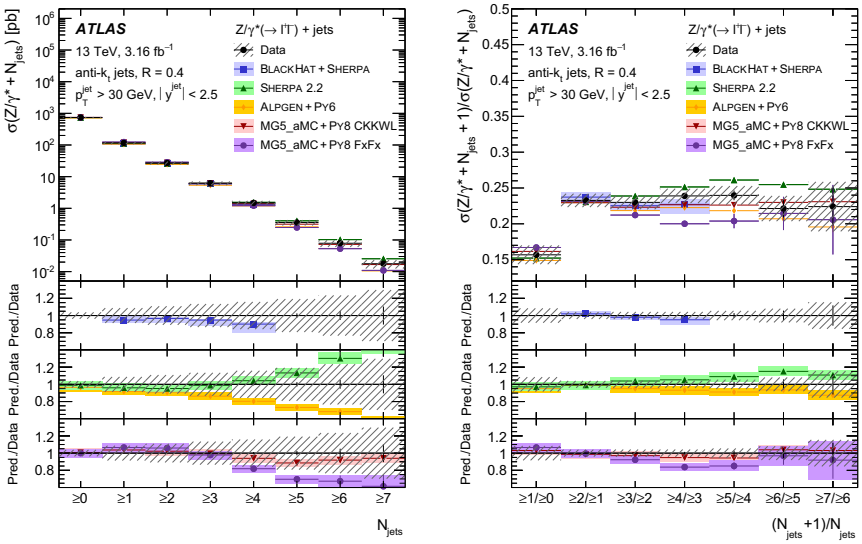

Fig. 4 Measured cross section as a function of the inclusive jet multiplicity (*left*) and ratio for successive inclusive jet multiplicities (*right*) for inclusive $Z +$ jets events. The data are compared to the predictions from BLACKHAT+SHERPA, SHERPA 2.2, ALPGEN+PY6, MG5_aMC+PY8 CKKWL, and MG5_aMC+PY8 FxFx. The *error bars* correspond to the statistical uncertainty, and the *hatched bands* to the data statistical and systematic uncertainties (including luminosity) added in quadrature. A constant 5% theoretical uncertainty is used for SHERPA 2.2, ALPGEN+PY6, MG5_aMC+PY8 CKKWL, and MG5_aMC+PY8 FxFx. Uncertainties from the parton distribution functions and QCD scale variations are included in the BLACKHAT+SHERPA predictions, as described in Sect. 3.3

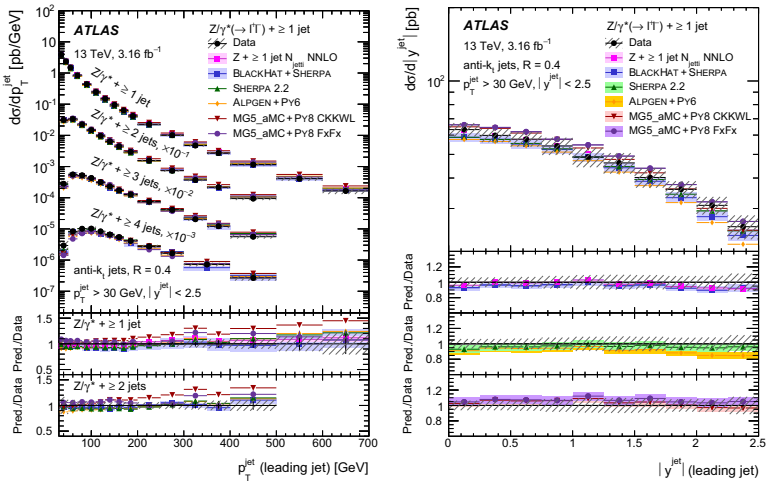

Fig. 5 Measured cross section as a function of the leading jet p_{T} for inclusive $Z+ \geq 1, 2, 3, 4$ jet events (*left*) and absolute value of the leading jet rapidity for inclusive $Z+ \geq 1$ jet events (*right*). The data are compared to the predictions from $Z+ \geq 1$ jet $\mathrm{N_{jetti}}$ NNLO, BLACKHAT+SHERPA, SHERPA 2.2, ALPGEN+PY6, MG5_aMC+PY8 CKKWL, and MG5_aMC+PY8 FxFx. The *error bars* correspond to the statistical uncertainty, and the *hatched bands* to the data statistical and systematic uncertainties (including luminosity) added in quadrature. The details of the prediction uncertainties are given in the text. For clarity, *uncertainty bands* are not shown for the Monte Carlo predictions in the *left-hand plot*. Uncertainties from the QCD scale variations for the $Z+ \geq 1$ jet $\mathrm{N_{jetti}}$ NNLO predictions are included, as described in Sect. 3.3

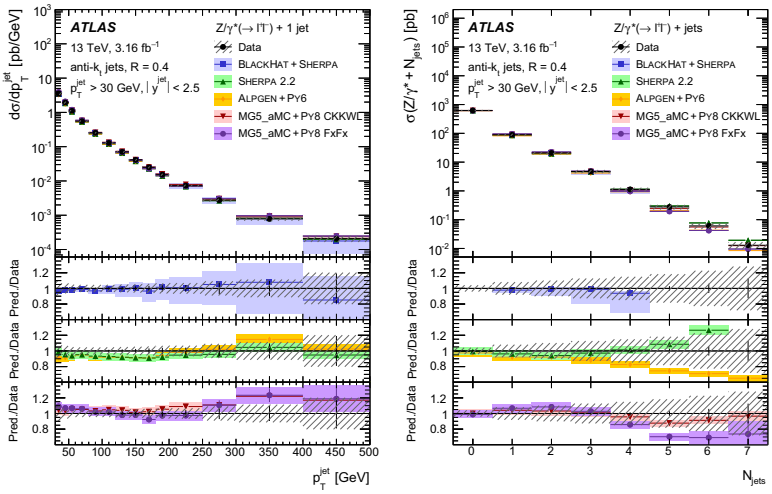

Fig. 6 Measured cross section as a function of jet p_{T} for exclusive $Z+1$ jet events (*left*) and exclusive jet multiplicity (*right*). The data are compared to the predictions from BLACKHAT+SHERPA, SHERPA 2.2, ALPGEN+PY6, MG5_aMC+PY8 CKKWL, and MG5_aMC+PY8 FxFx. The *error bars* correspond to the statistical uncertainty, and the *hatched bands* to the data statistical and systematic uncertainties (including luminosity) added in quadrature. The details of the prediction uncertainties are given in the text

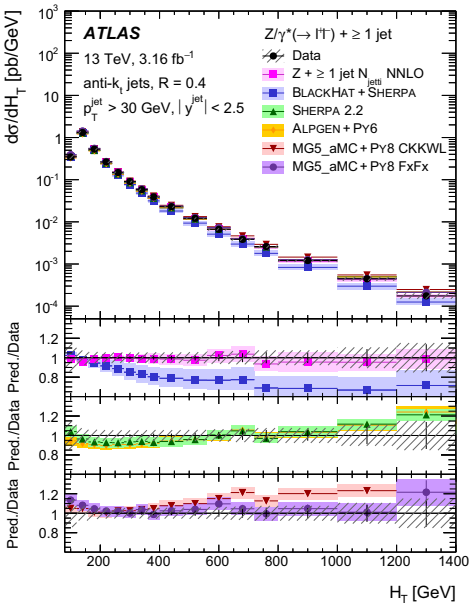

Fig. 7 Measured cross section as a function of H_T for inclusive $Z+ \geq 1$ jet events. The data are compared to the predictions from $Z+ \geq 1$ jet N_{jetti} NNLO, BLACKHAT+SHERPA, SHERPA 2.2, ALPGEN+PY6, MG5_aMC+PY8 CKKWL, and MG5_aMC+PY8 FxFx. The *error bars* correspond to the statistical uncertainty, and the *hatched bands* to the data statistical and systematic uncertainties (including luminosity) added in quadrature. The details of the prediction uncertainties are given in the text

inclusive jet multiplicity decreases logarithmically while the ratio is flat in the presence of at least one jet. The predictions are in agreement with the observed cross sections and their ratios, except for SHERPA 2.2, ALPGEN+PY6 and MG5_aMC+PY8 FxFx for high jet multiplicity, where a non-negligible fraction of the jets are produced by the parton shower.

The jet transverse momentum is a fundamental observable of the Z + jets process and probes pQCD over a wide range of scales. Moreover, understanding the kinematics of jets in events with vector bosons associated with several jets is essential for the modelling of backgrounds for other SM processes and searches beyond the SM. The leading jet p_T distribution (which is correlated with the p_T of the Z boson) in inclusive $Z+ \geq 1, 2, 3, 4$ jet events is shown in Fig. 5 and ranges up to 700 GeV. The LO generator MG5_aMC+PY8 CKKWL models a too-hard jet p_T spectrum. This feature is known from studies of LO generators in pp collisions at lower centre-of-mass energies [11], and can be interpreted as an indication that the dynamic factorisation and renormalisation scale used in the generation is not appropriate for the full jet p_T range. In contrast, the predictions from BLACKHAT+SHERPA, SHERPA 2.2, and MG5_aMC+PY8 FxFx, which are based on NLO matrix elements, are in agreement with the measured cross section within the systematic uncertainties over the full leading jet p_T range. ALPGEN+PY6 also shows good agreement with the measured data. The $Z+ \geq 1$ jet N_{jetti} NNLO prediction models the spectrum for the $Z+ \geq 1$ jet events well. Uncertainties from the QCD scale variations for the $Z+ \geq 1$ jet N_{jetti} NNLO predictions are included in the uncertainty band, as described in Sect. 3.3. For the leading jet rapidity distribution in inclusive $Z+ \geq 1$ jet events, also shown in this figure, all predictions show good agreement with the measured data within the uncertainties.

The exclusive jet p_T distribution probes the validity of $Z + 1$ jet predictions at increasing QCD scales represented by the jet p_T in the presence of a jet veto at a constant low scale; for a jet p_T range of several hundred GeV, accessible with the current data set, the jet scale is of order ten times larger than the veto scale (30 GeV). Figure 6 demonstrates that all predictions studied are consistent with the data within systematic uncertainties over the full jet p_T range (up to 500 GeV). This figure also shows the measured cross section as a function of the exclusive jet multiplicity, which decreases logarithmically. Similar trends as for the inclusive jet multiplicity (Fig. 4) are observed.

Quantities based on inclusive p_T sums of final-state objects, such as H_T, the scalar p_T sum of all visible objects in the final state, are often employed in searches for physics beyond the Standard Model, to enrich final states resulting from the decay of heavy particles. The values H_T or $H_T/2$ are also commonly used choices for scales for higher-order perturbative QCD calculations. Large values for this quantity can result either from a small number of very energetic particles or from a large number of less energetic particles. Figure 7 shows the measured cross sections as a function of the H_T distribution (up to 1400 GeV) in inclusive $Z+ \geq 1$ jet events. The predictions from SHERPA 2.2, ALPGEN+PY6 and MG5_aMC+PY8 FxFx describe well the H_T distribution. The prediction from MG5_aMC+PY8 CKKWL describes well the turn-over in the softer part of the H_T spectrum, but overestimates the contribution at large values of H_T, in line with the overestimate of the cross sections for hard jets. The fixed-order $Z+ \geq 1$ jet prediction from BLACKHAT+SHERPA underestimates the cross section for values of $H_T > 300$ GeV, as observed in similar measurements at lower centre-of-mass energies [11,81], due to the missing contributions from events with higher parton multiplicities, which for large values of H_T constitute a substantial portion of the data. Agreement is recovered by adding higher orders

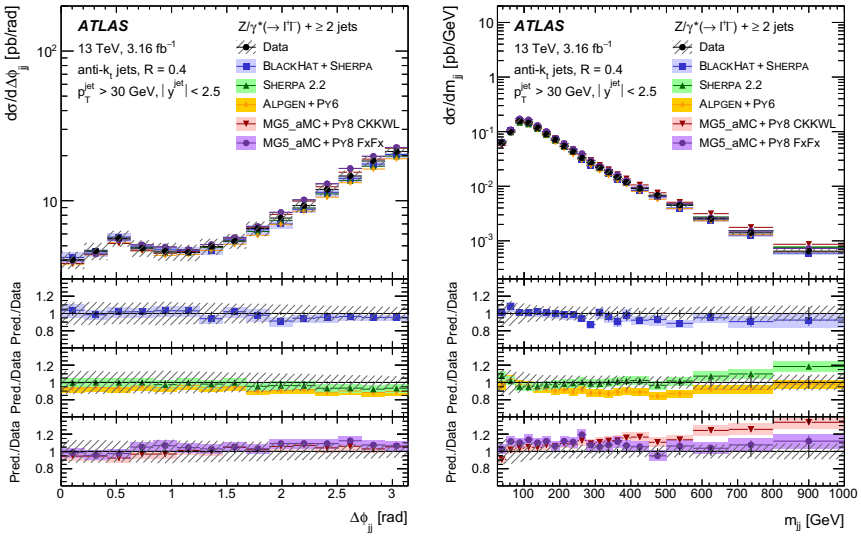

Fig. 8 Measured cross section as a function of $\Delta\phi_{\mathrm{jj}}$ (*left*) and m_{jj} (*right*) for inclusive $Z+\geq 2$ jet events. The data are compared to the predictions from BLACKHAT+SHERPA, SHERPA 2.2, ALPGEN+PY6, MG5_aMC+PY8 CKKWL, and MG5_aMC+PY8 FxFx. The *error bars* correspond to the statistical uncertainty, and the *hatched bands* to the data statistical and systematic uncertainties (including luminosity) added in quadrature. The details of the prediction uncertainties are given in the text

in perturbative QCD, as demonstrated by the good description of H_{T} by $Z+\geq 1$ jet $\mathrm{N_{jetti}}$ NNLO.

Angular relations between the two leading jets and the dijet mass are frequently used to separate either heavier SM particles or beyond-SM physics from the $Z+$ jets process. Figure 8 shows the differential cross section as a function of azimuthal angular difference between the two leading jets for $Z+\geq 2$ jet events, $\Delta\phi_{\mathrm{jj}}$. The tendency of the two jets to be back-to-back in the transverse plane is well modelled by all predictions. This figure also shows the measured cross sections as a function of the invariant mass m_{jj} of the two leading jets for $Z+\geq 2$ jet events. The shape of the dijet mass is modelled well by BLACKHAT+SHERPA, SHERPA 2.2, ALPGEN+PY6, and MG5_aMC+PY8 FxFx, whereas MG5_aMC+PY8 CKKWL shows a harder spectrum.

9 Conclusion

Proton–proton collision data at $\sqrt{s}=13\,\mathrm{TeV}$ from the LHC, corresponding to a total integrated luminosity of $3.16\,\mathrm{fb}^{-1}$, have been analysed by the ATLAS collaboration to study events with Z bosons decaying to electron or muon pairs, produced in association with one or more jets. The fiducial production cross sections for $Z+\geq 0$–7 jets have been measured, within the acceptance region defined by $p_{\mathrm{T}}^{\ell}>25\,\mathrm{GeV}$, $|\eta^{\ell}|<2.5$, $71<m_{\ell\ell}<111\,\mathrm{GeV}$, $p_{\mathrm{T}}^{\mathrm{jet}}>30\,\mathrm{GeV}$, $|y^{\mathrm{jet}}|<2.5$, and $\Delta R(\ell,\mathrm{jet})>0.4$, with a precision ranging from 4 to 30%. Ratios of cross sections for successive jet multiplicities and cross-section measurements as a function of different key variables such as the jet multiplicities, jet p_{T} for exclusive $Z+1$ jet events, leading jet p_{T} for $Z+\geq 1, 2, 3, 4$ jet events, leading jet rapidity for $Z+\geq 1$ jet events, H_{T}, $\Delta\phi_{\mathrm{jj}}$ and m_{jj} have also been derived.

The measurements have been compared to fixed-order calculations at NLO from BLACKHAT+SHERPA and at NNLO from the $Z+\geq 1$ jet $\mathrm{N_{jetti}}$ NNLO calculation, and to predictions from the generators SHERPA 2.2, ALPGEN+PY6, MG5_aMC+PY8 CKKWL, and MG5_aMC+PY8 FxFx. In general, the predictions are in good agreement with the observed cross sections and cross-section ratios within the uncertainties. Distributions which are dominated by a single jet multiplicity are modelled well by fixed-order NLO calculations, even in the presence of a jet veto at a low scale. The ME+PS generator MG5_aMC+PY8 CKKWL, which is based on LO matrix elements, models a too-hard jet spectrum, as observed in $\sqrt{s}=7\,\mathrm{TeV}$ pp collisions. It however models well the inclusive jet multiplicity distribution over the full multiplicity range. The modelling of the jet p_{T} and related

observables is significantly improved by the ME+PS@NLO generators SHERPA 2.2 and MG5_aMC+PY8 FxFx, which use NLO matrix elements for up to two additional partons. The recent $Z+ \geq 1$ jet N_{jetti} NNLO predictions describe well key distributions such as the leading jet p_T and H_T. The results presented in this paper provide essential input for the further optimisation of the Monte Carlo generators of Z+ jets production and constitute a powerful test of perturbative QCD for processes with a higher number of partons in the final state.

Acknowledgements We thank CERN for the very successful operation of the LHC, as well as the support staff from our institutions without whom ATLAS could not be operated efficiently. We acknowledge the support of ANPCyT, Argentina; YerPhI, Armenia; ARC, Australia; BMWFW and FWF, Austria; ANAS, Azerbaijan; SSTC, Belarus; CNPq and FAPESP, Brazil; NSERC, NRC and CFI, Canada; CERN; CONICYT, Chile; CAS, MOST and NSFC, China; COLCIENCIAS, Colombia; MSMT CR, MPO CR and VSC CR, Czech Republic; DNRF and DNSRC, Denmark; IN2P3-CNRS, CEA-DSM/IRFU, France; SRNSF, Georgia; BMBF, HGF, and MPG, Germany; GSRT, Greece; RGC, Hong Kong SAR, China; ISF, I-CORE and Benoziyo Center, Israel; INFN, Italy; MEXT and JSPS, Japan; CNRST, Morocco; NWO, Netherlands; RCN, Norway; MNiSW and NCN, Poland; FCT, Portugal; MNE/IFA, Romania; MES of Russia and NRC KI, Russian Federation; JINR; MESTD, Serbia; MSSR, Slovakia; ARRS and MIZŠ, Slovenia; DST/NRF, South Africa; MINECO, Spain; SRC and Wallenberg Foundation, Sweden; SERI, SNSF and Cantons of Bern and Geneva, Switzerland; MOST, Taiwan; TAEK, Turkey; STFC, United Kingdom; DOE and NSF, United States of America. In addition, individual groups and members have received support from BCKDF, the Canada Council, CANARIE, CRC, Compute Canada, FQRNT, and the Ontario Innovation Trust, Canada; EPLANET, ERC, ERDF, FP7, Horizon 2020 and Marie Skłodowska-Curie Actions, European Union; Investissements d'Avenir Labex and Idex, ANR, Région Auvergne and Fondation Partager le Savoir, France; DFG and AvH Foundation, Germany; Herakleitos, Thales and Aristeia programmes co-financed by EU-ESF and the Greek NSRF; BSF, GIF and Minerva, Israel; BRF, Norway; CERCA Programme Generalitat de Catalunya, Generalitat Valenciana, Spain; the Royal Society and Leverhulme Trust, United Kingdom. The crucial computing support from all WLCG partners is acknowledged gratefully, in particular from CERN, the ATLAS Tier-1 facilities at TRIUMF (Canada), NDGF (Denmark, Norway, Sweden), CC-IN2P3 (France), KIT/GridKA (Germany), INFN-CNAF (Italy), NL-T1 (Netherlands), PIC (Spain), ASGC (Taiwan), RAL (UK) and BNL (USA), the Tier-2 facilities worldwide and large non-WLCG resource providers. Major contributors of computing resources are listed in Ref. [82].

Funded by SCOAP[3].

References

1. D.J. Gross, F. Wilczek, Asymptotically free Gauge theories. Phys. Rev. D **8**, 3633 (1973). doi:10.1103/PhysRevD.8.3633
2. H.D. Politzer, Asymptotic freedom: an approach to strong interactions. Phys. Rep. **14**, 129 (1974). doi:10.1016/0370-1573(74)90014-3
3. R. Boughezal et al., Z-boson production in association with a jet at next-to-next-to-leading order in perturbative QCD. Phys. Rev. Lett. **116**, 152001 (2016). doi:10.1103/PhysRevLett.116.152001. arXiv:1512.01291 [hep-ph]
4. R. Boughezal, X. Liu, F. Petriello, Phenomenology of the Z-boson plus jet process at NNLO. Phys. Rev. D **94**, 074015 (2016). doi:10.1103/PhysRevD.94.074015. arXiv:1602.08140 [hep-ph]
5. A. Gehrmann-De Ridder, T. Gehrmann, E.W.N. Glover, A. Huss, T.A. Morgan, Precise QCD predictions for the production of a Z boson in association with a hadronic jet. Phys. Rev. Lett. **117**, 022001 (2016). doi:10.1103/PhysRevLett.117.022001. arXiv:1507.02850 [hep-ph]
6. A. Gehrmann-De Ridder, T. Gehrmann, E.W.N. Glover, A. Huss, T.A. Morgan, The NNLO QCD corrections to Z boson production at large transverse momentum. JHEP **07**, 133 (2016). doi:10.1007/JHEP07(2016)133. arXiv:1605.04295 [hep-ph]
7. ATLAS Collaboration, The ATLAS Experiment at the CERN Large Hadron Collider. JINST **3**, S08003 (2008). doi:10.1088/1748-0221/3/08/S08003
8. CMS Collaboration, The CMS experiment at the CERN LHC. JINST **3**, S08004 (2008). doi:10.1088/1748-0221/3/08/S08004
9. LHCb Collaboration, The LHCb detector at the LHC. JINST **3**, S08005 (2008). doi:10.1088/1748-0221/3/08/S08005
10. L. Evans, P. Bryant, LHC Machine, JINST **3**, S08001 (2008). doi:10.1088/1748-0221/3/08/S08001
11. ATLAS Collaboration, Measurement of the production cross section of jets in association with a Z boson in pp collisions at $\sqrt{s} = 7$ TeV with the ATLAS detector. JHEP **07**, 032 (2013). doi:10.1007/JHEP07(2013)032. arXiv:1304.7098 [hep-ex]
12. CMS Collaboration, Rapidity distributions in exclusive Z + jet and γ + jet events in pp collisions at $\sqrt{s} = 7$ TeV. Phys. Rev. D **88**, 112009 (2013). doi:10.1103/PhysRevD.88.112009. arXiv:1310.3082 [hep-ex]
13. CMS Collaboration, Event shapes and azimuthal correlations in Z + jets events in pp collisions at $\sqrt{s} = 7$ TeV. Phys. Lett. B **722**, 238 (2013). doi:10.1016/j.physletb.2013.04.025. arXiv:1301.1646 [hep-ex]
14. CMS Collaboration, Measurements of jet multiplicity and differential production cross sections of $Z+$ jets events in proton-proton collisions at $\sqrt{s} = 7$ TeV. Phys. Rev. D **91**, 052008 (2015). doi:10.1103/PhysRevD.91.052008. arXiv:1408.3104 [hep-ex]
15. LHCb Collaboration, Study of forward Z + jet production in pp collisions at $\sqrt{s} = 7$ TeV. JHEP **01**, 033 (2014). doi:10.1007/JHEP01(2014)033. arXiv:1310.8197 [hep-ex]
16. CMS Collaboration, Comparison of the Z/γ^* + jets to γ + jets cross sections in pp collisions at $\sqrt{s} = 8$ TeV. JHEP **10**, 128 (2015). doi:10.1007/JHEP04(2016)010, doi:10.1007/JHEP10(2015)128, arXiv:1505.06520 [hep-ex] [Erratum: JHEP 04 (2016) 010]
17. CMS Collaboration, Measurements of the differential production cross sections for a Z boson in association with jets in pp collisions at $\sqrt{s} = 8$ TeV (2016). arXiv:1611.03844 [hep-ex]
18. LHCb Collaboration, Measurement of forward W and Z boson production in association with jets in proton-proton collisions at $\sqrt{s} =$ 8 TeV. JHEP **05**, 131 (2016). doi:10.1007/JHEP05(2016)131. arXiv:1605.00951 [hep-ex]
19. T.A. Aaltonen et al., Measurement of differential production cross section for Z/γ^* bosons in association with jets in $p\bar{p}$ collisions at $\sqrt{s} = 1.96$ TeV. Phys. Rev. D **91**, 012002 (2015). doi:10.1103/PhysRevD.91.012002. arXiv:1409.4359 [hep-ex]
20. V.M. Abazov et al., Measurement of $Z/\gamma*$+jet+X angular distributions in p anti-p collisions at $\sqrt{s} = 1.96$ TeV. Phys. Lett. B **682**, 370 (2010). doi:10.1016/j.physletb.2009.11.012. arXiv:0907.4286 [hep-ex]

21. ATLAS Collaboration, Performance of the ATLAS trigger system in 2015 (2016). arXiv:1611.09661 [hep-ex]
22. S. Agostinelli et al., GEANT4: a simulation toolkit. Nucl. Instrum. Meth. A **506**, 250 (2003). doi:10.1016/S0168-9002(03)01368-8
23. ATLAS Collaboration, The ATLAS simulation infrastructure. Eur. Phys. J. C **70**, 823 (2010). doi:10.1140/epjc/s10052-010-1429-9, arXiv:1005.4568 [hep-ex]
24. C. Anastasiou, L.J. Dixon, K. Melnikov, F. Petriello, High precision QCD at hadron colliders: electroweak gauge boson rapidity distributions at NNLO. Phys. Rev. D **69**, 094008 (2004). doi:10.1103/PhysRevD.69.094008. arXiv:hep-ph/0312266
25. R. Gavin et al., FEWZ 2.0: a code for hadronic Z production at next-to-next-to-leading order. Comput. Phys. Commun. **182**, 2388 (2011). doi:10.1016/j.cpc.2011.06.008. arXiv:1011.3540 [hep-ph]
26. R. Gavin et al., W physics at the LHC with FEWZ 2.1. Comput. Phys. Commun. **184**, 208 (2013). doi:10.1016/j.cpc.2012.09.005. arXiv:1201.5896 [hep-ph]
27. Y. Li, F. Petriello, Combining QCD and electroweak corrections to dilepton production in FEWZ. Phys. Rev. D **86**, 094034 (2012). doi:10.1103/PhysRevD.86.094034. arXiv:1208.5967 [hep-ph]
28. M. Czakon, A. Mitov, Top++: a program for the calculation of the top-pair cross-section at Hadron colliders. Comput. Phys. Commun. **185**, 2930 (2014). doi:10.1016/j.cpc.2014.06.021. arXiv:1112.5675 [hep-ph]
29. N. Kidonakis, Two-loop soft anomalous dimensions for single top quark associated production with a W^- or H^-. Phys. Rev. D **82**, 054018 (2010). doi:10.1103/PhysRevD.82.054018. arXiv:1005.4451 [hep-ph]
30. N. Kidonakis, Next-to-next-to-leading-order collinear and soft gluon corrections for t-channel single top quark production. Phys. Rev. D **83**, 091503 (2011). doi:10.1103/PhysRevD.83.091503. arXiv:1103.2792 [hep-ph]
31. T. Gleisberg et al., Event generation with SHERPA 1.1. JHEP **02**, 007 (2009). doi:10.1088/1126-6708/2009/02/007. arXiv:0811.4622 [hep-ph]
32. M. Grazzini et al., $W^{\pm}Z$ production at hadron colliders in NNLO QCD. Phys. Lett. B **761**, 179 (2016). doi:10.1016/j.physletb.2016.08.017. arXiv:1604.08576 [hep-ph]
33. T. Gehrmann et al., W^+W^- Production at Hadron colliders in next to next to leading order QCD. Phys. Rev. Lett. **113**, 212001 (2014). doi:10.1103/PhysRevLett.113.212001. arXiv:1408.5243 [hep-ph]
34. T. Gleisberg, S. Höche, Comix, a new matrix element generator. JHEP **12**, 039 (2008). doi:10.1088/1126-6708/2008/12/039. arXiv:0808.3674 [hep-ph]
35. F. Cascioli, P. Maierhofer, S. Pozzorini, Scattering amplitudes with open loops. Phys. Rev. Lett. **108**, 111601 (2012). doi:10.1103/PhysRevLett.108.111601. arXiv:1111.5206 [hep-ph]
36. S. Schumann, F. Krauss, A Parton shower algorithm based on Catani-Seymour dipole factorisation. JHEP **03**, 038 (2008). doi:10.1088/1126-6708/2008/03/038. arXiv:0709.1027 [hep-ph]
37. S. Höche, F. Krauss, M. Schönherr, F. Siegert, QCD matrix elements + parton showers: the NLO case. JHEP **04**, 027 (2013). doi:10.1007/JHEP04(2013)027. arXiv:1207.5030 [hep-ph]
38. R.D. Ball et al., Parton distributions for the LHC Run II. JHEP **04**, 040 (2015). doi:10.1007/JHEP04(2015)040. arXiv:1410.8849 [hep-ph]
39. J. Alwall et al., The automated computation of tree-level and next-to-leading order differential cross sections, and their matching to parton shower simulations. JHEP **07**, 079 (2014). doi:10.1007/JHEP07(2014)079. arXiv:1405.0301 [hep-ph]
40. T. Sjöstrand, S. Mrenna, P.Z. Skands, A brief introduction to PYTHIA 8.1. Comput. Phys. Commun. **178**, 852 (2008). doi:10.1016/j.cpc.2008.01.036. arXiv:0710.3820 [hep-ph]
41. L. Lönnblad, Correcting the color dipole cascade model with fixed order matrix elements. JHEP **05**, 046 (2002). doi:10.1088/1126-6708/2002/05/046. arXiv:hep-ph/0112284
42. ATLAS Collaboration, ATLAS Pythia 8 tunes to 7 TeV data, ATL-PHYS-PUB-2014-021 (2014). https://cdsweb.cern.ch/record/1966419
43. R.D. Ball et al., Parton distributions with LHC data. Nucl. Phys. B **867**, 244 (2013). doi:10.1016/j.nuclphysb.2012.10.003. arXiv:1207.1303 [hep-ph]
44. R. Frederix, S. Frixione, Merging meets matching in MC@NLO. JHEP **12**, 061 (2012). doi:10.1007/JHEP12(2012)061. arXiv:1209.6215 [hep-ph]
45. R. Frederix, S. Frixione, A. Papaefstathiou, S. Prestel, P. Torrielli, A study of multi-jet production in association with an electroweak vector boson. JHEP **02**, 131 (2016). doi:10.1007/JHEP02(2016)131. arXiv:1511.00847 [hep-ph]
46. M.L. Mangano, M. Moretti, F. Piccinini, R. Pittau, A.D. Polosa, ALPGEN, a generator for hard multiparton processes in hadronic collisions. JHEP **07**, 001 (2003). doi:10.1088/1126-6708/2003/07/001. arXiv:hep-ph/0206293
47. T. Sjöstrand, S. Mrenna, P.Z. Skands, PYTHIA 6.4 physics and manual. JHEP **05**, 026 (2006). doi:10.1088/1126-6708/2006/05/026. arXiv:hep-ph/0603175
48. P.Z. Skands, Tuning Monte Carlo generators: the Perugia tunes. Phys. Rev. D **82**, 074018 (2010). doi:10.1103/PhysRevD.82.074018. arXiv:1005.3457 [hep-ph]
49. J. Pumplin et al., New generation of parton distributions with uncertainties from global QCD analysis. JHEP **07**, 012 (2002). doi:10.1088/1126-6708/2002/07/012. arXiv:hep-ph/0201195
50. H.-L. Lai et al., New parton distributions for collider physics. Phys. Rev. D **82**, 074024 (2010). doi:10.1103/PhysRevD.82.074024. arXiv:1007.2241 [hep-ph]
51. P. Nason, A new method for combining NLO QCD with shower Monte Carlo algorithms. JHEP **11**, 040 (2004). doi:10.1088/1126-6708/2004/11/040. arXiv:hep-ph/0409146
52. S. Frixione, P. Nason, C. Oleari, Matching NLO QCD computations with Parton shower simulations: the POWHEG method. JHEP **11**, 070 (2007). doi:10.1088/1126-6708/2007/11/070. arXiv:0709.2092 [hep-ph]
53. S. Alioli, P. Nason, C. Oleari, E. Re, A general framework for implementing NLO calculations in shower Monte Carlo programs: the POWHEG BOX. JHEP **06**, 043 (2010). doi:10.1007/JHEP06(2010)043. arXiv:1002.2581 [hep-ph]
54. M. Bahr et al., Herwig++ physics and manual. Eur. Phys. J. C **58**, 639 (2008). doi:10.1140/epjc/s10052-008-0798-9. arXiv:0803.0883 [hep-ph]
55. S. Gieseke, C. Rohr, A. Siodmok, Colour reconnections in Herwig++. Eur. Phys. J. C **72**, 2225 (2012). doi:10.1140/epjc/s10052-012-2225-5. arXiv:1206.0041 [hep-ph]
56. ATLAS Collaboration, Multi-boson simulation for 13 TeV ATLAS analyses, ATL-PHYS-PUB-2016-002 (2015). https://cdsweb.cern.ch/record/2119986
57. ATLAS Collaboration, Summary of ATLAS Pythia 8 tunes, ATLAS-PHYS-PUB-2012-003 (2012). https://cdsweb.cern.ch/record/1474107
58. A.D. Martin, W.J. Stirling, R.S. Thorne, G. Watt, Parton distributions for the LHC. Eur. Phys. J. C **63**, 189 (2009). doi:10.1140/epjc/s10052-009-1072-5. arXiv:0901.0002 [hep-ph]
59. C.F. Berger et al., Next-to-leading order QCD predictions for Z, γ^* + 3-Jet distributions at the Tevatron. Phys. Rev. D **82**, 074002 (2010). doi:10.1103/PhysRevD.82.074002. arXiv:1004.1659 [hep-ph]
60. H. Ita et al., Precise predictions for Z + 4 jets at Hadron colliders. Phys. Rev. D **85**, 031501 (2012). doi:10.1103/PhysRevD.85.031501. arXiv:1108.2229 [hep-ph]
61. S. Dulat et al., New parton distribution functions from a global analysis of quantum chromodynamics. Phys. Rev. D **93**, 033006 (2016). doi:10.1103/PhysRevD.93.033006. arXiv:1506.07443 [hep-ph]

62. R. Boughezal, C. Focke, X. Liu, F. Petriello, W-boson production in association with a jet at next-to-next-to-leading order in perturbative QCD. Phys. Rev. Lett. **115**, 062002 (2015). doi:10.1103/PhysRevLett.115.062002. arXiv:1504.02131 [hep-ph]
63. ATLAS Collaboration, Electron efficiency measurements with the ATLAS detector using the 2015 LHC proton-proton collision data, ATLAS-CONF-2016-024 (2016). https://cdsweb.cern.ch/record/2157687
64. ATLAS Collaboration, Electron identification measurements in ATLAS using $\sqrt{s}$ = 13 TeV data with 50 ns bunch spacing, ATL-PHYS-PUB-2015-041 (2015). https://cdsweb.cern.ch/record/2048202
65. ATLAS Collaboration, Muon reconstruction performance of the ATLAS detector in proton–proton collision data at $\sqrt{s}$ = 13 TeV. Eur. Phys. J. C **76**, 292 (2016). doi:10.1140/epjc/s10052-016-4120-y. arXiv:1603.05598 [hep-ex]
66. ATLAS Collaboration, Measurements of fiducial cross-sections for $t\bar{t}$ production with one or two additional b-jets in pp collisions at $\sqrt{s}$ = 8 TeV using the ATLAS detector. Eur. Phys. J. C **76**, 11 (2016). doi:10.1140/epjc/s10052-015-3852-4. arXiv:1508.06868 [hep-ex]
67. ATLAS Collaboration, Measurements of fiducial and differential cross sections for Higgs boson production in the diphoton decay channel at $\sqrt{s} = 8$ TeV with ATLAS. JHEP **09**, 112 (2014). doi:10.1007/JHEP09(2014)112. arXiv:1407.4222 [hep-ex]
68. M. Cacciari, G.P. Salam, G. Soyez, The anti-k_t jet clustering algorithm. JHEP **04**, 063 (2008). doi:10.1088/1126-6708/2008/04/063. arXiv:0802.1189 [hep-ph]
69. ATLAS Collaboration, Topological cell clustering in the ATLAS calorimeters and its performance in LHC Run 1 (2016). arXiv:1603.02934 [hep-ex]
70. ATLAS Collaboration, Jet Calibration and Systematic Uncertainties for Jets Reconstructed in the ATLAS Detector at $\sqrt{s}$ = 13 TeV, ATL-PHYS-PUB-2015-015 (2015). https://cdsweb.cern.ch/record/2028594
71. ATLAS Collaboration, Tagging and suppression of pileup jets with the ATLAS detector, ATLAS-CONF-2014-018 (2014). https://cds.cern.ch/record/1700870
72. ATLAS Collaboration, Performance of pile-up mitigation techniques for jets in pp collisions at $\sqrt{s}$ = 8 TeV using the ATLAS detector. Eur. Phys. J. C **76**, 581 (2016). doi:10.1140/epjc/s10052-016-4395-z. arXiv:1510.03823 [hep-ex]
73. ATLAS Collaboration, Improved luminosity determination in pp collisions at $\sqrt{s}$ = 7 TeV using the ATLAS detector at the LHC. Eur. Phys. J. C **73**, 2518 (2013). doi:10.1140/epjc/s10052-013-2518-3. arXiv:1302.4393 [hep-ex]
74. ATLAS Collaboration, Luminosity determination in pp collisions at $\sqrt{s}$ = 8 TeV using the ATLAS detector at the LHC, Eur. Phys. J. C **76**, 653 (2016). doi:10.1140/epjc/s10052-016-4466-1. arXiv:1608.03953 [hep-ex]
75. ATLAS Collaboration, Measurement of jets produced in top quark events using the di-lepton final state with 2 b-tagged jets in pp collisions at $\sqrt{s}$ = 13 TeV with the ATLAS detector, ATLAS-CONF-2015-065 (2015). https://cds.cern.ch/record/2114832
76. ATLAS Collaboration, Measurement of the $W^{\pm}Z$ boson pair-production cross section in pp collisions at $\sqrt{s}$ = 13 TeV with the ATLAS detector. Phys. Lett. B **762**, 1 (2016). doi:10.1016/j.physletb.2016.08.052. arXiv:1606.04017 [hep-ex]
77. G. D'Agostini, A multidimensional unfolding method based on Bayes' theorem. Nucl. Instrum. Meth. A **362**, 487 (1995). doi:10.1016/0168-9002(95)00274-X
78. The RooUnfold package and documentation are available from. http://hepunx.rl.ac.uk/~adye/software/unfold/RooUnfold.html
79. A. Glazov, Averaging of DIS cross section data. AIP Conf. Proc. **792**, 237 (2005). doi:10.1063/1.2122026
80. F.D. Aaron et al., Measurement of the Inclusive ep Scattering Cross Section at Low Q^2 and x at HERA. Eur. Phys. J. C **63**, 625 (2009). doi:10.1140/epjc/s10052-009-1128-6. arXiv:0904.0929 [hep-ex]
81. ATLAS Collaboration, Measurements of the W production cross sections in association with jets with the ATLAS detector. Eur. Phys. J. C **75**, 82 (2015). doi:10.1140/epjc/s10052-015-3262-7. arXiv:1409.8639 [hep-ex]
82. ATLAS Collaboration, ATLAS Computing Acknowledgements 2016–2017, ATL-GEN-PUB-2016-002. https://cdsweb.cern.ch/record/2202407

ATLAS Collaboration

M. Aaboud[137d], G. Aad[88], B. Abbott[115], J. Abdallah[8], O. Abdinov[12], B. Abeloos[119], R. Aben[109], O. S. AbouZeid[139], N. L. Abraham[151], H. Abramowicz[155], H. Abreu[154], R. Abreu[118], Y. Abulaiti[148a,148b], B. S. Acharya[167a,167b,a], S. Adachi[157], L. Adamczyk[41a], D. L. Adams[27], J. Adelman[110], S. Adomeit[102], T. Adye[133], A. A. Affolder[77], T. Agatonovic-Jovin[14], J. A. Aguilar-Saavedra[128a,128f], S. P. Ahlen[24], F. Ahmadov[68,b], G. Aielli[135a,135b], H. Akerstedt[148a,148b], T. P. A. Åkesson[84], A. V. Akimov[98], G. L. Alberghi[22a,22b], J. Albert[172], S. Albrand[58], M. J. Alconada Verzini[74], M. Aleksa[32], I. N. Aleksandrov[68], C. Alexa[28b], G. Alexander[155], T. Alexopoulos[10], M. Alhroob[115], B. Ali[130], M. Aliev[76a,76b], G. Alimonti[94a], J. Alison[33], S. P. Alkire[38], B. M. M. Allbrooke[151], B. W. Allen[118], P. P. Allport[19], A. Aloisio[106a,106b], A. Alonso[39], F. Alonso[74], C. Alpigiani[140], A. A. Alshehri[56], M. Alstaty[88], B. Alvarez Gonzalez[32], D. Álvarez Piqueras[170], M. G. Alviggi[106a,106b], B. T. Amadio[16], Y. Amaral Coutinho[26a], C. Amelung[25], D. Amidei[92], S. P. Amor Dos Santos[128a,128c], A. Amorim[128a,128b], S. Amoroso[32], G. Amundsen[25], C. Anastopoulos[141], L. S. Ancu[52], N. Andari[19], T. Andeen[11], C. F. Anders[60b], G. Anders[32], J. K. Anders[77], K. J. Anderson[33], A. Andreazza[94a,94b], V. Andrei[60a], S. Angelidakis[9], I. Angelozzi[109], A. Angerami[38], F. Anghinolfi[32], A. V. Anisenkov[111,c], N. Anjos[13], A. Annovi[126a,126b], C. Antel[60a], M. Antonelli[50], A. Antonov[100,*], D. J. Antrim[166], F. Anulli[134a], M. Aoki[69], L. Aperio Bella[19], G. Arabidze[93], Y. Arai[69], J. P. Araque[128a], A. T. H. Arce[48], F. A. Arduh[74], J-F. Arguin[97], S. Argyropoulos[66], M. Arik[20a], A. J. Armbruster[145], L. J. Armitage[79], O. Arnaez[32], H. Arnold[51], M. Arratia[30], O. Arslan[23], A. Artamonov[99], G. Artoni[122], S. Artz[86], S. Asai[157], N. Asbah[45], A. Ashkenazi[155], B. Åsman[148a,148b], L. Asquith[151], K. Assamagan[27], R. Astalos[146a], M. Atkinson[169], N. B. Atlay[143], K. Augsten[130], G. Avolio[32], B. Axen[16], M. K. Ayoub[119], G. Azuelos[97,d], M. A. Baak[32], A. E. Baas[60a], M. J. Baca[19], H. Bachacou[138], K. Bachas[76a,76b], M. Backes[122], M. Backhaus[32], P. Bagiacchi[134a,134b], P. Bagnaia[134a,134b], Y. Bai[35a], J. T. Baines[133], M. Bajic[39], O. K. Baker[179], E. M. Baldin[111,c], P. Balek[175], T. Balestri[150], F. Balli[138], W. K. Balunas[124], E. Banas[42], Sw. Banerjee[176,e], A. A. E. Bannoura[178], L. Barak[32], E. L. Barberio[91], D. Barberis[53a,53b], M. Barbero[88], T. Barillari[103], M-S Barisits[32], T. Barklow[145], N. Barlow[30], S. L. Barnes[87], B. M. Barnett[133], R. M. Barnett[16], Z. Barnovska-Blenessy[36a], A. Baroncelli[136a], G. Barone[25], A. J. Barr[122], L. Barranco Navarro[170], F. Barreiro[85], J. Barreiro Guimarães da Costa[35a], R. Bartoldus[145], A. E. Barton[75], P. Bartos[146a], A. Basalaev[125], A. Bassalat[119,f], R. L. Bates[56], S. J. Batista[161], J. R. Batley[30], M. Battaglia[139], M. Bauce[134a,134b], F. Bauer[138], H. S. Bawa[145,g], J. B. Beacham[113], M. D. Beattie[75], T. Beau[83], P. H. Beauchemin[165], P. Bechtle[23], H. P. Beck[18,h], K. Becker[122], M. Becker[86], M. Beckingham[173], C. Becot[112], A. J. Beddall[20d], A. Beddall[20b], V. A. Bednyakov[68], M. Bedognetti[109], C. P. Bee[150], L. J. Beemster[109], T. A. Beermann[32], M. Begel[27], J. K. Behr[45], A. S. Bell[81], G. Bella[155], L. Bellagamba[22a], A. Bellerive[31], M. Bellomo[89], K. Belotskiy[100], O. Beltramello[32], N. L. Belyaev[100], O. Benary[155,*], D. Benchekroun[137a], M. Bender[102], K. Bendtz[148a,148b], N. Benekos[10], Y. Benhammou[155], E. Benhar Noccioli[179], J. Benitez[66], D. P. Benjamin[48], J. R. Bensinger[25], S. Bentvelsen[109], L. Beresford[122], M. Beretta[50], D. Berge[109], E. Bergeaas Kuutmann[168], N. Berger[5], J. Beringer[16], S. Berlendis[58], N. R. Bernard[89], C. Bernius[112], F. U. Bernlochner[23], T. Berry[80], P. Berta[131], C. Bertella[86], G. Bertoli[148a,148b], F. Bertolucci[126a,126b], I. A. Bertram[75], C. Bertsche[45], D. Bertsche[115], G. J. Besjes[39], O. Bessidskaia Bylund[148a,148b], M. Bessner[45], N. Besson[138], C. Betancourt[51], A. Bethani[58], S. Bethke[103], A. J. Bevan[79], R. M. Bianchi[127], M. Bianco[32], O. Biebel[102], D. Biedermann[17], R. Bielski[87], N. V. Biesuz[126a,126b], M. Biglietti[136a], J. Bilbao De Mendizabal[52], T. R. V. Billoud[97], H. Bilokon[50], M. Bindi[57], A. Bingul[20b], C. Bini[134a,134b], S. Biondi[22a,22b], T. Bisanz[57], D. M. Bjergaard[48], C. W. Black[152], J. E. Black[145], K. M. Black[24], D. Blackburn[140], R. E. Blair[6], T. Blazek[146a], I. Bloch[45], C. Blocker[25], A. Blue[56], W. Blum[86,*], U. Blumenschein[57], S. Blunier[34a], G. J. Bobbink[109], V. S. Bobrovnikov[111,c], S. S. Bocchetta[84], A. Bocci[48], C. Bock[102], M. Boehler[51], D. Boerner[178], J. A. Bogaerts[32], D. Bogavac[14], A. G. Bogdanchikov[111], C. Bohm[148a], V. Boisvert[80], P. Bokan[14], T. Bold[41a], A. S. Boldyrev[101], M. Bomben[83], M. Bona[79], M. Boonekamp[138], A. Borisov[132], G. Borissov[75], J. Bortfeldt[32], D. Bortoletto[122], V. Bortolotto[62a,62b,62c], K. Bos[109], D. Boscherini[22a], M. Bosman[13], J. D. Bossio Sola[29], J. Boudreau[127], J. Bouffard[2], E. V. Bouhova-Thacker[75], D. Boumediene[37], C. Bourdarios[119], S. K. Boutle[56], A. Boveia[32], J. Boyd[32], I. R. Boyko[68], J. Bracinik[19], A. Brandt[8], G. Brandt[57], O. Brandt[60a], U. Bratzler[158], B. Brau[89], J. E. Brau[118], W. D. Breaden Madden[56], K. Brendlinger[124], A. J. Brennan[91], L. Brenner[109], R. Brenner[168], S. Bressler[175], T. M. Bristow[49], D. Britton[56], D. Britzger[45], F. M. Brochu[30], I. Brock[23], R. Brock[93], G. Brooijmans[38], T. Brooks[80], W. K. Brooks[34b], J. Brosamer[16], E. Brost[110], J. H Broughton[19], P. A. Bruckman de Renstrom[42], D. Bruncko[146b], R. Bruneliere[51], A. Bruni[22a], G. Bruni[22a], L. S. Bruni[109], BH Brunt[30], M. Bruschi[22a], N. Bruscino[23], P. Bryant[33], L. Bryngemark[84], T. Buanes[15], Q. Buat[144], P. Buchholz[143], A. G. Buckley[56], I. A. Budagov[68], F. Buehrer[51], M. K. Bugge[121], O. Bulekov[100], D. Bullock[8], H. Burckhart[32], S. Burdin[77], C. D. Burgard[51], A. M. Burger[5], B. Burghgrave[110], K. Burka[42], S. Burke[133], I. Burmeister[46], J. T. P. Burr[122], E. Busato[37], D. Büscher[51], V. Büscher[86], P. Bussey[56], J. M. Butler[24], C. M. Buttar[56], J. M. Butterworth[81], P. Butti[109], W. Buttinger[27], A. Buzatu[56], A. R. Buzykaev[111,c], S. Cabrera Urbán[170], D. Caforio[130],

V. M. Cairo[40a,40b], O. Cakir[4a], N. Calace[52], P. Calafiura[16], A. Calandri[88], G. Calderini[83], P. Calfayan[64], G. Callea[40a,40b], L. P. Caloba[26a], S. Calvente Lopez[85], D. Calvet[37], S. Calvet[37], T. P. Calvet[88], R. Camacho Toro[33], S. Camarda[32], P. Camarri[135a,135b], D. Cameron[121], R. Caminal Armadans[169], C. Camincher[58], S. Campana[32], M. Campanelli[81], A. Camplani[94a,94b], A. Campoverde[143], V. Canale[106a,106b], A. Canepa[163a], M. Cano Bret[36c], J. Cantero[116], T. Cao[43], M. D. M. Capeans Garrido[32], I. Caprini[28b], M. Caprini[28b], M. Capua[40a,40b], R. M. Carbone[38], R. Cardarelli[135a], F. Cardillo[51], I. Carli[131], T. Carli[32], G. Carlino[106a], L. Carminati[94a,94b], R. M. D. Carney[148a,148b], S. Caron[108], E. Carquin[34b], G. D. Carrillo-Montoya[32], J. R. Carter[30], J. Carvalho[128a,128c], D. Casadei[19], M. P. Casado[13,i], M. Casolino[13], D. W. Casper[166], E. Castaneda-Miranda[147a], R. Castelijn[109], A. Castelli[109], V. Castillo Gimenez[170], N. F. Castro[128a,j], A. Catinaccio[32], J. R. Catmore[121], A. Cattai[32], J. Caudron[23], V. Cavaliere[169], E. Cavallaro[13], D. Cavalli[94a], M. Cavalli-Sforza[13], V. Cavasinni[126a,126b], F. Ceradini[136a,136b], L. Cerda Alberich[170], A. S. Cerqueira[26b], A. Cerri[151], L. Cerrito[135a,135b], F. Cerutti[16], A. Cervelli[18], S. A. Cetin[20c], A. Chafaq[137a], D. Chakraborty[110], S. K. Chan[59], Y. L. Chan[62a], P. Chang[169], J. D. Chapman[30], D. G. Charlton[19], A. Chatterjee[52], C. C. Chau[161], C. A. Chavez Barajas[151], S. Che[113], S. Cheatham[167a,167c], A. Chegwidden[93], S. Chekanov[6], S. V. Chekulaev[163a], G. A. Chelkov[68,k], M. A. Chelstowska[92], C. Chen[67], H. Chen[27], K. Chen[150], S. Chen[35b], S. Chen[157], X. Chen[35c,l], Y. Chen[70], H. C. Cheng[92], H. J. Cheng[35a], Y. Cheng[33], A. Cheplakov[68], E. Cheremushkina[132], R. Cherkaoui El Moursli[137e], V. Chernyatin[27,*], E. Cheu[7], L. Chevalier[138], V. Chiarella[50], G. Chiarelli[126a,126b], G. Chiodini[76a], A. S. Chisholm[32], A. Chitan[28b], M. V. Chizhov[68], K. Choi[64], A. R. Chomont[37], S. Chouridou[9], B. K. B. Chow[102], V. Christodoulou[81], D. Chromek-Burckhart[32], J. Chudoba[129], A. J. Chuinard[90], J. J. Chwastowski[42], L. Chytka[117], G. Ciapetti[134a,134b], A. K. Ciftci[4a], D. Cinca[46], V. Cindro[78], I. A. Cioara[23], C. Ciocca[22a,22b], A. Ciocio[16], F. Cirotto[106a,106b], Z. H. Citron[175], M. Citterio[94a], M. Ciubancan[28b], A. Clark[52], B. L. Clark[59], M. R. Clark[38], P. J. Clark[49], R. N. Clarke[16], C. Clement[148a,148b], Y. Coadou[88], M. Cobal[167a,167c], A. Coccaro[52], J. Cochran[67], L. Colasurdo[108], B. Cole[38], A. P. Colijn[109], J. Collot[58], T. Colombo[166], G. Compostella[103], P. Conde Muiño[128a,128b], E. Coniavitis[51], S. H. Connell[147b], I. A. Connelly[80], V. Consorti[51], S. Constantinescu[28b], G. Conti[32], F. Conventi[106a,m], M. Cooke[16], B. D. Cooper[81], A. M. Cooper-Sarkar[122], F. Cormier[171], K. J. R. Cormier[161], T. Cornelissen[178], M. Corradi[134a,134b], F. Corriveau[90,n], A. Cortes-Gonzalez[32], G. Cortiana[103], G. Costa[94a], M. J. Costa[170], D. Costanzo[141], G. Cottin[30], G. Cowan[80], B. E. Cox[87], K. Cranmer[112], S. J. Crawley[56], G. Cree[31], S. Crépé-Renaudin[58], F. Crescioli[83], W. A. Cribbs[148a,148b], M. Crispin Ortuzar[122], M. Cristinziani[23], V. Croft[108], G. Crosetti[40a,40b], A. Cueto[85], T. Cuhadar Donszelmann[141], J. Cummings[179], M. Curatolo[50], J. Cúth[86], H. Czirr[143], P. Czodrowski[3], G. D'amen[22a,22b], S. D'Auria[56], M. D'Onofrio[77], M. J. Da Cunha Sargedas De Sousa[128a,128b], C. Da Via[87], W. Dabrowski[41a], T. Dado[146a], T. Dai[92], O. Dale[15], F. Dallaire[97], C. Dallapiccola[89], M. Dam[39], J. R. Dandoy[33], N. P. Dang[51], A. C. Daniells[19], N. S. Dann[87], M. Danninger[171], M. Dano Hoffmann[138], V. Dao[51], G. Darbo[53a], S. Darmora[8], J. Dassoulas[3], A. Dattagupta[118], W. Davey[23], C. David[172], T. Davidek[131], M. Davies[155], P. Davison[81], E. Dawe[91], I. Dawson[141], K. De[8], R. de Asmundis[106a], A. De Benedetti[115], S. De Castro[22a,22b], S. De Cecco[83], N. De Groot[108], P. de Jong[109], H. De la Torre[93], F. De Lorenzi[67], A. De Maria[57], D. De Pedis[134a], A. De Salvo[134a], U. De Sanctis[151], A. De Santo[151], J. B. De Vivie De Regie[119], W. J. Dearnaley[75], R. Debbe[27], C. Debenedetti[139], D. V. Dedovich[68], N. Dehghanian[3], I. Deigaard[109], M. Del Gaudio[40a,40b], J. Del Peso[85], T. Del Prete[126a,126b], D. Delgove[119], F. Deliot[138], C. M. Delitzsch[52], A. Dell'Acqua[32], L. Dell'Asta[24], M. Dell'Orso[126a,126b], M. Della Pietra[106a,m], D. della Volpe[52], M. Delmastro[5], P. A. Delsart[58], D. A. DeMarco[161], S. Demers[179], M. Demichev[68], A. Demilly[83], S. P. Denisov[132], D. Denysiuk[138], D. Derendarz[42], J. E. Derkaoui[137d], F. Derue[83], P. Dervan[77], K. Desch[23], C. Deterre[45], K. Dette[46], P. O. Deviveiros[32], A. Dewhurst[133], S. Dhaliwal[25], A. Di Ciaccio[135a,135b], L. Di Ciaccio[5], W. K. Di Clemente[124], C. Di Donato[106a,106b], A. Di Girolamo[32], B. Di Girolamo[32], B. Di Micco[136a,136b], R. Di Nardo[32], K. F. Di Petrillo[59], A. Di Simone[51], R. Di Sipio[161], D. Di Valentino[31], C. Diaconu[88], M. Diamond[161], F. A. Dias[49], M. A. Diaz[34a], E. B. Diehl[92], J. Dietrich[17], S. Díez Cornell[45], A. Dimitrievska[14], J. Dingfelder[23], P. Dita[28b], S. Dita[28b], F. Dittus[32], F. Djama[88], T. Djobava[54b], J. I. Djuvsland[60a], M. A. B. do Vale[26c], D. Dobos[32], M. Dobre[28b], C. Doglioni[84], J. Dolejsi[131], Z. Dolezal[131], M. Donadelli[26d], S. Donati[126a,126b], P. Dondero[123a,123b], J. Donini[37], J. Dopke[133], A. Doria[106a], M. T. Dova[74], A. T. Doyle[56], E. Drechsler[57], M. Dris[10], Y. Du[36b], J. Duarte-Campderros[155], E. Duchovni[175], G. Duckeck[102], O. A. Ducu[97,o], D. Duda[109], A. Dudarev[32], A. Chr. Dudder[86], E. M. Duffield[16], L. Duflot[119], M. Dührssen[32], M. Dumancic[175], A. K. Duncan[56], M. Dunford[60a], H. Duran Yildiz[4a], M. Düren[55], A. Durglishvili[54b], D. Duschinger[47], B. Dutta[45], M. Dyndal[45], C. Eckardt[45], K. M. Ecker[103], R. C. Edgar[92], N. C. Edwards[49], T. Eifert[32], G. Eigen[15], K. Einsweiler[16], T. Ekelof[168], M. El Kacimi[137c], V. Ellajosyula[88], M. Ellert[168], S. Elles[5], F. Ellinghaus[178], A. A. Elliot[172], N. Ellis[32], J. Elmsheuser[27], M. Elsing[32], D. Emeliyanov[133], Y. Enari[157], O. C. Endner[86], J. S. Ennis[173], J. Erdmann[46], A. Ereditato[18], G. Ernis[178], J. Ernst[2], M. Ernst[27], S. Errede[169], E. Ertel[86], M. Escalier[119], H. Esch[46], C. Escobar[127], B. Esposito[50], A. I. Etienvre[138], E. Etzion[155], H. Evans[64], A. Ezhilov[125], F. Fabbri[22a,22b], L. Fabbri[22a,22b], G. Facini[33], R. M. Fakhrutdinov[132], S. Falciano[134a], R. J. Falla[81], J. Faltova[32], Y. Fang[35a], M. Fanti[94a,94b], A. Farbin[8],

V. M. Cairo[40a,40b], O. Cakir[4a], N. Calace[52], P. Calafiura[16], A. Calandri[88], G. Calderini[83], P. Calfayan[64], G. Callea[40a,40b], L. P. Caloba[26a], S. Calvente Lopez[85], D. Calvet[37], S. Calvet[37], T. P. Calvet[88], R. Camacho Toro[33], S. Camarda[32], P. Camarri[135a,135b], D. Cameron[121], R. Caminal Armadans[169], C. Camincher[58], S. Campana[32], M. Campanelli[81], A. Camplani[94a,94b], A. Campoverde[143], V. Canale[106a,106b], A. Canepa[163a], M. Cano Bret[36c], J. Cantero[116], T. Cao[43], M. D. M. Capeans Garrido[32], I. Caprini[28b], M. Caprini[28b], M. Capua[40a,40b], R. M. Carbone[38], R. Cardarelli[135a], F. Cardillo[51], I. Carli[131], T. Carli[32], G. Carlino[106a], L. Carminati[94a,94b], R. M. D. Carney[148a,148b], S. Caron[108], E. Carquin[34b], G. D. Carrillo-Montoya[32], J. R. Carter[30], J. Carvalho[128a,128c], D. Casadei[19], M. P. Casado[13,i], M. Casolino[13], D. W. Casper[166], E. Castaneda-Miranda[147a], R. Castelijn[109], A. Castelli[109], V. Castillo Gimenez[170], N. F. Castro[128a,j], A. Catinaccio[32], J. R. Catmore[121], A. Cattai[32], J. Caudron[23], V. Cavaliere[169], E. Cavallaro[13], D. Cavalli[94a], M. Cavalli-Sforza[13], V. Cavasinni[126a,126b], F. Ceradini[136a,136b], L. Cerda Alberich[170], A. S. Cerqueira[26b], A. Cerri[151], L. Cerrito[135a,135b], F. Cerutti[16], A. Cervelli[18], S. A. Cetin[20c], A. Chafaq[137a], D. Chakraborty[110], S. K. Chan[59], Y. L. Chan[62a], P. Chang[169], J. D. Chapman[30], D. G. Charlton[19], A. Chatterjee[52], C. C. Chau[161], C. A. Chavez Barajas[151], S. Che[113], S. Cheatham[167a,167c], A. Chegwidden[93], S. Chekanov[6], S. V. Chekulaev[163a], G. A. Chelkov[68,k], M. A. Chelstowska[92], C. Chen[67], H. Chen[27], K. Chen[150], S. Chen[35b], S. Chen[157], X. Chen[35c,l], Y. Chen[70], H. C. Cheng[92], H. J. Cheng[35a], Y. Cheng[33], A. Cheplakov[68], E. Cheremushkina[132], R. Cherkaoui El Moursli[137e], V. Chernyatin[27,*], E. Cheu[7], L. Chevalier[138], V. Chiarella[50], G. Chiarelli[126a,126b], G. Chiodini[76a], A. S. Chisholm[32], A. Chitan[28b], M. V. Chizhov[68], K. Choi[64], A. R. Chomont[37], S. Chouridou[9], B. K. B. Chow[102], V. Christodoulou[81], D. Chromek-Burckhart[32], J. Chudoba[129], A. J. Chuinard[90], J. J. Chwastowski[42], L. Chytka[117], G. Ciapetti[134a,134b], A. K. Ciftci[4a], D. Cinca[46], V. Cindro[78], I. A. Cioara[23], C. Ciocca[22a,22b], A. Ciocio[16], F. Cirotto[106a,106b], Z. H. Citron[175], M. Citterio[94a], M. Ciubancan[28b], A. Clark[52], B. L. Clark[59], M. R. Clark[38], P. J. Clark[49], R. N. Clarke[16], C. Clement[148a,148b], Y. Coadou[88], M. Cobal[167a,167c], A. Coccaro[52], J. Cochran[67], L. Colasurdo[108], B. Cole[38], A. P. Colijn[109], J. Collot[58], T. Colombo[166], G. Compostella[103], P. Conde Muiño[128a,128b], E. Coniavitis[51], S. H. Connell[147b], I. A. Connelly[80], V. Consorti[51], S. Constantinescu[28b], G. Conti[32], F. Conventi[106a,m], M. Cooke[16], B. D. Cooper[81], A. M. Cooper-Sarkar[122], F. Cormier[171], K. J. R. Cormier[161], T. Cornelissen[178], M. Corradi[134a,134b], F. Corriveau[90,n], A. Cortes-Gonzalez[32], G. Cortiana[103], G. Costa[94a], M. J. Costa[170], D. Costanzo[141], G. Cottin[30], G. Cowan[80], B. E. Cox[87], K. Cranmer[112], S. J. Crawley[56], G. Cree[31], S. Crépé-Renaudin[58], F. Crescioli[83], W. A. Cribbs[148a,148b], M. Crispin Ortuzar[122], M. Cristinziani[23], V. Croft[108], G. Crosetti[40a,40b], A. Cueto[85], T. Cuhadar Donszelmann[141], J. Cummings[179], M. Curatolo[50], J. Cúth[86], H. Czirr[143], P. Czodrowski[3], G. D'amen[22a,22b], S. D'Auria[56], M. D'Onofrio[77], M. J. Da Cunha Sargedas De Sousa[128a,128b], C. Da Via[87], W. Dabrowski[41a], T. Dado[146a], T. Dai[92], O. Dale[15], F. Dallaire[97], C. Dallapiccola[89], M. Dam[39], J. R. Dandoy[33], N. P. Dang[51], A. C. Daniells[19], N. S. Dann[87], M. Danninger[171], M. Dano Hoffmann[138], V. Dao[51], G. Darbo[53a], S. Darmora[8], J. Dassoulas[3], A. Dattagupta[118], W. Davey[23], C. David[172], T. Davidek[131], M. Davies[155], P. Davison[81], E. Dawe[91], I. Dawson[141], K. De[8], R. de Asmundis[106a], A. De Benedetti[115], S. De Castro[22a,22b], S. De Cecco[83], N. De Groot[108], P. de Jong[109], H. De la Torre[93], F. De Lorenzi[67], A. De Maria[57], D. De Pedis[134a], A. De Salvo[134a], U. De Sanctis[151], A. De Santo[151], J. B. De Vivie De Regie[119], W. J. Dearnaley[75], R. Debbe[27], C. Debenedetti[139], D. V. Dedovich[68], N. Dehghanian[3], I. Deigaard[109], M. Del Gaudio[40a,40b], J. Del Peso[85], T. Del Prete[126a,126b], D. Delgove[119], F. Deliot[138], C. M. Delitzsch[52], A. Dell'Acqua[32], L. Dell'Asta[24], M. Dell'Orso[126a,126b], M. Della Pietra[106a,m], D. della Volpe[52], M. Delmastro[5], P. A. Delsart[58], D. A. DeMarco[161], S. Demers[179], M. Demichev[68], A. Demilly[83], S. P. Denisov[132], D. Denysiuk[138], D. Derendarz[42], J. E. Derkaoui[137d], F. Derue[83], P. Dervan[77], K. Desch[23], C. Deterre[45], K. Dette[46], P. O. Deviveiros[32], A. Dewhurst[133], S. Dhaliwal[25], A. Di Ciaccio[135a,135b], L. Di Ciaccio[5], W. K. Di Clemente[124], C. Di Donato[106a,106b], A. Di Girolamo[32], B. Di Girolamo[32], B. Di Micco[136a,136b], R. Di Nardo[32], K. F. Di Petrillo[59], A. Di Simone[51], R. Di Sipio[161], D. Di Valentino[31], C. Diaconu[88], M. Diamond[161], F. A. Dias[49], M. A. Diaz[34a], E. B. Diehl[92], J. Dietrich[17], S. Díez Cornell[45], A. Dimitrievska[14], J. Dingfelder[23], P. Dita[28b], S. Dita[28b], F. Dittus[32], F. Djama[88], T. Djobava[54b], J. I. Djuvsland[60a], M. A. B. do Vale[26c], D. Dobos[32], M. Dobre[28b], C. Doglioni[84], J. Dolejsi[131], Z. Dolezal[131], M. Donadelli[26d], S. Donati[126a,126b], P. Dondero[123a,123b], J. Donini[37], J. Dopke[133], A. Doria[106a], M. T. Dova[74], A. T. Doyle[56], E. Drechsler[57], M. Dris[10], Y. Du[36b], J. Duarte-Campderros[155], E. Duchovni[175], G. Duckeck[102], O. A. Ducu[97,o], D. Duda[109], A. Dudarev[32], A. Chr. Dudder[86], E. M. Duffield[16], L. Duflot[119], M. Dührssen[32], M. Dumancic[175], A. K. Duncan[56], M. Dunford[60a], H. Duran Yildiz[4a], M. Düren[55], A. Durglishvili[54b], D. Duschinger[47], B. Dutta[45], M. Dyndal[45], C. Eckardt[45], K. M. Ecker[103], R. C. Edgar[92], N. C. Edwards[49], T. Eifert[32], G. Eigen[15], K. Einsweiler[16], T. Ekelof[168], M. El Kacimi[137c], V. Ellajosyula[88], M. Ellert[168], S. Elles[5], F. Ellinghaus[178], A. A. Elliot[172], N. Ellis[32], J. Elmsheuser[27], M. Elsing[32], D. Emeliyanov[133], Y. Enari[157], O. C. Endner[86], J. S. Ennis[173], J. Erdmann[46], A. Ereditato[18], G. Ernis[178], J. Ernst[2], M. Ernst[27], S. Errede[169], E. Ertel[86], M. Escalier[119], H. Esch[46], C. Escobar[127], B. Esposito[50], A. I. Etienvre[138], E. Etzion[155], H. Evans[64], A. Ezhilov[125], F. Fabbri[22a,22b], L. Fabbri[22a,22b], G. Facini[33], R. M. Fakhrutdinov[132], S. Falciano[134a], R. J. Falla[81], J. Faltova[32], Y. Fang[35a], M. Fanti[94a,94b], A. Farbin[8],

A. Farilla[136a], C. Farina[127], E. M. Farina[123a,123b], T. Farooque[13], S. Farrell[16], S. M. Farrington[173], P. Farthouat[32], F. Fassi[137e], P. Fassnacht[32], D. Fassouliotis[9], M. Faucci Giannelli[80], A. Favareto[53a,53b], W. J. Fawcett[122], L. Fayard[119], O. L. Fedin[125,p], W. Fedorko[171], S. Feigl[121], L. Feligioni[88], C. Feng[36b], E. J. Feng[32], H. Feng[92], A. B. Fenyuk[132], L. Feremenga[8], P. Fernandez Martinez[170], S. Fernandez Perez[13], J. Ferrando[45], A. Ferrari[168], P. Ferrari[109], R. Ferrari[123a], D. E. Ferreira de Lima[60b], A. Ferrer[170], D. Ferrere[52], C. Ferretti[92], F. Fiedler[86], A. Filipčič[78], M. Filipuzzi[45], F. Filthaut[108], M. Fincke-Keeler[172], K. D. Finelli[152], M. C. N. Fiolhais[128a,128c], L. Fiorini[170], A. Fischer[2], C. Fischer[13], J. Fischer[178], W. C. Fisher[93], N. Flaschel[45], I. Fleck[143], P. Fleischmann[92], G. T. Fletcher[141], R. R. M. Fletcher[124], T. Flick[178], B. M. Flierl[102], L. R. Flores Castillo[62a], M. J. Flowerdew[103], G. T. Forcolin[87], A. Formica[138], A. Forti[87], A. G. Foster[19], D. Fournier[119], H. Fox[75], S. Fracchia[13], P. Francavilla[83], M. Franchini[22a,22b], D. Francis[32], L. Franconi[121], M. Franklin[59], M. Frate[166], M. Fraternali[123a,123b], D. Freeborn[81], S. M. Fressard-Batraneanu[32], F. Friedrich[47], D. Froidevaux[32], J. A. Frost[122], C. Fukunaga[158], E. Fullana Torregrosa[86], T. Fusayasu[104], J. Fuster[170], C. Gabaldon[58], O. Gabizon[154], A. Gabrielli[22a,22b], A. Gabrielli[16], G. P. Gach[41a], S. Gadatsch[32], G. Gagliardi[53a,53b], L. G. Gagnon[97], P. Gagnon[64], C. Galea[108], B. Galhardo[128a,128c], E. J. Gallas[122], B. J. Gallop[133], P. Gallus[130], G. Galster[39], K. K. Gan[113], S. Ganguly[37], J. Gao[36a], Y. Gao[49], Y. S. Gao[145,g], F. M. Garay Walls[49], C. García[170], J. E. García Navarro[170], M. Garcia-Sciveres[16], R. W. Gardner[33], N. Garelli[145], V. Garonne[121], A. Gascon Bravo[45], K. Gasnikova[45], C. Gatti[50], A. Gaudiello[53a,53b], G. Gaudio[123a], L. Gauthier[97], I. L. Gavrilenko[98], C. Gay[171], G. Gaycken[23], E. N. Gazis[10], Z. Gecse[171], C. N. P. Gee[133], Ch. Geich-Gimbel[23], M. Geisen[86], M. P. Geisler[60a], K. Gellerstedt[148a,148b], C. Gemme[53a], M. H. Genest[58], C. Geng[36a,q], S. Gentile[134a,134b], C. Gentsos[156], S. George[80], D. Gerbaudo[13], A. Gershon[155], S. Ghasemi[143], M. Ghneimat[23], B. Giacobbe[22a], S. Giagu[134a,134b], P. Giannetti[126a,126b], S. M. Gibson[80], M. Gignac[171], M. Gilchriese[16], T. P. S. Gillam[30], D. Gillberg[31], G. Gilles[178], D. M. Gingrich[3,d], N. Giokaris[9,*], M. P. Giordani[167a,167c], F. M. Giorgi[22a], P. F. Giraud[138], P. Giromini[59], D. Giugni[94a], F. Giuli[122], C. Giuliani[103], M. Giulini[60b], B. K. Gjelsten[121], S. Gkaitatzis[156], I. Gkialas[9], E. L. Gkougkousis[119], L. K. Gladilin[101], C. Glasman[85], J. Glatzer[13], P. C. F. Glaysher[49], A. Glazov[45], M. Goblirsch-Kolb[25], J. Godlewski[42], S. Goldfarb[91], T. Golling[52], D. Golubkov[132], A. Gomes[128a,128b,128d], R. Gonçalo[128a], J. Goncalves Pinto Firmino Da Costa[138], G. Gonella[51], L. Gonella[19], A. Gongadze[68], S. González de la Hoz[170], S. Gonzalez-Sevilla[52], L. Goossens[32], P. A. Gorbounov[99], H. A. Gordon[27], I. Gorelov[107], B. Gorini[32], E. Gorini[76a,76b], A. Gorišek[78], E. Gornicki[42], A. T. Goshaw[48], C. Gössling[46], M. I. Gostkin[68], C. R. Goudet[119], D. Goujdami[137c], A. G. Goussiou[140], N. Govender[147b,r], E. Gozani[154], L. Graber[57], I. Grabowska-Bold[41a], P. O. J. Gradin[58], P. Grafström[22a,22b], J. Gramling[52], E. Gramstad[121], S. Grancagnolo[17], V. Gratchev[125], P. M. Gravila[28e], H. M. Gray[32], E. Graziani[136a], Z. D. Greenwood[82,s], C. Grefe[23], K. Gregersen[81], I. M. Gregor[45], P. Grenier[145], K. Grevtsov[5], J. Griffiths[8], A. A. Grillo[139], K. Grimm[75], S. Grinstein[13,t], Ph. Gris[37], J.-F. Grivaz[119], S. Groh[86], E. Gross[175], J. Grosse-Knetter[57], G. C. Grossi[82], Z. J. Grout[81], L. Guan[92], W. Guan[176], J. Guenther[65], F. Guescini[52], D. Guest[166], O. Gueta[155], B. Gui[113], E. Guido[53a,53b], T. Guillemin[5], S. Guindon[2], U. Gul[56], C. Gumpert[32], J. Guo[36c], Y. Guo[36a,q], R. Gupta[43], S. Gupta[122], G. Gustavino[134a,134b], P. Gutierrez[115], N. G. Gutierrez Ortiz[81], C. Gutschow[81], C. Guyot[138], C. Gwenlan[122], C. B. Gwilliam[77], A. Haas[112], C. Haber[16], H. K. Hadavand[8], A. Hadef[88], S. Hageböck[23], M. Hagihara[164], Z. Hajduk[42], H. Hakobyan[180,*], M. Haleem[45], J. Haley[116], G. Halladjian[93], G. D. Hallewell[88], K. Hamacher[178], P. Hamal[117], K. Hamano[172], A. Hamilton[147a], G. N. Hamity[141], P. G. Hamnett[45], L. Han[36a], K. Hanagaki[69,u], K. Hanawa[157], M. Hance[139], B. Haney[124], P. Hanke[60a], R. Hanna[138], J. B. Hansen[39], J. D. Hansen[39], M. C. Hansen[23], P. H. Hansen[39], K. Hara[164], A. S. Hard[176], T. Harenberg[178], F. Hariri[119], S. Harkusha[95], R. D. Harrington[49], P. F. Harrison[173], F. Hartjes[109], N. M. Hartmann[102], M. Hasegawa[70], Y. Hasegawa[142], A. Hasib[115], S. Hassani[138], S. Haug[18], R. Hauser[93], L. Hauswald[47], M. Havranek[129], C. M. Hawkes[19], R. J. Hawkings[32], D. Hayakawa[159], D. Hayden[93], C. P. Hays[122], J. M. Hays[79], H. S. Hayward[77], S. J. Haywood[133], S. J. Head[19], T. Heck[86], V. Hedberg[84], L. Heelan[8], S. Heim[124], T. Heim[16], B. Heinemann[16], J. J. Heinrich[102], L. Heinrich[112], C. Heinz[55], J. Hejbal[129], L. Helary[32], S. Hellman[148a,148b], C. Helsens[32], J. Henderson[122], R. C. W. Henderson[75], Y. Heng[176], S. Henkelmann[171], A. M. Henriques Correia[32], S. Henrot-Versille[119], G. H. Herbert[17], H. Herde[25], V. Herget[177], Y. Hernández Jiménez[147c], G. Herten[51], R. Hertenberger[102], L. Hervas[32], G. G. Hesketh[81], N. P. Hessey[109], J. W. Hetherly[43], E. Higón-Rodriguez[170], E. Hill[172], J. C. Hill[30], K. H. Hiller[45], S. J. Hillier[19], I. Hinchliffe[16], E. Hines[124], R. R. Hinman[16], M. Hirose[51], D. Hirschbuehl[178], X. Hoad[49], J. Hobbs[150], N. Hod[163a], M. C. Hodgkinson[141], P. Hodgson[141], A. Hoecker[32], M. R. Hoeferkamp[107], F. Hoenig[102], D. Hohn[23], T. R. Holmes[16], M. Homann[46], T. Honda[69], T. M. Hong[127], B. H. Hooberman[169], W. H. Hopkins[118], Y. Horii[105], A. J. Horton[144], J-Y. Hostachy[58], S. Hou[153], A. Hoummada[137a], J. Howarth[45], J. Hoya[74], M. Hrabovsky[117], I. Hristova[17], J. Hrivnac[119], T. Hryn'ova[5], A. Hrynevich[96], P. J. Hsu[63], S.-C. Hsu[140], Q. Hu[36a], S. Hu[36c], Y. Huang[45], Z. Hubacek[130], F. Hubaut[88], F. Huegging[23], T. B. Huffman[122], E. W. Hughes[38], G. Hughes[75], M. Huhtinen[32], P. Huo[150], N. Huseynov[68,b], J. Huston[93], J. Huth[59], G. Iacobucci[52], G. Iakovidis[27], I. Ibragimov[143], L. Iconomidou-Fayard[119], E. Ideal[179], P. Iengo[32], O. Igonkina[109,v],

T. Iizawa[174], Y. Ikegami[69], M. Ikeno[69], Y. Ilchenko[11,w], D. Iliadis[156], N. Ilic[145], G. Introzzi[123a,123b], P. Ioannou[9,*], M. Iodice[136a], K. Iordanidou[38], V. Ippolito[59], N. Ishijima[120], M. Ishino[157], M. Ishitsuka[159], R. Ishmukhametov[113], C. Issever[122], S. Istin[20a], F. Ito[164], J. M. Iturbe Ponce[87], R. Iuppa[162a,162b], W. Iwanski[65], H. Iwasaki[69], J. M. Izen[44], V. Izzo[106a], S. Jabbar[3], B. Jackson[124], P. Jackson[1], V. Jain[2], K. B. Jakobi[86], K. Jakobs[51], S. Jakobsen[32], T. Jakoubek[129], D. O. Jamin[116], D. K. Jana[82], R. Jansky[65], J. Janssen[23], M. Janus[57], P. A. Janus[41a], G. Jarlskog[84], N. Javadov[68,b], T. Javůrek[51], M. Javurkova[51], F. Jeanneau[138], L. Jeanty[16], J. Jejelava[54a,x], G.-Y. Jeng[152], D. Jennens[91], P. Jenni[51,y], C. Jeske[173], S. Jézéquel[5], H. Ji[176], J. Jia[150], H. Jiang[67], Y. Jiang[36a], Z. Jiang[145], S. Jiggins[81], J. Jimenez Pena[170], S. Jin[35a], A. Jinaru[28b], O. Jinnouchi[159], H. Jivan[147c], P. Johansson[141], K. A. Johns[7], W. J. Johnson[140], K. Jon-And[148a,148b], G. Jones[173], R. W. L. Jones[75], S. Jones[7], T. J. Jones[77], J. Jongmanns[60a], P. M. Jorge[128a,128b], J. Jovicevic[163a], X. Ju[176], A. Juste Rozas[13,t], M. K. Köhler[175], A. Kaczmarska[42], M. Kado[119], H. Kagan[113], M. Kagan[145], S. J. Kahn[88], T. Kaji[174], E. Kajomovitz[48], C. W. Kalderon[122], A. Kaluza[86], S. Kama[43], A. Kamenshchikov[132], N. Kanaya[157], S. Kaneti[30], L. Kanjir[78], V. A. Kantserov[100], J. Kanzaki[69], B. Kaplan[112], L. S. Kaplan[176], A. Kapliy[33], D. Kar[147c], K. Karakostas[10], A. Karamaoun[3], N. Karastathis[10], M. J. Kareem[57], E. Karentzos[10], M. Karnevskiy[86], S. N. Karpov[68], Z. M. Karpova[68], K. Karthik[112], V. Kartvelishvili[75], A. N. Karyukhin[132], K. Kasahara[164], L. Kashif[176], R. D. Kass[113], A. Kastanas[149], Y. Kataoka[157], C. Kato[157], A. Katre[52], J. Katzy[45], K. Kawade[105], K. Kawagoe[73], T. Kawamoto[157], G. Kawamura[57], V. F. Kazanin[111,c], R. Keeler[172], R. Kehoe[43], J. S. Keller[45], J. J. Kempster[80], H. Keoshkerian[161], O. Kepka[129], B. P. Kerševan[78], S. Kersten[178], R. A. Keyes[90], M. Khader[169], F. Khalil-zada[12], A. Khanov[116], A. G. Kharlamov[111,c], T. Kharlamova[111,c], T. J. Khoo[52], V. Khovanskiy[99], E. Khramov[68], J. Khubua[54b,z], S. Kido[70], C. R. Kilby[80], H. Y. Kim[8], S. H. Kim[164], Y. K. Kim[33], N. Kimura[156], O. M. Kind[17], B. T. King[77], M. King[170], J. Kirk[133], A. E. Kiryunin[103], T. Kishimoto[157], D. Kisielewska[41a], F. Kiss[51], K. Kiuchi[164], O. Kivernyk[138], E. Kladiva[146b], M. H. Klein[38], M. Klein[77], U. Klein[77], K. Kleinknecht[86], P. Klimek[110], A. Klimentov[27], R. Klingenberg[46], T. Klioutchnikova[32], E.-E. Kluge[60a], P. Kluit[109], S. Kluth[103], J. Knapik[42], E. Kneringer[65], E. B. F. G. Knoops[88], A. Knue[103], A. Kobayashi[157], D. Kobayashi[159], T. Kobayashi[157], M. Kobel[47], M. Kocian[145], P. Kodys[131], T. Koffas[31], E. Koffeman[109], N. M. Köhler[103], T. Koi[145], H. Kolanoski[17], M. Kolb[60b], I. Koletsou[5], A. A. Komar[98,*], Y. Komori[157], T. Kondo[69], N. Kondrashova[36c], K. Köneke[51], A. C. König[108], T. Kono[69,aa], R. Konoplich[112,ab], N. Konstantinidis[81], R. Kopeliansky[64], S. Koperny[41a], L. Köpke[86], A. K. Kopp[51], K. Korcyl[42], K. Kordas[156], A. Korn[81], A. A. Korol[111,c], I. Korolkov[13], E. V. Korolkova[141], O. Kortner[103], S. Kortner[103], T. Kosek[131], V. V. Kostyukhin[23], A. Kotwal[48], A. Koulouris[10], A. Kourkoumeli-Charalampidi[123a,123b], C. Kourkoumelis[9], V. Kouskoura[27], A. B. Kowalewska[42], R. Kowalewski[172], T. Z. Kowalski[41a], C. Kozakai[157], W. Kozanecki[138], A. S. Kozhin[132], V. A. Kramarenko[101], G. Kramberger[78], D. Krasnopevtsev[100], M. W. Krasny[83], A. Krasznahorkay[32], A. Kravchenko[27], M. Kretz[60c], J. Kretzschmar[77], K. Kreutzfeldt[55], P. Krieger[161], K. Krizka[33], K. Kroeninger[46], H. Kroha[103], J. Kroll[124], J. Kroseberg[23], J. Krstic[14], U. Kruchonak[68], H. Krüger[23], N. Krumnack[67], M. C. Kruse[48], M. Kruskal[24], T. Kubota[91], H. Kucuk[81], S. Kuday[4b], J. T. Kuechler[178], S. Kuehn[51], A. Kugel[60c], F. Kuger[177], T. Kuhl[45], V. Kukhtin[68], R. Kukla[138], Y. Kulchitsky[95], S. Kuleshov[34b], M. Kuna[134a,134b], T. Kunigo[71], A. Kupco[129], H. Kurashige[70], L. L. Kurchaninov[163a], Y. A. Kurochkin[95], M. G. Kurth[44], V. Kus[129], E. S. Kuwertz[172], M. Kuze[159], J. Kvita[117], T. Kwan[172], D. Kyriazopoulos[141], A. La Rosa[103], J. L. La Rosa Navarro[26d], L. La Rotonda[40a,40b], C. Lacasta[170], F. Lacava[134a,134b], J. Lacey[31], H. Lacker[17], D. Lacour[83], V. R. Lacuesta[170], E. Ladygin[68], R. Lafaye[5], B. Laforge[83], T. Lagouri[179], S. Lai[57], S. Lammers[64], W. Lampl[7], E. Lançon[138], U. Landgraf[51], M. P. J. Landon[79], M. C. Lanfermann[52], V. S. Lang[60a], J. C. Lange[13], A. J. Lankford[166], F. Lanni[27], K. Lantzsch[23], A. Lanza[123a], S. Laplace[83], C. Lapoire[32], J. F. Laporte[138], T. Lari[94a], F. Lasagni Manghi[22a,22b], M. Lassnig[32], P. Laurelli[50], W. Lavrijsen[16], A. T. Law[139], P. Laycock[77], T. Lazovich[59], M. Lazzaroni[94a,94b], B. Le[91], O. Le Dortz[83], E. Le Guirriec[88], E. P. Le Quilleuc[138], M. LeBlanc[172], T. LeCompte[6], F. Ledroit-Guillon[58], C. A. Lee[27], S. C. Lee[153], L. Lee[1], B. Lefebvre[90], G. Lefebvre[83], M. Lefebvre[172], F. Legger[102], C. Leggett[16], A. Lehan[77], G. Lehmann Miotto[32], X. Lei[7], W. A. Leight[31], A. G. Leister[179], M. A. L. Leite[26d], R. Leitner[131], D. Lellouch[175], B. Lemmer[57], K. J. C. Leney[81], T. Lenz[23], B. Lenzi[32], R. Leone[7], S. Leone[126a,126b], C. Leonidopoulos[49], S. Leontsinis[10], G. Lerner[151], C. Leroy[97], A. A. J. Lesage[138], C. G. Lester[30], M. Levchenko[125], J. Levêque[5], D. Levin[92], L. J. Levinson[175], M. Levy[19], D. Lewis[79], M. Leyton[44], B. Li[36a,q], C. Li[36a], H. Li[150], L. Li[48], L. Li[36c], Q. Li[35a], S. Li[48], X. Li[87], Y. Li[143], Z. Liang[35a], B. Liberti[135a], A. Liblong[161], P. Lichard[32], K. Lie[169], J. Liebal[23], W. Liebig[15], A. Limosani[152], S. C. Lin[153,ac], T. H. Lin[86], B. E. Lindquist[150], A. E. Lionti[52], E. Lipeles[124], A. Lipniacka[15], M. Lisovyi[60b], T. M. Liss[169], A. Lister[171], A. M. Litke[139], B. Liu[153,ad], D. Liu[153], H. Liu[92], H. Liu[27], J. Liu[36b], J. B. Liu[36a], K. Liu[88], L. Liu[169], M. Liu[36a], Y. L. Liu[36a], Y. Liu[36a], M. Livan[123a,123b], A. Lleres[58], J. Llorente Merino[35a], S. L. Lloyd[79], F. Lo Sterzo[153], E. M. Lobodzinska[45], P. Loch[7], F. K. Loebinger[87], K. M. Loew[25], A. Loginov[179,*], T. Lohse[17], K. Lohwasser[45], M. Lokajicek[129], B. A. Long[24], J. D. Long[169], R. E. Long[75], L. Longo[76a,76b], K. A. Looper[113], J. A. Lopez[34b], D. Lopez Mateos[59], B. Lopez Paredes[141], I. Lopez Paz[13], A. Lopez Solis[83], J. Lorenz[102], N. Lorenzo Martinez[64], M. Losada[21], P. J. Lösel[102], X. Lou[35a],

A. Lounis[119], J. Love[6], P. A. Love[75], H. Lu[62a], N. Lu[92], H. J. Lubatti[140], C. Luci[134a,134b], A. Lucotte[58], C. Luedtke[51], F. Luehring[64], W. Lukas[65], L. Luminari[134a], O. Lundberg[148a,148b], B. Lund-Jensen[149], P. M. Luzi[83], D. Lynn[27], R. Lysak[129], E. Lytken[84], V. Lyubushkin[68], H. Ma[27], L. L. Ma[36b], Y. Ma[36b], G. Maccarrone[50], A. Macchiolo[103], C. M. Macdonald[141], B. Maček[78], J. Machado Miguens[124,128b], D. Madaffari[88], R. Madar[37], H. J. Maddocks[168], W. F. Mader[47], A. Madsen[45], J. Maeda[70], S. Maeland[15], T. Maeno[27], A. Maevskiy[101], E. Magradze[57], J. Mahlstedt[109], C. Maiani[119], C. Maidantchik[26a], A. A. Maier[103], T. Maier[102], A. Maio[128a,128b,128d], S. Majewski[118], Y. Makida[69], N. Makovec[119], B. Malaescu[83], Pa. Malecki[42], V. P. Maleev[125], F. Malek[58], U. Mallik[66], D. Malon[6], C. Malone[145], C. Malone[30], S. Maltezos[10], S. Malyukov[32], J. Mamuzic[170], G. Mancini[50], L. Mandelli[94a], I. Mandić[78], J. Maneira[128a,128b], L. Manhaes de Andrade Filho[26b], J. Manjarres Ramos[163b], A. Mann[102], A. Manousos[32], B. Mansoulie[138], J. D. Mansour[35a], R. Mantifel[90], M. Mantoani[57], S. Manzoni[94a,94b], L. Mapelli[32], G. Marceca[29], L. March[52], G. Marchiori[83], M. Marcisovsky[129], M. Marjanovic[14], D. E. Marley[92], F. Marroquim[26a], S. P. Marsden[87], Z. Marshall[16], S. Marti-Garcia[170], B. Martin[93], T. A. Martin[173], V. J. Martin[49], B. Martin dit La tour[15], M. Martinez[13,t], V. I. Martinez Outschoorn[169], S. Martin-Haugh[133], V. S. Martoiu[28b], A. C. Martyniuk[81], A. Marzin[32], L. Masetti[86], T. Mashimo[157], R. Mashinistov[98], J. Masik[87], A. L. Maslennikov[111,c], I. Massa[22a,22b], L. Massa[22a,22b], P. Mastrandrea[5], A. Mastroberardino[40a,40b], T. Masubuchi[157], P. Mättig[178], J. Mattmann[86], J. Maurer[28b], S. J. Maxfield[77], D. A. Maximov[111,c], R. Mazini[153], I. Maznas[156], S. M. Mazza[94a,94b], N. C. Mc Fadden[107], G. Mc Goldrick[161], S. P. Mc Kee[92], A. McCarn[92], R. L. McCarthy[150], T. G. McCarthy[103], L. I. McClymont[81], E. F. McDonald[91], J. A. Mcfayden[81], G. Mchedlidze[57], S. J. McMahon[133], R. A. McPherson[172,n], M. Medinnis[45], S. Meehan[140], S. Mehlhase[102], A. Mehta[77], K. Meier[60a], C. Meineck[102], B. Meirose[44], D. Melini[170,ae], B. R. Mellado Garcia[147c], M. Melo[146a], F. Meloni[18], S. B. Menary[87], L. Meng[77], X. T. Meng[92], A. Mengarelli[22a,22b], S. Menke[103], E. Meoni[165], S. Mergelmeyer[17], P. Mermod[52], L. Merola[106a,106b], C. Meroni[94a], F. S. Merritt[33], A. Messina[134a,134b], J. Metcalfe[6], A. S. Mete[166], C. Meyer[86], C. Meyer[124], J-P. Meyer[138], J. Meyer[109], H. Meyer Zu Theenhausen[60a], F. Miano[151], R. P. Middleton[133], S. Miglioranzi[53a,53b], L. Mijović[49], G. Mikenberg[175], M. Mikestikova[129], M. Mikuž[78], M. Milesi[91], A. Milic[27], D. W. Miller[33], C. Mills[49], A. Milov[175], D. A. Milstead[148a,148b], A. A. Minaenko[132], Y. Minami[157], I. A. Minashvili[68], A. I. Mincer[112], B. Mindur[41a], M. Mineev[68], Y. Minegishi[157], Y. Ming[176], L. M. Mir[13], K. P. Mistry[124], T. Mitani[174], J. Mitrevski[102], V. A. Mitsou[170], A. Miucci[18], P. S. Miyagawa[141], A. Mizukami[69], J. U. Mjörnmark[84], M. Mlynarikova[131], T. Moa[148a,148b], K. Mochizuki[97], P. Mogg[51], S. Mohapatra[38], S. Molander[148a,148b], R. Moles-Valls[23], R. Monden[71], M. C. Mondragon[93], K. Mönig[45], J. Monk[39], E. Monnier[88], A. Montalbano[150], J. Montejo Berlingen[32], F. Monticelli[74], S. Monzani[94a,94b], R. W. Moore[3], N. Morange[119], D. Moreno[21], M. Moreno Llácer[57], P. Morettini[53a], S. Morgenstern[32], D. Mori[144], T. Mori[157], M. Morii[59], M. Morinaga[157], V. Morisbak[121], S. Moritz[86], A. K. Morley[152], G. Mornacchi[32], J. D. Morris[79], L. Morvaj[150], P. Moschovakos[10], M. Mosidze[54b], H. J. Moss[141], J. Moss[145,af], K. Motohashi[159], R. Mount[145], E. Mountricha[27], E. J. W. Moyse[89], S. Muanza[88], R. D. Mudd[19], F. Mueller[103], J. Mueller[127], R. S. P. Mueller[102], T. Mueller[30], D. Muenstermann[75], P. Mullen[56], G. A. Mullier[18], F. J. Munoz Sanchez[87], J. A. Murillo Quijada[19], W. J. Murray[173,133], H. Musheghyan[57], M. Muškinja[78], A. G. Myagkov[132,ag], M. Myska[130], B. P. Nachman[145], O. Nackenhorst[52], K. Nagai[122], R. Nagai[69,aa], K. Nagano[69], Y. Nagasaka[61], K. Nagata[164], M. Nagel[51], E. Nagy[88], A. M. Nairz[32], Y. Nakahama[105], K. Nakamura[69], T. Nakamura[157], I. Nakano[114], R. F. Naranjo Garcia[45], R. Narayan[11], D. I. Narrias Villar[60a], I. Naryshkin[125], T. Naumann[45], G. Navarro[21], R. Nayyar[7], H. A. Neal[92], P. Yu. Nechaeva[98], T. J. Neep[87], A. Negri[123a,123b], M. Negrini[22a], S. Nektarijevic[108], C. Nellist[119], A. Nelson[166], S. Nemecek[129], P. Nemethy[112], A. A. Nepomuceno[26a], M. Nessi[32,ah], M. S. Neubauer[169], M. Neumann[178], R. M. Neves[112], P. Nevski[27], P. R. Newman[19], D. H. Nguyen[6], T. Nguyen Manh[97], R. B. Nickerson[122], R. Nicolaidou[138], J. Nielsen[139], A. Nikiforov[17], V. Nikolaenko[132,ag], I. Nikolic-Audit[83], K. Nikolopoulos[19], J. K. Nilsen[121], P. Nilsson[27], Y. Ninomiya[157], A. Nisati[134a], R. Nisius[103], T. Nobe[157], M. Nomachi[120], I. Nomidis[31], T. Nooney[79], S. Norberg[115], M. Nordberg[32], N. Norjoharuddeen[122], O. Novgorodova[47], S. Nowak[103], M. Nozaki[69], L. Nozka[117], K. Ntekas[166], E. Nurse[81], F. Nuti[91], F. O'grady[7], D. C. O'Neil[144], A. A. O'Rourke[45], V. O'Shea[56], F. G. Oakham[31,d], H. Oberlack[103], T. Obermann[23], J. Ocariz[83], A. Ochi[70], I. Ochoa[38], J. P. Ochoa-Ricoux[34a], S. Oda[73], S. Odaka[69], H. Ogren[64], A. Oh[87], S. H. Oh[48], C. C. Ohm[16], H. Ohman[168], H. Oide[53a,53b], H. Okawa[164], Y. Okumura[157], T. Okuyama[69], A. Olariu[28b], L. F. Oleiro Seabra[128a], S. A. Olivares Pino[49], D. Oliveira Damazio[27], A. Olszewski[42], J. Olszowska[42], A. Onofre[128a,128e], K. Onogi[105], P. U. E. Onyisi[11,w], M. J. Oreglia[33], Y. Oren[155], D. Orestano[136a,136b], N. Orlando[62b], R. S. Orr[161], B. Osculati[53a,53b,*], R. Ospanov[87], G. Otero y Garzon[29], H. Otono[73], M. Ouchrif[137d], F. Ould-Saada[121], A. Ouraou[138], K. P. Oussoren[109], Q. Ouyang[35a], M. Owen[56], R. E. Owen[19], V. E. Ozcan[20a], N. Ozturk[8], K. Pachal[144], A. Pacheco Pages[13], L. Pacheco Rodriguez[138], C. Padilla Aranda[13], S. Pagan Griso[16], M. Paganini[179], F. Paige[27], P. Pais[89], K. Pajchel[121], G. Palacino[64], S. Palazzo[40a,40b], S. Palestini[32], M. Palka[41b], D. Pallin[37], E. St. Panagiotopoulou[10], I. Panagoulias[10], C. E. Pandini[83], J. G. Panduro Vazquez[80], P. Pani[148a,148b], S. Panitkin[27], D. Pantea[28b], L. Paolozzi[52], Th. D. Papadopoulou[10],

K. Papageorgiou[9], A. Paramonov[6], D. Paredes Hernandez[179], A. J. Parker[75], M. A. Parker[30], K. A. Parker[141], F. Parodi[53a,53b], J. A. Parsons[38], U. Parzefall[51], V. R. Pascuzzi[161], E. Pasqualucci[134a], S. Passaggio[53a], Fr. Pastore[80], G. Pásztor[31,ai], S. Pataraia[178], J. R. Pater[87], T. Pauly[32], J. Pearce[172], B. Pearson[115], L. E. Pedersen[39], S. Pedraza Lopez[170], R. Pedro[128a,128b], S. V. Peleganchuk[111,c], O. Penc[129], C. Peng[35a], H. Peng[36a], J. Penwell[64], B. S. Peralva[26b], M. M. Perego[138], D. V. Perepelitsa[27], E. Perez Codina[163a], L. Perini[94a,94b], H. Pernegger[32], S. Perrella[106a,106b], R. Peschke[45], V. D. Peshekhonov[68], K. Peters[45], R. F. Y. Peters[87], B. A. Petersen[32], T. C. Petersen[39], E. Petit[58], A. Petridis[1], C. Petridou[156], P. Petroff[119], E. Petrolo[134a], M. Petrov[122], F. Petrucci[136a,136b], N. E. Pettersson[89], A. Peyaud[138], R. Pezoa[34b], P. W. Phillips[133], G. Piacquadio[145,aj], E. Pianori[173], A. Picazio[89], E. Piccaro[79], M. Piccinini[22a,22b], M. A. Pickering[122], R. Piegaia[29], J. E. Pilcher[33], A. D. Pilkington[87], A. W. J. Pin[87], M. Pinamonti[167a,167c,ak], J. L. Pinfold[3], A. Pingel[39], S. Pires[83], H. Pirumov[45], M. Pitt[175], L. Plazak[146a], M.-A. Pleier[27], V. Pleskot[86], E. Plotnikova[68], D. Pluth[67], R. Poettgen[148a,148b], L. Poggioli[119], D. Pohl[23], G. Polesello[123a], A. Poley[45], A. Policicchio[40a,40b], R. Polifka[161], A. Polini[22a], C. S. Pollard[56], V. Polychronakos[27], K. Pommès[32], L. Pontecorvo[134a], B. G. Pope[93], G. A. Popeneciu[28c], A. Poppleton[32], S. Pospisil[130], K. Potamianos[16], I. N. Potrap[68], C. J. Potter[30], C. T. Potter[118], G. Poulard[32], J. Poveda[32], V. Pozdnyakov[68], M. E. Pozo Astigarraga[32], P. Pralavorio[88], A. Pranko[16], S. Prell[67], D. Price[87], L. E. Price[6], M. Primavera[76a], S. Prince[90], K. Prokofiev[62c], F. Prokoshin[34b], S. Protopopescu[27], J. Proudfoot[6], M. Przybycien[41a], D. Puddu[136a,136b], M. Purohit[27,al], P. Puzo[119], J. Qian[92], G. Qin[56], Y. Qin[87], A. Quadt[57], W. B. Quayle[167a,167b], M. Queitsch-Maitland[45], D. Quilty[56], S. Raddum[121], V. Radeka[27], V. Radescu[122], S. K. Radhakrishnan[150], P. Radloff[118], P. Rados[91], F. Ragusa[94a,94b], G. Rahal[181], J. A. Raine[87], S. Rajagopalan[27], M. Rammensee[32], C. Rangel-Smith[168], M. G. Ratti[94a,94b], D. M. Rauch[45], F. Rauscher[102], S. Rave[86], T. Ravenscroft[56], I. Ravinovich[175], M. Raymond[32], A. L. Read[121], N. P. Readioff[77], M. Reale[76a,76b], D. M. Rebuzzi[123a,123b], A. Redelbach[177], G. Redlinger[27], R. Reece[139], R. G. Reed[147c], K. Reeves[44], L. Rehnisch[17], J. Reichert[124], A. Reiss[86], C. Rembser[32], H. Ren[35a], M. Rescigno[134a], S. Resconi[94a], O. L. Rezanova[111,c], P. Reznicek[131], R. Rezvani[97], R. Richter[103], S. Richter[81], E. Richter-Was[41b], O. Ricken[23], M. Ridel[83], P. Rieck[17], C. J. Riegel[178], J. Rieger[57], O. Rifki[115], M. Rijssenbeek[150], A. Rimoldi[123a,123b], M. Rimoldi[18], L. Rinaldi[22a], B. Ristić[52], E. Ritsch[32], I. Riu[13], F. Rizatdinova[116], E. Rizvi[79], C. Rizzi[13], S. H. Robertson[90,n], A. Robichaud-Veronneau[90], D. Robinson[30], J. E. M. Robinson[45], A. Robson[56], C. Roda[126a,126b], Y. Rodina[88,am], A. Rodriguez Perez[13], D. Rodriguez Rodriguez[170], S. Roe[32], C. S. Rogan[59], O. Røhne[121], J. Roloff[59], A. Romaniouk[100], M. Romano[22a,22b], S. M. Romano Saez[37], E. Romero Adam[170], N. Rompotis[140], M. Ronzani[51], L. Roos[83], E. Ros[170], S. Rosati[134a], K. Rosbach[51], P. Rose[139], N.-A. Rosien[57], V. Rossetti[148a,148b], E. Rossi[106a,106b], L. P. Rossi[53a], J. H. N. Rosten[30], R. Rosten[140], M. Rotaru[28b], I. Roth[175], J. Rothberg[140], D. Rousseau[119], A. Rozanov[88], Y. Rozen[154], X. Ruan[147c], F. Rubbo[145], M. S. Rudolph[161], F. Rühr[51], A. Ruiz-Martinez[31], Z. Rurikova[51], N. A. Rusakovich[68], A. Ruschke[102], H. L. Russell[140], J. P. Rutherfoord[7], N. Ruthmann[32], Y. F. Ryabov[125], M. Rybar[169], G. Rybkin[119], S. Ryu[6], A. Ryzhov[132], G. F. Rzehorz[57], A. F. Saavedra[152], G. Sabato[109], S. Sacerdoti[29], H. F-W. Sadrozinski[139], R. Sadykov[68], F. Safai Tehrani[134a], P. Saha[110], M. Sahinsoy[60a], M. Saimpert[138], T. Saito[157], H. Sakamoto[157], Y. Sakurai[174], G. Salamanna[136a,136b], A. Salamon[135a,135b], J. E. Salazar Loyola[34b], D. Salek[109], P. H. Sales De Bruin[140], D. Salihagic[103], A. Salnikov[145], J. Salt[170], D. Salvatore[40a,40b], F. Salvatore[151], A. Salvucci[62a,62b,62c], A. Salzburger[32], D. Sammel[51], D. Sampsonidis[156], J. Sánchez[170], V. Sanchez Martinez[170], A. Sanchez Pineda[106a,106b], H. Sandaker[121], R. L. Sandbach[79], M. Sandhoff[178], C. Sandoval[21], D. P. C. Sankey[133], M. Sannino[53a,53b], A. Sansoni[50], C. Santoni[37], R. Santonico[135a,135b], H. Santos[128a], I. Santoyo Castillo[151], K. Sapp[127], A. Sapronov[68], J. G. Saraiva[128a,128d], B. Sarrazin[23], O. Sasaki[69], K. Sato[164], E. Sauvan[5], G. Savage[80], P. Savard[161,d], N. Savic[103], C. Sawyer[133], L. Sawyer[82,s], J. Saxon[33], C. Sbarra[22a], A. Sbrizzi[22a,22b], T. Scanlon[81], D. A. Scannicchio[166], M. Scarcella[152], V. Scarfone[40a,40b], J. Schaarschmidt[175], P. Schacht[103], B. M. Schachtner[102], D. Schaefer[32], L. Schaefer[124], R. Schaefer[45], J. Schaeffer[86], S. Schaepe[23], S. Schaetzel[60b], U. Schäfer[86], A. C. Schaffer[119], D. Schaile[102], R. D. Schamberger[150], V. Scharf[60a], V. A. Schegelsky[125], D. Scheirich[131], M. Schernau[166], C. Schiavi[53a,53b], S. Schier[139], C. Schillo[51], M. Schioppa[40a,40b], S. Schlenker[32], K. R. Schmidt-Sommerfeld[103], K. Schmieden[32], C. Schmitt[86], S. Schmitt[45], S. Schmitz[86], B. Schneider[163a], U. Schnoor[51], L. Schoeffel[138], A. Schoening[60b], B. D. Schoenrock[93], E. Schopf[23], M. Schott[86], J. F. P. Schouwenberg[108], J. Schovancova[8], S. Schramm[52], M. Schreyer[177], N. Schuh[86], A. Schulte[86], M. J. Schultens[23], H.-C. Schultz-Coulon[60a], H. Schulz[17], M. Schumacher[51], B. A. Schumm[139], Ph. Schune[138], A. Schwartzman[145], T. A. Schwarz[92], H. Schweiger[87], Ph. Schwemling[138], R. Schwienhorst[93], J. Schwindling[138], T. Schwindt[23], G. Sciolla[25], F. Scuri[126a,126b], F. Scutti[91], J. Searcy[92], P. Seema[23], S. C. Seidel[107], A. Seiden[139], F. Seifert[130], J. M. Seixas[26a], G. Sekhniaidze[106a], K. Sekhon[92], S. J. Sekula[43], D. M. Seliverstov[125,*], N. Semprini-Cesari[22a,22b], C. Serfon[121], L. Serin[119], L. Serkin[167a,167b], M. Sessa[136a,136b], R. Seuster[172], H. Severini[115], T. Sfiligoj[78], F. Sforza[32], A. Sfyrla[52], E. Shabalina[57], N. W. Shaikh[148a,148b], L. Y. Shan[35a], R. Shang[169], J. T. Shank[24], M. Shapiro[16], P. B. Shatalov[99], K. Shaw[167a,167b], S. M. Shaw[87], A. Shcherbakova[148a,148b], C. Y. Shehu[151], P. Sherwood[81], L. Shi[153,an], S. Shimizu[70], C. O. Shimmin[166], M. Shimojima[104],

S. Shirabe[73], M. Shiyakova[68,ao], A. Shmeleva[98], D. Shoaleh Saadi[97], M. J. Shochet[33], S. Shojaii[94a], D. R. Shope[115], S. Shrestha[113], E. Shulga[100], M. A. Shupe[7], P. Sicho[129], A. M. Sickles[169], P. E. Sidebo[149], E. Sideras Haddad[147c], O. Sidiropoulou[177], D. Sidorov[116], A. Sidoti[22a,22b], F. Siegert[47], Dj. Sijacki[14], J. Silva[128a,128d], S. B. Silverstein[148a], V. Simak[130], Lj. Simic[14], S. Simion[119], E. Simioni[86], B. Simmons[81], D. Simon[37], M. Simon[86], P. Sinervo[161], N. B. Sinev[118], M. Sioli[22a,22b], G. Siragusa[177], S. Yu. Sivoklokov[101], J. Sjölin[148a,148b], M. B. Skinner[75], H. P. Skottowe[59], P. Skubic[115], M. Slater[19], T. Slavicek[130], M. Slawinska[109], K. Sliwa[165], R. Slovak[131], V. Smakhtin[175], B. H. Smart[5], L. Smestad[15], J. Smiesko[146a], S. Yu. Smirnov[100], Y. Smirnov[100], L. N. Smirnova[101,ap], O. Smirnova[84], J. W. Smith[57], M. N. K. Smith[38], R. W. Smith[38], M. Smizanska[75], K. Smolek[130], A. A. Snesarev[98], I. M. Snyder[118], S. Snyder[27], R. Sobie[172,n], F. Socher[47], A. Soffer[155], D. A. Soh[153], G. Sokhrannyi[78], C. A. Solans Sanchez[32], M. Solar[130], E. Yu. Soldatov[100], U. Soldevila[170], A. A. Solodkov[132], A. Soloshenko[68], O. V. Solovyanov[132], V. Solovyev[125], P. Sommer[51], H. Son[165], H. Y. Song[36a,aq], A. Sood[16], A. Sopczak[130], V. Sopko[130], V. Sorin[13], D. Sosa[60b], C. L. Sotiropoulou[126a,126b], R. Soualah[167a,167c], A. M. Soukharev[111,c], D. South[45], B. C. Sowden[80], S. Spagnolo[76a,76b], M. Spalla[126a,126b], M. Spangenberg[173], F. Spanò[80], D. Sperlich[17], F. Spettel[103], R. Spighi[22a], G. Spigo[32], L. A. Spiller[91], M. Spousta[131], R. D. St. Denis[56,*], A. Stabile[94a], R. Stamen[60a], S. Stamm[17], E. Stanecka[42], R. W. Stanek[6], C. Stanescu[136a], M. Stanescu-Bellu[45], M. M. Stanitzki[45], S. Stapnes[121], E. A. Starchenko[132], G. H. Stark[33], J. Stark[58], S. H Stark[39], P. Staroba[129], P. Starovoitov[60a], S. Stärz[32], R. Staszewski[42], P. Steinberg[27], B. Stelzer[144], H. J. Stelzer[32], O. Stelzer-Chilton[163a], H. Stenzel[55], G. A. Stewart[56], J. A. Stillings[23], M. C. Stockton[90], M. Stoebe[90], G. Stoicea[28b], P. Stolte[57], S. Stonjek[103], A. R. Stradling[8], A. Straessner[47], M. E. Stramaglia[18], J. Strandberg[149], S. Strandberg[148a,148b], A. Strandlie[121], M. Strauss[115], P. Strizenec[146b], R. Ströhmer[177], D. M. Strom[118], R. Stroynowski[43], A. Strubig[108], S. A. Stucci[27], B. Stugu[15], N. A. Styles[45], D. Su[145], J. Su[127], S. Suchek[60a], Y. Sugaya[120], M. Suk[130], V. V. Sulin[98], S. Sultansoy[4c], T. Sumida[71], S. Sun[59], X. Sun[35a], J. E. Sundermann[51], K. Suruliz[151], C. J. E. Suster[152], M. R. Sutton[151], S. Suzuki[69], M. Svatos[129], M. Swiatlowski[33], S. P. Swift[2], I. Sykora[146a], T. Sykora[131], D. Ta[51], C. Taccini[136a,136b], K. Tackmann[45], J. Taenzer[161], A. Taffard[166], R. Tafirout[163a], N. Taiblum[155], H. Takai[27], R. Takashima[72], T. Takeshita[142], Y. Takubo[69], M. Talby[88], A. A. Talyshev[111,c], K. G. Tan[91], J. Tanaka[157], M. Tanaka[159], R. Tanaka[119], S. Tanaka[69], R. Tanioka[70], B. B. Tannenwald[113], S. Tapia Araya[34b], S. Tapprogge[86], S. Tarem[154], G. F. Tartarelli[94a], P. Tas[131], M. Tasevsky[129], T. Tashiro[71], E. Tassi[40a,40b], A. Tavares Delgado[128a,128b], Y. Tayalati[137e], A. C. Taylor[107], G. N. Taylor[91], P. T. E. Taylor[91], W. Taylor[163b], F. A. Teischinger[32], P. Teixeira-Dias[80], K. K. Temming[51], D. Temple[144], H. Ten Kate[32], P. K. Teng[153], J. J. Teoh[120], F. Tepel[178], S. Terada[69], K. Terashi[157], J. Terron[85], S. Terzo[13], M. Testa[50], R. J. Teuscher[161,n], T. Theveneaux-Pelzer[88], J. P. Thomas[19], J. Thomas-Wilsker[80], P. D. Thompson[19], A. S. Thompson[56], L. A. Thomsen[179], E. Thomson[124], M. J. Tibbetts[16], R. E. Ticse Torres[88], V. O. Tikhomirov[98,ar], Yu. A. Tikhonov[111,c], S. Timoshenko[100], P. Tipton[179], S. Tisserant[88], K. Todome[159], T. Todorov[5,*], S. Todorova-Nova[131], J. Tojo[73], S. Tokár[146a], K. Tokushuku[69], E. Tolley[59], L. Tomlinson[87], M. Tomoto[105], L. Tompkins[145,as], K. Toms[107], B. Tong[59], P. Tornambe[51], E. Torrence[118], H. Torres[144], E. Torró Pastor[140], J. Toth[88,at], F. Touchard[88], D. R. Tovey[141], T. Trefzger[177], A. Tricoli[27], I. M. Trigger[163a], S. Trincaz-Duvoid[83], M. F. Tripiana[13], W. Trischuk[161], B. Trocmé[58], A. Trofymov[45], C. Troncon[94a], M. Trottier-McDonald[16], M. Trovatelli[172], L. Truong[167a,167c], M. Trzebinski[42], A. Trzupek[42], J. C-L. Tseng[122], P. V. Tsiareshka[95], G. Tsipolitis[10], N. Tsirintanis[9], S. Tsiskaridze[13], V. Tsiskaridze[51], E. G. Tskhadadze[54a], K. M. Tsui[62a], I. I. Tsukerman[99], V. Tsulaia[16], S. Tsuno[69], D. Tsybychev[150], Y. Tu[62b], A. Tudorache[28b], V. Tudorache[28b], T. T. Tulbure[28a], A. N. Tuna[59], S. A. Tupputi[22a,22b], S. Turchikhin[68], D. Turgeman[175], I. Turk Cakir[4b,au], R. Turra[94a,94b], P. M. Tuts[38], G. Ucchielli[22a,22b], I. Ueda[157], M. Ughetto[148a,148b], F. Ukegawa[164], G. Unal[32], A. Undrus[27], G. Unel[166], F. C. Ungaro[91], Y. Unno[69], C. Unverdorben[102], J. Urban[146b], P. Urquijo[91], P. Urrejola[86], G. Usai[8], J. Usui[69], L. Vacavant[88], V. Vacek[130], B. Vachon[90], C. Valderanis[102], E. Valdes Santurio[148a,148b], N. Valencic[109], S. Valentinetti[22a,22b], A. Valero[170], L. Valery[13], S. Valkar[131], J. A. Valls Ferrer[170], W. Van Den Wollenberg[109], P. C. Van Der Deijl[109], H. van der Graaf[109], N. van Eldik[154], P. van Gemmeren[6], J. Van Nieuwkoop[144], I. van Vulpen[109], M. C. van Woerden[109], M. Vanadia[134a,134b], W. Vandelli[32], R. Vanguri[124], A. Vaniachine[160], P. Vankov[109], G. Vardanyan[180], R. Vari[134a], E. W. Varnes[7], T. Varol[43], D. Varouchas[83], A. Vartapetian[8], K. E. Varvell[152], J. G. Vasquez[179], G. A. Vasquez[34b], F. Vazeille[37], T. Vazquez Schroeder[90], J. Veatch[57], V. Veeraraghavan[7], L. M. Veloce[161], F. Veloso[128a,128c], S. Veneziano[134a], A. Ventura[76a,76b], M. Venturi[172], N. Venturi[161], A. Venturini[25], V. Vercesi[123a], M. Verducci[134a,134b], W. Verkerke[109], J. C. Vermeulen[109], A. Vest[47,av], M. C. Vetterli[144,d], O. Viazlo[84], I. Vichou[169,*], T. Vickey[141], O. E. Vickey Boeriu[141], G. H. A. Viehhauser[122], S. Viel[16], L. Vigani[122], M. Villa[22a,22b], M. Villaplana Perez[94a,94b], E. Vilucchi[50], M. G. Vincter[31], V. B. Vinogradov[68], C. Vittori[22a,22b], I. Vivarelli[151], S. Vlachos[10], M. Vlasak[130], M. Vogel[178], P. Vokac[130], G. Volpi[126a,126b], M. Volpi[91], H. von der Schmitt[103], E. von Toerne[23], V. Vorobel[131], K. Vorobev[100], M. Vos[170], R. Voss[32], J. H. Vossebeld[77], N. Vranjes[14], M. Vranjes Milosavljevic[14], V. Vrba[129], M. Vreeswijk[109], R. Vuillermet[32], I. Vukotic[33], P. Wagner[23], W. Wagner[178], H. Wahlberg[74], S. Wahrmund[47], J. Wakabayashi[105], J. Walder[75], R. Walker[102], W. Walkowiak[143], V. Wallangen[148a,148b], C. Wang[35b], C. Wang[36b,aw], F. Wang[176], H. Wang[16], H. Wang[43], J. Wang[45], J. Wang[152], K. Wang[90],

R. Wang[6], S. M. Wang[153], T. Wang[38], W. Wang[36a], C. Wanotayaroj[118], A. Warburton[90], C. P. Ward[30], D. R. Wardrope[81], A. Washbrook[49], P. M. Watkins[19], A. T. Watson[19], M. F. Watson[19], G. Watts[140], S. Watts[87], B. M. Waugh[81], S. Webb[86], M. S. Weber[18], S. W. Weber[177], S. A. Weber[31], J. S. Webster[6], A. R. Weidberg[122], B. Weinert[64], J. Weingarten[57], C. Weiser[51], H. Weits[109], P. S. Wells[32], T. Wenaus[27], T. Wengler[32], S. Wenig[32], N. Wermes[23], M. D. Werner[67], P. Werner[32], M. Wessels[60a], J. Wetter[165], K. Whalen[118], N. L. Whallon[140], A. M. Wharton[75], A. White[8], M. J. White[1], R. White[34b], D. Whiteson[166], F. J. Wickens[133], W. Wiedenmann[176], M. Wielers[133], C. Wiglesworth[39], L. A. M. Wiik-Fuchs[23], A. Wildauer[103], F. Wilk[87], H. G. Wilkens[32], H. H. Williams[124], S. Williams[109], C. Willis[93], S. Willocq[89], J. A. Wilson[19], I. Wingerter-Seez[5], F. Winklmeier[118], O. J. Winston[151], B. T. Winter[23], M. Wittgen[145], T. M. H. Wolf[109], R. Wolff[88], M. W. Wolter[42], H. Wolters[128a,128c], S. D. Worm[133], B. K. Wosiek[42], J. Wotschack[32], M. J. Woudstra[87], K. W. Wozniak[42], M. Wu[58], M. Wu[33], S. L. Wu[176], X. Wu[52], Y. Wu[92], T. R. Wyatt[87], B. M. Wynne[49], S. Xella[39], Z. Xi[92], D. Xu[35a], L. Xu[27], B. Yabsley[152], S. Yacoob[147a], D. Yamaguchi[159], Y. Yamaguchi[120], A. Yamamoto[69], S. Yamamoto[157], T. Yamanaka[157], K. Yamauchi[105], Y. Yamazaki[70], Z. Yan[24], H. Yang[36c], H. Yang[176], Y. Yang[153], Z. Yang[15], W-M. Yao[16], Y. C. Yap[83], Y. Yasu[69], E. Yatsenko[5], K. H. Yau Wong[23], J. Ye[43], S. Ye[27], I. Yeletskikh[68], E. Yildirim[86], K. Yorita[174], R. Yoshida[6], K. Yoshihara[124], C. Young[145], C. J. S. Young[32], S. Youssef[24], D. R. Yu[16], J. Yu[8], J. M. Yu[92], J. Yu[67], L. Yuan[70], S. P. Y. Yuen[23], I. Yusuff[30,ax], B. Zabinski[42], G. Zacharis[10], R. Zaidan[66], A. M. Zaitsev[132,ag], N. Zakharchuk[45], J. Zalieckas[15], A. Zaman[150], S. Zambito[59], L. Zanello[134a,134b], D. Zanzi[91], C. Zeitnitz[178], M. Zeman[130], A. Zemla[41a], J. C. Zeng[169], Q. Zeng[145], O. Zenin[132], T. Ženiš[146a], D. Zerwas[119], D. Zhang[92], F. Zhang[176], G. Zhang[36a,aq], H. Zhang[35b], J. Zhang[6], L. Zhang[51], L. Zhang[36a], M. Zhang[169], R. Zhang[23], R. Zhang[36a,aw], X. Zhang[36b], Z. Zhang[119], X. Zhao[43], Y. Zhao[36b,ay], Z. Zhao[36a], A. Zhemchugov[68], J. Zhong[122], B. Zhou[92], C. Zhou[176], L. Zhou[38], L. Zhou[43], M. Zhou[150], N. Zhou[35c], C. G. Zhu[36b], H. Zhu[35a], J. Zhu[92], Y. Zhu[36a], X. Zhuang[35a], K. Zhukov[98], A. Zibell[177], D. Zieminska[64], N. I. Zimine[68], C. Zimmermann[86], S. Zimmermann[51], Z. Zinonos[57], M. Zinser[86], M. Ziolkowski[143], L. Živković[14], G. Zobernig[176], A. Zoccoli[22a,22b], M. zur Nedden[17], L. Zwalinski[32]

[1] Department of Physics, University of Adelaide, Adelaide, SA, Australia
[2] Physics Department, SUNY Albany, Albany, NY, USA
[3] Department of Physics, University of Alberta, Edmonton, AB, Canada
[4] [(a)]Department of Physics, Ankara University, Ankara, Turkey; [(b)]Istanbul Aydin University, Istanbul, Turkey; [(c)]Division of Physics, TOBB University of Economics and Technology, Ankara, Turkey
[5] LAPP, CNRS/IN2P3 and Université Savoie Mont Blanc, Annecy-le-Vieux, France
[6] High Energy Physics Division, Argonne National Laboratory, Argonne, IL, USA
[7] Department of Physics, University of Arizona, Tucson, AZ, USA
[8] Department of Physics, The University of Texas at Arlington, Arlington, TX, USA
[9] Physics Department, National and Kapodistrian University of Athens, Athens, Greece
[10] Physics Department, National Technical University of Athens, Zografou, Greece
[11] Department of Physics, The University of Texas at Austin, Austin, TX, USA
[12] Institute of Physics, Azerbaijan Academy of Sciences, Baku, Azerbaijan
[13] Institut de Física d'Altes Energies (IFAE), The Barcelona Institute of Science and Technology, Barcelona, Spain
[14] Institute of Physics, University of Belgrade, Belgrade, Serbia
[15] Department for Physics and Technology, University of Bergen, Bergen, Norway
[16] Physics Division, Lawrence Berkeley National Laboratory and University of California, Berkeley, CA, USA
[17] Department of Physics, Humboldt University, Berlin, Germany
[18] Albert Einstein Center for Fundamental Physics and Laboratory for High Energy Physics, University of Bern, Bern, Switzerland
[19] School of Physics and Astronomy, University of Birmingham, Birmingham, UK
[20] [(a)]Department of Physics, Bogazici University, Istanbul, Turkey; [(b)]Department of Physics Engineering, Gaziantep University, Gaziantep, Turkey; [(c)]Faculty of Engineering and Natural Sciences, Istanbul Bilgi University, Istanbul, Turkey; [(d)]Faculty of Engineering and Natural Sciences, Bahcesehir University, Istanbul, Turkey
[21] Centro de Investigaciones, Universidad Antonio Narino, Bogota, Colombia
[22] [(a)]INFN Sezione di Bologna, Bologna, Italy; [(b)]Dipartimento di Fisica e Astronomia, Università di Bologna, Bologna, Italy
[23] Physikalisches Institut, University of Bonn, Bonn, Germany
[24] Department of Physics, Boston University, Boston, MA, USA
[25] Department of Physics, Brandeis University, Waltham, MA, USA

[26] [(a)]Universidade Federal do Rio De Janeiro COPPE/EE/IF, Rio de Janeiro, Brazil; [(b)]Electrical Circuits Department, Federal University of Juiz de Fora (UFJF), Juiz de Fora, Brazil; [(c)]Federal University of Sao Joao del Rei (UFSJ), Sao Joao del Rei, Brazil; [(d)]Instituto de Fisica, Universidade de Sao Paulo, Sao Paulo, Brazil
[27] Physics Department, Brookhaven National Laboratory, Upton, NY, USA
[28] [(a)]Transilvania University of Brasov, Brasov, Romania; [(b)]Horia Hulubei National Institute of Physics and Nuclear Engineering, Bucharest, Romania; [(c)]Physics Department, National Institute for Research and Development of Isotopic and Molecular Technologies, Cluj-Napoca, Romania; [(d)]University Politehnica Bucharest, Bucharest, Romania; [(e)]West University in Timisoara, Timisoara, Romania
[29] Departamento de Física, Universidad de Buenos Aires, Buenos Aires, Argentina
[30] Cavendish Laboratory, University of Cambridge, Cambridge, UK
[31] Department of Physics, Carleton University, Ottawa, ON, Canada
[32] CERN, Geneva, Switzerland
[33] Enrico Fermi Institute, University of Chicago, Chicago, IL, USA
[34] [(a)]Departamento de Física, Pontificia Universidad Católica de Chile, Santiago, Chile; [(b)]Departamento de Física, Universidad Técnica Federico Santa María, Valparaíso, Chile
[35] [(a)]Institute of High Energy Physics, Chinese Academy of Sciences, Beijing, China; [(b)]Department of Physics, Nanjing University, Nanjing, Jiangsu, China; [(c)]Physics Department, Tsinghua University, Beijing 100084, China
[36] [(a)]Department of Modern Physics, University of Science and Technology of China, Anhui, China; [(b)]School of Physics, Shandong University, Shandong, China; [(c)]Department of Physics and Astronomy, Key Laboratory for Particle Physics, Astrophysics and Cosmology,Ministry of Education,Shanghai Key Laboratory for Particle Physics and Cosmology, Shanghai Jiao Tong University (also at PKU-CHEP), Shanghai, China
[37] Laboratoire de Physique Corpusculaire, Université Clermont Auvergne, Université Blaise Pascal, CNRS/IN2P3, Clermont-Ferrand, France
[38] Nevis Laboratory, Columbia University, Irvington, NY, USA
[39] Niels Bohr Institute, University of Copenhagen, Kobenhavn, Denmark
[40] [(a)]INFN Gruppo Collegato di Cosenza, Laboratori Nazionali di Frascati, Frascati, Italy; [(b)]Dipartimento di Fisica, Università della Calabria, Rende, Italy
[41] [(a)]Faculty of Physics and Applied Computer Science, AGH University of Science and Technology, Kraków, Poland; [(b)]Marian Smoluchowski Institute of Physics, Jagiellonian University, Krakow, Poland
[42] Institute of Nuclear Physics Polish Academy of Sciences, Krakow, Poland
[43] Physics Department, Southern Methodist University, Dallas, TX, USA
[44] Physics Department, University of Texas at Dallas, Richardson, TX, USA
[45] DESY, Hamburg and Zeuthen, Germany
[46] Lehrstuhl für Experimentelle Physik IV, Technische Universität Dortmund, Dortmund, Germany
[47] Institut für Kern- und Teilchenphysik, Technische Universität Dresden, Dresden, Germany
[48] Department of Physics, Duke University, Durham, NC, USA
[49] SUPA-School of Physics and Astronomy, University of Edinburgh, Edinburgh, UK
[50] INFN Laboratori Nazionali di Frascati, Frascati, Italy
[51] Fakultät für Mathematik und Physik, Albert-Ludwigs-Universität, Freiburg, Germany
[52] Departement de Physique Nucleaire et Corpusculaire, Université de Genève, Geneva, Switzerland
[53] [(a)]INFN Sezione di Genova, Genoa, Italy; [(b)]Dipartimento di Fisica, Università di Genova, Genova, Italy
[54] [(a)]E. Andronikashvili Institute of Physics, Iv. Javakhishvili Tbilisi State University, Tbilisi, Georgia; [(b)]High Energy Physics Institute, Tbilisi State University, Tbilisi, Georgia
[55] II Physikalisches Institut, Justus-Liebig-Universität Giessen, Giessen, Germany
[56] SUPA-School of Physics and Astronomy, University of Glasgow, Glasgow, UK
[57] II Physikalisches Institut, Georg-August-Universität, Göttingen, Germany
[58] Laboratoire de Physique Subatomique et de Cosmologie, Université Grenoble-Alpes, CNRS/IN2P3, Grenoble, France
[59] Laboratory for Particle Physics and Cosmology, Harvard University, Cambridge, MA, USA
[60] [(a)]Kirchhoff-Institut für Physik, Ruprecht-Karls-Universität Heidelberg, Heidelberg, Germany; [(b)]Physikalisches Institut, Ruprecht-Karls-Universität Heidelberg, Heidelberg, Germany; [(c)]ZITI Institut für technische Informatik, Ruprecht-Karls-Universität Heidelberg, Mannheim, Germany
[61] Faculty of Applied Information Science, Hiroshima Institute of Technology, Hiroshima, Japan

[62] [(a)]Department of Physics, The Chinese University of Hong Kong, Shatin, NT, Hong Kong; [(b)]Department of Physics, The University of Hong Kong, Hong Kong, China; [(c)]Department of Physics and Institute for Advanced Study, The Hong Kong University of Science and Technology, Clear Water Bay, Kowloon, Hong Kong, China
[63] Department of Physics, National Tsing Hua University, Taiwan, Taiwan
[64] Department of Physics, Indiana University, Bloomington, IN, USA
[65] Institut für Astro- und Teilchenphysik, Leopold-Franzens-Universität, Innsbruck, Austria
[66] University of Iowa, Iowa city, IA, USA
[67] Department of Physics and Astronomy, Iowa State University, Ames, IA, USA
[68] Joint Institute for Nuclear Research, JINR Dubna, Dubna, Russia
[69] KEK, High Energy Accelerator Research Organization, Tsukuba, Japan
[70] Graduate School of Science, Kobe University, Kobe, Japan
[71] Faculty of Science, Kyoto University, Kyoto, Japan
[72] Kyoto University of Education, Kyoto, Japan
[73] Department of Physics, Kyushu University, Fukuoka, Japan
[74] Instituto de Física La Plata, Universidad Nacional de La Plata and CONICET, La Plata, Argentina
[75] Physics Department, Lancaster University, Lancaster, UK
[76] [(a)]INFN Sezione di Lecce, Lecce, Italy; [(b)]Dipartimento di Matematica e Fisica, Università del Salento, Lecce, Italy
[77] Oliver Lodge Laboratory, University of Liverpool, Liverpool, UK
[78] Department of Experimental Particle Physics, Jožef Stefan Institute and Department of Physics, University of Ljubljana, Ljubljana, Slovenia
[79] School of Physics and Astronomy, Queen Mary University of London, London, UK
[80] Department of Physics, Royal Holloway University of London, Surrey, UK
[81] Department of Physics and Astronomy, University College London, London, UK
[82] Louisiana Tech University, Ruston, LA, USA
[83] Laboratoire de Physique Nucléaire et de Hautes Energies, UPMC and Université Paris-Diderot and CNRS/IN2P3, Paris, France
[84] Fysiska institutionen, Lunds universitet, Lund, Sweden
[85] Departamento de Fisica Teorica C-15, Universidad Autonoma de Madrid, Madrid, Spain
[86] Institut für Physik, Universität Mainz, Mainz, Germany
[87] School of Physics and Astronomy, University of Manchester, Manchester, UK
[88] CPPM, Aix-Marseille Université and CNRS/IN2P3, Marseille, France
[89] Department of Physics, University of Massachusetts, Amherst, MA, USA
[90] Department of Physics, McGill University, Montreal, QC, Canada
[91] School of Physics, University of Melbourne, Melbourne, VIC, Australia
[92] Department of Physics, The University of Michigan, Ann Arbor, MI, USA
[93] Department of Physics and Astronomy, Michigan State University, East Lansing, MI, USA
[94] [(a)]INFN Sezione di Milano, Milan, Italy; [(b)]Dipartimento di Fisica, Università di Milano, Milano, Italy
[95] B.I. Stepanov Institute of Physics, National Academy of Sciences of Belarus, Minsk, Republic of Belarus
[96] Research Institute for Nuclear Problems of Byelorussian State University, Minsk, Republic of Belarus
[97] Group of Particle Physics, University of Montreal, Montreal, QC, Canada
[98] P.N. Lebedev Physical Institute of the Russian Academy of Sciences, Moscow, Russia
[99] Institute for Theoretical and Experimental Physics (ITEP), Moscow, Russia
[100] National Research Nuclear University MEPhI, Moscow, Russia
[101] D.V. Skobeltsyn Institute of Nuclear Physics, M.V. Lomonosov Moscow State University, Moscow, Russia
[102] Fakultät für Physik, Ludwig-Maximilians-Universität München, München, Germany
[103] Max-Planck-Institut für Physik (Werner-Heisenberg-Institut), München, Germany
[104] Nagasaki Institute of Applied Science, Nagasaki, Japan
[105] Graduate School of Science and Kobayashi-Maskawa Institute, Nagoya University, Nagoya, Japan
[106] [(a)]INFN Sezione di Napoli, Napoli, Italy; [(b)]Dipartimento di Fisica, Università di Napoli, Napoli, Italy
[107] Department of Physics and Astronomy, University of New Mexico, Albuquerque, NM, USA
[108] Institute for Mathematics, Astrophysics and Particle Physics, Radboud University Nijmegen/Nikhef, Nijmegen, Netherlands
[109] Nikhef National Institute for Subatomic Physics and University of Amsterdam, Amsterdam, Netherlands

[110] Department of Physics, Northern Illinois University, DeKalb, IL, USA
[111] Budker Institute of Nuclear Physics, SB RAS, Novosibirsk, Russia
[112] Department of Physics, New York University, New York, NY, USA
[113] Ohio State University, Columbus, OH, USA
[114] Faculty of Science, Okayama University, Okayama, Japan
[115] Homer L. Dodge Department of Physics and Astronomy, University of Oklahoma, Norman, OK, USA
[116] Department of Physics, Oklahoma State University, Stillwater, OK, USA
[117] Palacký University, RCPTM, Olomouc, Czech Republic
[118] Center for High Energy Physics, University of Oregon, Eugene, OR, USA
[119] LAL, University of Paris-Sud, CNRS/IN2P3, Université Paris-Saclay, Orsay, France
[120] Graduate School of Science, Osaka University, Osaka, Japan
[121] Department of Physics, University of Oslo, Oslo, Norway
[122] Department of Physics, Oxford University, Oxford, UK
[123] [(a)]INFN Sezione di Pavia, Pavia, Italy; [(b)]Dipartimento di Fisica, Università di Pavia, Pavia, Italy
[124] Department of Physics, University of Pennsylvania, Philadelphia, PA, USA
[125] National Research Centre "Kurchatov Institute" B.P. Konstantinov Petersburg Nuclear Physics Institute, St. Petersburg, Russia
[126] [(a)]INFN Sezione di Pisa, Pisa, Italy; [(b)]Dipartimento di Fisica E. Fermi, Università di Pisa, Pisa, Italy
[127] Department of Physics and Astronomy, University of Pittsburgh, Pittsburgh, PA, USA
[128] [(a)]Laboratório de Instrumentação e Física Experimental de Partículas-LIP, Lisboa, Portugal; [(b)]Faculdade de Ciências, Universidade de Lisboa, Lisboa, Portugal; [(c)]Department of Physics, University of Coimbra, Coimbra, Portugal; [(d)]Centro de Física Nuclear da Universidade de Lisboa, Lisboa, Portugal; [(e)]Departamento de Fisica, Universidade do Minho, Braga, Portugal; [(f)]Departamento de Fisica Teorica y del Cosmos and CAFPE, Universidad de Granada, Granada, Spain; [(g)]Dep Fisica and CEFITEC of Faculdade de Ciencias e Tecnologia, Universidade Nova de Lisboa, Caparica, Portugal
[129] Institute of Physics, Academy of Sciences of the Czech Republic, Praha, Czech Republic
[130] Czech Technical University in Prague, Praha, Czech Republic
[131] Charles University, Faculty of Mathematics and Physics, Prague, Czech Republic
[132] State Research Center Institute for High Energy Physics (Protvino), NRC KI, Moscow, Russia
[133] Particle Physics Department, Rutherford Appleton Laboratory, Didcot, UK
[134] [(a)]INFN Sezione di Roma, Roma, Italy; [(b)]Dipartimento di Fisica, Sapienza Università di Roma, Roma, Italy
[135] [(a)]INFN Sezione di Roma Tor Vergata, Roma, Italy; [(b)]Dipartimento di Fisica, Università di Roma Tor Vergata, Roma, Italy
[136] [(a)]INFN Sezione di Roma Tre, Roma, Italy; [(b)]Dipartimento di Matematica e Fisica, Università Roma Tre, Roma, Italy
[137] [(a)]Faculté des Sciences Ain Chock, Réseau Universitaire de Physique des Hautes Energies-Université Hassan II, Casablanca, Morocco; [(b)]Centre National de l'Energie des Sciences Techniques Nucleaires, Rabat, Morocco; [(c)]Faculté des Sciences Semlalia, Université Cadi Ayyad, LPHEA-Marrakech, Marrakech, Morocco; [(d)]Faculté des Sciences, Université Mohamed Premier and LPTPM, Oujda, Morocco; [(e)]Faculté des Sciences, Université Mohammed V, Rabat, Morocco
[138] DSM/IRFU (Institut de Recherches sur les Lois Fondamentales de l'Univers), CEA Saclay (Commissariat à l'Energie Atomique et aux Energies Alternatives), Gif-sur-Yvette, France
[139] Santa Cruz Institute for Particle Physics, University of California Santa Cruz, Santa Cruz, CA, USA
[140] Department of Physics, University of Washington, Seattle, WA, USA
[141] Department of Physics and Astronomy, University of Sheffield, Sheffield, UK
[142] Department of Physics, Shinshu University, Nagano, Japan
[143] Fachbereich Physik, Universität Siegen, Siegen, Germany
[144] Department of Physics, Simon Fraser University, Burnaby, BC, Canada
[145] SLAC National Accelerator Laboratory, Stanford, CA, USA
[146] [(a)]Faculty of Mathematics, Physics and Informatics, Comenius University, Bratislava, Slovak Republic; [(b)]Department of Subnuclear Physics, Institute of Experimental Physics of the Slovak Academy of Sciences, Kosice, Slovak Republic
[147] [(a)]Department of Physics, University of Cape Town, Cape Town, South Africa; [(b)]Department of Physics, University of Johannesburg, Johannesburg, South Africa; [(c)]School of Physics, University of the Witwatersrand, Johannesburg, South Africa

[148] [(a)]Department of Physics, Stockholm University, Stockholm, Sweden; [(b)]The Oskar Klein Centre, Stockholm, Sweden
[149] Physics Department, Royal Institute of Technology, Stockholm, Sweden
[150] Departments of Physics and Astronomy and Chemistry, Stony Brook University, Stony Brook, NY, USA
[151] Department of Physics and Astronomy, University of Sussex, Brighton, UK
[152] School of Physics, University of Sydney, Sydney, SA, Australia
[153] Institute of Physics, Academia Sinica, Taipei, Taiwan
[154] Department of Physics, Technion: Israel Institute of Technology, Haifa, Israel
[155] Raymond and Beverly Sackler School of Physics and Astronomy, Tel Aviv University, Tel Aviv, Israel
[156] Department of Physics, Aristotle University of Thessaloniki, Thessaloníki, Greece
[157] International Center for Elementary Particle Physics and Department of Physics, The University of Tokyo, Tokyo, Japan
[158] Graduate School of Science and Technology, Tokyo Metropolitan University, Tokyo, Japan
[159] Department of Physics, Tokyo Institute of Technology, Tokyo, Japan
[160] Tomsk State University, Tomsk, Russia
[161] Department of Physics, University of Toronto, Toronto, ON, Canada
[162] [(a)]INFN-TIFPA, Trento, Italy; [(b)]University of Trento, Trento, Italy
[163] [(a)]TRIUMF, Vancouver, BC, Canada; [(b)]Department of Physics and Astronomy, York University, Toronto, ON, Canada
[164] Faculty of Pure and Applied Sciences, and Center for Integrated Research in Fundamental Science and Engineering, University of Tsukuba, Tsukuba, Japan
[165] Department of Physics and Astronomy, Tufts University, Medford, MA, USA
[166] Department of Physics and Astronomy, University of California Irvine, Irvine, CA, USA
[167] [(a)]INFN Gruppo Collegato di Udine, Sezione di Trieste, Udine, Italy; [(b)]ICTP, Trieste, Italy; [(c)]Dipartimento di Chimica, Fisica e Ambiente, Università di Udine, Udine, Italy
[168] Department of Physics and Astronomy, University of Uppsala, Uppsala, Sweden
[169] Department of Physics, University of Illinois, Urbana, IL, USA
[170] Instituto de Fisica Corpuscular (IFIC) and Departamento de Fisica Atomica, Molecular y Nuclear and Departamento de Ingeniería Electrónica and Instituto de Microelectrónica de Barcelona (IMB-CNM), University of Valencia and CSIC, Valencia, Spain
[171] Department of Physics, University of British Columbia, Vancouver, BC, Canada
[172] Department of Physics and Astronomy, University of Victoria, Victoria, BC, Canada
[173] Department of Physics, University of Warwick, Coventry, UK
[174] Waseda University, Tokyo, Japan
[175] Department of Particle Physics, The Weizmann Institute of Science, Rehovot, Israel
[176] Department of Physics, University of Wisconsin, Madison, WI, USA
[177] Fakultät für Physik und Astronomie, Julius-Maximilians-Universität, Würzburg, Germany
[178] Fakultät für Mathematik und Naturwissenschaften, Fachgruppe Physik, Bergische Universität Wuppertal, Wuppertal, Germany
[179] Department of Physics, Yale University, New Haven, CT, USA
[180] Yerevan Physics Institute, Yerevan, Armenia
[181] Centre de Calcul de l'Institut National de Physique Nucléaire et de Physique des Particules (IN2P3), Villeurbanne, France

[a] Also at Department of Physics, King's College London, London, UK
[b] Also at Institute of Physics, Azerbaijan Academy of Sciences, Baku, Azerbaijan
[c] Also at Novosibirsk State University, Novosibirsk, Russia
[d] Also at TRIUMF, Vancouver BC, Canada
[e] Also at Department of Physics and Astronomy, University of Louisville, Louisville, KY, USA
[f] Also at Physics Department, An-Najah National University, Nablus, Palestine
[g] Also at Department of Physics, California State University, Fresno CA, USA
[h] Also at Department of Physics, University of Fribourg, Fribourg, Switzerland
[i] Also at Departament de Fisica de la Universitat Autonoma de Barcelona, Barcelona, Spain
[j] Also at Departamento de Fisica e Astronomia, Faculdade de Ciencias, Universidade do Porto, Portugal
[k] Also at Tomsk State University, Tomsk, Russia, Russia
[l] Also at The Collaborative Innovation Center of Quantum Matter (CICQM), Beijing, China
[m] Also at Universita di Napoli Parthenope, Napoli, Italy

[n] Also at Institute of Particle Physics (IPP), Victoria, BC, Canada
[o] Also at Horia Hulubei National Institute of Physics and Nuclear Engineering, Bucharest, Romania
[p] Also at Department of Physics, St. Petersburg State Polytechnical University, St. Petersburg, Russia
[q] Also at Department of Physics, The University of Michigan, Ann Arbor MI, USA
[r] Also at Centre for High Performance Computing, CSIR Campus, Rosebank, Cape Town, South Africa
[s] Also at Louisiana Tech University, Ruston LA, USA
[t] Also at Institucio Catalana de Recerca i Estudis Avancats, ICREA, Barcelona, Spain
[u] Also at Graduate School of Science, Osaka University, Osaka, Japan
[v] Also at Institute for Mathematics, Astrophysics and Particle Physics, Radboud University Nijmegen/Nikhef, Nijmegen, Netherlands
[w] Also at Department of Physics, The University of Texas at Austin, Austin TX, USA
[x] Also at Institute of Theoretical Physics, Ilia State University, Tbilisi, Georgia
[y] Also at CERN, Geneva, Switzerland
[z] Also at Georgian Technical University (GTU), Tbilisi, Georgia
[aa] Also at Ochadai Academic Production, Ochanomizu University, Tokyo, Japan
[ab] Also at Manhattan College, New York NY, USA
[ac] Also at Academia Sinica Grid Computing, Institute of Physics, Academia Sinica, Taipei, Taiwan
[ad] Also at School of Physics, Shandong University, Shandong, China
[ae] Also at Departamento de Fisica Teorica y del Cosmos and CAFPE, Universidad de Granada, Granada, Spain
[af] Also at Department of Physics, California State University, Sacramento CA, USA
[ag] Also at Moscow Institute of Physics and Technology State University, Dolgoprudny, Russia
[ah] Also at Departement de Physique Nucleaire et Corpusculaire, Université de Genève, Geneva, Switzerland
[ai] Also at Eotvos Lorand University, Budapest, Hungary
[aj] Also at Departments of Physics and Astronomy and Chemistry, Stony Brook University, Stony Brook NY, USA
[ak] Also at International School for Advanced Studies (SISSA), Trieste, Italy
[al] Also at Department of Physics and Astronomy, University of South Carolina, Columbia SC, USA
[am] Also at Institut de Física d'Altes Energies (IFAE), The Barcelona Institute of Science and Technology, Barcelona, Spain
[an] Also at School of Physics, Sun Yat-sen University, Guangzhou, China
[ao] Also at Institute for Nuclear Research and Nuclear Energy (INRNE) of the Bulgarian Academy of Sciences, Sofia, Bulgaria
[ap] Also at Faculty of Physics, M.V.Lomonosov Moscow State University, Moscow, Russia
[aq] Also at Institute of Physics, Academia Sinica, Taipei, Taiwan
[ar] Also at National Research Nuclear University MEPhI, Moscow, Russia
[as] Also at Department of Physics, Stanford University, Stanford CA, USA
[at] Also at Institute for Particle and Nuclear Physics, Wigner Research Centre for Physics, Budapest, Hungary
[au] Also at Giresun University, Faculty of Engineering, Turkey
[av] Also at Flensburg University of Applied Sciences, Flensburg, Germany
[aw] Also at CPPM, Aix-Marseille Université and CNRS/IN2P3, Marseille, France
[ax] Also at University of Malaya, Department of Physics, Kuala Lumpur, Malaysia
[ay] Also at LAL, Univ. Paris-Sud, CNRS/IN2P3, Université Paris-Saclay, Orsay, France
*Deceased

Eur. Phys. J. C (2017) 77:292
DOI 10.1140/epjc/s10052-017-4821-x

THE EUROPEAN PHYSICAL JOURNAL C

Regular Article - Experimental Physics

Measurements of top-quark pair differential cross-sections in the $e\mu$ channel in pp collisions at $\sqrt{s} = 13$ TeV using the ATLAS detector

ATLAS Collaboration[*]

CERN, 1211 Geneva 23, Switzerland

Received: 16 December 2016 / Accepted: 12 April 2017 / Published online: 8 May 2017

Abstract This article presents measurements of $t\bar{t}$ differential cross-sections in a fiducial phase-space region, using an integrated luminosity of 3.2 fb^{-1} of proton–proton data at a centre-of-mass energy of $\sqrt{s} = 13$ TeV recorded by the ATLAS experiment at the LHC in 2015. Differential cross-sections are measured as a function of the transverse momentum and absolute rapidity of the top quark, and of the transverse momentum, absolute rapidity and invariant mass of the $t\bar{t}$ system. The $t\bar{t}$ events are selected by requiring one electron and one muon of opposite electric charge, and at least two jets, one of which must be tagged as containing a b-hadron. The measured differential cross-sections are compared to predictions of next-to-leading order generators matched to parton showers and the measurements are found to be consistent with all models within the experimental uncertainties with the exception of the POWHEG-BOX + Herwig++ predictions, which differ significantly from the data in both the transverse momentum of the top quark and the mass of the $t\bar{t}$ system.

Contents

[*] e-mail: atlas.publications@cern.ch

1 Introduction

The top quark is the heaviest fundamental particle in the standard model (SM) of particle physics. Understanding the production cross-section and kinematics of $t\bar{t}$ pairs is an important test of SM predictions. Furthermore, $t\bar{t}$ production is often an important background in searches for new physics and a detailed understanding of this process is therefore crucial.

At the large hadron collider (LHC), $t\bar{t}$ pair production in proton–proton (pp) collisions at a centre-of-mass energy of $\sqrt{s} = 13$ TeV occurs predominantly via gluon fusion (90%) with small contributions from $q\bar{q}$ annihilation (10%). Significant progress has been made in the precision of the calculations of the cross-section of this process, both inclusive and differential. Currently, calculations are available at next-to-next-to-leading order (NNLO) in perturbative QCD, including the resummation of next-to-next-to-leading logarithmic (NNLL) soft gluon terms [1–11].

Differential cross-sections for $t\bar{t}$ production have been measured by the ATLAS [12–14] and CMS [15,16] experiments, in events containing either one or two charged leptons, at $\sqrt{s} = 7$ TeV and $\sqrt{s} = 8$ TeV. Measurements of $t\bar{t}$ differential cross-sections at $\sqrt{s} = 13$ TeV have also been made at the CMS experiment [17] in events containing one charged lepton. The integrated luminosity of 3.2 fb^{-1} of pp collision data collected by the ATLAS experiment at $\sqrt{s} = 13$ TeV allows the measurement of the differential cross-section as a function of the kinematic variables of the $t\bar{t}$ system in a different kinematic regime compared to the previous LHC measurements. The inclusive cross-section has been measured at $\sqrt{s} = 13$ TeV by both the ATLAS [18] and CMS [19,20] experiments and was found to be in agreement with the theoretical predictions. This article presents measurements of $t\bar{t}$ differential cross-sections in terms of five different kinematic observables, both absolute and normalised to the fiducial cross-section. These observables are the transverse momen-

tum of the top quark ($p_{\mathrm{T}}(t)$), the absolute rapidity of the top quark ($|y(t)|$), the transverse momentum of the $t\bar{t}$ system ($p_{\mathrm{T}}(t\bar{t})$), the absolute rapidity of the $t\bar{t}$ system ($|y(t\bar{t})|$), and the invariant mass of the $t\bar{t}$ system ($m(t\bar{t})$). The distributions of these variables are unfolded to the particle level in a fiducial volume. The $p_{\mathrm{T}}(t)$ and $m(t\bar{t})$ observables are expected to be sensitive to the modelling of higher-order corrections in QCD, whereas the rapidity of the top quark and $t\bar{t}$ system are expected to have sensitivity to the parton distribution functions (PDF) used in the simulations. The $p_{\mathrm{T}}(t\bar{t})$ observable is sensitive to the amount of gluon radiation in the event and can be useful for the tuning of Monte Carlo (MC) generators. Top quarks and anti-top quarks are measured in one combined distribution for the $p_{\mathrm{T}}(t)$ and $|y(t)|$ observables, rather than studying them separately. The $t\bar{t}$ system is reconstructed in events containing exactly one electron and one muon. Events in which a τ lepton decays to an electron or muon are also included.

2 ATLAS detector

The ATLAS detector [21] at the LHC covers nearly the entire solid angle around the interaction point. It consists of an inner tracking detector surrounded by a thin superconducting solenoid, electromagnetic and hadronic calorimeters, and a muon spectrometer incorporating three large superconducting toroidal magnet systems. The inner-detector system is immersed in a 2 T axial magnetic field and provides charged-particle tracking in the range $|\eta| < 2.5$.[1]

The high-granularity silicon pixel detector surrounds the collision region and provides four measurements per track. The closest layer, known as the Insertable B-Layer [22,23], was added in 2014 and provides high-resolution hits at small radius to improve the tracking performance. The pixel detector is followed by the silicon microstrip tracker, which provides four three-dimensional measurement points per track. These silicon detectors are complemented by the transition radiation tracker, which enables radially extended track reconstruction up to $|\eta| = 2.0$. The transition radiation tracker also provides electron identification information based on the fraction of hits (typically 30 in total) passing a higher charge threshold indicative of transition radiation.

The calorimeter system covers the pseudorapidity range $|\eta|<4.9$. Within the region $|\eta|<3.2$, electromagnetic calorimetry is provided by barrel and endcap high-granularity lead/liquid-argon (LAr) electromagnetic calorimeters, with an additional thin LAr presampler covering $|\eta| < 1.8$ to correct for energy loss in material upstream of the calorimeters. Hadronic calorimetry is provided by the steel/scintillator-tile calorimeter, segmented into three barrel structures within $|\eta| < 1.7$, and two copper/LAr hadronic endcap calorimeters that cover $1.5 < |\eta| < 3.2$. The solid angle coverage is completed with forward copper/LAr and tungsten/LAr calorimeter modules optimised for electromagnetic and hadronic measurements respectively, in the region $3.1 < |\eta| < 4.9$.

The muon spectrometer comprises separate trigger and high-precision tracking chambers measuring the deflection of muons in a magnetic field generated by superconducting air-core toroids. The precision chamber system covers the region $|\eta| < 2.7$ with three layers of monitored drift tubes, complemented by cathode strip chambers in the forward region, where the background is highest. The muon trigger system covers the range $|\eta| < 2.4$ with resistive-plate chambers in the barrel, and thin-gap chambers in the endcap regions.

A two-level trigger system is used to select interesting events [24,25]. The Level-1 trigger is implemented in hardware and uses a subset of detector information to reduce the event rate to a design value of at most 100 kHz. This is followed by the software-based high-level trigger, which reduces the event rate to 1 kHz.

3 Data and simulation samples

The pp collision data used in this analysis were collected during 2015 by ATLAS and correspond to an integrated luminosity of 3.2 fb^{-1} at $\sqrt{s} = 13$ TeV. The data considered in this analysis were collected under stable beam conditions, and requiring all subdetectors to be operational. Each selected event includes additional interactions from, on average, 14 inelastic pp collisions in the same proton bunch crossing, as well as residual detector signals from previous bunch crossings with a 25 ns bunch spacing, collectively referred to as "pile-up". Events are required to pass a single-lepton trigger, either electron or muon. Multiple triggers are used to select events: either triggers with low p_{T} thresholds of 24 GeV that utilise isolation requirements to reduce the trigger rate, or higher p_{T} thresholds of 50 GeV for muons or 60 and 120 GeV for electrons, with no isolation requirements to increase event acceptance.

MC simulations are used to model background processes and to correct the data for detector acceptance and resolution effects. The ATLAS detector is simulated [26] using GEANT 4 [27]. A "fast simulation" [28], utilising parameterised showers in the calorimeter, but with full simulation of the inner detector and muon spectrometer, is used

[1] ATLAS uses a right-handed coordinate system with its origin at the nominal interaction point (IP) in the centre of the detector and the z-axis along the beam pipe. The x-axis points from the IP to the centre of the LHC ring, and the y-axis points upwards. Cylindrical coordinates (r, ϕ) are used in the transverse plane, ϕ being the azimuthal angle around the z-axis. The pseudorapidity is defined in terms of the polar angle θ as $\eta = -\ln\tan(\theta/2)$. Angular distance is measured in units of $\Delta R \equiv \sqrt{(\Delta\eta)^2 + (\Delta\phi)^2}$.

in the samples generated to estimate $t\bar{t}$ modelling uncertainties. Additional pp interactions are generated using PYTHIA 8 (v8.186) [29] and overlaid on signal and background processes in order to simulate the effect of pile-up. The MC simulations are reweighted to match the distribution of the average number of interactions per bunch crossing that are observed in data. This process is referred to as "pile-up reweighting". The same reconstruction algorithms and analysis procedures are applied to both data and MC simulation. Corrections derived from dedicated data samples are applied to the MC simulation in order to improve agreement with data.

The nominal $t\bar{t}$ sample is simulated using the next-to-leading order (NLO) POWHEG-Box (v2) matrix-element event generator [30–32] using PYTHIA 6 (v6.427) [33] for the parton shower (PS). POWHEG-Box is interfaced to the CT10 [34] NLO PDF set while PYTHIA 6 uses the CTEQ6L1 PDF set [35]. A set of tuned parameters called the Perugia 2012 tune [36] is used in the simulation of the underlying event. The "h_{damp}" parameter, which controls the p_{T} of the first additional gluon emission beyond the Born configuration, is set to the mass of the top quark (m_t). The main effect of this is to regulate the high-p_{T} emission against which the $t\bar{t}$ system recoils. The choice of this h_{damp} value was found to improve the modelling of the $t\bar{t}$ system kinematics with respect to data in previous analyses [37]. In order to investigate the effects of initial- and final-state radiation, alternative POWHEG-Box + PYTHIA 6 samples are generated with the renormalisation and factorisation scales varied by a factor of 2 (0.5) and using low (high) radiation variations of the Perugia 2012 tune and an h_{damp} value of m_t ($2m_t$), corresponding to less (more) parton-shower radiation [37], referred to as "radHi" and "radLo". These variations were selected to cover the uncertainties in the measurements of differential distributions in $\sqrt{s} = 7$ TeV data [12]. The h_{damp} value for the low radiation sample is not decreased as it was found to disagree with previously published data. Alternative samples are generated using POWHEG-Box (v2) and MADGRAPH5_aMC@NLO (v2.2.1) [38], referred to as MG5_aMC@NLO hereafter, both interfaced to Herwig++ (v2.7.1) [39], in order to estimate the effects of the choice of matrix-element event generator and parton-shower algorithm. Additional $t\bar{t}$ samples are generated for comparisons with unfolded data using SHERPA (v2.2.0) [40], POWHEG-Box (v2) + PYTHIA 8 as well as POWHEG-Box (v2) and MG5_aMC@NLO interfaced to HERWIG 7 [39,41]. In all $t\bar{t}$ samples, the mass of the top quark is set to 172.5 GeV. These $t\bar{t}$ samples are described in further detail in Ref. [37].

Background processes are simulated using a variety of MC event generators. Single-top quark production in association with a W boson (Wt) is simulated using POWHEG-Box v1 + PYTHIA 6 with the same parameters and PDF sets as those used for the nominal $t\bar{t}$ sample and is normalised to the theoretical cross-section [42]. The higher-order overlap with $t\bar{t}$ production is addressed using the "diagram removal" (DR) generation scheme [43]. A sample generated using an alternative "diagram subtraction" (DS) method is used to evaluate systematic uncertainties [43].

SHERPA (v2.1.1), interfaced to the CT10 PDF set, is used to model Drell–Yan production, where the dominant contribution is from $Z/\gamma^* \to \tau^+\tau^-$. For this process, SHERPA calculates matrix elements at NLO for up to two partons and at leading order (LO) for up to four partons using the OpenLoops [44] and Comix [45] matrix-element event generators. The matrix elements are merged with the SHERPA parton shower [46] using the ME + PS@NLO prescription [47]. The total cross-section is normalised to the NNLO predictions [48]. SHERPA (v2.1.1) with the CT10 PDF set is also used to simulate electroweak diboson production [49] (WW, WZ, ZZ), where both bosons decay leptonically. For these samples, SHERPA calculates matrix elements at NLO for zero additional partons, at LO for one to three additional partons (with the exception of ZZ production, for which the one additional parton is also at NLO), and using PS for all parton multiplicities of four or more. All samples are normalised using the cross-section computed by the event generator.

Events with $t\bar{t}$ production in association with a vector boson are simulated using MG5_aMC@NLO + PYTHIA 8 [50], using the NNPDF2.3 PDF set and the A14 tune, as described in Ref. [51].

Background contributions containing one prompt lepton and one misidentified ("fake") lepton, arising from either a heavy-flavour hadron decay, photon conversion, jet misidentification or light-meson decay, are estimated using samples from MC simulation. The history of the stable particles in the generator-level record is used to identify fake leptons from these processes by identifying leptons that originated from hadrons. The majority (∼90%) of fake-lepton events originate from the single-lepton $t\bar{t}$ process, with smaller contributions arising from W + jets and $t\bar{t}$ + vector-boson events. W + jets events are simulated using POWHEG-Box + PYTHIA 8 with the CT10 PDF set and the AZNLO tune [52]. The t-channel single-top quark process is generated using POWHEG-Box v1 + PYTHIA 6 with the same parameters and PDF sets as those used for the nominal $t\bar{t}$ sample. EVTGEN (v1.2.0) [53] is used for the heavy-flavour hadron decays in all samples. Other possible processes with fake leptons, such as multi-jet and Drell–Yan production, are negligible for the event selection used in this analysis.

4 Object and event selection

This analysis utilises reconstructed electrons, muons, jets and missing transverse momentum (with magnitude $E_{\text{T}}^{\text{miss}}$). Electron candidates are identified by matching an inner-detector track to an isolated energy deposit in the electromagnetic

calorimeter, within the fiducial region of transverse momentum $p_{\mathrm{T}} > 25$ GeV and pseudorapidity $|\eta| < 2.47$. Electron candidates are excluded if the calorimeter cluster is within the transition region between the barrel and the endcap of the electromagnetic calorimeter, $1.37 < |\eta| < 1.52$. Electrons are selected using a multivariate algorithm and are required to satisfy a likelihood-based quality criterion, in order to provide high efficiency and good rejection of fake electrons [54,55]. Electron candidates must have tracks that pass the requirements of transverse impact parameter significance[2] $|d_0^{\mathrm{sig}}| < 5$ and longitudinal impact parameter $|z_0 \sin\theta| < 0.5$ mm. Electrons must pass isolation requirements based on inner-detector tracks and topological clusters in the calorimeter which depend on η and p_{T}. These requirements result in an isolation efficiency of 95% for an electron p_{T} of 25 GeV and 99% for an electron p_{T} above 60 GeV when determined in simulated $Z \to e^+e^-$ events. The fake-electron rate determined in simulated $t\bar{t}$ events is 2%. Electrons that share a track with a muon are discarded. Double counting of electron energy deposits as jets is prevented by removing the closest jet within $\Delta R = 0.2$ of a reconstructed electron. Following this, the electron is discarded if a jet exists within $\Delta R = 0.4$ of the electron to ensure sufficient separation from nearby jet activity.

Muon candidates are identified from muon-spectrometer tracks that match tracks in the inner detector, with $p_{\mathrm{T}} > 25$ GeV and $|\eta| < 2.5$ [56]. The tracks of muon candidates are required to have a transverse impact parameter significance $|d_0^{\mathrm{sig}}| < 3$ and longitudinal impact parameter $|z_0 \sin\theta| < 0.5$ mm. Muons must satisfy quality criteria and isolation requirements based on inner-detector tracks and topological clusters in the calorimeter which depend on η and p_{T}. These requirements reduce the contributions from fake muons and provide the same efficiency as for electrons when determined in simulated $t\bar{t}$ events. Muons may leave energy deposits in the calorimeter that could be misidentified as a jet, so jets with fewer than three associated tracks are removed if they are within $\Delta R = 0.4$ of a muon. Muons are discarded if they are separated from the nearest jet by $\Delta R < 0.4$ to reduce the background from muons from heavy-flavour hadron decays inside jets.

Jets are reconstructed with the anti-k_t algorithm [57,58], using a radius parameter of $R = 0.4$, from topological clusters of energy deposits in the calorimeters. Jets are accepted within the range $p_{\mathrm{T}} > 25$ GeV and $|\eta| < 2.5$, and are calibrated using simulation with corrections derived from data [59]. Jets likely to originate from pile-up are suppressed using a multivariate jet-vertex-tagger (JVT) [60,61] for candidates with $p_{\mathrm{T}} < 60$ GeV and $|\eta| < 2.4$. Jets are identified as candidates for containing b-hadrons using a multivariate discriminant [62], which uses track impact parameters, track invariant mass, track multiplicity and secondary vertex information to discriminate b-jets from light-quark or gluon jets (light jets). The average b-tagging efficiency is 76%, with a purity of 90%, for b-jets in simulated dileptonic $t\bar{t}$ events.

$E_{\mathrm{T}}^{\mathrm{miss}}$ is reconstructed using calibrated electrons, muons and jets [63], where the electrons and muons are required to satisfy the selection criteria above. Tracks associated with the primary vertex are used for the computation of $E_{\mathrm{T}}^{\mathrm{miss}}$ from energy not associated with electrons, muons or jets. The primary vertex is defined as the vertex with the highest sum of p_{T}^2 of tracks associated with it.

Signal events are selected by requiring exactly one electron and one muon of opposite electric charge, and at least two jets, at least one of which must be b-tagged. No requirements are made on the $E_{\mathrm{T}}^{\mathrm{miss}}$ in the event. Using this selection, 85% of events are expected to be $t\bar{t}$ events. The other processes that pass the signal selection are Drell–Yan ($Z/\gamma^* \to \tau^+\tau^-$), diboson and single-top quark (Wt) production and fake-lepton events.

The event yields after the signal selection are listed in Table 1. The number of events observed in the signal region exceeds the prediction, but the excess is within the uncertainties. Distributions of lepton and jet p_{T} and $E_{\mathrm{T}}^{\mathrm{miss}}$ are shown in Fig. 1. The $t\bar{t}$ contribution is normalised using the predicted cross-section, calculated with the Top++2.0 program at next-to-next-to-leading order in perturbative QCD, including soft-gluon resummation to next-to-next-to-leading-logarithm order [6] and assuming a top-quark mass of 172.5 GeV. The data and prediction agree within the total uncertainty for all distributions. The p_{T} observables show a small deficit in the simulation prediction at low p_{T} which was found to be correlated with the modelling of the top-quark p_{T}.

Table 1 Event yields in the signal selection, and after requiring that neutrino weighting (NW) reconstructs the event. The quoted uncertainties include uncertainties from leptons, jets, missing transverse momentum, luminosity, statistics, background modelling and pile-up modelling. They do not include uncertainties from PDF or signal $t\bar{t}$ modelling. The results and uncertainties are rounded according to recommendations from the Particle Data Group (PDG)

Process	Signal region	Signal region + NW
$Z/\gamma^* \to \tau^+\tau^-$	22 ± 9	10 ± 8
Diboson	44 ± 4	17 ± 2
Fake lepton	200 ± 60	150 ± 50
Wt	860 ± 60	480 ± 40
$t\bar{t}$	$15{,}800 \pm 900$	$13{,}300 \pm 800$
Expected	$17{,}000 \pm 900$	$13{,}900 \pm 800$
Observed	17,501	14,387

[2] The transverse impact parameter significance is defined as $d_0^{\mathrm{sig}} = d_0/\sigma_{d_0}$, where σ_{d_0} is the uncertainty in the transverse impact parameter d_0.

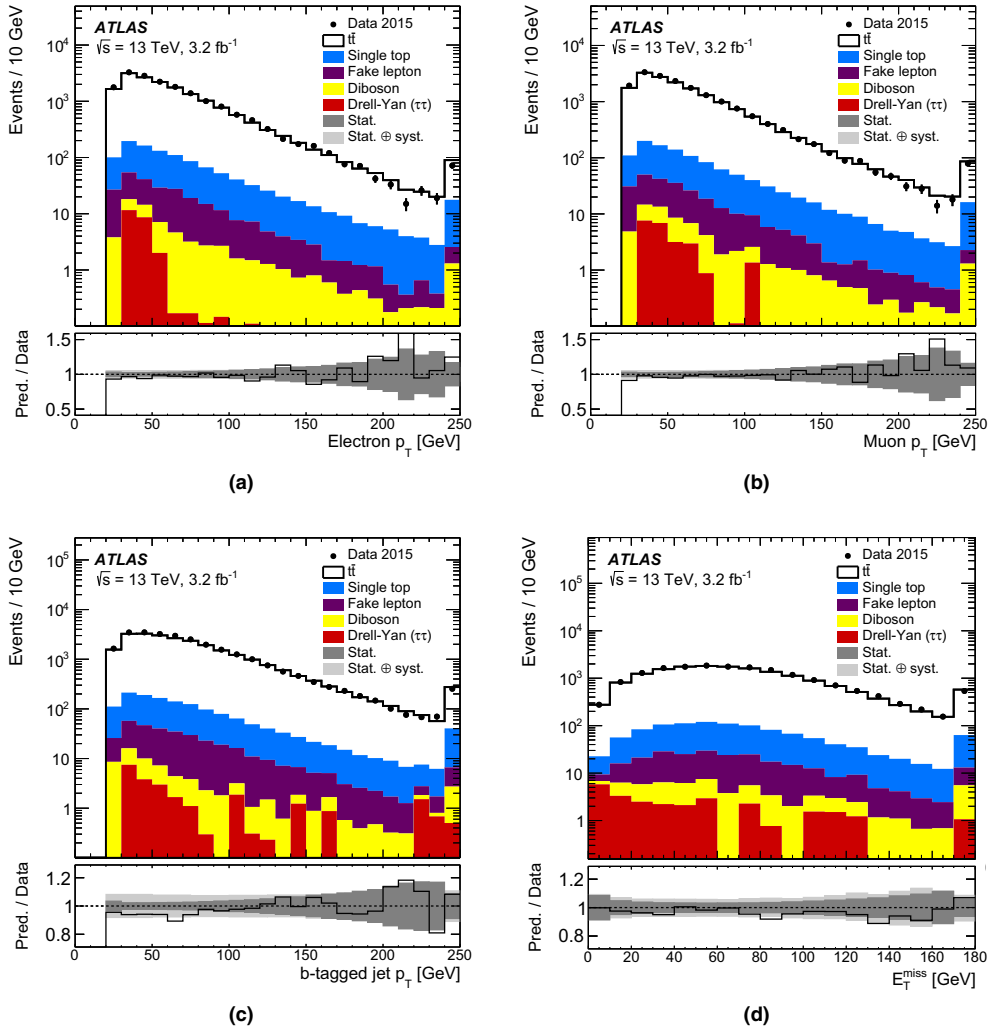

Fig. 1 Kinematic distributions for the electron p_{T} (**a**), muon p_{T} (**b**), b-jet p_{T} (**c**), and $E_{\mathrm{T}}^{\mathrm{miss}}$ (**d**) for the $e^{\pm}\mu^{\mp}$ signal selection. In all figures, the rightmost bin also contains events that are above the x-axis range. The *dark uncertainty bands* in the ratio plots represent the statistical uncertainties while the *light uncertainty bands* represent the statistical, systematic and luminosity uncertainties added in quadrature. The uncertainties quoted include uncertainties from leptons, jets, missing transverse momentum, background modelling and pile-up modelling. They do not include uncertainties from PDF or signal $t\bar{t}$ modelling

Particle-level objects are constructed using generator-level information in the MC simulation, using a procedure intended to correspond as closely as possible to the reconstructed object and event selection. Only objects in the MC simulation with a lifetime longer than 3×10^{-11} s (stable) in the generator-level information are used. Particle-level electrons and muons are identified as those originating from a W-boson decay, including those via intermediate τ leptons.

The four-momenta of each electron or muon is summed with the four-momenta of all radiated photons, excluding those from hadron decays, within a cone of size $\Delta R = 0.1$, and the resulting objects are required to have $p_{\mathrm{T}} > 25$ GeV and $|\eta| < 2.5$. Particle-level jets are constructed using stable particles, with the exception of selected particle-level electrons and muons and particle-level neutrinos originating from W-boson decays, using the anti-k_t algorithm with a radius parameter of $R = 0.4$, in the region $p_{\mathrm{T}} > 25$ GeV and $|\eta| < 2.5$. Intermediate b-hadrons in the MC decay chain history are clustered in the stable-particle jets with their energies set to zero. If, after clustering, a particle-level jet contains one or more of these "ghost" b-hadrons, the jet is said to have originated from a b-quark. This technique is referred to as "ghost matching" [64]. Particle-level $E_{\mathrm{T}}^{\mathrm{miss}}$ is calculated using the vector transverse-momentum sum of all neutrinos in the event, excluding those originating from hadron decays, either directly or via a τ lepton.

Events are selected at the particle level in a fiducial phase space region with similar requirements to the phase space region at reconstruction level. Events are selected by requiring exactly one particle-level electron and one particle-level muon of opposite electric charge, and at least two particle-level jets, at least one of which must originate from a b-quark.

5 Reconstruction

The t, $\bar{t}$, and $t\bar{t}$ are reconstructed using both the particle-level objects and the reconstructed objects in order to measure their kinematic distributions. The reconstructed system is built using the neutrino weighting (NW) method [65].

Whereas the individual four-momenta of the two neutrinos in the final state are not directly measured in the detector, the sum of their transverse momenta is measured as $E_{\mathrm{T}}^{\mathrm{miss}}$. The absence of the measured four-momenta of the two neutrinos leads to an under-constrained system that cannot be solved analytically. However, if additional constraints are placed on the mass of the top-quark, the mass of the W boson, and on the pseudorapidities of the two neutrinos, the system can be solved using the following equations:

$$\begin{aligned} (\ell_{1,2} + \nu_{1,2})^2 &= m_W^2 = (80.2\,\mathrm{GeV})^2, \\ (\ell_{1,2} + \nu_{1,2} + b_{1,2})^2 &= m_t^2 = (172.5\,\mathrm{GeV})^2, \\ \eta(\nu),\ \eta(\bar{\nu}) &= \eta_1,\ \eta_2, \end{aligned} \tag{1}$$

where $\ell_{1,2}$ are the charged leptons, $\nu_{1,2}$ are the neutrinos, and $b_{1,2}$ are the b-jets (or jets), representing four-momentum vectors, and η_1, η_2 are the assumed η values of the two neutrinos. Since the neutrino η's are unknown, many different assumptions of their values are tested. The possible values for $\eta(\nu)$ and $\eta(\bar{\nu})$ are scanned between -5 and 5 in steps of 0.2.

With the assumptions about m_t, m_W, and values for $\eta(\nu)$ and $\eta(\bar{\nu})$, Eq. (1) can now be solved, leading to two possible solutions for each assumption of $\eta(\nu)$ and $\eta(\bar{\nu})$. Only real solutions without an imaginary component are considered. The observed $E_{\mathrm{T}}^{\mathrm{miss}}$ value in each event is used to determine which solutions are more likely to be correct. A "reconstructed" $E_{\mathrm{T}}^{\mathrm{miss}}$ value resulting from the neutrinos for each solution is compared to the $E_{\mathrm{T}}^{\mathrm{miss}}$ observed in the event. If this reconstructed $E_{\mathrm{T}}^{\mathrm{miss}}$ value matches the observed $E_{\mathrm{T}}^{\mathrm{miss}}$ value in the event, then the solution with those values for $\eta(\nu)$ and $\eta(\bar{\nu})$ is likely to be the correct one. A weight is introduced in order to quantify this agreement:

$$w = \exp\left(\frac{-\Delta E_x^2}{2\sigma_x^2}\right) \cdot \exp\left(\frac{-\Delta E_y^2}{2\sigma_y^2}\right), \tag{2}$$

where $\Delta E_{x,y}$ is the difference between the missing transverse momentum computed from Eq. (1) and the observed missing transverse momentum in the x–y plane and $\sigma_{x,y}$ is the resolution of the observed $E_{\mathrm{T}}^{\mathrm{miss}}$ in the detector in the x–y plane. The assumption for $\eta(\nu)$ and $\eta(\bar{\nu})$ that gives the highest weight is used to reconstruct the t and $\bar{t}$ for that event. The $E_{\mathrm{T}}^{\mathrm{miss}}$ resolution is taken to be 15 GeV for both the x and y directions [63]. This choice has little effect on which solution is picked in each event. The highest-weight solution remains the same regardless of the choice of $\sigma_{x,y}$.

In each event, there may be more than two jets and therefore many possible combinations of jets to use in the kinematic reconstruction. In addition, there is an ambiguity in assigning a jet to the t or to the $\bar{t}$ candidate. In events with only one b-tagged jet, the b-tagged jet and the highest-p_{T} non-b-tagged jet are used to reconstruct the t and $\bar{t}$, whereas in events with two or more b-tagged jets, the two b-tagged jets with the highest weight from the b-tagging algorithm are used.

Equation (1) cannot always be solved for a particular assumption of $\eta(\nu)$ and $\eta(\bar{\nu})$. This can be caused by misassignment of the input objects or through mismeasurement of the input object four-momenta. It is also possible that the assumed m_t is sufficiently different from the true value to prevent a valid solution for that event. To mitigate these effects, the assumed value of m_t is varied between the values of 168 and 178 GeV, in steps of 1 GeV, and the p_{T} of the measured jets are smeared using a Gaussian function with a width of 10% of their measured p_{T}. This smearing is repeated 20 times. This allows the NW algorithm to shift the four-momenta (of the electron, muon and the two jets) and m_t assumption to see if a solution can be found. The solution which produces the highest w is taken as the reconstructed system.

For a fraction of events, even smearing does not help to find a solution. Such events are not included in the signal

selection and are counted as an inefficiency of the reconstruction. For the signal $t\bar{t}$ MC samples, the inefficiency is ∼20%. Due to the implicit assumptions about the m_t and m_W, the reconstruction inefficiency found in simulated background samples is much higher (∼40% for Wt and Drell–Yan processes) and leads to a suppression of background events. Table 1 shows the event yields before and after reconstruction in the signal region. The purity of $t\bar{t}$ events increases after reconstruction. The distributions of the experimental observables after reconstruction are shown in Fig. 2.

Particle-level t, $\bar{t}$, and $t\bar{t}$ objects are reconstructed following the prescriptions from the LHCTopWG, with the exception that only events with at least one b-tagged jet are allowed. Events are required to have exactly two leptons of opposite-sign electric charge (one electron and one muon), and at least two jets. The t and $\bar{t}$ are reconstructed by considering the two particle-level neutrinos with the highest p_{T} and the two particle-level charged leptons. The charged leptons and the neutrinos are paired such that $|m_{\nu_1,\ell_1} - m_W| + |m_{\nu_2,\ell_2} - m_W|$ is minimised. These pairs are then used as pseudo W bosons and are paired with particle-level jets such that $|m_{W_1,j_1} - m_t| + |m_{W_2,j_2} - m_t|$ is minimised, where at least one of the jets must be b-tagged. In cases where only one particle-level b-jet is present, the particle-level jet with the highest p_{T} among the non-b-tagged jets is used as the second jet. In cases with two particle-level b-jets, both are taken. In the rare case of events with more than two particle-level b-jets, the two highest-p_{T} particle-level b-jets are used. The particle-level $t\bar{t}$ object is constructed using the sum of the four-momenta of the particle-level t and $\bar{t}$.

6 Unfolding

To obtain the absolute and normalised differential cross-sections in the fiducial phase space region (see Sect. 4) with respect to the $t\bar{t}$ system variables, the distributions are unfolded to particle level using an iterative Bayesian method [66] implemented in the RooUnfold package [67]. In the unfolding, background-subtracted data are corrected for detector acceptance and resolution effects as well as for the efficiency to pass the event selection requirements in order to obtain the absolute differential cross-sections. The fiducial differential cross-sections are divided by the measured total cross-section, obtained by integrating over all bins in the differential distribution, in order to obtain the normalised differential cross-sections.

The differential cross-sections are calculated using the equation:

$$\frac{\mathrm{d}\sigma_{t\bar{t}}}{\mathrm{d}X_i} = \frac{1}{\mathcal{L}\cdot\mathcal{B}\cdot\Delta X_i\cdot\epsilon_i}\cdot\sum_j R_{ij}^{-1}\cdot\epsilon_j^{\mathrm{fid}}\cdot(N_j^{\mathrm{obs}} - N_j^{\mathrm{bkg}}), \tag{3}$$

where i indicates the bin for the observable X, ΔX_i is the width of bin i, $\mathcal{L}$ is the integrated luminosity, $\mathcal{B}$ is the branching ratio of the process ($t\bar{t} \rightarrow b\bar{b}e^{\pm}\nu_e\mu^{\mp}\nu_\mu$), R is the response matrix, N_j^{obs} is the number of observed events in data in bin j, and N_j^{bkg} is the estimated number of background events in bin j. The efficiency parameter, ϵ_i ($\epsilon_j^{\mathrm{fid}}$), is used to correct for events passing the reconstructed (fiducial) event selection but not the fiducial (reconstructed) selection.

The response matrix, R, describes the detector response, and is determined by mapping the bin-to-bin migration of events from particle level to reconstruction level in the nominal $t\bar{t}$ MC simulation. Figure 3 shows the response matrices that are used for each experimental observable, normalised such that the sum of entries in each row is equal to one. The values represent the fraction of events at particle level in bin i that are reconstructed in bin j at reconstruction level.

The binning for the observables is chosen such that approximately half of the events are reconstructed in the same bin at reconstruction level as at the particle level (corresponding to a value of approximately 0.5 in the diagonal elements of the migration matrix). Pseudo-data are constructed by randomly sampling events from the nominal $t\bar{t}$ MC sample, to provide a number of events similar to the number expected from data. These pseudo-data are used to establish the stability of unfolding with respect to the choice of binning with pull tests. The binning choice must result in pulls consistent with a mean of zero and a standard deviation of one, within uncertainties. The choice of binning does not introduce any bias or underestimation of the statistical uncertainties. The number of iterations used in the iterative Bayesian unfolding is also optimised using pseudo-experiments. Iterations are performed until the χ^2 per degree of freedom, calculated by comparing the unfolded pseudo-data to the corresponding generator-level distribution for that pseudo-data set, is less than unity. The optimum number of iterations is determined to be six. Tests are performed to establish that the unfolding procedure is able to successfully unfold distributions other than those predicted by the nominal MC simulation.

7 Systematic uncertainties

The measured differential cross-sections are affected by systematic uncertainties arising from detector response, signal modelling, and background modelling. The contributions from various sources of uncertainty are described in this section. Summaries of the sources of uncertainty for the absolute and normalised differential cross-sections for the $p_{\mathrm{T}}(t)$ are presented in Tables 2 and 3. The total systematic uncertainties are calculated by summing all of the individual systematic uncertainties in quadrature and the total uncertainty is calculated by summing the systematic and statistical uncertainties

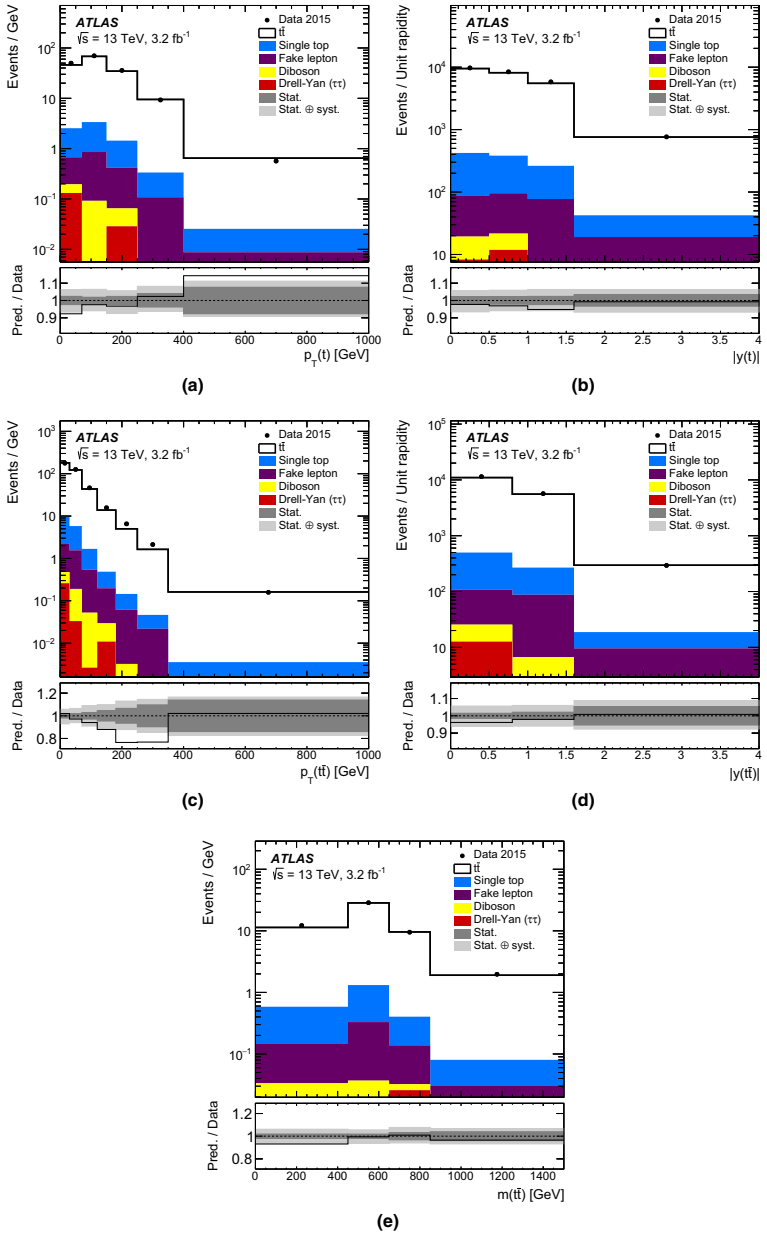

Fig. 2 Kinematic distributions for the $p_{\mathrm{T}}(t)$ (**a**), $|y(t)|$ (**b**), $p_{\mathrm{T}}(t\bar{t})$ (**c**), $t\bar{t}$ $|y_{t\bar{t}}|$ (**d**), and $m(t\bar{t})$ (**e**) after reconstruction of the $t\bar{t}$ system. In all figures, the rightmost bin also contains events that are above the x-axis range. The *uncertainty bands* represent the statistical uncertainties (*dark*) and the statistical, systematic and luminosity uncertainties added in quadrature (*light*). The uncertainties quoted include uncertainties on leptons, jets, $E_{\mathrm{T}}^{\mathrm{miss}}$, background and pile-up modelling, and luminosity. They do not include uncertainties on PDF or signal $t\bar{t}$ modelling

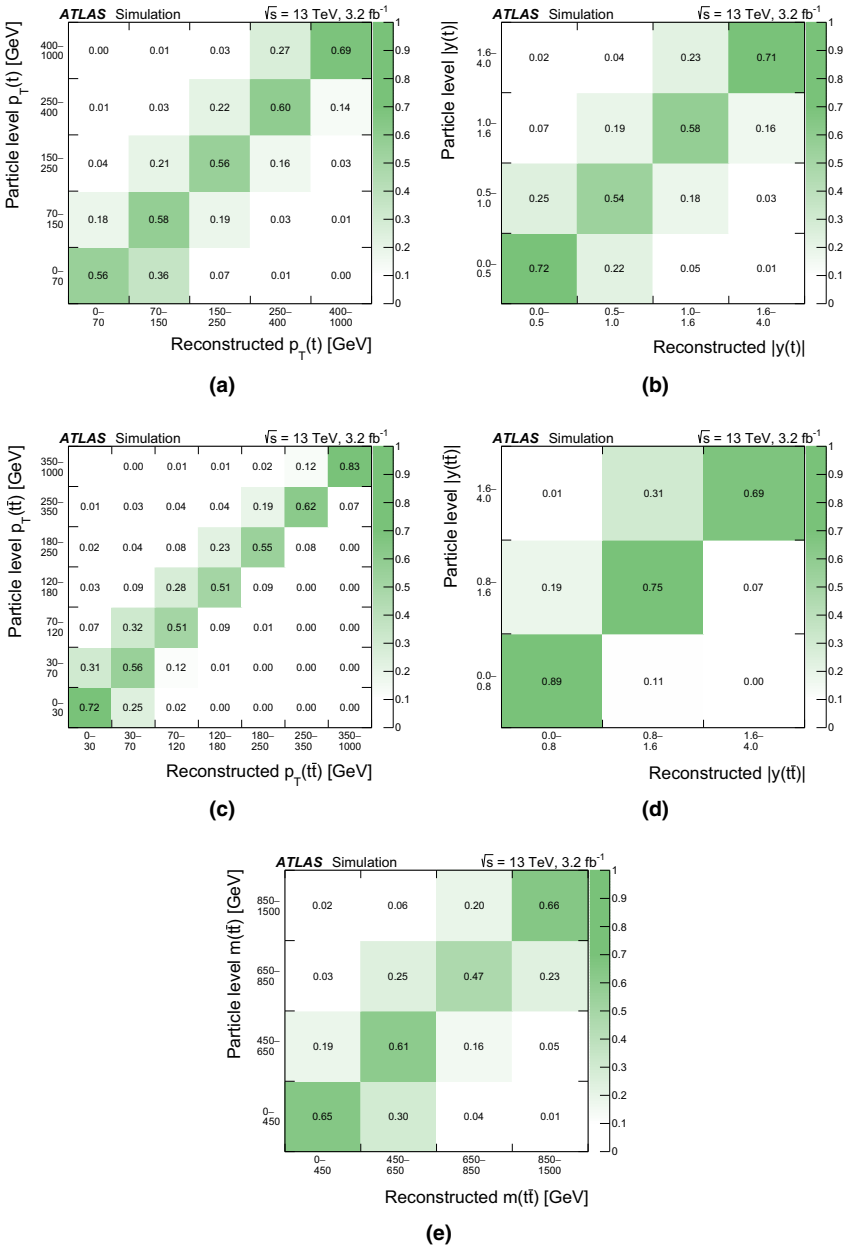

Fig. 3 The response matrices for the observables obtained from the nominal $t\bar{t}$ MC, normalised by row to unity. *Each bin* shows the probability for a particle-level event in bin j to be observed in a reconstruction-level bin i. White corresponds to 0 probability and the *darkest green* to a probability of one, where the other probabilities lie in between those *shades*

Table 2 Summary of the sources of uncertainty in the absolute fiducial differential cross-section as a function of $p_{\mathrm{T}}(t)$. The uncertainties are presented as a percentage of the measured cross-section in each bin. Entries with 0.0 are uncertainties that are less than 0.05 in magnitude. For systematic uncertainties that have only one variation, $\pm(\mp)$ indicate that the systematic shift is positive (negative) and then symmetrised. All uncertainties are rounded to two digits

$p_{\mathrm{T}}(t)$	0–70 GeV	70–150 GeV	150–250 GeV	250–400 GeV	400–1000 GeV
Source	Systematic uncertainty (%)				
Radiation scale	$+4.0\ -3.9$	$+1.1\ -3.9$	$+1.9\ -3.5$	$+1.4\ -5.0$	$+5.0\ -5.4$
MC generator	∓ 0.9	∓ 1.2	∓ 1.4	± 1.6	∓ 6.7
PDF extrapolation	∓ 2.9	∓ 2.8	∓ 1.9	∓ 0.3	∓ 2.4
PDF4LHC 100	± 2.2	± 2.5	± 2.8	± 3.7	± 6.1
Parton shower	∓ 8.0	∓ 7.7	∓ 3.9	± 3.1	± 34
Background	$+0.3\ -0.5$	$+0.2\ -0.4$	± 0.2	± 0.2	$+0.4\ -1.5$
Pile-up	$+0.7\ -1.4$	$+0.2\ -0.6$	$+0.0\ -0.4$	$+0.0\ -0.4$	$+4.1\ -0.0$
Lepton	$+0.8\ -0.7$	± 0.8	± 1.0	± 1.6	$+3.2\ -3.0$
b-tagging	$+3.1\ -3.6$	$+3.4\ -3.9$	$+3.4\ -4.0$	$+4.0\ -4.7$	$+6.2\ -7.2$
Jet	± 2.8	$+2.6\ -3.4$	$+2.0\ -1.8$	$+1.9\ -1.1$	$+4.5\ -5.1$
E_{T}^{miss}	$+0.2\ -0.1$	± 0.1	$+0.2\ -0.1$	$+0.3\ -0.5$	$+1.0\ -0.3$
Luminosity	$+2.0\ -2.1$	$+2.1\ -2.2$	$+2.1\ -2.2$	$+2.3\ -2.4$	$+3.0\ -3.1$
MC stat. unc.	± 0.4	± 0.3	± 0.5	± 0.9	± 3.2
Total syst. unc.	$+11\ -11$	$+9\ -11$	$+7.3\ -8.1$	$+7.5\ -9.1$	$+37\ -37$
Data statistics	± 1.8	± 1.3	± 1.8	± 3.4	± 10
Total uncertainty	$+11\ -11$	$+10\ -11$	$+7.5\ -8.3$	$+8.2\ -9.8$	$+38\ -39$

Table 3 Summary of the sources of uncertainty in the normalised fiducial differential cross-section as a function of $p_{\mathrm{T}}(t)$. The uncertainties are presented as a percentage of the measured cross-section in each bin. Entries with 0.0 are uncertainties that are less than 0.05 in magnitude. For systematic uncertainties that have only one variation, $\pm(\mp)$ indicate that the systematic shift is positive (negative) and then symmetrised. All uncertainties are rounded to two digits

$p_{\mathrm{T}}(t)$	0–70 GeV	70–150 GeV	150–250 GeV	250–400 GeV	400–1000 GeV
Source	Systematic uncertainty (%)				
Radiation scale	$+2.1\ -0.3$	$+0.0\ -1.1$	$+0.4\ -0.3$	$+0.0\ -1.2$	$+2.1\ -0.0$
MC generator	± 0.2	∓ 0.2	∓ 0.4	± 2.7	∓ 5.4
PDF extrapolation	∓ 0.5	∓ 0.4	± 0.4	± 2.4	± 0.8
PDF4LHC 100	± 0.6	± 0.3	± 0.5	± 1.7	± 4.0
Parton shower	∓ 2.8	∓ 2.1	± 1.6	± 8.9	± 41
Background	$+0.1\ -0.2$	$+0.0\ -0.1$	$+0.3\ -0.0$	$+0.3\ -0.1$	$+0.1\ -1.2$
Pile-up	$+0.4\ -0.8$	± 0.0	$+0.3\ -0.2$	$+0.8\ -0.7$	$+5.1\ -0.0$
Lepton	$+0.4\ -0.3$	$+0.1\ -0.3$	$+0.3\ -0.1$	± 0.7	$+2.3\ -1.9$
b-tagging	± 0.2	± 0.2	± 0.2	± 0.9	$+2.3\ -2.4$
Jet	$+0.9\ -0.8$	$+0.4\ -1.0$	$+0.8\ -0.6$	$+3.0\ -2.4$	$+6.9\ -7.3$
E_{T}^{miss}	$+0.2\ -0.1$	$+0.0\ -0.1$	$+0.2\ -0.1$	$+0.3\ -0.5$	$+1.0\ -0.4$
Luminosity	± 0.0	± 0.0	± 0.0	± 0.0	± 0.0
MC stat. unc.	± 0.0	± 0.2	± 0.0	± 0.4	± 2.6
Total syst. unc.	$+3.8\ -3.2$	$+2.2\ -2.7$	$+2.1\ -2.0$	$+10\ -10$	$+42\ -42$
Data statistics	± 1.8	± 1.3	± 1.8	± 3.4	± 10
Total uncertainty	$+4.2\ -3.6$	$+2.6\ -2.9$	$+2.8\ -2.7$	$+11\ -11$	$+44\ -43$

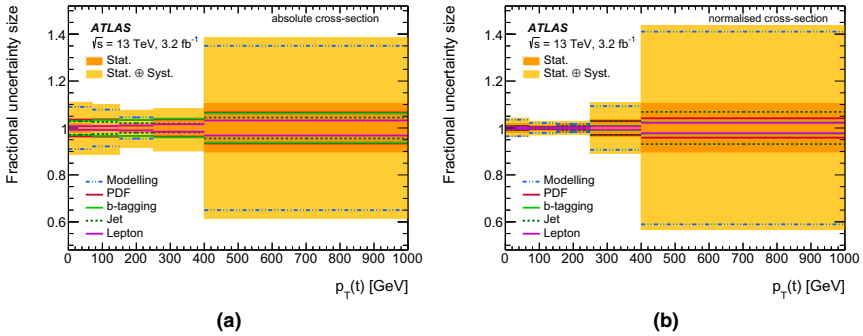

Fig. 4 Summary of the fractional size of the absolute (**a**) and normalised (**b**) fiducial differential cross-sections as a function of $p_{\mathrm{T}}(t)$. Systematic uncertainties which are symmetric are represented by *solid lines* and asymmetric uncertainties are represented by *dashed* or *dot–dashed lines*. Systematic uncertainties from common sources, such as modelling of the $t\bar{t}$ production, have been grouped together. Uncertainties due to luminosity or background modelling are not included. The statistical and total uncertainty sizes are indicated by the *shaded bands*

in quadrature. The effect of different groups of systematic uncertainties is shown graphically for $p_{\mathrm{T}}(t)$ in Fig. 4.

7.1 Signal modelling uncertainties

The following systematic uncertainties related to the modelling of the $t\bar{t}$ system in the MC generators are considered: the choice of matrix-element generator, the hadronisation model, the choice of PDF, and the amount of initial- and final-state radiation.

Each source is estimated by using a different MC sample in the unfolding procedure. In particular, a chosen baseline MC sample is unfolded using response matrices and corrections derived from an alternative sample. The difference between the unfolded distribution in the baseline sample and the true distribution in the baseline sample is taken as the systematic uncertainty due to the signal modelling.

The choice of NLO generator (MC generator) affects the kinematic properties of the simulated $t\bar{t}$ events and the reconstruction efficiencies. To estimate this uncertainty, a comparison between POWHEG-Box and MG5_aMC@NLO (both using Herwig++ for the parton-shower simulation) is performed, with the POWHEG-Box sample used as the baseline. The resulting systematic shift is used to define a symmetric uncertainty, where deviations from the nominal sample are also considered to be mirrored in the opposite direction, resulting in equal and opposite symmetric uncertainties (called symmetrising).

To evaluate the uncertainty arising from the choice of parton-shower algorithm, a sample generated using POWHEG-Box + PYTHIA 6 is compared to the alternative sample generated with POWHEG-Box + Herwig++, where both samples use "fast simulation". The resulting uncertainty is symmetrised. The choices of NLO generator and parton-shower algorithm are dominant sources of systematic uncertainty in all observables.

The uncertainty due to the choice of PDF is evaluated using the PDF4LHC15 prescription [68]. The prescription utilises 100 eigenvector shifts derived from fits to the CT14 [69], MMHT [69] and NNPDF3.0 [70] PDF sets (PDF4LHC 100). The nominal MC sample used in the analysis is generated using the CT10 PDF set. Therefore, the uncertainty is taken to be the standard deviation of all eigenvector variations summed in quadrature with the difference between the central values of the CT14 and CT10 PDF sets (PDF extrapolation). The resulting uncertainty is symmetrised. Both PDF-based uncertainties contribute as one of the dominant systematic uncertainties.

Uncertainties arising from varying the amount of initial- and final-state radiation (radiation scale), which alters the jet multiplicity in events and the transverse momentum of the $t\bar{t}$ system, are estimated by comparing the nominal POWHEG-Box + PYTHIA 6 sample to samples generated with high and low radiation settings, as discussed in Sect. 3. The uncertainty is taken as the difference between the nominal and the increased radiation sample, and the nominal and the decreased radiation sample. The initial- and final-state radiation is a significant source of uncertainty in the absolute cross-section measurements but only a moderate source of uncertainty in the normalised cross-sections.

7.2 Background modelling uncertainties

The uncertainties in the background processes are assessed by repeating the full analysis using pseudo-data sets and by varying the background predictions by one standard devi-

Table 4 Summary of the measured absolute ($\frac{d\sigma_{t\bar{t}}}{dX}$) and normalised ($\frac{1}{\sigma_{t\bar{t}}}\frac{d\sigma_{t\bar{t}}}{dX}$) differential cross-sections, along with the relative statistical (Stat.) and systematic (Syst.) uncertainties for both the absolute (abs.) and normalised (norm.) cross-sections. The results and uncertainties are rounded according to recommendations from the Particle Data Group (PDG)

X	$\frac{d\sigma_{t\bar{t}}}{dX}$ [$\frac{pb}{GeV}$]	$\frac{1}{\sigma_{t\bar{t}}}\frac{d\sigma_{t\bar{t}}}{dX}$ [$\frac{1}{GeV}$]	Stat. (abs.) (%)	Stat. (norm.) (%)	Syst. (abs.) (%)	Syst. (norm.) (%)
$p_T(t)$ (GeV)						
0–70	7.1	0.371	±1.8	±1.7	+11 −11	+4 −3.2
70–150	9.9	0.515	±1.3	±1.2	+10 −11	+2.3 −2.7
150–250	4.61	0.239	±1.8	±1.7	+7 −8	+2.1 −2.0
250–400	0.97	0.051	±3.4	±3.3	+7 −9	+10 −11
400–1000	0.042	0.0022	±10	±9	+40 −40	+40 −40
$p_T(t\bar{t})$ (GeV)						
0–30	9.6	0.99	±2.2	±2.0	+15 −16	+12 −13
30–70	8.6	0.88	±1.9	±1.7	+8 −8	+9 −9
70–120	3.6	0.368	±3.0	±2.7	+10 −11	+8 −9
120–180	0.139	0.143	±5	±5	+24 −24	+19 −18
180–250	0.064	0.066	±7	±6	+40 −40	+32 −32
250–350	0.023	0.024	±10	±9	+24 −24	+30 −19
350–1000	0.0017	0.0018	±14	±13	+50 −50	+40 −40
$m(t\bar{t})$ (GeV)						
0–450	0.94	0.097	±1.8	±1.6	+12 −13	+5 −5
450–650	1.76	0.183	±2.0	±1.9	+8 −9	+2.8 −3.0
650–850	0.57	0.059	±4	±3.3	+10 −12	+8 −8
850–1500	0.111	0.0115	±6	±5	+11 −11	+14 −14
X	$\frac{d\sigma_{t\bar{t}}}{dX}$ [pb]	$\frac{1}{\sigma_{t\bar{t}}}\frac{d\sigma_{t\bar{t}}}{dX}$	Stat. (abs.) (%)	Stat. (norm.) (%)	Syst. (abs.) (%)	Syst. (norm.) (%)
$\lvert y(t\bar{t})\rvert$						
0.0–0.8	7.7	0.797	±1.3	±1.1	+8 −9	+1.8 −1.8
0.8–1.6	3.9	0.400	±2.2	±2.0	+9 −10	+3.4 −3.4
1.6–4.0	0.170	0.0176	±7	±7	+13 −13	+8 −8
$\lvert y(t)\rvert$						
0.0–0.5	12.9	0.665	±1.5	±1.4	+8 −10	+1.0 −1.3
0.5–1.0	11.5	0.595	±1.6	±1.5	+10 −10	+2.2 −1.9
1.0–1.6	8.1	0.421	±1.8	±1.7	+8 −9	+1.4 −1.2
1.6–4.0	0.95	0.0489	±2.9	±2.7	+8 −9	+6 −6

ation of their nominal values. The difference between the nominal pseudo-data set result and the shifted result is taken as the systematic uncertainty.

Each background prediction has an uncertainty associated with its theoretical cross-section. The cross-section for the Wt process is varied by ±5.3% [42], the diboson cross-section is varied by ±6%, and the Drell–Yan $Z/\gamma^* \to \tau^+\tau^-$ background is varied by ±5% based on studies of different MC generators. A 30% uncertainty is assigned to the normalisation of the fake-lepton background based on comparisons between data and MC simulation in a fake-dominated control region, which is selected in the same way as the $t\bar{t}$ signal region but the leptons are required to have same-sign electric charges.

An additional uncertainty is evaluated for the Wt process by replacing the nominal DR sample with a DS sample, as discussed in Sect. 3, and taking the difference between the two as the systematic uncertainty.

7.3 Detector modelling uncertainties

Systematic uncertainties due to the modelling of the detector response affect the signal reconstruction efficiency, the unfolding procedure, and the background estimation. In order to evaluate their impact, the full analysis is repeated with variations of the detector modelling and the difference between the nominal and the shifted results is taken as the systematic uncertainty.

Table 5 χ^2 values between the normalised unfolded fiducial cross-section and various predictions from the MC simulation. The number of degrees of freedom (NDF) is equal to one less than the number of bins in the distribution. POWHEG refers to POWHEG-Box v2

Predictions	$p_{\mathrm{T}}(t)$		$\lvert y(t)\rvert$		$p_{\mathrm{T}}(t\bar{t})$		$\lvert y(t\bar{t})\rvert$		$m(t\bar{t})$	
	χ^2/NDF	p-value	χ^2/NDF	p-value	χ^2/NDF	p-value	χ^2/NDF	p-value	χ^2/NDF	p-value
POWHEG + PYTHIA 6	5.2/4	0.27	0.5/3	0.92	5.5/6	0.48	0.6/2	0.74	3.9/4	0.42
POWHEG + PYTHIA 8	4.6/4	0.33	1.3/3	0.73	5.1/6	0.53	0.0/2	1.00	5.7/4	0.22
POWHEG + HERWIG++	14.6/4	0.01	1.4/3	0.71	4.1/6	0.66	1.0/2	0.61	12.0/4	0.02
MG5_aMC@NLO + HERWIG++	2.0/4	0.74	1.3/3	0.73	0.6/6	1.00	0.2/2	0.90	0.9/4	0.92
MG5_aMC@NLO + PYTHIA 8	3.6/4	0.46	0.6/3	0.90	10.7/6	0.10	0.1/2	0.95	2.7/4	0.61
SHERPA	3.8/4	0.43	0.8/3	0.85	0.7/6	0.99	0.0/2	1.00	2.3/4	0.68
POWHEG + PYTHIA 6 (radHi)	7.8/4	0.10	0.6/3	0.90	0.9/6	0.99	0.4/2	0.82	3.8/4	0.43
POWHEG + PYTHIA 6 (radLow)	5.5/4	0.24	0.8/3	0.85	9.6/6	0.14	0.8/2	0.67	4.5/4	0.34

The uncertainties due to lepton isolation, trigger, identification, and reconstruction requirements are evaluated in 2015 data using a tag-and-probe method in leptonically decaying Z-boson events [56]. These uncertainties are summarised as "Lepton" in Tables 2 and 3.

The uncertainties due to the jet energy scale and resolution are extrapolated to $\sqrt{s} = 13$ TeV using a combination of test beam data, simulation and $\sqrt{s} = 8$ TeV dijet data [59]. To account for potential mismodelling of the JVT distribution in simulation, a 2% systematic uncertainty is applied to the jet efficiency. These uncertainties are summarised as "Jet" in Tables 2 and 3. Uncertainties due to b-tagging, summarised under "b-tagging", are determined using $\sqrt{s} = 8$ TeV data as described in Ref. [71] for b-jets and Ref. [72] for c- and light-jets, with additional uncertainties to account for the presence of the new Insertable B-Layer detector and the extrapolation from $\sqrt{s} = 8$ TeV to $\sqrt{s} = 13$ TeV [62].

The systematic uncertainty due to the track-based terms (i.e. those tracks not associated with other reconstructed objects such as leptons and jets) used in the calculation of $E_{\mathrm{T}}^{\mathrm{miss}}$ is evaluated by comparing the $E_{\mathrm{T}}^{\mathrm{miss}}$ in $Z \to \mu\mu$ events, which do not contain prompt neutrinos from the hard process, using different generators. Uncertainties associated with energy scales and resolutions of leptons and jets are propagated to the $E_{\mathrm{T}}^{\mathrm{miss}}$ calculation.

The uncertainty due to the integrated luminosity is $\pm 2.1\%$. It is derived, following a methodology similar to that detailed in Ref. [73], from a calibration of the luminosity scale using x–y beam-separation scans performed in August 2015. The uncertainty in the pile-up reweighting is evaluated by varying the scale factors by $\pm 1\sigma$ based on the reweighting of the average number of interactions per bunch crossing.

The uncertainties due to lepton and $E_{\mathrm{T}}^{\mathrm{miss}}$ modelling are not large for any observable. For the absolute cross-sections, the uncertainty due to luminosity is not a dominant systematic uncertainty, and this uncertainty mainly cancels in the normalised cross-sections. The luminosity uncertainty does not cancel fully since it affects the background subtraction. The uncertainty due to jet energy scale and JVT is a significant source of uncertainty in the absolute cross-sections and in some of the normalised cross-sections such as for $p_{\mathrm{T}}(t\bar{t})$. The uncertainties due to the limited number of MC events are evaluated using pseudo-experiments. The data statistical uncertainty is evaluated using the full covariance matrix from the unfolding.

8 Results

The unfolded particle-level distributions for the absolute and normalised fiducial differential cross-sections are presented in Table 4. The total systematic uncertainties include all sources discussed in Sect. 7.

The unfolded normalised data are used to compare with different generator predictions. The significance of the differences of various generators, with respect to the data in each observable, are evaluated by calculating the χ^2 and determining p-values using the number of degrees of freedom (NDF). The χ^2 is determined using:

$$\chi^2 = S^{\mathrm{T}}_{(N-1)} \cdot \mathrm{Cov}^{-1}_{(N-1)} \cdot S_{(N-1)}, \tag{4}$$

where Cov^{-1} is the inverse of the full bin-to-bin covariance matrix, including all statistical and systematic uncertainties, N is the number of bins, and S is a column vector of the differences between the unfolded data and the prediction. The NDF is equal to the number of bins minus one in the observable for the normalised cross-sections. In Cov and S, a single bin is removed from the calculation to account for the normalisation of the observable, signified by the $(N-1)$ subscript. The χ^2, NDF, and associated p-values are presented in Table 5 for the normalised cross-sections. Most generators studied agree with the unfolded data in each observable within the experimental uncertainties, with the exception of the POWHEG-Box + Herwig++ MC simulation, which differs significantly from the data in both $p_{\mathrm{T}}(t)$ and $m(t\bar{t})$.

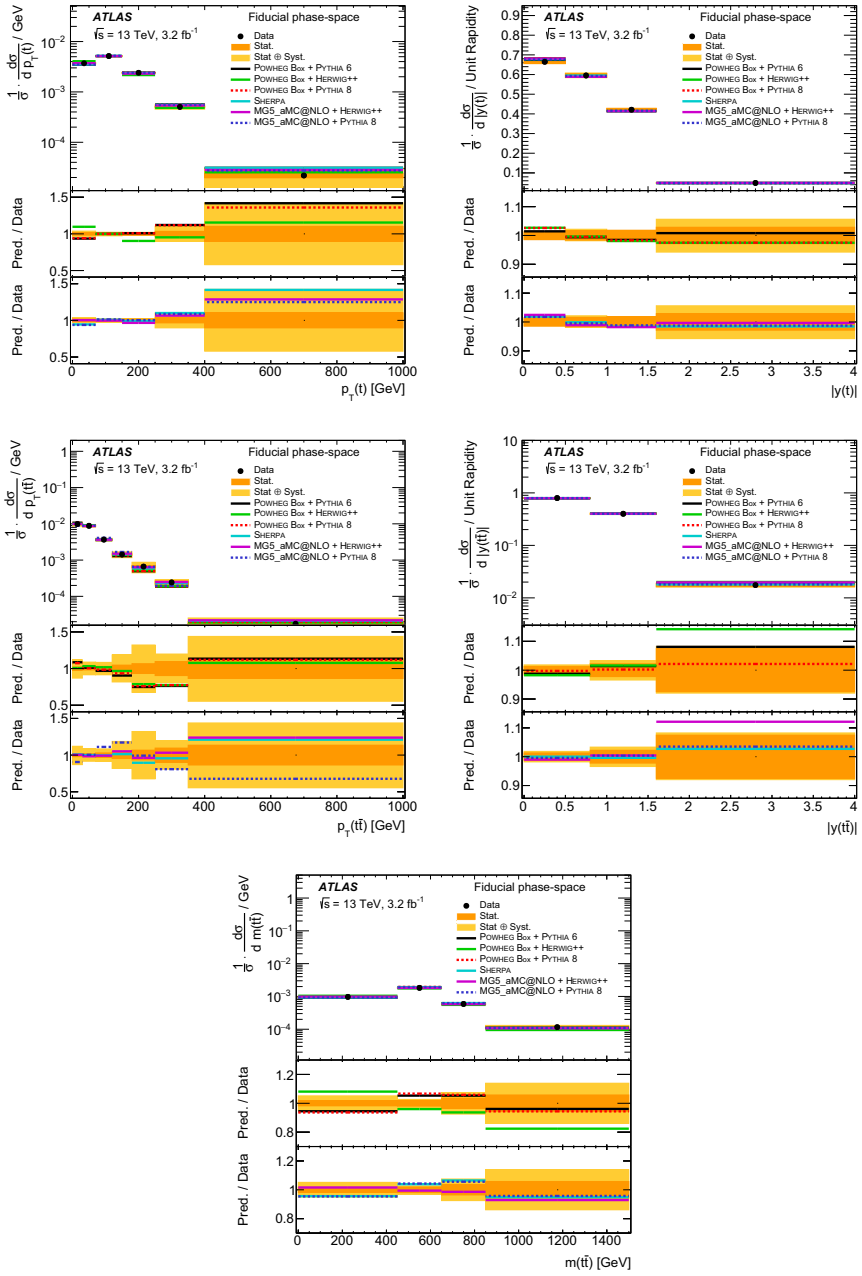

Fig. 5 The measured normalised fiducial differential cross-sections compared to predictions from POWHEG-BOX (*top ratio panel*), MG5_aMC@NLO, and SHERPA (*bottom ratio panel*) interfaced to various parton shower programs

The normalised differential cross-sections for all observables are compared to predictions of different MC generators in Fig. 5.

The POWHEG-Box generator tends to predict a harder $p_{\mathrm{T}}(t)$ spectrum for the top quark than is observed in data, although the data are still consistent with the prediction within the experimental uncertainties. The MG5_aMC@NLO generator appears to agree better with the observed $p_{\mathrm{T}}(t)$ spectrum, particularly when interfaced to Herwig++. For the $p_{\mathrm{T}}(t\bar{t})$ spectrum, again little difference is observed between POWHEG-Box + PYTHIA 6 and PYTHIA 8, and both generally predict a softer spectrum than the data but are also consistent within the experimental uncertainties. The MG5_aMC@NLO generator, interfaced to PYTHIA 8 or Herwig++ seems to agree with the data at low to medium values of p_{T} but MG5_aMC@NLO + Herwig++ disagrees at higher values. For the $m(t\bar{t})$ observable, although the uncertainties are quite large, predictions from POWHEG-Box interfaced to PYTHIA 6 or PYTHIA 8 and the MG5_aMC@NLO + PYTHIA 8 prediction seem higher than the observed data around 600 GeV. For the rapidity observables, all MC predictions appear to agree with the observed data, except for the high $|y(t\bar{t})|$ region, where some of the predictions are slightly higher than the data.

9 Conclusions

Absolute and normalised differential top-quark pair-production cross-sections in a fiducial phase-space region are measured using 3.2 fb^{-1} of $\sqrt{s} = 13$ TeV proton–proton collisions recorded by the ATLAS detector at the LHC in 2015. The differential cross-sections are determined in the $e^{\pm}\mu^{\mp}$ channel, for the transverse momentum and the absolute rapidity of the top quark, as well as the transverse momentum, the absolute rapidity, and the invariant mass of the top-quark pair. The measured differential cross-sections are compared to predictions of NLO generators matched to parton showers and the results are found to be consistent with all models within the experimental uncertainties, with the exception of POWHEG-Box + Herwig++, which deviates from the data in the $p_{\mathrm{T}}(t)$ and $m(t\bar{t})$ observables.

Acknowledgements We thank CERN for the very successful operation of the LHC, as well as the support staff from our institutions without whom ATLAS could not be operated efficiently. We acknowledge the support of ANPCyT, Argentina; YerPhI, Armenia; ARC, Australia; BMWFW and FWF, Austria; ANAS, Azerbaijan; SSTC, Belarus; CNPq and FAPESP, Brazil; NSERC, NRC and CFI, Canada; CERN; CONICYT, Chile; CAS, MOST and NSFC, China; COLCIENCIAS, Colombia; MSMT CR, MPO CR and VSC CR, Czech Republic; DNRF and DNSRC, Denmark; IN2P3-CNRS, CEA-DSM/IRFU, France; SRNSF, Georgia; BMBF, HGF, and MPG, Germany; GSRT, Greece; RGC, Hong Kong SAR, China; ISF, I-CORE and Benoziyo Center, Israel; INFN, Italy; MEXT and JSPS, Japan; CNRST, Morocco; NWO, Netherlands; RCN, Norway; MNiSW and NCN, Poland; FCT, Portugal; MNE/IFA, Romania; MES of Russia and NRC KI, Russian Federation; JINR; MESTD, Serbia; MSSR, Slovakia; ARRS and MIZŠ, Slovenia; DST/NRF, South Africa; MINECO, Spain; SRC and Wallenberg Foundation, Sweden; SERI, SNSF and Cantons of Bern and Geneva, Switzerland; MOST, Taiwan; TAEK, Turkey; STFC, United Kingdom; DOE and NSF, United States of America. In addition, individual groups and members have received support from BCKDF, the Canada Council, CANARIE, CRC, Compute Canada, FQRNT, and the Ontario Innovation Trust, Canada; EPLANET, ERC, ERDF, FP7, Horizon 2020 and Marie Skłodowska-Curie Actions, European Union; Investissements d'Avenir Labex and Idex, ANR, Région Auvergne and Fondation Partager le Savoir, France; DFG and AvH Foundation, Germany; Herakleitos, Thales and Aristeia programmes co-financed by EU-ESF and the Greek NSRF; BSF, GIF and Minerva, Israel; BRF, Norway; CERCA Programme Generalitat de Catalunya, Generalitat Valenciana, Spain; the Royal Society and Leverhulme Trust, United Kingdom. The crucial computing support from all WLCG partners is acknowledged gratefully, in particular from CERN, the ATLAS Tier-1 facilities at TRIUMF (Canada), NDGF (Denmark, Norway, Sweden), CC-IN2P3 (France), KIT/GridKA (Germany), INFN-CNAF (Italy), NL-T1 (Netherlands), PIC (Spain), ASGC (Taiwan), RAL (UK) and BNL (USA), the Tier-2 facilities worldwide and large non-WLCG resource providers. Major contributors of computing resources are listed in Ref. [74].

Funded by SCOAP^3.

References

1. M. Cacciari, M. Czakon, M. Mangano, A. Mitov, P. Nason, Top-pair production at hadron colliders with next-to-next-to-leading logarithmic soft-gluon resummation. Phys. Lett. B **710**, 612–622 (2012). doi:10.1016/j.physletb.2012.03.013. arXiv:1111.5869 [hep-ph]
2. P. Bärnreuther, M. Czakon, A. Mitov, Percent level precision physics at the tevatron: first genuine NNLO QCD corrections to $q\bar{q} \to t\bar{t} + X$. Phys. Rev. Lett. **109**, 132001 (2012). doi:10.1103/PhysRevLett.109.132001. arXiv:1204.5201 [hep-ph]
3. M. Czakon, A. Mitov, NNLO corrections to top-pair production at hadron colliders: the all-fermionic scattering channels. JHEP **12**, 054 (2012). doi:10.1007/JHEP12(2012)054. arXiv:1207.0236 [hep-ph]
4. M. Czakon, A. Mitov, NNLO corrections to top pair production at hadron colliders: the quark-gluon reaction. JHEP **01**, 080 (2013). doi:10.1007/JHEP01(2013)080. arXiv:1210.6832 [hep-ph]
5. M. Czakon, P. Fiedler, A. Mitov, Total top-quark pair-production cross section at hadron colliders through $O(\alpha_S^4)$. Phys. Rev. Lett. **110**, 252004 (2013). doi:10.1103/PhysRevLett.110.252004. arXiv:1303.6254 [hep-ph]
6. M. Czakon, A. Mitov, Top++: a program for the calculation of the top-pair cross-section at hadron colliders. Comput. Phys. Commun. **185**, 2930 (2014). doi:10.1016/j.cpc.2014.06.021. arXiv:1112.5675 [hep-ph]
7. M. Guzzi, K. Lipka, S.-O. Moch, Top-quark pair production at hadron colliders: differential cross section and phenomenological applications with DiffTop. JHEP **01**, 082 (2015). doi:10.1007/JHEP01(2015)082. arXiv:1406.0386 [hep-ph]

8. N. Kidonakis, NNNLO soft-gluon corrections for the top-quark p_T and rapidity distributions. Phys. Rev. D **91**, 031501 (2015). doi:10.1103/PhysRevD.91.031501. arXiv:1411.2633 [hep-ph]
9. V. Ahrens, A. Ferroglia, M. Neubert, B.D. Pecjak, L.L. Yang, Renormalization-group improved predictions for top-quark pair production at hadron colliders. JHEP **09**, 097 (2010). doi:10.1007/JHEP09(2010)097. arXiv:1003.5827 [hep-ph]
10. M. Czakon, D. Heymes, A. Mitov, High-precision differential predictions for top-quark pairs at the LHC. Phys. Rev. Lett. **116**, 082003 (2016). doi:10.1103/PhysRevLett.116.082003. arXiv:1511.00549 [hep-ph]
11. M. Czakon, D. Heymes, A. Mitov, Dynamical scales for multi-TeV top-pair production at the LHC (2016). arXiv:1606.03350 [hep-ph]
12. ATLAS Collaboration, Measurements of normalized differential cross sections for $t\bar{t}$ production in pp collisions at $\sqrt{s} = 7$ TeV using the ATLAS detector. Phys. Rev. D **90**, 072004 (2014). doi:10.1103/PhysRevD.90.072004. arXiv:1407.0371 [hep-ex]
13. ATLAS Collaboration, Measurements of top-quark pair differential cross-sections in the lepton+jets channel in pp collisions at $\sqrt{s} = 8$ TeV using the ATLAS detector. Eur. Phys. J. C **76**, 538 (2016). doi:10.1140/epjc/s10052-016-4366-4. arXiv:1511.04716 [hep-ex]
14. ATLAS Collaboration, Differential top-antitop cross-section measurements as a function of observables constructed from final-state particles using pp collisions at $\sqrt{s} = 7$ TeV in the ATLAS detector. JHEP **06**, 100 (2015). doi:10.1007/JHEP06(2015)100. arXiv:1502.05923 [hep-ex]
15. CMS Collaboration, Measurement of differential top-quark pair production cross sections in pp colisions at $\sqrt{s} = 7$ TeV. Eur. Phys. J. C **73**, 2339 (2013). doi:10.1140/epjc/s10052-013-2339-4. arXiv:1211.2220 [hep-ex]
16. CMS Collaboration, Measurement of the differential cross section for top quark pair production in pp collisions at $\sqrt{s} = 8$ TeV. Eur. Phys. J. C **75**, 542 (2015). doi:10.1140/epjc/s10052-015-3709-x. arXiv:1505.04480 [hep-ex]
17. CMS Collaboration, Measurement of differential cross sections for top quark pair production using the lepton+jets final state in proton–proton collisions at 13 TeV Submitted to: Phys. Rev. D (2016). arXiv:1610.04191 [hep-ex]
18. ATLAS Collaboration, Measurement of the $t\bar{t}$ production cross-section using $e\mu$ events with b-tagged jets in pp collisions at $\sqrt{s} = 13$ TeV with the ATLAS detector. Phys. Lett. B **761**, 136–157 (2016). doi:10.1016/j.physletb.2016.08.019. arXiv:1606.02699 [hep-ex]
19. CMS Collaboration, Measurement of the top quark pair production cross section in proton–proton collisions at $\sqrt{s} = 13$ TeV. Phys. Rev. Lett. **116**, 052002 (2016). doi:10.1103/PhysRevLett.116.052002
20. CMS Collaboration, Measurement of the $t\bar{t}$ production cross section using events in the eμ final state in pp collisions at $\sqrt{s} = 13$ TeV. Accepted by: Eur. Phys. J. C (2016). arXiv:1611.04040 [hep-ex]
21. ATLAS Collaboration, The ATLAS experiment at the CERN large hadron collider. JINST **3**, S08003 (2008). doi:10.1088/1748-0221/3/08/S08003
22. ATLAS Collaboration, ATLAS insertable B-layer technical design report. ATLAS-TDR-19 (2010). http://cds.cern.ch/record/1291633
23. ATLAS Collaboration, ATLAS insertable B-layer technical design report addendum. ATLAS-TDR-19-ADD-1 (2012). http://cds.cern.ch/record/1451888
24. ATLAS Collaboration, Performance of the ATLAS trigger system in 2010. Eur. Phys. J. C **72**, 1849 (2012). doi:10.1140/epjc/s10052-011-1849-1. arXiv:1110.1530 [hep-ex]
25. ATLAS Collaboration, 2015 start-up trigger menu and initial performance assessment of the ATLAS trigger using Run-2 data. ATL-DAQ-PUB-2016-001 (2016). http://cds.cern.ch/record/2136007
26. ATLAS Collaboration, The ATLAS simulation infrastructure. Eur. Phys. J. C **70**, 823–874 (2010). doi:10.1140/epjc/s10052-010-1429-9. arXiv:1005.4568 [physics.ins-det]
27. S. Agostinelli et al., GEANT4: a simulation toolkit. Nucl. Instrum. Methods A **506**, 250–303 (2003). doi:10.1016/S0168-9002(03)01368-8
28. ATLAS Collaboration, The simulation principle and performance of the ATLAS fast calorimeter simulation FastCaloSim. ATL-PHYS-PUB-2010-013 (2010). http://cds.cern.ch/record/1300517
29. T. Sjöstrand, S. Mrenna, P.Z. Skands, A brief introduction to PYTHIA 8.1. Comput. Phys. Commun. **178**, 852–867 (2008). doi:10.1016/j.cpc.2008.01.036. arXiv:0710.3820 [hep-ph]
30. P. Nason, A New method for combining NLO QCD with shower Monte Carlo algorithms. JHEP **11**, 040 (2004). doi:10.1088/1126-6708/2004/11/040. arXiv:hep-ph/0409146
31. S. Frixione, P. Nason, C. Oleari, Matching NLO QCD computations with parton shower simulations: the POWHEG method. JHEP **11**, 070 (2007). doi:10.1088/1126-6708/2007/11/070. arXiv:0709.2092 [hep-ph]
32. S. Alioli, P. Nason, C. Oleari, E. Re, A general framework for implementing NLO calculations in shower Monte Carlo programs: the POWHEG BOX. JHEP **06**, 043 (2010). doi:10.1007/JHEP06(2010)043. arXiv:1002.2581 [hep-ph]
33. T. Sjöstrand, S. Mrenna, P.Z. Skands, PYTHIA 6.4 physics and manual. JHEP **0605**, 026 (2006). doi:10.1088/1126-6708/2006/05/026. arXiv:hep-ph/0603175
34. H.-L. Lai, M. Guzzi, J. Huston, Z. Li, P.M. Nadolsky et al., New parton distributions for collider physics. Phys. Rev. D **82**, 074024 (2010). doi:10.1103/PhysRevD.82.074024. arXiv:1007.2241 [hep-ph]
35. D. Stump et al., Inclusive jet production, parton distributions, and the search for new physics. JHEP **10**, 046 (2003). doi:10.1088/1126-6708/2003/10/046. arXiv:hep-ph/0303013
36. P.Z. Skands, Tuning Monte Carlo generators: the Perugia tunes. Phys. Rev. D **82**, 074018 (2010). doi:10.1103/PhysRevD.82.074018. arXiv:1005.3457 [hep-ph]
37. ATLAS Collaboration, Simulation of top quark production for the ATLAS experiment at $\sqrt{s} = 13$ TeV. ATL-PHYS-PUB-2016-004 (2016). http://cds.cern.ch/record/2120417
38. J. Alwall et al., The automated computation of tree-level and next-to-leading order differential cross sections, and their matching to parton shower simulations. JHEP **07**, 079 (2014). doi:10.1007/JHEP07(2014)079. arXiv:1405.0301 [hep-ph]
39. M. Bahr et al., Herwig++ physics and manual. Eur. Phys. J. C **58**, 639–707 (2008). doi:10.1140/epjc/s10052-008-0798-9. arXiv:0803.0883 [hep-ph]
40. T. Gleisberg, S. Hoeche, F. Krauss, M. Schonherr, S. Schumann et al., Event generation with SHERPA 1.1. JHEP **02**, 007 (2009). doi:10.1088/1126-6708/2009/02/007. arXiv:0811.4622 [hep-ph]
41. J. Bellm et al., Herwig 7.0/Herwig++ 3.0 release note. Eur. Phys. J. C **76**, 196 (2016). doi:10.1140/epjc/s10052-016-4018-8. arXiv:1512.01178
42. N. Kidonakis, Two-loop soft anomalous dimensions for single top quark associated production with a W$-$ or H$-$. Phys. Rev. D **82**, 054018 (2010). doi:10.1103/PhysRevD.82.054018. arXiv:1005.4451 [hep-ph]
43. S. Frixione, E. Laenen, P. Motylinski, B.R. Webber, C.D. White, Single-top hadroproduction in association with a W boson. JHEP **07**, 029 (2008). doi:10.1088/1126-6708/2008/07/029. arXiv:0805.3067 [hep-ph]
44. F. Cascioli, P. Maierhofer, S. Pozzorini, Scattering amplitudes with open loops. Phys. Rev. Lett. **108**, 111601 (2012). doi:10.1103/PhysRevLett.108.111601. arXiv:1111.5206 [hep-ph]

45. T. Gleisberg, S. Hoeche, Comix, a new matrix element generator. JHEP **12**, 039 (2008). doi:10.1088/1126-6708/2008/12/039. arXiv:0808.3674 [hep-ph]
46. S. Schumann, F. Krauss, A parton shower algorithm based on Catani-Seymour dipole factorisation. JHEP **03**, 038 (2008). doi:10.1088/1126-6708/2008/03/038. arXiv:0709.1027 [hep-ph]
47. S. Hoeche, F. Krauss, M. Schonherr, F. Siegert, QCD matrix elements + parton showers: the NLO case. JHEP **04**, 027 (2013). doi:10.1007/JHEP04(2013)027. arXiv:1207.5030 [hep-ph]
48. ATLAS Collaboration, Monte Carlo generators for the production of a W or Z/γ^* Boson in association with Jets at ATLAS in Run 2. ATL-PHYS-PUB-2016-003 (2016). http://cds.cern.ch/record/2120133
49. ATLAS Collaboration, Multi-boson simulation for 13 TeV ATLAS analyses. ATL-PHYS-PUB-2016-002 (2016). http://cds.cern.ch/record/2119986
50. J. Alwall, M. Herquet, F. Maltoni, O. Mattelaer, T. Stelzer, MadGraph 5: going beyond. JHEP **06**, 128 (2011). doi:10.1007/JHEP06(2011)128. arXiv:1106.0522 [hep-ph]
51. ATLAS Collaboration, Modelling of the $t\bar{t}H$ and $t\bar{t}V$ ($V = W, Z$) processes for $\sqrt{s} = 13$ TeV ATLAS analyses. ATL-PHYS-PUB-2016-005 (2016). http://cds.cern.ch/record/2120826
52. ATLAS Collaboration, Measurement of the Z/γ^* boson transverse momentum distribution in pp collisions at $\sqrt{s} = 7$ TeV with the ATLAS detector. JHEP **09**, 55 (2014). doi:10.1007/JHEP09(2014)145. arXiv:1406.3660 [hep-ex]
53. D.J. Lange, The EvtGen particle decay simulation package. Nucl. Instrum. Methods A **462**, 152–155 (2001). doi:10.1016/S0168-9002(01)00089-4
54. ATLAS Collaboration, Electron reconstruction and identification efficiency measurements with the ATLAS detector using the 2011 LHC proton–proton collision data. Eur. Phys. J. C **74**, 2941 (2014). doi:10.1140/epjc/s10052-014-2941-0. arXiv:1404.2240 [hep-ex]
55. ATLAS Collaboration, Electron efficiency measurements with the ATLAS detector using the 2015 LHC proton–proton collision data. ATLAS-CONF-2016-024 (2016). http://cdsweb.cern.ch/record/2157687
56. ATLAS Collaboration, Muon reconstruction performance of the ATLAS detector in proton–proton collision data at $\sqrt{s} = 13$ TeV. Eur. Phys. J. C **76**, 292 (2016). doi:10.1140/epjc/s10052-016-4120-y. arXiv:1603.05598 [hep-ex]
57. M. Cacciari, G.P. Salam, Dispelling the N^3 myth for the k_t jet-finder. Phys. Lett. B **641**, 57–61 (2006). doi:10.1016/j.physletb.2006.08.037. arXiv:hep-ph/0512210
58. M. Cacciari, G.P. Salam, G. Soyez, The anti-k_t jet clustering algorithm. JHEP **04**, 063 (2008). doi:10.1088/1126-6708/2008/04/063. arXiv:0802.1189. [hep-ph]
59. ATLAS Collaboration, Jet calibration and systematic uncertainties for jets reconstructed in the ATLAS detector at $\sqrt{s} = 13$ TeV. ATL-PHYS-PUB-2015-015 (2015). http://cds.cern.ch/record/2037613
60. ATLAS Collaboration, Tagging and suppression of pileup jets with the ATLAS detector. ATLAS-CONF-2014-018 (2014). http://cds.cern.ch/record/1700870
61. ATLAS Collaboration, Performance of pile-up mitigation techniques for jets in pp collisions at $\sqrt{s} = 8$ TeV using the ATLAS detector. CERN-PH-EP-2015-20 (2015). arXiv:1510.03823 [hep-ex]
62. ATLAS Collaboration, Expected performance of the ATLAS b-tagging algorithms in Run-2. ATL-PHYS-PUB-2015-022 (2015). http://cds.cern.ch/record/2037697
63. ATLAS Collaboration, Performance of missing transverse momentum reconstruction for the ATLAS detector in the first proton–proton collisions at at $\sqrt{s} = 13$ TeV. ATL-PHYS-PUB-2015-027 (2015). http://cds.cern.ch/record/2037904
64. M. Cacciari, G.P. Salam, Pileup subtraction using jet areas. Phys. Lett. BB **659**, 119–126 (2008). doi:10.1016/j.physletb.2007.09.077. arXiv:0707.1378 [hep-ph]
65. D0 Collaboration, Measurement of the top quark mass using dilepton events. Phys. Rev. Lett. **80**, 2063–2068 (1998). doi:10.1103/PhysRevLett.80.2063. arXiv:hep-ex/9706014
66. G. D'Agostini, A multidimensional unfolding method based on Bayes' theorem. Nucl. Instrum. Methods A **362**, 487–498 (1995). doi:10.1016/0168-9002(95)00274-X
67. T. Adye, Unfolding algorithms and tests using RooUnfold. In *Proceedings of the PHYSTAT 2011 Workshop, CERN, Geneva, Switzerland, January 2011, CERN-2011-006*, pp. 313–318. arXiv:1105.1160 [physics.data-an]
68. J. Butterworth et al., PDF4LHC recommendations for LHC Run II. J. Phys. G **43**, 023001 (2016). doi:10.1088/0954-3899/43/2/023001. arXiv:1510.03865 [hep-ph]
69. S. Dulat et al., New parton distribution functions from a global analysis of quantum chromodynamics. Phys. Rev. D **93**, 033006 (2016). doi:10.1103/PhysRevD.93.033006. arXiv:1506.07443 [hep-ph]
70. NNPDF Collaboration, R.D. Ball et al., Parton distributions for the LHC Run II. JHEP **04**, 040 (2015). doi:10.1007/JHEP04(2015)040. arXiv:1410.8849 [hep-ph]
71. ATLAS Collaboration, Calibration of b-tagging using dileptonic top pair events in a combinatorial likelihood approach with the ATLAS experiment. ATLAS-CONF-2014-004 (2014). http://cds.cern.ch/record/1664335
72. ATLAS Collaboration, Calibration of the performance of b-tagging for c and light-flavour jets in the 2012 ATLAS data. ATLAS-CONF-2014-046 (2014). http://cds.cern.ch/record/1741020
73. ATLAS Collaboration, Luminosity determination in pp collisions at $\sqrt{s} = 8$ TeV using the ATLAS detector at the LHC (2016). arXiv:1608.03953 [hep-ex]
74. ATLAS Collaboration, ATLAS computing acknowledgements 2016–2017. ATL-GEN-PUB-2016-002 (2016). http://cds.cern.ch/record/2202407

ATLAS Collaboration

M. Aaboud[136d], G. Aad[87], B. Abbott[114], J. Abdallah[8], O. Abdinov[12], B. Abeloos[118], R. Aben[108], O. S. AbouZeid[138], N. L. Abraham[152], H. Abramowicz[156], H. Abreu[155], R. Abreu[117], Y. Abulaiti[149a,149b], B. S. Acharya[168a,168b,a], S. Adachi[158], L. Adamczyk[40a], D. L. Adams[27], J. Adelman[109], S. Adomeit[101], T. Adye[132], A. A. Affolder[76], T. Agatonovic-Jovin[14], J. A. Aguilar-Saavedra[127a,127f], S. P. Ahlen[24], F. Ahmadov[67,b], G. Aielli[134a,134b], H. Akerstedt[149a,149b], T. P. A. Åkesson[83], A. V. Akimov[97], G. L. Alberghi[22a,22b], J. Albert[173], S. Albrand[57], M. J. Alconada Verzini[73], M. Aleksa[32], I. N. Aleksandrov[67], C. Alexa[28b], G. Alexander[156], T. Alexopoulos[10], M. Alhroob[114], B. Ali[129], M. Aliev[75a,75b], G. Alimonti[93a], J. Alison[33], S. P. Alkire[37], B. M. M. Allbrooke[152], B. W. Allen[117], P. P. Allport[19], A. Aloisio[105a,105b], A. Alonso[38], F. Alonso[73], C. Alpigiani[139], A. A. Alshehri[55], M. Alstaty[87], B. Alvarez Gonzalez[32], D. Álvarez Piqueras[171], M. G. Alviggi[105a,105b], B. T. Amadio[16], K. Amako[68], Y. Amaral Coutinho[26a], C. Amelung[25], D. Amidei[91], S. P. Amor Dos Santos[127a,127c], A. Amorim[127a,127b], S. Amoroso[32], G. Amundsen[25], C. Anastopoulos[142], L. S. Ancu[51], N. Andari[19], T. Andeen[11], C. F. Anders[60b], G. Anders[32], J. K. Anders[76], K. J. Anderson[33], A. Andreazza[93a,93b], V. Andrei[60a], S. Angelidakis[9], I. Angelozzi[108], A. Angerami[37], F. Anghinolfi[32], A. V. Anisenkov[110,c], N. Anjos[13], A. Annovi[125a,125b], C. Antel[60a], M. Antonelli[49], A. Antonov[99,*], F. Anulli[133a], M. Aoki[68], L. Aperio Bella[19], G. Arabidze[92], Y. Arai[68], J. P. Araque[127a], A. T. H. Arce[47], F. A. Arduh[73], J-F. Arguin[96], S. Argyropoulos[65], M. Arik[20a], A. J. Armbruster[146], L. J. Armitage[78], O. Arnaez[32], H. Arnold[50], M. Arratia[30], O. Arslan[23], A. Artamonov[98], G. Artoni[121], S. Artz[85], S. Asai[158], N. Asbah[44], A. Ashkenazi[156], B. Åsman[149a,149b], L. Asquith[152], K. Assamagan[27], R. Astalos[147a], M. Atkinson[170], N. B. Atlay[144], K. Augsten[129], G. Avolio[32], B. Axen[16], M. K. Ayoub[118], G. Azuelos[96,d], M. A. Baak[32], A. E. Baas[60a], M. J. Baca[19], H. Bachacou[137], K. Bachas[75a,75b], M. Backes[121], M. Backhaus[32], P. Bagiacchi[133a,133b], P. Bagnaia[133a,133b], Y. Bai[35a], J. T. Baines[132], O. K. Baker[180], E. M. Baldin[110,c], P. Balek[176], T. Balestri[151], F. Balli[137], W. K. Balunas[123], E. Banas[41], Sw. Banerjee[177,e], A. A. E. Bannoura[179], L. Barak[32], E. L. Barberio[90], D. Barberis[52a,52b], M. Barbero[87], T. Barillari[102], M-S. Barisits[32], T. Barklow[146], N. Barlow[30], S. L. Barnes[86], B. M. Barnett[132], R. M. Barnett[16], Z. Barnovska-Blenessy[59], A. Baroncelli[135a], G. Barone[25], A. J. Barr[121], L. Barranco Navarro[171], F. Barreiro[84], J. Barreiro Guimarães da Costa[35a], R. Bartoldus[146], A. E. Barton[74], P. Bartos[147a], A. Basalaev[124], A. Bassalat[118,f], R. L. Bates[55], S. J. Batista[162], J. R. Batley[30], M. Battaglia[138], M. Bauce[133a,133b], F. Bauer[137], H. S. Bawa[146,g], J. B. Beacham[112], M. D. Beattie[74], T. Beau[82], P. H. Beauchemin[166], P. Bechtle[23], H. P. Beck[18,h], K. Becker[121], M. Becker[85], M. Beckingham[174], C. Becot[111], A. J. Beddall[20e], A. Beddall[20b], V. A. Bednyakov[67], M. Bedognetti[108], C. P. Bee[151], L. J. Beemster[108], T. A. Beermann[32], M. Begel[27], J. K. Behr[44], C. Belanger-Champagne[89], A. S. Bell[80], G. Bella[156], L. Bellagamba[22a], A. Bellerive[31], M. Bellomo[88], K. Belotskiy[99], O. Beltramello[32], N. L. Belyaev[99], O. Benary[156,*], D. Benchekroun[136a], M. Bender[101], K. Bendtz[149a,149b], N. Benekos[10], Y. Benhammou[156], E. Benhar Noccioli[180], J. Benitez[65], D. P. Benjamin[47], J. R. Bensinger[25], S. Bentvelsen[108], L. Beresford[121], M. Beretta[49], D. Berge[108], E. Bergeaas Kuutmann[169], N. Berger[5], J. Beringer[16], S. Berlendis[57], N. R. Bernard[88], C. Bernius[111], F. U. Bernlochner[23], T. Berry[79], P. Berta[130], C. Bertella[85], G. Bertoli[149a,149b], F. Bertolucci[125a,125b], I. A. Bertram[74], C. Bertsche[44], D. Bertsche[114], G. J. Besjes[38], O. Bessidskaia Bylund[149a,149b], M. Bessner[44], N. Besson[137], C. Betancourt[50], A. Bethani[57], S. Bethke[102], A. J. Bevan[78], R. M. Bianchi[126], L. Bianchini[25], M. Bianco[32], O. Biebel[101], D. Biedermann[17], R. Bielski[86], N. V. Biesuz[125a,125b], M. Biglietti[135a], J. Bilbao De Mendizabal[51], T. R. V. Billoud[96], H. Bilokon[49], M. Bindi[56], S. Binet[118], A. Bingul[20b], C. Bini[133a,133b], S. Biondi[22a,22b], T. Bisanz[56], D. M. Bjergaard[47], C. W. Black[153], J. E. Black[146], K. M. Black[24], D. Blackburn[139], R. E. Blair[6], J.-B. Blanchard[137], T. Blazek[147a], I. Bloch[44], C. Blocker[25], A. Blue[55], W. Blum[85,*], U. Blumenschein[56], S. Blunier[34a], G. J. Bobbink[108], V. S. Bobrovnikov[110,c], S. S. Bocchetta[83], A. Bocci[47], C. Bock[101], M. Boehler[50], D. Boerner[179], J. A. Bogaerts[32], D. Bogavac[14], A. G. Bogdanchikov[110], C. Bohm[149a], V. Boisvert[79], P. Bokan[14], T. Bold[40a], A. S. Boldyrev[168a,168c], M. Bomben[82], M. Bona[78], M. Boonekamp[137], A. Borisov[131], G. Borissov[74], J. Bortfeldt[32], D. Bortoletto[121], V. Bortolotto[62a,62b,62c], K. Bos[108], D. Boscherini[22a], M. Bosman[13], J. D. Bossio Sola[29], J. Boudreau[126], J. Bouffard[2], E. V. Bouhova-Thacker[74], D. Boumediene[36], C. Bourdarios[118], S. K. Boutle[55], A. Boveia[32], J. Boyd[32], I. R. Boyko[67], J. Bracinik[19], A. Brandt[8], G. Brandt[56], O. Brandt[60a], U. Bratzler[159], B. Brau[88], J. E. Brau[117], W. D. Breaden Madden[55], K. Brendlinger[123], A. J. Brennan[90], L. Brenner[108], R. Brenner[169], S. Bressler[176], T. M. Bristow[48], D. Britton[55], D. Britzger[44], F. M. Brochu[30], I. Brock[23], R. Brock[92], G. Brooijmans[37], T. Brooks[79], W. K. Brooks[34b], J. Brosamer[16], E. Brost[109], J. H Broughton[19], P. A. Bruckman de Renstrom[41], D. Bruncko[147b], R. Bruneliere[50], A. Bruni[22a], G. Bruni[22a], L. S. Bruni[108], BH. Brunt[30], M. Bruschi[22a], N. Bruscino[23], P. Bryant[33], L. Bryngemark[83], T. Buanes[15], Q. Buat[145], P. Buchholz[144], A. G. Buckley[55], I. A. Budagov[67], F. Buehrer[50], M. K. Bugge[120], O. Bulekov[99], D. Bullock[8], H. Burckhart[32], S. Burdin[76], C. D. Burgard[50], B. Burghgrave[109], K. Burka[41], S. Burke[132], I. Burmeister[45], J. T. P. Burr[121], E. Busato[36], D. Büscher[50], V. Büscher[85], P. Bussey[55], J. M. Butler[24], C. M. Buttar[55], J. M. Butterworth[80], P. Butti[108], W. Buttinger[27], A. Buzatu[55], A. R. Buzykaev[110,c], S. Cabrera Urbán[171],

D. Caforio[129], V. M. Cairo[39a,39b], O. Cakir[4a], N. Calace[51], P. Calafiura[16], A. Calandri[87], G. Calderini[82], P. Calfayan[63], G. Callea[39a,39b], L. P. Caloba[26a], S. Calvente Lopez[84], D. Calvet[36], S. Calvet[36], T. P. Calvet[87], R. Camacho Toro[33], S. Camarda[32], P. Camarri[134a,134b], D. Cameron[120], R. Caminal Armadans[170], C. Camincher[57], S. Campana[32], M. Campanelli[80], A. Camplani[93a,93b], A. Campoverde[144], V. Canale[105a,105b], A. Canepa[164a], M. Cano Bret[141], J. Cantero[115], T. Cao[42], M. D. M. Capeans Garrido[32], I. Caprini[28b], M. Caprini[28b], M. Capua[39a,39b], R. M. Carbone[37], R. Cardarelli[134a], F. Cardillo[50], I. Carli[130], T. Carli[32], G. Carlino[105a], L. Carminati[93a,93b], R. M. D. Carney[149a,149b], S. Caron[107], E. Carquin[34b], G. D. Carrillo-Montoya[32], J. R. Carter[30], J. Carvalho[127a,127c], D. Casadei[19], M. P. Casado[13,i], M. Casolino[13], D. W. Casper[167], E. Castaneda-Miranda[148a], R. Castelijn[108], A. Castelli[108], V. Castillo Gimenez[171], N. F. Castro[127a,j], A. Catinaccio[32], J. R. Catmore[120], A. Cattai[32], J. Caudron[23], V. Cavaliere[170], E. Cavallaro[13], D. Cavalli[93a], M. Cavalli-Sforza[13], V. Cavasinni[125a,125b], F. Ceradini[135a,135b], L. Cerda Alberich[171], A. S. Cerqueira[26b], A. Cerri[152], L. Cerrito[134a,134b], F. Cerutti[16], M. Cerv[32], A. Cervelli[18], S. A. Cetin[20d], A. Chafaq[136a], D. Chakraborty[109], S. K. Chan[58], Y. L. Chan[62a], P. Chang[170], J. D. Chapman[30], D. G. Charlton[19], A. Chatterjee[51], C. C. Chau[162], C. A. Chavez Barajas[152], S. Che[112], S. Cheatham[168a,168c], A. Chegwidden[92], S. Chekanov[6], S. V. Chekulaev[164a], G. A. Chelkov[67,k], M. A. Chelstowska[91], C. Chen[66], H. Chen[27], K. Chen[151], S. Chen[35b], S. Chen[158], X. Chen[35c], Y. Chen[69], H. C. Cheng[91], H. J Cheng[35a], Y. Cheng[33], A. Cheplakov[67], E. Cheremushkina[131], R. Cherkaoui El Moursli[136e], V. Chernyatin[27,*], E. Cheu[7], L. Chevalier[137], V. Chiarella[49], G. Chiarelli[125a,125b], G. Chiodini[75a], A. S. Chisholm[32], A. Chitan[28b], M. V. Chizhov[67], K. Choi[63], A. R. Chomont[36], S. Chouridou[9], B. K. B. Chow[101], V. Christodoulou[80], D. Chromek-Burckhart[32], J. Chudoba[128], A. J. Chuinard[89], J. J. Chwastowski[41], L. Chytka[116], G. Ciapetti[133a,133b], A. K. Ciftci[4a], D. Cinca[45], V. Cindro[77], I. A. Cioara[23], C. Ciocca[22a,22b], A. Ciocio[16], F. Cirotto[105a,105b], Z. H. Citron[176], M. Citterio[93a], M. Ciubancan[28b], A. Clark[51], B. L. Clark[58], M. R. Clark[37], P. J. Clark[48], R. N. Clarke[16], C. Clement[149a,149b], Y. Coadou[87], M. Cobal[168a,168c], A. Coccaro[51], J. Cochran[66], L. Colasurdo[107], B. Cole[37], A. P. Colijn[108], J. Collot[57], T. Colombo[167], G. Compostella[102], P. Conde Muiño[127a,127b], E. Coniavitis[50], S. H. Connell[148b], I. A. Connelly[79], V. Consorti[50], S. Constantinescu[28b], G. Conti[32], F. Conventi[105a,l], M. Cooke[16], B. D. Cooper[80], A. M. Cooper-Sarkar[121], K. J. R. Cormier[162], T. Cornelissen[179], M. Corradi[133a,133b], F. Corriveau[89,m], A. Cortes-Gonzalez[32], G. Cortiana[102], G. Costa[93a], M. J. Costa[171], D. Costanzo[142], G. Cottin[30], G. Cowan[79], B. E. Cox[86], K. Cranmer[111], S. J. Crawley[55], G. Cree[31], S. Crépé-Renaudin[57], F. Crescioli[82], W. A. Cribbs[149a,149b], M. Crispin Ortuzar[121], M. Cristinziani[23], V. Croft[107], G. Crosetti[39a,39b], A. Cueto[84], T. Cuhadar Donszelmann[142], J. Cummings[180], M. Curatolo[49], J. Cúth[85], H. Czirr[144], P. Czodrowski[3], G. D'amen[22a,22b], S. D'Auria[55], M. D'Onofrio[76], M. J. Da Cunha Sargedas De Sousa[127a,127b], C. Da Via[86], W. Dabrowski[40a], T. Dado[147a], T. Dai[91], O. Dale[15], F. Dallaire[96], C. Dallapiccola[88], M. Dam[38], J. R. Dandoy[33], N. P. Dang[50], A. C. Daniells[19], N. S. Dann[86], M. Danninger[172], M. Dano Hoffmann[137], V. Dao[50], G. Darbo[52a], S. Darmora[8], J. Dassoulas[3], A. Dattagupta[117], W. Davey[23], C. David[173], T. Davidek[130], M. Davies[156], P. Davison[80], E. Dawe[90], I. Dawson[142], K. De[8], R. de Asmundis[105a], A. De Benedetti[114], S. De Castro[22a,22b], S. De Cecco[82], N. De Groot[107], P. de Jong[108], H. De la Torre[92], F. De Lorenzi[66], A. De Maria[56], D. De Pedis[133a], A. De Salvo[133a], U. De Sanctis[152], A. De Santo[152], J. B. De Vivie De Regie[118], W. J. Dearnaley[74], R. Debbe[27], C. Debenedetti[138], D. V. Dedovich[67], N. Dehghanian[3], I. Deigaard[108], M. Del Gaudio[39a,39b], J. Del Peso[84], T. Del Prete[125a,125b], D. Delgove[118], F. Deliot[137], C. M. Delitzsch[51], A. Dell'Acqua[32], L. Dell'Asta[24], M. Dell'Orso[125a,125b], M. Della Pietra[105a,l], D. della Volpe[51], M. Delmastro[5], P. A. Delsart[57], D. A. DeMarco[162], S. Demers[180], M. Demichev[67], A. Demilly[82], S. P. Denisov[131], D. Denysiuk[137], D. Derendarz[41], J. E. Derkaoui[136d], F. Derue[82], P. Dervan[76], K. Desch[23], C. Deterre[44], K. Dette[45], P. O. Deviveiros[32], A. Dewhurst[132], S. Dhaliwal[25], A. Di Ciaccio[134a,134b], L. Di Ciaccio[5], W. K. Di Clemente[123], C. Di Donato[105a,105b], A. Di Girolamo[32], B. Di Girolamo[32], B. Di Micco[135a,135b], R. Di Nardo[32], A. Di Simone[50], R. Di Sipio[162], D. Di Valentino[31], C. Diaconu[87], M. Diamond[162], F. A. Dias[48], M. A. Diaz[34a], E. B. Diehl[91], J. Dietrich[17], S. Díez Cornell[44], A. Dimitrievska[14], J. Dingfelder[23], P. Dita[28b], S. Dita[28b], F. Dittus[32], F. Djama[87], T. Djobava[53b], J. I. Djuvsland[60a], M. A. B. do Vale[26c], D. Dobos[32], M. Dobre[28b], C. Doglioni[83], J. Dolejsi[130], Z. Dolezal[130], M. Donadelli[26d], S. Donati[125a,125b], P. Dondero[122a,122b], J. Donini[36], J. Dopke[132], A. Doria[105a], M. T. Dova[73], A. T. Doyle[55], E. Drechsler[56], M. Dris[10], Y. Du[140], J. Duarte-Campderros[156], E. Duchovni[176], G. Duckeck[101], O. A. Ducu[96,n], D. Duda[108], A. Dudarev[32], A. Chr. Dudder[85], E. M. Duffield[16], L. Duflot[118], M. Dührssen[32], M. Dumancic[176], M. Dunford[60a], H. Duran Yildiz[4a], M. Düren[54], A. Durglishvili[53b], D. Duschinger[46], B. Dutta[44], M. Dyndal[44], C. Eckardt[44], K. M. Ecker[102], R. C. Edgar[91], N. C. Edwards[48], T. Eifert[32], G. Eigen[15], K. Einsweiler[16], T. Ekelof[169], M. El Kacimi[136c], V. Ellajosyula[87], M. Ellert[169], S. Elles[5], F. Ellinghaus[179], A. A. Elliot[173], N. Ellis[32], J. Elmsheuser[27], M. Elsing[32], D. Emeliyanov[132], Y. Enari[158], O. C. Endner[85], J. S. Ennis[174], J. Erdmann[45], A. Ereditato[18], G. Ernis[179], J. Ernst[2], M. Ernst[27], S. Errede[170], E. Ertel[85], M. Escalier[118], H. Esch[45], C. Escobar[126], B. Esposito[49], A. I. Etienvre[137], E. Etzion[156], H. Evans[63], A. Ezhilov[124], M. Ezzi[136e], F. Fabbri[22a,22b], L. Fabbri[22a,22b], G. Facini[33], R. M. Fakhrutdinov[131], S. Falciano[133a], R. J. Falla[80], J. Faltova[32], Y. Fang[35a], M. Fanti[93a,93b], A. Farbin[8],

A. Farilla[135a], C. Farina[126], E. M. Farina[122a,122b], T. Farooque[13], S. Farrell[16], S. M. Farrington[174], P. Farthouat[32], F. Fassi[136e], P. Fassnacht[32], D. Fassouliotis[9], M. Faucci Giannelli[79], A. Favareto[52a,52b], W. J. Fawcett[121], L. Fayard[118], O. L. Fedin[124,o], W. Fedorko[172], S. Feigl[120], L. Feligioni[87], C. Feng[140], E. J. Feng[32], H. Feng[91], A. B. Fenyuk[131], L. Feremenga[8], P. Fernandez Martinez[171], S. Fernandez Perez[13], J. Ferrando[44], A. Ferrari[169], P. Ferrari[108], R. Ferrari[122a], D. E. Ferreira de Lima[60b], A. Ferrer[171], D. Ferrere[51], C. Ferretti[91], A. Ferretto Parodi[52a,52b], F. Fiedler[85], A. Filipčič[77], M. Filipuzzi[44], F. Filthaut[107], M. Fincke-Keeler[173], K. D. Finelli[153], M. C. N. Fiolhais[127a,127c], L. Fiorini[171], A. Firan[42], A. Fischer[2], C. Fischer[13], J. Fischer[179], W. C. Fisher[92], N. Flaschel[44], I. Fleck[144], P. Fleischmann[91], G. T. Fletcher[142], R. R. M. Fletcher[123], T. Flick[179], L. R. Flores Castillo[62a], M. J. Flowerdew[102], G. T. Forcolin[86], A. Formica[137], A. Forti[86], A. G. Foster[19], D. Fournier[118], H. Fox[74], S. Fracchia[13], P. Francavilla[82], M. Franchini[22a,22b], D. Francis[32], L. Franconi[120], M. Franklin[58], M. Frate[167], M. Fraternali[122a,122b], D. Freeborn[80], S. M. Fressard-Batraneanu[32], F. Friedrich[46], D. Froidevaux[32], J. A. Frost[121], C. Fukunaga[159], E. Fullana Torregrosa[85], T. Fusayasu[103], J. Fuster[171], C. Gabaldon[57], O. Gabizon[155], A. Gabrielli[22a,22b], A. Gabrielli[16], G. P. Gach[40a], S. Gadatsch[32], S. Gadomski[79], G. Gagliardi[52a,52b], L. G. Gagnon[96], P. Gagnon[63], C. Galea[107], B. Galhardo[127a,127c], E. J. Gallas[121], B. J. Gallop[132], P. Gallus[129], G. Galster[38], K. K. Gan[112], S. Ganguly[36], J. Gao[59], Y. Gao[48], Y. S. Gao[146,g], F. M. Garay Walls[48], C. García[171], J. E. García Navarro[171], M. Garcia-Sciveres[16], R. W. Gardner[33], N. Garelli[146], V. Garonne[120], A. Gascon Bravo[44], K. Gasnikova[44], C. Gatti[49], A. Gaudiello[52a,52b], G. Gaudio[122a], L. Gauthier[96], I. L. Gavrilenko[97], C. Gay[172], G. Gaycken[23], E. N. Gazis[10], Z. Gecse[172], C. N. P. Gee[132], Ch. Geich-Gimbel[23], M. Geisen[85], M. P. Geisler[60a], K. Gellerstedt[149a,149b], C. Gemme[52a], M. H. Genest[57], C. Geng[59,p], S. Gentile[133a,133b], C. Gentsos[157], S. George[79], D. Gerbaudo[13], A. Gershon[156], S. Ghasemi[144], M. Ghneimat[23], B. Giacobbe[22a], S. Giagu[133a,133b], P. Giannetti[125a,125b], B. Gibbard[27], S. M. Gibson[79], M. Gignac[172], M. Gilchriese[16], T. P. S. Gillam[30], D. Gillberg[31], G. Gilles[179], D. M. Gingrich[3,d], N. Giokaris[9,*], M. P. Giordani[168a,168c], F. M. Giorgi[22a], F. M. Giorgi[17], P. F. Giraud[137], P. Giromini[58], D. Giugni[93a], F. Giuli[121], C. Giuliani[102], M. Giulini[60b], B. K. Gjelsten[120], S. Gkaitatzis[157], I. Gkialas[157], E. L. Gkougkousis[118], L. K. Gladilin[100], C. Glasman[84], J. Glatzer[50], P. C. F. Glaysher[48], A. Glazov[44], M. Goblirsch-Kolb[25], J. Godlewski[41], S. Goldfarb[90], T. Golling[51], D. Golubkov[131], A. Gomes[127a,127b,127d], R. Gonçalo[127a], J. Goncalves Pinto Firmino Da Costa[137], G. Gonella[50], L. Gonella[19], A. Gongadze[67], S. González de la Hoz[171], S. Gonzalez-Sevilla[51], L. Goossens[32], P. A. Gorbounov[98], H. A. Gordon[27], I. Gorelov[106], B. Gorini[32], E. Gorini[75a,75b], A. Gorišek[77], E. Gornicki[41], A. T. Goshaw[47], C. Gössling[45], M. I. Gostkin[67], C. R. Goudet[118], D. Goujdami[136c], A. G. Goussiou[139], N. Govender[148b,q], E. Gozani[155], L. Graber[56], I. Grabowska-Bold[40a], P. O. J. Gradin[57], P. Grafström[22a,22b], J. Gramling[51], E. Gramstad[120], S. Grancagnolo[17], V. Gratchev[124], P. M. Gravila[28e], H. M. Gray[32], E. Graziani[135a], Z. D. Greenwood[81,r], C. Grefe[23], K. Gregersen[80], I. M. Gregor[44], P. Grenier[146], K. Grevtsov[5], J. Griffiths[8], A. A. Grillo[138], K. Grimm[74], S. Grinstein[13,s], Ph. Gris[36], J.-F. Grivaz[118], S. Groh[85], E. Gross[176], J. Grosse-Knetter[56], G. C. Grossi[81], Z. J. Grout[80], L. Guan[91], W. Guan[177], J. Guenther[64], F. Guescini[51], D. Guest[167], O. Gueta[156], B. Gui[112], E. Guido[52a,52b], T. Guillemin[5], S. Guindon[2], U. Gul[55], C. Gumpert[32], J. Guo[141], Y. Guo[59,p], R. Gupta[42], S. Gupta[121], G. Gustavino[133a,133b], P. Gutierrez[114], N. G. Gutierrez Ortiz[80], C. Gutschow[46], C. Guyot[137], C. Gwenlan[121], C. B. Gwilliam[76], A. Haas[111], C. Haber[16], H. K. Hadavand[8], N. Haddad[136e], A. Hadef[87], S. Hageböck[23], M. Hagihara[165], Z. Hajduk[41], H. Hakobyan[181,*], M. Haleem[44], J. Haley[115], G. Halladjian[92], G. D. Hallewell[87], K. Hamacher[179], P. Hamal[116], K. Hamano[173], A. Hamilton[148a], G. N. Hamity[142], P. G. Hamnett[44], L. Han[59], K. Hanagaki[68,t], K. Hanawa[158], M. Hance[138], B. Haney[123], P. Hanke[60a], R. Hanna[137], J. B. Hansen[38], J. D. Hansen[38], M. C. Hansen[23], P. H. Hansen[38], K. Hara[165], A. S. Hard[177], T. Harenberg[179], F. Hariri[118], S. Harkusha[94], R. D. Harrington[48], P. F. Harrison[174], F. Hartjes[108], N. M. Hartmann[101], M. Hasegawa[69], Y. Hasegawa[143], A. Hasib[114], S. Hassani[137], S. Haug[18], R. Hauser[92], L. Hauswald[46], M. Havranek[128], C. M. Hawkes[19], R. J. Hawkings[32], D. Hayakawa[160], D. Hayden[92], C. P. Hays[121], J. M. Hays[78], H. S. Hayward[76], S. J. Haywood[132], S. J. Head[19], T. Heck[85], V. Hedberg[83], L. Heelan[8], S. Heim[123], T. Heim[16], B. Heinemann[16], J. J. Heinrich[101], L. Heinrich[111], C. Heinz[54], J. Hejbal[128], L. Helary[32], S. Hellman[149a,149b], C. Helsens[32], J. Henderson[121], R. C. W. Henderson[74], Y. Heng[177], S. Henkelmann[172], A. M. Henriques Correia[32], S. Henrot-Versille[118], G. H. Herbert[17], H. Herde[25], V. Herget[178], Y. Hernández Jiménez[148c], G. Herten[50], R. Hertenberger[101], L. Hervas[32], G. G. Hesketh[80], N. P. Hessey[108], J. W. Hetherly[42], R. Hickling[78], E. Higón-Rodriguez[171], E. Hill[173], J. C. Hill[30], K. H. Hiller[44], S. J. Hillier[19], I. Hinchliffe[16], E. Hines[123], R. R. Hinman[16], M. Hirose[50], D. Hirschbuehl[179], J. Hobbs[151], N. Hod[164a], M. C. Hodgkinson[142], P. Hodgson[142], A. Hoecker[32], M. R. Hoeferkamp[106], F. Hoenig[101], D. Hohn[23], T. R. Holmes[16], M. Homann[45], T. Honda[68], T. M. Hong[126], B. H. Hooberman[170], W. H. Hopkins[117], Y. Horii[104], A. J. Horton[145], J-Y. Hostachy[57], S. Hou[154], A. Hoummada[136a], J. Howarth[44], J. Hoya[73], M. Hrabovsky[116], I. Hristova[17], J. Hrivnac[118], T. Hryn'ova[5], A. Hrynevich[95], C. Hsu[148c], P. J. Hsu[154,u], S.-C. Hsu[139], Q. Hu[59], S. Hu[141], Y. Huang[44], Z. Hubacek[129], F. Hubaut[87], F. Huegging[23], T. B. Huffman[121], E. W. Hughes[37], G. Hughes[74], M. Huhtinen[32], P. Huo[151], N. Huseynov[67,b], J. Huston[92], J. Huth[58], G. Iacobucci[51], G. Iakovidis[27], I. Ibragimov[144], L. Iconomidou-Fayard[118], E. Ideal[180],

Z. Idrissi[136e], P. Iengo[32], O. Igonkina[108,v], T. Iizawa[175], Y. Ikegami[68], M. Ikeno[68], Y. Ilchenko[11,w], D. Iliadis[157], N. Ilic[146], T. Ince[102], G. Introzzi[122a,122b], P. Ioannou[9,*], M. Iodice[135a], K. Iordanidou[37], V. Ippolito[58], N. Ishijima[119], M. Ishino[158], M. Ishitsuka[160], R. Ishmukhametov[112], C. Issever[121], S. Istin[20a], F. Ito[165], J. M. Iturbe Ponce[86], R. Iuppa[163a,163b], W. Iwanski[64], H. Iwasaki[68], J. M. Izen[43], V. Izzo[105a], S. Jabbar[3], B. Jackson[123], P. Jackson[1], V. Jain[2], K. B. Jakobi[85], K. Jakobs[50], S. Jakobsen[32], T. Jakoubek[128], D. O. Jamin[115], D. K. Jana[81], R. Jansky[64], J. Janssen[23], M. Janus[56], G. Jarlskog[83], N. Javadov[67,b], T. Javůrek[50], F. Jeanneau[137], L. Jeanty[16], G.-Y. Jeng[153], D. Jennens[90], P. Jenni[50,x], C. Jeske[174], S. Jézéquel[5], H. Ji[177], J. Jia[151], H. Jiang[66], Y. Jiang[59], Z. Jiang[146], S. Jiggins[80], J. Jimenez Pena[171], S. Jin[35a], A. Jinaru[28b], O. Jinnouchi[160], H. Jivan[148c], P. Johansson[142], K. A. Johns[7], W. J. Johnson[139], K. Jon-And[149a,149b], G. Jones[174], R. W. L. Jones[74], S. Jones[7], T. J. Jones[76], J. Jongmanns[60a], P. M. Jorge[127a,127b], J. Jovicevic[164a], X. Ju[177], A. Juste Rozas[13,s], M. K. Köhler[176], A. Kaczmarska[41], M. Kado[118], H. Kagan[112], M. Kagan[146], S. J. Kahn[87], T. Kaji[175], E. Kajomovitz[47], C. W. Kalderon[121], A. Kaluza[85], S. Kama[42], A. Kamenshchikov[131], N. Kanaya[158], S. Kaneti[30], L. Kanjir[77], V. A. Kantserov[99], J. Kanzaki[68], B. Kaplan[111], L. S. Kaplan[177], A. Kapliy[33], D. Kar[148c], K. Karakostas[10], A. Karamaoun[3], N. Karastathis[10], M. J. Kareem[56], E. Karentzos[10], M. Karnevskiy[85], S. N. Karpov[67], Z. M. Karpova[67], K. Karthik[111], V. Kartvelishvili[74], A. N. Karyukhin[131], K. Kasahara[165], L. Kashif[177], R. D. Kass[112], A. Kastanas[150], Y. Kataoka[158], C. Kato[158], A. Katre[51], J. Katzy[44], K. Kawade[104], K. Kawagoe[72], T. Kawamoto[158], G. Kawamura[56], V. F. Kazanin[110,c], R. Keeler[173], R. Kehoe[42], J. S. Keller[44], J. J. Kempster[79], H. Keoshkerian[162], O. Kepka[128], B. P. Kerševan[77], S. Kersten[179], R. A. Keyes[89], M. Khader[170], F. Khalil-zada[12], A. Khanov[115], A. G. Kharlamov[110,c], T. Kharlamova[110], T. J. Khoo[51], V. Khovanskiy[98], E. Khramov[67], J. Khubua[53b,y], S. Kido[69], C. R. Kilby[79], H. Y. Kim[8], S. H. Kim[165], Y. K. Kim[33], N. Kimura[157], O. M. Kind[17], B. T. King[76], M. King[171], J. Kirk[132], A. E. Kiryunin[102], T. Kishimoto[158], D. Kisielewska[40a], F. Kiss[50], K. Kiuchi[165], O. Kivernyk[137], E. Kladiva[147b], M. H. Klein[37], M. Klein[76], U. Klein[76], K. Kleinknecht[85], P. Klimek[109], A. Klimentov[27], R. Klingenberg[45], J. A. Klinger[142], T. Klioutchnikova[32], E.-E. Kluge[60a], P. Kluit[108], S. Kluth[102], J. Knapik[41], E. Kneringer[64], E. B. F. G. Knoops[87], A. Knue[102], A. Kobayashi[158], D. Kobayashi[160], T. Kobayashi[158], M. Kobel[46], M. Kocian[146], P. Kodys[130], T. Koffas[31], E. Koffeman[108], N. M. Köhler[102], T. Koi[146], H. Kolanoski[17], M. Kolb[60b], I. Koletsou[5], A. A. Komar[97,*], Y. Komori[158], T. Kondo[68], N. Kondrashova[44], K. Köneke[50], A. C. König[107], T. Kono[68,z], R. Konoplich[111,aa], N. Konstantinidis[80], R. Kopeliansky[63], S. Koperny[40a], L. Köpke[85], A. K. Kopp[50], K. Korcyl[41], K. Kordas[157], A. Korn[80], A. A. Korol[110,c], I. Korolkov[13], E. V. Korolkova[142], O. Kortner[102], S. Kortner[102], T. Kosek[130], V. V. Kostyukhin[23], A. Kotwal[47], A. Koulouris[10], A. Kourkoumeli-Charalampidi[122a,122b], C. Kourkoumelis[9], V. Kouskoura[27], A. B. Kowalewska[41], R. Kowalewski[173], T. Z. Kowalski[40a], C. Kozakai[158], W. Kozanecki[137], A. S. Kozhin[131], V. A. Kramarenko[100], G. Kramberger[77], D. Krasnopevtsev[99], M. W. Krasny[82], A. Krasznahorkay[32], A. Kravchenko[27], M. Kretz[60c], J. Kretzschmar[76], K. Kreutzfeldt[54], P. Krieger[162], K. Krizka[33], K. Kroeninger[45], H. Kroha[102], J. Kroll[123], J. Kroseberg[23], J. Krstic[14], U. Kruchonak[67], H. Krüger[23], N. Krumnack[66], M. C. Kruse[47], M. Kruskal[24], T. Kubota[90], H. Kucuk[80], S. Kuday[4b], J. T. Kuechler[179], S. Kuehn[50], A. Kugel[60c], F. Kuger[178], A. Kuhl[138], T. Kuhl[44], V. Kukhtin[67], R. Kukla[137], Y. Kulchitsky[94], S. Kuleshov[34b], M. Kuna[133a,133b], T. Kunigo[70], A. Kupco[128], H. Kurashige[69], Y. A. Kurochkin[94], V. Kus[128], E. S. Kuwertz[173], M. Kuze[160], J. Kvita[116], T. Kwan[173], D. Kyriazopoulos[142], A. La Rosa[102], J. L. La Rosa Navarro[26d], L. La Rotonda[39a,39b], C. Lacasta[171], F. Lacava[133a,133b], J. Lacey[31], H. Lacker[17], D. Lacour[82], V. R. Lacuesta[171], E. Ladygin[67], R. Lafaye[5], B. Laforge[82], T. Lagouri[180], S. Lai[56], S. Lammers[63], W. Lampl[7], E. Lançon[137], U. Landgraf[50], M. P. J. Landon[78], M. C. Lanfermann[51], V. S. Lang[60a], J. C. Lange[13], A. J. Lankford[167], F. Lanni[27], K. Lantzsch[23], A. Lanza[122a], S. Laplace[82], C. Lapoire[32], J. F. Laporte[137], T. Lari[93a], F. Lasagni Manghi[22a,22b], M. Lassnig[32], P. Laurelli[49], W. Lavrijsen[16], A. T. Law[138], P. Laycock[76], T. Lazovich[58], M. Lazzaroni[93a,93b], B. Le[90], O. Le Dortz[82], E. Le Guirriec[87], E. P. Le Quilleuc[137], M. LeBlanc[173], T. LeCompte[6], F. Ledroit-Guillon[57], C. A. Lee[27], S. C. Lee[154], L. Lee[1], B. Lefebvre[89], G. Lefebvre[82], M. Lefebvre[173], F. Legger[101], C. Leggett[16], A. Lehan[76], G. Lehmann Miotto[32], X. Lei[7], W. A. Leight[31], A. G. Leister[180], M. A. L. Leite[26d], R. Leitner[130], D. Lellouch[176], B. Lemmer[56], K. J. C. Leney[80], T. Lenz[23], B. Lenzi[32], R. Leone[7], S. Leone[125a,125b], C. Leonidopoulos[48], S. Leontsinis[10], G. Lerner[152], C. Leroy[96], A. A. J. Lesage[137], C. G. Lester[30], M. Levchenko[124], J. Levêque[5], D. Levin[91], L. J. Levinson[176], M. Levy[19], D. Lewis[78], A. M. Leyko[23], M. Leyton[43], B. Li[59,p], C. Li[59], H. Li[151], H. L. Li[33], L. Li[47], L. Li[141], Q. Li[35a], S. Li[47], X. Li[86], Y. Li[144], Z. Liang[35a], B. Liberti[134a], A. Liblong[162], P. Lichard[32], K. Lie[170], J. Liebal[23], W. Liebig[15], A. Limosani[153], S. C. Lin[154,ab], T. H. Lin[85], B. E. Lindquist[151], A. E. Lionti[51], E. Lipeles[123], A. Lipniacka[15], M. Lisovyi[60b], T. M. Liss[170], A. Lister[172], A. M. Litke[138], B. Liu[154,ac], D. Liu[154], H. Liu[91], H. Liu[27], J. Liu[87], J. B. Liu[59], K. Liu[87], L. Liu[170], M. Liu[47], M. Liu[59], Y. L. Liu[59], Y. Liu[59], M. Livan[122a,122b], A. Lleres[57], J. Llorente Merino[35a], S. L. Lloyd[78], F. Lo Sterzo[154], E. M. Lobodzinska[44], P. Loch[7], F. K. Loebinger[86], K. M. Loew[25], A. Loginov[180,*], T. Lohse[17], K. Lohwasser[44], M. Lokajicek[128], B. A. Long[24], J. D. Long[170], R. E. Long[74], L. Longo[75a,75b], K. A. Looper[112], J. A. Lopez Lopez[34b], D. Lopez Mateos[58], B. Lopez Paredes[142], I. Lopez Paz[13], A. Lopez Solis[82], J. Lorenz[101], N. Lorenzo Martinez[63],

M. Losada[21], P. J. Lösel[101], X. Lou[35a], A. Lounis[118], J. Love[6], P. A. Love[74], H. Lu[62a], N. Lu[91], H. J. Lubatti[139], C. Luci[133a,133b], A. Lucotte[57], C. Luedtke[50], F. Luehring[63], W. Lukas[64], L. Luminari[133a], O. Lundberg[149a,149b], B. Lund-Jensen[150], P. M. Luzi[82], D. Lynn[27], R. Lysak[128], E. Lytken[83], V. Lyubushkin[67], H. Ma[27], L. L. Ma[140], Y. Ma[140], G. Maccarrone[49], A. Macchiolo[102], C. M. Macdonald[142], B. Maček[77], J. Machado Miguens[123,127b], D. Madaffari[87], R. Madar[36], H. J. Maddocks[169], W. F. Mader[46], A. Madsen[44], J. Maeda[69], S. Maeland[15], T. Maeno[27], A. Maevskiy[100], E. Magradze[56], J. Mahlstedt[108], C. Maiani[118], C. Maidantchik[26a], A. A. Maier[102], T. Maier[101], A. Maio[127a,127b,127d], S. Majewski[117], Y. Makida[68], N. Makovec[118], B. Malaescu[82], Pa. Malecki[41], V. P. Maleev[124], F. Malek[57], U. Mallik[65], D. Malon[6], C. Malone[146], C. Malone[30], S. Maltezos[10], S. Malyukov[32], J. Mamuzic[171], G. Mancini[49], L. Mandelli[93a], I. Mandić[77], J. Maneira[127a,127b], L. Manhaes de Andrade Filho[26b], J. Manjarres Ramos[164b], A. Mann[101], A. Manousos[32], B. Mansoulie[137], J. D. Mansour[35a], R. Mantifel[89], M. Mantoani[56], S. Manzoni[93a,93b], L. Mapelli[32], G. Marceca[29], L. March[51], G. Marchiori[82], M. Marcisovsky[128], M. Marjanovic[14], D. E. Marley[91], F. Marroquim[26a], S. P. Marsden[86], Z. Marshall[16], S. Marti-Garcia[171], B. Martin[92], T. A. Martin[174], V. J. Martin[48], B. Martin dit Latour[15], M. Martinez[13,s], V. I. Martinez Outschoorn[170], S. Martin-Haugh[132], V. S. Martoiu[28b], A. C. Martyniuk[80], A. Marzin[32], L. Masetti[85], T. Mashimo[158], R. Mashinistov[97], J. Masik[86], A. L. Maslennikov[110,c], I. Massa[22a,22b], L. Massa[22a,22b], P. Mastrandrea[5], A. Mastroberardino[39a,39b], T. Masubuchi[158], P. Mättig[179], J. Mattmann[85], J. Maurer[28b], S. J. Maxfield[76], D. A. Maximov[110,c], R. Mazini[154], I. Maznas[157], S. M. Mazza[93a,93b], N. C. Mc Fadden[106], G. Mc Goldrick[162], S. P. Mc Kee[91], A. McCarn[91], R. L. McCarthy[151], T. G. McCarthy[102], L. I. McClymont[80], E. F. McDonald[90], J. A. Mcfayden[80], G. Mchedlidze[56], S. J. McMahon[132], R. A. McPherson[173,m], M. Medinnis[44], S. Meehan[139], S. Mehlhase[101], A. Mehta[76], K. Meier[60a], C. Meineck[101], B. Meirose[43], D. Melini[171], B. R. Mellado Garcia[148c], M. Melo[147a], F. Meloni[18], X. T. Meng[91], A. Mengarelli[22a,22b], S. Menke[102], E. Meoni[166], S. Mergelmeyer[17], P. Mermod[51], L. Merola[105a,105b], C. Meroniınst93a, F. S. Merritt[33], A. Messina[133a,133b], J. Metcalfe[6], A. S. Mete[167], C. Meyer[85], C. Meyer[123], J-P. Meyer[137], J. Meyer[108], H. Meyer Zu Theenhausen[60a], F. Miano[152], R. P. Middleton[132], S. Miglioranzi[52a,52b], L. Mijović[48], G. Mikenberg[176], M. Mikestikova[128], M. Mikuž[77], M. Milesi[90], A. Milic[64], D. W. Miller[33], C. Mills[48], A. Milov[176], D. A. Milstead[149a,149b], A. A. Minaenko[131], Y. Minami[158], I. A. Minashvili[67], A. I. Mincer[111], B. Mindur[40a], M. Mineev[67], Y. Minegishi[158], Y. Ming[177], L. M. Mir[13], K. P. Mistry[123], T. Mitani[175], J. Mitrevski[101], V. A. Mitsou[171], A. Miucci[18], P. S. Miyagawa[142], J. U. Mjörnmark[83], M. Mlynarikova[130], T. Moa[149a,149b], K. Mochizuki[96], S. Mohapatra[37], S. Molander[149a,149b], R. Moles-Valls[23], R. Monden[70], M. C. Mondragon[92], K. Mönig[44], J. Monk[38], E. Monnier[87], A. Montalbano[151], J. Montejo Berlingen[32], F. Monticelli[73], S. Monzani[93a,93b], R. W. Moore[3], N. Morange[118], D. Moreno[21], M. Moreno Llácer[56], P. Morettini[52a], S. Morgenstern[32], D. Mori[145], T. Mori[158], M. Morii[58], M. Morinaga[158], V. Morisbak[120], S. Moritz[85], A. K. Morley[153], G. Mornacchi[32], J. D. Morris[78], S. S. Mortensen[38], L. Morvaj[151], M. Mosidze[53b], J. Moss[146,ad], K. Motohashi[160], R. Mount[146], E. Mountricha[27], E. J. W. Moyse[88], S. Muanza[87], R. D. Mudd[19], F. Mueller[102], J. Mueller[126], R. S. P. Mueller[101], T. Mueller[30], D. Muenstermann[74], P. Mullen[55], G. A. Mullier[18], F. J. Munoz Sanchez[86], J. A. Murillo Quijada[19], W. J. Murray[174,132], H. Musheghyan[56], M. Muškinja[77], A. G. Myagkov[131,ae], M. Myska[129], B. P. Nachman[146], O. Nackenhorst[51], K. Nagai[121], R. Nagai[68,z], K. Nagano[68], Y. Nagasaka[61], K. Nagata[165], M. Nagel[50], E. Nagy[87], A. M. Nairz[32], Y. Nakahama[104], K. Nakamura[68], T. Nakamura[158], I. Nakano[113], R. F. Naranjo Garcia[44], R. Narayan[11], D. I. Narrias Villar[60a], I. Naryshkin[124], T. Naumann[44], G. Navarro[21], R. Nayyar[7], H. A. Neal[91], P. Yu. Nechaeva[97], T. J. Neep[86], A. Negri[122a,122b], M. Negrini[22a], S. Nektarijevic[107], C. Nellist[118], A. Nelson[167], S. Nemecek[128], P. Nemethy[111], A. A. Nepomuceno[26a], M. Nessi[32,af], M. S. Neubauer[170], M. Neumann[179], R. M. Neves[111], P. Nevski[27], P. R. Newman[19], D. H. Nguyen[6], T. Nguyen Manh[96], R. B. Nickerson[121], R. Nicolaidou[137], J. Nielsen[138], A. Nikiforov[17], V. Nikolaenko[131,ae], I. Nikolic-Audit[82], K. Nikolopoulos[19], J. K. Nilsen[120], P. Nilsson[27], Y. Ninomiya[158], A. Nisati[133a], R. Nisius[102], T. Nobe[158], M. Nomachi[119], I. Nomidis[31], T. Nooney[78], S. Norberg[114], M. Nordberg[32], N. Norjoharuddeen[121], O. Novgorodova[46], S. Nowak[102], M. Nozaki[68], L. Nozka[116], K. Ntekas[167], E. Nurse[80], F. Nuti[90], F. O'grady[7], D. C. O'Neil[145], A. A. O'Rourke[44], V. O'Shea[55], F. G. Oakham[31,d], H. Oberlack[102], T. Obermann[23], J. Ocariz[82], A. Ochi[69], I. Ochoa[37], J. P. Ochoa-Ricoux[34a], S. Oda[72], S. Odaka[68], H. Ogren[63], A. Oh[86], S. H. Oh[47], C. C. Ohm[16], H. Ohman[169], H. Oide[52a,52b], H. Okawa[165], Y. Okumura[158], T. Okuyama[68], A. Olariu[28b], L. F. Oleiro Seabra[127a], S. A. Olivares Pino[48], D. Oliveira Damazio[27], A. Olszewski[41], J. Olszowska[41], A. Onofre[127a,127e], K. Onogi[104], P. U. E. Onyisi[11,w], M. J. Oreglia[33], Y. Oren[156], D. Orestano[135a,135b], N. Orlando[62b], R. S. Orr[162], B. Osculati[52a,52b,*], R. Ospanov[86], G. Otero y Garzon[29], H. Otono[72], M. Ouchrif[136d], F. Ould-Saada[120], A. Ouraou[137], K. P. Oussoren[108], Q. Ouyang[35a], M. Owen[55], R. E. Owen[19], V. E. Ozcan[20a], N. Ozturk[8], K. Pachal[145], A. Pacheco Pages[13], L. Pacheco Rodriguez[137], C. Padilla Aranda[13], M. Pagáčová[50], S. Pagan Griso[16], M. Paganini[180], F. Paige[27], P. Pais[88], K. Pajchel[120], G. Palacino[164b], S. Palazzo[39a,39b], S. Palestini[32], M. Palka[40b], D. Pallin[36], E. St. Panagiotopoulou[10], C. E. Pandini[82], J. G. Panduro Vazquez[79], P. Pani[149a,149b], S. Panitkin[27], D. Pantea[28b], L. Paolozzi[51], Th. D. Papadopoulou[10], K. Papageorgiou[157], A. Paramonov[6],

D. Paredes Hernandez[180], A. J. Parker[74], M. A. Parker[30], K. A. Parker[142], F. Parodi[52a,52b], J. A. Parsons[37], U. Parzefall[50], V. R. Pascuzzi[162], E. Pasqualucci[133a], S. Passaggio[52a], Fr. Pastore[79], G. Pásztor[31,ag], S. Pataraia[179], J. R. Pater[86], T. Pauly[32], J. Pearce[173], B. Pearson[114], L. E. Pedersen[38], M. Pedersen[120], S. Pedraza Lopez[171], R. Pedro[127a,127b], S. V. Peleganchuk[110,c], O. Penc[128], C. Peng[35a], H. Peng[59], J. Penwell[63], B. S. Peralva[26b], M. M. Perego[137], D. V. Perepelitsa[27], E. Perez Codina[164a], L. Perini[93a,93b], H. Pernegger[32], S. Perrella[105a,105b], R. Peschke[44], V. D. Peshekhonov[67], K. Peters[44], R. F. Y. Peters[86], B. A. Petersen[32], T. C. Petersen[38], E. Petit[57], A. Petridis[1], C. Petridou[157], P. Petroff[118], E. Petrolo[133a], M. Petrov[121], F. Petrucci[135a,135b], N. E. Pettersson[88], A. Peyaud[137], R. Pezoa[34b], P. W. Phillips[132], G. Piacquadio[146,ah], E. Pianori[174], A. Picazio[88], E. Piccaro[78], M. Piccinini[22a,22b], M. A. Pickering[121], R. Piegaia[29], J. E. Pilcher[33], A. D. Pilkington[86], A. W. J. Pin[86], M. Pinamonti[168a,168c,ai], J. L. Pinfold[3], A. Pingel[38], S. Pires[82], H. Pirumov[44], M. Pitt[176], L. Plazak[147a], M.-A. Pleier[27], V. Pleskot[85], E. Plotnikova[67], P. Plucinski[92], D. Pluth[66], R. Poettgen[149a,149b], L. Poggioli[118], D. Pohl[23], G. Polesello[122a], A. Poley[44], A. Policicchio[39a,39b], R. Polifka[162], A. Polini[22a], C. S. Pollard[55], V. Polychronakos[27], K. Pommès[32], L. Pontecorvo[133a], B. G. Pope[92], G. A. Popeneciu[28c], A. Poppleton[32], S. Pospisil[129], K. Potamianos[16], I. N. Potrap[67], C. J. Potter[30], C. T. Potter[117], G. Poulard[32], J. Poveda[32], V. Pozdnyakov[67], M. E. Pozo Astigarraga[32], P. Pralavorio[87], A. Pranko[16], S. Prell[66], D. Price[86], L. E. Price[6], M. Primavera[75a], S. Prince[89], K. Prokofiev[62c], F. Prokoshin[34b], S. Protopopescu[27], J. Proudfoot[6], M. Przybycien[40a], D. Puddu[135a,135b], M. Purohit[27,aj], P. Puzo[118], J. Qian[91], G. Qin[55], Y. Qin[86], A. Quadt[56], W. B. Quayle[168a,168b], M. Queitsch-Maitland[44], D. Quilty[55], S. Raddum[120], V. Radeka[27], V. Radescu[121], S. K. Radhakrishnan[151], P. Radloff[117], P. Rados[90], F. Ragusa[93a,93b], G. Rahal[182], J. A. Raine[86], S. Rajagopalan[27], M. Rammensee[32], C. Rangel-Smith[169], M. G. Ratti[93a,93b], D. M. Rauch[44], F. Rauscher[101], S. Rave[85], T. Ravenscroft[55], I. Ravinovich[176], M. Raymond[32], A. L. Read[120], N. P. Readioff[76], M. Reale[75a,75b], D. M. Rebuzzi[122a,122b], A. Redelbach[178], G. Redlinger[27], R. Reece[138], R. G. Reed[148c], K. Reeves[43], L. Rehnisch[17], J. Reichert[123], A. Reiss[85], C. Rembser[32], H. Ren[35a], M. Rescigno[133a], S. Resconi[93a], O. L. Rezanova[110,c], P. Reznicek[130], R. Rezvani[96], R. Richter[102], S. Richter[80], E. Richter-Was[40b], O. Ricken[23], M. Ridel[82], P. Rieck[17], C. J. Riegel[179], J. Rieger[56], O. Rifki[114], M. Rijssenbeek[151], A. Rimoldi[122a,122b], M. Rimoldi[18], L. Rinaldi[22a], B. Ristić[51], E. Ritsch[32], I. Riu[13], F. Rizatdinova[115], E. Rizvi[78], C. Rizzi[13], S. H. Robertson[89,m], A. Robichaud-Veronneau[89], D. Robinson[30], J. E. M. Robinson[44], A. Robson[55], C. Roda[125a,125b], Y. Rodina[87,ak], A. Rodriguez Perez[13], D. Rodriguez Rodriguez[171], S. Roe[32], C. S. Rogan[58], O. Røhne[120], J. Roloff[58], A. Romaniouk[99], M. Romano[22a,22b], S. M. Romano Saez[36], E. Romero Adam[171], N. Rompotis[139], M. Ronzani[50], L. Roos[82], E. Ros[171], S. Rosati[133a], K. Rosbach[50], P. Rose[138], N.-A. Rosien[56], V. Rossetti[149a,149b], E. Rossi[105a,105b], L. P. Rossi[52a], J. H. N. Rosten[30], R. Rosten[139], M. Rotaru[28b], I. Roth[176], J. Rothberg[139], D. Rousseau[118], A. Rozanov[87], Y. Rozen[155], X. Ruan[148c], F. Rubbo[146], M. S. Rudolph[162], F. Rühr[50], A. Ruiz-Martinez[31], Z. Rurikova[50], N. A. Rusakovich[67], A. Ruschke[101], H. L. Russell[139], J. P. Rutherfoord[7], N. Ruthmann[32], Y. F. Ryabov[124], M. Rybar[170], G. Rybkin[118], S. Ryu[6], A. Ryzhov[131], G. F. Rzehorz[56], A. F. Saavedra[153], G. Sabato[108], S. Sacerdoti[29], H. F-W. Sadrozinski[138], R. Sadykov[67], F. Safai Tehrani[133a], P. Saha[109], M. Sahinsoy[60a], M. Saimpert[137], T. Saito[158], H. Sakamoto[158], Y. Sakurai[175], G. Salamanna[135a,135b], A. Salamon[134a,134b], J. E. Salazar Loyola[34b], D. Salek[108], P. H. Sales De Bruin[139], D. Salihagic[102], A. Salnikov[146], J. Salt[171], D. Salvatore[39a,39b], F. Salvatore[152], A. Salvucci[62a,62b,62c], A. Salzburger[32], D. Sammel[50], D. Sampsonidis[157], J. Sánchez[171], V. Sanchez Martinez[171], A. Sanchez Pineda[105a,105b], H. Sandaker[120], R. L. Sandbach[78], M. Sandhoff[179], C. Sandoval[21], D. P. C. Sankey[132], M. Sannino[52a,52b], A. Sansoni[49], C. Santoni[36], R. Santonico[134a,134b], H. Santos[127a], I. Santoyo Castillo[152], K. Sapp[126], A. Sapronov[67], J. G. Saraiva[127a,127d], B. Sarrazin[23], O. Sasaki[68], K. Sato[165], E. Sauvan[5], G. Savage[79], P. Savard[162,d], N. Savic[102], C. Sawyer[132], L. Sawyer[81,r], J. Saxon[33], C. Sbarra[22a], A. Sbrizzi[22a,22b], T. Scanlon[80], D. A. Scannicchio[167], M. Scarcella[153], V. Scarfone[39a,39b], J. Schaarschmidt[176], P. Schacht[102], B. M. Schachtner[101], D. Schaefer[32], L. Schaefer[123], R. Schaefer[44], J. Schaeffer[85], S. Schaepe[23], S. Schaetzel[60b], U. Schäfer[85], A. C. Schaffer[118], D. Schaile[101], R. D. Schamberger[151], V. Scharf[60a], V. A. Schegelsky[124], D. Scheirich[130], M. Schernau[167], C. Schiavi[52a,52b], S. Schier[138], C. Schillo[50], M. Schioppa[39a,39b], S. Schlenker[32], K. R. Schmidt-Sommerfeld[102], K. Schmieden[32], C. Schmitt[85], S. Schmitt[44], S. Schmitz[85], B. Schneider[164a], U. Schnoor[50], L. Schoeffel[137], A. Schoening[60b], B. D. Schoenrock[92], E. Schopf[23], M. Schott[85], J. F. P. Schouwenberg[107], J. Schovancova[8], S. Schramm[51], M. Schreyer[178], N. Schuh[85], A. Schulte[85], M. J. Schultens[23], H.-C. Schultz-Coulon[60a], H. Schulz[17], M. Schumacher[50], B. A. Schumm[138], Ph. Schune[137], A. Schwartzman[146], T. A. Schwarz[91], H. Schweiger[86], Ph. Schwemling[137], R. Schwienhorst[92], J. Schwindling[137], T. Schwindt[23], G. Sciolla[25], F. Scuri[125a,125b], F. Scutti[90], J. Searcy[91], P. Seema[23], S. C. Seidel[106], A. Seiden[138], F. Seifert[129], J. M. Seixas[26a], G. Sekhniaidze[105a], K. Sekhon[91], S. J. Sekula[42], D. M. Seliverstov[124,*], N. Semprini-Cesari[22a,22b], C. Serfon[120], L. Serin[118], L. Serkin[168a,168b], M. Sessa[135a,135b], R. Seuster[173], H. Severini[114], T. Sfiligoj[77], F. Sforza[32], A. Sfyrla[51], E. Shabalina[56], N. W. Shaikh[149a,149b], L. Y. Shan[35a], R. Shang[170], J. T. Shank[24], M. Shapiro[16], P. B. Shatalov[98], K. Shaw[168a,168b], S. M. Shaw[86], A. Shcherbakova[149a,149b], C. Y. Shehu[152], P. Sherwood[80], L. Shi[154,al], S. Shimizu[69], C. O. Shimmin[167], M. Shimojima[103],

S. Shirabe[72], M. Shiyakova[67,am], A. Shmeleva[97], D. Shoaleh Saadi[96], M. J. Shochet[33], S. Shojaii[93a], D. R. Shope[114], S. Shrestha[112], E. Shulga[99], M. A. Shupe[7], P. Sicho[128], A. M. Sickles[170], P. E. Sidebo[150], E. Sideras Haddad[148c], O. Sidiropoulou[178], D. Sidorov[115], A. Sidoti[22a,22b], F. Siegert[46], Dj. Sijacki[14], J. Silva[127a,127d], S. B. Silverstein[149a], V. Simak[129], Lj. Simic[14], S. Simion[118], E. Simioni[85], B. Simmons[80], D. Simon[36], M. Simon[85], P. Sinervo[162], N. B. Sinev[117], M. Sioli[22a,22b], G. Siragusa[178], S. Yu. Sivoklokov[100], J. Sjölin[149a,149b], M. B. Skinner[74], H. P. Skottowe[58], P. Skubic[114], M. Slater[19], T. Slavicek[129], M. Slawinska[108], K. Sliwa[166], R. Slovak[130], V. Smakhtin[176], B. H. Smart[5], L. Smestad[15], J. Smiesko[147a], S. Yu. Smirnov[99], Y. Smirnov[99], L. N. Smirnova[100,an], O. Smirnova[83], M. N. K. Smith[37], R. W. Smith[37], M. Smizanska[74], K. Smolek[129], A. A. Snesarev[97], I. M. Snyder[117], S. Snyder[27], R. Sobie[173,m], F. Socher[46], A. Soffer[156], D. A. Soh[154], G. Sokhrannyi[77], C. A. Solans Sanchez[32], M. Solar[129], E. Yu. Soldatov[99], U. Soldevila[171], A. A. Solodkov[131], A. Soloshenko[67], O. V. Solovyanov[131], V. Solovyev[124], P. Sommer[50], H. Son[166], H. Y. Song[59,ao], A. Sood[16], A. Sopczak[129], V. Sopko[129], V. Sorin[13], D. Sosa[60b], C. L. Sotiropoulou[125a,125b], R. Soualah[168a,168c], A. M. Soukharev[110,c], D. South[44], B. C. Sowden[79], S. Spagnolo[75a,75b], M. Spalla[125a,125b], M. Spangenberg[174], F. Spanò[79], D. Sperlich[17], F. Spettel[102], R. Spighi[22a], G. Spigo[32], L. A. Spiller[90], M. Spousta[130], R. D. St. Denis[55,*], A. Stabile[93a], R. Stamen[60a], S. Stamm[17], E. Stanecka[41], R. W. Stanek[6], C. Stanescu[135a], M. Stanescu-Bellu[44], M. M. Stanitzki[44], S. Stapnes[120], E. A. Starchenko[131], G. H. Stark[33], J. Stark[57], P. Staroba[128], P. Starovoitov[60a], S. Stärz[32], R. Staszewski[41], P. Steinberg[27], B. Stelzer[145], H. J. Stelzer[32], O. Stelzer-Chilton[164a], H. Stenzel[54], G. A. Stewart[55], J. A. Stillings[23], M. C. Stockton[89], M. Stoebe[89], G. Stoicea[28b], P. Stolte[56], S. Stonjek[102], A. R. Stradling[8], A. Straessner[46], M. E. Stramaglia[18], J. Strandberg[150], S. Strandberg[149a,149b], A. Strandlie[120], M. Strauss[114], P. Strizenec[147b], R. Ströhmer[178], D. M. Strom[117], R. Stroynowski[42], A. Strubig[107], S. A. Stucci[27], B. Stugu[15], N. A. Styles[44], D. Su[146], J. Su[126], S. Suchek[60a], Y. Sugaya[119], M. Suk[129], V. V. Sulin[97], S. Sultansoy[4c], T. Sumida[70], S. Sun[58], X. Sun[35a], J. E. Sundermann[50], K. Suruliz[152], G. Susinno[39a,39b], M. R. Sutton[152], S. Suzuki[68], M. Svatos[128], M. Swiatlowski[33], I. Sykora[147a], T. Sykora[130], D. Ta[50], C. Taccini[135a,135b], K. Tackmann[44], J. Taenzer[162], A. Taffard[167], R. Tafirout[164a], N. Taiblum[156], H. Takai[27], R. Takashima[71], T. Takeshita[143], Y. Takubo[68], M. Talby[87], A. A. Talyshev[110,c], K. G. Tan[90], J. Tanaka[158], M. Tanaka[160], R. Tanaka[118], S. Tanaka[68], R. Tanioka[69], B. B. Tannenwald[112], S. Tapia Araya[34b], S. Tapprogge[85], S. Tarem[155], G. F. Tartarelli[93a], P. Tas[130], M. Tasevsky[128], T. Tashiro[70], E. Tassi[39a,39b], A. Tavares Delgado[127a,127b], Y. Tayalati[136e], A. C. Taylor[106], G. N. Taylor[90], P. T. E. Taylor[90], W. Taylor[164b], F. A. Teischinger[32], P. Teixeira-Dias[79], K. K. Temming[50], D. Temple[145], H. Ten Kate[32], P. K. Teng[154], J. J. Teoh[119], F. Tepel[179], S. Terada[68], K. Terashi[158], J. Terron[84], S. Terzo[13], M. Testa[49], R. J. Teuscher[162,m], T. Theveneaux-Pelzer[87], J. P. Thomas[19], J. Thomas-Wilsker[79], P. D. Thompson[19], A. S. Thompson[55], L. A. Thomsen[180], E. Thomson[123], M. J. Tibbetts[16], R. E. Ticse Torres[87], V. O. Tikhomirov[97,ap], Yu. A. Tikhonov[110,c], S. Timoshenko[99], P. Tipton[180], S. Tisserant[87], K. Todome[160], T. Todorov[5,*], S. Todorova-Nova[130], J. Tojo[72], S. Tokár[147a], K. Tokushuku[68], E. Tolley[58], L. Tomlinson[86], M. Tomoto[104], L. Tompkins[146,aq], K. Toms[106], B. Tong[58], P. Tornambe[50], E. Torrence[117], H. Torres[145], E. Torró Pastor[139], J. Toth[87,ar], F. Touchard[87], D. R. Tovey[142], T. Trefzger[178], A. Tricoli[27], I. M. Trigger[164a], S. Trincaz-Duvoid[82], M. F. Tripiana[13], W. Trischuk[162], B. Trocmé[57], A. Trofymov[44], C. Troncon[93a], M. Trottier-McDonald[16], M. Trovatelli[173], L. Truong[168a,168c], M. Trzebinski[41], A. Trzupek[41], J. C-L. Tseng[121], P. V. Tsiareshka[94], G. Tsipolitis[10], N. Tsirintanis[9], S. Tsiskaridze[13], V. Tsiskaridze[50], E. G. Tskhadadze[53a], K. M. Tsui[62a], I. I. Tsukerman[98], V. Tsulaia[16], S. Tsuno[68], D. Tsybychev[151], Y. Tu[62b], A. Tudorache[28b], V. Tudorache[28b], A. N. Tuna[58], S. A. Tupputi[22a,22b], S. Turchikhin[67], D. Turecek[129], D. Turgeman[176], R. Turra[93a,93b], P. M. Tuts[37], M. Tyndel[132], G. Ucchielli[22a,22b], I. Ueda[158], M. Ughetto[149a,149b], F. Ukegawa[165], G. Unal[32], A. Undrus[27], G. Unel[167], F. C. Ungaro[90], Y. Unno[68], C. Unverdorben[101], J. Urban[147b], P. Urquijo[90], P. Urrejola[85], G. Usai[8], J. Usui[68], L. Vacavant[87], V. Vacek[129], B. Vachon[89], C. Valderanis[101], E. Valdes Santurio[149a,149b], N. Valencic[108], S. Valentinetti[22a,22b], A. Valero[171], L. Valery[13], S. Valkar[130], J. A. Valls Ferrer[171], W. Van Den Wollenberg[108], P. C. Van Der Deijl[108], H. van der Graaf[108], N. van Eldik[155], P. van Gemmeren[6], J. Van Nieuwkoop[145], I. van Vulpen[108], M. C. van Woerden[108], M. Vanadia[133a,133b], W. Vandelli[32], R. Vanguri[123], A. Vaniachine[161], P. Vankov[108], G. Vardanyan[181], R. Vari[133a], E. W. Varnes[7], T. Varol[42], D. Varouchas[82], A. Vartapetian[8], K. E. Varvell[153], J. G. Vasquez[180], G. A. Vasquez[34b], F. Vazeille[36], T. Vazquez Schroeder[89], J. Veatch[56], V. Veeraraghavan[7], L. M. Veloce[162], F. Veloso[127a,127c], S. Veneziano[133a], A. Ventura[75a,75b], M. Venturi[173], N. Venturi[162], A. Venturini[25], V. Vercesi[122a], M. Verducci[133a,133b], W. Verkerke[108], J. C. Vermeulen[108], A. Vest[46,as], M. C. Vetterli[145,d], O. Viazlo[83], I. Vichou[170,*], T. Vickey[142], O. E. Vickey Boeriu[142], G. H. A. Viehhauser[121], S. Viel[16], L. Vigani[121], M. Villa[22a,22b], M. Villaplana Perez[93a,93b], E. Vilucchi[49], M. G. Vincter[31], V. B. Vinogradov[67], C. Vittori[22a,22b], I. Vivarelli[152], S. Vlachos[10], M. Vlasak[129], M. Vogel[179], P. Vokac[129], G. Volpi[125a,125b], M. Volpi[90], H. von der Schmitt[102], E. von Toerne[23], V. Vorobel[130], K. Vorobev[99], M. Vos[171], R. Voss[32], J. H. Vossebeld[76], N. Vranjes[14], M. Vranjes Milosavljevic[14], V. Vrba[128], M. Vreeswijk[108], R. Vuillermet[32], I. Vukotic[33], Z. Vykydal[129], P. Wagner[23], W. Wagner[179], H. Wahlberg[73], S. Wahrmund[46], J. Wakabayashi[104], J. Walder[74], R. Walker[101], W. Walkowiak[144], V. Wallangen[149a,149b], C. Wang[35b], C. Wang[140,87], F. Wang[177], H. Wang[16], H. Wang[42], J. Wang[44], J. Wang[153], K. Wang[89],

R. Wang[6], S. M. Wang[154], T. Wang[23], T. Wang[37], W. Wang[59], C. Wanotayaroj[117], A. Warburton[89], C. P. Ward[30], D. R. Wardrope[80], A. Washbrook[48], P. M. Watkins[19], A. T. Watson[19], M. F. Watson[19], G. Watts[139], S. Watts[86], B. M. Waugh[80], S. Webb[85], M. S. Weber[18], S. W. Weber[178], S. A. Weber[31], J. S. Webster[6], A. R. Weidberg[121], B. Weinert[63], J. Weingarten[56], C. Weiser[50], H. Weits[108], P. S. Wells[32], T. Wenaus[27], T. Wengler[32], S. Wenig[32], N. Wermes[23], M. Werner[50], M. D. Werner[66], P. Werner[32], M. Wessels[60a], J. Wetter[166], K. Whalen[117], N. L. Whallon[139], A. M. Wharton[74], A. White[8], M. J. White[1], R. White[34b], D. Whiteson[167], F. J. Wickens[132], W. Wiedenmann[177], M. Wielers[132], C. Wiglesworth[38], L. A. M. Wiik-Fuchs[23], A. Wildauer[102], F. Wilk[86], H. G. Wilkens[32], H. H. Williams[123], S. Williams[108], C. Willis[92], S. Willocq[88], J. A. Wilson[19], I. Wingerter-Seez[5], F. Winklmeier[117], O. J. Winston[152], B. T. Winter[23], M. Wittgen[146], J. Wittkowski[101], T. M. H. Wolf[108], M. W. Wolter[41], H. Wolters[127a,127c], S. D. Worm[132], B. K. Wosiek[41], J. Wotschack[32], M. J. Woudstra[86], K. W. Wozniak[41], M. Wu[57], M. Wu[33], S. L. Wu[177], X. Wu[51], Y. Wu[91], T. R. Wyatt[86], B. M. Wynne[48], S. Xella[38], D. Xu[35a], L. Xu[27], B. Yabsley[153], S. Yacoob[148a], D. Yamaguchi[160], Y. Yamaguchi[119], A. Yamamoto[68], S. Yamamoto[158], T. Yamanaka[158], K. Yamauchi[104], Y. Yamazaki[69], Z. Yan[24], H. Yang[141], H. Yang[177], Y. Yang[154], Z. Yang[15], W-M. Yao[16], Y. C. Yap[82], Y. Yasu[68], E. Yatsenko[5], K. H. Yau Wong[23], J. Ye[42], S. Ye[27], I. Yeletskikh[67], E. Yildirim[85], K. Yorita[175], R. Yoshida[6], K. Yoshihara[123], C. Young[146], C. J. S. Young[32], S. Youssef[24], D. R. Yu[16], J. Yu[8], J. M. Yu[91], J. Yu[66], L. Yuan[69], S. P. Y. Yuen[23], I. Yusuff[30,at], B. Zabinski[41], R. Zaidan[65], A. M. Zaitsev[131,ae], N. Zakharchuk[44], J. Zalieckas[15], A. Zaman[151], S. Zambito[58], L. Zanello[133a,133b], D. Zanzi[90], C. Zeitnitz[179], M. Zeman[129], A. Zemla[40a], J. C. Zeng[170], Q. Zeng[146], O. Zenin[131], T. Ženiš[147a], D. Zerwas[118], D. Zhang[91], F. Zhang[177], G. Zhang[59,ao], H. Zhang[35b], J. Zhang[6], L. Zhang[50], M. Zhang[170], R. Zhang[23], R. Zhang[59,au], X. Zhang[140], Z. Zhang[118], X. Zhao[42], Y. Zhao[140], Z. Zhao[59], A. Zhemchugov[67], J. Zhong[121], B. Zhou[91], C. Zhou[177], L. Zhou[37], L. Zhou[42], M. Zhou[151], N. Zhou[35c], C. G. Zhu[140], H. Zhu[35a], J. Zhu[91], Y. Zhu[59], X. Zhuang[35a], K. Zhukov[97], A. Zibell[178], D. Zieminska[63], N. I. Zimine[67], C. Zimmermann[85], S. Zimmermann[50], Z. Zinonos[56], M. Zinser[85], M. Ziolkowski[144], L. Živković[14], G. Zobernig[177], A. Zoccoli[22a,22b], M. zur Nedden[17], L. Zwalinski[32]

[1] Department of Physics, University of Adelaide, Adelaide, Australia
[2] Physics Department, SUNY Albany, Albany, NY, USA
[3] Department of Physics, University of Alberta, Edmonton, AB, Canada
[4] [(a)]Department of Physics, Ankara University, Ankara, Turkey; [(b)]Istanbul Aydin University, Istanbul, Turkey; [(c)]Division of Physics, TOBB University of Economics and Technology, Ankara, Turkey
[5] LAPP, CNRS/IN2P3 and Université Savoie Mont Blanc, Annecy-le-Vieux, France
[6] High Energy Physics Division, Argonne National Laboratory, Argonne, IL, USA
[7] Department of Physics, University of Arizona, Tucson, AZ, USA
[8] Department of Physics, The University of Texas at Arlington, Arlington, TX, USA
[9] Physics Department, National and Kapodistrian University of Athens, Athens, Greece
[10] Physics Department, National Technical University of Athens, Zografou, Greece
[11] Department of Physics, The University of Texas at Austin, Austin, TX, USA
[12] Institute of Physics, Azerbaijan Academy of Sciences, Baku, Azerbaijan
[13] Institut de Física d'Altes Energies (IFAE), The Barcelona Institute of Science and Technology, Barcelona, Spain
[14] Institute of Physics, University of Belgrade, Belgrade, Serbia
[15] Department for Physics and Technology, University of Bergen, Bergen, Norway
[16] Physics Division, Lawrence Berkeley National Laboratory and University of California, Berkeley, CA, USA
[17] Department of Physics, Humboldt University, Berlin, Germany
[18] Albert Einstein Center for Fundamental Physics and Laboratory for High Energy Physics, University of Bern, Bern, Switzerland
[19] School of Physics and Astronomy, University of Birmingham, Birmingham, UK
[20] [(a)]Department of Physics, Bogazici University, Istanbul, Turkey; [(b)]Department of Physics Engineering, Gaziantep University, Gaziantep, Turkey; [(c)]Faculty of Engineering and Natural Sciences, Istanbul Bilgi University, Istanbul, Turkey; [(d)]Faculty of Engineering and Natural Sciences, Bahcesehir University, Istanbul, Turkey
[21] Centro de Investigaciones, Universidad Antonio Narino, Bogotá, Colombia
[22] [(a)]INFN Sezione di Bologna, Bologna, Italy; [(b)]Dipartimento di Fisica e Astronomia, Università di Bologna, Bologna, Italy
[23] Physikalisches Institut, University of Bonn, Bonn, Germany
[24] Department of Physics, Boston University, Boston, MA, USA
[25] Department of Physics, Brandeis University, Waltham, MA, USA

[26] [(a)]Universidade Federal do Rio De Janeiro COPPE/EE/IF, Rio de Janeiro, Brazil; [(b)]Electrical Circuits Department, Federal University of Juiz de Fora (UFJF), Juiz de Fora, Brazil; [(c)]Federal University of Sao Joao del Rei (UFSJ), Sao Joao del Rei, Brazil; [(d)]Instituto de Fisica, Universidade de Sao Paulo, Sao Paulo, Brazil
[27] Physics Department, Brookhaven National Laboratory, Upton, NY, USA
[28] [(a)]Transilvania University of Brasov, Brasov, Romania; [(b)]National Institute of Physics and Nuclear Engineering, Bucharest, Romania; [(c)]Physics Department, National Institute for Research and Development of Isotopic and Molecular Technologies, Cluj-Napoca, Romania; [(d)]University Politehnica Bucharest, Bucharest, Romania; [(e)]West University in Timisoara, Timisoara, Romania
[29] Departamento de Física, Universidad de Buenos Aires, Buenos Aires, Argentina
[30] Cavendish Laboratory, University of Cambridge, Cambridge, UK
[31] Department of Physics, Carleton University, Ottawa, ON, Canada
[32] CERN, Geneva, Switzerland
[33] Enrico Fermi Institute, University of Chicago, Chicago, IL, USA
[34] [(a)]Departamento de Física, Pontificia Universidad Católica de Chile, Santiago, Chile; [(b)]Departamento de Física, Universidad Técnica Federico Santa María, Valparaiso, Chile
[35] [(a)]Institute of High Energy Physics, Chinese Academy of Sciences, Beijing, China; [(b)]Department of Physics, Nanjing University, Jiangsu, China; [(c)]Physics Department, Tsinghua University, Beijing 100084, China
[36] Laboratoire de Physique Corpusculaire, Université Clermont Auvergne, Université Blaise Pascal, CNRS/IN2P3, Clermont-Ferrand, France
[37] Nevis Laboratory, Columbia University, Irvington, NY, USA
[38] Niels Bohr Institute, University of Copenhagen, Kobenhavn, Denmark
[39] [(a)]INFN Gruppo Collegato di Cosenza, Laboratori Nazionali di Frascati, Frascati, Italy; [(b)]Dipartimento di Fisica, Università della Calabria, Rende, Italy
[40] [(a)]Faculty of Physics and Applied Computer Science, AGH University of Science and Technology, Kraków, Poland; [(b)]Marian Smoluchowski Institute of Physics, Jagiellonian University, Kraków, Poland
[41] Institute of Nuclear Physics Polish Academy of Sciences, Kraków, Poland
[42] Physics Department, Southern Methodist University, Dallas, TX, USA
[43] Physics Department, University of Texas at Dallas, Richardson, TX, USA
[44] DESY, Hamburg and Zeuthen, Germany
[45] Lehrstuhl für Experimentelle Physik IV, Technische Universität Dortmund, Dortmund, Germany
[46] Institut für Kern- und Teilchenphysik, Technische Universität Dresden, Dresden, Germany
[47] Department of Physics, Duke University, Durham, NC, USA
[48] SUPA-School of Physics and Astronomy, University of Edinburgh, Edinburgh, UK
[49] INFN Laboratori Nazionali di Frascati, Frascati, Italy
[50] Fakultät für Mathematik und Physik, Albert-Ludwigs-Universität, Freiburg, Germany
[51] Departement de Physique Nucleaire et Corpusculaire, Université de Genève, Geneva, Switzerland
[52] [(a)]INFN Sezione di Genova, Genoa, Italy; [(b)]Dipartimento di Fisica, Università di Genova, Genoa, Italy
[53] [(a)]E. Andronikashvili Institute of Physics, Iv. Javakhishvili Tbilisi State University, Tbilisi, Georgia; [(b)]High Energy Physics Institute, Tbilisi State University, Tbilisi, Georgia
[54] II Physikalisches Institut, Justus-Liebig-Universität Giessen, Giessen, Germany
[55] SUPA-School of Physics and Astronomy, University of Glasgow, Glasgow, UK
[56] II Physikalisches Institut, Georg-August-Universität, Göttingen, Germany
[57] Laboratoire de Physique Subatomique et de Cosmologie, Université Grenoble-Alpes, CNRS/IN2P3, Grenoble, France
[58] Laboratory for Particle Physics and Cosmology, Harvard University, Cambridge, MA, USA
[59] Department of Modern Physics, University of Science and Technology of China, Anhui, China
[60] [(a)]Kirchhoff-Institut für Physik, Ruprecht-Karls-Universität Heidelberg, Heidelberg, Germany; [(b)]Physikalisches Institut, Ruprecht-Karls-Universität Heidelberg, Heidelberg, Germany; [(c)]ZITI Institut für technische Informatik, Ruprecht-Karls-Universität Heidelberg, Mannheim, Germany
[61] Faculty of Applied Information Science, Hiroshima Institute of Technology, Hiroshima, Japan
[62] [(a)]Department of Physics, The Chinese University of Hong Kong, Shatin, N.T., Hong Kong; [(b)]Department of Physics, The University of Hong Kong, Hong Kong, China; [(c)]Department of Physics and Institute for Advanced Study, The Hong Kong University of Science and Technology, Clear Water Bay, Kowloon, Hong Kong, China
[63] Department of Physics, Indiana University, Bloomington, IN, USA

[64] Institut für Astro- und Teilchenphysik, Leopold-Franzens-Universität, Innsbruck, Austria
[65] University of Iowa, Iowa City, IA, USA
[66] Department of Physics and Astronomy, Iowa State University, Ames, IA, USA
[67] Joint Institute for Nuclear Research, JINR Dubna, Dubna, Russia
[68] KEK, High Energy Accelerator Research Organization, Tsukuba, Japan
[69] Graduate School of Science, Kobe University, Kobe, Japan
[70] Faculty of Science, Kyoto University, Kyoto, Japan
[71] Kyoto University of Education, Kyoto, Japan
[72] Department of Physics, Kyushu University, Fukuoka, Japan
[73] Instituto de Física La Plata, Universidad Nacional de La Plata and CONICET, La Plata, Argentina
[74] Physics Department, Lancaster University, Lancaster, UK
[75] [(a)]INFN Sezione di Lecce, Lecce, Italy; [(b)]Dipartimento di Matematica e Fisica, Università del Salento, Lecce, Italy
[76] Oliver Lodge Laboratory, University of Liverpool, Liverpool, UK
[77] Department of Experimental Particle Physics, Jožef Stefan Institute and Department of Physics, University of Ljubljana, Ljubljana, Slovenia
[78] School of Physics and Astronomy, Queen Mary University of London, London, UK
[79] Department of Physics, Royal Holloway University of London, Surrey, UK
[80] Department of Physics and Astronomy, University College London, London, UK
[81] Louisiana Tech University, Ruston, LA, USA
[82] Laboratoire de Physique Nucléaire et de Hautes Energies, UPMC and Université Paris-Diderot and CNRS/IN2P3, Paris, France
[83] Fysiska institutionen, Lunds universitet, Lund, Sweden
[84] Departamento de Fisica Teorica C-15, Universidad Autonoma de Madrid, Madrid, Spain
[85] Institut für Physik, Universität Mainz, Mainz, Germany
[86] School of Physics and Astronomy, University of Manchester, Manchester, UK
[87] CPPM, Aix-Marseille Université and CNRS/IN2P3, Marseille, France
[88] Department of Physics, University of Massachusetts, Amherst, MA, USA
[89] Department of Physics, McGill University, Montreal, QC, Canada
[90] School of Physics, University of Melbourne, Victoria, Australia
[91] Department of Physics, The University of Michigan, Ann Arbor, MI, USA
[92] Department of Physics and Astronomy, Michigan State University, East Lansing, MI, USA
[93] [(a)]INFN Sezione di Milano, Milan, Italy; [(b)]Dipartimento di Fisica, Università di Milano, Milan, Italy
[94] B.I. Stepanov Institute of Physics, National Academy of Sciences of Belarus, Minsk, Republic of Belarus
[95] Research Institute for Nuclear Problems of Byelorussian State University, Minsk, Republic of Belarus
[96] Group of Particle Physics, University of Montreal, Montreal, QC, Canada
[97] P.N. Lebedev Physical Institute of the Russian Academy of Sciences, Moscow, Russia
[98] Institute for Theoretical and Experimental Physics (ITEP), Moscow, Russia
[99] National Research Nuclear University MEPhI, Moscow, Russia
[100] D.V. Skobeltsyn Institute of Nuclear Physics, M.V. Lomonosov Moscow State University, Moscow, Russia
[101] Fakultät für Physik, Ludwig-Maximilians-Universität München, Munich, Germany
[102] Max-Planck-Institut für Physik (Werner-Heisenberg-Institut), München, Germany
[103] Nagasaki Institute of Applied Science, Nagasaki, Japan
[104] Graduate School of Science and Kobayashi-Maskawa Institute, Nagoya University, Nagoya, Japan
[105] [(a)]INFN Sezione di Napoli, Napoli, Italy; [(b)]Dipartimento di Fisica, Università di Napoli, Napoli, Italy
[106] Department of Physics and Astronomy, University of New Mexico, Albuquerque, NM, USA
[107] Institute for Mathematics, Astrophysics and Particle Physics, Radboud University Nijmegen/Nikhef, Nijmegen, The Netherlands
[108] Nikhef National Institute for Subatomic Physics and University of Amsterdam, Amsterdam, The Netherlands
[109] Department of Physics, Northern Illinois University, DeKalb, IL, USA
[110] Budker Institute of Nuclear Physics, SB RAS, Novosibirsk, Russia
[111] Department of Physics, New York University, New York, NY, USA
[112] Ohio State University, Columbus, OH, USA
[113] Faculty of Science, Okayama University, Okayama, Japan

[114] Homer L. Dodge Department of Physics and Astronomy, University of Oklahoma, Norman, OK, USA
[115] Department of Physics, Oklahoma State University, Stillwater, OK, USA
[116] Palacký University, RCPTM, Olomouc, Czech Republic
[117] Center for High Energy Physics, University of Oregon, Eugene, OR, USA
[118] LAL, Univ. Paris-Sud, CNRS/IN2P3, Université Paris-Saclay, Orsay, France
[119] Graduate School of Science, Osaka University, Osaka, Japan
[120] Department of Physics, University of Oslo, Oslo, Norway
[121] Department of Physics, Oxford University, Oxford, UK
[122] [(a)]INFN Sezione di Pavia, Pavia, Italy; [(b)]Dipartimento di Fisica, Università di Pavia, Pavia, Italy
[123] Department of Physics, University of Pennsylvania, Philadelphia, PA, USA
[124] National Research Centre "Kurchatov Institute" B.P. Konstantinov Petersburg Nuclear Physics Institute, St. Petersburg, Russia
[125] [(a)]INFN Sezione di Pisa, Pisa, Italy; [(b)]Dipartimento di Fisica E. Fermi, Università di Pisa, Pisa, Italy
[126] Department of Physics and Astronomy, University of Pittsburgh, Pittsburgh, PA, USA
[127] [(a)]Laboratório de Instrumentação e Física Experimental de Partículas-LIP, Lisbon, Portugal; [(b)]Faculdade de Ciências, Universidade de Lisboa, Lisbon, Portugal; [(c)]Department of Physics, University of Coimbra, Coimbra, Portugal; [(d)]Centro de Física Nuclear da Universidade de Lisboa, Lisbon, Portugal; [(e)]Departamento de Fisica, Universidade do Minho, Braga, Portugal; [(f)]Departamento de Fisica Teorica y del Cosmos and CAFPE, Universidad de Granada, Granada, Spain; [(g)]Dep Fisica and CEFITEC of Faculdade de Ciencias e Tecnologia, Universidade Nova de Lisboa, Caparica, Portugal
[128] Institute of Physics, Academy of Sciences of the Czech Republic, Praha, Czech Republic
[129] Czech Technical University in Prague, Praha, Czech Republic
[130] Faculty of Mathematics and Physics, Charles University in Prague, Praha, Czech Republic
[131] State Research Center Institute for High Energy Physics (Protvino), NRC KI, Protvino, Russia
[132] Particle Physics Department, Rutherford Appleton Laboratory, Didcot, UK
[133] [(a)]INFN Sezione di Roma, Rome, Italy; [(b)]Dipartimento di Fisica, Sapienza Università di Roma, Rome, Italy
[134] [(a)]INFN Sezione di Roma Tor Vergata, Rome, Italy; [(b)]Dipartimento di Fisica, Università di Roma Tor Vergata, Rome, Italy
[135] [(a)]INFN Sezione di Roma Tre, Rome, Italy; [(b)]Dipartimento di Matematica e Fisica, Università Roma Tre, Rome, Italy
[136] [(a)]Faculté des Sciences Ain Chock, Réseau Universitaire de Physique des Hautes Energies-Université Hassan II, Casablanca, Morocco; [(b)]Centre National de l'Energie des Sciences Techniques Nucleaires, Rabat, Morocco; [(c)]Faculté des Sciences Semlalia, Université Cadi Ayyad, LPHEA-Marrakech, Marrakech, Morocco; [(d)]Faculté des Sciences, Université Mohamed Premier and LPTPM, Oujda, Morocco; [(e)]Faculté des Sciences, Université Mohammed V, Rabat, Morocco
[137] DSM/IRFU (Institut de Recherches sur les Lois Fondamentales de l'Univers), CEA Saclay (Commissariat à l'Energie Atomique et aux Energies Alternatives), Gif-sur-Yvette, France
[138] Santa Cruz Institute for Particle Physics, University of California Santa Cruz, Santa Cruz, CA, USA
[139] Department of Physics, University of Washington, Seattle, WA, USA
[140] School of Physics, Shandong University, Shandong, China
[141] Department of Physics and Astronomy, Shanghai Key Laboratory for Particle Physics and Cosmology, Shanghai Jiao Tong University; (Also Affiliated with PKU-CHEP), Shanghai, China
[142] Department of Physics and Astronomy, University of Sheffield, Sheffield, UK
[143] Department of Physics, Shinshu University, Nagano, Japan
[144] Fachbereich Physik, Universität Siegen, Siegen, Germany
[145] Department of Physics, Simon Fraser University, Burnaby, BC, Canada
[146] SLAC National Accelerator Laboratory, Stanford, CA, USA
[147] [(a)]Faculty of Mathematics, Physics and Informatics, Comenius University, Bratislava, Slovak Republic; [(b)]Department of Subnuclear Physics, Institute of Experimental Physics of the Slovak Academy of Sciences, Kosice, Slovak Republic
[148] [(a)]Department of Physics, University of Cape Town, Cape Town, South Africa; [(b)]Department of Physics, University of Johannesburg, Johannesburg, South Africa; [(c)]School of Physics, University of the Witwatersrand, Johannesburg, South Africa
[149] [(a)]Department of Physics, Stockholm University, Stockholm, Sweden; [(b)]The Oskar Klein Centre, Stockholm, Sweden
[150] Physics Department, Royal Institute of Technology, Stockholm, Sweden

[151] Departments of Physics and Astronomy and Chemistry, Stony Brook University, Stony Brook, NY, USA
[152] Department of Physics and Astronomy, University of Sussex, Brighton, UK
[153] School of Physics, University of Sydney, Sydney, Australia
[154] Institute of Physics, Academia Sinica, Taipei, Taiwan
[155] Department of Physics, Technion: Israel Institute of Technology, Haifa, Israel
[156] Raymond and Beverly Sackler School of Physics and Astronomy, Tel Aviv University, Tel Aviv, Israel
[157] Department of Physics, Aristotle University of Thessaloniki, Thessaloniki, Greece
[158] International Center for Elementary Particle Physics and Department of Physics, The University of Tokyo, Tokyo, Japan
[159] Graduate School of Science and Technology, Tokyo Metropolitan University, Tokyo, Japan
[160] Department of Physics, Tokyo Institute of Technology, Tokyo, Japan
[161] Tomsk State University, Tomsk, Russia
[162] Department of Physics, University of Toronto, Toronto, ON, Canada
[163] [(a)]INFN-TIFPA, Trento, Italy; [(b)]University of Trento, Trento, Italy
[164] [(a)]TRIUMF, Vancouver, BC, Canada; [(b)]Department of Physics and Astronomy, York University, Toronto, ON, Canada
[165] Faculty of Pure and Applied Sciences, and Center for Integrated Research in Fundamental Science and Engineering, University of Tsukuba, Tsukuba, Japan
[166] Department of Physics and Astronomy, Tufts University, Medford, MA, USA
[167] Department of Physics and Astronomy, University of California Irvine, Irvine, CA, USA
[168] [(a)]INFN Gruppo Collegato di Udine, Sezione di Trieste, Udine, Italy; [(b)]ICTP, Trieste, Italy; [(c)]Dipartimento di Chimica, Fisica e Ambiente, Università di Udine, Udine, Italy
[169] Department of Physics and Astronomy, University of Uppsala, Uppsala, Sweden
[170] Department of Physics, University of Illinois, Urbana, IL, USA
[171] Instituto de Fisica Corpuscular (IFIC) and Departamento de Fisica Atomica, Molecular y Nuclear and Departamento de Ingeniería Electrónica and Instituto de Microelectrónica de Barcelona (IMB-CNM), University of Valencia and CSIC, Valencia, Spain
[172] Department of Physics, University of British Columbia, Vancouver, BC, Canada
[173] Department of Physics and Astronomy, University of Victoria, Victoria, BC, Canada
[174] Department of Physics, University of Warwick, Coventry, UK
[175] Waseda University, Tokyo, Japan
[176] Department of Particle Physics, The Weizmann Institute of Science, Rehovot, Israel
[177] Department of Physics, University of Wisconsin, Madison, WI, USA
[178] Fakultät für Physik und Astronomie, Julius-Maximilians-Universität, Würzburg, Germany
[179] Fakultät für Mathematik und Naturwissenschaften, Fachgruppe Physik, Bergische Universität Wuppertal, Wuppertal, Germany
[180] Department of Physics, Yale University, New Haven, CT, USA
[181] Yerevan Physics Institute, Yerevan, Armenia
[182] Centre de Calcul de l'Institut National de Physique Nucléaire et de Physique des Particules (IN2P3), Villeurbanne, France

[a] Also at Department of Physics, King's College London, London, UK
[b] Also at Institute of Physics, Azerbaijan Academy of Sciences, Baku, Azerbaijan
[c] Also at Novosibirsk State University, Novosibirsk, Russia
[d] Also at TRIUMF, Vancouver, BC, Canada
[e] Also at Department of Physics and Astronomy, University of Louisville, Louisville, KY, USA
[f] Also at Physics Department, An-Najah National University, Nablus, Palestine
[g] Also at Department of Physics, California State University, Fresno, CA, USA
[h] Also at Department of Physics, University of Fribourg, Fribourg, Switzerland
[i] Also at Departament de Fisica de la Universitat Autonoma de Barcelona, Barcelona, Spain
[j] Also at Departamento de Fisica e Astronomia, Faculdade de Ciencias, Universidade do Porto, Portugal
[k] Also at Tomsk State University, Tomsk, Russia
[l] Also at Universita di Napoli Parthenope, Napoli, Italy
[m] Also at Institute of Particle Physics (IPP), Canada
[n] Also at National Institute of Physics and Nuclear Engineering, Bucharest, Romania
[o] Also at Department of Physics, St. Petersburg State Polytechnical University, St. Petersburg, Russia

[p] Also at Department of Physics, The University of Michigan, Ann Arbor, MI, USA
[q] Also at Centre for High Performance Computing, CSIR Campus, Rosebank, Cape Town, South Africa
[r] Also at Louisiana Tech University, Ruston, LA, USA
[s] Also at Institucio Catalana de Recerca i Estudis Avancats, ICREA, Barcelona, Spain
[t] Also at Graduate School of Science, Osaka University, Osaka, Japan
[u] Also at Department of Physics, National Tsing Hua University, Taiwan
[v] Also at Institute for Mathematics, Astrophysics and Particle Physics, Radboud University Nijmegen/Nikhef, Nijmegen, The Netherlands
[w] Also at Department of Physics, The University of Texas at Austin, Austin, TX, USA
[x] Also at CERN, Geneva, Switzerland
[y] Also at Georgian Technical University (GTU), Tbilisi, Georgia
[z] Also at Ochadai Academic Production, Ochanomizu University, Tokyo, Japan
[aa] Also at Manhattan College, New York, NY, USA
[ab] Also at Academia Sinica Grid Computing, Institute of Physics, Academia Sinica, Taipei, Taiwan
[ac] Also at School of Physics, Shandong University, Shandong, China
[ad] Also at Department of Physics, California State University, Sacramento CA, USA
[ae] Also at Moscow Institute of Physics and Technology, State University, Dolgoprudny, Russia
[af] Also at Departement de Physique Nucleaire et Corpusculaire, Université de Genève, Geneva, Switzerland
[ag] Also at Eotvos Lorand University, Budapest, Hungary
[ah] Also at Departments of Physics and Astronomy and Chemistry, Stony Brook University, Stony Brook NY, USA
[ai] Also at International School for Advanced Studies (SISSA), Trieste, Italy
[aj] Also at Department of Physics and Astronomy, University of South Carolina, Columbia, SC, USA
[ak] Also at Institut de Física d'Altes Energies (IFAE), The Barcelona Institute of Science and Technology, Barcelona, Spain
[al] Also at School of Physics and Engineering, Sun Yat-sen University, Guangzhou, China
[am] Also at Institute for Nuclear Research and Nuclear Energy (INRNE) of the Bulgarian Academy of Sciences, Sofia, Bulgaria
[an] Also at Faculty of Physics, M.V. Lomonosov Moscow State University, Moscow, Russia
[ao] Also at Institute of Physics, Academia Sinica, Taipei, Taiwan
[ap] Also at National Research Nuclear University MEPhI, Moscow, Russia
[aq] Also at Department of Physics, Stanford University, Stanford, CA, USA
[ar] Also at Institute for Particle and Nuclear Physics, Wigner Research Centre for Physics, Budapest, Hungary
[as] Also at Flensburg University of Applied Sciences, Flensburg, Germany
[at] Also at University of Malaya, Department of Physics, Kuala Lumpur, Malaysia
[au] Also at CPPM, Aix-Marseille Université and CNRS/IN2P3, Marseille, France
*Deceased

Eur. Phys. J. C (2017) 77:40
DOI 10.1140/epjc/s10052-016-4574-y

THE EUROPEAN PHYSICAL JOURNAL C

Regular Article - Experimental Physics

Measurement of the $t\bar{t}Z$ and $t\bar{t}W$ production cross sections in multilepton final states using 3.2 fb^{-1} of pp collisions at $\sqrt{s}$ = 13 TeV with the ATLAS detector

ATLAS Collaboration[⋆]

CERN, 1211 Geneva 23, Switzerland

Received: 7 September 2016 / Accepted: 13 December 2016 / Published online: 20 January 2017

Abstract A measurement of the $t\bar{t}Z$ and $t\bar{t}W$ production cross sections in final states with either two same-charge muons, or three or four leptons (electrons or muons) is presented. The analysis uses a data sample of proton–proton collisions at $\sqrt{s} = 13$ TeV recorded with the ATLAS detector at the Large Hadron Collider in 2015, corresponding to a total integrated luminosity of 3.2 fb^{-1}. The inclusive cross sections are extracted using likelihood fits to signal and control regions, resulting in $\sigma_{t\bar{t}Z} = 0.9 \pm 0.3$ pb and $\sigma_{t\bar{t}W} = 1.5 \pm 0.8$ pb, in agreement with the Standard Model predictions.

1 Introduction

At the Large Hadron Collider (LHC), top quarks are copiously produced in quark–antiquark pairs ($t\bar{t}$). This process has been extensively studied in proton–proton collisions at 7 and 8 TeV, and recently at 13 TeV [1,2] centre-of-mass energy. Measurements of the associated production of $t\bar{t}$ with a Z boson ($t\bar{t}Z$) allow the extraction of information about the neutral-current coupling of the top quark. The production rate of a top-quark pair with a massive vector boson could be altered in the presence of physics beyond the Standard Model (SM), such as vector-like quarks [3,4], strongly coupled Higgs bosons [5] or technicolour [6–10], and therefore the measurements of $\sigma_{t\bar{t}Z}$ and $\sigma_{t\bar{t}W}$ are important checks of the validity of the SM at this new energy regime. The $t\bar{t}Z$ and $t\bar{t}W$ processes have been established by ATLAS [11] and CMS [12] using the Run-1 dataset at $\sqrt{s} = 8$ TeV, with measured cross sections compatible with the SM prediction and having uncertainties of ∼30%. At $\sqrt{s} = 13$ TeV, the SM cross sections of the $t\bar{t}Z$ and $t\bar{t}W$ processes increase by factors of 3.5 and 2.4, respectively, compared to $\sqrt{s} = 8$ TeV. The cross sections, computed at next-to-leading-order (NLO) QCD precision, using MadGraph5_aMC@NLO (referred to in the following as MG5_aMC), are $\sigma_{t\bar{t}Z} = 0.84$ pb and $\sigma_{t\bar{t}W} = 0.60$ pb with an uncertainty of ∼12% [13,14], primarily due to higher-order corrections, estimated by varying the renormalisation and factorisation scales.

This paper presents measurements of the $t\bar{t}Z$ and $t\bar{t}W$ cross sections using 3.2 fb^{-1} of proton–proton (pp) collision data at $\sqrt{s} = 13$ TeV collected by the ATLAS detector in 2015. The final states of top-quark pairs produced in association with a Z or a W boson comprise up to four isolated, prompt leptons.[1] Decay modes with two same-sign (SS) charged muons, or three or four leptons are considered in this analysis. The analysis strategy follows the strategy adopted for the 8 TeV dataset [11], excluding the lower sensitivity SS dilepton channels. Table 1 lists the analysis channels and the targeted decay modes of the $t\bar{t}Z$ and $t\bar{t}W$ processes. Each channel is divided into multiple analysis regions in order to enhance the sensitivity to the signal. Simultaneous fits are performed to the signal regions and selected control regions in order to extract the cross sections for $t\bar{t}Z$ and $t\bar{t}W$ production. Additional validation regions are defined to check that the background estimate agrees with the data and are not used in the fit.

2 The ATLAS detector

The ATLAS detector [15] consists of four main subsystems: an inner tracking system, electromagnetic (EM) and hadronic calorimeters, and a muon spectrometer (MS). The inner detector (ID) consists of a high-granularity silicon pixel detector, including the newly installed Insertable B-Layer [16], which is the innermost layer of the tracking system, and a silicon microstrip tracker, together providing pre-

⋆ e-mail: atlas.publications@cern.ch

[1] In this paper, lepton is used to denote electron or muon, and prompt lepton is used to denote a lepton produced in a Z or W boson or τ-lepton decay.

Table 1 List of $t\bar{t}W$ and $t\bar{t}Z$ decay modes and analysis channels targeting them

Process	$t\bar{t}$ decay	Boson decay	Channel
$t\bar{t}W$	$(\mu^{\pm}\nu b)(q\bar{q}b)$	$\mu^{\pm}\nu$	SS dimuon
	$(\ell^{\pm}\nu b)(\ell^{\mp}\nu b)$	$\ell^{\pm}\nu$	Trilepton
$t\bar{t}Z$	$(\ell^{\pm}\nu b)(q\bar{q}b)$	$\ell^{+}\ell^{-}$	Trilepton
	$(\ell^{\pm}\nu b)(\ell^{\mp}\nu b)$	$\ell^{+}\ell^{-}$	Tetralepton

cision tracking in the pseudorapidity[2] range $|\eta| < 2.5$ and of a transition radiation tracker covering $|\eta| < 2.0$. All the systems are immersed in a 2 T magnetic field provided by a superconducting solenoid. The EM sampling calorimeter uses lead and liquid argon (LAr) and is divided into barrel ($|\eta| < 1.475$) and endcap ($1.375 < |\eta| < 3.2$) regions. Hadron calorimetry is provided by a steel/scintillator-tile calorimeter, segmented into three barrel structures, in the range $|\eta| < 1.7$, and by two copper/LAr hadronic endcap calorimeters that cover the region $1.5 < |\eta| < 3.2$. The solid angle coverage is completed with forward copper/LAr and tungsten/LAr calorimeter modules, optimised for EM and hadronic measurements respectively, covering the region $3.1 < |\eta| < 4.9$. The muon spectrometer measures the deflection of muon tracks in the range $|\eta| < 2.7$ using multiple layers of high-precision tracking chambers located in toroidal magnetic fields. The field integral of the toroids ranges between 2.0 and 6.0 Tm for most of the detector. The muon spectrometer is also instrumented with separate trigger chambers covering $|\eta| < 2.4$. A two-level trigger system, using custom hardware followed by a software-based trigger level, is used to reduce the event rate to an average of around 1 kHz for offline storage.

3 Data and simulated event samples

The data were collected with the ATLAS detector during 2015 with a bunch spacing of 25 ns and a mean number of 14 pp interactions per bunch crossing (pile-up). With strict data-quality requirements, the integrated luminosity considered corresponds to 3.2 fb^{-1} with an uncertainty of 2.1% [17].

Monte Carlo simulation samples (MC) are used to model the expected signal and background distributions in the different control, validation and signal regions described below. The heavy-flavour decays involving b- and c-quarks, particularly important to this measurement, are modelled using the EvtGen [18] program, except for processes modelled using the Sherpa generator. In all samples the top-quark mass is set to 172.5 GeV and the Higgs boson mass is set to 125 GeV. The response of the detector to stable[3] particles is emulated by a dedicated simulation [19] based either fully on Geant [20] or on a faster parameterisation [21] for the calorimeter response and Geant for other detector systems. To account for additional pp interactions from the same and close-by bunch crossings, a set of minimum-bias interactions generated using Pythia v8.210 [22], referred to as Pythia 8 in the following, with the A2 [23] set of tuned MC parameters (A2 tune) is superimposed on the hard-scattering events. In order to reproduce the same pile-up levels present in the data, the distribution of the number of additional pp interactions in the MC samples is reweighted to match the one in the data. All samples are processed through the same reconstruction software as the data. Simulated events are corrected so that the object identification, reconstruction and trigger efficiencies, energy scales and energy resolutions match those determined from data control samples.

The associated production of a top-quark pair with one or two vector bosons is generated at leading order (LO) with MG5_aMC interfaced to Pythia 8, with up to two ($t\bar{t}W$), one ($t\bar{t}Z$) or no ($t\bar{t}WW$) extra partons included in the matrix elements. The γ^* contribution and the Z/γ^* interference are included in the $t\bar{t}Z$ samples. The A14 [24] set of tuned MC parameters (A14 tune) is used together with the NNPDF2.3LO parton distribution function (PDF) set [25]. The samples are normalised using cross sections computed at NLO in QCD [26].

The t-channel production of a single top quark in association with a Z boson (tZ) is generated using MG5_aMC interfaced with Pythia v6.427 [27], referred to as Pythia 6 in the following, with the CTEQ6L1 PDF [28] set and the Perugia2012 [29] set of tuned MC parameters at NLO in QCD. The Z/γ^* interference is included, and the four-flavour scheme is used in the computation.

The Wt-channel production of a single top quark together with a Z boson (tWZ) is generated with MG5_aMC and showered with Pythia 8, using the NNPDF3.0NLO PDF set [30] and the A14 tune. The generation is performed at NLO in QCD using the five-flavour scheme. Diagrams containing a top-quark pair are removed to avoid overlap with the $t\bar{t}Z$ process.

Diboson processes with four charged leptons (4ℓ), three charged leptons and one neutrino ($\ell\ell\ell\nu$) or two charged leptons and two neutrinos ($\ell\ell\nu\nu$) are simulated using the Sherpa 2.1 generator [31]. The matrix elements include all diagrams with four electroweak vertices. They are calculated for up to one ($4\ell, \ell\ell\nu\nu$) or no additional partons ($\ell\ell\ell\nu$) at

[2] ATLAS uses a right-handed coordinate system with its origin at the nominal interaction point (IP) in the centre of the detector and the z-axis along the beam pipe. The x-axis points from the IP to the centre of the LHC ring, and the y-axis points upward. Cylindrical coordinates (r, ϕ) are used in the transverse plane, ϕ being the azimuthal angle around the z-axis. The pseudorapidity is defined in terms of the polar angle θ as $\eta = -\ln\tan(\theta/2)$.

[3] A particle is considered stable if $c\tau \geq 1$ cm.

NLO and up to three partons at LO using the COMIX [32] and OPENLOOPS [33] matrix element generators and merged with the SHERPA parton shower using the ME+PS@NLO prescription [34]. The CT10nlo PDF set [35] is used in conjunction with a dedicated parton-shower tuning developed by the SHERPA authors. The NLO cross sections calculated by the generator are used to normalise diboson processes. Alternative diboson samples are simulated using the POWHEG-BOX v2 [36] generator, interfaced to the PYTHIA 8 parton shower model, and for which the CT10nlo PDF set is used in the matrix element, while the CTEQ6L1 PDF set is used for the parton shower along with the AZNLO [37] set of tuned MC parameters.

The production of three massive vector bosons with subsequent leptonic decays of all three bosons is modelled at LO with the SHERPA 2.1 generator and the CT10 PDF set [35]. Up to two additional partons are included in the matrix element at LO and the full NLO accuracy is used for the inclusive process.

Electroweak processes involving the vector-boson scattering (VBS) diagram and producing two same-sign leptons, two neutrinos and two partons are modelled using SHERPA 2.1 at LO accuracy and the CT10 PDF set. Processes of orders four and six in the electroweak coupling constant are considered, and up to one additional parton is included in the matrix element.

For the generation of $t\bar{t}$ events and Wt-channel single-top-quark events the POWHEG-BOX v2 generator is used with the CT10 PDF set. The parton shower and the underlying event are simulated using PYTHIA 6 with the CTEQ6L1 PDF set and the corresponding Perugia2012 tune. The $t\bar{t}$ samples are normalised to their next-to-next-to-leading-order (NNLO) cross-section predictions, including soft-gluon resummation to next-to-next-to-leading-log order, as calculated with the TOP++2.0 program (see Ref. [38] and references therein). For more efficient sample generation, the $t\bar{t}$ sample is produced by selecting only true dilepton events in the final state. Moreover, an additional dilepton $t\bar{t}$ sample requiring a b-hadron not coming from top-quark decays is generated after b-jet selection. Diagram removal is employed to remove the overlap between $t\bar{t}$ and Wt [39].

Samples of $t\bar{t}$ events produced in association with a Higgs boson ($t\bar{t}H$) are generated using NLO matrix elements in MG5_aMC with the CT10NLO PDF set and interfaced with PYTHIA 8 for the modelling of the parton shower. Higgs boson production via gluon–gluon fusion (ggF) and vector boson fusion (VBF) is generated using the POWHEG-BOX v2 generator with CT10 PDF set. The parton shower and underlying event are simulated using PYTHIA 8 with the CTEQ6L1 PDF set and AZNLO tune. Higgs boson production with a vector boson is generated at LO using PYTHIA 8 with the CTEQ6L1 PDF. All Higgs boson samples are normalised using theoretical calculations of Ref. [40].

Events containing Z or W bosons with associated jets, referred to as Z+jets and W+jets in the following, are simulated using the SHERPA 2.1 generator. Matrix elements are calculated for up to two partons at NLO and four partons at LO. The CT10 PDF set is used in conjunction with a dedicated parton-shower tuning developed by the SHERPA authors [31]. The Z/W+jets samples are normalised to the NNLO cross sections [41–44]. Alternative Z/W+jets samples are simulated using MG5_aMC at LO interfaced to the PYTHIA 8 parton shower model. The A14 tune is used together with the NNPDF2.3LO PDF set.

The SM production of three and four top quarks is generated at LO with MG5_aMC+PYTHIA 8, using the A14 tune together with the NNPDF2.3LO PDF set. The samples are normalised using cross sections computed at NLO [45,46].

4 Object reconstruction

The final states of interest in this analysis contain electrons, muons, jets, b-jets and missing transverse momentum.

Electron candidates [47] are reconstructed from energy deposits (clusters) in the EM calorimeter that are associated with reconstructed tracks in the inner detector. The electron identification relies on a likelihood-based selection [48,49]. Electrons are required to pass the "medium" likelihood identification requirements described in Ref. [49]. These include requirements on the shapes of the electromagnetic shower in the calorimeter as well as tracking and track-to-cluster matching quantities. The electrons are also required to have transverse momentum $p_{\mathrm{T}} > 7$ GeV and $|\eta_{\mathrm{cluster}}| < 2.47$, where η_{cluster} is the pseudorapidity of the calorimeter energy deposit associated with the electron candidate. Candidates in the EM calorimeter barrel/endcap transition region $1.37 < |\eta_{\mathrm{cluster}}| < 1.52$ are excluded.

Muon candidates are reconstructed from a fit to track segments in the various layers of the muon spectrometer, matched with tracks identified in the inner detector. Muons are required to have $p_{\mathrm{T}} > 7$ GeV and $|\eta| < 2.4$ and to pass the "medium" identification requirements defined in Ref. [50]. The medium requirement includes selections on the numbers of hits in the ID and MS as well as a compatibility requirement between momentum measurements in the ID and MS. It provides a high efficiency and purity of selected muons. Electron candidates sharing a track with a muon candidate are removed.

To reduce the non-prompt lepton background from hadron decays or jets misidentified as leptons (labelled as "fake leptons" throughout this paper), electron and muon candidates are required to be isolated. The total sum of track transverse momenta in a surrounding cone of size $\min(10\,\mathrm{GeV}/p_{\mathrm{T}}, r_{e,\mu})$, excluding the track of the candidate from the sum, is required to be less than 6% of the candidate p_{T}, where $r_e = 0.2$ and $r_\mu = 0.3$. In addition, the sum of the

cluster transverse energies in the calorimeter within a cone of size $\Delta R_\eta \equiv \sqrt{(\Delta\eta)^2 + (\Delta\phi)^2} = 0.2$ of any electron candidate, excluding energy deposits of the candidate itself, is required to be less than 6% of the candidate p_{T}.

For both electrons and muons, the longitudinal impact parameter of the associated track with respect to the primary vertex,[4] z_0, is required to satisfy $|z_0 \sin\theta| < 0.5$ mm. The significance of the transverse impact parameter d_0 is required to satisfy $|d_0|/\sigma(d_0) < 5$ for electrons and $|d_0|/\sigma(d_0) < 3$ for muons, where $\sigma(d_0)$ is the uncertainty in d_0.

Jets are reconstructed using the anti-k_t algorithm [51,52] with radius parameter $R = 0.4$, starting from topological clusters in the calorimeters [53]. The effect of pile-up on jet energies is accounted for by a jet-area-based correction [54] and the energy resolution of the jets is improved by using global sequential corrections [55]. Jets are calibrated to the hadronic energy scale using E- and η-dependent calibration factors based on MC simulations, with in-situ corrections based on Run-1 data [56,57] and checked with early Run-2 data [58]. Jets are accepted if they fulfil the requirements $p_{\mathrm{T}} > 25$ GeV and $|\eta| < 2.5$. To reduce the contribution from jets associated with pile-up, jets with $p_{\mathrm{T}} < 60$ GeV and $|\eta| < 2.4$ are required to satisfy pile-up rejection criteria (JVT), based on a multivariate combination of track-based variables [59].

Jets are b-tagged as likely to contain b-hadrons using the MV2c20 algorithm, a multivariate discriminant making use of the long lifetime, large decay multiplicity, hard fragmentation and high mass of b-hadrons [60]. The average efficiency to correctly tag a b-jet is approximately 77%, as determined in simulated $t\bar{t}$ events, but it varies as a function of p_{T} and η. In simulation, the tagging algorithm gives a rejection factor of about 130 against light-quark and gluon jets, and about 4.5 against jets containing charm quarks [61]. The efficiency of b-tagging in simulation is corrected to that in data using a $t\bar{t}$-based calibration using Run-1 data [62] and validated with Run-2 data [63].

The missing transverse momentum $\mathbf{p}_{\mathrm{T}}^{\mathrm{miss}}$, with magnitude $E_{\mathrm{T}}^{\mathrm{miss}}$, is a measure of the transverse momentum imbalance due to particles escaping detection. It is computed [64] as the negative sum of the transverse momenta of all electrons, muons and jets and an additional soft term. The soft term is constructed from all tracks that are associated with the primary vertex but not with any physics object. In this way, the $E_{\mathrm{T}}^{\mathrm{miss}}$ is adjusted for the best calibration of the jets and the other identified physics objects above, while maintaining pile-up independence in the soft term [65,66].

To prevent double-counting of electron energy deposits as jets, the closest jet within $\Delta R_y = 0.2$ of a reconstructed electron is removed, where $\Delta R_y \equiv \sqrt{(\Delta y)^2 + (\Delta\phi)^2}$. If the nearest jet surviving the above selection is within $\Delta R_y = 0.4$ of an electron, the electron is discarded to ensure that selected electrons are sufficiently separated from nearby jet activity. To reduce the background from muons originating from heavy-flavour particle decays inside jets, muons are removed if they are separated from the nearest jet by $\Delta R_y < 0.4$. However, if this jet has fewer than three associated tracks, the muon is kept and the jet is removed instead; this avoids an inefficiency for high-energy muons undergoing significant energy loss in the calorimeter.

5 Event selection and background estimation

Only events collected using single-electron or single-muon triggers are accepted. The trigger thresholds, $p_{\mathrm{T}} > 24$ GeV for electrons and $p_{\mathrm{T}} > 20$ GeV for muons, are set to be almost fully efficient for reconstructed leptons with $p_{\mathrm{T}} > 25$ GeV. Events are required to have at least one reconstructed primary vertex. In all selections considered, at least one reconstructed lepton with $p_{\mathrm{T}} > 25$ GeV is required to match ($\Delta R_\eta < 0.15$) a lepton with the same flavour reconstructed by the trigger algorithm. Three channels are defined based on the number of reconstructed leptons, which are sorted according to their transverse momentum in decreasing order.

Background events containing well-identified prompt leptons are modelled by simulation. The normalisations for the WZ and ZZ processes are taken from data control regions and included in the fit. The yields in these data control regions are extrapolated to the signal regions using simulation. Systematic uncertainties in the extrapolation are taken into account in the overall uncertainty in the background estimate.

Background sources involving one or more fake leptons are modelled using data events from control regions. For the same-sign dimuon (2μ-SS) analysis and the trilepton analysis the fake-lepton background is estimated using the matrix method [67], where any combination of fake leptons among the selected leptons is considered. However, compared to Ref. [67], the real- and fake-lepton efficiencies used by the matrix method are estimated in a different way in this measurement. The lepton efficiencies are measured by applying the matrix method in control regions, where the lepton efficiencies are extracted in a likelihood fit as free parameters using the matrix method as model, assuming Poisson statistics, and assuming that events with two fake leptons are negligible. In this way the parameters are by construction the actual parameters of the matrix model itself, instead of relying on external lepton efficiency measurements, which are not guaranteed to be fully consistent with the matrix model. The control regions are defined in dilepton events, separately for b-tagged and b-vetoed events

[4] A primary vertex candidate is defined as a vertex with at least five associated tracks, consistent with the beam collision region. If more than one such vertex is found, the vertex candidate with the largest sum of squared transverse momenta of its associated tracks is taken as the primary vertex.

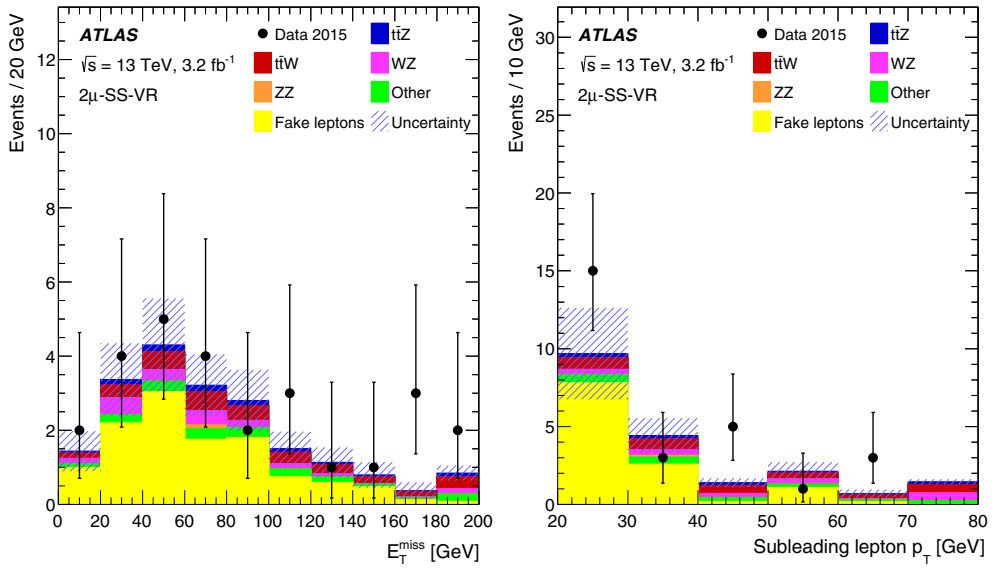

Fig. 1 The (*left*) $E_{\mathrm{T}}^{\mathrm{miss}}$ and (*right*) subleading lepton p_{T} distributions shown for the b-tagged 2μ-SS channel where the signal region requirements on subleading lepton p_{T}, number of b-tags, and $E_{\mathrm{T}}^{\mathrm{miss}}$ are relaxed. The shaded band represents the total uncertainty. The background denoted 'Other' contains other SM processes producing two same-sign prompt leptons. The last bin in each of the distributions includes the overflow

to take into account the different fake-lepton efficiencies depending on whether the source is a light-flavour jet or a heavy-flavour jet. The real-lepton efficiencies are measured in inclusive opposite-sign events, and fake-lepton efficiencies in events with same-sign leptons and $E_{\mathrm{T}}^{\mathrm{miss}} > 40\,\mathrm{GeV}$ (for b-tagged events $E_{\mathrm{T}}^{\mathrm{miss}} > 20\,\mathrm{GeV}$), after subtracting the estimated contribution from events with misidentification of the charge of a lepton (referred to as "charge-flip" in the following), and excluding the same-sign dimuon signal region. The charge-flip events are subtracted using simulation. The extracted fake-lepton efficiencies are found to be compatible with fake-lepton efficiencies from a fully data-driven procedure where the charge-flip events are estimated from data. For the tetralepton channel, the contribution from backgrounds containing fake leptons is estimated from simulation and corrected with scale factors determined in control regions.

The full selection requirements and the background evaluation strategies in the different channels are described below.

5.1 Same-sign dimuon analysis

The same-sign dimuon signal region targets the $t\bar{t}W$ process and has the highest sensitivity among all same-sign dilepton regions [11]. The main reason for this is that electrons have a much larger charge misidentification probability, inducing a significant background from top-quark pairs. Events are required to have two muon candidates with the same charge and $p_{\mathrm{T}} > 25\,\mathrm{GeV}$, $E_{\mathrm{T}}^{\mathrm{miss}} > 40\,\mathrm{GeV}$, the scalar sum of the p_{T} of selected leptons and jets, H_{T}, above 240 GeV, and at least two b-tagged jets. Events containing additional leptons (with $p_{\mathrm{T}} > 7\,\mathrm{GeV}$) are vetoed.

The dominant background in the 2μ-SS region arises from events containing fake leptons, where the main source is $t\bar{t}$ events. Backgrounds from the production of prompt leptons with correctly identified charge come primarily from WZ production, but the relative contribution of this background is small compared to the fake-lepton background. The charge-flip background is negligible in this signal region, as the probability of misidentifying the charge of a muon in the relevant p_{T} range is negligible. For the validation of the fake-lepton background estimate a region is defined based on the signal region selection but omitting the $E_{\mathrm{T}}^{\mathrm{miss}}$ requirement, reducing the p_{T} threshold of the subleading lepton to 20 GeV and requiring at least one b-tagged jet. The distributions of $E_{\mathrm{T}}^{\mathrm{miss}}$ and subleading lepton p_{T} in this validation region (2μ-SS-VR) are shown in Fig. 1. The expected numbers of events in the 2μ-SS signal region are shown in Table 4. Nine events are observed in data for this signal region.

Table 2 Summary of event selections in the trilepton signal regions

Variable	3ℓ-Z-1b4j	3ℓ-Z-2b3j	3ℓ-Z-2b4j	3ℓ-noZ-2b
Leading leptons p_{T}	>25 GeV	>25 GeV	>25 GeV	>25 GeV
Other leptons' p_{T}	>20 GeV	>20 GeV	>20 GeV	>20 GeV
Sum of leptons' charges	±1	±1	±1	±1
OSSF $\lvert m_{\ell\ell} - m_Z \rvert$	<10 GeV	<10 GeV	<10 GeV	>10 GeV
n_{jets}	≥4	3	≥4	≥2 and ≤4
$n_{b\text{-jets}}$	1	≥2	≥2	≥2

5.2 Trilepton analysis

Four signal regions with exactly three leptons are considered. The first three are sensitive to $t\bar{t}Z$; each of these requires an opposite-sign same-flavour (OSSF) pair of leptons whose invariant mass is within 10 GeV of the Z boson mass. The signal regions are categorised by their jet and b-jet multiplicities and have different signal-to-background ratios. In the 3ℓ-Z-1b4j region, at least four jets are required, exactly one of which is b-tagged. In the 3ℓ-Z-2b3j region, exactly three jets with at least two b-tagged jets are required. In the 3ℓ-Z-2b4j region, at least four jets are required, of which at least two are b-tagged.

In the 3ℓ-noZ-2b region at least two and at most four jets are required, of which at least two are b-tagged, no OSSF lepton pair is allowed in the Z boson mass window, and the sum of the lepton charges must be ±1. This region primarily targets the $t\bar{t}W$ process but also has a sizeable $t\bar{t}Z$ contribution.

The signal region definitions for the trilepton channel are summarised in Table 2, while the expected numbers of events in the signal regions are shown in Table 4. The dominant backgrounds in the 3ℓ-Z-1b4j, 3ℓ-Z-2b3j and 3ℓ-Z-2b4j signal regions arise from Z+jets production with a fake lepton, diboson production and the production of a single top quark in association with a Z boson.

A control region is used to constrain the normalisation of the WZ background in data. Exactly three leptons are required, at least one pair of which must be an OSSF pair with an invariant mass within 10 GeV of the Z boson mass.

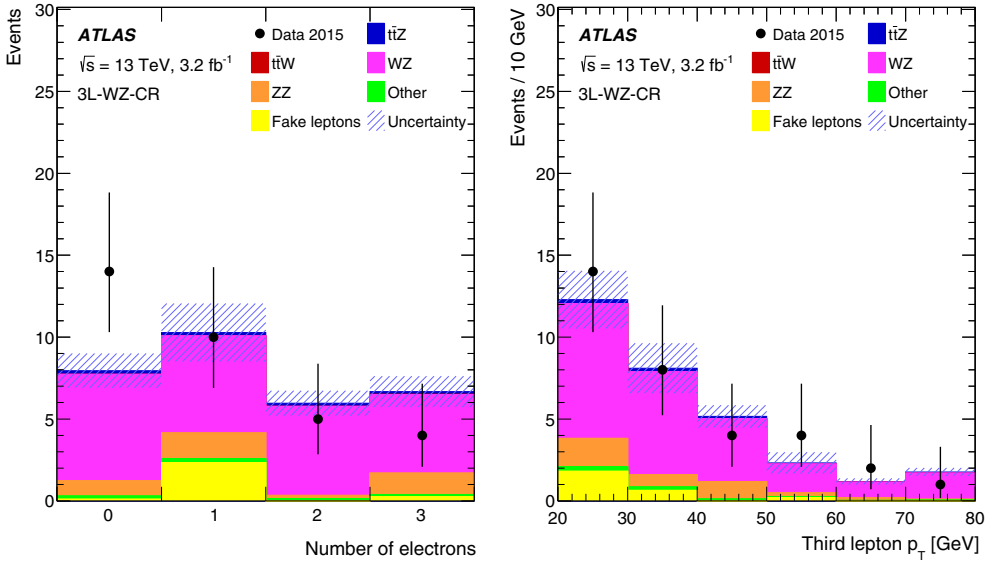

Fig. 2 Distributions of (*left*) the number of electrons and (*right*) the third-lepton p_{T} in the 3ℓ-WZ-CR control region before the fit. The background denoted 'Other' contains other SM processes producing three prompt leptons. The shaded band represents the total uncertainty. The last bin of the distribution shown in the *right panel* includes the overflow

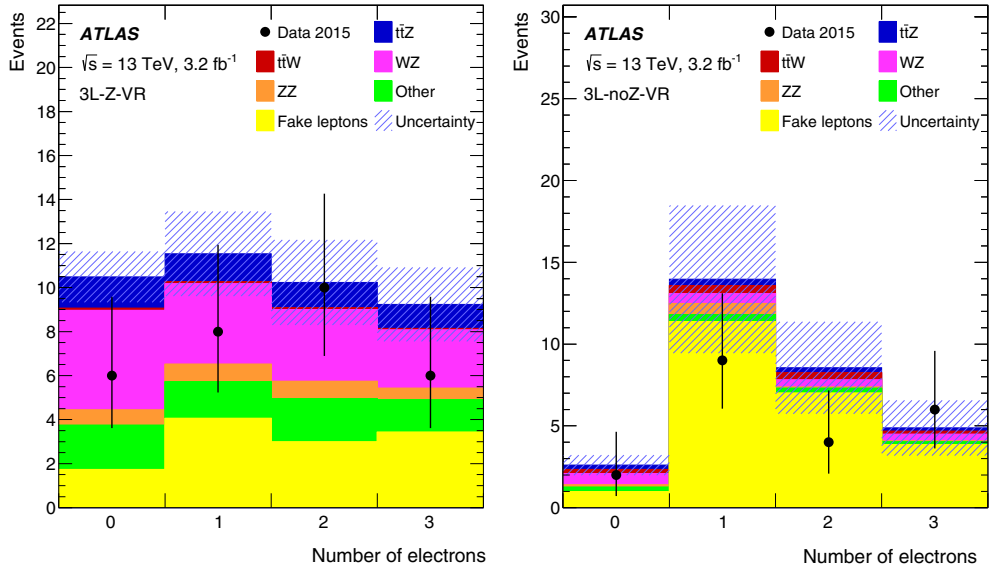

Fig. 3 Distributions of the number of electrons in the (*left*) 3ℓ-Z-VR and (*right*) 3ℓ-noZ-VR validation regions, shown before the fit. The background denoted 'Other' contains other SM processes producing three prompt leptons. The shaded band represents the total uncertainty

There must be exactly three jets, none of which pass the b-tagging requirement. With these requirements, the expected $t\bar{t}Z$ signal contribution is roughly 1% of the total number of events. This region is referred to as 3ℓ-WZ-CR and it is included in the fit. Distributions comparing data and SM prediction are shown in Fig. 2.

Two background validation regions are defined for the trilepton channel. In the first region, 3ℓ-Z-VR, the presence of two OSSF leptons with an invariant mass within 10 GeV of the mass of the Z boson is required. The region requires the events to have at most three jets where exactly one is b-tagged, or exactly two jets where both jets are b-tagged. The main backgrounds are WZ production and Z+jets events with fake leptons. In the second region, 3ℓ-noZ-VR, events with such a pair of leptons are vetoed. This region requires the events to have at most three jets where exactly one is b-tagged, and it is dominated by the fake-lepton background from top-quark pair production. Neither validation region is used in the fit. The distributions of the number of electrons in each of the two validation regions are shown in Fig. 3, demonstrating that data and background modelling are in good agreement within statistical uncertainties.

In total, 29 events are observed in the four signal regions. Distributions of the number of jets, number of b-tagged jets, missing transverse momentum and transverse momentum of the third lepton are shown in Fig. 4.

5.3 Tetralepton analysis

The tetralepton channel targets the $t\bar{t}Z$ process for the case where both W bosons resulting from top-quark decays and the Z boson decay leptonically. Events with two pairs of opposite-sign leptons are selected, and at least one pair must be of same flavour. The OSSF lepton pair with reconstructed invariant mass closest to m_Z is attributed to the Z boson decay and denoted in the following by Z_1. The two remaining leptons are used to define Z_2. Four signal regions are defined according to the relative flavour of the two Z_2 leptons, different flavour (DF) or same flavour (SF), and the number of b-tagged jets: one, or at least two ($1b$, $2b$). The signal regions are thus 4ℓ-DF-1b, 4ℓ-DF-2b, 4ℓ-SF-1b and 4ℓ-SF-2b.

To suppress events with fake leptons in the 1-b-tag multiplicity regions, additional requirements on the scalar sum of the transverse momenta of the third and fourth leptons ($p_{\mathrm{T}34}$) are imposed. In the 4ℓ-SF-1b and 4ℓ-DF-1b regions, events are required to satisfy $p_{\mathrm{T}34} > 25$ GeV and $p_{\mathrm{T}34} > 35$ GeV, respectively. In all regions, the invariant mass of any two reconstructed OS leptons is required to be larger than 10 GeV. The signal region definitions for the tetralepton channel are summarised in Table 3.

A control region used to constrain the ZZ normalisation, referred to as 4ℓ-ZZ-CR, is included in the fit and is defined to have exactly four reconstructed leptons, a Z_2 pair with

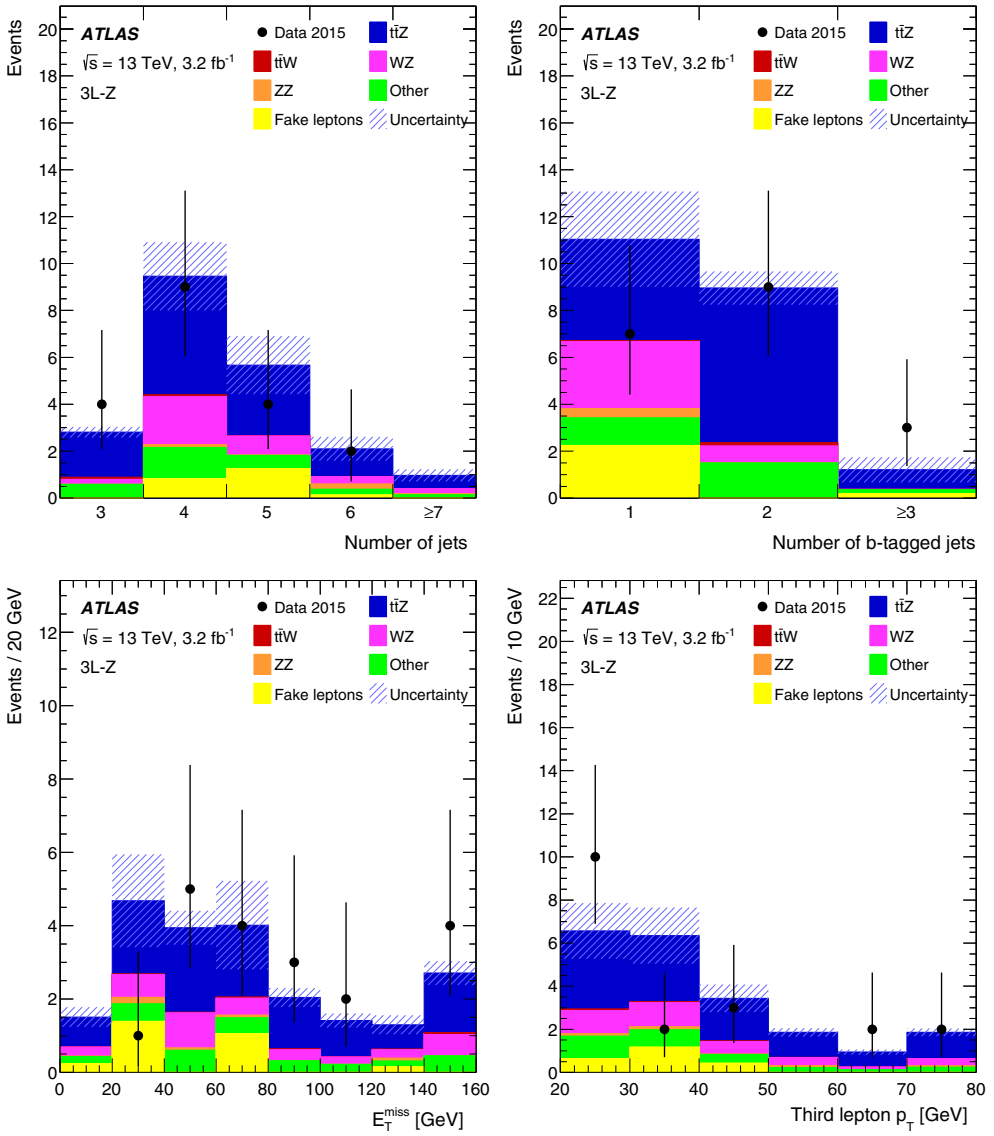

Fig. 4 Distributions of (*top left*) the number of jets, (*top right*) the number of b-tagged jets, (*bottom left*) the missing transverse momentum and (*bottom right*) the third-lepton p_{T}, for events contained in any of the three signal regions 3ℓ-Z-1b4j, 3ℓ-Z-2b3j or 3ℓ-Z-2b4j. The distributions are shown before the fit. The background denoted 'Other' contains other SM processes producing three prompt leptons. The shaded band represents the total uncertainty. The last bin in each of the distributions shown in the *bottom panels* includes the overflow

OSSF leptons, the value of both m_{Z_1} and m_{Z_2} within 10 GeV of the mass of the Z boson, and $E_{\mathrm{T}}^{\mathrm{miss}} < 40$ GeV. The leading lepton p_{T}, the invariant mass of the Z_2 lepton pair, the missing transverse momentum and the jet multiplicity in this control region are shown in Fig. 5, and good agreement is seen between data and prediction.

Table 3 Definitions of the four signal regions in the tetralepton channel. All leptons are required to satisfy $p_{\mathrm{T}} > 7$ GeV and at least one lepton with $p_{\mathrm{T}} > 25$ GeV is required to be trigger matched. The invariant mass of any two reconstructed OS leptons is required to be larger than 10 GeV

Region	Z_2 leptons	$p_{\mathrm{T}34}$	$\lvert m_{Z_2} - m_Z \rvert$	$E_{\mathrm{T}}^{\mathrm{miss}}$	$n_{b\text{-tags}}$
4ℓ-DF-1b	$e^{\pm}\mu^{\mp}$	>35 GeV	–	–	1
4ℓ-DF-2b	$e^{\pm}\mu^{\mp}$	–	–	–	≥ 2
4ℓ-SF-1b	$e^{\pm}e^{\mp}$, $\mu^{\pm}\mu^{\mp}$	>25 GeV	$\left\{\begin{array}{l}>10\,\mathrm{GeV}\\<10\,\mathrm{GeV}\end{array}\right.$	$\left\{\begin{array}{l}>40\,\mathrm{GeV}\\>80\,\mathrm{GeV}\end{array}\right.$	1
4ℓ-SF-2b	$e^{\pm}e^{\mp}$, $\mu^{\pm}\mu^{\mp}$	–	$\left\{\begin{array}{l}>10\,\mathrm{GeV}\\<10\,\mathrm{GeV}\end{array}\right.$	$\left\{\begin{array}{l}-\\>40\,\mathrm{GeV}\end{array}\right.$	≥ 2

The contribution from backgrounds containing fake leptons is estimated from simulation and corrected with scale factors determined in two control regions: one region enriched in $t\bar{t}$ events and thus in heavy-flavour jets, and one region enriched in Z+jets events, and thus in light-flavour jets. The scale factors are calibrated separately for electron and muon fake-lepton candidates. The scale factors are applied to all MC simulation events with fewer than four prompt leptons according to the number and the flavour of the fake leptons. The $t\bar{t}$ scale factors are applied to MC processes with real top quarks, while for all other processes the Z+jets scale factors are applied. Different generators are used when determining the scale factors and when applying them. It is verified that the uncertainties in the scale factors include the differences between these generators.

The expected yields in the signal and control regions in the tetralepton channel are shown in Table 4. Five events are observed in the four signal regions. Figure 6 shows the data superimposed to the expected distributions for all four signal regions combined. Overall the acceptance times efficiency for the $t\bar{t}Z$ and $t\bar{t}W$ processes is 6‰ and 2‰, respectively.

6 Systematic uncertainties

The normalisation of signal and background in each channel can be affected by several sources of systematic uncertainty. These are described in the following subsections.

6.1 Luminosity

The uncertainty in the integrated luminosity in the 2015 dataset is 2.1%. It is derived, following a methodology similar to that detailed in Ref. [68], from a calibration of the luminosity scale using x–y beam-separation scans performed in August 2015. This systematic uncertainty is applied to all processes modelled using Monte Carlo simulations.

6.2 Uncertainties associated with reconstructed objects

Uncertainties associated with the lepton selection arise from imperfect knowledge of the trigger, reconstruction, identification and isolation efficiencies, and lepton momentum scale and resolution [47–50,69]. The uncertainty in the electron identification efficiency is the largest systematic uncertainty in the trilepton channel and among the most important ones in the tetralepton channel.

Uncertainties associated with the jet selection arise from the jet energy scale (JES), the JVT requirement and the jet energy resolution (JER). Their estimations are based on Run-1 data and checked with early Run-2 data. The JES and its uncertainty are derived by combining information from test-beam data, collision data and simulation [70]. JES uncertainty components arising from the in-situ calibration and the jet flavour composition are among the dominant uncertainties in the 2μ-SS and trilepton channels. The uncertainties in the JER and JVT have a significant effect at low jet p_{T}. The JER uncertainty results in the second largest uncertainty in the trilepton channel.

The efficiency of the flavour-tagging algorithm is measured for each jet flavour using control samples in data and in simulation. From these measurements, correction factors are defined to correct the tagging rates in the simulation. In the case of b-jets, correction factors and their uncertainties are estimated based on observed and simulated b-tagging rates in $t\bar{t}$ dilepton events [62]. In the case of c-jets, they are derived based on jets with identified D^* mesons [71]. In the case of light-flavour jets, correction factors are derived using dijet events [71]. Sources of uncertainty affecting the b- and c-tagging efficiencies are considered as a function of jet p_{T}, including bin-to-bin correlations [62]. An additional uncertainty is assigned to account for the extrapolation of the b-tagging efficiency measurement from the p_{T} region used to determine the scale factors to regions with higher p_{T}. For the efficiency to tag light-flavour jets, the dependence of the uncertainty on the jet p_{T} and η is considered. These systematic uncertainties are taken as uncorrelated between b-jets, c-jets, and light-flavour jets.

The treatment of the uncertainties associated with reconstructed objects is common to all three channels, and thus these are considered as correlated among different regions.

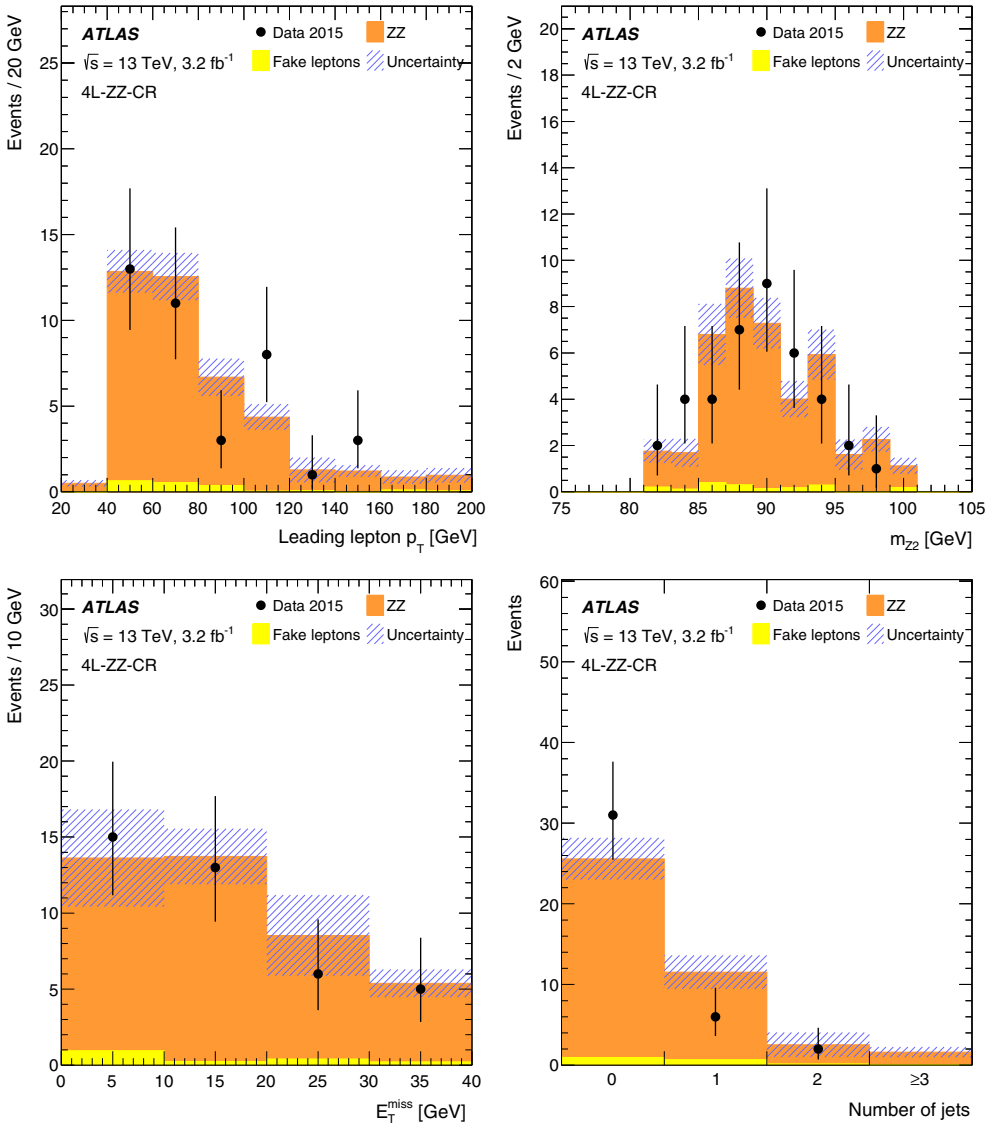

Fig. 5 (*Top left*) Leading lepton p_{T}, (*top right*) m_{Z_2}, (*bottom left*) missing transverse momentum and (*bottom right*) jet multiplicity distributions in the 4ℓ-ZZ-CR control region. The distributions are shown before the fit. The shaded band represents the total uncertainty. The last bin of the distribution shown in the *top left panel* includes the overflow

Table 4 Expected event yields for signal and backgrounds, and the observed data in all control and signal regions used in the fit to extract the $t\bar{t}Z$ and $t\bar{t}W$ cross sections. The quoted uncertainties in the expected event yields represent systematic uncertainties including MC statistical uncertainties. The tZ, tWZ, $t\bar{t}H$, three- and four-top-quark processes are denoted $t+X$. The WZ, ZZ, $H \to ZZ$ (ggF and VBF), HW and HZ and VBS processes are denoted 'Bosons'

Region	$t+X$	Bosons	Fake leptons	Total bkg.	$t\bar{t}W$	$t\bar{t}Z$	Data
3ℓ-WZ-CR	0.52 ± 0.13	26.9 ± 2.2	2.2 ± 1.8	29.5 ± 2.8	0.015 ± 0.004	0.80 ± 0.13	33
4ℓ-ZZ-CR	<0.001	39.5 ± 2.6	1.8 ± 0.6	41.2 ± 2.7	<0.001	0.026 ± 0.007	39
2μ-SS	0.94 ± 0.08	0.12 ± 0.05	1.5 ± 1.3	2.5 ± 1.3	2.32 ± 0.33	0.70 ± 0.10	9
3ℓ-Z-2b4j	1.08 ± 0.25	0.5 ± 0.4	<0.001	1.6 ± 0.5	0.065 ± 0.013	5.5 ± 0.7	8
3ℓ-Z-1b4j	1.14 ± 0.24	3.3 ± 2.2	2.2 ± 1.7	6.7 ± 2.8	0.036 ± 0.011	4.3 ± 0.6	7
3ℓ-Z-2b3j	0.58 ± 0.19	0.22 ± 0.18	<0.001	0.80 ± 0.26	0.083 ± 0.014	1.93 ± 0.28	4
3ℓ-noZ-2b	0.95 ± 0.11	0.14 ± 0.12	3.6 ± 2.2	4.7 ± 2.2	1.59 ± 0.28	1.45 ± 0.20	10
4ℓ-SF-1b	0.212 ± 0.032	0.09 ± 0.07	0.113 ± 0.022	0.42 ± 0.08	<0.001	0.66 ± 0.09	1
4ℓ-SF-2b	0.121 ± 0.021	0.07 ± 0.06	0.062 ± 0.012	0.25 ± 0.07	<0.001	0.63 ± 0.09	1
4ℓ-DF-1b	0.25 ± 0.04	0.0131 ± 0.0032	0.114 ± 0.019	0.37 ± 0.04	<0.001	0.75 ± 0.10	2
4ℓ-DF-2b	0.16 ± 0.05	<0.001	0.063 ± 0.013	0.23 ± 0.05	<0.001	0.64 ± 0.09	1

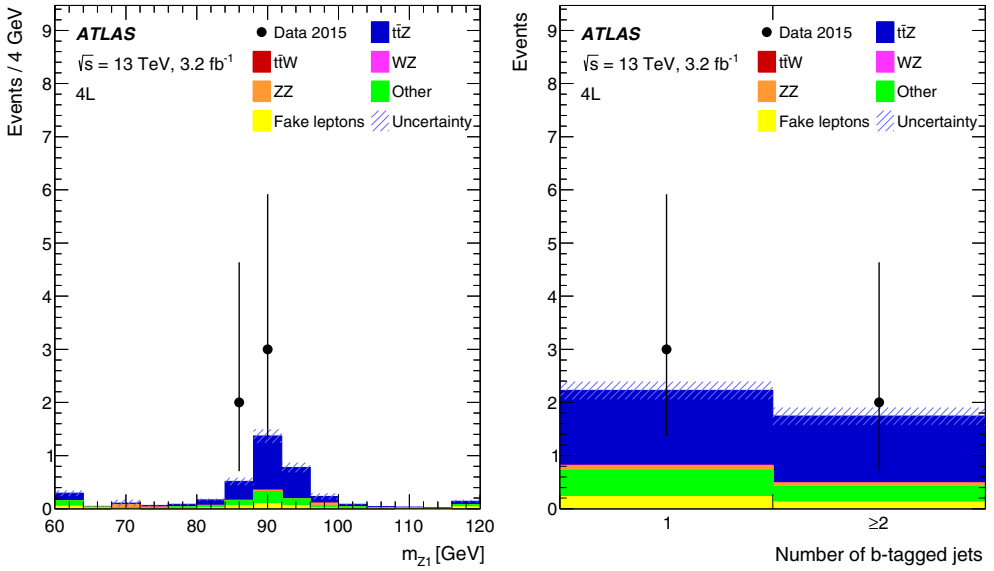

Fig. 6 Distributions (*left*) of the invariant mass of the OSSF lepton pair closest to the Z boson mass, m_{Z_1}, and (*right*) of the number of b-tagged jets, for events in the tetralepton signal regions. The distributions are shown before the fit. The background denoted 'Other' contains other SM processes producing four prompt leptons. The shaded band represents the total uncertainty. The first and last bin of the distribution shown in the *left panel* include the underflow and overflow, respectively

6.3 Uncertainties in signal modelling

From the nominal MG5_aMC+PYTHIA 8 (A14 tune) configuration, two parameters are varied to investigate uncertainties from the modelling of the $t\bar{t}Z$ and $t\bar{t}W$ processes: the renormalisation (μ_R) and factorisation (μ_F) scales. A simultaneous variation of $\mu_R = \mu_F$ by factors 2.0 and 0.5 is performed. In addition, the effects of a set of variations in the tune parameters (A14 eigentune variations), sensitive to initial- and final-state radiation, multiple parton interactions and colour reconnection, are evaluated. Studies performed at particle level show that the largest impact comes

from variations in initial-state radiation [26]. The systematic uncertainty due to the choice of generator for the $t\bar{t}Z$ and $t\bar{t}W$ signals is estimated by comparing the nominal sample with one generated with SHERPA v2.2. The SHERPA sample uses the LO matrix element with up to one (two) additional parton(s) included in the matrix element calculation for $t\bar{t}Z$ ($t\bar{t}W$) and merged with the SHERPA parton shower [72] using the ME+PS@LO prescription. The NNPDF3.0NLO PDF set is used in conjunction with a dedicated parton shower tune developed by the SHERPA authors. Signal modelling uncertainties are treated as correlated among channels.

6.4 Uncertainties in background modelling

In the trilepton and 2μ-SS channels, the diboson background is dominated by WZ production, while ZZ production is dominant in the tetralepton channel. While the inclusive cross sections for these processes are known to better than 10%, they contribute to the background in these channels if additional b-jets and other jets are produced and thus have a significantly larger uncertainty.

In the trilepton and 2μ-SS channels, the normalisation of the WZ background is treated as a free parameter in the fit used to extract the $t\bar{t}Z$ and $t\bar{t}W$ signals. The uncertainty in the extrapolation of the WZ background estimate from the control region to signal regions with specific jet and b-tag multiplicities is evaluated by comparing predictions obtained by varying the renormalisation, factorisation and resummation scales used in MC generation. The uncertainties vary across the different regions and an overall uncertainty of -50% and $+100\%$ is used.

The normalisation of the ZZ background is treated as a free parameter in the fit used to extract the $t\bar{t}Z$ and $t\bar{t}W$ signals. In the tetralepton channel, several uncertainties in the ZZ background estimate are considered. They arise from the extrapolation from the 4ℓ-ZZ-CR control region (corresponding to on-shell ZZ production) to the signal region (with off-shell ZZ background) and from the extrapolation from the control region without jets to the signal region with at least one jet. They are found to be 30% and 20%, respectively. An additional uncertainty of 10–30% is assigned to the normalisation of the heavy-flavour content of the ZZ background, based on a data-to-simulation comparison of events with one Z boson and additional jets and cross-checked with a comparison between different ZZ simulations [11].

The uncertainty in the $t\bar{t}H$ background is evaluated by varying the factorisation and renormalisation scales up and down by a factor of two with respect to the nominal value, $H_{\mathrm{T}}/2$, where H_{T} is defined as the scalar sum of the transverse masses $\sqrt{p_{\mathrm{T}}^2 + m^2}$ of all final state particles.

For the tZ background, an overall normalisation uncertainty of 50% is assumed. An additional uncertainty affecting the distribution of this background as a function of jet and b-jet multiplicity is evaluated by varying the factorisation and renormalisation scales, as well as the amount of radiation in the Perugia2012 parton-shower tune.

An uncertainty of $+10\%$ and -22% is assigned to the tWZ background cross section. The uncertainty is asymmetric due to an alternative estimate of the interference effect between this process and the $t\bar{t}Z$ production. The shape uncertainty is evaluated by varying the factorisation and renormalisation scales up and down by a factor of two with respect to the nominal value $H_{\mathrm{T}}/2$.

For other prompt-lepton backgrounds, uncertainties of 20% are assigned to the normalisations of the WH and ZH processes, based on calculations from Ref. [73]. An uncertainty of 50% is considered for triboson and same-sign WW processes.

The fake-lepton background uncertainty is evaluated as follows. The uncertainty due to the matrix method is estimated by propagating the statistical uncertainty on the measurement of the fake-lepton efficiencies. Additionally, a 20% uncertainty is added to the subtracted charge-flip yields estimated as the difference between data-driven charge-flips and simulation, and the $E_{\mathrm{T}}^{\mathrm{miss}}$ requirement used to enhance the single-fake-lepton fraction is varied by 20 GeV. The main sources of fake muons are decays of light-flavour or heavy-flavour hadrons inside jets. For the 2μ-SS region, the flavour composition of the jets faking leptons is assumed to be unknown. To cover this uncertainty, the central values of the fake-lepton efficiencies extracted from the b-veto and the b-tag control regions are used, with the efficiency difference assigned as an extra uncertainty. For the tetralepton channel, fake-lepton systematic uncertainties are covered by the scale-factor uncertainties used to calibrate the simulated fake-lepton yield in the control regions. Within a fake-lepton estimation method, all systematic uncertainties are considered to be correlated among analysis channels and regions. Thus 2μ-SS and trilepton fake-lepton systematic uncertainties that use the matrix method are not correlated with the tetralepton systematic uncertainties. The expected uncertainties in the fake-lepton backgrounds relative to the total backgrounds vary in each channel and signal region: 50% for the 2μ-SS region, 25–50% for the trilepton channel and 5–10% for the tetralepton channel.

7 Results

In order to extract the $t\bar{t}Z$ and $t\bar{t}W$ cross sections, nine signal regions (2μ-SS, 3ℓ-Z-1b4j, 3ℓ-Z-2b3j, 3ℓ-Z-2b4j, 3ℓ-noZ-2b, 4ℓ-DF-1b, 4ℓ-DF-2b, 4ℓ-SF-1b, 4ℓ-SF-2b) and two control regions (3ℓ-WZ-CR, 4ℓ-ZZ-CR) are simultaneously fitted. The 2μ-SS signal region is particularly sensitive to $t\bar{t}W$, the 3ℓ-noZ-2b signal region is sensitive to both, $t\bar{t}W$

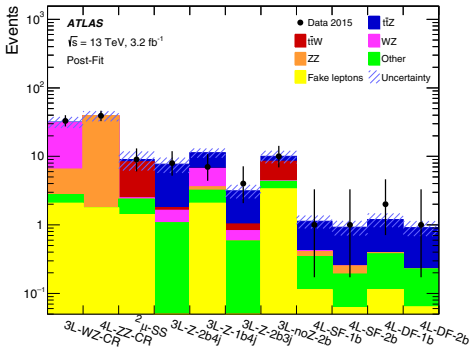

Fig. 7 Expected yields after the fit compared to data for the fit to extract $\sigma_{t\bar{t}Z}$ and $\sigma_{t\bar{t}W}$ in the signal regions and in the control regions used to constrain the WZ and ZZ backgrounds. The 'Other' background summarises all other backgrounds described in Sect. 3. The shaded band represents the total uncertainty

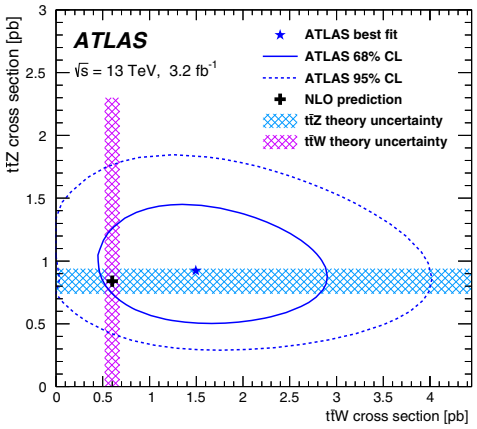

Fig. 8 The result of the simultaneous fit to the $t\bar{t}Z$ and $t\bar{t}W$ cross sections along with the 68 and 95% confidence level (CL) contours. The *shaded areas* correspond to the theoretical uncertainties in the Standard Model predictions, and include renormalisation and factorisation scale uncertainties as well as PDF uncertainties including α_S variations

and $t\bar{t}Z$, while all other signal regions aim at the determination of the $t\bar{t}Z$ cross section. The cross sections $\sigma_{t\bar{t}Z}$ and $\sigma_{t\bar{t}W}$ are determined using a binned maximum-likelihood fit to the numbers of events in these regions. The fit is based on the profile-likelihood technique, where systematic uncertainties are allowed to vary as nuisance parameters and take on their best-fit values. None of the uncertainties are found to be significantly constrained or pulled from their initial values. The calculation of confidence intervals and hypothesis testing is performed using a modified frequentist method as implemented in RooStats [74,75].

A summary of the fit to all regions used to measure the $t\bar{t}Z$ and $t\bar{t}W$ production cross sections are shown in Fig. 7. The normalisation corrections for the WZ and ZZ backgrounds with respect to the Standard Model predictions are obtained from the fits as described in Sect. 5 and found to be compatible with unity: 1.11 ± 0.30 for the WZ background and 0.94 ± 0.17 for the ZZ background.

The results of the fit are $\sigma_{t\bar{t}Z} = 0.92 \pm 0.29$ (stat.) $\pm$ 0.10 (syst.) pb and $\sigma_{t\bar{t}W} = 1.50 \pm 0.72$ (stat.) ± 0.33 (syst.) pb with a correlation of -0.13 and are shown in Fig. 8. The fit yields significances of 3.9σ and 2.2σ over the background-only hypothesis for the $t\bar{t}Z$ and $t\bar{t}W$ processes, respectively. The expected significances are 3.4σ for $t\bar{t}Z$ and 1.0σ for $t\bar{t}W$ production. The significance values are computed using the asymptotic approximation described in Ref. [76]. In the two channels most sensitive to the $t\bar{t}W$ signal the observed relative number of events with two positively or two negatively charged leptons is compatible with expectation. In the 3ℓ-noZ-2b channel the observed distribution of the number of events with a given amount of electrons and muons match expectation, as well.

Table 5 shows the leading and total uncertainties in the measured $t\bar{t}Z$ and $t\bar{t}W$ cross sections. In estimating the uncertainties for $t\bar{t}Z$ ($t\bar{t}W$), the cross section for $t\bar{t}W$ ($t\bar{t}Z$) is fixed to its Standard Model value. For both processes, the precision of the measurement is dominated by statistical uncertainties. For the $t\bar{t}Z$ determination, the different sources contribute with similar size to the total systematic uncertainty. For the $t\bar{t}W$ determination, the dominant systematic uncertainty source is the limited amount of data available for the estimation of the fake leptons.

Table 5 List of dominant and total uncertainties in the measured cross sections of the $t\bar{t}Z$ and $t\bar{t}W$ processes from the fit. All uncertainties are symmetrised

Uncertainty	$\sigma_{t\bar{t}Z}$(%)	$\sigma_{t\bar{t}W}$(%)
Luminosity	2.6	3.1
Reconstructed objects	8.3	9.3
Backgrounds from simulation	5.3	3.1
Fake leptons and charge misID	3.0	19
Signal modelling	2.3	4.2
Total systematic	11	22
Statistical	31	48
Total	32	53

8 Conclusion

Measurements of the production cross sections of a top-quark pair in association with a Z or W boson using 3.2 fb^{-1} of

data collected by the ATLAS detector in $\sqrt{s} = 13$ TeV pp collisions at the LHC are presented. Final states with either two same-charge muons, or three or four leptons are analysed. From a simultaneous fit to nine signal regions and two control regions, the $t\bar{t}Z$ and $t\bar{t}W$ production cross sections are determined to be $\sigma_{t\bar{t}Z} = 0.9 \pm 0.3$ pb and $\sigma_{t\bar{t}W} = 1.5 \pm 0.8$ pb. Both measurements are consistent with the NLO QCD theoretical calculations, $\sigma_{t\bar{t}Z} = 0.84 \pm 0.09$ pb and $\sigma_{t\bar{t}W} = 0.60 \pm 0.08$ pb.

Acknowledgements We thank CERN for the very successful operation of the LHC, as well as the support staff from our institutions without whom ATLAS could not be operated efficiently.
We acknowledge the support of ANPCyT, Argentina; YerPhI, Armenia; ARC, Australia; BMWFW and FWF, Austria; ANAS, Azerbaijan; SSTC, Belarus; CNPq and FAPESP, Brazil; NSERC, NRC and CFI, Canada; CERN; CONICYT, Chile; CAS, MOST and NSFC, China; COLCIENCIAS, Colombia; MSMT CR, MPO CR and VSC CR, Czech Republic; DNRF and DNSRC, Denmark; IN2P3-CNRS, CEA-DSM/IRFU, France; GNSF, Georgia; BMBF, HGF, and MPG, Germany; GSRT, Greece; RGC, Hong Kong SAR, China; ISF, I-CORE and Benoziyo Center, Israel; INFN, Italy; MEXT and JSPS, Japan; CNRST, Morocco; FOM and NWO, Netherlands; RCN, Norway; MNiSW and NCN, Poland; FCT, Portugal; MNE/IFA, Romania; MES of Russia and NRC KI, Russian Federation; JINR; MESTD, Serbia; MSSR, Slovakia; ARRS and MIZŠ, Slovenia; DST/NRF, South Africa; MINECO, Spain; SRC and Wallenberg Foundation, Sweden; SERI, SNSF and Cantons of Bern and Geneva, Switzerland; MOST, Taiwan; TAEK, Turkey; STFC, United Kingdom; DOE and NSF, United States of America. In addition, individual groups and members have received support from BCKDF, the Canada Council, CANARIE, CRC, Compute Canada, FQRNT, and the Ontario Innovation Trust, Canada; EPLANET, ERC, FP7, Horizon 2020 and Marie Skłodowska-Curie Actions, European Union; Investissements d'Avenir Labex and Idex, ANR, Région Auvergne and Fondation Partager le Savoir, France; DFG and AvH Foundation, Germany; Herakleitos, Thales and Aristeia programmes co-financed by EU-ESF and the Greek NSRF; BSF, GIF and Minerva, Israel; BRF, Norway; Generalitat de Catalunya, Generalitat Valenciana, Spain; the Royal Society and Leverhulme Trust, United Kingdom.
The crucial computing support from all WLCG partners is acknowledged gratefully, in particular from CERN, the ATLAS Tier-1 facilities at TRIUMF (Canada), NDGF (Denmark, Norway, Sweden), CC-IN2P3 (France), KIT/GridKA (Germany), INFN-CNAF (Italy), NL-T1 (Netherlands), PIC (Spain), ASGC (Taiwan), RAL (UK) and BNL (USA), the Tier-2 facilities worldwide and large non-WLCG resource providers. Major contributors of computing resources are listed in Ref. [77].

Funded by SCOAP[3].

References

1. ATLAS Collaboration, Measurement of the $t\bar{t}$ production cross-section using $e\mu$ events with b-tagged jets in pp collisions at $\sqrt{s} =$ 13 TeV with the ATLAS detector. Phys. Lett. B **761**, 136 (2016). doi:10.1016/j.physletb.2016.08.019, arXiv:1606.02699 [hep-ex]
2. CMS Collaboration, Measurement of the top quark pair production cross section in proton-proton collisions at $\sqrt{s} = 13$ TeV Phys. Rev. Lett. **116**, 052002 (2016). doi:10.1103/PhysRevLett.116.052002. arXiv:1510.05302 [hep-ex]
3. J.A. Aguilar-Saavedra, Identifying top partners at LHC. JHEP **11**, 030 (2009). doi:10.1088/1126-6708/2009/11/030. arXiv:0907.3155 [hep-ph]
4. J.A. Aguilar-Saavedra et al., Handbook of vectorlike quarks: mixing and single production. Phys. Rev. D **88**, 094010 (2013). doi:10.1103/PhysRevD.88.094010. arXiv:1306.0572 [hep-ph]
5. M. Perelstein, Little Higgs models and their phenomenology. Prog. Part. Nucl. Phys. **58**, 247 (2007). doi:10.1016/j.ppnp.2006.04.001. arXiv:hep-ph/0512128
6. R.S. Chivukula, S.B. Selipsky, E.H. Simmons, Nonoblique effects in the $Zb\bar{b}$ vertex from ETC dynamics. Phys. Rev. Lett. **69**, 575 (1992). doi:10.1103/PhysRevLett.69.575. arXiv:hep-ph/9204214
7. R.S. Chivukula, E.H. Simmons, J. Terning, A heavy top quark and the $Zb\bar{b}$ vertex in noncommuting extended technicolor. Phys. Lett. B **331**, 383 (1994). doi:10.1016/0370-2693(94)91068-5. arXiv:hep-ph/9404209
8. K. Hagiwara, N. Kitazawa, Extended technicolor contribution to the Zbb vertex. Phys. Rev. D **52**, 5374 (1995). doi:10.1103/PhysRevD.52.5374. arXiv:hep-ph/9504332
9. U. Mahanta, Noncommuting ETC corrections to $Zt\bar{t}$ vertex. Phys. Rev. D **55**, 5848 (1997). doi:10.1103/PhysRevD.55.5848. arXiv:hep-ph/9611289
10. U. Mahanta, Probing noncommuting ETC effects by $e^+e^- \to t\bar{t}$ at NLC. Phys. Rev. D **56**, 402 (1997). doi:10.1103/PhysRevD.56.402
11. ATLAS Collaboration, Measurement of the $t\bar{t}W$ and $t\bar{t}Z$ production cross sections in pp collisions at $\sqrt{s} = 8$ TeV with the ATLAS detector. JHEP **11**, 172 (2015). doi:10.1007/JHEP11(2015)172, arXiv:1509.05276 [hep-ex]
12. CMS Collaboration, Observation of top quark pairs produced in association with a vector boson in pp collisions at $\sqrt{s} = 8$ TeV. JHEP **01**, 096 (2016). doi:10.1007/JHEP01(2016)096, arXiv:1510.01131 [hep-ex]
13. S. Frixione et al., Electroweak and QCD corrections to top-pair hadroproduction in association with heavy bosons. JHEP **06**, 184 (2015). doi:10.1007/JHEP06(2015)184. arXiv:1504.03446 [hep-ph]
14. J. Alwall et al., The automated computation of tree-level and next-to-leading order differential cross sections, and their matching to parton shower simulations. JHEP **07**, 079 (2014). doi:10.1007/JHEP07(2014)079. arXiv:1405.0301 [hep-ph]
15. ATLAS Collaboration, The ATLAS experiment at the CERN Large Hadron Collider. JINST **3**, S08003 (2008). doi:10.1088/1748-0221/3/08/S08003
16. ATLAS Collaboration, ATLAS Insertable B-Layer Technical Design Report, ATLAS-TDR-19,2010. http://cds.cern.ch/record/1291633, ATLAS Insertable B-Layer Technical Design Report Addendum, ATLAS-TDR-19-ADD-1,2012. http://cds.cern.ch/record/1451888
17. ATLAS Collaboration, Luminosity determination in pp collisions at $\sqrt{s} = 8$ TeV using the ATLAS detector at the LHC. Eur. Phys. J. C **76**, 653 (2016). doi:10.1140/epjc/s10052-016-4466-1. arXiv:1608.03953 [hep-ex]
18. D.J. Lange, The EvtGen particle decay simulation package. Nucl. Instrum. Meth. A **462**, 152 (2001). doi:10.1016/S0168-9002(01)00089-4
19. ATLAS Collaboration, The ATLAS simulation infrastructure. Eur. Phys. J. C **70**, 823 (2010). doi:10.1140/epjc/s10052-010-1429-9, arXiv:1005.4568 [hep-ex]

20. S. Agostinelli et al., GEANT4—a simulation toolkit. Nucl. Instrum. Meth. A **506**, 250 (2003). doi:10.1016/S0168-9002(03)01368-8
21. ATLAS Collaboration, The simulation principle and performance of the ATLAS fast calorimeter simulation FastCaloSim, ATL-PHYS-PUB-2010-013 (2010). http://cds.cern.ch/record/1300517
22. T. Sjöstrand et al., An introduction to PYTHIA 8.2. Comput. Phys. Commun. **191**, 159 (2015). doi:10.1016/j.cpc.2015.01.024. arXiv:1410.3012 [hep-ph]
23. ATLAS Collaboration, Further ATLAS tunes of PYTHIA 6 and PYTHIA 8, ATL-PHYS-PUB-2011-014 (2011). http://cds.cern.ch/record/1400677
24. ATLAS Collaboration, ATLAS PYTHIA 8 tunes to 7 TeV data, ATL-PHYS-PUB-2014-021 (2014). http://cdsweb.cern.ch/record/1966419
25. R.D. Ball et al., Parton distributions with LHC data. Nucl. Phys. B **867**, 244 (2013). doi:10.1016/j.nuclphysb.2012.10.003. arXiv:1207.1303 [hep-ph]
26. ATLAS Collaboration, Modelling of the $t\bar{t}H$ and $t\bar{t}V$ ($V = W, Z$) processes for $\sqrt{s} = 13$ TeV ATLAS analyses, ATL-PHYS-PUB-2016-005 (2016). http://cds.cern.ch/record/2120826
27. T. Sjöstrand, S. Mrenna, P.Z. Skands, PYTHIA 6.4 Physics and Manual. JHEP **05**, 026 (2006). doi:10.1088/1126-6708/2006/05/026, arXiv:hep-ph/0603175
28. J. Pumplin et al., New generation of parton distributions with uncertainties from global QCD analysis. JHEP **07**, 012 (2002). doi:10.1088/1126-6708/2002/07/012. arXiv:hep-ph/0201195
29. P.Z. Skands, Tuning Monte Carlo generators: the Perugia tunes. Phys. Rev. D **82**, 074018 (2010). doi:10.1103/PhysRevD.82.074018. arXiv:1005.3457 [hep-ph]
30. R.D. Ball et al., Parton distributions for the LHC Run II. JHEP **04**, 040 (2015). doi:10.1007/JHEP04(2015)040. arXiv:1410.8849 [hep-ph]
31. T. Gleisberg et al., Event generation with SHERPA 1.1. JHEP **02**, 007 (2009). doi:10.1088/1126-6708/2009/02/007, arXiv:0811.4622 [hep-ph]
32. T. Gleisberg, S. Höche, Comix, a new matrix element generator. JHEP **12**, 039 (2008). doi:10.1088/1126-6708/2008/12/039. arXiv:0808.3674 [hep-ph]
33. F. Cascioli, P. Maierhofer, S. Pozzorini, Scattering amplitudes with open loops. Phys. Rev. Lett. **108**, 111601 (2012). doi:10.1103/PhysRevLett.108.111601. arXiv:1111.5206 [hep-ph]
34. S. Höche et al., QCD matrix elements + parton showers: the NLO case. JHEP **04**, 027 (2013). doi:10.1007/JHEP04(2013)027. arXiv:1207.5030 [hep-ph]
35. H.-L. Lai et al., New parton distributions for collider physics. Phys. Rev. D **82**, 074024 (2010). doi:10.1103/PhysRevD.82.074024. arXiv:1007.2241
36. S. Alioli et al., A general framework for implementing NLO calculations in shower Monte Carlo programs: the POWHEG BOX. JHEP **06**, 043 (2010). doi:10.1007/JHEP06043. arXiv:1002.2581 [hep-ph]
37. ATLAS Collaboration, Measurement of the Z/γ^* boson transverse momentum distribution in pp collisions at $\sqrt{s} = 7$ TeV with the ATLAS detector. JHEP **09**, 145 (2014). doi:10.1007/JHEP09(2014)145, arXiv:1406.3660 [hep-ex]
38. M. Czakon, A. Mitov, Top++: a program for the calculation of the top-pair cross-section at hadron colliders. Comput. Phys. Commun. **185**, 2930 (2014). doi:10.1016/j.cpc.2014.06.021. arXiv:1112.5675 [hep-ph]
39. E. Re, Single-top Wt-channel production matched with parton showers using the POWHEG method. Eur. Phys. J. C **71**, 1547 (2011). doi:10.1140/epjc/s10052-011-1547-z. arXiv:1009.2450 [hep-ph]
40. D. de Florian et al., Handbook of LHC Higgs cross sections: 4. Deciphering the nature of the Higgs sector (2016). arXiv:1610.07922 [hep-ph]
41. C. Anastasiou et al., High precision QCD at hadron colliders: Electroweak gauge boson rapidity distributions at NNLO. Phys. Rev. D **69**, 094008 (2004). doi:10.1103/PhysRevD.69.094008. arXiv:hep-ph/0312266
42. R. Gavin et al., FEWZ 2.0: A code for hadronic Z production at next-to-next-to-leading order. Comput. Phys. Commun. **182**, 2388 (2011). doi:10.1016/j.cpc.2011.06.008. arXiv:1011.3540 [hep-ph]
43. R. Gavin et al., W Physics at the LHC with FEWZ 2.1. Comput. Phys. Commun. **184**, 208 (2013). doi:10.1016/j.cpc.2012.09.005. arXiv:1201.5896 [hep-ph]
44. Y. Li, F. Petriello, Combining QCD and electroweak corrections to dilepton production in FEWZ. Phys. Rev. D **86**, 094034 (2012). doi:10.1103/PhysRevD.86.094034. arXiv:1208.5967 [hep-ph]
45. V. Barger, W.-Y. Keung, B. Yencho, Triple-top signal of new physics at the LHC. Phys. Lett. B **687**, 70 (2010). doi:10.1016/j.physletb.2010.03.001. arXiv:1001.0221 [hep-ph]
46. G. Bevilacqua, M. Worek, Constraining BSM Physics at the LHC: four top final states with NLO accuracy in perturbative QCD. JHEP **07**, 111 (2012). doi:10.1007/JHEP07(2012)111. arXiv:1206.3064 [hep-ph]
47. ATLAS Collaboration, Electron reconstruction and identification efficiency measurements with the ATLAS detector using the 2011 LHC proton–proton collision data. Eur. Phys. J. C **74**, 2941 (2014). doi:10.1140/epjc/s10052-014-2941-0, arXiv:1404.2240 [hep-ex]
48. ATLAS Collaboration, Electron efficiency measurements with the ATLAS detector using the 2012 LHC proton–proton collision data, ATLAS-CONF-2014-032 (2014). http://cdsweb.cern.ch/record/1706245
49. ATLAS Collaboration, Electron identification measurements in ATLAS using $\sqrt{s} = 13$ TeV data with 50 ns bunch spacing, ATL-PHYS-PUB-2015-041 (2015). http://cdsweb.cern.ch/record/2048202
50. ATLAS Collaboration, Muon reconstruction performance of the ATLAS detector in proton–proton collision data at $\sqrt{s} = 13$ TeV. Eur. Phys. J. C **76**, 292 (2016). doi:10.1140/epjc/s10052-016-4120-y, arXiv:1603.05598 [hep-ex]
51. M. Cacciari, G.P. Salam, G. Soyez, The anti-k_t jet clustering algorithm. JHEP **04**, 063 (2008). doi:10.1088/1126-6708/2008/04/063. arXiv:0802.1189 [hep-ph]
52. M. Cacciari, G.P. Salam, Dispelling the N^3 myth for the k_t jet-finder. Phys. Lett. B **641**, 57 (2006). doi:10.1016/j.physletb.2006.08.037. arXiv:hep-ph/0512210
53. ATLAS Collaboration, Topological cell clustering in the ATLAS calorimeters and its performance in LHC Run 1, (2016), arXiv:1603.02934 [hep-ex]
54. M. Cacciari, G.P. Salam, G. Soyez, The catchment area of jets. JHEP **04**, 005 (2008). doi:10.1088/1126-6708/2008/04/005. arXiv:0802.1188 [hep-ph]
55. ATLAS Collaboration, Jet global sequential corrections with the ATLAS detector in proton–proton collisions at $\sqrt{s} = 8$ TeV, ATLAS-CONF-2015-002 (2015). http://cdsweb.cern.ch/record/2001682
56. ATLAS Collaboration, Jet energy measurement with the ATLAS detector in proton–proton collisions at $\sqrt{s} = 7$ TeV, Eur. Phys. J. C **73** (2013) 2304, doi:10.1140/epjc/s10052-013-2304-2, arXiv:1112.6426 [hep-ex]
57. ATLAS Collaboration, Monte Carlo calibration and combination of in-situ measurements of jet energy scale, jet energy resolution and jet mass in ATLAS, ATLAS-CONF-2015-037 (2015). http://cdsweb.cern.ch/record/2044941
58. ATLAS Collaboration, Jet calibration and systematic uncertainties for jets reconstructed in the ATLAS detector at $\sqrt{s} = 13$ TeV, ATL-PHYS-PUB-2015-015 (2015). http://cds.cern.ch/record/2037613

59. ATLAS Collaboration, Performance of pile-up mitigation techniques for jets in pp collisions at $\sqrt{s} = 8$ TeV using the ATLAS detector. Eur. Phys. J. C **76**, 581 (2016). doi:10.1140/epjc/s10052-016-4395-1. arXiv:1510.03823 [hep-ex]
60. ATLAS Collaboration, Performance of b-jet identification in the ATLAS experiment. JINST **11**, P04008 (2016). doi:10.1088/1748-0221/11/04/P04008, arXiv:1512.01094 [hep-ex]
61. ATLAS Collaboration, Expected performance of the ATLAS b-tagging algorithms in Run-2, ATL-PHYS-PUB-2015-022 (2015). http://cdsweb.cern.ch/record/2037697
62. ATLAS Collaboration, Calibration of b-tagging using dileptonic top pair events in a combinatorial likelihood approach with the ATLAS experiment, ATLAS-CONF-2014-004 (2014). http://cdsweb.cern.ch/record/1664335
63. ATLAS Collaboration, Commissioning of the ATLAS b-tagging algorithms using $t\bar{t}$ events in early Run-2 data, ATL-PHYS-PUB-2015-039 (2015). http://cdsweb.cern.ch/record/2047871
64. ATLAS Collaboration, Performance of missing transverse momentum reconstruction in proton–proton collisions at $\sqrt{s} = 7$ TeV with ATLAS. Eur. Phys. J. C **72**, 1844 (2012). doi:10.1140/epjc/s10052-011-1844-6, arXiv:1108.5602 [hep-ex]
65. ATLAS Collaboration, Performance of missing transverse momentum reconstruction with the ATLAS detector in the first proton–proton collisions at $\sqrt{s} = 13$ TeV, ATL-PHYS-PUB-2015-027 (2015). http://cdsweb.cern.ch/record/2037904
66. ATLAS Collaboration, Expected performance of missing transverse momentum reconstruction for the ATLAS detector at $\sqrt{s} = 13$ TeV, ATL-PHYS-PUB-2015-023 (2015). http://cdsweb.cern.ch/record/2037700
67. ATLAS Collaboration, Measurement of the top quark-pair production cross section with ATLAS in pp collisions at $\sqrt{s} = 7$ TeV. Eur. Phys. J. C **71** (2011) 1577. doi:10.1140/epjc/s10052-011-1577-6, arXiv:1012.1792 [hep-ex]
68. ATLAS Collaboration, Improved luminosity determination in pp collisions at $\sqrt{s} = 7$ TeV using the ATLAS detector at the LHC. Eur. Phys. J. C **73** (2013) 2518, doi:10.1140/epjc/s10052-013-2518-3, arXiv:1302.4393 [hep-ex]
69. ATLAS Collaboration, Expected electron performance in the ATLAS experiment, ATL-PHYS-PUB-2011-006 (2011). http://cdsweb.cern.ch/record/1345327
70. ATLAS Collaboration, Jet energy measurement and its systematic uncertainty in proton–proton collisions at $\sqrt{s} = 7$ TeV with the ATLAS detector. Eur. Phys. J. C **75**, 17 (2015). doi:10.1140/epjc/s10052-014-3190-y, arXiv:1406.0076 [hep-ex]
71. ATLAS Collaboration, Calibration of the performance of b-tagging for c and light-flavour jets in the 2012 ATLAS data, ATLAS-CONF-2014-046 (2014). http://cdsweb.cern.ch/record/1741020
72. S. Schumann, F. Krauss, A parton shower algorithm based on Catani–Seymour dipole factorisation. JHEP **03**, 038 (2008). doi:10.1088/1126-6708/2008/03/038. arXiv:0709.1027 [hep-ph]
73. S Heinemeyer et al., Handbook of LHC Higgs cross sections: 3. Higgs Properties. arXiv:1307.1347 [hep-ph]
74. W. Verkerke, D. Kirkby, 'The RooFit toolkit for data modeling'. arXiv:physics/0306116
75. W. Verkerke, D. Kirkby, RooFit Users Manual v2.91. http://rootfit.sourceforge.net
76. G. Cowan et al., Asymptotic formulae for likelihood-based tests of new physics. Eur. Phys. J. C **71** (2011) 1554 (Erratum: C **73** (2013) 2501, doi:10.1140/epjc/s10052-011-1554-0, 10.1140/epjc/s10052-013-2501-z, arXiv:1007.1727)
77. ATLAS Collaboration, ATLAS computing acknowledgements 2016–2017, ATL-GEN-PUB-2016-002 (2016). http://cds.cern.ch/record/2202407

ATLAS Collaboration

M. Aaboud[137d], G. Aad[88], B. Abbott[115], J. Abdallah[66], O. Abdinov[12], B. Abeloos[119], R. Aben[109], O. S. AbouZeid[139], N. L. Abraham[153], H. Abramowicz[157], H. Abreu[156], R. Abreu[118], Y. Abulaiti[150a,150b], B. S. Acharya[167a,167b,a], L. Adamczyk[40a], D. L. Adams[27], J. Adelman[110], S. Adomeit[102], T. Adye[133], A. A. Affolder[77], T. Agatonovic-Jovin[14], J. Agricola[56], J. A. Aguilar-Saavedra[128a,128f], S. P. Ahlen[24], F. Ahmadov[68,b], G. Aielli[135a,135b], H. Akerstedt[150a,150b], T. P. A. Åkesson[84], A. V. Akimov[98], G. L. Alberghi[22a,22b], J. Albert[172], S. Albrand[57], M. J. Alconada Verzini[74], M. Aleksa[32], I. N. Aleksandrov[68], C. Alexa[28b], G. Alexander[157], T. Alexopoulos[10], M. Alhroob[115], B. Ali[130], M. Aliev[76a,76b], G. Alimonti[94a], J. Alison[33], S. P. Alkire[37], B. M. M. Allbrooke[153], B. W. Allen[118], P. P. Allport[19], A. Aloisio[106a,106b], A. Alonso[38], F. Alonso[74], C. Alpigiani[140], M. Alstaty[88], B. Alvarez Gonzalez[32], D. Álvarez Piqueras[170], M. G. Alviggi[106a,106b], B. T. Amadio[16], K. Amako[69], Y. Amaral Coutinho[26a], C. Amelung[25], D. Amidei[92], S. P. Amor Dos Santos[128a,128c], A. Amorim[128a,128b], S. Amoroso[32], G. Amundsen[25], C. Anastopoulos[143], L. S. Ancu[51], N. Andari[110], T. Andeen[11], C. F. Anders[61b], G. Anders[32], J. K. Anders[77], K. J. Anderson[33], A. Andreazza[94a,94b], V. Andrei[61a], S. Angelidakis[9], I. Angelozzi[109], P. Anger[46], A. Angerami[37], F. Anghinolfi[32], A. V. Anisenkov[111,c], N. Anjos[13], A. Annovi[126a,126b], C. Antel[61a], M. Antonelli[49], A. Antonov[100,*], F. Anulli[134a], M. Aoki[69], L. Aperio Bella[19], G. Arabidze[93], Y. Arai[69], J. P. Araque[128a], A. T. H. Arce[47], F. A. Arduh[74], J.-F. Arguin[97], S. Argyropoulos[66], M. Arik[20a], A. J. Armbruster[147], L. J. Armitage[79], O. Arnaez[32], H. Arnold[50], M. Arratia[30], O. Arslan[23], A. Artamonov[99], G. Artoni[122], S. Artz[86], S. Asai[159], N. Asbah[44], A. Ashkenazi[157], B. Åsman[150a,150b], L. Asquith[153], K. Assamagan[27], R. Astalos[148a], M. Atkinson[169], N. B. Atlay[145], K. Augsten[130], G. Avolio[32], B. Axen[16], M. K. Ayoub[119], G. Azuelos[97,d], M. A. Baak[32], A. E. Baas[61a], M. J. Baca[19], H. Bachacou[138], K. Bachas[76a,76b], M. Backes[32], M. Backhaus[32], P. Bagiacchi[134a,134b], P. Bagnaia[134a,134b], Y. Bai[35a], J. T. Baines[133], O. K. Baker[179], E. M. Baldin[111,c], P. Balek[131], T. Balestri[152], F. Balli[138], W. K. Balunas[124], E. Banas[41], Sw. Banerjee[176,e], A. A. E. Bannoura[178], L. Barak[32], E. L. Barberio[91], D. Barberis[52a,52b], M. Barbero[88], T. Barillari[103], T. Barklow[147], N. Barlow[30], S. L. Barnes[87], B. M. Barnett[133], R. M. Barnett[16], Z. Barnovska-Blenessy[5], A. Baroncelli[136a], G. Barone[25], A. J. Barr[122], L. Barranco Navarro[170], F. Barreiro[85], J. Barreiro Guimarães da Costa[35a], R. Bartoldus[147], A. E. Barton[75], P. Bartos[148a], A. Basalaev[125], A. Bassalat[119,f],

R. L. Bates[55], S. J. Batista[162], J. R. Batley[30], M. Battaglia[139], M. Bauce[134a,134b], F. Bauer[138], H. S. Bawa[147,g], J. B. Beacham[113], M. D. Beattie[75], T. Beau[83], P. H. Beauchemin[165], P. Bechtle[23], H. P. Beck[18,h], K. Becker[122], M. Becker[86], M. Beckingham[173], C. Becot[112], A. J. Beddall[20d], A. Beddall[20b], V. A. Bednyakov[68], M. Bedognetti[109], C. P. Bee[152], L. J. Beemster[109], T. A. Beermann[32], M. Begel[27], J. K. Behr[44], C. Belanger-Champagne[90], A. S. Bell[81], G. Bella[157], L. Bellagamba[22a], A. Bellerive[31], M. Bellomo[89], K. Belotskiy[100], O. Beltramello[32], N. L. Belyaev[100], O. Benary[157,*], D. Benchekroun[137a], M. Bender[102], K. Bendtz[150a,150b], N. Benekos[10], Y. Benhammou[157], E. Benhar Noccioli[179], J. Benitez[66], D. P. Benjamin[47], J. R. Bensinger[25], S. Bentvelsen[109], L. Beresford[122], M. Beretta[49], D. Berge[109], E. Bergeaas Kuutmann[168], N. Berger[5], J. Beringer[16], S. Berlendis[57], N. R. Bernard[89], C. Bernius[112], F. U. Bernlochner[23], T. Berry[80], P. Berta[131], C. Bertella[86], G. Bertoli[150a,150b], F. Bertolucci[126a,126b], I. A. Bertram[75], C. Bertsche[44], D. Bertsche[115], G. J. Besjes[38], O. Bessidskaia Bylund[150a,150b], M. Bessner[44], N. Besson[138], C. Betancourt[50], S. Bethke[103], A. J. Bevan[79], W. Bhimji[16], R. M. Bianchi[127], L. Bianchini[25], M. Bianco[32], O. Biebel[102], D. Biedermann[17], R. Bielski[87], N. V. Biesuz[126a,126b], M. Biglietti[136a], J. Bilbao De Mendizabal[51], H. Bilokon[49], M. Bindi[56], S. Binet[119], A. Bingul[20b], C. Bini[134a,134b], S. Biondi[22a,22b], D. M. Bjergaard[47], C. W. Black[154], J. E. Black[147], K. M. Black[24], D. Blackburn[140], R. E. Blair[6], J.-B. Blanchard[138], J. E. Blanco[80], T. Blazek[148a], I. Bloch[44], C. Blocker[25], W. Blum[86,*], U. Blumenschein[56], S. Blunier[34a], G. J. Bobbink[109], V. S. Bobrovnikov[111,c], S. S. Bocchetta[84], A. Bocci[47], C. Bock[102], M. Boehler[50], D. Boerner[178], J. A. Bogaerts[32], D. Bogavac[14], A. G. Bogdanchikov[111], C. Bohm[150a], V. Boisvert[80], P. Bokan[14], T. Bold[40a], A. S. Boldyrev[167a,167c], M. Bomben[83], M. Bona[79], M. Boonekamp[138], A. Borisov[132], G. Borissov[75], J. Bortfeldt[32], D. Bortoletto[122], V. Bortolotto[63a,63b,63c], K. Bos[109], D. Boscherini[22a], M. Bosman[13], J. D. Bossio Sola[29], J. Boudreau[127], J. Bouffard[2], E. V. Bouhova-Thacker[75], D. Boumediene[36], C. Bourdarios[119], S. K. Boutle[55], A. Boveia[32], J. Boyd[32], I. R. Boyko[68], J. Bracinik[19], A. Brandt[8], G. Brandt[56], O. Brandt[61a], U. Bratzler[160], B. Brau[89], J. E. Brau[118], H. M. Braun[178,*], W. D. Breaden Madden[55], K. Brendlinger[124], A. J. Brennan[91], L. Brenner[109], R. Brenner[168], S. Bressler[175], T. M. Bristow[48], D. Britton[55], D. Britzger[44], F. M. Brochu[30], I. Brock[23], R. Brock[93], G. Brooijmans[37], T. Brooks[80], W. K. Brooks[34b], J. Brosamer[16], E. Brost[118], J. H Broughton[19], P. A. Bruckman de Renstrom[41], D. Bruncko[148b], R. Bruneliere[50], A. Bruni[22a], G. Bruni[22a], L. S. Bruni[109], BH Brunt[30], M. Bruschi[22a], N. Bruscino[23], P. Bryant[33], L. Bryngemark[84], T. Buanes[15], Q. Buat[146], P. Buchholz[145], A. G. Buckley[55], I. A. Budagov[68], F. Buehrer[50], M. K. Bugge[121], O. Bulekov[100], D. Bullock[8], H. Burckhart[32], S. Burdin[77], C. D. Burgard[50], B. Burghgrave[110], K. Burka[41], S. Burke[133], I. Burmeister[45], J. T. P. Burr[122], E. Busato[36], D. Büscher[50], V. Büscher[86], P. Bussey[55], J. M. Butler[24], C. M. Buttar[55], J. M. Butterworth[81], P. Butti[109], W. Buttinger[27], A. Buzatu[55], A. R. Buzykaev[111,c], S. Cabrera Urbán[170], D. Caforio[130], V. M. Cairo[39a,39b], O. Cakir[4a], N. Calace[51], P. Calafiura[16], A. Calandri[88], G. Calderini[83], P. Calfayan[102], L. P. Caloba[26a], S. Calvente Lopez[85], D. Calvet[36], S. Calvet[36], T. P. Calvet[88], R. Camacho Toro[33], S. Camarda[32], P. Camarri[135a,135b], D. Cameron[121], R. Caminal Armadans[169], C. Camincher[57], S. Campana[32], M. Campanelli[81], A. Camplani[94a,94b], A. Campoverde[145], V. Canale[106a,106b], A. Canepa[163a], M. Cano Bret[142], J. Cantero[116], R. Cantrill[128a], T. Cao[42], M. D. M. Capeans Garrido[32], I. Caprini[28b], M. Caprini[28b], M. Capua[39a,39b], R. Caputo[86], R. M. Carbone[37], R. Cardarelli[135a], F. Cardillo[50], I. Carli[131], T. Carli[32], G. Carlino[106a], L. Carminati[94a,94b], S. Caron[108], E. Carquin[34b], G. D. Carrillo-Montoya[32], J. R. Carter[30], J. Carvalho[128a,128c], D. Casadei[19], M. P. Casado[13,i], M. Casolino[13], D. W. Casper[166], E. Castaneda-Miranda[149a], R. Castelijn[109], A. Castelli[109], V. Castillo Gimenez[170], N. F. Castro[128a,j], A. Catinaccio[32], J. R. Catmore[121], A. Cattai[32], J. Caudron[86], V. Cavaliere[169], E. Cavallaro[13], D. Cavalli[94a], M. Cavalli-Sforza[13], V. Cavasinni[126a,126b], F. Ceradini[136a,136b], L. Cerda Alberich[170], B. C. Cerio[47], A. S. Cerqueira[26b], A. Cerri[153], L. Cerrito[79], F. Cerutti[16], M. Cerv[32], A. Cervelli[18], S. A. Cetin[20c], A. Chafaq[137a], D. Chakraborty[110], S. K. Chan[59], Y. L. Chan[63a], P. Chang[169], J. D. Chapman[30], D. G. Charlton[19], A. Chatterjee[51], C. C. Chau[162], C. A. Chavez Barajas[153], S. Che[113], S. Cheatham[75], A. Chegwidden[93], S. Chekanov[6], S. V. Chekulaev[163a], G. A. Chelkov[68,k], M. A. Chelstowska[92], C. Chen[67], H. Chen[27], K. Chen[152], S. Chen[35b], S. Chen[159], X. Chen[35c], Y. Chen[70], H. C. Cheng[92], H. J Cheng[35a], Y. Cheng[33], A. Cheplakov[68], E. Cheremushkina[132], R. Cherkaoui El Moursli[137e], V. Chernyatin[27,*], E. Cheu[7], L. Chevalier[138], V. Chiarella[49], G. Chiarelli[126a,126b], G. Chiodini[76a], A. S. Chisholm[19], A. Chitan[28b], M. V. Chizhov[68], K. Choi[64], A. R. Chomont[36], S. Chouridou[9], B. K. B. Chow[102], V. Christodoulou[81], D. Chromek-Burckhart[32], J. Chudoba[129], A. J. Chuinard[90], J. J. Chwastowski[41], L. Chytka[117], G. Ciapetti[134a,134b], A. K. Ciftci[4a], D. Cinca[45], V. Cindro[78], I. A. Cioara[23], C. Ciocca[22a,22b], A. Ciocio[16], F. Cirotto[106a,106b], Z. H. Citron[175], M. Citterio[94a], M. Ciubancan[28b], A. Clark[51], B. L. Clark[59], M. R. Clark[37], P. J. Clark[48], R. N. Clarke[16], C. Clement[150a,150b], Y. Coadou[88], M. Cobal[167a,167c], A. Coccaro[51], J. Cochran[67], L. Coffey[25], L. Colasurdo[108], B. Cole[37], A. P. Colijn[109], J. Collot[57], T. Colombo[32], G. Compostella[103], P. Conde Muiño[128a,128b], E. Coniavitis[50], S. H. Connell[149b], I. A. Connelly[80], V. Consorti[50], S. Constantinescu[28b], G. Conti[32], F. Conventi[106a,l], M. Cooke[16], B. D. Cooper[81], A. M. Cooper-Sarkar[122], K. J. R. Cormier[162], T. Cornelissen[178], M. Corradi[134a,134b], F. Corriveau[90,m], A. Corso-Radu[166], A. Cortes-Gonzalez[13], G. Cortiana[103], G. Costa[94a], M. J. Costa[170], D. Costanzo[143],

G. Cottin[30], G. Cowan[80], B. E. Cox[87], K. Cranmer[112], S. J. Crawley[55], G. Cree[31], S. Crépé-Renaudin[57], F. Crescioli[83], W. A. Cribbs[150a,150b], M. Crispin Ortuzar[122], M. Cristinziani[23], V. Croft[108], G. Crosetti[39a,39b], T. Cuhadar Donszelmann[143], J. Cummings[179], M. Curatolo[49], J. Cúth[86], C. Cuthbert[154], H. Czirr[145], P. Czodrowski[3], G. D'amen[22a,22b], S. D'Auria[55], M. D'Onofrio[77], M. J. Da Cunha Sargedas De Sousa[128a,128b], C. Da Via[87], W. Dabrowski[40a], T. Dado[148a], T. Dai[92], O. Dale[15], F. Dallaire[97], C. Dallapiccola[89], M. Dam[38], J. R. Dandoy[33], N. P. Dang[50], A. C. Daniells[19], N. S. Dann[87], M. Danninger[171], M. Dano Hoffmann[138], V. Dao[50], G. Darbo[52a], S. Darmora[8], J. Dassoulas[3], A. Dattagupta[64], W. Davey[23], C. David[172], T. Davidek[131], M. Davies[157], P. Davison[81], E. Dawe[91], I. Dawson[143], R. K. Daya-Ishmukhametova[89], K. De[8], R. de Asmundis[106a], A. De Benedetti[115], S. De Castro[22a,22b], S. De Cecco[83], N. De Groot[108], P. de Jong[109], H. De la Torre[85], F. De Lorenzi[67], A. De Maria[56], D. De Pedis[134a], A. De Salvo[134a], U. De Sanctis[153], A. De Santo[153], J. B. De Vivie De Regie[119], W. J. Dearnaley[75], R. Debbe[27], C. Debenedetti[139], D. V. Dedovich[68], N. Dehghanian[3], I. Deigaard[109], M. Del Gaudio[39a,39b], J. Del Peso[85], T. Del Prete[126a,126b], D. Delgove[119], F. Deliot[138], C. M. Delitzsch[51], M. Deliyergiyev[78], A. Dell'Acqua[32], L. Dell'Asta[24], M. Dell'Orso[126a,126b], M. Della Pietra[106a,l], D. della Volpe[51], M. Delmastro[5], P. A. Delsart[57], D. A. DeMarco[162], S. Demers[179], M. Demichev[68], A. Demilly[83], S. P. Denisov[132], D. Denysiuk[138], D. Derendarz[41], J. E. Derkaoui[137d], F. Derue[83], P. Dervan[77], K. Desch[23], C. Deterre[44], K. Dette[45], P. O. Deviveiros[32], A. Dewhurst[133], S. Dhaliwal[25], A. Di Ciaccio[135a,135b], L. Di Ciaccio[5], W. K. Di Clemente[124], C. Di Donato[134a,134b], A. Di Girolamo[32], B. Di Girolamo[32], B. Di Micco[136a,136b], R. Di Nardo[32], A. Di Simone[50], R. Di Sipio[162], D. Di Valentino[31], C. Diaconu[88], M. Diamond[162], F. A. Dias[48], M. A. Diaz[34a], E. B. Diehl[92], J. Dietrich[17], S. Diglio[88], A. Dimitrievska[14], J. Dingfelder[23], P. Dita[28b], S. Dita[28b], F. Dittus[32], F. Djama[88], T. Djobava[53b], J. I. Djuvsland[61a], M. A. B. do Vale[26c], D. Dobos[32], M. Dobre[28b], C. Doglioni[84], T. Dohmae[159], J. Dolejsi[131], Z. Dolezal[131], B. A. Dolgoshein[100,*], M. Donadelli[26d], S. Donati[126a,126b], P. Dondero[123a,123b], J. Donini[36], J. Dopke[133], A. Doria[106a], M. T. Dova[74], A. T. Doyle[55], E. Drechsler[56], M. Dris[10], Y. Du[141], J. Duarte-Campderros[157], E. Duchovni[175], G. Duckeck[102], O. A. Ducu[97,n], D. Duda[109], A. Dudarev[32], E. M. Duffield[16], L. Duflot[119], L. Duguid[80], M. Dührssen[32], M. Dumancic[175], M. Dunford[61a], H. Duran Yildiz[4a], M. Düren[54], A. Durglishvili[53b], D. Duschinger[46], B. Dutta[44], M. Dyndal[44], C. Eckardt[44], K. M. Ecker[103], R. C. Edgar[92], N. C. Edwards[48], T. Eifert[32], G. Eigen[15], K. Einsweiler[16], T. Ekelof[168], M. El Kacimi[137c], V. Ellajosyula[88], M. Ellert[168], S. Elles[5], F. Ellinghaus[178], A. A. Elliot[172], N. Ellis[32], J. Elmsheuser[27], M. Elsing[32], D. Emeliyanov[133], Y. Enari[159], O. C. Endner[86], M. Endo[120], J. S. Ennis[173], J. Erdmann[45], A. Ereditato[18], G. Ernis[178], J. Ernst[2], M. Ernst[27], S. Errede[169], E. Ertel[86], M. Escalier[119], H. Esch[45], C. Escobar[127], B. Esposito[49], A. I. Etienvre[138], E. Etzion[157], H. Evans[64], A. Ezhilov[125], F. Fabbri[22a,22b], L. Fabbri[22a,22b], G. Facini[33], R. M. Fakhrutdinov[132], S. Falciano[134a], R. J. Falla[81], J. Faltova[32], Y. Fang[35a], M. Fanti[94a,94b], A. Farbin[8], A. Farilla[136a], C. Farina[127], E. M. Farina[123a,123b], T. Farooque[13], S. Farrell[16], S. M. Farrington[173], P. Farthouat[32], F. Fassi[137e], P. Fassnacht[32], D. Fassouliotis[9], M. Faucci Giannelli[80], A. Favareto[52a,52b], W. J. Fawcett[122], L. Fayard[119], O. L. Fedin[125,o], W. Fedorko[171], S. Feigl[121], L. Feligioni[88], C. Feng[141], E. J. Feng[32], H. Feng[92], A. B. Fenyuk[132], L. Feremenga[8], P. Fernandez Martinez[170], S. Fernandez Perez[13], J. Ferrando[55], A. Ferrari[168], P. Ferrari[109], R. Ferrari[123a], D. E. Ferreira de Lima[61b], A. Ferrer[170], D. Ferrere[51], C. Ferretti[92], A. Ferretto Parodi[52a,52b], F. Fiedler[86], A. Filipčič[78], M. Filipuzzi[44], F. Filthaut[108], M. Fincke-Keeler[172], K. D. Finelli[154], M. C. N. Fiolhais[128a,128c], L. Fiorini[170], A. Firan[42], A. Fischer[2], C. Fischer[13], J. Fischer[178], W. C. Fisher[93], N. Flaschel[44], I. Fleck[145], P. Fleischmann[92], G. T. Fletcher[143], R. R. M. Fletcher[124], T. Flick[178], A. Floderus[84], L. R. Flores Castillo[63a], M. J. Flowerdew[103], G. T. Forcolin[87], A. Formica[138], A. Forti[87], A. G. Foster[19], D. Fournier[119], H. Fox[75], S. Fracchia[13], P. Francavilla[83], M. Franchini[22a,22b], D. Francis[32], L. Franconi[121], M. Franklin[59], M. Frate[166], M. Fraternali[123a,123b], D. Freeborn[81], S. M. Fressard-Batraneanu[32], F. Friedrich[46], D. Froidevaux[32], J. A. Frost[122], C. Fukunaga[160], E. Fullana Torregrosa[86], T. Fusayasu[104], J. Fuster[170], C. Gabaldon[57], O. Gabizon[178], A. Gabrielli[22a,22b], A. Gabrielli[16], G. P. Gach[40a], S. Gadatsch[32], S. Gadomski[51], G. Gagliardi[52a,52b], L. G. Gagnon[97], P. Gagnon[64], C. Galea[108], B. Galhardo[128a,128c], E. J. Gallas[122], B. J. Gallop[133], P. Gallus[130], G. Galster[38], K. K. Gan[113], J. Gao[60], Y. Gao[48], Y. S. Gao[147,g], F. M. Garay Walls[48], C. García[170], J. E. García Navarro[170], M. Garcia-Sciveres[16], R. W. Gardner[33], N. Garelli[147], V. Garonne[121], A. Gascon Bravo[44], C. Gatti[49], A. Gaudiello[52a,52b], G. Gaudio[123a], B. Gaur[145], L. Gauthier[97], I. L. Gavrilenko[98], C. Gay[171], G. Gaycken[23], E. N. Gazis[10], Z. Gecse[171], C. N. P. Gee[133], Ch. Geich-Gimbel[23], M. Geisen[86], M. P. Geisler[61a], C. Gemme[52a], M. H. Genest[57], C. Geng[60,p], S. Gentile[134a,134b], S. George[80], D. Gerbaudo[13], A. Gershon[157], S. Ghasemi[145], H. Ghazlane[137b], M. Ghneimat[23], B. Giacobbe[22a], S. Giagu[134a,134b], P. Giannetti[126a,126b], B. Gibbard[27], S. M. Gibson[80], M. Gignac[171], M. Gilchriese[16], T. P. S. Gillam[30], D. Gillberg[31], G. Gilles[178], D. M. Gingrich[3,d], N. Giokaris[9], M. P. Giordani[167a,167c], F. M. Giorgi[22a], F. M. Giorgi[17], P. F. Giraud[138], P. Giromini[59], D. Giugni[94a], F. Giuli[122], C. Giuliani[103], M. Giulini[61b], B. K. Gjelsten[121], S. Gkaitatzis[158], I. Gkialas[158], E. L. Gkougkousis[119], L. K. Gladilin[101], C. Glasman[85], J. Glatzer[50], P. C. F. Glaysher[48], A. Glazov[44], M. Goblirsch-Kolb[103], J. Godlewski[41], S. Goldfarb[91], T. Golling[51], D. Golubkov[132], A. Gomes[128a,128b,128d], R. Gonçalo[128a], J. Goncalves Pinto Firmino Da Costa[138],

G. Gonella[50], L. Gonella[19], A. Gongadze[68], S. González de la Hoz[170], G. Gonzalez Parra[13], S. Gonzalez-Sevilla[51], L. Goossens[32], P. A. Gorbounov[99], H. A. Gordon[27], I. Gorelov[107], B. Gorini[32], E. Gorini[76a,76b], A. Gorišek[78], E. Gornicki[41], A. T. Goshaw[47], C. Gössling[45], M. I. Gostkin[68], C. R. Goudet[119], D. Goujdami[137c], A. G. Goussiou[140], N. Govender[149b,q], E. Gozani[156], L. Graber[56], I. Grabowska-Bold[40a], P. O. J. Gradin[57], P. Grafström[22a,22b], J. Gramling[51], E. Gramstad[121], S. Grancagnolo[17], V. Gratchev[125], P. M. Gravila[28e], H. M. Gray[32], E. Graziani[136a], Z. D. Greenwood[82,r], C. Grefe[23], K. Gregersen[81], I. M. Gregor[44], P. Grenier[147], K. Grevtsov[5], J. Griffiths[8], A. A. Grillo[139], K. Grimm[75], S. Grinstein[13,s], Ph. Gris[36], J.-F. Grivaz[119], S. Groh[86], J. P. Grohs[46], E. Gross[175], J. Grosse-Knetter[56], G. C. Grossi[82], Z. J. Grout[153], L. Guan[92], W. Guan[176], J. Guenther[65], F. Guescini[51], D. Guest[166], O. Gueta[157], E. Guido[52a,52b], T. Guillemin[5], S. Guindon[2], U. Gul[55], C. Gumpert[32], J. Guo[142], Y. Guo[60,p], S. Gupta[122], G. Gustavino[134a,134b], P. Gutierrez[115], N. G. Gutierrez Ortiz[81], C. Gutschow[46], C. Guyot[138], C. Gwenlan[122], C. B. Gwilliam[77], A. Haas[112], C. Haber[16], H. K. Hadavand[8], N. Haddad[137e], A. Hadef[88], P. Haefner[23], S. Hageböck[23], Z. Hajduk[41], H. Hakobyan[180,*], M. Haleem[44], J. Haley[116], G. Halladjian[93], G. D. Hallewell[88], K. Hamacher[178], P. Hamal[117], K. Hamano[172], A. Hamilton[149a], G. N. Hamity[143], P. G. Hamnett[44], L. Han[60], K. Hanagaki[69,t], K. Hanawa[159], M. Hance[139], B. Haney[124], P. Hanke[61a], R. Hanna[138], J. B. Hansen[38], J. D. Hansen[38], M. C. Hansen[23], P. H. Hansen[38], K. Hara[164], A. S. Hard[176], T. Harenberg[178], F. Hariri[119], S. Harkusha[95], R. D. Harrington[48], P. F. Harrison[173], F. Hartjes[109], N. M. Hartmann[102], M. Hasegawa[70], Y. Hasegawa[144], A. Hasib[115], S. Hassani[138], S. Haug[18], R. Hauser[93], L. Hauswald[46], M. Havranek[129], C. M. Hawkes[19], R. J. Hawkings[32], D. Hayden[93], C. P. Hays[122], J. M. Hays[79], H. S. Hayward[77], S. J. Haywood[133], S. J. Head[19], T. Heck[86], V. Hedberg[84], L. Heelan[8], S. Heim[124], T. Heim[16], B. Heinemann[16], J. J. Heinrich[102], L. Heinrich[112], C. Heinz[54], J. Hejbal[129], L. Helary[24], S. Hellman[150a,150b], C. Helsens[32], J. Henderson[122], R. C. W. Henderson[75], Y. Heng[176], S. Henkelmann[171], A. M. Henriques Correia[32], S. Henrot-Versille[119], G. H. Herbert[17], Y. Hernández Jiménez[170], G. Herten[50], R. Hertenberger[102], L. Hervas[32], G. G. Hesketh[81], N. P. Hessey[109], J. W. Hetherly[42], R. Hickling[79], E. Higón-Rodriguez[170], E. Hill[172], J. C. Hill[30], K. H. Hiller[44], S. J. Hillier[19], I. Hinchliffe[16], E. Hines[124], R. R. Hinman[16], M. Hirose[50], D. Hirschbuehl[178], J. Hobbs[152], N. Hod[163a], M. C. Hodgkinson[143], P. Hodgson[143], A. Hoecker[32], M. R. Hoeferkamp[107], F. Hoenig[102], D. Hohn[23], T. R. Holmes[16], M. Homann[45], T. M. Hong[127], B. H. Hooberman[169], W. H. Hopkins[118], Y. Horii[105], A. J. Horton[146], J.-Y. Hostachy[57], S. Hou[155], A. Hoummada[137a], J. Howarth[44], M. Hrabovsky[117], I. Hristova[17], J. Hrivnac[119], T. Hryn'ova[5], A. Hrynevich[96], C. Hsu[149c], P. J. Hsu[155,u], S.-C. Hsu[140], D. Hu[37], Q. Hu[60], Y. Huang[44], Z. Hubacek[130], F. Hubaut[88], F. Huegging[23], T. B. Huffman[122], E. W. Hughes[37], G. Hughes[75], M. Huhtinen[32], P. Huo[152], N. Huseynov[68,b], J. Huston[93], J. Huth[59], G. Iacobucci[51], G. Iakovidis[27], I. Ibragimov[145], L. Iconomidou-Fayard[119], E. Ideal[179], Z. Idrissi[137e], P. Iengo[32], O. Igonkina[109,v], T. Iizawa[174], Y. Ikegami[69], M. Ikeno[69], Y. Ilchenko[11,w], D. Iliadis[158], N. Ilic[147], T. Ince[103], G. Introzzi[123a,123b], P. Ioannou[9,*], M. Iodice[136a], K. Iordanidou[37], V. Ippolito[59], N. Ishijima[120], M. Ishino[71], M. Ishitsuka[161], R. Ishmukhametov[113], C. Issever[122], S. Istin[20a], F. Ito[164], J. M. Iturbe Ponce[87], R. Iuppa[135a,135b], W. Iwanski[65], H. Iwasaki[69], J. M. Izen[43], V. Izzo[106a], S. Jabbar[3], B. Jackson[124], M. Jackson[77], P. Jackson[1], V. Jain[2], K. B. Jakobi[86], K. Jakobs[50], S. Jakobsen[32], T. Jakoubek[129], D. O. Jamin[116], D. K. Jana[82], E. Jansen[81], R. Jansky[65], J. Janssen[23], M. Janus[56], G. Jarlskog[84], N. Javadov[68,b], T. Javůrek[50], F. Jeanneau[138], L. Jeanty[16], G.-Y. Jeng[154], D. Jennens[91], P. Jenni[50,x], J. Jentzsch[45], C. Jeske[173], S. Jézéquel[5], H. Ji[176], J. Jia[152], H. Jiang[67], Y. Jiang[60], S. Jiggins[81], J. Jimenez Pena[170], S. Jin[35a], A. Jinaru[28b], O. Jinnouchi[161], P. Johansson[143], K. A. Johns[7], W. J. Johnson[140], K. Jon-And[150a,150b], G. Jones[173], R. W. L. Jones[75], S. Jones[7], T. J. Jones[77], J. Jongmanns[61a], P. M. Jorge[128a,128b], J. Jovicevic[163a], X. Ju[176], A. Juste Rozas[13,s], M. K. Köhler[175], A. Kaczmarska[41], M. Kado[119], H. Kagan[113], M. Kagan[147], S. J. Kahn[88], E. Kajomovitz[47], C. W. Kalderon[122], A. Kaluza[86], S. Kama[42], A. Kamenshchikov[132], N. Kanaya[159], S. Kaneti[30], L. Kanjir[78], V. A. Kantserov[100], J. Kanzaki[69], B. Kaplan[112], L. S. Kaplan[176], A. Kapliy[33], D. Kar[149c], K. Karakostas[10], A. Karamaoun[3], N. Karastathis[10], M. J. Kareem[56], E. Karentzos[10], M. Karnevskiy[86], S. N. Karpov[68], Z. M. Karpova[68], K. Karthik[112], V. Kartvelishvili[75], A. N. Karyukhin[132], K. Kasahara[164], L. Kashif[176], R. D. Kass[113], A. Kastanas[15], Y. Kataoka[159], C. Kato[159], A. Katre[51], J. Katzy[44], K Kawade[105], K. Kawagoe[73], T. Kawamoto[159], G. Kawamura[56], S. Kazama[159], V. F. Kazanin[111,c], R. Keeler[172], R. Kehoe[42], J. S. Keller[44], J. J. Kempster[80], H. Keoshkerian[162], O. Kepka[129], B. P. Kerševan[78], S. Kersten[178], R. A. Keyes[90], M. Khader[169], F. Khalil-zada[12], A. Khanov[116], A. G. Kharlamov[111,c], T. J. Khoo[51], V. Khovanskiy[99], E. Khramov[68], J. Khubua[53b,y], S. Kido[70], H. Y. Kim[8], S. H. Kim[164], Y. K. Kim[33], N. Kimura[158], O. M. Kind[17], B. T. King[77], M. King[170], S. B. King[171], J. Kirk[133], A. E. Kiryunin[103], T. Kishimoto[70], D. Kisielewska[40a], F. Kiss[50], K. Kiuchi[164], O. Kivernyk[138], E. Kladiva[148b], M. H. Klein[37], M. Klein[77], U. Klein[77], K. Kleinknecht[86], P. Klimek[110], A. Klimentov[27], R. Klingenberg[45], J. A. Klinger[143], T. Klioutchnikova[32], E.-E. Kluge[61a], P. Kluit[109], S. Kluth[103], J. Knapik[41], E. Kneringer[65], E. B. F. G. Knoops[88], A. Knue[55], A. Kobayashi[159], D. Kobayashi[161], T. Kobayashi[159], M. Kobel[46], M. Kocian[147], P. Kodys[131], T. Koffas[31], E. Koffeman[109], T. Koi[147], H. Kolanoski[17], M. Kolb[61b], I. Koletsou[5], A. A. Komar[98,*], Y. Komori[159], T. Kondo[69], N. Kondrashova[44], K. Köneke[50], A. C. König[108],

T. Kono[69,z], R. Konoplich[112,aa], N. Konstantinidis[81], R. Kopeliansky[64], S. Koperny[40a], L. Köpke[86], A. K. Kopp[50], K. Korcyl[41], K. Kordas[158], A. Korn[81], A. A. Korol[111,c], I. Korolkov[13], E. V. Korolkova[143], O. Kortner[103], S. Kortner[103], T. Kosek[131], V. V. Kostyukhin[23], A. Kotwal[47], A. Kourkoumeli-Charalampidi[158], C. Kourkoumelis[9], V. Kouskoura[27], A. B. Kowalewska[41], R. Kowalewski[172], T. Z. Kowalski[40a], C. Kozakai[159], W. Kozanecki[138], A. S. Kozhin[132], V. A. Kramarenko[101], G. Kramberger[78], D. Krasnopevtsev[100], M. W. Krasny[83], A. Krasznahorkay[32], J. K. Kraus[23], A. Kravchenko[27], M. Kretz[61c], J. Kretzschmar[77], K. Kreutzfeldt[54], P. Krieger[162], K. Krizka[33], K. Kroeninger[45], H. Kroha[103], J. Kroll[124], J. Kroseberg[23], J. Krstic[14], U. Kruchonak[68], H. Krüger[23], N. Krumnack[67], A. Kruse[176], M. C. Kruse[47], M. Kruskal[24], T. Kubota[91], H. Kucuk[81], S. Kuday[4b], J. T. Kuechler[178], S. Kuehn[50], A. Kugel[61c], F. Kuger[177], A. Kuhl[139], T. Kuhl[44], V. Kukhtin[68], R. Kukla[138], Y. Kulchitsky[95], S. Kuleshov[34b], M. Kuna[134a,134b], T. Kunigo[71], A. Kupco[129], H. Kurashige[70], Y. A. Kurochkin[95], V. Kus[129], E. S. Kuwertz[172], M. Kuze[161], J. Kvita[117], T. Kwan[172], D. Kyriazopoulos[143], A. La Rosa[103], J. L. La Rosa Navarro[26d], L. La Rotonda[39a,39b], C. Lacasta[170], F. Lacava[134a,134b], J. Lacey[31], H. Lacker[17], D. Lacour[83], V. R. Lacuesta[170], E. Ladygin[68], R. Lafaye[5], B. Laforge[83], T. Lagouri[179], S. Lai[56], S. Lammers[64], W. Lampl[7], E. Lançon[138], U. Landgraf[50], M. P. J. Landon[79], V. S. Lang[61a], J. C. Lange[13], A. J. Lankford[166], F. Lanni[27], K. Lantzsch[23], A. Lanza[123a], S. Laplace[83], C. Lapoire[32], J. F. Laporte[138], T. Lari[94a], F. Lasagni Manghi[22a,22b], M. Lassnig[32], P. Laurelli[49], W. Lavrijsen[16], A. T. Law[139], P. Laycock[77], T. Lazovich[59], M. Lazzaroni[94a,94b], B. Le[91], O. Le Dortz[83], E. Le Guirriec[88], E. P. Le Quilleuc[138], M. LeBlanc[172], T. LeCompte[6], F. Ledroit-Guillon[57], C. A. Lee[27], S. C. Lee[155], L. Lee[1], G. Lefebvre[83], M. Lefebvre[172], F. Legger[102], C. Leggett[16], A. Lehan[77], G. Lehmann Miotto[32], X. Lei[7], W. A. Leight[31], A. Leisos[158,ab], A. G. Leister[179], M. A. L. Leite[26d], R. Leitner[131], D. Lellouch[175], B. Lemmer[56], K. J. C. Leney[81], T. Lenz[23], B. Lenzi[32], R. Leone[7], S. Leone[126a,126b], C. Leonidopoulos[48], S. Leontsinis[10], G. Lerner[153], C. Leroy[97], A. A. J. Lesage[138], C. G. Lester[30], M. Levchenko[125], J. Levêque[5], D. Levin[92], L. J. Levinson[175], M. Levy[19], D. Lewis[79], A. M. Leyko[23], M. Leyton[43], B. Li[60,p], H. Li[152], H. L. Li[33], L. Li[47], L. Li[142], Q. Li[35a], S. Li[47], X. Li[87], Y. Li[145], Z. Liang[35a], B. Liberti[135a], A. Liblong[162], P. Lichard[32], K. Lie[169], J. Liebal[23], W. Liebig[15], A. Limosani[154], S. C. Lin[155,ac], T. H. Lin[86], B. E. Lindquist[152], A. E. Lionti[51], E. Lipeles[124], A. Lipniacka[15], M. Lisovyi[61b], T. M. Liss[169], A. Lister[171], A. M. Litke[139], B. Liu[155,ad], D. Liu[155], H. Liu[92], H. Liu[27], J. Liu[88], J. B. Liu[60], K. Liu[88], L. Liu[169], M. Liu[47], M. Liu[60], Y. L. Liu[60], Y. Liu[60], M. Livan[123a,123b], A. Lleres[57], J. Llorente Merino[35a], S. L. Lloyd[79], F. Lo Sterzo[155], E. M. Lobodzinska[44], P. Loch[7], W. S. Lockman[139], F. K. Loebinger[87], A. E. Loevschall-Jensen[38], K. M. Loew[25], A. Loginov[179,*], T. Lohse[17], K. Lohwasser[44], M. Lokajicek[129], B. A. Long[24], J. D. Long[169], R. E. Long[75], L. Longo[76a,76b], K. A. Looper[113], L. Lopes[128a], D. Lopez Mateos[59], B. Lopez Paredes[143], I. Lopez Paz[13], A. Lopez Solis[83], J. Lorenz[102], N. Lorenzo Martinez[64], M. Losada[21], P. J. Lösel[102], X. Lou[35a], A. Lounis[119], J. Love[6], P. A. Love[75], H. Lu[63a], N. Lu[92], H. J. Lubatti[140], C. Luci[134a,134b], A. Lucotte[57], C. Luedtke[50], F. Luehring[64], W. Lukas[65], L. Luminari[134a], O. Lundberg[150a,150b], B. Lund-Jensen[151], P. M. Luzi[83], D. Lynn[27], R. Lysak[129], E. Lytken[84], V. Lyubushkin[68], H. Ma[27], L. L. Ma[141], Y. Ma[141], G. Maccarrone[49], A. Macchiolo[103], C. M. Macdonald[143], B. Maček[78], J. Machado Miguens[124,128b], D. Madaffari[88], R. Madar[36], H. J. Maddocks[168], W. F. Mader[46], A. Madsen[44], J. Maeda[70], S. Maeland[15], T. Maeno[27], A. Maevskiy[101], E. Magradze[56], J. Mahlstedt[109], C. Maiani[119], C. Maidantchik[26a], A. A. Maier[103], T. Maier[102], A. Maio[128a,128b,128d], S. Majewski[118], Y. Makida[69], N. Makovec[119], B. Malaescu[83], Pa. Malecki[41], V. P. Maleev[125], F. Malek[57], U. Mallik[66], D. Malon[6], C. Malone[147], S. Maltezos[10], S. Malyukov[32], J. Mamuzic[170], G. Mancini[49], B. Mandelli[32], L. Mandelli[94a], I. Mandić[78], J. Maneira[128a,128b], L. Manhaes de Andrade Filho[26b], J. Manjarres Ramos[163b], A. Mann[102], A. Manousos[32], B. Mansoulie[138], J. D. Mansour[35a], R. Mantifel[90], M. Mantoani[56], S. Manzoni[94a,94b], L. Mapelli[32], G. Marceca[29], L. March[51], G. Marchiori[83], M. Marcisovsky[129], M. Marjanovic[14], D. E. Marley[92], F. Marroquim[26a], S. P. Marsden[87], Z. Marshall[16], S. Marti-Garcia[170], B. Martin[93], T. A. Martin[173], V. J. Martin[48], B. Martin dit Latour[15], M. Martinez[13,s], V. I. Martinez Outschoorn[169], S. Martin-Haugh[133], V. S. Martoiu[28b], A. C. Martyniuk[81], M. Marx[140], A. Marzin[32], L. Masetti[86], T. Mashimo[159], R. Mashinistov[98], J. Masik[87], A. L. Maslennikov[111,c], I. Massa[22a,22b], L. Massa[22a,22b], P. Mastrandrea[5], A. Mastroberardino[39a,39b], T. Masubuchi[159], P. Mättig[178], J. Mattmann[86], J. Maurer[28b], S. J. Maxfield[77], D. A. Maximov[111,c], R. Mazini[155], S. M. Mazza[94a,94b], N. C. Mc Fadden[107], G. Mc Goldrick[162], S. P. Mc Kee[92], A. McCarn[92], R. L. McCarthy[152], T. G. McCarthy[103], L. I. McClymont[81], E. F. McDonald[91], K. W. McFarlane[58,*], J. A. Mcfayden[81], G. Mchedlidze[56], S. J. McMahon[133], R. A. McPherson[172,m], M. Medinnis[44], S. Meehan[140], S. Mehlhase[102], A. Mehta[77], K. Meier[61a], C. Meineck[102], B. Meirose[43], D. Melini[170], B. R. Mellado Garcia[149c], M. Melo[148a], F. Meloni[18], A. Mengarelli[22a,22b], S. Menke[103], E. Meoni[165], S. Mergelmeyer[17], P. Mermod[51], L. Merola[106a,106b], C. Meroni[94a], F. S. Merritt[33], A. Messina[134a,134b], J. Metcalfe[6], A. S. Mete[166], C. Meyer[86], C. Meyer[124], J.-P. Meyer[138], J. Meyer[109], H. Meyer Zu Theenhausen[61a], F. Miano[153], R. P. Middleton[133], S. Miglioranzi[52a,52b], L. Mijović[23], G. Mikenberg[175], M. Mikestikova[129], M. Mikuž[78], M. Milesi[91], A. Milic[65], D. W. Miller[33], C. Mills[48], A. Milov[175], D. A. Milstead[150a,150b], A. A. Minaenko[132], Y. Minami[159], I. A. Minashvili[68], A. I. Mincer[112], B. Mindur[40a], M. Mineev[68], Y. Ming[176], L. M. Mir[13], K. P. Mistry[124],

T. Mitani[174], J. Mitrevski[102], V. A. Mitsou[170], A. Miucci[51], P. S. Miyagawa[143], J. U. Mjörnmark[84], T. Moa[150a,150b], K. Mochizuki[97], S. Mohapatra[37], S. Molander[150a,150b], R. Moles-Valls[23], R. Monden[71], M. C. Mondragon[93], K. Mönig[44], J. Monk[38], E. Monnier[88], A. Montalbano[152], J. Montejo Berlingen[32], F. Monticelli[74], S. Monzani[94a,94b], R. W. Moore[3], N. Morange[119], D. Moreno[21], M. Moreno Llácer[56], P. Morettini[52a], S. Morgenstern[32], D. Mori[146], T. Mori[159], M. Morii[59], M. Morinaga[159], V. Morisbak[121], S. Moritz[86], A. K. Morley[154], G. Mornacchi[32], J. D. Morris[79], S. S. Mortensen[38], L. Morvaj[152], M. Mosidze[53b], J. Moss[147,ae], K. Motohashi[161], R. Mount[147], E. Mountricha[27], S. V. Mouraviev[98,*], E. J. W. Moyse[89], S. Muanza[88], R. D. Mudd[19], F. Mueller[103], J. Mueller[127], R. S. P. Mueller[102], T. Mueller[30], D. Muenstermann[75], P. Mullen[55], G. A. Mullier[18], F. J. Munoz Sanchez[87], J. A. Murillo Quijada[19], W. J. Murray[173,133], H. Musheghyan[56], M. Muškinja[78], A. G. Myagkov[132,af], M. Myska[130], B. P. Nachman[147], O. Nackenhorst[51], K. Nagai[122], R. Nagai[69,z], K. Nagano[69], Y. Nagasaka[62], K. Nagata[164], M. Nagel[50], E. Nagy[88], A. M. Nairz[32], Y. Nakahama[32], K. Nakamura[69], T. Nakamura[159], I. Nakano[114], H. Namasivayam[43], R. F. Naranjo Garcia[44], R. Narayan[11], D. I. Narrias Villar[61a], I. Naryshkin[125], T. Naumann[44], G. Navarro[21], R. Nayyar[7], H. A. Neal[92], P. Yu. Nechaeva[98], T. J. Neep[87], P. D. Nef[147], A. Negri[123a,123b], M. Negrini[22a], S. Nektarijevic[108], C. Nellist[119], A. Nelson[166], S. Nemecek[129], P. Nemethy[112], A. A. Nepomuceno[26a], M. Nessi[32,ag], M. S. Neubauer[169], M. Neumann[178], R. M. Neves[112], P. Nevski[27], P. R. Newman[19], D. H. Nguyen[6], T. Nguyen Manh[97], R. B. Nickerson[122], R. Nicolaidou[138], J. Nielsen[139], A. Nikiforov[17], V. Nikolaenko[132,af], I. Nikolic-Audit[83], K. Nikolopoulos[19], J. K. Nilsen[121], P. Nilsson[27], Y. Ninomiya[159], A. Nisati[134a], R. Nisius[103], T. Nobe[159], L. Nodulman[6], M. Nomachi[120], I. Nomidis[31], T. Nooney[79], S. Norberg[115], M. Nordberg[32], N. Norjoharuddeen[122], O. Novgorodova[46], S. Nowak[103], M. Nozaki[69], L. Nozka[117], K. Ntekas[10], E. Nurse[81], F. Nuti[91], F. O'grady[7], D. C. O'Neil[146], A. A. O'Rourke[44], V. O'Shea[55], F. G. Oakham[31,d], H. Oberlack[103], T. Obermann[23], J. Ocariz[83], A. Ochi[70], I. Ochoa[37], J. P. Ochoa-Ricoux[34a], S. Oda[73], S. Odaka[69], H. Ogren[64], A. Oh[87], S. H. Oh[47], C. C. Ohm[16], H. Ohman[168], H. Oide[32], H. Okawa[164], Y. Okumura[33], T. Okuyama[69], A. Olariu[28b], L. F. Oleiro Seabra[128a], S. A. Olivares Pino[48], D. Oliveira Damazio[27], A. Olszewski[41], J. Olszowska[41], A. Onofre[128a,128e], K. Onogi[105], P. U. E. Onyisi[11,w], M. J. Oreglia[33], Y. Oren[157], D. Orestano[136a,136b], N. Orlando[63b], R. S. Orr[162], B. Osculati[52a,52b,*], R. Ospanov[87], G. Otero y Garzon[29], H. Otono[73], M. Ouchrif[137d], F. Ould-Saada[121], A. Ouraou[138], K. P. Oussoren[109], Q. Ouyang[35a], M. Owen[55], R. E. Owen[19], V. E. Ozcan[20a], N. Ozturk[8], K. Pachal[146], A. Pacheco Pages[13], L. Pacheco Rodriguez[138], C. Padilla Aranda[13], M. Pagáčová[50], S. Pagan Griso[16], F. Paige[27], P. Pais[89], K. Pajchel[121], G. Palacino[163b], S. Palazzo[39a,39b], S. Palestini[32], M. Palka[40b], D. Pallin[36], A. Palma[128a,128b], E. St. Panagiotopoulou[10], C. E. Pandini[83], J. G. Panduro Vazquez[80], P. Pani[150a,150b], S. Panitkin[27], D. Pantea[28b], L. Paolozzi[51], Th. D. Papadopoulou[10], K. Papageorgiou[158], A. Paramonov[6], D. Paredes Hernandez[179], A. J. Parker[75], M. A. Parker[30], K. A. Parker[143], F. Parodi[52a,52b], J. A. Parsons[37], U. Parzefall[50], V. R. Pascuzzi[162], E. Pasqualucci[134a], S. Passaggio[52a], Fr. Pastore[80], G. Pásztor[31,ah], S. Pataraia[178], J. R. Pater[87], T. Pauly[32], J. Pearce[172], B. Pearson[115], L. E. Pedersen[38], M. Pedersen[121], S. Pedraza Lopez[170], R. Pedro[128a,128b], S. V. Peleganchuk[111,c], D. Pelikan[168], O. Penc[129], C. Peng[35a], H. Peng[60], J. Penwell[64], B. S. Peralva[26b], M. M. Perego[138], D. V. Perepelitsa[27], E. Perez Codina[163a], L. Perini[94a,94b], H. Pernegger[32], S. Perrella[106a,106b], R. Peschke[44], V. D. Peshekhonov[68], K. Peters[44], R. F. Y. Peters[87], B. A. Petersen[32], T. C. Petersen[38], E. Petit[57], A. Petridis[1], C. Petridou[158], P. Petroff[119], E. Petrolo[134a], M. Petrov[122], F. Petrucci[136a,136b], N. E. Pettersson[89], A. Peyaud[138], R. Pezoa[34b], P. W. Phillips[133], G. Piacquadio[147,ai], E. Pianori[173], A. Picazio[89], E. Piccaro[79], M. Piccinini[22a,22b], M. A. Pickering[122], R. Piegaia[29], J. E. Pilcher[33], A. D. Pilkington[87], A. W. J. Pin[87], M. Pinamonti[167a,167c,aj], J. L. Pinfold[3], A. Pingel[38], S. Pires[83], H. Pirumov[44], M. Pitt[175], L. Plazak[148a], M.-A. Pleier[27], V. Pleskot[86], E. Plotnikova[68], P. Plucinski[93], D. Pluth[67], R. Poettgen[150a,150b], L. Poggioli[119], D. Pohl[23], G. Polesello[123a], A. Poley[44], A. Policicchio[39a,39b], R. Polifka[162], A. Polini[22a], C. S. Pollard[55], V. Polychronakos[27], K. Pommès[32], L. Pontecorvo[134a], B. G. Pope[93], G. A. Popeneciu[28c], D. S. Popovic[14], A. Poppleton[32], S. Pospisil[130], K. Potamianos[16], I. N. Potrap[68], C. J. Potter[30], C. T. Potter[118], G. Poulard[32], J. Poveda[32], V. Pozdnyakov[68], M. E. Pozo Astigarraga[32], P. Pralavorio[88], A. Pranko[16], S. Prell[67], D. Price[87], L. E. Price[6], M. Primavera[76a], S. Prince[90], M. Proissl[48], K. Prokofiev[63c], F. Prokoshin[34b], S. Protopopescu[27], J. Proudfoot[6], M. Przybycien[40a], D. Puddu[136a,136b], M. Purohit[27,ak], P. Puzo[119], J. Qian[92], G. Qin[55], Y. Qin[87], A. Quadt[56], W. B. Quayle[167a,167b], M. Queitsch-Maitland[87], D. Quilty[55], S. Raddum[121], V. Radeka[27], V. Radescu[61b], S. K. Radhakrishnan[152], P. Radloff[118], P. Rados[91], F. Ragusa[94a,94b], G. Rahal[181], J. A. Raine[87], S. Rajagopalan[27], M. Rammensee[32], C. Rangel-Smith[168], M. G. Ratti[94a,94b], F. Rauscher[102], S. Rave[86], T. Ravenscroft[55], I. Ravinovich[175], M. Raymond[32], A. L. Read[121], N. P. Readioff[77], M. Reale[76a,76b], D. M. Rebuzzi[123a,123b], A. Redelbach[177], G. Redlinger[27], R. Reece[139], K. Reeves[43], L. Rehnisch[17], J. Reichert[124], H. Reisin[29], C. Rembser[32], H. Ren[35a], M. Rescigno[134a], S. Resconi[94a], O. L. Rezanova[111,c], P. Reznicek[131], R. Rezvani[97], R. Richter[103], S. Richter[81], E. Richter-Was[40b], O. Ricken[23], M. Ridel[83], P. Rieck[17], C. J. Riegel[178], J. Rieger[56], O. Rifki[115], M. Rijssenbeek[152], A. Rimoldi[123a,123b], M. Rimoldi[18], L. Rinaldi[22a], B. Ristić[51], E. Ritsch[32], I. Riu[13], F. Rizatdinova[116], E. Rizvi[79], C. Rizzi[13], S. H. Robertson[90,m], A. Robichaud-Veronneau[90], D. Robinson[30], J. E. M. Robinson[44], A. Robson[55],

C. Roda[126a,126b], Y. Rodina[88], A. Rodriguez Perez[13], D. Rodriguez Rodriguez[170], S. Roe[32], C. S. Rogan[59], O. Røhne[121], A. Romaniouk[100], M. Romano[22a,22b], S. M. Romano Saez[36], E. Romero Adam[170], N. Rompotis[140], M. Ronzani[50], L. Roos[83], E. Ros[170], S. Rosati[134a], K. Rosbach[50], P. Rose[139], O. Rosenthal[145], N.-A. Rosien[56], V. Rossetti[150a,150b], E. Rossi[106a,106b], L. P. Rossi[52a], J. H. N. Rosten[30], R. Rosten[140], M. Rotaru[28b], I. Roth[175], J. Rothberg[140], D. Rousseau[119], C. R. Royon[138], A. Rozanov[88], Y. Rozen[156], X. Ruan[149c], F. Rubbo[147], M. S. Rudolph[162], F. Rühr[50], A. Ruiz-Martinez[31], Z. Rurikova[50], N. A. Rusakovich[68], A. Ruschke[102], H. L. Russell[140], J. P. Rutherfoord[7], N. Ruthmann[32], Y. F. Ryabov[125], M. Rybar[169], G. Rybkin[119], S. Ryu[6], A. Ryzhov[132], G. F. Rzehorz[56], A. F. Saavedra[154], G. Sabato[109], S. Sacerdoti[29], H. F.-W. Sadrozinski[139], R. Sadykov[68], F. Safai Tehrani[134a], P. Saha[110], M. Sahinsoy[61a], M. Saimpert[138], T. Saito[159], H. Sakamoto[159], Y. Sakurai[174], G. Salamanna[136a,136b], A. Salamon[135a,135b], J. E. Salazar Loyola[34b], D. Salek[109], P. H. Sales De Bruin[140], D. Salihagic[103], A. Salnikov[147], J. Salt[170], D. Salvatore[39a,39b], F. Salvatore[153], A. Salvucci[63a], A. Salzburger[32], D. Sammel[50], D. Sampsonidis[158], A. Sanchez[106a,106b], J. Sánchez[170], V. Sanchez Martinez[170], H. Sandaker[121], R. L. Sandbach[79], H. G. Sander[86], M. Sandhoff[178], C. Sandoval[21], R. Sandstroem[103], D. P. C. Sankey[133], M. Sannino[52a,52b], A. Sansoni[49], C. Santoni[36], R. Santonico[135a,135b], H. Santos[128a], I. Santoyo Castillo[153], K. Sapp[127], A. Sapronov[68], J. G. Saraiva[128a,128d], B. Sarrazin[23], O. Sasaki[69], Y. Sasaki[159], K. Sato[164], G. Sauvage[5,*], E. Sauvan[5], G. Savage[80], P. Savard[162,d], C. Sawyer[133], L. Sawyer[82,r], J. Saxon[33], C. Sbarra[22a], A. Sbrizzi[22a,22b], T. Scanlon[81], D. A. Scannicchio[166], M. Scarcella[154], V. Scarfone[39a,39b], J. Schaarschmidt[175], P. Schacht[103], B. M. Schachtner[102], D. Schaefer[32], R. Schaefer[44], J. Schaeffer[86], S. Schaepe[23], S. Schaetzel[61b], U. Schäfer[86], A. C. Schaffer[119], D. Schaile[102], R. D. Schamberger[152], V. Scharf[61a], V. A. Schegelsky[125], D. Scheirich[131], M. Schernau[166], C. Schiavi[52a,52b], S. Schier[139], C. Schillo[50], M. Schioppa[39a,39b], S. Schlenker[32], K. R. Schmidt-Sommerfeld[103], K. Schmieden[32], C. Schmitt[86], S. Schmitt[44], S. Schmitz[86], B. Schneider[163a], U. Schnoor[50], L. Schoeffel[138], A. Schoening[61b], B. D. Schoenrock[93], E. Schopf[23], M. Schott[86], J. Schovancova[8], S. Schramm[51], M. Schreyer[177], N. Schuh[86], A. Schulte[86], M. J. Schultens[23], H.-C. Schultz-Coulon[61a], H. Schulz[17], M. Schumacher[50], B. A. Schumm[139], Ph. Schune[138], A. Schwartzman[147], T. A. Schwarz[92], Ph. Schwegler[103], H. Schweiger[87], Ph. Schwemling[138], R. Schwienhorst[93], J. Schwindling[138], T. Schwindt[23], G. Sciolla[25], F. Scuri[126a,126b], F. Scutti[91], J. Searcy[92], P. Seema[23], S. C. Seidel[107], A. Seiden[139], F. Seifert[130], J. M. Seixas[26a], G. Sekhniaidze[106a], K. Sekhon[92], S. J. Sekula[42], D. M. Seliverstov[125,*], N. Semprini-Cesari[22a,22b], C. Serfon[121], L. Serin[119], L. Serkin[167a,167b], M. Sessa[136a,136b], R. Seuster[172], H. Severini[115], T. Sfiligoj[78], F. Sforza[32], A. Sfyrla[51], E. Shabalina[56], N. W. Shaikh[150a,150b], L. Y. Shan[35a], R. Shang[169], J. T. Shank[24], M. Shapiro[16], P. B. Shatalov[99], K. Shaw[167a,167b], S. M. Shaw[87], A. Shcherbakova[150a,150b], C. Y. Shehu[153], P. Sherwood[81], L. Shi[155,al], S. Shimizu[70], C. O. Shimmin[166], M. Shimojima[104], M. Shiyakova[68,am], A. Shmeleva[98], D. Shoaleh Saadi[97], M. J. Shochet[33], S. Shojaii[94a,94b], S. Shrestha[113], E. Shulga[100], M. A. Shupe[7], P. Sicho[129], A. M. Sickles[169], P. E. Sidebo[151], O. Sidiropoulou[177], D. Sidorov[116], A. Sidoti[22a,22b], F. Siegert[46], Dj. Sijacki[14], J. Silva[128a,128d], S. B. Silverstein[150a], V. Simak[130], O. Simard[5], Lj. Simic[14], S. Simion[119], E. Simioni[86], B. Simmons[81], D. Simon[36], M. Simon[86], P. Sinervo[162], N. B. Sinev[118], M. Sioli[22a,22b], G. Siragusa[177], S. Yu. Sivoklokov[101], J. Sjölin[150a,150b], M. B. Skinner[75], H. P. Skottowe[59], P. Skubic[115], M. Slater[19], T. Slavicek[130], M. Slawinska[109], K. Sliwa[165], R. Slovak[131], V. Smakhtin[175], B. H. Smart[5], L. Smestad[15], J. Smiesko[148a], S. Yu. Smirnov[100], Y. Smirnov[100], L. N. Smirnova[101,an], O. Smirnova[84], M. N. K. Smith[37], R. W. Smith[37], M. Smizanska[75], K. Smolek[130], A. A. Snesarev[98], S. Snyder[27], R. Sobie[172,m], F. Socher[46], A. Soffer[157], D. A. Soh[155], G. Sokhrannyi[78], C. A. Solans Sanchez[32], M. Solar[130], E. Yu. Soldatov[100], U. Soldevila[170], A. A. Solodkov[132], A. Soloshenko[68], O. V. Solovyanov[132], V. Solovyev[125], P. Sommer[50], H. Son[165], H. Y. Song[60,ao], A. Sood[16], A. Sopczak[130], V. Sopko[130], V. Sorin[13], D. Sosa[61b], C. L. Sotiropoulou[126a,126b], R. Soualah[167a,167c], A. M. Soukharev[111,c], D. South[44], B. C. Sowden[80], S. Spagnolo[76a,76b], M. Spalla[126a,126b], M. Spangenberg[173], F. Spanò[80], D. Sperlich[17], F. Spettel[103], R. Spighi[22a], G. Spigo[32], L. A. Spiller[91], M. Spousta[131], R. D. St. Denis[55,*], A. Stabile[94a], R. Stamen[61a], S. Stamm[17], E. Stanecka[41], R. W. Stanek[6], C. Stanescu[136a], M. Stanescu-Bellu[44], M. M. Stanitzki[44], S. Stapnes[121], E. A. Starchenko[132], G. H. Stark[33], J. Stark[57], P. Staroba[129], P. Starovoitov[61a], S. Stärz[32], R. Staszewski[41], P. Steinberg[27], B. Stelzer[146], H. J. Stelzer[32], O. Stelzer-Chilton[163a], H. Stenzel[54], G. A. Stewart[55], J. A. Stillings[23], M. C. Stockton[90], M. Stoebe[90], G. Stoicea[28b], P. Stolte[56], S. Stonjek[103], A. R. Stradling[8], A. Straessner[46], M. E. Stramaglia[18], J. Strandberg[151], S. Strandberg[150a,150b], A. Strandlie[121], M. Strauss[115], P. Strizenec[148b], R. Ströhmer[177], D. M. Strom[118], R. Stroynowski[42], A. Strubig[108], S. A. Stucci[18], B. Stugu[15], N. A. Styles[44], D. Su[147], J. Su[127], R. Subramaniam[82], S. Suchek[61a], Y. Sugaya[120], M. Suk[130], V. V. Sulin[98], S. Sultansoy[4c], T. Sumida[71], S. Sun[59], X. Sun[35a], J. E. Sundermann[50], K. Suruliz[153], G. Susinno[39a,39b], M. R. Sutton[153], S. Suzuki[69], M. Svatos[129], M. Swiatlowski[33], I. Sykora[148a], T. Sykora[131], D. Ta[50], C. Taccini[136a,136b], K. Tackmann[44], J. Taenzer[162], A. Taffard[166], R. Tafirout[163a], N. Taiblum[157], H. Takai[27], R. Takashima[72], T. Takeshita[144], Y. Takubo[69], M. Talby[88], A. A. Talyshev[111,c], K. G. Tan[91], J. Tanaka[159], R. Tanaka[119], S. Tanaka[69], B. B. Tannenwald[113], S. Tapia Araya[34b], S. Tapprogge[86], S. Tarem[156], G. F. Tartarelli[94a], P. Tas[131], M. Tasevsky[129], T. Tashiro[71], E. Tassi[39a,39b], A. Tavares Delgado[128a,128b],

Y. Tayalati[137d], A. C. Taylor[107], G. N. Taylor[91], P. T. E. Taylor[91], W. Taylor[163b], F. A. Teischinger[32], P. Teixeira-Dias[80], K. K. Temming[50], D. Temple[146], H. Ten Kate[32], P. K. Teng[155], J. J. Teoh[120], F. Tepel[178], S. Terada[69], K. Terashi[159], J. Terron[85], S. Terzo[103], M. Testa[49], R. J. Teuscher[162,m], T. Theveneaux-Pelzer[88], J. P. Thomas[19], J. Thomas-Wilsker[80], E. N. Thompson[37], P. D. Thompson[19], A. S. Thompson[55], L. A. Thomsen[179], E. Thomson[124], M. Thomson[30], M. J. Tibbetts[16], R. E. Ticse Torres[88], V. O. Tikhomirov[98,ap], Yu. A. Tikhonov[111,c], S. Timoshenko[100], P. Tipton[179], S. Tisserant[88], K. Todome[161], T. Todorov[5,*], S. Todorova-Nova[131], J. Tojo[73], S. Tokár[148a], K. Tokushuku[69], E. Tolley[59], L. Tomlinson[87], M. Tomoto[105], L. Tompkins[147,aq], K. Toms[107], B. Tong[59], E. Torrence[118], H. Torres[146], E. Torró Pastor[140], J. Toth[88,ar], F. Touchard[88], D. R. Tovey[143], T. Trefzger[177], A. Tricoli[27], I. M. Trigger[163a], S. Trincaz-Duvoid[83], M. F. Tripiana[13], W. Trischuk[162], B. Trocmé[57], A. Trofymov[44], C. Troncon[94a], M. Trottier-McDonald[16], M. Trovatelli[172], L. Truong[167a,167c], M. Trzebinski[41], A. Trzupek[41], J. C.-L. Tseng[122], P. V. Tsiareshka[95], G. Tsipolitis[10], N. Tsirintanis[9], S. Tsiskaridze[13], V. Tsiskaridze[50], E. G. Tskhadadze[53a], K. M. Tsui[63a], I. I. Tsukerman[99], V. Tsulaia[16], S. Tsuno[69], D. Tsybychev[152], A. Tudorache[28b], V. Tudorache[28b], A. N. Tuna[59], S. A. Tupputi[22a,22b], S. Turchikhin[101,an], D. Turecek[130], D. Turgeman[175], R. Turra[94a,94b], A. J. Turvey[42], P. M. Tuts[37], M. Tyndel[133], G. Ucchielli[22a,22b], I. Ueda[159], M. Ughetto[150a,150b], F. Ukegawa[164], G. Unal[32], A. Undrus[27], G. Unel[166], F. C. Ungaro[91], Y. Unno[69], C. Unverdorben[102], J. Urban[148b], P. Urquijo[91], P. Urrejola[86], G. Usai[8], A. Usanova[65], L. Vacavant[88], V. Vacek[130], B. Vachon[90], C. Valderanis[102], E. Valdes Santurio[150a,150b], N. Valencic[109], S. Valentinetti[22a,22b], A. Valero[170], L. Valery[13], S. Valkar[131], S. Vallecorsa[51], J. A. Valls Ferrer[170], W. Van Den Wollenberg[109], P. C. Van Der Deijl[109], R. van der Geer[109], H. van der Graaf[109], N. van Eldik[156], P. van Gemmeren[6], J. Van Nieuwkoop[146], I. van Vulpen[109], M. C. van Woerden[32], M. Vanadia[134a,134b], W. Vandelli[32], R. Vanguri[124], A. Vaniachine[6,k], P. Vankov[109], G. Vardanyan[180], R. Vari[134a], E. W. Varnes[7], T. Varol[42], D. Varouchas[83], A. Vartapetian[8], K. E. Varvell[154], J. G. Vasquez[179], F. Vazeille[36], T. Vazquez Schroeder[90], J. Veatch[56], L. M. Veloce[162], F. Veloso[128a,128c], S. Veneziano[134a], A. Ventura[76a,76b], M. Venturi[172], N. Venturi[162], A. Venturini[25], V. Vercesi[123a], M. Verducci[134a,134b], W. Verkerke[109], J. C. Vermeulen[109], A. Vest[46,as], M. C. Vetterli[146,d], O. Viazlo[84], I. Vichou[169,*], T. Vickey[143], O. E. Vickey Boeriu[143], G. H. A. Viehhauser[122], S. Viel[16], L. Vigani[122], R. Vigne[65], M. Villa[22a,22b], M. Villaplana Perez[94a,94b], E. Vilucchi[49], M. G. Vincter[31], V. B. Vinogradov[68], C. Vittori[22a,22b], I. Vivarelli[153], S. Vlachos[10], M. Vlasak[130], M. Vogel[178], P. Vokac[130], G. Volpi[126a,126b], M. Volpi[91], H. von der Schmitt[103], E. von Toerne[23], V. Vorobel[131], K. Vorobev[100], M. Vos[170], R. Voss[32], J. H. Vossebeld[77], N. Vranjes[14], M. Vranjes Milosavljevic[14], V. Vrba[129], M. Vreeswijk[109], R. Vuillermet[32], I. Vukotic[33], Z. Vykydal[130], P. Wagner[23], W. Wagner[178], H. Wahlberg[74], S. Wahrmund[46], J. Wakabayashi[105], J. Walder[75], R. Walker[102], W. Walkowiak[145], V. Wallangen[150a,150b], C. Wang[35b], C. Wang[141,88], F. Wang[176], H. Wang[16], H. Wang[42], J. Wang[44], J. Wang[154], K. Wang[90], R. Wang[6], S. M. Wang[155], T. Wang[23], T. Wang[37], W. Wang[60], X. Wang[179], C. Wanotayaroj[118], A. Warburton[90], C. P. Ward[30], D. R. Wardrope[81], A. Washbrook[48], P. M. Watkins[19], A. T. Watson[19], M. F. Watson[19], G. Watts[140], S. Watts[87], B. M. Waugh[81], S. Webb[86], M. S. Weber[18], S. W. Weber[177], J. S. Webster[6], A. R. Weidberg[122], B. Weinert[64], J. Weingarten[56], C. Weiser[50], H. Weits[109], P. S. Wells[32], T. Wenaus[27], T. Wengler[32], S. Wenig[32], N. Wermes[23], M. Werner[50], M. D. Werner[67], P. Werner[32], M. Wessels[61a], J. Wetter[165], K. Whalen[118], N. L. Whallon[140], A. M. Wharton[75], A. White[8], M. J. White[1], R. White[34b], D. Whiteson[166], F. J. Wickens[133], W. Wiedenmann[176], M. Wielers[133], P. Wienemann[23], C. Wiglesworth[38], L. A. M. Wiik-Fuchs[23], A. Wildauer[103], F. Wilk[87], H. G. Wilkens[32], H. H. Williams[124], S. Williams[109], C. Willis[93], S. Willocq[89], J. A. Wilson[19], I. Wingerter-Seez[5], F. Winklmeier[118], O. J. Winston[153], B. T. Winter[23], M. Wittgen[147], J. Wittkowski[102], M. W. Wolter[41], H. Wolters[128a,128c], S. D. Worm[133], B. K. Wosiek[41], J. Wotschack[32], M. J. Woudstra[87], K. W. Wozniak[41], M. Wu[57], M. Wu[33], S. L. Wu[176], X. Wu[51], Y. Wu[92], T. R. Wyatt[87], B. M. Wynne[48], S. Xella[38], D. Xu[35a], L. Xu[27], B. Yabsley[154], S. Yacoob[149a], R. Yakabe[70], D. Yamaguchi[161], Y. Yamaguchi[120], A. Yamamoto[69], S. Yamamoto[159], T. Yamanaka[159], K. Yamauchi[105], Y. Yamazaki[70], Z. Yan[24], H. Yang[142], H. Yang[176], Y. Yang[155], Z. Yang[15], W.-M. Yao[16], Y. C. Yap[83], Y. Yasu[69], E. Yatsenko[5], K. H. Yau Wong[23], J. Ye[42], S. Ye[27], I. Yeletskikh[68], A. L. Yen[59], E. Yildirim[86], K. Yorita[174], R. Yoshida[6], K. Yoshihara[124], C. Young[147], C. J. S. Young[32], S. Youssef[24], D. R. Yu[16], J. Yu[8], J. M. Yu[92], J. Yu[67], L. Yuan[70], S. P. Y. Yuen[23], I. Yusuff[30,at], B. Zabinski[41], R. Zaidan[141], A. M. Zaitsev[132,af], N. Zakharchuk[44], J. Zalieckas[15], A. Zaman[152], S. Zambito[59], L. Zanello[134a,134b], D. Zanzi[91], C. Zeitnitz[178], M. Zeman[130], A. Zemla[40a], J. C. Zeng[169], Q. Zeng[147], K. Zengel[25], O. Zenin[132], T. Ženiš[148a], D. Zerwas[119], D. Zhang[92], F. Zhang[176], G. Zhang[60,ao], H. Zhang[35b], J. Zhang[6], L. Zhang[50], R. Zhang[23], R. Zhang[60,au], X. Zhang[141], Z. Zhang[119], X. Zhao[42], Y. Zhao[141], Z. Zhao[60], A. Zhemchugov[68], J. Zhong[122], B. Zhou[92], C. Zhou[47], L. Zhou[37], L. Zhou[42], M. Zhou[152], N. Zhou[35c], C. G. Zhu[141], H. Zhu[35a], J. Zhu[92], Y. Zhu[60], X. Zhuang[35a], K. Zhukov[98], A. Zibell[177], D. Zieminska[64], N. I. Zimine[68], C. Zimmermann[86], S. Zimmermann[50], Z. Zinonos[56], M. Zinser[86], M. Ziolkowski[145], L. Živković[14], G. Zobernig[176], A. Zoccoli[22a,22b], M. zur Nedden[17], L. Zwalinski[32]

[1] Department of Physics, University of Adelaide, Adelaide, SA, Australia
[2] Physics Department, SUNY Albany, Albany, NY, USA
[3] Department of Physics, University of Alberta, Edmonton, AB, Canada
[4] [(a)] Department of Physics, Ankara University, Ankara, Turkey; [(b)] Istanbul Aydin University, Istanbul, Turkey; [(c)] Division of Physics, TOBB University of Economics and Technology, Ankara, Turkey
[5] LAPP, CNRS/IN2P3 and Université Savoie Mont Blanc, Annecy-le-Vieux, France
[6] High Energy Physics Division, Argonne National Laboratory, Argonne, IL, USA
[7] Department of Physics, University of Arizona, Tucson, AZ, USA
[8] Department of Physics, The University of Texas at Arlington, Arlington, TX, USA
[9] Physics Department, University of Athens, Athens, Greece
[10] Physics Department, National Technical University of Athens, Zografou, Greece
[11] Department of Physics, The University of Texas at Austin, Austin, TX, USA
[12] Institute of Physics, Azerbaijan Academy of Sciences, Baku, Azerbaijan
[13] Institut de Física d'Altes Energies (IFAE), The Barcelona Institute of Science and Technology, Barcelona, Spain
[14] Institute of Physics, University of Belgrade, Belgrade, Serbia
[15] Department for Physics and Technology, University of Bergen, Bergen, Norway
[16] Physics Division, Lawrence Berkeley National Laboratory and University of California, Berkeley, CA, USA
[17] Department of Physics, Humboldt University, Berlin, Germany
[18] Albert Einstein Center for Fundamental Physics and Laboratory for High Energy Physics, University of Bern, Bern, Switzerland
[19] School of Physics and Astronomy, University of Birmingham, Birmingham, UK
[20] [(a)] Department of Physics, Bogazici University, Istanbul, Turkey; [(b)] Department of Physics Engineering, Gaziantep University, Gaziantep, Turkey; [(c)] Istanbul Bilgi University, Faculty of Engineering and Natural Sciences, Istanbul, Turkey; [(d)] Bahcesehir University, Faculty of Engineering and Natural Sciences, Istanbul, Turkey
[21] Centro de Investigaciones, Universidad Antonio Narino, Bogota, Colombia
[22] [(a)] INFN Sezione di Bologna, Bologna, Italy; [(b)] Dipartimento di Fisica e Astronomia, Università di Bologna, Bologna, Italy
[23] Physikalisches Institut, University of Bonn, Bonn, Germany
[24] Department of Physics, Boston University, Boston, MA, USA
[25] Department of Physics, Brandeis University, Waltham, MA, USA
[26] [(a)] Universidade Federal do Rio De Janeiro COPPE/EE/IF, Rio de Janeiro, Brazil; [(b)] Electrical Circuits Department, Federal University of Juiz de Fora (UFJF), Juiz de Fora, Brazil; [(c)] Federal University of Sao Joao del Rei (UFSJ), Sao Joao del Rei, Brazil; [(d)] Instituto de Fisica, Universidade de Sao Paulo, Sao Paulo, Brazil
[27] Physics Department, Brookhaven National Laboratory, Upton, NY, USA
[28] [(a)] Transilvania University of Brasov, Brasov, Romania; [(b)] National Institute of Physics and Nuclear Engineering, Bucharest, Romania; [(c)] Physics Department, National Institute for Research and Development of Isotopic and Molecular Technologies, Cluj Napoca, Romania; [(d)] University Politehnica Bucharest, Bucharest, Romania; [(e)] West University in Timisoara, Timisoara, Romania
[29] Departamento de Física, Universidad de Buenos Aires, Buenos Aires, Argentina
[30] Cavendish Laboratory, University of Cambridge, Cambridge, UK
[31] Department of Physics, Carleton University, Ottawa, ON, Canada
[32] CERN, Geneva, Switzerland
[33] Enrico Fermi Institute, University of Chicago, Chicago, IL, USA
[34] [(a)] Departamento de Física, Pontificia Universidad Católica de Chile, Santiago, Chile; [(b)] Departamento de Física, Universidad Técnica Federico Santa María, Valparaiso, Chile
[35] [(a)] Institute of High Energy Physics, Chinese Academy of Sciences, Beijing, China; [(b)] Department of Physics, Nanjing University, Jiangsu, China; [(c)] Physics Department, Tsinghua University, Beijing 100084, China
[36] Laboratoire de Physique Corpusculaire, Clermont Université and Université Blaise Pascal and CNRS/IN2P3, Clermont-Ferrand, France
[37] Nevis Laboratory, Columbia University, Irvington, NY, USA
[38] Niels Bohr Institute, University of Copenhagen, Copenhagen, Denmark
[39] [(a)] INFN Gruppo Collegato di Cosenza, Laboratori Nazionali di Frascati, Frascati, Italy; [(b)] Dipartimento di Fisica, Università della Calabria, Rende, Italy

[40] [(a)]Faculty of Physics and Applied Computer Science, AGH University of Science and Technology, Krakow, Poland; [(b)]Marian Smoluchowski Institute of Physics, Jagiellonian University, Krakow, Poland
[41] Institute of Nuclear Physics, Polish Academy of Sciences, Krakow, Poland
[42] Physics Department, Southern Methodist University, Dallas, TX, USA
[43] Physics Department, University of Texas at Dallas, Richardson, TX, USA
[44] DESY, Hamburg and Zeuthen, Germany
[45] Lehrstuhl für Experimentelle Physik IV, Technische Universität Dortmund, Dortmund, Germany
[46] Institut für Kern-und Teilchenphysik, Technische Universität Dresden, Dresden, Germany
[47] Department of Physics, Duke University, Durham, NC, USA
[48] SUPA-School of Physics and Astronomy, University of Edinburgh, Edinburgh, UK
[49] INFN Laboratori Nazionali di Frascati, Frascati, Italy
[50] Fakultät für Mathematik und Physik, Albert-Ludwigs-Universität, Freiburg, Germany
[51] Section de Physique, Université de Genève, Geneva, Switzerland
[52] [(a)]INFN Sezione di Genova, Genoa, Italy; [(b)]Dipartimento di Fisica, Università di Genova, Genoa, Italy
[53] [(a)]E. Andronikashvili Institute of Physics, Iv. Javakhishvili Tbilisi State University, Tbilisi, Georgia; [(b)]High Energy Physics Institute, Tbilisi State University, Tbilisi, Georgia
[54] II Physikalisches Institut, Justus-Liebig-Universität Giessen, Giessen, Germany
[55] SUPA-School of Physics and Astronomy, University of Glasgow, Glasgow, UK
[56] II Physikalisches Institut, Georg-August-Universität, Göttingen, Germany
[57] Laboratoire de Physique Subatomique et de Cosmologie, Université Grenoble-Alpes, CNRS/IN2P3, Grenoble, France
[58] Department of Physics, Hampton University, Hampton, VA, USA
[59] Laboratory for Particle Physics and Cosmology, Harvard University, Cambridge, MA, USA
[60] Department of Modern Physics, University of Science and Technology of China, Anhui, China
[61] [(a)]Kirchhoff-Institut für Physik, Ruprecht-Karls-Universität Heidelberg, Heidelberg, Germany; [(b)]Physikalisches Institut, Ruprecht-Karls-Universität Heidelberg, Heidelberg, Germany; [(c)]ZITI Institut für technische Informatik, Ruprecht-Karls-Universität Heidelberg, Mannheim, Germany
[62] Faculty of Applied Information Science, Hiroshima Institute of Technology, Hiroshima, Japan
[63] [(a)]Department of Physics, The Chinese University of Hong Kong, Shatin, NT, Hong Kong; [(b)]Department of Physics, The University of Hong Kong, Hong Kong, China; [(c)]Department of Physics, The Hong Kong University of Science and Technology, Clear Water Bay, Kowloon, Hong Kong, China
[64] Department of Physics, Indiana University, Bloomington, IN, USA
[65] Institut für Astro- und Teilchenphysik, Leopold-Franzens-Universität, Innsbruck, Austria
[66] University of Iowa, Iowa City, IA, USA
[67] Department of Physics and Astronomy, Iowa State University, Ames, IA, USA
[68] Joint Institute for Nuclear Research, JINR Dubna, Dubna, Russia
[69] KEK, High Energy Accelerator Research Organization, Tsukuba, Japan
[70] Graduate School of Science, Kobe University, Kobe, Japan
[71] Faculty of Science, Kyoto University, Kyoto, Japan
[72] Kyoto University of Education, Kyoto, Japan
[73] Department of Physics, Kyushu University, Fukuoka, Japan
[74] Instituto de Física La Plata, Universidad Nacional de La Plata and CONICET, La Plata, Argentina
[75] Physics Department, Lancaster University, Lancaster, UK
[76] [(a)]INFN Sezione di Lecce, Lecce, Italy; [(b)]Dipartimento di Matematica e Fisica, Università del Salento, Lecce, Italy
[77] Oliver Lodge Laboratory, University of Liverpool, Liverpool, UK
[78] Department of Physics, Jožef Stefan Institute and University of Ljubljana, Ljubljana, Slovenia
[79] School of Physics and Astronomy, Queen Mary University of London, London, UK
[80] Department of Physics, Royal Holloway University of London, Surrey, UK
[81] Department of Physics and Astronomy, University College London, London, UK
[82] Louisiana Tech University, Ruston, LA, USA
[83] Laboratoire de Physique Nucléaire et de Hautes Energies, UPMC and Université Paris-Diderot and CNRS/IN2P3, Paris, France
[84] Fysiska institutionen, Lunds universitet, Lund, Sweden
[85] Departamento de Fisica Teorica C-15, Universidad Autonoma de Madrid, Madrid, Spain

[86] Institut für Physik, Universität Mainz, Mainz, Germany
[87] School of Physics and Astronomy, University of Manchester, Manchester, UK
[88] CPPM, Aix-Marseille Université and CNRS/IN2P3, Marseille, France
[89] Department of Physics, University of Massachusetts, Amherst, MA, USA
[90] Department of Physics, McGill University, Montreal, QC, Canada
[91] School of Physics, University of Melbourne, Melbourne, VIC, Australia
[92] Department of Physics, The University of Michigan, Ann Arbor, MI, USA
[93] Department of Physics and Astronomy, Michigan State University, East Lansing, MI, USA
[94] [(a)]INFN Sezione di Milano, Milan, Italy; [(b)]Dipartimento di Fisica, Università di Milano, Milan, Italy
[95] B.I. Stepanov Institute of Physics, National Academy of Sciences of Belarus, Minsk, Republic of Belarus
[96] National Scientific and Educational Centre for Particle and High Energy Physics, Minsk, Republic of Belarus
[97] Group of Particle Physics, University of Montreal, Montreal, QC, Canada
[98] P.N. Lebedev Physical Institute of the Russian Academy of Sciences, Moscow, Russia
[99] Institute for Theoretical and Experimental Physics (ITEP), Moscow, Russia
[100] National Research Nuclear University MEPhI, Moscow, Russia
[101] D.V. Skobeltsyn Institute of Nuclear Physics, M.V. Lomonosov Moscow State University, Moscow, Russia
[102] Fakultät für Physik, Ludwig-Maximilians-Universität München, München, Germany
[103] Max-Planck-Institut für Physik (Werner-Heisenberg-Institut), München, Germany
[104] Nagasaki Institute of Applied Science, Nagasaki, Japan
[105] Graduate School of Science and Kobayashi-Maskawa Institute, Nagoya University, Nagoya, Japan
[106] [(a)]INFN Sezione di Napoli, Naples, Italy; [(b)]Dipartimento di Fisica, Università di Napoli, Naples, Italy
[107] Department of Physics and Astronomy, University of New Mexico, Albuquerque, NM, USA
[108] Institute for Mathematics, Astrophysics and Particle Physics, Radboud University Nijmegen/Nikhef, Nijmegen, The Netherlands
[109] Nikhef National Institute for Subatomic Physics and University of Amsterdam, Amsterdam, The Netherlands
[110] Department of Physics, Northern Illinois University, DeKalb, IL, USA
[111] Budker Institute of Nuclear Physics, SB RAS, Novosibirsk, Russia
[112] Department of Physics, New York University, New York, NY, USA
[113] Ohio State University, Columbus, OH, USA
[114] Faculty of Science, Okayama University, Okayama, Japan
[115] Homer L. Dodge Department of Physics and Astronomy, University of Oklahoma, Norman, OK, USA
[116] Department of Physics, Oklahoma State University, Stillwater, OK, USA
[117] Palacký University, RCPTM, Olomouc, Czech Republic
[118] Center for High Energy Physics, University of Oregon, Eugene, OR, USA
[119] LAL, Univ. Paris-Sud, CNRS/IN2P3, Université Paris-Saclay, Orsay, France
[120] Graduate School of Science, Osaka University, Osaka, Japan
[121] Department of Physics, University of Oslo, Oslo, Norway
[122] Department of Physics, Oxford University, Oxford, UK
[123] [(a)]INFN Sezione di Pavia, Pavia, Italy; [(b)]Dipartimento di Fisica, Università di Pavia, Pavia, Italy
[124] Department of Physics, University of Pennsylvania, Philadelphia, PA, USA
[125] National Research Centre "Kurchatov Institute" B.P.Konstantinov Petersburg Nuclear Physics Institute, St. Petersburg, Russia
[126] [(a)]INFN Sezione di Pisa, Pisa, Italy; [(b)]Dipartimento di Fisica E. Fermi, Università di Pisa, Pisa, Italy
[127] Department of Physics and Astronomy, University of Pittsburgh, Pittsburgh, PA, USA
[128] [(a)]Laboratório de Instrumentação e Física Experimental de Partículas -LIP, Lisbon, Portugal; [(b)]Faculdade de Ciências, Universidade de Lisboa, Lisbon, Portugal; [(c)]Department of Physics, University of Coimbra, Coimbra, Portugal; [(d)]Centro de Física Nuclear da Universidade de Lisboa, Lisbon, Portugal; [(e)]Departamento de Fisica, Universidade do Minho, Braga, Portugal; [(f)]Departamento de Fisica Teorica y del Cosmos and CAFPE, Universidad de Granada, Granada, Spain; [(g)]Dep Fisica and CEFITEC of Faculdade de Ciencias e Tecnologia, Universidade Nova de Lisboa, Caparica, Portugal
[129] Institute of Physics, Academy of Sciences of the Czech Republic, Prague, Czech Republic
[130] Czech Technical University in Prague, Prague, Czech Republic
[131] Faculty of Mathematics and Physics, Charles University in Prague, Prague, Czech Republic

[132] State Research Center Institute for High Energy Physics (Protvino), NRC KI, Russia
[133] Particle Physics Department, Rutherford Appleton Laboratory, Didcot, UK
[134] [(a)]INFN Sezione di Roma, Rome, Italy; [(b)]Dipartimento di Fisica, Sapienza Università di Roma, Rome, Italy
[135] [(a)]INFN Sezione di Roma Tor Vergata, Rome, Italy; [(b)]Dipartimento di Fisica, Università di Roma Tor Vergata, Rome, Italy
[136] [(a)]INFN Sezione di Roma Tre, Rome, Italy; [(b)]Dipartimento di Matematica e Fisica, Università Roma Tre, Rome, Italy
[137] [(a)]Faculté des Sciences Ain Chock, Réseau Universitaire de Physique des Hautes Energies-Université Hassan II, Casablanca, Morocco; [(b)]Centre National de l'Energie des Sciences Techniques Nucleaires, Rabat, Morocco; [(c)]Faculté des Sciences Semlalia, Université Cadi Ayyad, LPHEA-Marrakech, Marrakech, Morocco; [(d)]Faculté des Sciences, Université Mohamed Premier and LPTPM, Oujda, Morocco; [(e)]Faculté des Sciences, Université Mohammed V, Rabat, Morocco
[138] DSM/IRFU (Institut de Recherches sur les Lois Fondamentales de l'Univers), CEA Saclay (Commissariat à l'Energie Atomique et aux Energies Alternatives), Gif-sur-Yvette, France
[139] Santa Cruz Institute for Particle Physics, University of California Santa Cruz, Santa Cruz, CA, USA
[140] Department of Physics, University of Washington, Seattle, WA, USA
[141] School of Physics, Shandong University, Shandong, China
[142] Department of Physics and Astronomy, Shanghai Key Laboratory for Particle Physics and Cosmology, Shanghai Jiao Tong University, (also affiliated with PKU-CHEP), Shanghai, China
[143] Department of Physics and Astronomy, University of Sheffield, Sheffield, UK
[144] Department of Physics, Shinshu University, Nagano, Japan
[145] Fachbereich Physik, Universität Siegen, Siegen, Germany
[146] Department of Physics, Simon Fraser University, Burnaby, BC, Canada
[147] SLAC National Accelerator Laboratory, Stanford, CA, USA
[148] [(a)]Faculty of Mathematics, Physics and Informatics, Comenius University, Bratislava, Slovak Republic; [(b)]Department of Subnuclear Physics, Institute of Experimental Physics of the Slovak Academy of Sciences, Kosice, Slovak Republic
[149] [(a)]Department of Physics, University of Cape Town, Cape Town, South Africa; [(b)]Department of Physics, University of Johannesburg, Johannesburg, South Africa; [(c)]School of Physics, University of the Witwatersrand, Johannesburg, South Africa
[150] [(a)]Department of Physics, Stockholm University, Stockholm, Sweden; [(b)]The Oskar Klein Centre, Stockholm, Sweden
[151] Physics Department, Royal Institute of Technology, Stockholm, Sweden
[152] Departments of Physics and Astronomy and Chemistry, Stony Brook University, Stony Brook, NY, USA
[153] Department of Physics and Astronomy, University of Sussex, Brighton, UK
[154] School of Physics, University of Sydney, Sydney, NSW, Australia
[155] Institute of Physics, Academia Sinica, Taipei, Taiwan
[156] Department of Physics, Technion: Israel Institute of Technology, Haifa, Israel
[157] Raymond and Beverly Sackler School of Physics and Astronomy, Tel Aviv University, Tel Aviv, Israel
[158] Department of Physics, Aristotle University of Thessaloniki, Thessaloniki, Greece
[159] International Center for Elementary Particle Physics and Department of Physics, The University of Tokyo, Tokyo, Japan
[160] Graduate School of Science and Technology, Tokyo Metropolitan University, Tokyo, Japan
[161] Department of Physics, Tokyo Institute of Technology, Tokyo, Japan
[162] Department of Physics, University of Toronto, Toronto, ON, Canada
[163] [(a)]TRIUMF, Vancouver, BC, Canada; [(b)]Department of Physics and Astronomy, York University, Toronto, ON, Canada
[164] Faculty of Pure and Applied Sciences, and Center for Integrated Research in Fundamental Science and Engineering, University of Tsukuba, Tsukuba, Japan
[165] Department of Physics and Astronomy, Tufts University, Medford, MA, USA
[166] Department of Physics and Astronomy, University of California Irvine, Irvine, CA, USA
[167] [(a)]INFN Gruppo Collegato di Udine, Sezione di Trieste, Udine, Italy; [(b)]ICTP, Trieste, Italy; [(c)]Dipartimento di Chimica Fisica e Ambiente, Università di Udine, Udine, Italy
[168] Department of Physics and Astronomy, University of Uppsala, Uppsala, Sweden
[169] Department of Physics, University of Illinois, Urbana, IL, USA
[170] Instituto de Fisica Corpuscular (IFIC) and Departamento de Fisica Atomica, Molecular y Nuclear and Departamento de Ingeniería Electrónica and Instituto de Microelectrónica de Barcelona (IMB-CNM), University of Valencia and CSIC, Valencia, Spain

[171] Department of Physics, University of British Columbia, Vancouver, BC, Canada
[172] Department of Physics and Astronomy, University of Victoria, Victoria, BC, Canada
[173] Department of Physics, University of Warwick, Coventry, UK
[174] Waseda University, Tokyo, Japan
[175] Department of Particle Physics, The Weizmann Institute of Science, Rehovot, Israel
[176] Department of Physics, University of Wisconsin, Madison, WI, USA
[177] Fakultät für Physik und Astronomie, Julius-Maximilians-Universität, Würzburg, Germany
[178] Fakultät für Mathematik und Naturwissenschaften, Fachgruppe Physik, Bergische Universität Wuppertal, Wuppertal, Germany
[179] Department of Physics, Yale University, New Haven, CT, USA
[180] Yerevan Physics Institute, Yerevan, Armenia
[181] Centre de Calcul de l'Institut National de Physique Nucléaire et de Physique des Particules (IN2P3), Villeurbanne, France

[a] Also at Department of Physics, King's College London, London, United Kingdom
[b] Also at Institute of Physics, Azerbaijan Academy of Sciences, Baku, Azerbaijan
[c] Also at Novosibirsk State University, Novosibirsk, Russia
[d] Also at TRIUMF, Vancouver BC, Canada
[e] Also at Department of Physics and Astronomy, University of Louisville, Louisville, KY, USA
[f] Also at Physics Department, An-Najah National University, Nablus, Palestine
[g] Also at Department of Physics, California State University, Fresno, CA, USA
[h] Also at Department of Physics, University of Fribourg, Fribourg, Switzerland
[i] Also at Departament de Fisica de la Universitat Autonoma de Barcelona, Barcelona, Spain
[j] Also at Departamento de Fisica e Astronomia, Faculdade de Ciencias, Universidade do Porto, Porto, Portugal
[k] Also at Tomsk State University, Tomsk, Russia
[l] Also at Universita di Napoli Parthenope, Napoli, Italy
[m] Also at Institute of Particle Physics (IPP), Victoria, BC, Canada
[n] Also at National Institute of Physics and Nuclear Engineering, Bucharest, Romania
[o] Also at Department of Physics, St. Petersburg State Polytechnical University, St. Petersburg, Russia
[p] Also at Department of Physics, The University of Michigan, Ann Arbor, MI, USA
[q] Also at Centre for High Performance Computing, CSIR Campus, Rosebank, Cape Town, South Africa
[r] Also at Louisiana Tech University, Ruston, LA, USA
[s] Also at Institucio Catalana de Recerca i Estudis Avancats, ICREA, Barcelona, Spain
[t] Also at Graduate School of Science, Osaka University, Osaka, Japan
[u] Also at Department of Physics, National Tsing Hua University, Hsinchu, Taiwan
[v] Also at Institute for Mathematics, Astrophysics and Particle Physics, Radboud University Nijmegen/Nikhef, Nijmegen, Netherlands
[w] Also at Department of Physics, The University of Texas at Austin, Austin TX, USA
[x] Also at CERN, Geneva, Switzerland
[y] Also at Georgian Technical University (GTU), Tbilisi, Georgia
[z] Also at Ochadai Academic Production, Ochanomizu University, Tokyo, Japan
[aa] Also at Manhattan College, New York NY, USA
[ab] Also at Hellenic Open University, Patras, Greece
[ac] Also at Academia Sinica Grid Computing, Institute of Physics, Academia Sinica, Taipei, Taiwan
[ad] Also at School of Physics, Shandong University, Shandong, China
[ae] Also at Department of Physics, California State University, Sacramento CA, USA
[af] Also at Moscow Institute of Physics and Technology State University, Dolgoprudny, Russia
[ag] Also at Section de Physique, Université de Genève, Geneva, Switzerland
[ah] Also at Eotvos Lorand University, Budapest, Hungary
[ai] Also at Departments of Physics and Astronomy and Chemistry, Stony Brook University, Stony Brook NY, USA
[aj] Also at International School for Advanced Studies (SISSA), Trieste, Italy
[ak] Also at Department of Physics and Astronomy, University of South Carolina, Columbia SC, USA
[al] Also at School of Physics and Engineering, Sun Yat-sen University, Guangzhou, China

[am] Also at Institute for Nuclear Research and Nuclear Energy (INRNE) of the Bulgarian Academy of Sciences, Sofia, Bulgaria
[an] Also at Faculty of Physics, M.V.Lomonosov Moscow State University, Moscow, Russia
[ao] Also at Institute of Physics, Academia Sinica, Taipei, Taiwan
[ap] Also at National Research Nuclear University MEPhI, Moscow, Russia
[aq] Also at Department of Physics, Stanford University, Stanford CA, USA
[ar] Also at Institute for Particle and Nuclear Physics, Wigner Research Centre for Physics, Budapest, Hungary
[as] Also at Flensburg University of Applied Sciences, Flensburg, Germany
[at] Also at University of Malaya, Department of Physics, Kuala Lumpur, Malaysia
[au] Also at CPPM, Aix-Marseille Université and CNRS/IN2P3, Marseille, France
* Deceased

From: **Atlas Analysis Glance** atlas-analysis-glance@cern.ch
Subject: Analysis TOPQ-2016-03 "MS dilepton top mass at 8 TeV" - EdBoard formed
Date: 25 January 2016 at 11:26
To: Thorsten.Kuhl@cern.ch, Tancredi.Carli@cern.ch, nenad.vranjes@cern.ch, Richard.Nisius@cern.ch, andreas.alexander.maier@cern.ch, cortiana@mppmu.mpg.de, frederic.deliot@cern.ch, mark.andrew.owen@cern.ch
Cc: Giacomo.Polesello@cern.ch, d.r.tovey@sheffield.ac.uk, h26@nikhef.nl, kado@lal.in2p3.fr, atlas-TOPQ-MASS-conveners@cern.ch

Dear colleagues,

The EdBoard for:

TOPQ-2016-03
"MS dilepton top mass at 8 TeV"
https://atglance.web.cern.ch/atglance/analysis/detailAnalysis.php?readonly=true&id=7982

is formed now.

Members are:
- Editorial board: Nenad Vranjes (Belgrade IP),Thorsten Kuhl (DESY),Tancredi Carli (CERN)
- Chair: Thorsten Kuhl (DESY)

The supporting documents should be already available at
https://atglance.web.cern.ch/atglance/analysis/detailAnalysis.php?readonly=true&id=7982 (in phase 1)

or directly at:
supporting notes:
https://cds.cern.ch/record/2124214/

Editorial board members can find guidelines for the work on edboards at:

https://twiki.cern.ch/twiki/bin/view/AtlasProtected/EditorialBoardGuidelines

Editorial board members and analysis team: a checklist to follow for the review of your note is stored at:

https://twiki.cern.ch/twiki/bin/view/AtlasProtected/PubComConfCheckList

Please have look at the guidelines also when you worked on edboards recently. We try to keep this page up to date with recent information. We invite the chair to organize a meeting of the edboard with the group conveners and the authors to discuss the analysis and the following draft.
Thank you.

Best wishes
Paul De Jong
(email generated via glance)

PS. For the Group Conveners (if not done already):
Please go in glance and when ready fill the relevant fields under the section Analysis review and production of draft.
Then click on the "Proceed and release of draft" button.
THANKS.

From: **Atlas Analysis Glance** atlas-analysis-glance@cern.ch
Subject: Analysis Paper HIGG-2016-33 'HZZ mass 2015+2016' - Editorial Board Formed
Date: 13 January 2017 at 13:37
To: Fabio.Cerutti@cern.ch, michael.duehrssen@cern.ch, kortner@mppmu.mpg.de, ioannis.nomidis@cern.ch, Gaetano.Barone@cern.ch, Gerald.Eigen@cern.ch, shassani@hep.saclay.cea.fr, nicolaid@hep.saclay.cea.fr, Kirill.Prokofiev@cern.ch, Christos.Anastopoulos@cern.ch, sau.lan.wu@cern.ch, luis.flores.castillo@cern.ch, ryszard@physics.smu.edu, daits@umich.edu, zhaozg@ustc.edu.cn, bzhou@umich.edu, lfayard@lal.in2p3.fr, schaffer@mail.cern.ch, Sandra.Kortner@cern.ch, ckourk@mail.cern.ch, fassoul@mail.cern.ch, thomas.koffas@cern.ch, Reisaburo.Tanaka@cern.ch, gabriella.sciolla@cern.ch, williams@hep.upenn.edu, alexei.maslennikov@cern.ch, stefano.rosati@cern.ch, Rostislav.Konoplich@cern.ch, roberto.di.nardo@cern.ch, eleni.mountricha@cern.ch, sarah.heim@cern.ch, Antonio.Salvucci@cern.ch, Susumu.Oda@cern.ch, Jochen.Meyer@cern.ch, giacomo.artoni@cern.ch, hulin.wang@cern.ch, xiangyang.ju@cern.ch, ludovica.aperio.bella@cern.ch, Joany.Andreina.Manjarres.Ramos@cern.ch, Valerio.Bortolotto@cern.ch, Stylianos.Angelidakis@cern.ch, goblirsc@cern.ch, cyril.becot@cern.ch, justas.zalieckas@cern.ch, bijan.haney@cern.ch, andrea.gabrielli@cern.ch, ddivalen@physics.carleton.ca, gcree@physics.carleton.ca, mcanobre@cern.ch, katharina.maria.ecker@cern.ch, nanlu@umich.edu, karolos.potamianos@cern.ch, giada.mancini@cern.ch, nikita.belyaev@cern.ch, william.axel.leight@cern.ch, xiandong.zhao@cern.ch, syed.haider.abidi@cern.ch, Haonan.lu@cern.ch, zongchang.yang@cern.ch, ppodberezko@gmail.com, hherde@brandeis.edu, denys.denysiuk@cern.ch, antoine.laudrain@cern.ch, ngtszyu@gmail.com, cong.geng@cern.ch, arthur.lesage@cea.fr, lauts.hk@gmail.com, walbrech@mpp.mpg.de, joseph.william.carter@cern.ch, marco.scodeggio@student.unife.it, simona.gargiulo15@gmail.com, pan.bellos@hotmail.com, christian.weber@yale.edu, tdpowell@sheffield.ac.uk, nenad.vranjes@cern.ch, alexandre.glazov@desy.de, montoya@cern.ch
Cc: d.r.tovey@sheffield.ac.uk, Tancredi.Carli@cern.ch, atlas-publication-committee-chair@cern.ch, atlas-higg-hsg2-conveners@cern.ch

Dear colleagues,

The EdBoard for HIGG-2016-33 "HZZ mass 2015+2016" is formed now.

Link: https://glance.cern.ch/atlas/analysis/papers/details.php?id=9923

Members are:

- Editorial board:

  - CARRILLO MONTOYA, German David
  - GLAZOV, Alexandre
  - VRANJES, Nenad

- Chair:

  - GLAZOV, Alexandre

Best wishes,

(Automatic e-mail generated by Stephane Willocq)

This message was automatically generated by Glance (hash d65810ca7dc7c996decad1a2fbf85c43).